Dose Calculation and Verification in External Beam Therapy –Warsaw, Poland – 2017

- **Course Directors**
- Tommy Knöös (SE)
- Brendan McClean (IE)

- **Faculty**
- Anders Ahnesjö (SE)
- Ceberg Crister (SE)
- Maria Mania Aspradakis (CH)
- Núria Jornet I Sala (ES)

History

- 1st Teaching course dedicated to Physicists ONLY
  - initiated by H. Svensson and A. Dutreix after an ESTRO workshop on "MU calculation and verification for therapy machines" in 1995 in Gardone Riviera (Italy) during the 3rd ESTRO biennial physics

- The first courses held from 1998
  - Mainly on "Monitor Unit Calculations" which mainly covered factor based models for dose calculation (ESTRO booklet #3 and #6)
  - Since 2002 a much broader physics ("dose determination and verification") content was aimed for photon and electron beam physics, beam modeling and dose calculation algorithms, …

- From 1998 to 2017, the course has been given 19 times (including this week) and about 1600 physicists have participated so far.

Faculty history

- Andrée Dutreix France
- Hans Svensson Sweden
- Gerald Kutcher U.S.A.
- André Bridier France
- Dietmar Georg Austria
- Ben Mijnheer The Netherlands
- Joanna Izewska Austria (IAEA)
- Jörgen Olofsson Sweden
- Günther Hartmann Germany
- **Anders Ahnesjö - Sweden**
- **Maria Aspradakis - Greece**
- **Brendan McClean - Ireland**
- **Tommy Knöös - Sweden**
- **Nuria Jornet - Spain**
- **Crister Ceberg - Sweden**
- **Gabriella Axelsson and Elena Giusti - Course Coordinators ESTRO**

Locations

1 : Santorini (GR) 26-30 April 1998
2 : Santorini (GR) 07-11 May 2000
3 : Coimbra (P) 20-24 May 2001
4 : Perugia (I) 21-25 April 2002
5 : Barcelona (E) 06-10 May 2003
6 : Nice (F) 02-06 May 2004
7 : Poznan (PL) 24 -28 April 2005
8 : Izmir (TU) 7 - 11 May 2006
9: Budapest (H) 29 April – 3 May 2007
10: Dublin (IRE) 19 April – 24 April 2008
11: Munich (D) 15 March-19 March 2009
12: Sevilla (ESP) 14 -18 March, 2010
13: Athens (GR) 27-31 March 2011
14:Izmir (TU) 11-15 March 2012
15: Firenze (IT) 10-14 March 2013
16: Prague (Cz) 9-13 March 2014
17: Barcelona (E) 15-19 March 2015
18: Utrecht (NL) 6-10 March 2016
19: Warsaw (Pl) 2-6 April 2017

ESTRO School

Participants

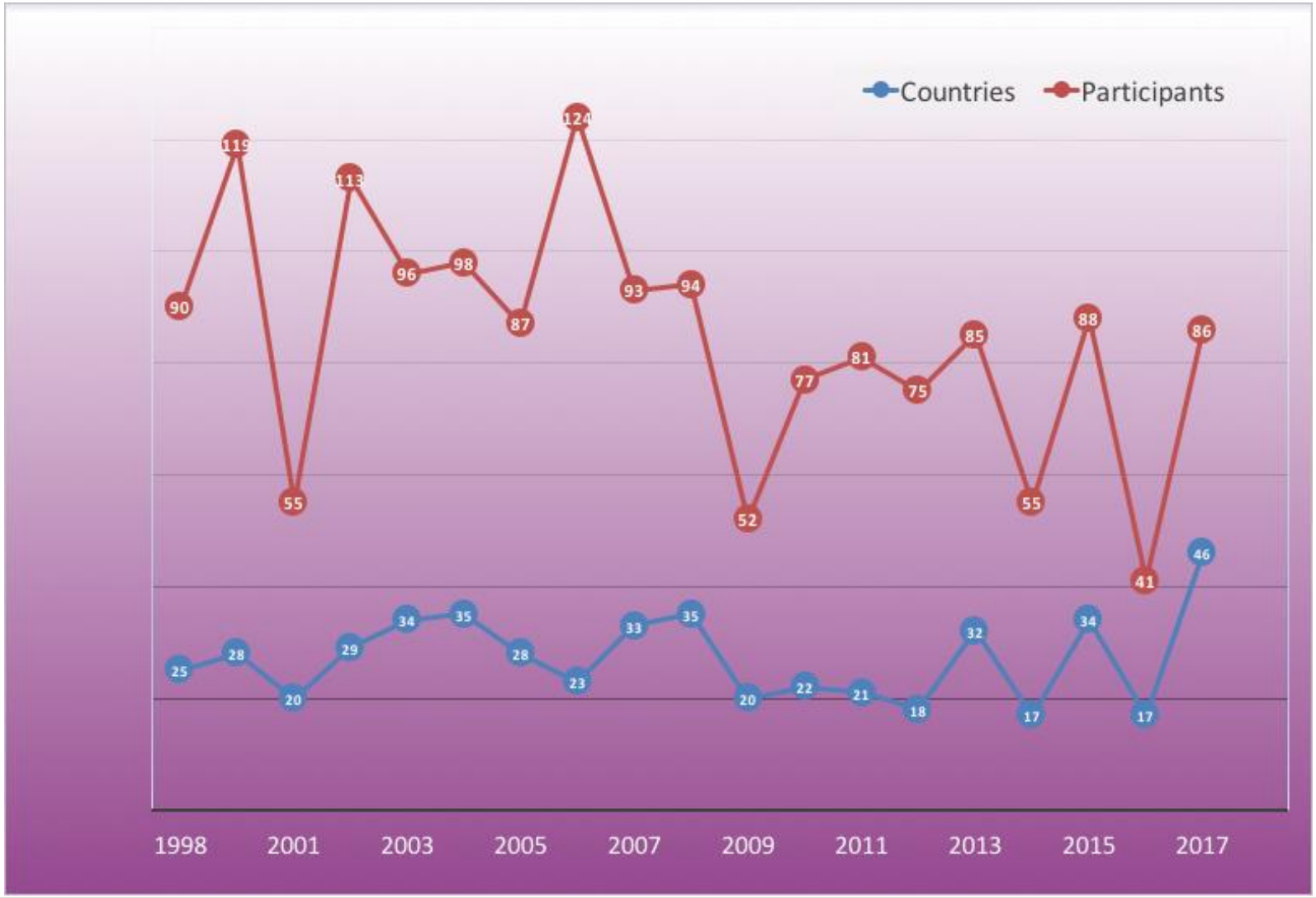

ESTRO School

Why this course?

ESTRO School

What do we know about our systems and safety?

There are recurring themes in reported incidents and accidents

Skills and Rules (Training)
'cookbook' QC is still required

Important to do this with **alertness**, **attention** to detail, **Vigilence**

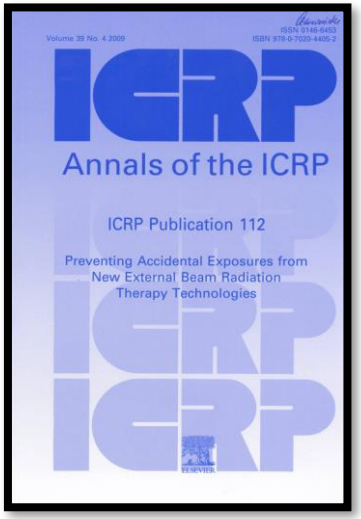

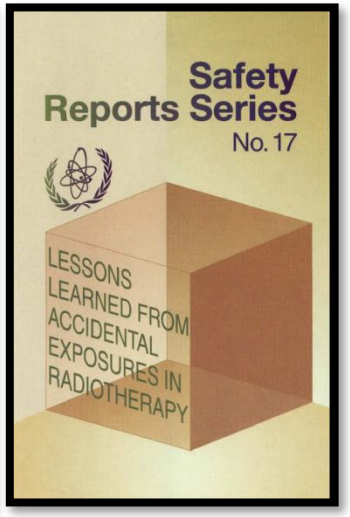

Most (80%?) of what we do falls into these two categories
Need vendor input (applications training)

What do we know about our systems and safety?

There are recurring themes in reported incidents and accidents

Knowledge (Education)
Need to **analyse**, **interpret**, **apply** to new approaches (**critical thinking**)
Real life situations are 'Tangled', dynamically changing – how do you 'train' for that?
Understanding (TP dose calc, optimisation, clinical objectives etc)

Objective of this course!

Commissioning

Inappropriate commissioning

- Reported 2007 at Hôpital de Rangueil in Toulouse, France
- In April 2006, the physicist in the clinic commissioned the new BrainLAB Novalis stereotactic unit
  - Possible to use small fields (6x6mm)
  - "…an ionisation chamber of inappropriate dimensions…" for calibrating the smallest microbeams was used (Farmer chamber was used)
  - The incorrect data was entered into the TPS
  - 145 patients affected

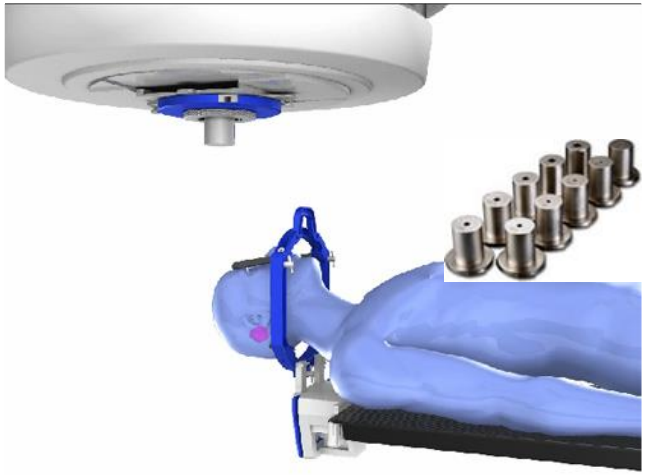

Calibration of TPS - Australia

The incident was discovered in 2006 when an independent measure of machine output, external to the linear accelerator quality assurance process, was performed to implement some new quality assurance software.

These measurements highlighted that there was an under-dosing of 5% when they used data from one of the linacs.

Further investigation at the time of the detection of this anomaly was able to trace back to the TPS beam calibration ratio as the likely cause of the consistent 5% dose discrepancy.

It involved 869 patients between 2004 and 2006.

CT calibration

- Transfer of CT# or HU# to density (physical or electron density depending on TPS)
- Usually performed by scanning

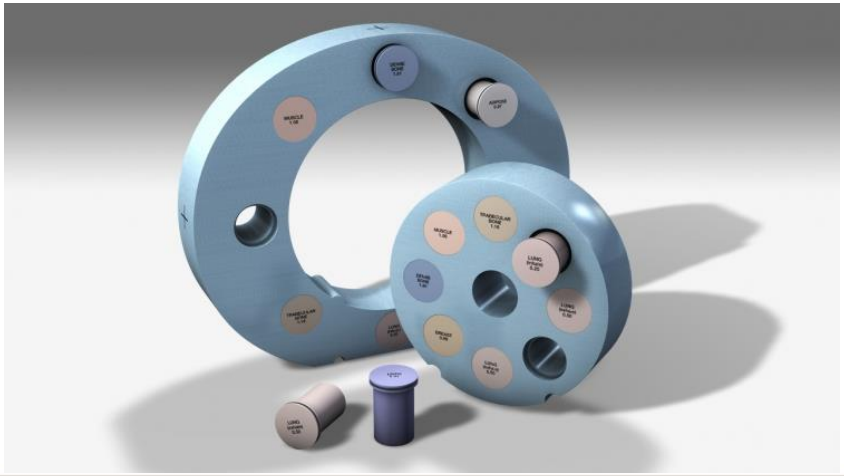

Density vs Hounsfield Number

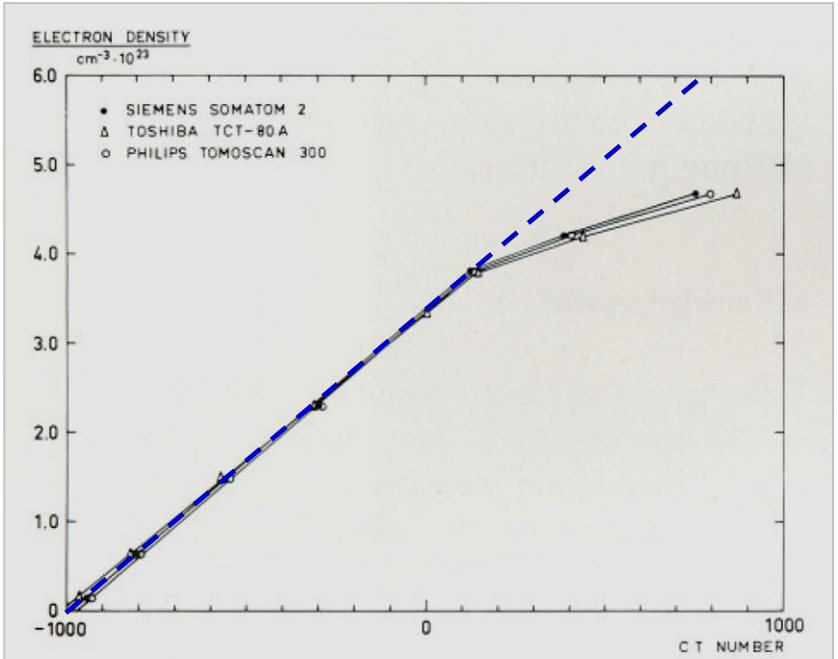

Fig. 3. Relation between CT number and electron density for three different CT scanners. Knöös et al RO 1986

- Lost the dependence of high Z for bone
- Medium not dense enough
- Too low dose
- Most significant for phantoms i.e. IMRT QA
  - -5%

Found during audit

Lessons learned from Epinal

- Potential errors
  - Wrong use of TPS due to lack of training + unsafe screen display #1
  - Dose due to verification imaging (MV portal) not taken into account #2
  - Calculation error due to in-house software, not tested, not qualified #3
  - Sole physicist
- Prevention
  - Time and organisation for continuous training
  - Team of physicists (at least 2)
  - QA for software
  - Software with safe human-computer interaction
  - In vivo dosimetry and second independent calculation

S. Derreumaux, B. Aubert and P. Gourmelon

Institut de Radioprotection et de Sûreté Nucléaire

Radiation Oncologists and physicist in JAIL

- A French court on Wednesday sentenced two doctors and a radiophysicist to 18 months in prison for their role in radiation overdoses given to nearly 450 cancer patients.
- At least 12 people have died as a result of the overdoses administered to patients at the Jean Monnet hospital in Epinal in northeastern France between 2001 and 2006.
- Dozens more are seriously ill as a result of calibration errors that produced the most serious radiation overdose incident France has known.
- The doctors and the radiophysicist had been charged with manslaughter, failure to help people in danger and destroying evidence.

From
The Sunday Times

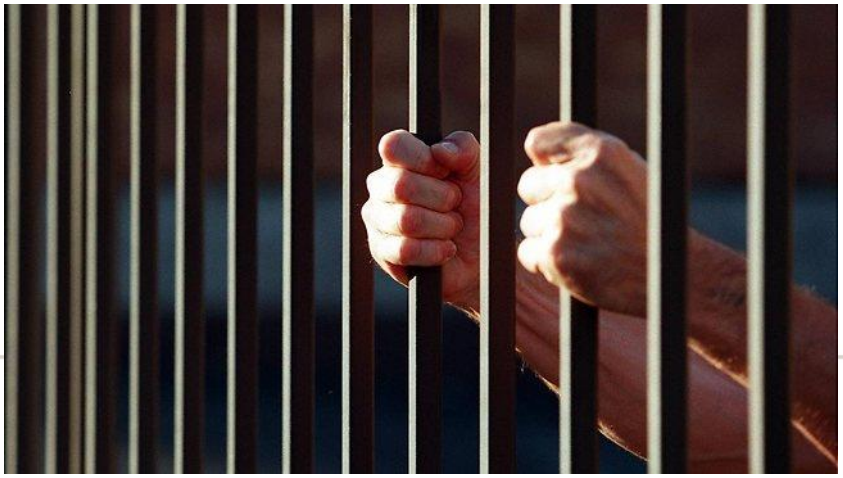

Aim of this course I

- To review external therapy beam physics and beam modelling
- To understand the concepts behind dose algorithms and modelling in state-of-the-art TPS (today' s system)
- To understand the process of commissioning of TP systems

Aim of this course II

- To review dosimetry methods of importance for commissioning and verification
- To review dose verification methods and to offer an overview of available technologies and evaluation methods
- To enable practical implementation of concepts for dose verification in advanced external beam therapy including SRT and IMRT

Programme structure

- Introduction
  - Basic concepts
  - Convolution/superposition
- Input data
  - Linac head design
  - Multisource models
  - Patient characterisation and phantoms
- Modelling 1
  - Point kernels and pencil kernels
  - Grid based approaches
  - Relative dose away from reference conditions
- Verification 1
  - Detectors for measurement; The best detector for different jobs.
  - Uncertainties in our measurements

Programme structure

- Modelling 2
  - How is collected data used in the Beam Model?
  - Small fields
  - Electrons modelling
  - Factor based MU calculations
- MU Calculation Workshop
- Verification 2
  - Methods for data comparison
  - Commissioning, performance and periodic TPS tests
- Modelling 3
  - DVH and dose based metrics
  - Out of field dose modelling
- Practical on Modelling

Programme structure

- In-vivo dosimetry
- Margins in dose calculation
- Guest lecture
- Interactive MCQ

Basic concepts

Crister Ceberg

Medical Radiation Physics

Lund University

Sweden

Learning objectives

The aim of this module is to refresh basic concepts such as

- Radiometric and dosimetric quantities
- Conversion and deposition of energy
- Delta-particle equilibrium
- Raytracing
- Convolution
- The radiation transport equation

The problem

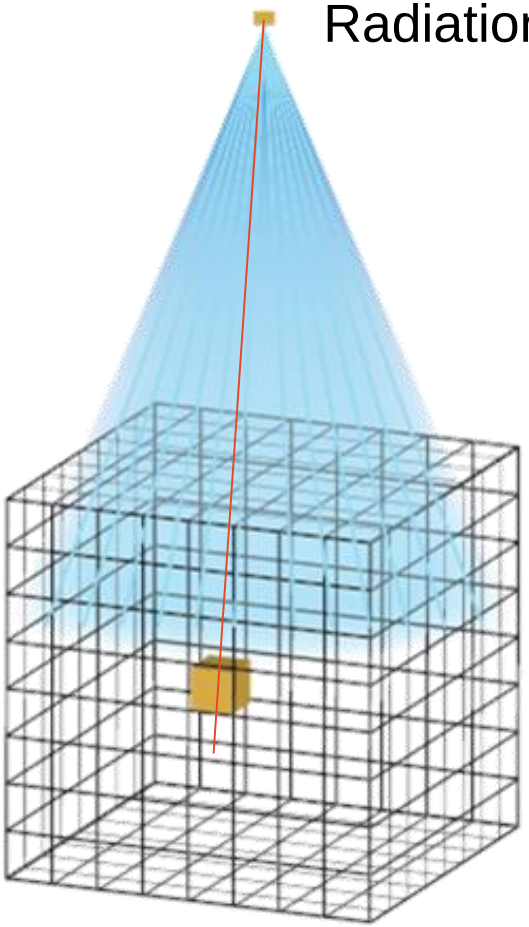

Image from the RayStation manual

- Incident particle fluence
- Raytracing
- Redistribution of energy

Absorbed dose

Source of primary particles

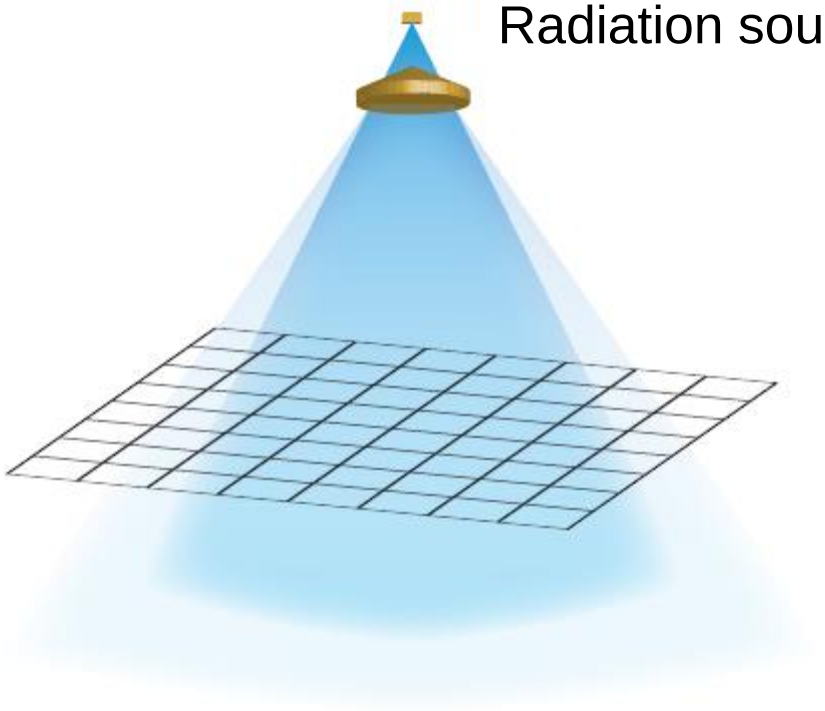

- Incident particle fluence
- Raytracing
- Redistribution of energy

Image from the RayStation manual

RADIOMETRIC QUANTITIES

Particle number

Phase space coordinates $(\vec{r}; \vec{\Omega}; E)$

Spatial coordinate	$\vec{r}$
Direction	$\vec{\Omega}$
Energy	E

Number of particles of type j: $N_j = N_j(\vec{r}; \vec{\Omega}; E)$

Direction

$$\vec{\Omega} = (sin\theta cos\varphi, sin\theta sin\varphi, cos\theta)$$

θ *is the polar angle*

φ *is the azimuth angle*

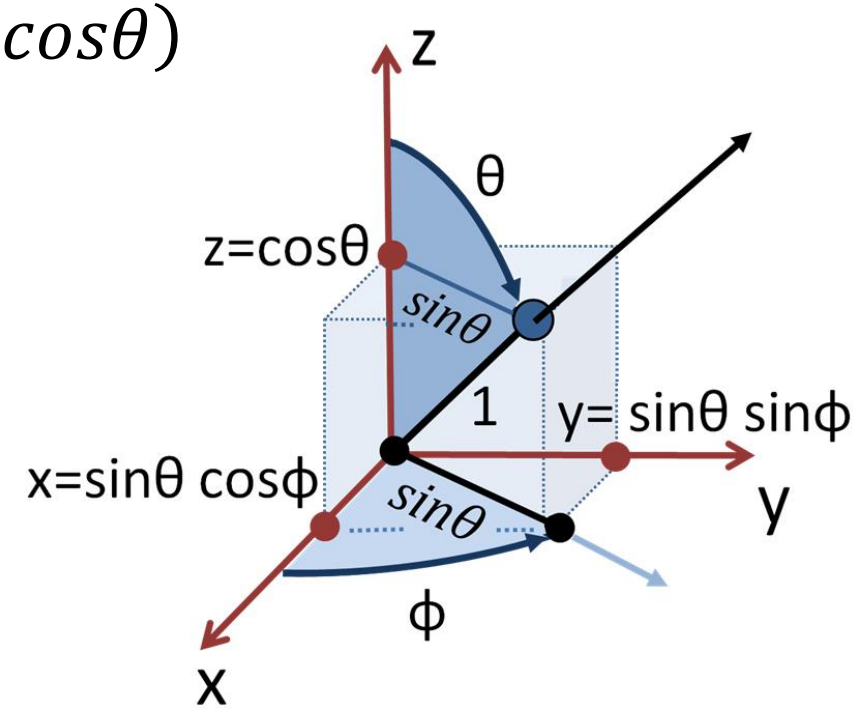

Fluence

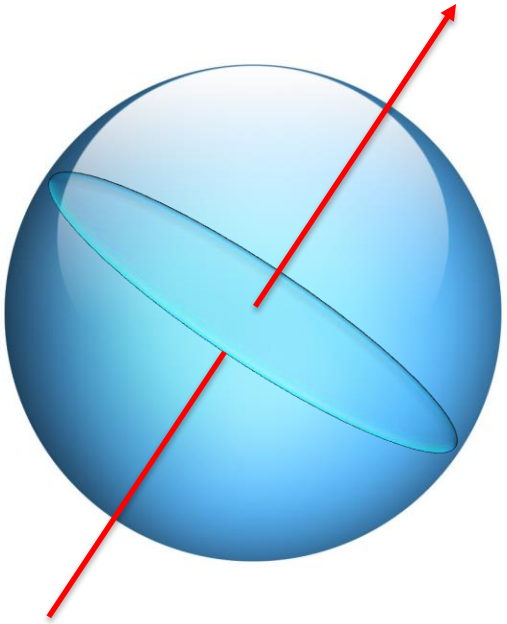

$$\Phi_j = \frac{dN_j}{da_\perp} = \frac{dN_j}{da}$$

Fluence

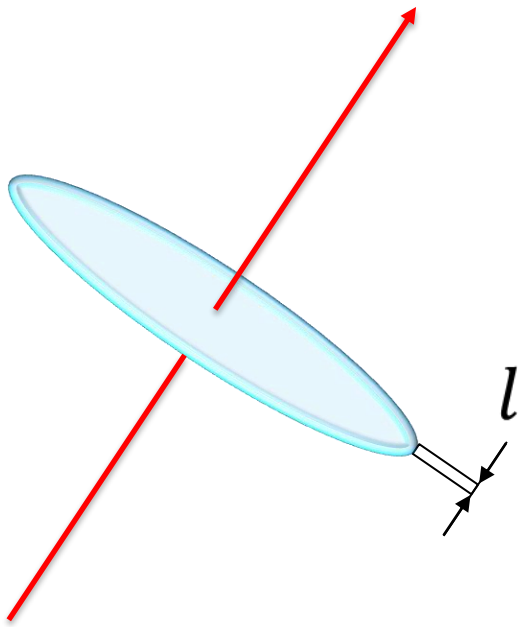

$$\Phi_j = \frac{dN_j}{da_\perp} = \frac{dN_j l}{da_\perp l} = \frac{dL_j}{dV}$$

Energy distribution

$$N_{j,E} = \frac{dN_j(\vec{r};\vec{\Omega};E)}{dE}$$

$$\Phi_{j,E} = \frac{dN_{j,E}}{da} = \frac{d^2N_j(\vec{r};\vec{\Omega};E)}{dEda}$$

Angular distribution

$$N_{j,\Omega,E} = \frac{d^2 N_j(\vec{r};\vec{\Omega};E)}{d\Omega dE}$$

$$\Phi_{j,\Omega,E} = \frac{dN_{j,\Omega,E}}{da} = \frac{d^3 N_j(\vec{r};\vec{\Omega};E)}{d\Omega dE da}$$

"Phase flux": $\dot{\Phi}_{j,\Omega,E} = \frac{d\Phi_{j,\Omega,E}}{dt}$

Incorporating particle energy

Radiant energy: $R_j = N_j E$

Energy fluence: $\psi_j = \frac{dR_j}{da} = \frac{dN_j}{da} E = \Phi_j E$

Angular and energy distribution:

$$\psi_{j,\Omega,E} = \Phi_{j,\Omega,E} E = \frac{d^3 N_j(\vec{r};\vec{\Omega};E)}{d\Omega dE da} E$$

DOSIMETRIC QUANTITIES

Conversion and deposition of energy

Conversion of energy (green)

- Energy transferred to secondary particles

Deposition of energy (yellow)

- Energy not re-emitted by ionizing particles

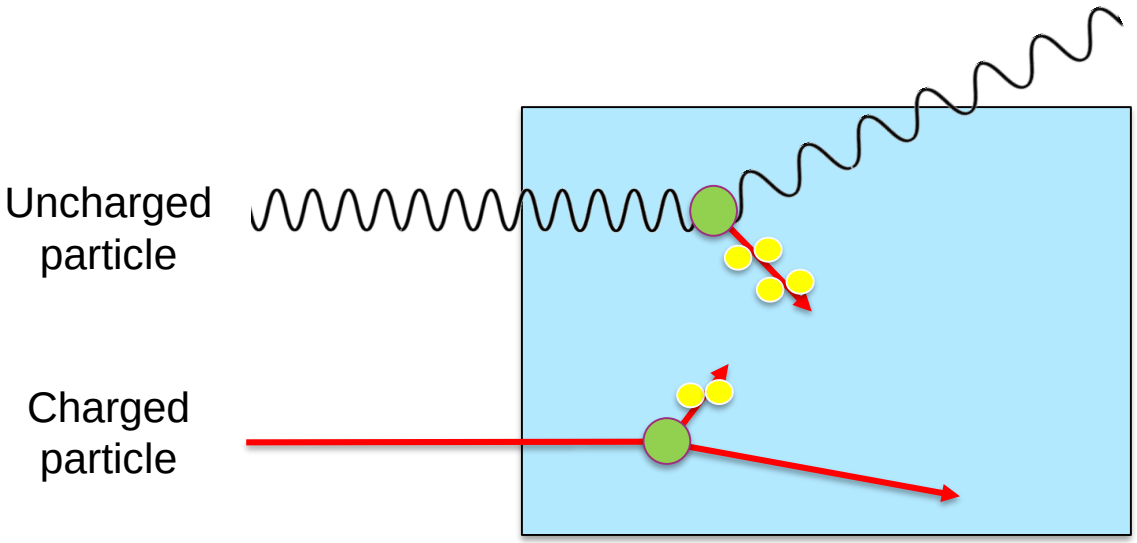

Conversion of energy (uncharged particles)

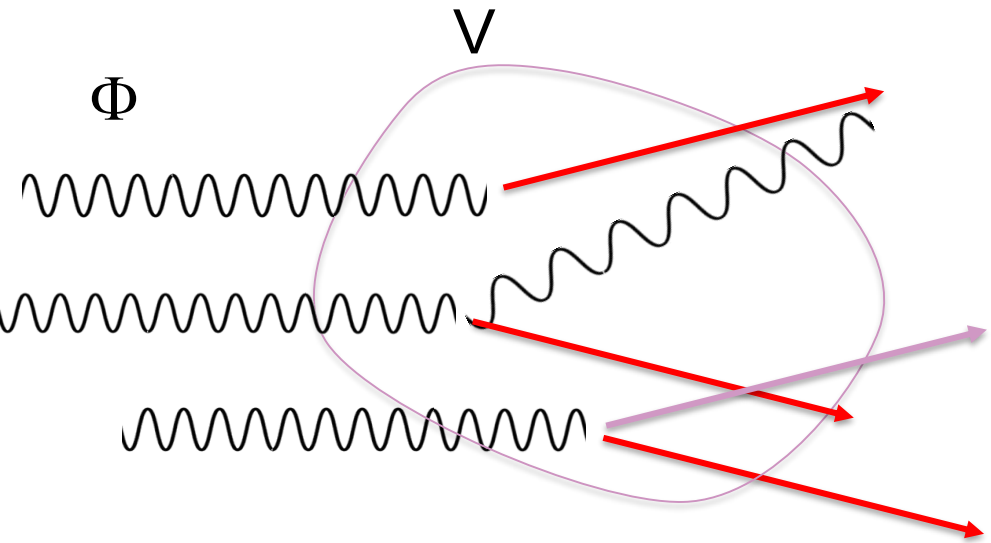

$$f = \frac{\sum_i f_i \sigma_i}{\sum_i \sigma_i}$$

Energy transferred to charged particles: $E_{tr} = \Phi E \mu V f = \Psi \frac{\mu_{tr}}{\rho} m$

Conversion of energy (uncharged particles)

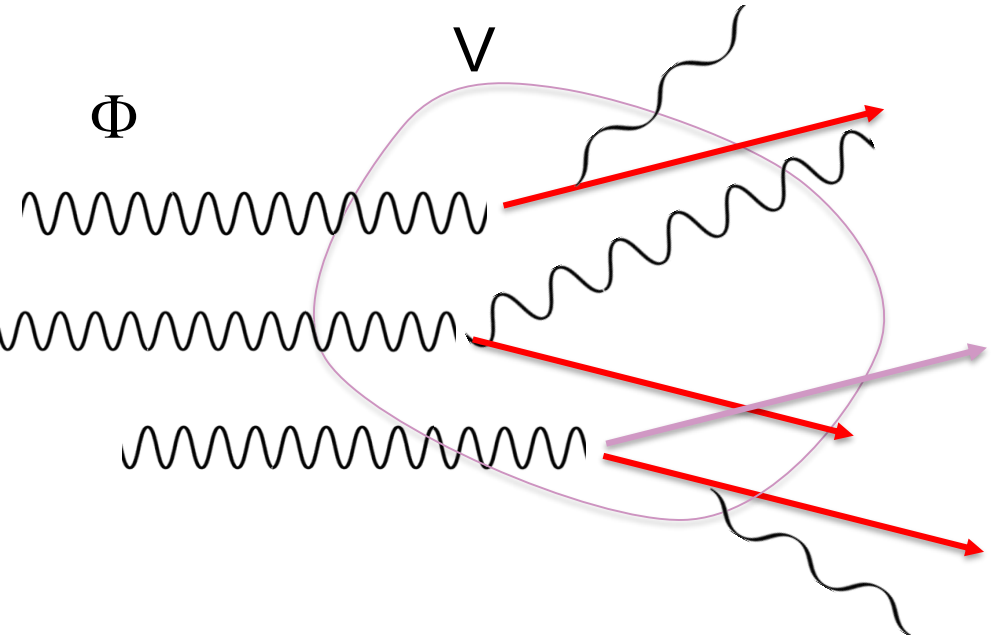

$$f = \frac{\sum_i f_i \sigma_i}{\sum_i \sigma_i}$$

Energy transferred to charged particles: $E_{tr} = \Phi E \mu V f = \Psi \frac{\mu_{tr}}{\rho} m$

$$E_{tr,net} = E_{tr}(1 - \bar{g}) = \Psi \frac{\mu_{en}}{\rho} m$$

Conversion of energy (uncharged particles)

The **TERMA**, T, for ionizing uncharged particles, is the quotient of dE by dm, where dE is the mean sum of the initial kinetic energies of **all charged and uncharged particles** liberated in a mass dm of a material by the uncharged particles incident on dm

$$T = \frac{dE}{dm} = \Psi \frac{\mu}{\rho}; \quad T = \int_E \Psi_E \frac{\mu}{\rho} dE$$

Conversion of energy (uncharged particles)

The **kerma**, K, for ionizing uncharged particles, is the quotient of dE_{tr} by dm, where dE_{tr} is the mean sum of the initial kinetic energies of all the charged particles liberated in a mass dm of a material by the uncharged particles incident on dm (ICRU 85, 2011)

$$K = \frac{dE_{tr}}{dm} = \Psi \frac{\mu_{tr}}{\rho}; \quad K = \int_E \Psi_E \frac{\mu_{tr}}{\rho} dE$$

$$K_{col} = \frac{dE_{tr,net}}{dm}; \qquad K_{col} = \int_E \Psi_E \frac{\mu_{en}}{\rho} dE$$

Conversion of energy (charged particles)

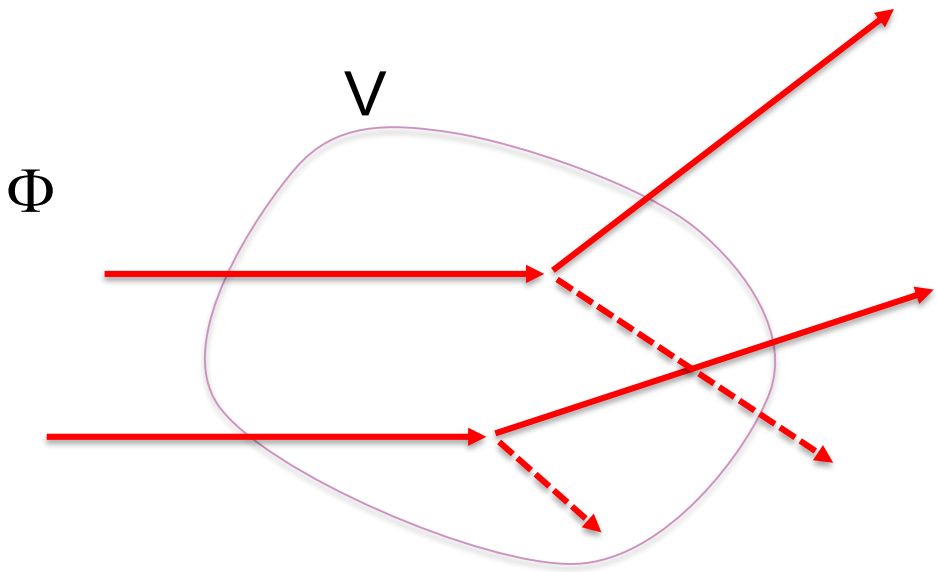

Energy lost in electronic interactions: $E_{el} = \Phi S_{el} V$

Conversion of energy (charged particles)

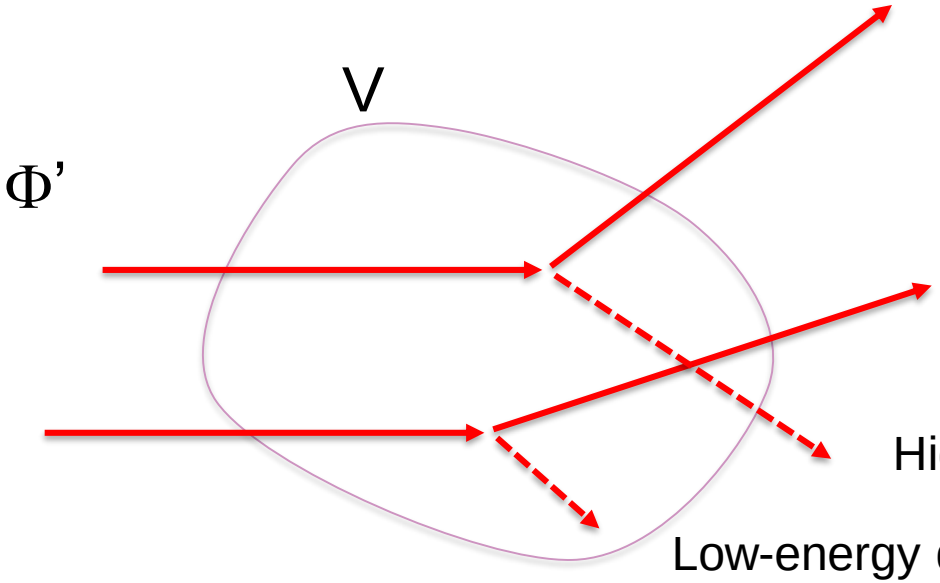

High-energy delta particle , $E_\delta > \Delta$

Low-energy delta particle, $E_\delta < \Delta$

Energy lost in electronic interactions: $E_{el} = \Phi S_{el} V$

$E_{el,\Delta} = \Phi' L_\Delta V$

Conversion of energy (charged particles)

The **cema**, C, for ionizing charged particles, is the quotient of dE_{el} by dm, where dE_{el} is the mean energy lost in electronic interactions in a mass dm of a material by the charged particles, except secondary electrons, incident on dm (ICRU 85, 2011)

$$C = \frac{dE_{el}}{dm} = \Phi \frac{S_{el}}{\rho}; \quad C = \int_E \Phi_E \frac{S_{el}}{\rho} dE$$

$$C_\Delta = \frac{dE_{el,\Delta}}{dm}; \qquad C_\Delta = \int_E \Phi'_E \frac{L_\Delta}{\rho} dE$$

Deposition of energy

The **energy deposit**, ε_i, is the energy deposited in a single interaction, *i*,

$$\varepsilon_i = \varepsilon_{in} - \varepsilon_{out} + Q$$

where ε_{in} is the energy of the incident ionizing particle (excluding rest energy), ε_{out} is the sum of the energies of all charged and uncharged ionizing particles leaving the interaction (excluding rest energy), and *Q* is the change in rest energies of the nucleus and of all elementary particles involved in the interaction (ICRU 85, 2011)

Deposition of energy

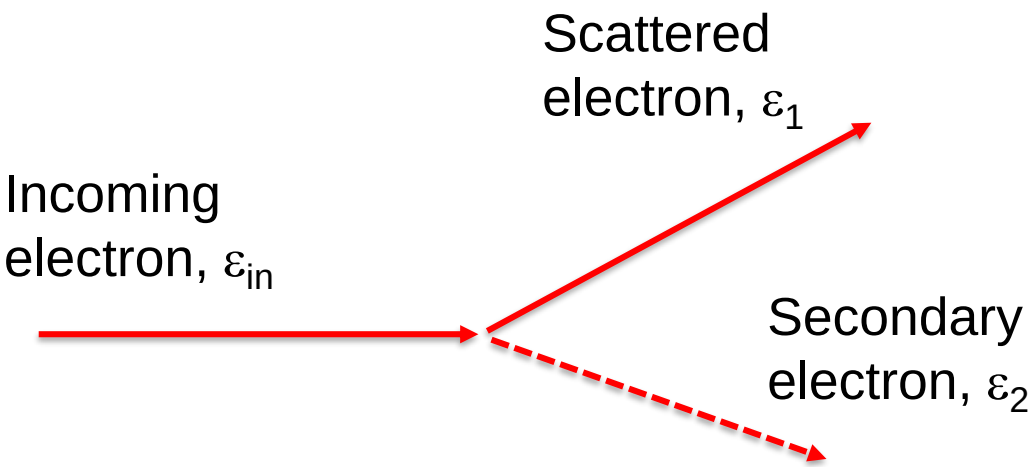

Energy deposit: $\varepsilon_i = \varepsilon_{in} - \varepsilon_{out} + Q$

Example: Coulomb interaction, Q=0

Deposition of energy

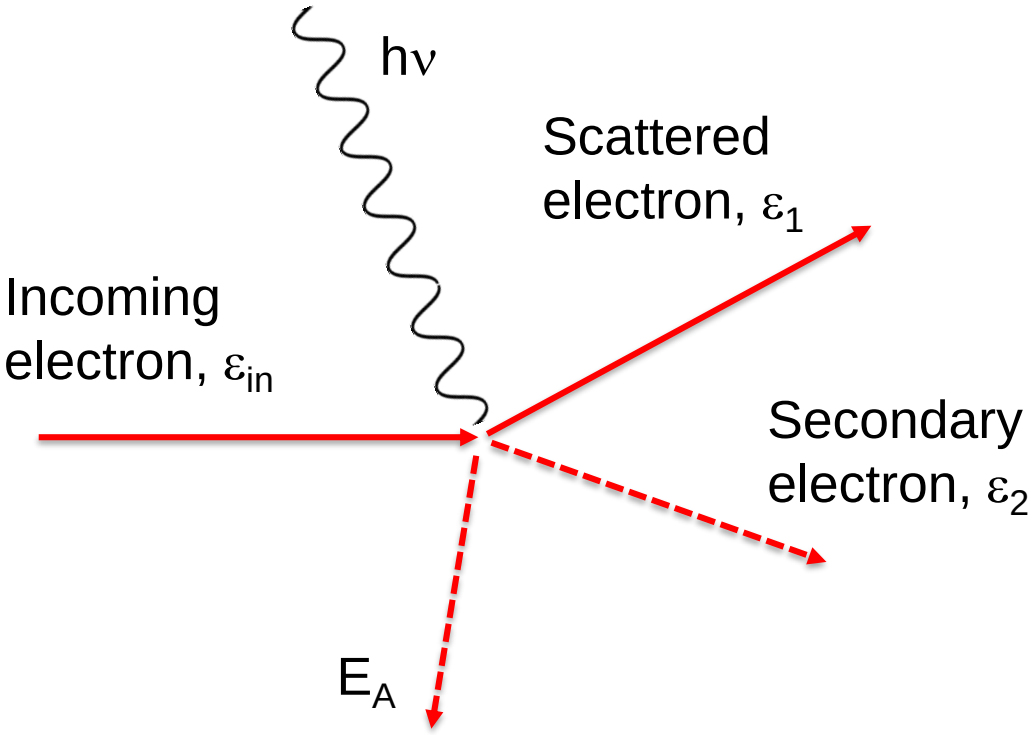

Energy deposit: $\varepsilon_i = \varepsilon_{in} - \varepsilon_{out} + Q$

$\varepsilon_i = \varepsilon_{in} - (\varepsilon_1 + \varepsilon_2 + h\nu + E_A)$

Example: Coulomb interaction, Q=0

Deposition of energy

The **energy imparted**, ε, to the matter in a given volume is the sum of all energy deposits in the volume

$$\varepsilon = \sum_i \varepsilon_i$$

where the summation is performed over all energy deposits, ε_i, in that volume (ICRU 85, 2011)

Deposition of energy

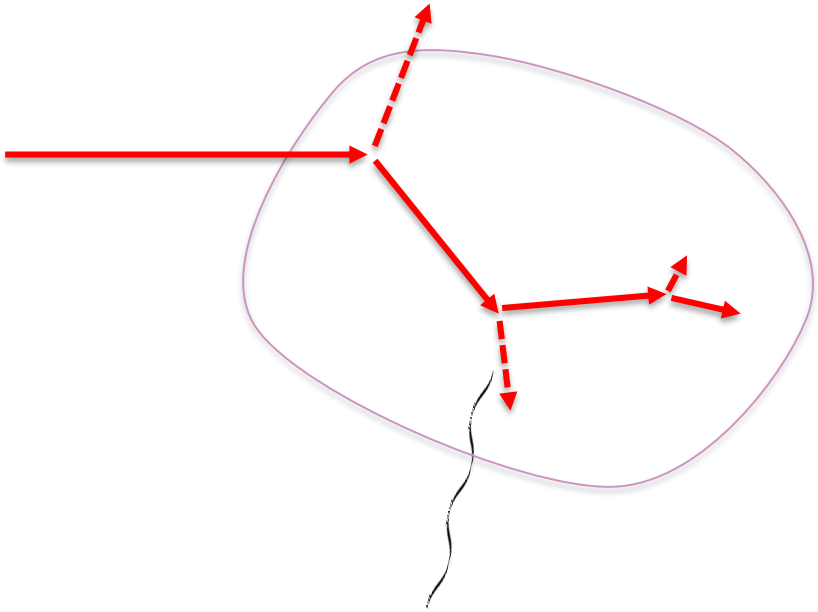

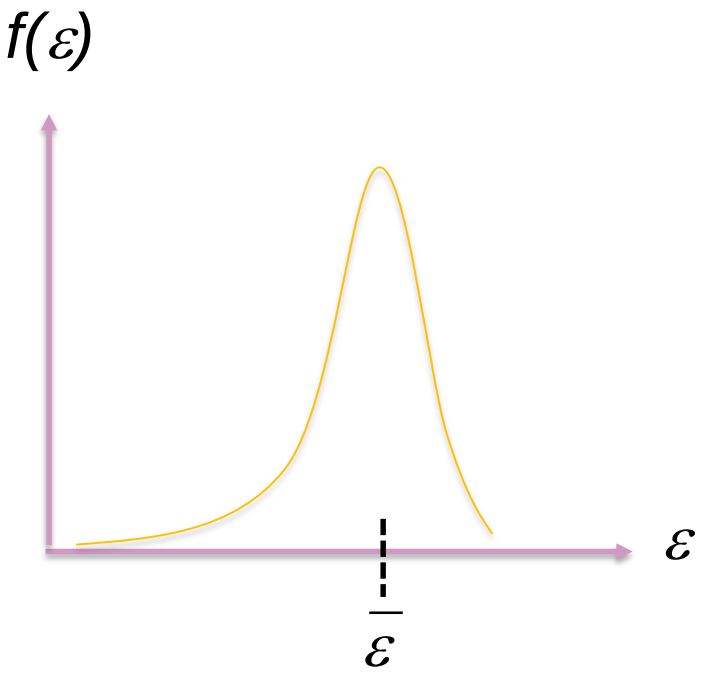

$$\varepsilon = \sum_i \varepsilon_i = n\frac{1}{n}\sum_i \varepsilon_i = n\bar{\varepsilon}_i$$

Deposition of energy

The **absorbed dose**, *D*, is the quotient of $d\bar{\varepsilon}$ by *dm*, where $d\bar{\varepsilon}$ is the mean energy imparted by ionizing radiation to matter of mass *dm* (ICRU 85, 2011)

$$D = \frac{d\bar{\varepsilon}}{dm}$$

$$D = \frac{d(\bar{n}\bar{\varepsilon_i})}{dm}; \quad D = \int_E \Phi_E \frac{\mu}{\rho} \bar{\varepsilon_i} dE + \overline{n_s}\overline{\varepsilon_s}$$

Deposition of energy

Neglecting energy deposit in

- interactions of uncharged particles
- nuclear or elementary particle interactions
- spontaneous nuclear transformations
- bremsstrahlung processes

$$D = \int_E \Phi_E \frac{S_{el}}{\rho} k \, dE$$

Delta-particle equilibrium

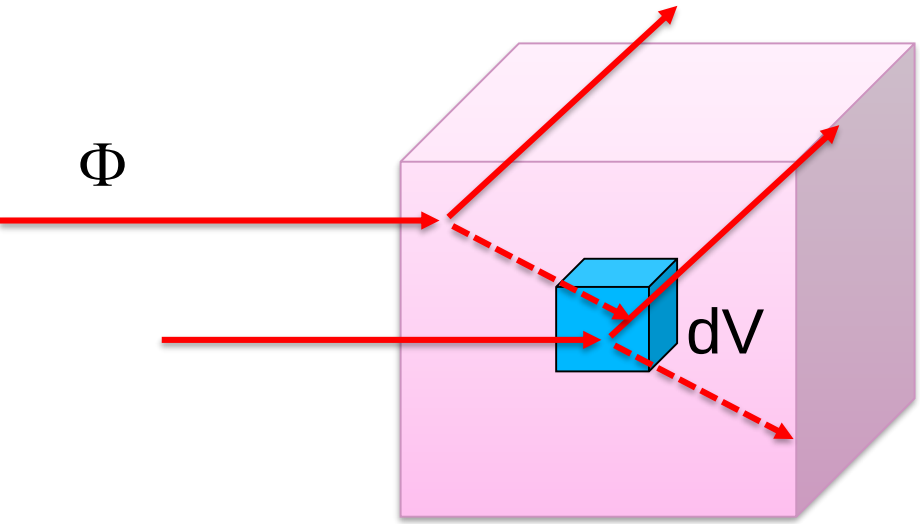

High-energy delta particle , $E_\delta > \Delta$

δ-particle equilibrium, k=1:

$$D = C = \int_E \Phi_E \frac{S_{el}}{\rho} dE$$

Partial delta-particle equilibrium

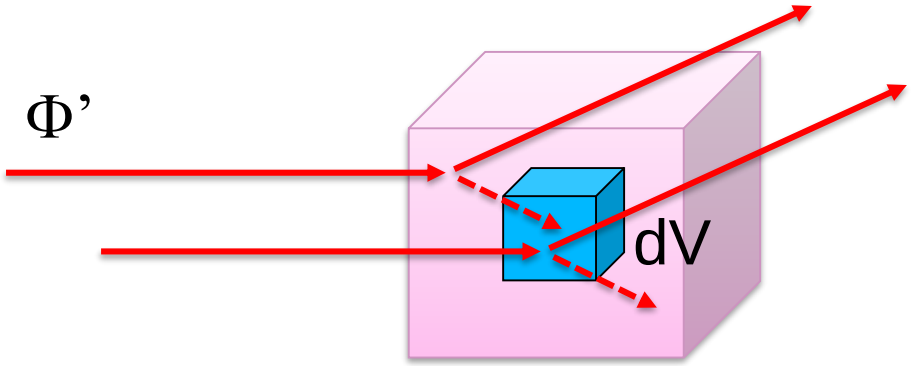

Low-energy delta particle , $E_\delta < \Delta$

Partial δ-particle equilibrium, k<1:

$$D = C_\Delta = \int_E \Phi'_E \frac{L_\Delta}{\rho} dE$$

The problem

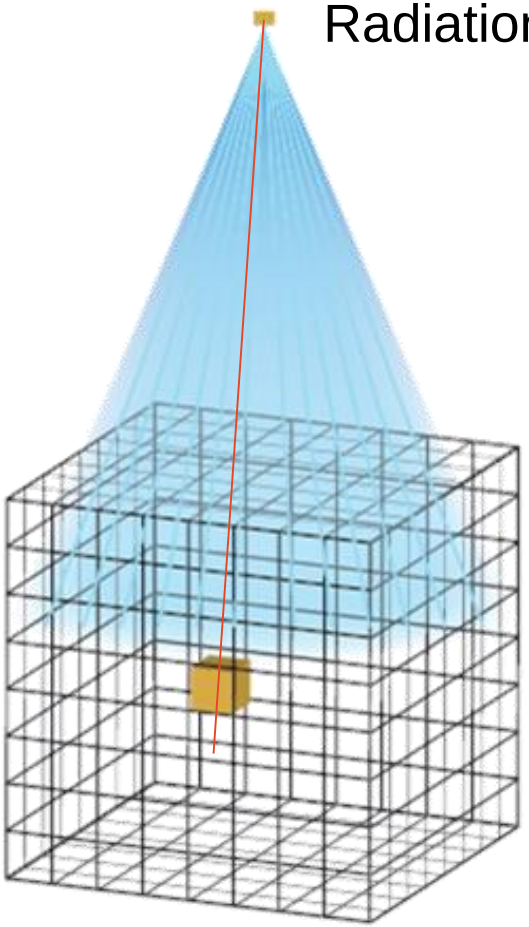

RayStation

- Incident particle fluence
- Raytracing
- Redistribution of energy

Absorbed dose $D = \int_E \Phi_E \frac{S_{el}}{\rho} dE$

RAYTRACING

Raytracing in heterogeneous media

$$\Phi_E = \Phi_{E,0} e^{-\int_{\vec{r}_0}^{\vec{r}} \mu(\vec{r}')dl}$$

$$e^{-\int_{\vec{r}_0}^{\vec{r}} \mu(\vec{r}')dl} = e^{-\mu z_{rad}}$$

$$z_{rad} = \frac{1}{\mu} \sum_{i,j,k} z_{i,j,k} \mu_{i,j,k}$$

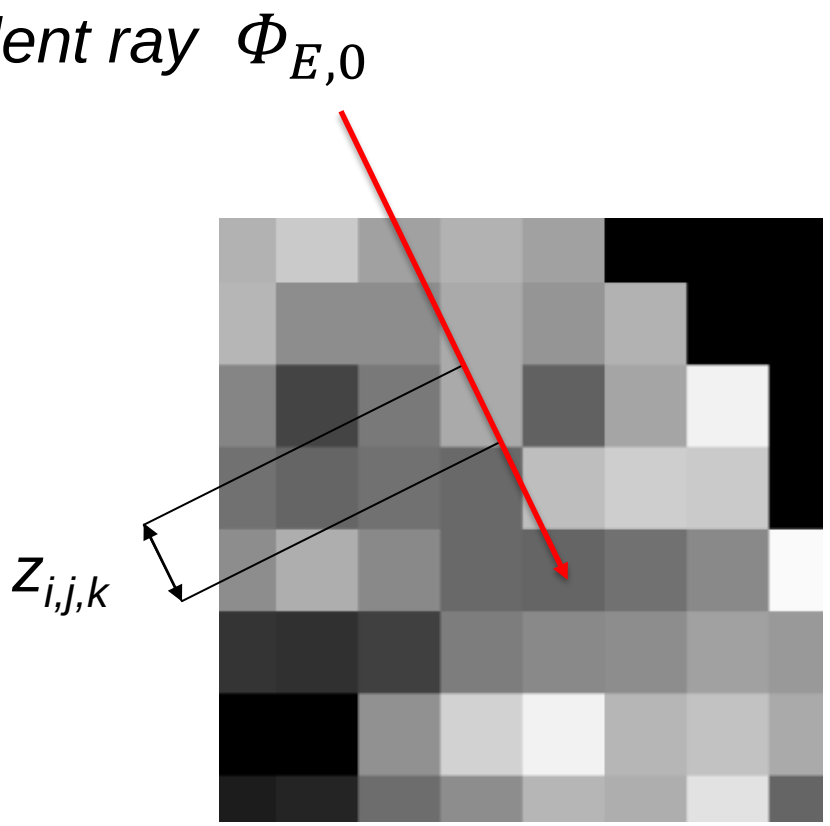

Siddon's raytracing algorithm

The ray from A to B

$$x(\alpha) = x_A + \alpha(x_B - x_A)$$
$$y(\alpha) = y_A + \alpha(y_B - y_A)$$
$$L = \sqrt{(x_B - x_A)^2 + (y_B - y_A)^2}$$

The planes

$$X_i = X_1 + (i-1)d_x$$
$$Y_j = Y_1 + (j-1)d_y$$

Intersections

$$\alpha_{x,i} = (X_i - x_A)/(x_B - x_A)$$
$$\alpha_{y,j} = (Y_j - y_A)/(y_B - y_A)$$
$$\{\alpha\} = merge[\{\alpha_x\}, \{\alpha_y\}]$$

$$z_{rad} = \frac{1}{\mu}\sum_n L(\alpha_n - \alpha_{n-1})\,\mu_{i(n),j(n),k(n)}$$

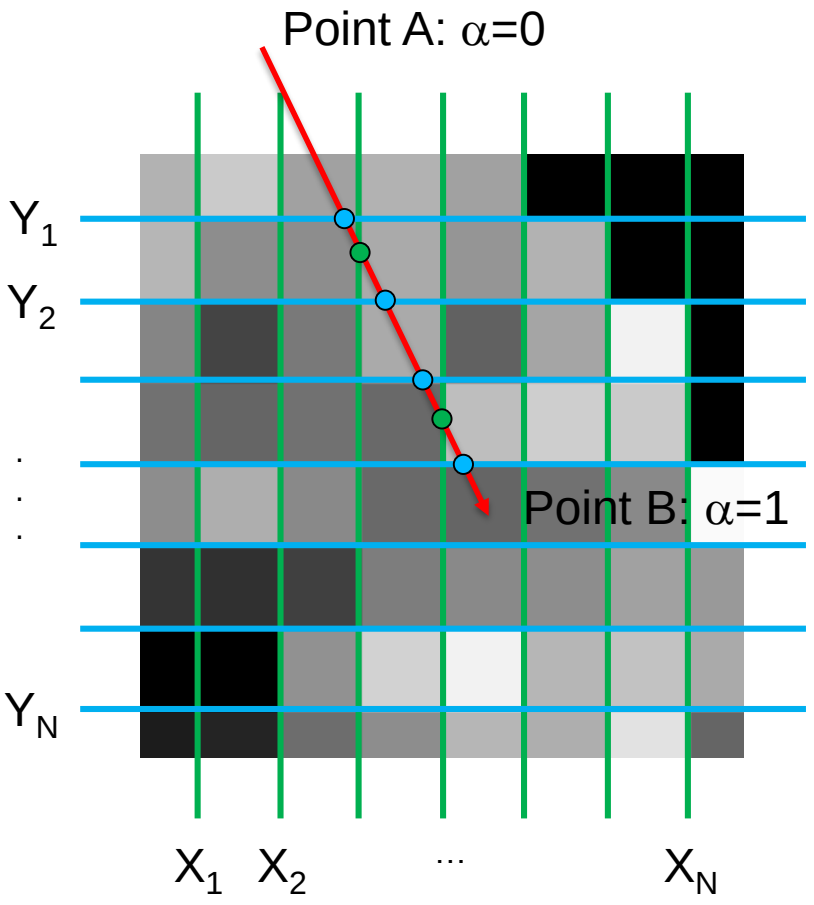

Siddon, Med Phys 12:252, 1985

ESTRO School

CONVOLUTION

Raytracing

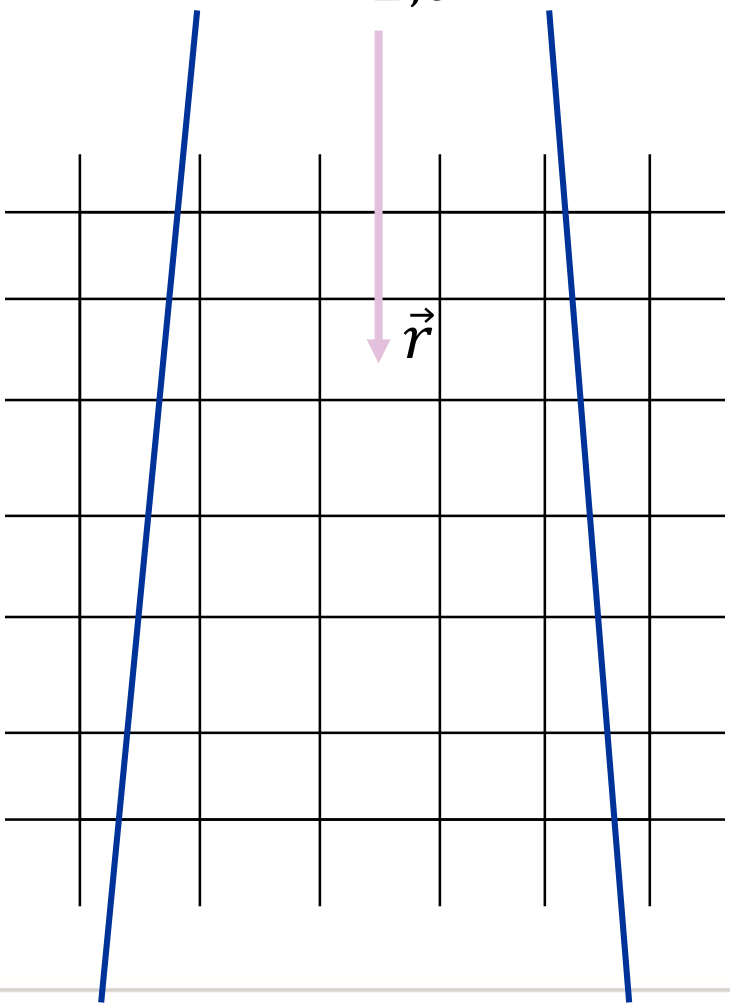

Raytracing

$\Phi_E(\vec{r})$

Conversion quantity

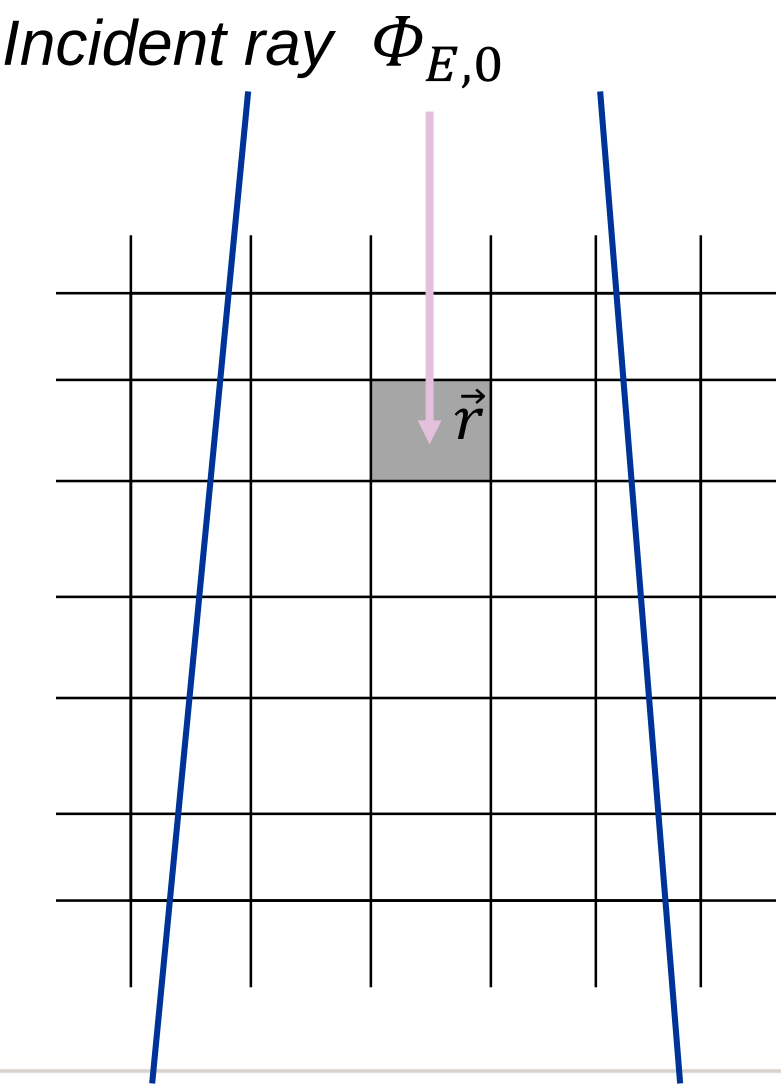

Raytracing

$$\Phi_E(\vec{r})$$

Conversion of energy

$$T(\vec{r}) = \int_E \Phi_E(\vec{r}) E \frac{\mu}{\rho} dE$$

Redistribution kernel

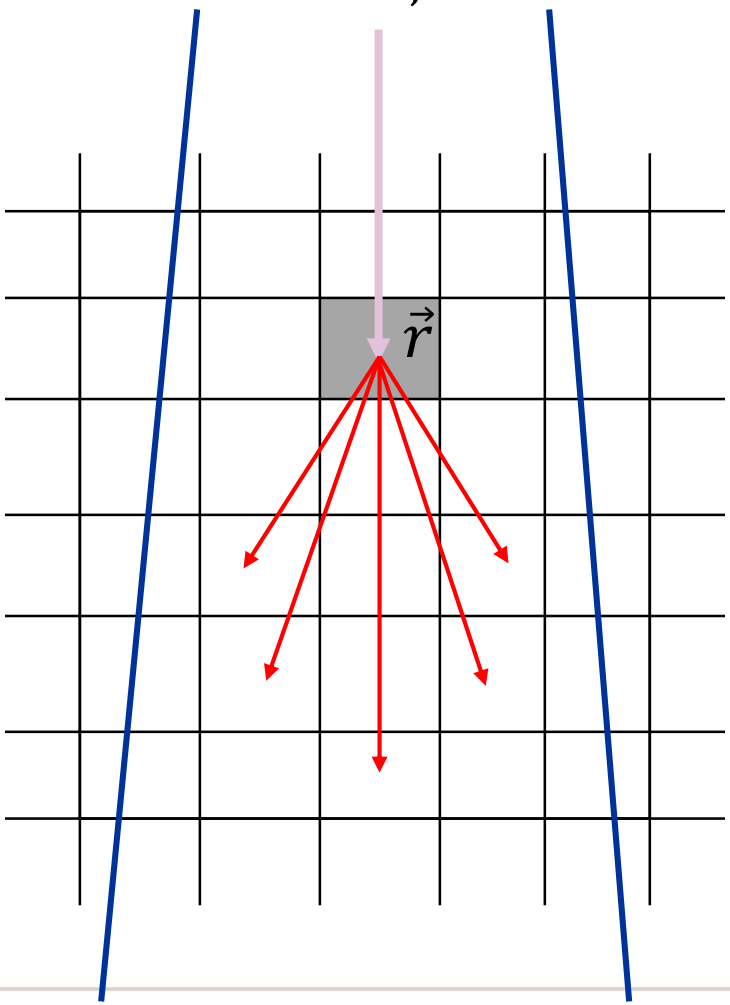

Raytracing

$$\Phi_E(\vec{r})$$

Conversion of energy

$$T(\vec{r}) = \int_E \Phi_E(\vec{r}) E \frac{\mu}{\rho} dE$$

Redistribution of energy

$$A(\vec{r}_c, \vec{r})$$

Redistribution kernel

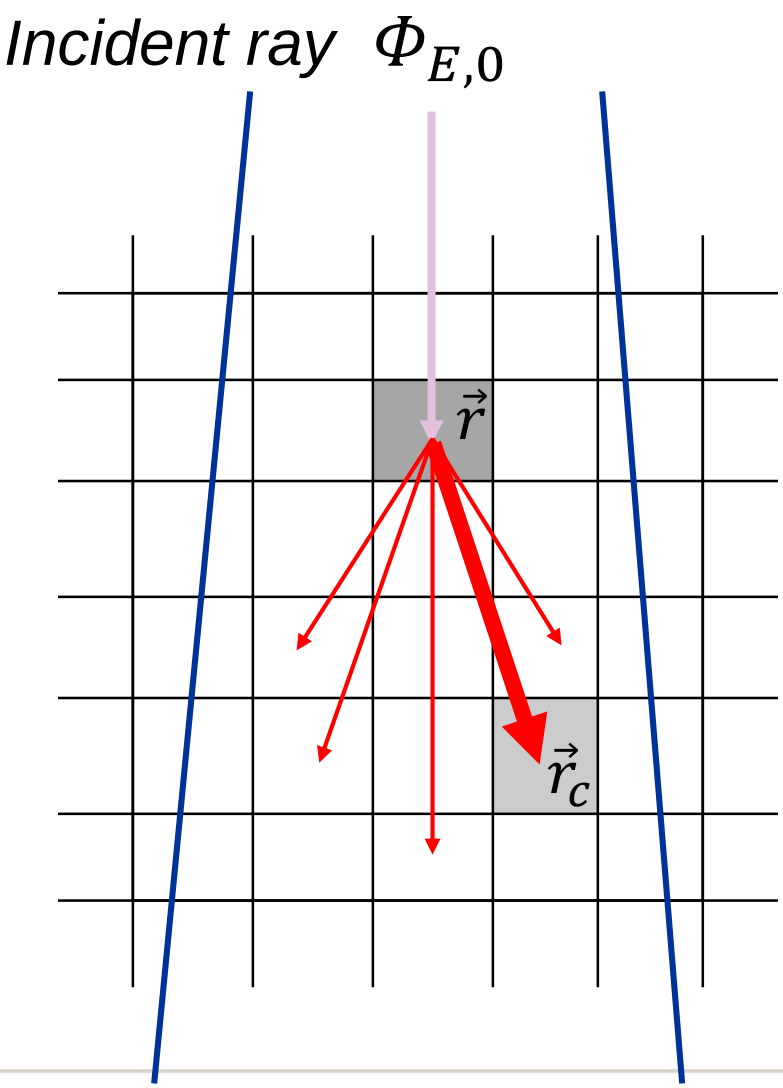

Raytracing

$$\Phi_E(\vec{r})$$

Conversion of energy

$$T(\vec{r}) = \int_E \Phi_E(\vec{r}) E \frac{\mu}{\rho} dE$$

Redistribution of energy

$$A(\vec{r}_c, \vec{r})$$

Deposition of energy

$$dD(\vec{r}_c) = T(\vec{r}) A(\vec{r}_c, \vec{r}) dV$$

Volume integration

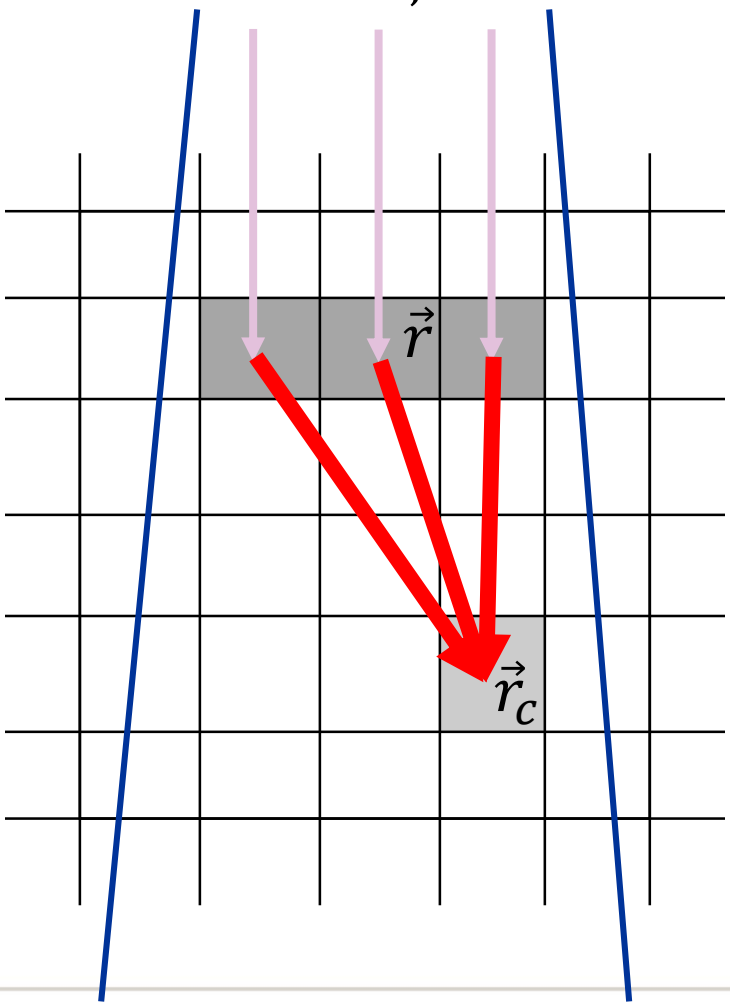

Raytracing

$$\Phi_E(\vec{r})$$

Conversion of energy

$$T(\vec{r}) = \int_E \Phi_E(\vec{r}) E \frac{\mu}{\rho} dE$$

Redistribution of energy

$$A(\vec{r}_c, \vec{r})$$

Deposition of energy

$$D(\vec{r}_c) = \iiint_V T(\vec{r})\, A(\vec{r}_c, \vec{r}) dV$$

Convolution

$$D(\vec{r}_c) = \iiint_V T(\vec{r})\, A(\vec{r}_c, \vec{r})\, dV$$

This is an integral transform of $T(\vec{r})$ with $A(\vec{r}_c, \vec{r})$ as the kernel function

If the kernel is invariant, such that $A(\vec{r}_c, \vec{r}) = A(\vec{r}_c - \vec{r})$, the transform becomes a convolution, and (following the convolution theorem)

$$D(\vec{r}_c) = T(\vec{r}) * A(\vec{r}_c, \vec{r}) = FFT^{-1}[FFT(T) \cdot FFT(A)]$$

In general, however, the kernel varies with position, due to divergence, changes in energy, and the heterogeneity of the medium

THE RADIATION TRANSPORT EQUATION

Vector fluence

$$\vec{\Phi}_{j,\Omega,E} = \vec{\Omega}\Phi_{j,\Omega,E}$$

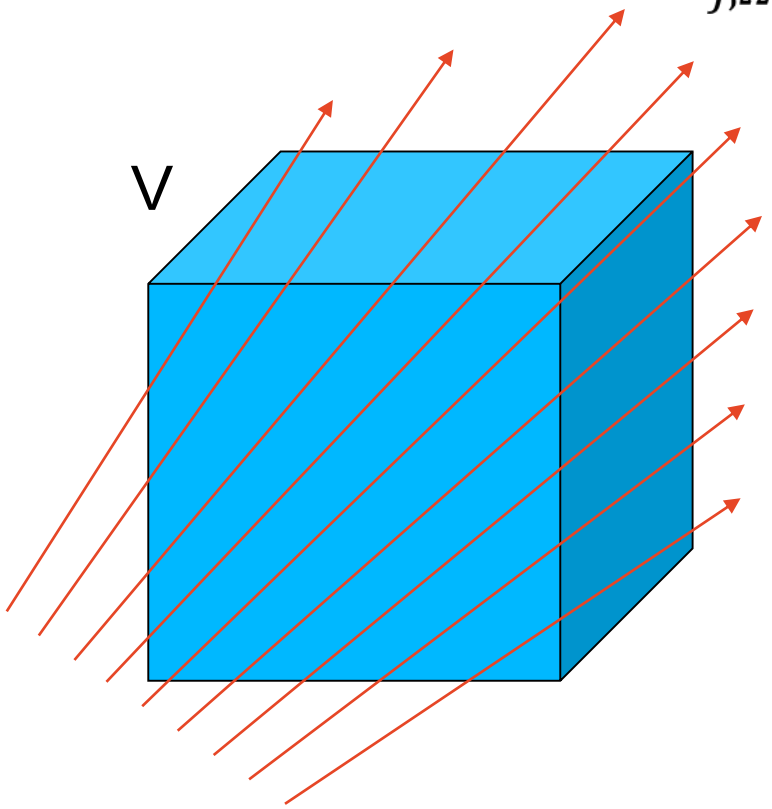

Net transport of particles out of a volume

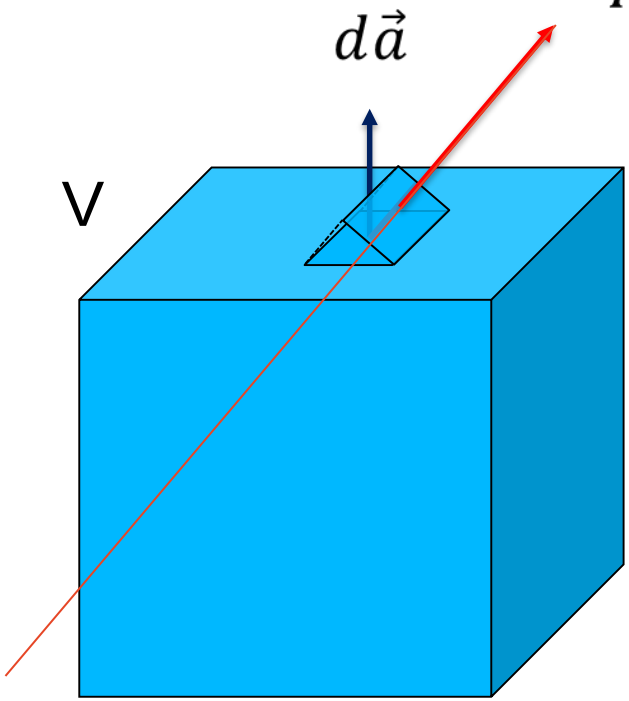

$$\vec{\Phi}_{j,\Omega,E} = \vec{\Omega}\Phi_{j,\Omega,E}$$

$$dn_{j,\Omega,E} = \vec{\Phi}_{j,\Omega,E} \cdot \overrightarrow{da}$$

$$n_{j,\Omega,E} = N^{in}_{j,\Omega,E} - N^{out}_{j,\Omega,E} = \oiint_A dn_{j,\Omega,E}$$

$$n_{j,\Omega,E} = \oiint_A \vec{\Phi}_{j,\Omega,E} \cdot \overrightarrow{da}$$

$$n_{j,\Omega,E} = \iiint_V \nabla \cdot \vec{\Phi}_{j,\Omega,E} dV$$

For an infinitesimal volume

$$\frac{dn_{j,\Omega,E}}{dV} = \frac{d}{dV}\iiint_V \nabla \cdot \vec{\Phi}_{j,\Omega,E} dV = \nabla \cdot \vec{\Phi}_{j,\Omega,E}$$

Sink term

- Outscatter

Source terms

- Inscatter
- Radiation production

For an infinitesimal volume

$$\frac{dn_{j,\Omega,E}}{dV} = \frac{d}{dV}\iiint_V \nabla \cdot \vec{\Phi}_{j,\Omega,E} dV = \nabla \cdot \vec{\Phi}_{j,\Omega,E}$$

Sink term

- Outscatter

Source terms

- Inscatter
- Radiation production

$$If\ equal, there\ is\ radiation\ equilibrium: \nabla \cdot \vec{\Phi}_{j,\Omega,E} = 0$$

Outscatter

$$Outscatter: \; -\Phi_{j,\Omega,E}(\vec{\Omega}, E)\, \mu_j(E)$$

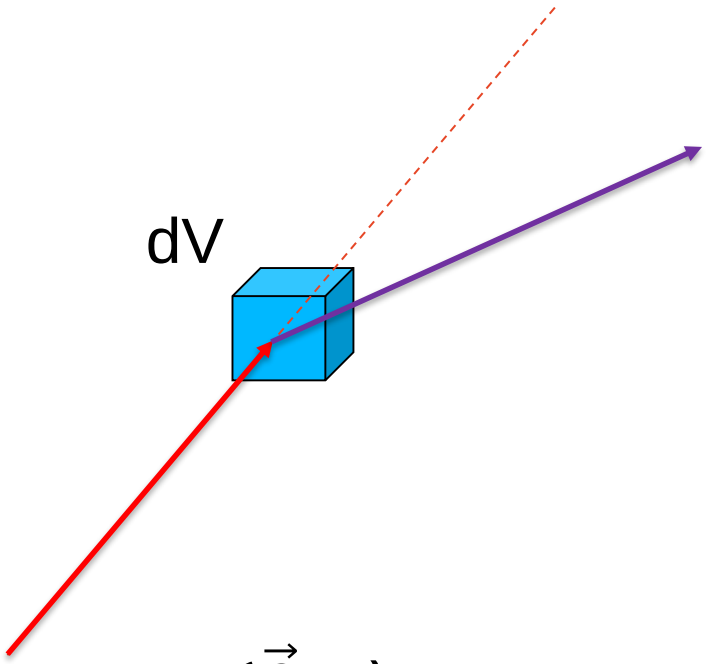

$$\mu = \rho \frac{N_A}{M} \sigma$$

Inscatter

$$Inscatter: +\sum_{j'} \int_{4\pi} d\Omega' \int_{E_{cut}}^{\infty} dE'\, \Phi_{j',\Omega,E}(\vec{\Omega}', E')\mu_{j'\to j,\Omega,E}(\vec{\Omega}', E'; \vec{\Omega}, E)$$

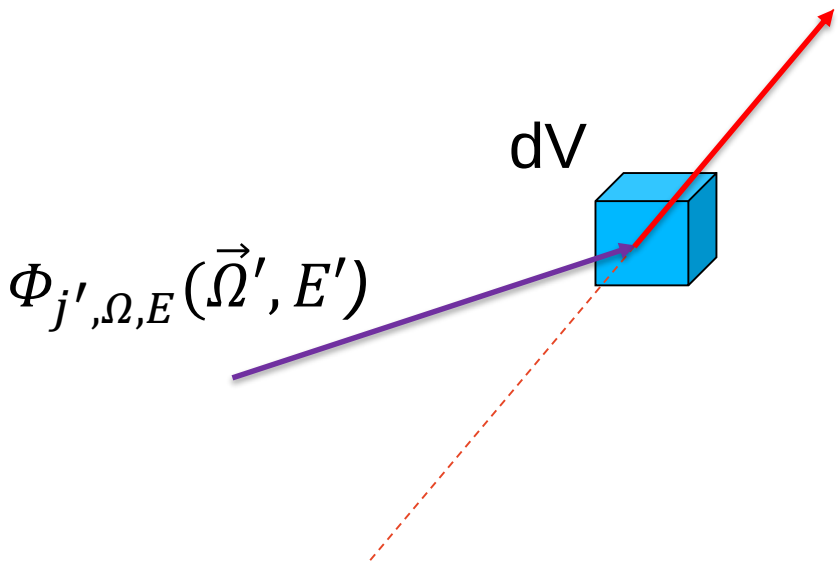

Radiation production

$$Radiation\ production: \quad + S_{j,\Omega,E}$$

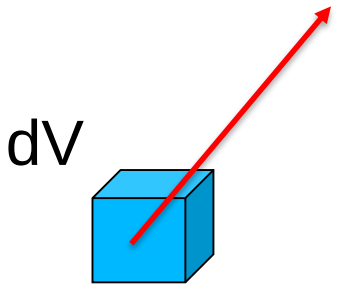

The radiation transport equation

For all particle types:

$$\nabla \cdot \vec{\Phi}_{j,\Omega,E}(\vec{\Omega},E) = -\Phi_{j,\Omega,E}(\vec{\Omega},E)\mu_j(E)$$

$$+\sum_{j'}\int_{4\pi} d\Omega' \int_{E_{cut}}^{\infty} dE'\, \Phi_{j',\Omega,E}(\vec{\Omega}',E')\mu_{j'\to j,\Omega,E}(\vec{\Omega}',E';\vec{\Omega},E)$$

$$+S_{j,\Omega,E}$$

Solving the radiation transport equation

$$\nabla \cdot \vec{\Phi}_{j,\Omega,E}(\vec{\Omega},E) = -\Phi_{j,\Omega,E}(\vec{\Omega},E)\mu_j(E) + \sum_{j'} \int_{4\pi} d\Omega' \int_{E_{cut}}^{\infty} dE'\, \Phi_{j',\Omega,E}(\vec{\Omega}',E')\mu_{j'\to j,\Omega,E}(\vec{\Omega}',E';\vec{\Omega},E) + S_{j,\Omega,E}$$

- Solve for $\Phi_{j,\Omega,E}(\vec{\Omega},E)$
  - Analytical solution is generally not feasible
- Convergent techniques
  - Monte Carlo
  - Deterministic methods

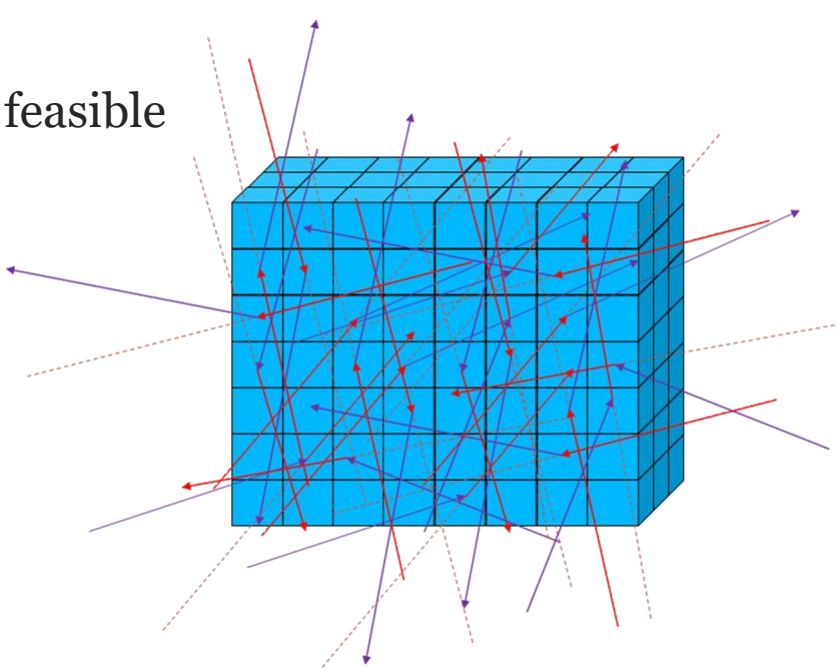

Convergent techniques

Monte Carlo

- Implicit solution
- Stochastic errors
- Limited by noise due to finite number of particles

Deterministic methods

- Explicit solution
- Modelling errors
- Limited by discretization in space, angle, and energy

Summary

We have been talking about

- Radiometric and dosimetric quantities
- Conversion and deposition of energy
- Delta-particle equilibrium
- Raytracing
- Convolution
- The radiation transport equation

References

- ICRU. Fundamental quantities and units for ionizing radiation. ICRU Report 85. Bethesda; 2011.
- R L Siddon. Fast calculation of the exact radiological path for a three-dimensional CT. Med Phys 12:252, 1985.

Linac head designs: Photon and electron beams

Tommy Knöös

Sweden

Learning objectives

- To know how a clinical high-energy photon beam is produced.
- To learn about basic photon beam characteristics, such as beam quality and lateral distributions.
- To understand how the photon beam is shaped and modulated in collimators and wedges.
- To understand how the “raw” electron beam is converted into a flat and clinically useable electron beam through scattering foils.
- To learn about electron beam collimation.
- To understand the basic characteristics of a clinical electron beam.

A typical linac of today

Varian Clinac®
Engineered for Clinical Benefits

1 **Gridded Electron Gun**
Controls dose rate rapidly and accurately. Permits precise beam control for dynamic treatments, since gun can be gated. Removable for cost-effective replacement.

2 **Energy Switch**
Patented switch provides energies within the full therapeutic range, at consistently high, stable dose rates, even with low energy x-ray beams. Ensures optimum performance and spectral purity at both energies.

3 **Wave Guide**
High efficiency, side coupled standing wave accelerator guide with demountable electron gun and energy switch.

4 **Achromatic 3-Field Bending Magnet**
Unique design with fixed ± 3 % energy slits ensures exact replication of the input beam for every treatment. The 270° bending system, coupled with Varian's 3-dimensional servo system, provides for a 2 mm circular focal spot size for optimal portal imaging.

5 **Real-Time Beam Control Steering System**
Radial and transverse steering coils and a real-time feedback system ensure that beam symmetry is within ± 2 % at all gantry angles.

6 **Focal Spot Size**
Even at maximum dose rate – and any gantry angle – the circular focal spot remains less than 2 mm, held constant by a focus solenoid. Assures optimum image quality for portal imaging.

7 **10-Port Carousel**
New electron scattering foils provide homogeneous electron beams at therapeutic depths. Extra ports allow for future development of specialized beams.

8 **Ion Chamber**
Dual sealed ion chambers with 8 sectors for rigourous beam control provide two independent channels, impervious to changes in temperature and pressure. Beam dosimetry is monitored to be within ± 2 % for longterm consistency and stability.

9 **Asymmetric Jaws**
Four independent collimators provide flexible beam definition of symmetric and asymmetric fields.

10 **Millennium™ Multi-Leaf Collimator**
Dynamic full field high resolution 120 leaf MLC with dual redundant safety readout for most accurate conformal beam shaping and IMRT treatments.

11 **Electronic Portal Imager**
High-resolution PortalVision™ aS1000 Megavoltage imager mounted on a robotic arm for efficient patient setup verification and IMRT plan QA.

12 **On-Board Imager®**
kV X-ray source (12a) and high-speed, high-resolution X-ray detector (12b) mounted on two robotic arms orthogonal to the treatment beam for Image Guided Radio Therapy (IGRT). The unique system provides kV imaging at treatment and includes radiographic, fluoroscopic and Cone Beam CT image acquisition and patient repositioning applications.

A typical linac of today

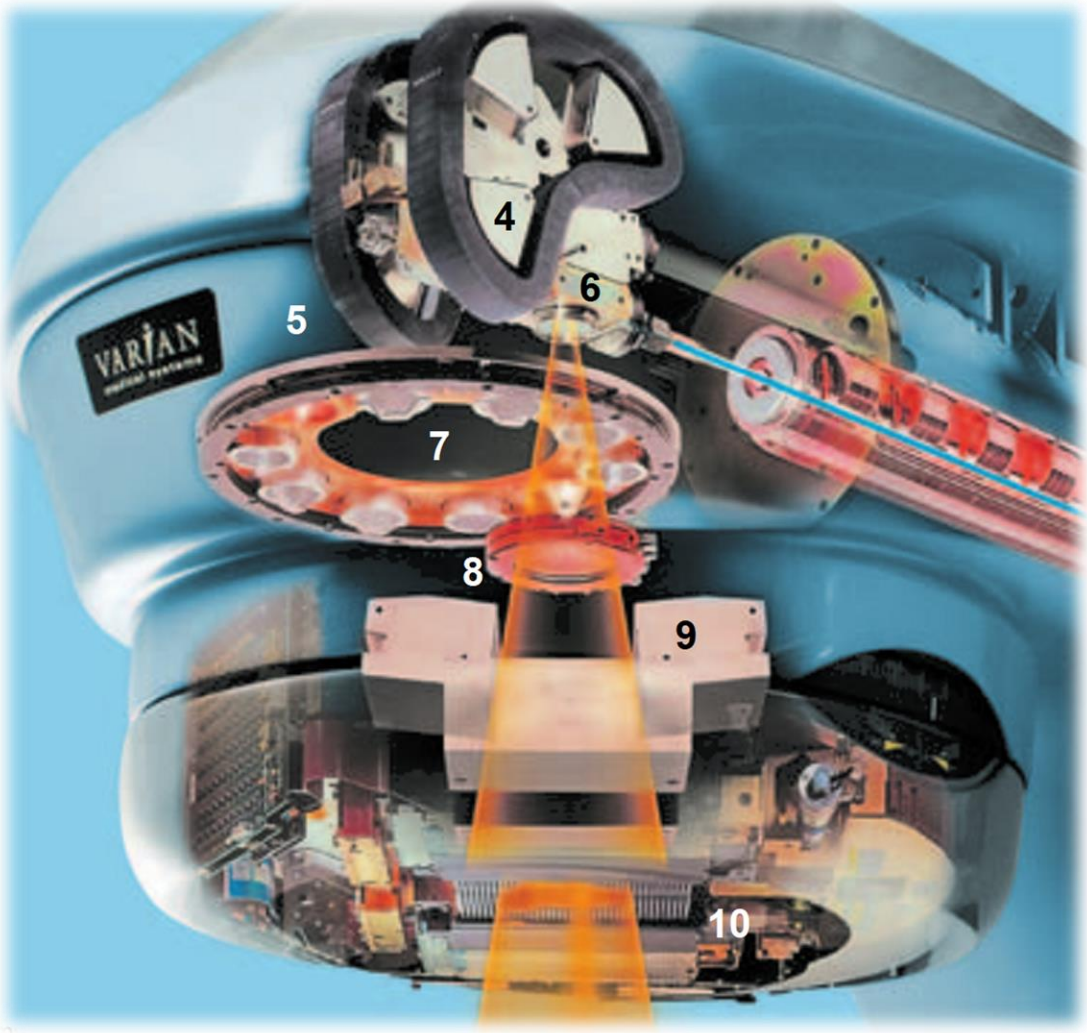

ESTRO School

Bending magnets

Critical component as it controls the electron beam energy.
Why not use a simple 90° bending magnet?

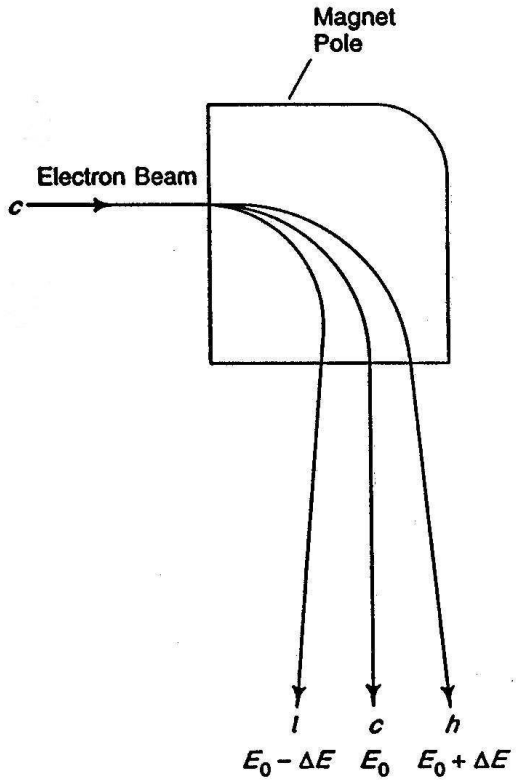

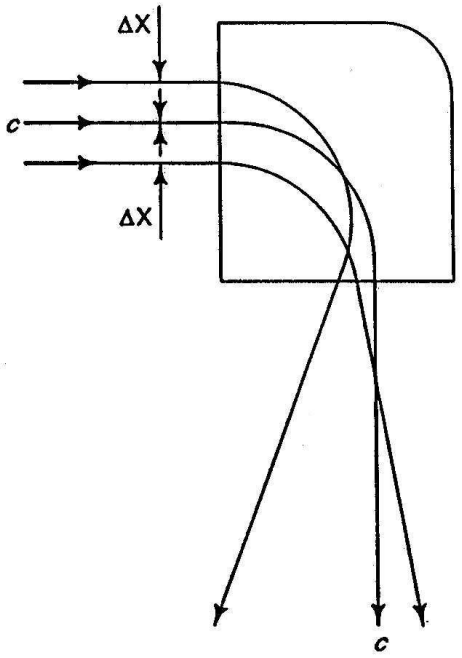

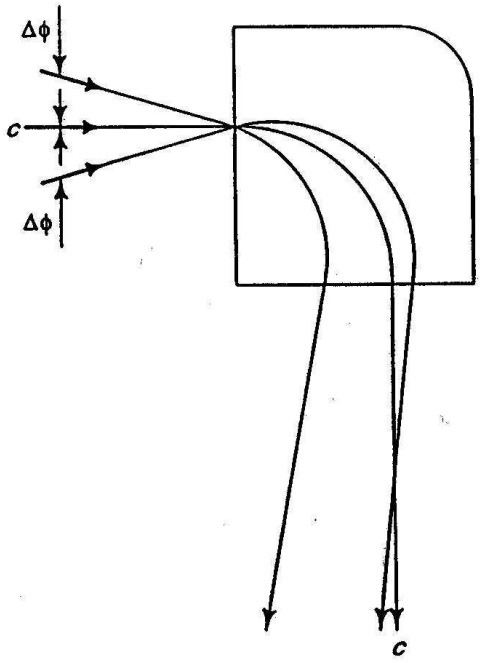

Not all treatment machines have a bending magnet.

Karzmark *et al* [1]

Achromatic bending magnets

3×90° (Varian Clinac, high energy)

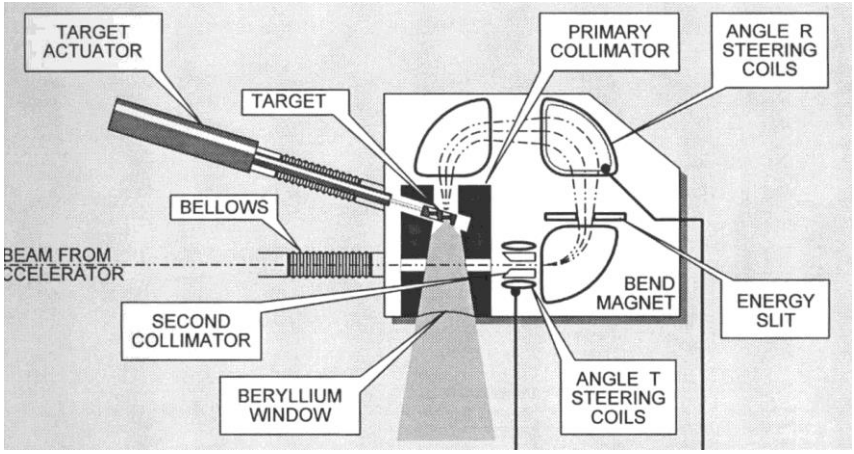

270° (Siemens Primus)

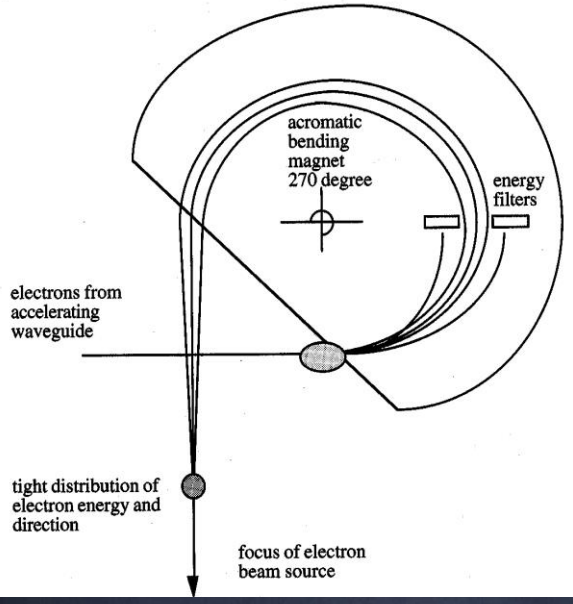

112° Slalom (Elekta)

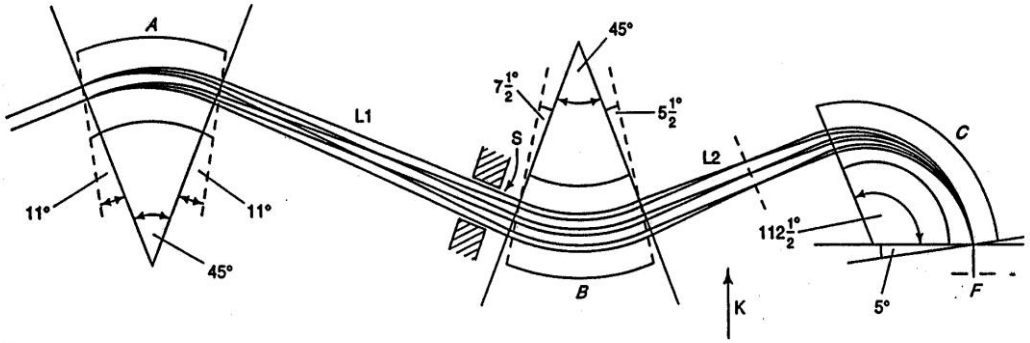

Karzmark *et al* [1]

ESTRO School

Other designs exist without bending magnet

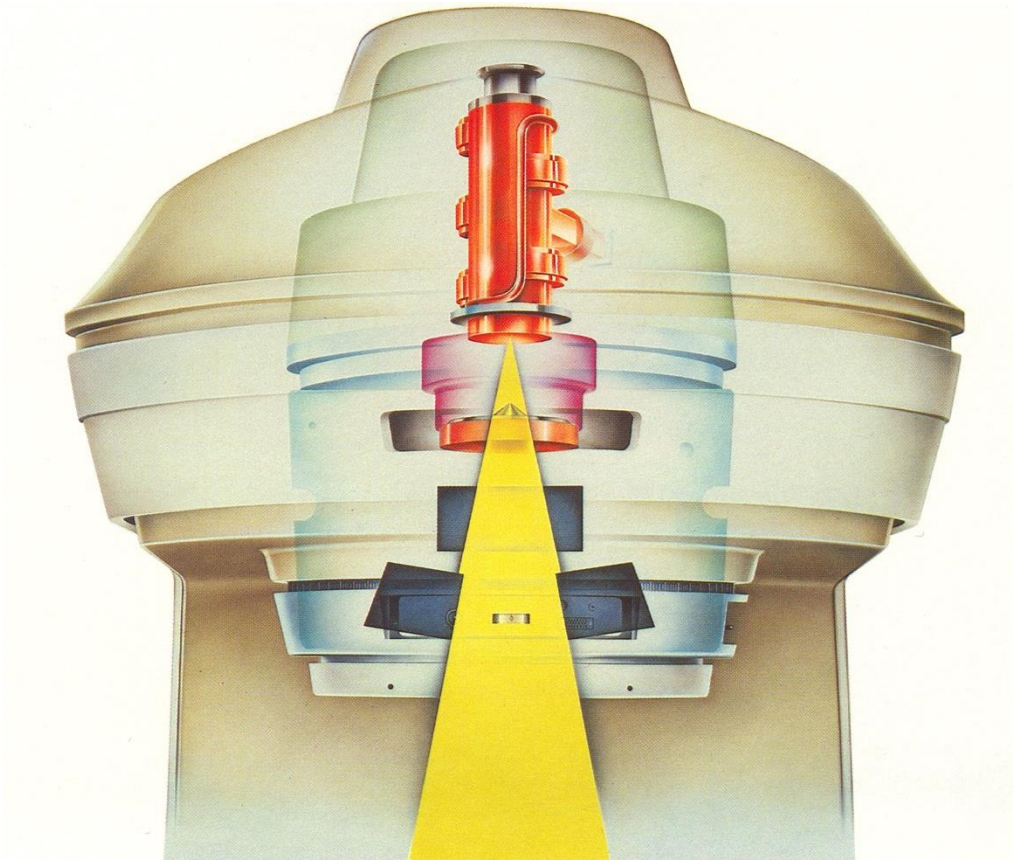

Example – Varian low energy machine 4/6 MV

Target materials

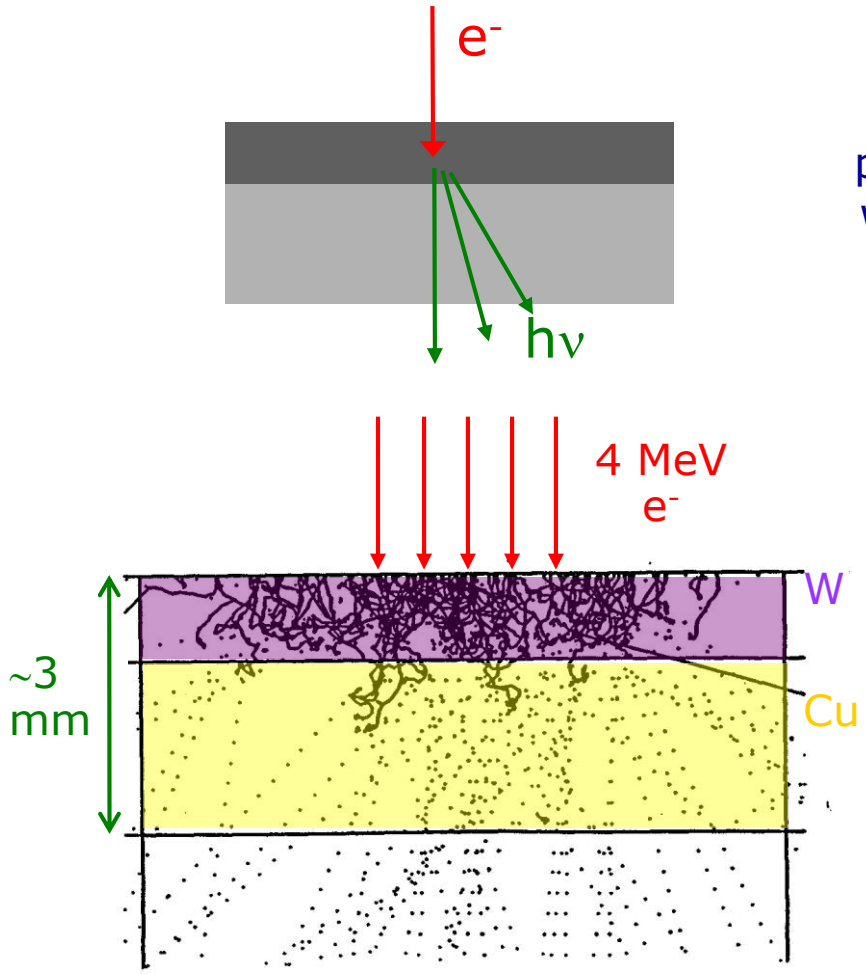

X-ray targets can be constructed in two layers; one high-*Z* (W, Au) for photon production and a second layer with lower *Z* (Cu, Al) to fully stop the electrons and harden the photon spectrum. (and providing cooling)

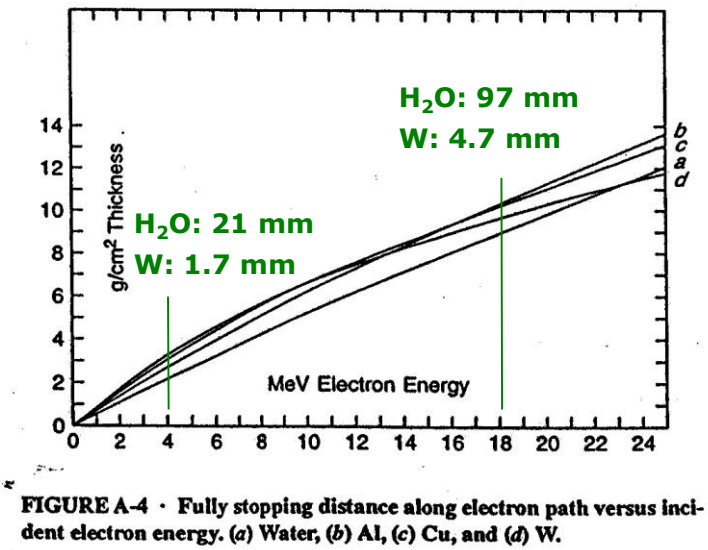

FIGURE A-4 · Fully stopping distance along electron path versus incident electron energy. (*a*) Water, (*b*) Al, (*c*) Cu, and (*d*) W.

Karzmark *et al* [1]

ESTRO School

The Focal source spot

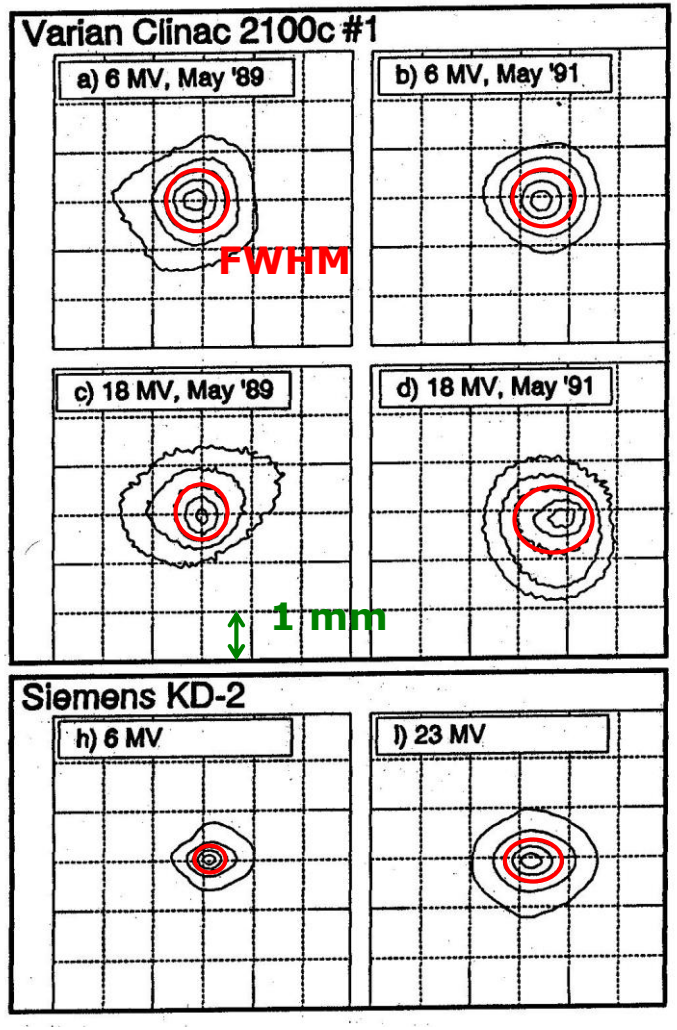

Approximately Gaussian source distributions, in some cases elliptical. Typical FWHM is 1-2 mm.

(Measured using a rotated slit camera and a diode.)

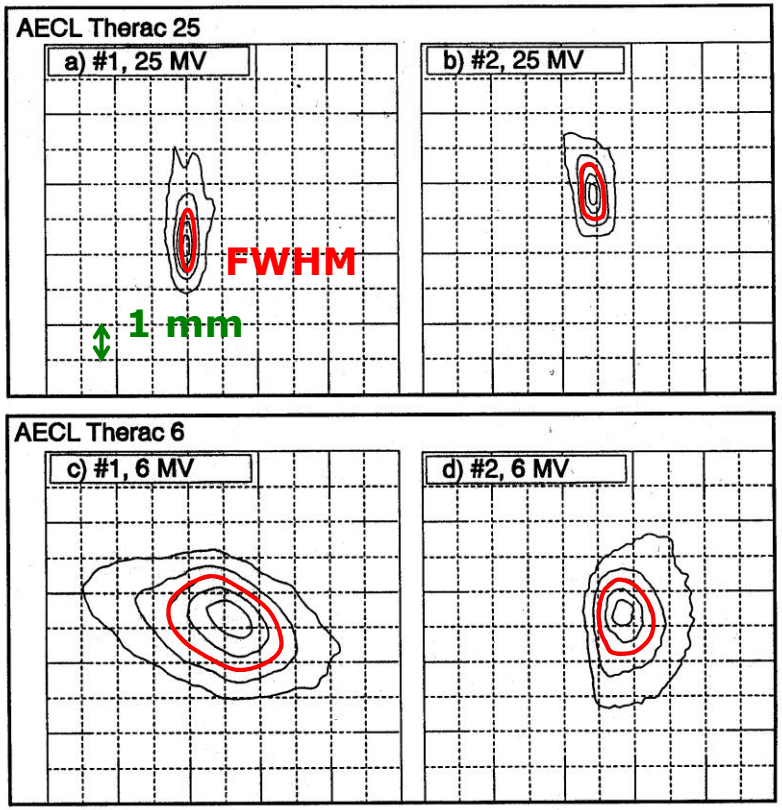

Jaffray *et al* [2]

ESTRO School

Geometric penumbra

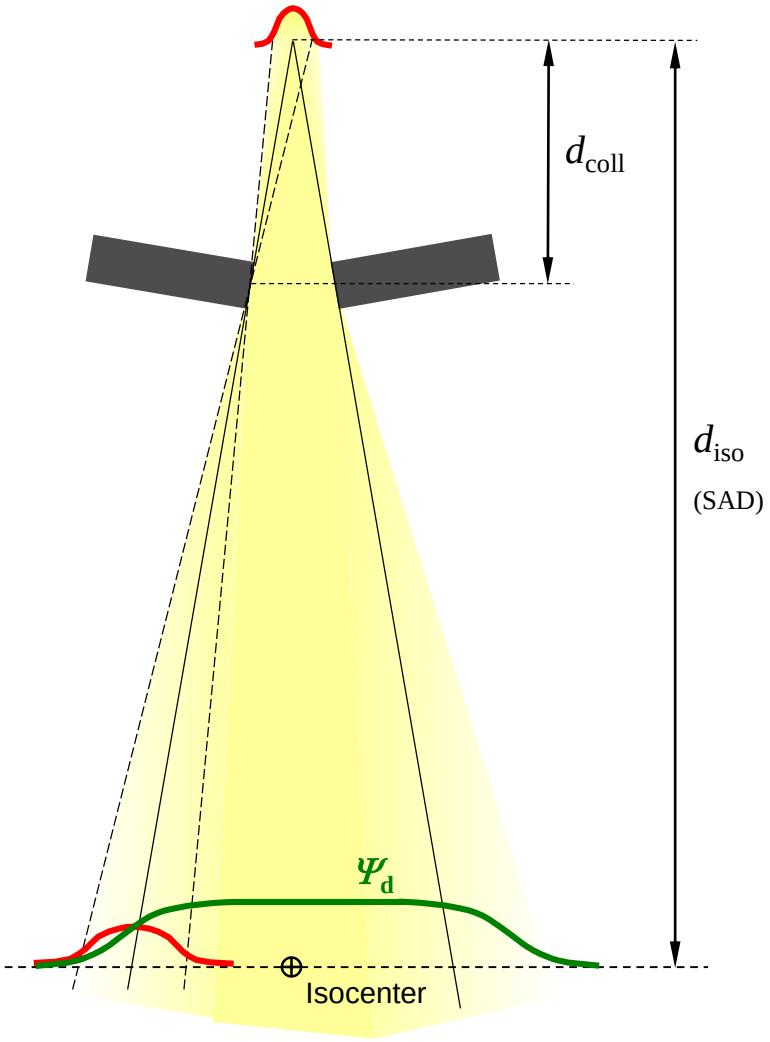

The source related *geometric penumbra* (10-90%) typically has a width of 3-5 mm at isocenter level, but can in more extreme cases extend up to about 10 mm.

Particularly important for small beams and IMRT.

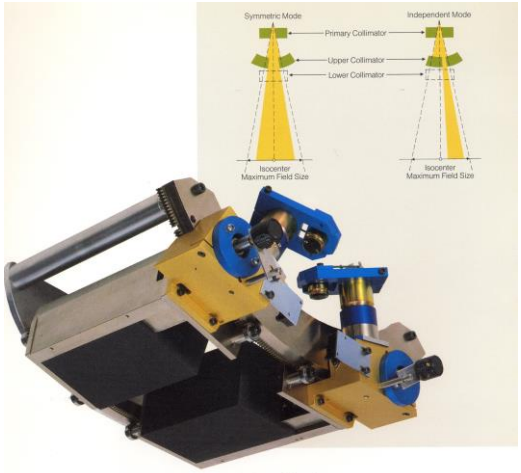

Focal/direct fluence characteristics

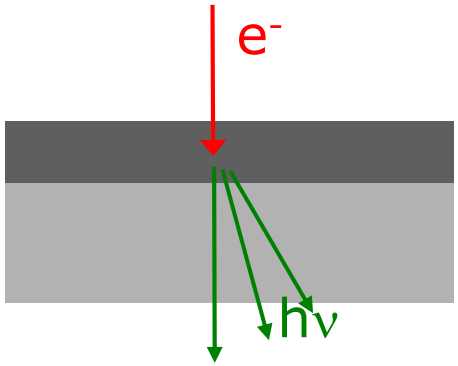

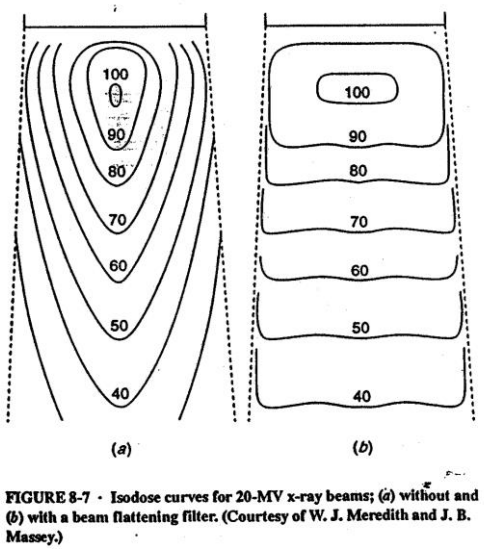

FIGURE 8-7 · Isodose curves for 20-MV x-ray beams; (*a*) without and (*b*) with a beam flattening filter. (Courtesy of W. J. Meredith and J. B. Massey.)

Lateral fluence distribution

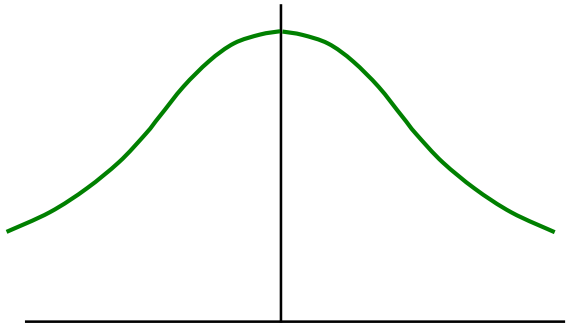

Mean energy - lateral variation
(Off-axis softening)

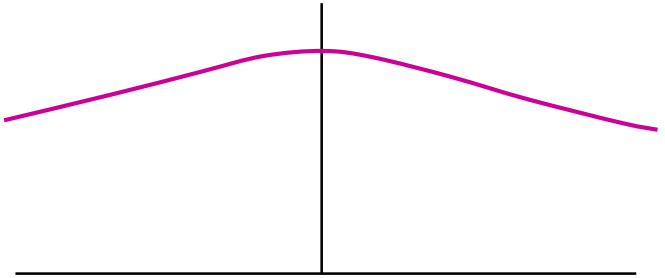

Karzmark *et al* [1]

ESTRO School

Flattening of the direct photon beam

The conical *flattening filter* absorbs 50-90% of the direct photons on the central axis.
In addition, it works as a scatter source located 7-15 cm downstream from the target, adding 5-10% at isocenter.

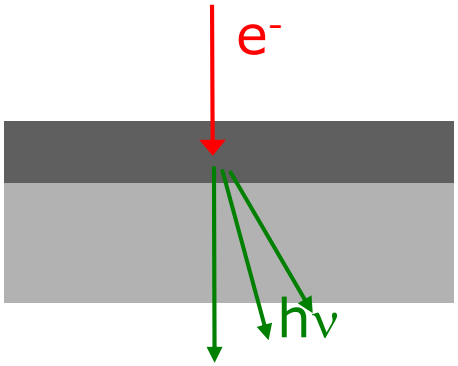

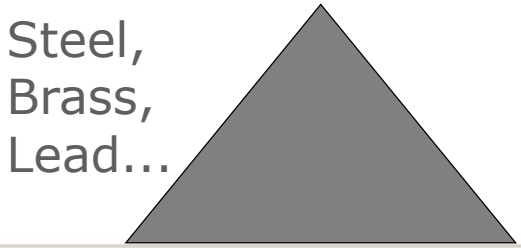

Lateral fluence distribution

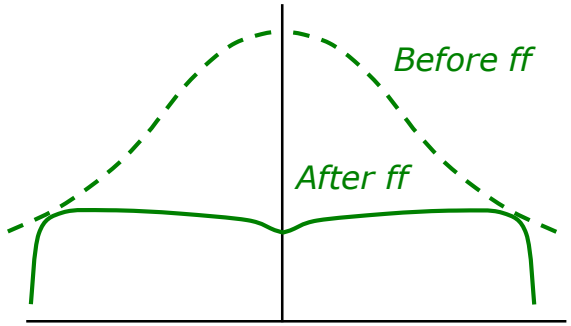

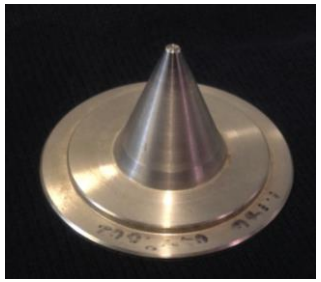

ESTRO School

Consequences of a flattening filter

Head scatter

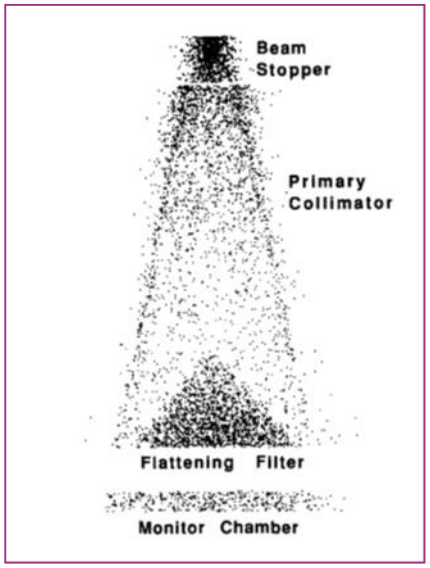

From Chaney 1994

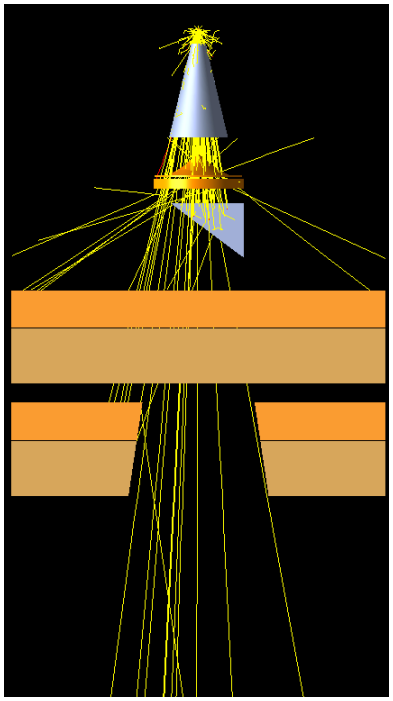

Energy variations off-axis

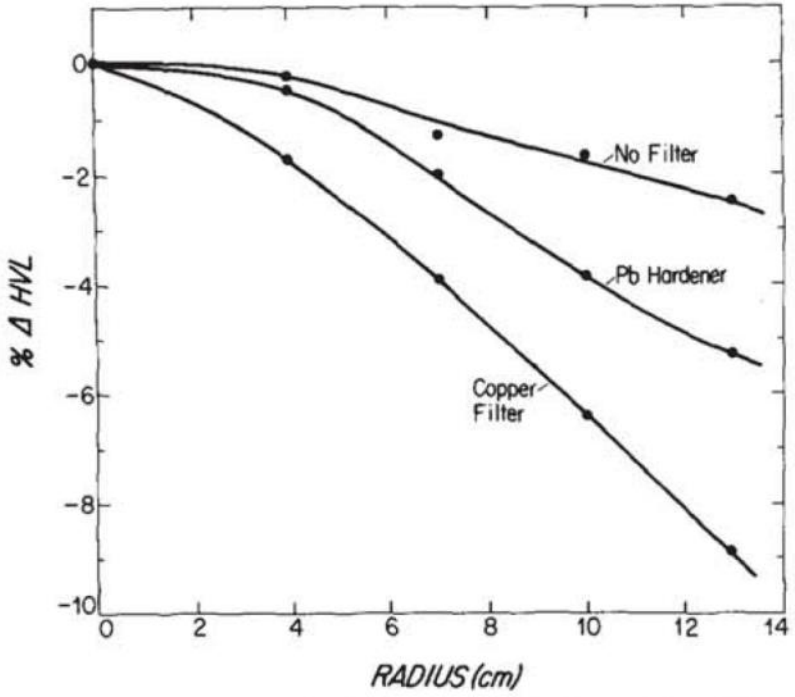

FIG. 4. Percentage changes in HVL, measured in brass, but with each curve normalized to its value on the central axis.

From Lutz and Larsen 1984

Flattening filters

Elekta

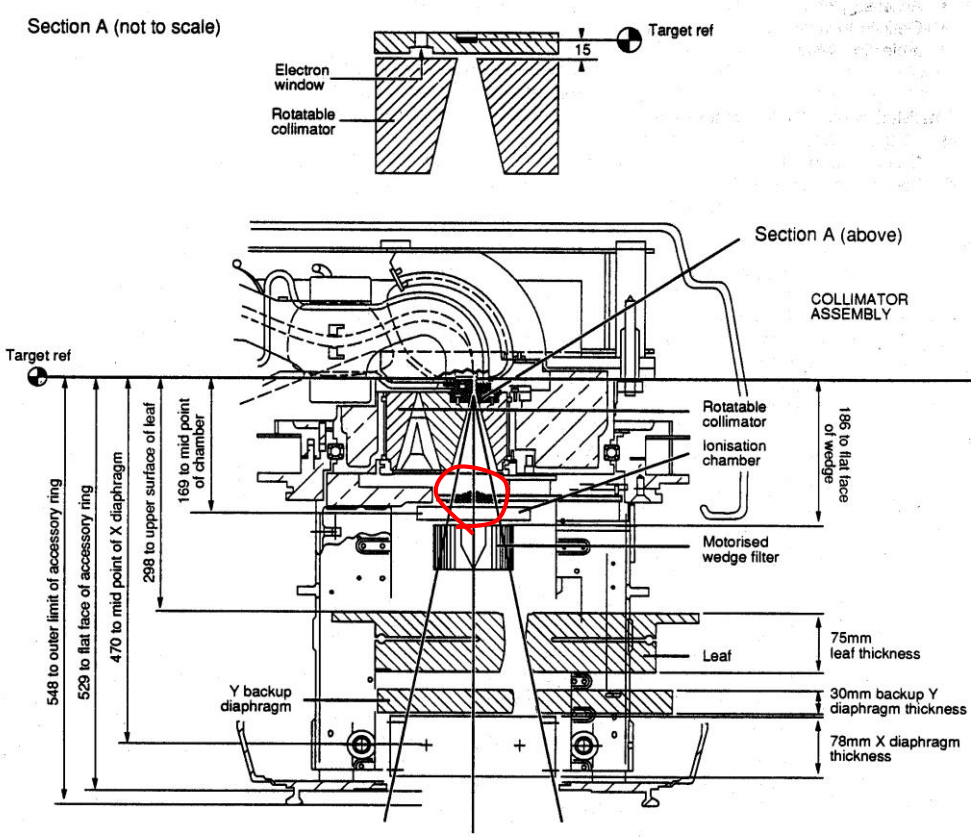

Varian (Clinac, high energy)

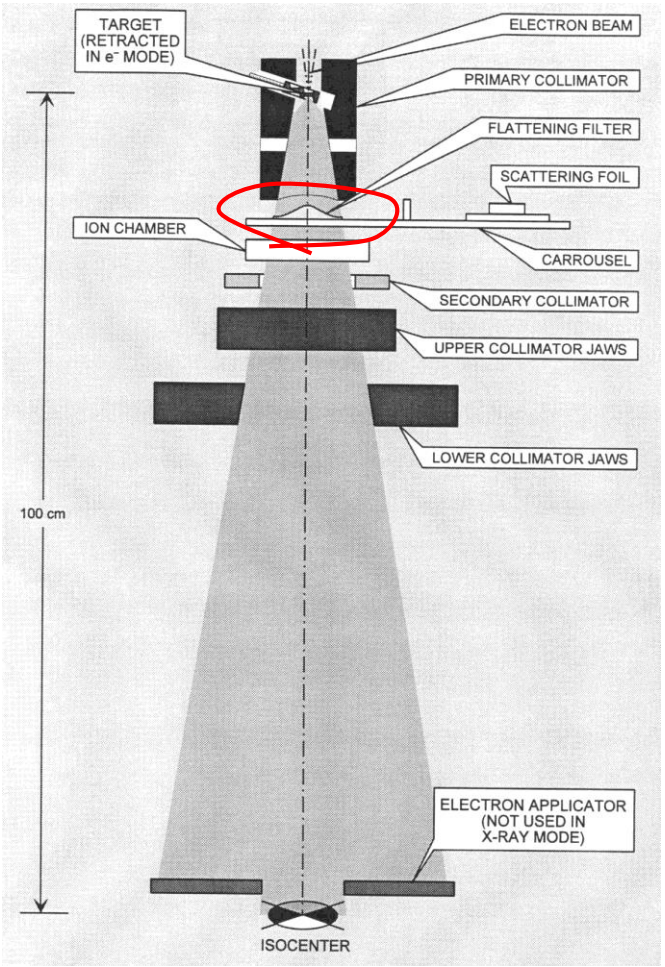

ESTRO School

Carousel from Elekta Precise

TrueBeam carousel

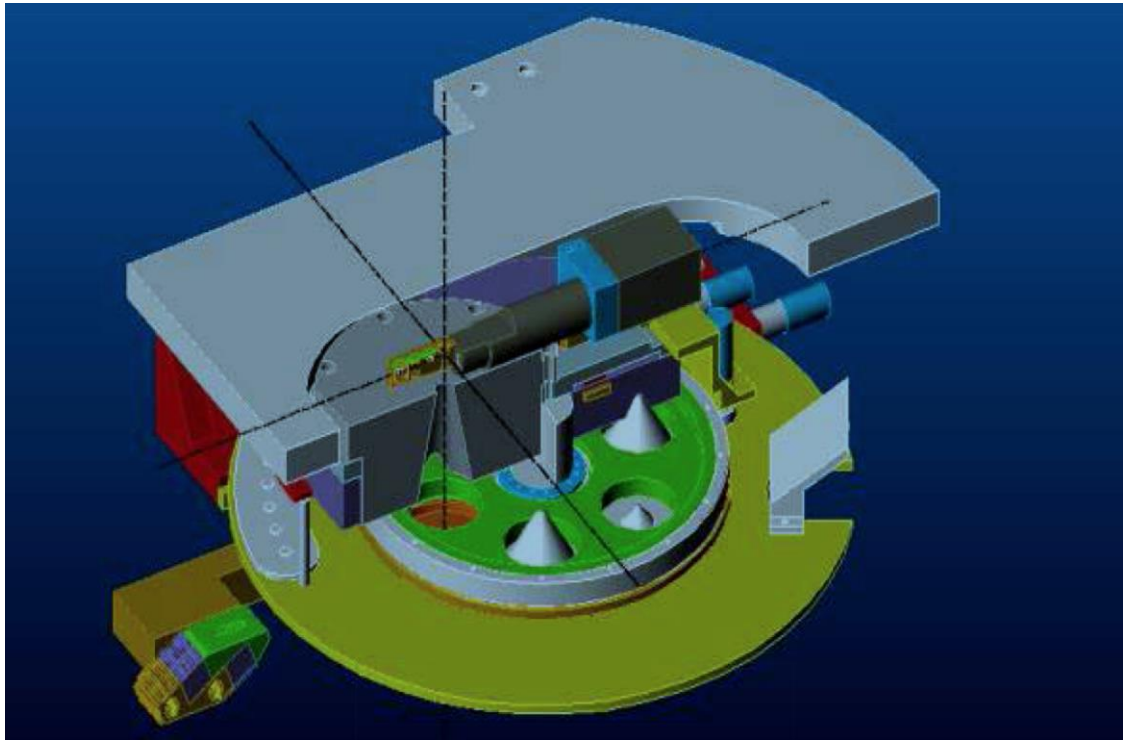

Resulting photon spectra at isocenter

Average photon energies (in MeV):

≤10MV: ~ MV/3

>10MV: ~ MV/3.5-4

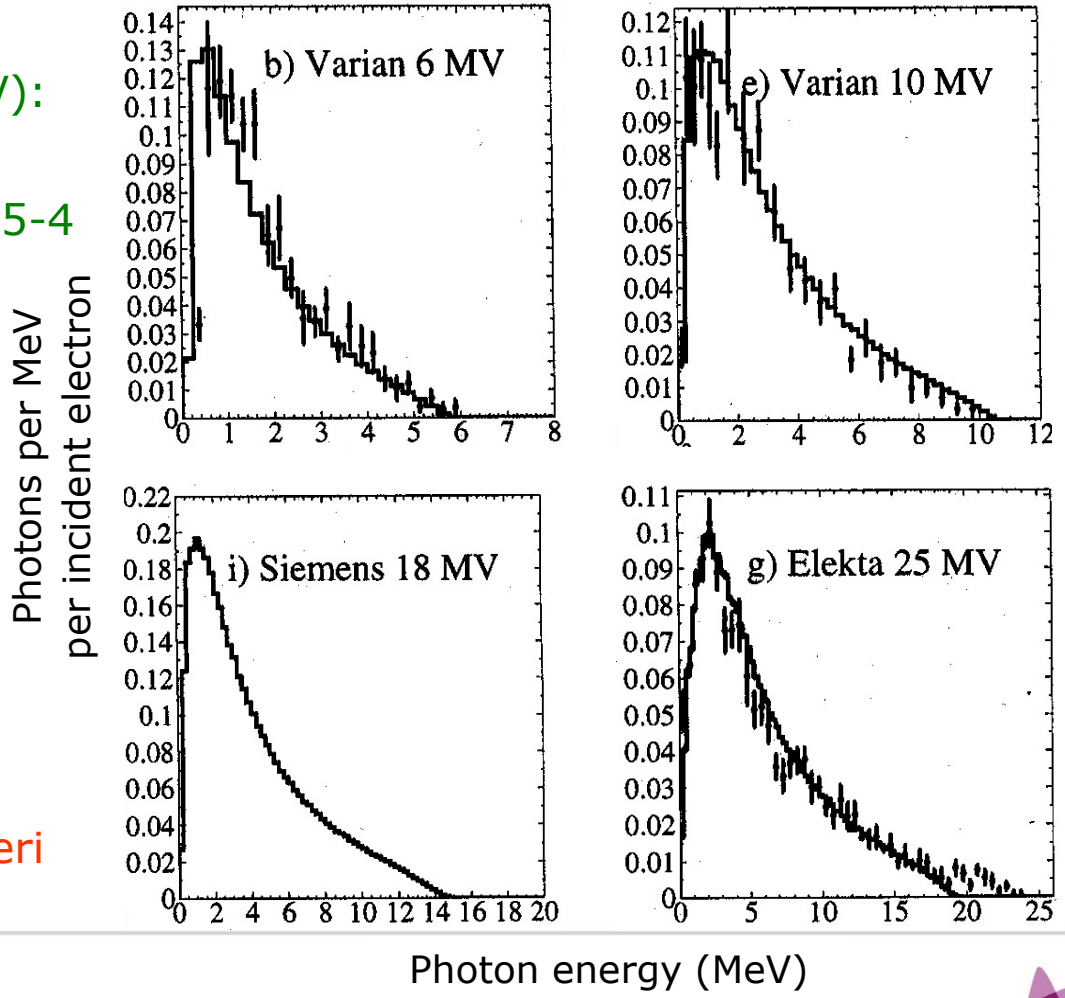

Sheikh-Bagheri *et al* [4]

ESTRO School

Resulting energy fluence spectra at isocenter (in log scale)

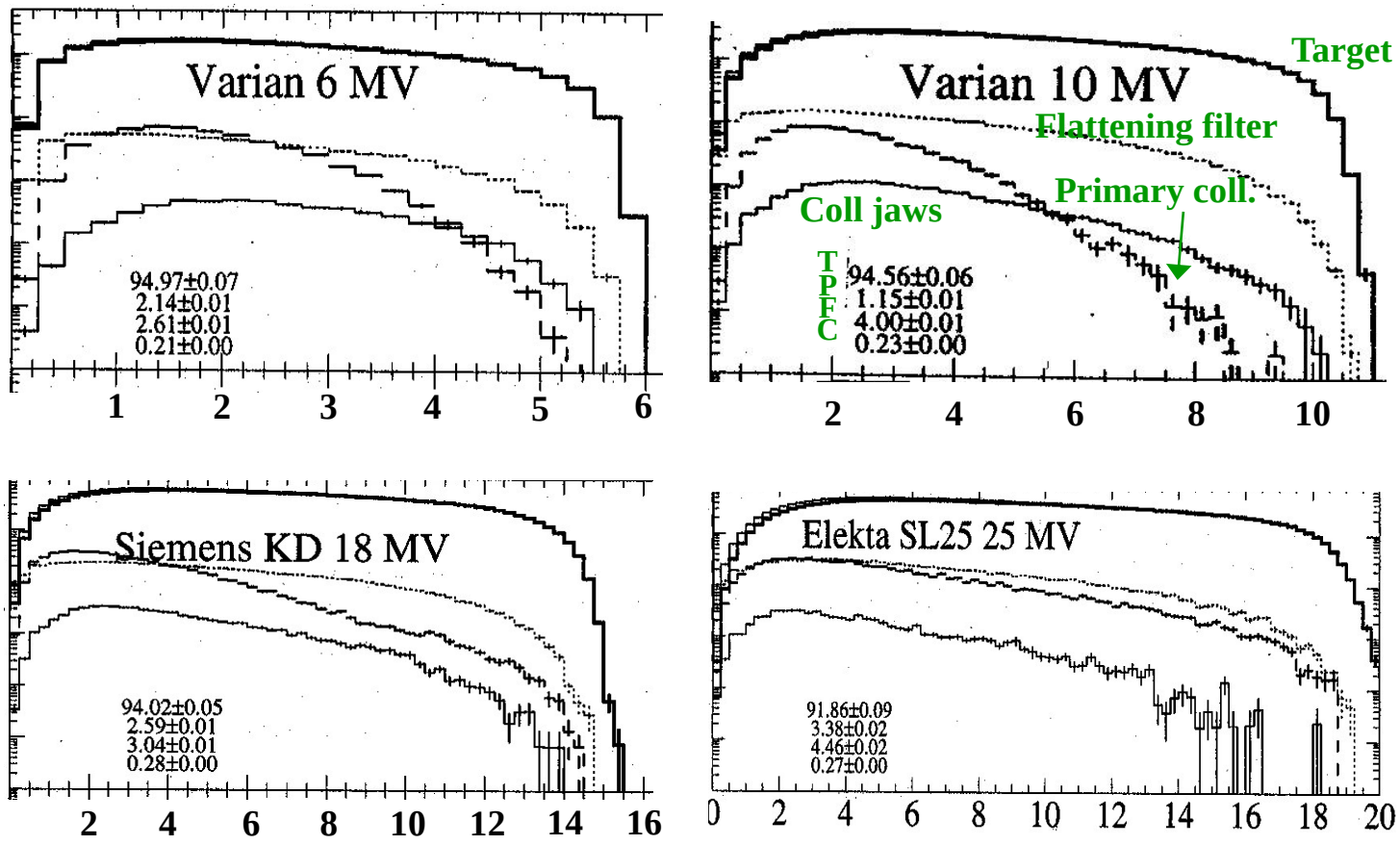

Sheikh-Bagheri *et al* [4]

ESTRO School

Photon fluence w/wo FF

Flattened

Unflattened

6 MV

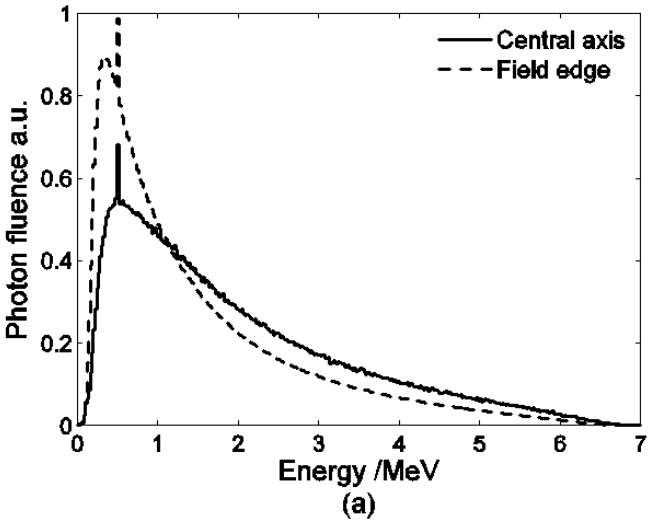

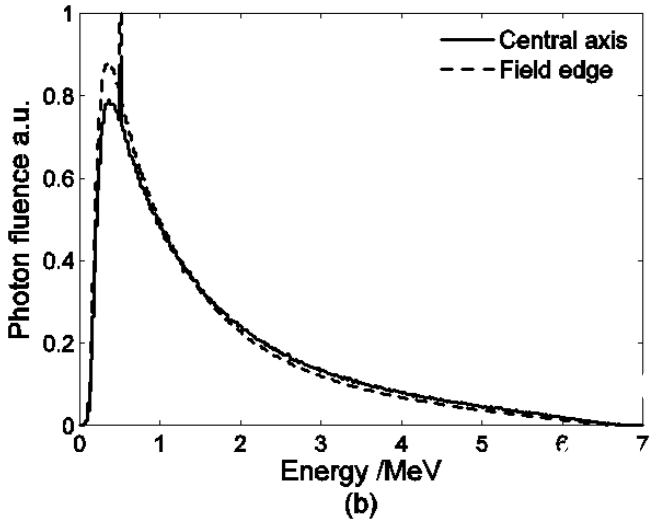

10 MV

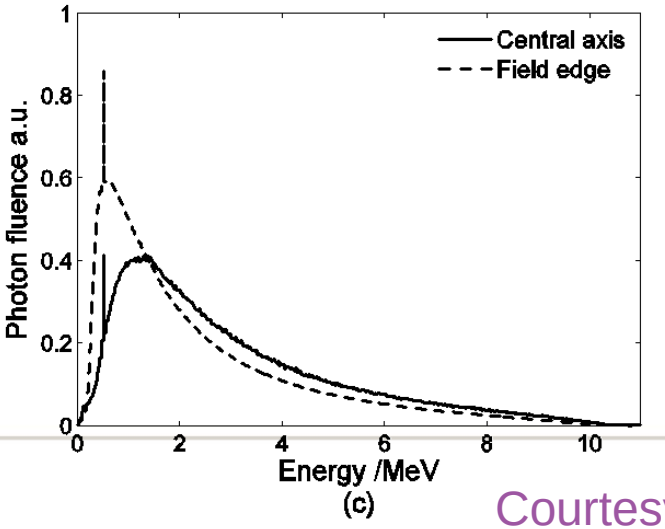

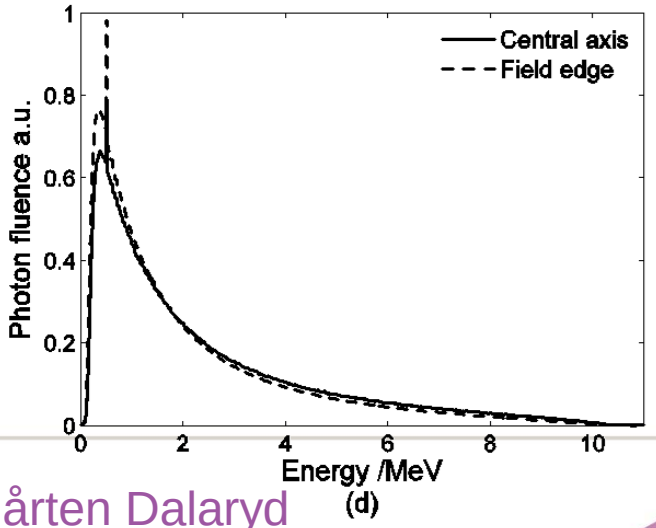

Courtesy Mårten Dalaryd

ESTRO School

Beam quality variations off axis

6 MV

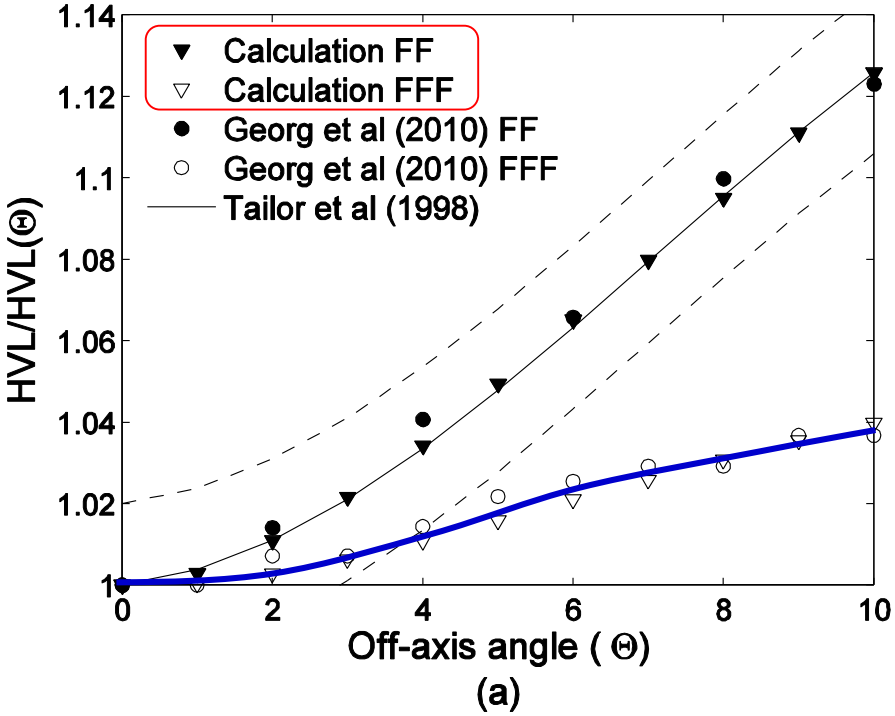

10 MV

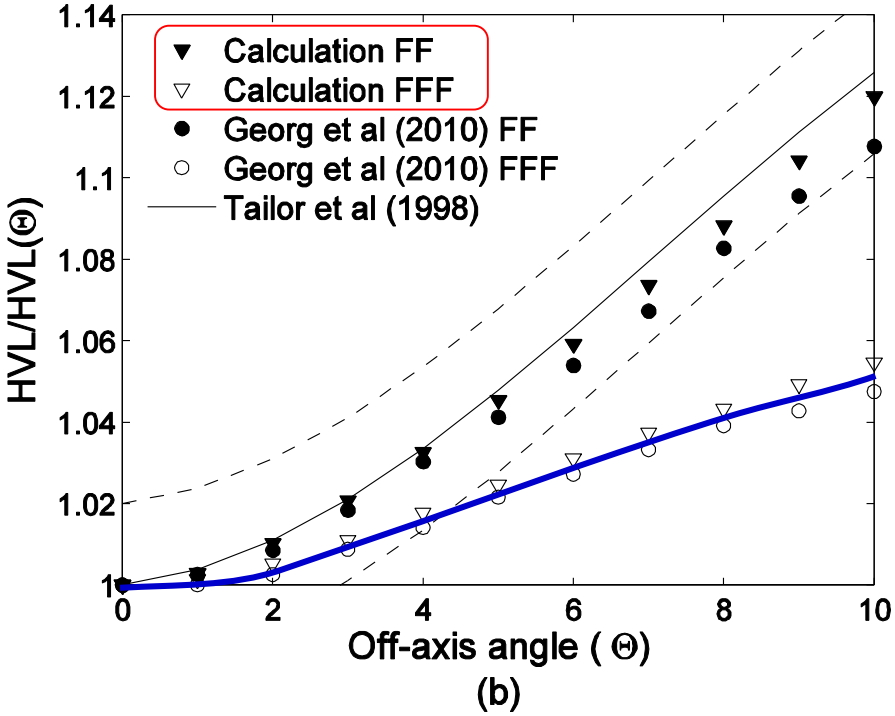

Courtesy Mårten Dalaryd

ESTRO School

Significance of off-axis softening

MC simulation of a clinical 4 MV photon beam, dose reconstruction at 10 cm depth.

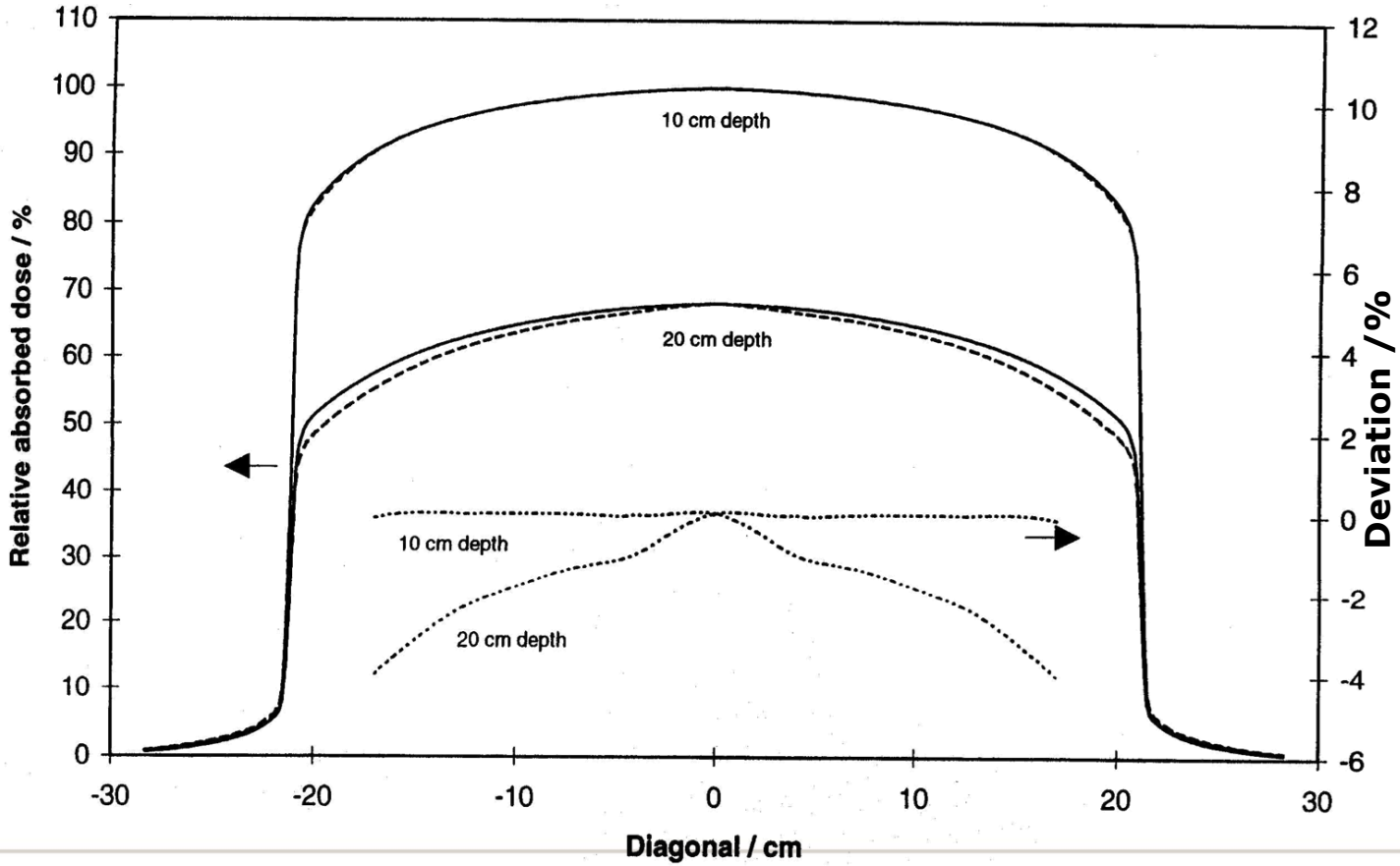

Sätherberg *et al* [3]

ESTRO School

Flattening filter free megavoltage photon beams
Lateral dose profile – 10 MV

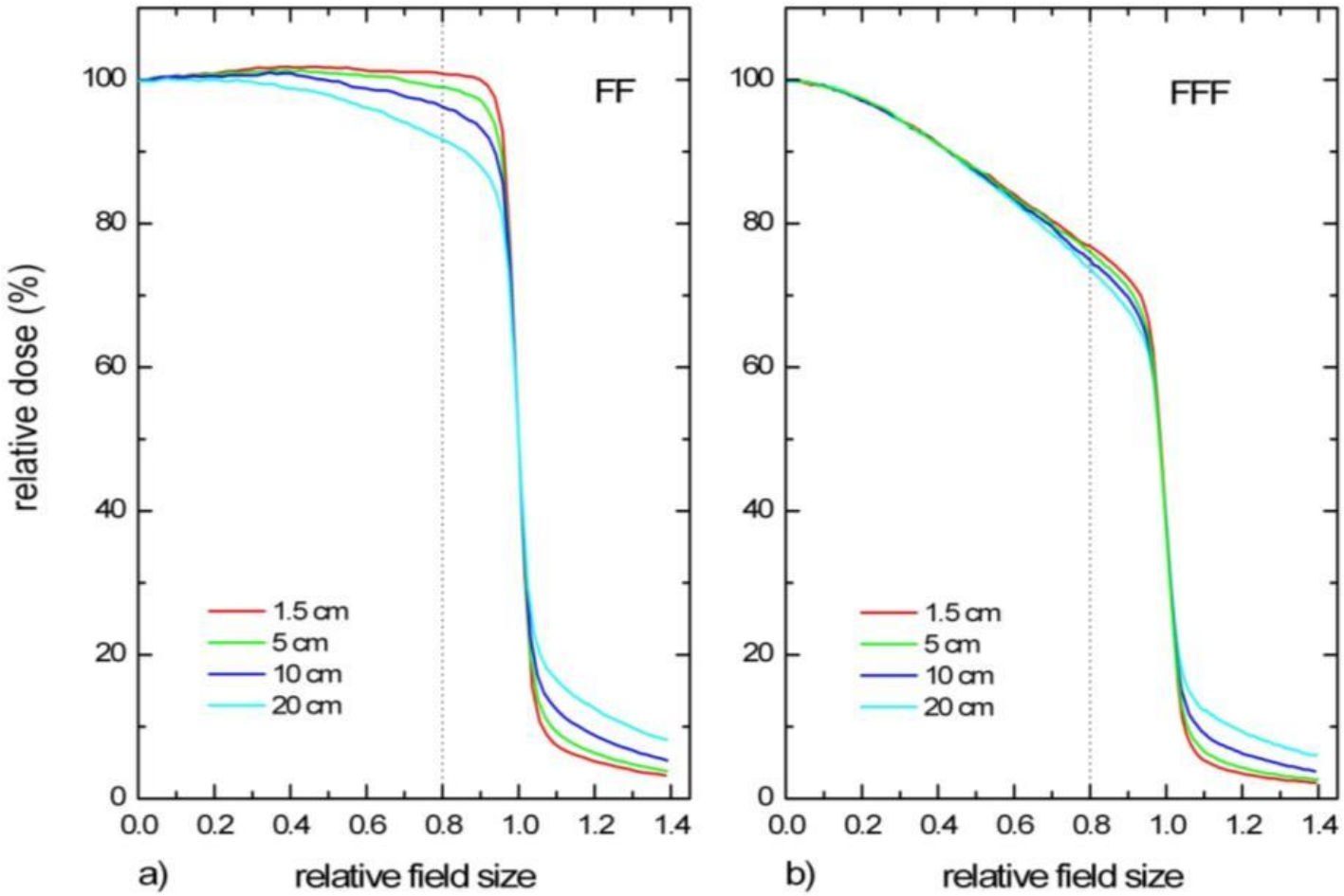

Kragl *et al* [10]

ESTRO School

The TomoTherapy treatment unit

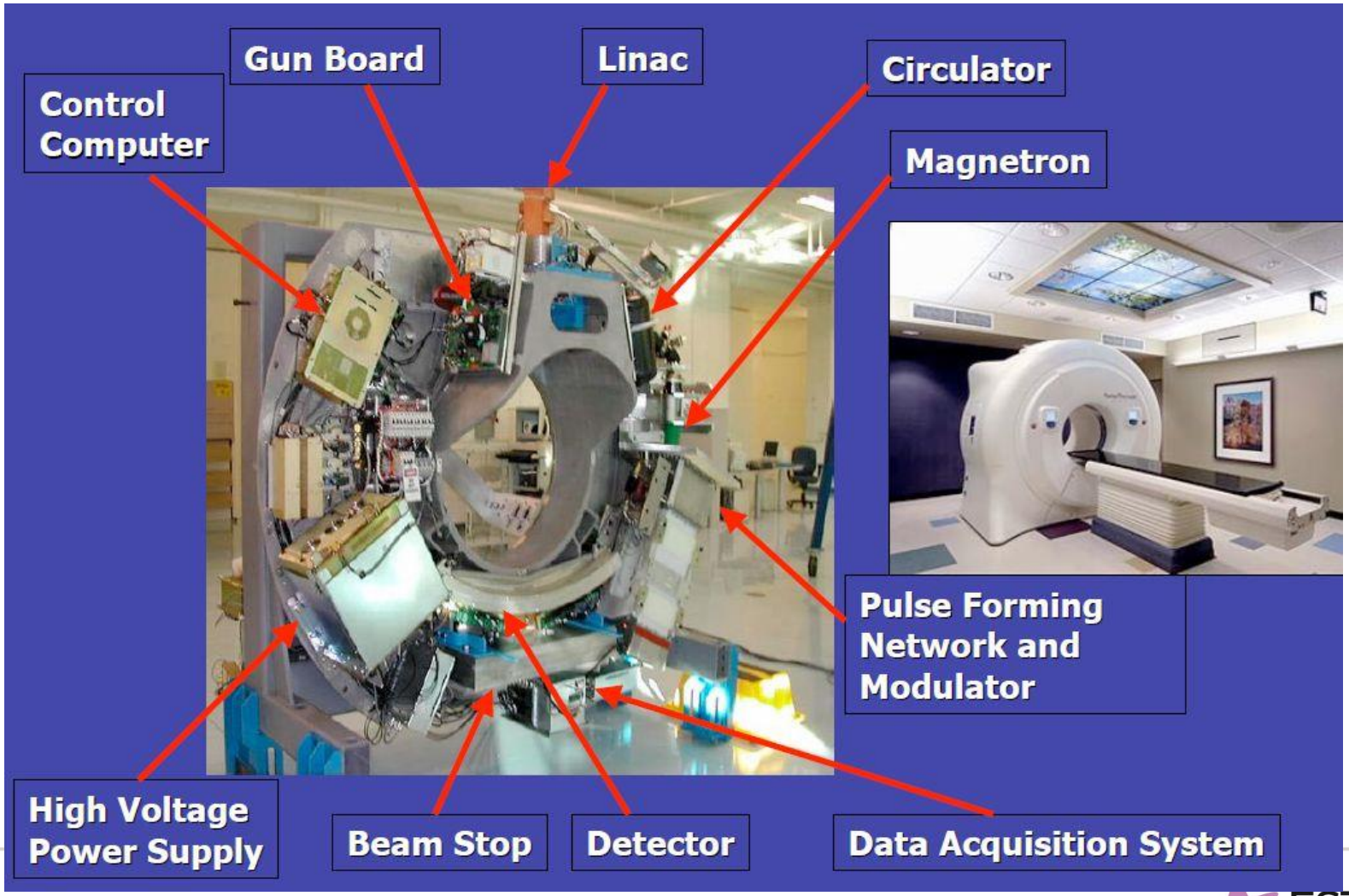

The TomoTherapy treatment head

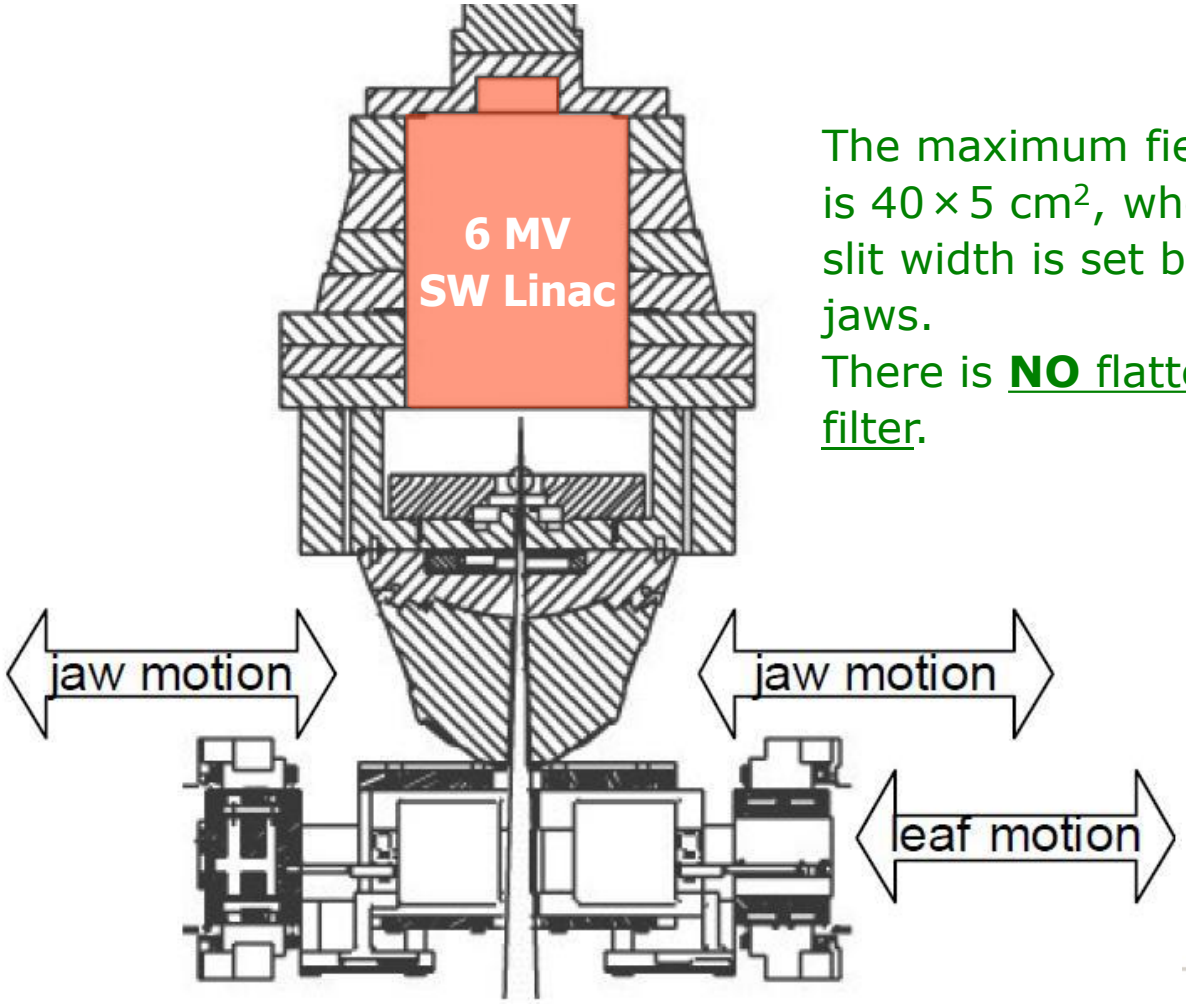

The maximum field size is 40×5 cm^2, where the slit width is set by the jaws.
There is **NO** flattening filter.

TomoTherapy treatment beam

40 cm long slits on film (1, 2.5, and 5 cm wide).

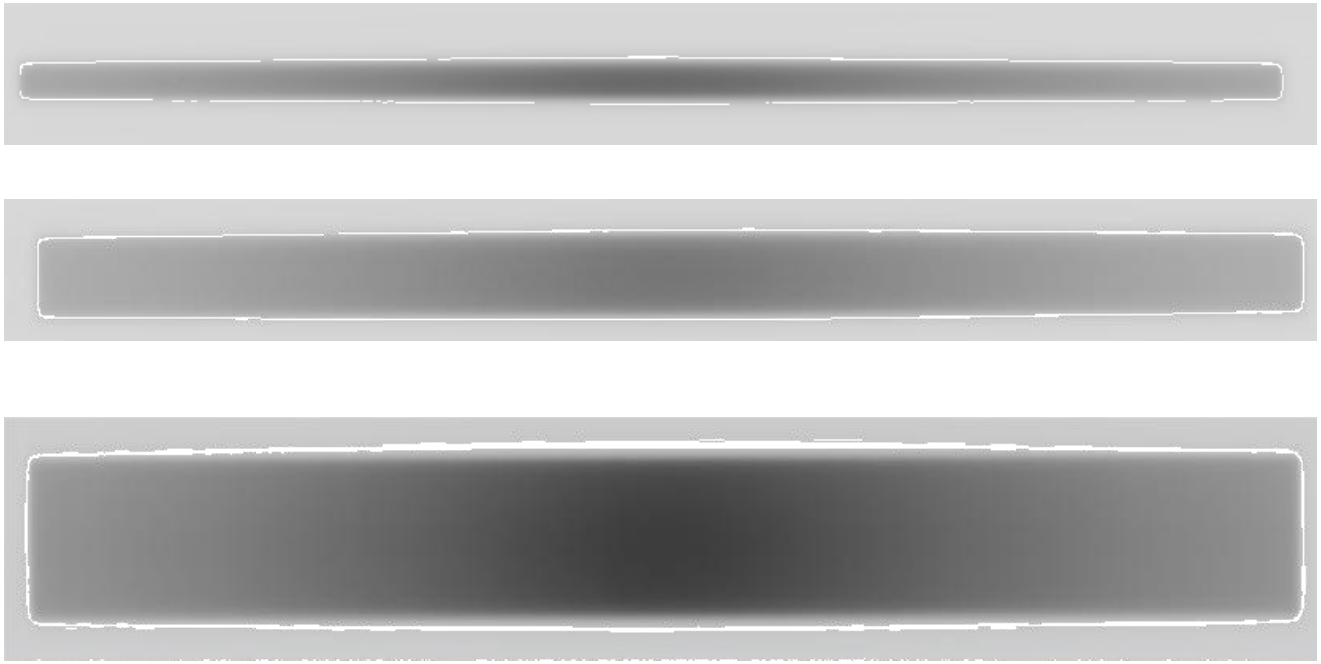

TomoTherapy dose profiles

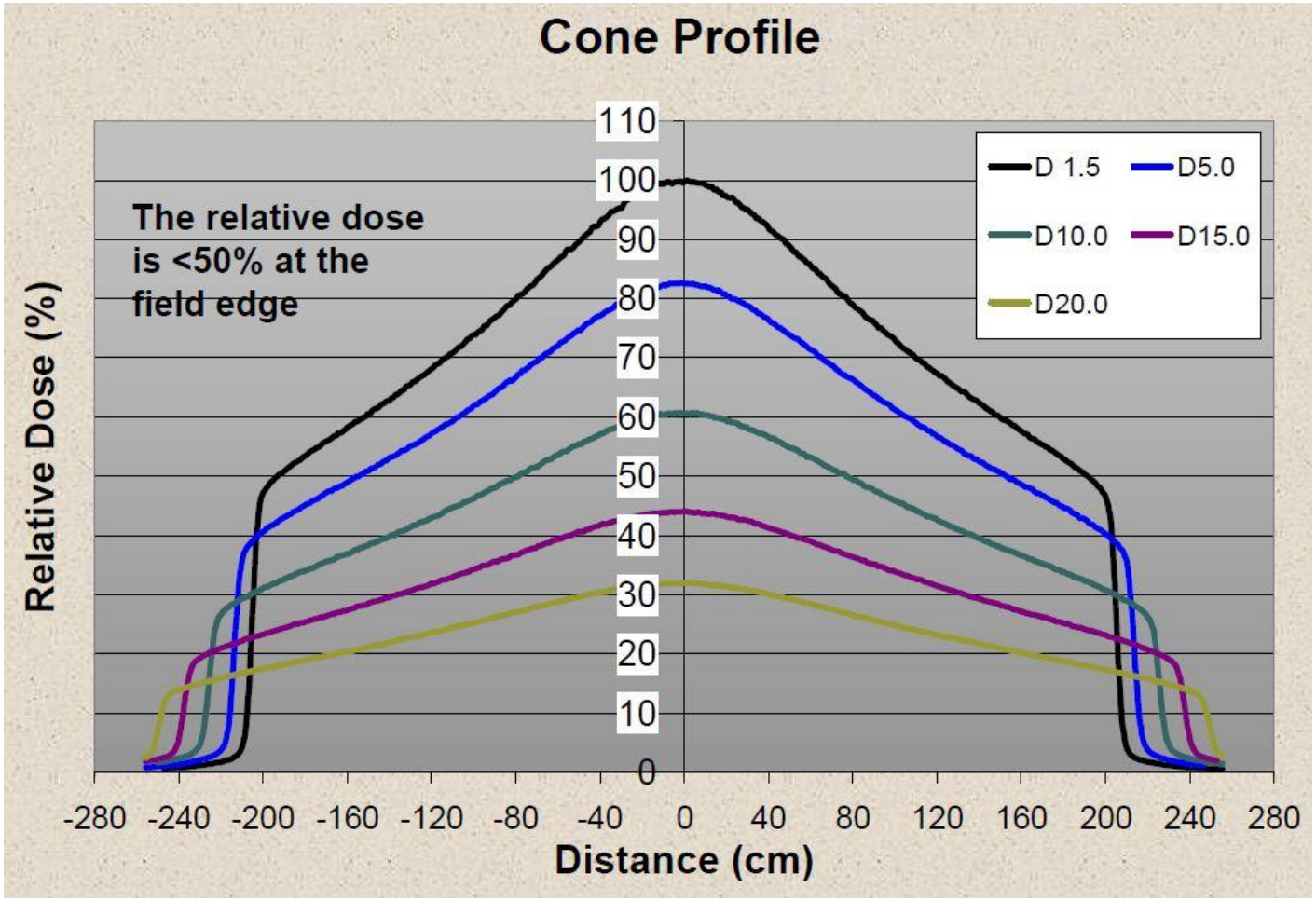

Beam alignment on flattening filter

Perfect alignment

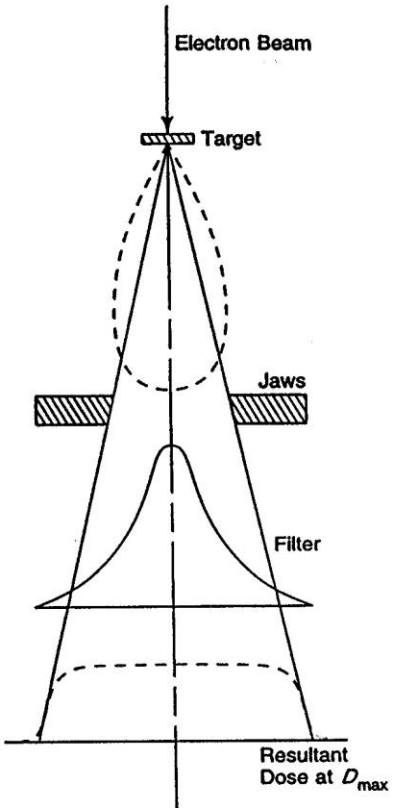

Angle error

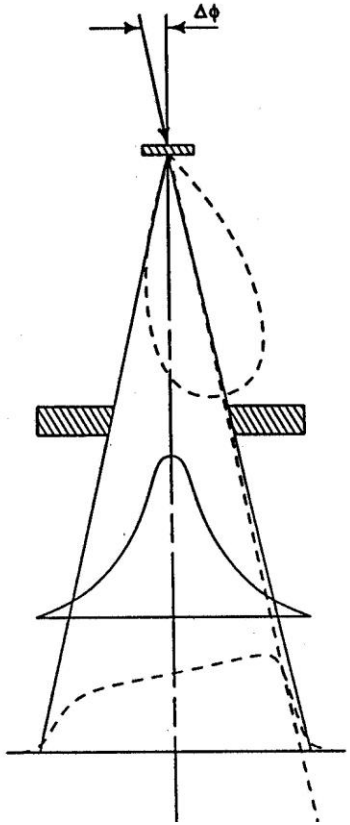

Position error

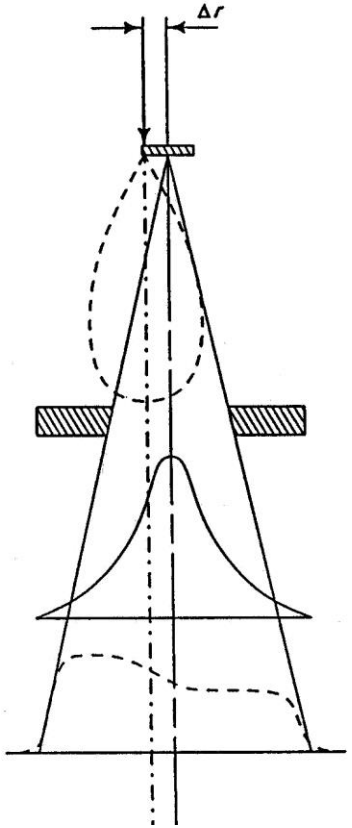

Karzmark *et al* [1]

ESTRO School

Lateral dose distributions

max field size at d_{max} and 10 cm depth

Beam flatness is normally optimized at 10 cm depth, which means that there will be "horns" at d_{max}.

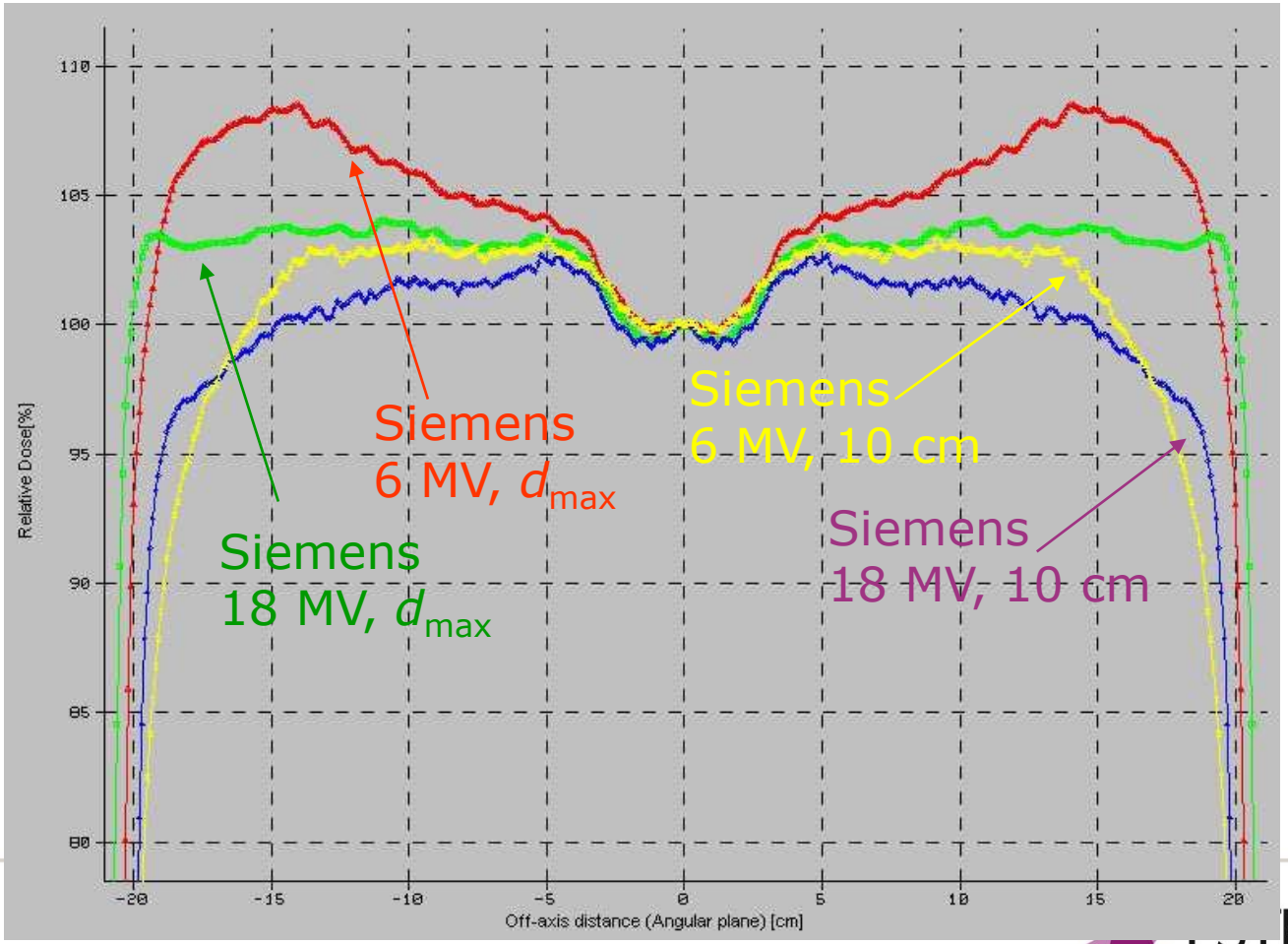

Lateral dose distributions

10x10 cm² at d_{max} and 10 cm depth

In smaller fields the "horns" contributes to the dose close to the field edges, yielding better beam flatness.

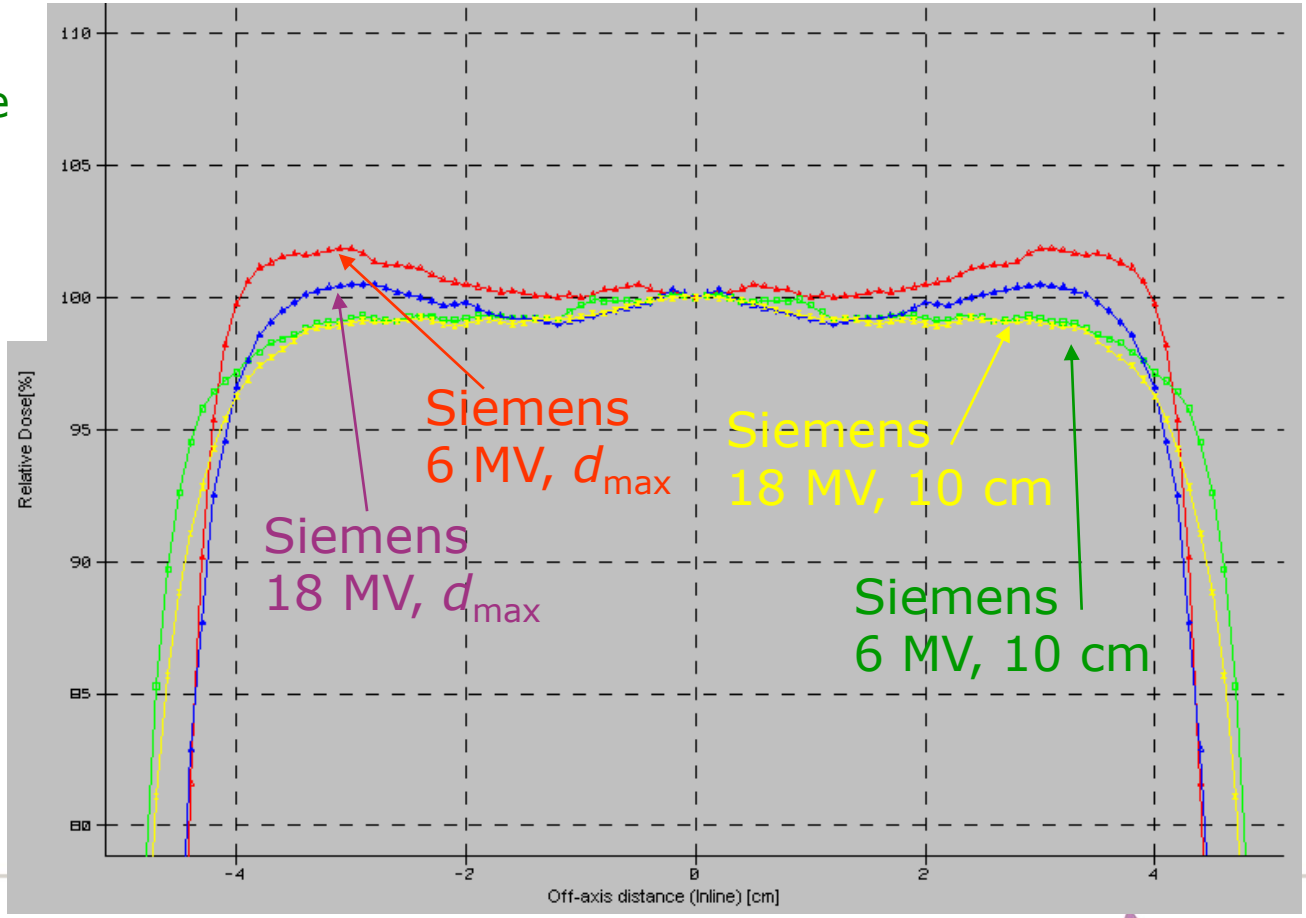

ESTRO School

Dose monitor chamber

Transmission ionization chamber that monitors and controls delivered dose (MU), dose rate, beam symmetry and flatness.

Varian

Elekta

The dosimetry system must contain two independent channels.

Sealed or open compensated chambers ⇒ no dosimetric influence from ambient air pressure or temperature.

The E-field (bias voltage) should be high (~ 500 V/mm) in order to minimize recombination/dose rate dependence.

Commonly layered through thin and strong foils with condensed Au or Cu. Total thickness ~ 0.2 mm.

Dose monitor chamber

Transmission ionization chamber that monitors and controls delivered dose (MU), dose rate, beam symmetry and flatness.

Varian True beam

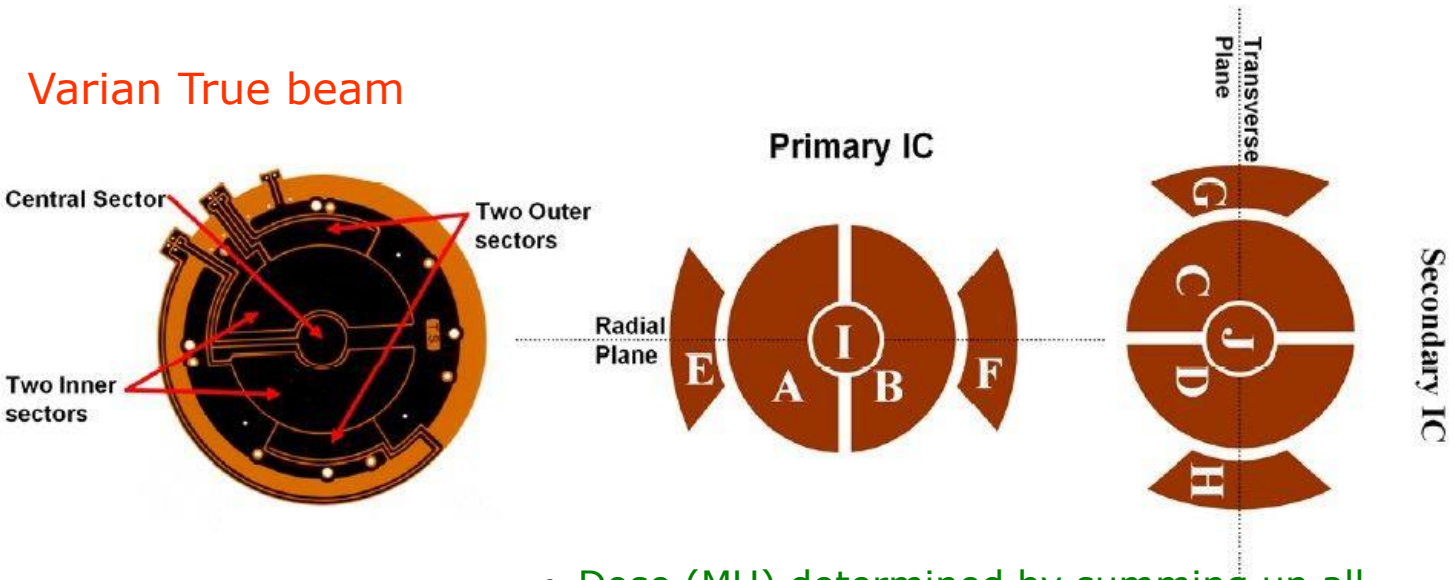

- Dose (MU) determined by summing up all sectors, divided into two independent channels.
- Symmetry determined through comparisons between left/upper and right/lower side.
- Flatness (new on True Beam) is determined by comparing ratios between (A+B) and I or (C+D) and J.

Monitor feedback/Beam symmetry servo

The monitor signal can be used as feedback to the electron beam transport, i.e. steering magnets, to optimize beam symmetry.

Varian
(*Clinac HE*)

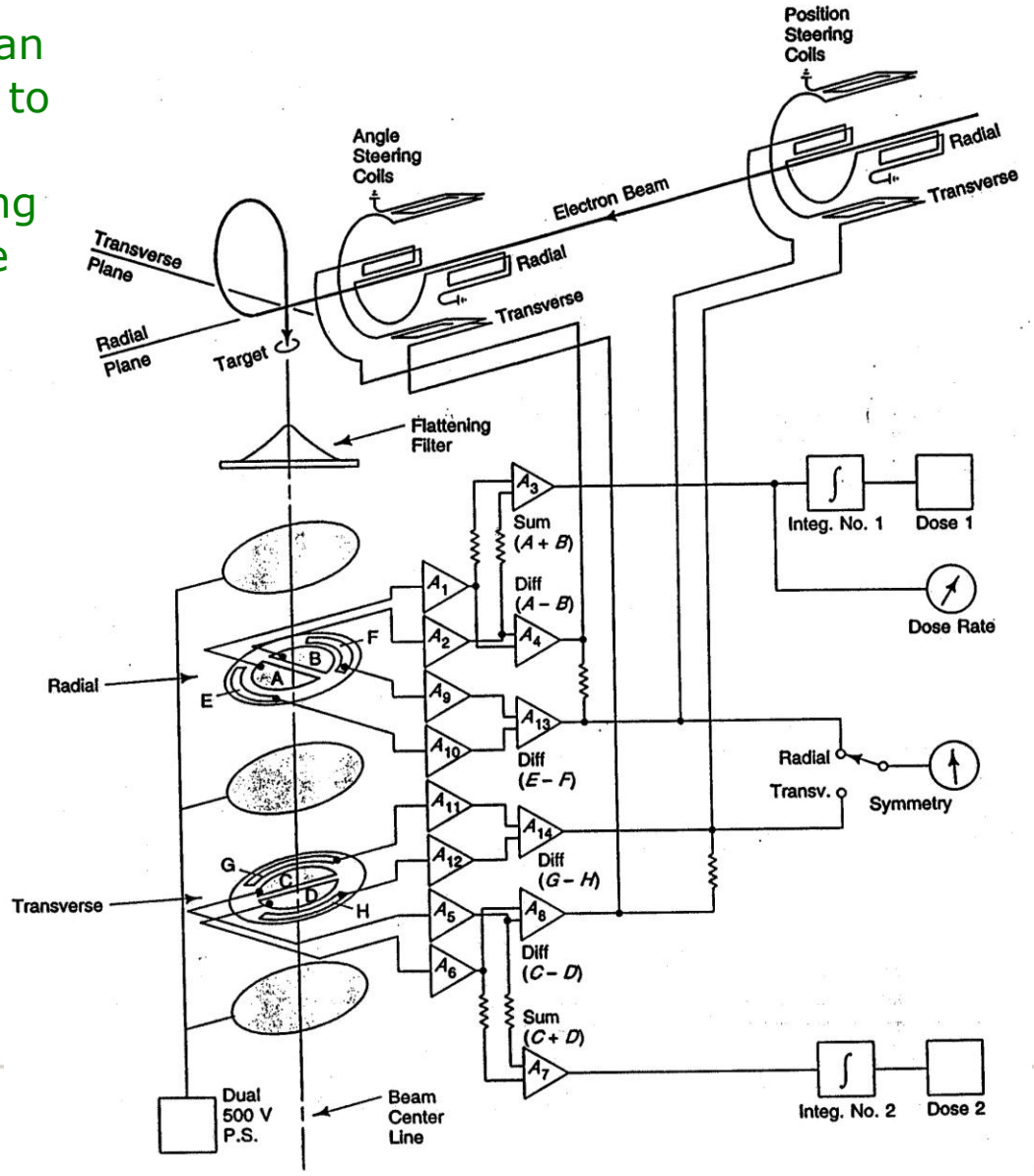

ESTRO School

Monitor feedback/Beam energy servo

An increase in beam energy causes a rise in the dose rate in the center of the field, and vice versa.
The X-ray gun servo system of an Elekta linac uses this property to detect energy changes by using the two hump plates.
The difference between the two hump plates is used to produce an error signal, which gives a correction to the nominal level of gun current set by the operator.

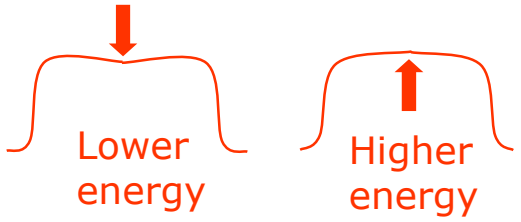

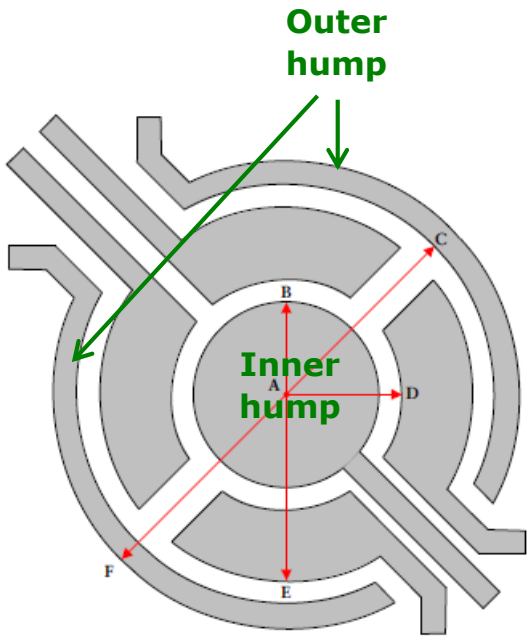

Elekta Dosimetry System

A → B = 5.8 cm
A → C = 16.5 cm
A → D = 7.3 cm
A → E = 15.3 cm
A → F = 18.2 cm

Figure 3.4 *Servo plate coverage at the isocenter*

MLC design – I – Lower jaw replacement

EXAMPLES:

(*Siemens*)

(*GE*)

(*Scanditronix*)

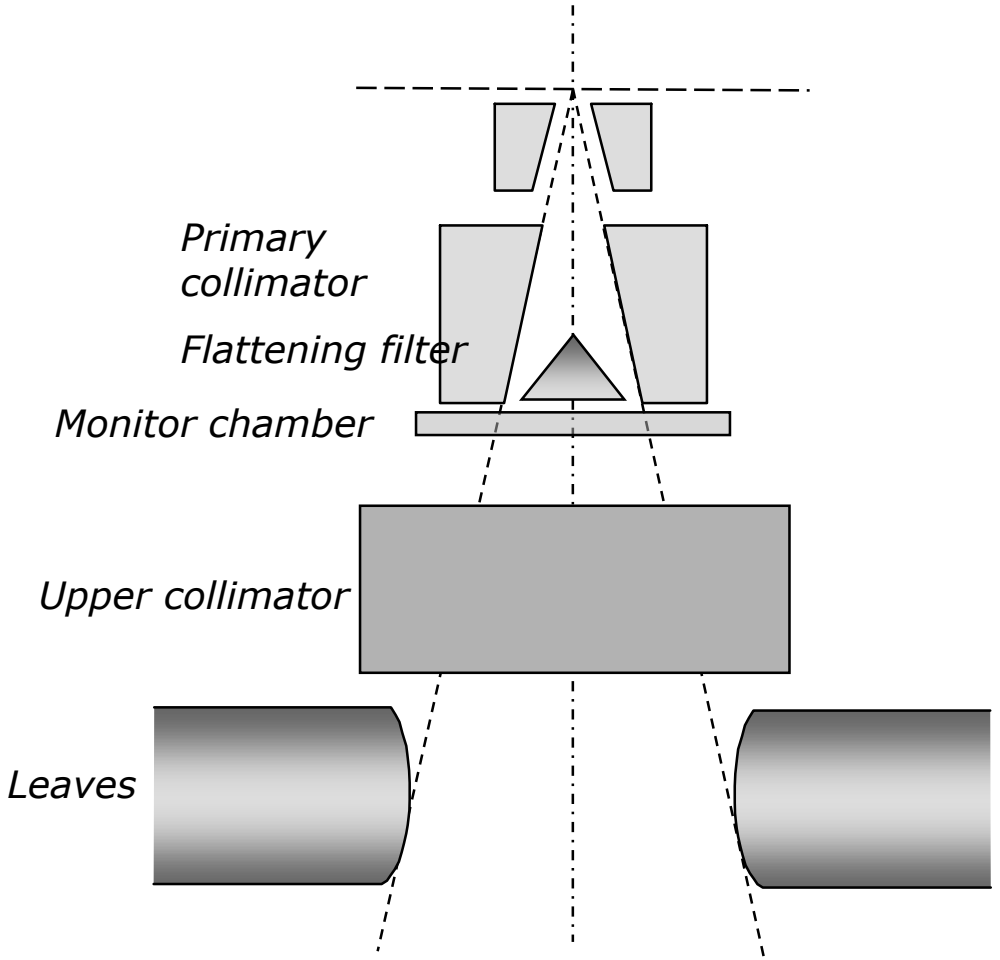

MLC design – II – Upper jaw replacement

EXAMPLE:

ELEKTA

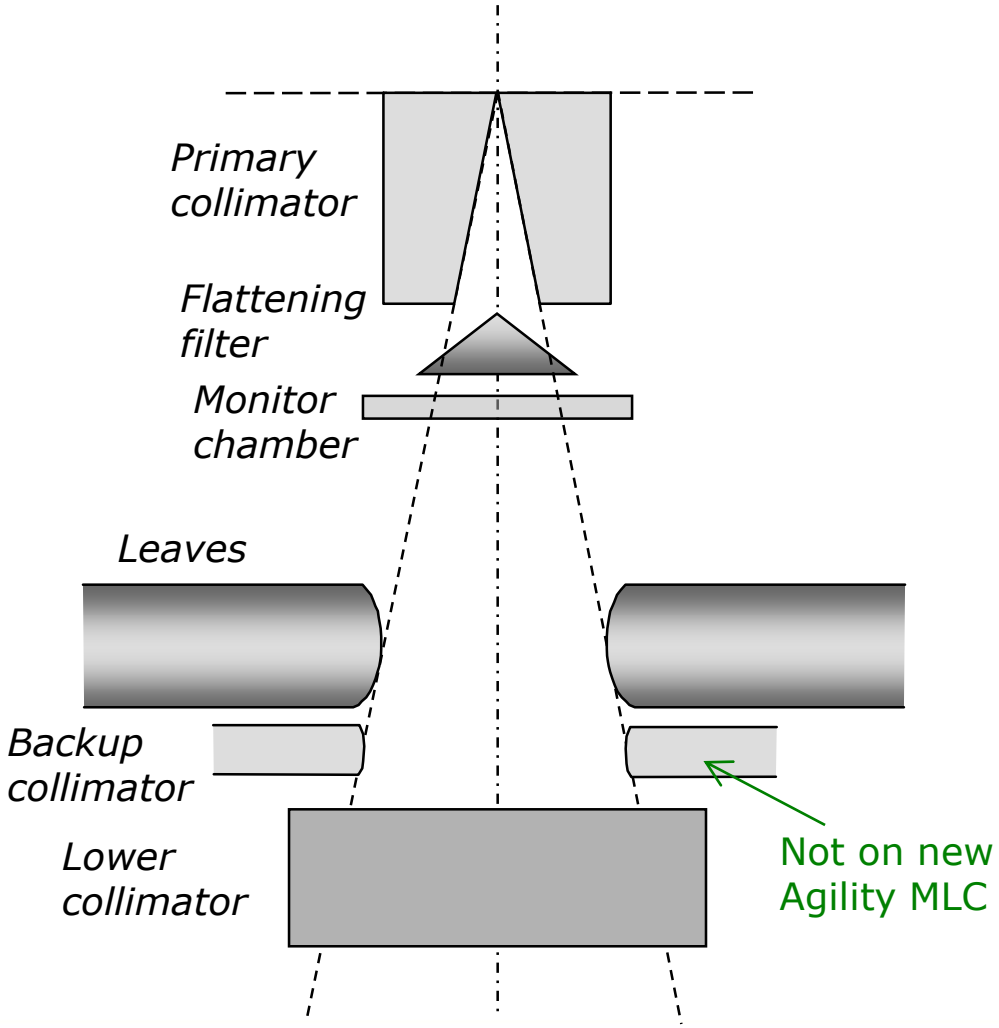

ESTRO School

MLC design – III – Third level configuration

EXAMPLES:

VARIAN medical systems

μMLCs

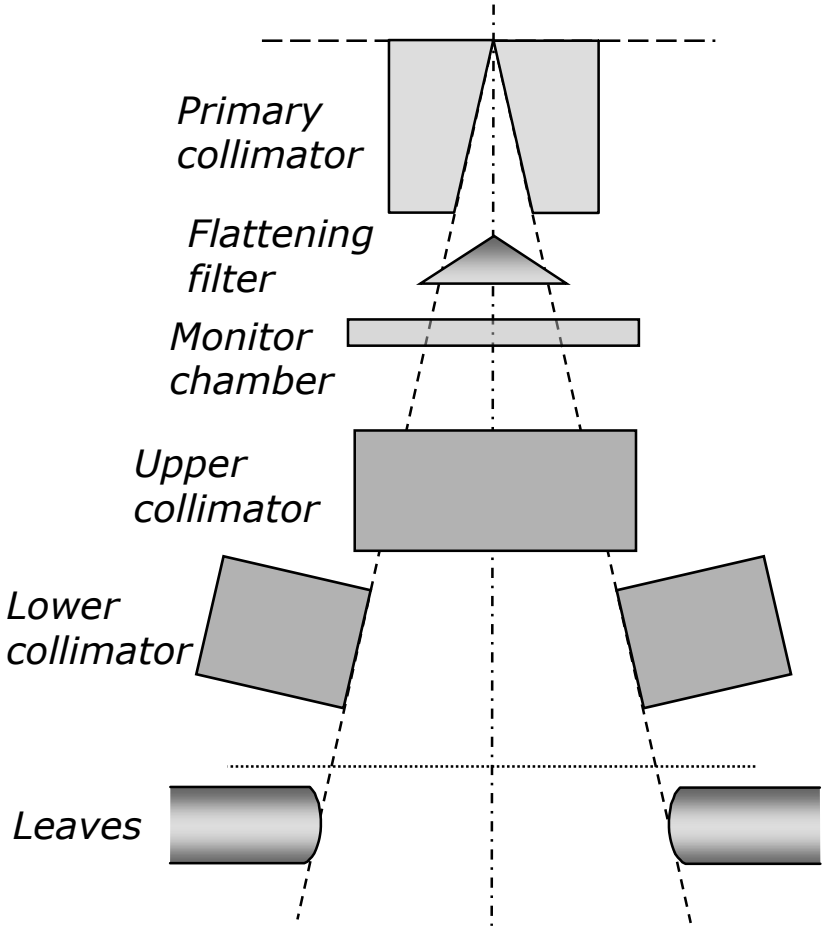

ESTRO School

Collimator alignment

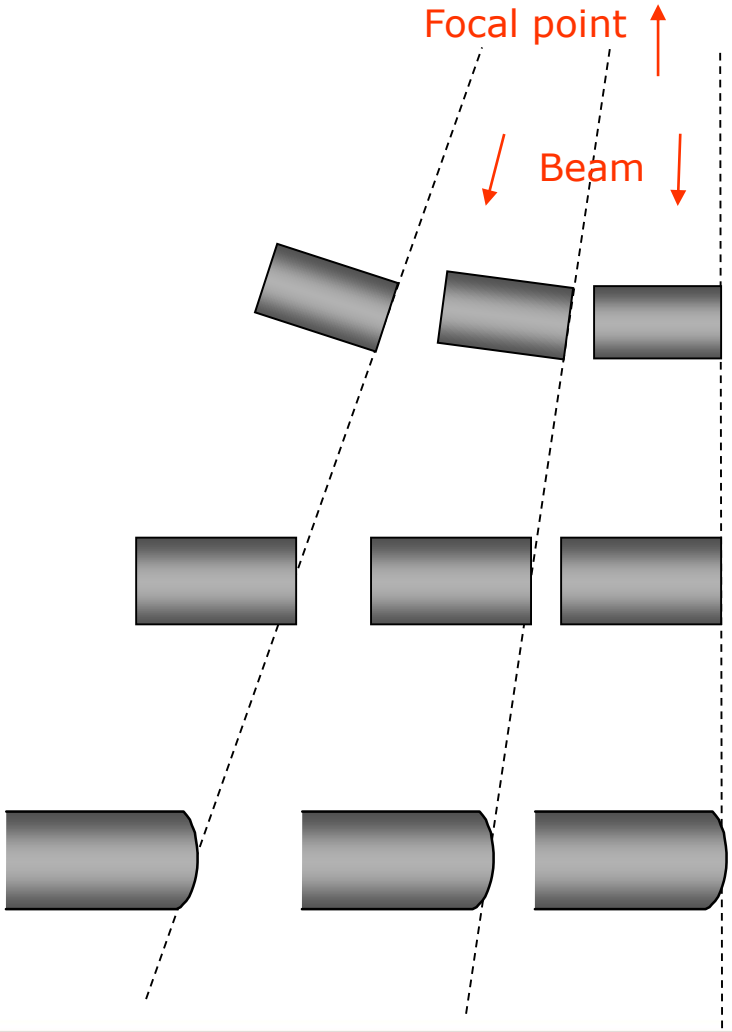

Collimator alignment	Geometric penumbra
Focused leaf edge *advanced mechanics*	
Straight leaf edge *Not used for large fields*	
Rounded leaf edge *Most common solution for MLC*	

Positioning rounded collimator edges

Important for dose calculations in small fields and IMRT.

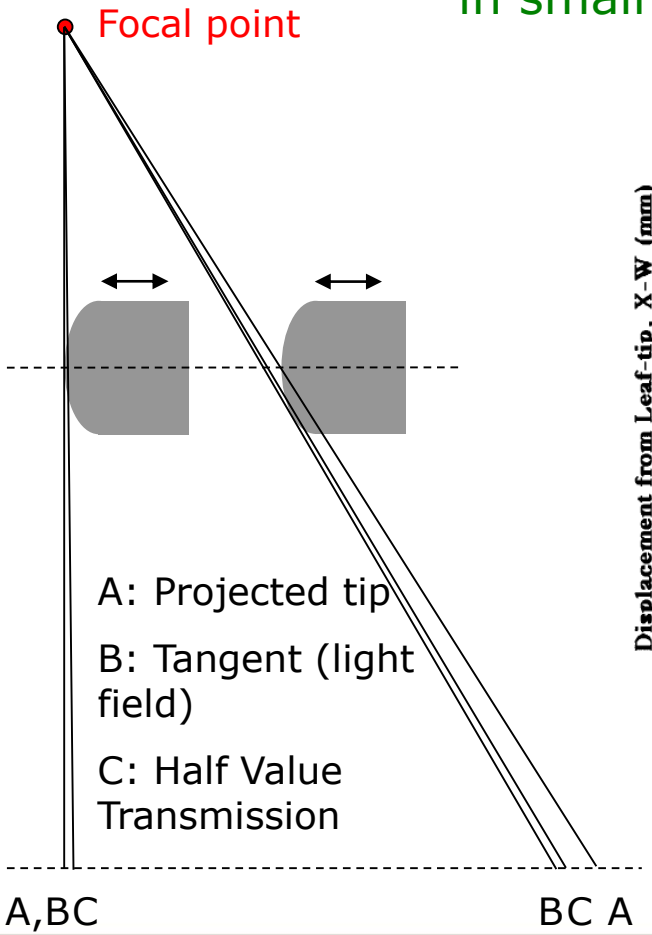

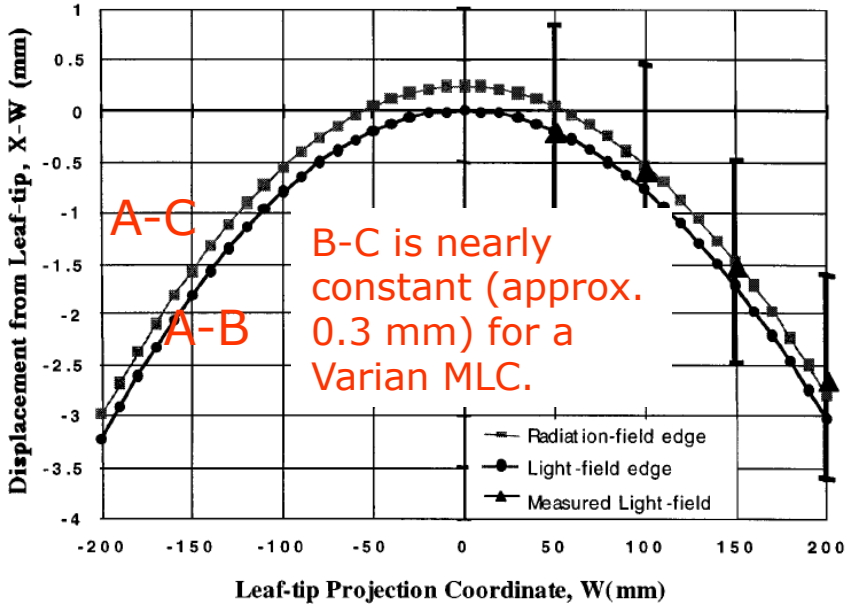

Boyer and Li [6]

Rounded collimator edges

The design of the rounded edge can vary, depending on the geometry (thickness, location and maximum over-travel).

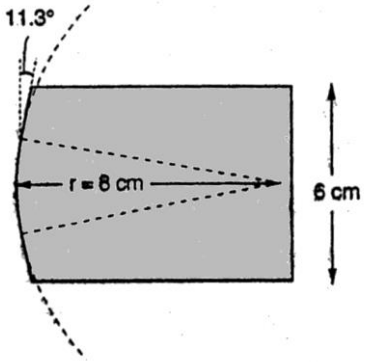

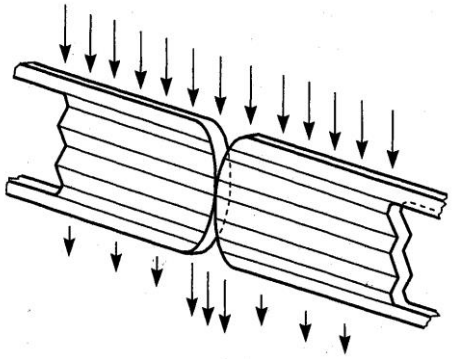

Increased leakage if no backup collimator is present

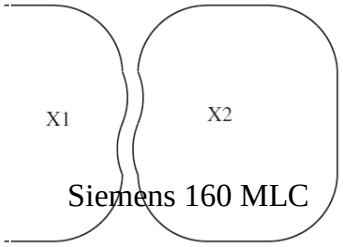

Tacke *et al* [11]

Penumbra widening due to rounded leaf edges

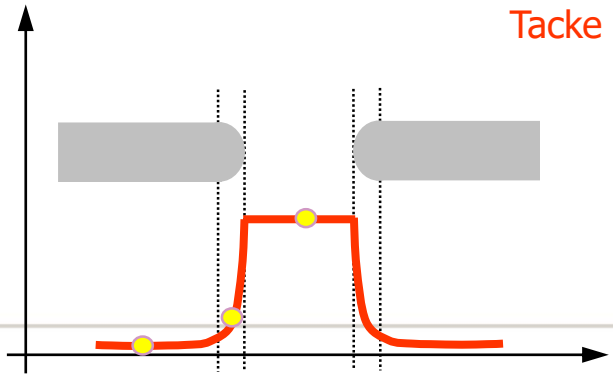

ESTRO School

MLC penumbras (motion direction)

The resulting penumbra is not only dependent on the leaf edges, but also on the location of the MLC in the treatment head.

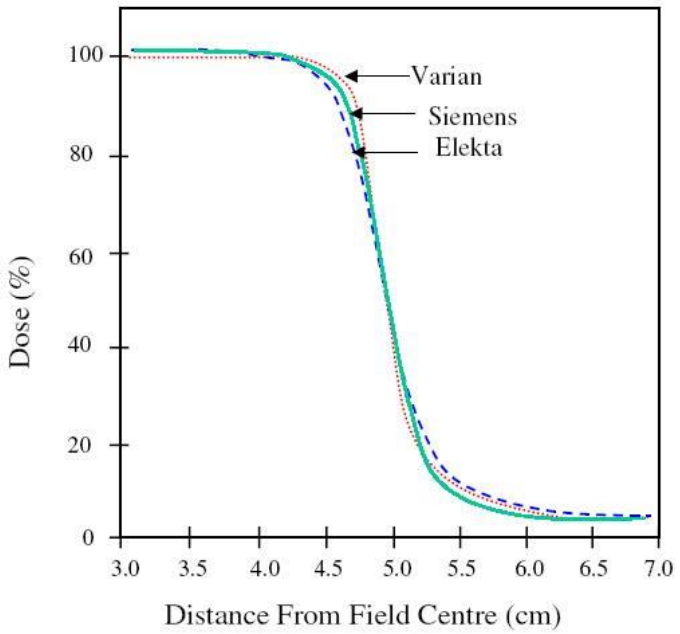

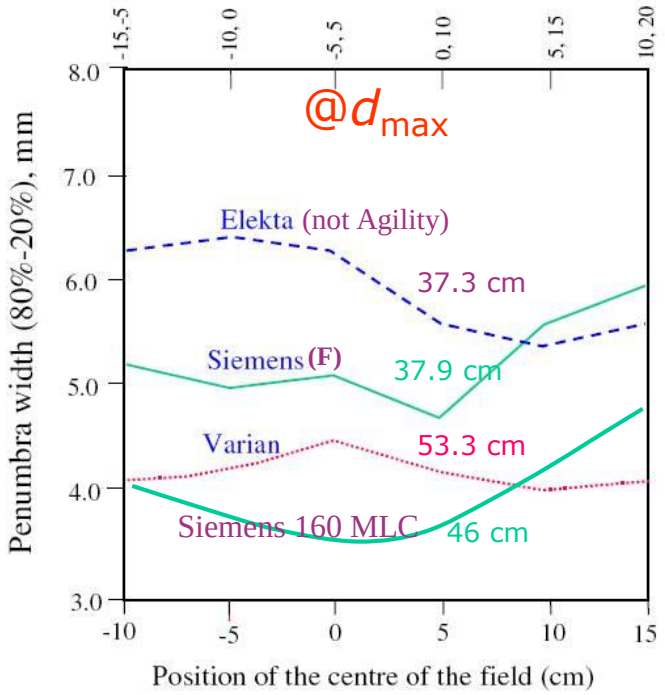

Numbers equal SCD (outer edge)

Huq *et al* [5]

Leaf design in the width direction

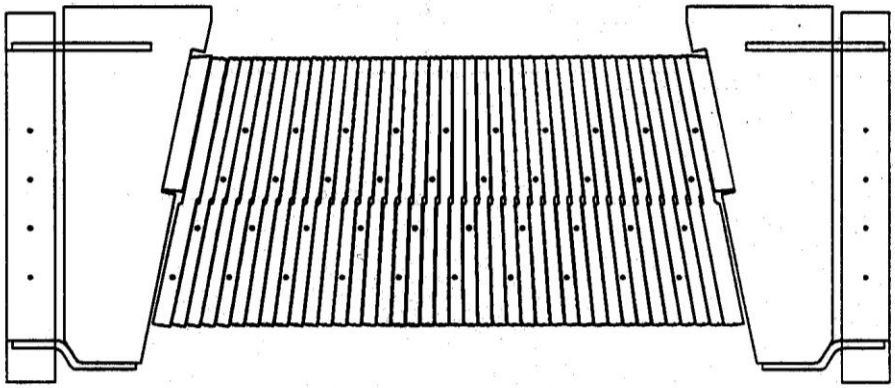

The leaves are thicker at the base in order to follow the divergence of the beam.

Inter-leaf leakage is minimized through "tongues" and "grooves".

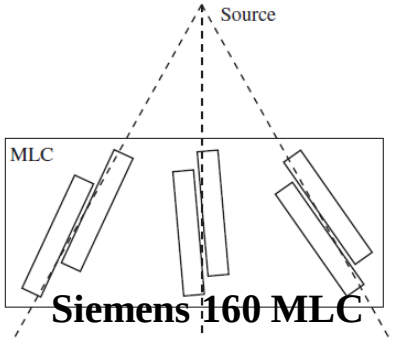

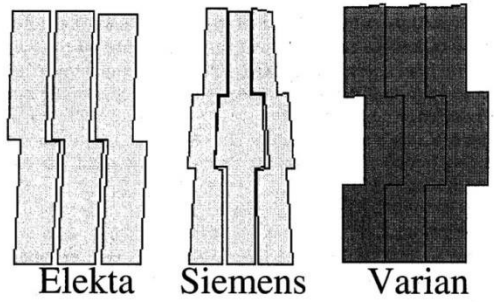

No backup collimators in place!

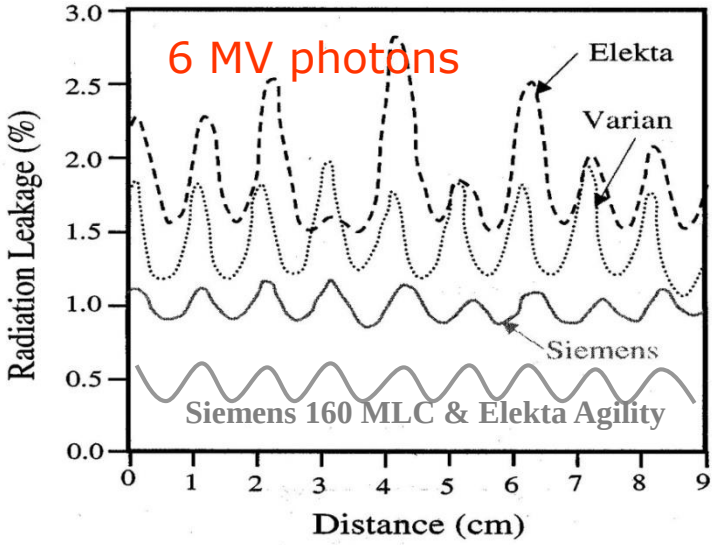

Huq *et al* [5]

ESTRO School

Tongue and groove effect

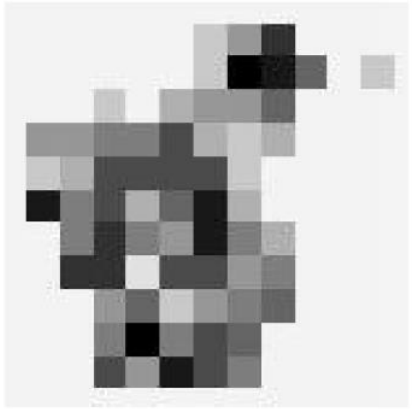

(a)

(b)

W/o T/G

MC calculations

MLC

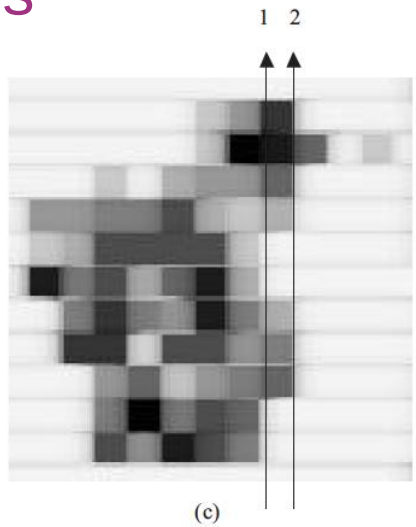

(c)

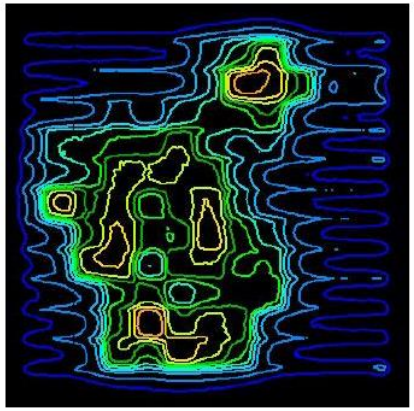

(d)

With T/G

Deng et al [15]

ESTRO School

MLC design – IV – TomoTherapy MLC

Pneumatic "binary" MLC, opening/closing in 20 ms.

The 64 Tungsten leaves are 10 cm thick and 0.625 cm wide (at isocenter distance =85 cm), <0.5% transmission.

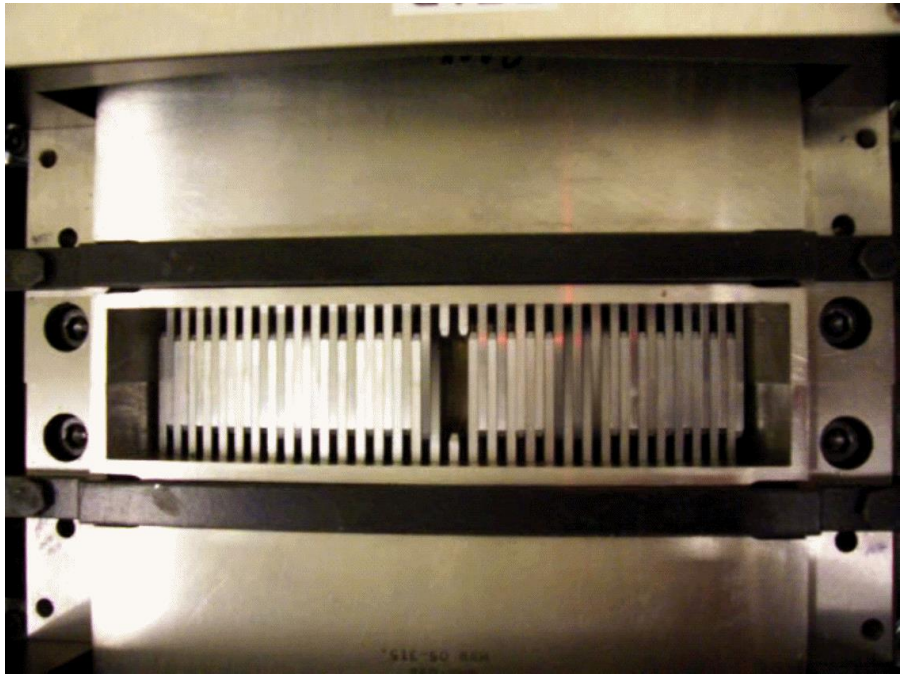

Different methods for creating wedged dose distributions

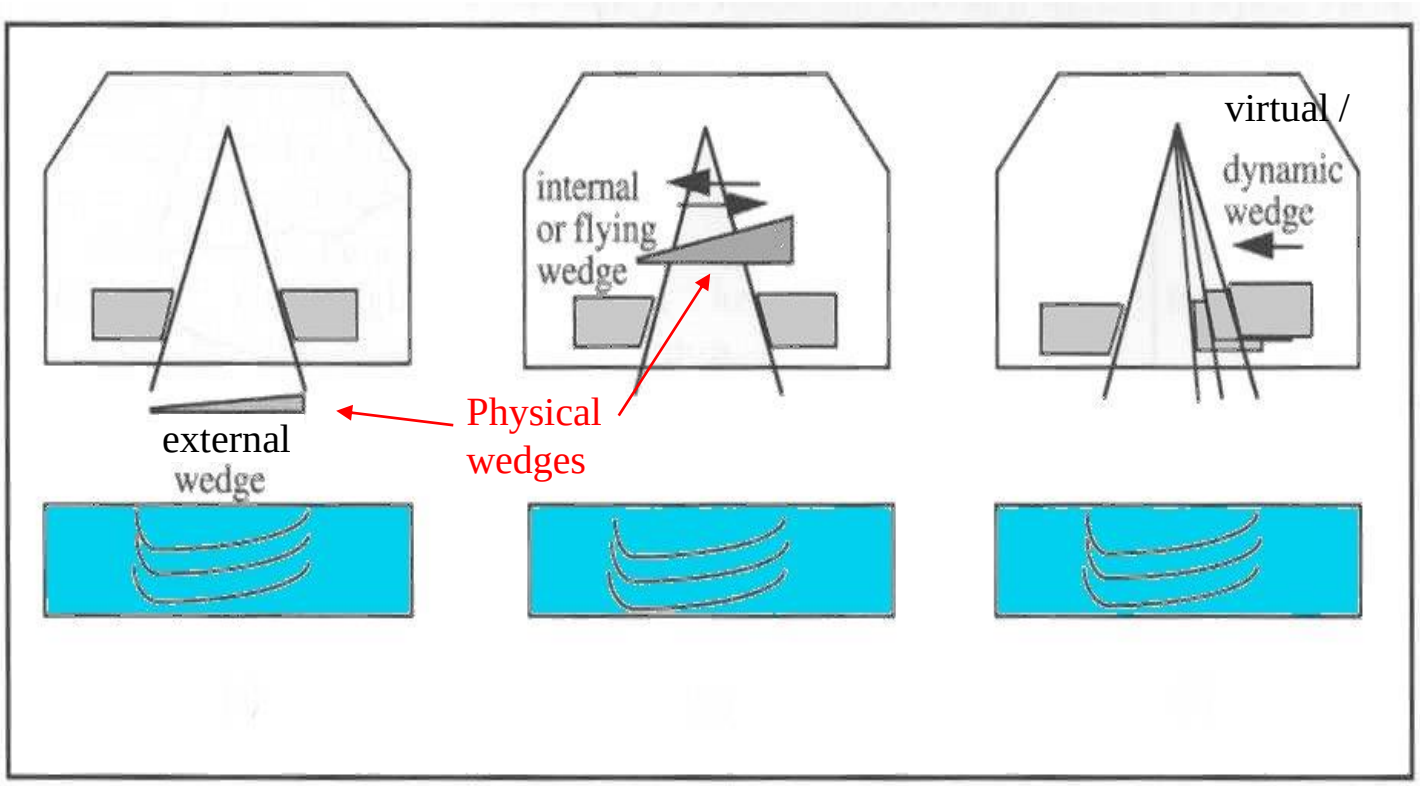

Wedge induced beam quality shifts

Physical wedges filter the beam, yielding beam hardening. Although, above approx. 15 MV the pair production process will balance the hardening, resulting in unaffected (or even softer) beam quality.

Zhu *et al* [9]

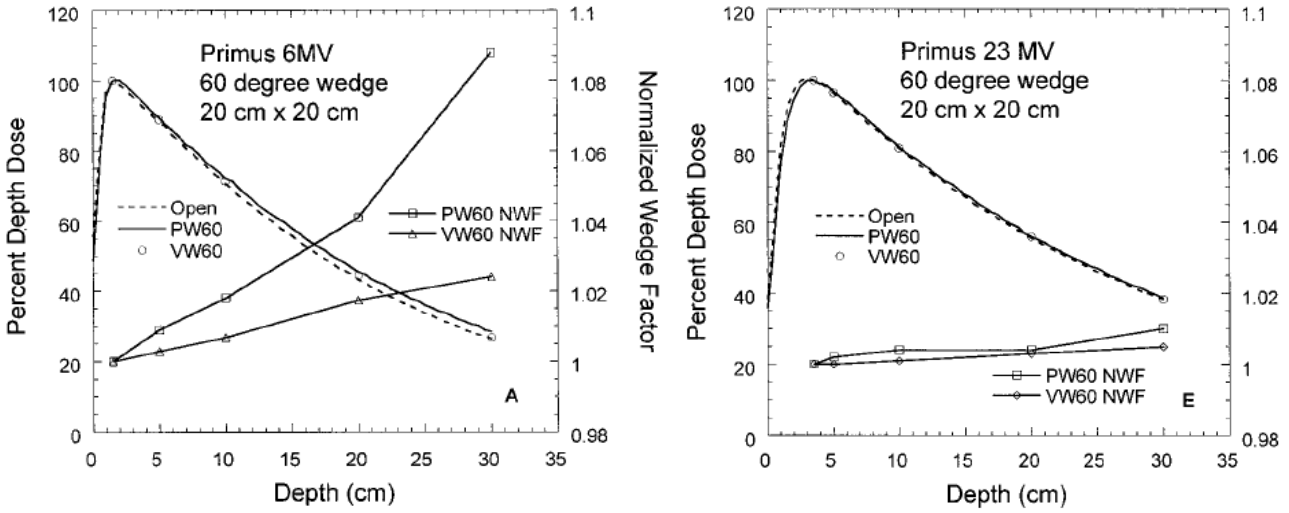

Knöös and Wittgren [16]

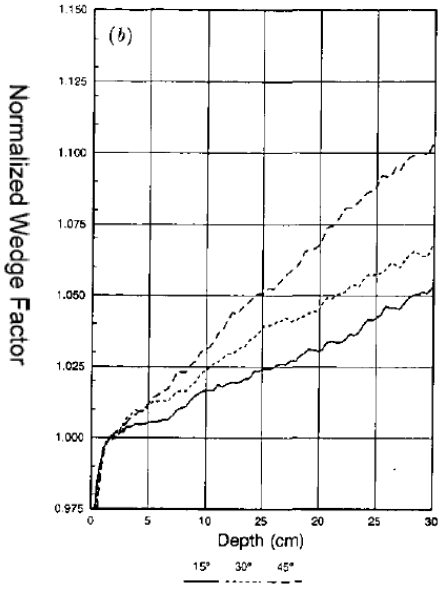

PW60=60 deg Physical wedge
VW60=60 deg Virtual wedge

Wedge induced head scatter

A physical wedge acts as a scatter source. For external wedges, i.e. located below the collimators, the wedge scatter will result in increased doses outside the beam edges.

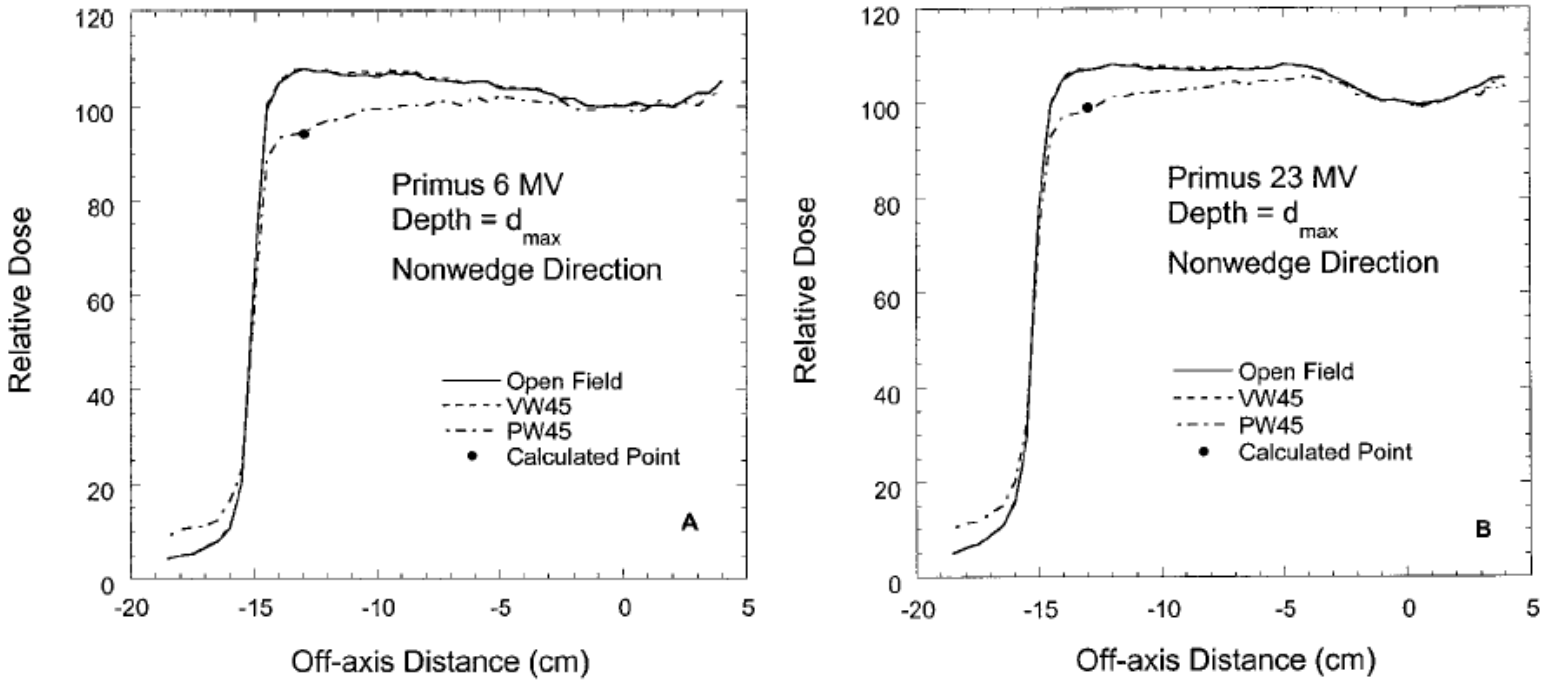

VW45=45 deg Virtual wedge
PW45=45 deg Physical wedge

Zhu *et al* [9]

Hard wedges

Manual mounted - Varian

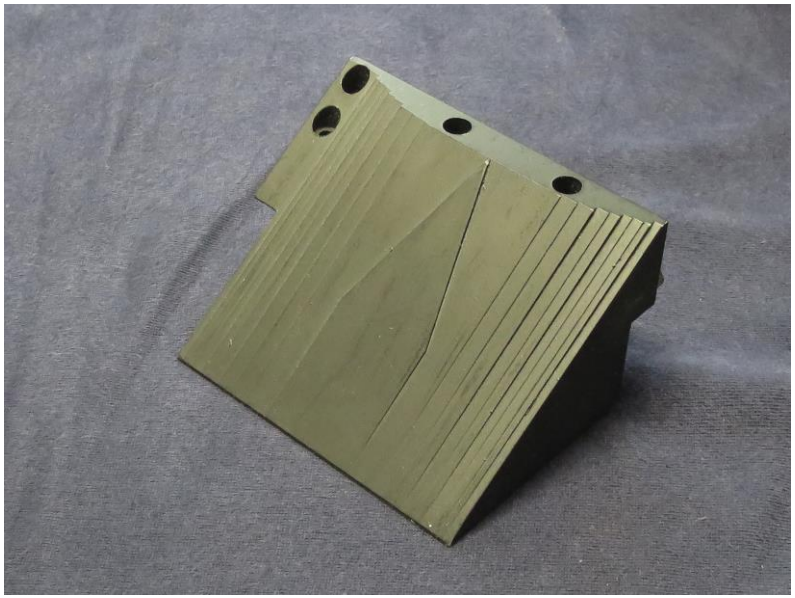

Remote controlled - Elekta

Resuming an interrupted wedge treatment

The time varying fluence distribution means that an interrupted treatment can not be resumed without information about the delivered fraction (not necessary for physical wedges).

Hence, both delivered and remaining/given MUs must be known by the accelerator control software.

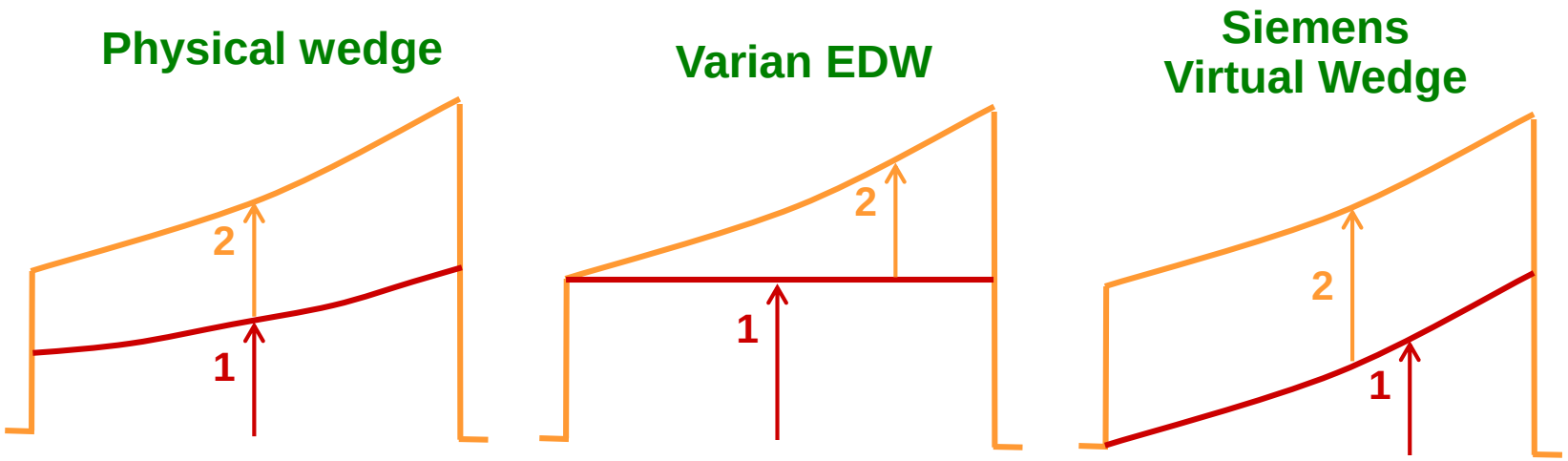

Note: Impossible to deliver few MUs using dynamic/virtual wedge!

Electron treatment heads

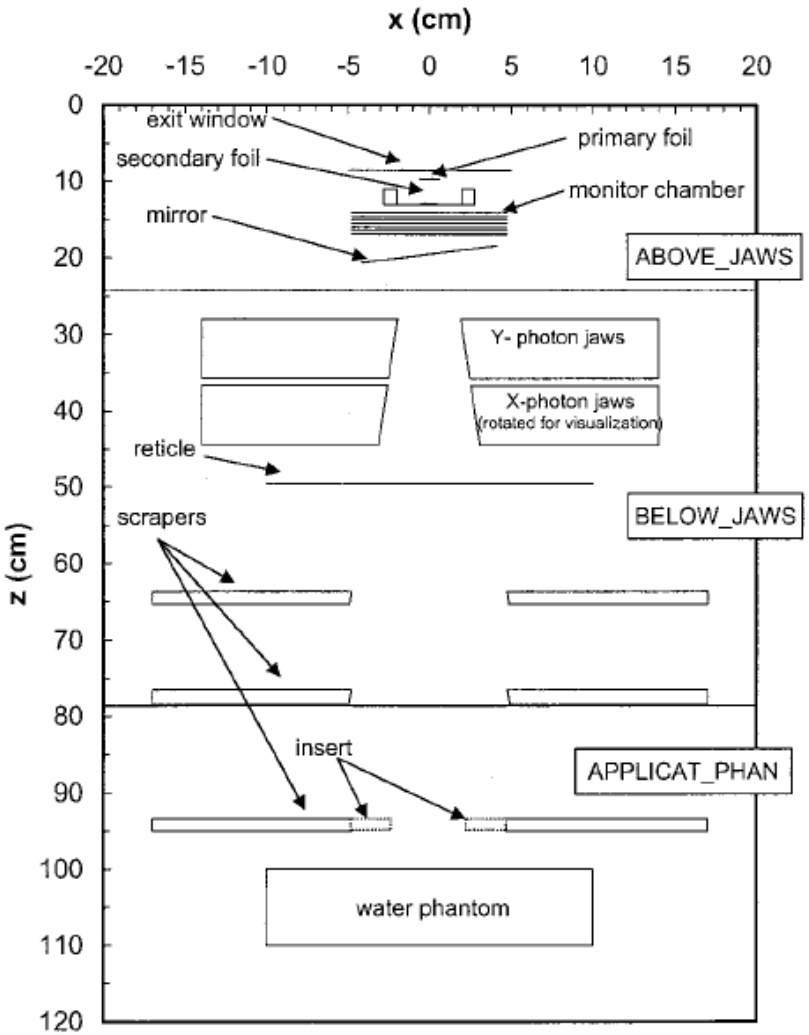

Bieda *et al* [12]

Electrons are much more influenced by scattering and energy loss interactions than photons.

The shape of the electron dose distribution depends therefore more on treatment head design parameters than it does for photons.

Creating a clinically useable electron beam

Traditionally a single foil technique was used ⇒

To get a broad enough beam the single foil has to be quite thick ⇒

Significant energy loss and spread.

The introduction of a secondary foil downstream reduces these problems since the total foil thickness can be reduced considerably.

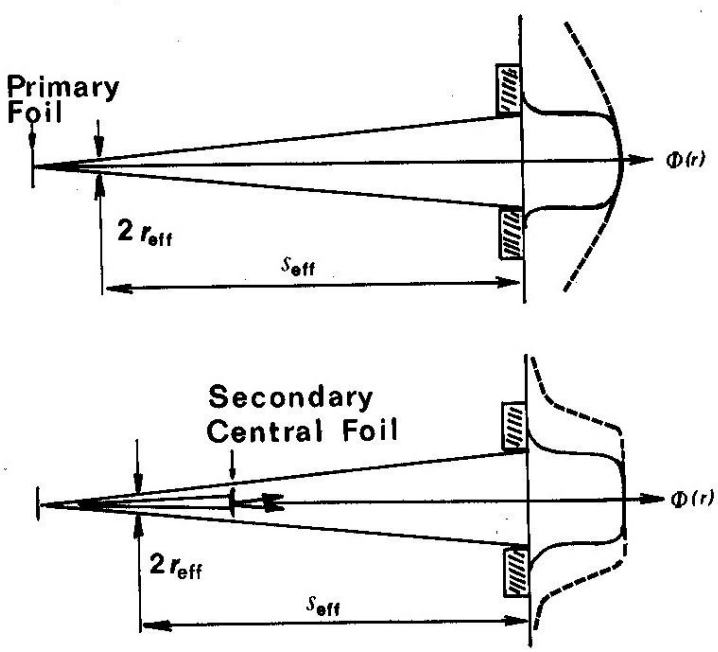

ICRU 35 [8]

Design of scattering foils

Primary foil: High *Z*-mtrl, e.g. Au or Ta, gives the highest linear scattering power vs. collision stopping power, i.e. the most effective scattering. Thickness (t) ≈ 0.05-0.4 mm (energy dependent).

Secondary foil: Lower *Z*-mtrl, e.g. Al, often used in order to reduce bremsstrahlung production. Thickness (h) $\lesssim$ 3 mm.

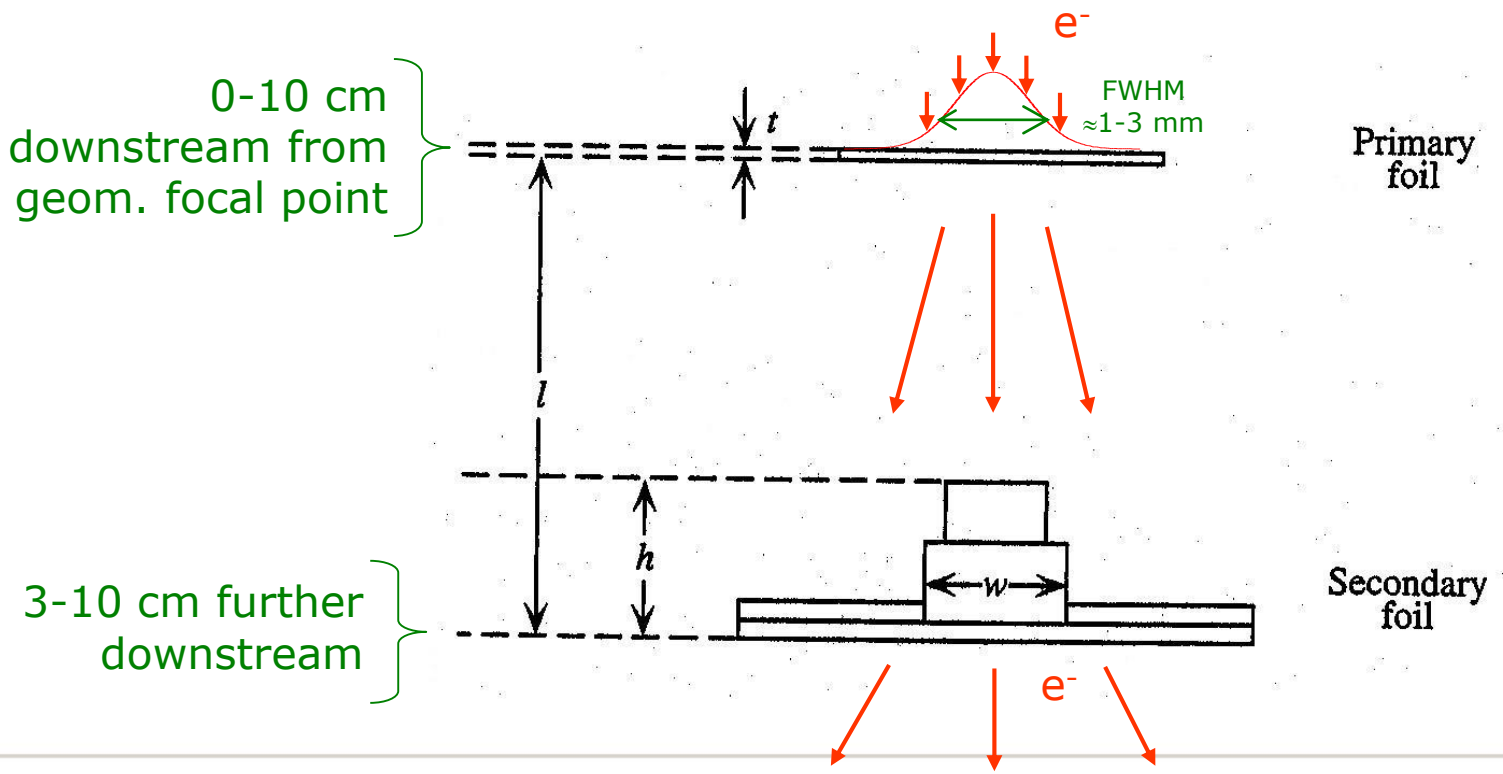

Bieda *et al* [12]

ESTRO School

Filter assembly for a Varian Clinac

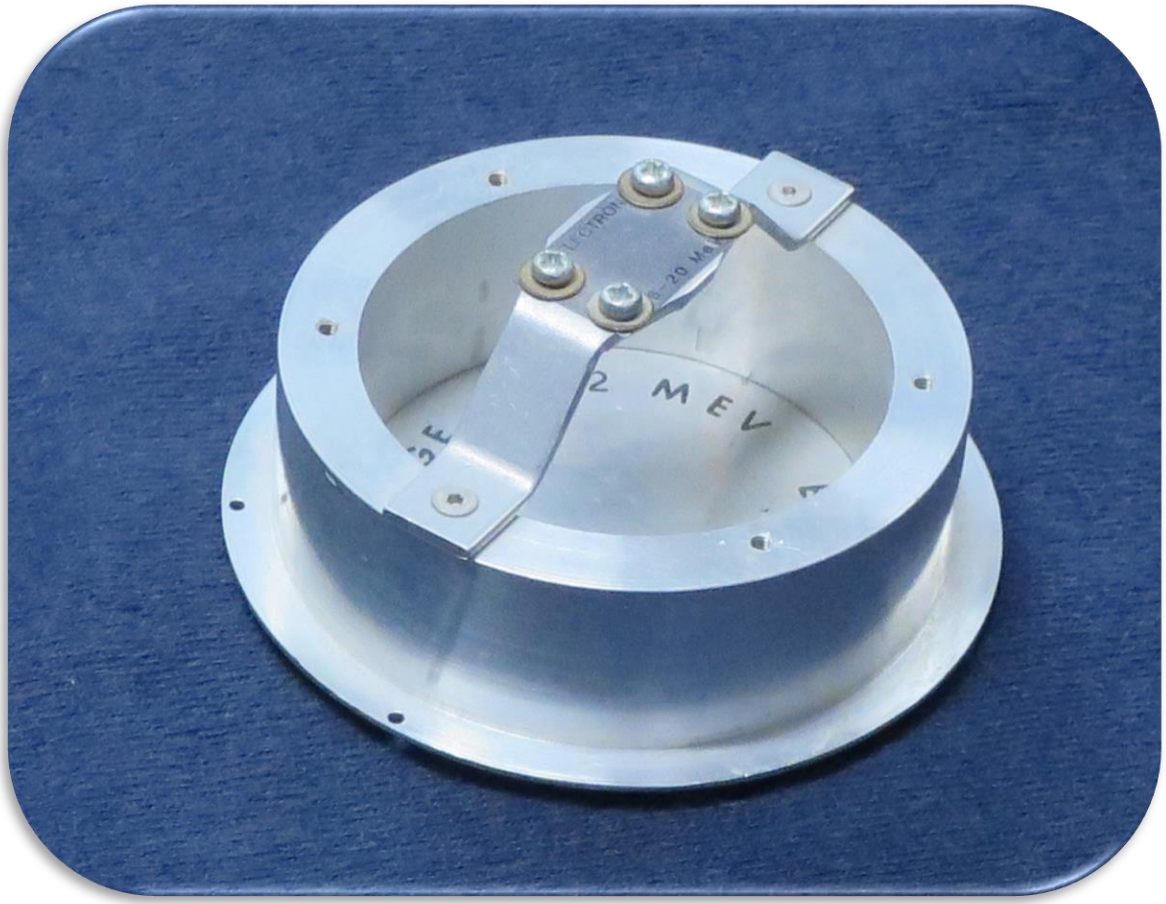

ESTRO School

Secondary scattering foils

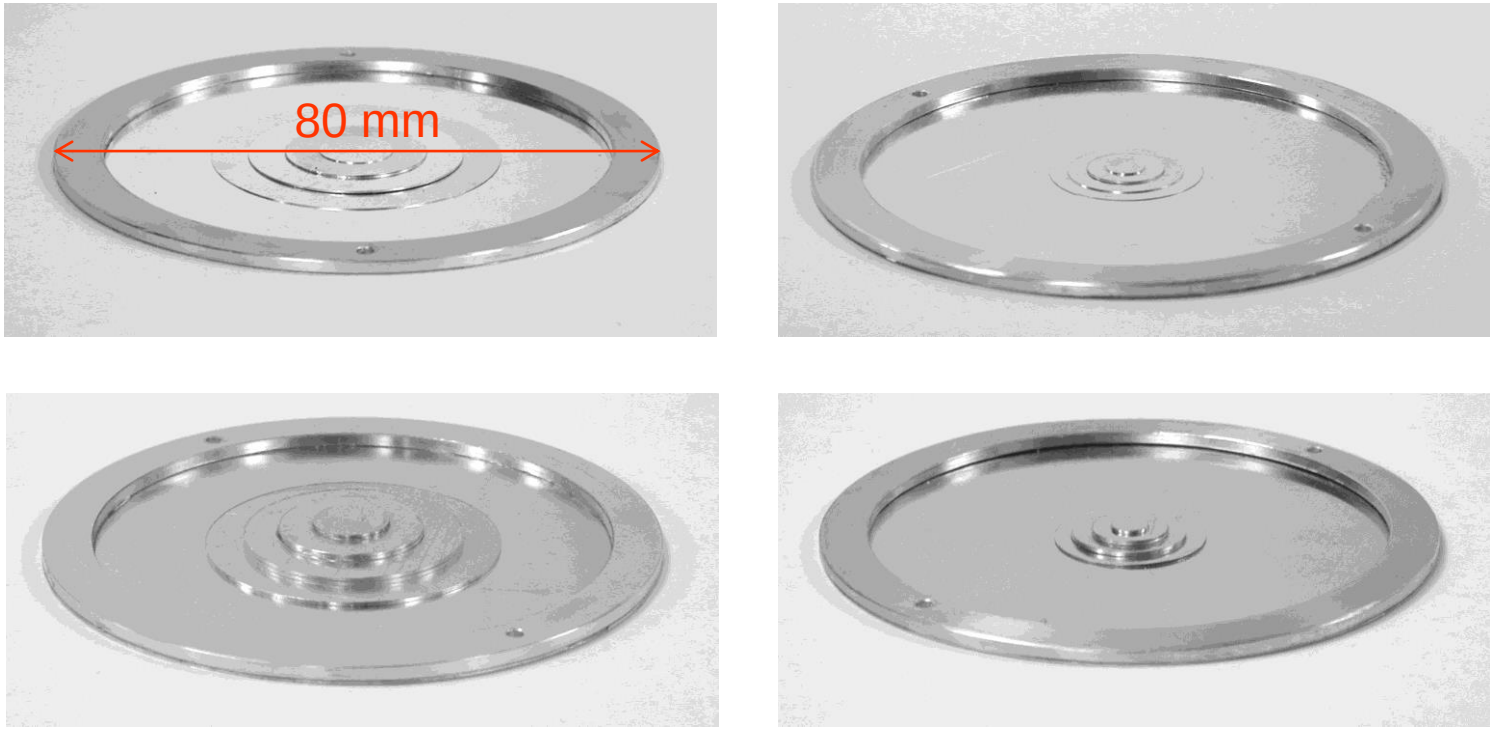

Scattering foils from research work by Magnus G Karlsson (Umeå)

Different electron collimators

Cone/tube collimator

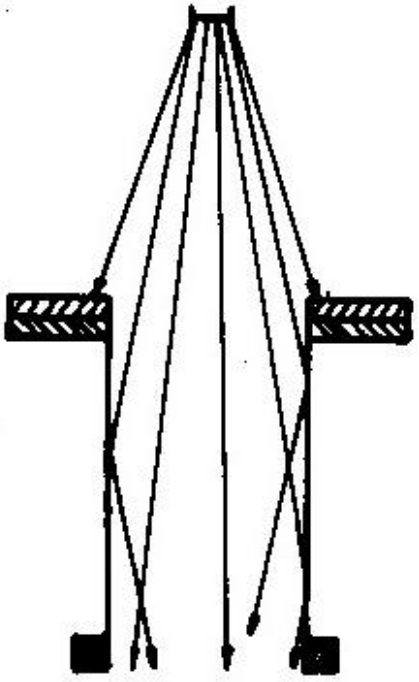

Modified tube collimator

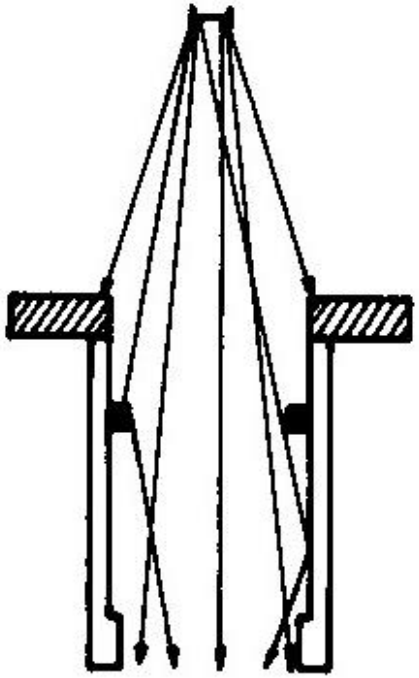

Diaphragm collimator

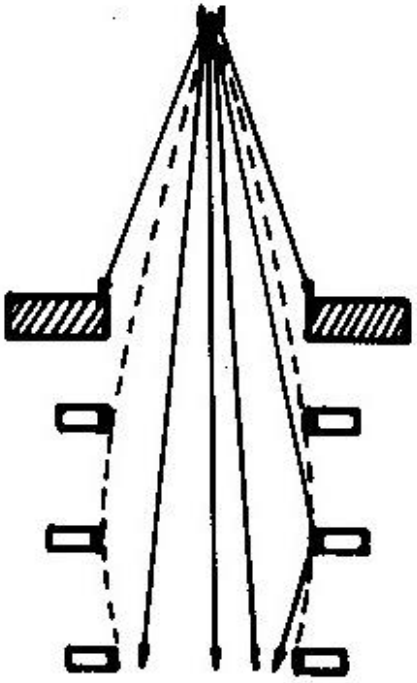

ICRU 35 [8]

More scattered electrons

Actual electron collimators

Siemens

Varian

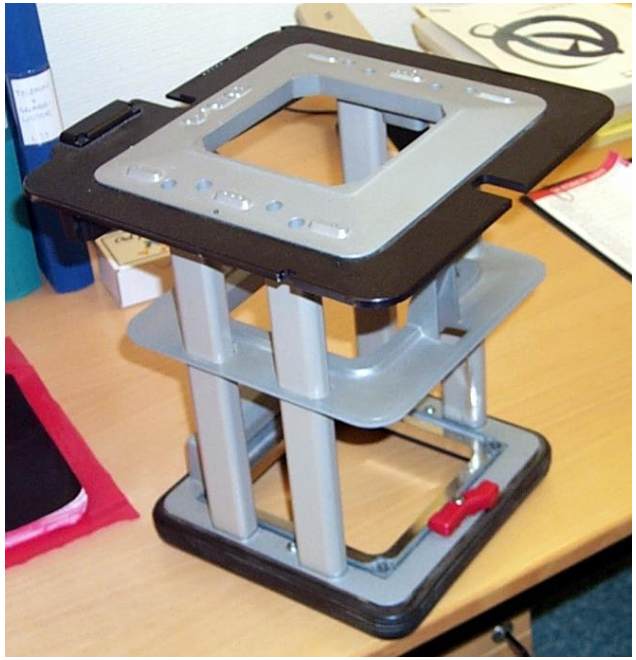

Elekta

Typical insert

20 MeV electron w/wo applicator

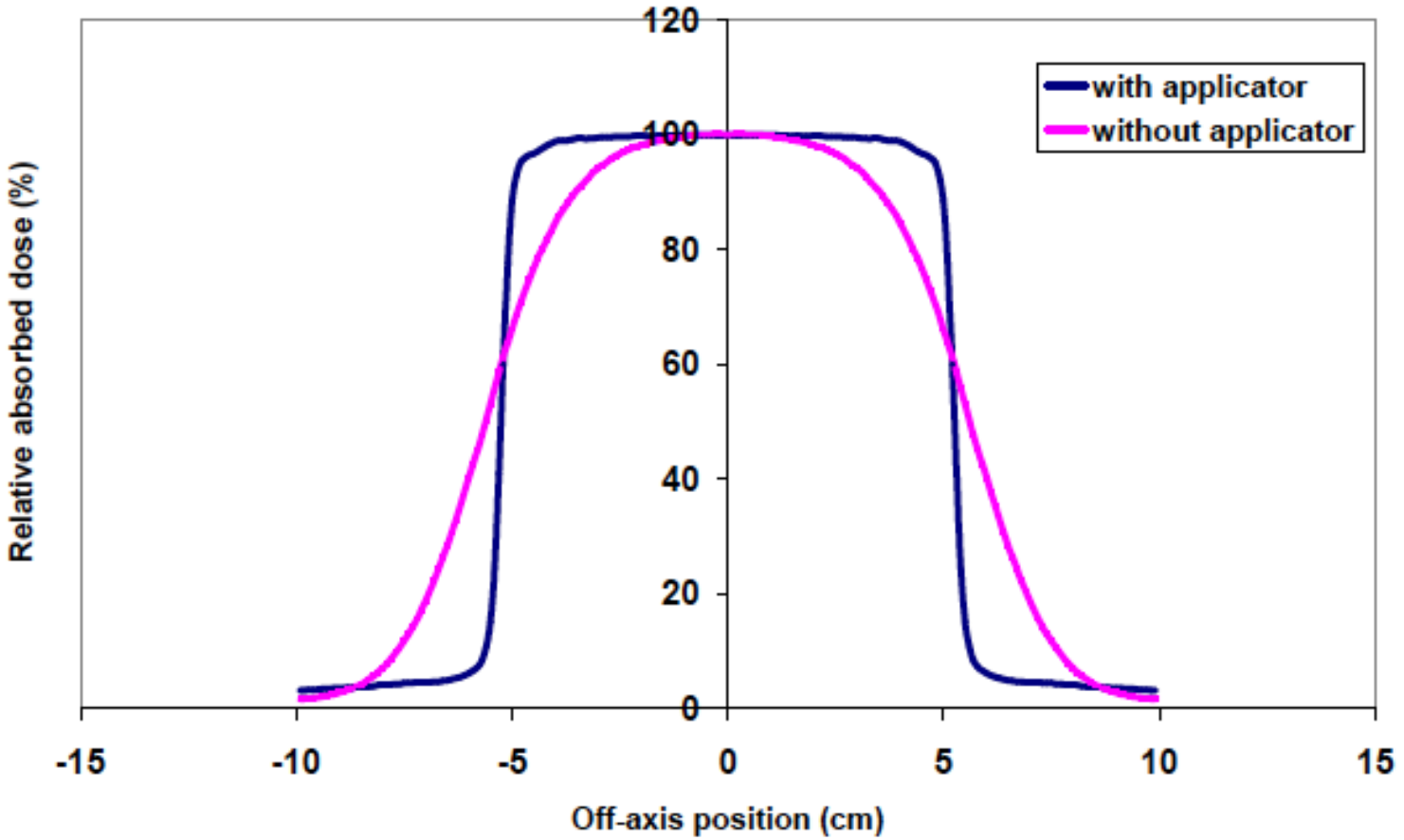

Figure 1. Absorbed dose profiles with and without an electron applicator for an Elekta SLi Plus machine. The applicator size is 10×10 cm^2 and the nominal energy is 20 MeV. The measurements were performed with a diode detector at 1 cm depth in a water phantom. SSD= 100 cm.

Olsson 2003 [17]

Summary

- The focal spot size (FWHM typically 1-2 mm) influences the photon beam penumbra width.
- Lateral photon beam flattening through a conical flattening filter also creates additional scatter and increases the off-axis softening effect.
- Mean photon energy [MeV] at isocenter roughly equals MV/3, somewhat lower for high-energy beams.
- The geometrical beam alignment is not trivial for rounded leaf edges. It may vary between accelerator vendors and should be better known among users and TPS vendors.
- Electron beams are strongly influenced by scattering and energy loss interactions inside the treatment head and depends therefore more on treatment head design than photons.

References I

1. Karzmark CJ, Nunan CS, and Tanabe E (1993) Medical Electron Accelerators. McGraw-Hill, Inc. ISBN 0-07-105410-3.
2. Jaffray DA and Battista JJ (1993) X-ray sources of medical linear accelerators: Focal and extra-focal radiation. Med Phys 20, 1417-27.
3. Sätherberg A, Karlsson MG, and Karlsson M (1996) Theoretical and experimental determination of phantom scatter factors for photon fields with different radial energy variation. Phys Med Biol 41, 2687-94.
4. Sheikh-Bagheri D and Rogers DW (2002) Monte Carlo calculation of nine megavoltage photon beam spectra using the BEAM code. Med Phys 29, 391-402.
5. Huq MS, Das IJ, Steinberg T, and Galvin JM (2002) A dosimetric comparison of various multileaf collimators. Phys Med Biol 47, N159-70.
6. Boyer AL and Li S (1997) Geometric analysis of light-field position of a multileaf collimator with curved ends. Med Phys 24, 757-62.
7. Vassiliev ON, Titt U, Pönisch F, Kry SF, Mohan R, and Gillin MT (2006) Dosimetric properties of photon beams from a flattening filter free clinical accelerator. Phys Med Biol 51, 1907-17.
8. ICRU Report 35 (1984) Radiation Dosimetry: Electron Beams with Energies Between 1 and 50 MeV. ISBN 0-913394-29-7.

References II

9. Zhu XR, Gillin MT, Jursinic PA, Lopez F, Grimm DF, and Rownd JJ (2000) Comparison of dosimetric characteristics of Siemens virtual and physical wedges. Med Phys 27, 2267-77.
10. Kragl G, af Wetterstedt S, Knäusl B, Lind M, McCavana P, Knöös T, McClean B, and Georg D (2009) Dosimetric characteristics of 6 and 10 MV unflattened photon beams. Radiother Oncol 93, 141-6.
11. Tacke MB, Nill S, Häring P, and Oelfke U (2008) 6 MV dosimetric characterization of the 160 MLCTM, the new Siemens multileaf collimator. Med Phys 35, 1634-42.
12. Bieda MR, Antolak JA, Hogstrom KR (2001) The effect of scattering foil parameters on electron-beam Monte Carlo calculations. Med Phys 28, 2527-34.
13. Brahme A, Svensson H (1979) Radiation beam characteristics of a 22 MeV microtron. Acta Radiol Oncol Radiat Phys Biol 18, 244-72.
14. van Battum LJ, van der Zee W, Huizenga H (2003) Scattered radiation from applicators in clinical electron beams. Phys Med Biol 48, 2493-507.
15. Deng J, Pawlicki T, Chen Y et al, The MLC tongue-and-groove effect on IMRT dose distributions, Phys Med Biol 46 (2001) 1039-1060.
16. Knöös T and Wittgren L, Which depth dose data should be used for dose planning with wedge filters? Phys Med Biol 36 (1991) 255-267.
17. Olsson M-L, Monte Carlo simulations of the Elekta Sli Plus electron applicator system – A base for a new applicator design to reduce radiation leakage, MSc Thesis, Lund University, 2003.

ESTRO

Multi-source beam modeling and TPS data commissioning for photons

Anders Ahnesjö
Uppsala University
Sweden

UPPSALA
UNIVERSITY

Learning objectives

To understand:

1. the different roles in a modern TPS of fluence engines versus dose engines

2. how a multisource fluence engine for photons can be designed

3. the role of measured data in beam modelling

Model based dose calculations

Energy fluence engine, multisource models

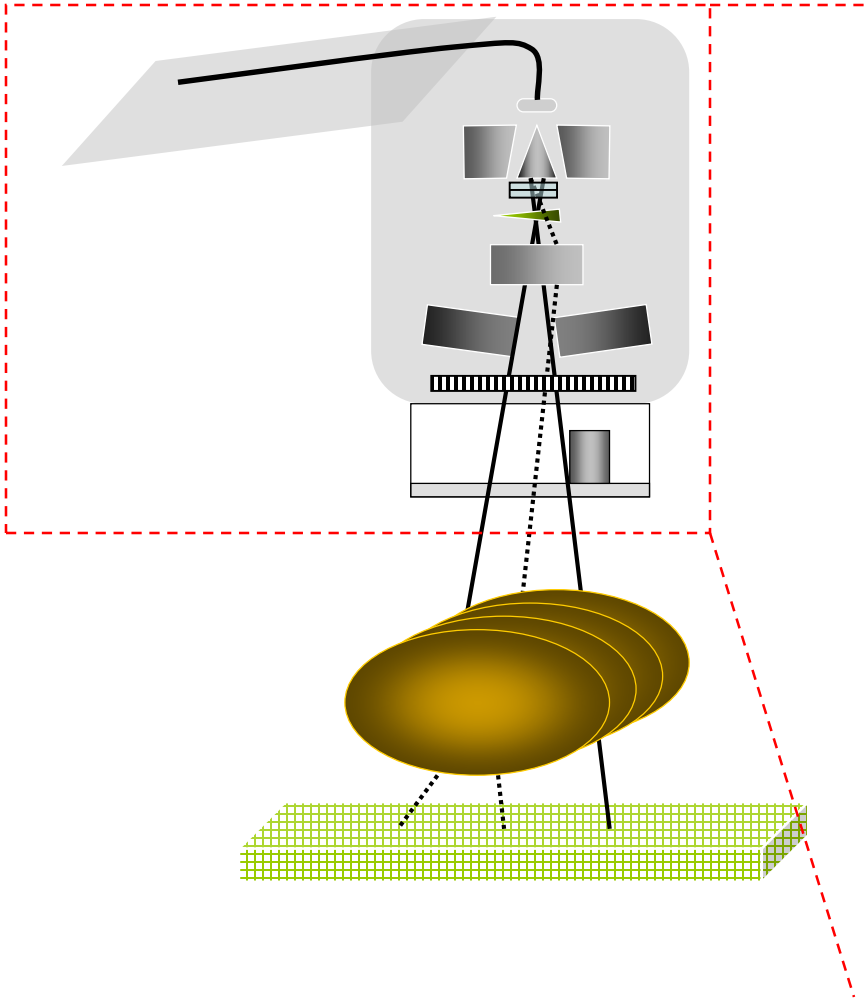

- Finite photon source size
- Open fluence distribution
- Fluence modulation
  - Step&shot
  - Dynamic
  - Wedges
- Head scatter sources
  - flattening filter
  - collimators
  - wedges
- Monitor back scatter
- Collimator leakage, including
  - MLC interleaf leakage
  - shape of MLC leaf ends
- Beam spectra
- Spectral changes
- Electron contamination

Processes to include

What algorithms can different beam data sets support?

Beam data objects	***Fluence/Dose engines***
Dose profiles & Output factors	•No explicit treatment head modelling •Dose calculations based on correction factors from geometrical scaling and attenuation
Description of individual particles	•Explicit treatment head modelling yielding *phase space* of individual particles
Description of multiple sources	•Explicit treatment head modelling yielding fluence distributions •Dose calculations from fluence using kernel superpositions OR explicit transport calculations
Mixed approaches also possible!	

A feasible energy fluence engine should

- **be simple enough to understand the behaviour of the model**
- **have only a small number of free parameters**
- **the model parameters should be determined by measurements that are not too complicated and time consuming i.e. output factors, profiles or depth dose curves in water and air**
- **be complex enough to confirm all measurements in agreement with the accuracy demands**
- **fast in sampling the particle properties (if used for Monte Carlo dose engines)**

(Fippel *et al.* MedPhys(30)2003: 301-311):

Alt 1: Using Dose profiles & Output factors

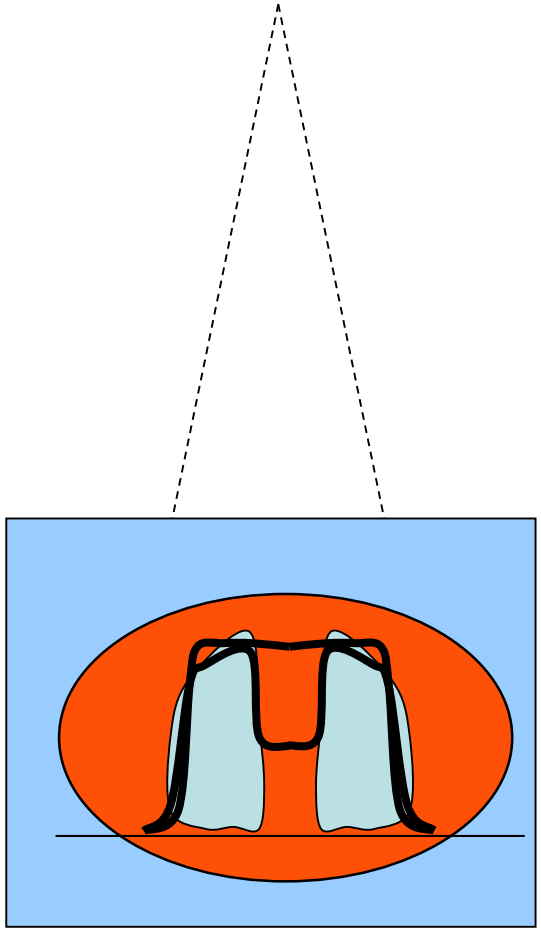

- Dose profiles reshaped using factors deduced from first order, point source fluence changes
- Workhorse in old time “2D” TPS and some Monitor Unit Check programs
- OK for a limited set of field geometries at non-violated equilibrium conditions, e.g. stereotactical treatments
- **Breaks down for general CRT/IMRT/VMAT conditions!**

Alt 2: Describing individual particles – Phase Space

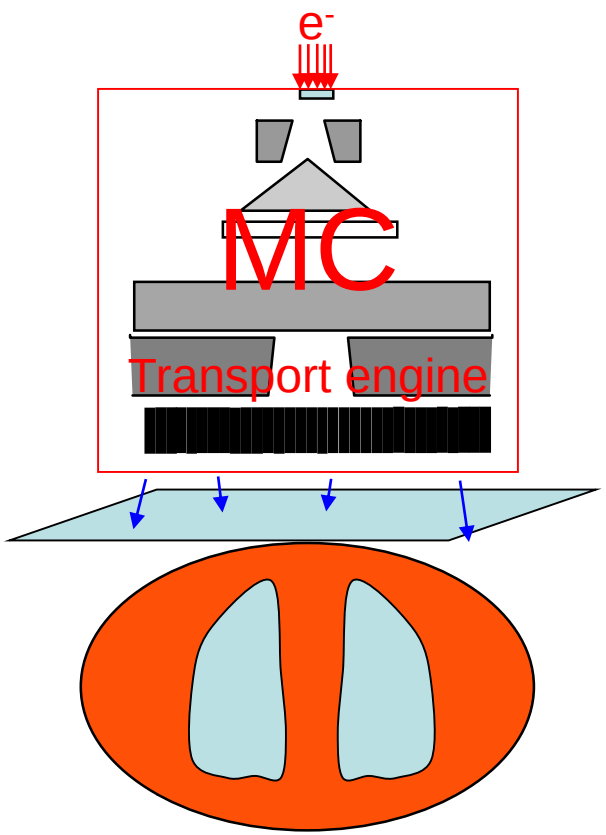

- Monte Carlo transport engine used to yield long list (millions…) of output particles at an exit interface
- Each output particle specified to type, energy, lateral position and direction
- Electron source onto target tweaked to match the output to dose measured in water
- Excellent research tool, **less practical for routine work**

Energy fluence engine based on Multi-Source models

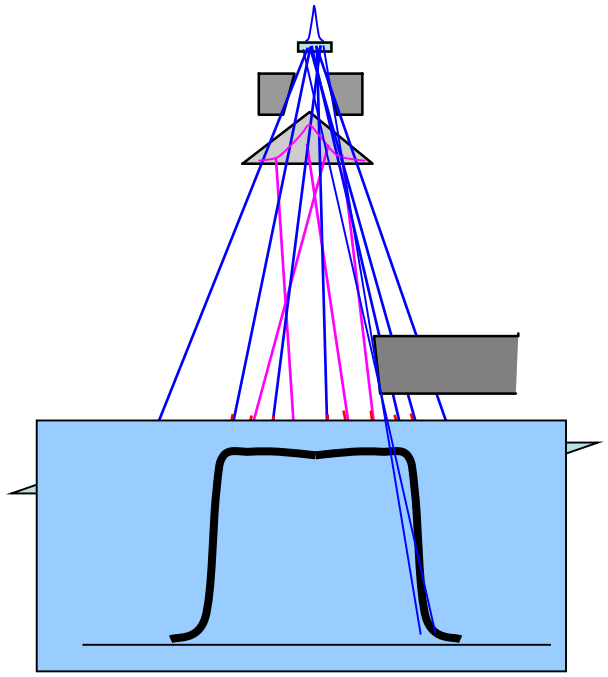

- Back trace the particles of a Monte Carlo generated phase space to their sites of last interaction (i.e. particle source positions)
- Group dense locations of last interaction sites into sources, calculate emission characteristics of each source

OR

- **Use *a priori* information about the sources and fit parameterized models versus measurements**

- **Measurements can be specialized for explicit source data OR standard dose and output data**

Multi-Source model implementation concept

Multi-source modelling give energy fluence maps for the direct beam and the head scattered beam. Particle characteristics to feed the dose engine are then deduced through:

- **Number of particles** – matrix element value (which has to consider partial source blocking while being computed!)
- **Position** – matrix element location
- **Direction** – as if the particles were coming directly from respective source to the matrix element, angular spread can be included
- **Energy** – given by a beam spectrum, off axis variations may be included
- **Extended sources** to model partial blocking

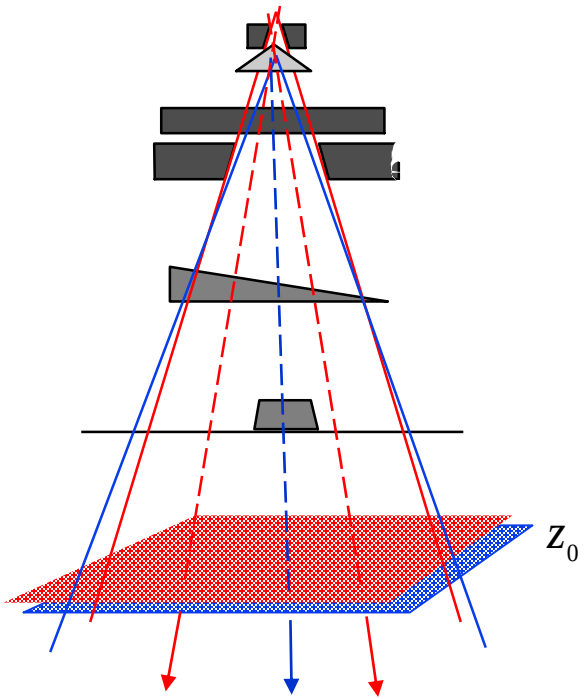

Calculate the value of a fluence matrix element

The width, shape and other radiative properties of the source

Collimators can be raytraced, or approximated as ideal beam blockers

For each element, find the contributions from the relevant sources

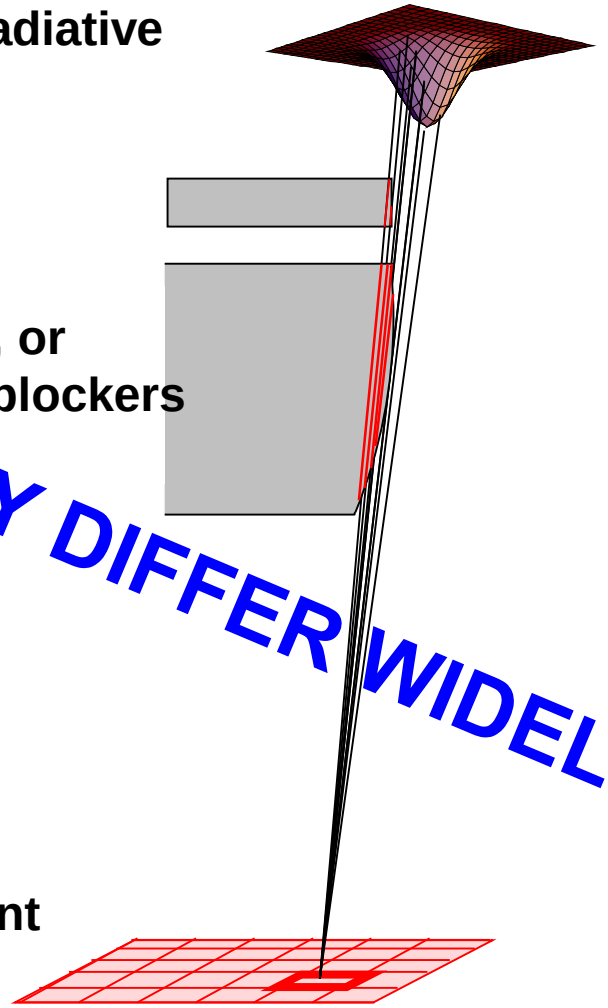

IMPLEMENTATIONS MAY DIFFER WIDELY!

Properties of the direct beam source

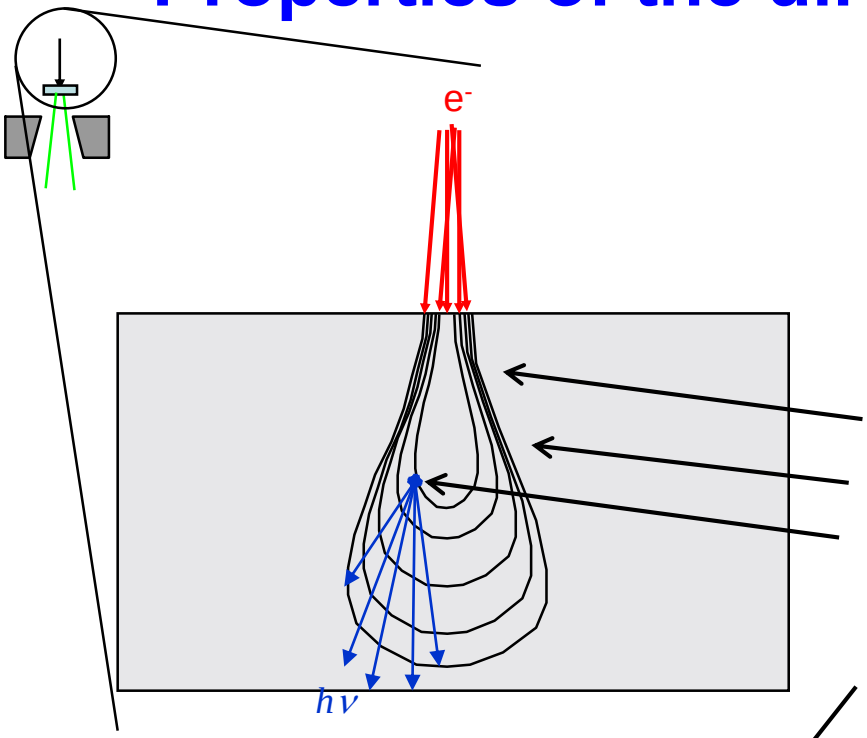

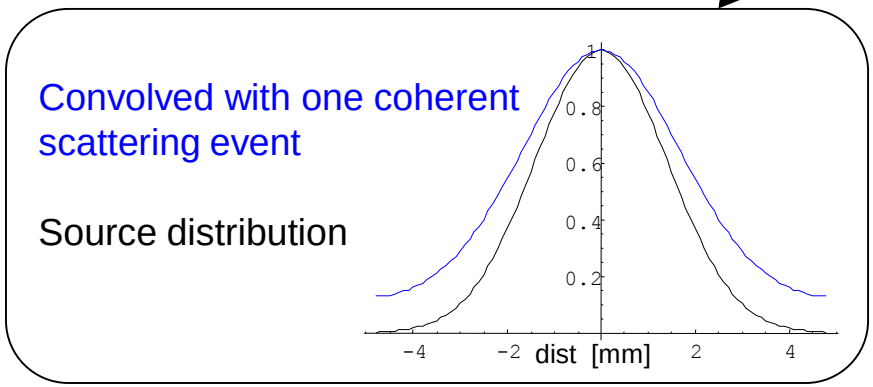

Four blurring steps:

1. **Electron beam distribution**
2. **Electron scattering in target**
3. **Brems X-section angular distribution**
4. **Coherent scatter in flattening filter (affecting the view of the source from downstream)**

Beam source size

reconstruction using beam-spot camera

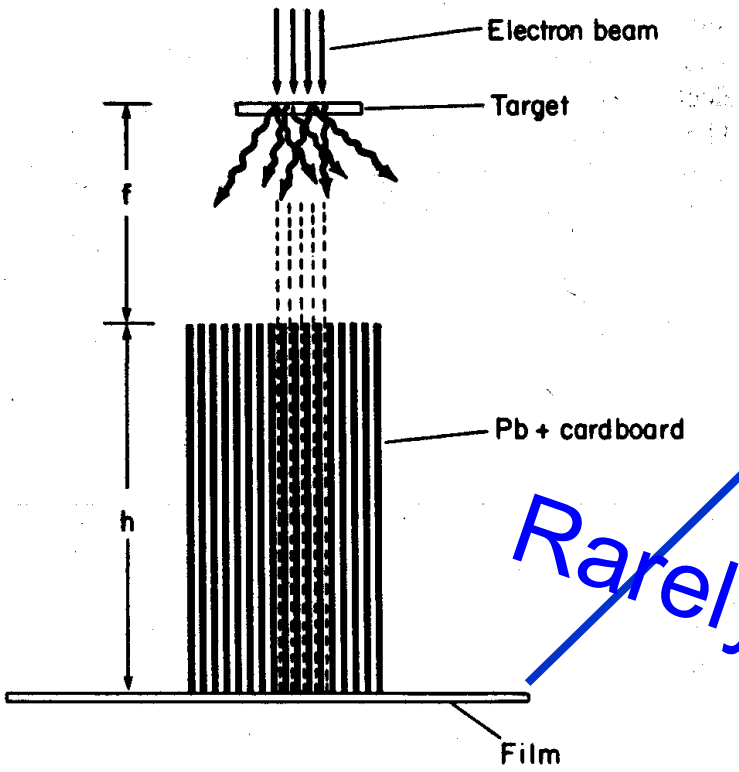

FIG. 1. Diagram illustrating the principle and function of the beam-spot camera.

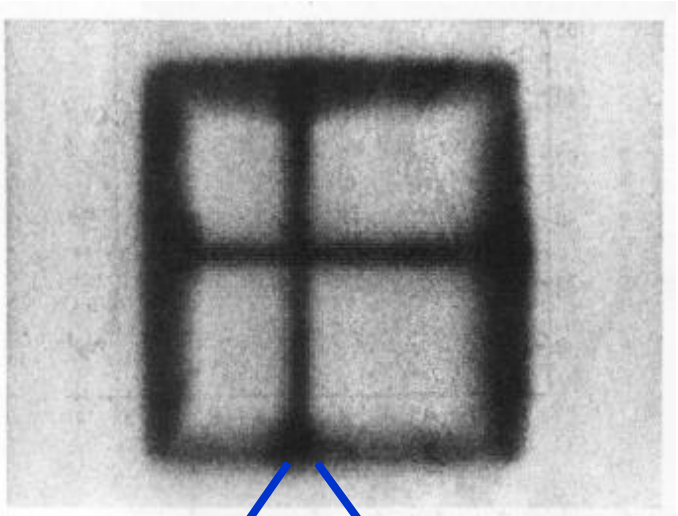

FIG. 2. Magnified image of the x-ray source of a linear accelerator producing 8-MV x rays. The camera was turned 90° between the two exposures. The actual distance between adjacent parallel dark lines is 0.47 mm.

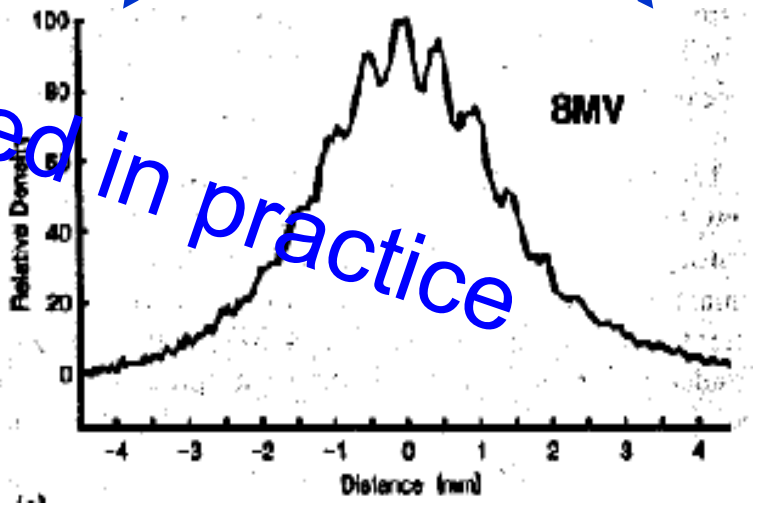

Rarely used in practice

from Lutz, Maleki & Bjärngard, Med.Phys. **15**, p 614-617

Beam source size
reconstruction from slit images

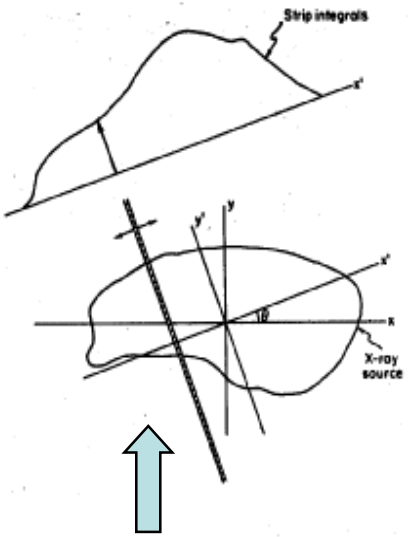

CT algorithms

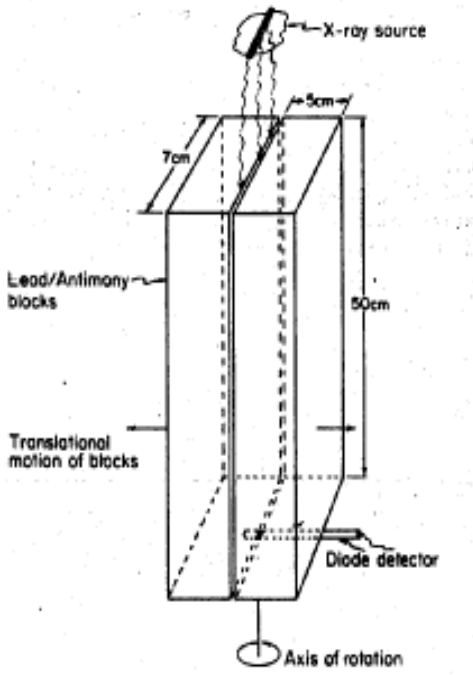

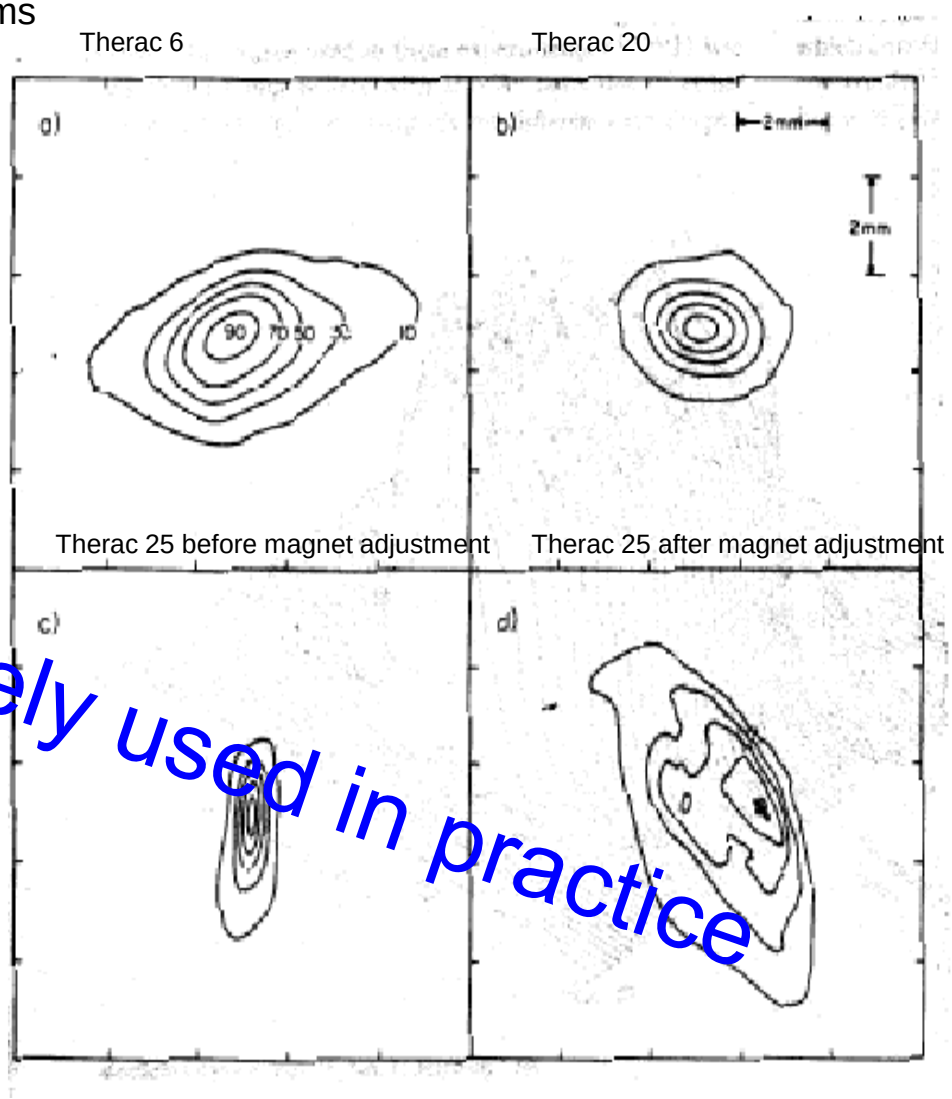

Rarely used in practice

from Munro & Rawlinson, Med. Phys. **15**,1988, p517-524

Beam source size

by fitting calculated profiles to measured profiles by varying the source size

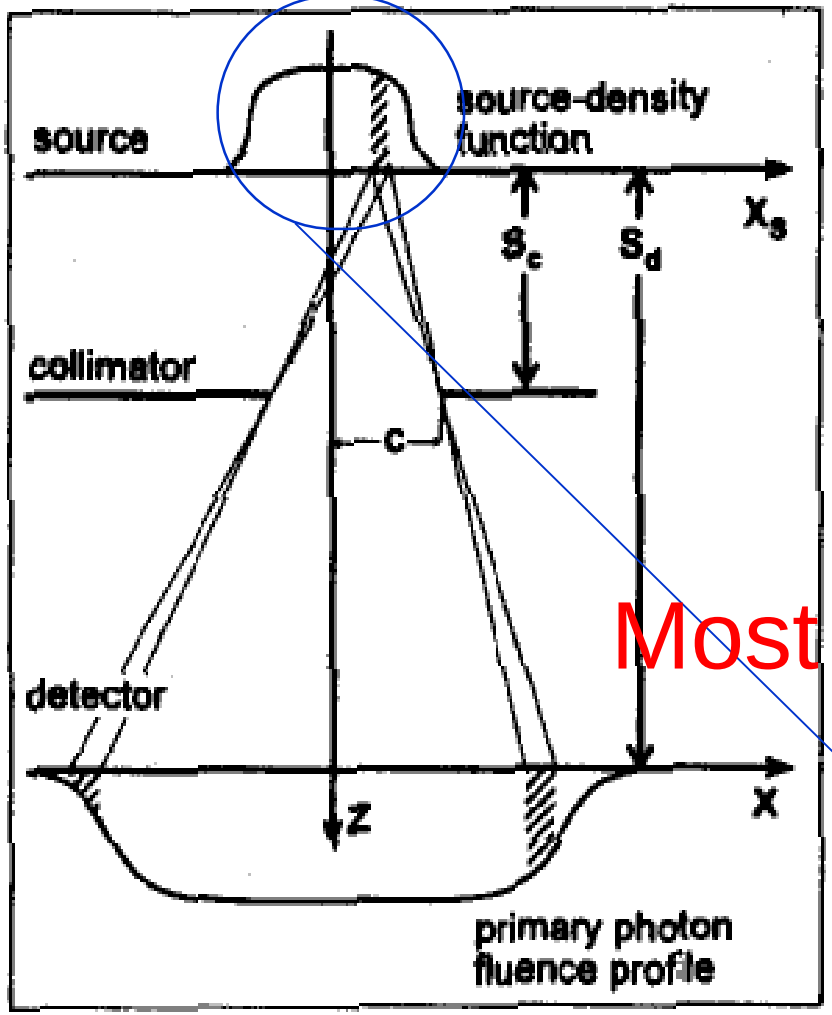

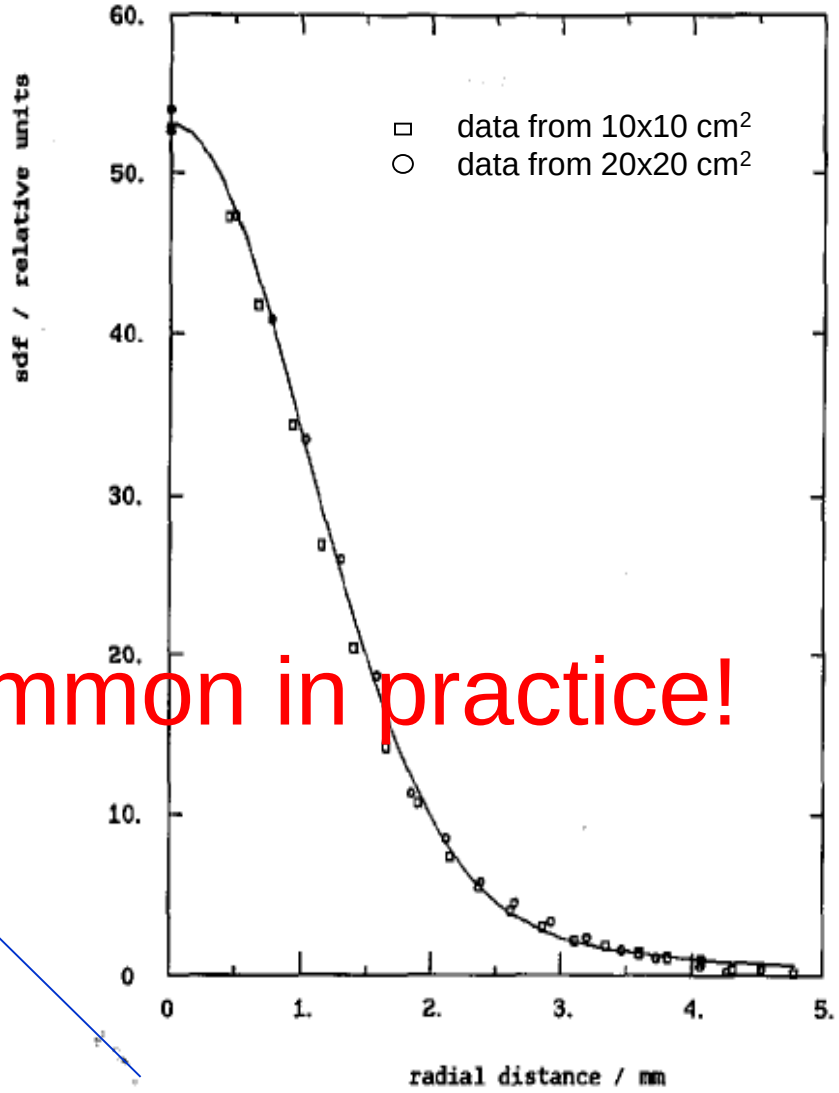

Most common in practice!

from Treuer *et al*, Mediz. Physik,1987, p375-80

Source size determination by fitting calculated dose profiles to measured profiles for 10x10 cm^2 fields.

Results from 59 clinical Siemens machines in Nucletrons customer database

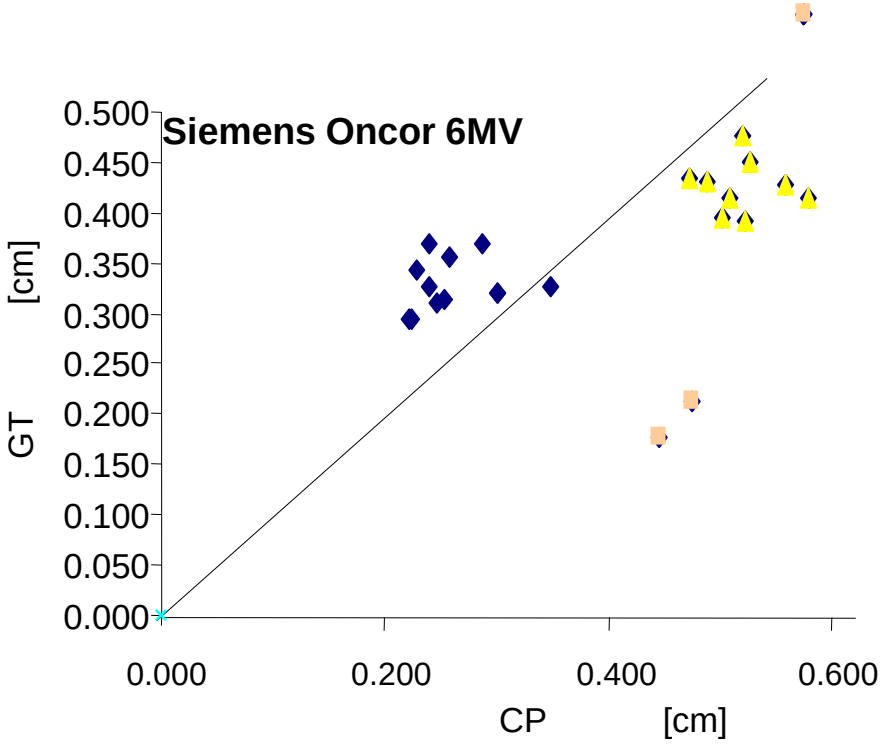

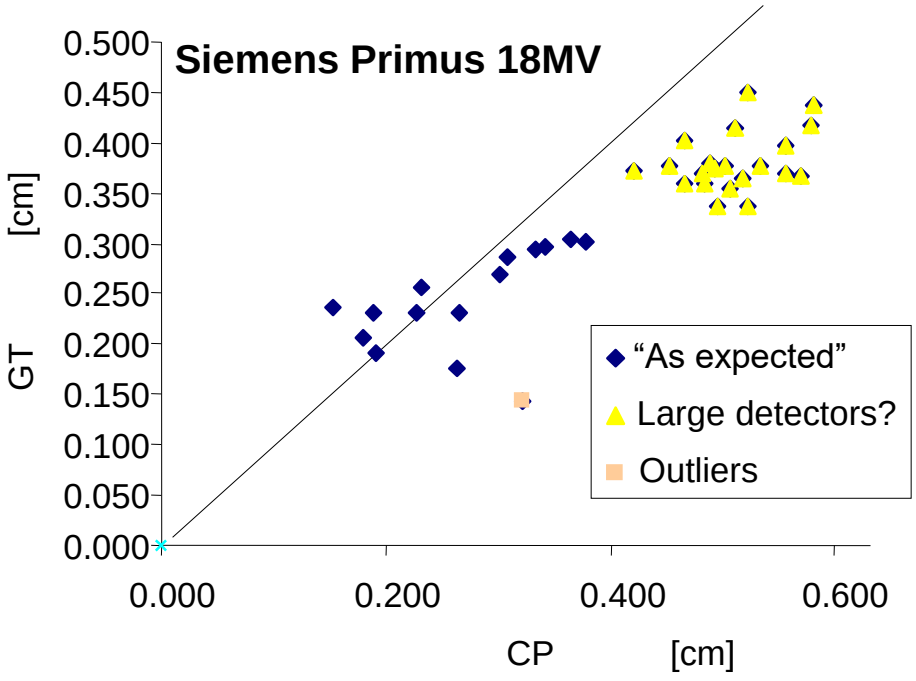

Source size effects, focused leafs

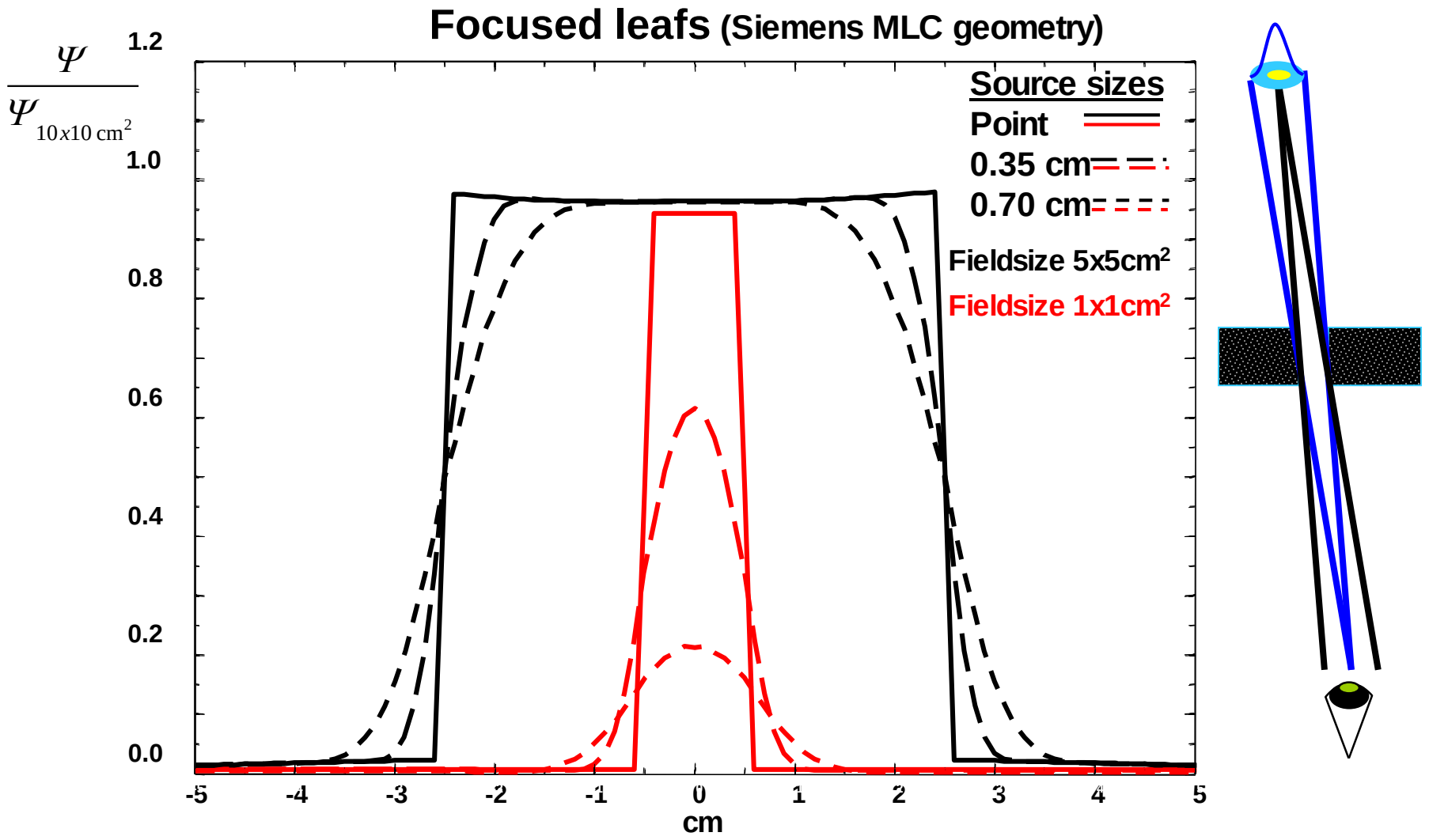

When the source "fills" the "inverse" view we get dramatic decrease in fluence output with increasing source size!

Upper and lower penumbra parts have different slopes

Focused leafs (Siemens MLC geometry)

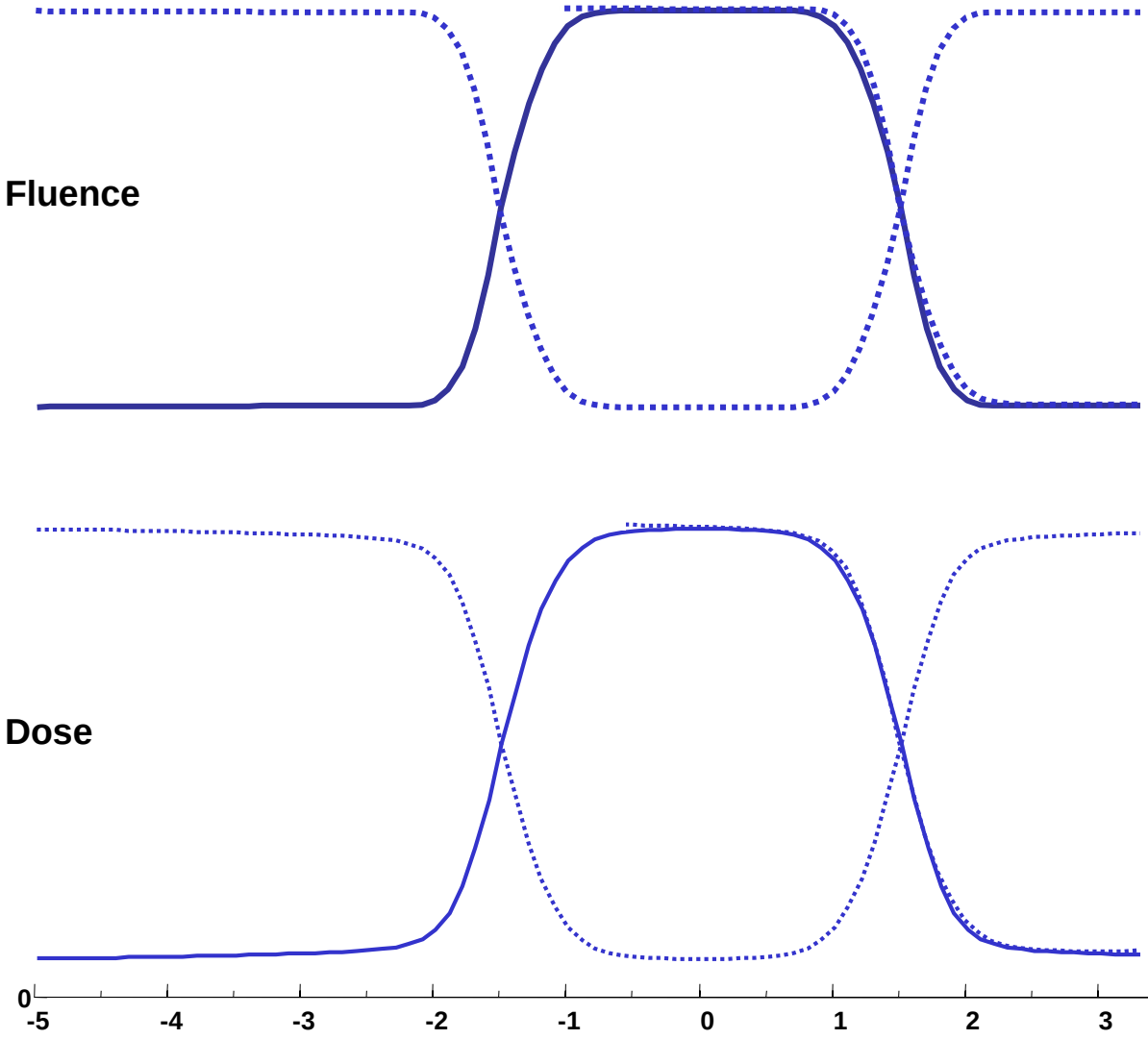

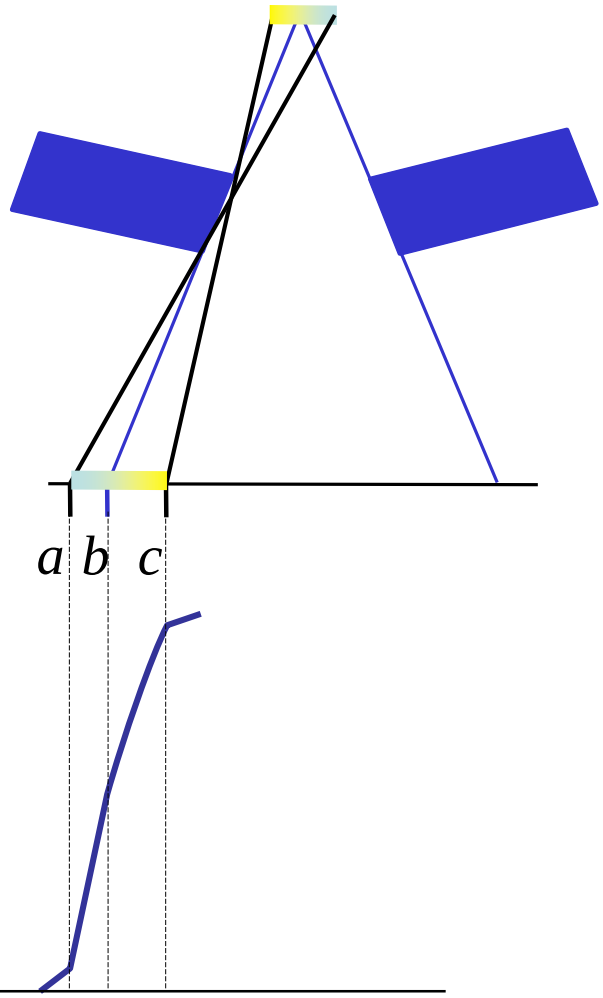

Alignement of multiple collimators – potential issue for delivery robustness & calculation consistency

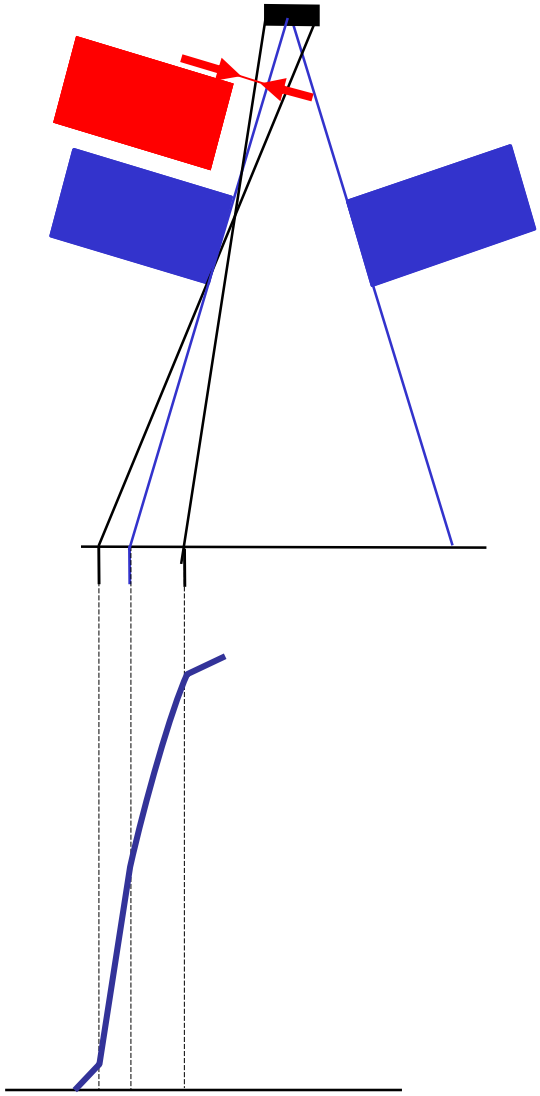

A margin for setting additional jaws make penumbra conditions more robust!

Direct beam source
- open beam fluence distribution

The joint effect of

- **angular variations of the direct beam source radiance**
- **flattening filter absorption/modulation**

commonly expressed as an open beam fluence matrix

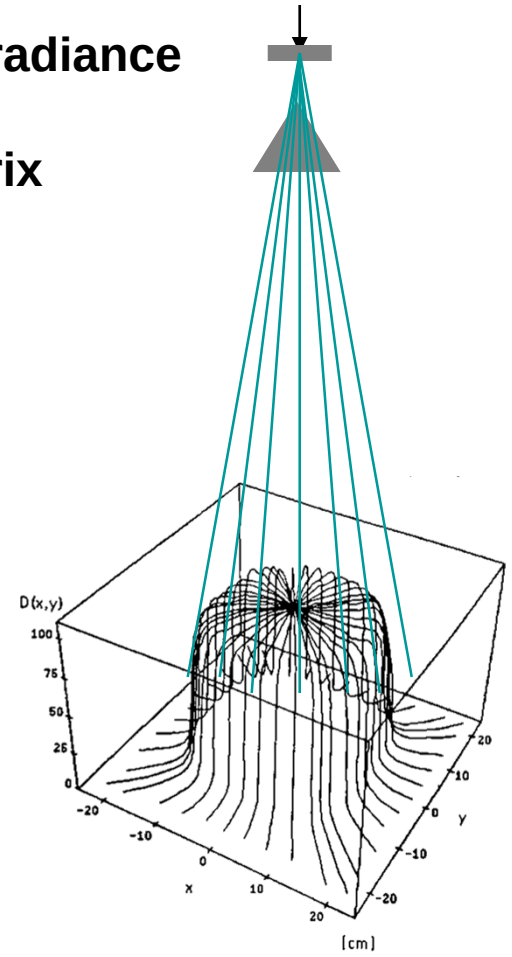

Can be acquired through a variaty of means:

- **”in air” scanning**
- **diagonal dose profiles in a water phantom**
- **”star” dose measurements and subsequent deconvolution/fluence fitting**

In air scanning of lateral profiles

The signal scored by a scanned detector is directly proportional to the energy fluence only if the spectrum is constant!

Signal is proportional to $\text{response}(x,y)\cdot\Psi(x,y)$

The energy absorption coefficient μ_{en} of any buildup material varies with lateral spectral shifts.

Since primary dose for CPE is very close to $\mu_{\text{en}}^{\text{wat}}(x,y)\cdot\Psi(x,y)$ **scanning in air could yield results that decribes how the primary dose will vary laterally!**

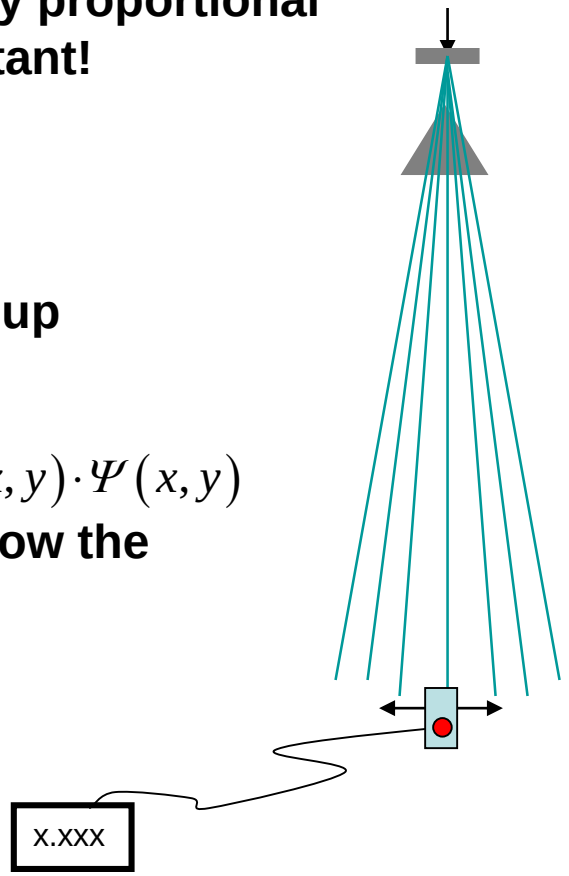

Star dose measurements – machine variability

58 of Varian Clinac 2100 6 MV

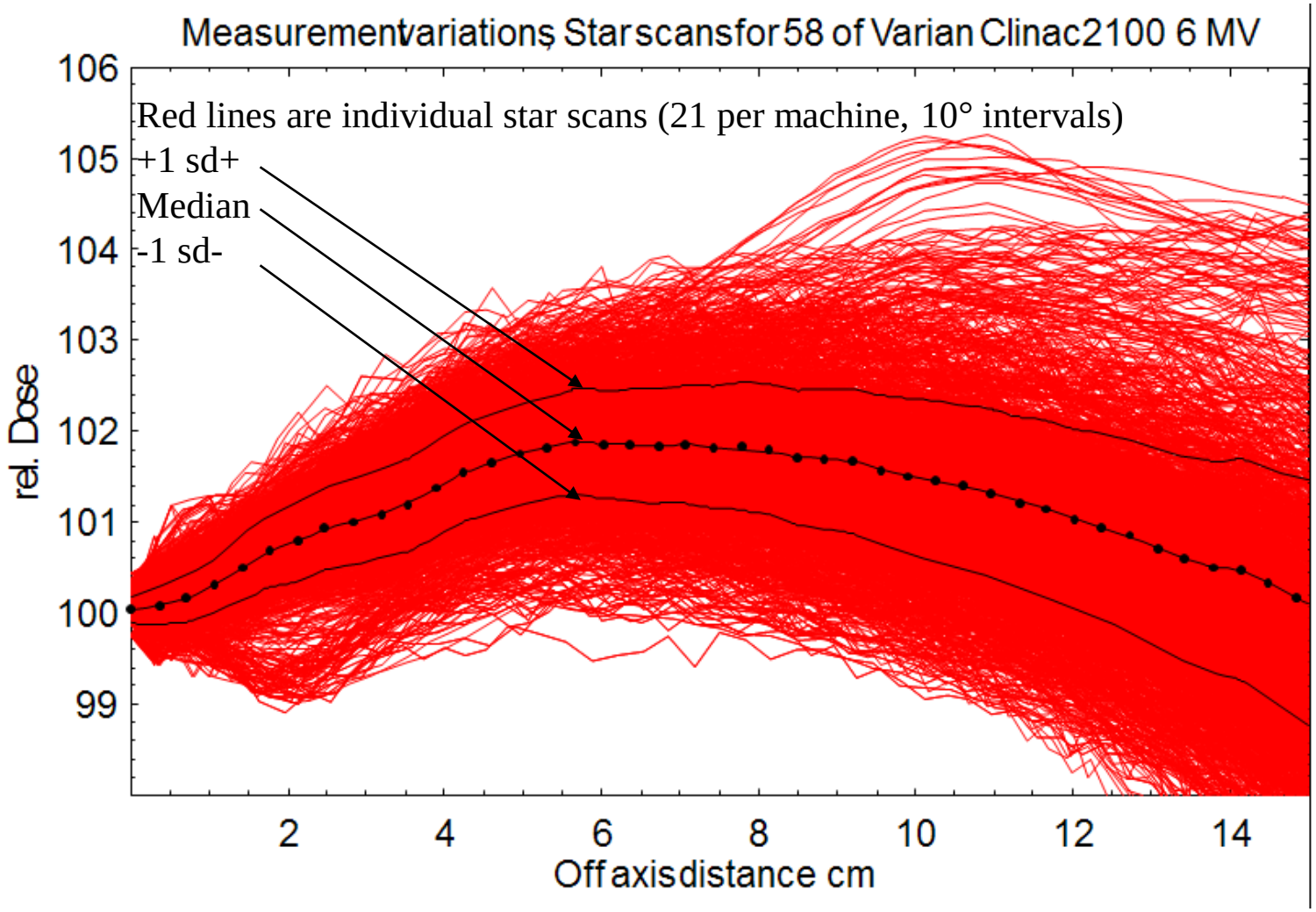

Star dose measurements – machine variability

12 Siemens Primus 10 MV

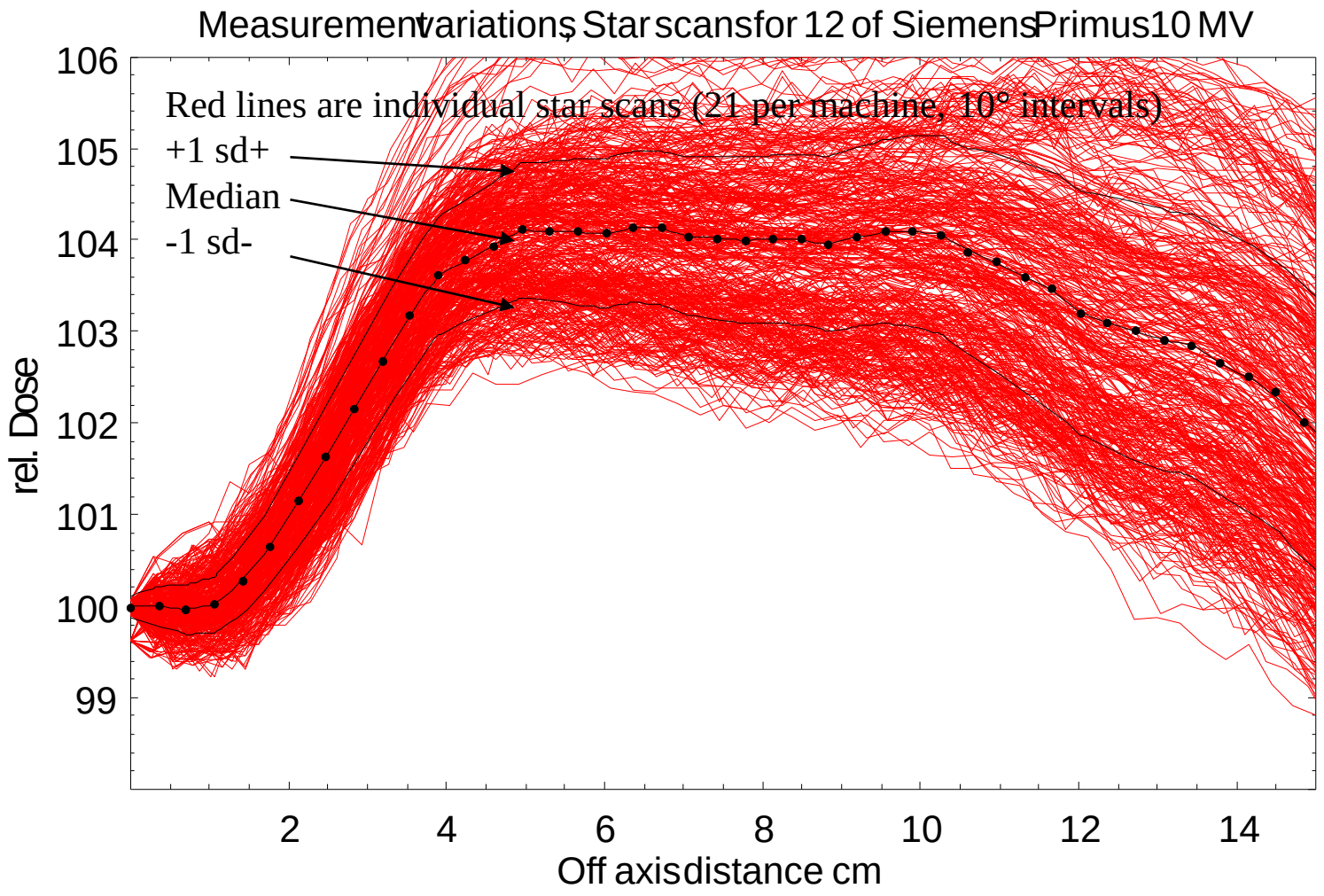

Beam energy spectra
- spectral filtering by the flattening filter

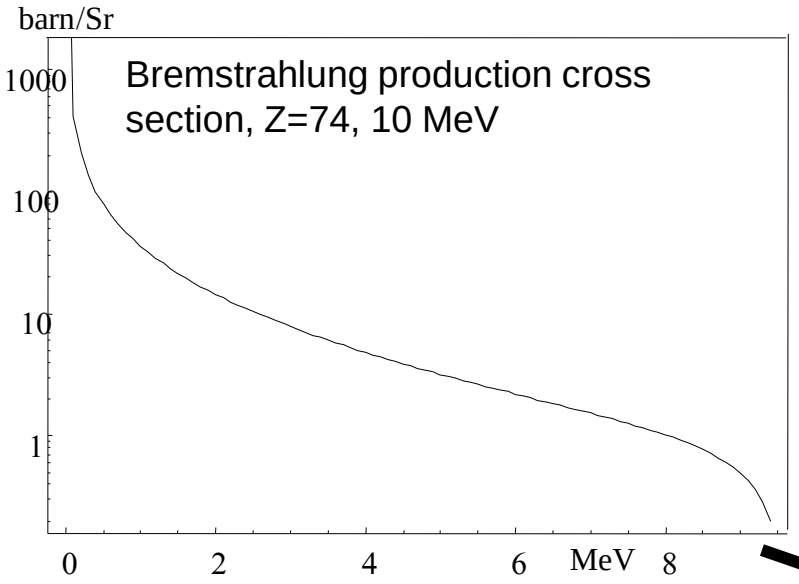

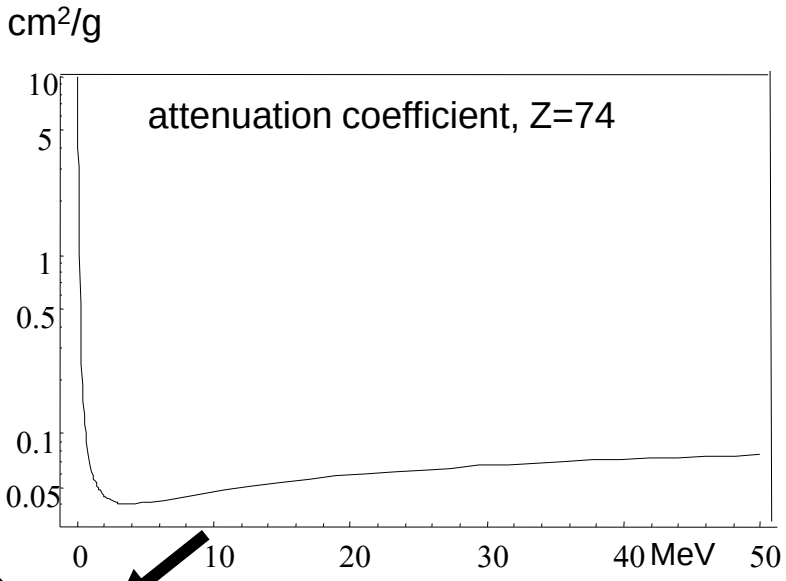

Direct beam spectrum, principal shape.
Spectrum distorted offaxis towards lower energies due to less filtration & decreasing energy with increasing brem angle

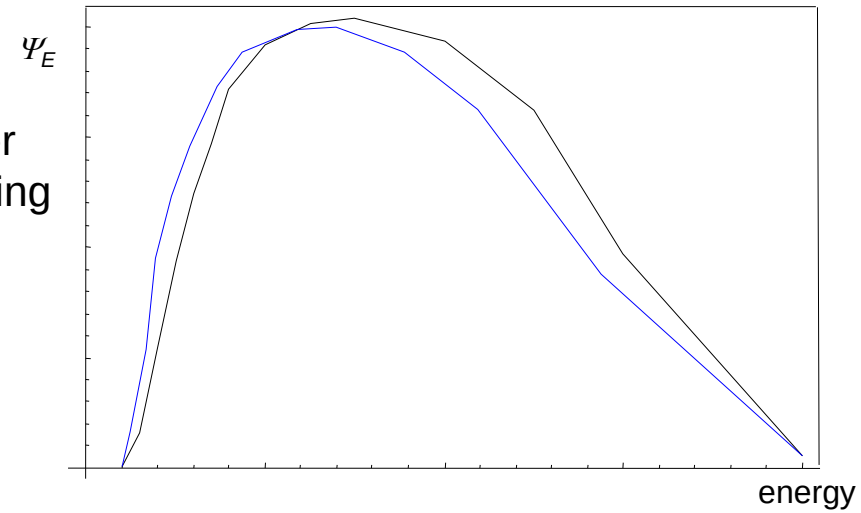

Beam energy spectra
- methods to determine spectra for clinical beams

require trimming of the resulting spectrum so that measured dose matches calculated dose

Measurements
- Low beam current and/or Compton scatter methods
- Not practical for clinical use

Monte Carlo methods
- Mohan et al MedPhys 12 p 592 1985 widely used for testing
- BEAM (EGS4/nrc) standard tool
- Other codes also used, PENELOPE, GEANT, etc.
- Still not practical for routine use
- MC data to be standard part of linac purchase procedure?

Analytical modelling from cross sections
- Target designs requires use of ‘thick target theory’, i.e. must model the electron transport prior to bremsstrahlung interactions

Unfolding from transmission through attenuators
- Based on ‘in air’ measurements
- Requires good control of attenuator purity
- Most methods use some support of spectral shape constrains

Unfolding from depth dose distributions in water
- **Requires access to monoenergetic depth dose data (Monte Carlo)**
- **Unfolding methods needs spectral shape constrains**

Beam energy spectra
Measurements – Compton spectroscopy

Reduce the fluence to a countable level by Compton scattering. Spectrum derived by correcting for energy loss during scattering. Setup complexity makes it unpractical for clinical use.

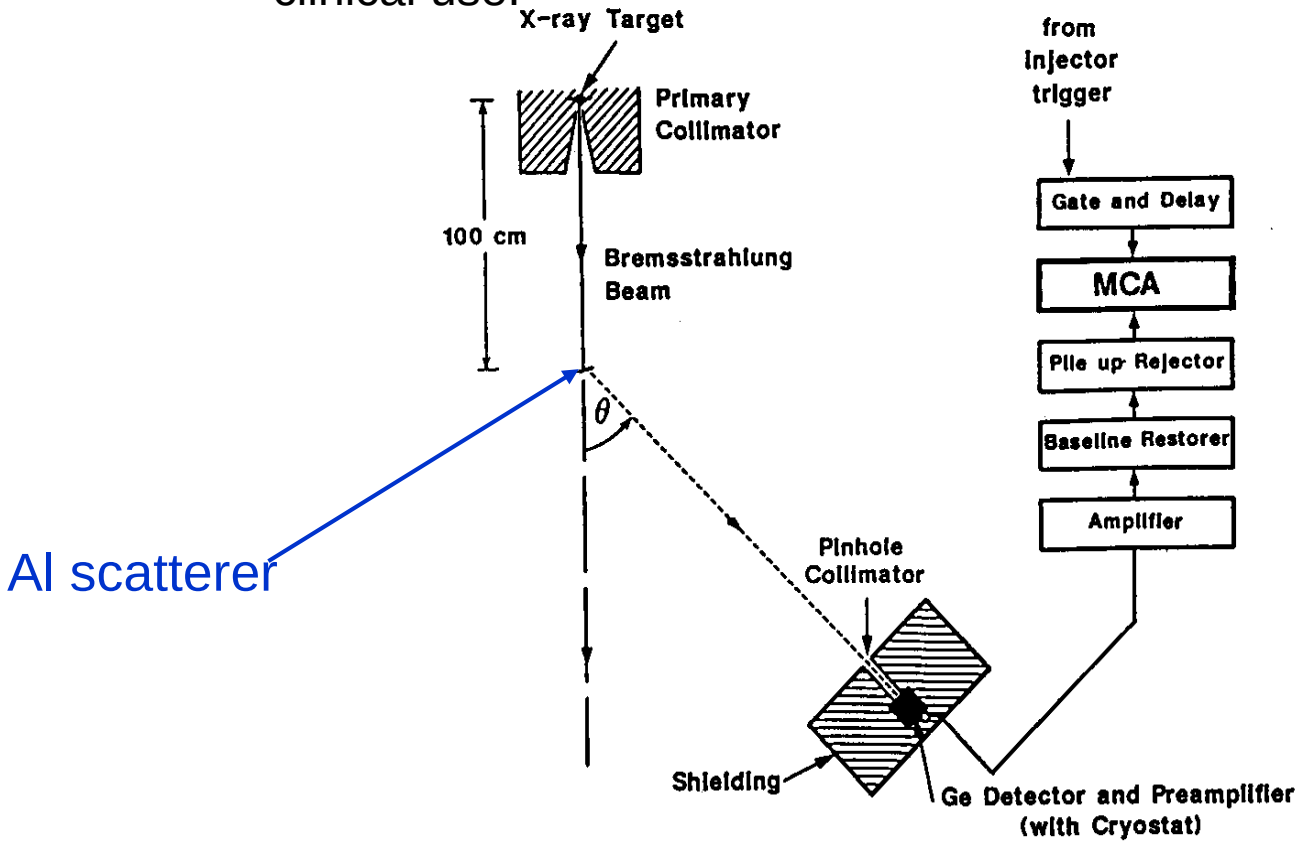

from Landry and Anderson, MedPhys 18, 1991, p 527

Beam energy spectra analytical modeling

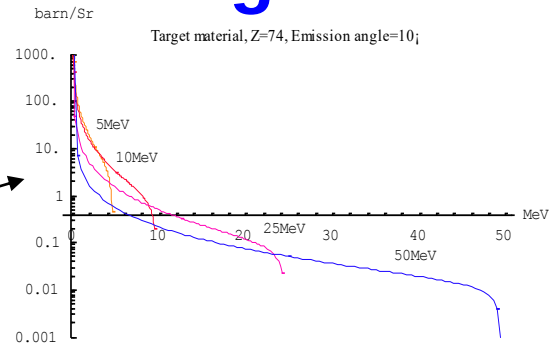

Numerical integration of X-sections and attenuation data, results similar to Monte Carlo

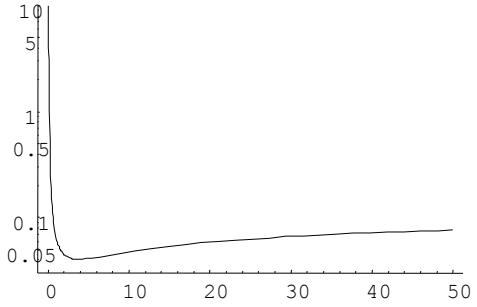

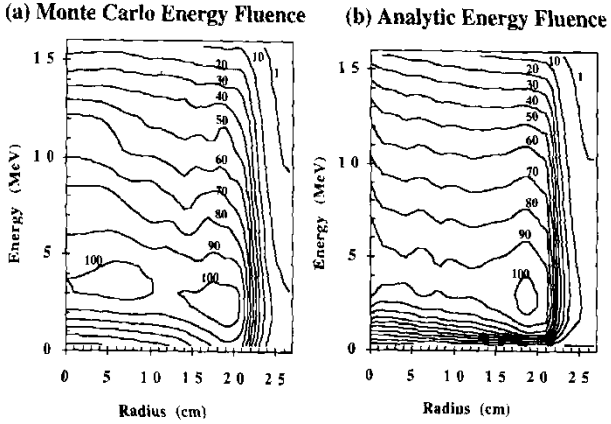

Simple models, parametric control of spectral shape $\Psi_E = \Psi_E(p_1, p_2, p_3)$

from Desobry & Boyer, MedPhys 21, 1994, p 1943

Beam energy spectra
Unfolding measured transmission data

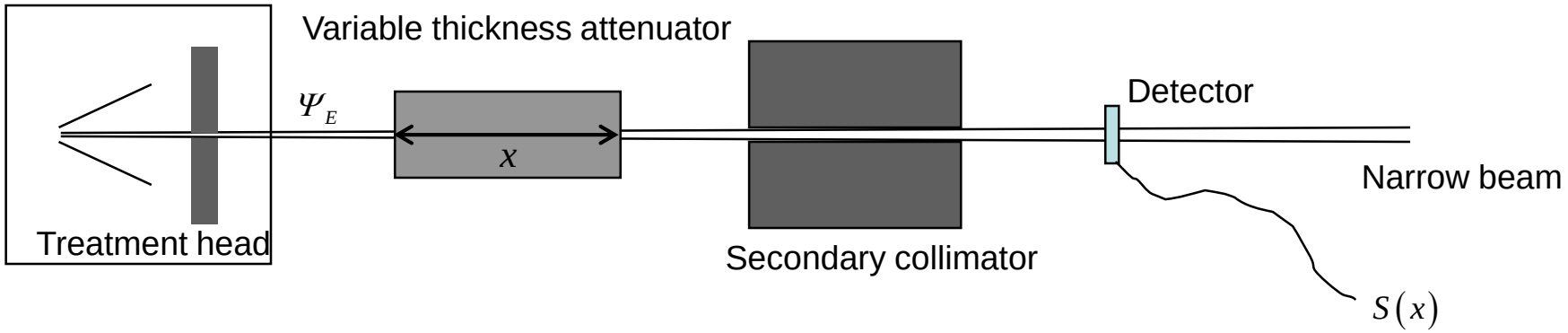

General:

$$\frac{S(x)}{S(0)} = \frac{\int_0^{E_{\max}} R(E)\Psi_E \, \mathrm{e}^{-\mu(E)\cdot x} \, \mathrm{d}E}{\int_0^{E_{\max}} R(E)\Psi_E \mathrm{d}E}$$

$R(E)$ Detector response

Ψ_E Energy fluence spectrum

Simple approach:
(neglects energy response variations)

$$S(x_j) = \sum_i \Psi_{E_i} \, \mathrm{e}^{-\mu(E_i)\cdot x_j} \, \Delta E_i \quad \Leftrightarrow \quad \underbrace{S_j = \sum_i \Psi_i A_{i,j}}_{\text{to be solved by numerical methods (linear algebra)}}$$

Beam energy spectra

Constrained unfolding of spectra from depth dose measured in water

Recipe:

Minimize the difference between measured depth dose and spectral weighted monoenergetic Monte Carlo calculated depth dose. Explicitly consider electron contamination depth dose in the buildup region (or exclude the buildup zone from depth doses!):

$$\delta(s_1, s_2 \ldots, e_1, e_2 \ldots) = \sum_{\text{fsize}} \sum_{\text{depth}} \left| c_{\text{fsize}} D_{\text{depth, fsize}} - \left(\left(\sum_{\text{ebin}} \Psi_{\text{ebin}}(s_1, s_2 \ldots) \cdot d_{\text{depth, fsize, ebin}} \right) + d_{\text{depth}}^{\text{electron cont}}(e_1, e_2 \ldots) \right) \right|$$

Measured depth dose, phantom scatter normalized

MC calc depth doses for monoenergetic photons

Error norm to minimize by varying parameters

Spectrum model, constrained to a "physical" shape

Electron contamination model

Ahnesjö & Andreo, 1989 PMB 34, p 1451-64

Beam energy spectra
- results from constrained unfolding

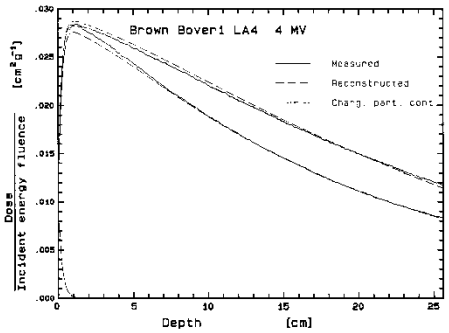

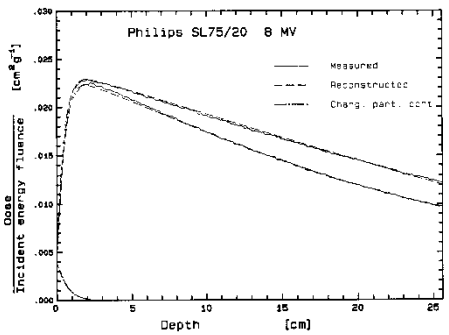

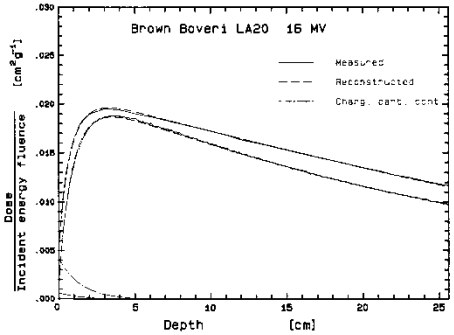

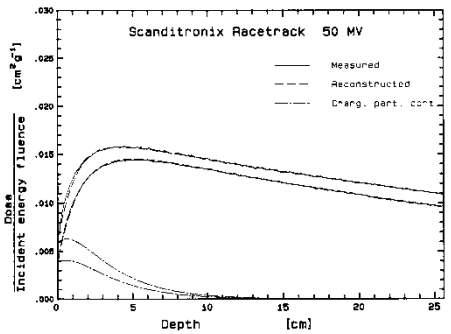

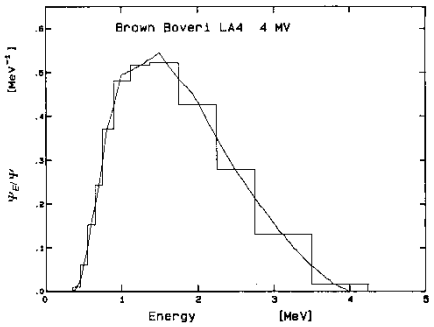

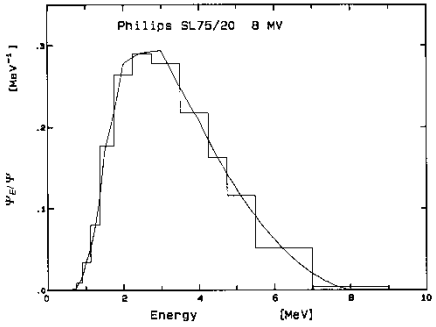

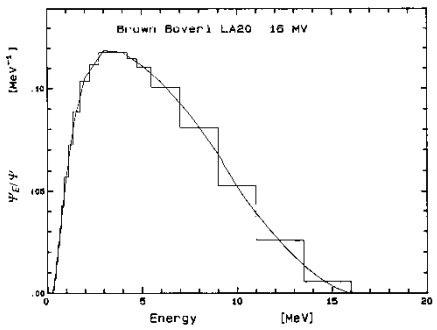

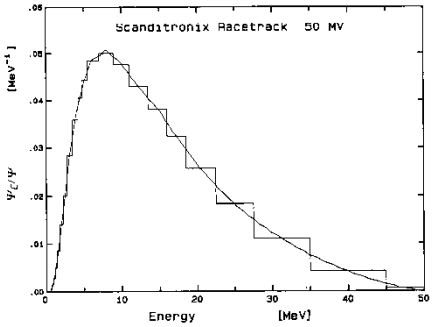

Ahnesjö & Andreo, 1989 PMB 34, p 1451-64

Spectral changes from off axis filtration

Lateral variation of the spectrum, such as off axis softening can be modelled by varying coefficients of attenuation and energy release.

Off axis HVL values can therefore be modelled without explicit knowledge of the spectrum change causing it!

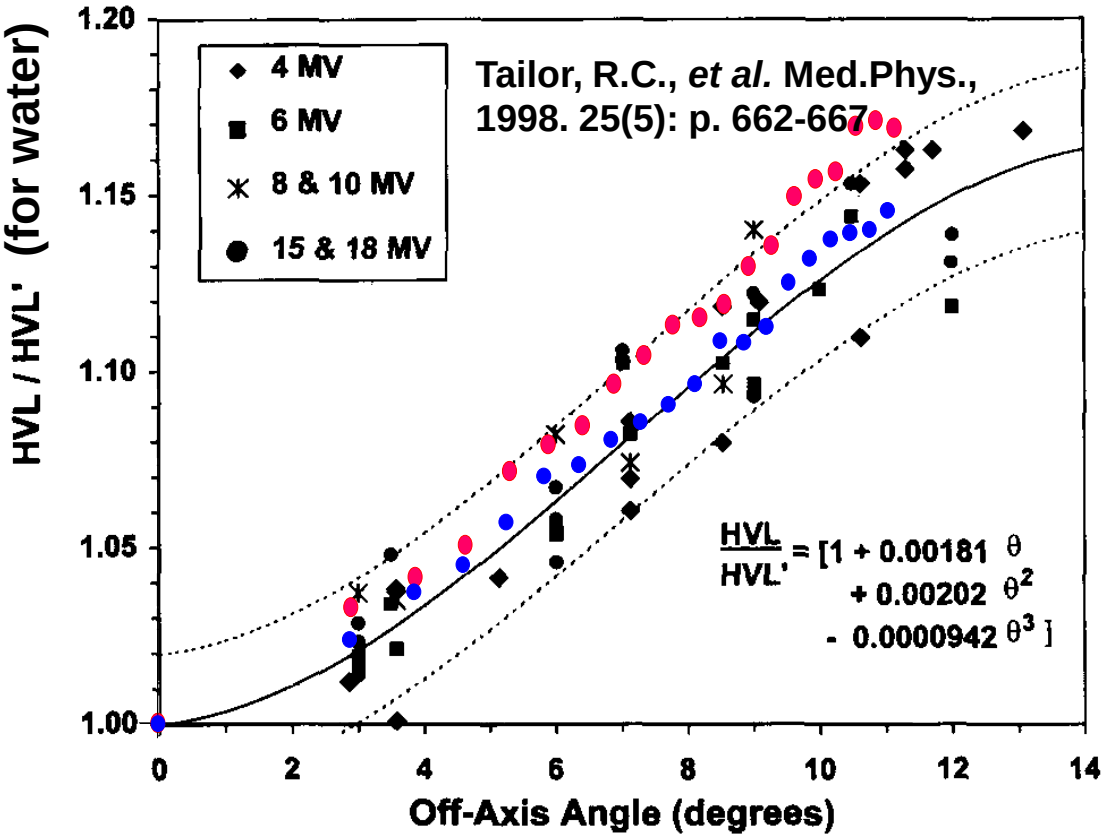

$$\mu(\text{direct beam}) \approx \frac{\ln 2}{\text{HVL}}$$

Monte Carlo data
Sheikh-Bagheri priv. com.

BEAM (EGS4) Elekta SL 25, 25 MV

BEAM (EGS4) Elekta SL 25, 6 MV

Depth dose – machine variability

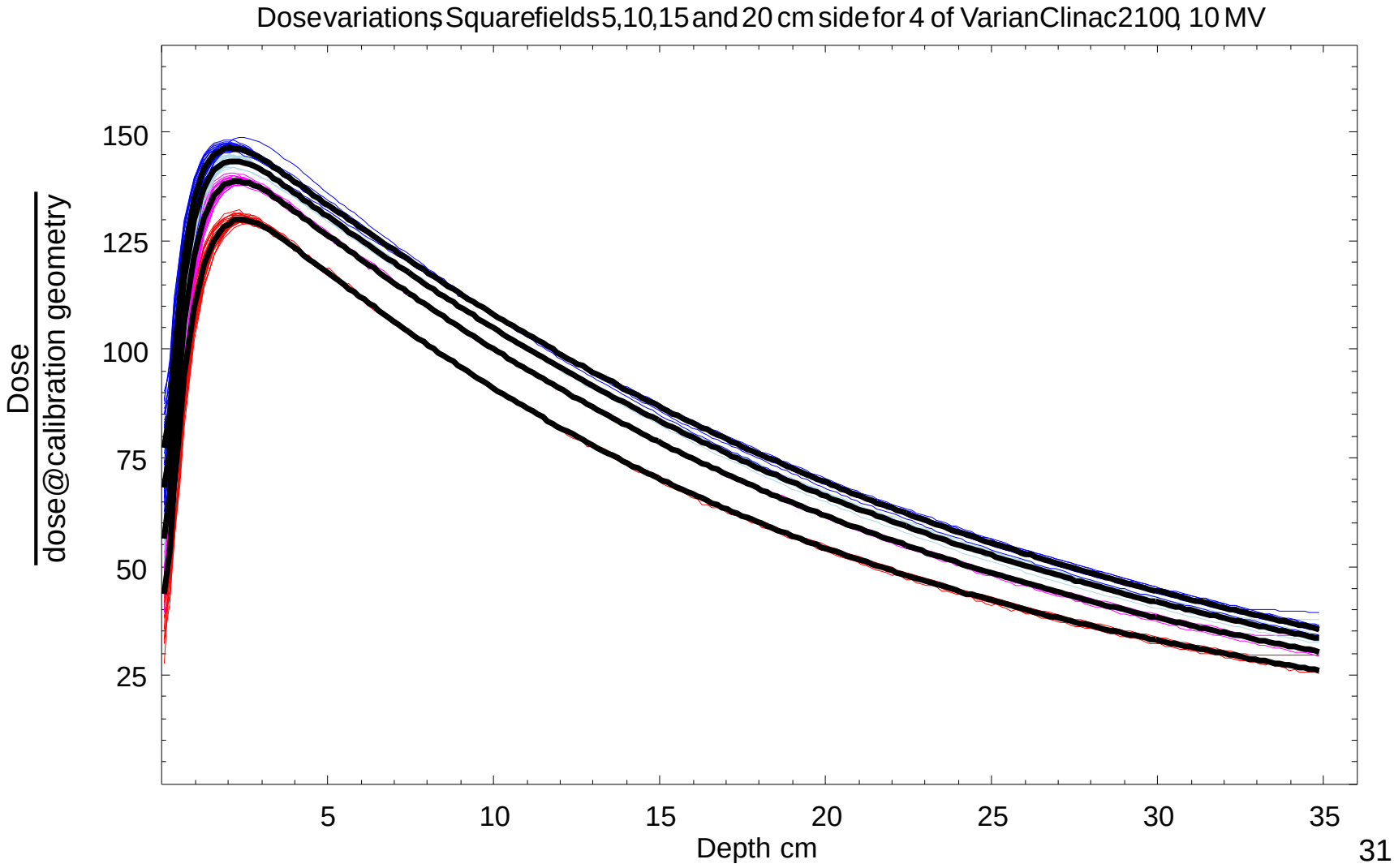

Electron contamination

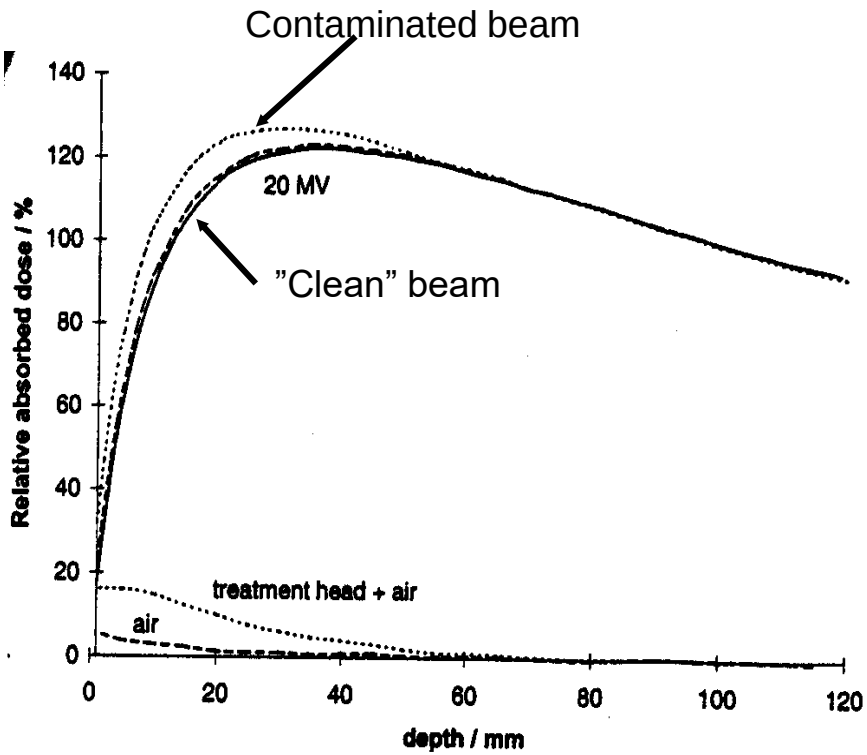

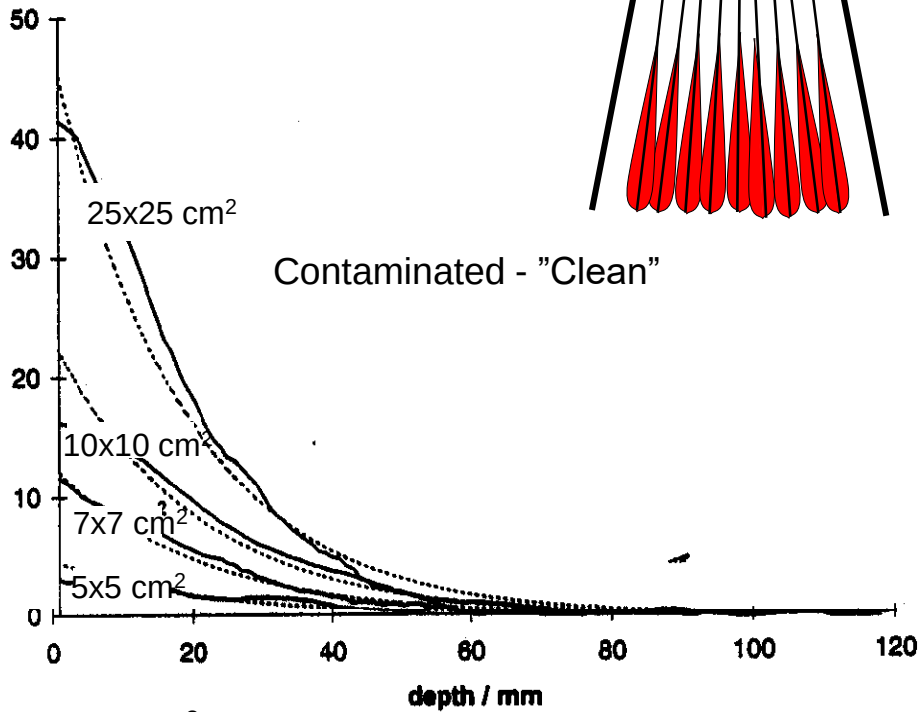

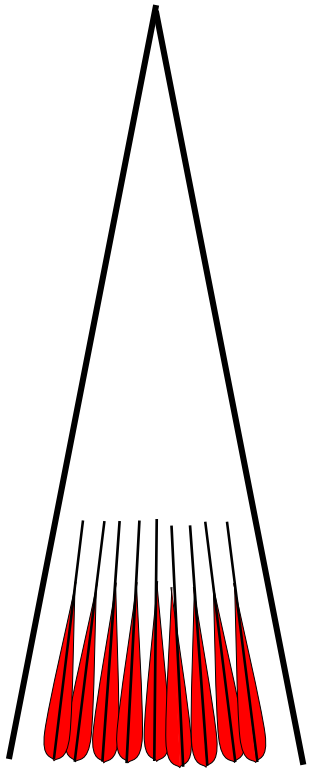

Maximum penetration depth appr. MV/3 [cm^2/g], i.e. deeper than d_{max}....
Field size most important factor for magnitude, no impact on penetration depth.

Sjögren & Karlsson, Med. Phys. **23** 1996 p 1873-1881

Electron contamination, cont…

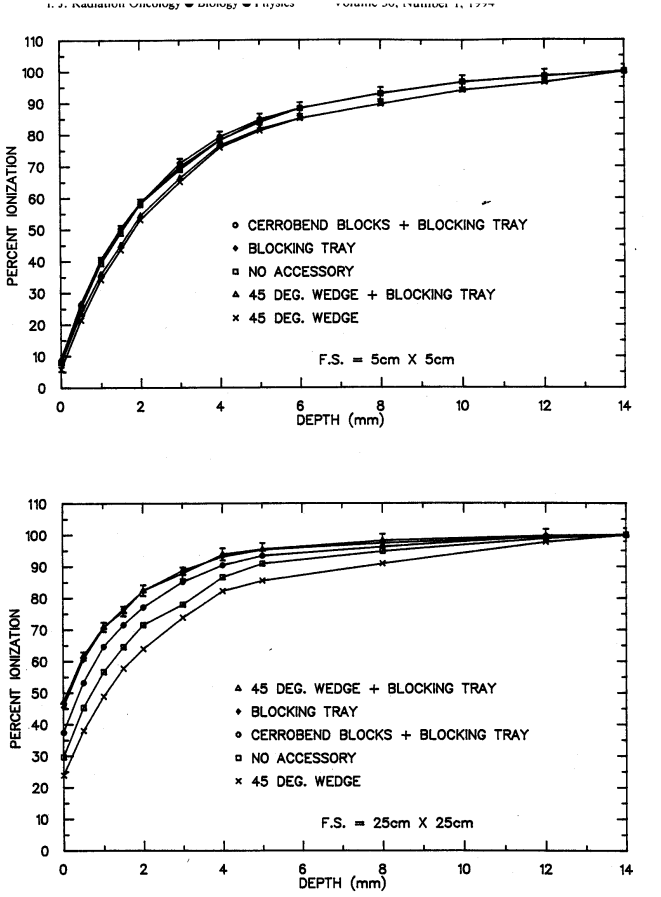

Fig. 2. Comparison of accessory effects on build-up for 6 MV photons; field sizes: 5 × 5 cm and 25 × 25 cm.

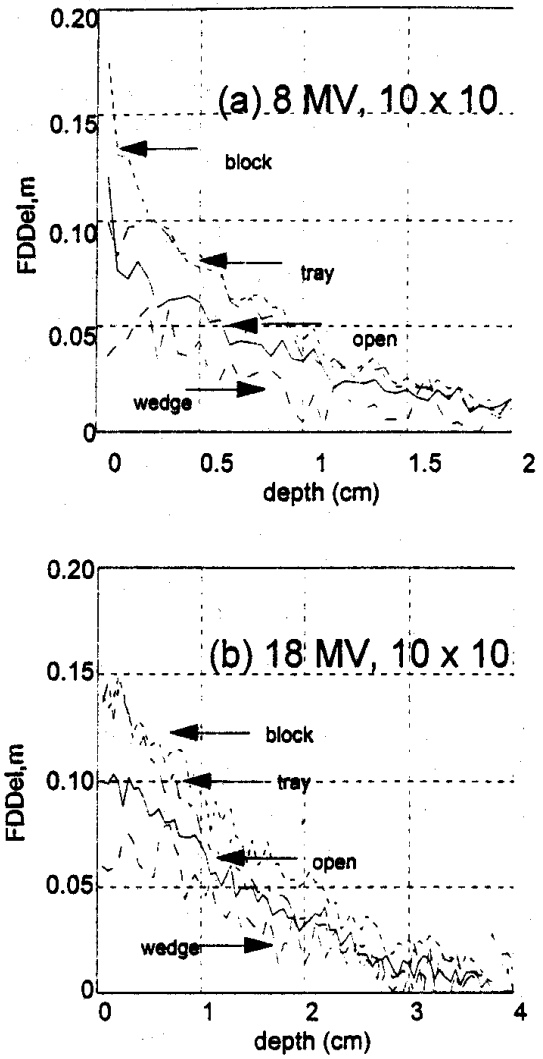

Everything in the beam path has an impact, still field size is most important single factor!

Zhu & Palta, 1998 Med. Phys. **25** p 12-19

Fontenla *et al* IJROBP. 1994 **30** p 211-219

Flattening filter scatter the major extrafocal contribution *Monte Carlo proof:*

Mevatron & EGS4

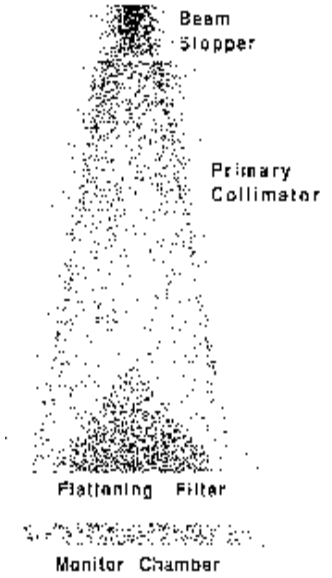

Distribution of origin site. Note clouds at beam stopper, primary collimator and flattening filter

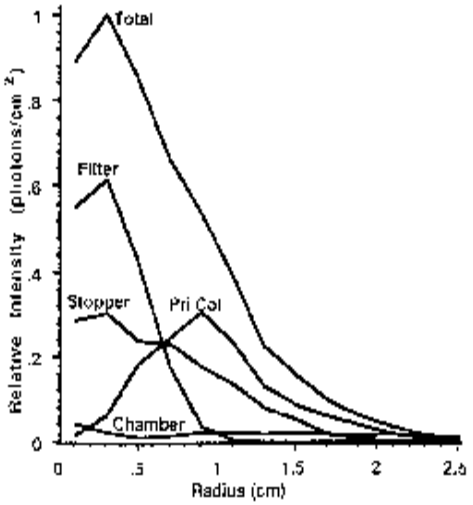

Lateral distribution of origin sites, projected to a common distance from the target.

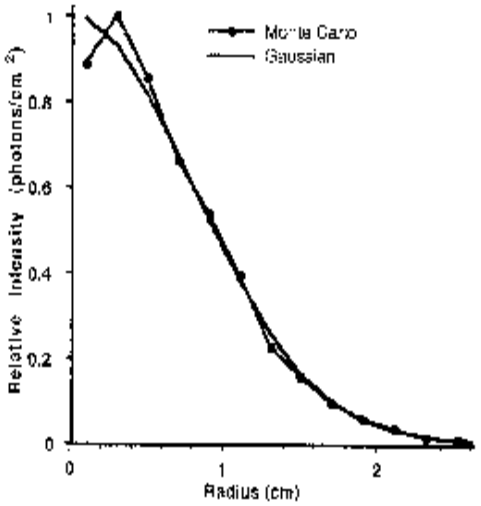

All scatter sources merged to an effective source distribution.

Chaney E L *et al* 1994 A Monte Carlo study of accelerator head scatter *Med. Phys.* **21** 1383-9

Flattening filter scatter, semi-analytical approach

$$\frac{\Psi_f}{\Psi_0} = \iint_{\text{area as viewed backward through the aperture}} \underbrace{k_\sigma(\phi)\,k_C(\phi)}\;\underbrace{\frac{(c_0 - c_1\theta)}{(z_{calc} - z_{filt})^2}}\,dA$$

Assumptions (Med. Phys. 21 p 1227-1235):

- Predominantly first order scatter
- Triangular source distribution over the *visible* filter area
  - Fit parameters c_0 and c_1 from measured output factors.
- Correction factors for:
  - Energy loss in Compton scattering.
  - Klein-Nishina cross section angular variation.
- Modulate the resultant fluence if modulators are present

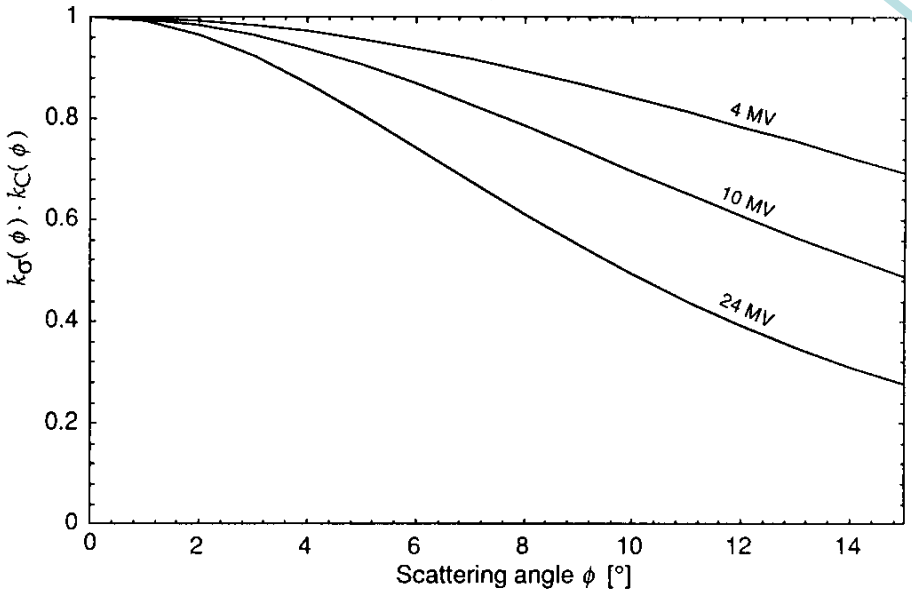

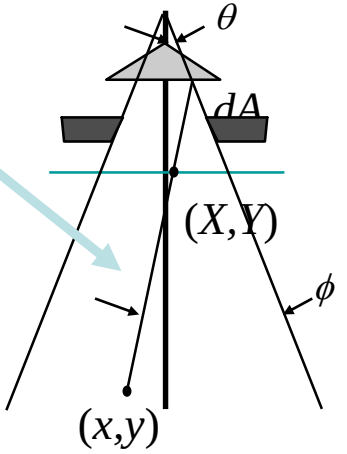

$$\eta = \prod_i \eta_i(X_i, Y_i)$$

Head scatter fluence calculation - integration over extended sources

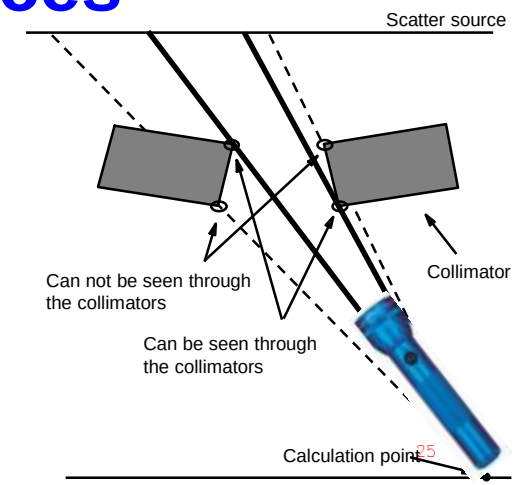

Main steps in the OOPS (Object Oriented Pixel Shadowing) back projection algorithm for head scatter geometry integrations:

I. **Cover scattering surface by a pixel matrix.**
II. **Set all pixels as scattering.**
III. **Illuminate the matrix by a light source place in the calculation point.**
IV. **Construct the shadow cast on the matrix from each collimating element (collimator, MLC, block,…).**
V. **Combine all shadows (reset shadowed pixels).**

Only visible pixels remains set !

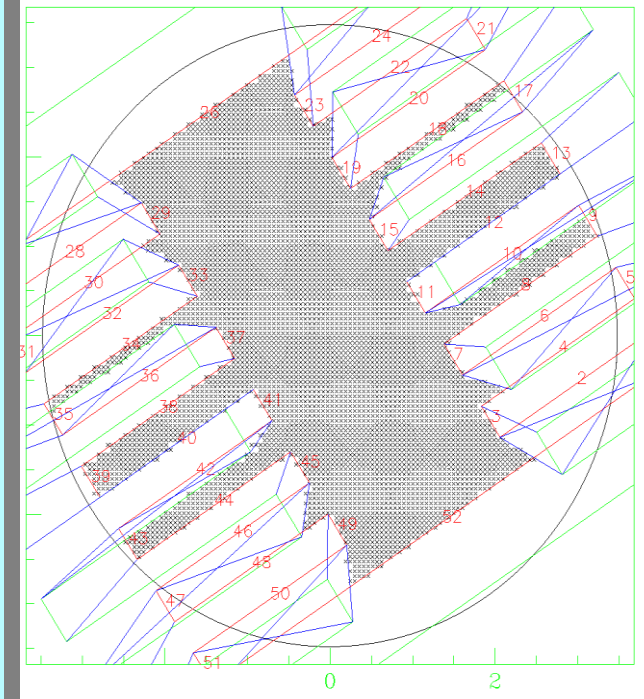

Flattening filter scatter cause variation of S_c - used for source data acquisition!

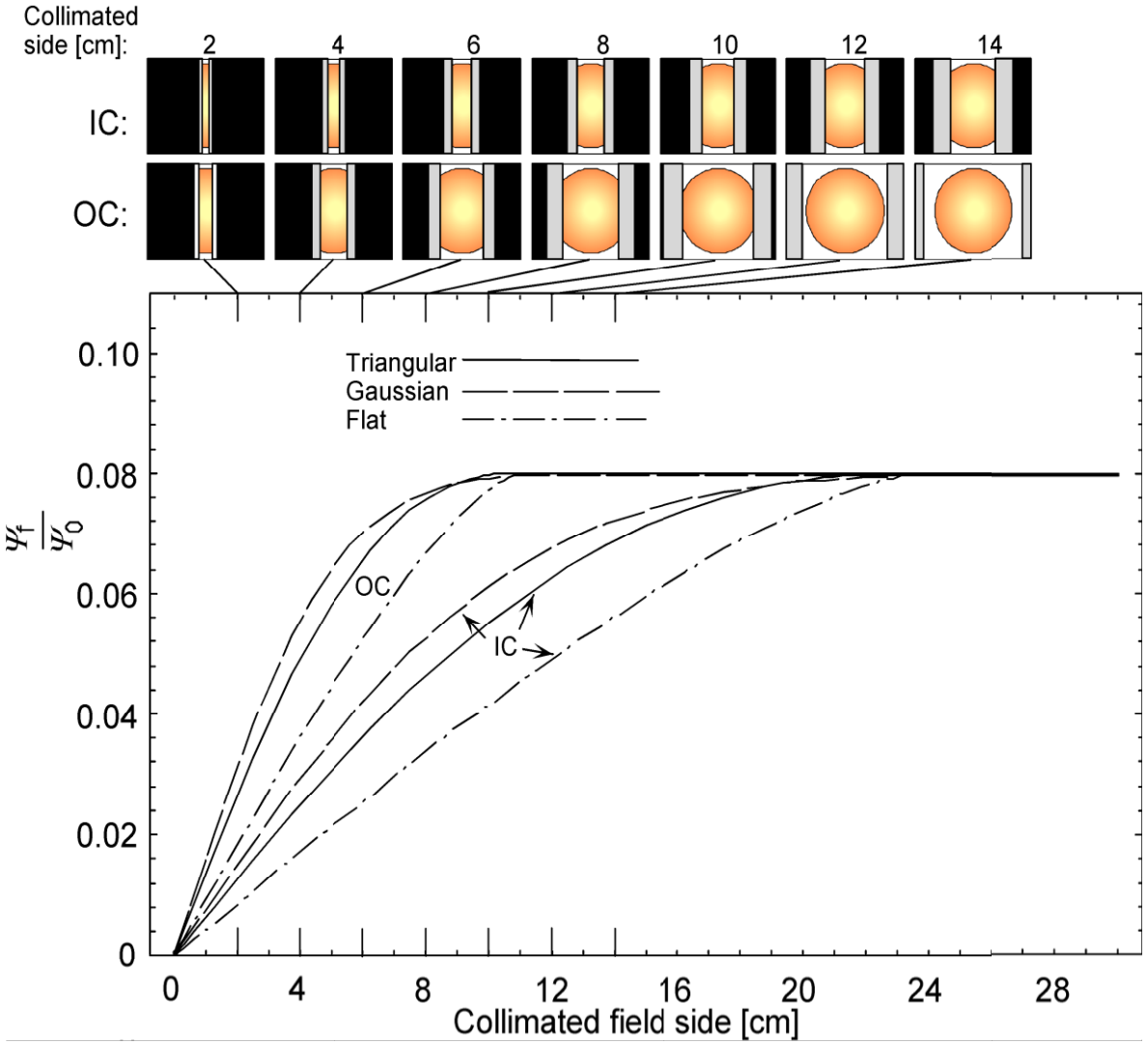

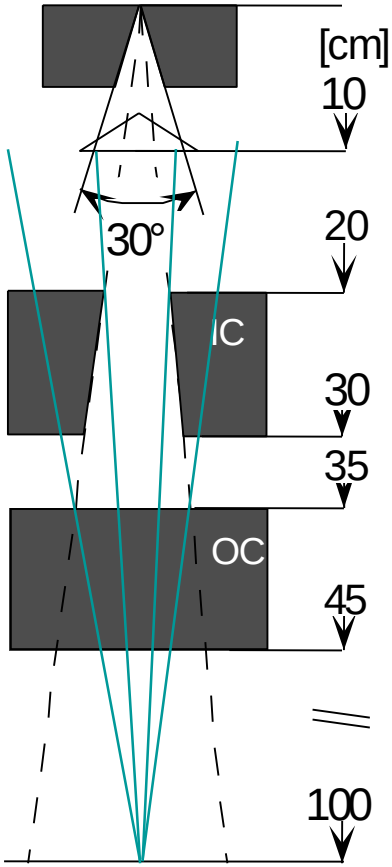

Ahnesjö 1994 Med. Phys. **21** 1227-35

Flattening filter scatter varies laterally !

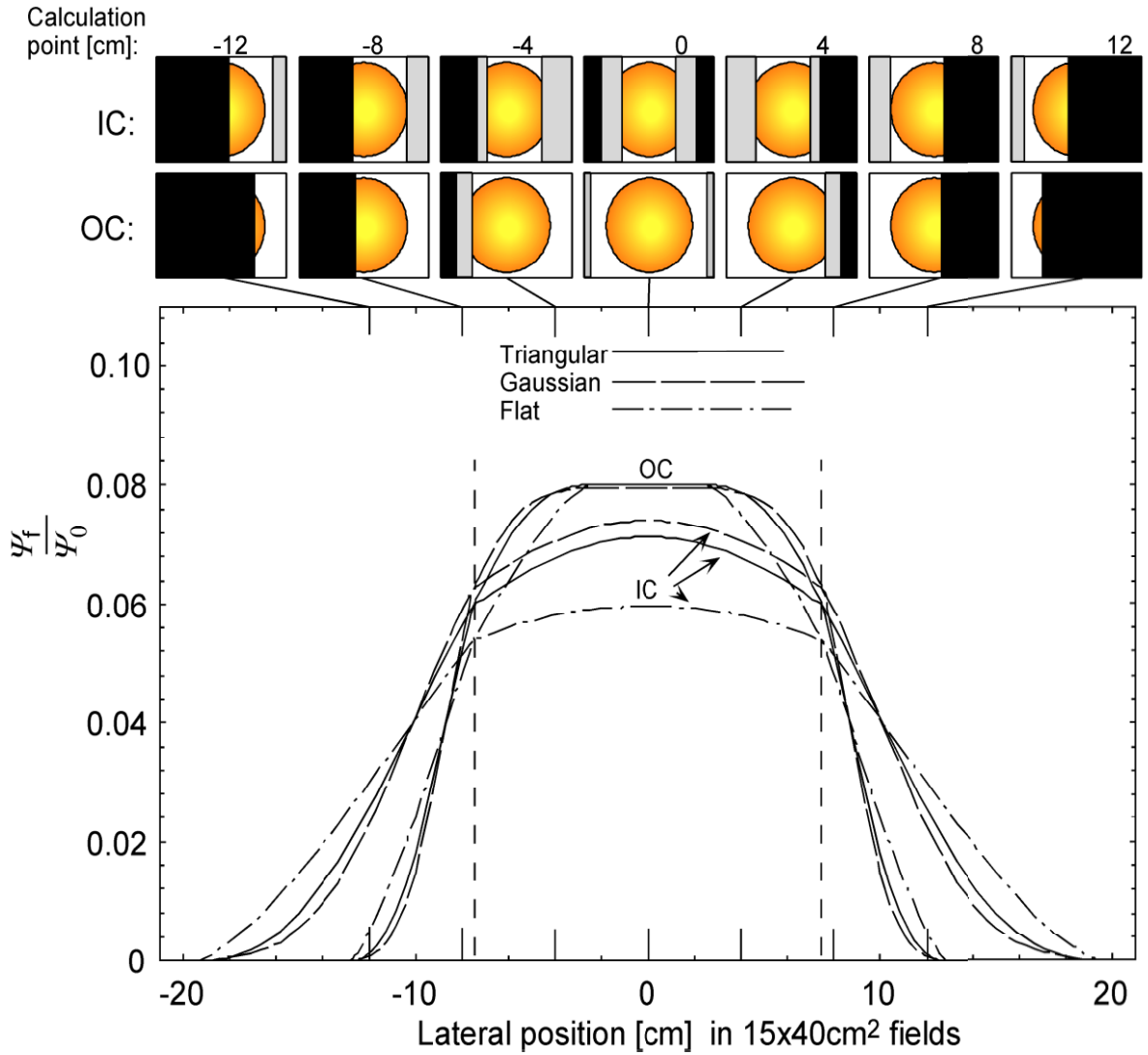

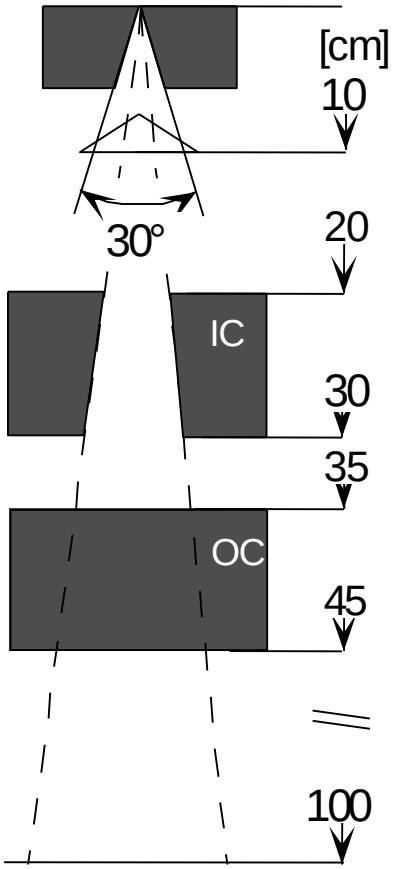

Ahnesjö 1994 Med. Phys. **21** 1227-35

Head scatter machine (man?) variability

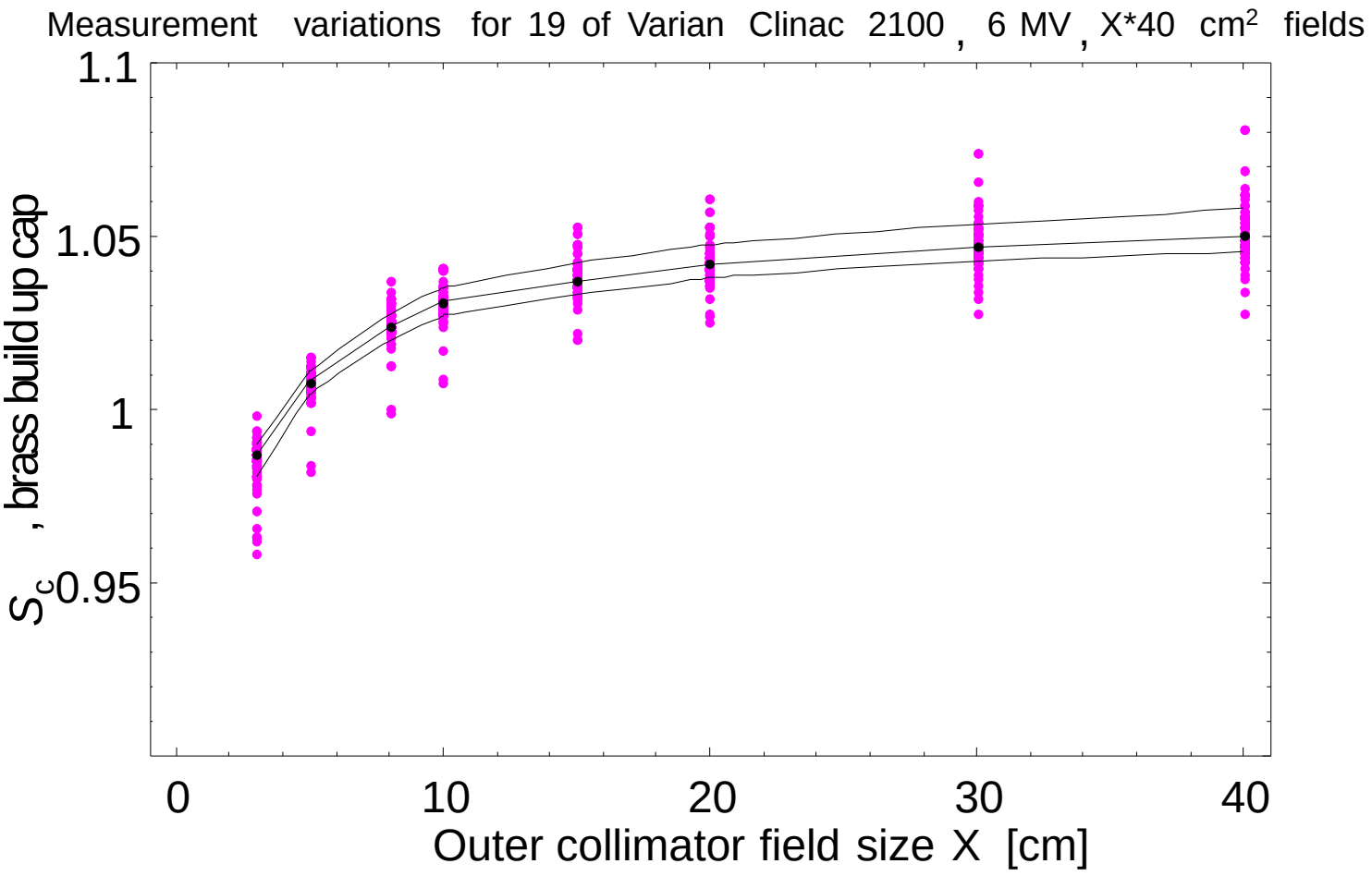

Collimator scatter

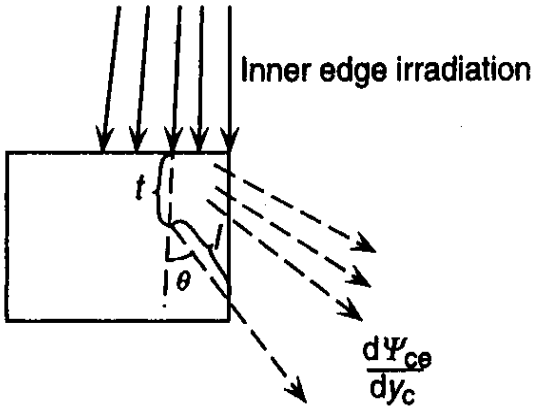

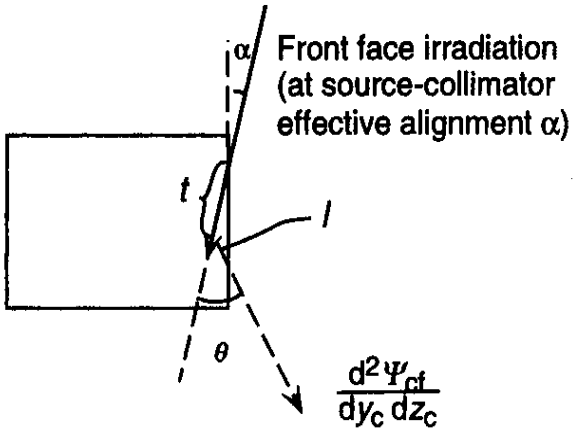

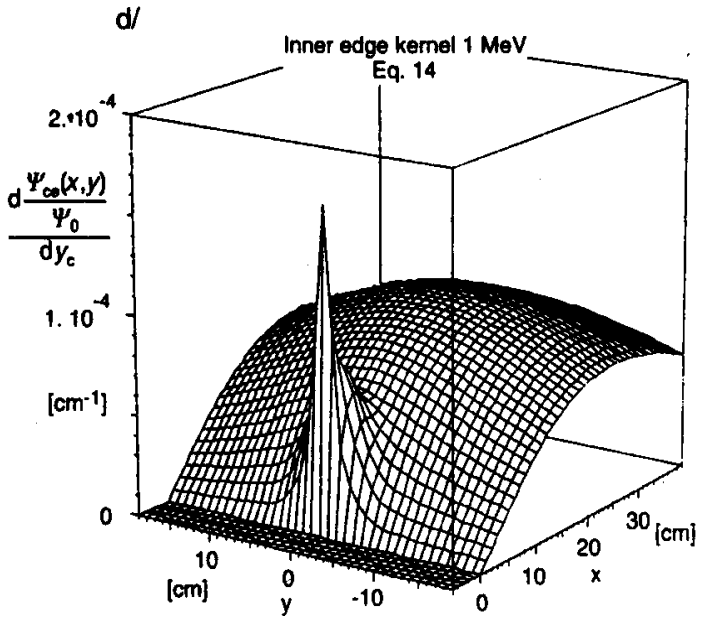

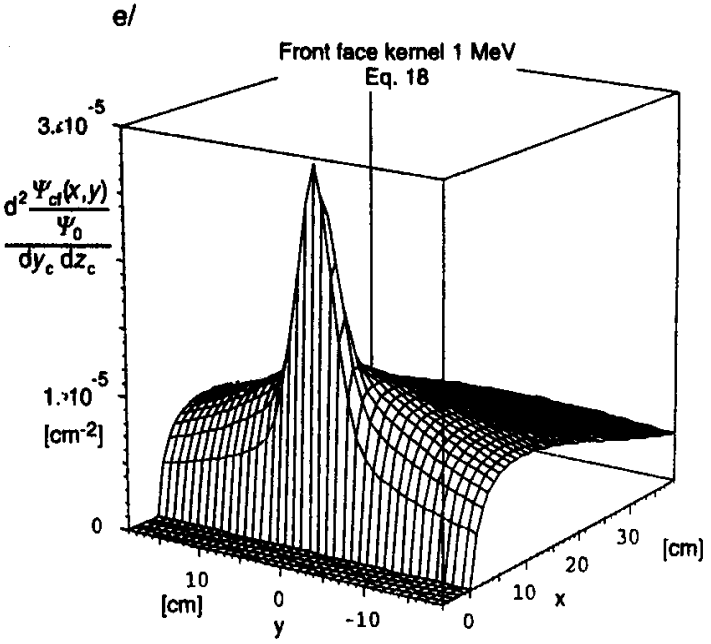

Ahnesjö, Med. Phys. **22** p 267-278

Collimator scatter, cont…

- minor influence

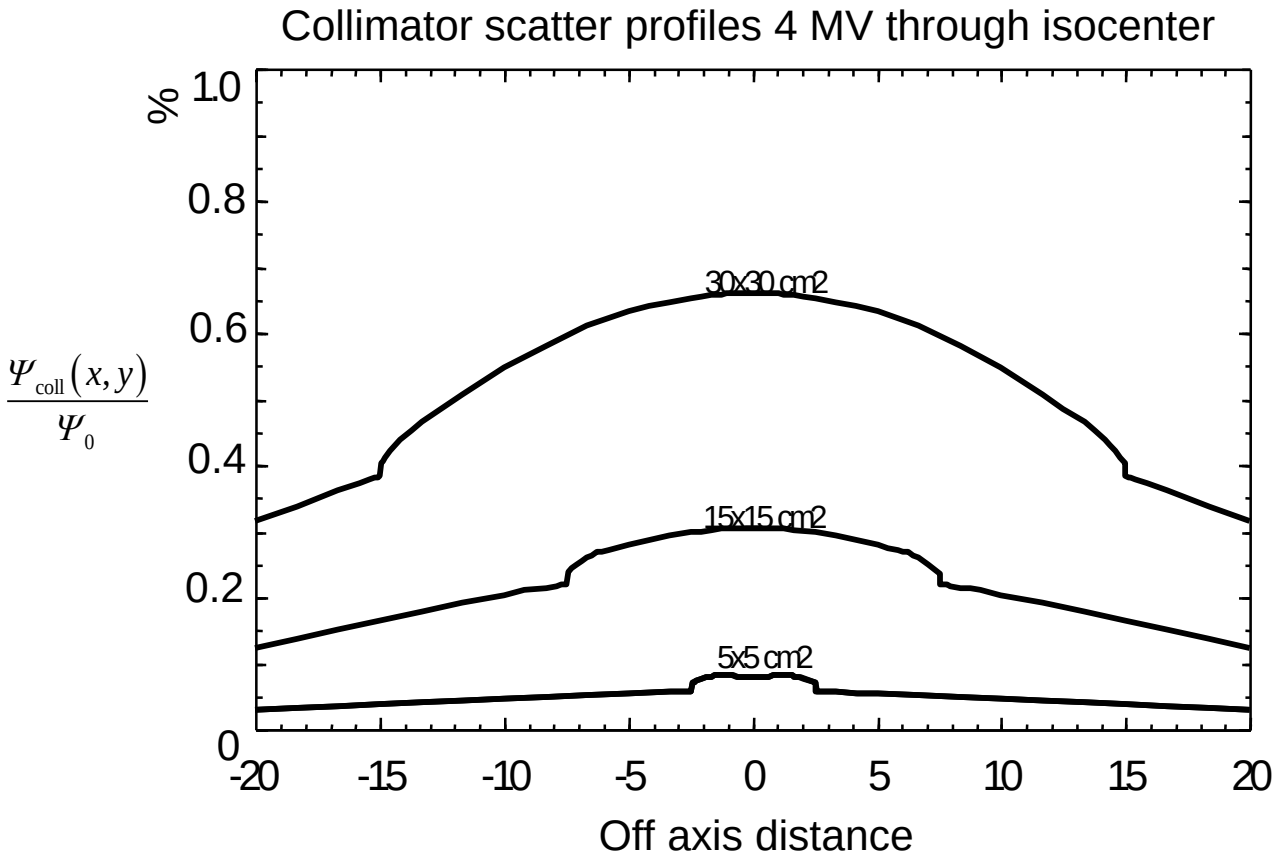

Ahnesjö, Med. Phys. **22** p 267-278

Monitor back scatter

$$\frac{\Psi_0}{M} = \frac{\Psi_0}{M_0 + M_b(A)} = \frac{\Psi_0}{M_0}\left[\frac{1}{1+b(A)}\right]$$

- Usually a very small effect
- Dominated by low energy charged particles, can be stopped by a protection sheet.
- Can be modelled by a monitor's-eye-view of the collimators:
  - Distance source to monitor and collimator.
  - Shape of visible collimator surface.
  - Empirical constant, 0.3 to 0.4.

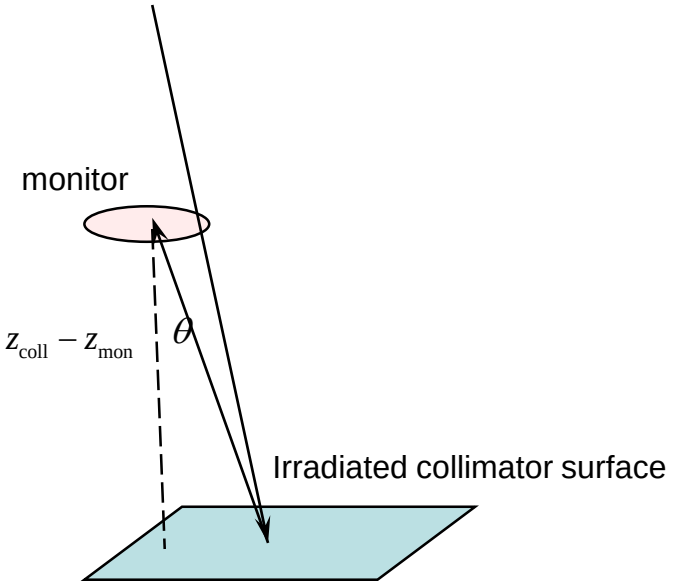

$$b(A) = k_{back}\, F\, \frac{z_{mon}^2}{z_{coll}^2}$$

$$F = \iint_{\substack{\text{Irradiated}\\ \text{collimator}\\ \text{area}}} \frac{\cos^3\theta}{\pi\left(z_{coll} - z_{mon}\right)^2}\, \mathrm{d}A$$

PMB 44 p R99-R155

Monitor back scatter

Table 2. Relative BSR-related output changes for the indicated ranges of jaw-defined field sizes measured by the pulse-counting method.

Photon beam energy, linear accelerator	Square fields from 5 × 5 cm^2 to 40 × 40 cm^2 (%)	Rectangular fields, x = 40 cm, y from 5–40 cm (%)	Rectangular fields, y = 40 cm, x from 5–40 cm (%)
6 MV, Clinac 600C	−0.1 ± 0.4	0.0 ± 0.4	0.0 ± 0.4
6 MV, Clinac 2100C (No 1)	1.6 ± 0.4	1.2 ± 0.4	0.7 ± 0.4
18 MV, Clinac 2100C (No 1)	2.4 ± 0.4	1.7 ± 0.4	1.2 ± 0.4
6 MV, Clinac 2100C (No 2)	1.7 ± 0.4	1.4 ± 0.4	0.6 ± 0.4
18 MV, Clinac 2100C (No 2)	2.1 ± 0.3	2.0 ± 0.3	1.1 ± 0.3
6 MV, Clinac 2300CD	1.2 ± 0.3	1.0 ± 0.3	0.5 ± 0.3
15 MV, Clinac 2300CD	1.8 ± 0.3	1.6 ± 0.3	0.5 ± 0.3
6 MV, Clinac 2300CD (MLC)	—	—	−0.2 ± 0.3[a]

[a] MLC-defined field width varied from 5–25 cm with X jaws retracted and Y jaws defining a fixed length of 25 cm.

Yu *et al* 1996 *PMB* **41** 1107-1117

Head scatter model parameterization example

Scatter component	Model	Model parameters
Flattening filter scatter	Triangular source distribution	c_0 and c_1
Collimator scatter	Scatter kernel integration around the field edge	None
Backscatter to monitor	Monitor's eye view factors of irradiated block areas	Backscatter coefficient k_b
		Σ 3 *parameters*

The parameters are determined by fitting measured S_c (OF_{air}) to calculations!

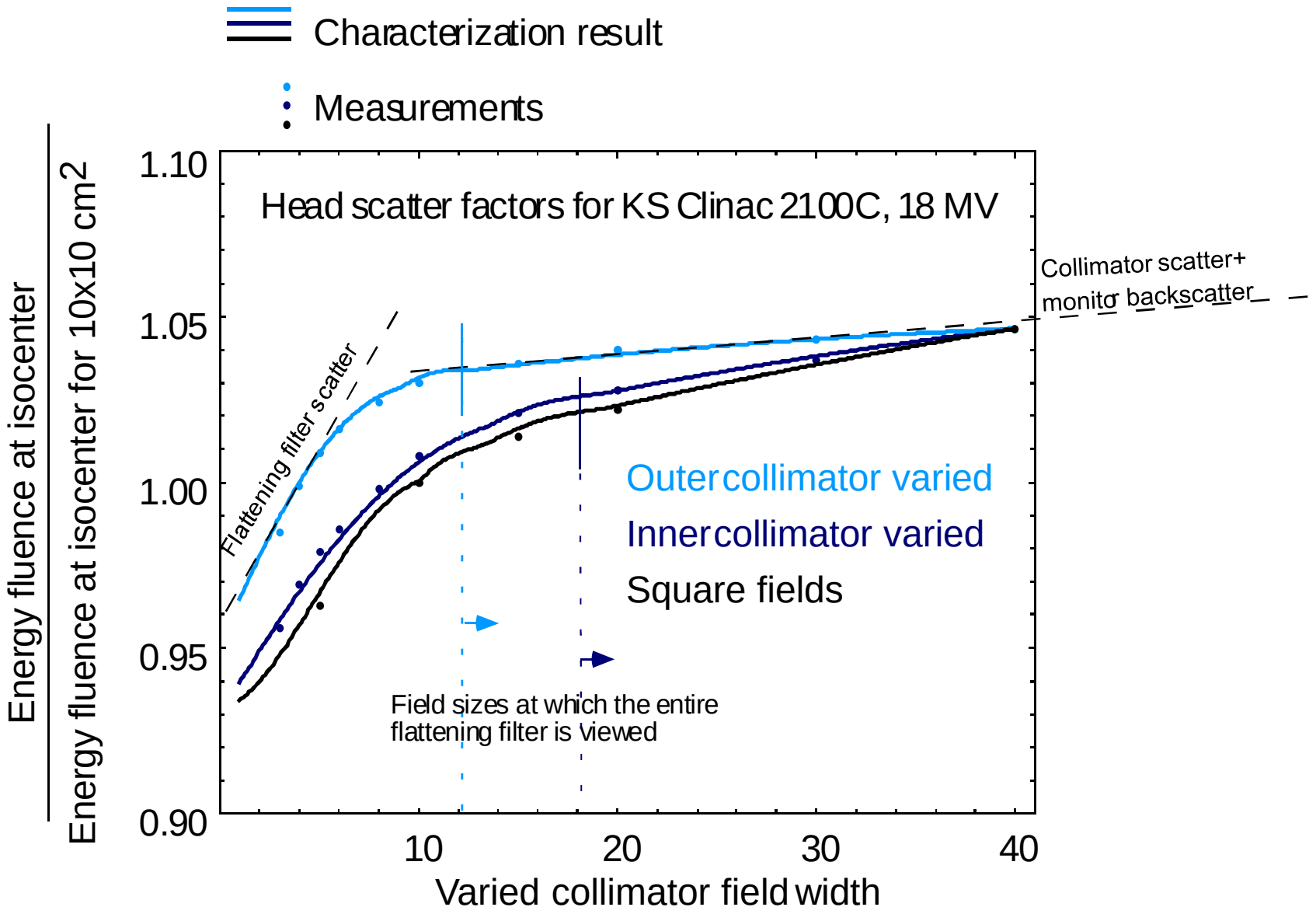
Characterization result
Measurements
Head scatter factors for KS Clinac 2100C, 18 MV
Energy fluence at isocenter
Energy fluence at isocenter for 10x10 cm2
1.10
1.05
1.00
0.95
0.90
10
20
30
40
Varied collimator field width
Flattening filter scatter
Collimator scatter+
monitor backscatter
Outer collimator varied
Inner collimator varied
Square fields
Field sizes at which the entire
flattening filter is viewed

Collimator leakage

MLC intraleaf and interleaf

Two effects:

- Diffused dose from spiky interleaf fluence leakage
- *Intraleaf* attenuation

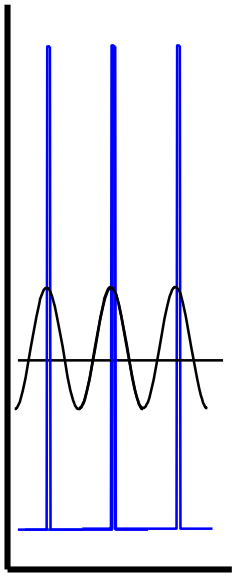

Intraleaf leakage very small:

$$e^{-\frac{\mu}{\rho}\rho \cdot t} \xrightarrow[\text{8 cm tungsten at 3 MeV}]{} e^{-0.0408\times 18.0\times 8.0} = 0.28\%$$

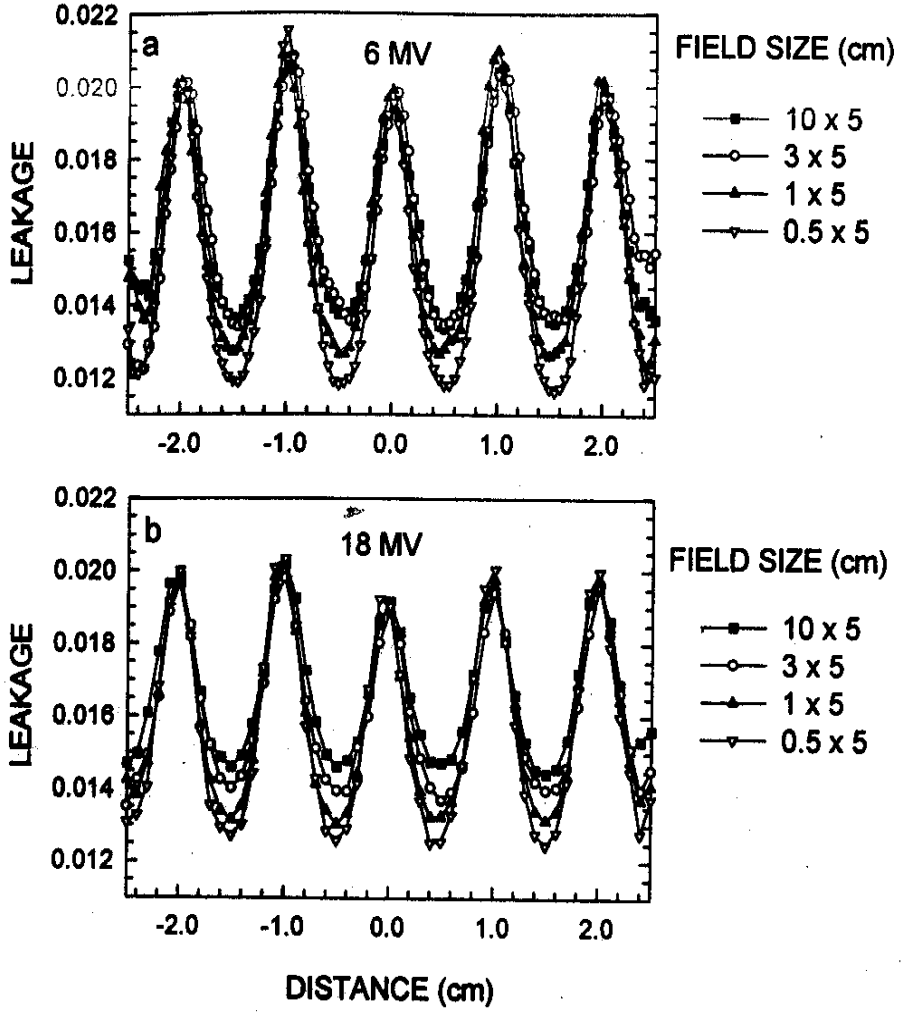

Measuements from
Arnfield *et al*, 2000 Med. Phys. **27** p 2231-2241

Summary

Multisource beam representations

- allow modelling of individual machines by parameter settings
- actual implementations **varies between TPS** with great impact on e.g. small field and VMAT/IMRT performance
- automated methods exist for parameter setting from measured data
- parameters can also be readily derived from Monte Carlo phase space data
- developed for several beam modalities

Be critical to your data!

For new, well controlled and standardized machines one may consider using a standard set of data!

Some practical considerations in beam data commissioning

1. Understand the use/purpose of **all** your data items!
   - Checked TPS vendor information?
   - How are the data driving the dose calculations?
   - Used to verify a resulting source parameterization?
   - Error propagation analysis?

2. Be critical to your beam data!
   - Best practice used?
   - Are they qualatively correct?
   - ”Common” errors checked?
   - Compared with similar data?
   - Reviewed by somebody else?

3. Be critical to your TPS!
   - What are the approximations?
   - What are your acceptance levels?
   - How to handle exceded levels?

Understanding the purpose... *Oncentra*

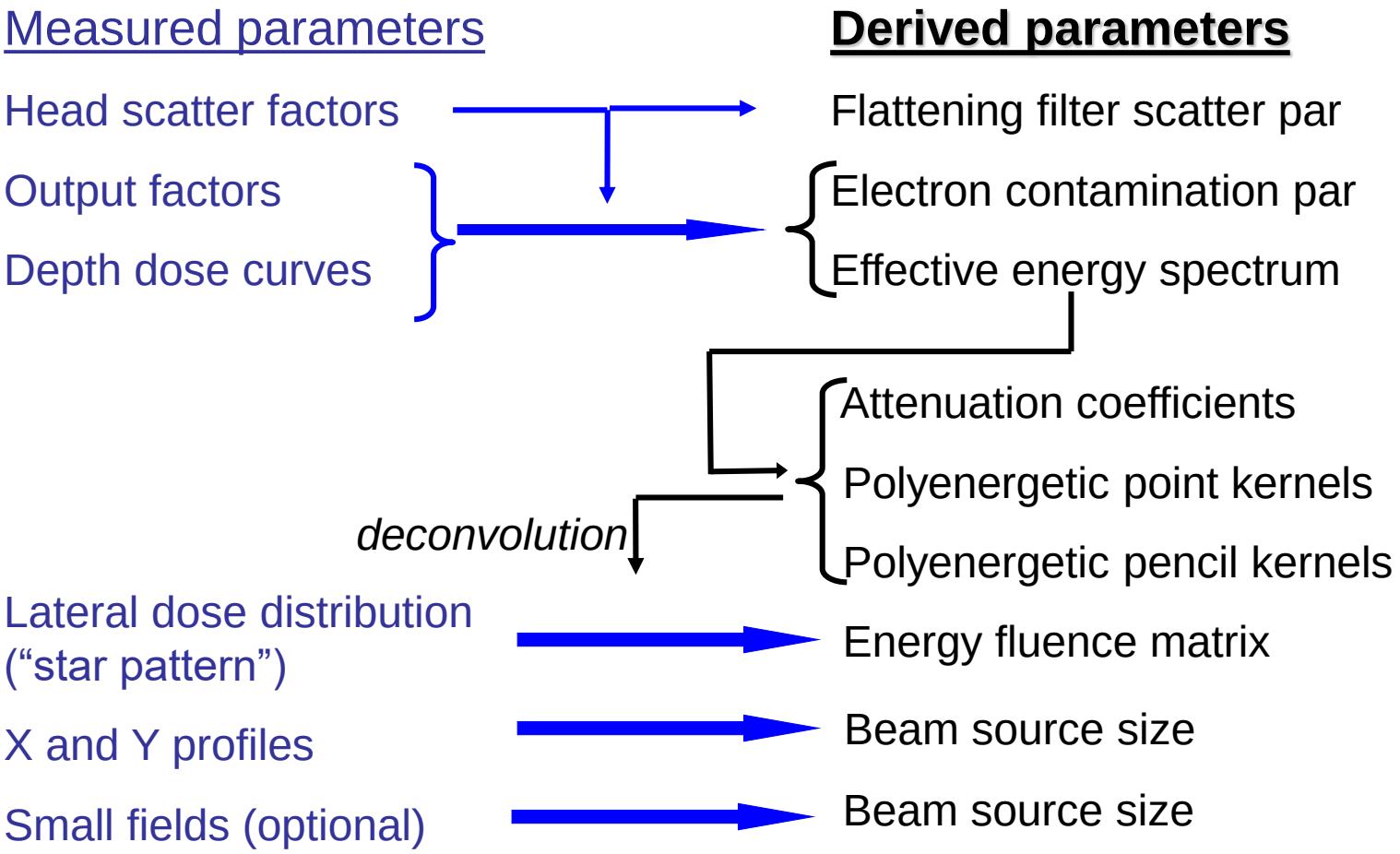

Ahnesjö *etal*, 2005 MedPhys 32 pp 1722-37

Possible errors and expected consequences
Oncentra examples

- Build-up blurring from finite sized ion chambers
  => *bad electron contamination fit*
- Penumbra blurring due to ion chamber long axis along beam edge
  => *bad effective source size fit =>bad small field D/MU*
- Partly blocked ion chambers for small fields OFair
  => *bad effective source size fit =>bad small field D/MU*
- Depth offset
  => *bad effective spectrum fit, wrong depth doses (but not as measured!)*
- Noisy data
  => *error analysis difficult*
- Too thin or too low density of build-up cap for S_c meas.
  =>*bad values of flat.filt.scat. parameters=>overestimated output variation*

What to expect from your TPS ... *Oncentra*

Mean error±1.s.d. for appr. 1000 linacs

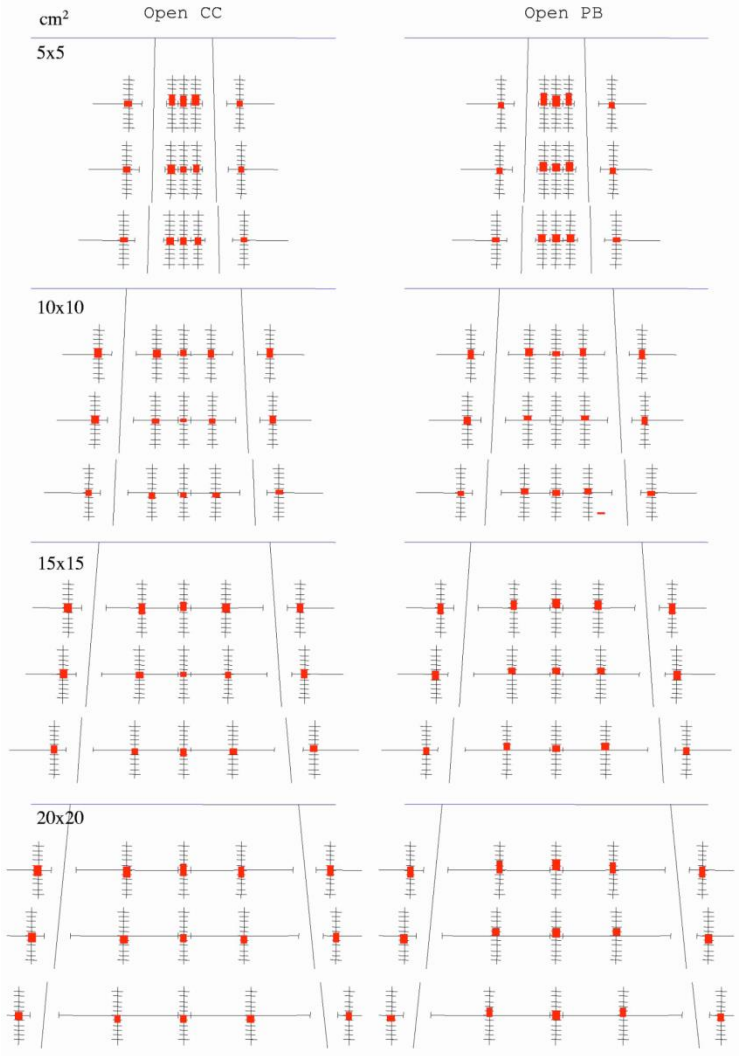

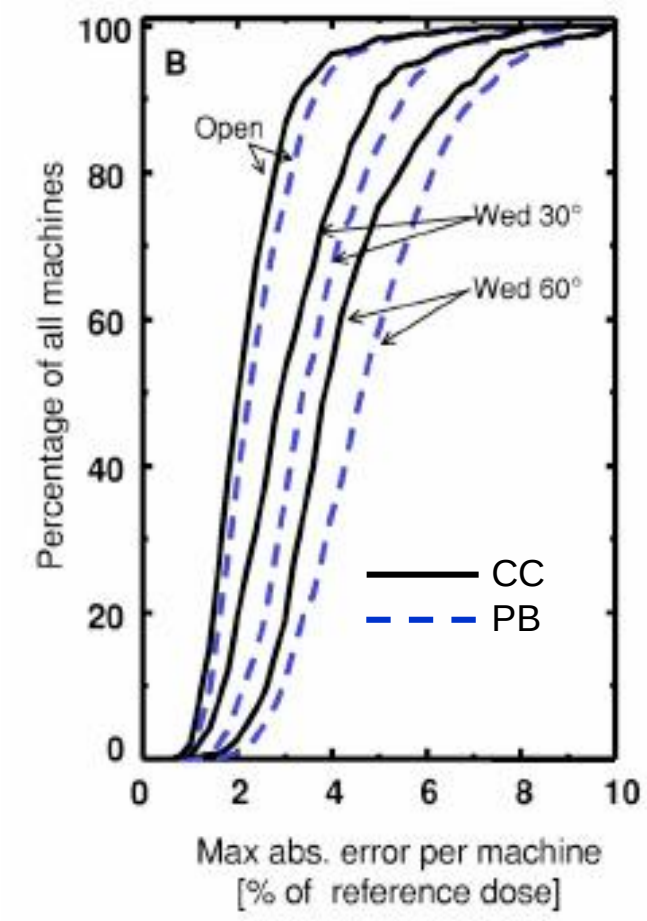

Ahnesjö *et al,* 2005 Med. Phys., Vol. 32, pp1722-37

Understanding the purpose... *Pinnacle*

Gaussian height	An increase in the value of this parameter decreases the sharpness of the transition between the low-dose gradient region outside the radiation field and the high-dose gradient region.	The accuracy of monitor unit calculations for elongated fields decreases with an increase in the value of this parameter of around 0.05. The value of this parameter increases with field size.
Gaussian width	This parameter has a similar effect on the off-axis profile as the Gaussian height parameter.	Because of the low value of the Gaussian height parameter required for accurate monitor unit calculations, this parameter has little effect on off-axis profile.
Jaw transmission	An increase in the value of this parameter increases the value of the off-axis profile in the low-dose gradient region outside the radiation field.	Changes in this parameter of 0.005 have a noticeable effect on the off-axis profile in the low-dose gradient region outside the radiation field. The value of this parameter typically increases with field size.
Modifiers		
Modifier Scatter Factor	This parameter affects off-axis profiles for wedged fields. An increase in the value of this parameter decreases the value of the off-axis ratio in the region of the thin end of the wedge and increases the off-axis ratio in the region of the thick end of the wedge.	Changes in this parameter of 0.1 are needed to have a noticeable effect on the off-axis profile. The value of this parameter typically increases with field size.
Electron Contamination		
Maximum Depth (cm)	The value of this parameter is determined by the energy of the radiation beam and is typically set to be approximately $2 \times d_{max}$.	The exact value of this parameter is not too critical. It is independent of field size.
Surface dose (Dose/Fluence)	Increasing the value of this parameter increases the dose at very shallow depths to the region of electron	The exact value of this parameter is not critical, as the tolerance of the accuracy of the model near the surface is significantly looser than elsewhere.

Understanding the purpose... *Pinnacle – ABMOS*

(automated beam model optimization system)
Létourneau *etal* Med. Phys. 37 „5, 2010, pp2110

TABLE I. Description of the beam model parameters a

	Available for optimization
Description	Abbre
- MLC transmission	%
- Jaw transmission	$\%T_{X\text{-jaws}}$
- MLC interleaf leakage	L_{height} and
- Orthogonal source size	S_X a
- Extrafocal scatter source	G_{height} and
- Geometric correction for rounded leaf MLC leaf-end	Pc

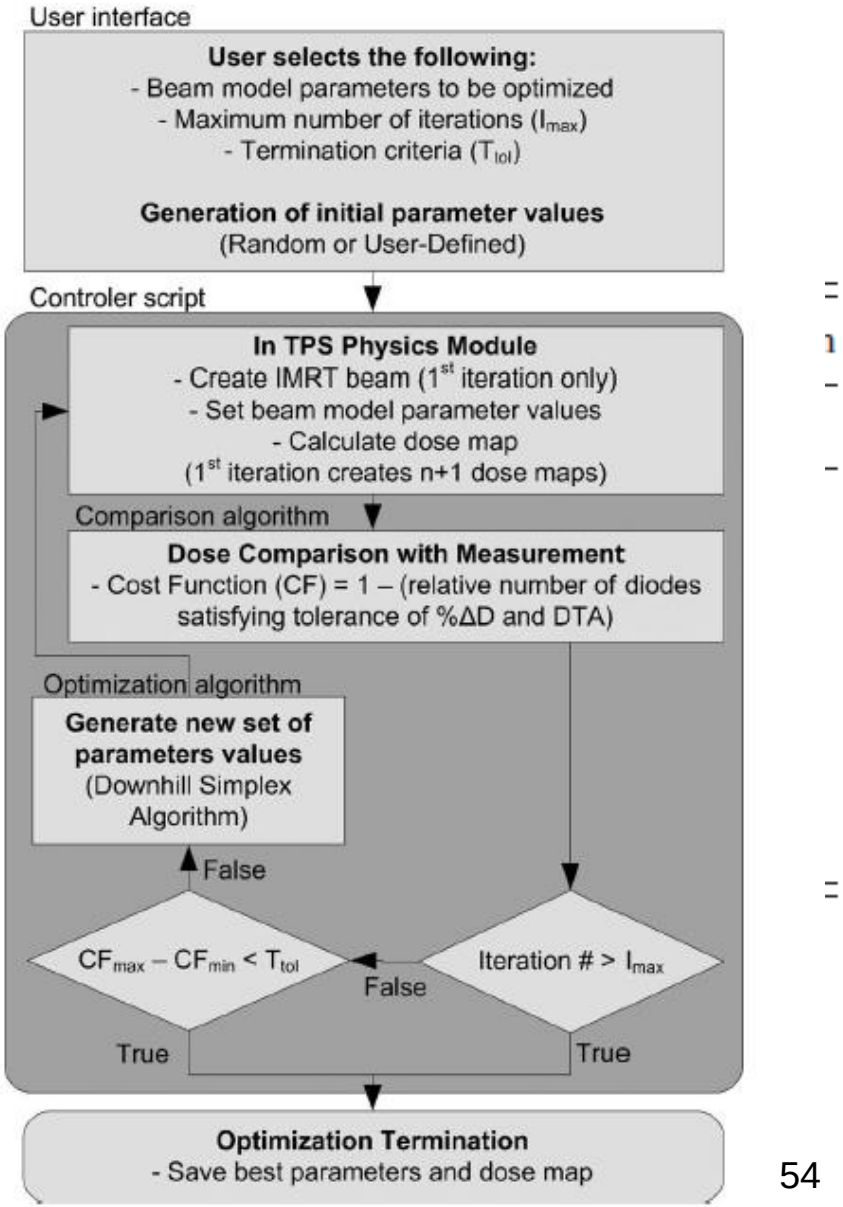

Understanding the procedure... *RayStation*

10.5.2 A step-by-step instruction for beam commissioning

Step 1 – Perform the steps which are prerequisites for auto-modeling

Step 2 – Remove electrons

Step 3 – Output Factor Corrections Auto Modeling

Step 4 – Photon Energy Spectrum Auto Modeling To constrain the auto-modeling towards physically feasible shapes use the auto-modeling step Energy spectrum (Parameterized) described in *section 8.5.6 Energy spectrum (Parameterized) on page 137*.

Step 5 – Electron Contamination Auto Modeling

Step 6 – Beam Profile and Off Axis Softening

Step 7 – Sources

Step 8 – Collimator calibrations

Step 9 – Off axis

Step 10 – Depth dose curves revisited

Step 11 – MLC parameters

If MLC collimated fields are used, try to tune the MLC parameters **Tongue and groove**, **Leaf tip width** and **MLC Collimator calibration x-position**. The MLC x-position **Offset** can be compared to a MLC leaf gap.

Understanding the purpose... *Eclipse*

2.3. The optimization procedure for parameter derivation

The proposed automatic optimization procedure is based on the minimization of an objective function measuring the deviation between dose calculations and measurements. To obtain acceptable calculation times, a fast point dose calculation method ($M_{\text{p.d.}}$) presented in section 2.2.2 is used during the optimization instead of the volumetric calculation method ($M_{\text{v.d.}}$) presented in section 2.2.1. Since $M_{\text{p.d.}}$ is only capable of calculating the photon dose, $M_{\text{v.d.}}$ is still used to derive the electron contamination parameters. The procedure consists of the following phases:

(i) Resampling, adjustment and scaling of the measured beam data.
(ii) Initial optimization of photon parameters $\bar{E}(r)$, $I(r)$, σ_{ef}, w_{ef} and $\bar{E}_{\text{ef}}$ using Powell's direction search method. The measurements in the build-up region are ignored in this phase.
(iii) Optimization of the electron contamination parameters $\sigma_{\text{e},1}$, $\sigma_{\text{e},2}$, c, and the weights $w_{\text{e},i}$ $(i = 1, \ldots, 6)$ for $c_{\text{e}}(z)$ based on the differences between the measured PDDs and calculated PDDs without electron contamination.
(iv) To allow the use of $M_{\text{p.d.}}$ also in the build-up region, the differences between $M_{\text{p.d.}}$ and $M_{\text{v.d.}}$ are evaluated at the current parameter values. The differences are mostly due to the inability of $M_{\text{p.d.}}$ to calculate the electron dose. The measured beam data, which are used as an optimization target, are replaced by the original measurements subtracted by the differences.
(v) Refining the optimization based on the modified measurement data to take the measurements in the build-up region into account.

The optimization process is not sensitive to the initial parameter values used in step (ii), which is demonstrated with an example case in section 3.1. In the following sections the above steps are described in more detail.

Tillikainen *etal*, 2007 PhysMedBiol 52 pp 1441-67

Be critical to your data – compare with others...

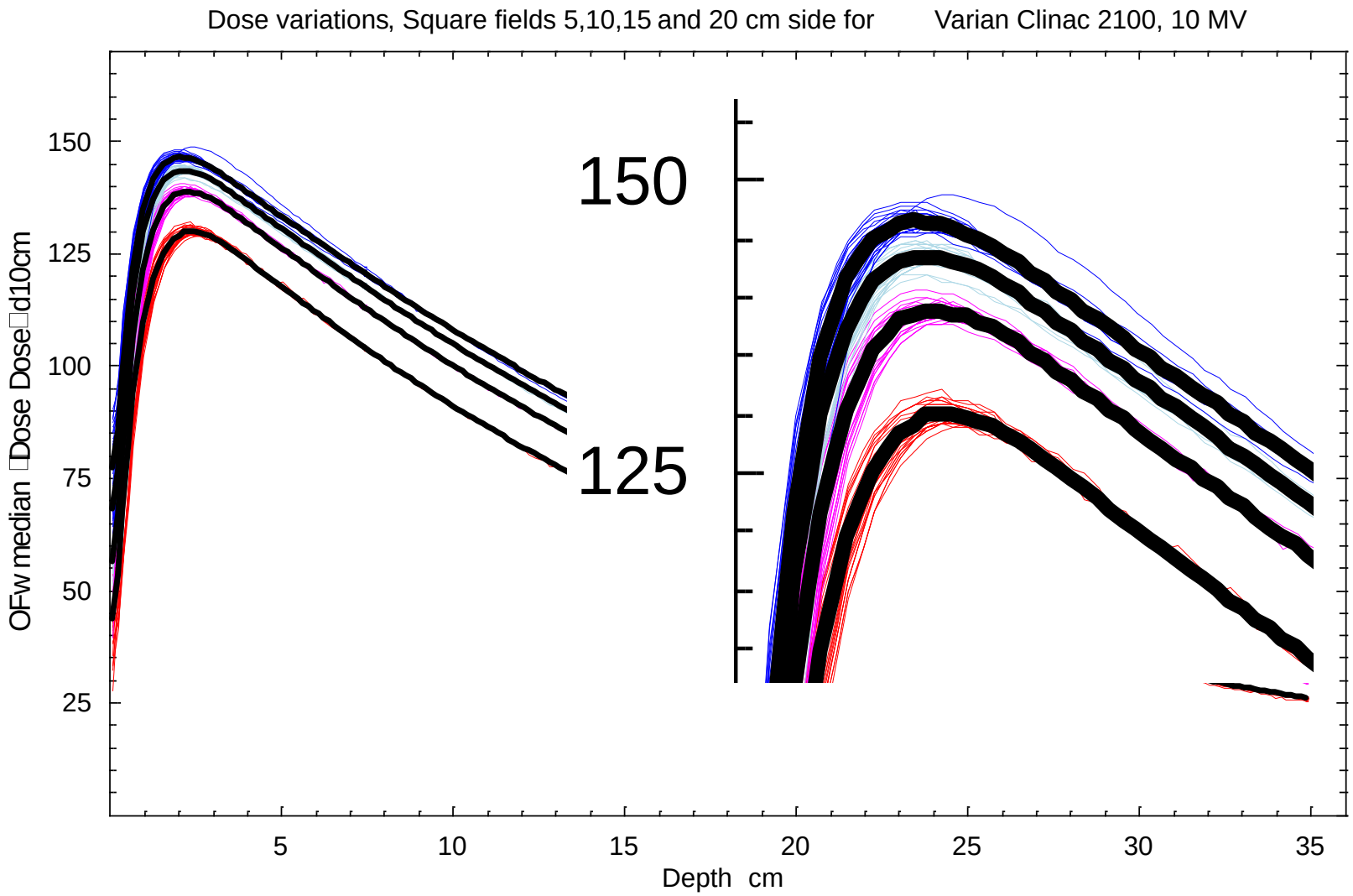

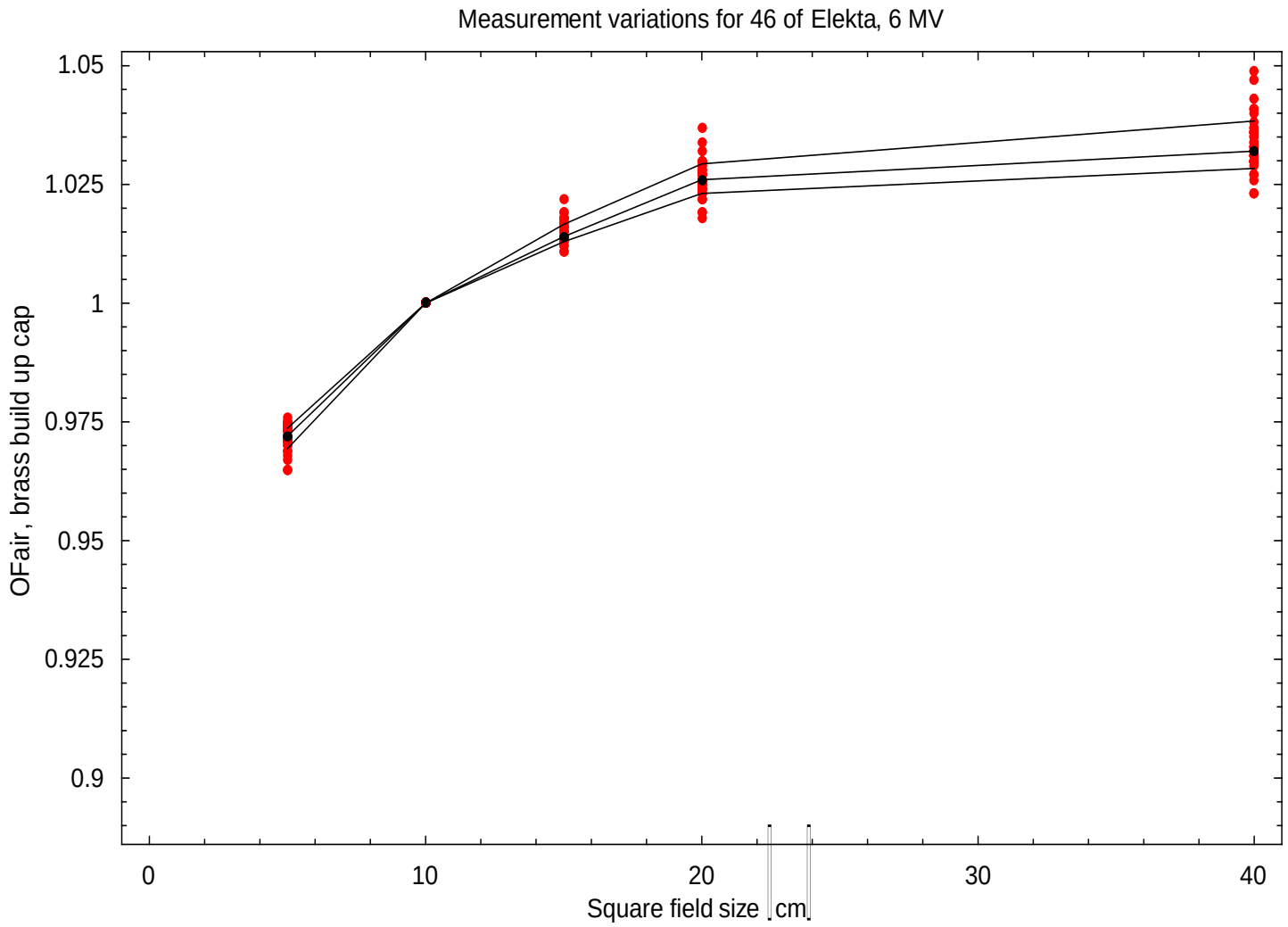
Measurement variations for 46 of Elekta, 6 MV
OFair, brass build up cap
1.05
1.025
1
0.975
0.95
0.925
0.9
0
10
20
30
40
Square field size cm

Be critical to your data – best practice used?

Report of AAPM Therapy Physics Committee Task Group 74: In-air output ratio, S_c, for megavoltage photon beams

The **in-air output ratio**, S_c is now defined as the ratio of primary collision water kerma in free-space, K_p, per monitor unit between an arbitrary collimator setting, c, and the reference collimator setting, c_{ref}, at the same location on the central axis,

$$S_c(c) \equiv \frac{K_p(c;z_{ref})/\mathrm{MU}}{K_p(c_{ref};z_{ref})/\mathrm{MU}}, \quad (3)$$

where z_{ref} is the reference source-to-detector distance (usu-

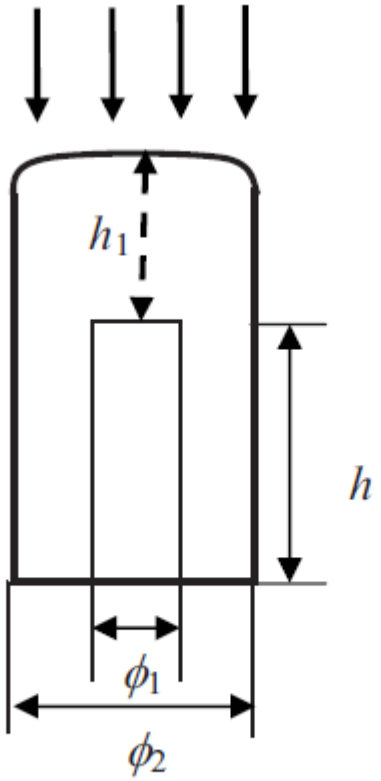

FIG. 10. Schematics of a brass miniphantom recommended for measurements of S_c for square fields larger than 1.5×1.5 cm^2 and photon energy less than 25 MV.

Be critical to your data – best practice used?

Accelerator beam data commissioning equipment and procedures: Report of the TG-106 of the Therapy Physics Committee of the AAPM

IPEM Report: Small Field MV Photon Dosimetry

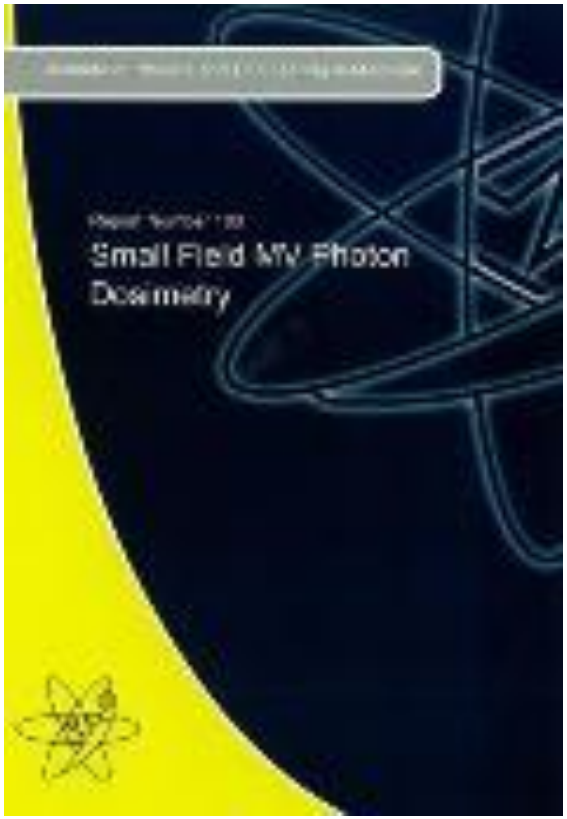

The most practical item is to have a good theory (and to understand it...)!

ESTRO School

WWW.ESTRO.ORG/SCHOOL

Small MV photon fields

Measurement challenges

Maria.Aspradakis@luks.ch

Learning objectives

- The physics of small MV photon fields: small field conditions and characteristics
- Determination of dose in small fields: reference and relative dosimetry
- IAEA/AAPM formalism for dosimetry in static and composite fields

The physics of small MV photon fields

The conditions that determine whether a field is classified as small are:

1. Loss of lateral charged particle equilibrium (CPE)
2. Partial occlusion of the primary photon source by the collimating device
3. The detector perturbs particle fluence because of its size (too large in comparison to the field size) and/or its composition

1. Lateral electron disequilibrium (lack of lateral CPE)

Lateral charged particle loss

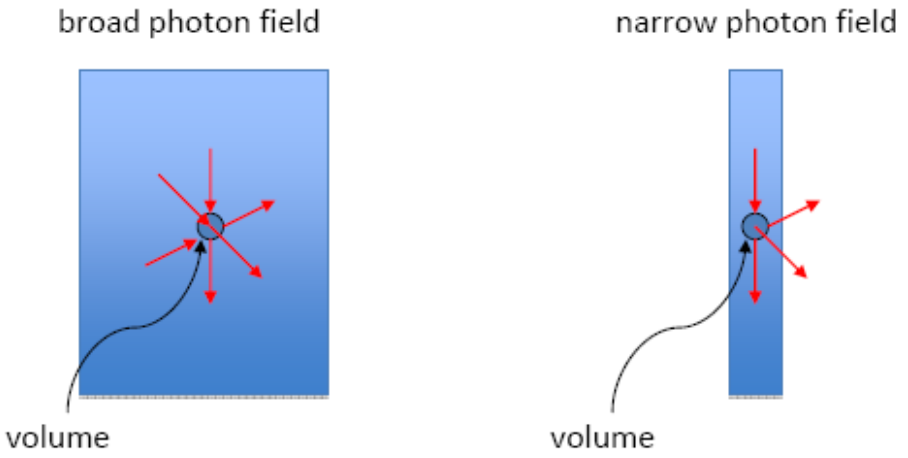

A small field can be defined as a field with a size smaller than the "lateral range" of charged particles

$\frac{D}{K_{\text{coll}}}$ *is a measure of the degree of equilibrium or transient equilibrium*

1. Lateral electron disequilibrium (lack of lateral CPE)

Minimum field radius required for lateral electron equilibrium (r_{LEE})

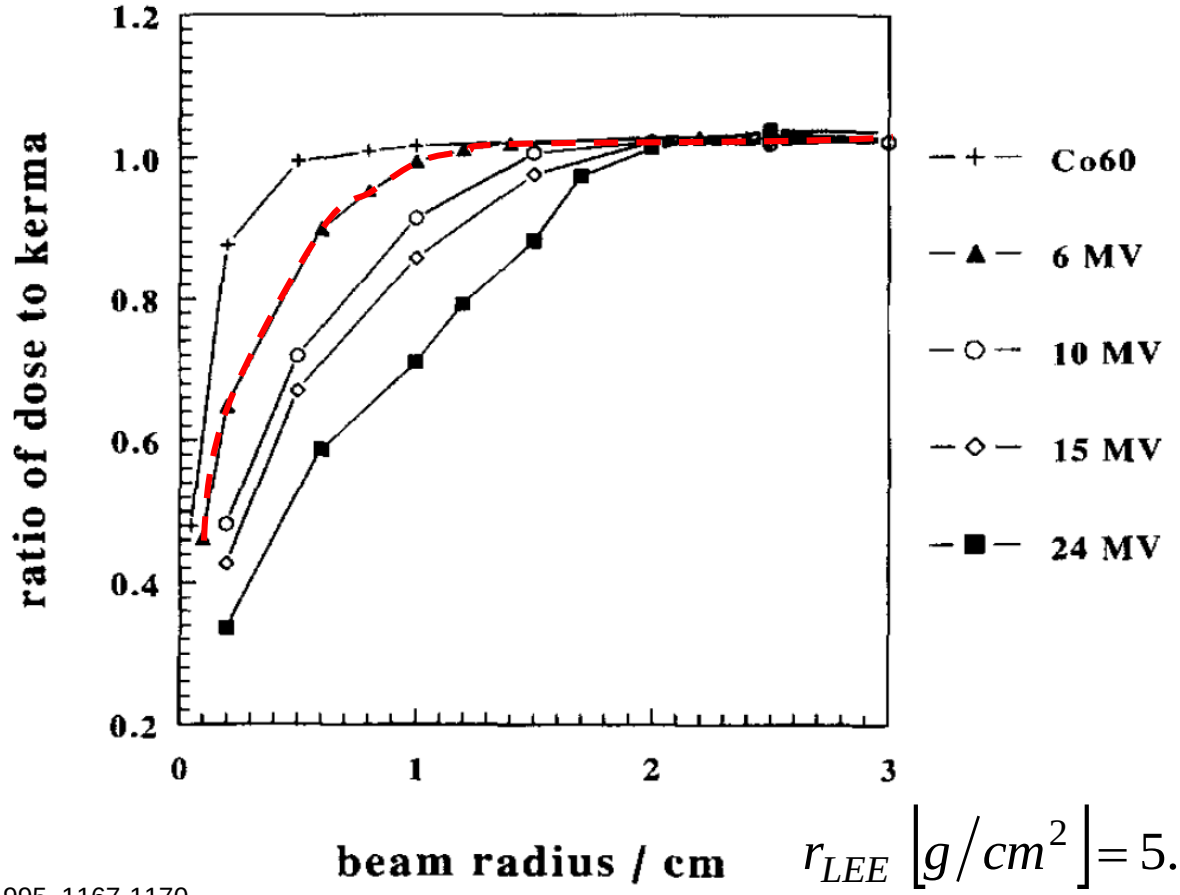

$$r_{LEE}\left[g/cm^2\right] = 5.973 \times TPR_{10}^{20} - 2.688$$

Li et al MedPhys **22**, 1995, 1167-1170

2. Occlusion of the primary source

In broad fields:

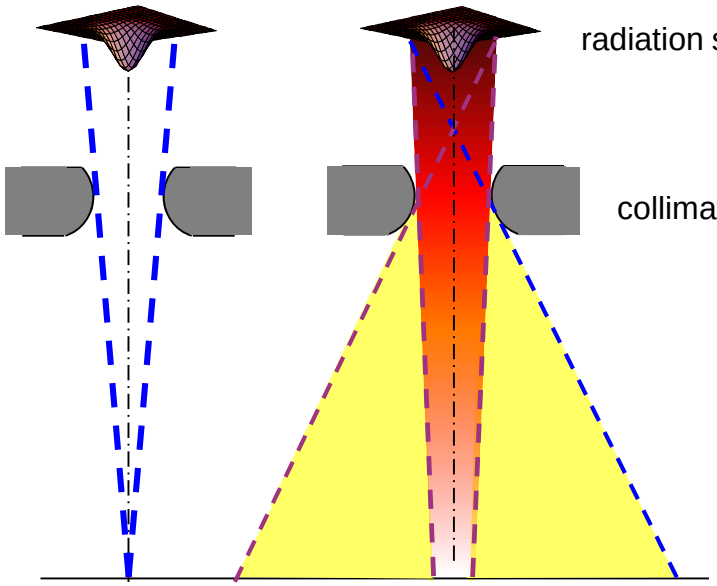

Full view of extended direct beam source from the point of measurement

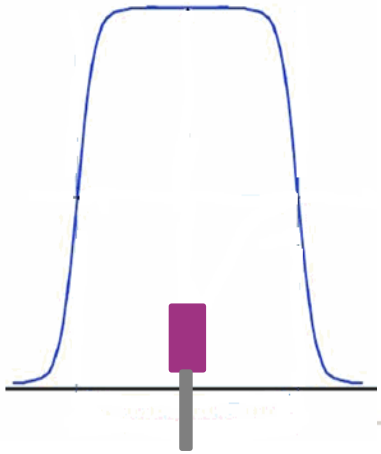

Dose variation across a broad field (‘dose profile’)

Radiation detector measures in region of uniform dose

ESTRO School

2. Occlusion of the primary source

In narrow fields:

Occlusion of the beam
focal spot
with decreasing collimator
setting

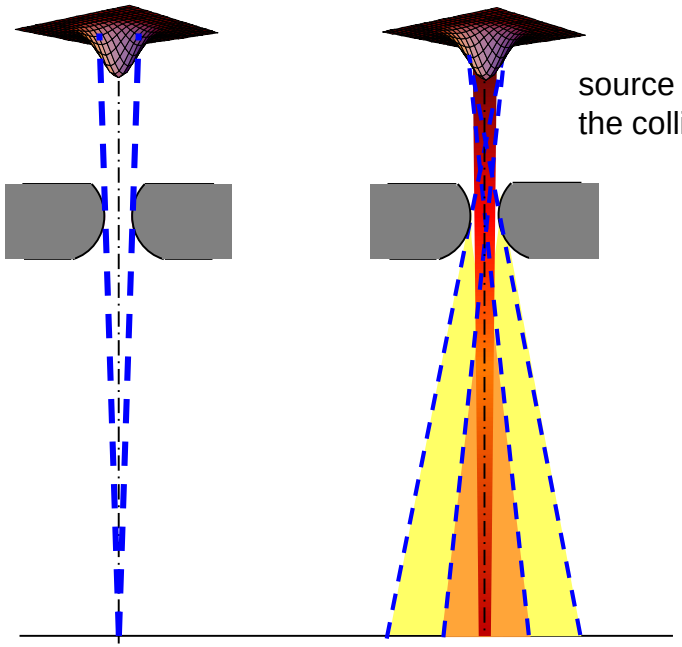

source occlusion by
the collimators

Partial view of
extended direct
beam source from
the point of
measurement

Very narrow dose profile

Radiation detector
measures in non-uniform
dose region

ESTRO School

2. Occlusion of the primary source

Overlapping penumbras

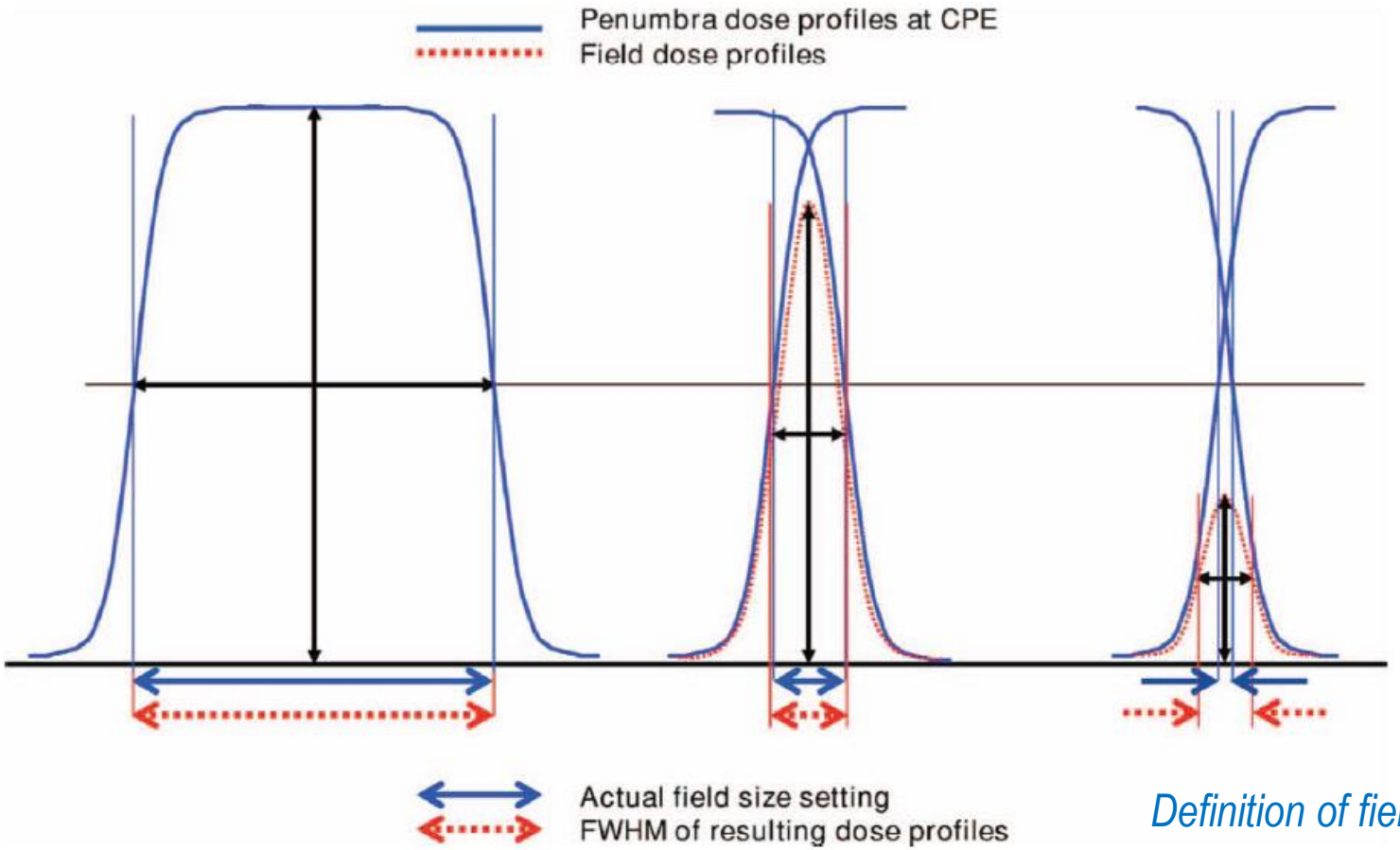

Definition of field size?

3. Detector response (detector perturbation effects)

Detector size:

a) Volume averaging (the size of the detector relative to the size of the radiation field)

Detector composition:

b) Density of sensitive volume of the detector

c) Atomic properties of the sensitive volume of the detector

d) Influence of detector components other than its sensitive volume (extra-cameral components)

Detector size: a) volume averaging

The detector produces a signal that is proportional to the mean absorbed dose over its sensitive volume and this signal is affected by the homogeneity of the absorbed dose over the detection volume

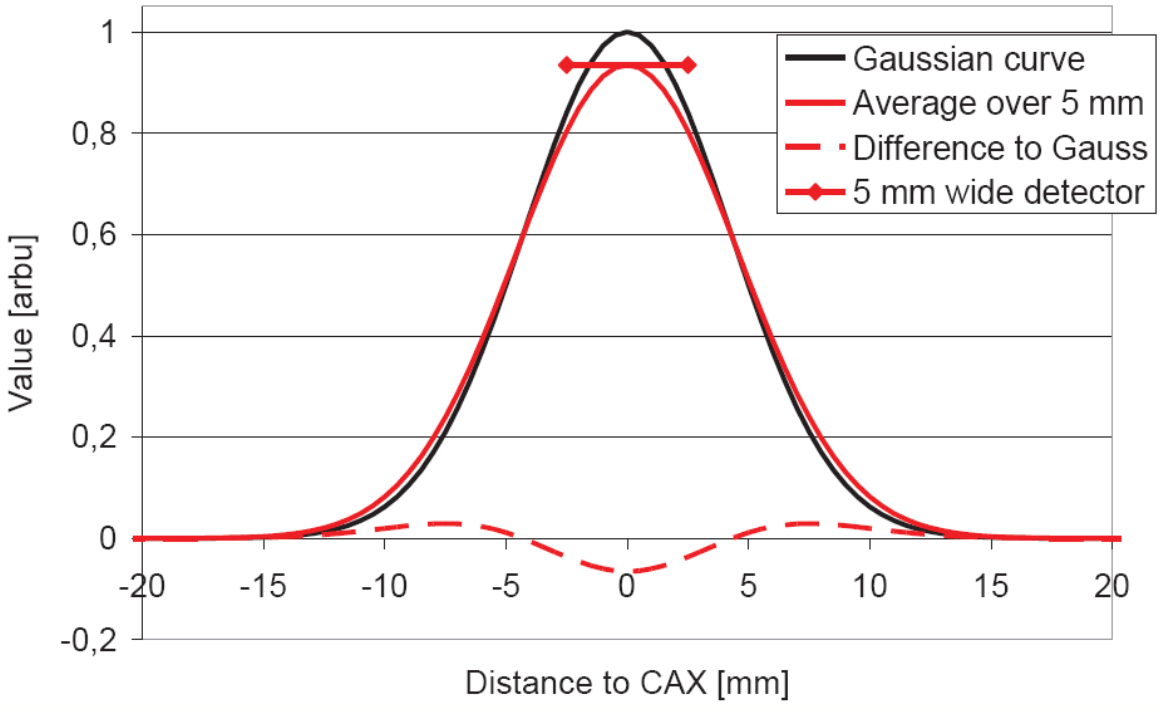

Wuerfel, J. U., Medical Physics International Journal, vol 1, no 1, 2013

ESTRO School

Detector size: a) volume averaging

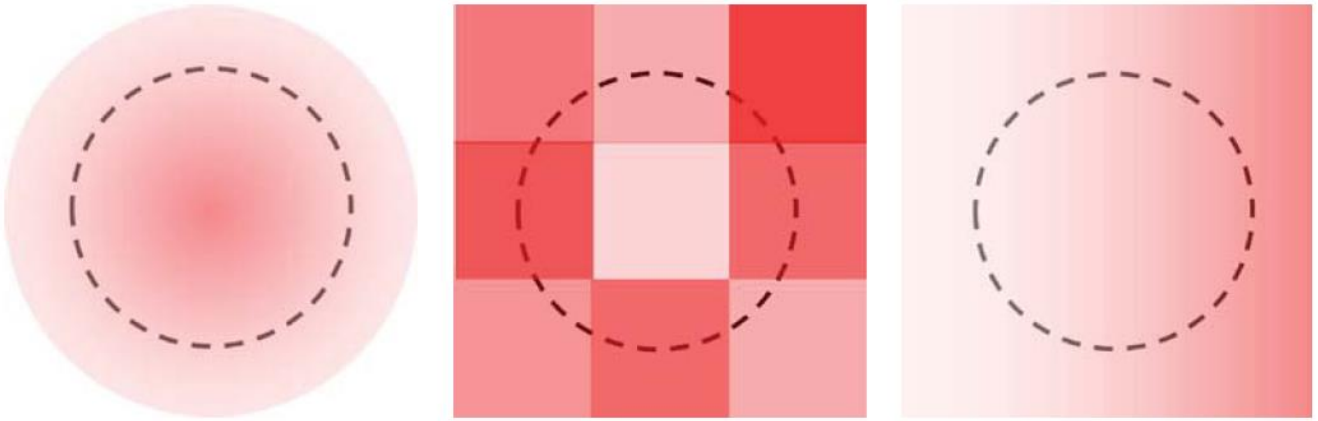

FIG. 4. Beam's-eye view illustrations of the lateral volume averaging effects in a pancake-like detector (sketched in a dashed line): (a) the maximum absorbed dose being at the point of measurement (the centroid of the pancake), (b) a modulated beam where absorbed dose of interest is smaller than the average absorbed dose over the detector cavity, and (c) a wedged beam with linear lateral fluence gradient.

Bouchard H et. al ., Med. Phys. 42 (10), 6033-47, Oct 2015

3. Detector response (detector perturbation effects)

Detector size:

a) Volume averaging (the size of the detector relative to the size of the radiation field)

Detector composition:

b) Density of sensitive volume of the detector

c) Atomic properties of the sensitive volume of the detector

d) Influence of detector components other than its sensitive volume (extra-cameral components)

Detector composition

Ionization chambers

wall, central electrode, air cavity

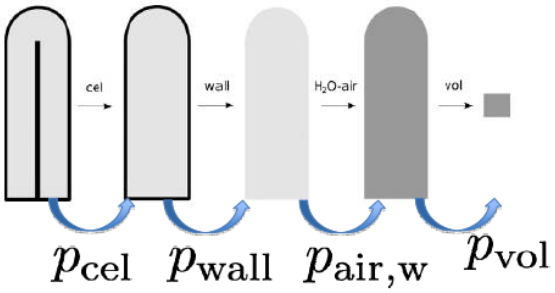

Crop *el al* (2009), PMB,54(9), 2951-2969, 2009

In recent years, Monte Carlo methods have been invaluable in analysing in detail various types of perturbation factors and from these deriving a total perturbation correction factor for ionisation chambers.

Diodes

housing, shielding, sensitive volume

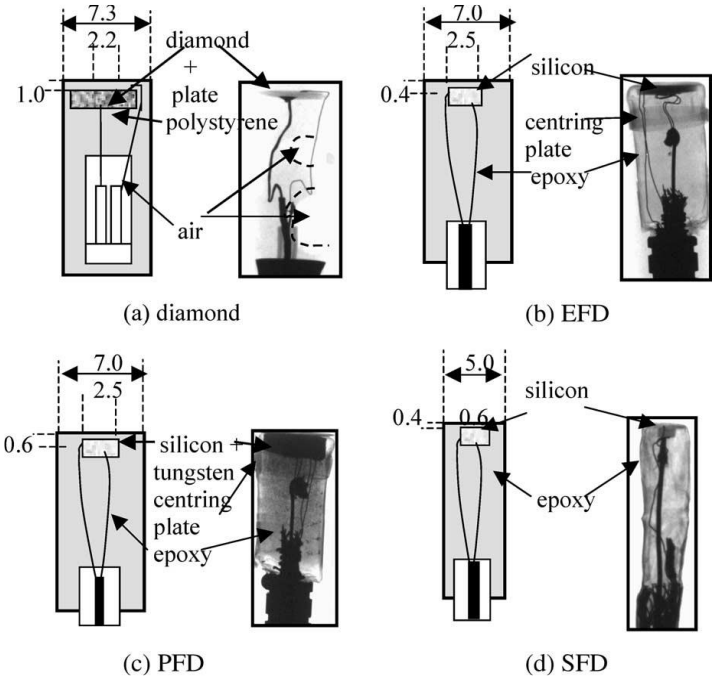

C. McKerracher, D.I. Thwaites /
Radiotherapy and Oncology 79 (2006) 348–351

Detector composition: perturbation effects in small fields

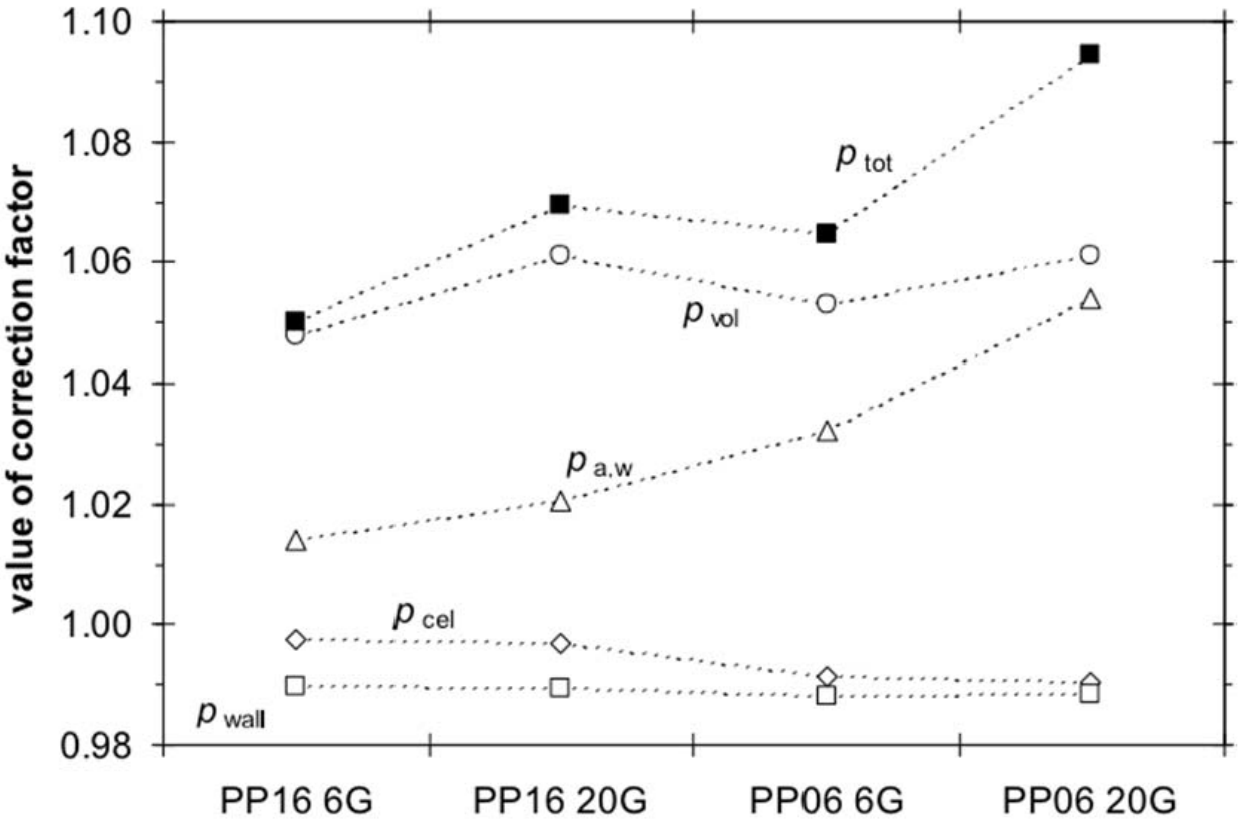

PinPoint 31016
0.016 cm^3

PinPoint 31015
0.015 cm^3

6MV

0.8 cm × 0.8cm

Calculations with Monte Carlo methods

Source sizes (FWHM) used in simulations:
0.6mm (6G)
2.0mm (20G)

Graph compiled with data from
Crop *el al* (2009), PMB,54(9), 2951-2969, 2009

Detector composition: b) density of sensitive volume

cavity theory:

$$\frac{D_{\text{water (at a point)}}}{D_{\text{detector (averaged over its sensitive volume)}}}$$

$$\frac{D_{\text{water-voxel in water}}}{D_{\text{detector-voxel in water}}}$$

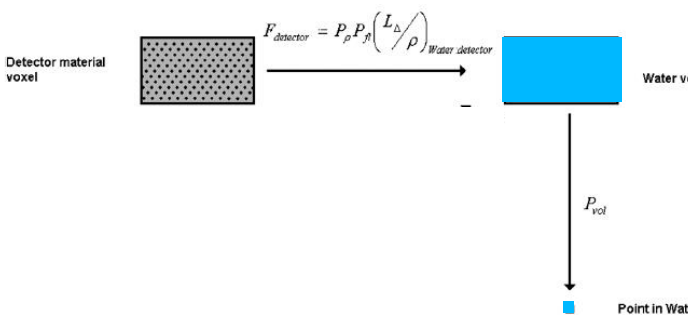

$$\frac{D_{\text{water-voxel in water}}}{D_{\text{water-voxel with detector density in water}}}$$

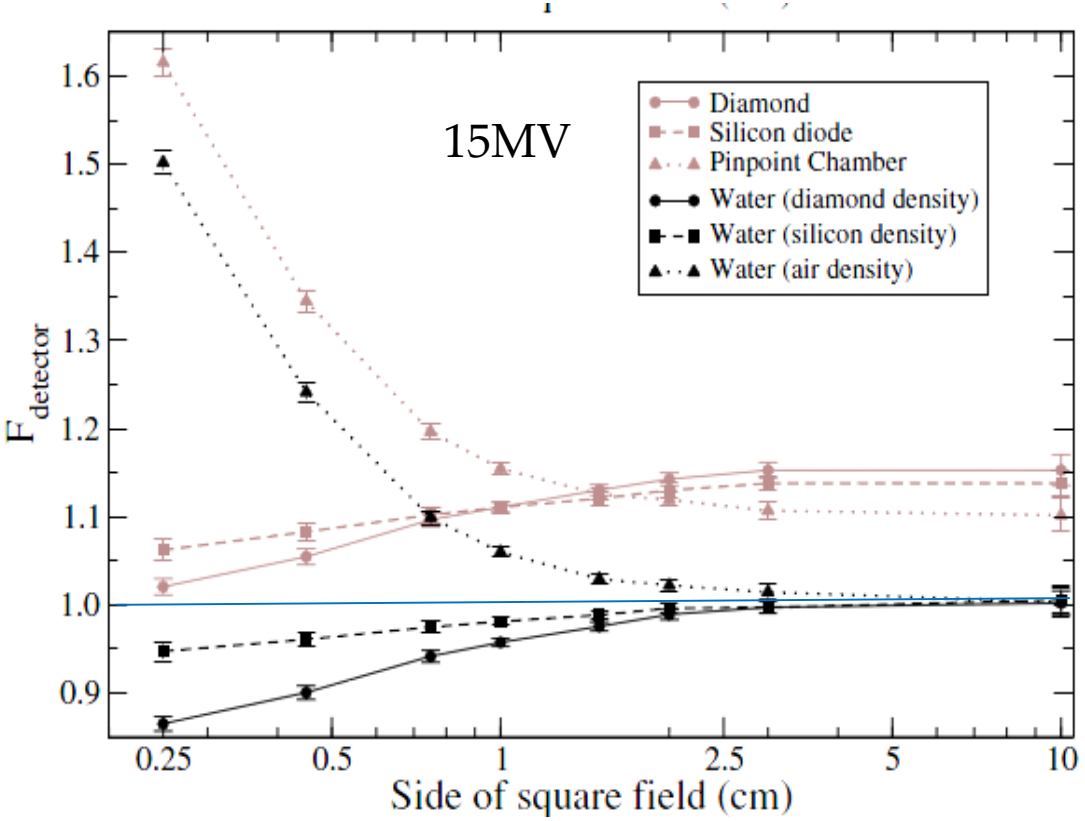

*Voxel has the size of the sensitive volume of the detector

Scott et al PMB, 57 (2012) 4461-4476

ESTRO School

Detector composition: b) density of sensitive volume

Detector response in small photon fields has been recently investigated in detail by Bouchard *et al* by calculating the absorbed dose in the detector cavity as a sum of absorbed doses from **1.25MeV pencil beams** incident on cavities with different densities (cavity of 5mm radius and 2mm thickness)

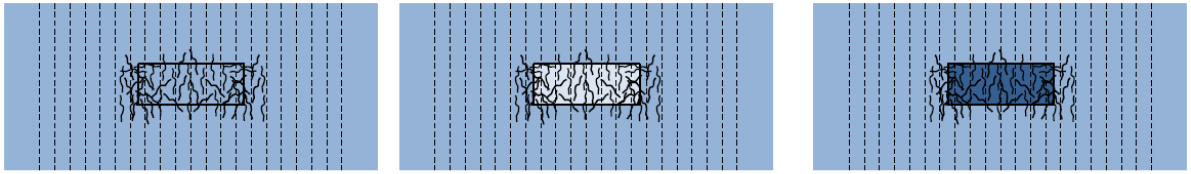

Water cavity | Vapor cavity | Dense-water cavity

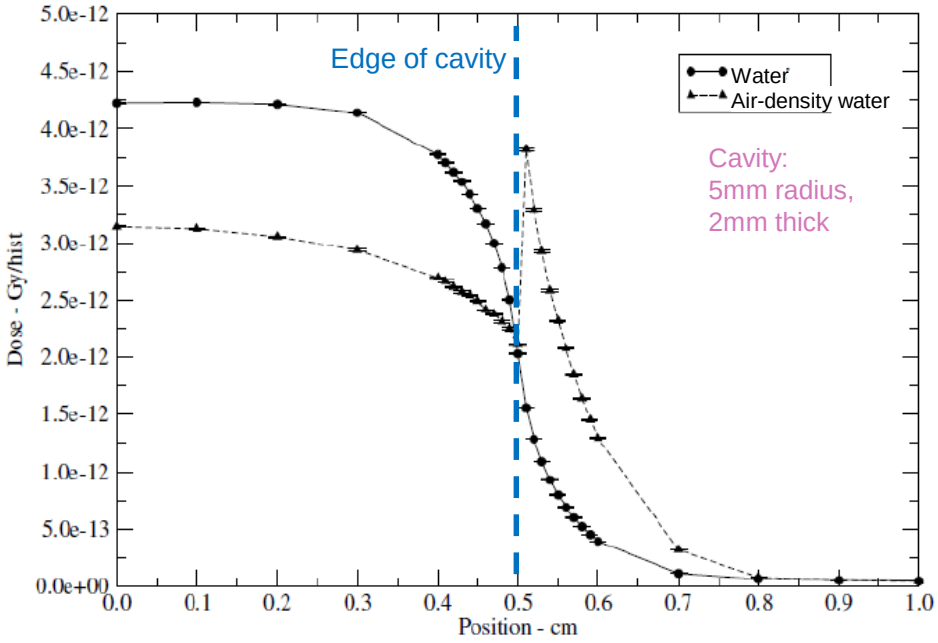

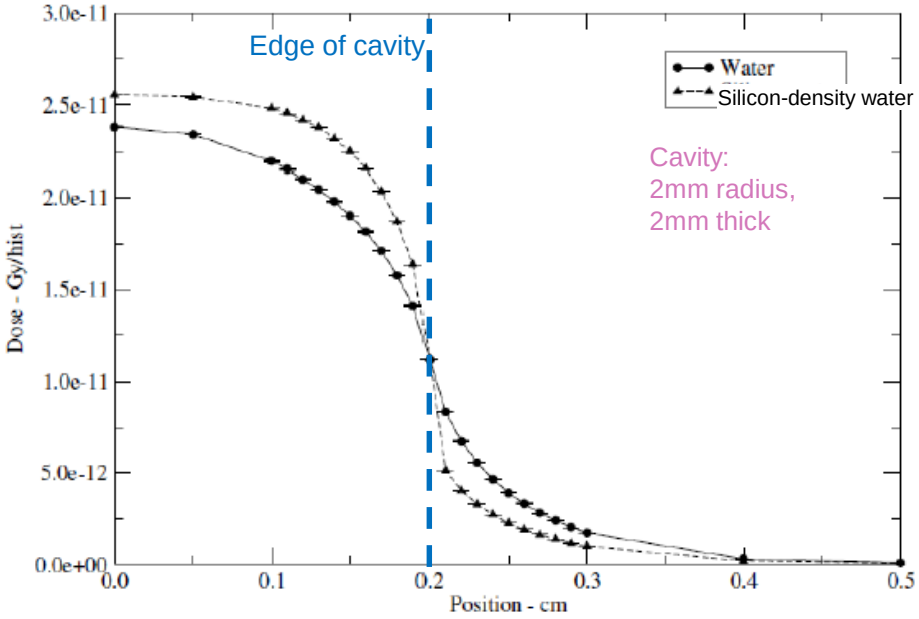

Bouchard et al, Med. Phys. 42 (10), 6048-61, Oct 2015
Hugo Bouchard, MV Photon Dosimetry; Small field considerations, NPL, Jan 2016

ESTRO School

Detector composition: c) atomic composition

Atomic properties of the detector also have an effect on the interaction cross sections and influence the response of the detector. These are:

- The atomic number Z (Z-dependence in photo-electric effect, pair production)
- The I-value (mean excitation energy or potential related to stopping power, linearly increasing with Z)
- The density effect parameter δ (reduction in the collision stopping power)

Monte Carlo simulations of cavity dose response to 1.25MeV photon pencil beams in cavity of identical electron density (water), but different atomic composition

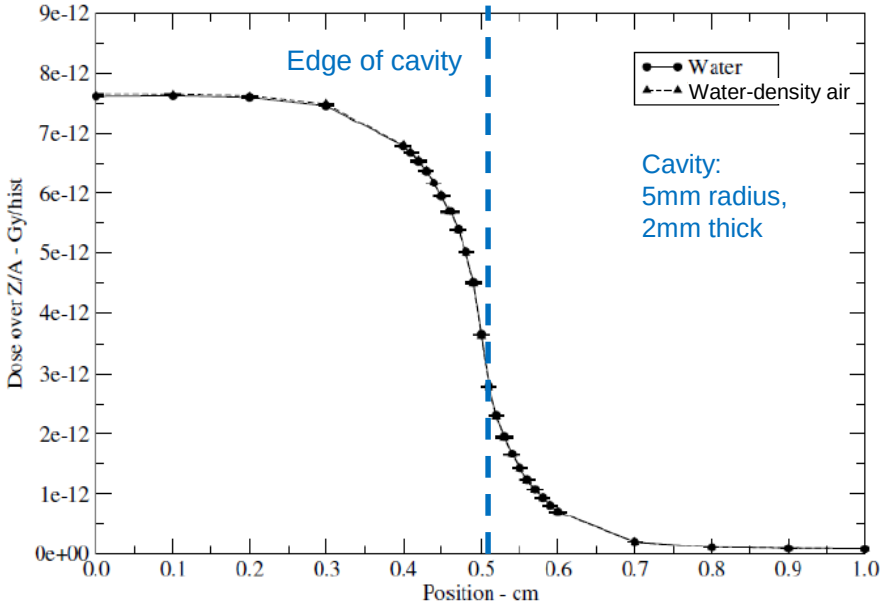

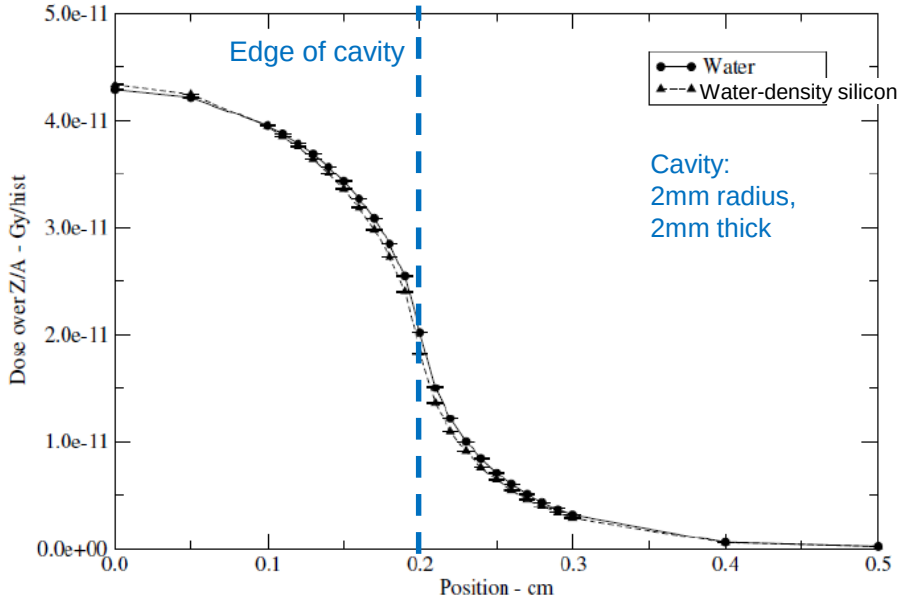

Atomic composition perturbation effects significantly smaller in comparison to density perturbation effects

Bouchard et al, Med. Phys. 42 (10), 6048-61, Oct 2015

ESTRO School

Detector composition: d) extracameral effects

Extra-cameral components refer to walls, electrodes, stems. These also affect detector response

Monte Carlo simulations of cavity dose response to 1.25MeV photon pencil beams with the cavity surrounded by a wall

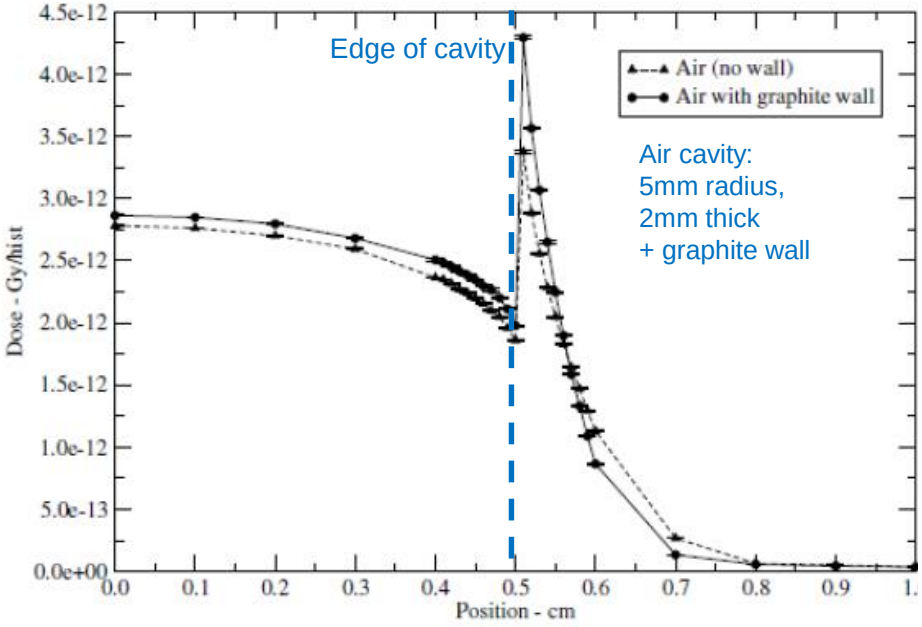

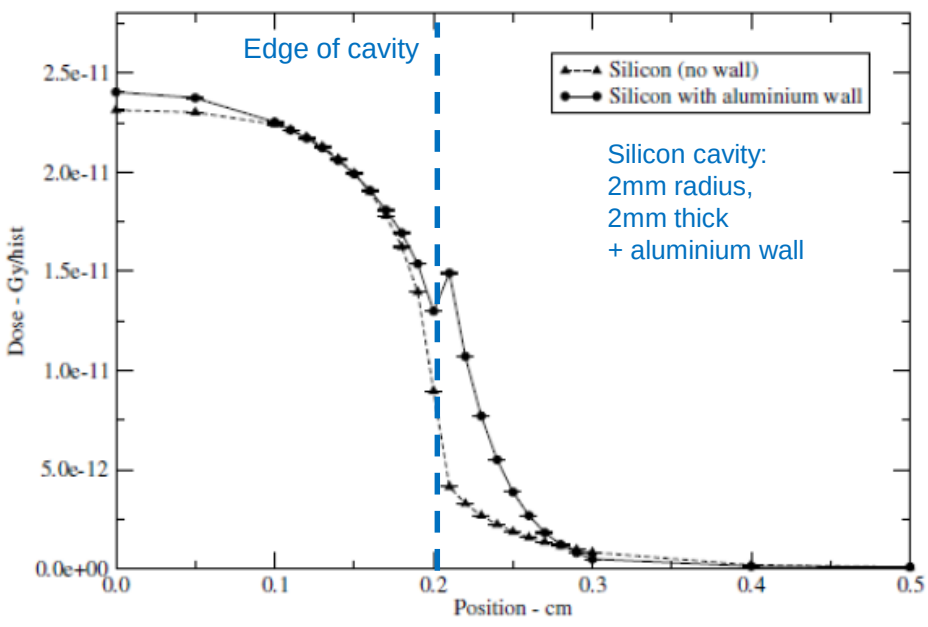

Extracameral perturbation effects can be significant in comparison to density perturbation effects

Bouchard et al, Med. Phys. 42 (10), 6048-61, Oct 2015

ESTRO School

Detector composition: b) density of sensitive volume

$$\frac{D_{\text{water-voxel in water}}}{D_{\text{detector-voxel in water}}}$$

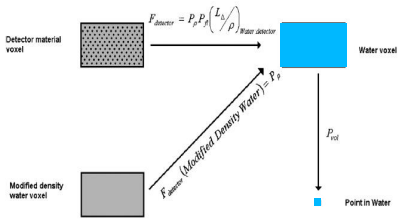

$$\frac{D_{\text{water-voxel in water}}}{D_{\text{water-voxel with detector density in water}}}$$

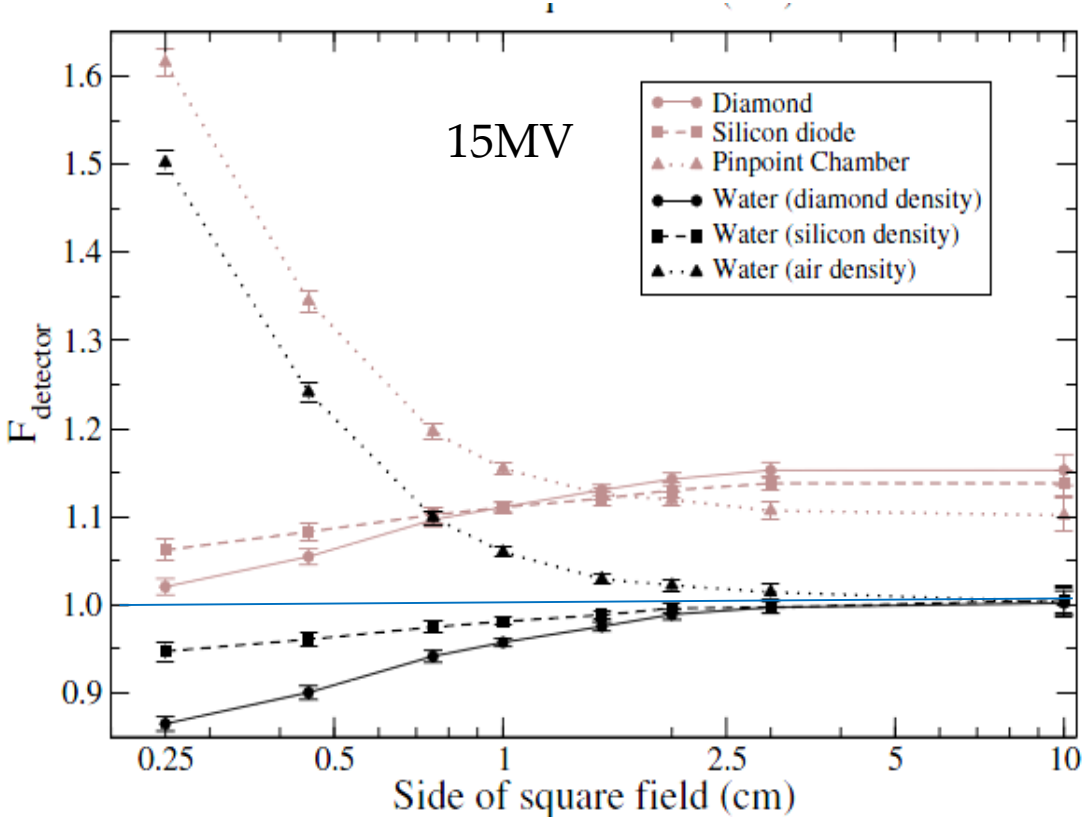

*Voxel has the size of the sensitive volume of the detector

Scott et al PMB, 57 (2012) 4461-4476

Small MV photon fields: characteristics

- changes in beam spectra with collimating method, accelerating potential, field size and depth
- dose profiles: overlapping penumbra & apparent widening of field
- drop in beam output

Small MV photon fields: characteristics

Photon energy fluence spectra in water - variation with field size and depth in water

6MV

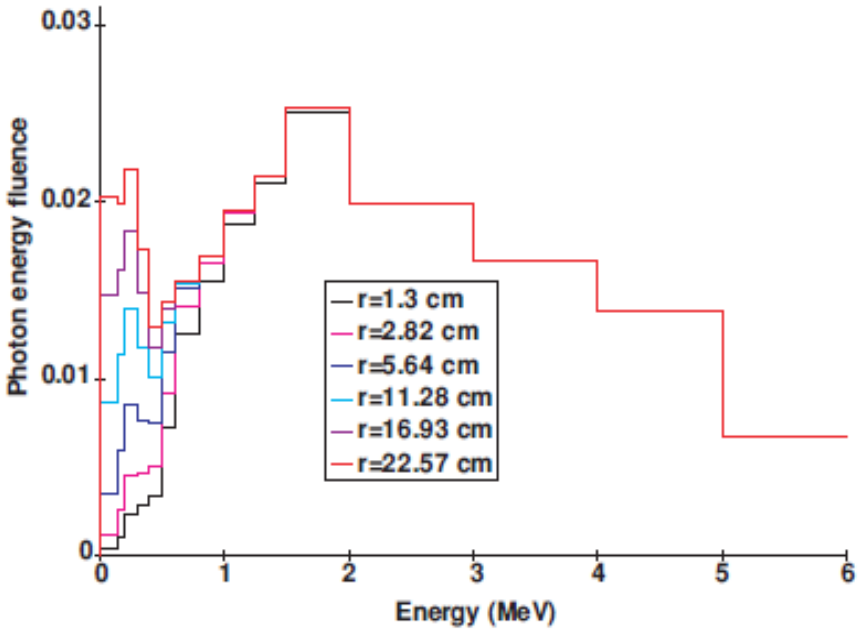

at depth of maximum build-up

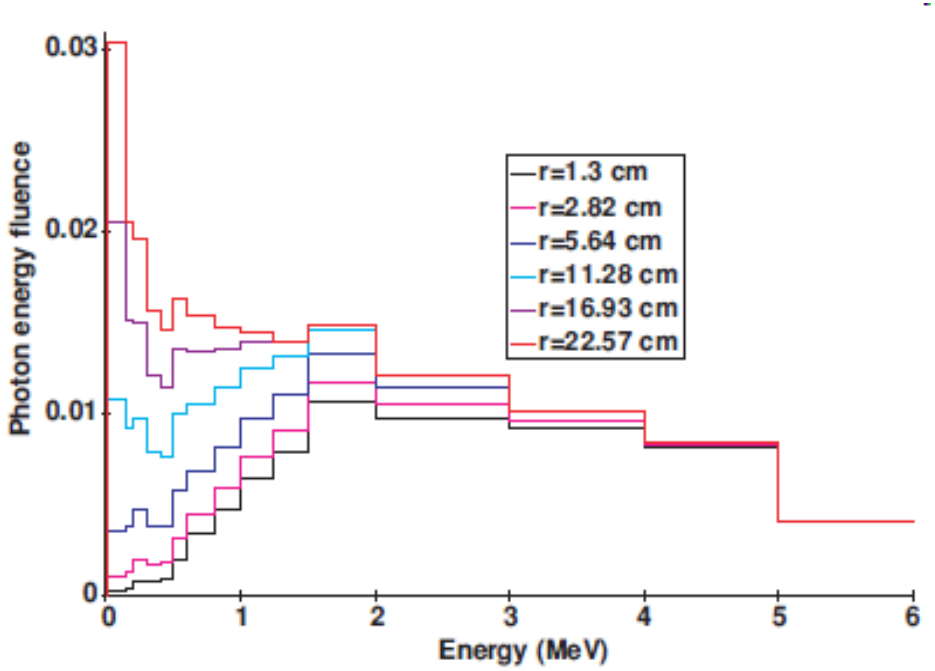

at 150mm depth

Yin et al Phys Med Biol 49(16) (2004)

Small MV photon fields: characteristics

Particle fluence spectra in water - variation with field size, 6MV 50mm depth

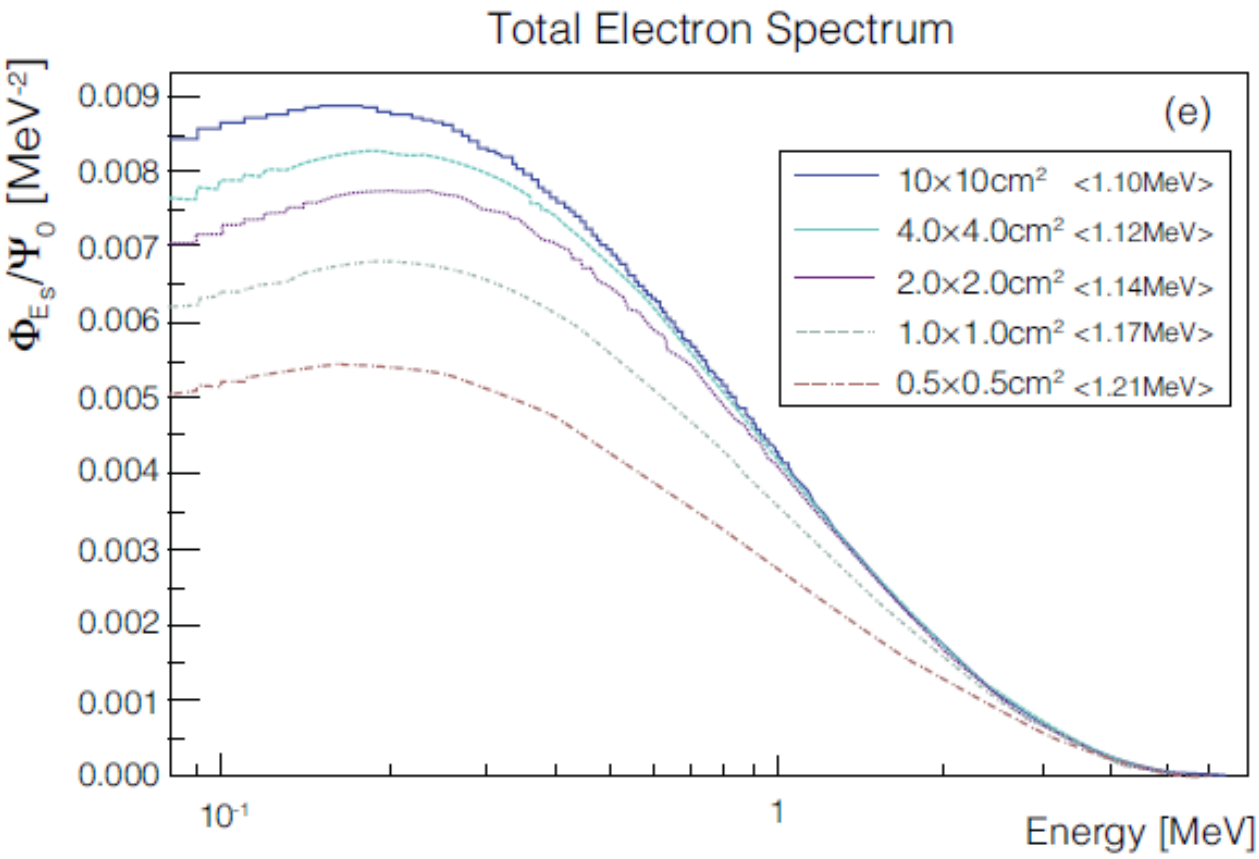

Eklund and Ahnesjö, PMB 53(16) 2008

ESTRO School

Small MV photon fields: characteristics

Overlapping penumbra, source occlusion → drop in output

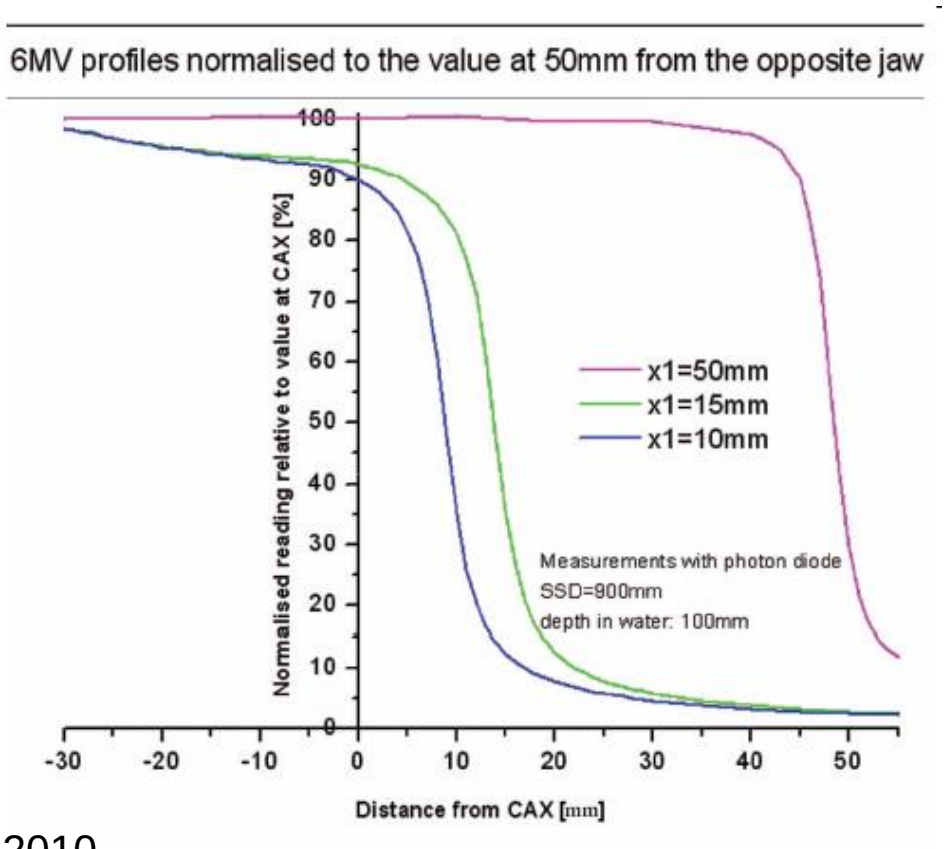

IPEM report 103, 2010

ESTRO School

Small MV photon fields: characteristics

Drop in output: detector dependence

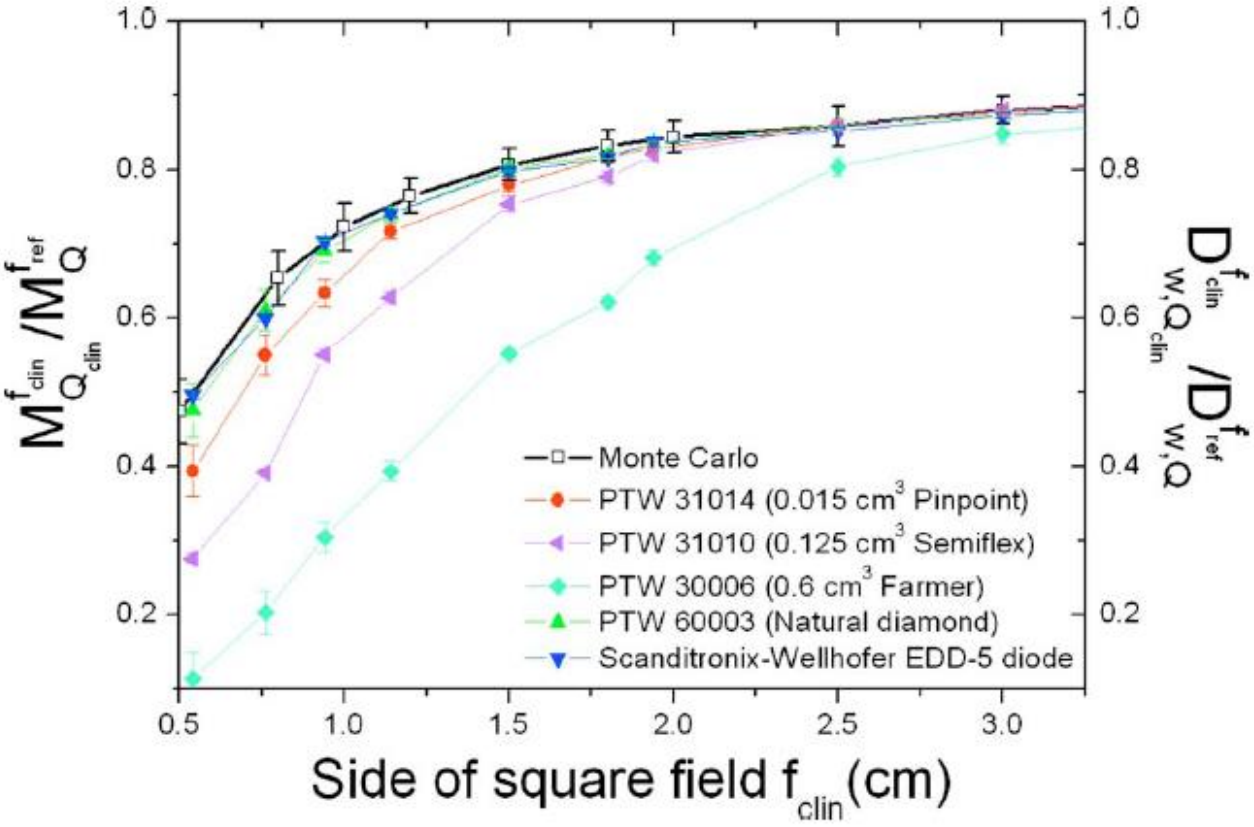

Sanchez-Doblado et al , Physica Medica, 23, 58-66, 2007

ESTRO School

Current practice and developments on the determination of dose in small fields

Determination of dose in small fields

Choice of detector & knowing its dependencies

- Energy dependence of detector response
- Perturbation effects
  - Volume averaging
  - Ionization chambers: wall, central electrode, air cavity different from water
  - Solid state detectors (e.g. diodes): housing, shielding, coating of silicon chip

Determination of dose in small fields

Energy dependence

μ for mass energy absorption coefficient ratios

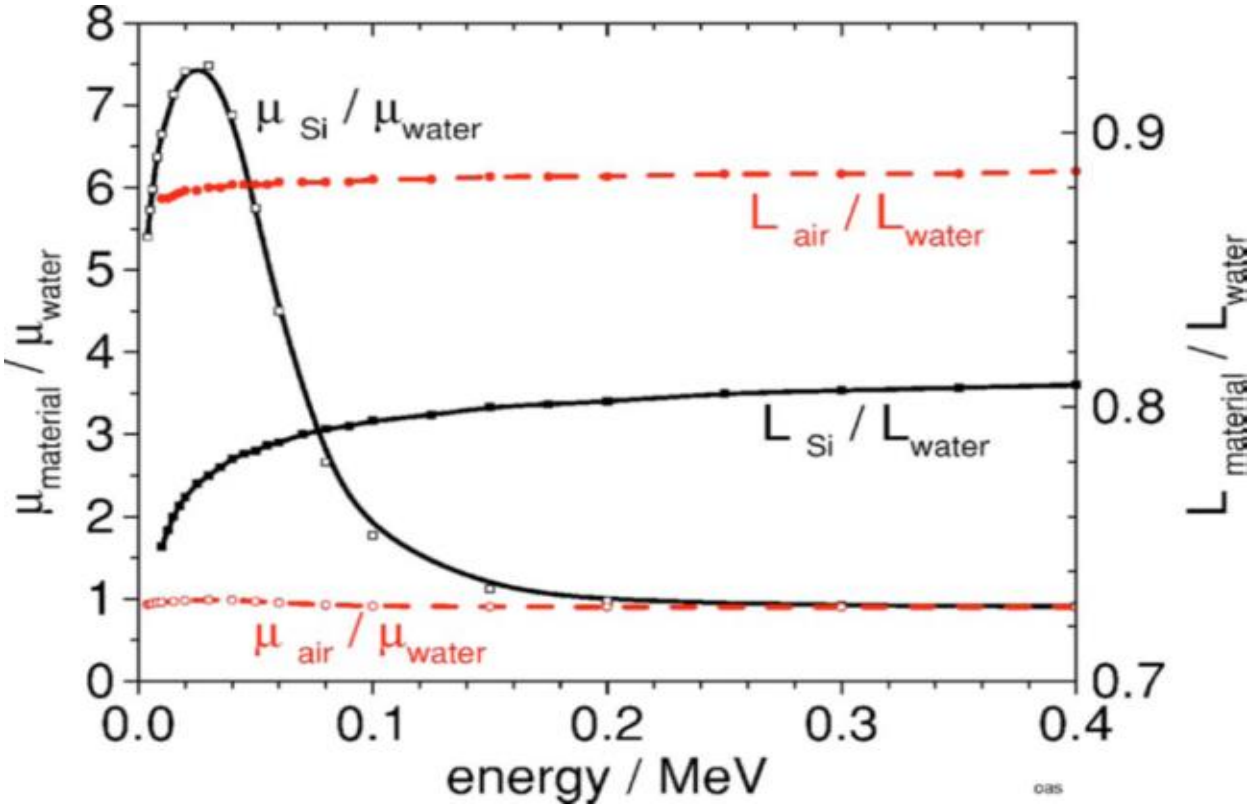

Sauer & Wilbert MP **34**, 2007, 1983-1988

L for stopping power ratios

ESTRO School

Relative dose - profiles

- To determine the penumbra correctly use a small detector (consider directional dependence)
- Check the detector response outside the geometrical field

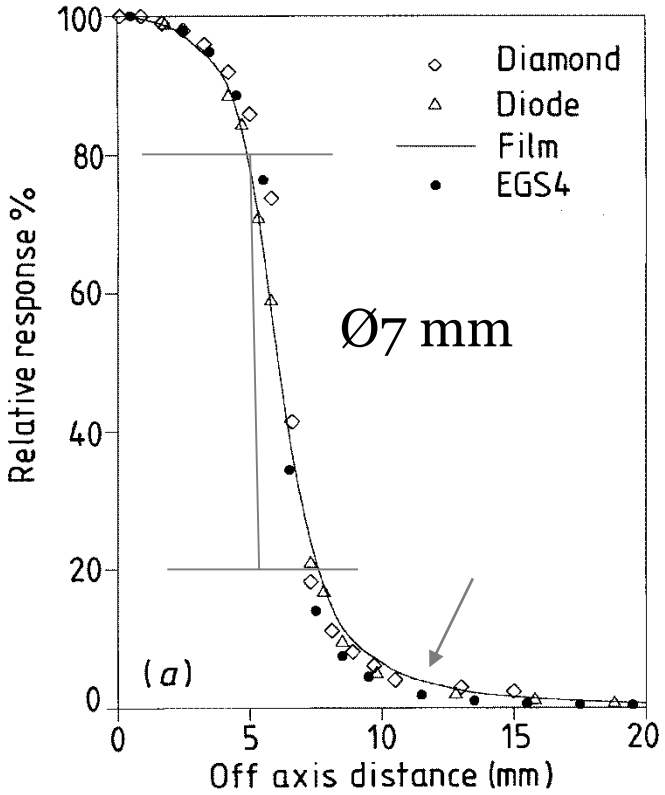

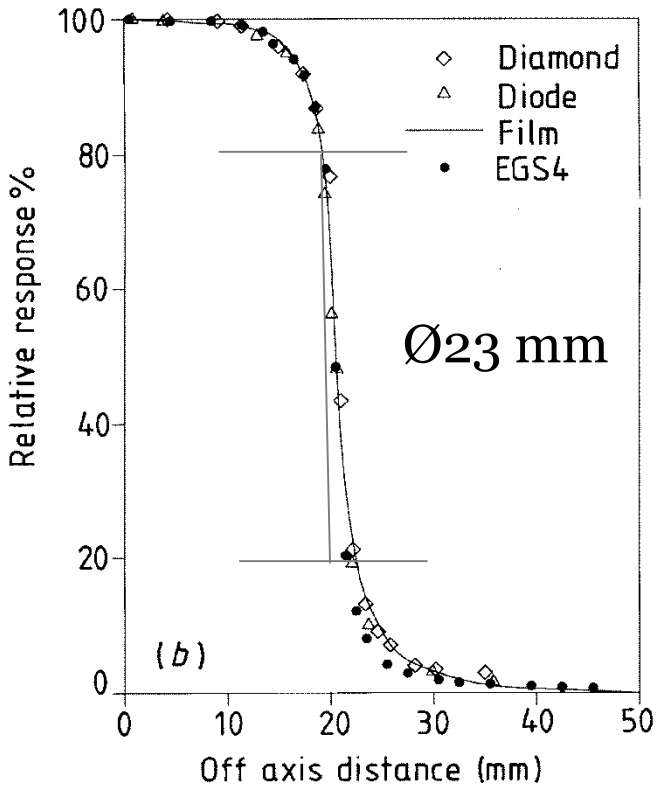

Heydarian et al PMB 41 (1996) 93–110

Determination of dose in small fields

Relative dose: PDDs → careful experimental setup

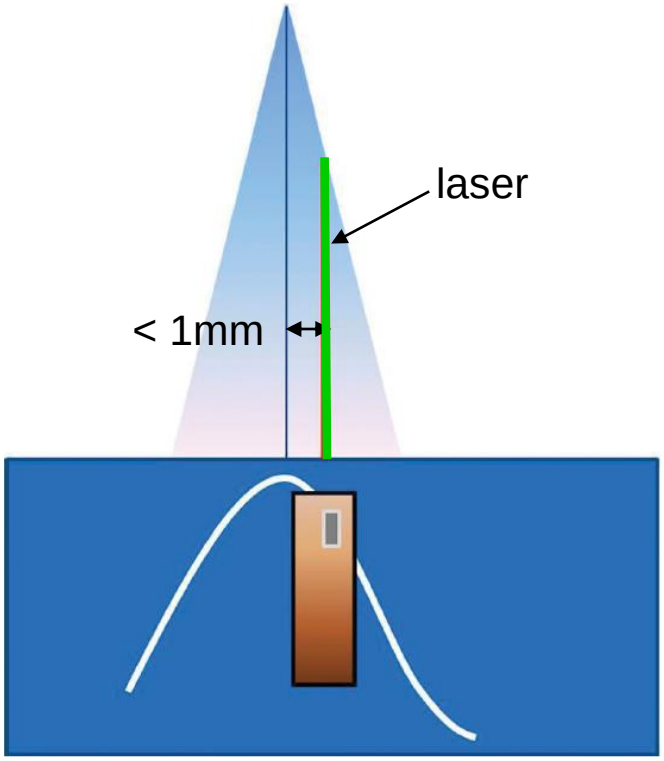

Dietrich & Sherouse Med Phys 38(7), 2011

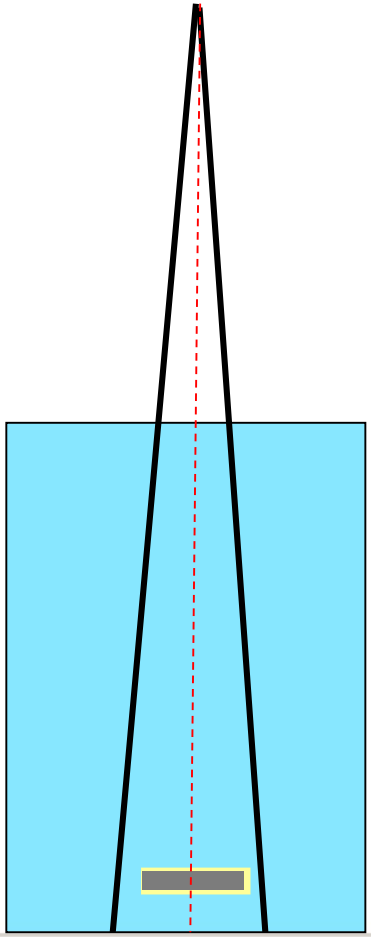

Determination of dose in small fields

Relative dose: output factors (field size factor), S_{cp}

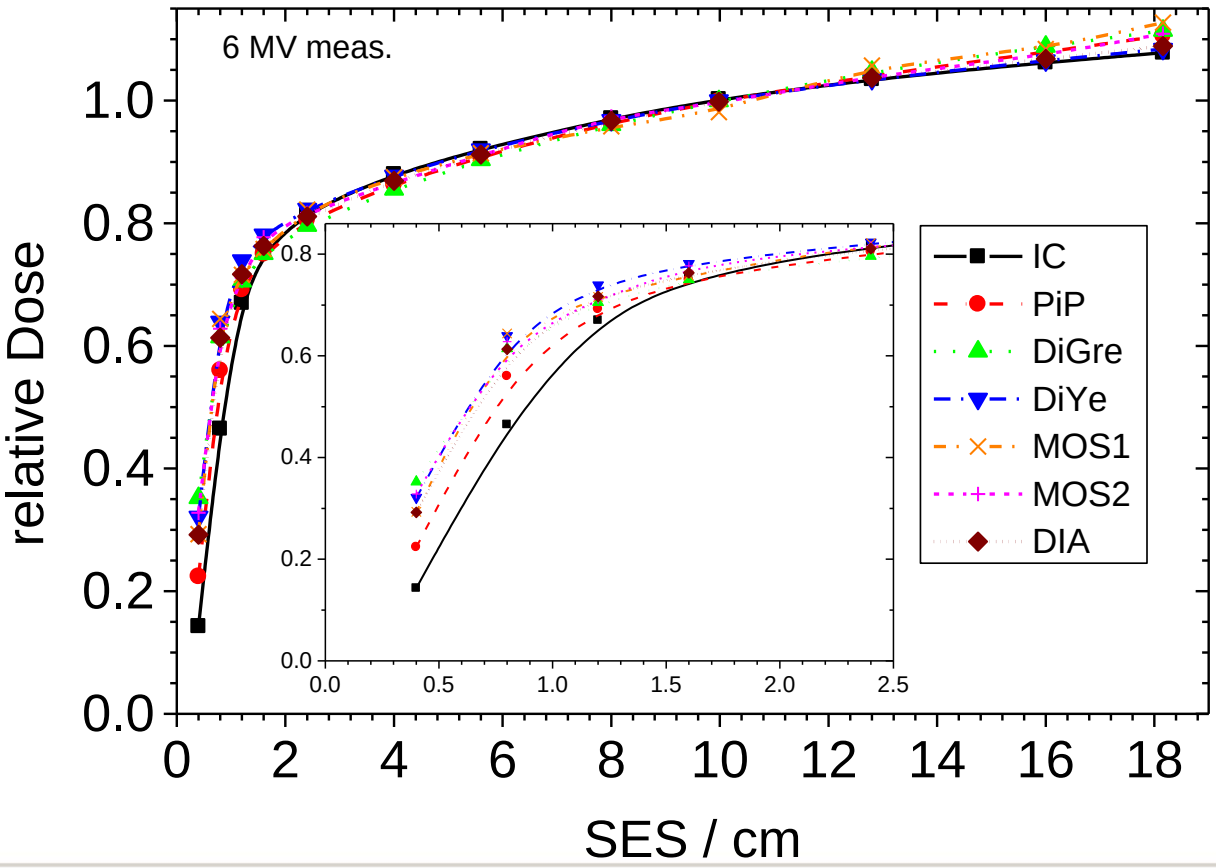

Sauer & Wilbert MP **34**, 2007, 1983-1988

ESTRO School

Determination of dose in small fields

$$\frac{\text{Dose to det}}{\text{Dose to water}} =$$

Detector response ratios normalised to the response of the ionisation chamber

Characterisation of the sensitivity of the diode

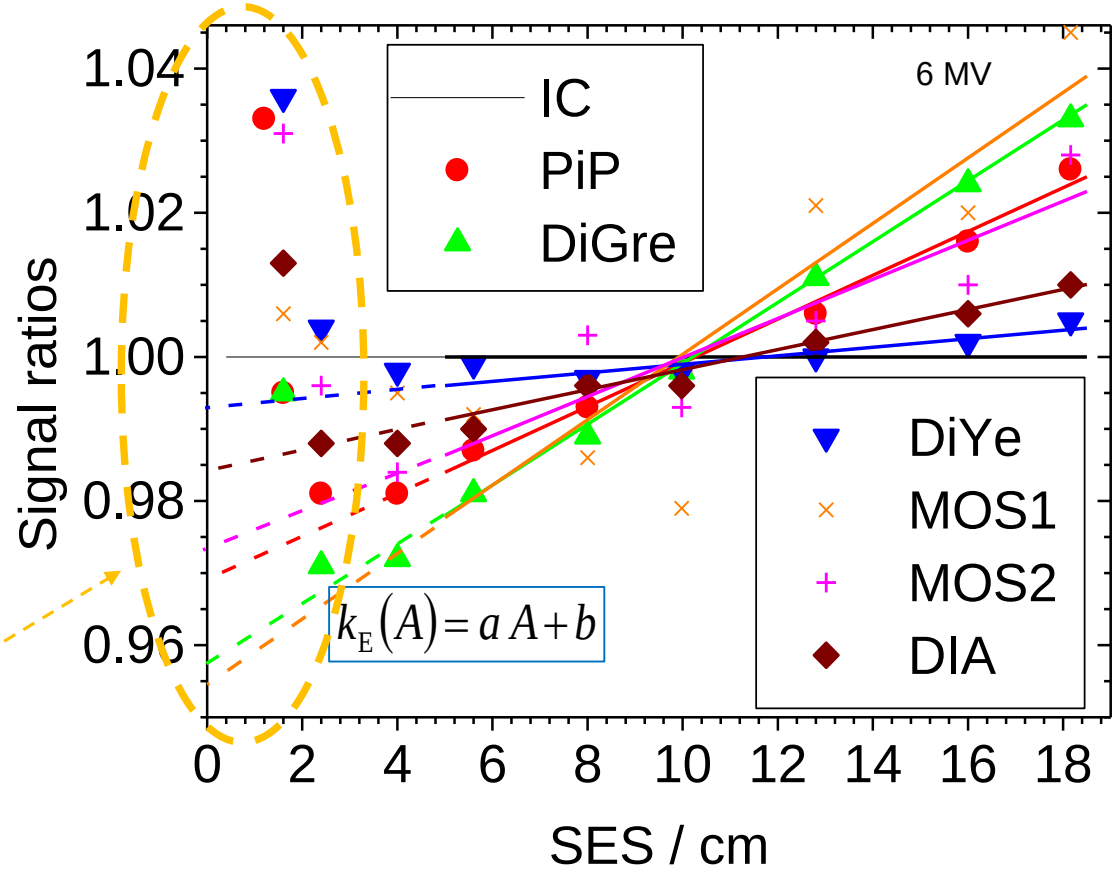

Unshielded diodes over respond at small fields!

Sauer & Wilbert MP **34**, 2007, 1983-1988

ESTRO School

Determination of dose in small fields

Reference dose with air-filled ionisation chambers

$$D_{w,Q}^{f_{ref}} = M_Q^{f_{ref}} \cdot N_{D,w,Q_o} \cdot k_{Q,Q_o}$$

IAEA, TRS-398 (2000)

$$k_{Q,Q_o} = \frac{\left(\frac{\overline{W}_{air}}{e}\right)_Q \left[\left(\frac{\overline{S}}{\rho}\right)_{air}^{water}\right]_Q p_Q}{\left(\frac{\overline{W}_{air}}{e}\right)_{Q_0} \left[\left(\frac{\overline{S}}{\rho}\right)_{air}^{water}\right]_{Q_0} p_{Q_0}} \approx \frac{\left[\left(\frac{\overline{S}}{\rho}\right)_{air}^{water}\right]_Q p_Q}{\left[\left(\frac{\overline{S}}{\rho}\right)_{air}^{water}\right]_{Q_0} p_{Q_0}}$$

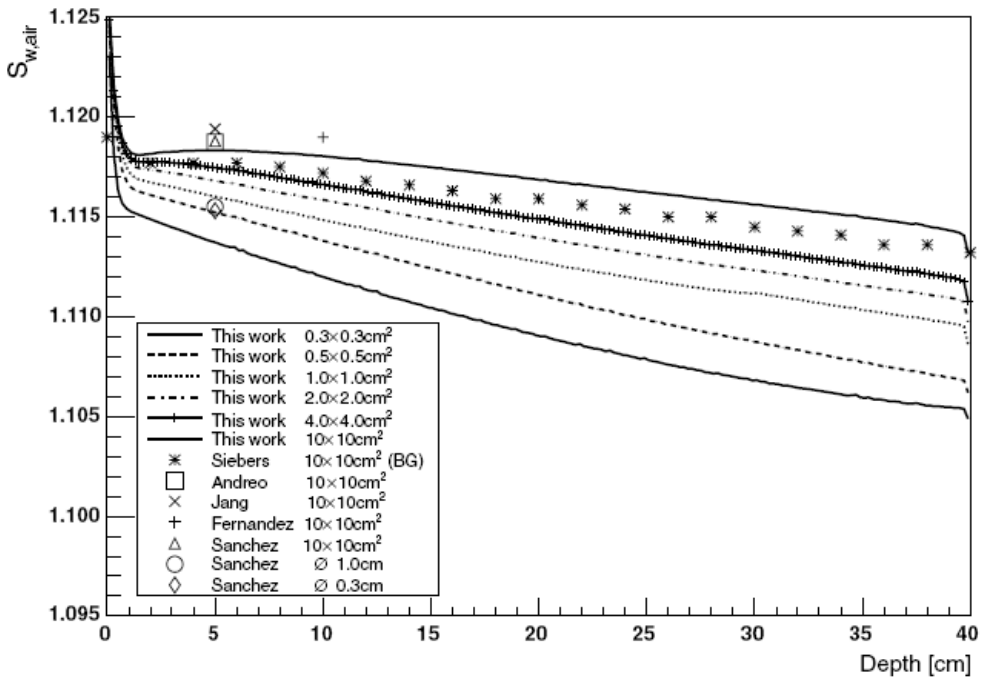

Eklund & Ahnesjo, PMB, 53 (2008) 4231-4247

ESTRO School

Small fields: relative dosimetry - field size factor, S_{cp}

measurement with an ionisation chamber

fluence perturbation

$$S_{cp}(A) = \frac{D_w(A, z_{ref})}{D_w(A_{ref}, z_{ref})} = \frac{M(A, z_{ref})}{M(A_{ref}, z_{ref})} \left[\left(\frac{\bar{S}}{\rho} \right)_{air}^{w} \right]_{A_{ref}}^{A} [p_{det}]_{A_{ref}}^{A}$$

Challenge: perturbation factors

A: field size (aperture)

z_{ref}: reference depth

ESTRO School

Small fields: relative dosimetry - field size factor, S_{cp}

measurement with a solid state detector (diode)

energy dependence & fluence perturbation

$$S_{cp}(A) = \frac{D(A, z_{ref})}{D(A_{ref}, z_{ref})} = \frac{M(A, z_{ref})}{M(A_{ref}, z_{ref})} \left[p_{E,det}\right]_{A_{ref}}^{A} \left[p_{det}\right]_{A_{ref}}^{A}$$

sensitivity of the detector

$\left[p_{E,det}\right]_{A_{ref}}^{A}$

≠1 for detector Ø <A

Challenge: perturbation factors!

ESTRO School

Small fields: relative dosimetry - field size factor, S_{cp}

Characterise the response of the diode

MC simulation of normalised response of unshielded diode PTW 60012

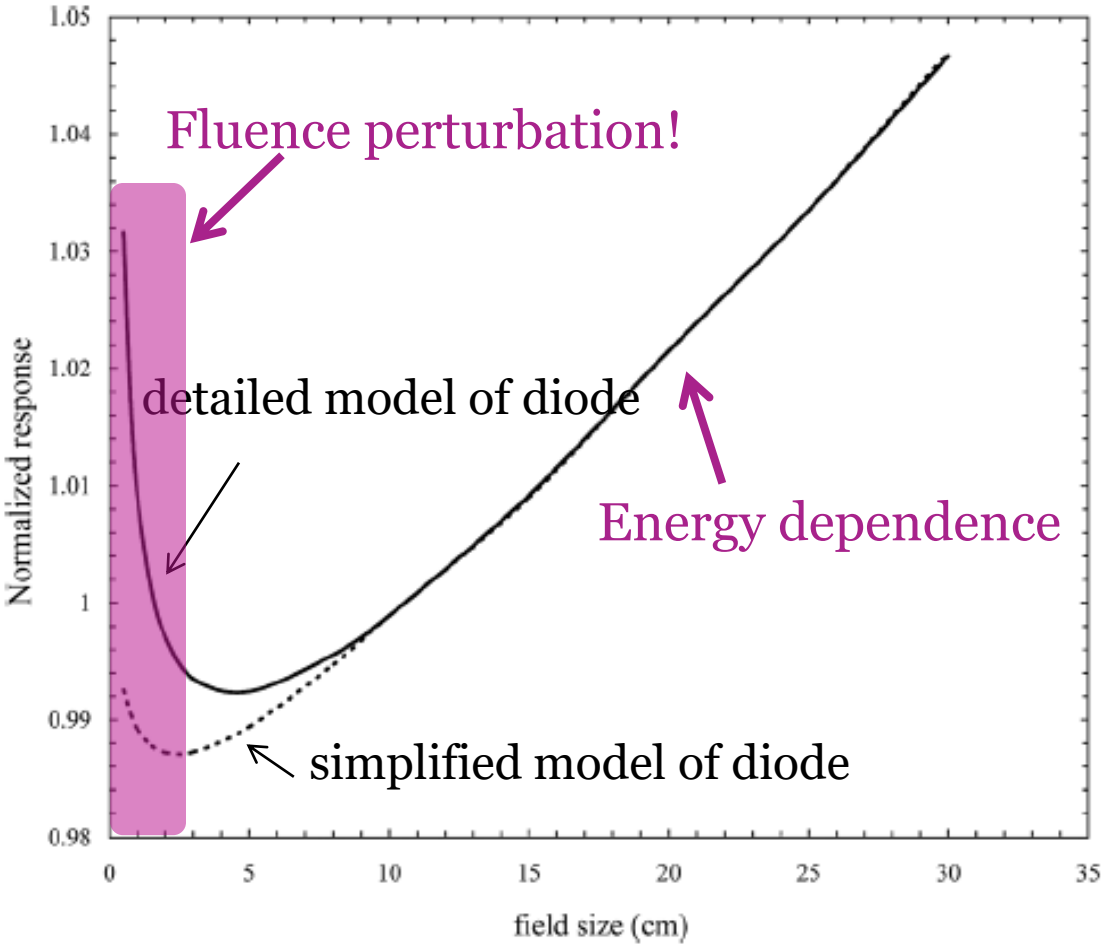

Franscescon et al MP 38(12), 2011

unshielded diode over-responds at small fields

correction to ratio of readings < 1

ESTRO School

Small fields: relative dosimetry - field size factor, S_{cp}

MC simulation of detector response

Correction to ratio of readings

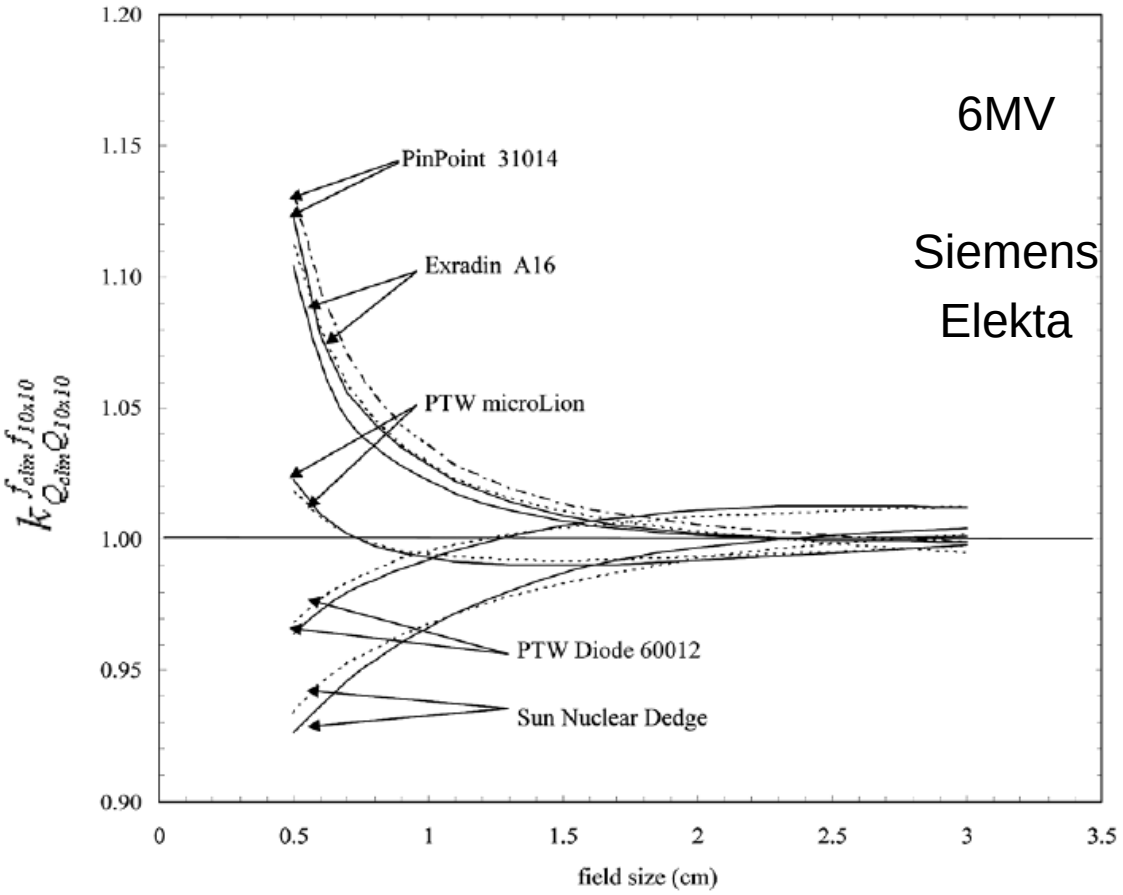

Franscescon et al MP 38(12), 2011

ESTRO School

Challenges in the determination of S_{cp}

- Volume averaging
- Energy dependence
- Fluence perturbation

Small fields: relative dosimetry in practice

Volume averaging is described mathematically using the profile shape and the detector geometry.

The **volume averaging correction** is defined as the ratio of the absorbed dose to water at the reference point in the water phantom in the absence of the detector to the mean absorbed dose to water over the sensitive volume of the detector (still in the absence of the detector).

Sensitive volume of detector, V

Point of dose determination

$D(x_o, y_o, z_o)$

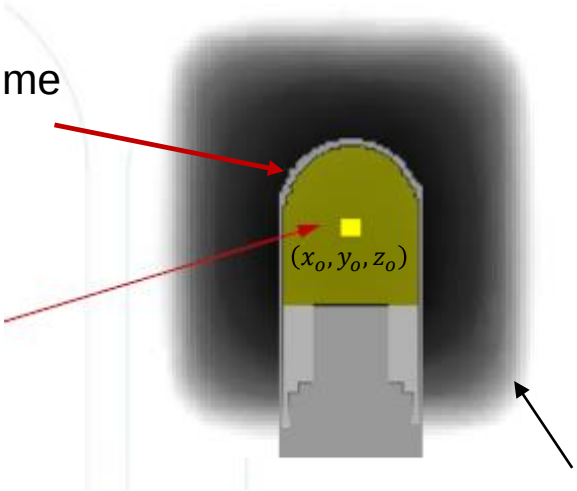

radiation field

$$k_{vol} = \frac{D(x_o, y_o, z_o)}{D_V}$$

$$D_V = \frac{1}{V} \iiint_V D(x, y, z) dV$$

Georg *et al*, 2nd ESTRO Forum, Pre-meeting workshop 2013

Small fields: relative dosimetry in practice

Detector size - the effect of volume averaging

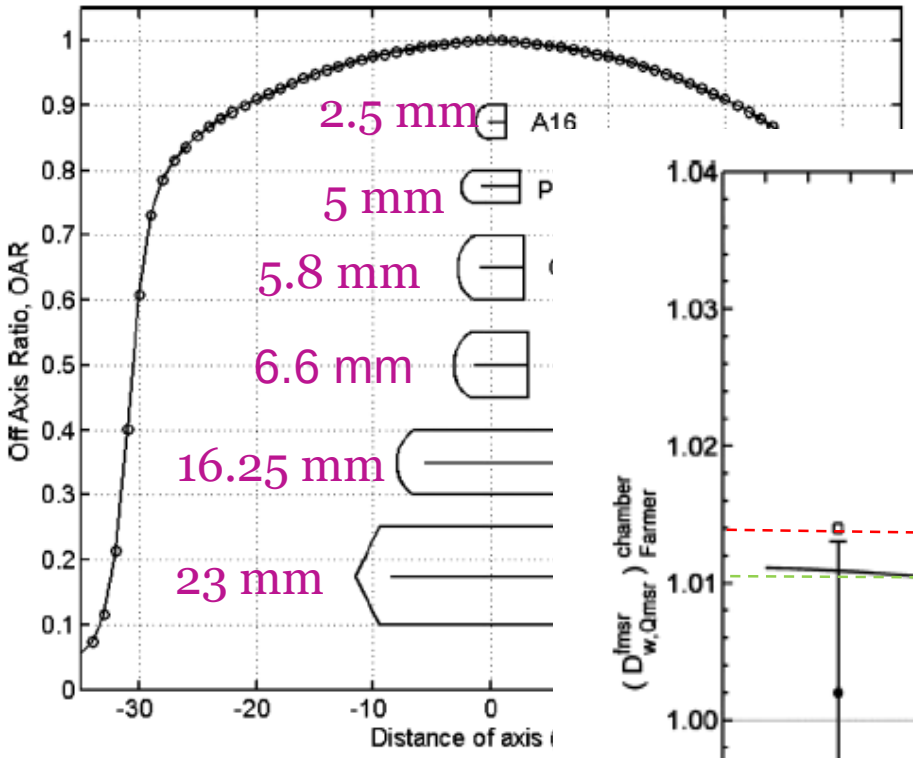

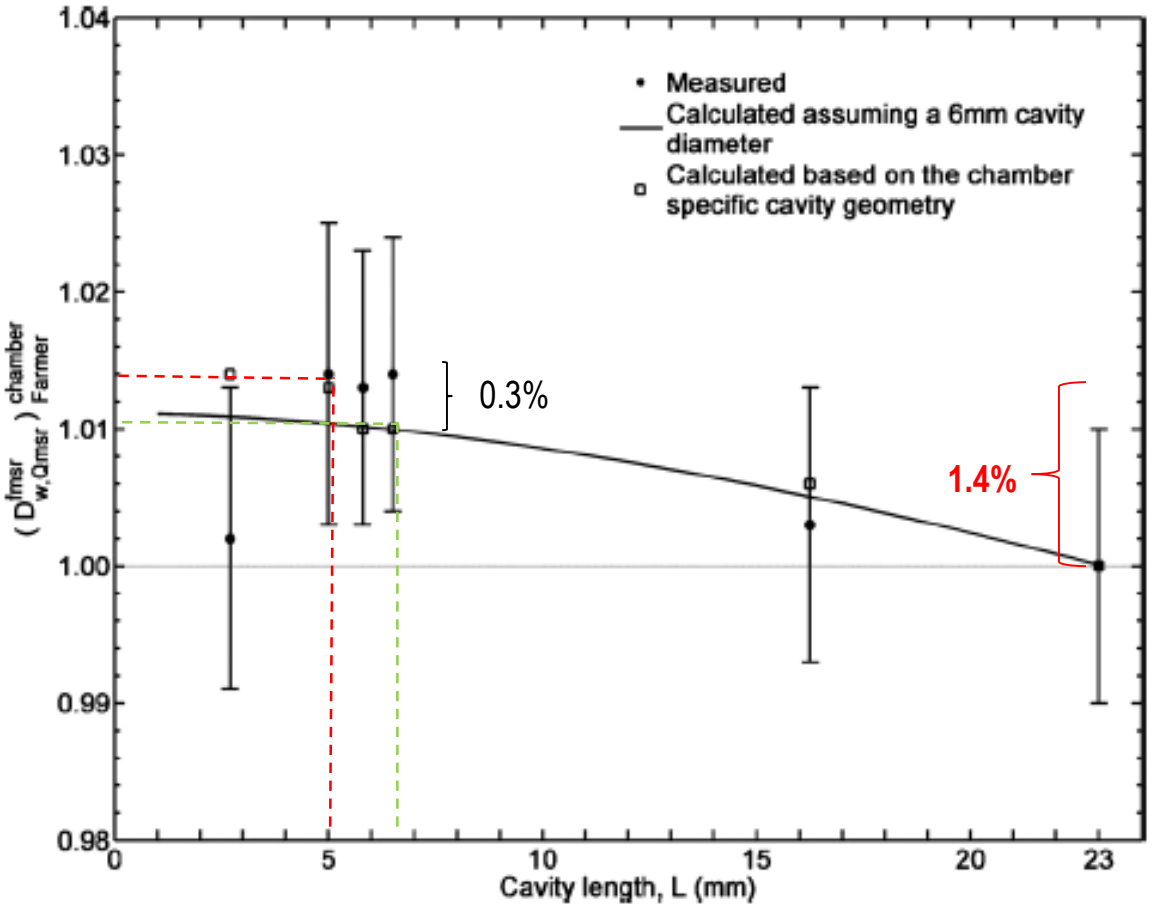

Pantelis *el al* (2010), Med Phys 37 (5)

Small fields: relative dosimetry in practice

Corrections for volume averaging

TABLE II. Calculated volume-averaging correction factors [$1/F_{average}$ in Eq. (3)] for each detector.

Detector	5-mm cone diameter	7.5-mm cone diameter	10-mm cone diameter
0.5-mm PSD	1.003	1.001	1.000
1.0-mm PSD	1.011	1.002	1.001
PTW 60008	1.014	1.003	1.001
PTW 60012	1.014	1.003	1.001
MicroLion chamber	1.068	1.016	1.007
SFD diode	1.004	1.001	1.000

Morin et al MP, 40(1), 2013

Detector	Stem orientation	Field size	Volume averaging correction factor
FOD	Perpendicular	4 mm cone, 5 mm MLC	1.009
SFD	Perpendicular	4 mm cone, 5 mm MLC	1.002
SFD	Parallel	4 mm cone, 5 mm MLC	1.003
60012	Perpendicular	4 mm cone, 5 mm MLC	1.004
60012	Parallel	4 mm cone, 5 mm MLC	1.007
EFD, PFD	Perpendicular	4 mm cone, 5 mm MLC	1.018
EFD, PFD	Parallel	4 mm cone, 5 mm MLC	1.037
EFD, PFD	Perpendicular	7.5 mm cone	1.004
EFD, PFD	Parallel	7.5 mm cone	1.007

Ralston et al PMB, 57, 2012

Minimise energy/field size dependence

An **approximation to account** for the influence of spectral changes between the 10cm × 10cm and a smaller field (e.g. 4cm × 4cm) on detector response would be to *cross-calibrate the small detector against a medium size detector in an intermediate field* (smaller than the reference field of 10cm × 10cm);

This is referred to as '**daisy-chaining'** by Dietrich & Sherouse MedPhys 38(7), 2011

$$S_{cp}(A) \cong \frac{M_{diode}(A)}{M_{diode}(A_{int})} \cdot \frac{M_{IC}(A_{int})}{M_{IC}(A_{ref})}$$

Small fields: relative dosimetry in practice

‘Daisy-chaining’
the normalisation of output factors through an intermediate field

Normalisation to value at 10cm ×10cm

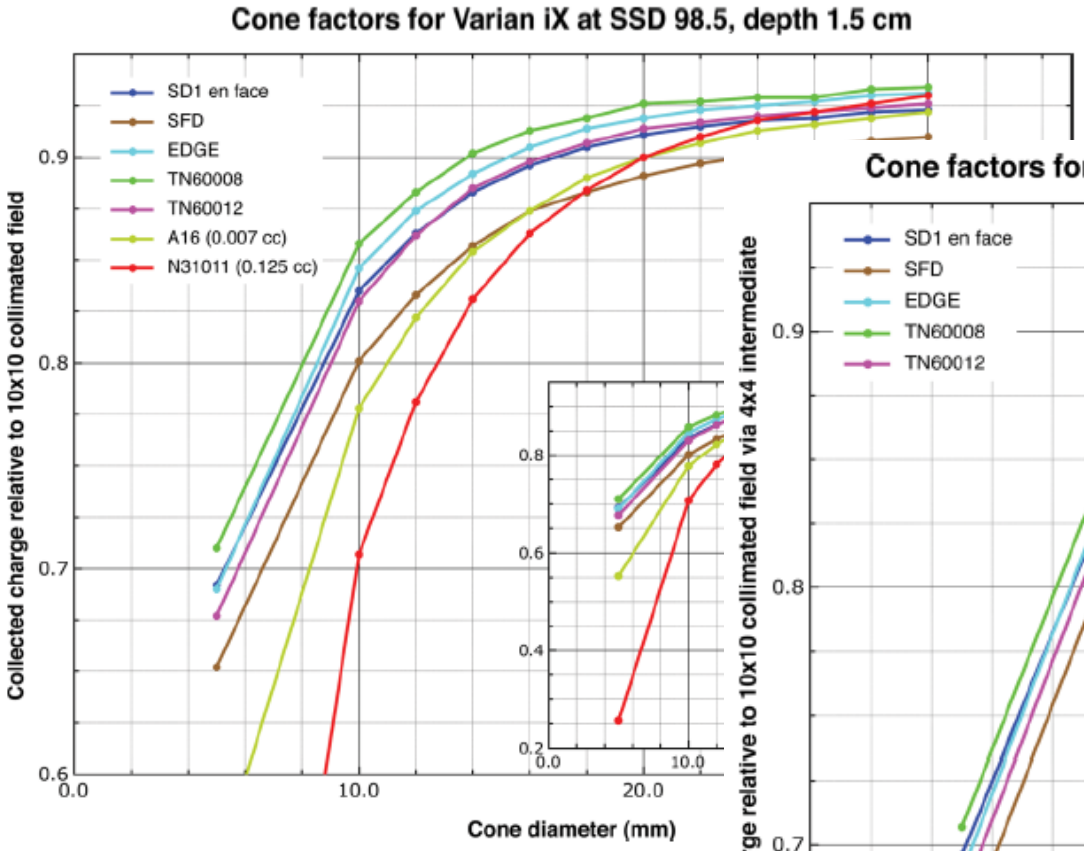

Normalisation to value at 4cm × 4cm

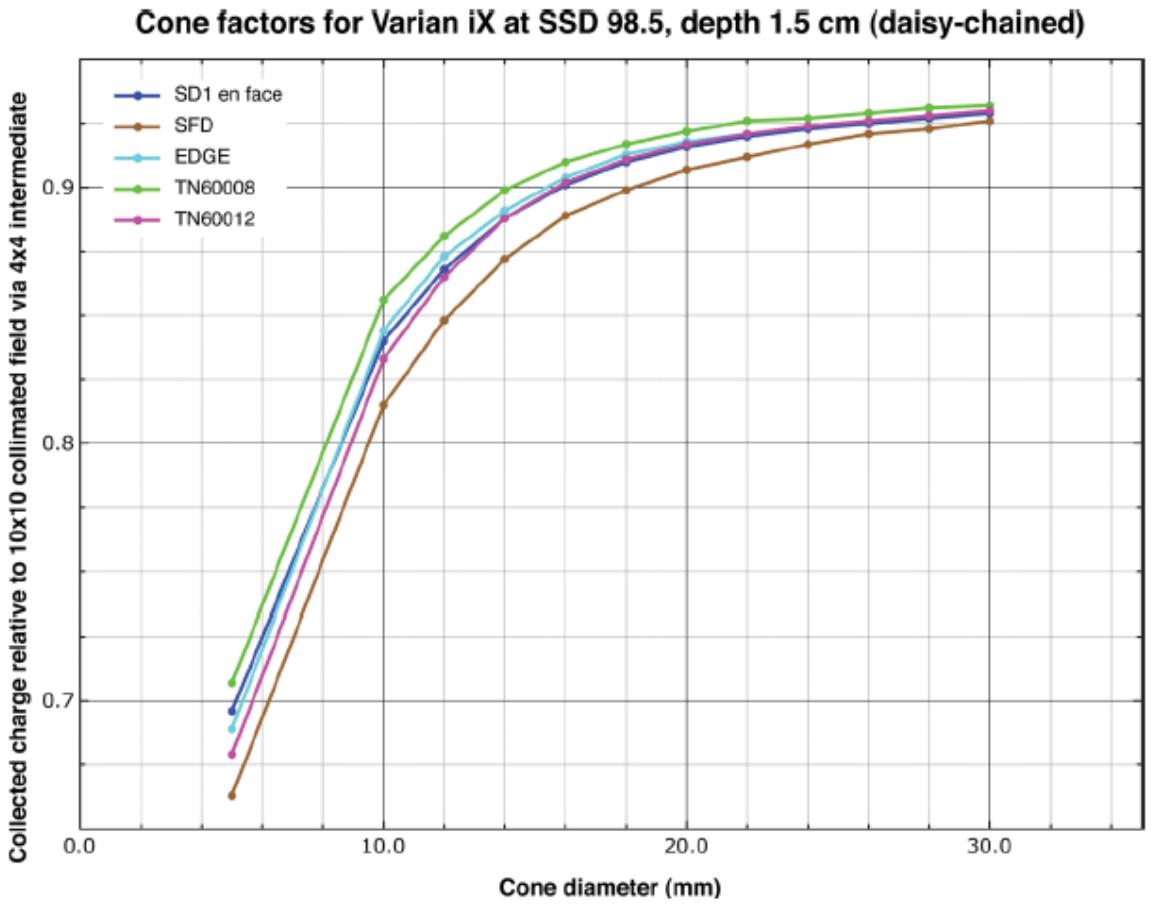

Dietrich & Sherouse Med Phys 38(7), 2011

IAEA/AAPM formalism for reference dosimetry

Small static MV fields: reference dose determination

Medical Physics Letter

A new formalism for reference dosimetry of small and nonstandard fields

R. Alfonso
International Atomic Energy Agency, A-1400 Vienna, Austria and Instituto Nacional de Oncologia y Radiobiologia, CP 10400 La Habana, Cuba

P. Andreo
International Atomic Energy Agency, A-1400 Vienna, Austria and University of Stockholm-Karolinska Institutet, SE-17176 Stockholm, Sweden

R. Capote
International Atomic Energy Agency, A-1400 Vienna, Austria

M. Saiful Huq
University of Pittsburgh Cancer Institute, Pittsburgh, Pennsylvania 15232

W. Kilby
Accuray Inc., Sunnyvale, California 94089

P. Kjäll
Elekta Instrument AB, SE-10393 Stockholm, Sweden

T. R. Mackie
Department of Medical Physics, University of Wisconsin, Madison, Wisconsin 53706

H. Palmans[a)]
National Physical Laboratory, Teddington, Middx TW11 0LW, United Kingdom and Slovenský Metrologický Ústav, SK-84255 Bratislava, Slovakia

K. Rosser
Royal Marsden NHS Foundation Trust, Sutton, Surrey SM2 5PT, United Kingdom

J. Seuntjens
Medical Physics, McGill University, Montreal, Québec H3G 1A4, Canada

W. Ullrich
BrainLAB AG, D-85622 Feldkirchen, Germany

S. Vatnitsky
International Atomic Energy Agency, A-1400 Vienna, Austria

(Received 2 June 2008; revised 2 October 2008; accepted for publication 2 October 2008; published 28 October 2008)

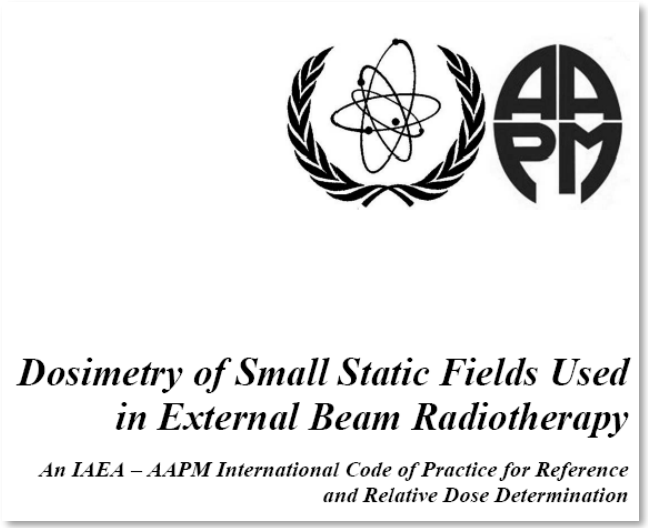

Alfonso el al (2008), Med Phys 35 (11)

Small static MV fields: reference dose determination

f_{msr} machine specific reference field

Q_{msr} beam quality of machine specific reference field

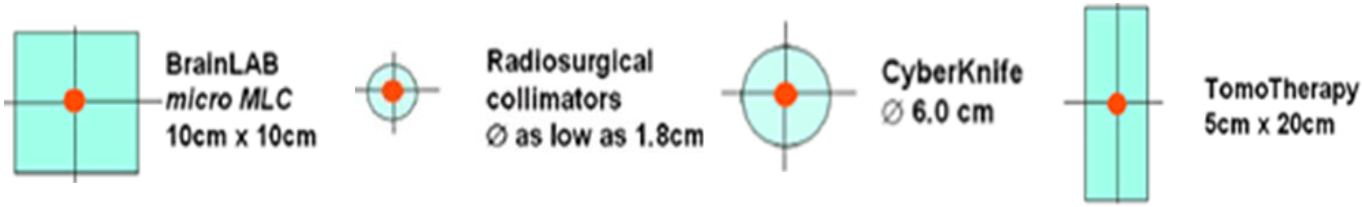

$$D_{w,Q_{msr}}^{f_{msr}} = M_{Q_{msr}}^{f_{msr}} \cdot N_{D,w,Q_o} \cdot k_{Q,Q_o} \cdot k_{Q_{msr},Q}^{f_{msr},f_{ref}}$$

where field output factors are defined as:

$$\Omega_{Q_{clin},Qmsr}^{f_{clin},f_{msr}} = \frac{D_{w,Q_{clin}}^{f_{clin}}}{D_{w,Q_{msr}}^{f_{msr}}}$$

Clin: any clinical field

Ref: 10cm ×10cm

Alfonso el al (2008), Med Phys 35 (11)

IAEA/AAPM formalism for relative dosimetry

output factor determination in small static fields

$$S_{cp} = \Omega^{f_{clin},\, f_{msr}}_{Q_{clin},Q_{msr}} = \frac{D^{f_{clin}}_{w,Q_{clin}}}{D^{f_{msr}}_{w,Q_{msr}}}$$

$$= \frac{M^{f_{clin}}_{Q_{clin}}}{M^{f_{msr}}_{Q_{msr}}} k^{f_{clin},\, f_{msr}}_{Q_{clin},Q_{msr}}$$

Small field detector-specific correction factor

Small field detector correction factors

Account for three main detector perturbation effects:

$$k_{Q_{clin},Q_{msr}}^{f_{clin},f_{msr}} \approx \left[p_{vol}\right]_{Q_{msr}}^{Q_{clin}} \left[p_{fluence}\right]_{Q_{msr}}^{Q_{clin}} \left[p_{spectrum}\right]_{Q_{msr}}^{Q_{clin}}$$

Ratio of volume averaging correction factors

Ratio of charged particle fluence perturbation correction factors

Ratio of correction factors to account for the spectral dependence of photon energy absorption in the detector medium

Small field detector correction factors

Only different degree in CPE & spectral effects considered

$$\left[p_{fluence}\right]_{Q_{msr}}^{Q_{clin}} \left[p_{spectrum}\right]_{Q_{msr}}^{Q_{clin}}$$

FS [cm]	0.6	0.9	1.2	1.8	2.4	3.0	4.2	10.0
TLD chips	1.000	…	1.003	1.008	1.004	1.000	1.005	1.010
TLD micro-cubes	0.998				9	1.000	1.001	1.007
IBA SFD diode	0.995				6	1.000	0.990	0.969
IBA PFD diode	0.936				9	1.000	1.000	1.001
IBA EFD diode	0.961				2	1.000	0.997	0.989
PTW 60003Diamond (Sensitive area ~ 15 mm^2)	0.995	…	0.983	0.992	1.002	1.000	0.996	0.995
PTW 60019 microDiamond	0.961	…	0.980	0.990				
RPLD (GDM-302M)	…	…	…	0.993				
Al_2O_3:C	0.980	0.982	0.985	0.991				
Scintillator 1	1.022	1.009	1.000	0.996				
Scintillator 2	1.028	1.015	1.006	1.000				
PTW 31018microLion	0.970	…	0.980	0.990				
IBA CC01	1.000	…	0.993	0.993				
IBA CC04	1.096	…	1.007	0.998				
IBA CC13[b]	…	…	1.033	1.008				
Wellhöfer IC10[b]			30	1.005	1.005	1.000	0.996	0.996
PTW 31014 PinPoint			07	1.002	1.000	1.000	0.998	1.002
PTW 31016 PinPoint 3D			13	1.000	1.001	1.000	0.998	0.999
PTW 31010 Semiflex[b]	…	…	1.027	1.002	1.004	1.000	0.996	0.997
PTW 31013 Semiflex[a,b]	…	…	…	…	1.013	1.000	0.992	0.993

These result confirm previous conclusions that unshielded diodes a better choice of detector than shielded diodes.

active volume > 0.1 cm^3 corrections of 20%-30% !

The corrections for mini-ionization chambers used in this study (active volume between 0.015 cm^3 and 0.05 cm^3) were generally lower than **10%** and for micro-chambers (active volume<0.015 cm^3) lower than **3%**.

[a]This chamber was included in the table for completeness but it is not recommended to use for small field dosimetry in fields smaller than 2.0 × 2.0 cm^2 because the volume averaging effect is unacceptably high.

[b]For these ionization chambers, corrections for the smallest field were unacceptably high (>20%) for field sizes smaller than 1 × 1 cm^2 and therefore were excluded from Table V.

Azangwe et al Med. Phys. 41 (7), 2014

Small field detector correction factors

$$k_{Q_{\text{clin}},Q_{\text{msr}}}^{f_{\text{clin}},f_{\text{msr}}}$$

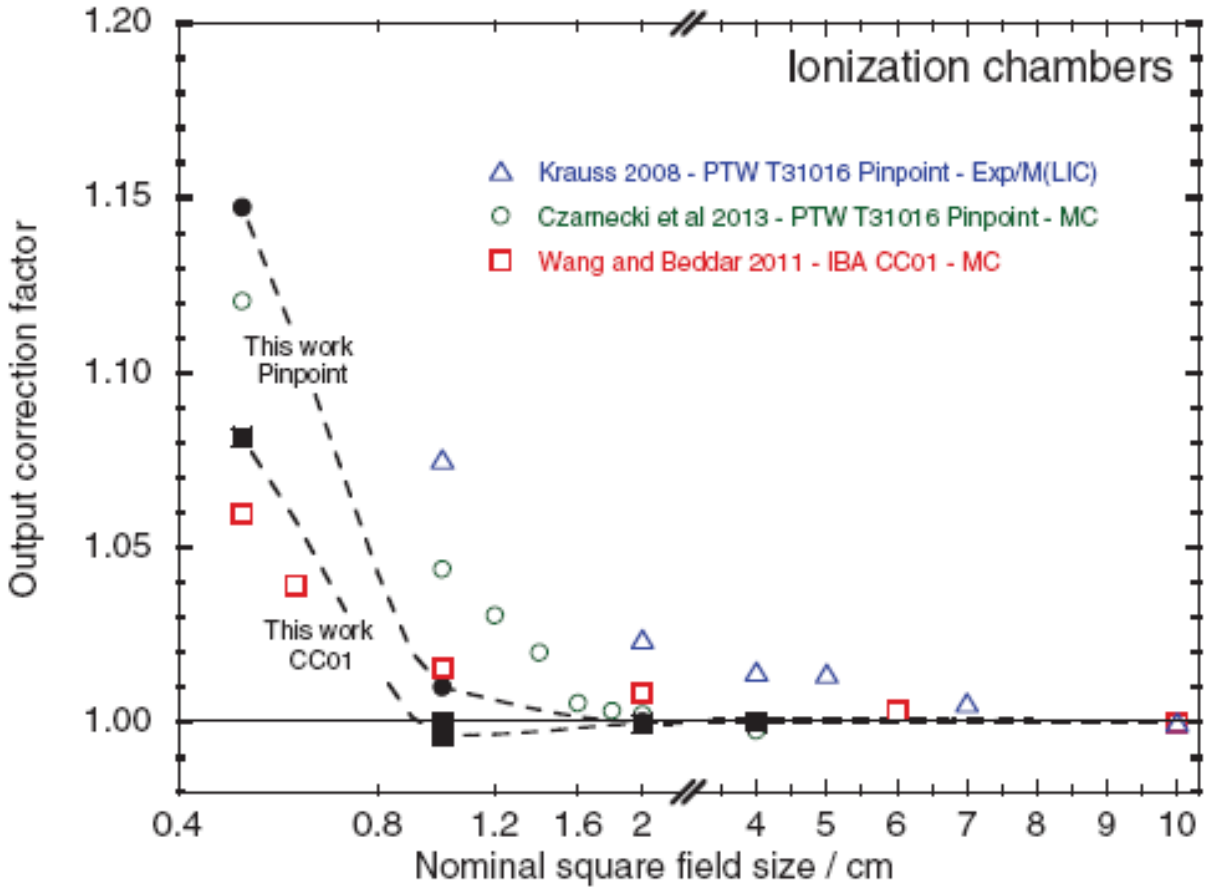

Benmakhlouf et al Med. Phys. 41 (4), 2014

IAEA/AAPM formalism for relative dosimetry

Small field detector correction factors

$$k_{Q_{clin},Q_{msr}}^{f_{clin},f_{msr}}$$

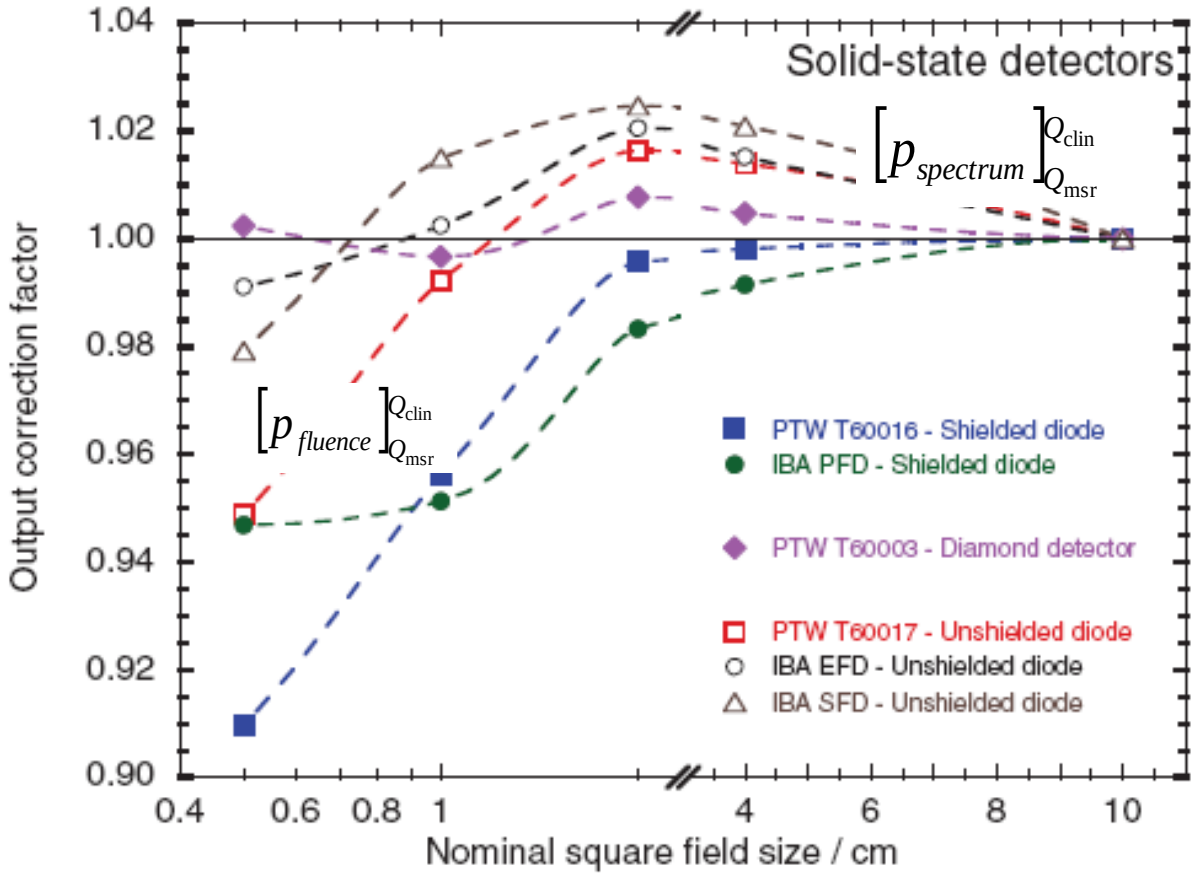

Benmakhlouf et al Med. Phys. 41 (4), 2014

ESTRO School

Summary: measurements in small static fields

- Consensus so far on current good practice for reference and relative dosimetry in static small MV photon fields:
  - ✓Careful experimental setup
  - ✓Choice of suitably small detector which is known to minimally perturb fluence
  - ✓Approximately correct for volume averaging and energy dependence of detector
  - ✓Corroboration of data

Summary: measurements in small static fields

- Consensus so far on current good practice for reference and relative dosimetry in static small MV photon fields:
  - ✓Careful experimental setup
  - ✓Choice of suitably small detector which is known to minimally perturb fluence
  - ✓Approximately correct for volume averaging and energy dependence of detector
  - ✓Corroboration of data
- Current research efforts in small field dosimetry focus on the determination of detector specific output correction factors.
- Detectors requiring output **corrections greater that 5%** will not be recommended for dose determination in small fields.
- The IAEA TECDOC will include a consistent set of such data and will be an international code of practice for small static field dosimetry.

Background and early reviews on small field dosimetry

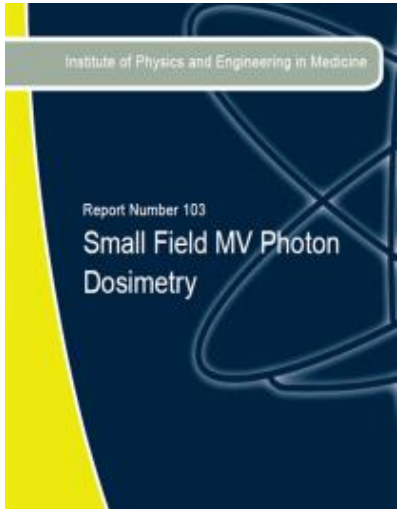

- IPEM Report 103, 2010
- R. Alfonso, P. Andreo, R. Capote, M. S. Huq, W. Kilby, P. Kjäll, T. R. Mackie, H. Palmans, K. Rosser, J. Seuntjens, W. Ullrich, and S. Vatnitsky, "A new formalism for reference dosimetry of small and nonstandard fields," *Med. Phys.* **35**, 5179–5187 (2008).
- I. J. Das, G. X. Ding, and A. Ahnesjö, "Small fields: Nonequilibrium radiation dosimetry," Med. Phys. 35, 206–215 (2008).
- H Palmans (2011) CN-182-INV006, Small and composite field dosimetry: the problems and recent progress. IDOS Conference, Vienna.

Note: There has been an explosion in the literature since 2008 on the topic of small field dosimetry!

In depth reading on the physics of small MV photon fields

- Bouchard H, Seuntjens, J., Palmans H., ‘On charge particle equilibrium violation in external photon fields’, Med. Phys. 39 (3), 1473-1480, Mar 2012

- Bouchard H, Seuntjens, J., Duane, S., Kamio, Y., Palmans H., ‘Detector dose response in megavoltage small photon beams. I Theroretical concepts’, Med. Phys. 42 (10), 6033-47, Oct 2015

- Bouchard H, Kamio, Y., Palmans H., Seuntjens, J., Duane, S., ‘Detector dose response in megavoltage small photon beams. II Pencil beams perturbation effects’, Med. Phys. 42 (10), 6048-61, Oct 2015

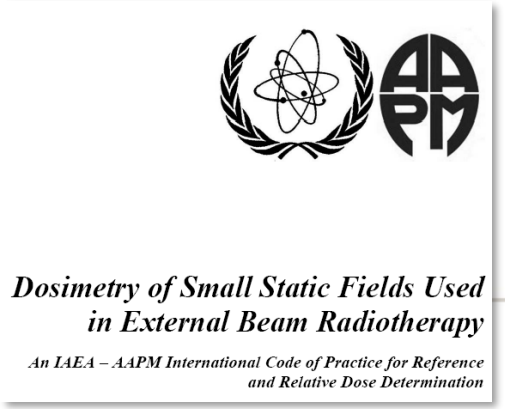

ESTRO School

ESTRO School

WWW.ESTRO.ORG/SCHOOL

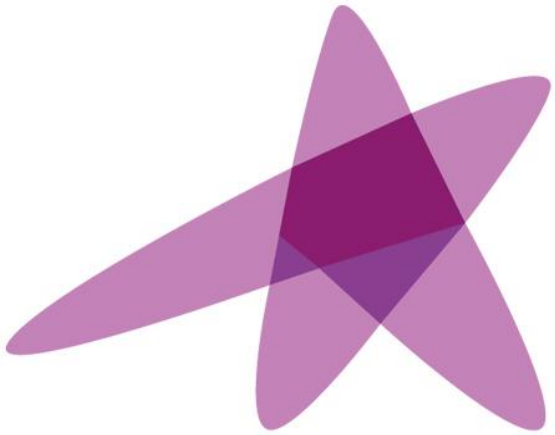

ESTRO School

WWW.ESTRO.ORG/SCHOOL

Dose measurements;

Part 1 The best detector for different jobs

detectors for input data collection

Núria Jornet

Servei de Radiofísica
Hospital Sant Pau, Barcelona

Learning objectives

1. To have an overview of the point detectors used for relative dose measurements
2. Understand their principle of detection, strengths and weaknesses
3. Be able to chose the best detector for a particular type of measurement

I will focus mainly on MV x-rays

I will mainly discuss the use of detectors for relative dose measurements.

I will compare detectors widely used to new kids on the market

I won't talk about detectors to be used in proton/ion dose measurements

I won't cover TLD/OSL

How to go from our reading to dose to media?

Dose measurements

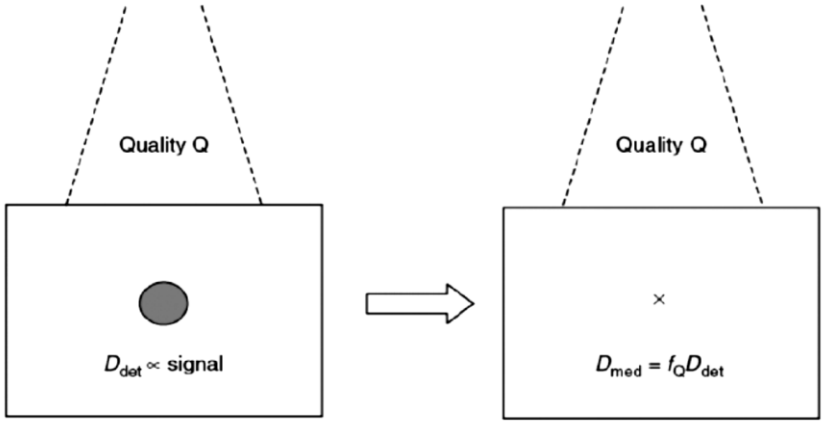

$D_{med} = M \times F_{cal} \times f_Q$

$f_Q = d \cdot S_{w,med} + (1-d) \cdot [\mu_{en}/\rho]_{w,med}$

d=1 small (Bragg Gray) cavities
d=0 large cavities (photon detectors)

-Bragg Gray Cavity [electron sensor, range of electrons>cavity] $f_Q = S_{w,med}$ → Ionisation chambers in High Energy X-ray Beams

-If it isn't a Bragg Gray Cavity $f_Q = [\mu_{en}/\rho]_{w,med}$ → High density detectors such as diodes, MOSFET, diamonds for High Energy X-ray beams

ESTRO School

Principle of absorbed dose measurements
Reference conditions

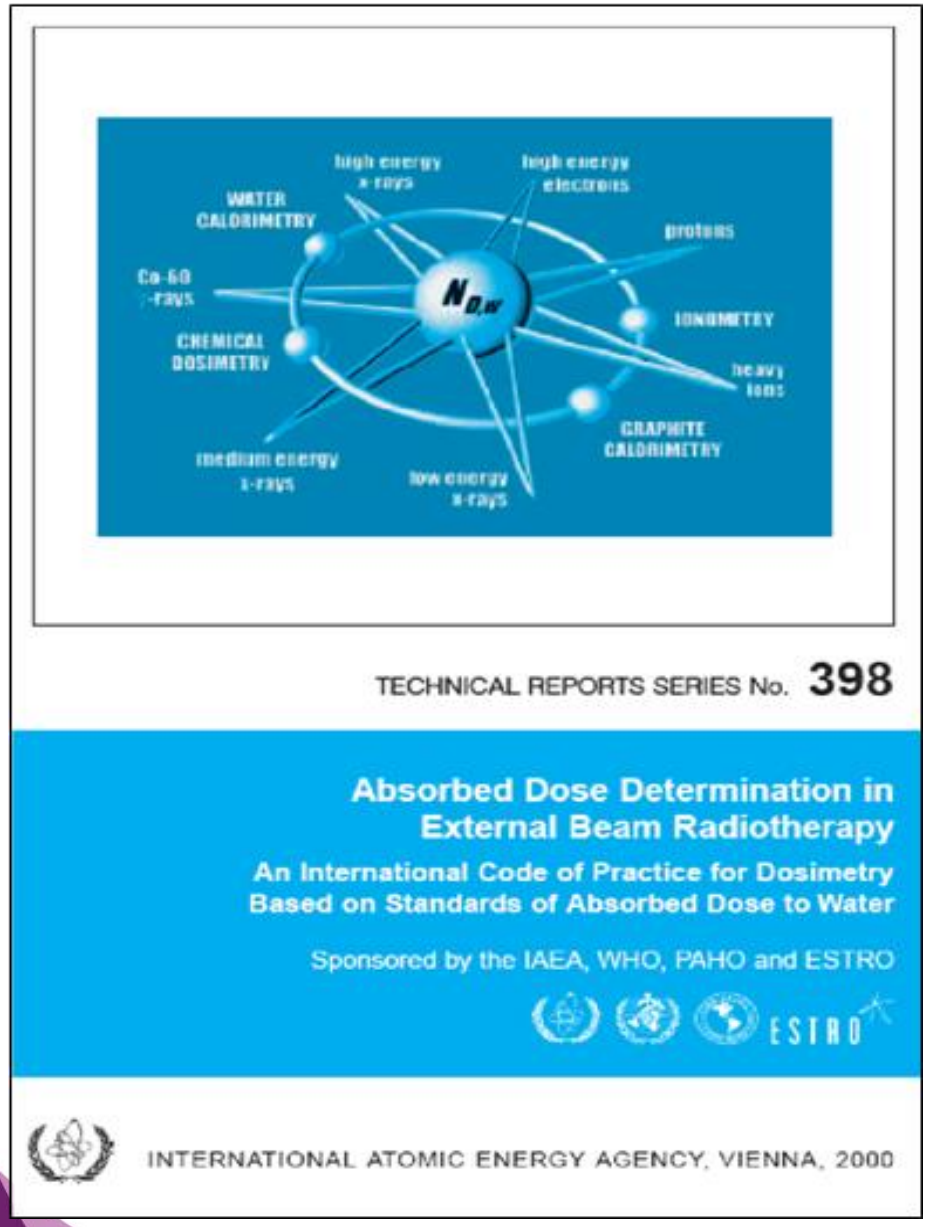

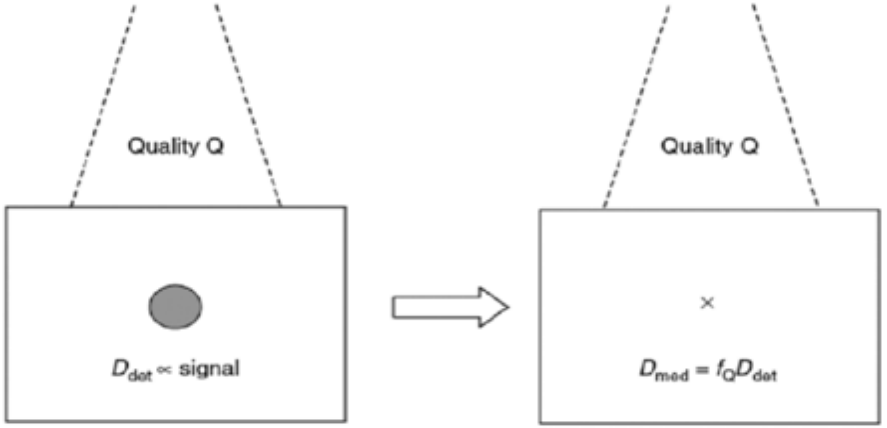

Detector: air (ionisation chamber)

Med: Water

For reference irradiation conditions:

Fixed field size 10x10 cm2

Fixed depth 10cm

Fixed SSD 100cm

$$D_{w,Q} = M^* \cdot k_i \cdot N_{D,w}$$

$$N_{D,w} = \alpha \cdot k_l \cdot f_{Q,ideal} \cdot P_Q$$

Calibrated in terms of water absorbed dose in ^{60}Co-radiation in units of Gray per Coulomb

ESTRO School

Challenges: reference versus relative dosimetry

Reference conditions
Reference dosimetry

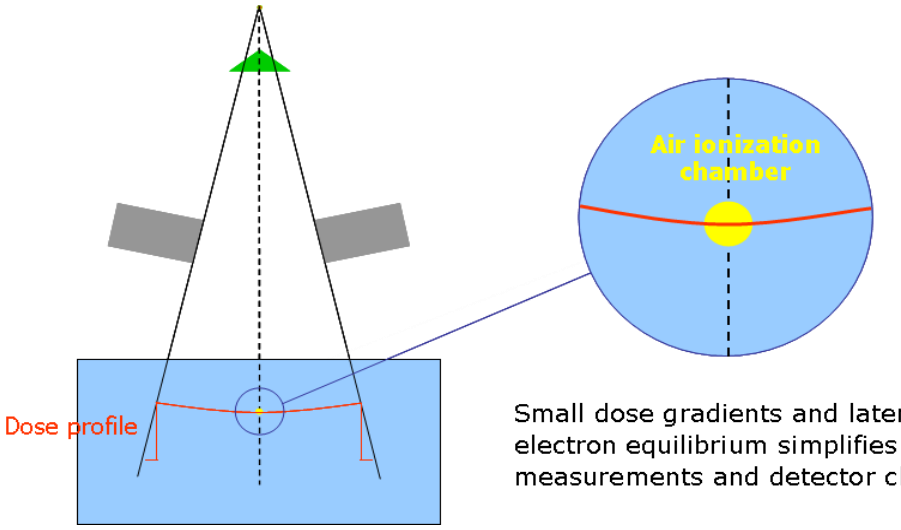

Small dose gradients and lateral electron equilibrium simplifies measurements and detector choice.

- Uniform electron fluence distribution over the detector.
- Beam spectra at the reference point in ref. conditions known.
- Detector of choice: **Ion Chambers**

Non reference conditions:
Relative dosimetry

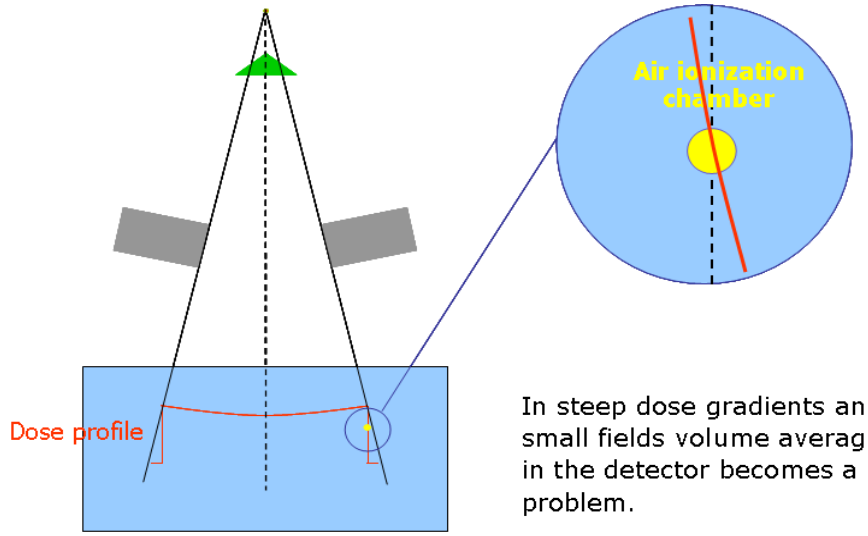

In steep dose gradients and small fields volume averaging in the detector becomes a problem.

- Non-Uniform electron fluence distribution over the detector. **VOLUME AVERAGING**
- Beam spectra at the reference point may differ from beam spectra at the measuring point. **ENERGY DEPENDENCE; PERTURBATION FACTORS**
- Perturbation in electron fluence caused by the detector itself **PERTURBATION FACTORS**

ESTRO School

When moving away from reference conditions the detector will face differences in:

Small fields

Less scatter photons, beam hardening

Energy fluence

For high energy x-rays

Photon energy fluence changes with field size and depth

Dose rate

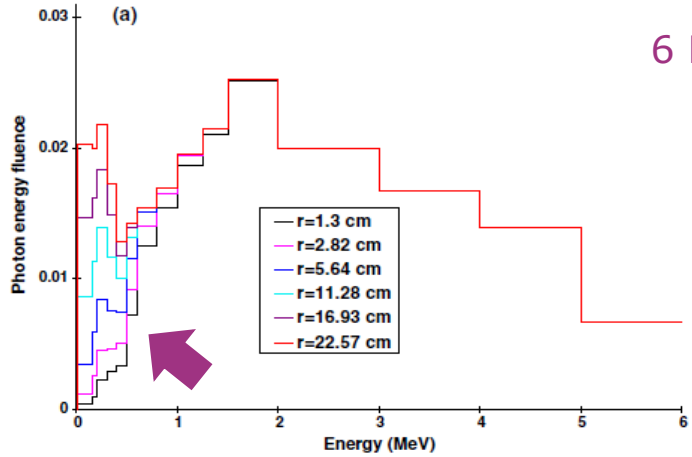

6 MV, d_{max}

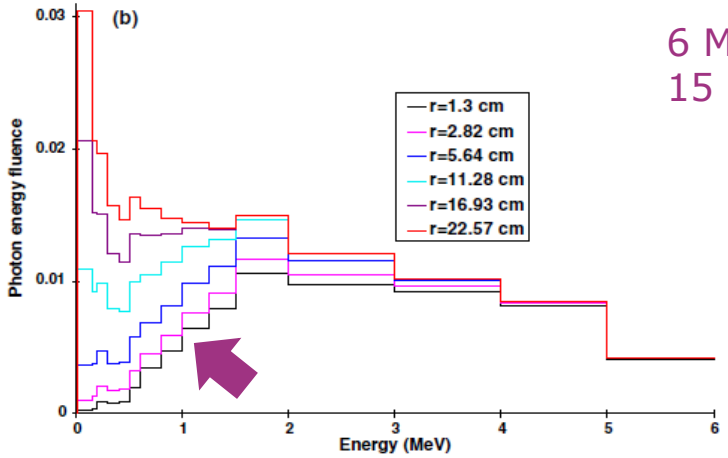

6 MV,
15 cm depth

Figure 1. Total 6 MV photon energy fluence calculated using Monte Carlo FLURZnrc (EGSnrc) code as a monotonically increasing function of field size at (a) peak and (b) 15 cm depth of water.

Yin et al. PMB 49 (2004)

ESTRO School

When moving away from reference conditions the detector will face differences in:

Large fields

More low energy scattered photons

Energy fluence

For high energy x-rays

Photon energy fluence changes with field size and depth

Dose rate

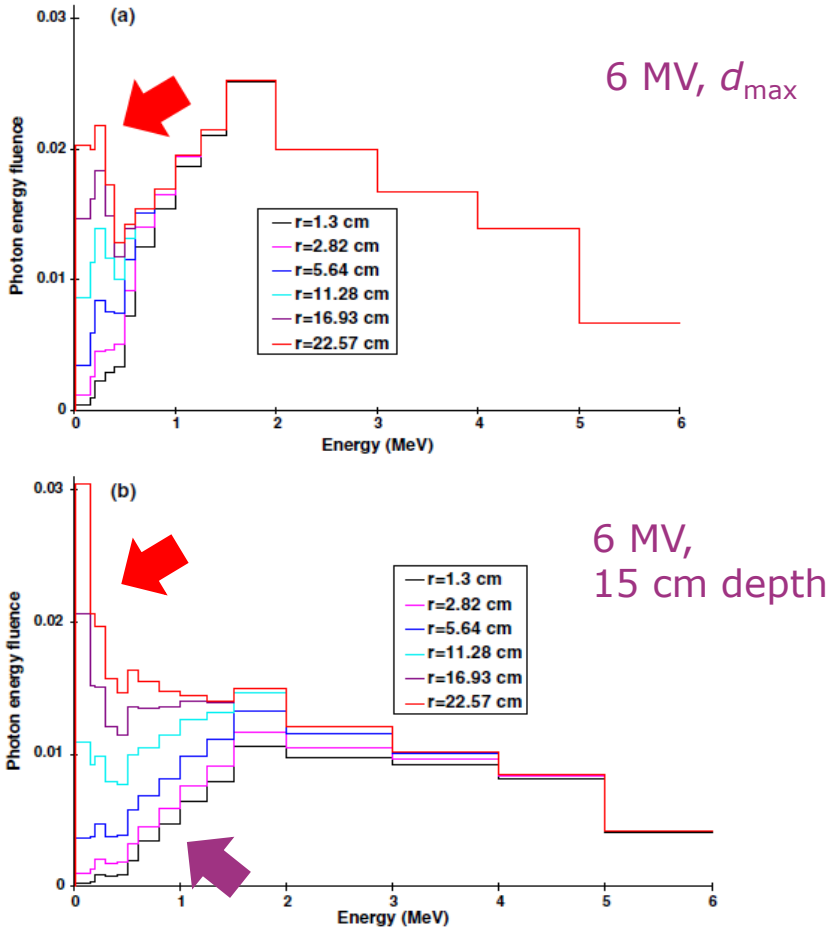

Figure 1. Total 6 MV photon energy fluence calculated using Monte Carlo FLURZnrc (EGSnrc) code as a monotonically increasing function of field size at (a) peak and (b) 15 cm depth of water.

Yin et al. PMB 49 (2004)

ESTRO School

When moving away from reference conditions the detector will face differences in:

Energy fluence

For high energy x-rays

Secondary electron fluence depends slightly on field size and depth

Dose rate

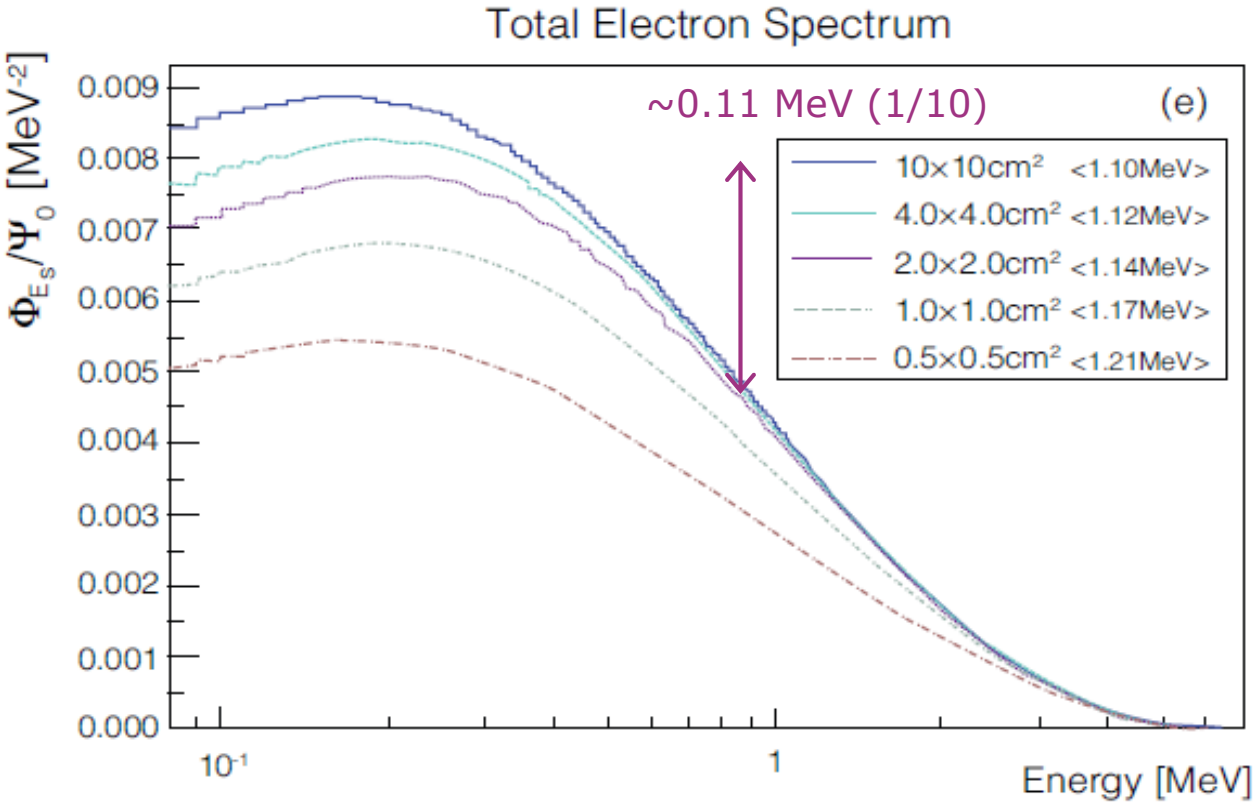

Eklund and Ahnesjö, PMB 53(16) 2008

ESTRO School

Mean energies in a 6 MV beam depending on field size and depth

Two counteracting effects as depth increases: Beam hardening of primary fluence and increasing amount of scattered photons.

photons

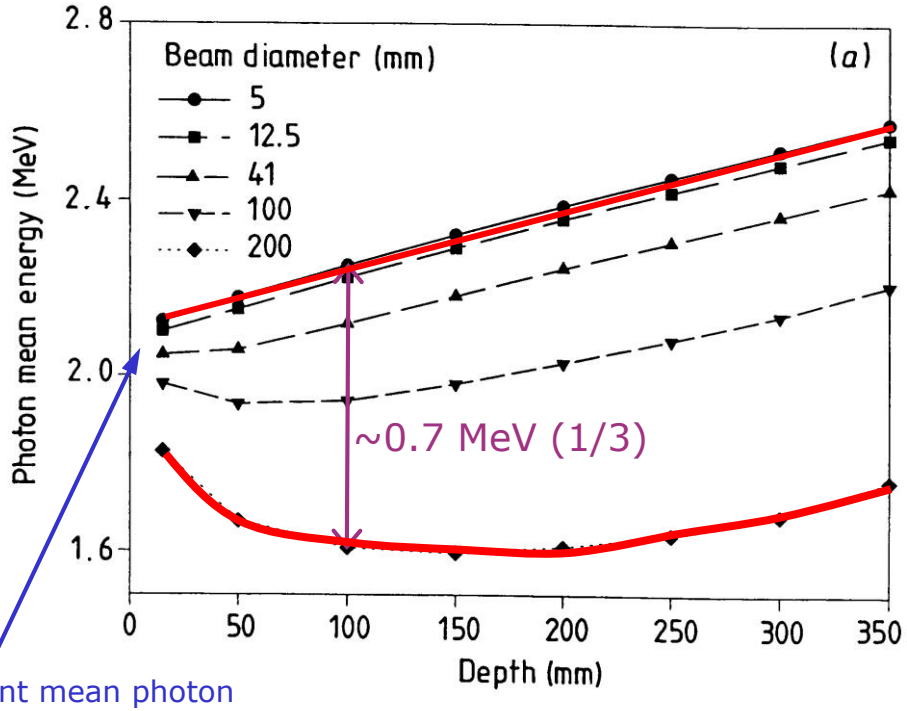

Incident mean photon energy = 2.11 MeV

electrons

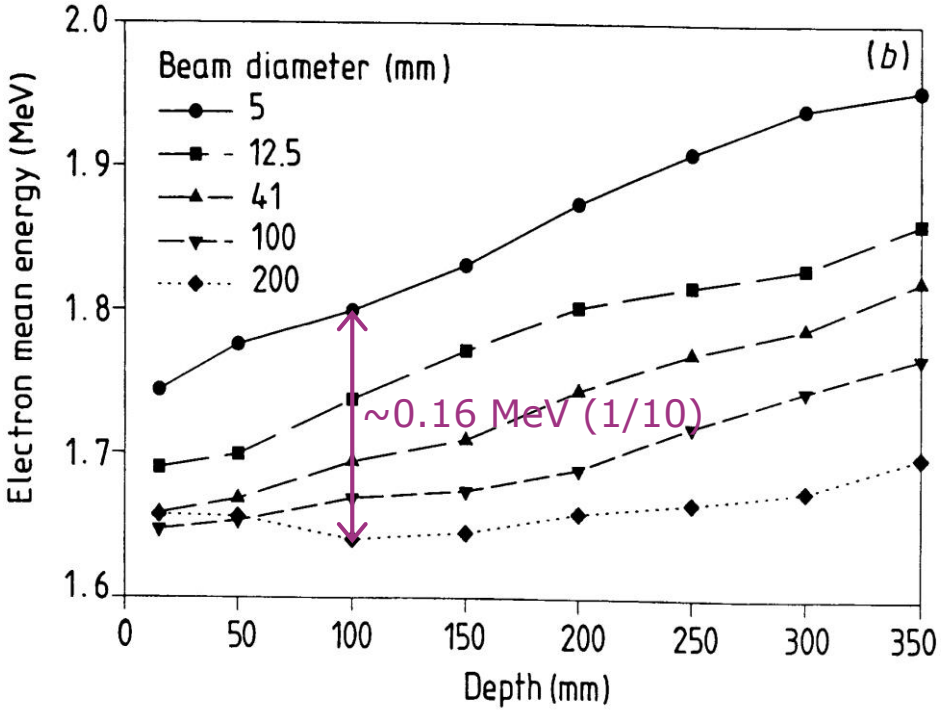

Heydarian *et al*

ESTRO School

Relative-absolute dose measurements

- Relative measurements (ion chambers, diodes, diamonds…)

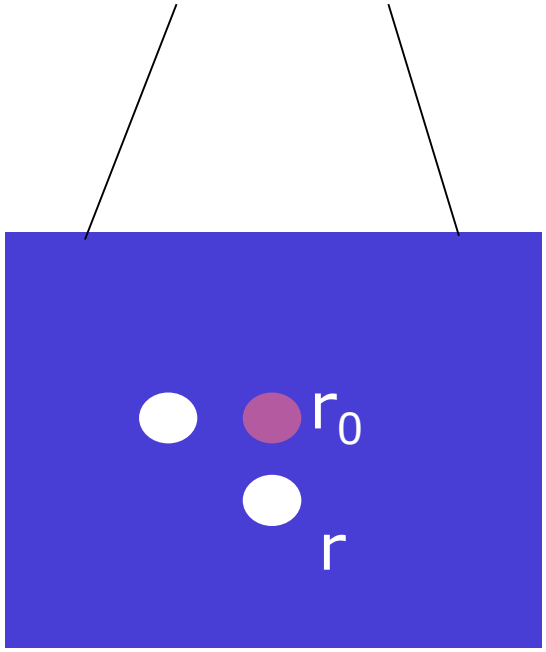

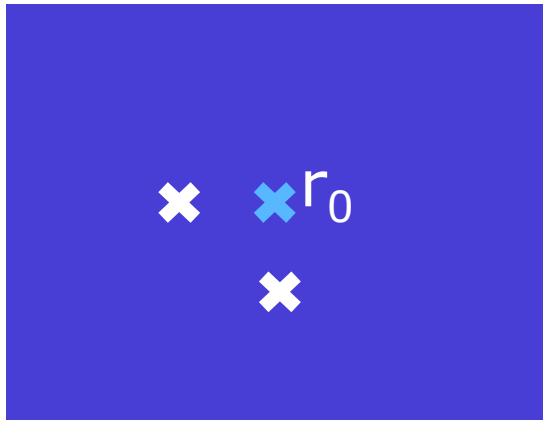

$D_{det} = R(r) \cdot F_{cal}(r)$

$D_{med} = D_{det} \cdot f_Q(r)$

$$\frac{D_{med}(r)}{D_{med}(r_0)} = \frac{R(r)}{R(r_0)} \times \frac{F_{cal}(r)}{F_{cal}(r_0)} \times \frac{f_Q(r)}{f_Q(r_0)}$$

$f_Q = [\mu_{en}/\rho]_{w,\,med}$

$f_Q = S_{w,med}$

ESTRO School

Energy Dependence

Intrinsic energy dependence

Detector reading to the average dose to the material of the sensitive detecting element

$D_{det}(Q) = F_{cal}(Q) \cdot M_{det}(Q)$

Ion chamber: $F_{cal} = 1$ (W/e constant)

TLD: TLD response per unit of dose varies between 5% and 15% for low energy photons

Absorbed dose- energy dependence

Relates the dose to the detector material to the dose to the medium

$D_{med}(Q) = f(Q) \cdot D_{det}(Q) = f_Q \cdot D_{det}(Q)$

Cavity Theory

$$\frac{\overline{D_{det}}}{D_{med}} = d\left(\frac{\overline{L_D}}{r}\right)_{med}^{det} + (1-d)\left(\frac{\overline{\mu_{en}}}{r}\right)_{med}^{det} \quad \textit{Burling}$$

f(Q) is calculated by MC

ESTRO School

Energy dependence of detector response (photon interactions within the detector)

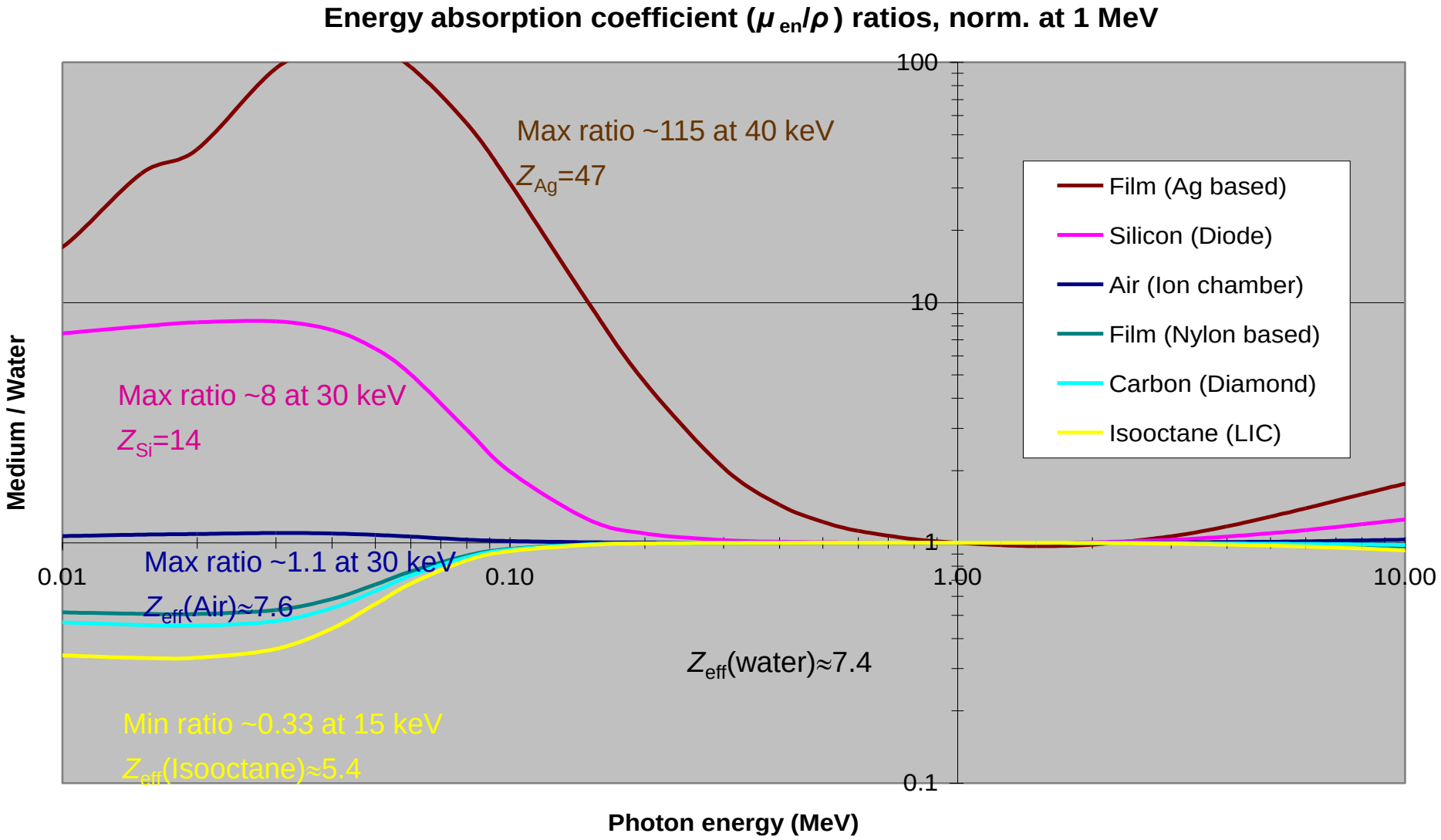

What is meant by "Energy dependence"?

A varying relation between the detector signal and the investigated dose (water), caused by spectral changes of the beam.

ESTRO School

Energy dependence due to changing Stopping-power ratios (dose deposition due to electrons)

What is meant by "Energy dependence"?

A varying relation between the detector signal and the investigated dose (water), caused by spectral changes of the beam.

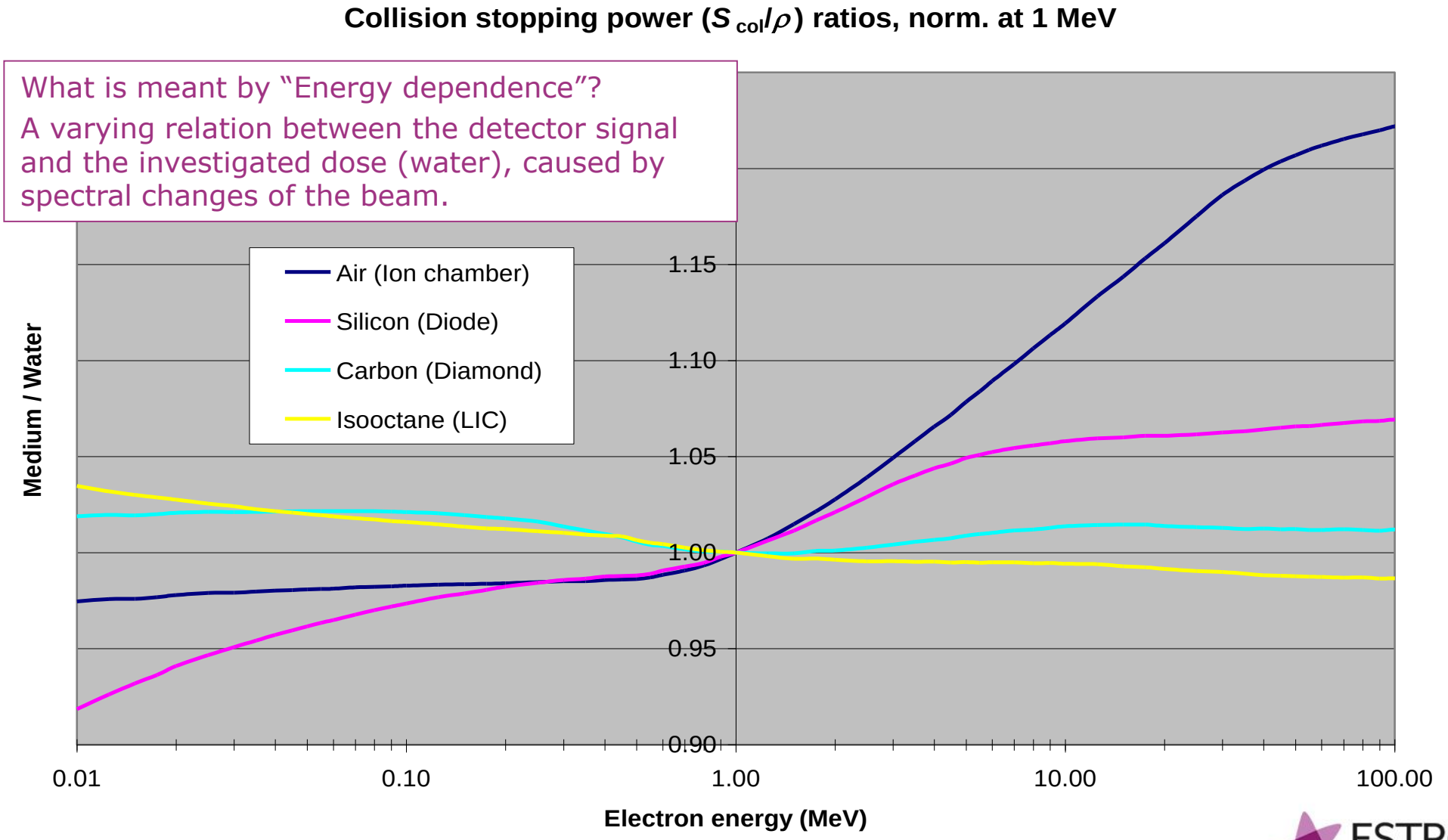

ESTRO School

Energy dependence of an air filled ion chamber response (secondary electrons within the detector)

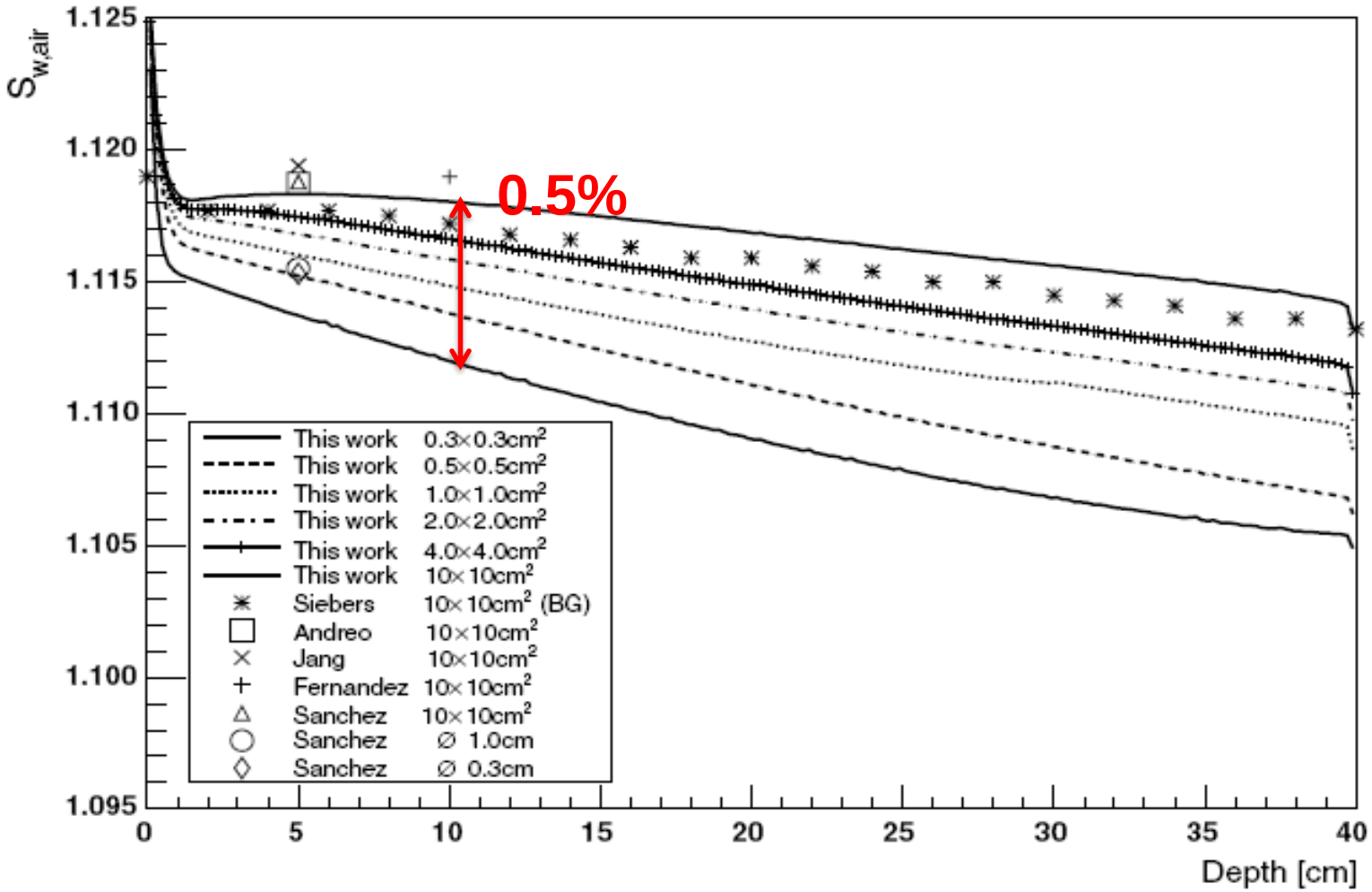

Small difference between field sizes <0.5%

Small difference when moving the detector in depth < 1% for the 0.3 cm field size

School

Variation of $s_{water,air}$ for ion chamber measurements

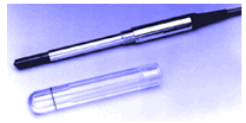

10^7 photons

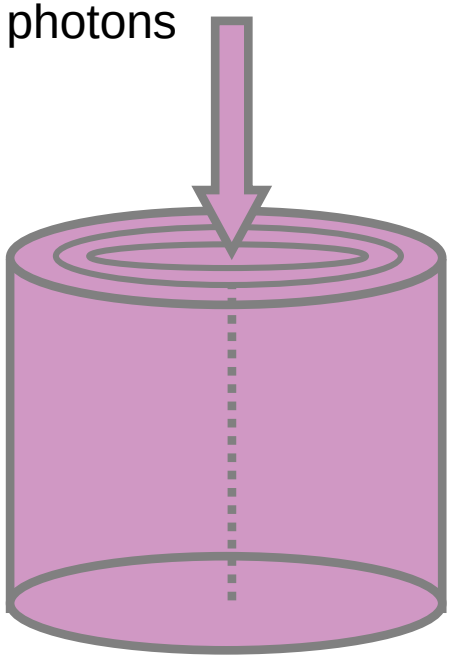

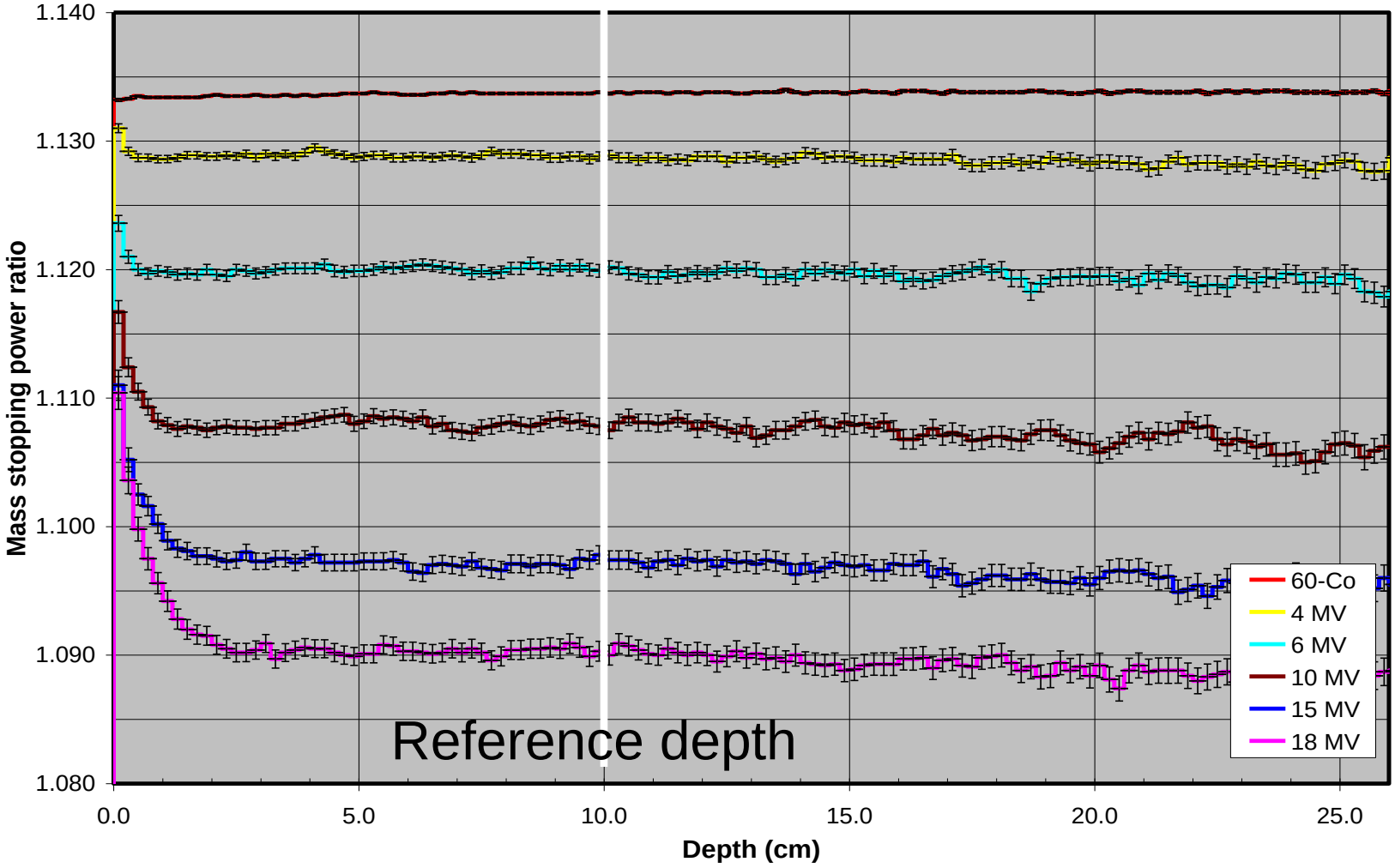

T Knöös

Calculations performed with SPRrznrc

ESTRO School

Variation of $s_{water,air}$ for ion chamber measurements

10^7 photons

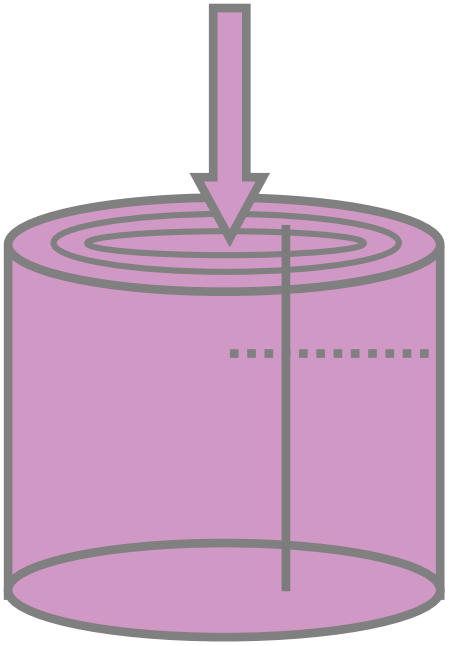

Constant spectra over the field

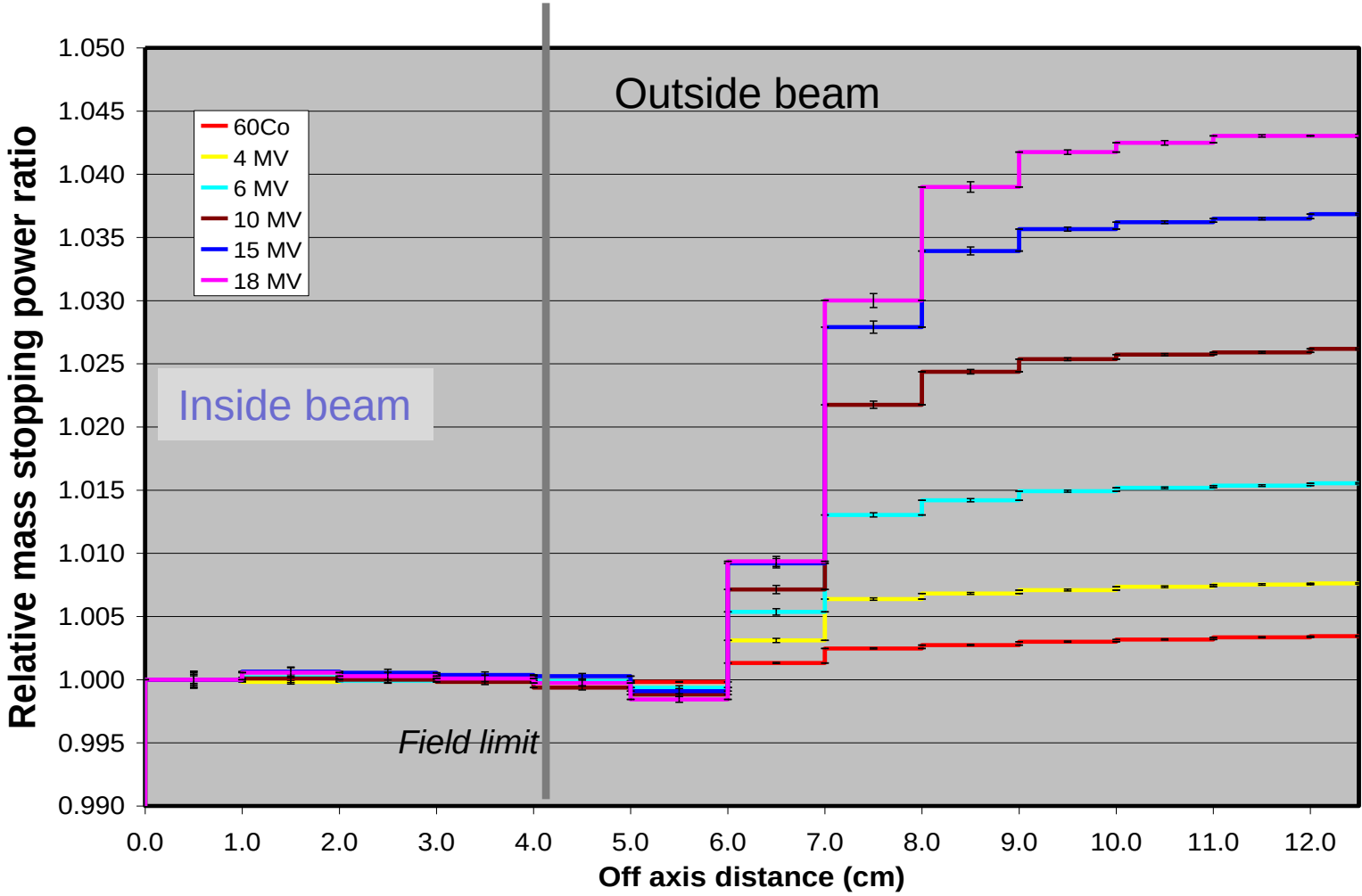

Stopping power ratios along a radii at 10 cm depth in water

Calculations performed with SPRrznrc

T Knöös

ESTRO School

Raiders of the perfect detector

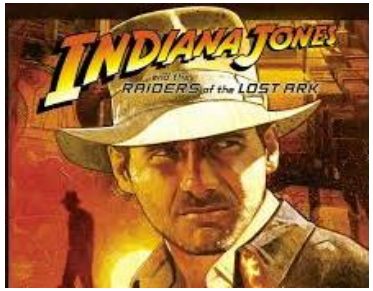

- High Repeatability
- High Reproducibility [no variation of response with i.e. accumulated dose]
- High Accuracy and precision
- High Sensitivity
- Adequate dose range and lineality of the response with dose
- Energy independence
- Insensitivity of the response to influence quantities (dose rate, temperature, pressure, direction…)
- Small dimensions

Precision: Statistical reproducibility of measurements+resolution of measuring system
Accuracy how closely the measurement value agrees with the true value.

Principle of absorbed dose measurements

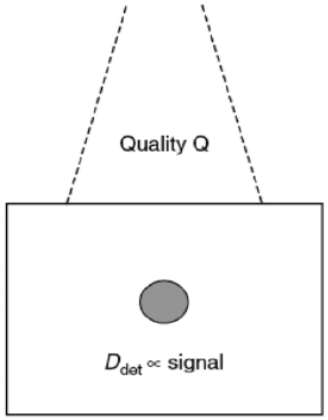

Ionisation chamber	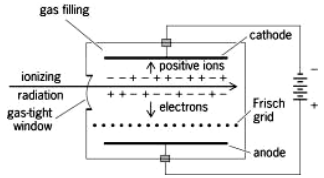	Charge
Diode	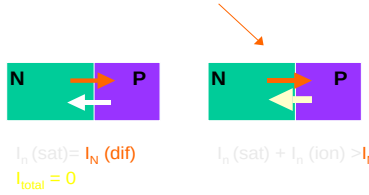	Charge
Diamond	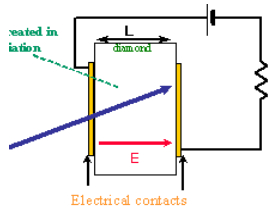	Charge
Scintillator	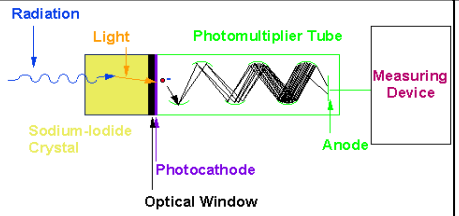	Light
Film	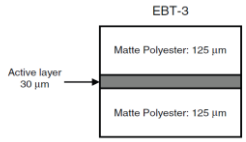	Chemical reaction changes opaqueness. Optical Density

Challenges: reference versus relative dosimetry

Reference conditions

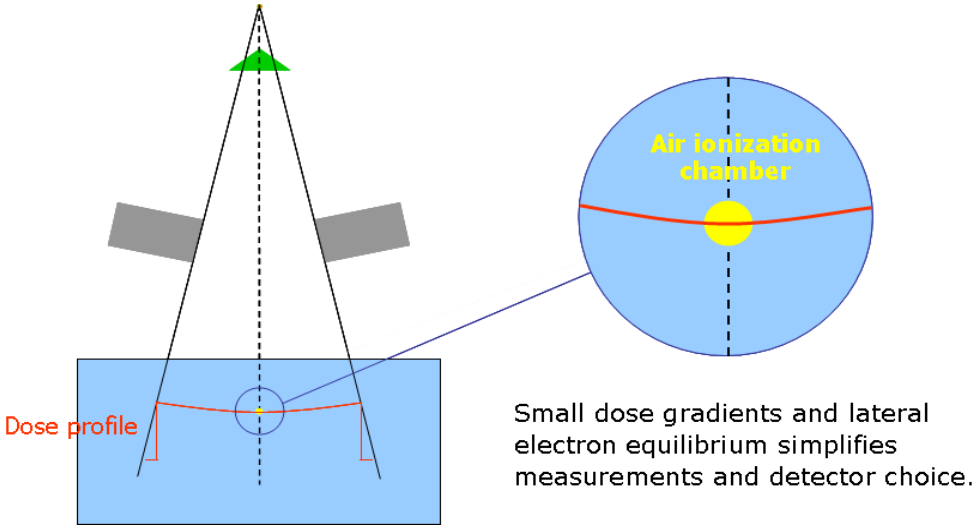

- Uniform electron fluence distribution over the detector.
- Beam spectra at the reference point in ref. conditions known.
- Detector of choice: Ion Chambers

Non reference conditions: *Relative dosimetry*

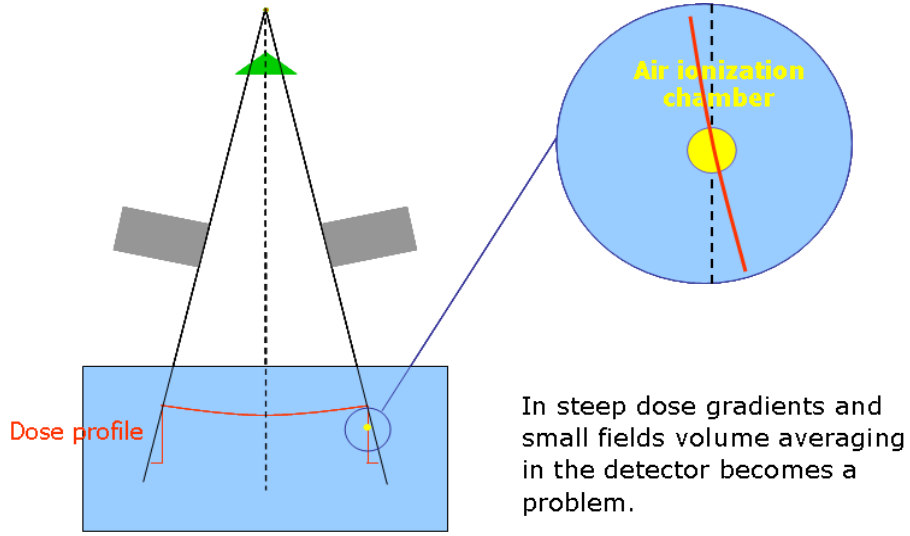

- Non-Uniform electron fluence distribution over the detector. VOLUME AVERAGING
- Beam spectra at the reference point may differ from beam spectra at the measuring point. ENERGY DEPENDENCE; PERTURBATION FACTORS
- Detector of choice: ???

ESTRO School

Does the detector used matter?

Accelerator beam data commissioning equipment and procedures: Report of the TG-106 of the Therapy Physics Committee of the AAPM

Indra J. Das[a)]
Department of Radiation Oncology, University of Pennsylvania, Philadelphia, Pennsylvania 19104

Chee-Wai Cheng
Department of Radiation Oncology, Morristown Memorial Hospital, Morristown, New Jersey 07962

Ronald J. Watts
International Medical Physics Services, San Antonio, Texas 78232

Anders Ahnesjö
Uppsala University and Nucletron Scandinavia AB, 751 47 Uppsala, Sweden

John Gibbons
Department of Radiation Oncology, Mary Bird Perkins Cancer Center, Baton Rouge, Louisiana 70809

X. Allen Li
Department of Radiation Oncology, Medical College of Wisconsin, Milwaukee, Wisconsin 53226

Jessica Lowenstein
Radiological Physics Center, MD Anderson Cancer Center, Houston, Texas 77030

Raj K. Mitra
Department of Radiation Oncology, Ochsner Clinic, New Orleans, Louisiana 70121

William E. Simon
Sun Nuclear Corporation, Melbourne, Florida 32940

Timothy C. Zhu
Department of Radiation Oncology, University of Pennsylvania, Philadelphia, Pennsylvania 19104

(Received 4 February 2008; revised 18 July 2008; accepted for publication 18 July 2008; published 22 August 2008)

ESTRO School

Type of data that we need to collect

- Beam profiles
- Depth dose
- Tissue maximum or phantom ratio TMR/TPR
- Surface dose and build up region
- Total scatter factors
- Phantom scatter factors
- Wedge factors/tray factors
- Dose/MU under reference conditions

RX

electrons

Does the detector used matter?

" Since commissioning beam data are treated as a reference and ultimately used by treatment planning systems, it is **vitally important that the collected data are of the highest quality to avoid dosimetric and patient treatment errors** that may subsequently lead to a poor radiation outcome. Beam data commissioning should be performed with appropriate knowl- edge and **proper tools** and should be independent of the person collecting the data."

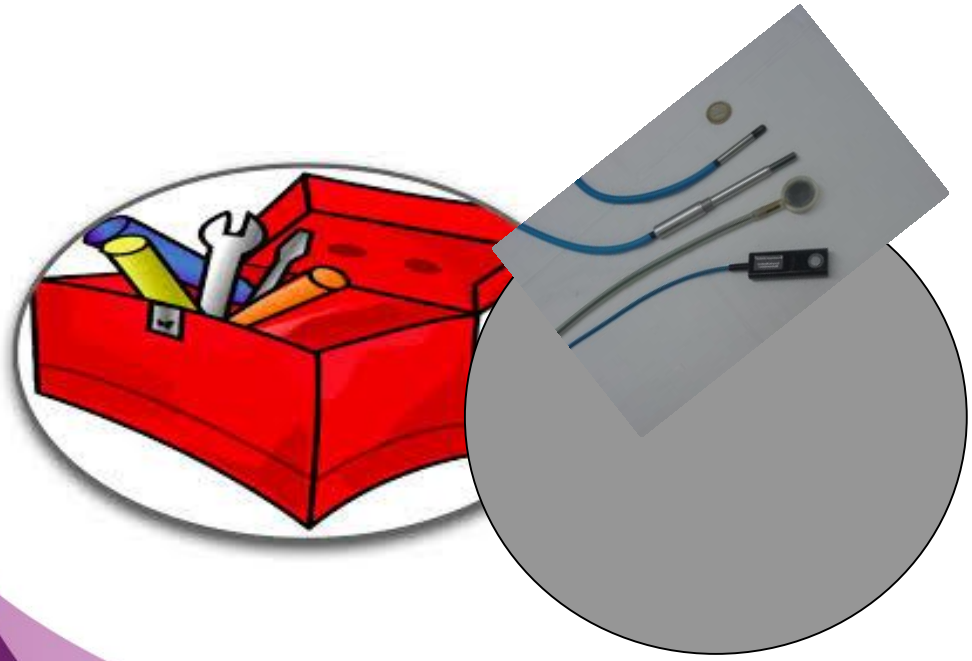

Das et al. **AAPM TG 106** Med.Phys. (2008)

Example: Source size measured by profile fitting

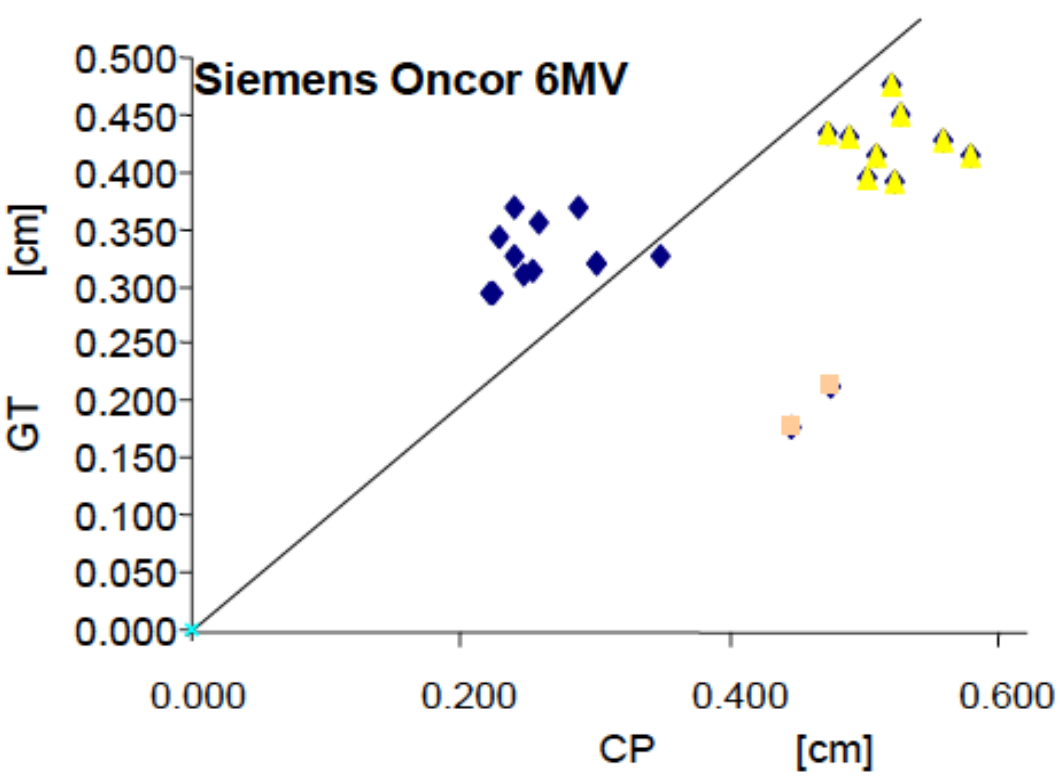

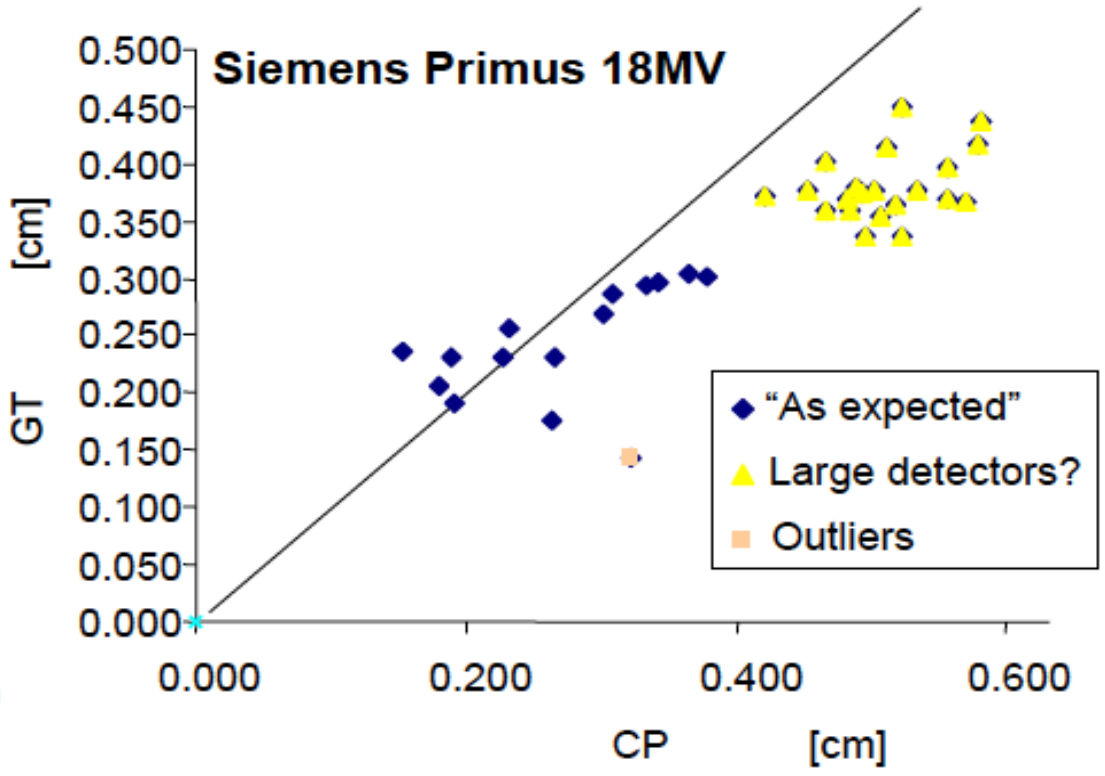

ESTRO School

Detector characteristics

- **Volume effects: Size of sensitive volume**
- Energy dependence: Interactions in detector material
- Cable/stem leakage, polarity effect
- Dose rate dependence: Recombination, bias voltage
- Temperature dependence
- Long term stability/irradiation effects

Does size matter?
Profiles

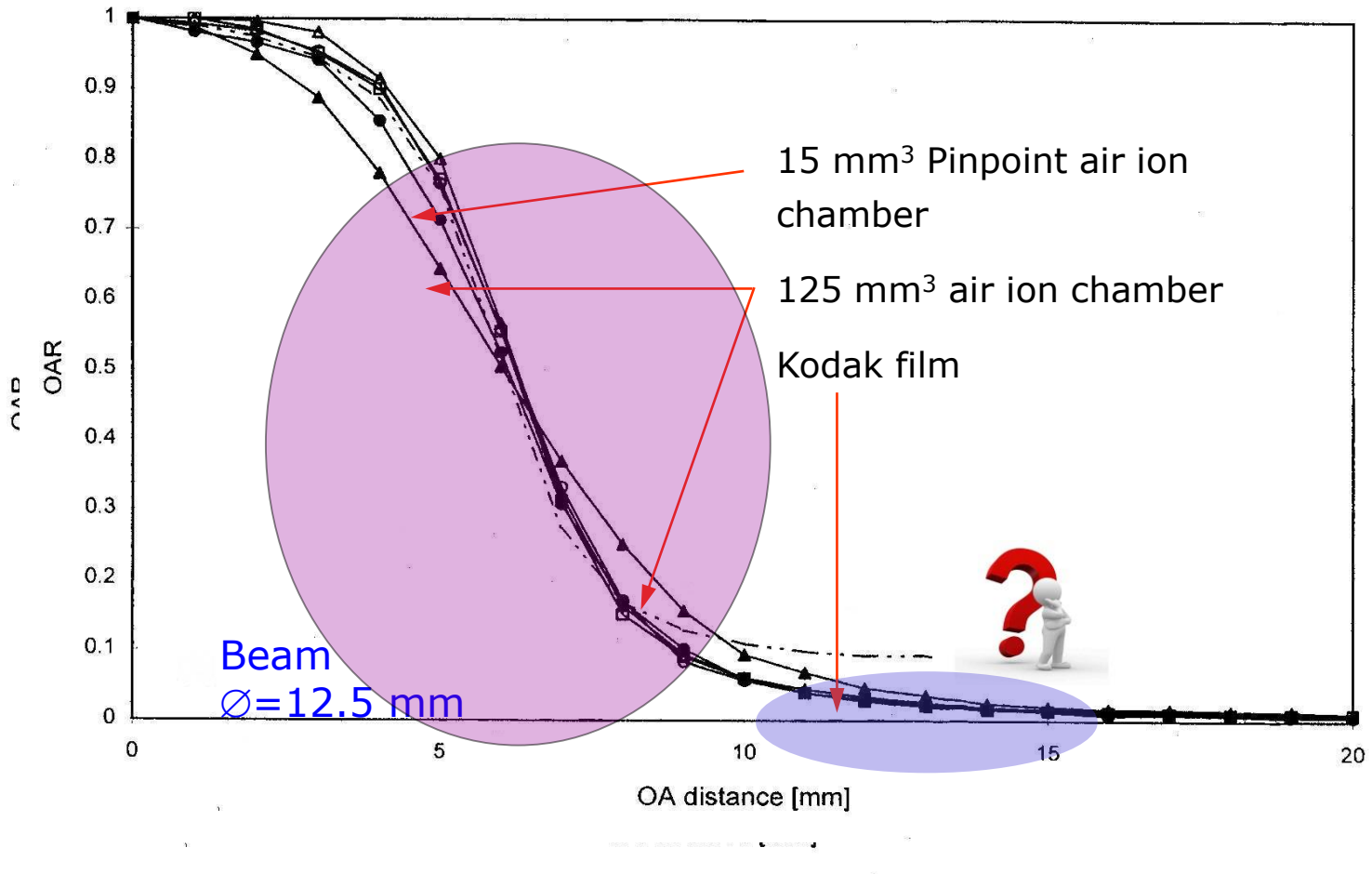

Film gold standard (resolution)

McKerracher *et al* [4]

Film gold standard (resolution)

ESTRO School

Beam Profiles: Penumbra measurements using detectors of different sizes
The volume effect

6 MV, d_{max} (1.4 cm depth)

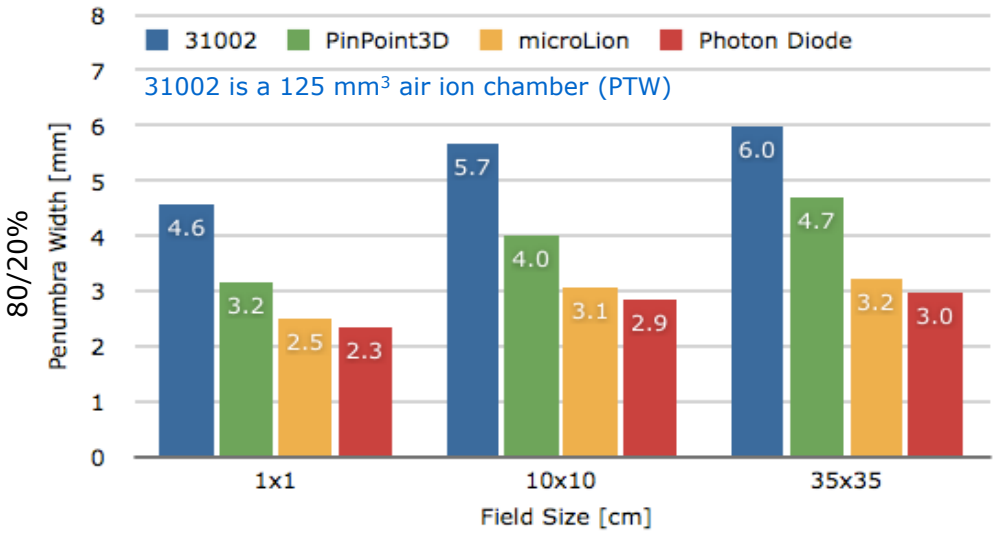

Krauss [20]

6 MV, 30 cm depth

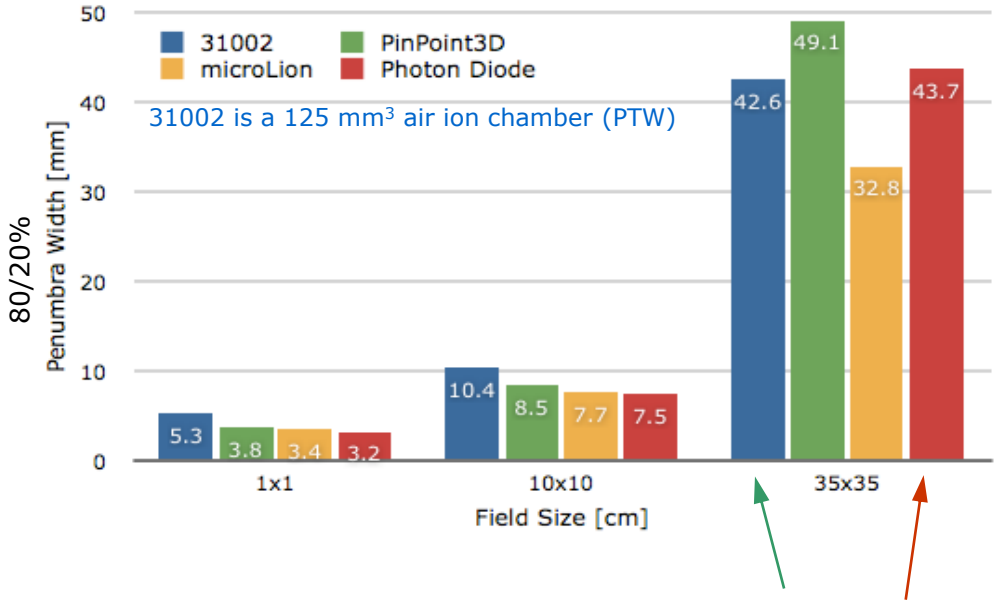

Penumbra widening due to overestimated beam tails (scattered radiation outside beam – energy dependence)

ESTRO School

Beam Profiles: Penumbra measurements using detectors of different sizes
The volume effect

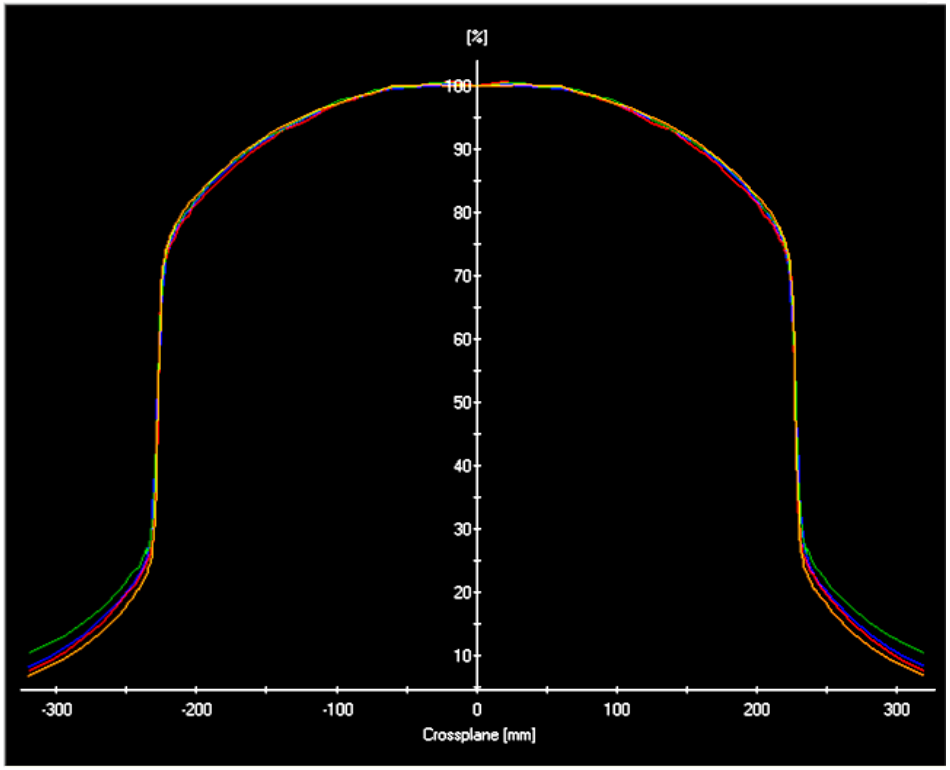

Krauss [20]

6 MV, 30 cm depth

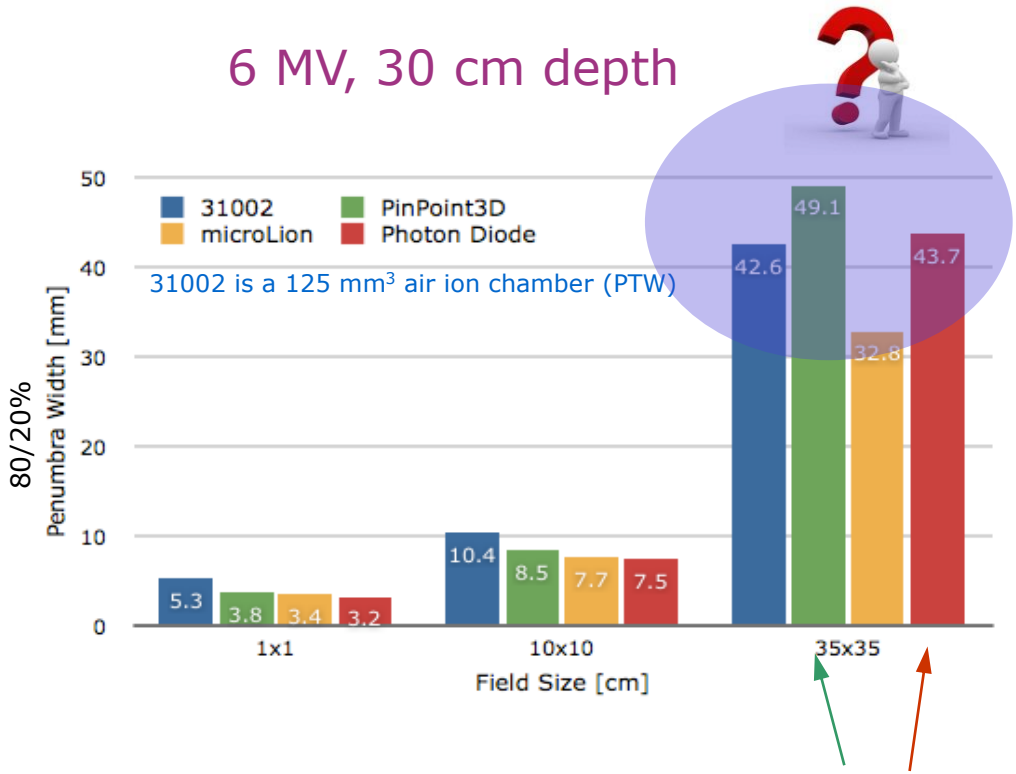

Penumbra widening due to overestimated beam tails (scattered radiation outside beam – energy dependence)

ESTRO School

Output factors: detectors of different sizes
The volume effect

(NACP is a plane parallel air ion chamber, ∅=20 mm)

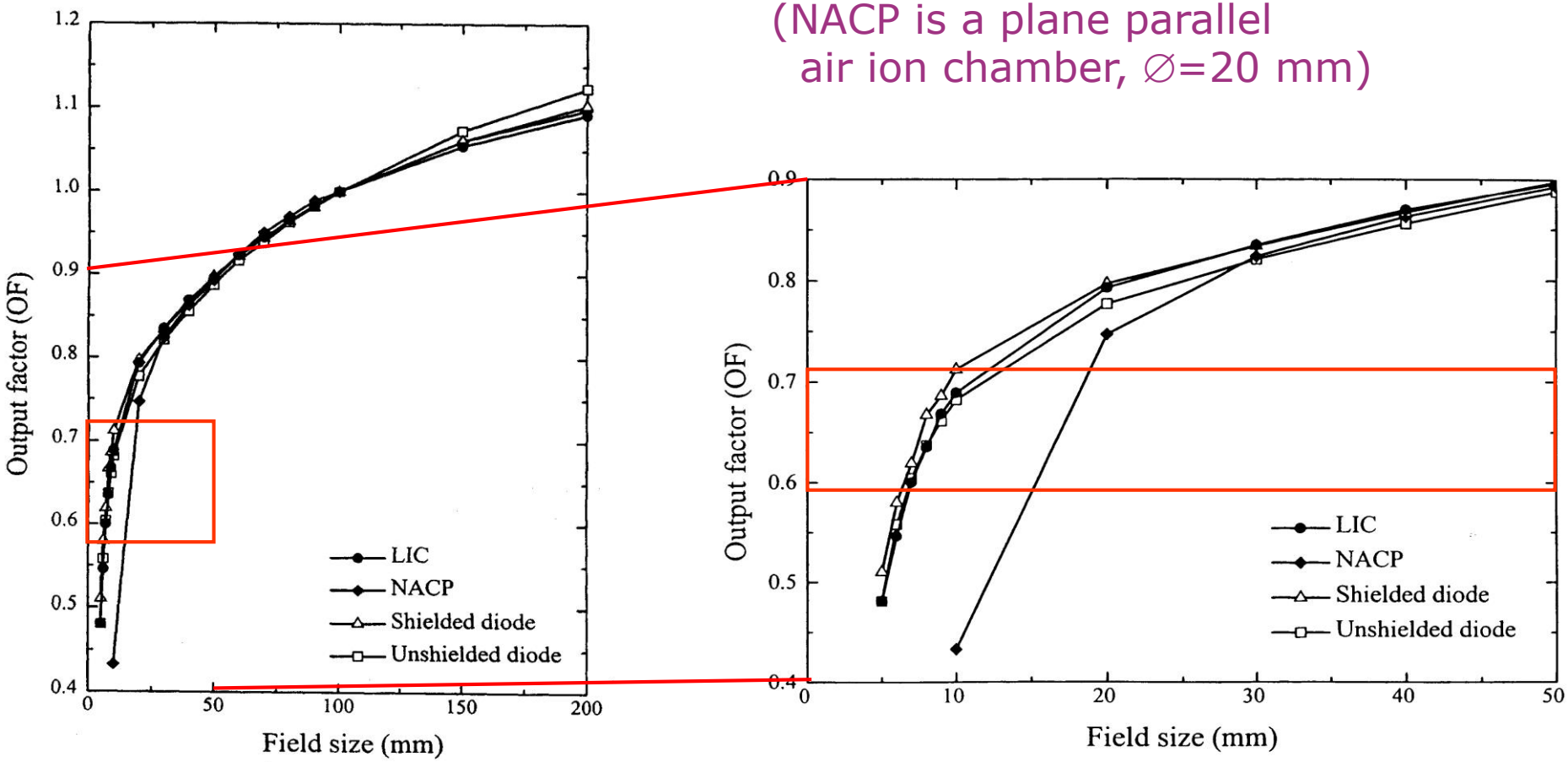

Dasu *et al* [5]

Does size matter?
Output factors

Volume effect detector dimension>1/4 field size

Incident beam direction

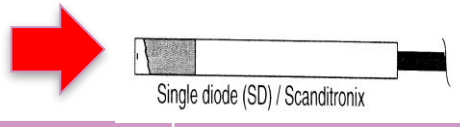

Detector			Φ (mm)	Length (mm)	Minimum field size (mm)
Pinpoint (PTW)	Air i.c.		2	5	8
RK (IBA)	Air i.c.	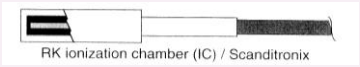	4	10	16
MicroLion (PTW)	Liquid i.c.	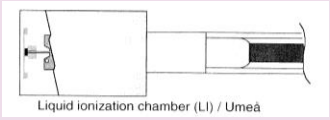	2.5	0.35	10
Diamond (PTW)	Diamond	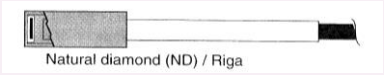	variable	0.3	
MicroDiamond (PTW)	Syntethic Diamond	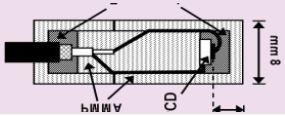	1.1	0.001	4.5
EDE diode (IBA)	Diode	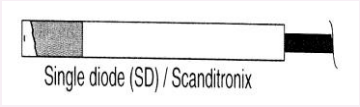	0.6	0.06	2.4
SFD diode (IBA)	Diode	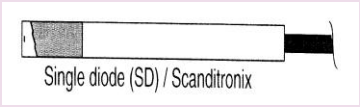	2	0.06	8
W1 (Standard Imaging)	Scintillator		2.8	3	12

Does size matter?
Output factors

Volume effect detector dimension>1/4 field size

Incident beam direction

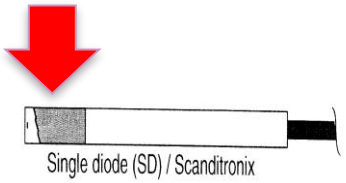

Detector			Φ (mm)	Length (mm)	Minimum field size (mm)
Pinpoint (PTW)	Air i.c.		2	5	20
RK (IBA)	Air i.c.	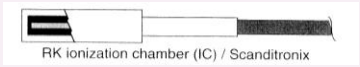	4	10	40
MicroLion (PTW)	Liquid i.c.	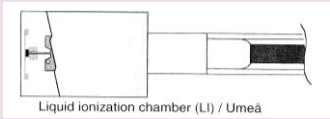	2.5	0.35	1.4
Diamond (PTW)	Diamond	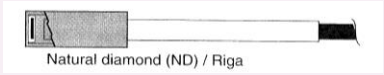	variable	0.3	1.2
MicroDiamond (PTW)	Syntethic Diamond		1.1	0.001	0.004
EDE diode (IBA)	Diode	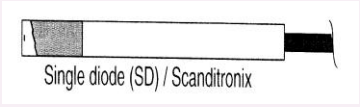	0.6	0.06	0.24
SFD diode (IBA)	Diode	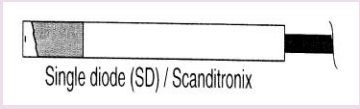	2	0.06	0.24
W1 (Standard Imaging)	Scintillator		2.8	3	12

Pushing volume to the lower limit

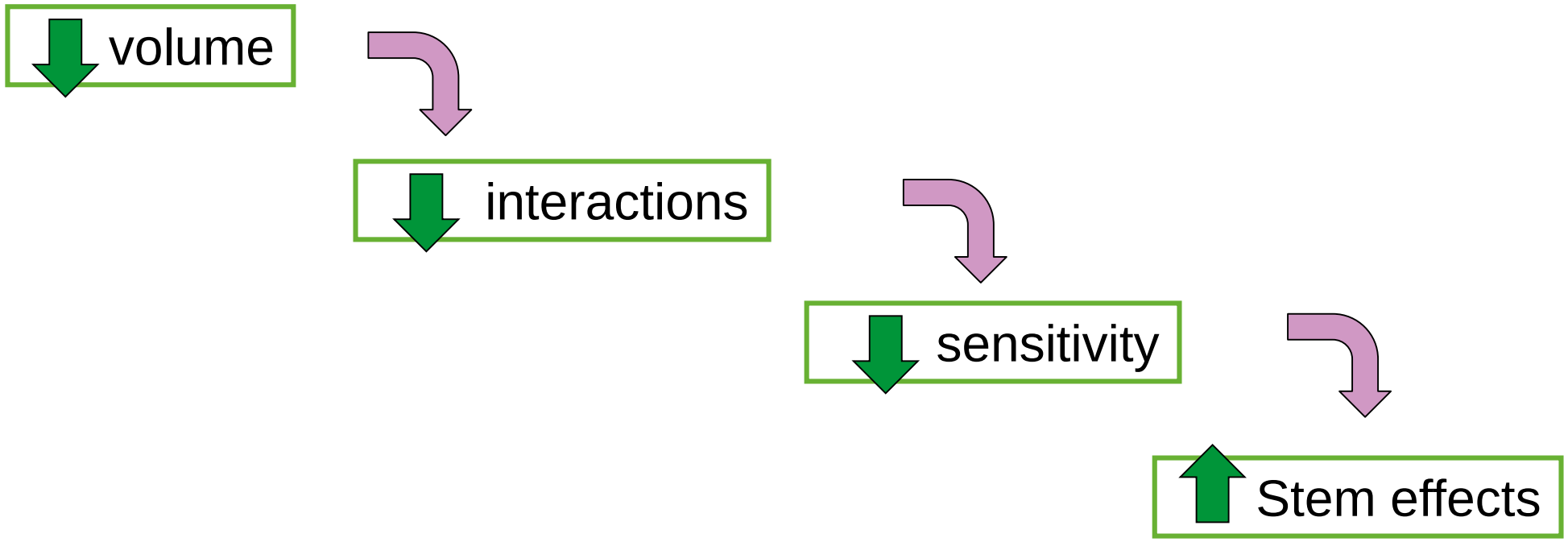

Pushing volume to the lower limit

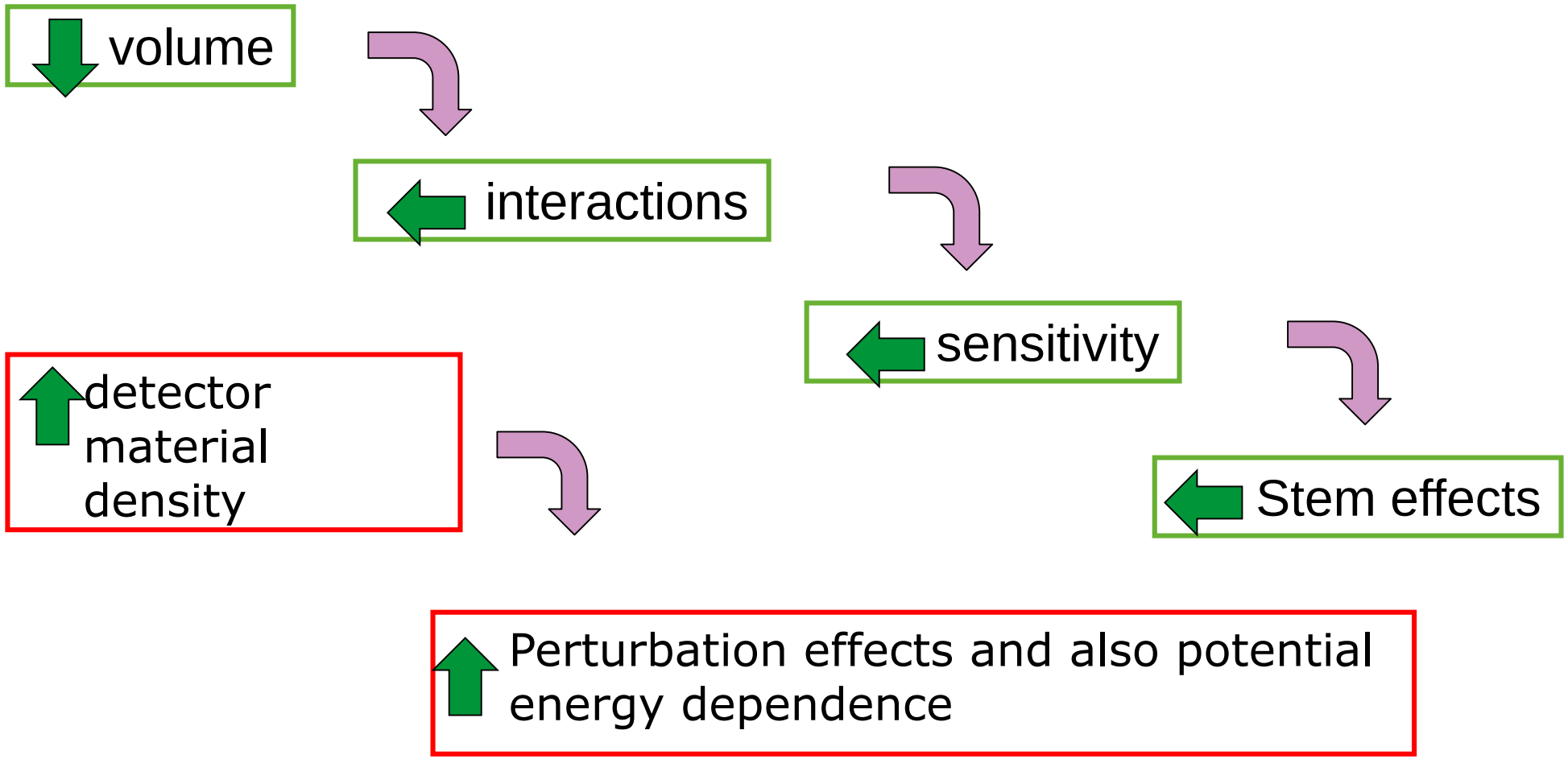

Detector characteristics

✓ Volume effects: Size of sensitive volume

- **Energy dependence: Interactions in detector material**
- Cable/stem leakage, polarity effect
- Dose rate dependence: Recombination, bias voltage
- Temperature dependence
- Long term stability/irradiation effects

ESTRO School

Output factors: Large fields

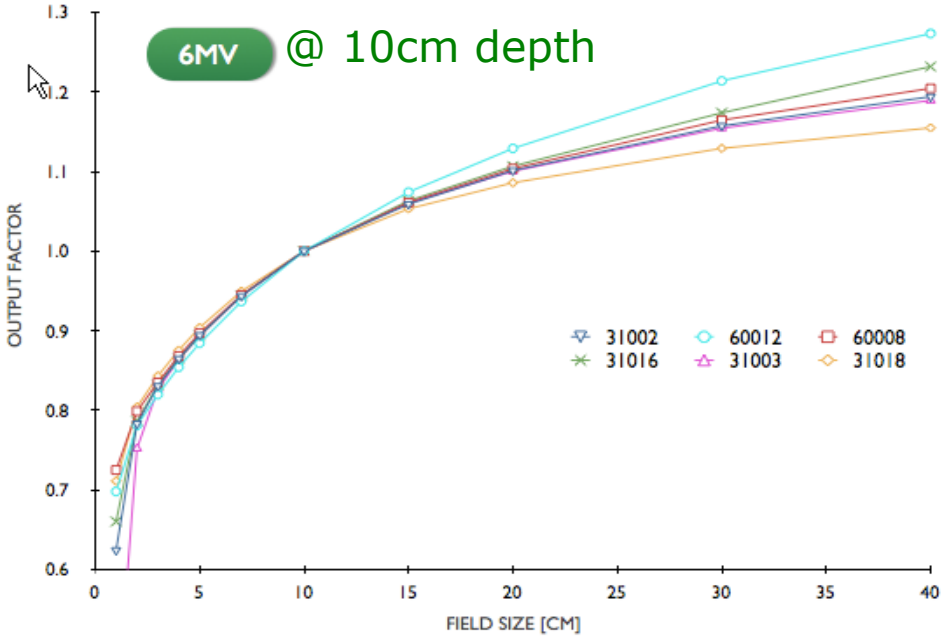

Unshielded Diode

0.125cc i.c.

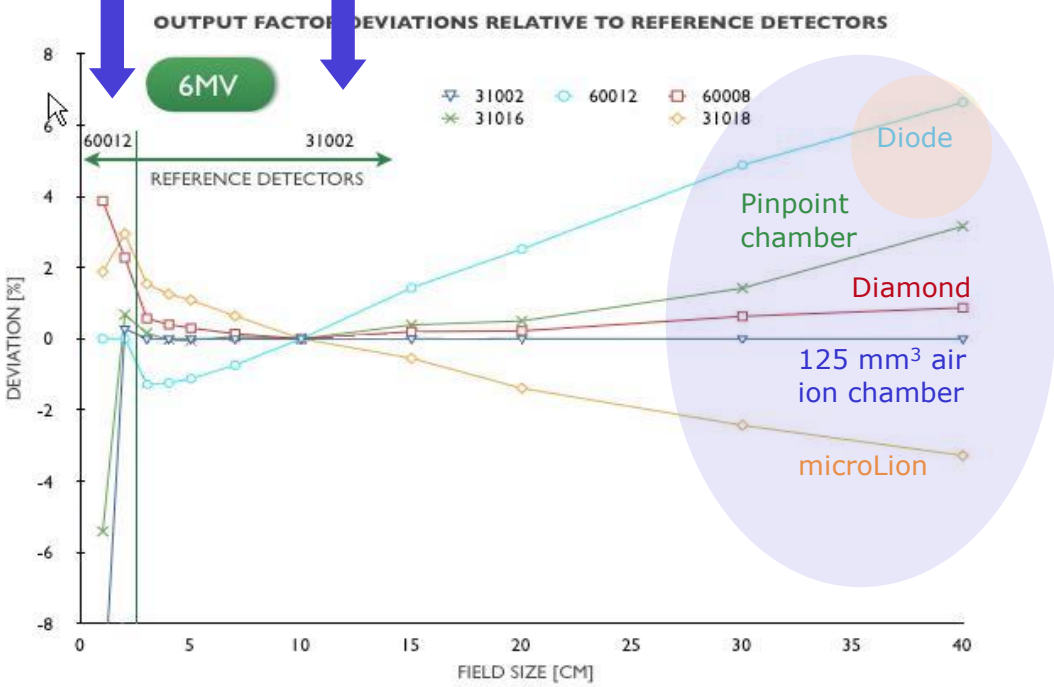

Krauss et al.

www.wienkav.at/kav/kfj/91033454/physik/PTW/liquid.htm

ESTRO School

Energy dependence due to changing Stopping-power ratios

6 MV photon beam
n=narrow beam (∅=0.5 cm)
b=broad beam (∅=10 cm)

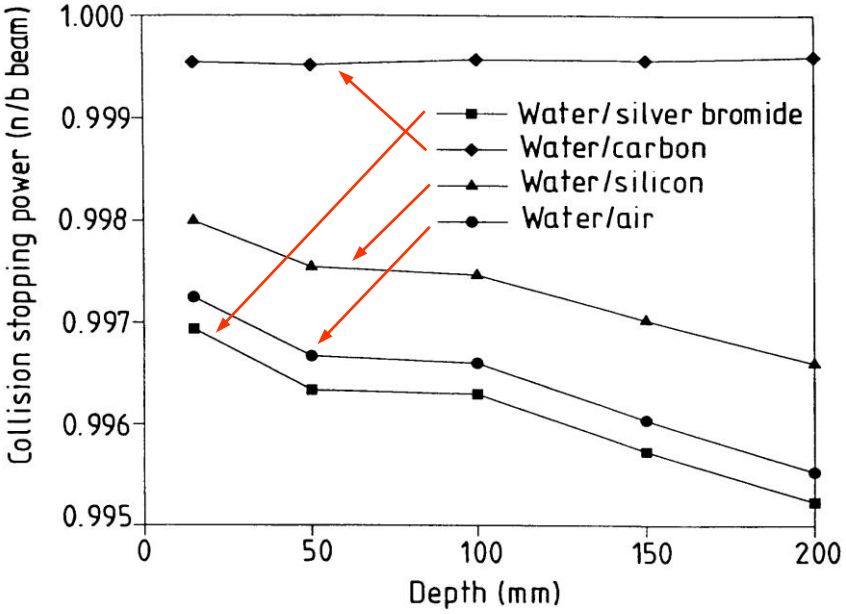

Heydarian *et al*

Cylindrical air ion chambers can be used without correction for energy variations in high energy photon beams, incl. Co-60 (IAEA TRS-398).

The secondary electron energy spectrum is not changing with depth.

Ratio narrow/large field depth dependence
Difference <0.5%

ESTRO School

Energy dependence at low photon energies (photon interactions in the detector medium)

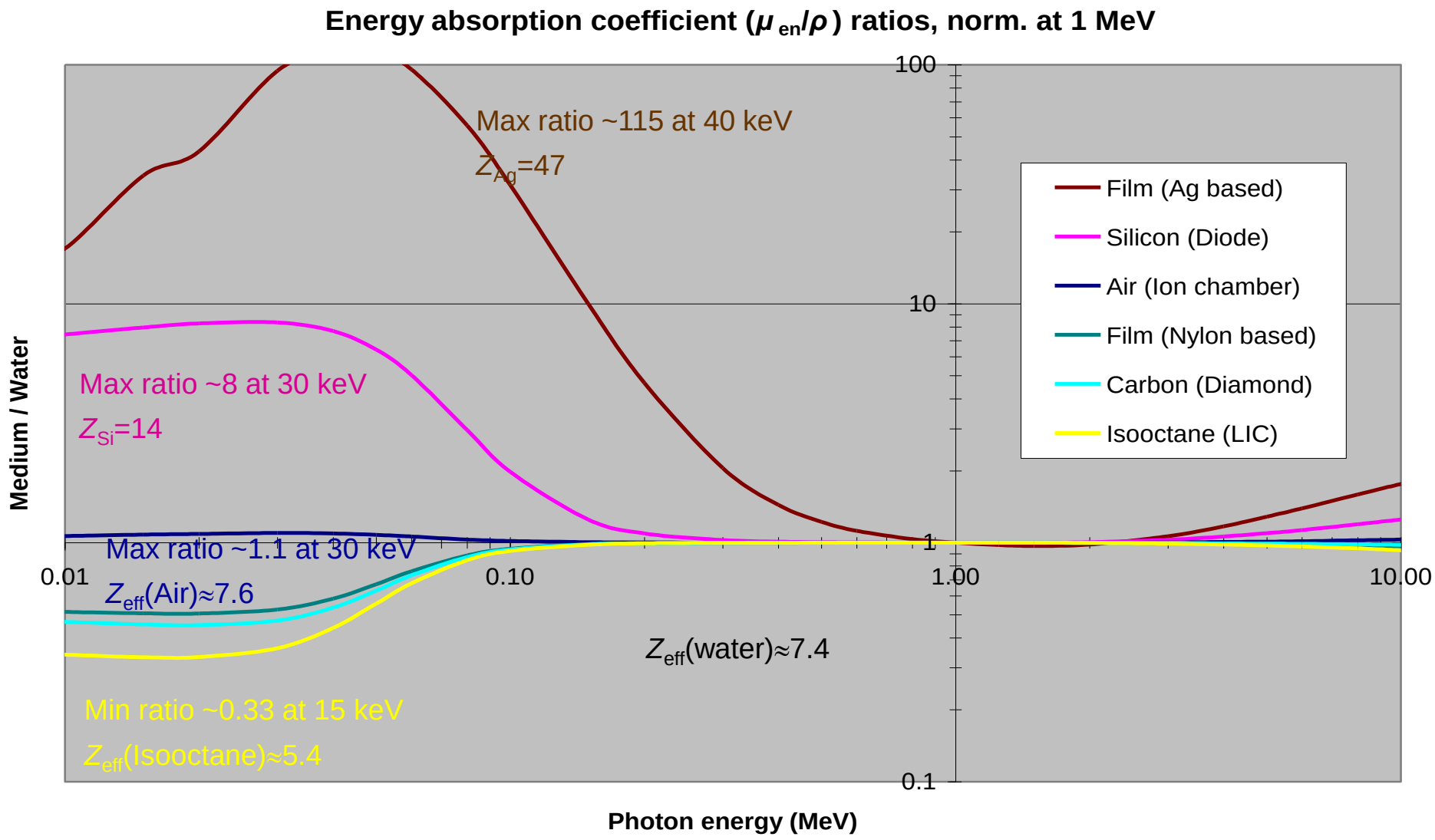

Output factors for large fields using diodes

Shielded Si diodes for compensation of photon energy dependence.

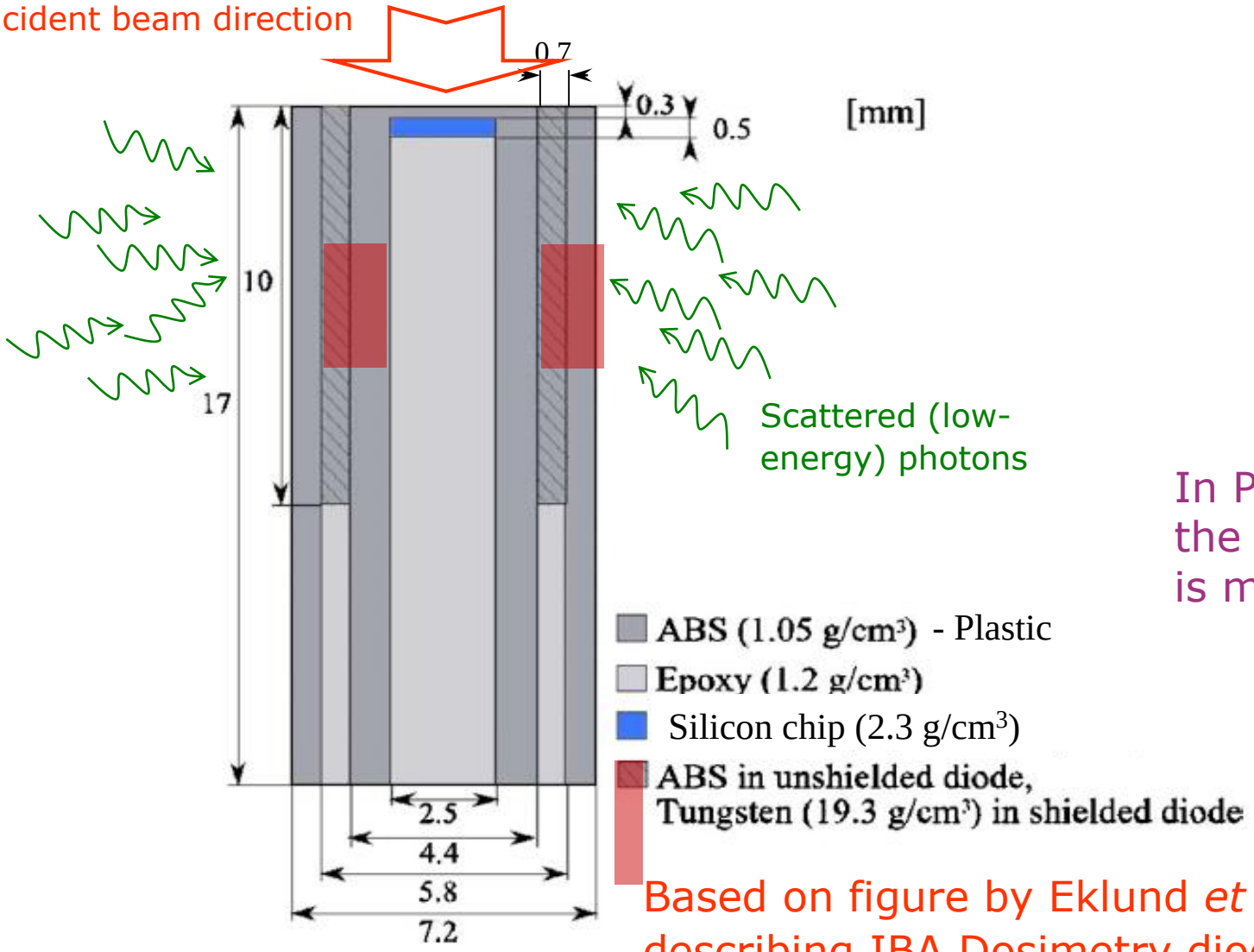

In PTW photon diodes the backscatter shield is made of steel instead.

Based on figure by Eklund *et al* [6] describing IBA Dosimetry diodes (EFD/PFD)

ESTRO School

Scanning results in a 5 MV X-ray beam using p-Si diodes.

Low energy in combination with large beams (here 5 MV and 40x40 cm^2) displays the largest deviations for Si diodes.

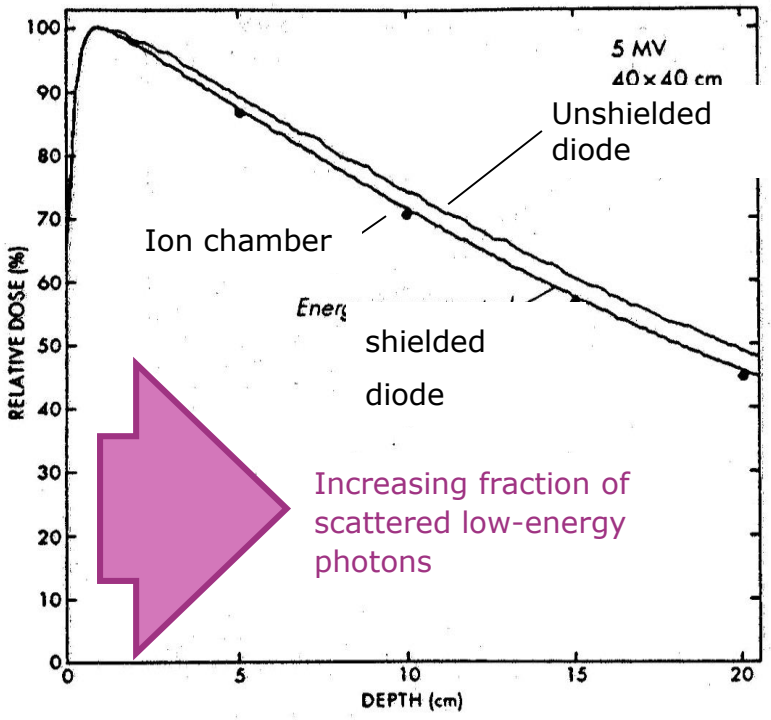

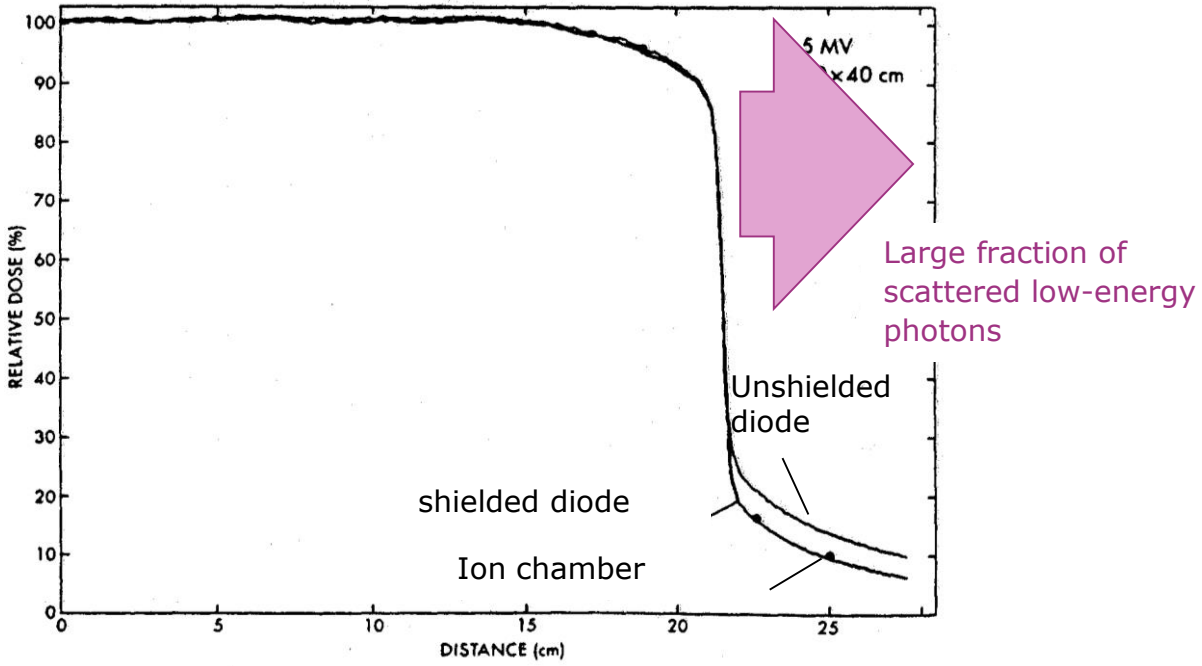

Data from Scanditronix

ESTRO School

OF measurements, incl. corrections, in a 6 MV X-ray beam using p-Si diodes

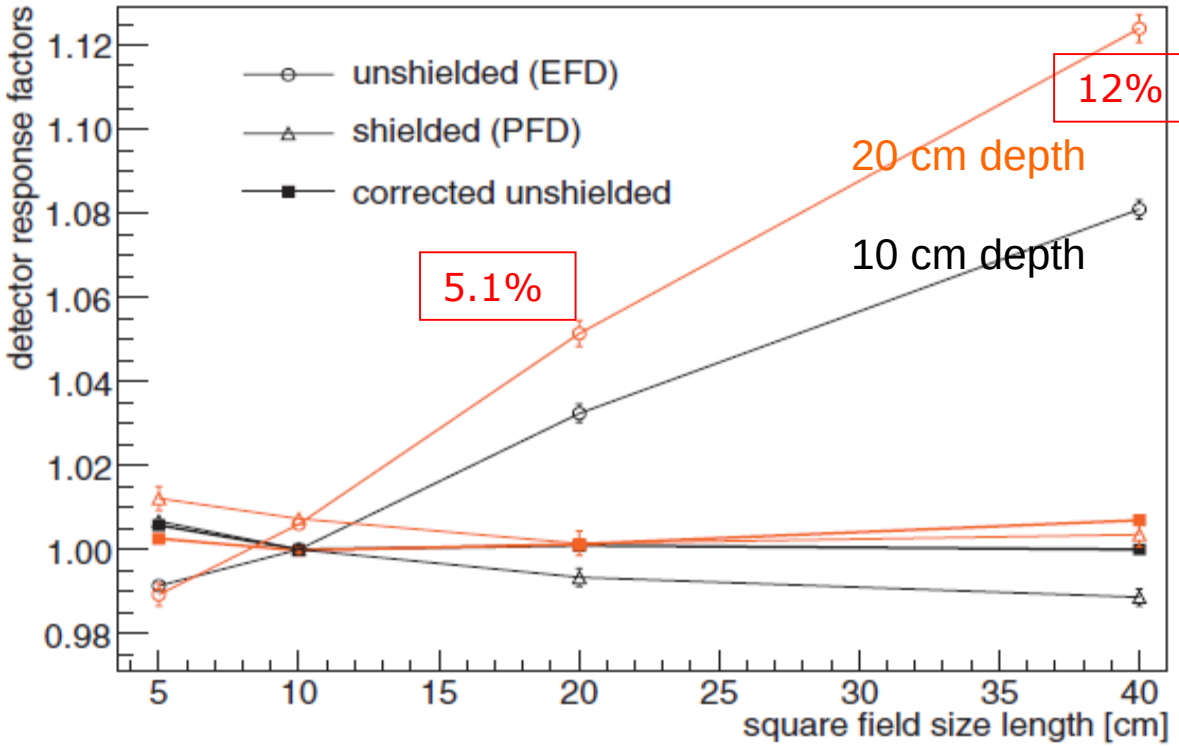

Eklund *et al* [6]

Use shielded diodes for x-ray dosimetry

Exception: Small fields (the shielding would perturbate the field)

ESTRO School

Output factor measurements using detectors of different materials

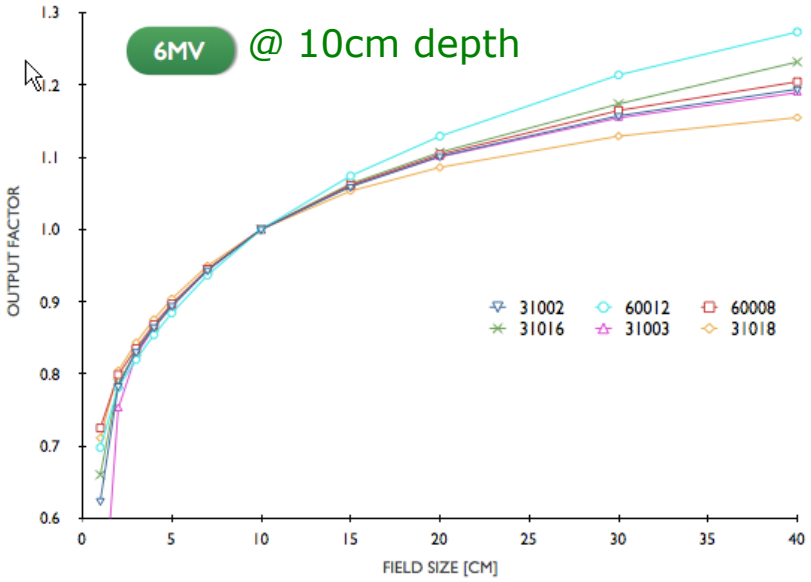

Krauss [20]

Aluminium central electrode

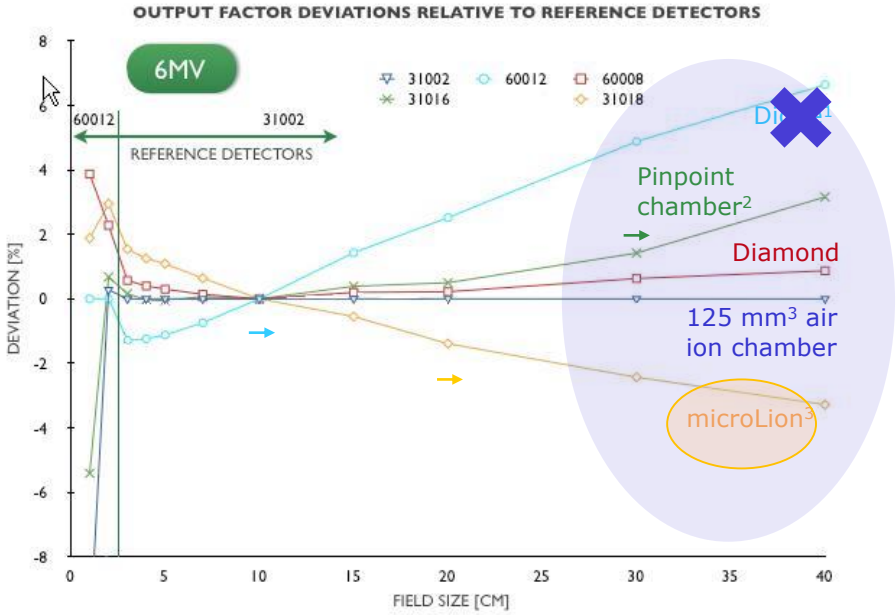

[1]PTW recommends max photon field size: 10x10 cm^2

[2]PTW recommends max photon field size: 30x30 cm^2

[3]PTW recommends max photon field size: 20x20 cm^2

ESTRO School

Energy dependence at low photon energies (photon interactions in the detector medium)

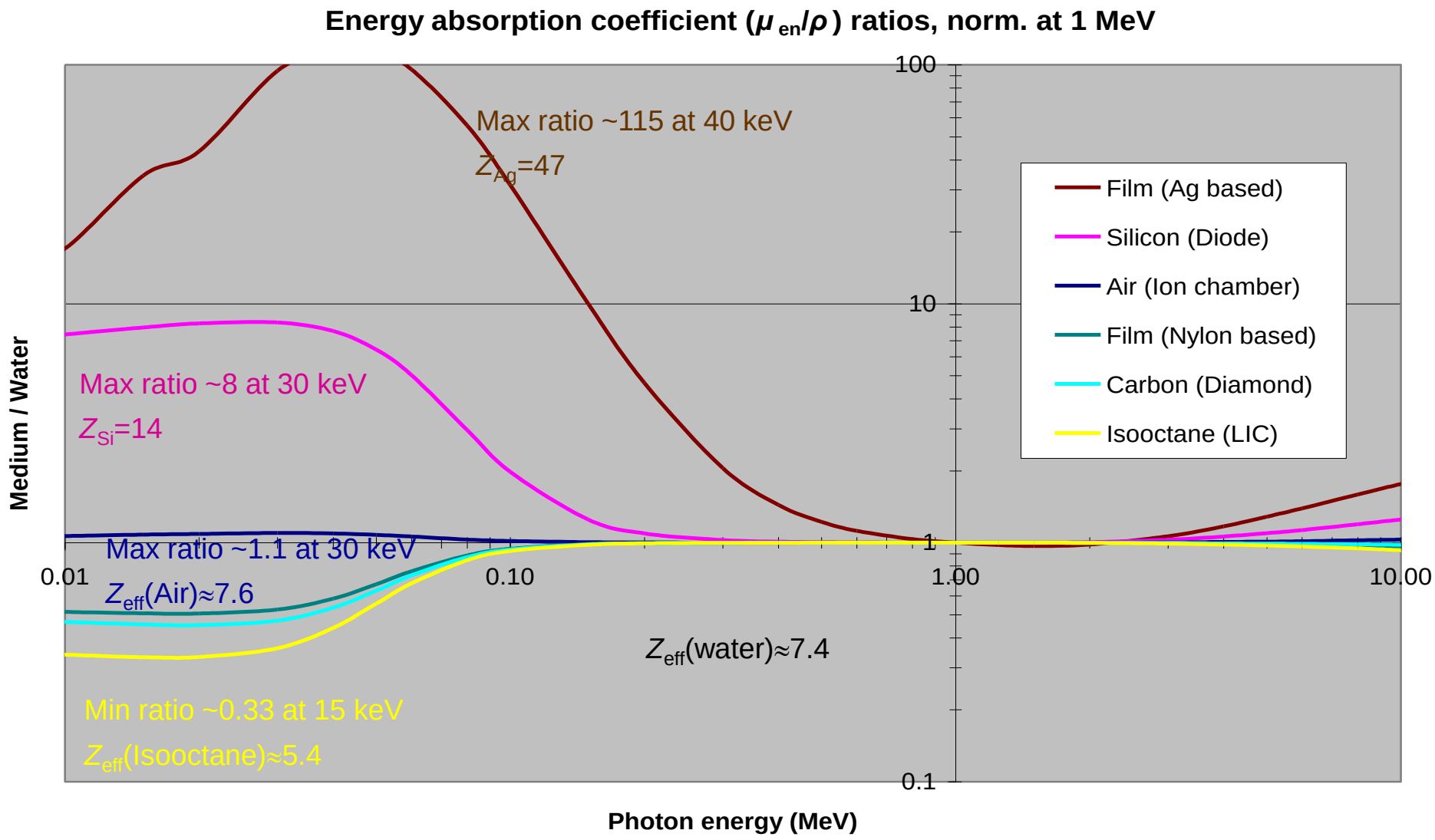

Detector characteristics

✓ Volume effects: Size of sensitive volume

✓ Energy dependence: Interactions in detector material

- **Cable/stem leakage, polarity effect**
- Dose rate dependence: Recombination, bias voltage
- Temperature dependence
- Long term stability/irradiation effects

ESTRO School

Output factor measurements using detectors of different materials

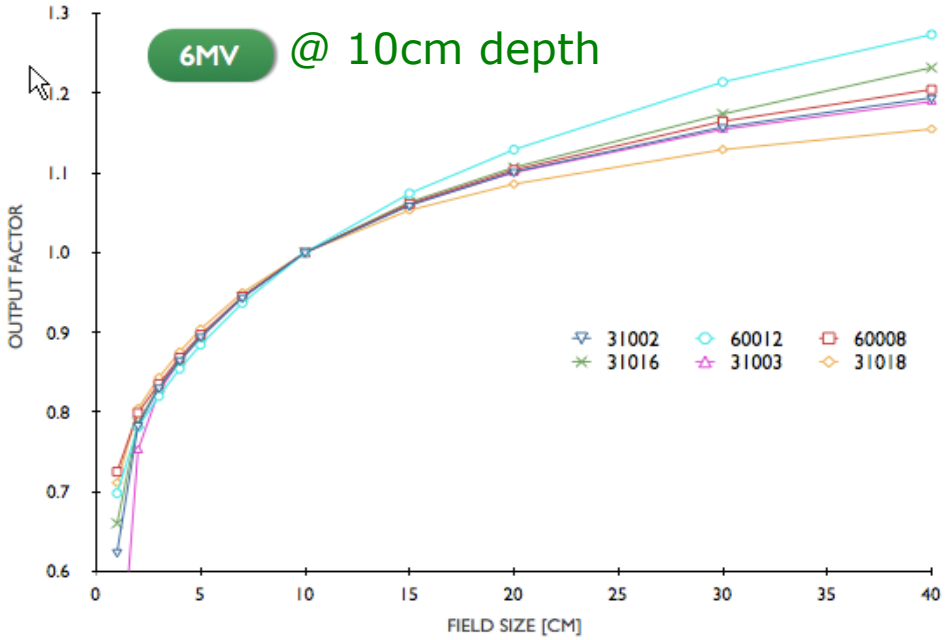

Krauss [20]

Aluminium central electrode

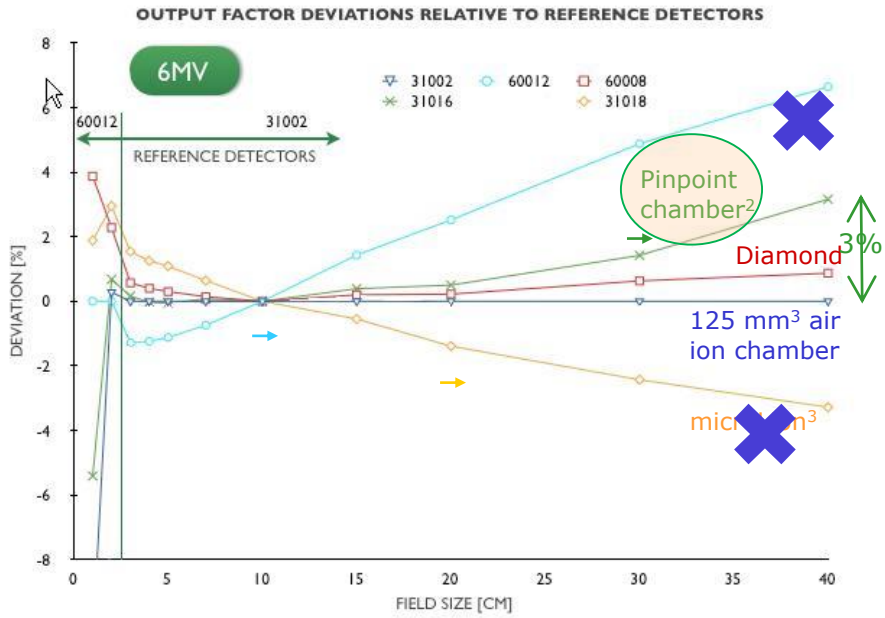

[1]PTW recommends max photon field size: 10x10 cm²

[2]PTW recommends max photon field size: 30x30 cm²

[3]PTW recommends max photon field size: 20x20 cm²

ESTRO School

OF measurements in a 6 MV beam using Pinpoint ion chamber (15 mm^3).

Energy dependence (non water equivalence central electrode)

Old PTW chamber 31006 with a central electrode of steel causing similar behaviour as an Si diode.

New PTW pinpoint chambers 31014-6 have aluminium central electrodes.

Measured OF rel. 125 mm^3 ion chamber

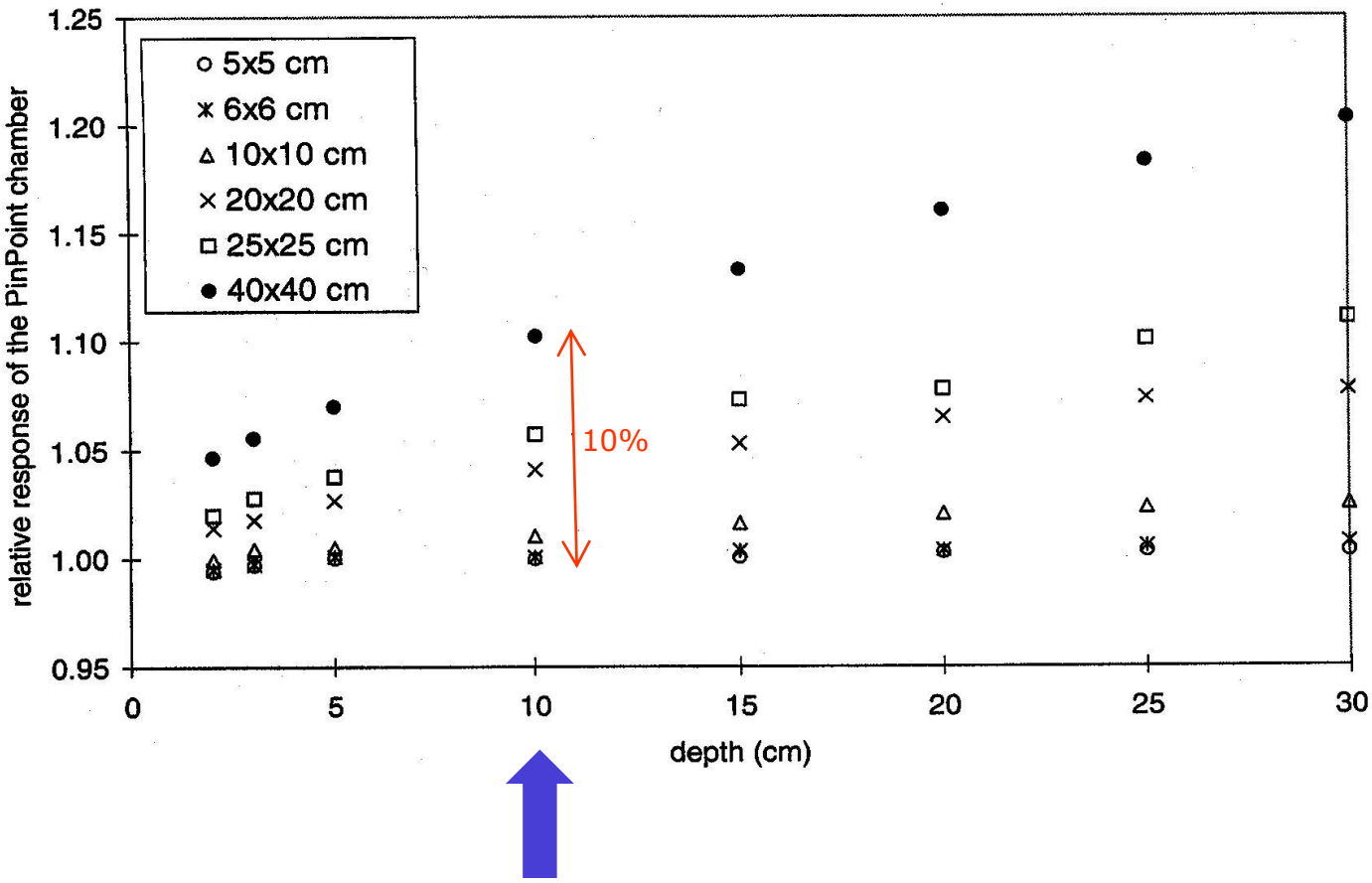

Martens *et al* [12]

ESTRO School

OF measurements
Pinpoint ion chamber (aluminium central electrode; 15 mm³)

Measured OF rel. 125 mm³ ion chamber

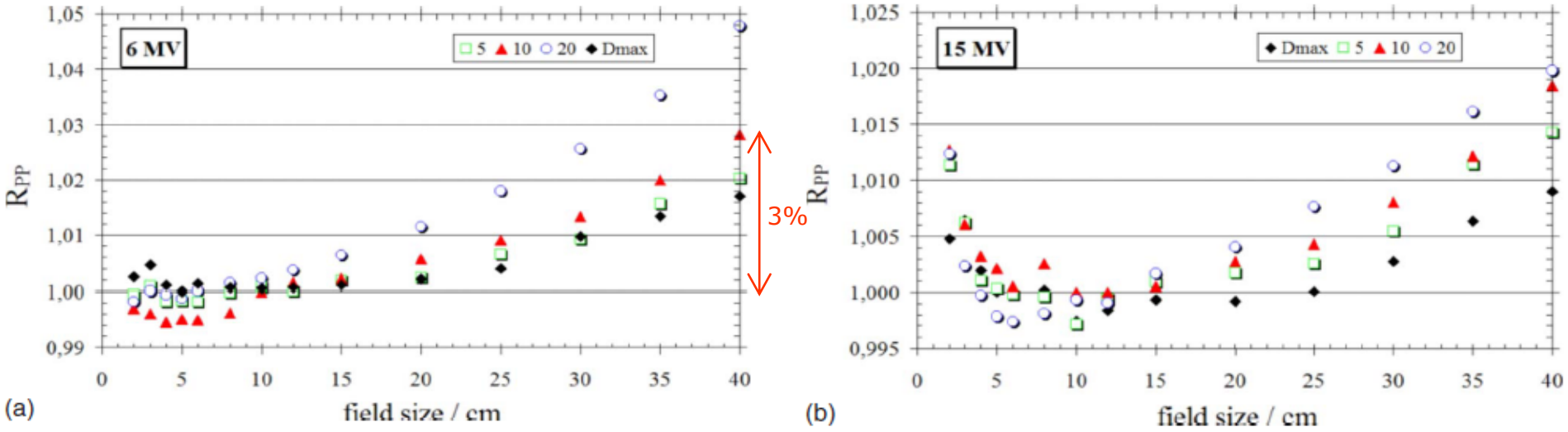

FIG. 5. Uncorrected relative response of type 31014 PinPoint chamber for 6 and 15 MV beams as a function of depth (D_{max} and 5, 10, and 20 cm) and field size.

Agostinelli *et al* [21]

ESTRO School

OF measurements using a Pinpoint ion chamber (15 mm³)

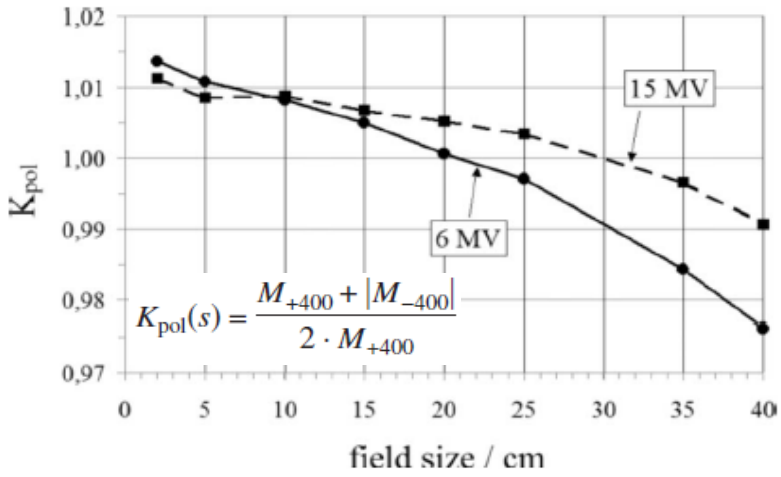

FIG. 3. Polarity correction factor K_{pol} at a 10 cm depth as a function of field size for type 31014 PinPoint chamber. 6 MV (circle solid line), 15 MV (square dashed line).

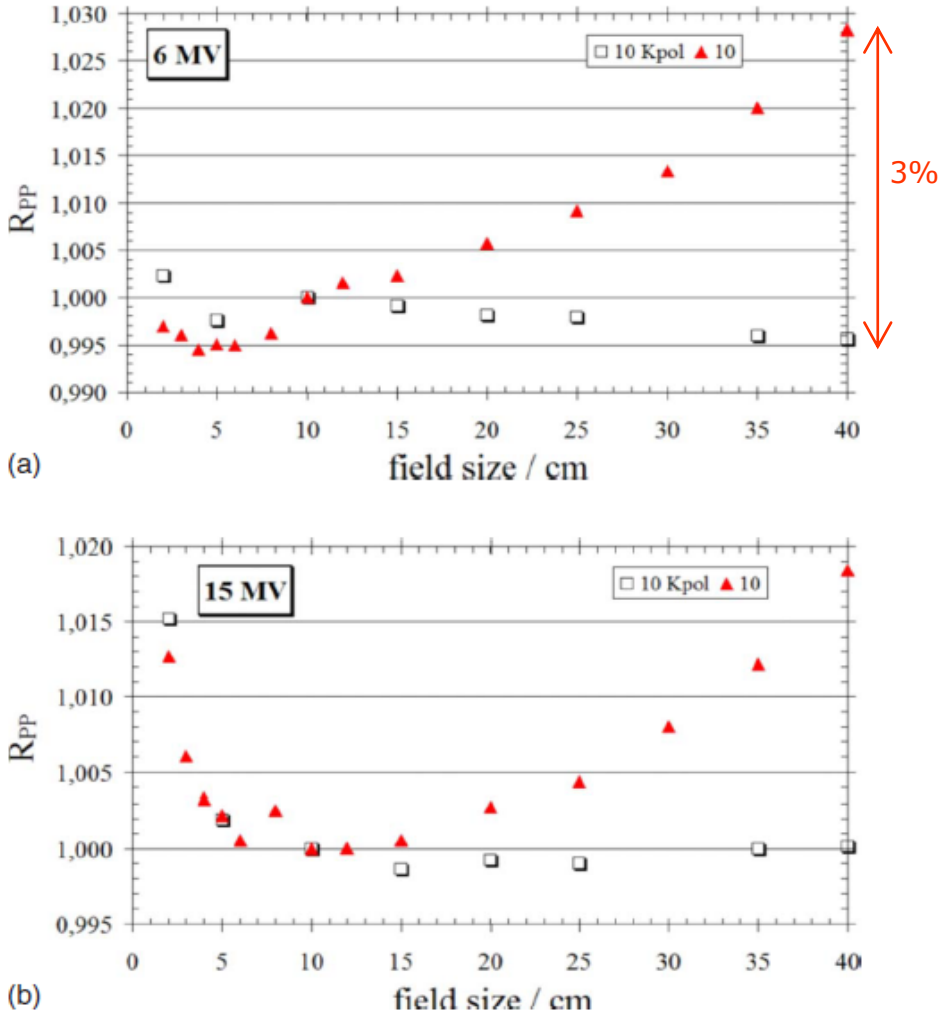

FIG. 4. Polarity-corrected (□) vs. uncorrected (▲) relative response of type 31014 PinPoint chamber for the 6 and 15 MV beams at a 10 cm depth.

Agostinelli *et al* [21]

ESTRO School

PDD measurements and the polarity effects X rays

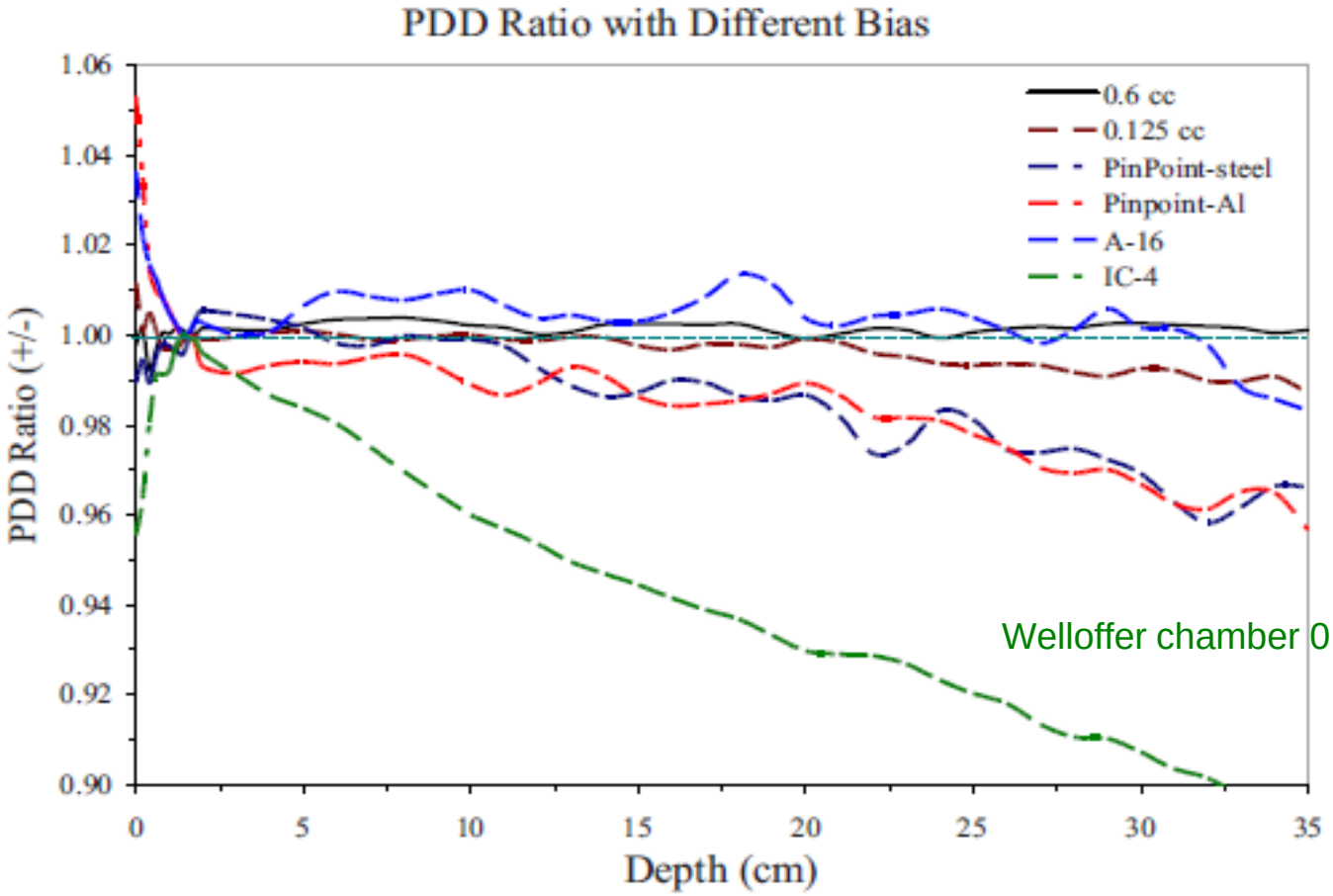

Welloffer chamber 0.04cc

- TG106 AAPM (2008)
- 6MV x-rays – cylindrical i.c.

ESTRO School

Cable leakage in a PinPoint chamber

Normally, the signal from stem and cable irradiation is small enough (< 1 pC/(Gy·cm)) to be neglected, but the small air volume yields a low detector signal level…

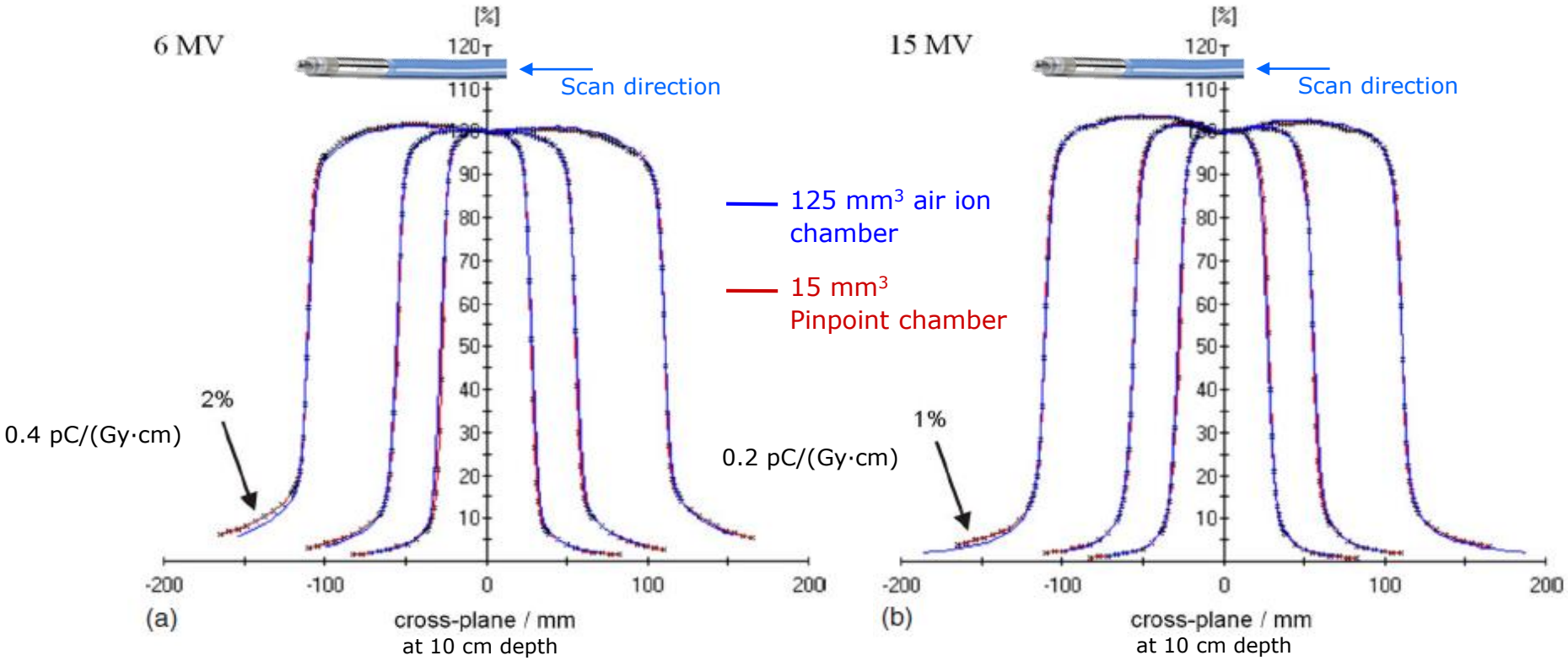

Agostinelli *et al* [21]

PDD build up region
Plane parallel chamber

Effective point of measurement well defined
Good resolution in depth

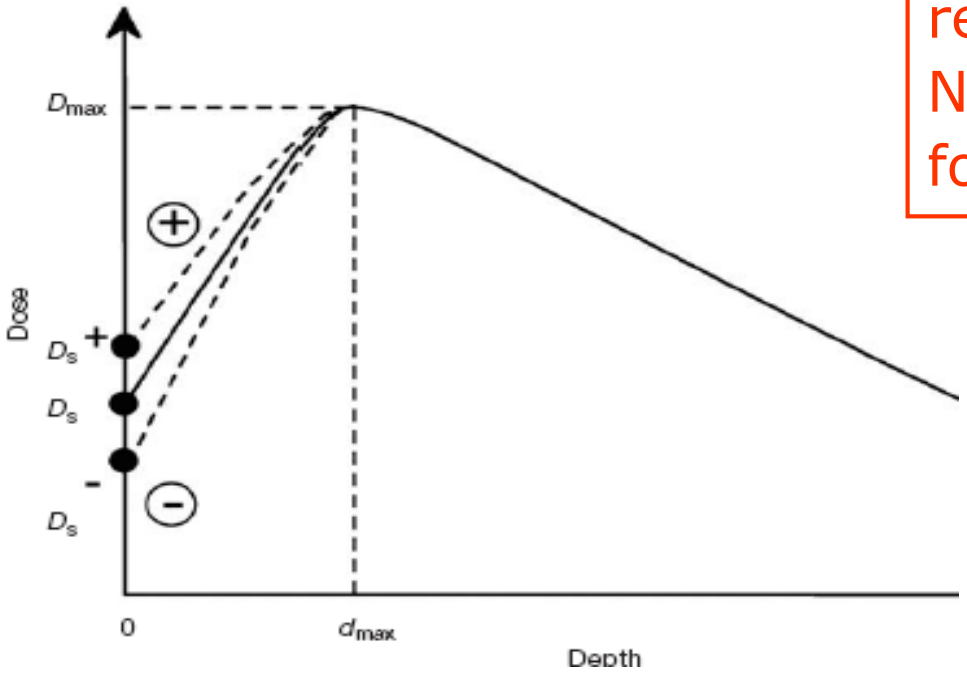

Need of correcting by the polarity factor on the build up region
Need to correct for in scatter for depths near the surface

ESTRO School

Detector characteristics

- ✓ Volume effects: Size of sensitive volume
- ✓ Energy dependence: Interactions in detector material
- ✓ Cable/stem leakage, polarity effect
- Dose rate dependence: Recombination, bias voltage
- Temperature dependence
- Long term stability/irradiation effects

Ion-recombination ionization measurements.

- Initial recombination: Recombination within one created ion cluster. Depends on material, temperature and bias voltage, not dose rate.
- Columnar recombination: Recombination within one particle track. Depends on ionization density of the radiation and bias voltage, not dose rate.
- General recombination: Recombination when ions in different particle tracks interact. Depends on bias voltage and dose rate.

Applied bias voltages for different detectors.

- Air ion chamber: 200-500 V
- Liquid ion chamber: 800 V (microLion)
- Diamond detector: 100 V
- p-Si diode: -

Perhaps obvious, but...

It is a good idea to always use the same bias voltage for a given detector to minimize differences when comparing measurement results.

ESTRO School

Dose rate dependence in photon beams

Diodes

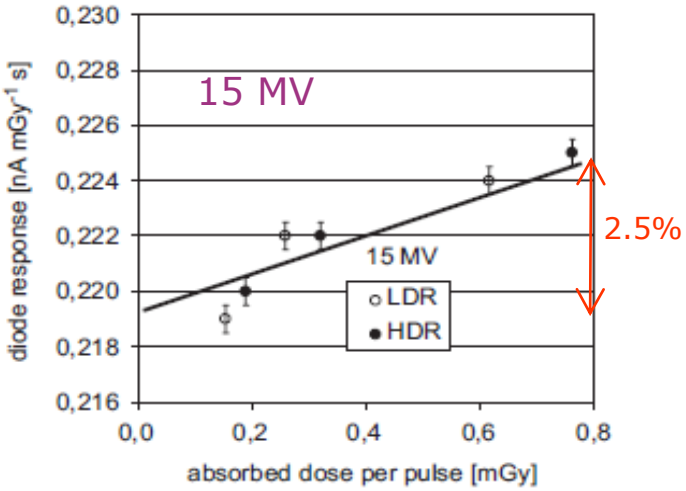

Djouguela *et al* [7]

This positive dose rate dependence is often referred to as *supralinear*.

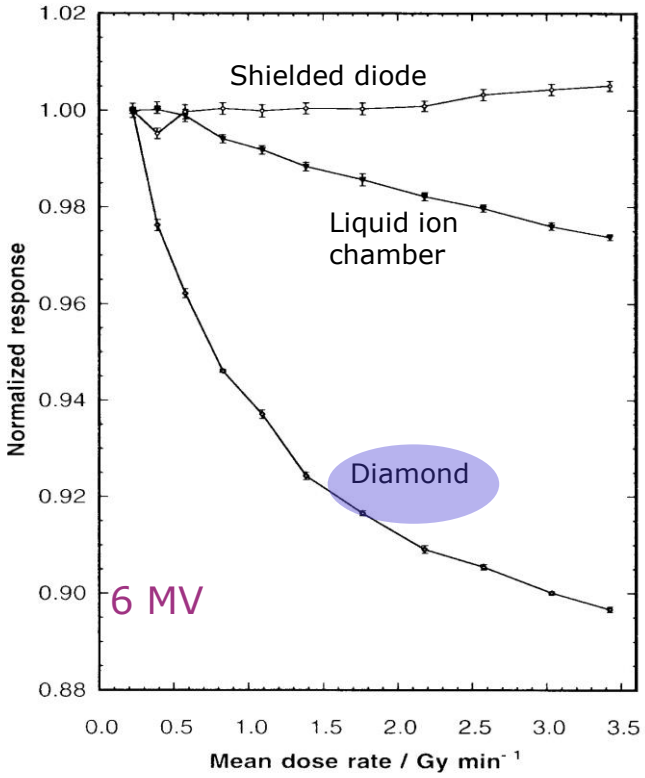

Dose per 4.5 μs pulse (150 Hz) between 0.03 and 0.38 mGy.

Westermark *et al* [3]

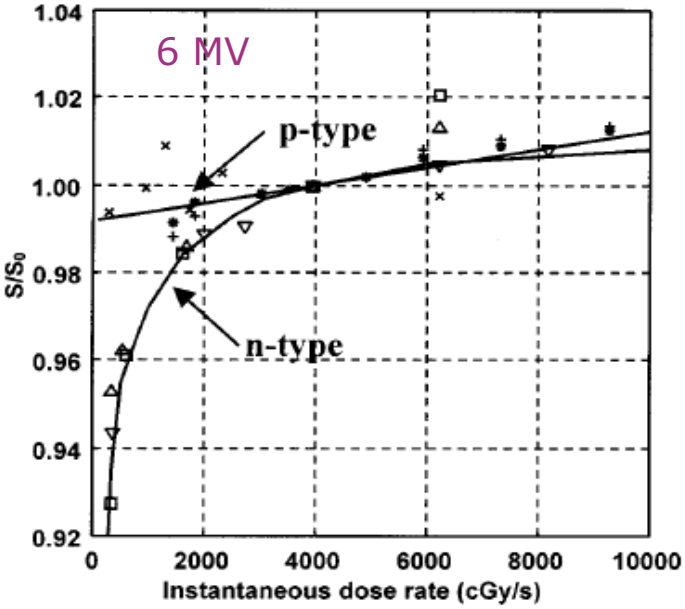

Dose per 3 μs pulse between 0 and 0.3 mGy.

Saini *et al* [8]

0.3 mGy per pulse corresponds to approximately 3-4 Gy/min on a regular medical accelerator.

ESTRO School

Dose rate dependence in photon beams

Diamond

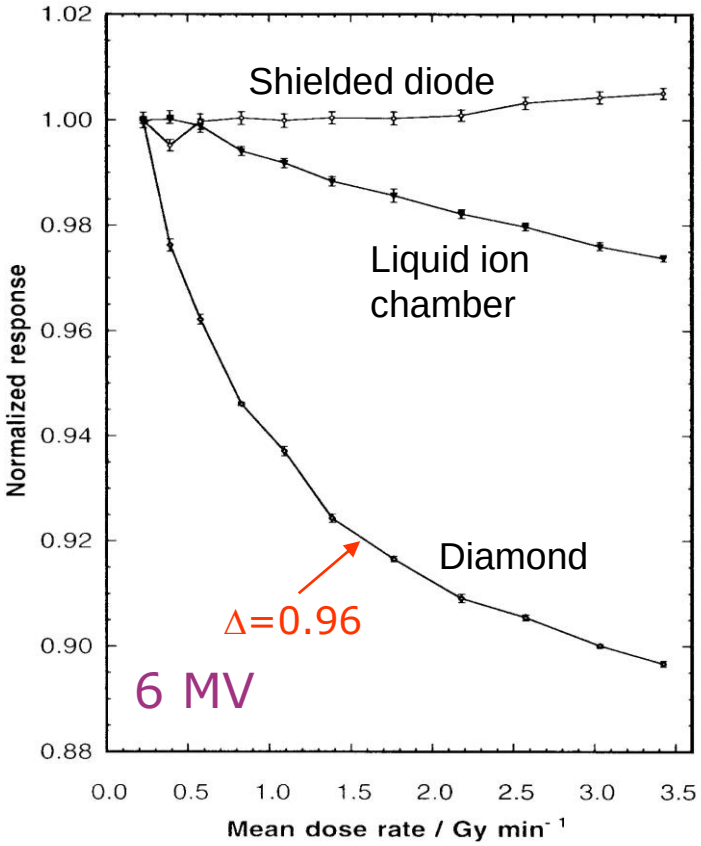

Westermark *et al* [3]

$$I = I_{dark} + k \cdot \dot{D}^{\Delta}$$

where k and Δ should be fitted for each individual diamond detector. Typical values of Δ range from 0.90 to 0.99.

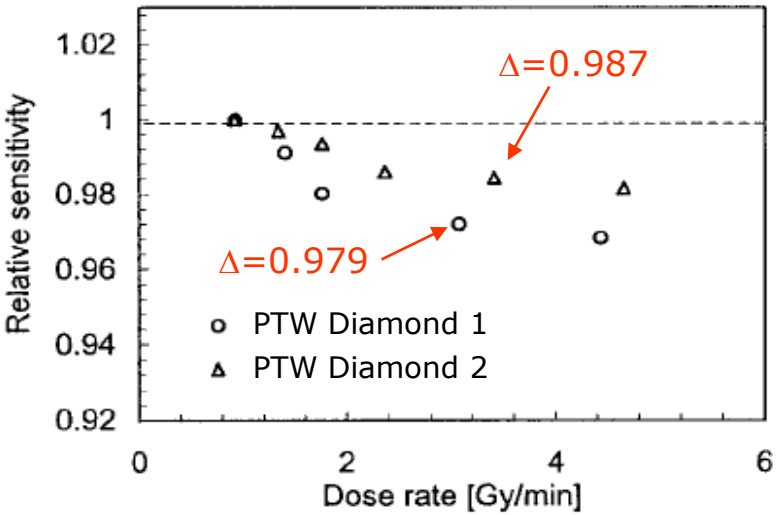

De Angelis *et al* [15]

ESTRO School

Effects from dose rate dependence

6 MV X-ray beams

10x10 cm^2

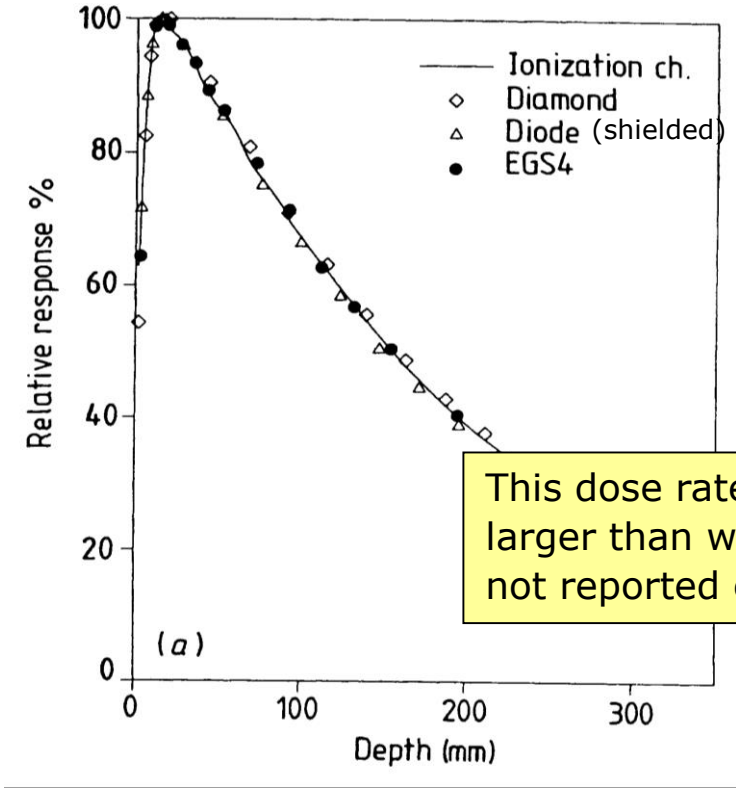

3x3 cm^2

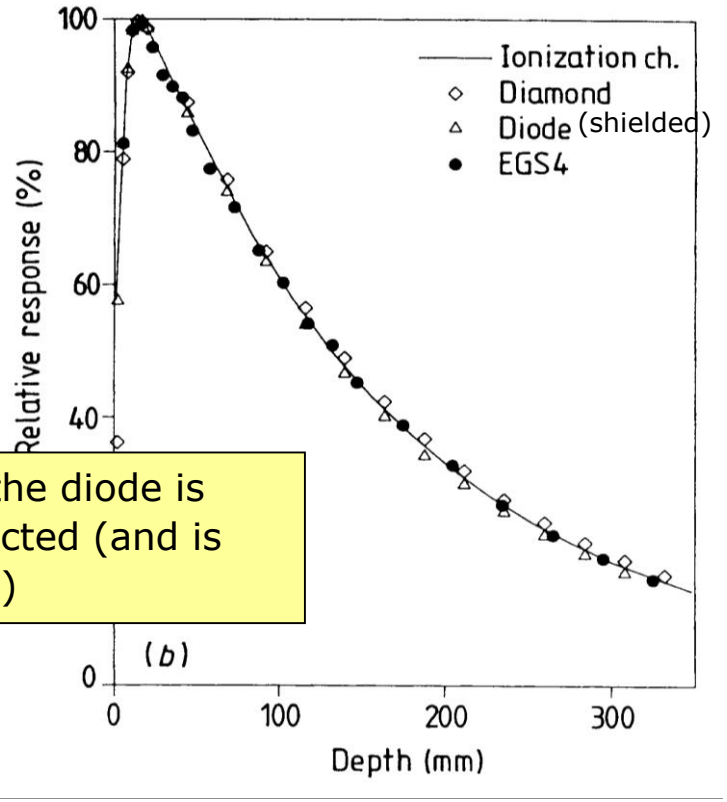

This dose rate effect of the diode is larger than what is expected (and is not reported elsewhere?)

Heydarian *et al* [2]

ESTRO School

Detector characteristics

- ✓ Volume effects: Size of sensitive volume
- ✓ Energy dependence: Interactions in detector material
- ✓ Cable/stem leakage, polarity effect
- ✓ Dose rate dependence: Recombination, bias voltage
- Temperature dependence
- Long term stability/irradiation effects

Temperature effects

- Diodes

TABLE III. Temperature coefficients for *n*- and *p*-type diodes. All measurement were made at depth of 5 cm, 10×10 cm^2, SSD = 100 cm.

Diode type	Temperature coefficient 6 MV (%/°C)	15 or 20 MV (%/°C)	Co-60 (%/°C)
Isorad Gold 1, unirradiated	0.06	0.05 (20 MV)	0.45 (T1000)
Isorad Gold 2, unirradiated	0.08	0.10 (20 MV)	0.16 (T1000)
Isorad Red	0.22	0.21 (20 MV)	0.37 (T1000)
QED unirradiated	0.27	0.25 (15 MV)	0.34 (TPhoenix)
QED Blue Diode	0.30	0.31 (15 MV)	0.30 (T780)
QED Red Diode	0.29	0.29 (15 MV)	0.29 (T780)
Scanditronix EDP 10	0.38	0.33 (20 MV)	0.36 (T1000)
Scanditronix EDP 30	0.36	0.34 (20 MV)	0.39 (T1000)
Average (pre-irradiated only):	0.31	0.30	0.34

Saini *et al* [8]

- Liquid ionisation chamber

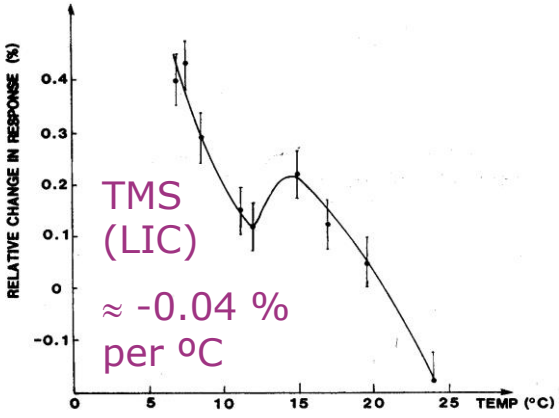

Figure 5. The relative response in TMS at different temperatures.

Wickman *et al* [9]

- Diamond

PTW diamond detector 60003 has a temperature dependence of approx. 0.1% per °C (De Angelis *et al* [15])

- Open air ion chamber

1/293 = -0.34 % per °C

In relative dosimetry during one single measurement session the effects caused by temperature variations can normally be neglected.
However, *in vivo* dosimetry…

ESTRO School

Detector characteristics

- ✓ Volume effects: Size of sensitive volume
- ✓ Energy dependence: Interactions in detector material
- ✓ Cable/stem leakage, polarity effect
- ✓ Dose rate dependence: Recombination, bias voltage
- ✓ Temperature dependence
- Long term stability/irradiation effects

Effects from dose accumulation in old p-Si diodes.

Sensitivity (8-10 kGy typically pre-irradiated on commercial diodes).

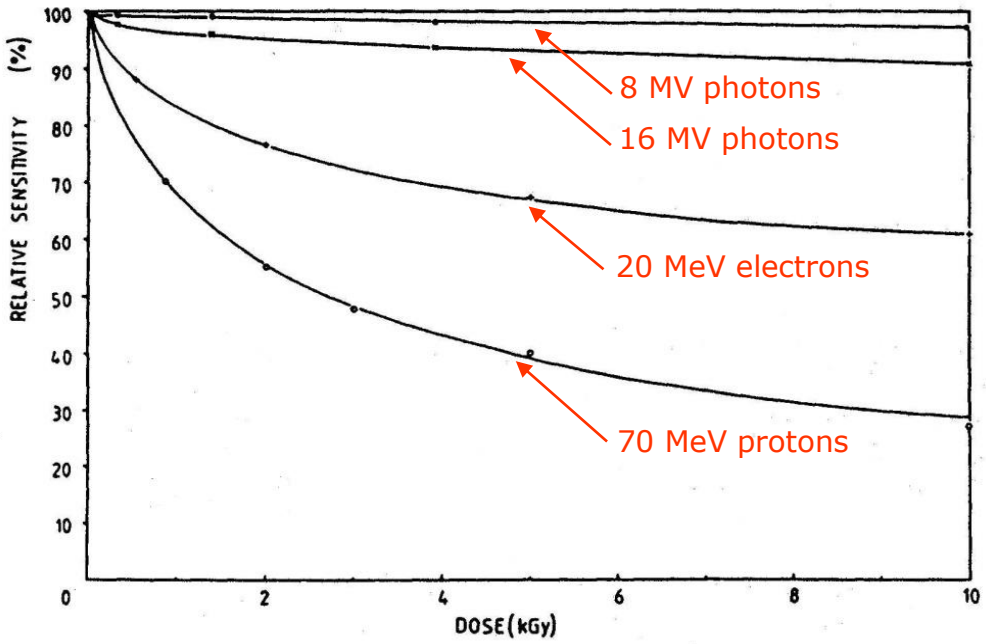

Rikner [10]

PTW states sensitivity losses of
<0.1% per kGy for Co-60 and
<10% per kGy for 23 MV photons

Temperature dependence.

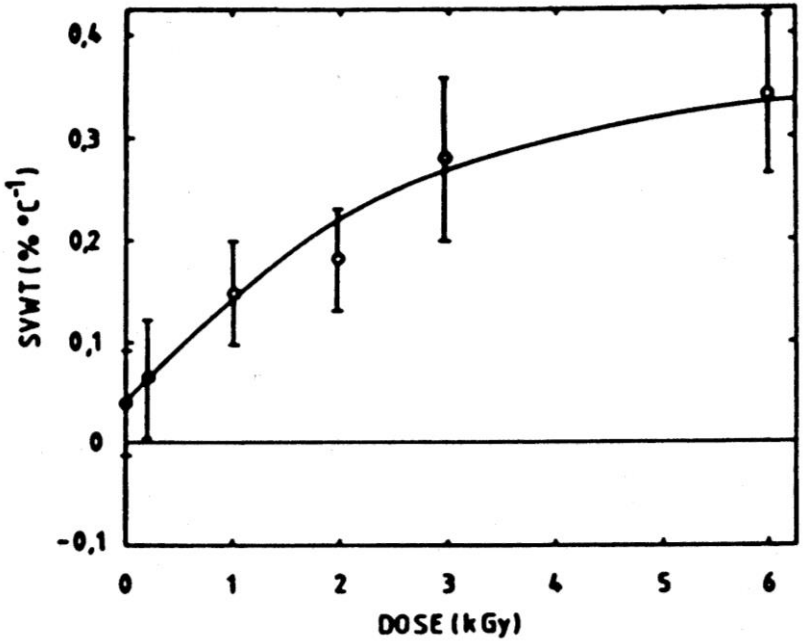

Rikner [10]

Pre-irradiation effects in PTW diamond detectors
(Type 60003)

PTW recommends 10 Gy of pre-irradiation. Mandatory if bias voltage has been turned off.

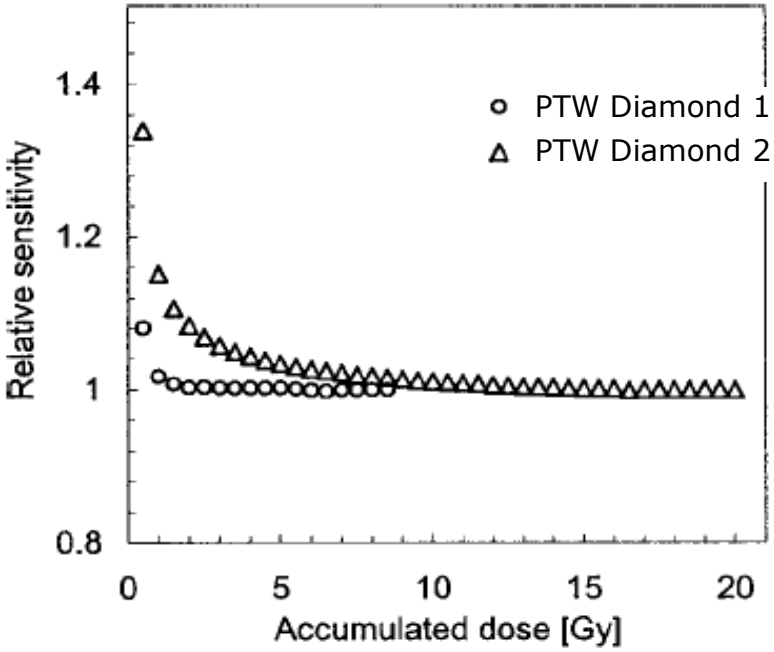

De Angelis *et al* [15]

Dark current after irradiation in a 6 MV beam. Initial level ≈0.4% rel. measurement signal.

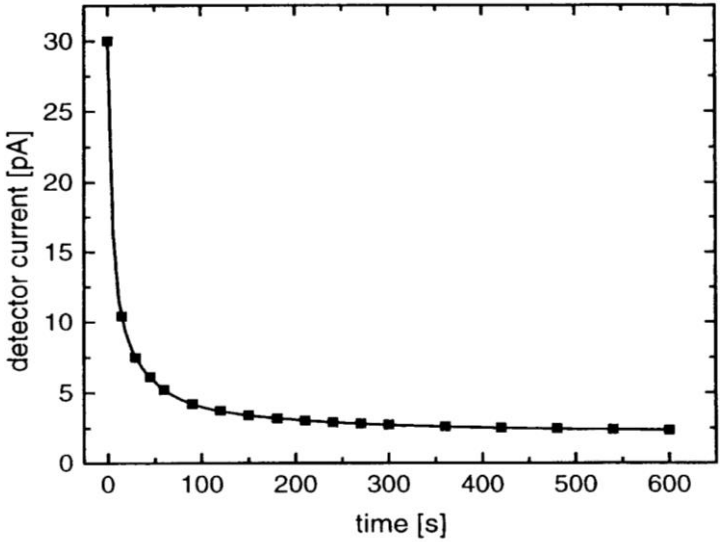

Laub *et al* [11]

Detector characteristics- New detectors

- Volume effects: Size of sensitive volume : Small/increase density
- Energy dependence: Interactions in the detector material

  As equivalent as possible to water
- Cable/stem leakage, polarity effect

  No polarisation/high response-low contribution from stem-cable
- Dose rate dependence: Recombination, bias voltage
- Temperature dependence

  In diodes try to increase gap and traps near conduction band
- Long term stability/irradiation effects

  Stable material/lattice with irradiation

Natural diamond → MicroDiamond

- Good water equivalence of Carbon for high energy photon and electron beams
- High sensitivity: 0.5uC/Gy (dimensions can be reduced)
- Low temperature dependence < 1%/K
- Stable response with accumulated dose (< 0.05% per kGy)

Natural Diamond (60003-PTW)	MicroDiamond (60019-PTW)
Polarization needed (100 V)	No Polarization (Schottky diode conf.)
High response variability between detectors	Reproducible production
Need of 5 Gy pre-irradiation before each set of measurements (response drop 19%)	No need of pre-irradiation
High dark current	Dark current negligible
Dose rate dependence	Low dose rate dependence

ESTRO School

OF measurements using a microDiamond detector

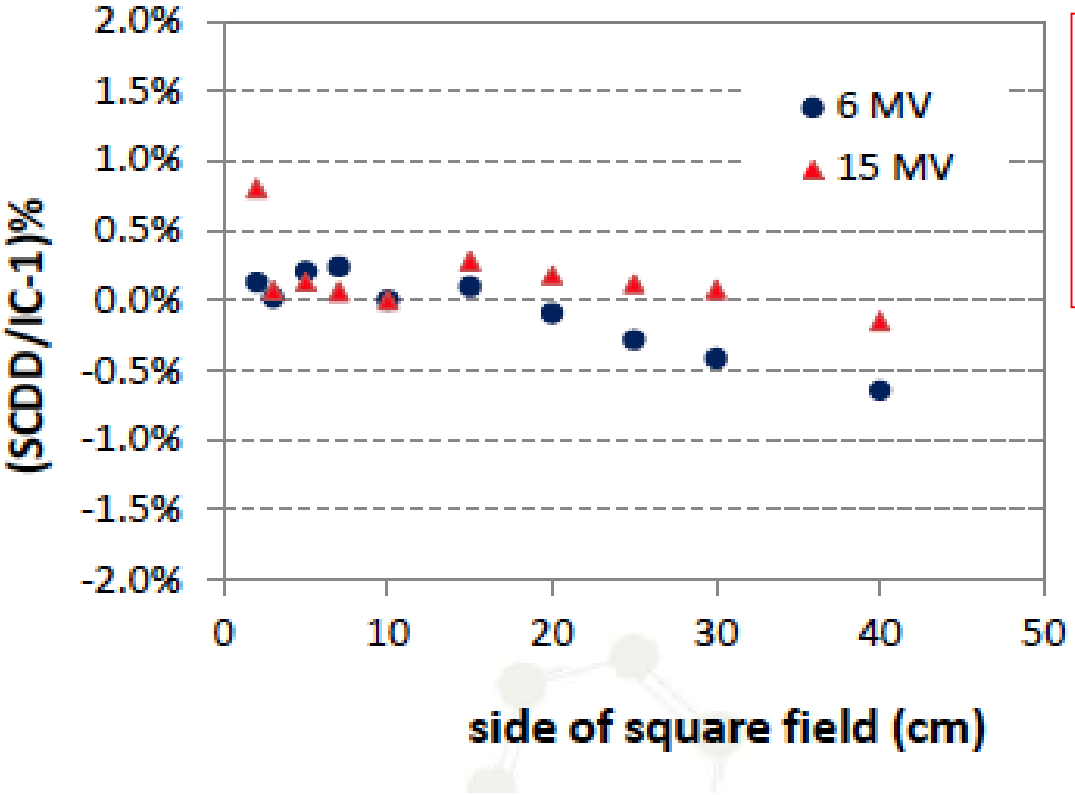

Reference dosimeter:

Field size 5-40 cm side: 0.6 cc cyl ion chamber

Field size <5 cm side: Pinpoint ion chamber

Differences < 1%

From Pimpinella, ESTRO33, Advances in synthetic diamond detector dosimetry

ESTRO School

Organic scintillator
(W1 Standard Imaging)

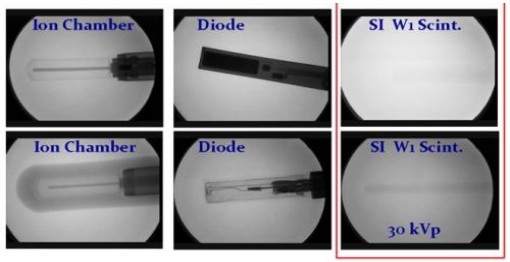

- Good water equivalence for high energy photon and electron beams

Test	Result	Uncertainty
Short-term repeatability (@0.75 Gy)	σ = 0.10%	0.07%
Short-term repeatability (@0.15 Gy)	σ = 0.25%	0.05%
Dose-response linearity	RMS = 0.61 %	0.20%
Angular dependence	RMS = 0.21 %	0.07%
Temperature dependence	-0.225 %·$^{0}C^{-1}$	0.008%·$^{0}C^{-1}$
Time to reach thermal equilibrium*	1 min 40 s	16 s
Repetition rate dependence	RMS = 0.53 %	0.06%
Deviation from ISL	RMS = 0.38 %	0.26%
Loss of sensitivity with accumulated dose	-0.28%·kGy^{-1} [0-15 kGy] -0.032%·kGy^{-1}[15-127 kGy]	0.06%·kGy^{-1} 0.018%·kGy^{-1}

ESTRO School

Organic scintillator
(W1 Standard Imaging)

Energy Dependence; reference conditions

(uncertainty k=1)

Modality	Nominal energy	Difference (%)
High-energy X-rays	6 MV	-
	15 MV	-0.2±0.6
Electrons	6 MeV	-0.5±0.7
	9 MeV	-1.2±0.6
	12 MeV	0.5±0.6
	16 MeV	-0.4±0.6
	20 MeV	-0.2±0.6

ESTRO School

Organic scintillator
(W1 Standard Imaging)

Irradiation produces luminiscence

Light is guided through optical fiber to a photomultiplier

The signal is proportional to absorbed dose

BUT

When we irradiate optical fiber Cerenkov light is produced

Cerenkov light depends on the length of fiber irradiated, not proportional to dose

Cerenkov light and luminiscence have different wave lenghts

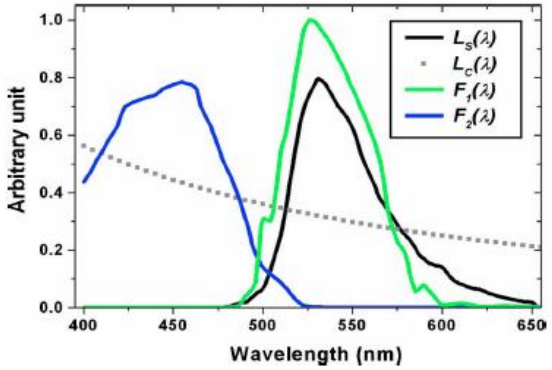

Spectral discrimination method

ESTRO School

Organic scintillator
(W1 Standard Imaging)

Cerenkov light and luminiscence have different wave lengths

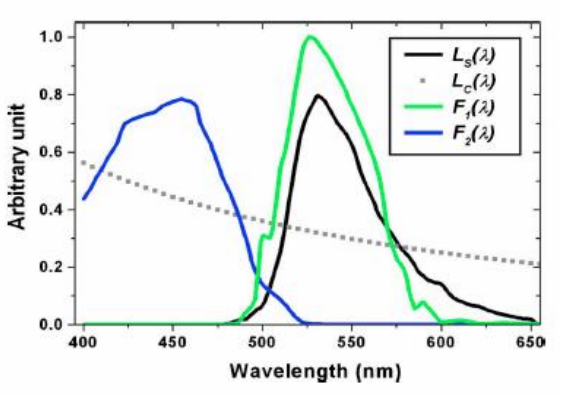

Spectral discrimination method

$CLR = (R_{1\_max\_f1} - R_{1\_min\_f1}) / (R_{2\_max\_f1} - R_{2\_min\_f1})$

$Gain = Dose_{f2} / (R_{1\_min\_f2} - R_{2\_min\_f2} * CLR)$

$Dose = Gain \cdot (R_1 - R_2 \cdot CLR)$

$R_{i\_j\_k}$ where:
R refers to the reading
i refers to channel
j to the fiber configuration (maximum or minimum)
k to the side (cm) of the square radiation field

Organic scintillator
(W1 Standard Imaging)

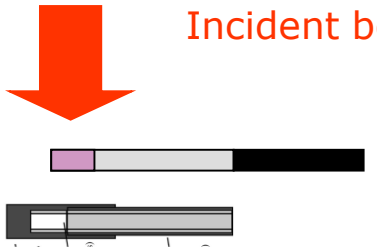

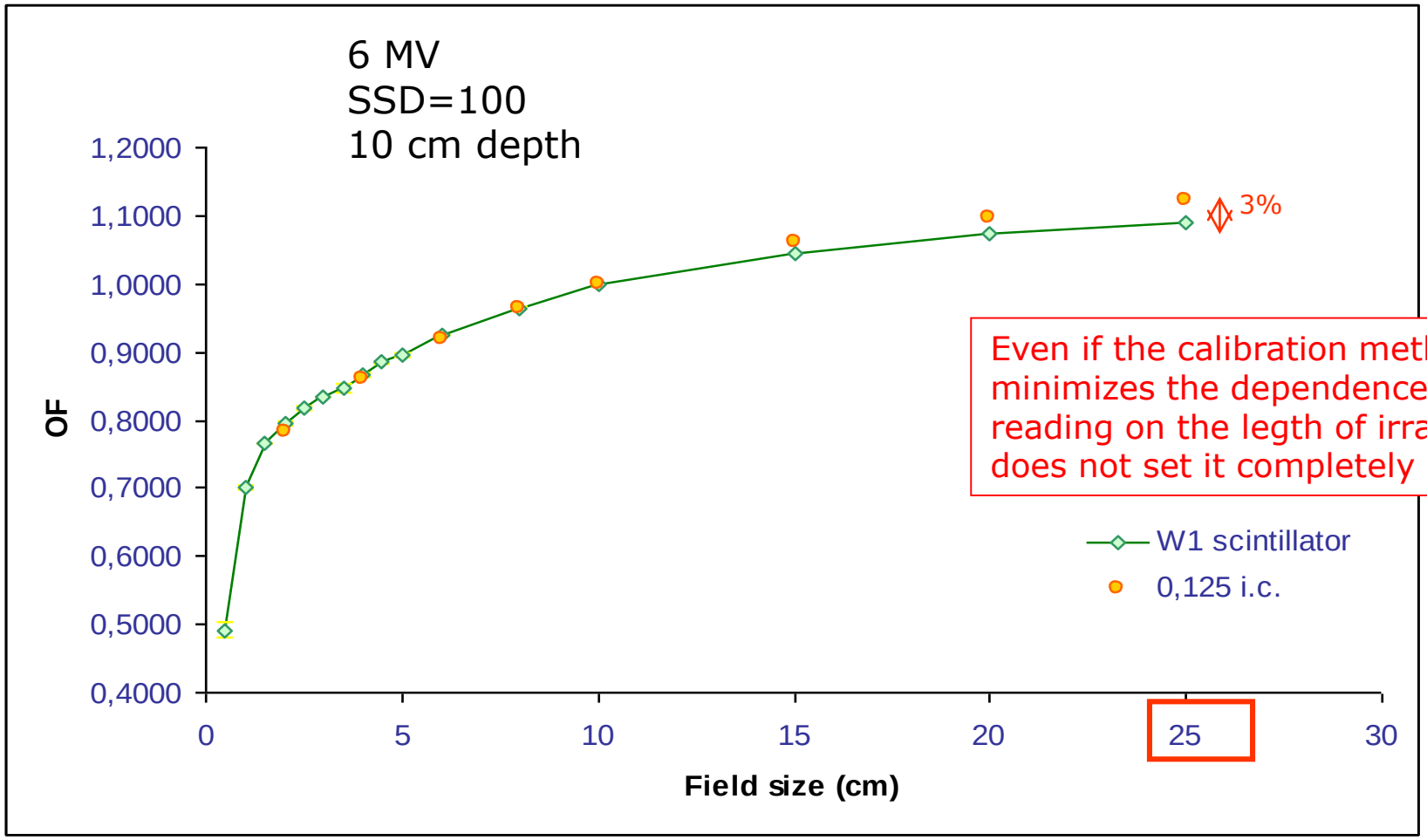

Even if the calibration methodology minimizes the dependence of the detector reading on the legth of irradiated fiber it does not set it completely independent

Organic scintillator
(W1 Standard Imaging)

OF: small fields

Perpendicular to beam axis

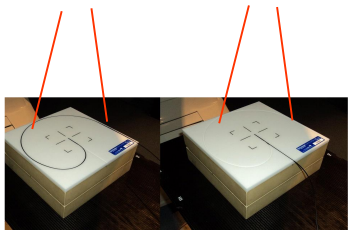

Parallel to beam axis

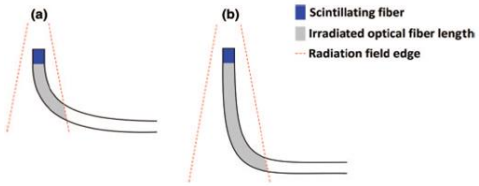

Calibration name	Detector orientation	Phantom	Depth (cm)	SSD (cm)	Field size CRL (f1) cm^2	Field size gain (f2) cm^2
"Standard" (A)	Perpendicular to beam axis	Calibration plate + Plastic water	10	100	40 x 40	10 x10
Small fields (B)	Parallel to beam axis	MP3 water	10	100	10 x 10	10 x 10
Small fields (C)	Parallel to beam axis	MP3 water	10	100	5 x 5	5 x 5

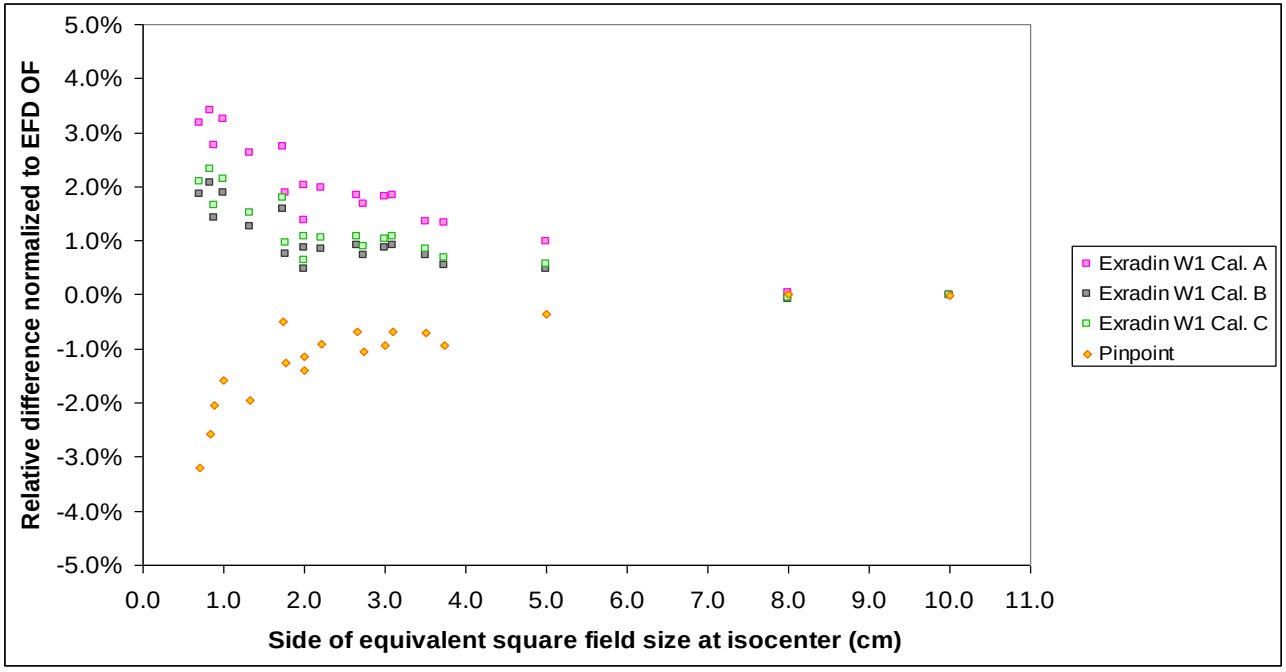

Relative differences of OF normalized to EFD-3G OF.

OF are referred to a 10 x 10 cm^2 field size.

The calibration methodology proposed by the manufacturer is not appropriate for measuring output factors for small fields. Calibration using smaller fields and the detector axis parallel to beam axis should be used.

These results show that the CRL and gain depend on field size and orientation of the scintillator.

ESTRO School

Detector	Appropiate for	Be careful
Ionization chambers	❑ **For x-ray depth dose measurements** ❑ **Plane-parallel chamber for build-up region** ❑ **Output factors large fields** ❑ **Output factors for small fields (micro-chambers)**	❑ Check polarity effect for both photon and electron beams ❑ Always measure with the same nominal V ❑ For micro-chambers the stem signal can be an issue ❑ Correct by Sw,air for electron depth dose measurements. ❑ Use small volume detectors for scanning ❑ Effective point of measurement ❑ Check stability temperature during measurements
Diodes	❑ **Depth dose measurements and profiles** ❑ **Shielded detector for x-rays** ❑ **Non-shielded for electron beams** ❑ **Output factors** ❑ **Shielded detector standard/large fields** ❑ **Non-shielded for small fields**	❑ Energy dependence ❑ Sensitivity variation with accumulated dose ❑ May present sensitivity variation with dose rate ❑ Check stability temperature during measurements

Detector	Appropiate for	Be careful
Diamond	❑ **Output factors small fields** ❑ **Profiles**	❑ Dose rate dependence ❑ Huge production spread ❑ Not really small > 3mm
Synthetic diamond	❑ **Output factors small fields** ❑ **Profiles**	❑ No dose rate dependence ❑ Production reproducible ❑ Small: 2.2 mm diameter
Organic scintillators	❑ **Depth dose measurements and profiles** ❑ **Output factors** ❑ **Profiles**	❑ Cerenkov radiation response contamination ❑ Commercial solution Standard Imaging

Looking for the perfect detector MV X-rays

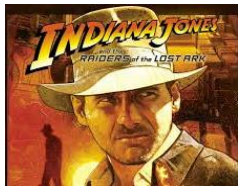

Property	Air i.c. ~10^{-1} cm ^{3}	Air Micro i.c. ~10^{-3} cm ^{3}	Si-Diode unshielded	Si-Diode shielded	Si-Diode SFD	W1 organic scintillator	MicroDiamond
Sensitivity	++++	++	+++	+++	+++	+	++
Repetability	++++	+++	+++	+++	++	+++	+++
Linearity	++++	++++	++++	++++	+++	++++	++++
Dose rate dep	+	+	+++	+++	+++	++	+++
Energy dep	++	++(+) Depends on chamber	++++	+++	++++	+	+
Volume effects	++++	+++	++	++	+	+	++
Density effects	+ Depends on chamber	+ Depends on chamber	++++	++++	++++	+	+++
Accumulated dose	-	-	++++	++++	++++	+	+
Polarity	+	Depends on chamber	-	-	-	-	-
Temp.			++++	++++	++++	++++	+

Which detector would you chose to measure…??:

1. PDD in a large 18MV X-ray field:
2. PDD in a 1x1 cm^2 X-ray field:
3. Profile in a 10x10 cm^2 X-ray field:
4. Output factor 2x2 cm^2 X-ray field:
5. PDD 10x10 cm^2 electron field:
6. Output factors electron beam:
7. Reference dose X-ray beam:

Summary

- No detector is (obviously) optimal for all situations ⇒
  Understanding strong and weak sides of the experimental setup, including the phantom, is vital.
- Be critical of your measurement results. Try to verify important data, such as TPS input, with independent measurements or calculations.

References 1

1. Yin Z, Hugtenburg RP, Beddoe AH (2004) Response corrections for solid-state detectors in megavoltage photon dosimetry. Phys Med Biol 49, 3691–702.
2. Heydarian M, Hoban PW, Beddoe AH (1996) A comparison of dosimetry techniques in stereotactic radiosurgery. Phys Med Biol 41, 93-110.
3. Westermark M, Arndt J, Nilsson B, Brahme A (2000) Comparative dosimetry in narrow high-energy photon beams.
Phys Med Biol 45, 685-702.
4. McKerracher C, Thwaites DI (1999) Assessment of new small-field detectors against standard-field detectors for practical stereotactic beam data acquisition. Phys Med Biol 44, 2143-60.
5. Dasu A, Löfroth PO, Wickman G (1998) Liquid ionization chamber measurements of dose distributions in small 6 MV photon beams. Phys Med Biol 43, 21-36.
6. Eklund A, Ahnesjö A (2010) Spectral perturbations from silicon diode detector encapsulation and shielding in photon fields. Med Phys 37, 6055-60.
7. Djouguela A, Griessbach I, Harder D, Kollhoff R, Chofor N, Rühmann A, Willborn K, Poppe B (2008) Dosimetric characteristics of an unshielded p-type Si diode: linearity, photon energy dependence and spatial resolution. Z Med Phys 18, 301-6
8. Saini AS, Zhu TC (2002) Temperature dependence of commercially available diode detectors. Med Phys 29, 622-30.

ESTRO School

References 2

9. Wickman G, Nyström H (1992) The use of liquids in ionization chambers for high precision radiotherapy dosimetry. Phys Med Biol 37, 1789-1812.
10. Rikner G (Year?) Symposium on Semiconductor Detectors. Inst. of Oncology, Dept. of Hospital Physics, Uppsala, Sweden
11. Laub WU, Kaulich TW, Nusslin F (1999) A diamond detector in the dosimetry of high-energy electron and photon beams.
Phys Med Biol 44, 2183-92.
12. Martens C, De Wagter C, De Neve W (2000) The value of the PinPoint ion chamber for characterization of small field segments used in intensity-modulated radiotherapy. Phys Med Biol 45, 2519-30.
13. IAEA (2000) Absorbed dose determination in external beam radiotherapy: An international code of practice for dosimetry based on standards of absorbed dose to water. IAEA Technical Report Series Report No. 398, International Atomic Energy Agency (Vienna)
14. Galbraith DM, Rawlinson JA, Munro P (1984) Dose errors due to charge storage in electron irradiated plastic phantoms. Med Phys 11, 197-203
15. De Angelis C, Onori S, Pacilio M, Cirrone GAP, Cuttone G, Raffaele L, Bucciolini M, Mazzocchi S (2002) An investigation of the operating characteristics of two PTW diamond detectors in photon and electron beams. Med Phys 29, 248-54

References 3

16. Zhu TC, Ahnesjö A, Lam KL, Li XA, Ma CM, Palta JR, Sharpe MB, Thomadsen B, Tailor RC (2009) Report of AAPM Therapy Physics Committee Task Group 74: in-air output ratio, Sc, for megavoltage photon beams. Med Phys 36, 5261-91
17. Jursinic PA (2006) Measurement of head scatter factors of linear accelerators with columnar miniphantoms. Med Phys 33, 1720-8
18. Frye DM, Paliwal BR, Thomadsen BR, Jursinic PA (1995) Intercomparison of normalized head-scatter factor measurement techniques. Med Phys 22, 249-53
19. Weber L, Nilsson P, Ahnesjö A (1997) Build-up cap materials for measurement of photon head-scatter factors. Phys Med Biol 42, 1875-86.
20. Krauss H (Institute for Radiooncology, Kaiser Franz Josef Hospital, Vienna, Austria) www.wienkav.at/kav/kfj/91033454/physik/PTW/liquid.htm
21. Agostinelli S, Garelli S, Piergentili M, Foppiano F (2008) Response to high-energy photons of PTW31014 PinPoint ion chamber with a central aluminum electrode. Med Phys 35, 3293-301
22. Aget H, Rosenwald JC (1991) Polarity effect for various ionization chambers with multiple irradiation conditions in electron beams. Med Phys 18, 67-72.

ESTRO School

Patient Characterisation for Radiotherapy

Brendan McClean

(and friends….)

Feidhmeannacht na Seirbhíse Sláinte
Health Service Executive

Saint Luke's
Radiation Oncology
Network

Objectives and aims

- To understand how patient anatomy and tissue is represented in a typical TPS
- To examine the implications of different ways of representation
- To distinguish between dose to water and dose to tissue calculations and the consequences of using either
  - (now dealt with by TK lecture!)

Outline

- What a CT image represents
- Methods of Calibration of CT images for radiotherapy
- Assigning tissue to in a TPS
- Limitations of CT data
- Dose to water/Dose to tissue
- Dosimetric impact of assumptions for:
  - MV
  - keV
  - Protons
- Developments

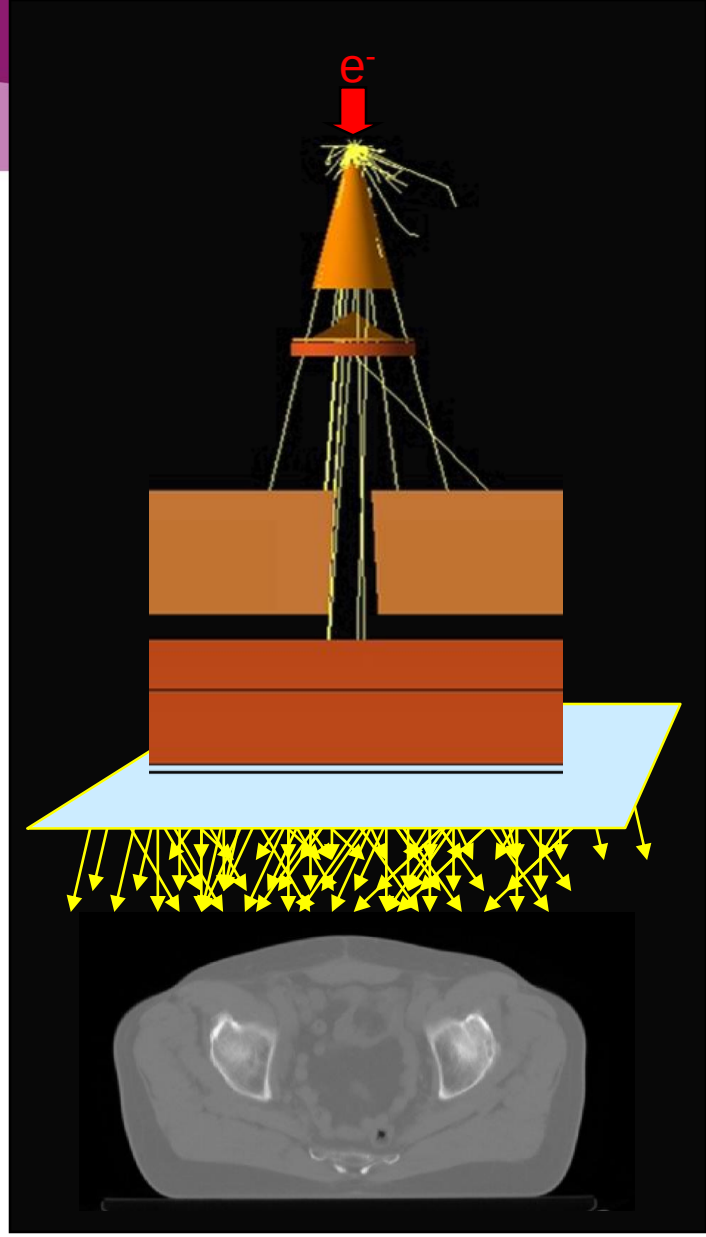

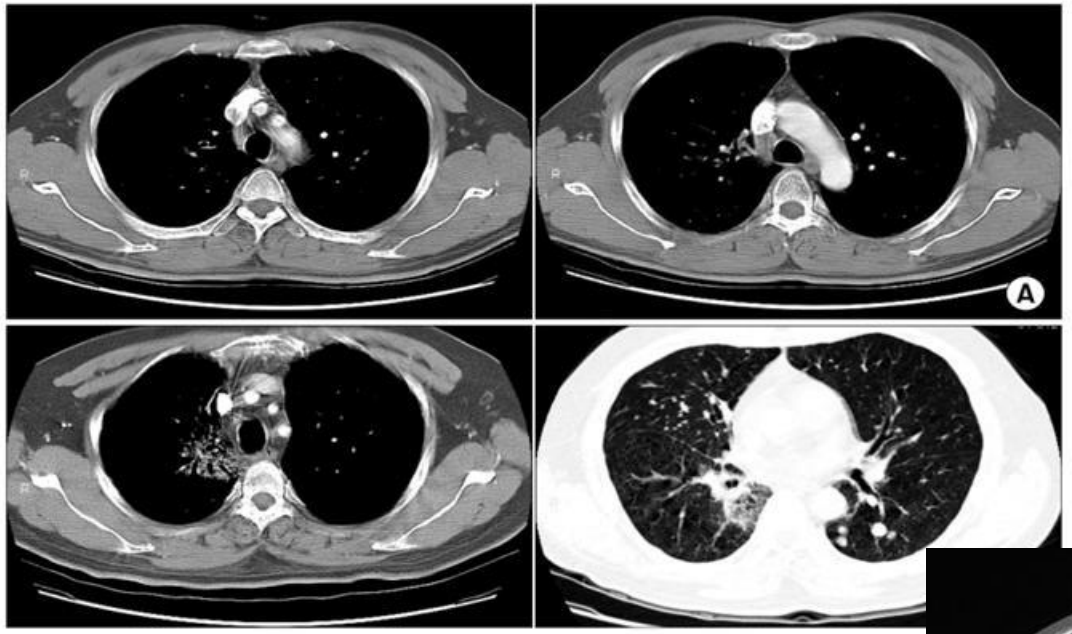

CT

- Accurate reconstruction of patient's anatomy
  - Exact anatomical location of inhomogeneities
- CT numbers contain quantitative information on radiological properties of different materials
- Dose calculations and DRR's

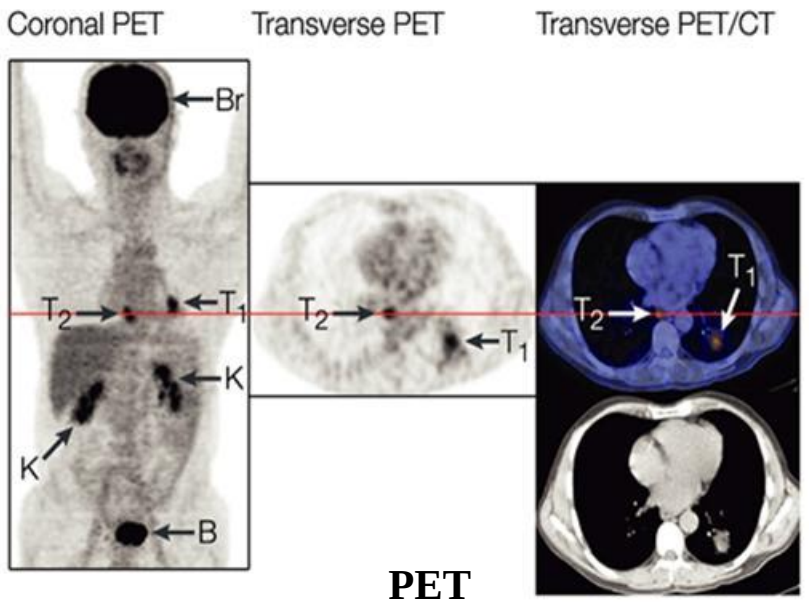

PET

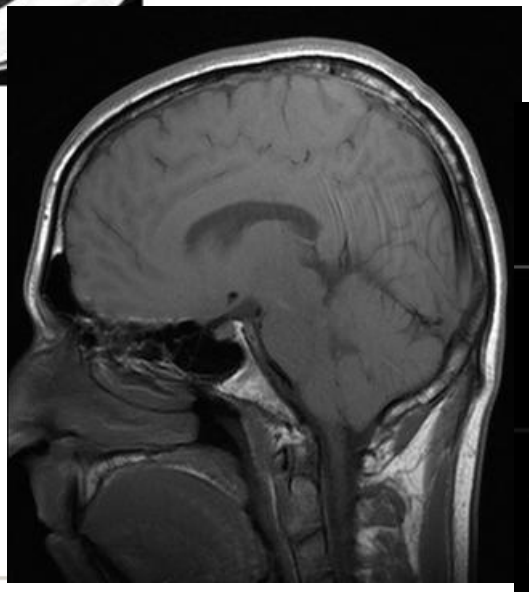

MRI

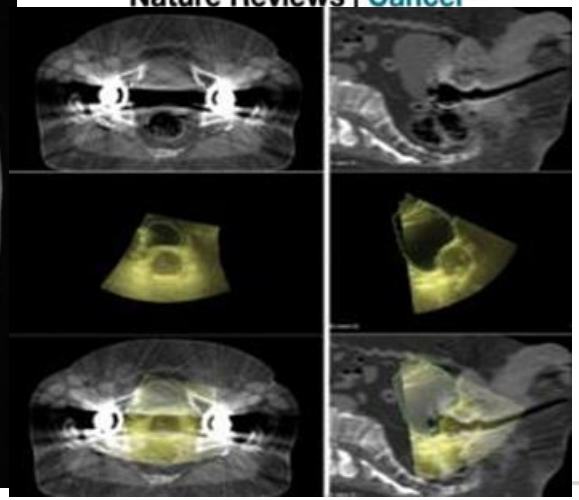

Ultrasound

ESTRO School

What the user sees….

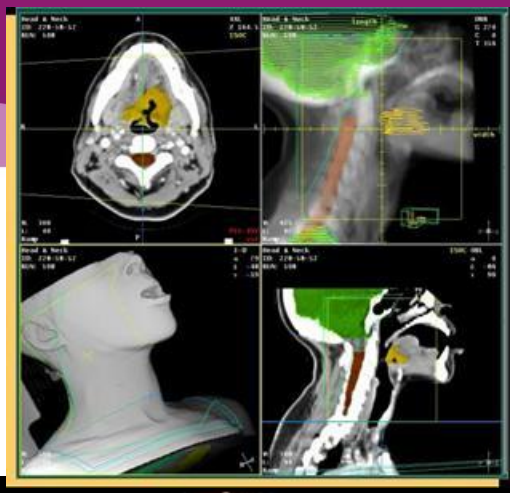

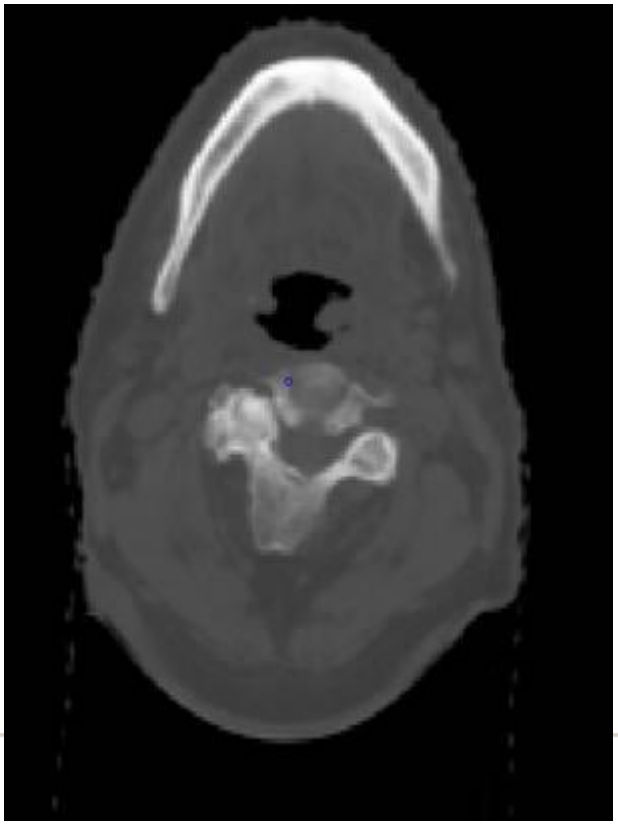

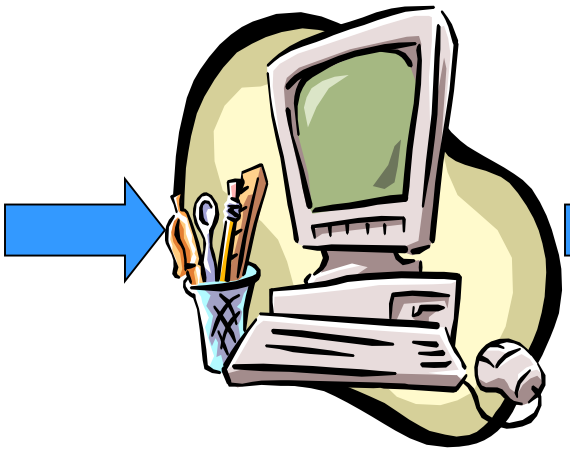

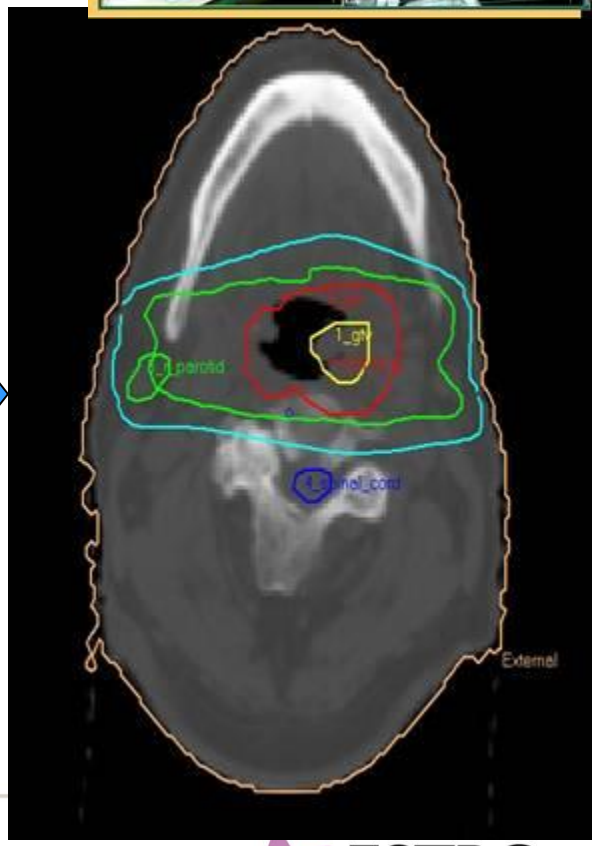

ESTRO School

What does the TPS 'see'? What impact does this have on dose calculation?

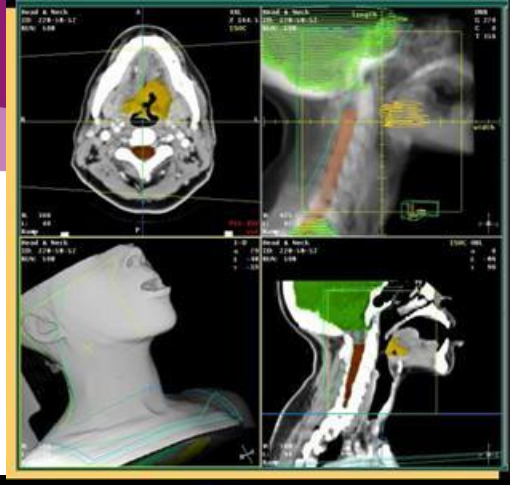

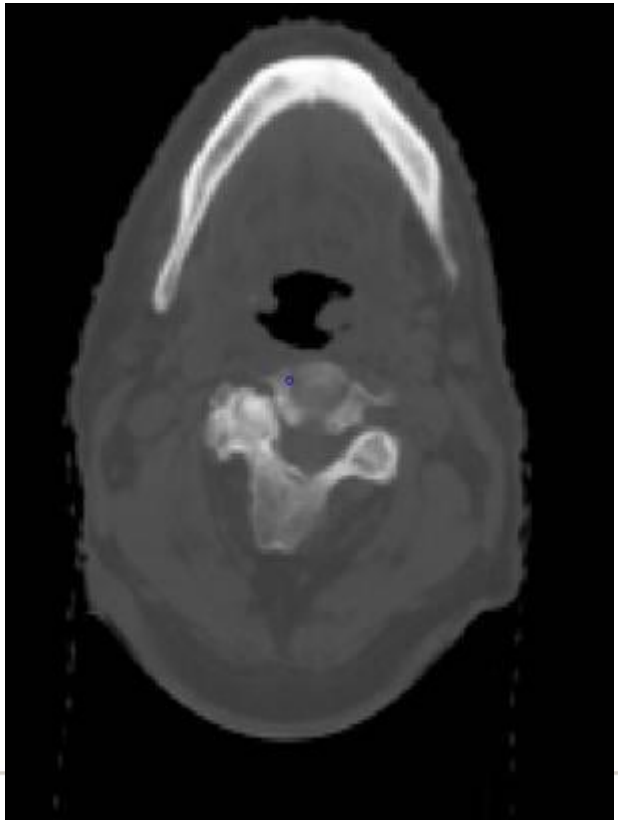

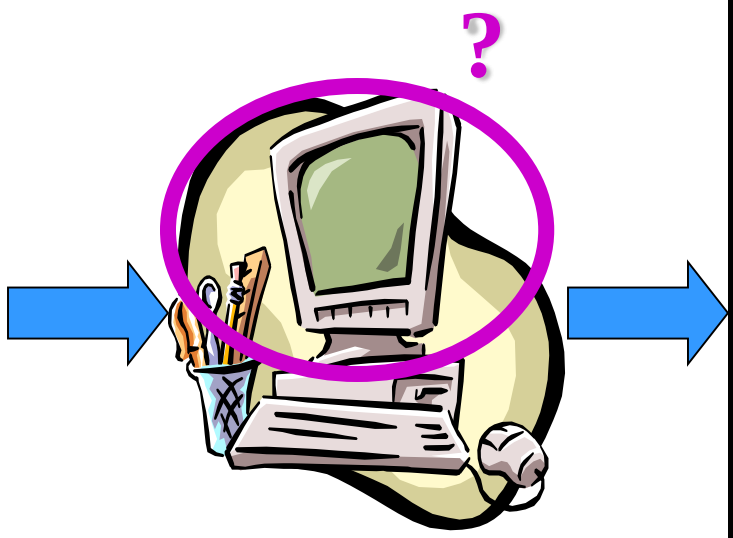

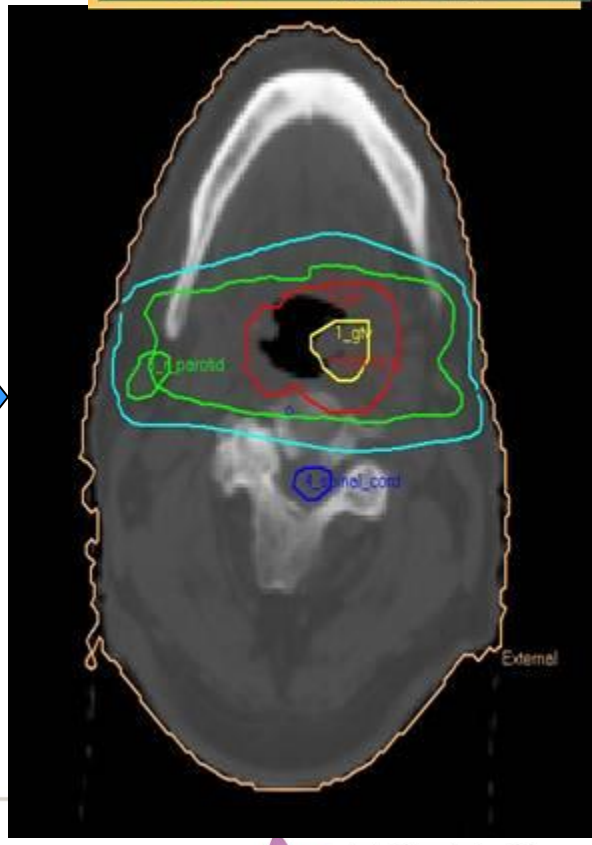

ESTRO School

Principle of CT operation

$$\Phi_{E,0}(E)$$

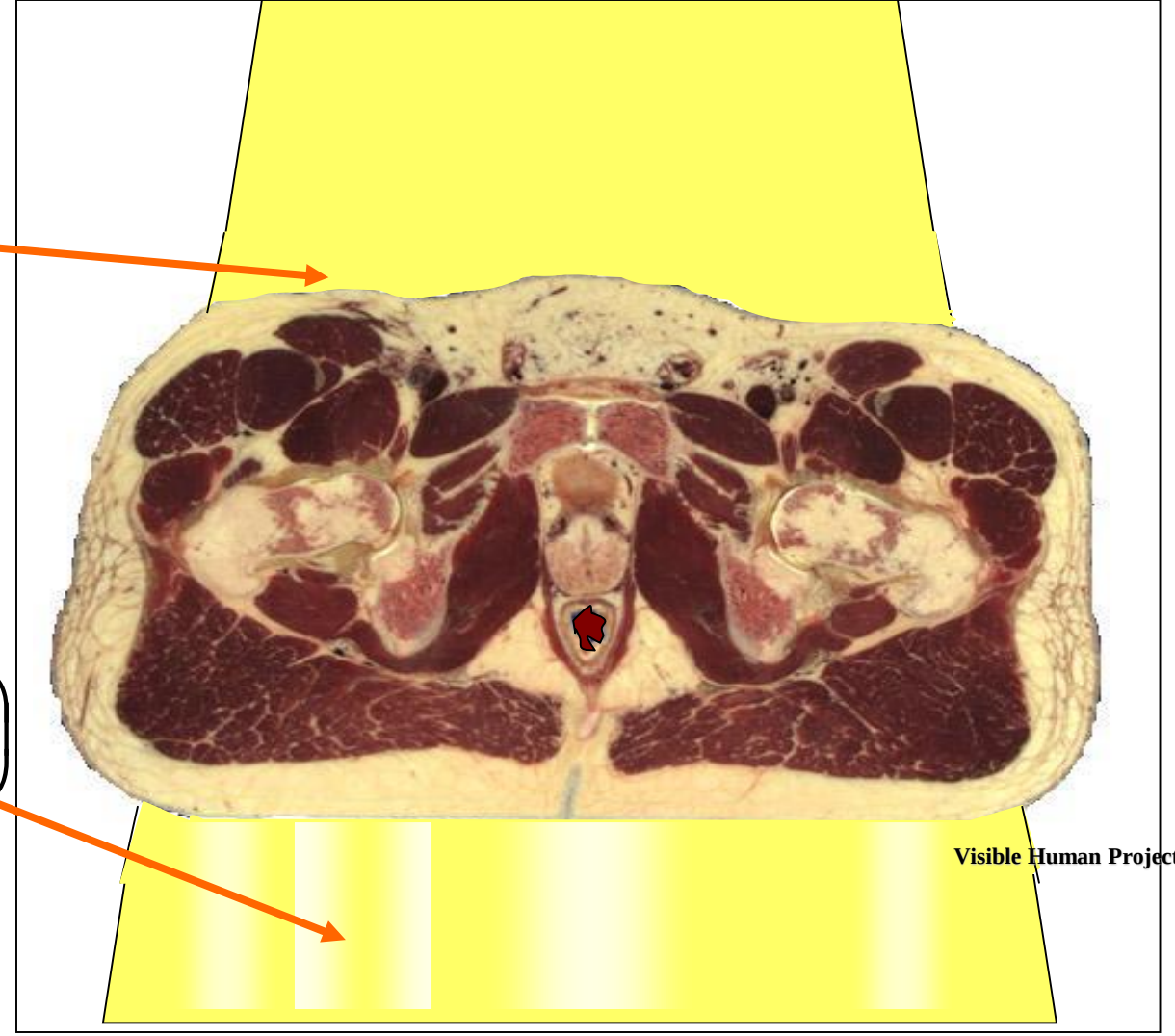

$$\Phi_E(E) = \Phi_{E,0}(E)\exp\left(-\int_0^s \mu(E,t)dt\right)$$

$$\mu(E) = \rho N_A \sum_i^N \left(\frac{w_i}{A_i}\sigma_i(E)\right)$$

$$\lambda = \ln\left(\frac{\Phi_0}{\Phi}\right) = \int_0^s \mu(E,t)dt$$

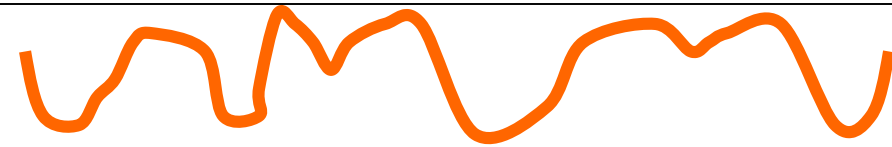

$\mu(E)$ depends on ρ_e (linear) and $Z_{eff}^{\ x}$ (x=3-4)

The End Point…

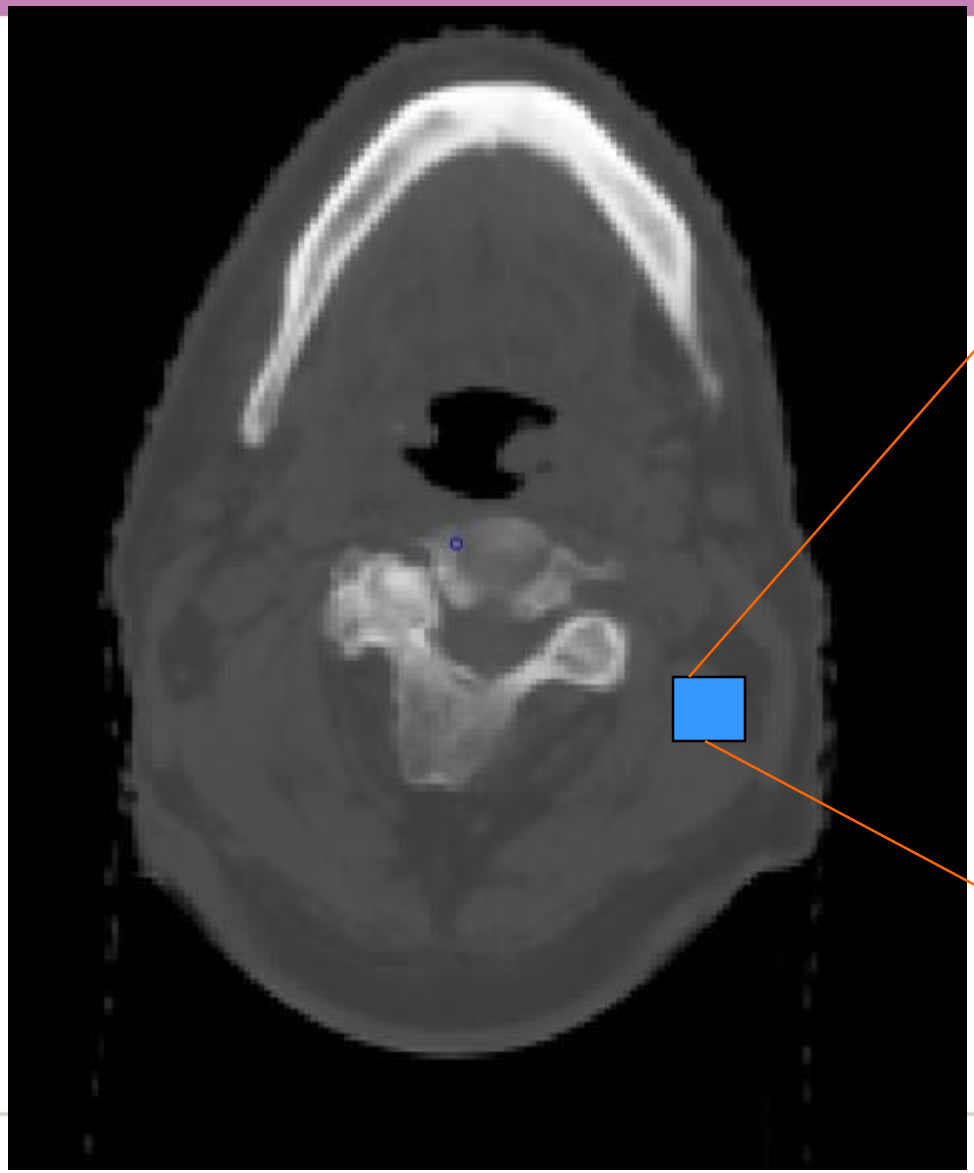

20	40	17	20	37	17	52	31
40	31	40	20	25	17	20	25
17	52	22	37	22	25	37	22
25	20	25	31	25	17	20	17
17	25	40	20	31	40	40	40
37	22	37	17	40	40	22	22
37	22	37	20	31	17	25	22
37	37	17	22	31	31	22	52

$$N_{CT} = \frac{\mu_m - \mu_w}{\mu_w} x\,1000$$

ESTRO School

Z-axis resolution

- Each two dimensional pixel in a CT image represents attenuation within a three-dimensional voxel

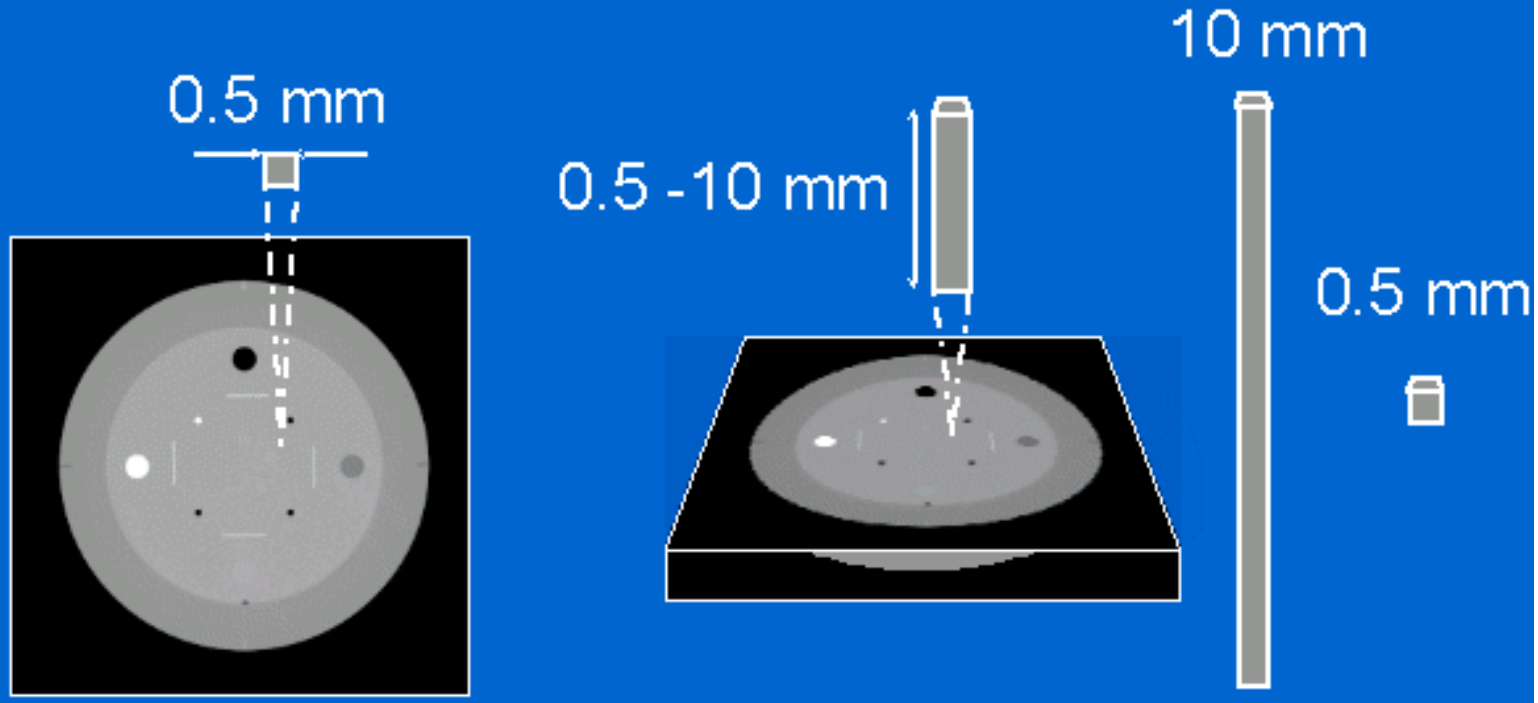

Each voxel assumed to have single Atomic composition and density

Now: Patient represented by large number of voxels each with a Hounsfield number

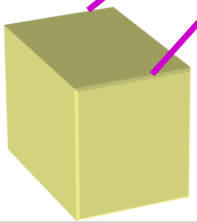

For non-water and direct simulation of radiation transport need:

- Electron Density
- Mass Density
- Chemical composition

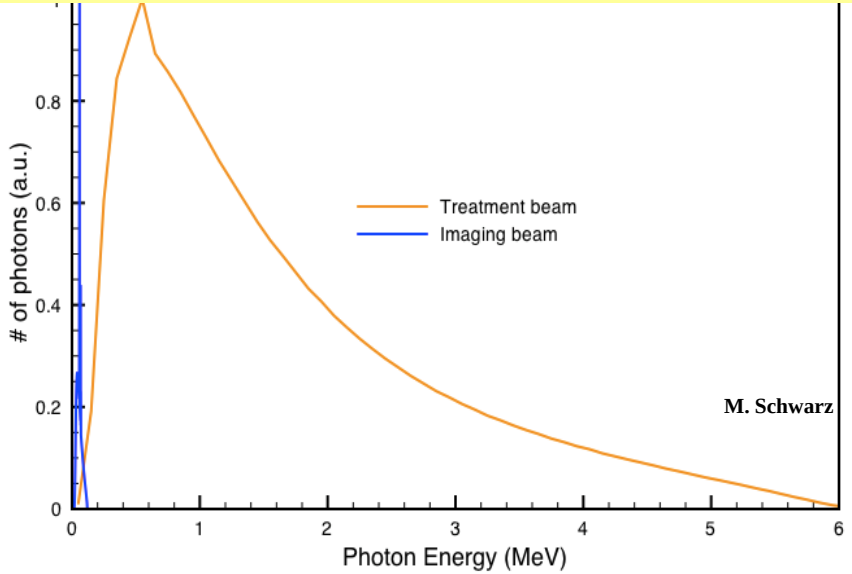

However CT is at kV energies → Radiological properties relevant to MV are not directly available

Each voxel assumed to have single atomic composition and density

Assigned by a calibration curve

ESTRO School

CT Calibration

Electron Density CT Phantom
Gammex 467

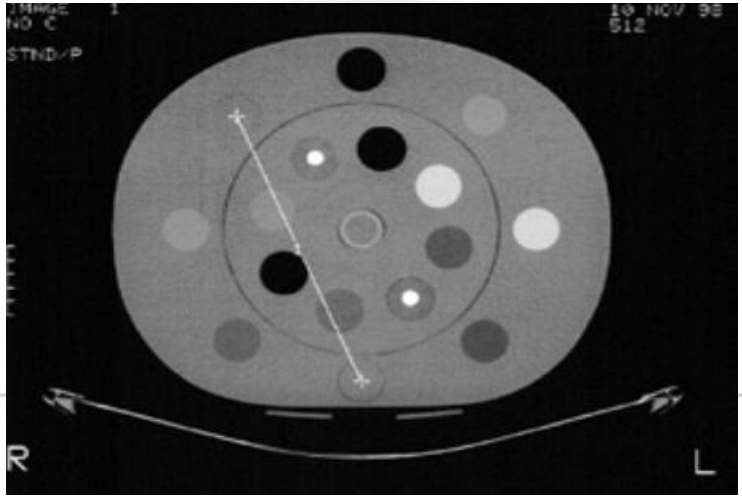

Rod Material	Electron Density Relative to Water	Physical Density g/cm³
Lung (LN-300)	0.28	0.30
Lung (LN-450)	0.40	0.45
Adipose (AP6)	0.90	0.92
Breast	0.96	0.99
CT Solid Water	0.99	1.02
Brain	1.05	1.05
Liver (LV1)	1.07	1.08
Inner Bone	1.09	1.12
Bone (B200)	1.11	1.15
Bone (CB2-30% Mineral)	1.28	1.34
Bone (CB2-50% Mineral)	1.47	1.56
Cortical Bone (SB3)	1.69	1.82
True Water	1.00	1.00

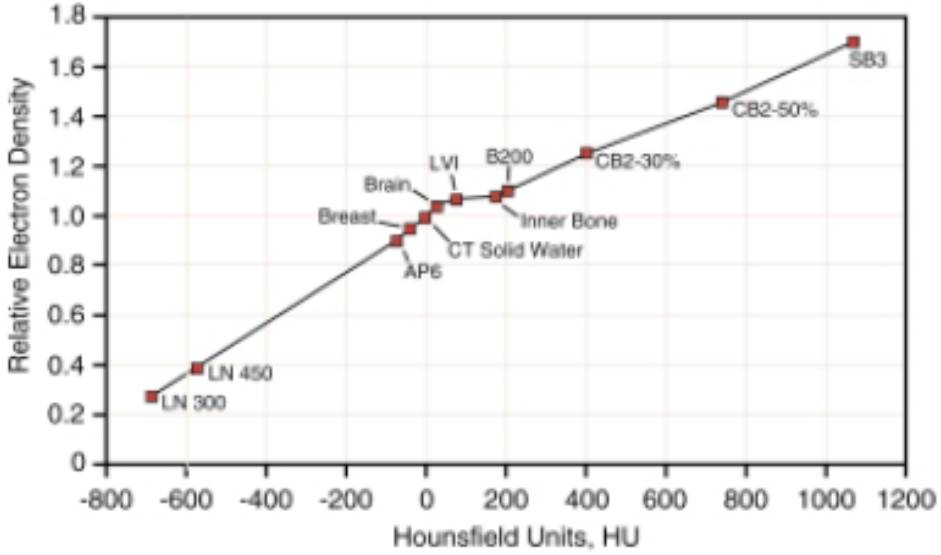

Relationship between the relative electron density and CT number (in Hounsfield Units, HU) of materials in the Electron Density CT Phantom as measured by a GE CT/i scanner.

CONVERTING CT NUMBERS TO DENSITY

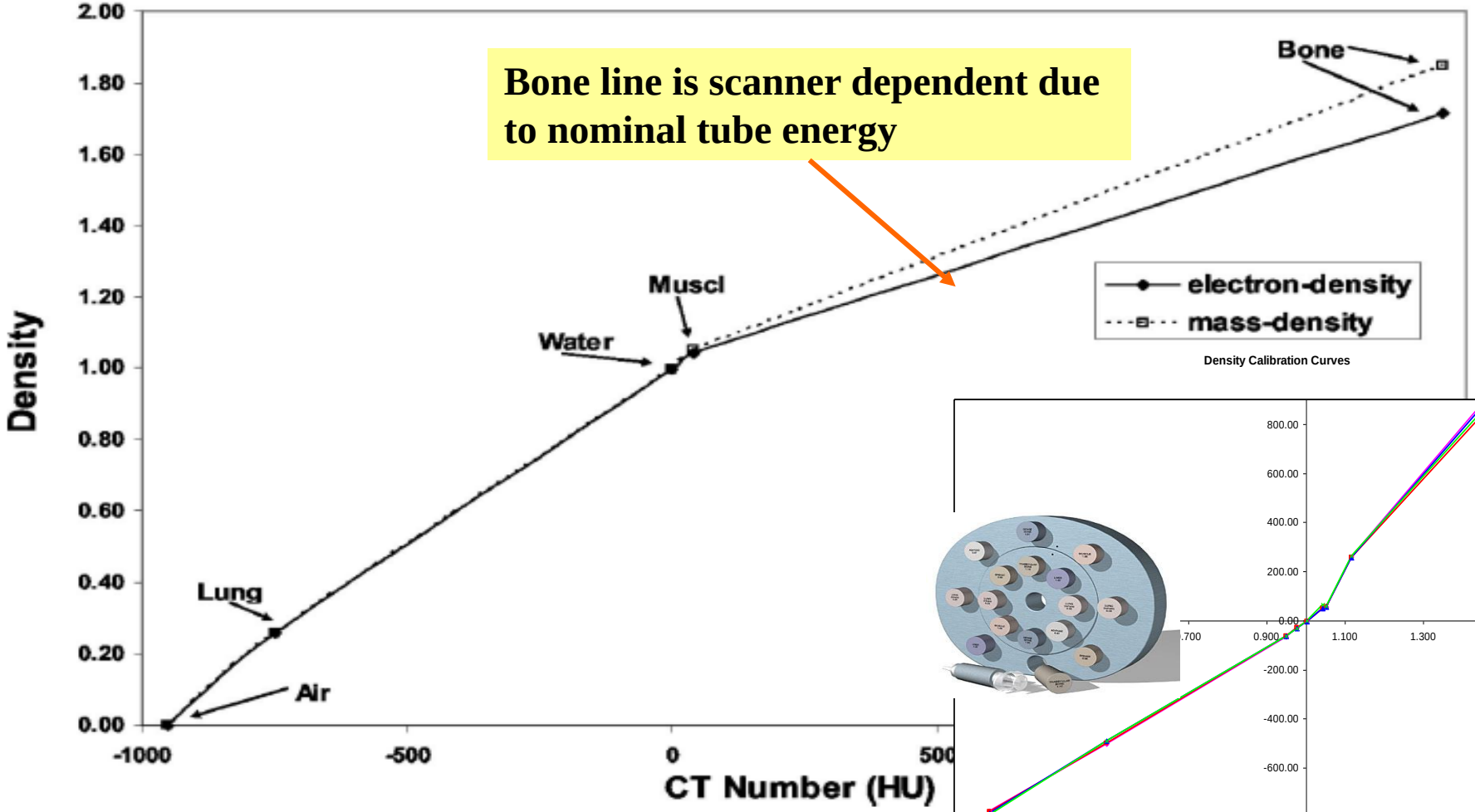

Note only one calibration per CT unit regardless of patient size

N_{CT} α electron density ρ^e_t

$$\rho_t^e = \rho_t N_A \sum_i w_i \frac{Z_i}{A_i}$$

ESTRO School

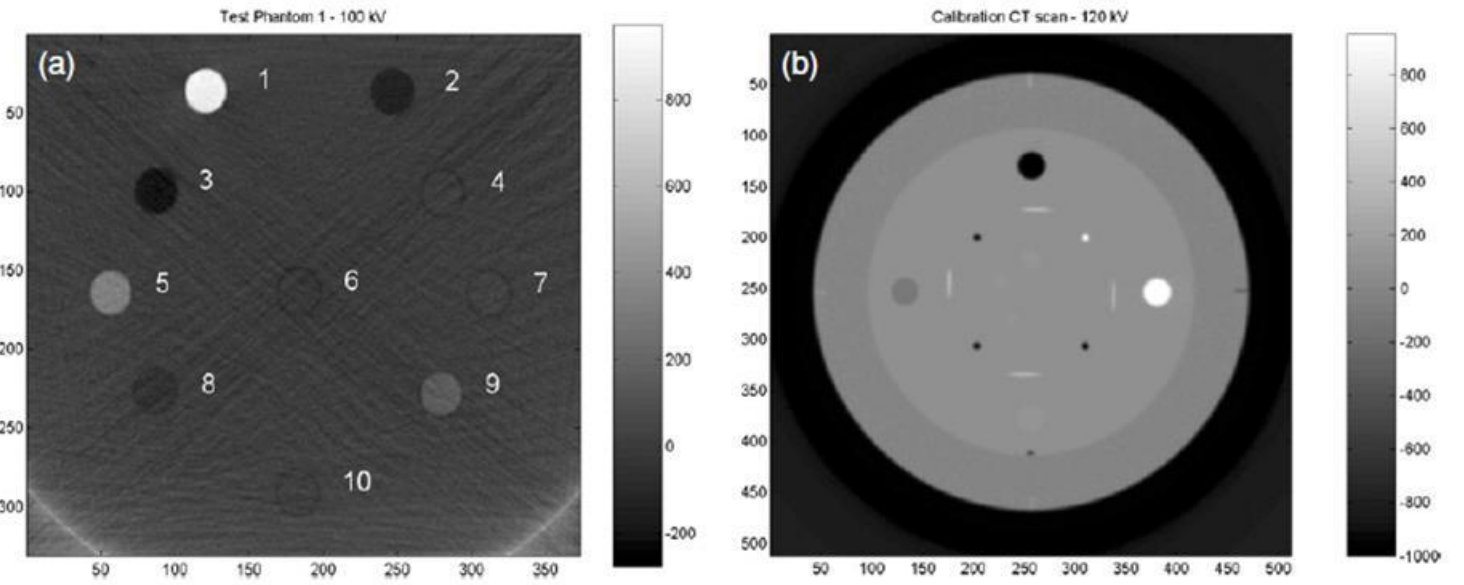

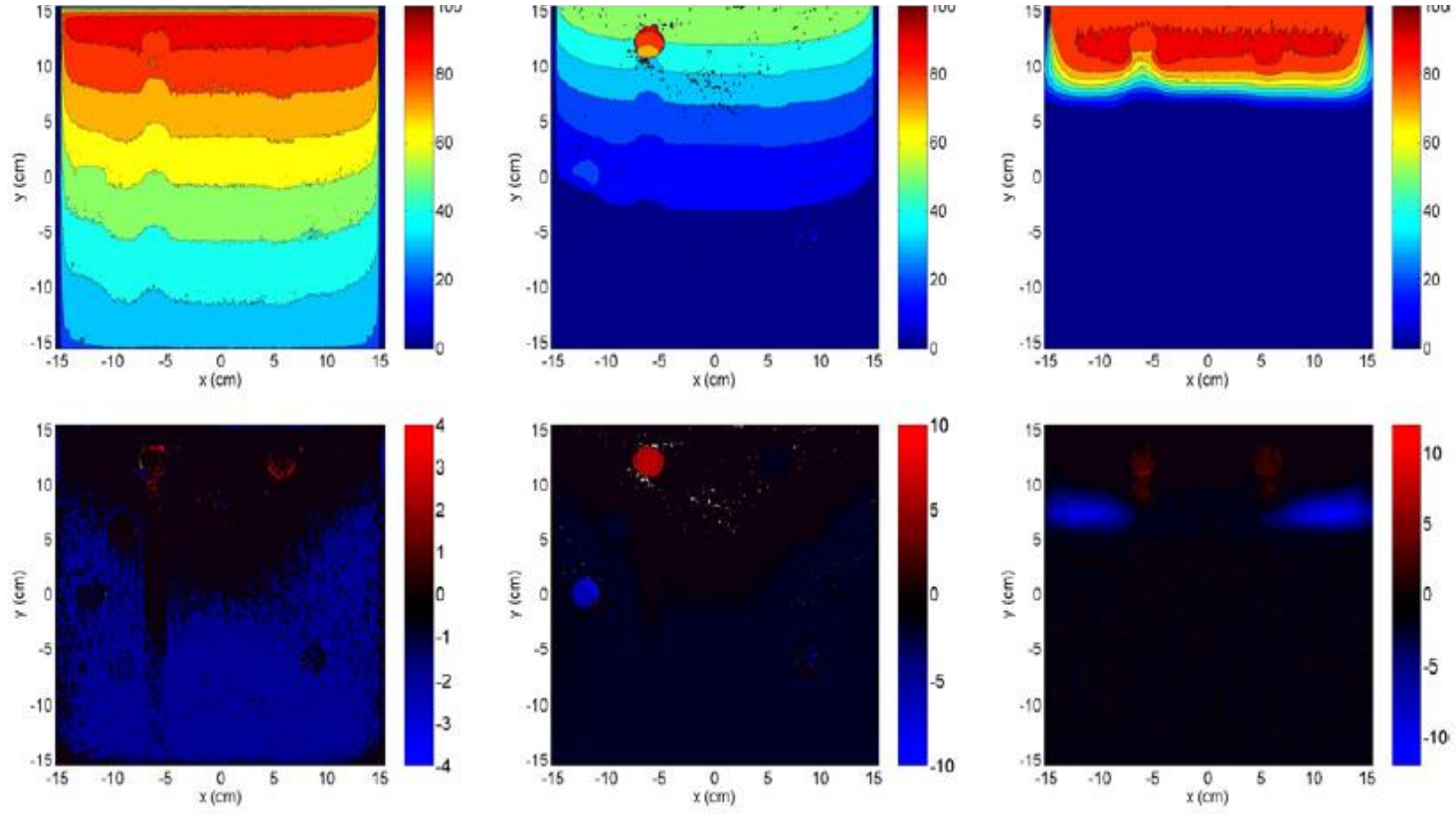

$$\frac{D_{exact} - D_{default}}{D_{default}}$$

10% 6MV and 15MV
30% 18MeV
40% kV

Verhaegen and Devic, PMB 2005

ESTRO School

Common misunderstandings in published literature:

Dose calculation engines on TPS (referred to as 'conventional' excluding Monte Carlo models):

- **use CT number calibration tables in terms of relative electron density**
- **calculate dose to water**

Not always the case!

Dose calculation models on TPS differ in implementation

Why do some TPSs require CT calibration tables in terms of relative mass density

e.g. in point kernel dose calculation engines it is TERMA and point kernels that are scaled

$$T(r) \approx \frac{\bar{\mu}}{\rho}(MV, r, medium(r))\ \Psi_o\ e^{-\int_0^r \frac{\bar{\mu}}{\rho}(MV, r', medium(r'))\, r' dr'}$$

Effective (spectrum averaged) mass attenuation coefficient at radiological distance r for the medium with certain density

Primary energy fluence at the surface

- **Mass attenuation coefficients usually pre-stored as weighted averages for an energy spectrum and for media with different composition and mass density**
- **$N_{CT} \Rightarrow$ relative mass density and material composition**

$\Rightarrow$ mass attenuation coefficient and linear attenuation coefficient

e.g. in Pinnacle, TomoTherapy PS

Tissue and Phantom Material Characterization

-as used in Oncentra MP-

Composition	$\frac{\rho_{mass}}{\rho_{mass,H_2O}}$	$\frac{\rho_{elec}}{\rho_{elec,H_2O}}$	H	H_{DCM}
Air (outside patient)	0.00121	0.00109	-992	-128
Air (inside patient)	0.00121	0.00109	-976	-127
Lung (ICRU 44)	0.50	0.50	-480	-96
Adipose (ICRU 44)	0.95	0.95	-96	-72
Muscle (ICRU 44)	1.05	1.04	48	-63
Cartilage (ICRP 23)	1.10	1.08	128	-58
2/3 Cartilage, 1/3 Bone	1.35	1.29	528	-33
1/3 Cartilage, 2/3 Bone	1.60	1.52	976	-5
Bone (ICRP 23)	1.85	1.72	1488	27
Bone (ICRP 23)	2.10	1.95	1824	48
½ Bone, ½ Aluminum	2.40	2.15	2224	73
Aluminum	2.70	2.34	2640	99
Aluminum	2.83	2.46	2832	111
Iron	7.87	6.60	>2832	112
Water	1.00	1.00	-	“127”

Note: Water is not part of an anatomical scale

The scale will interpret a water CT-image as a mixture of adipose and muscle

Plastics are not part of the scale either

Tissue and Phantom Material Characterization

-as used in Oncentra MP-

Composition	$\frac{\rho_{mass}}{\rho_{mass,H_2O}}$	$\frac{\rho_{elec}}{\rho_{elec,H_2O}}$	H	H_{DCM}
Air				-128
Air				-127
Lun				-96
Adi				-72
Mus				-63
Car				-58
2/3				-33
1/3 Cartilage, 2/3 Bone	1.60	1.52	976	-5
Bone (ICRP 23)	1.85	1.72	1488	27
Bone (ICRP 23)	2.10	1.95	1824	48
½ Bone, ½ Aluminum	2.40	2.15	2224	73
Aluminum	2.70	2.34	2640	99
Aluminum	2.83	2.46	2832	111
Iron	7.87	6.60	>2832	112
Water	1.00	1.00	-	“127”

- how many linear segments should be used?
- which tissue-equivalent materials are suitable for calibration?
- where should the boundaries between tissue types be set?

.....

Quality of conversion affects dose calculation

- one of the weakest links in the calculation chain!

ESTRO School

ICRP PUBLICATION 23: REFERENCE MAN: ANATOMICAL, PHYSIOLOGICAL AND METABOLIC CHARACTERISTICS, 23

International Commission on Radiation Units & Measurements

Tissue Substitutes in Radiation Dosimetry and Measurement (Report 44)

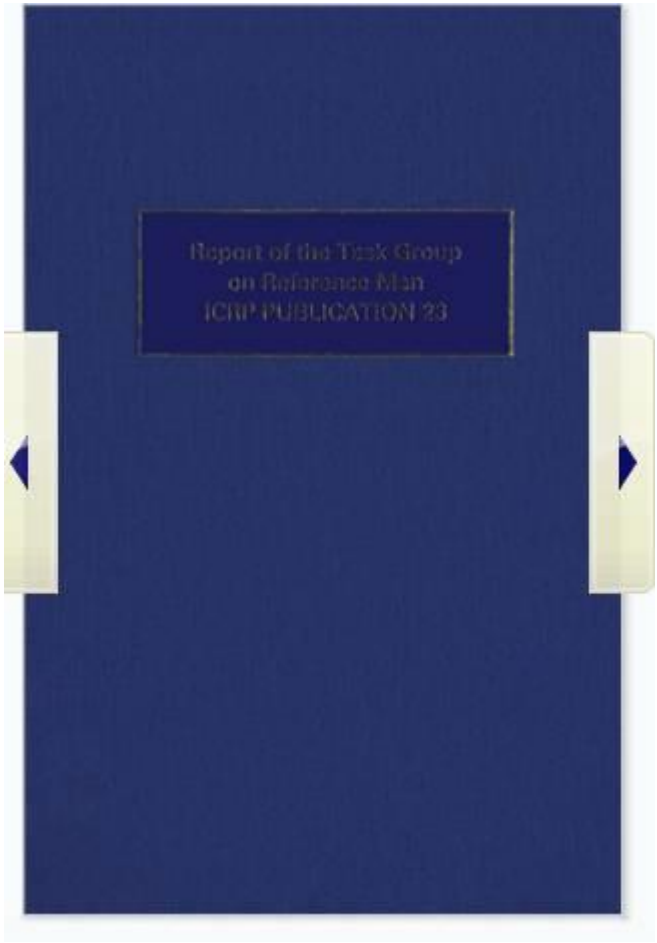

Note: implicit assumption that elemental composition, weights and density values correspond to 'standard' compositions as in ICRU 44 and ICRP23

This ignores patient to patient variation (~15%)

' body tissue compositions should not be given the standing of physical constants'

Gender? Ethnicity? Number of samples?

ESTRO School

Tissue composition

- How accurate are published 'reference' tissues?
- Variability over population?
- Variability with age (breast)
- The myth of the 50-50 breast (Yaffe et at MP 2009)

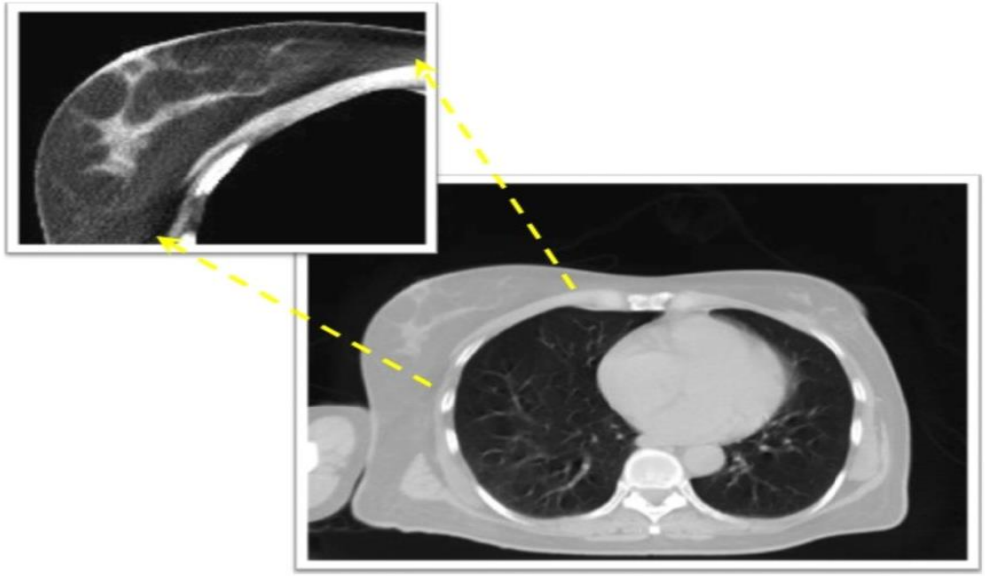

Afsharpour et al PMB 2011

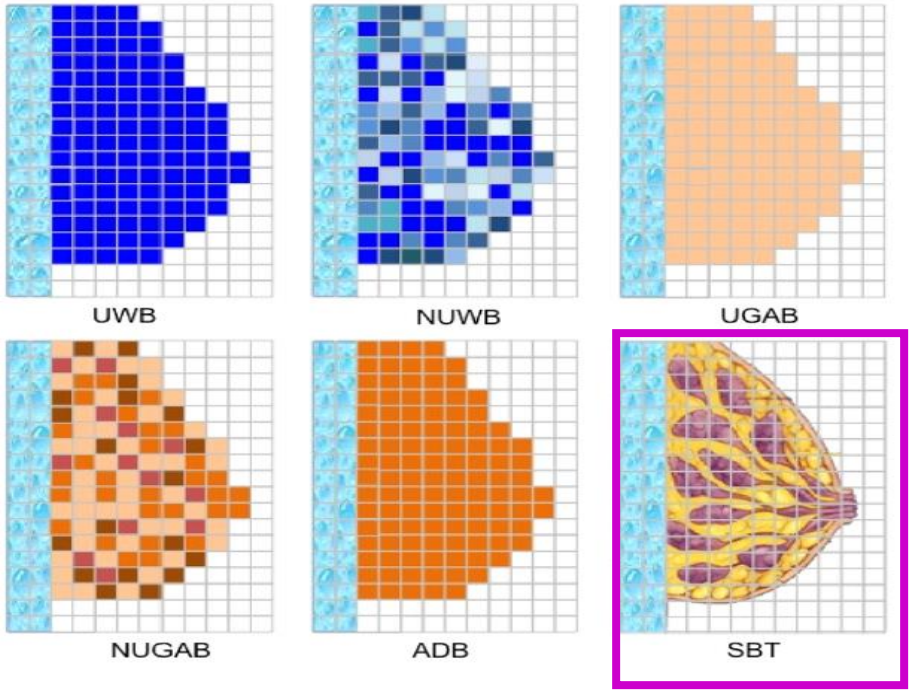

Breast was long assumed: 50% adipose, 50% gland (brighter above)

Reality: mean composition is much closer to 80% A / 20% G

ESTRO School

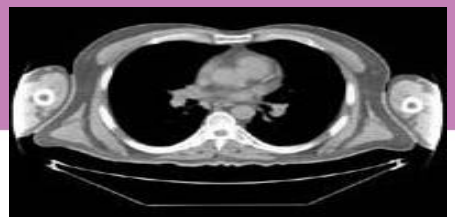

Voxelization based on dose grid resolution

Adapted from van Dyk

CTCREATE process

Read CT Data

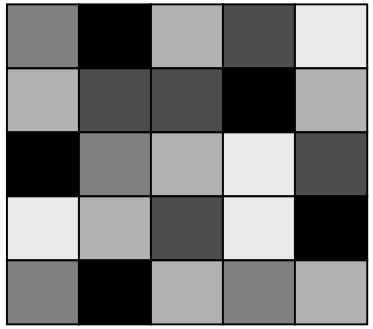

Apply Transport grid

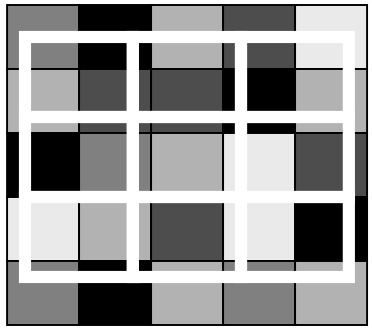

Resample CT

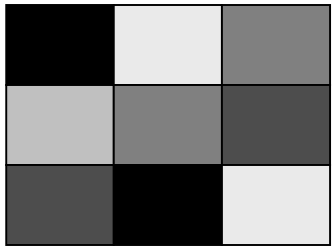

Convert to Densities

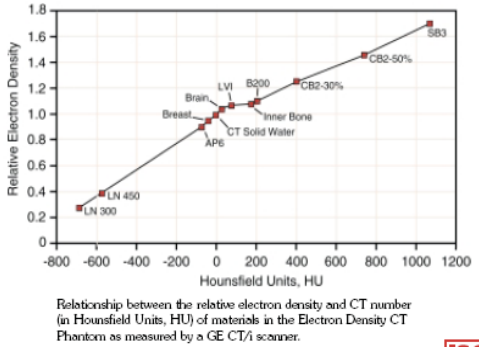

Relationship between the relative electron density and CT number (in Hounsfield Units, HU) of materials in the Electron Density CT Phantom as measured by a GE CT/i scanner.

Convert to materials

Rod Material	Electron Density Relative to Water	Physical Density g/cm³
Lung (LN-300)	0.28	0.30
Lung (LN-450)	0.40	0.45
Adipose (AP6)	0.90	0.92
Breast	0.96	0.99
CT Solid Water	0.99	1.02
Brain	1.05	1.05
Liver (LV1)	1.07	1.08
Inner Bone	1.09	1.12
Bone (B200)	1.11	1.15
Bone (CB2-30% Mineral)	1.28	1.34
Bone (CB2-50% Mineral)	1.47	1.56
Cortical Bone (SB3)	1.69	1.82
True Water	1.00	1.00

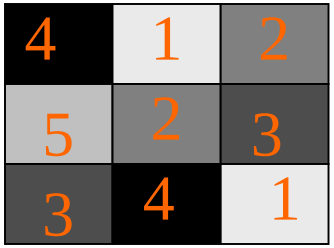

How accurate are CT numbers…?

- HU of homogeneous material can vary by 1-2%
- Depends on location (beam hardening) – up to 3%
- Variation across scanners for high density (>5% in cases)
- Electron Density of Tissue Substitutes
- Tissue substitutes=tissues?

- Tissue Assignment (ICRU and ICRP)?

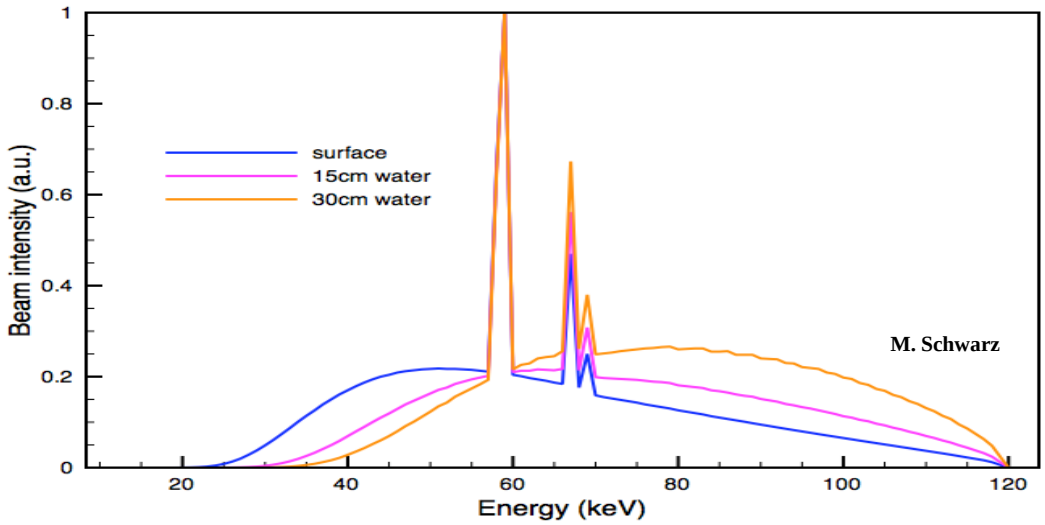

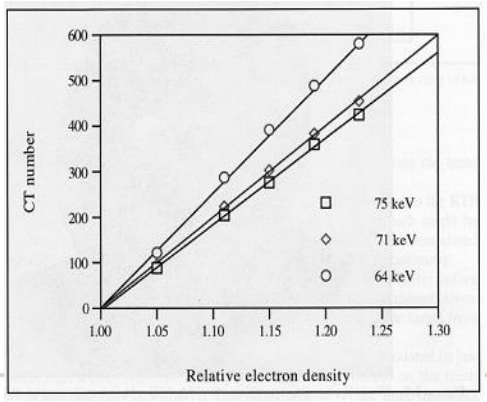

ESTRO School

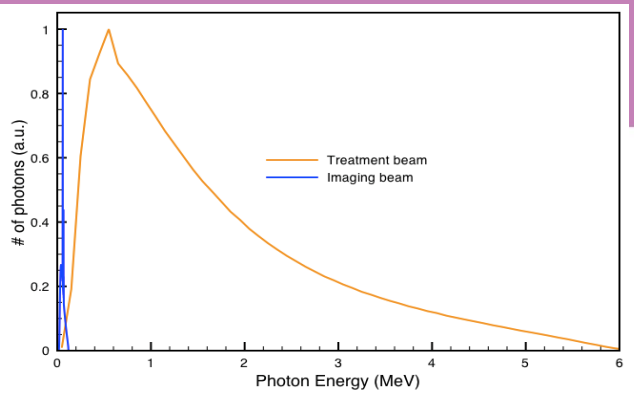

CT number is determined not only by electron density.

→ two media of identical ρ_e but different Z_{eff} will have different HU

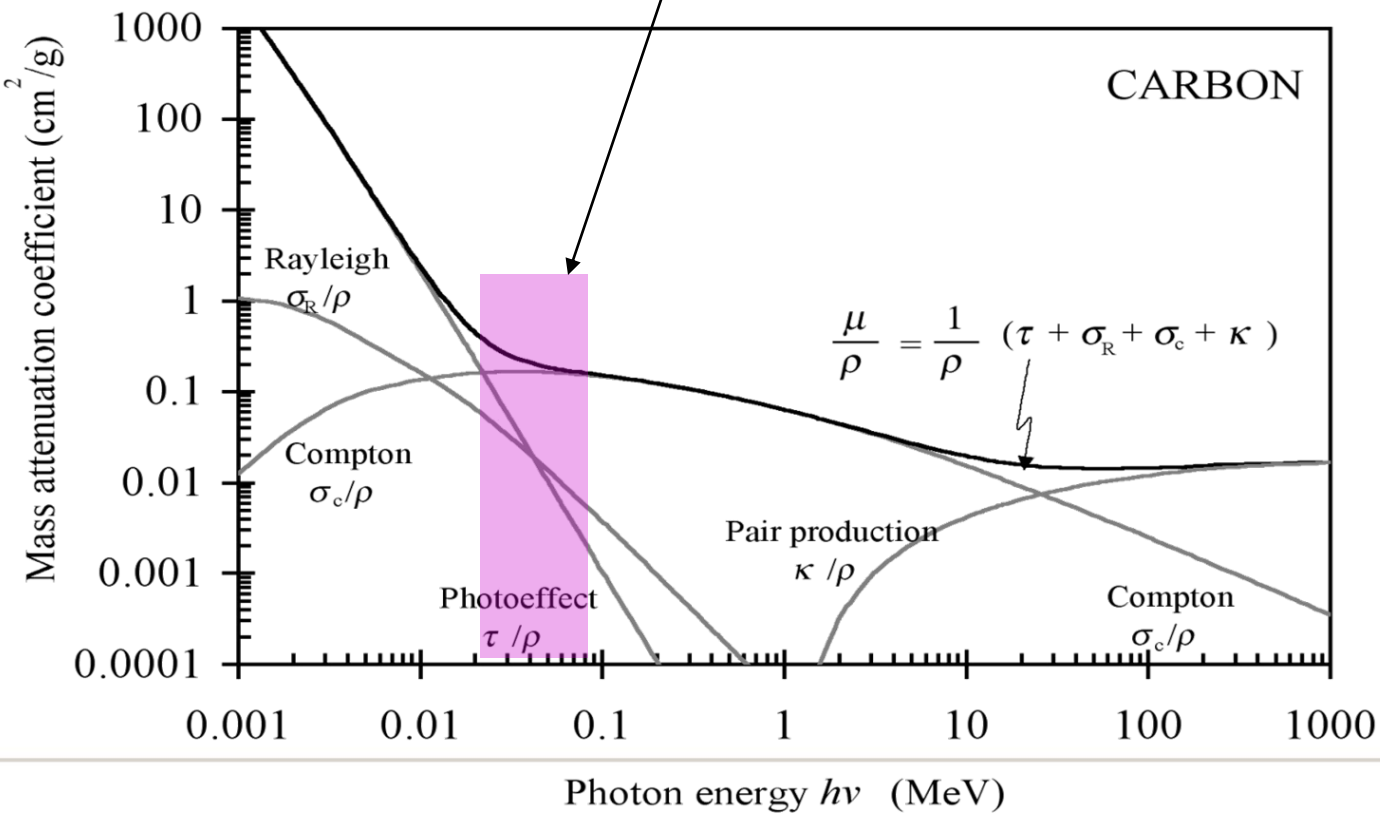

Adapted from Schwarz

Tissues with different Mass density and elemental weights can have same HN

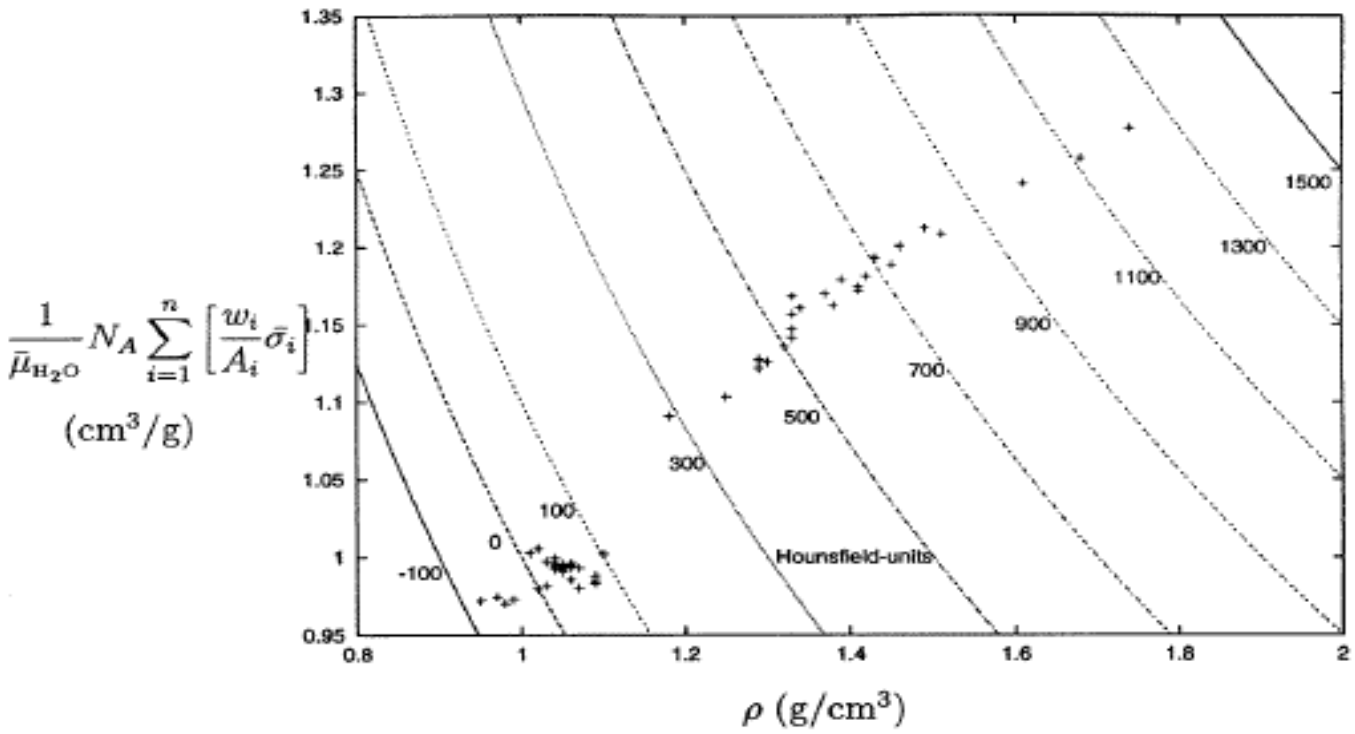

Figure 3. Projection of the space of tissue parameters (ρ, w_i). The data points are corresponding to the 71 human tissues. Along the hyperbolas, the CT number is constant.

W. Schneider et al PMB 45 2000

Tissues with different Mass density and elemental weights can have same HN

Where do we define boundaries between ρe of media?
How many media?

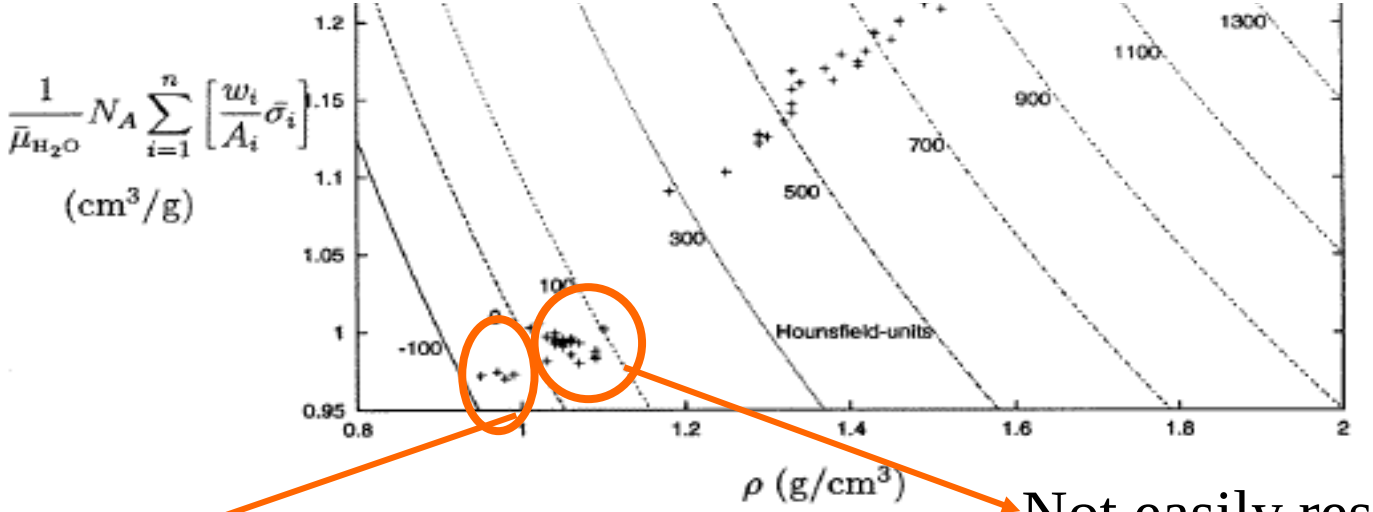

Resolved

Not easily resolved!

Figure 3. Projection of the space of tissue parameters (ρ, w_i). The data points are corresponding to the 71 human tissues. Along the hyperbolas, the CT number is constant.

W. Schneider et al PMB 45 2000

Uncertainties on CT calibration

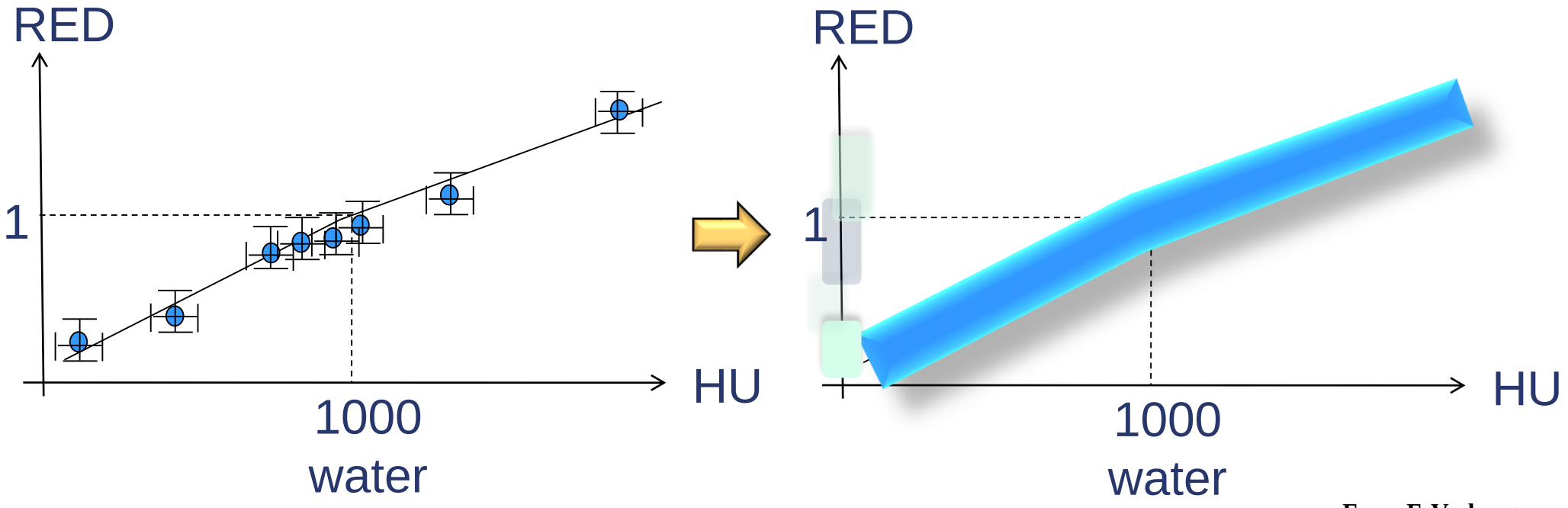

From F. Verhaegen

-uncertainty on (e-) density

-uncertainty on material assignment

ESTRO School

Stoichiometric calibration: An improved approach

U. Schneider et al PMB 1996

Calculate Relative Electron Density:

$$\rho_e = \frac{\rho N_g}{\rho^{water} N_g^{water}}$$

Using chemical composition:

$$N_g = \sum N_g^i = N_A \sum \frac{w_i Z_i}{A_i}$$

$$H = 1000 \frac{\mu}{\mu_w}$$

Relative proton stopping power

$$\rho_s = \rho_e \frac{\log\left[2m_e c^2 \beta^2 / I_m \left(1-\beta^2\right)\right] - \beta^2}{\log\left[2m_e c^2 \beta^2 / I_w \left(1-\beta^2\right)\right] - \beta^2} = \rho_e K$$

Rutherford et al 1976

$$\mu = \rho N_g (Z, A)\left\{K^{ph} \tilde{Z}^{3.62} + K^{coh} \hat{Z}^{1.86} + K^{KN}\right\}$$

By making measurements of H for different tissue substitutes of known composition one can get a fit of data to derive values for $K^{ph/coh/KN}$ which characterize the CT scanner

From this can plot a curve to predict H for range of tissues substitutes and real tissue

ESTRO School

Stoichiometric calibration: An improved approach

U. Schneider et al PMB 1996

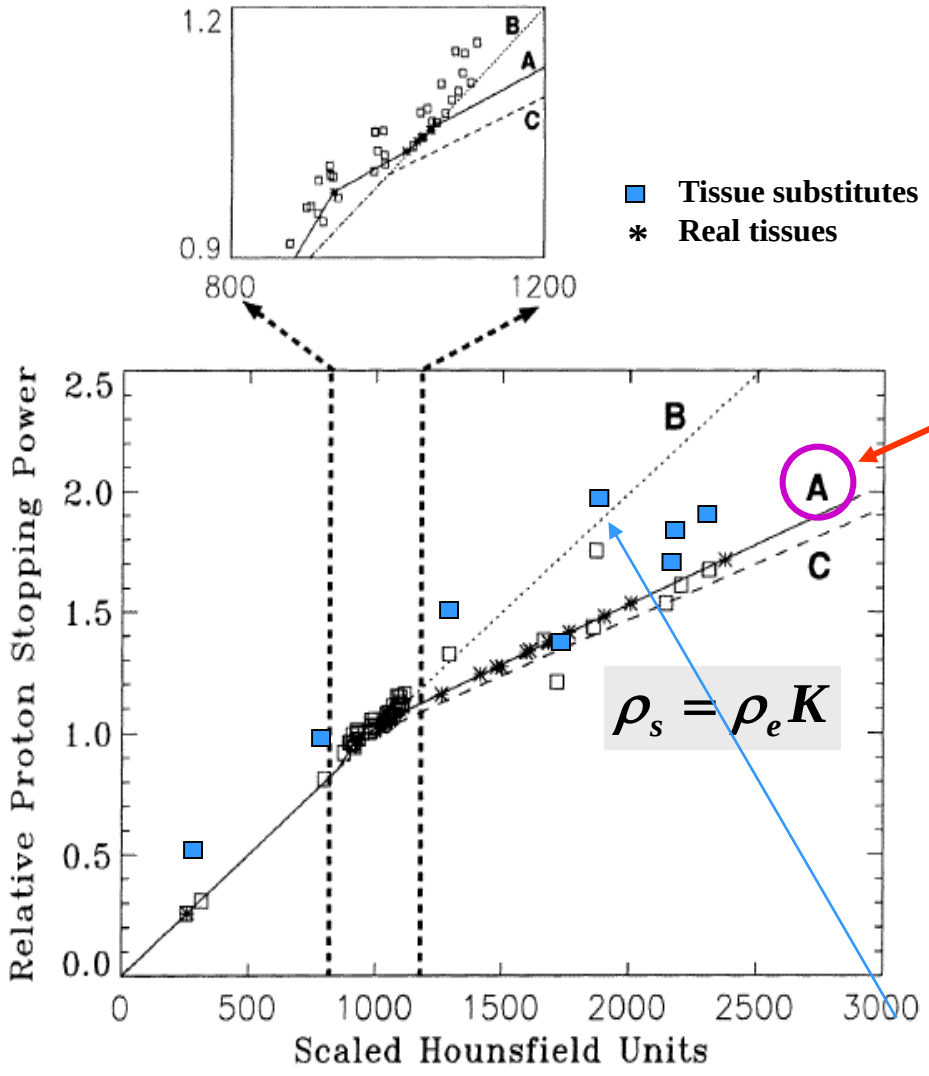

Verified for proton stopping power by measurements in a sheep head

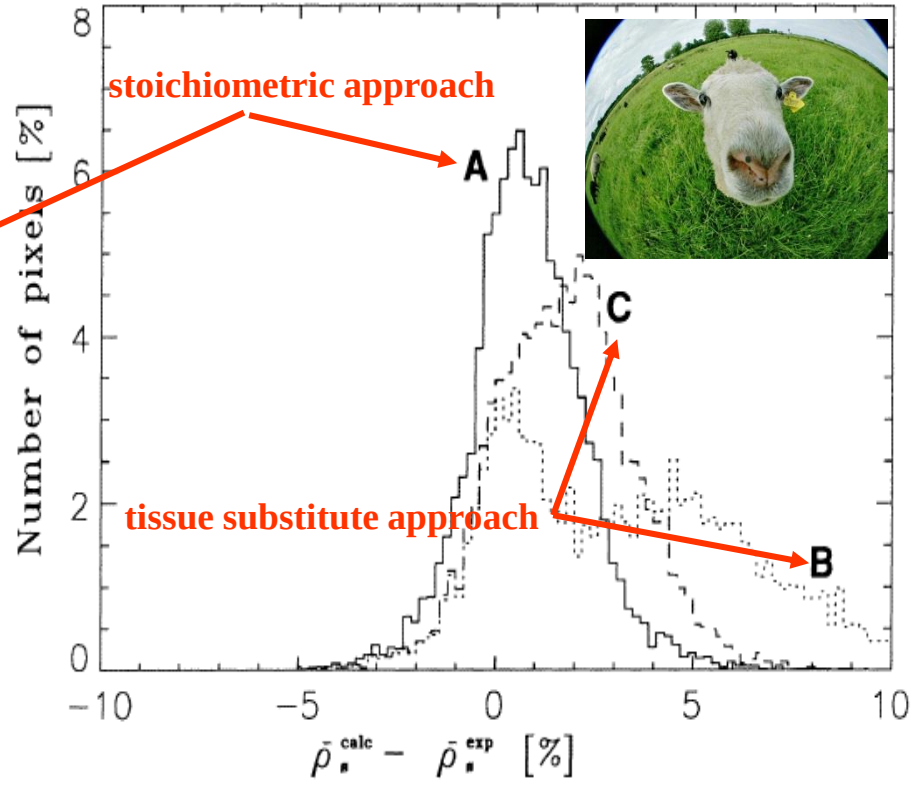

Calibration based on tissue substitutes only is very sensitive to material chosen. Different substitutes give different calibration curves

ESTRO School

How many materials are needed?

- Du Plessis et al (MP 25(7) 1998)
  - Combined 16 human tissues into 7 dosimetrically equivalent subsets with constant elemental composition to give dose accuracy of <1%.
  - Needed further subdivision in bone and lung (57) by varying density only
- W.Schneider (stoichiometric) calibrating H with mass density and elemental weights
  - Extended to 71 tissues
  - Grouped into 24 bins
  - Simplified using interpolation functions for 4 sections of calibration curve+
- 'Ctcreate' from BEAMnrc
  - 4 major tissue types (air, lung, soft tissue, bone)
  - ICRU tissue composition used and mass density from linear interpolation

D_w or D_m?

Now we have the patient tissue represented (in some way), do we report *Dose to Water* or *Dose to Tissue*?

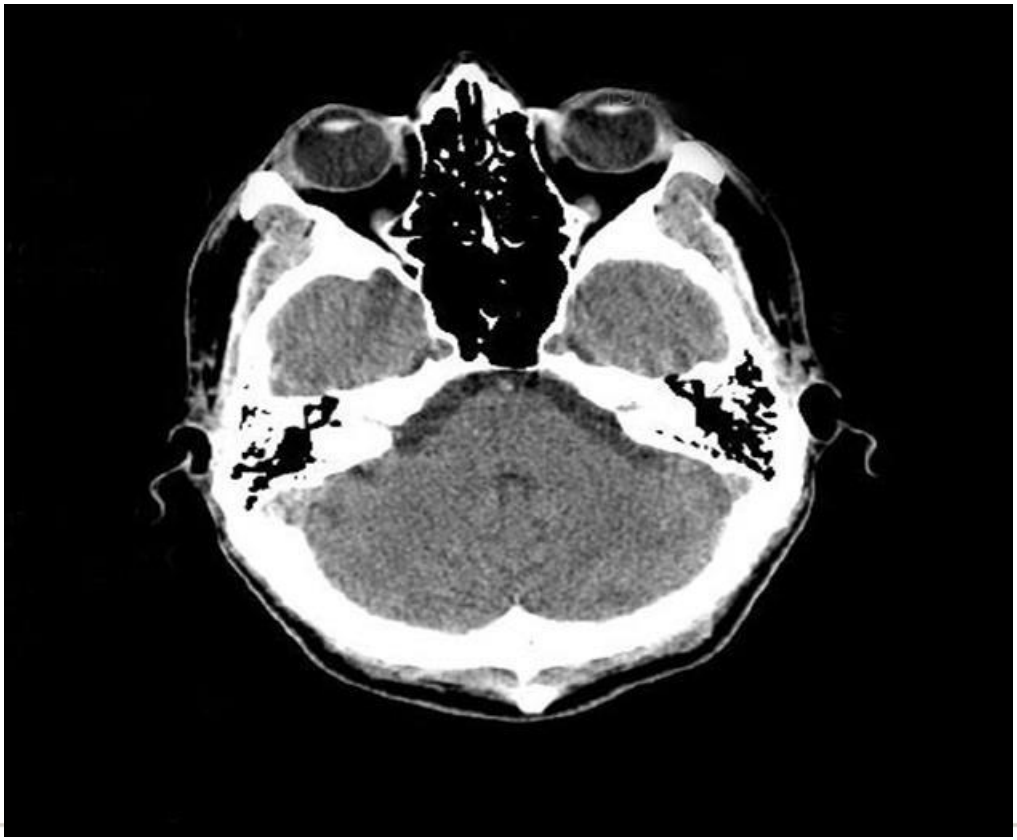

Dose to Water or Dose to Tissue?

$$D_{w,W} \cong \frac{\mu_{en,w}}{\rho} \Psi_o \, e^{-\mu_w z}$$

$$D_{w,M} \cong \frac{\mu_{en,m}}{\rho} \Psi_o \, e^{-\mu_m z} \left(\frac{\bar{S}}{\rho} \right)_m^w$$

$$D_{m,M} \cong \frac{\mu_{en,m}}{\rho} \Psi_o \, e^{-\mu_m z}$$

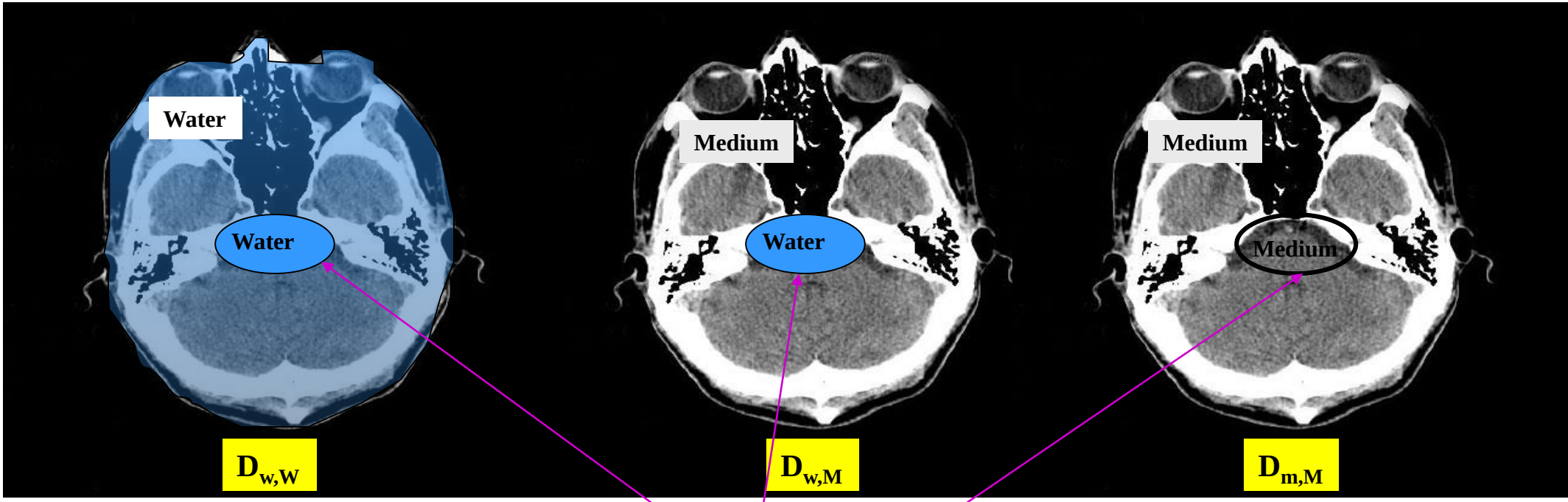

Scoring Volume

$\Rightarrow$ conversion of dose to medium to dose to water

$$D_{w,M} = D_{m,M} \left(\frac{\bar{S}}{\rho} \right)_m^w$$

from Anders Ahnesjö

ESTRO School

Recent Clinical Example SLRON

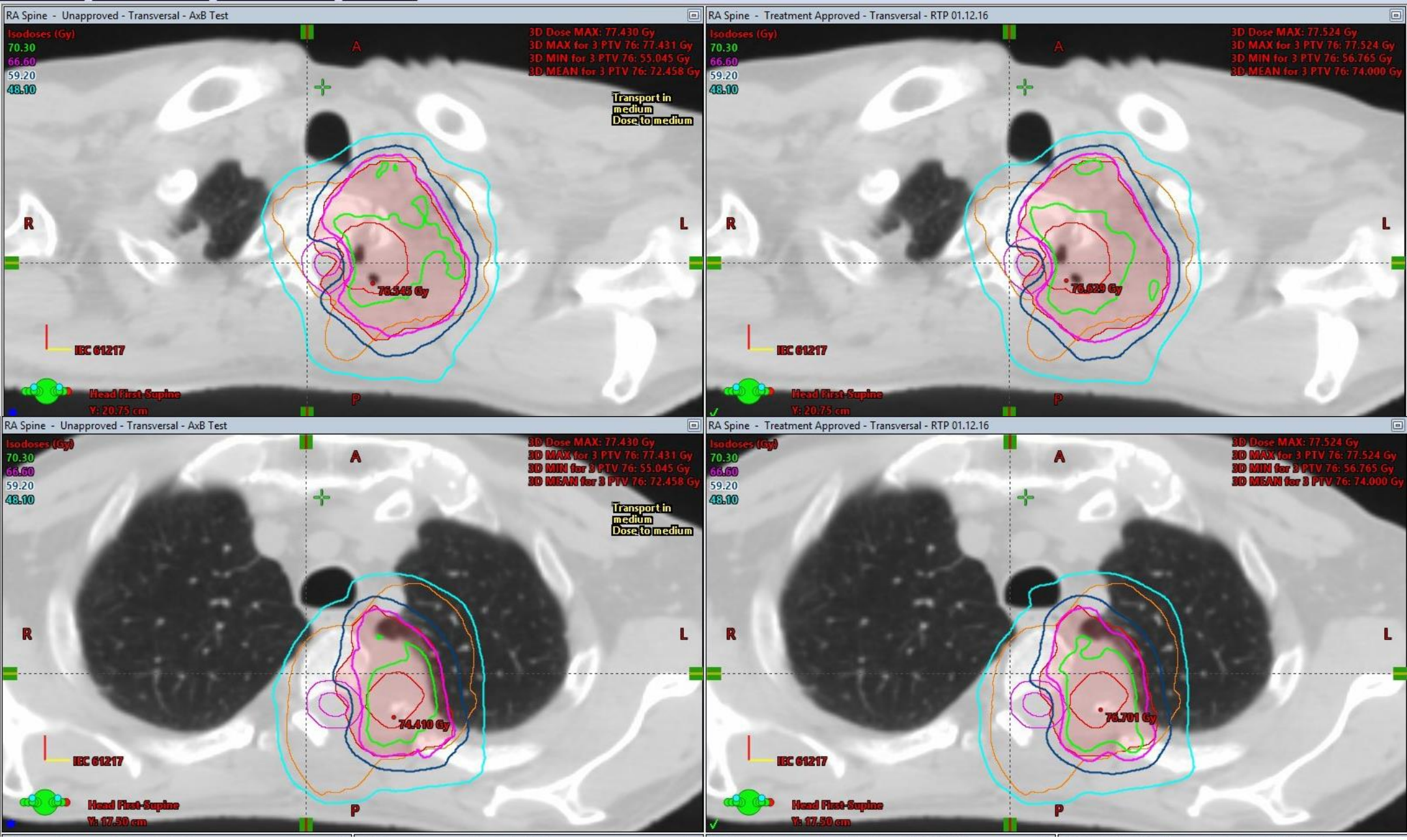

Recent Clinical Example SLRON

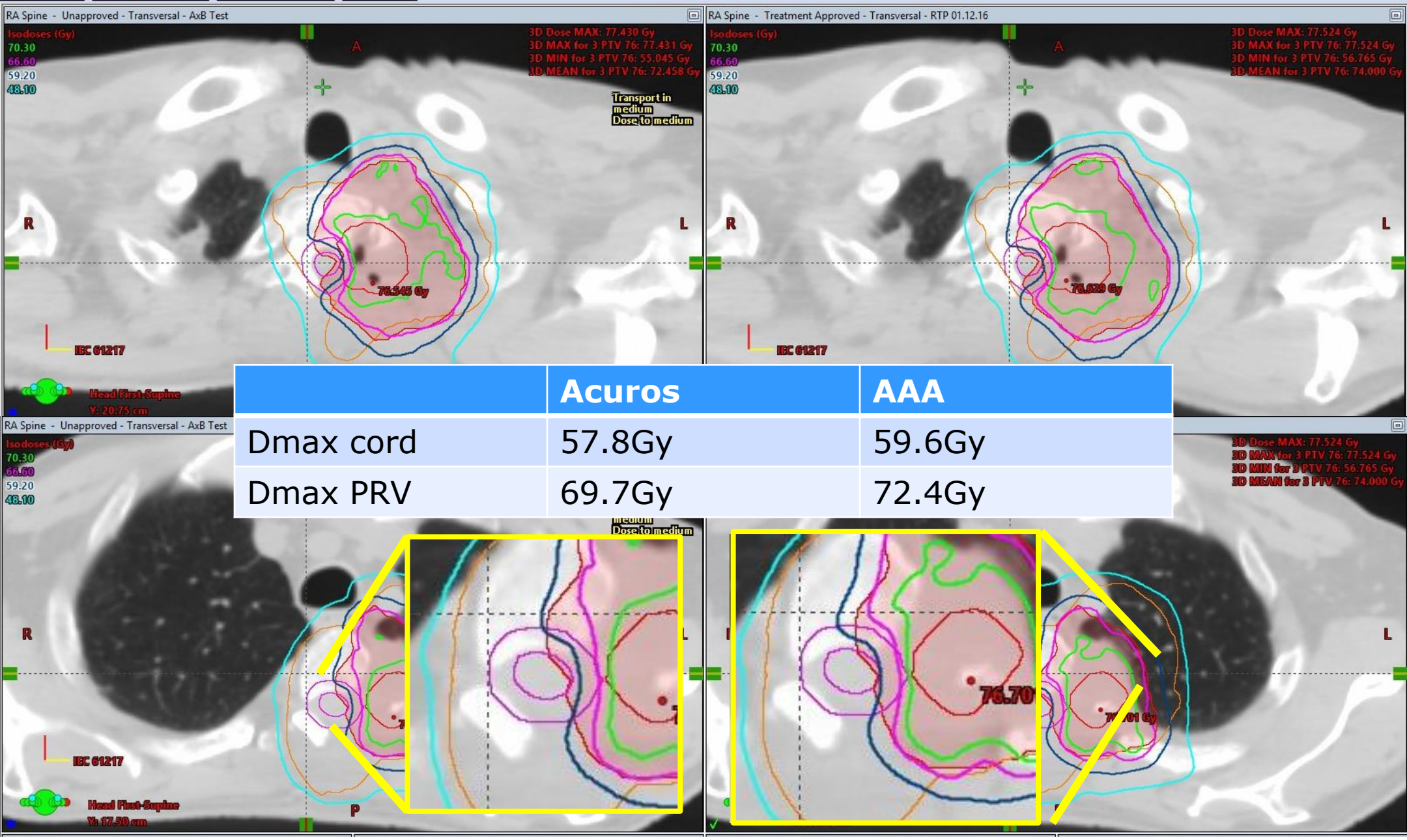

	Acuros	AAA
Dmax cord	57.8Gy	59.6Gy
Dmax PRV	69.7Gy	72.4Gy

Some developments: DECT

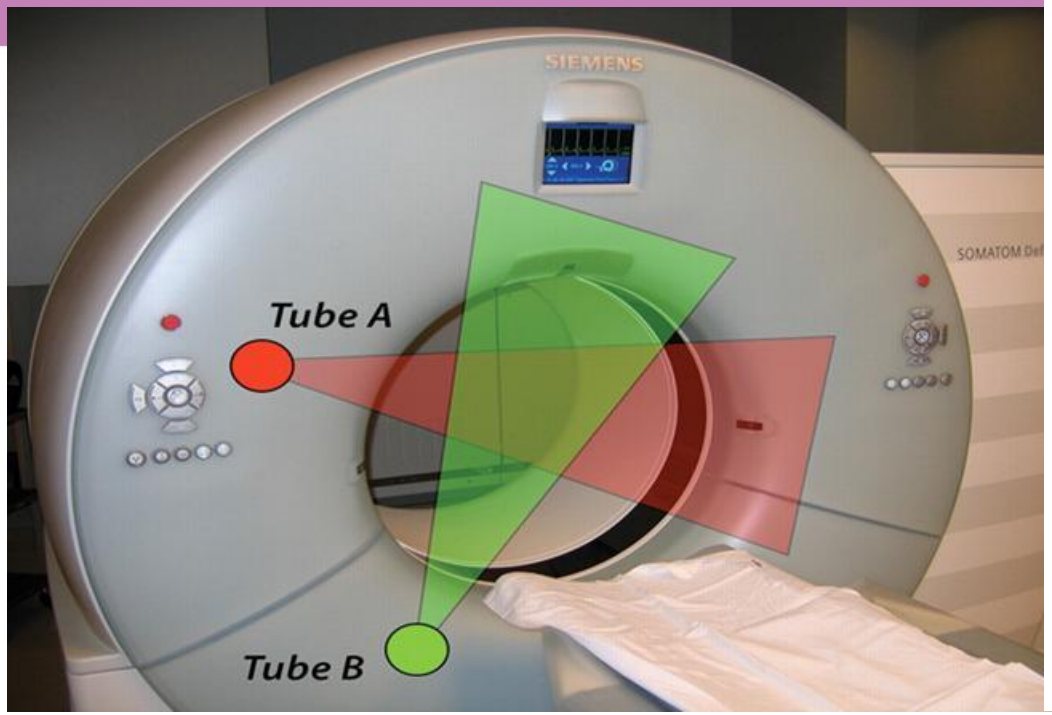

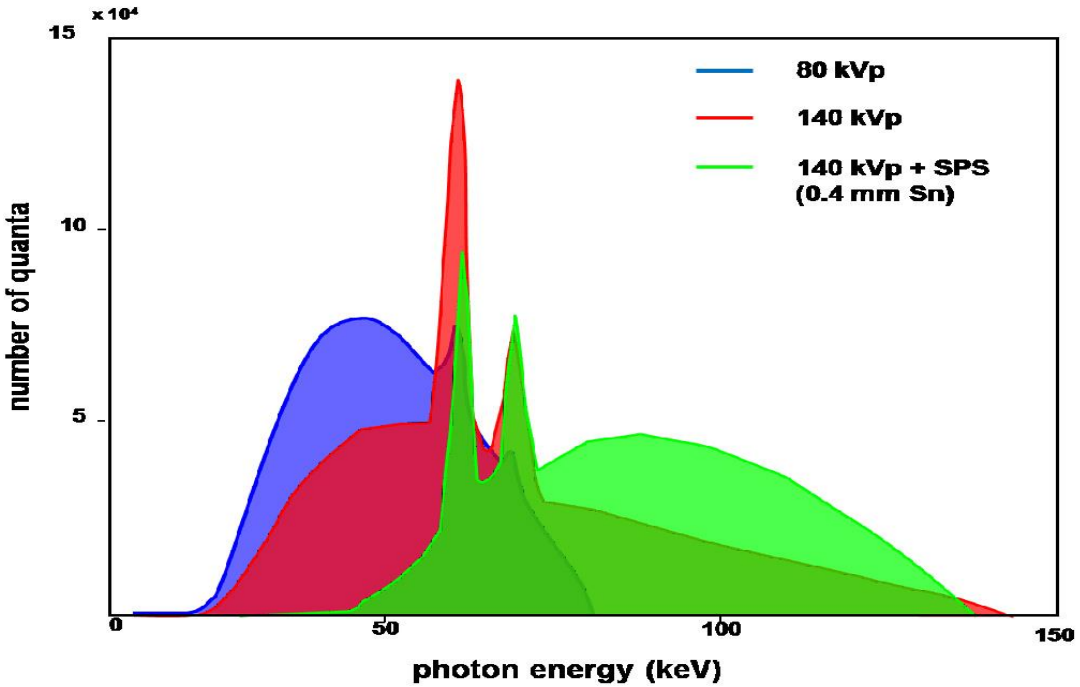

Attenuation is function of medium density and elemental composition
Several materials same HU but different densities and elemental compositions

DECT exploits energy and compositional dependence of μ at keV energies

$\mu(E) = \rho(af_{compton}(E) + bf_{PE}(E))$

a and b depend only on composition of material

Scan at 2 energies to give Z_{eff} and electron or mass density via simultaneous equations

ESTRO School

Dose uncertainties in MC MV photon dose calculations

- **Bazalova PMB 2008, *Dual-energy CT-based material extraction for tissue segmentation in Monte Carlo dose calculations***

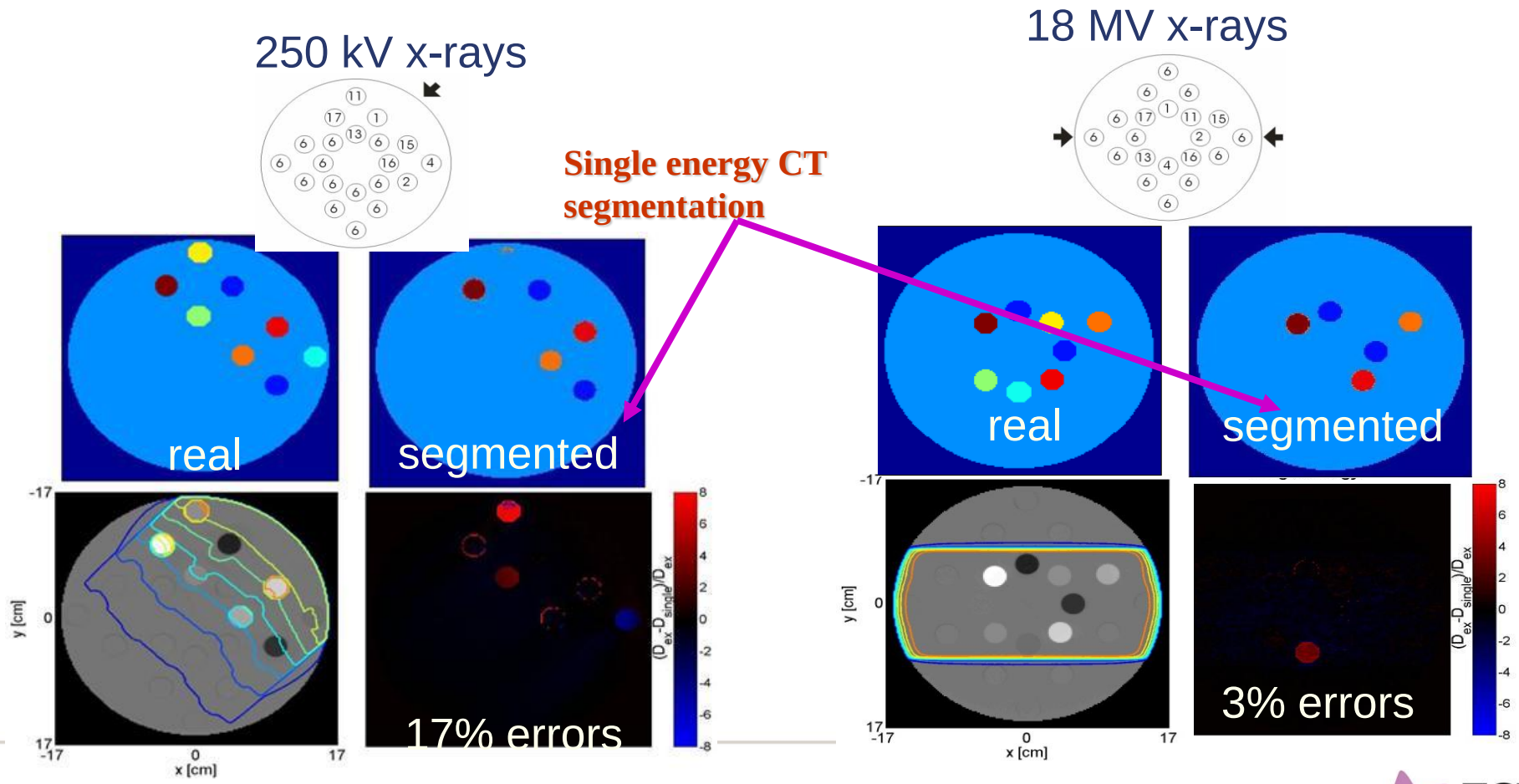

From F Verhaegen

But <1% when dual energy used

ESTRO School

Other image possibilities

Cone beam CT images?

- Image quality of CBCT images << CT images
  - $HU_{CT} \neq HU_{CBCT}$
  - Needs separate calibration
  - CBCT sensitive to motion artifacts
- Hatton PMB 54 (2007): 20% dose errors for MV photons based on CBCT

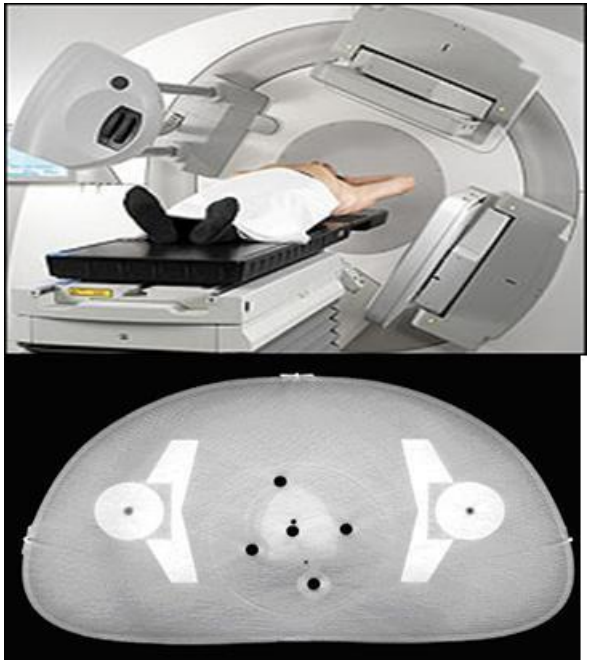

Other image possibilities

MRI images?

- MRI superior soft tissue contrast
  - Lower intraobserver variation
  - Smaller margins
- Bulk density assignment?
  - Bone must be delineated on the scans
  - Doses not as accurate as could be
  - DRR's difficult

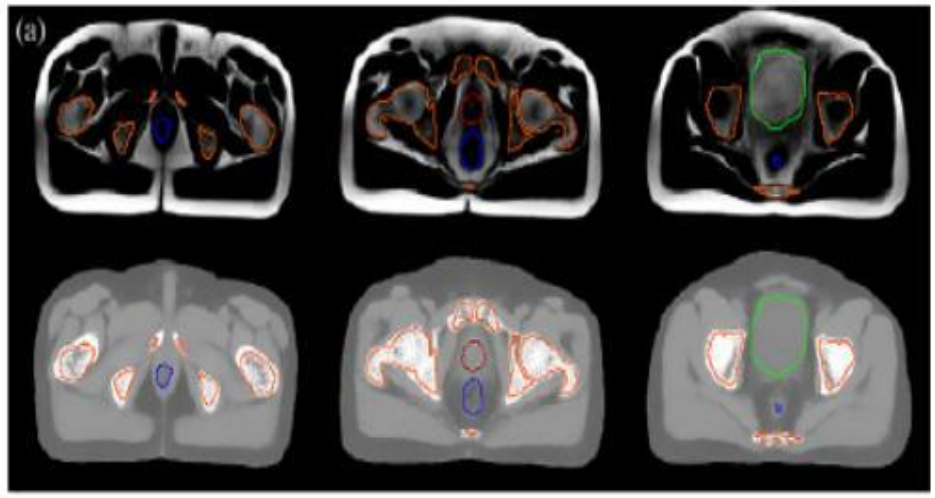

Dowling IJROBP 83 (2012). Prostate

- Atlas-based electron density mapping method
  - MRI atlas built up from number of patients
  - Corresponding CT data sets
  - Patient MRI mapped to atlas, same vectors applied to CT Atlas
- PseudoCT and planning CT dose differences 95% <2%/2mm.
- Full examination of uncertainties needed
  - How similar is anatomy of patients?

Table 2 Comparison of original CT and pseudo-CT-based HU (n = 39)*

Site	CT mean HU (±SD)	Pseudo-CT mean HU (±SD)	Two-tailed t-test p value result
Rectum	−54 (4)	−54 (143)	>0.9
Bladder	9 (0)	9 (6)	>0.9
Bone	339 (10)	340 (85)	>0.9
Prostate	42 (1)	42 (25)	>0.9

* The increased standard deviation (SD) in the pseudo-CT is due to the large number of CT scans used to generate the pseudo-CT atlas.

ESTRO School

Conclusions

Numerous approximations whose impact on the final dose accuracy should not be ignored!

- CT remains the preferred image modality
- CT calibration curves and tissue segmentation key to accurate dose calculation
  - More important for Protons and keV (and Brachytherapy)
  - Some common practices to establish tissue characterization can introduce systematic errors into dose planning
- Dw and Dm debate continues but important to specify medium in literature

Thank you!


IT WAS THE NEXT LOGICAL STEP... WE'VE NOW FULLY DIGITIZED OUR PATIENTS!

Point kernel based models

Anders Ahnesjö
Uppsala University
Sweden

ESTRO

UPPSALA
UNIVERSITY

Learning objectives

1. Understand the basic principles of the point kernel superposition/convolution/collapse cone family of dose engine models

2. Understand the expected performance of point kernel models versus MC, pencil kernel and grid based models in terms of speed versus accuracy for different clinical situations

3. Contribute to the understanding of the different roles in modern TPS of dose engines versus fluence engines

Physical processes in MV photon beams

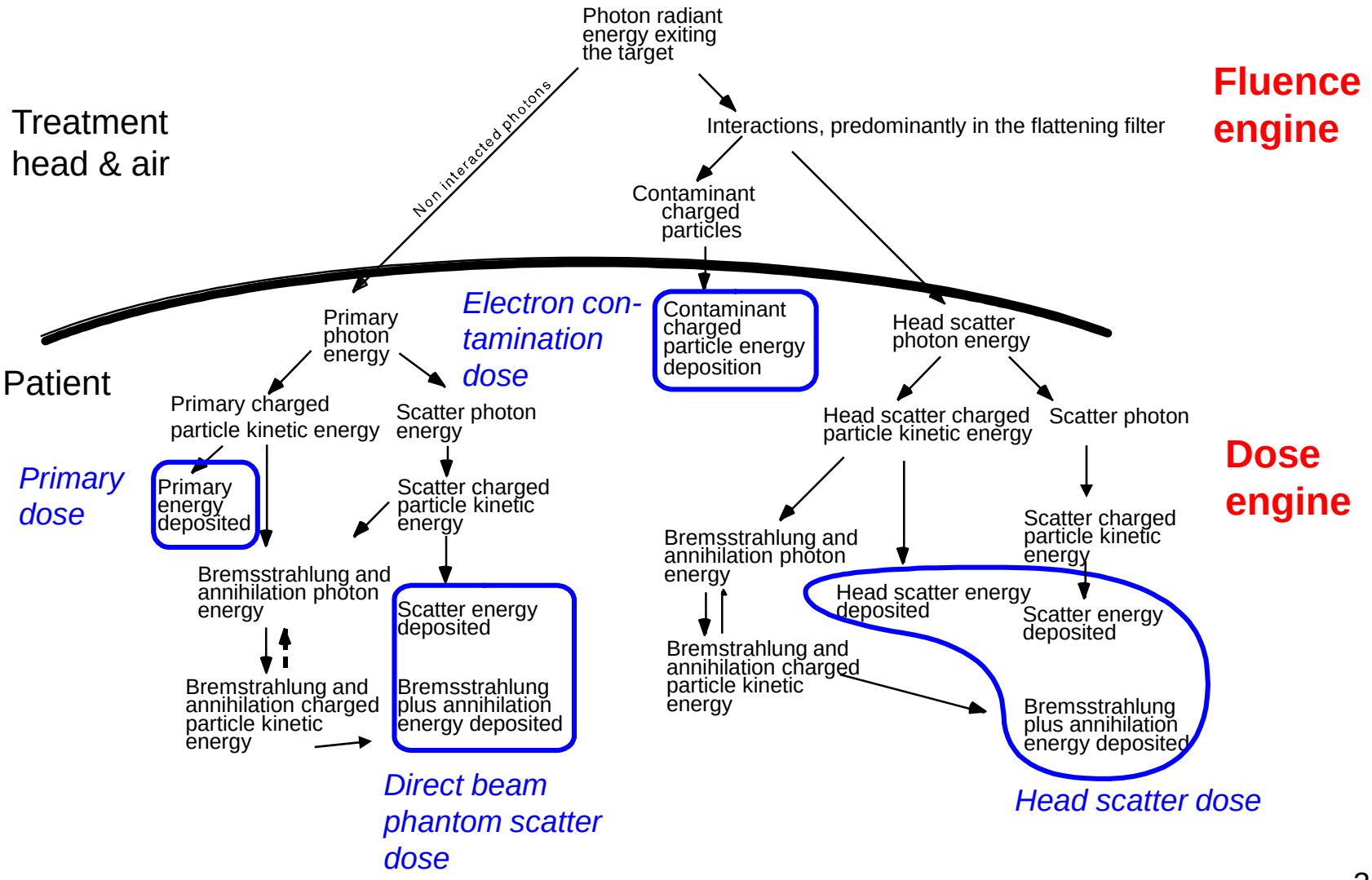

Ahnesjö and Aspradakis, PMB 44 (1999), R99-155

Dose deposition physics:

- Dose is deposited through electrons set in motion by the photon interactions
- Mean free path between electron interaction sites is nanometers (biomolecule size) - but the complete electron path length can be up to 10 cm in lung, less in other tissues
- For fields smaller than the actual electron range, the dose varies strongly with local density variations and field size
- For fields larger than the actual electron range, the dose varies less and is simpler to calculate

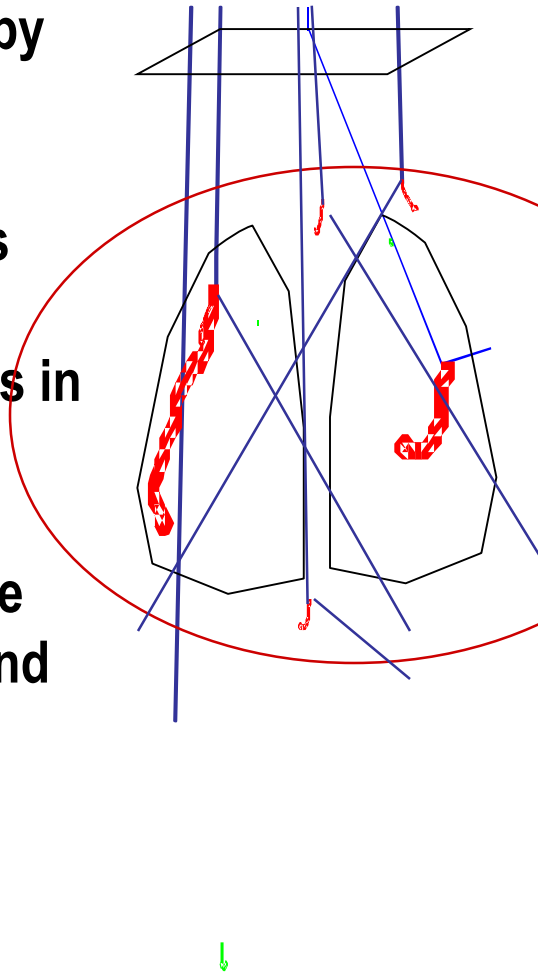

Photon dose calculation methods
Dose engines

”Model based”

“Factor based”

	Method characteristics	*Remarks*
Monte Carlo	Explicit particle transport simulation + Accurate - Noisy dose distributions	Standard research tool, clinical use under development
Analytic solvers	Solves numerically transport equtations + Accurate - Discretization effects	Standard tool in nuclear engineering, less common in medical physics
Point kernel methods ***“Convolution/superposition”*** ***“Collapsed Cone”***	Implicit particle transport + Accurate - Minor systematic errors	Current workhorse for accurate calculations in lung.
Pencil kernel methods	Heterogeneity impact through corrections	The workhorse for many applications, in particular IMRT optimization.
Scatter dose estimations	”Semi” pencil kernel metods	Often used for factorbased calculation schemes
1D heterogeneity corrections	Models what happen along the incident beam direction only	Can be used to correct dose calculated with any method for a homogeneous case

Hybrids possible

”Convolution/superposition”

Point kernel methods

”Collapsed Cone”

Primary Photon beam energy balance

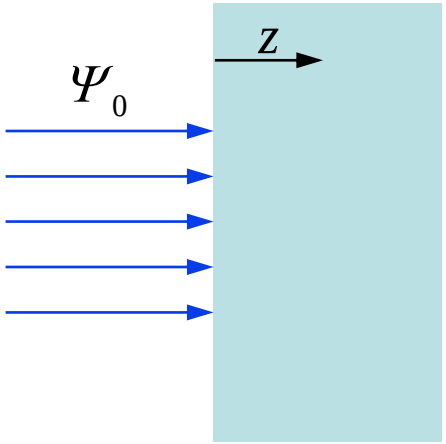

$\Psi_0 = E \cdot \Phi_0$ Incident energy fluence

$\Psi_0 \, e^{-\mu z}$ Attenuated energy fluence at depth *z*

$\frac{\mu}{\rho} \Psi_0 \, e^{-\mu z}$ Energy ”taken away” from the direct beam, TERMA, at depth *z*

$\frac{\mu_{en}}{\rho} \Psi_0 \, e^{-\mu z}$ Energy transfered into collision KERMA at *z*, it is appr. **Primary Dose**

$\frac{\mu - \mu_{en}}{\rho} \Psi_0 \, e^{-\mu z}$ Energy transfered into photon scatter, SCERMA, at depth *z*

TERMA, Total Energy Released per MAss
KERMA, Kinetic Energy Released per MAss
SCERMA, photon Scatter Energy Released per MAss
Collision KERMA+SCERMA=TERMA

Point Kernel methods:

- **Analytical solution of primary particle transport in the phantom**
- **Use pre-calculated point kernels from Monte Carlo to describe the dose deposition around a primary photon interaction site**
- **Calculate dose by superposition of all contributions**
- **Fast superposition methods by use of the Collapsed Cone approximation (any media) or Fast Fourier Transforms (homogeneous media only).**

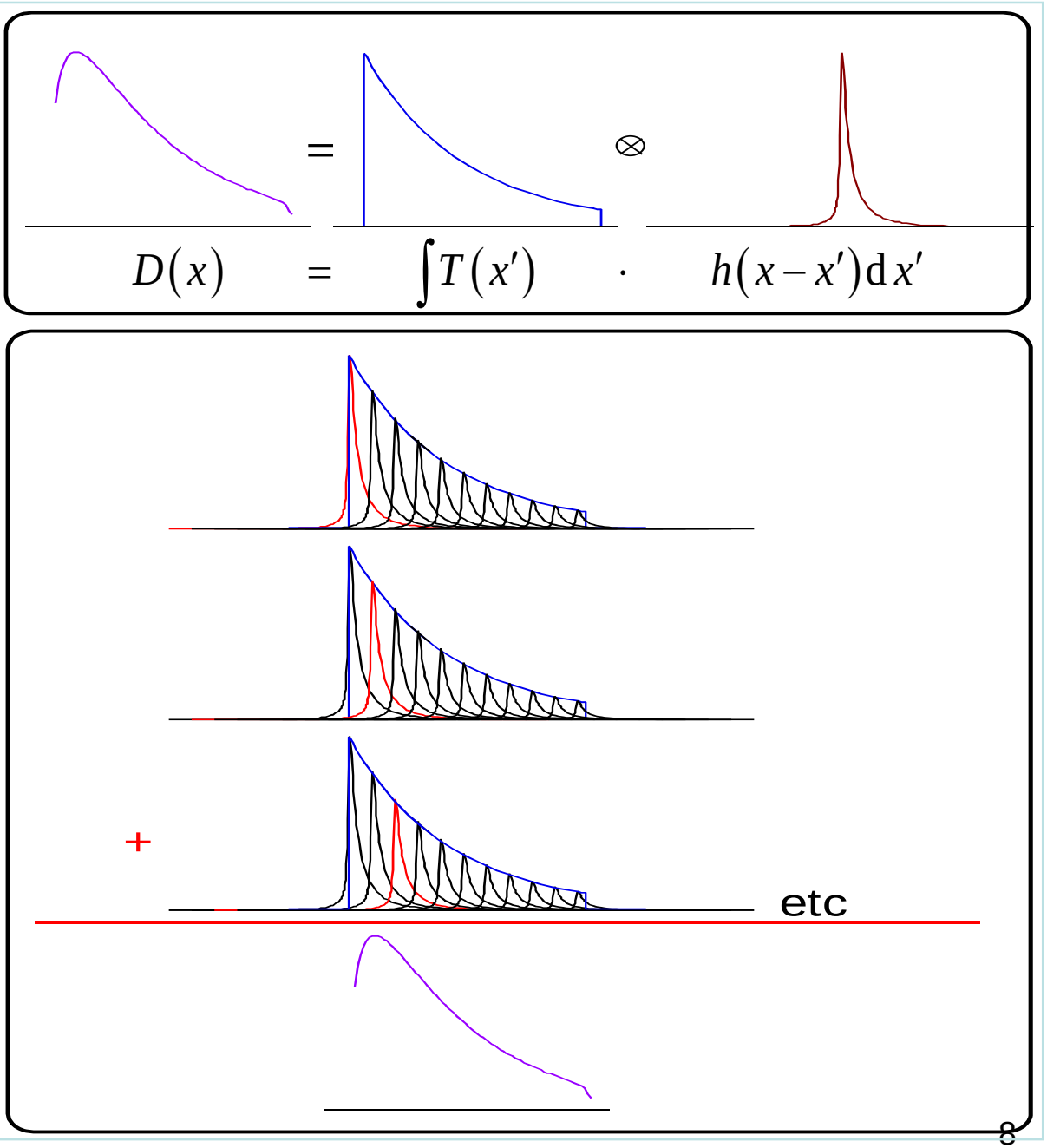

Point Kernel methods consist of two steps:

1. Trace the primary beam through the patient and calculate **how much, and where, the beam have "lost" energy** in the patient

2. **Redistribute ("blur")** that energy into patient absorbed dose **by means of point kernels** that describes the transport and energy absorption of the secondary particles set into motion via primary photon interactions

Tracing the primary beam to release energy (for later transport by point kernels)

Energy fluence

$$\Psi_E(\mathbf{r}) = \underbrace{\Psi_E(\mathbf{r}_0)}_{\text{Incident modulated and collimated energy fluence}} \underbrace{\left(\frac{\mathbf{r}_0}{\mathbf{r}}\right)^2}_{\text{Inverse square}} \mathrm{e}^{\overbrace{-\int_{l_{\mathbf{r}_0}}^{l_{\mathbf{r}}} \mu(l)\,\mathrm{d}l}^{\text{Raytrace integral through CT-matrix}}}$$

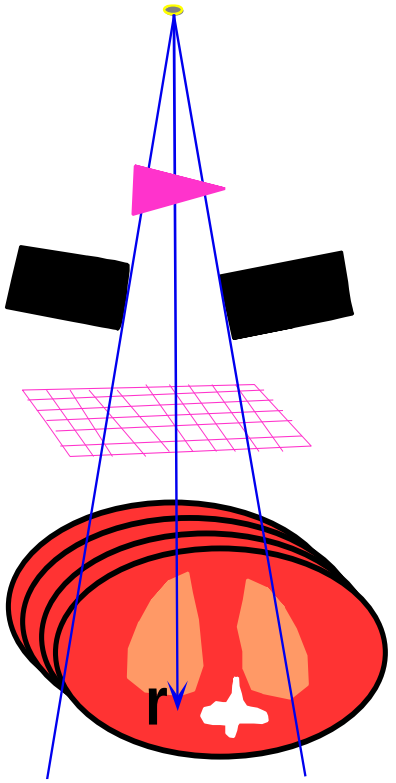

Collision KERMA (*the released energy to become primary dose*)

$$P(\mathbf{r}) = \int_E \frac{\mu_{\text{en}}}{\rho}(E,\mathbf{r})\,\Psi_E(\mathbf{r})\,\mathrm{d}E$$

SCERMA (*the released energy to become scatter dose*)

$$S(\mathbf{r}) = \int_E \frac{\mu-\mu_{\text{en}}}{\rho}(E,\mathbf{r})\,\Psi_E(\mathbf{r})\,\mathrm{d}E$$

TERMA=collision KERMA+SCERMA

The result for each ray is weigthed by the value of the energy fluence bixel it passes!

Handling the beam spectrum – depth changes

Instead of integrating over energy, the collision kerma and scerma distributions can be calculated directly by raytracing with parameterized exponentials. Effect of spectral changing with depth, i.e. ***depth hardening*** is described by means of the hardening coefficients κ_P and κ_S

e.g. Pinnacle, Raystation

$$\frac{P(z)}{\Psi_0} = \sum_{i=1}^{n} \frac{\Psi_{E_i}}{\Psi_0} \mu_{\text{en}}(E_i) e^{-\mu(E_i) z}$$

$$\frac{S(z)}{\Psi_0} = \sum_{i=1}^{n} \frac{\Psi_{E_i}}{\Psi_0} \left(\mu(E_i) - \mu_{\text{en}}(E_i)\right) e^{-\mu(E_i) z}$$

e.g. Oncentra

$$\overset{\text{parameterization}}{=} \frac{P_0}{\Psi_0} e^{-\mu_P (1-\kappa_P \cdot z) z}$$

$$\overset{\text{parametrization}}{=} \frac{S_0}{\Psi_0} e^{-\mu_S (1-\kappa_S \cdot z) z}$$

parameters

$$\frac{P_0}{\Psi_0}, \mu_P, \kappa_P$$

$$\frac{S_0}{\Psi_0}, \mu_S, \kappa_S$$

The parameters derived using a (depth dose effective) spectrum. Only μ_P and κ_P are directly measurable quantities.

Heterogeneities considered by using different sets of parameters for each tissue type, mapped by using lookup tables from the Hounsfield numbers!

Handling the beam spectrum – offaxis changes

Effect of spectral changing with lateral position can be modelled by lateral variation of the energy release parameters. The offaxis variation of μ_P is experimentally accessible, variation of the other raytracing parameters can be correlated to μ_P, see MedPhys, Vol32, pp1722-37.

$$\left(\frac{HVL(0)}{HVL(\delta)} = \frac{\mu_P(\delta)}{\mu_P(0)}\right):$$

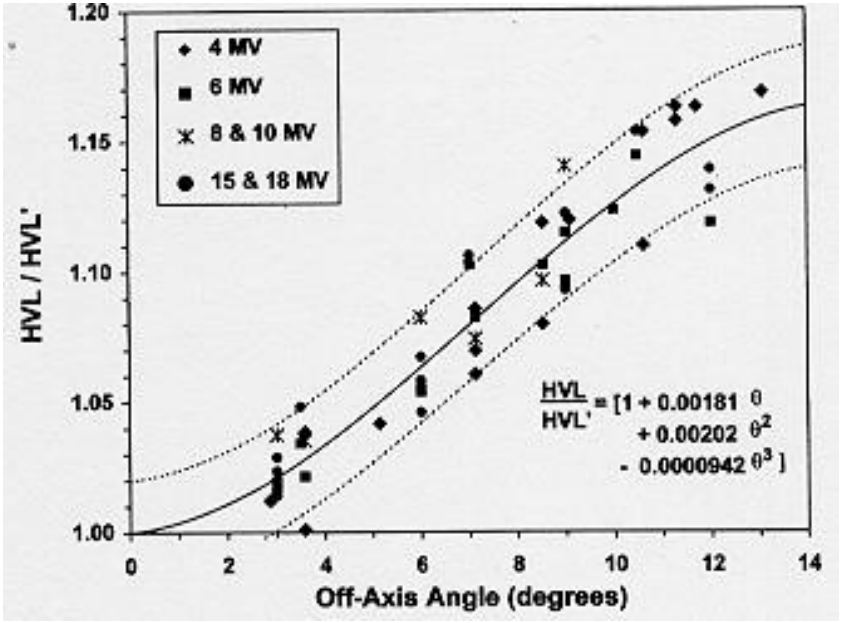

Tailor, R.C., *et al.* Medical Physics, 1998. **25**(5): p. 662-667

Heterogeneities considered by using different sets of parameters for each tissue type, mapped by using tissue lookup tables from the Hounsfield numbers!

Tissue and Phantom Material Characterization

-as used in Oncentra MP-

Composition	$\frac{\rho_{mass}}{\rho_{mass,H_2O}}$	$\frac{\rho_{elec}}{\rho_{elec,H_2O}}$	HN
Air (outside patient)	0.00121	0.00109	-992
Air (inside patient)	0.00121	0.00109	-976
Lung (ICRU 44)	0.50	0.50	-480
Adipose (ICRU 44)	0.95	0.95	-96
Muscle (ICRU 44)	1.05	1.04	48
Cartilage (ICRP 23)	1.10	1.08	128
2/3 Cartilage, 1/3 Bone	1.35	1.29	528
1/3 Cartilage, 2/3 Bone	1.60	1.52	976
Bone (ICRP 23)	1.85	1.72	1488
Bone (ICRP 23)	2.10	1.95	1824
½ Bone, ½ Aluminum	2.40	2.15	2224
Aluminum	2.70	2.34	2640
Aluminum	2.83	2.46	2832
Iron	7.87	6.60	>2832
Water	1.00	1.00	-

Note: *Water is not part of an anatomical scale!*

The scale will interpret a water CT-image as a mixture of adipose and muscle!

Tissue and Phantom Material interpolation

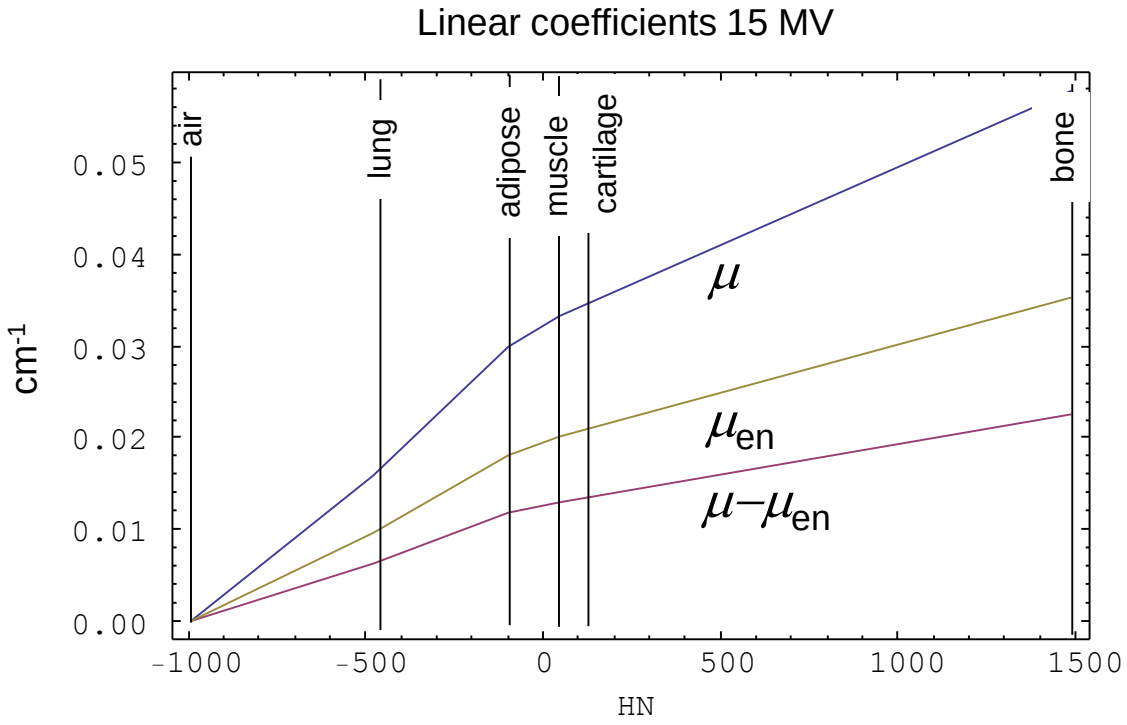

Dose Properties of Point Kernels

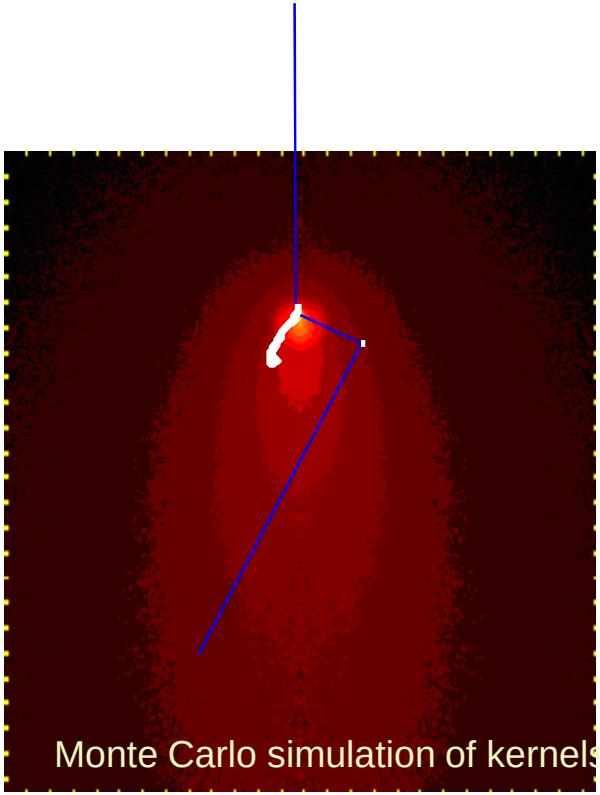

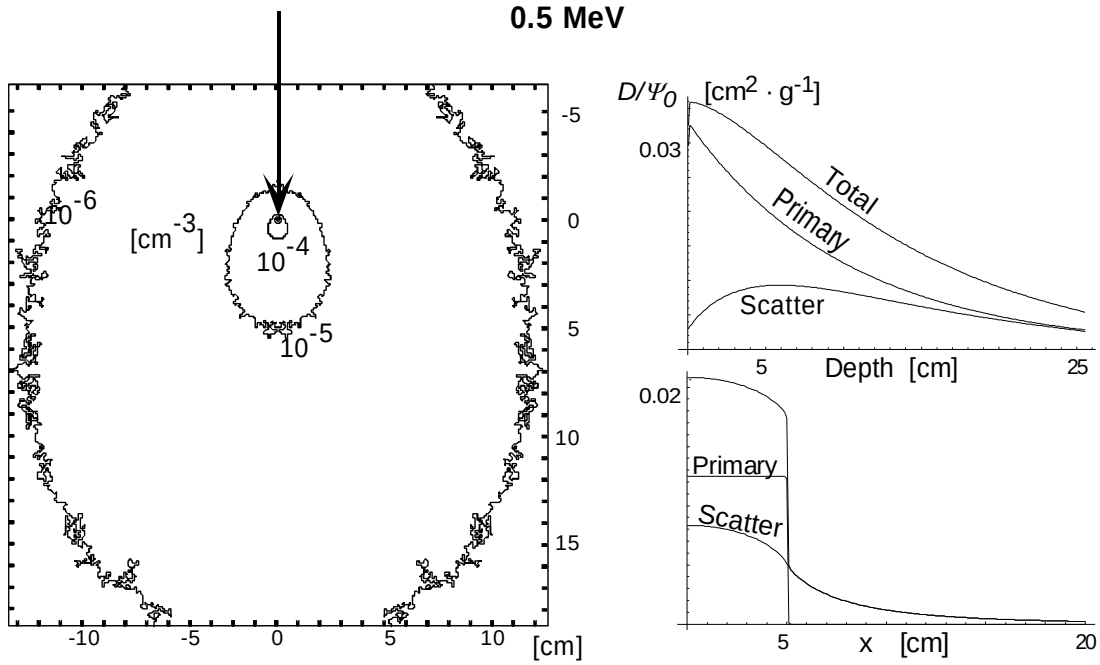

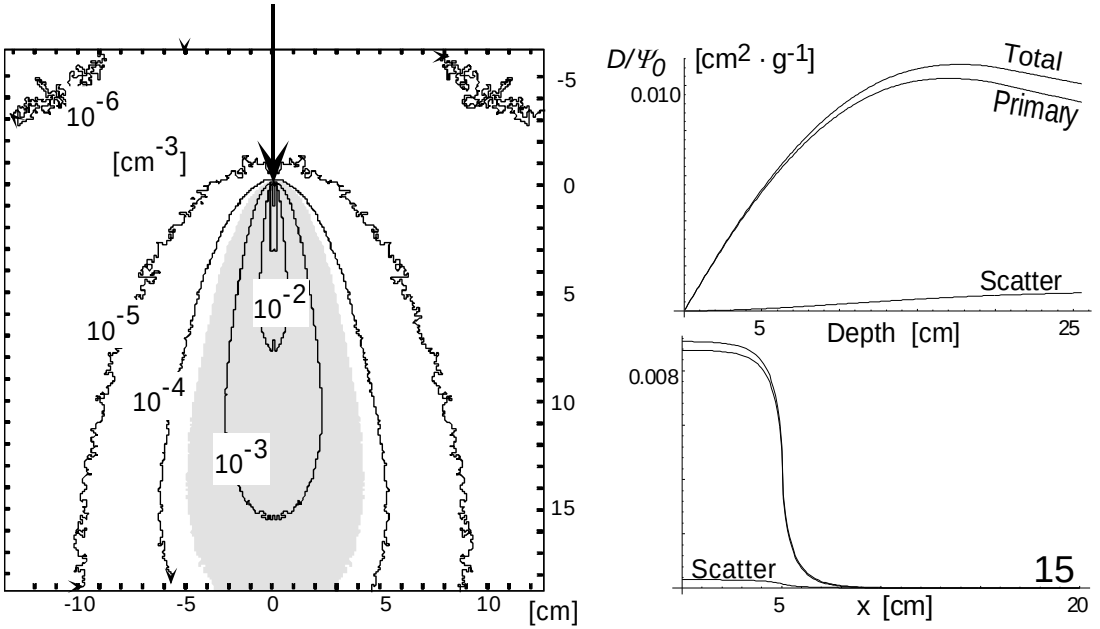

Dose properties for point kernels cont.:

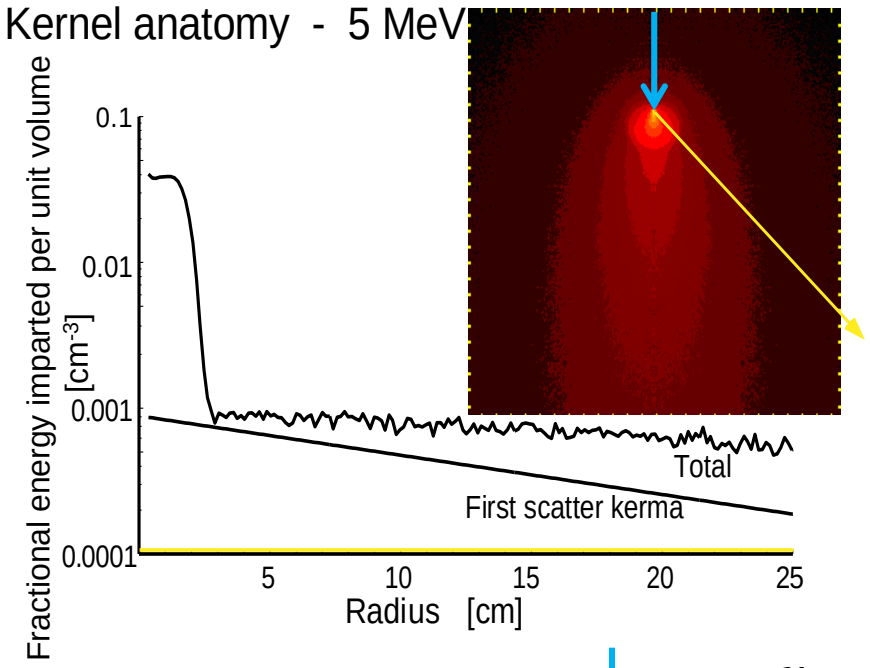

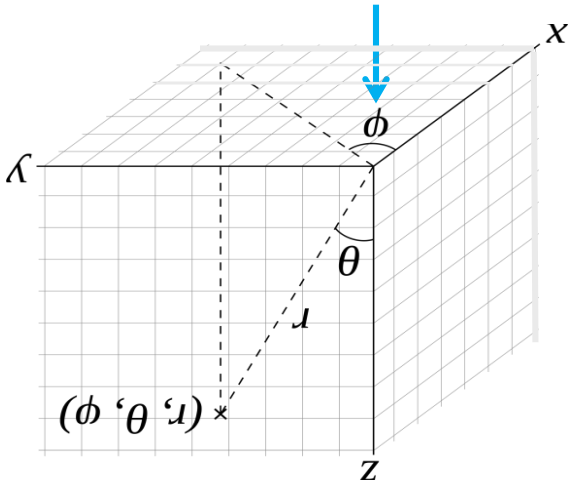

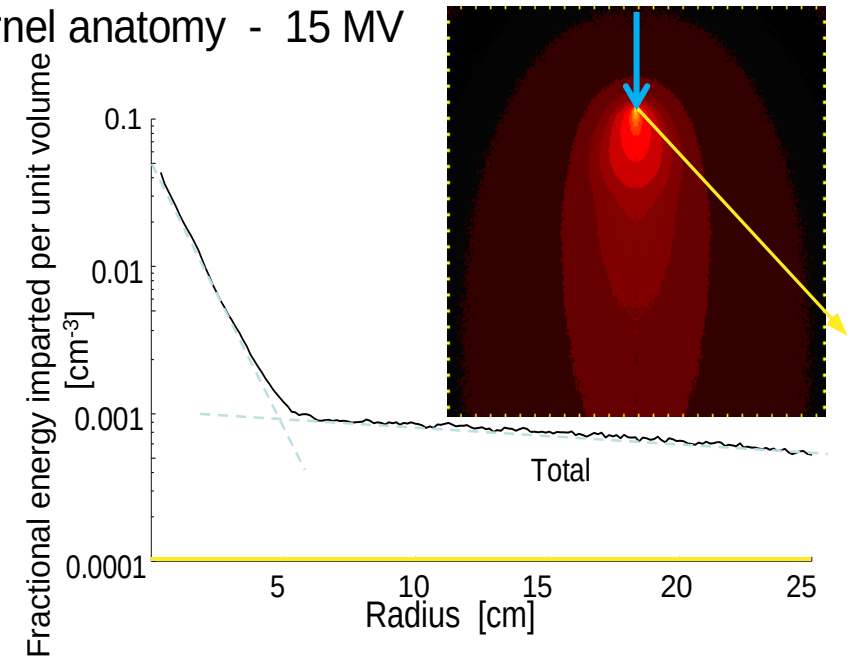

Suitable parameterization of polyenergetic point kernels

$$h(r,\theta) = \frac{A_\theta \, \mathrm{e}^{-a_\theta r} + B_\theta \, \mathrm{e}^{-b_\theta r}}{r^2}$$

Ahnesjö, *A. Med. Phys.* **16** 577–92

Discretizing the angular part of the point kernels: the collapsed cone approximation for superposition of point kernels

Discretization:

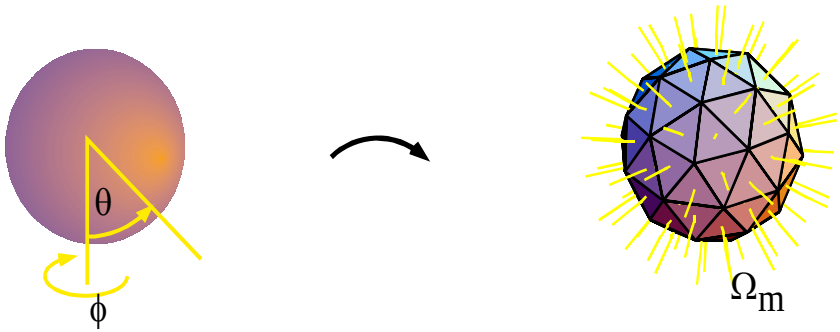

Consequence – displacement of energy deposition location that increase with distance from interaction point

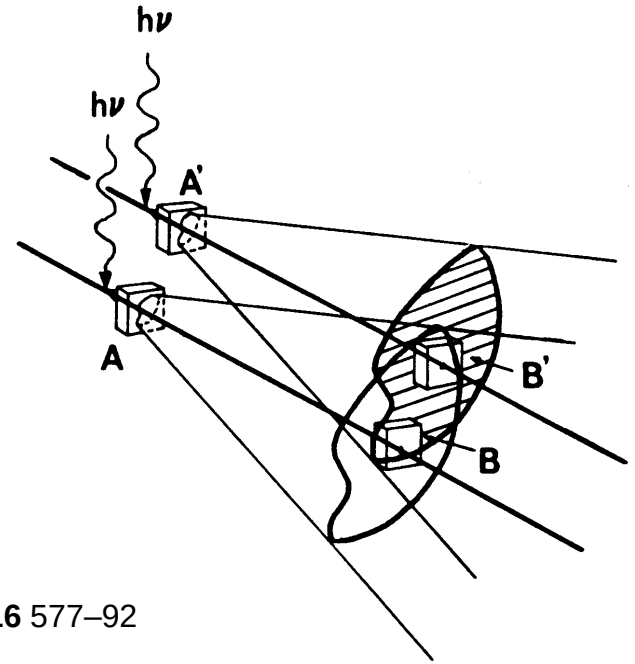

Ahnesjö, *A. Med. Phys.* **16** 577–92

Discretization and parameterization:

Most energy is transported in the forward direction, hence it make sense to have smaller bins in the forward direction.

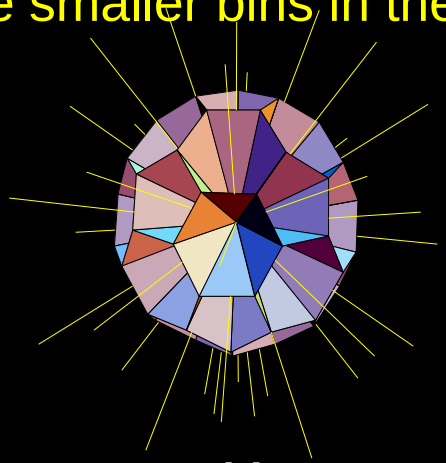

36 bins

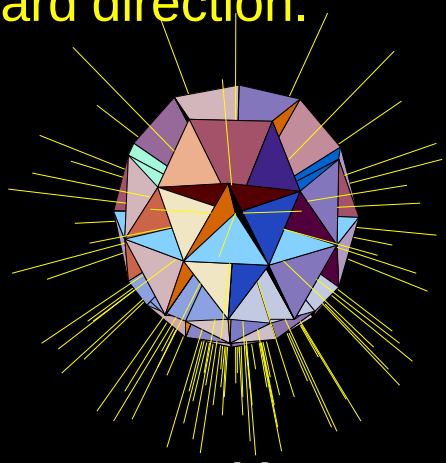

106 bins
(default in Oncentra, Monaco)

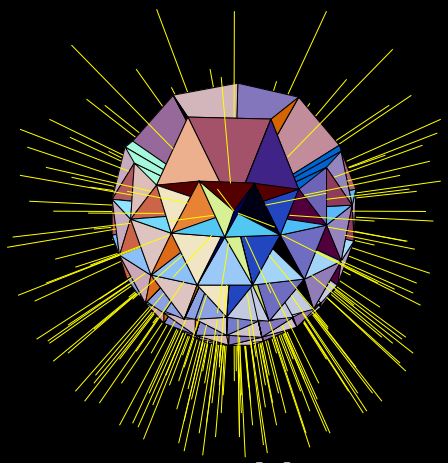

201 bins

Discretization into angular bins causes $1/r^2$ dependence in parameterization to vanish

$$h_m(r,\theta) = \iint_{\theta,\phi\in\Omega_m} \frac{A_\theta\, \mathrm{e}^{-a_\theta r} + B_\theta\, \mathrm{e}^{-b_\theta r}}{r^2} \cdot r^2 \sin\theta\, \mathrm{d}\theta\, \mathrm{d}\phi =$$

$$= \Omega_m \left(A_{\Omega_m}\, \mathrm{e}^{-a_{\Omega_m} r} + B_{\Omega_m}\, \mathrm{e}^{-b_{\Omega_m} r} \right)$$

Collapsed Cone transport scheme

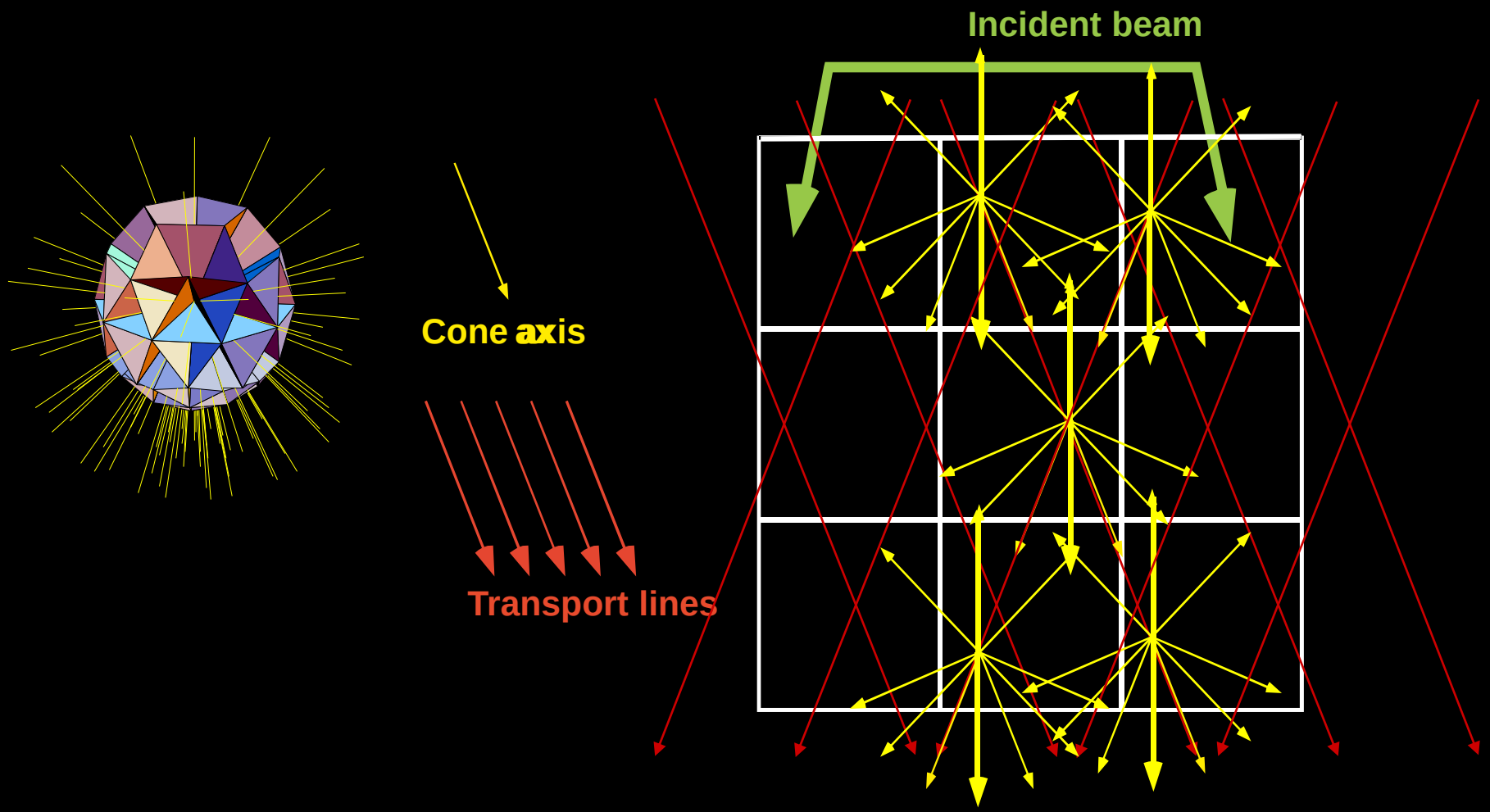

Radiant energy transport along a transport line

Analytical raytrace of kernel exponential through a voxel constitutes a transport step of the radiant energy:

$$R_{\text{out}}(\ell) = R_{\text{in}} \cdot \mathrm{e}^{-a\ell} + \frac{k}{a^2}\left(1 - \mathrm{e}^{-a\ell}\right)$$

attenuation of incoming energy

radiant energy contribution from the voxel considering intravoxel attenuation

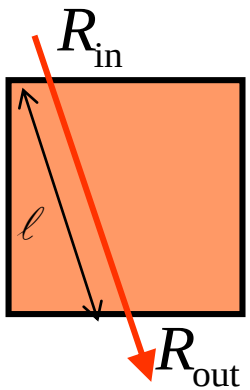

Energy deposited inside the voxel (appr. $a \cdot R$) becomes *the deposited dose*

- Parameter a from kernel parameterization and is scaled to represent the voxel medium, k stems from incident beam energy release (coll KERMA and SCERMA) and medium
- Performed separately for primary and scatter dose

More about transport along a line…

Factorization of attenuation:

$$L = \sum_i \ell_i$$

$$\mathrm{e}^{-aL} = \mathrm{e}^{-a\sum_i \ell_i} = \mathrm{e}^{-a\ell_1}\,\mathrm{e}^{-a\ell_2}\,\mathrm{e}^{-a\ell_3}\ldots = \prod_i \mathrm{e}^{-a\ell_i}$$

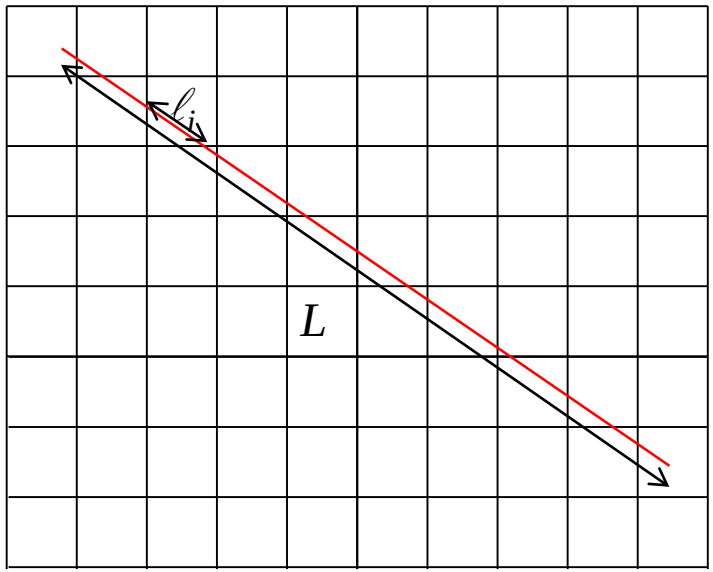

Transport of radiant energy along line:

$$R_i = R_{i-1}\,\mathrm{e}^{-a\cdot\ell_i} + \Delta R_i$$

Net energy release from a step ℓ_i ("collapsed" solid angle $\Delta\Omega$, kernel=$A\mathrm{e}^{-a\ell}$:

$$\Delta R_i = \int_0^{\ell_i} \underbrace{T_i \cdot \rho_i \cdot \Delta\Omega \cdot \frac{A}{a}}_{\text{energy release per length}} \underbrace{\mathrm{e}^{-a\cdot(\ell_i-\ell')}}_{\substack{\text{attenuation from point of release } \ell' \\ \text{to exit at } \ell_i}} \mathrm{d}\ell' = T_i \cdot \rho_i \cdot \Delta\Omega \cdot \frac{A}{a^2}\left(1-\mathrm{e}^{-a\cdot\ell_i}\right)$$

Local dose absorption:

$$D_i \approx a\,\frac{R_{i-1}+R_i}{2}$$

Kernel tilting

Consider a point kernel and a transport direction defined for one of the axes. In diverging beams, the kernel transport angle θ varies with location:

- Kernel *h(r)* = $\dfrac{A_\theta e^{-a_\theta r}}{r^2}$
- Define $\theta' = \theta + \delta$
- Approximate

$$A_{\theta'} = A_\theta + c_1\delta + c_1\delta^2$$

$$a_{\theta'} = a_\theta + d_1\delta + d_1\delta^2$$

- Parameters c_i and d_i determined from Monte Carlo data

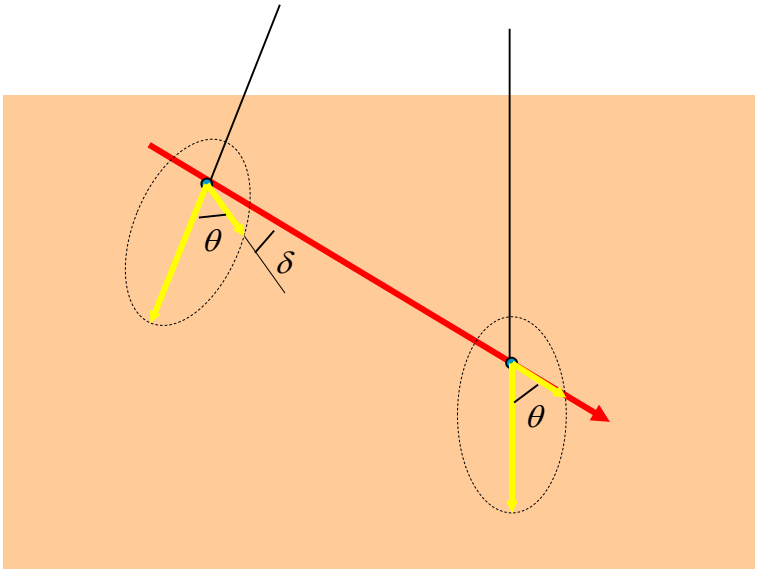

Tilting cont...

Effects increase with

- tilting angle, i.e.
  - shorter SSD
  - larger fields (and off axis segments)
- longer particle range, i.e.
  - low density regions (lung)
  - higher energies

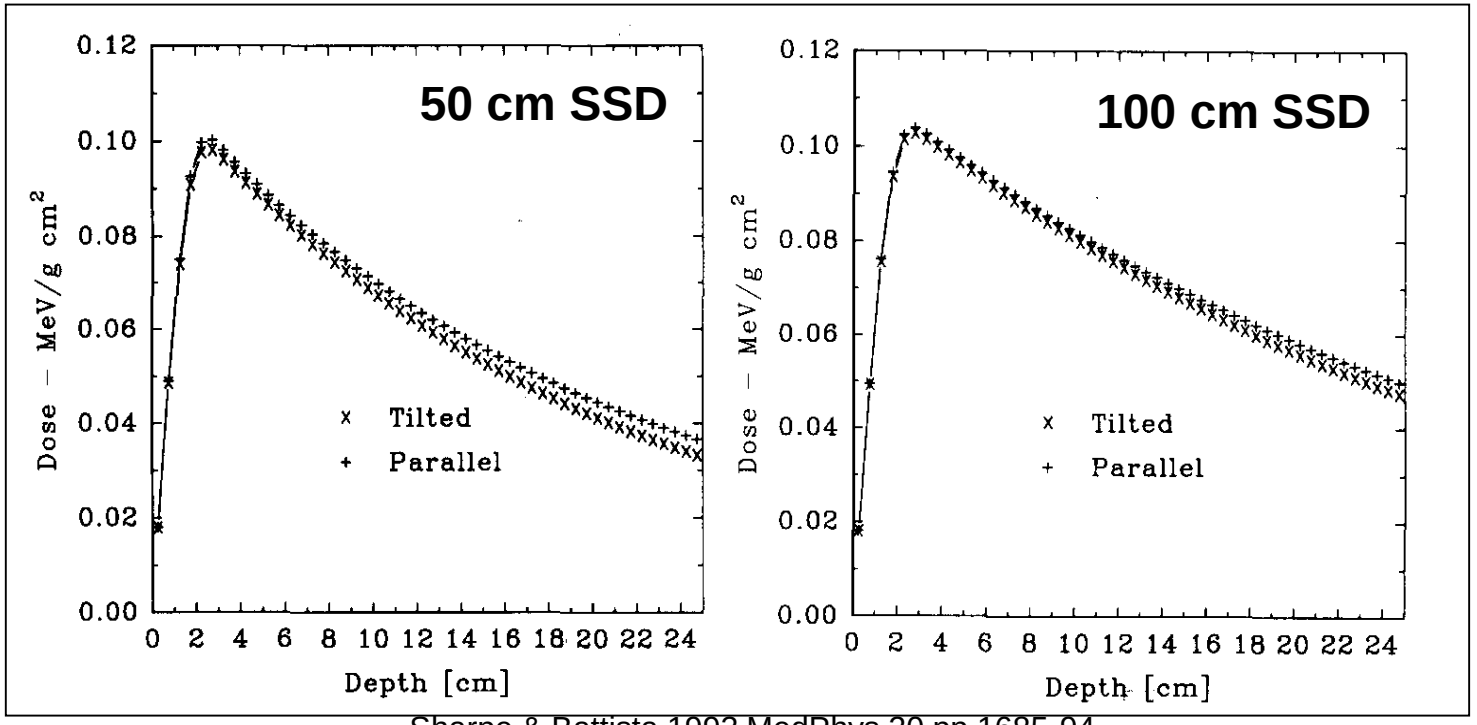

Sharpe & Battista 1993 MedPhys 20 pp 1685-94

18 MV on lung phantom

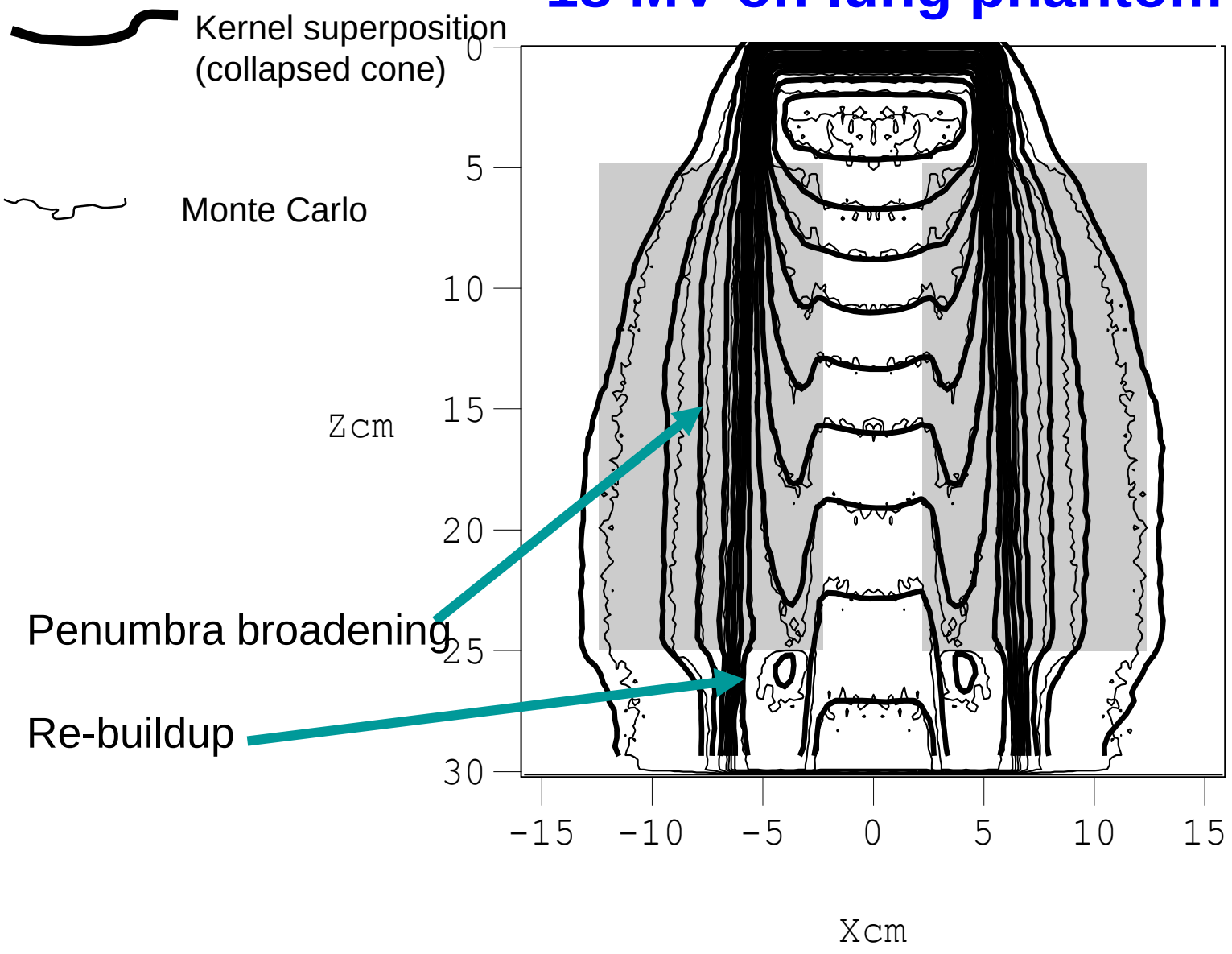

Modelling charged particle contamination

Has to be added as a separate model of the pencil kernel type:

Ahnesjö and Andreo [4]

$$\frac{p_{c_\pm}}{\rho}(r,z) = \alpha e^{-\beta z} e^{-\gamma r^2}$$

The parameters α, β, and γ can be determined through fitting to the difference between measurements and calculated photon dose.

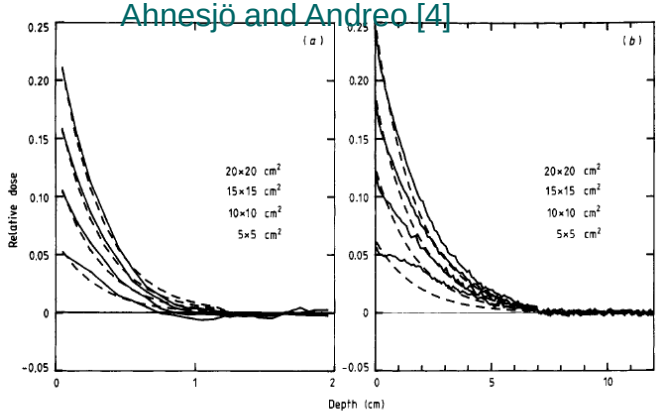

Figure 3. Contaminant dose distributions, expressed in fractions of the maximum total dose, for various field sizes of 4 MV (*a*) and 24 MV (*b*) photon beams. The dashed curves denote the simulated distributions (equation (9)) and the full curves the mean reconstructed distributions.

$$\frac{D_{c_\pm}(z,f)}{\psi} = \alpha e^{-\beta z} \int_{-f/2}^{f/2} \int_{-f/2}^{f/2} e^{-\gamma(x^2+y^2)} dx\, dy$$

$$= \alpha e^{-\beta z} \frac{\pi}{\gamma} \operatorname{erf}^2\left(\sqrt{\gamma}\frac{f}{2}\right),$$

where the error function is defined as

$$\operatorname{erf}(x) = \frac{2}{\sqrt{\pi}} \int_0^x e^{-t^2} dt.$$

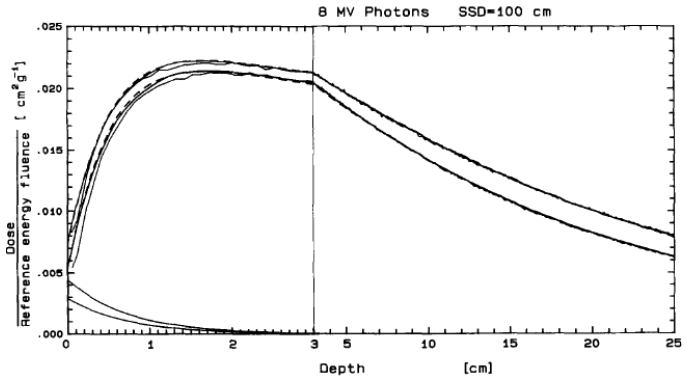

Ahnesjö *et al* Med Phys 19, 263-73

Summary of Point Kernel model properties

- Heterogeneities are considered through scaling of the rectilinear transport along all lines, hence it models:
  - loss of CPE for small fields and in lung
  - penumbra broadening in lung
  - rebuildup after low density media
- Major limitations:
  - rectilinear scaling coarse approximation for multiple scattering
  - angular discretization effects
- Use of media specific μ_{en} in primary raytrace yield dose to medium in medium (not water in medium) but is implementation dependent!
- The dose calculation time for N^3 voxels is with the Collapsed Cone approach reduced from being proportional to N^7 operations to to $M \cdot N^3$ where M is the number of transport directions
- Core calculation loops only a few hundred lines of code, much less complex than a multisource beam modelling code

What about calculation time and accuracy?

Several papers compare CC, PK, MC and measurements

Calculation times CC

(old data, so absolute timing obsolete...)

Calculation time is direct proportional to # voxels times # kernel directions:

Example: # voxels=128x128x128 (appr. $2 \cdot 10^6$), # directions=106

Configuration	**Time (s)**
Masterplan 3.0 Pentium 4 2.8 GHz	210
*Pentium 4 2.8 GHz, improved coding	114
*8 core Xeon 1.86 GHz (1 thread)	95
*8 core Xeon 1.86 GHz (8 threads)	13
*GPU GeForce 8800 GTX	2

The calculations for the parallel transport lines used in the CC approach are extremely suitable for implementation on parallel hardware!

Kloppenborg B and Loos R 2007 "Parallel collapsed cone dose calculations using a Graphics Processing Unit", Bachelor Thesis, Saxion Hogeschool (Enschede, Netherlands)

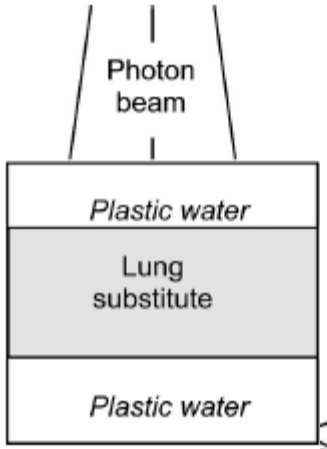

10x10 cm²

2x2 cm²

- Monte Carlo
- CC Helax-TMS
- Batho
- Batho/modified
- PB Helax-TMS
- ○ TLD
- ☆ △ ◆ IC (different kinds)

6 MV **18 MV**

Depth (cm)

PDD (%)

(a) (b) (e) (f)

Carrasco *et al* MedPhys 31 (2004) p2899

6 MV

Haedinger *et al* IJROBP 61 (2005) p239

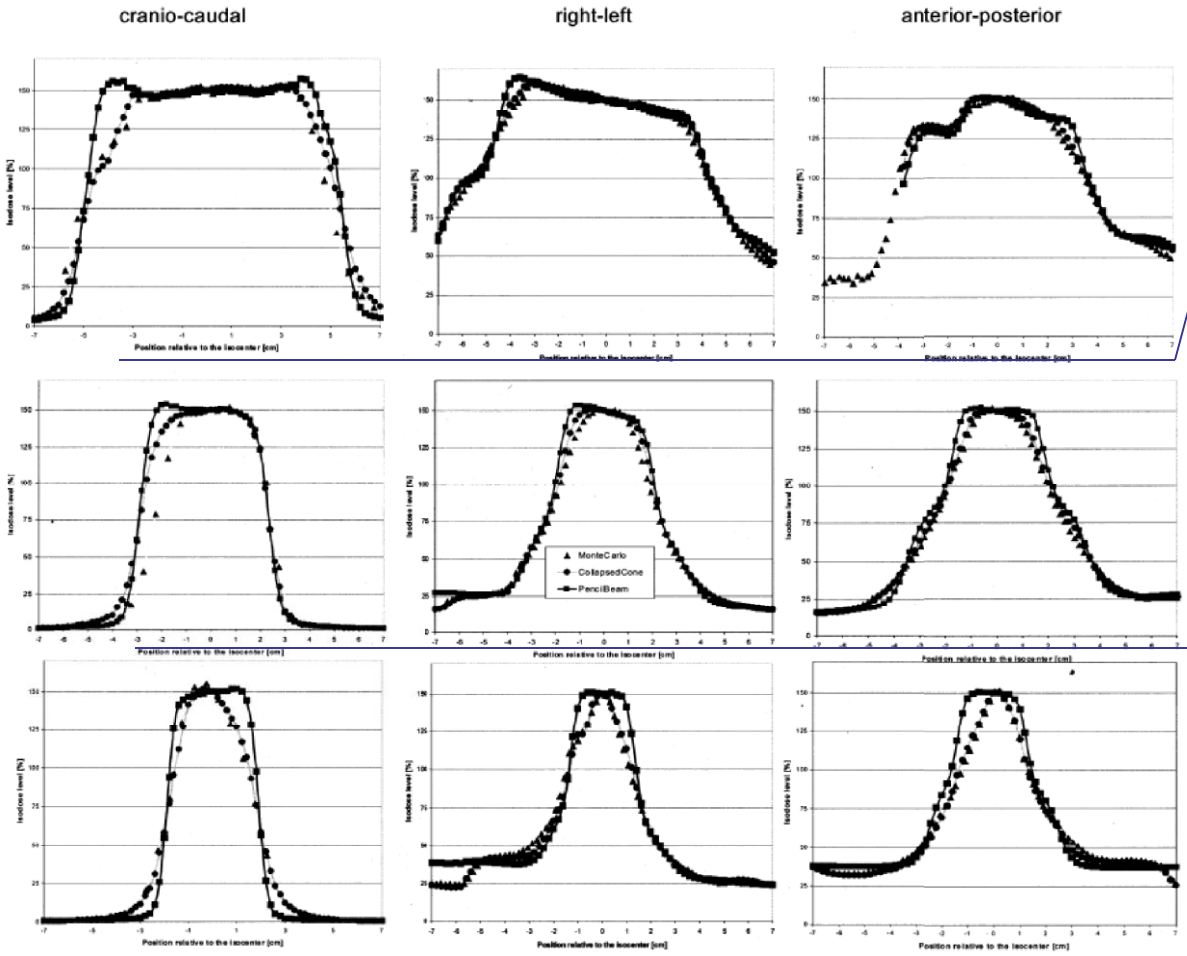

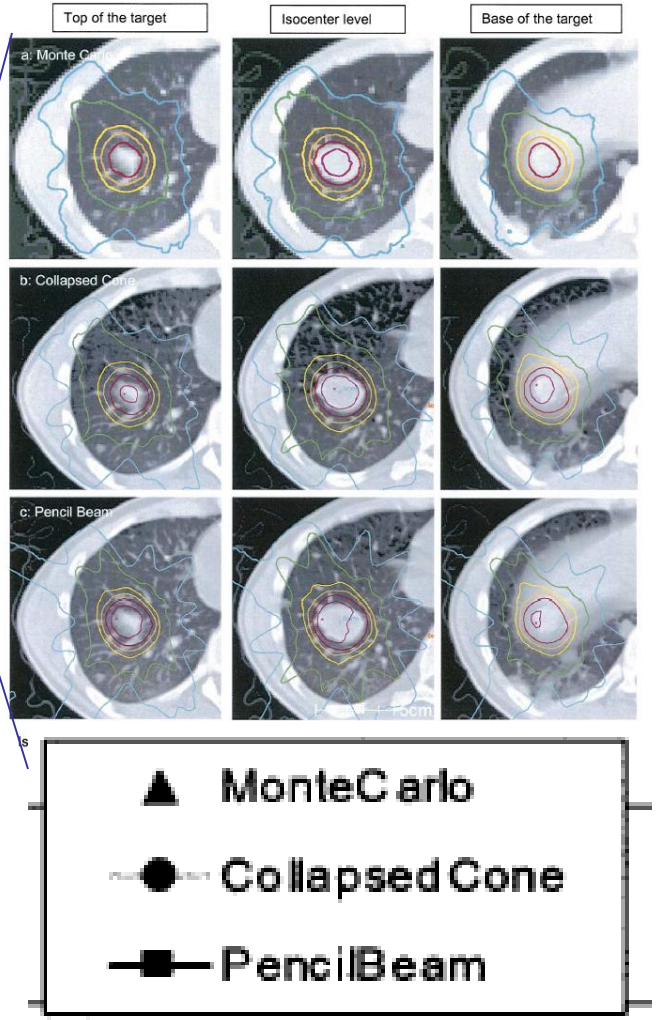

Krieger&Sauer PMB 50 (2005) p859
TMS

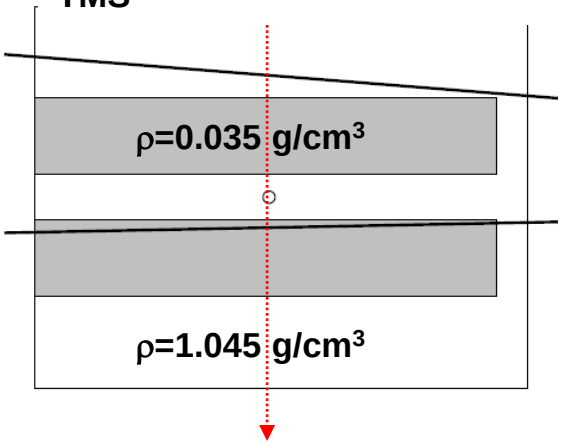

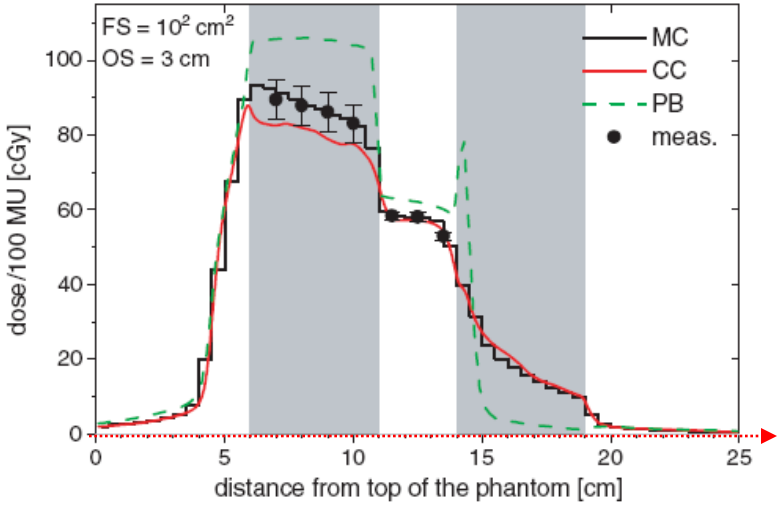

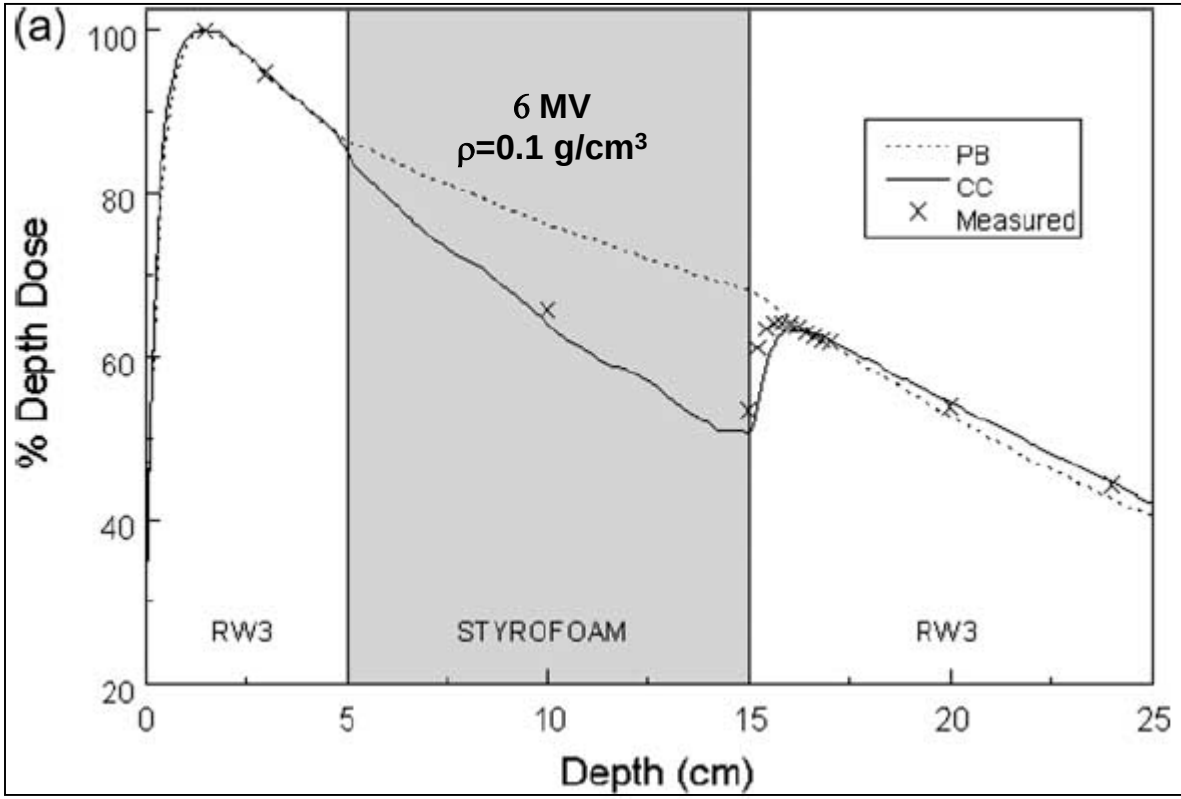

Nisbet *et al* RadOnc 73 (2004) p79
TMS

Dose rebuild-up behind a cylinder cavity

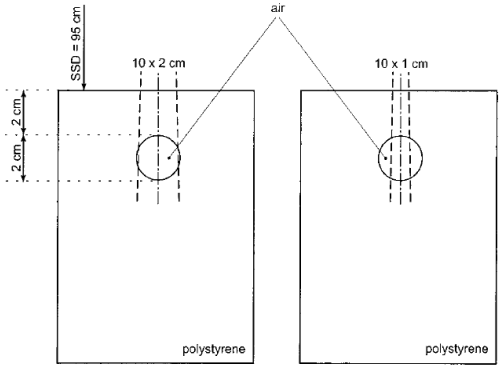

Martens *et al* MedPhys 29 (2002) p1528

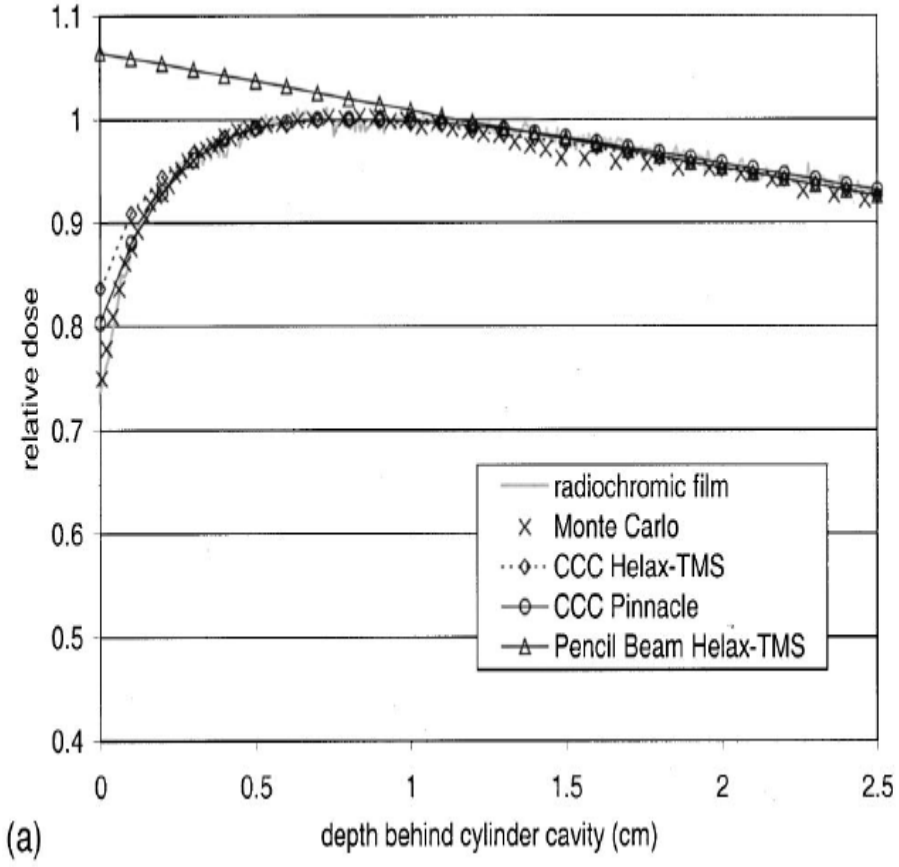

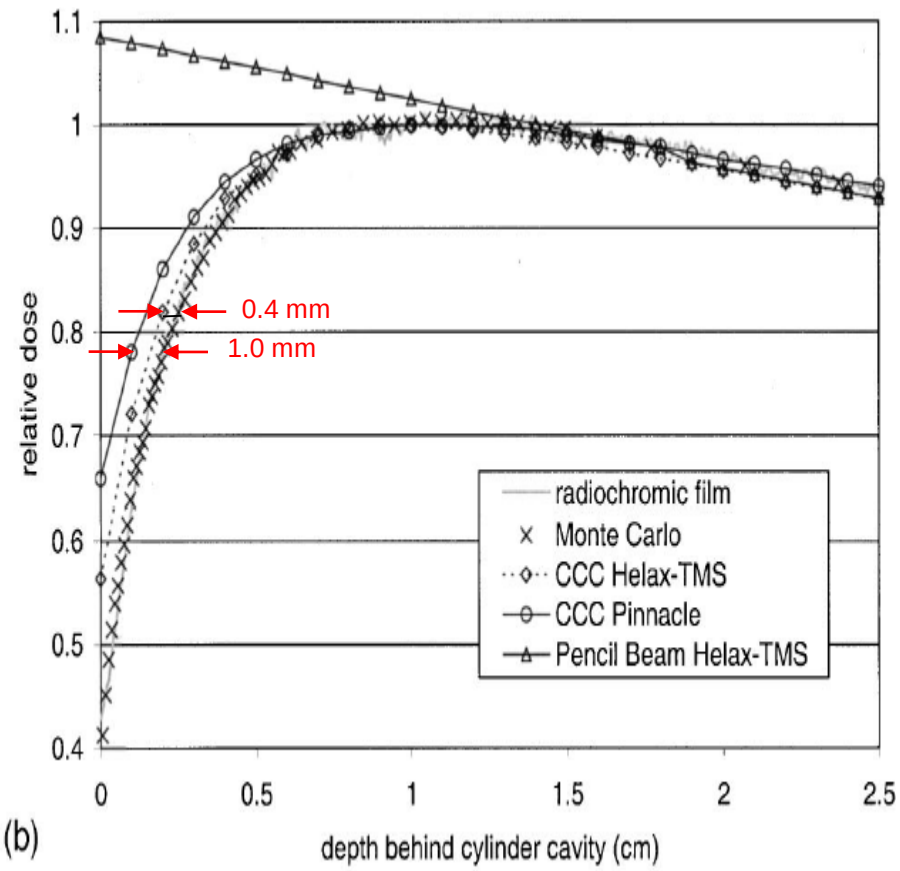

Monte Carlo simulations, PB calculations, CCC calculations and radiochromic film measurements (film strips along the beam axis) for a 10x2 cm^2 **(a)** and a 10x1 cm^2 **(b)** field.

Fogliata *et al* PMB 52 (2007) p1363-85

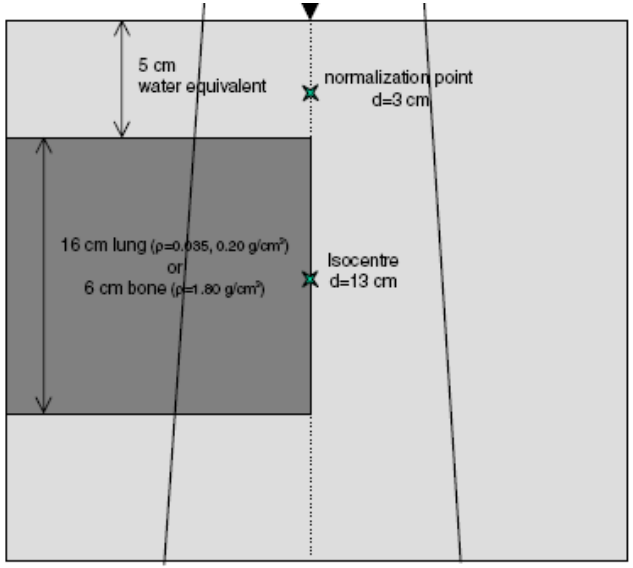

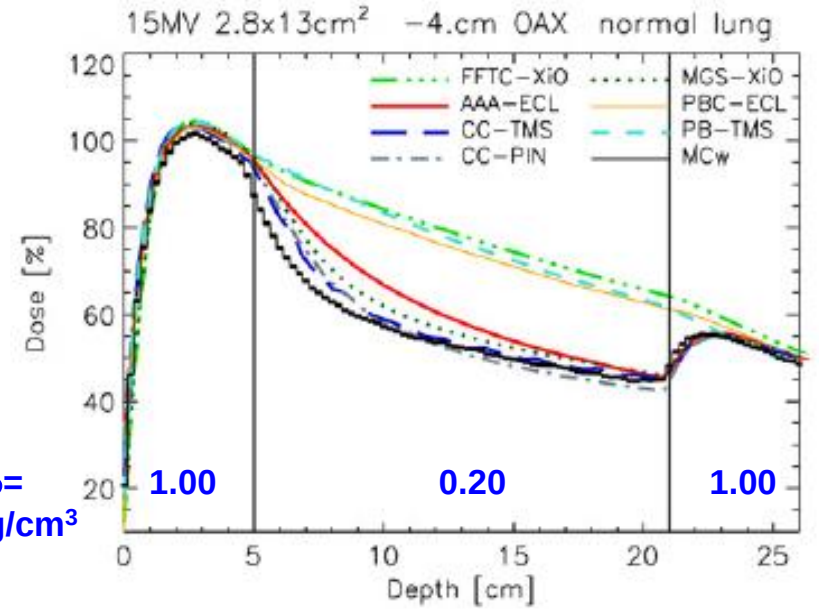

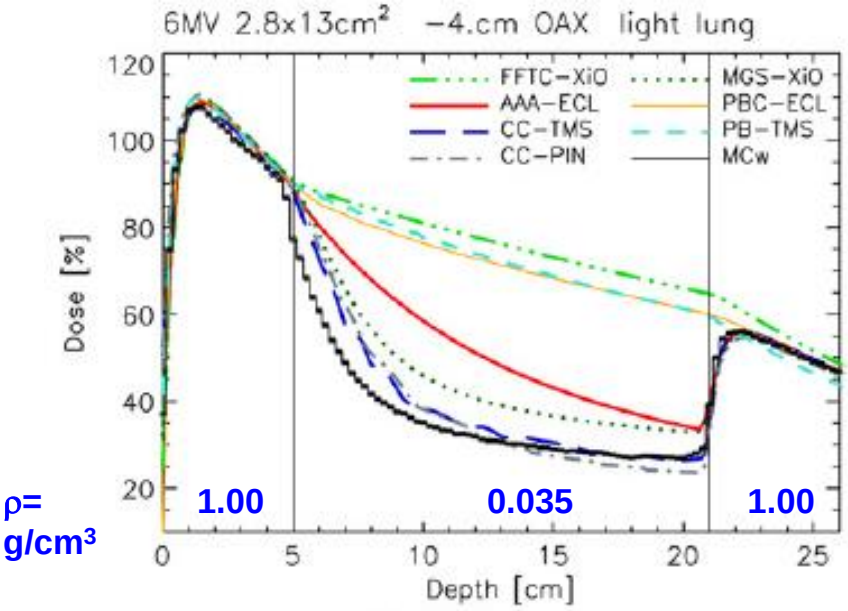

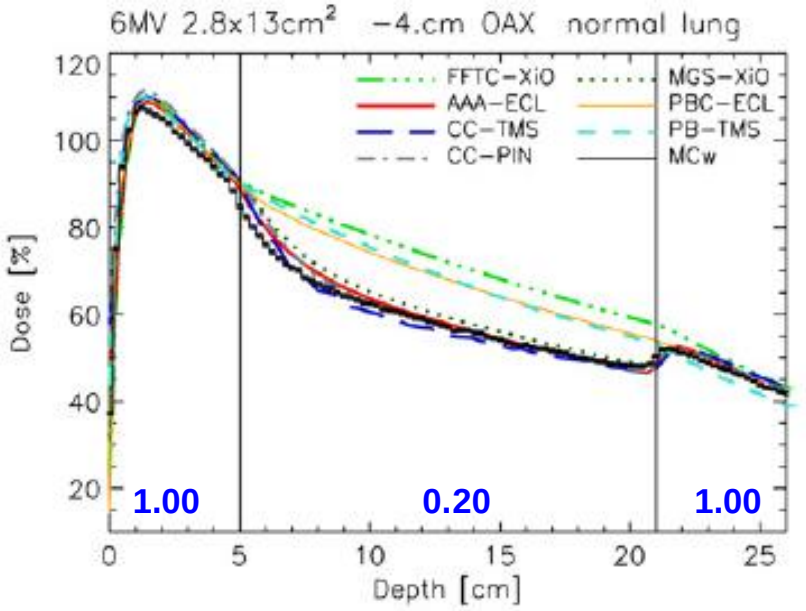

Irvine *et al* ClinOnc 16 (2004) p148

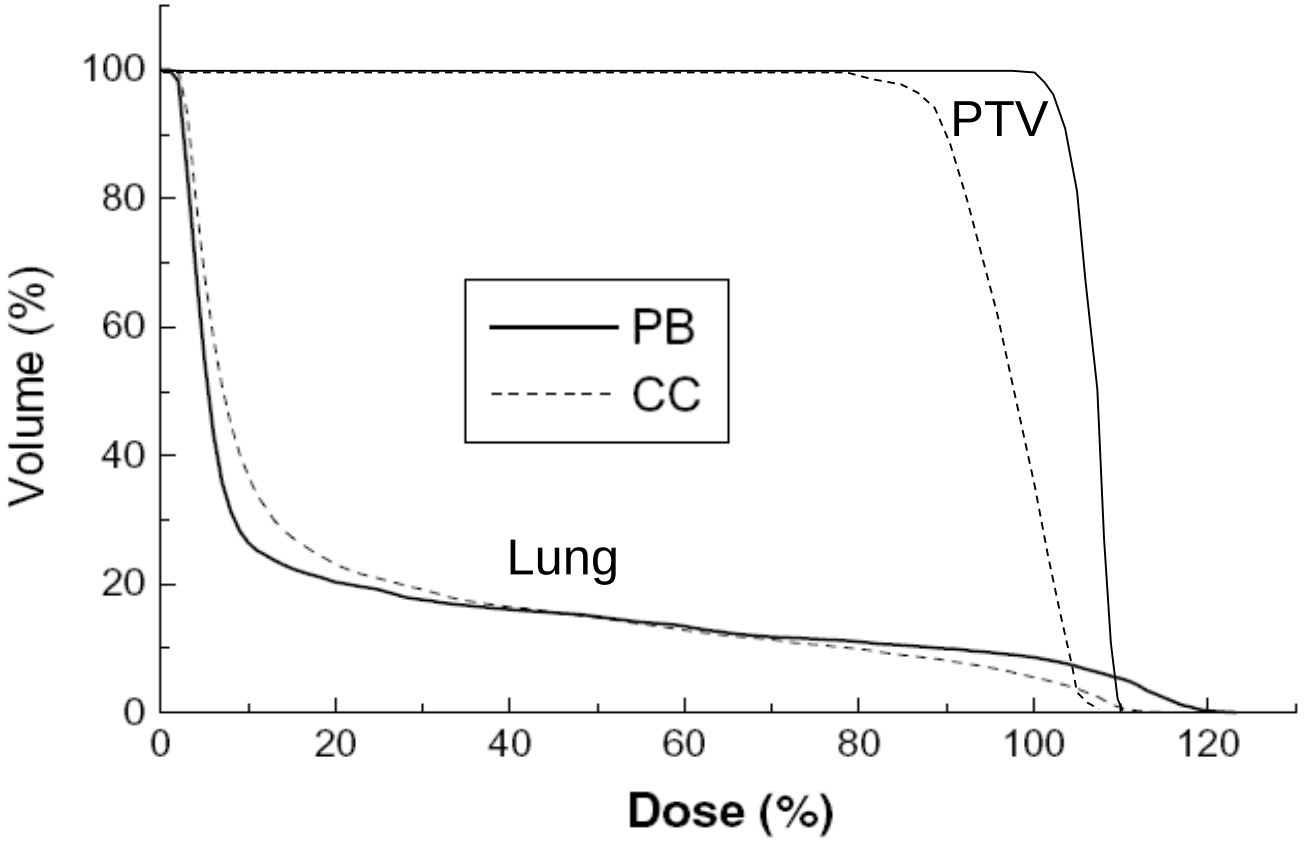

Target mean dose easy to compensate.
PTV is hard to make homogenous

Retrospective lung calculation study, Uppsala Akademiska Sjukhus

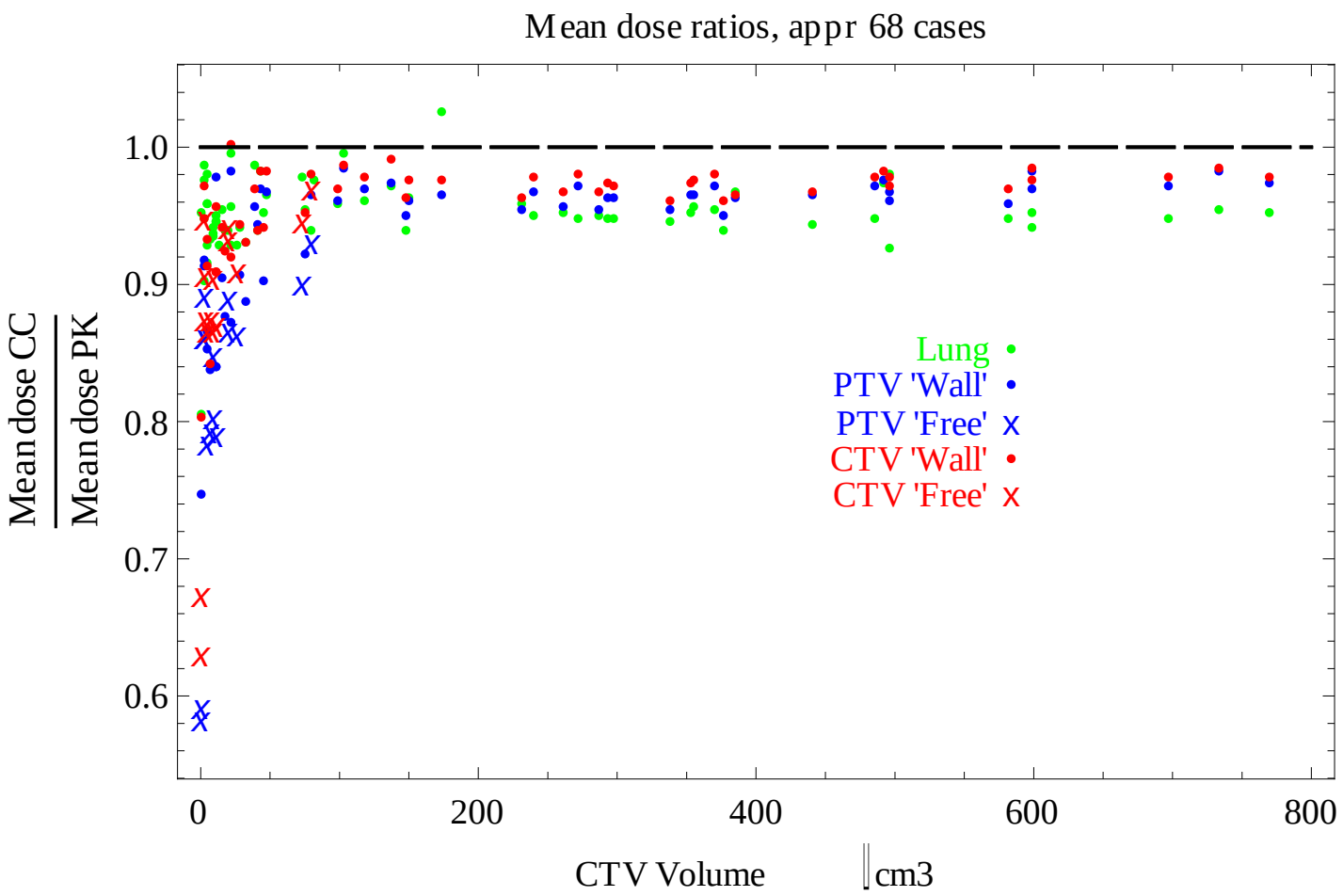

one dot – one patient

- is it the PTV or the CTV/GTV that matters for DVH optimization?

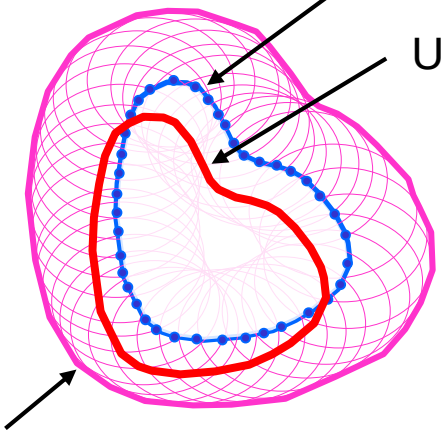

PTV formed from snapshot **CTV** using a translational margin ellipsoid to cover most possible positions of **CTV**

<u>Re-buildup dose makeup</u>: With sufficient beam margins, re-buildup will make DVH of the different CTV instances insensitive of where it is in a homogeneous PTV ”fluence bath” (of heterogeneous dose), cf ”flash” margins for tangential breast!

Simulation results of using multiple instances (~4000) of the same patient with ”moving target” for a 3-fraction treatment

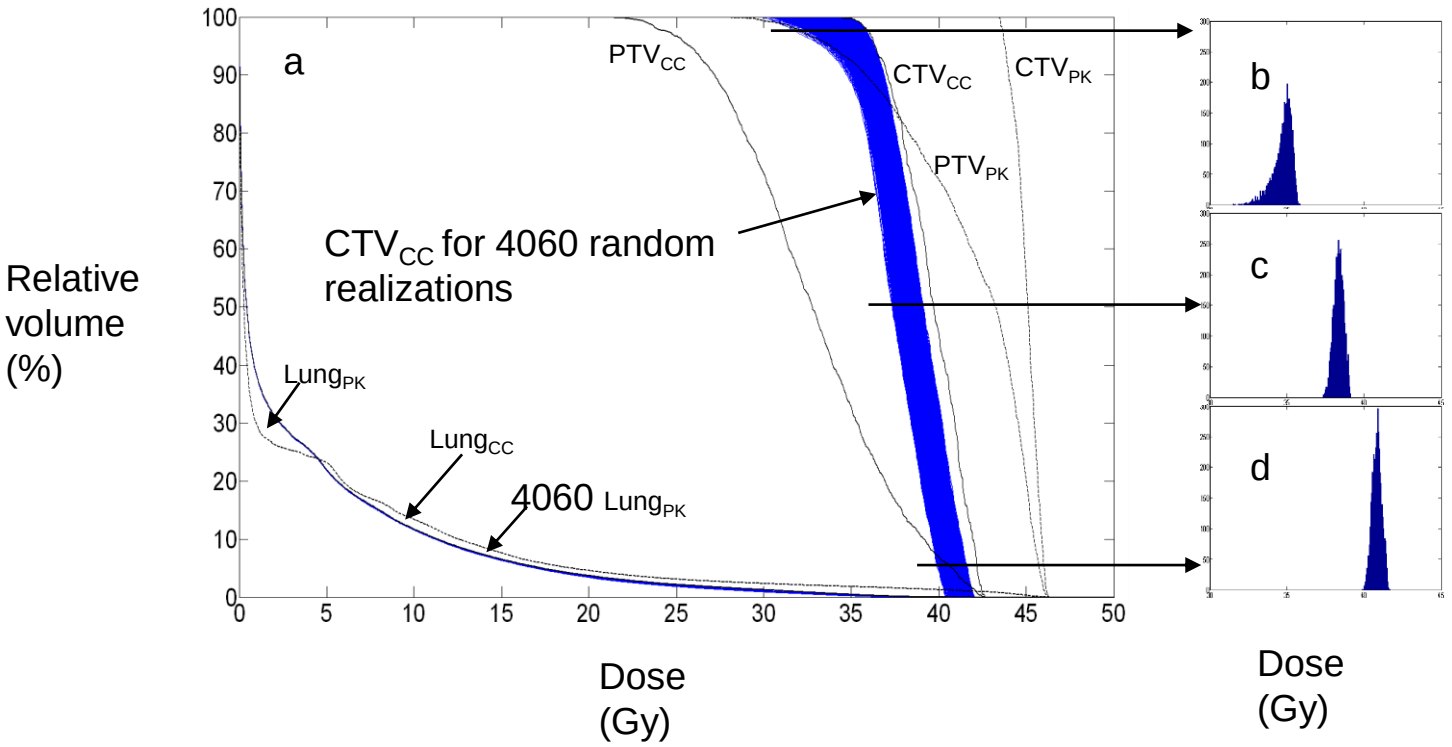

CT images defines the radiation transport arena

- **Imaging sequence must be relevant for the irradiation technique (breath hold, gating etc)**
- **Movements may yield large artifacts, and hence their calculated dose**

In lung, the dose to a small dense object (tumor) covered by large enough field margins is more determined by its size&chape than its position!

Wrong shape – wrong dose!

Wrong place – likely correct dose!

Summary

- Point Kernel algorithms show small deviations versus Monte Carlo for clinical cases, much more accurate than Pencil Kernel models
- Collapsed Cone inherent paralellism can efficiently use Graphical Processor Units for dose calculations literally in seconds
- Accuracy (and speed...) implemention dependent, depending on the approximations used
- Pencil kernel algorithms frequently used instead of point kernels, particularly in applications with optimizations, but will give errors particularly for lung cases

Spectrum corrections of raytraced collision kerma and scerma for attenuated beams (wedges)

Multiply cKERMA by $$k_{PQ}(depth, thickness) = \frac{\frac{(1-g)\,\mathrm{KERMA}}{\Psi}(\mathrm{mod})}{\frac{(1-g)\,\mathrm{KERMA}}{\Psi}(\mathrm{open})}$$

Multiply SCERMA by $$k_{SQ}(depth, thickness) = \frac{\frac{\mathrm{SCERMA}}{\Psi}(\mathrm{mod})}{\frac{\mathrm{SCERMA}}{\Psi}(\mathrm{open})}$$

i. e.

$$\frac{P}{\Psi_0}(\mathrm{mod}) = k_{PQ} \cdot \hat{\eta} \cdot \frac{P}{\Psi_0}(open)$$

$$\frac{S}{\Psi_0}(\mathrm{mod}) = k_{SQ} \cdot \hat{\eta} \cdot \frac{S}{\Psi_0}(open)$$

Where $\hat{\eta}$ is the modulation.

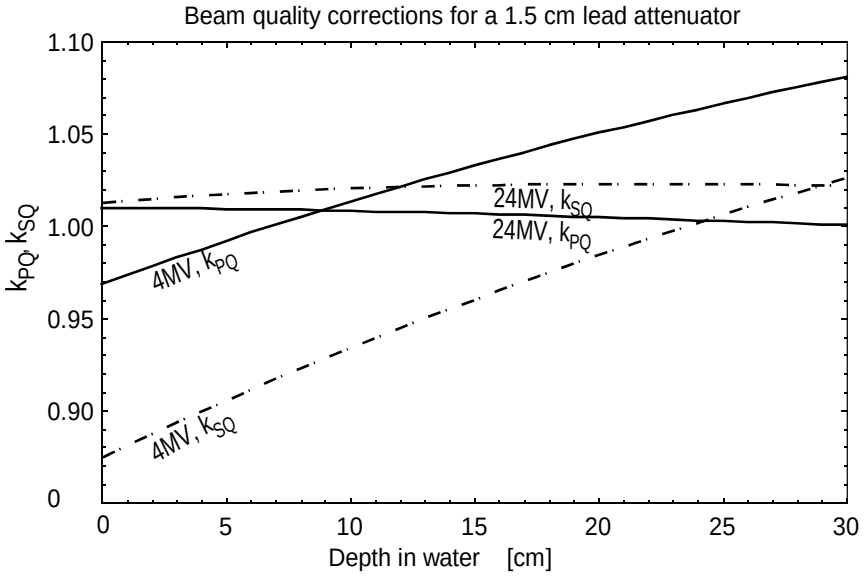

Pencil kernel models for photon dose calculations

Anders Ahnesjö

Acknowledgements
Mania Aspradakis, Luzerner Kantonsspital, Luzern, Switzerland
Jörgen Olofsson, Umeå University hospital, Umeå, Sweden

Learning objectives for the pencil kernel lecture

- To understand the concept of pencil kernel based dose calculations
- To know how pencil kernels can be determined for a beam
- To learn about common pencil kernel parameterizations
- To learn about calculation techniques from kernel&fluence to dose.
- To understand the most important approximations and limitations

concepts:

Pencil kernel

"Pencil" beam of photons

"pencil" beam = point monodirectional beam

Water phantom

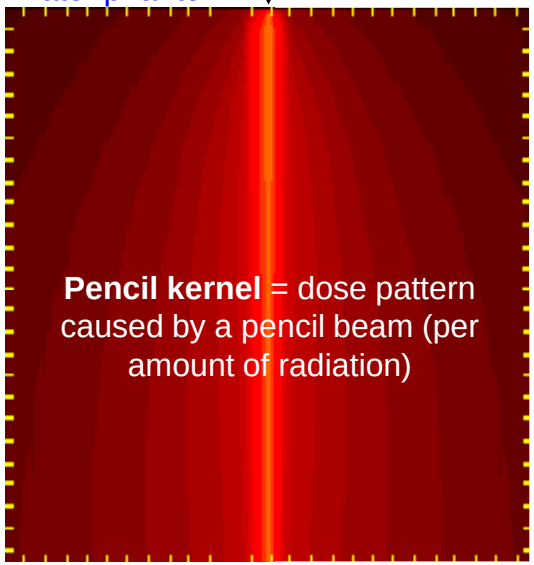

Dose calculation

View the incident photon fluence as composed (i.e. a sum) of pencil beams

Summing pencil kernels in the same way gives dose

$$D(x,y,z) = \iint_{\text{Field}} \Psi(x',y') \cdot \frac{p}{\rho}(x-x', y-y', z)\,\mathrm{d}x'\,\mathrm{d}y'$$

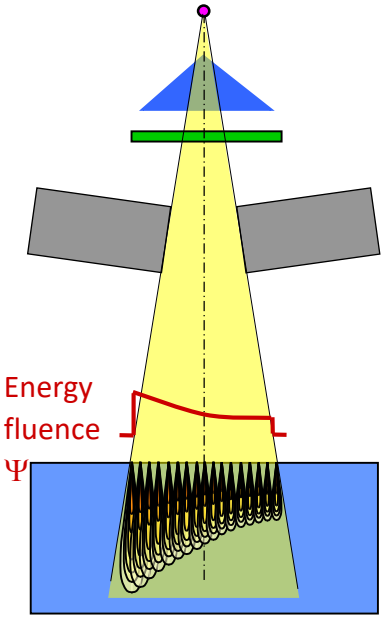

concepts:

Pencil and point energy deposition kernels

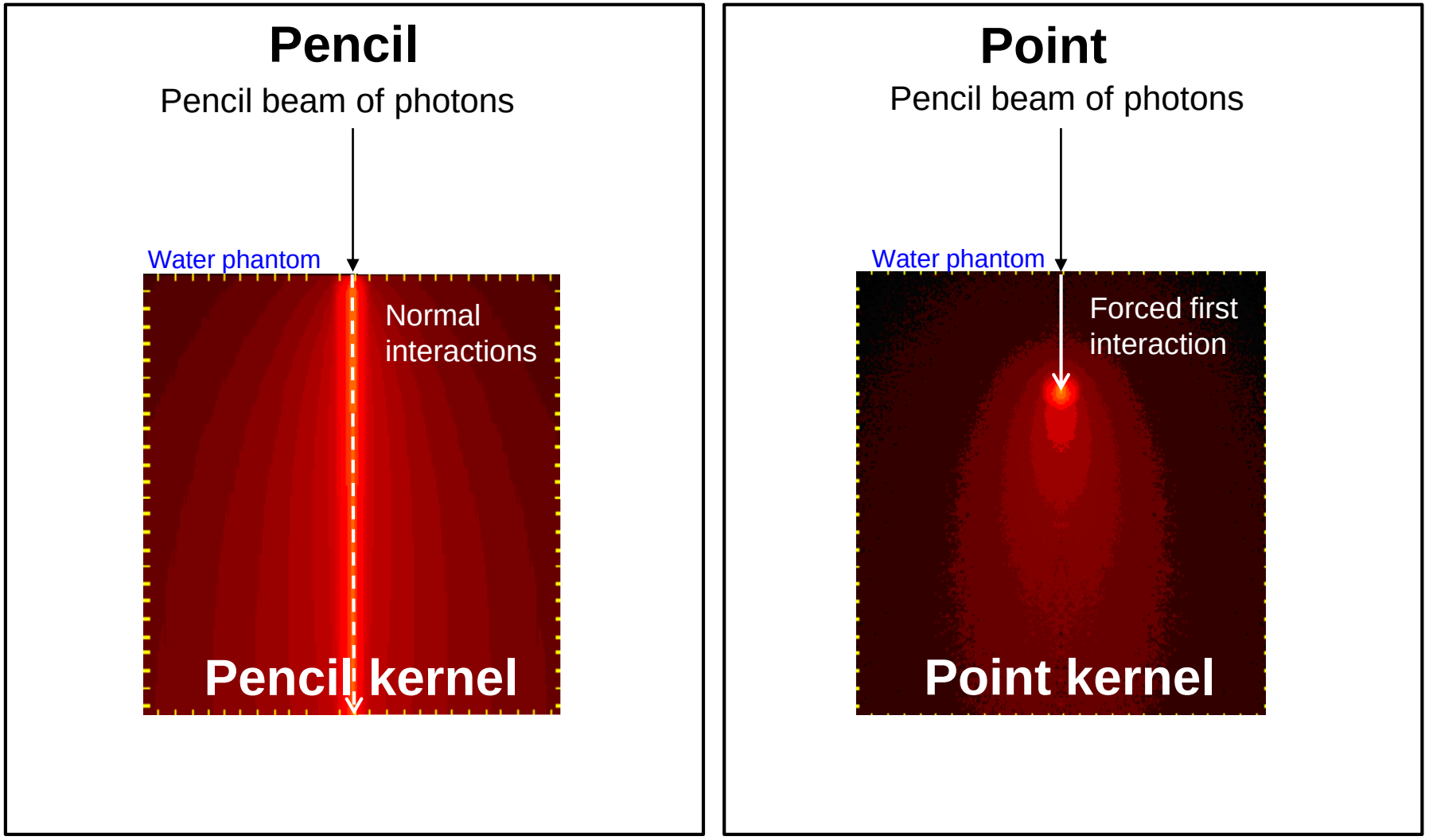

concepts:

Dimensions of a pencil kernel

Basic dose equation

$$D(x,y,z) = \iint_{\text{Field}} \Psi(x',y') \cdot \frac{p}{\rho}(x-x',y-y',z)\,\mathrm{d}x'\,\mathrm{d}y'$$

Dimensional analysis

$$\underbrace{\frac{\text{Energy}}{\text{mass}}}_{\text{dose}} = \iint_{\text{Field}} \underbrace{\frac{\text{Energy}}{\text{area}}}_{\text{energy fluence}} \cdot \underbrace{\frac{\dfrac{\text{deposited energy}}{\text{incident energy}}}{\text{mass}}}_{\text{pencil kernel}} \underbrace{\Delta\text{area}}_{\text{integration element}}$$

Hence, the dimension is energy fraction per mass, or mass^{-1} (since energy fraction is dimensionless).

concepts:

Finite sized pencil beams - beamlets

Pre-integrated over a finite beam area. Reduces time for super-position, assumes constant energy fluence over the beamlet area.

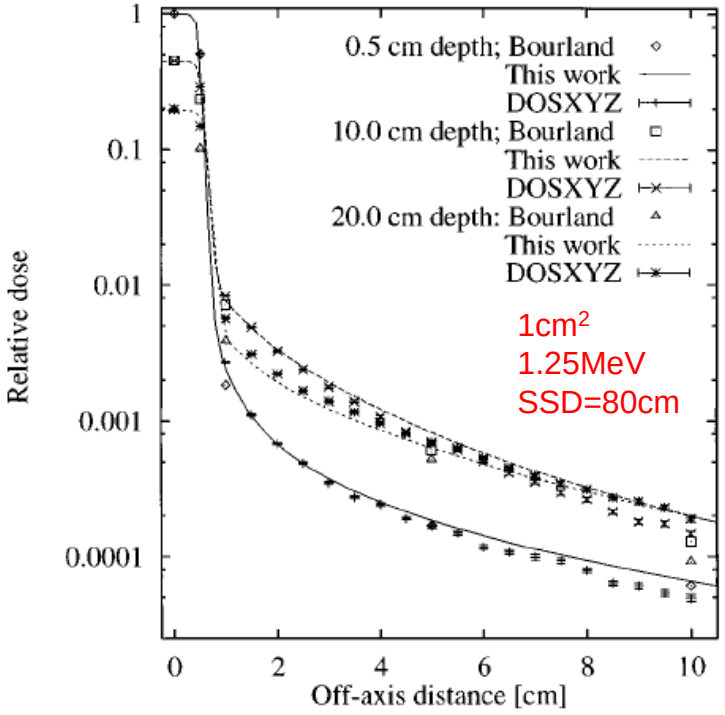

Ostapiak, et al (1997) *Med Phys 24*, 743-50.

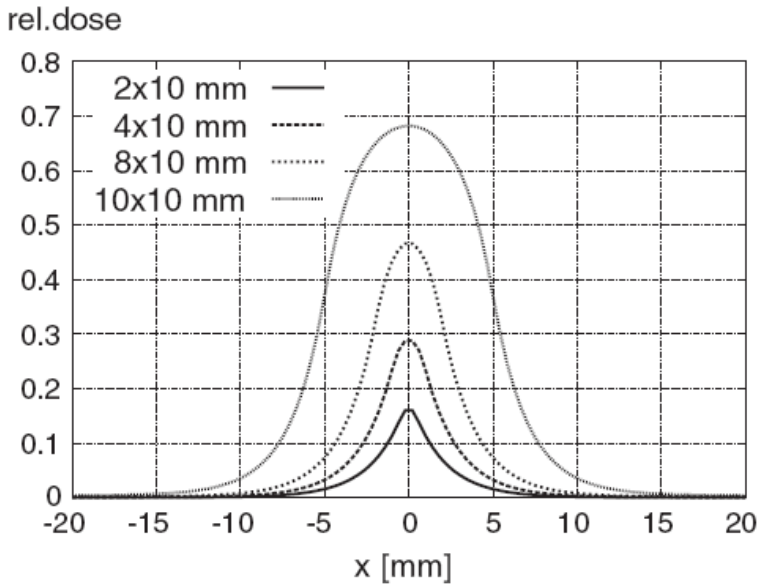

U Jelen, et al (2005) *Phys Med Biol 50*, 1747-66.

Mainly for fast calculations in IMRT optimization. The beamlet sizes must match the resolution of the fluence grid.

pencil kernel determination:

Most direct approach – Monte Carlo

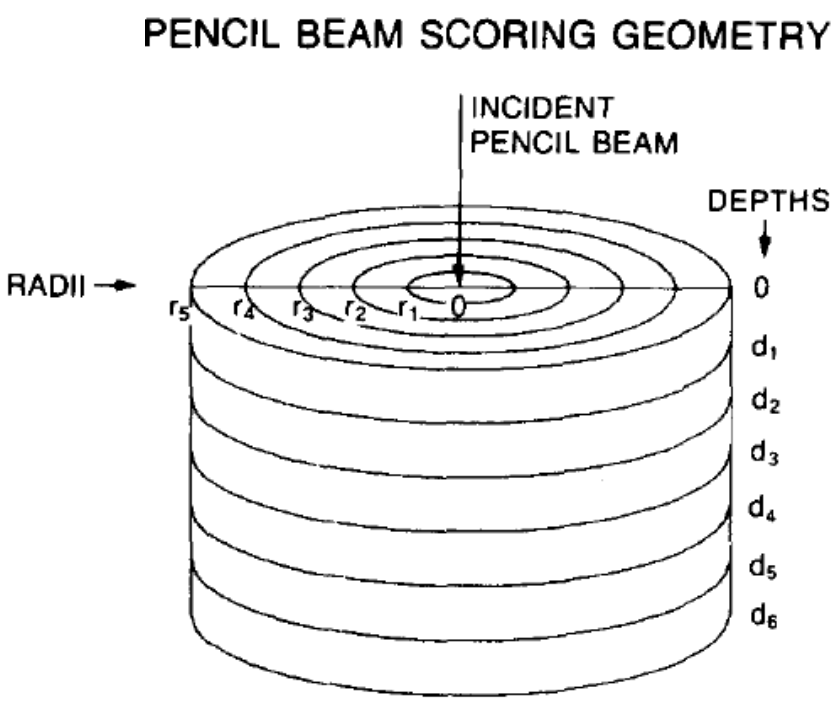

R Mohan and CS Chui (1987) *Med Phys 14*, 70-7

Beam spectrum necessary, either for direct MC simulation, or for adding mono-energetic kernels from a once calculated (MC) database

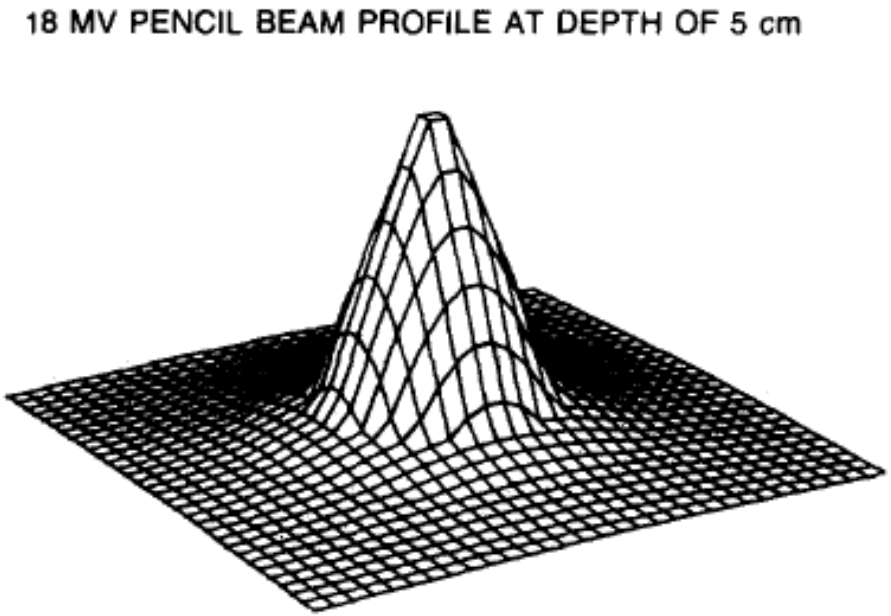

pencil kernel determination:

Beam modelling refresher: spectrum determination to make a polyenergetic kernel from a library of Monte Carlo generated monoenergetic kernel:

$$\delta\left(s_1, s_2 \ldots, e_1, e_2 \ldots\right) = \sum_{\text{fsize}} \sum_{\text{depth}} \left| c_{\text{fsize}} D_{\text{depth, fsize}} - \left(\left(\sum_{\text{ebin}} \Psi_{\text{ebin}}\left(s_1, s_2 \ldots\right) \cdot d_{\text{depth, fsize, ebin}} \right) + d_{\text{depth}}^{\text{electron cont}}\left(e_1, e_2 \ldots\right) \right) \right|$$

Measured depth dose, phantom scatter normalized

MC calc depth doses for monoenergetic photons

Error norm to minimize by varying parameters

Spectrum model, constrained to a "physical" shape

Electron contamination model

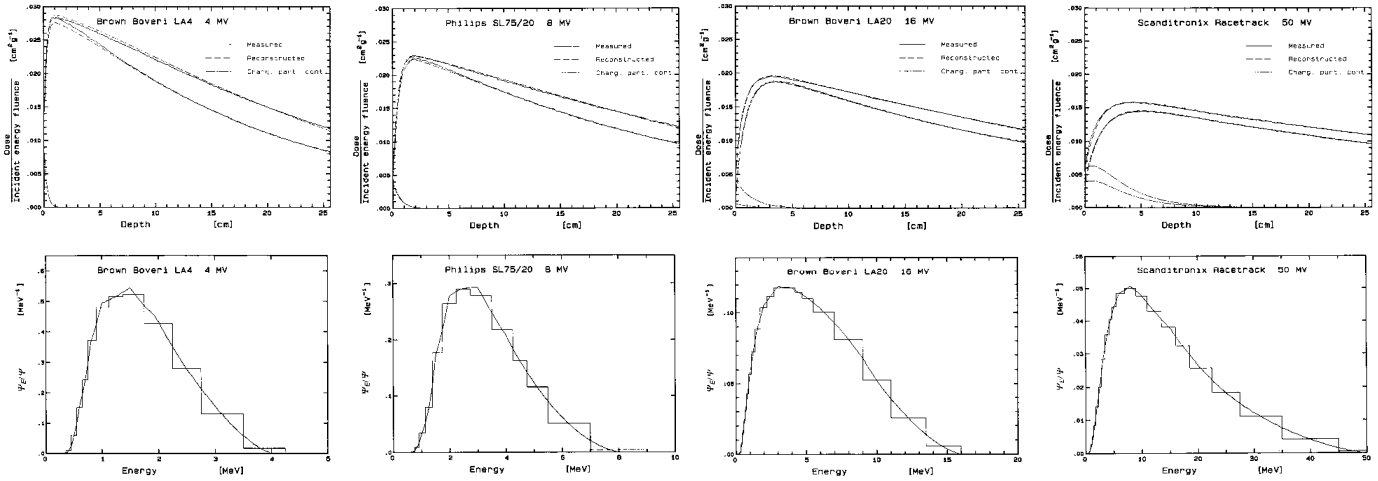

A Ahnesjö and P Andreo (1989) *Phys Med Biol 34*, 1451-64.

A Ahnesjö et al (1992) *Med Phys* 19, 263-273

pencil kernel determination:

Radial differentiation of measured dose for (equivalent) circular fields

$$\frac{p}{\rho}(r,z) = \frac{1}{2\pi\, r\, dr}\,\frac{D_{\text{meas}}}{\Psi}(r,z)$$

since

$$D(x,y,z) = \iint_{\text{Field}} \Psi(x',y')\cdot\frac{p}{\rho}(x-x',y-y',z)\,\mathrm{d}x'\,\mathrm{d}y' = \int_0^{2\pi}\int_0^{r} \underbrace{\Psi}_{\substack{\text{constant}\\ \text{within}\\ \text{field radius}}}\cdot\frac{p}{\rho}(r',z)\,\underbrace{r'\,\mathrm{d}r'\,\mathrm{d}\theta}_{\substack{\text{cylindrical}\\ \text{geometry}\\ \text{integrator}}}$$

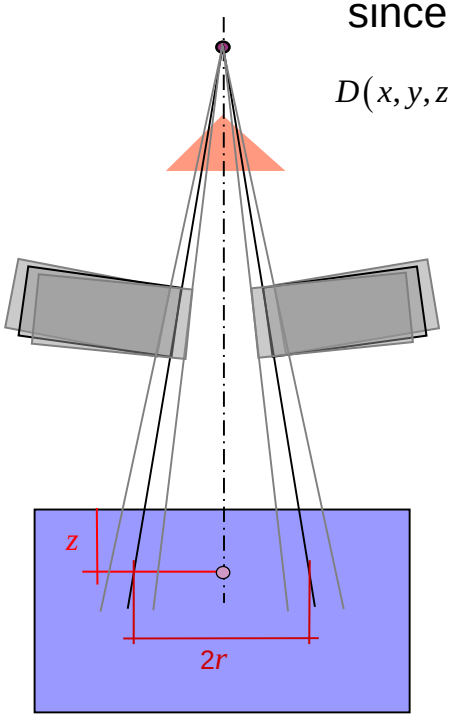

CP Ceberg, et al (1996) *Med Phys 23*, 505-11.

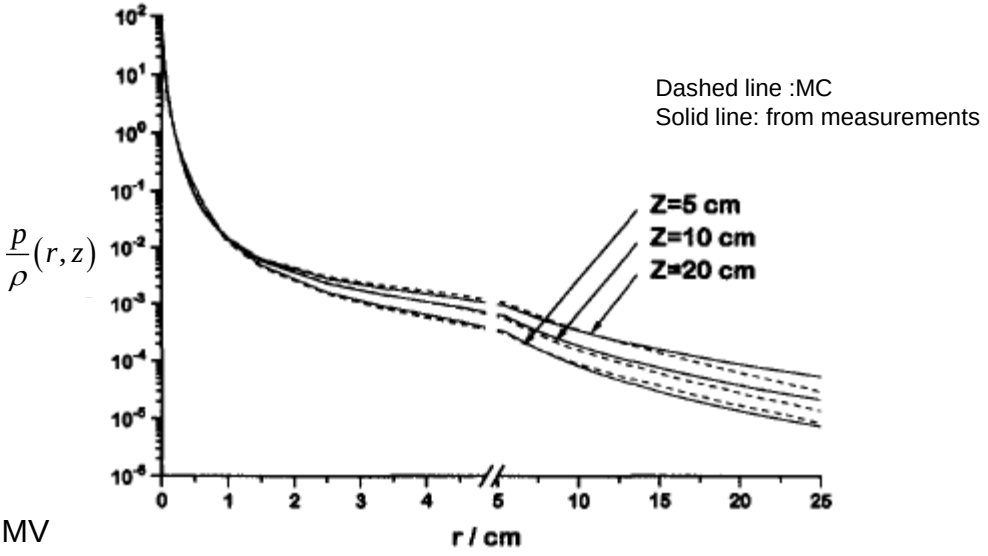

Dashed line :MC
Solid line: from measurements

6 MV

Absolute normalization is a problem, can be circumvented by phantom scatter normalized measured dose, and do renormalization via a reference field size of the calculated dose

pencil kernel parameterization:

Why parameterize kernels?

- Save memory
- Enable various (analytical) calculations
- Simplify commissioning

pencil kernel parameterization:

Monte Carlo PB kernel represented as double exponential over radius, tabulated for depths z. Motivations: lateral attenuation (a_z, b_z) and cylindrical geometry 1/r factor of the effective particle fluencies.

$$\frac{p}{\rho}(r,z) = \underbrace{\frac{A_z\, e^{-a_z r}}{r}}_{\text{primary dose}} + \underbrace{\frac{B_z\, e^{-b_z r}}{r}}_{\text{scatter dose}}$$

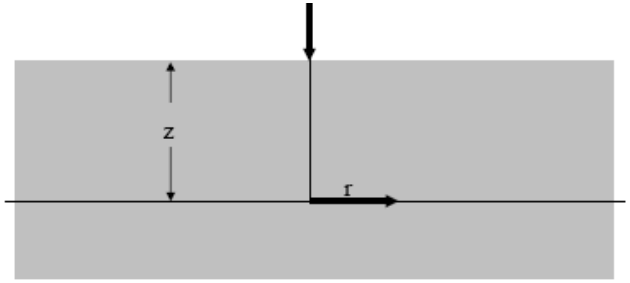

4 parameters required at each depth z for a given photon beam

	5 MV				8 MV				18 MV			
z [cm]	A_z [cm g^{-1}]	a_z [cm^{-1}]	B_z [cm g^{-1}]	b_z [cm^{-1}]	A_z [cm g^{-1}]	a_z [cm^{-1}]	B_z [cm g^{-1}]	b_z [cm^{-1}]	A_z [cm g^{-1}]	a_z [cm^{-1}]	B_z [cm g^{-1}]	b_z [cm^{-1}]
2	0.269E-1	6.95	0.506E-4	0.116	0.157E-1	4.59	0.344E-4	0.125	0.827	3.59	0.256	0.167
5	0.221E-1	6.59	0.112E-3	0.159	0.132E-1	4.29	0.754E-4	0.168	0.660	2.62	0.707	0.243
10	0.169E-1	6.64	0.163E-3	0.158	0.105E-1	4.24	0.122E-3	0.173	0.548	2.49	0.919	0.219
15	0.132E-1	6.75	0.162E-3	0.137	0.848E-2	4.26	0.130E-3	0.154	0.460	2.44	0.963	0.193
20	0.103E-1	6.80	0.142E-3	0.119	0.688E-2	4.26	0.121E-3	0.137	0.391	2.41	0.934	0.173

A Ahnesjö et al (1992) *Med Phys* 19, 263-273

This is the PK kernel parameterization used in Helax-TMS -> Oncentra -> etc

pencil kernel parameterization:

Math curiosity, $\frac{p}{\rho}(r,z) = \frac{A_z\, e^{-a_z r}}{r} + \frac{B_z\, e^{-b_z r}}{r}$ goes to infinity when r->0.

Dose on the main axis for a circular field of fluence Ψ:

$$D(z) = \int_0^{2\pi}\int_0^{R} \Psi \frac{p}{\rho}(r,z)\, r\, \mathrm{d}r =$$

$$= \int_0^{2\pi}\int_0^{R} \Psi \left(\frac{A_z\, e^{-a_z r}}{r} + \frac{B_z\, e^{-b_z r}}{r} \right) r\, \mathrm{d}r =$$

$$= \Psi 2\pi \left(\frac{A_z\left(1 - e^{-a_z R}\right)}{a_z} + \frac{B_z\left(1 - e^{-b_z R}\right)}{b_z} \right)$$

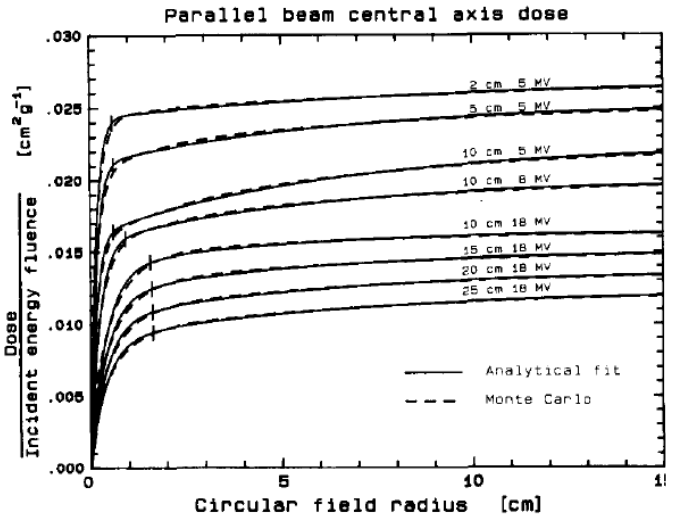

Ahnesjö et al (1992) *Med Phys* 19, 263-273

what happens when field size R goes to zero?

pencil kernel parameterization:

A further parameterization of $\frac{p}{\rho}(r) = \frac{A_z\, e^{-a_z r} + B_z\, e^{-b_z r}}{r}$, using the beam quality index TPR2010 as single input parameter:

$$\frac{A_z}{a_z} = A_1\left[1-\exp\left(A_2\sqrt{z^2+A_5^2}\right)\right]\exp\left(A_3 z + A_4 z^2\right) \qquad A_m = \sum_{i=1}^{5} C_{i,A_m}\cdot \mathrm{TPR}_{20/10}^{\,i}$$

$$\frac{B_z}{b_z} = B_1\left[1-\exp\left(B_2\sqrt{z^2+B_5^2}\right)\right]\exp\left(B_3 z + B_4 z^2\right) \qquad B_m = \sum_{i=1}^{5} C_{i,B_m}\cdot \mathrm{TPR}_{20/10}^{\,i}$$

$$a_z = a_1 + a_2 z \qquad a_m = \sum_{i=1}^{5} C_{i,a_m}\cdot \mathrm{TPR}_{20/10}^{\,i}$$

$$b_z = b_1\left[1-\exp\left(b_2\sqrt{z^2+b_5^2}\right)\right]\exp\left(b_3 z + b_4 z^2\right) \qquad b_m = \sum_{i=1}^{5} C_{i,b_m}\cdot \mathrm{TPR}_{20/10}^{\,i}$$

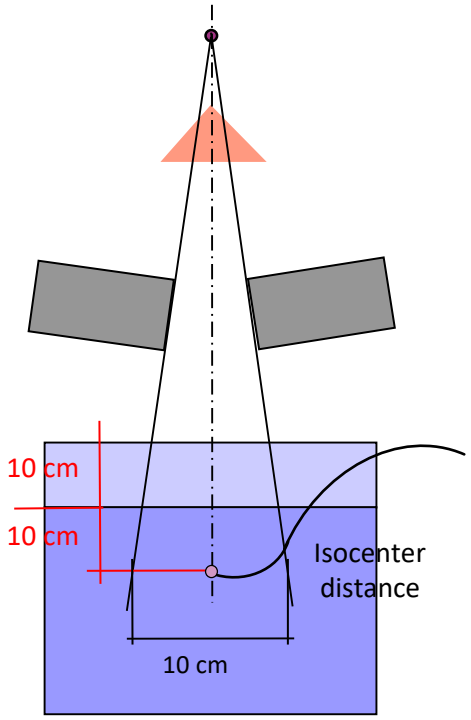

$$\mathrm{TPR}_{20/10} = \frac{D(10\times10, z = 20\,\mathrm{cm})}{D(10\times10, z = 10\,\mathrm{cm})}$$

Table 1
Coefficients used for to calculate pencil beam parameters as a function of $\mathrm{TPR}_{20/10}$

	C_0	C_1	C_2	C_3	C_4	C_5
A_1 ($\mathrm{cm^2\,g^{-1}}$)	0.0128018	−0.0577391	0.1790839	−0.2467955	0.1328192	−0.0194684
A_2 ($\mathrm{cm^{-1}}$)	16.7815028	−279.4672663	839.0016549	−978.4915013	470.5317337	−69.2485573
A_3 ($\mathrm{cm^{-1}}$)	−0.0889669	−0.2587584	0.7069203	−0.3654033	0.0029760	−0.0003786
A_4 ($\mathrm{cm^{-2}}$)	0.0017089	−0.0169150	0.0514650	−0.0639530	0.0324490	−0.0049121
A_5 (cm)	0.1431447	−0.2134626	0.5825546	−0.2969273	−0.0011436	0.0002219
B_1 ($\mathrm{cm^2\,g^{-1}}$)	−42.7607523	264.3424720	−633.4540368	731.5311577	−402.5280374	82.4936551
B_2 ($\mathrm{cm^{-1}}$)	0.2428359	−2.5029336	7.6128101	−9.5273454	4.8249840	−0.7097852
B_3 ($\mathrm{cm^{-1}}$)	−0.0910420	−0.2621605	0.7157244	−0.3664126	0.0000930	−0.0000232
B_4 ($\mathrm{cm^{-2}}$)	0.0017284	−0.0172146	0.0522109	−0.0643946	0.0322177	−0.0047015
B_5 (cm)	−30.4609625	354.2866078	−1073.2952368	1315.2670101	−656.3702845	96.5983711
a_1 ($\mathrm{cm^{-1}}$)	−0.0065985	0.0242136	−0.0647001	0.0265272	0.0072169	−0.0020479
a_2 ($\mathrm{cm^{-2}}$)	−26.3337419	435.6865552	−1359.8342546	1724.6602381	−972.7565415	200.3468023
b_1 ($\mathrm{cm^{-1}}$)	−80.7027159	668.1710175	−2173.2445309	3494.2393490	−2784.4670834	881.2276510
b_2 ($\mathrm{cm^{-1}}$)	3.4685991	−41.2468479	124.9729952	−153.2610078	76.5242757	−11.2624113
b_3 ($\mathrm{cm^{-1}}$)	−39.6550497	277.7202038	−777.0749505	1081.5724508	−747.1056558	204.5432666
b_4 ($\mathrm{cm^{-2}}$)	0.6514859	−4.7179961	13.6742202	−19.7521659	14.1873606	−4.0478845
b_5 (cm)	0.4695047	−3.6644336	10.0039321	−5.1195905	−0.0007387	0.0002360

The numerical values are given with a very high precision. Not because we claim this precision in the determination of specific parameters, but because of the bad conditioning of the problem, where just slight differences in the parameters can make large difference in the end.

T Nyholm, et al (2006) *Radiother Oncol 78*, 347-51.

This is the PK kernel parameterization used in e.g. Scandidos Delta4 software

pencil kernel parameterization:

The TPR2010 based parameterization can be extended to also consider off axis softening – modify the PK parameters based of the generic Tailor fit.

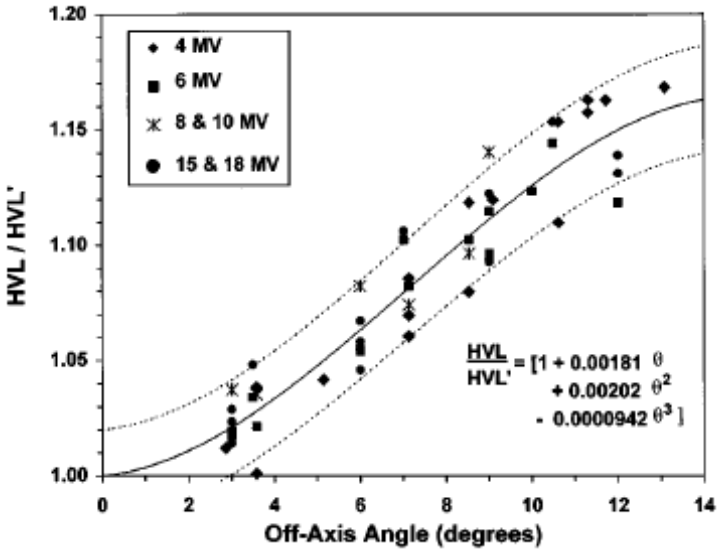

Tailor et al (1998) *Med Phys 25*, 662-7.

For details, see:

- Olofsson et al (2006) Med Phys 33, 3418-25
- Nyholm,et al (2006) Phys. Med. Biol. 51, 4111-8

Much smaller effect in FFF beams!

pencil kernel parameterization:

The lateral component $k_\beta(\theta, \lambda, p_z)$ is modelled as a superposition of six radial exponential functions:

$$k_\beta(\theta, \lambda, p_z) = \sum_{i=1}^{6} c_i \frac{1}{\lambda} \exp(-\mu_i \lambda) \ (\mathrm{m}^{-1}). \tag{6}$$

For each depth p_z and angle θ, this component describes the fraction of energy deposited into an infinitesimally small angular section at a distance λ to the beamlet central axis. The attenuation coefficients μ_i in (6) are fixed, and are chosen such that the effective ranges $1/\mu_i$ vary in between $0, \ldots, 200\,\mathrm{mm}$. The weight parameters c_i are fitted for each calculation plane to minimize deviations between the analytical kernel presentation in (6) and the poly-energetic kernel computed from the monoenergetic pre-calculated pencil beam kernels.

This is the PK kernel parameterization used in AAA Eclipse

Tillikainen et al Phys. Med. Biol. 52 (2007) 1441–1467

calculation techniques:

Calculation task – make dose out from given beam(s), a pencil kernel and the patient geometry

Theory: view the incident photon fluence as composed (i.e. a sum) of pencil beams, so summing pencil kernels in the same way should give give the dose

$$D(x,y,z) = \iint_{\text{Field}} \Psi(x',y') \cdot \frac{p}{\rho}(x-x', y-y', z)\,\mathrm{d}x'\,\mathrm{d}y'$$

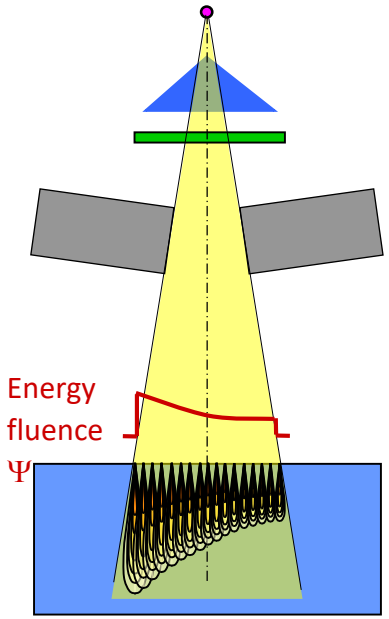

Reality:

- Do it fast!
- Do it faster!!
- Faster!!!!!
- Consider inverse square law
- Heterogeneties???
- Special cases of interest?

calculation techniques:

A particular simple case is dose at the main axis for circular fields of radius R with homogeneous energy fluence:

$$D(z) = \int_0^{2\pi}\int_0^{R} \Psi \frac{A_z\, e^{-a_z r} + B_z\, e^{-b_z r}}{r}\, r\, dr$$

$$\Downarrow$$

$$\frac{D}{\Psi}(z) = 2\pi\left(\frac{A_z\left(1-e^{-a_z R}\right)}{a_z} + \frac{B_z\left(1-e^{-b_z R}\right)}{b_z}\right)$$

In the same way, the dose to the central axis from a square field, with side s, can be calculated by employing the equivalent circle with R=0.561·s.

Bjärngard and Siddon (1982). *Med Phys* 9, 258-60

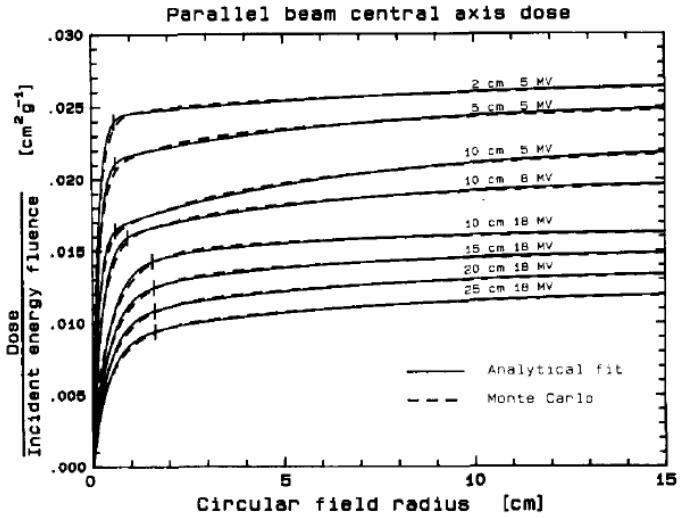

FIG. 4. Comparisons at various depths and beam energies between central axis dose for circular fields calculated directly with Monte Carlo pencil beam kernels (dashed lines) and analytical kernels (solid lines). The vertical bar on each curve marks the field radius for which lateral charged particle equilibrium is established, defined as the radius where the integral of the first term of Eq. (1) equals 98% of its value at infinite radius.

Ahnesjö et al (1992) *Med Phys* 19, 263-73

Calculation techniques:

Convolutions - many dose calculation problems can be approximated as convolutions (invariant kernel -> for homogeneous media):

Convolution - an averaging operation where at each point a weighted mean of the original function is calculated. The (invariant!!!) weighting function is often called kernel.

1D example

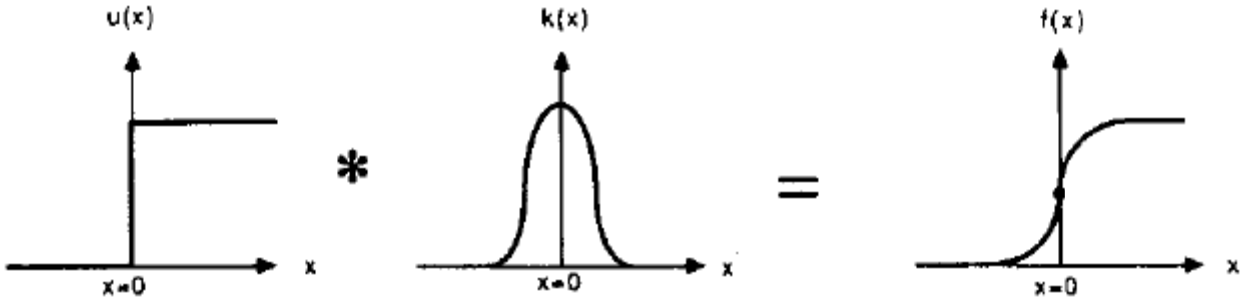

1D $[f \otimes g](x) = \int_{-\infty}^{\infty} f(x')\, g(x - x')\, \mathrm{d}x'$

2D cartesian $[f \otimes g](x, y) = \int_{-\infty}^{\infty} \int_{-\infty}^{\infty} f(x', y')\, g(x - x', y - y')\, \mathrm{d}x'\, \mathrm{d}y'$

2D polar Google Hankel transforms!

3D cartesian $[f \otimes g](x, y, z) = \int_{-\infty}^{\infty} \int_{-\infty}^{\infty} \int_{-\infty}^{\infty} f(x', y', z')\, g(x - x', y - y', z - z')\, \mathrm{d}x'\, \mathrm{d}y'\, \mathrm{d}z'$

calculation techniques:

The **convolution theorem** states that the Fourier transform of a convolution is the product of the Fourier transforms of the components.

$\mathcal{F}$ denotes Fourier transform operator

$$\mathcal{F}\{f\} = \int_{\mathbb{R}^n} f(x) e^{-2\pi i x \cdot \nu}\,\mathrm{d}x$$

$$\mathcal{F}\{g\} = \int_{\mathbb{R}^n} g(x) e^{-2\pi i x \cdot \nu}\,\mathrm{d}x$$

Pointwise multiplication

$$\mathcal{F}\{f * g\} = \mathcal{F}\{f\} \cdot \mathcal{F}\{g\}$$

$$\mathcal{F}\{f \cdot g\} = \mathcal{F}\{f\} * \mathcal{F}\{g\}$$

Applying the inverse Fourier transform $\mathcal{F}^{-1}$ gives the result:

$$f * g = \mathcal{F}^{-1}\{\mathcal{F}\{f\} \cdot \mathcal{F}\{g\}\}$$

calculation techniques:

Fast Fourier Transform (FFT) convolution

FFT is a way to compute the same result more quickly: operations proportional to $N \ln(N)$ per dimension instead of N^2 $\Rightarrow$ decrease calc burden from N^4 to $2N^2 \ln(N)$, a factor proportional to $2\ln(N)/N^2$ shorter time, with NxN fluence pixels.

Scaling example

N	factor
10	1
100	0.02
200	0.006

Calculation recipe for the lateral dose distribution at a given depth through FFT convolution.

1. Perform a 2D FFT on the pencil kernel (can be pre-stored!)
2. Perform a 2D FFT on the lateral energy fluence distribution
3. Mulitply the two transformed distributions
4. Perform an inverse 2D FFT (FFT^{-1}) on the resulting product
5. Done – for all points in a plane at a certain depth (not a 3D matrix, yet)!

R Mohan and CS Chui (1987) *Med Phys 14*, 70-7

Used at some stage in most TPS that use pencil kernels

calculation techniques:

Penumbra effects:

- electron transport effects – automatically by the kernel
- collimator transmission and finite source occlusion effects
  - should be considered during fluence modelling (dosimetric leaf gap addition not sufficient)
  - can also be approximated with a field edge blurring convolution of the primary part, example (in dose domain, direct blurring of idealized collimated fluence also possible):

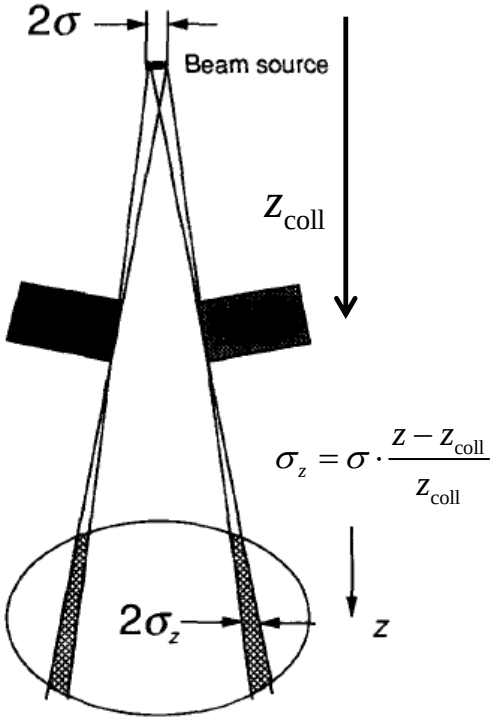

$$\frac{p}{\rho}(r,z) = \underbrace{\frac{A_z e^{-a_z r}}{r}} + \frac{B_z e^{-b_z r}}{r}$$

$$\Downarrow$$

$$\frac{1}{\pi\sigma_z^2} e^{-\frac{r^2}{\sigma_z^2}} \otimes \frac{A_z e^{-a_z r}}{r}$$

projected Gaussian source distribution

A Ahnesjö et al (1992) *Med Phys* 19, 263-273

calculation techniques:

Charged particle contamination, separate modelling needed when pencil kernels are derived from MC simulations

Charged particle contamination kernel

$$\frac{p_{c_{\pm}}}{\rho}(r,z) = \alpha e^{-\beta z} e^{-\gamma r^2}$$

The parameters α, β, and γ can be determined through fitting to the difference between measurements and calculated photon dose.

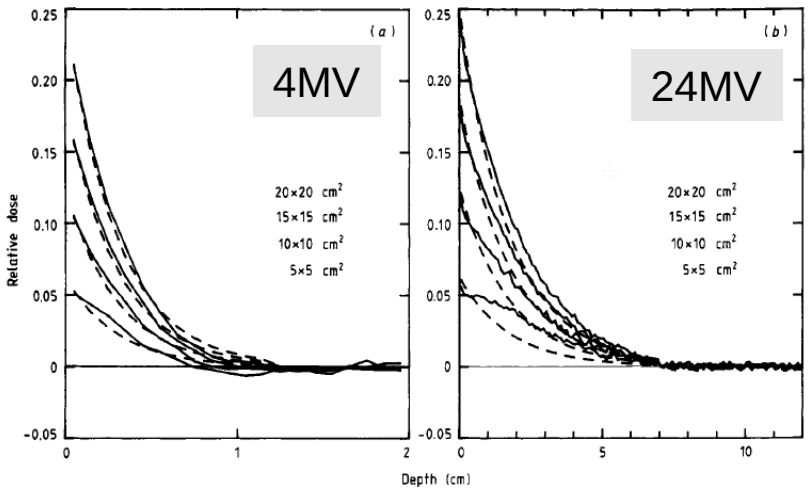

A Ahnesjö and P Andreo (1989) *Phys Med Biol 34*, 1451-64.

calculation techniques:

What about beam divergence and the inverse square law?

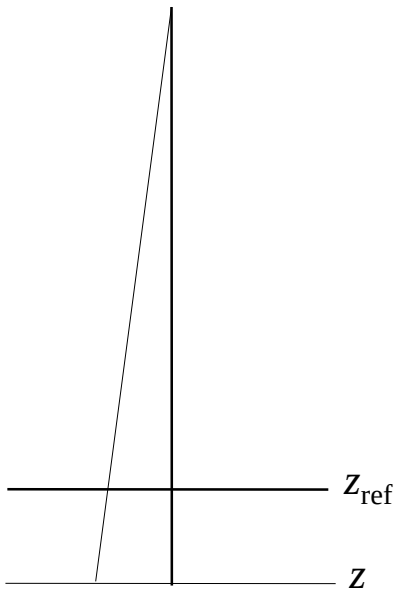

Fluence scaled to the depth of calculation and integration (convolution) carried out over the field size at depth:

$$D(x,y,z) = \iint_{\text{Field}} \Psi(x',y') \cdot \frac{p}{\rho}(x-x', y-y', z)\,\mathrm{d}x'\,\mathrm{d}y'$$

$$\Downarrow$$

$$D(x,y,z) = \iint_{\text{Field}} \left(\frac{z_{\text{ref}}}{z}\right)^2 \cdot \Psi_{\text{ref}}\left(\frac{z}{z_{\text{ref}}}x', \frac{z}{z_{\text{ref}}}y'\right) \cdot \frac{p}{\rho}(x-x', y-y', z)\,\mathrm{d}x'\,\mathrm{d}y'$$

calculation techniques:

Eclipse (AAA) use a spherical coordinate grid to deal with beam divergence/inverse square law

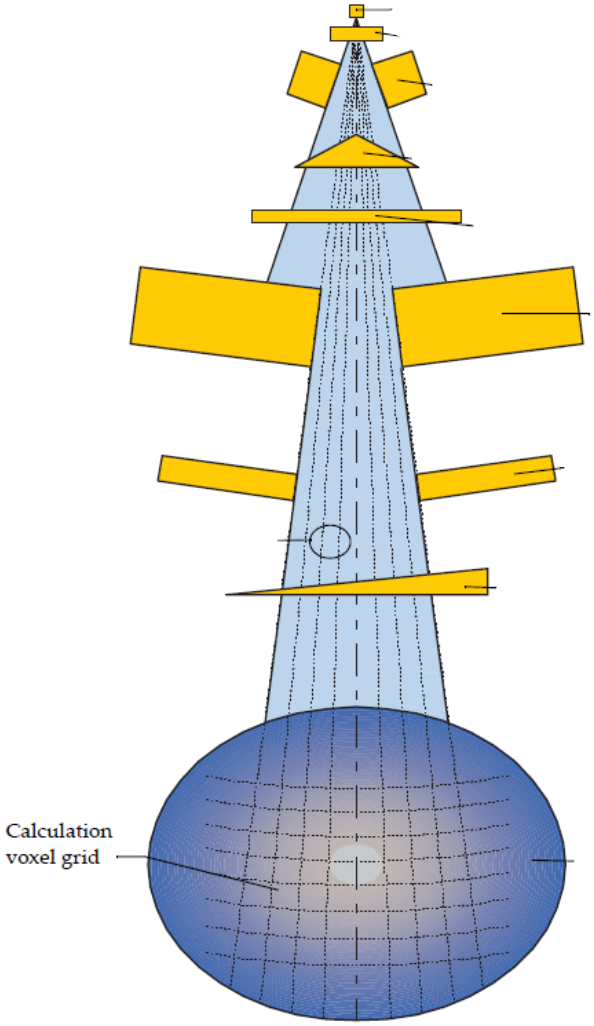

calculation techniques:

Depth invariant (almost) shape relative dose profile – use for interpolation to save convolutions?

Primary dose profiles for a 10x10 cm field at 1, 3, 5 and 10 cm depths
Scatter dose profiles at 5, 10, 15 and 20 cm depths

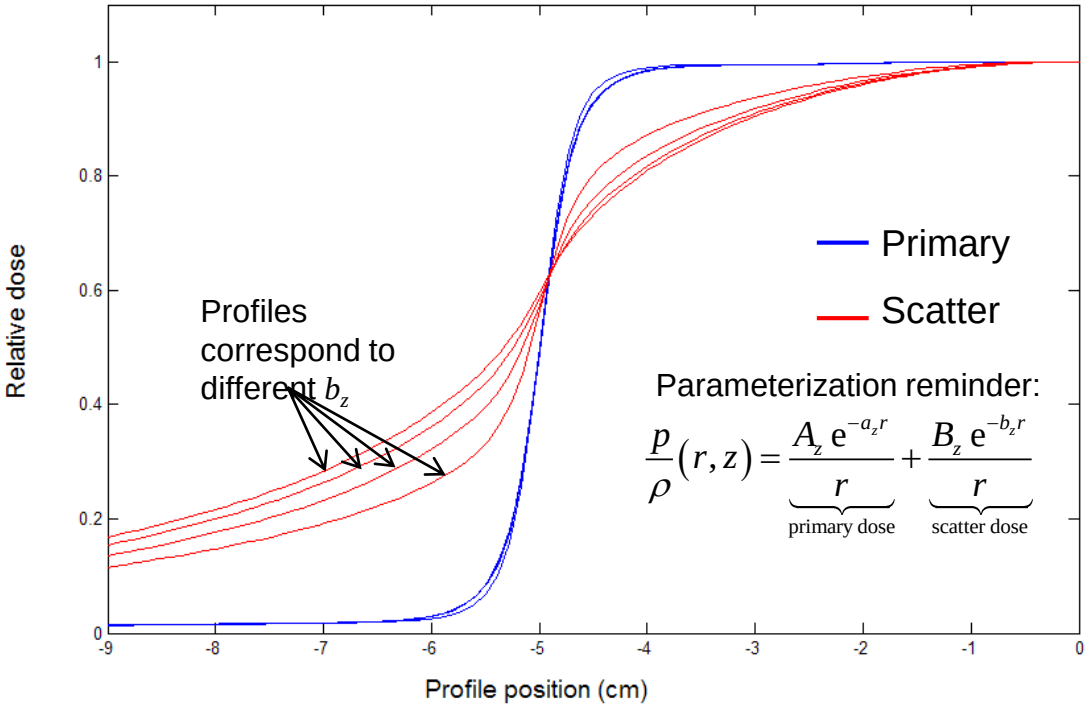

The profiles change smoothly as functions of a_z and b_z and hence are suitable for interpolation with a_z and b_z as interpolation variables!

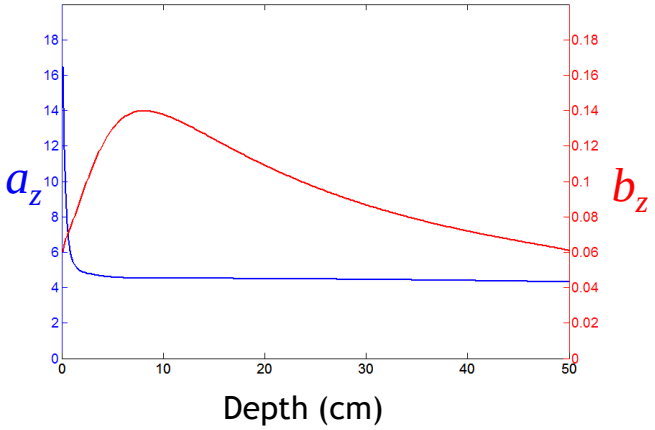

calculation techniques:

interpolation scheme to save convolutions, example (primary dose):

1. Pre-calculate lateral dose distributions, D_k, for a selected set of kernel parameters a_{z_k}, where k=1..n

2. Runtime operations per calculation point:
   - Calculate radiological depth $z \Rightarrow a_z$
   - Interpolate between lateral dose distributions, D_k and D_{k+1}

$$D = S_z^2 \frac{A_z}{a_z}\left((1-q)\cdot\frac{D_k}{A_{z_k}/a_{z_k}} + q\cdot\frac{D_{k+1}}{A_{z_{k+1}}/a_{z_{k+1}}}\right) \qquad q = \frac{a_z - a_{z_k}}{a_{z_{k+1}} - a_{z_k}}$$

S_z^2 = Inverse square factor

Two lateral distributions sufficient for primary dose and three for scatter dose. Only five convolutions per field!

This is the PK implementation in Oncentra

calculation techniques:

A singular value decomposition (SVD) trick based on the same profile invariance properties as the interpolation scheme:

Decomposition of pencil beam kernels for fast dose calculations in three-dimensional treatment planning

Thomas Bortfeld, Wolfgang Schlegel, and Bernhard Rhein
German Cancer Research Center, Research Program Radiologic Diagnostics and Therapy, Department of Biophysics and Medical Radiation Physics, Im Neuenheimer Feld 280, W-6900 Heidelberg, Germany

Med Phys 20(2) 1993, p311-318

This is the PK implementation (for intermediate results during optimization) in RayStation
Also used in Plato, and experimental systems (e.g. Voxelplan, Heidelberg)

calculation techniques:

Common approach for heterogeneity handling:

primary dose, use PK primary dose data for the depth z_{rad} :

$$z_{\mathrm{rad}} = \frac{1}{\mu_{\mathrm{water}}} \int_0^z \frac{\mu}{\rho}(z') \cdot \rho(z')\,\mathrm{d}z'$$

scatter dose, apply a 1D convolution derived correction factor:

$$\mathrm{CF_S} = \frac{\int_0^z \mu(z')\,\mathrm{d}z' \cdot \mathrm{e}^{-\int_0^z \mu(t)\,\mathrm{d}t}}{\int_0^z \mu_{\mathrm{w}}\,\mathrm{d}z' \cdot \mathrm{e}^{-\int_0^z \mu_{\mathrm{w}}\,\mathrm{d}t}} = \frac{z_{\mathrm{rad}}}{z} \cdot \mathrm{e}^{-\mu(z_{\mathrm{rad}}-z)}$$

This is the methods used for PK kernel in (at least) Oncentra

A Ahnesjö et al (1992) *Med Phys* 19, 263-273

calculation techniques:

Heterogeneities, comparison between different algorithms:

Standard Pencil beam

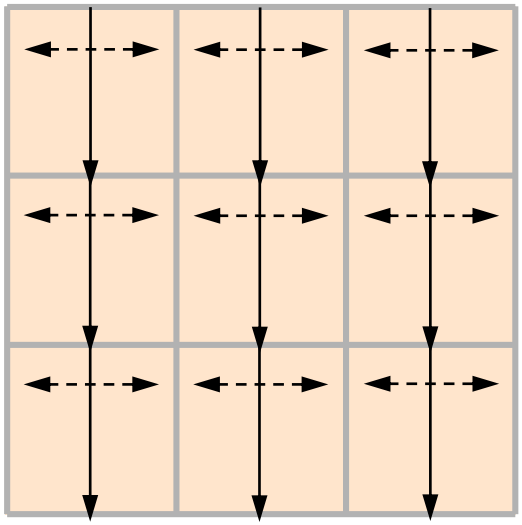

Kernel scaling by radiological pathlengths: Only along rayline.

Varian AAA
(Anisotropic Analytical Algorithm)

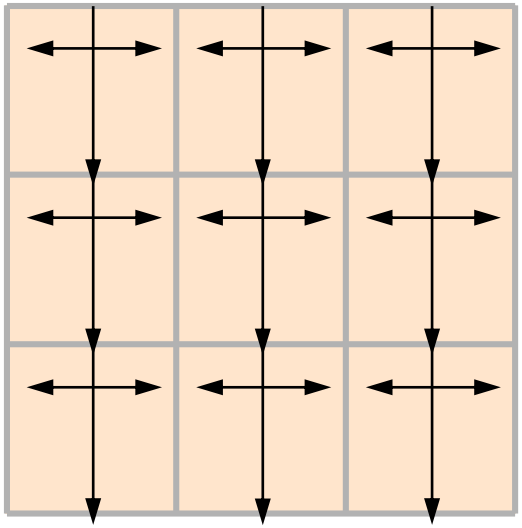

Kernel scaling by radiological pathlengths: In 16 direction lateral directions and along raylines.

Convolution superposition/ Collapsed cone

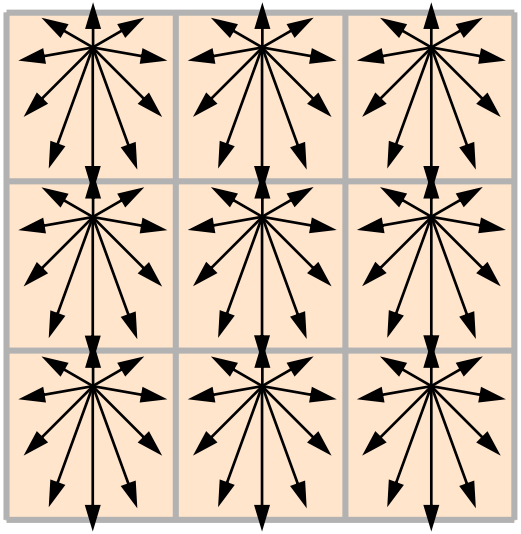

Kernel scaling by radiological pathlengths: In all directions, 100+

calculation techniques – heterogeneity handling in Eclipse AAA:

build-up/down filtering to mitigate discontinuities

Doses will change too fast at material/tissue interfaces when just applying an effective depth correction. To model gradual changes at material interfaces, a correction is introduced based on a convolution using a build-up kernel along the depth direction.

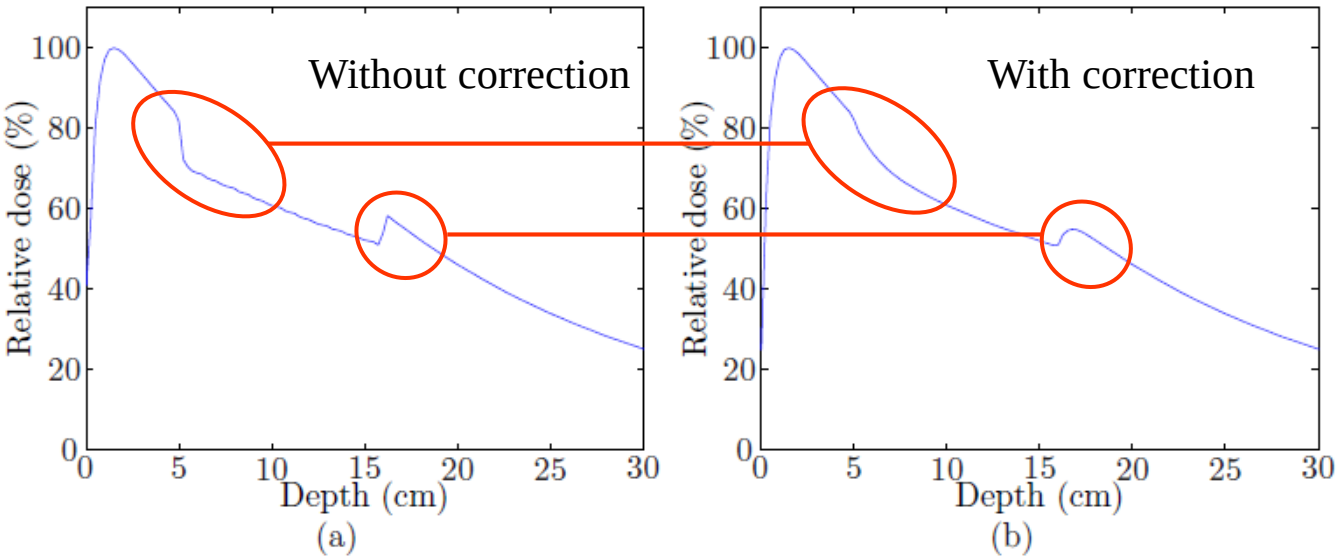

Fig. 11: The calculated dose for a 3×3 cm^2 field for a 6 MV beam incident on a water phantom with lung insert ($\rho_w = 0.3$) from $z = 5, \ldots, 15$ cm (a) without the build-up/build-down correction, and (b) with the correction turned on.

L Korhonen (2009) m *PhD thesis*, Department of Biomedical Engineering and Computational Science, Helsinki University of Technology

Approximations in PK dose calculations

Infinite slab approximation: doses at phantom boundaries

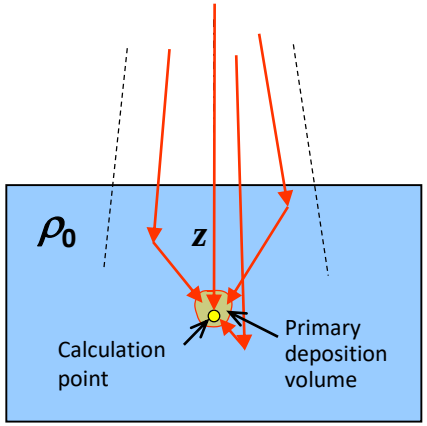

Ideal case

The depth (z) is generally assumed to be constant within the lateral integration plane during calculation of the scatter dose to a point.

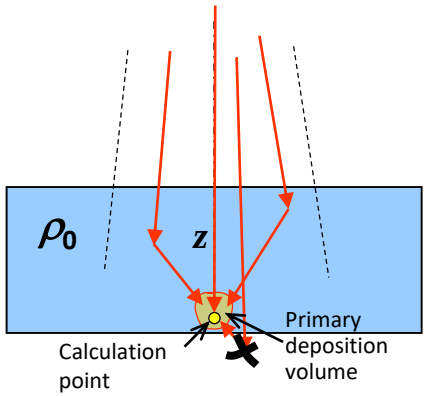

Backscatter overestimated

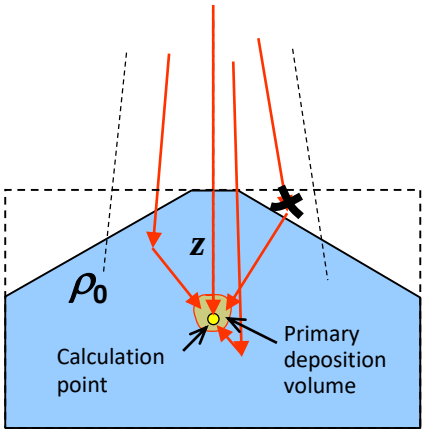

Scatter overestimated

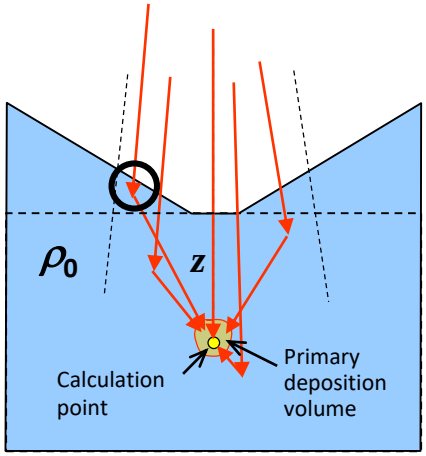

Scatter underestimated

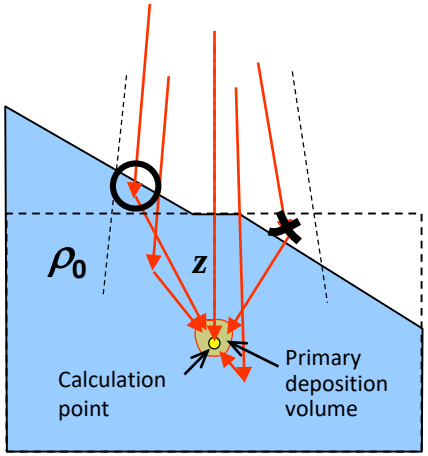

Errors cancel (roughly)

Approximations in PK dose calculations

Heterogeneous media: kernel scaling

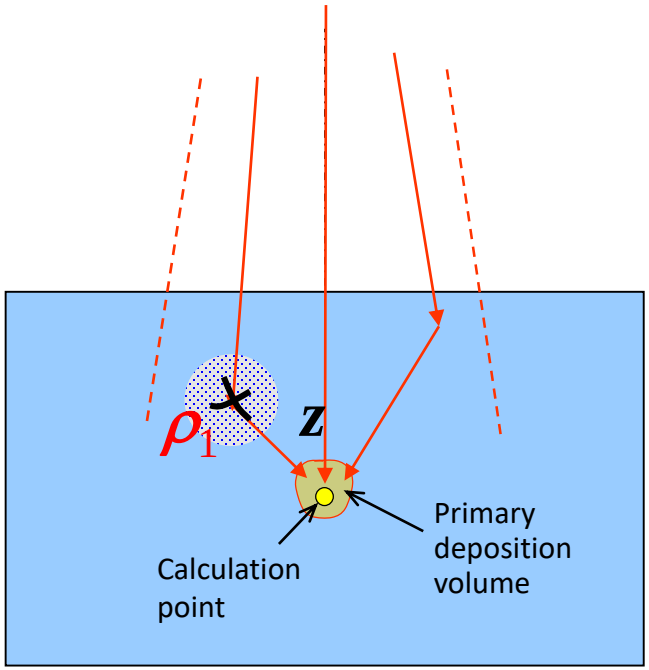

Scatter overestimated

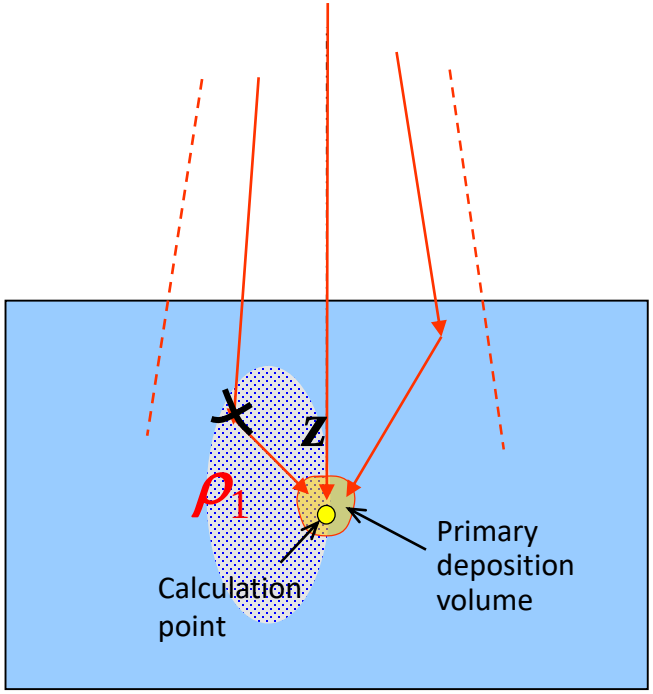

Scatter and primary overestimated

For $\rho_1 < \rho_{water}$

Approximations in dose calculation

Comparison of methods (pencil kernel, AAA, point kernel, MC)

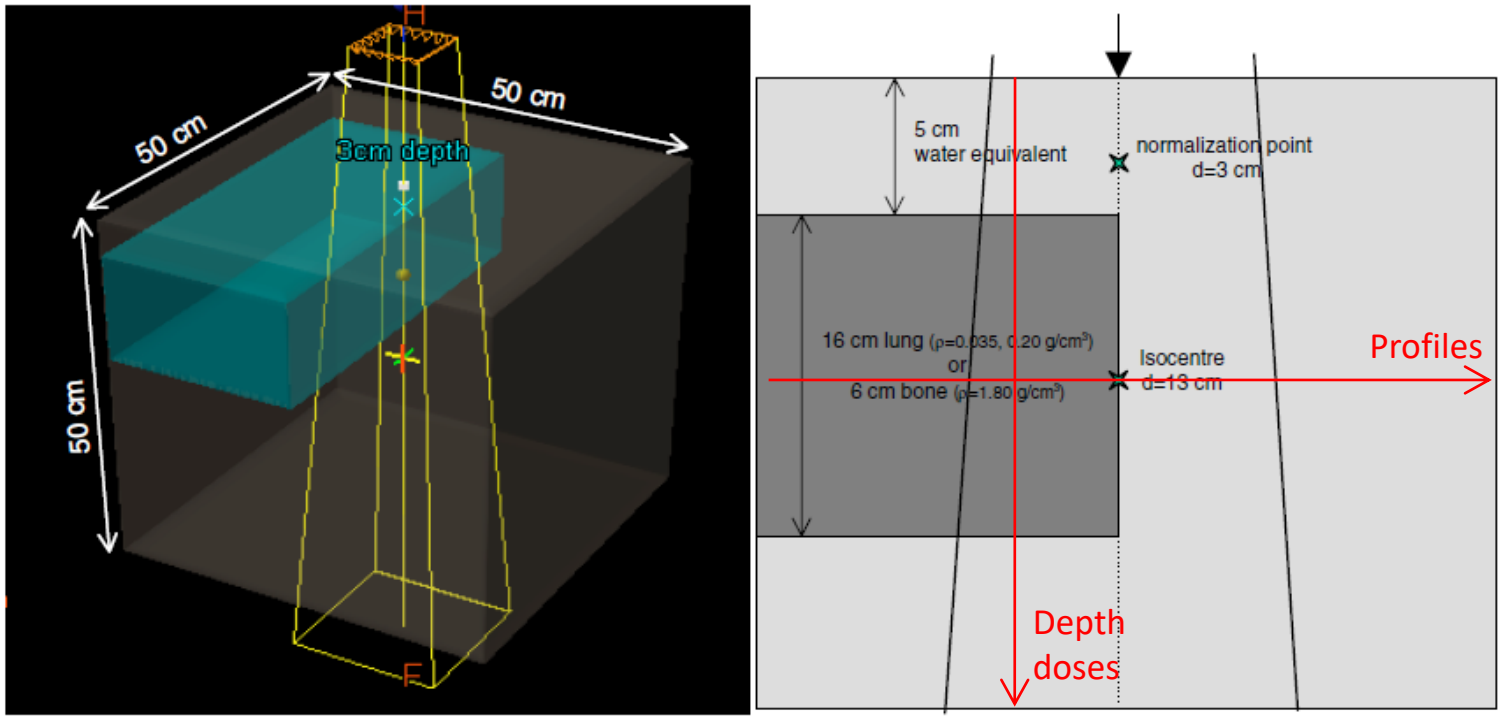

Fogliata A et al (2007) Phys Med Biol 52, 1363-85.

Approximations in dose calculation

Comparison of methods (pencil kernel, AAA, point kernel, MC)

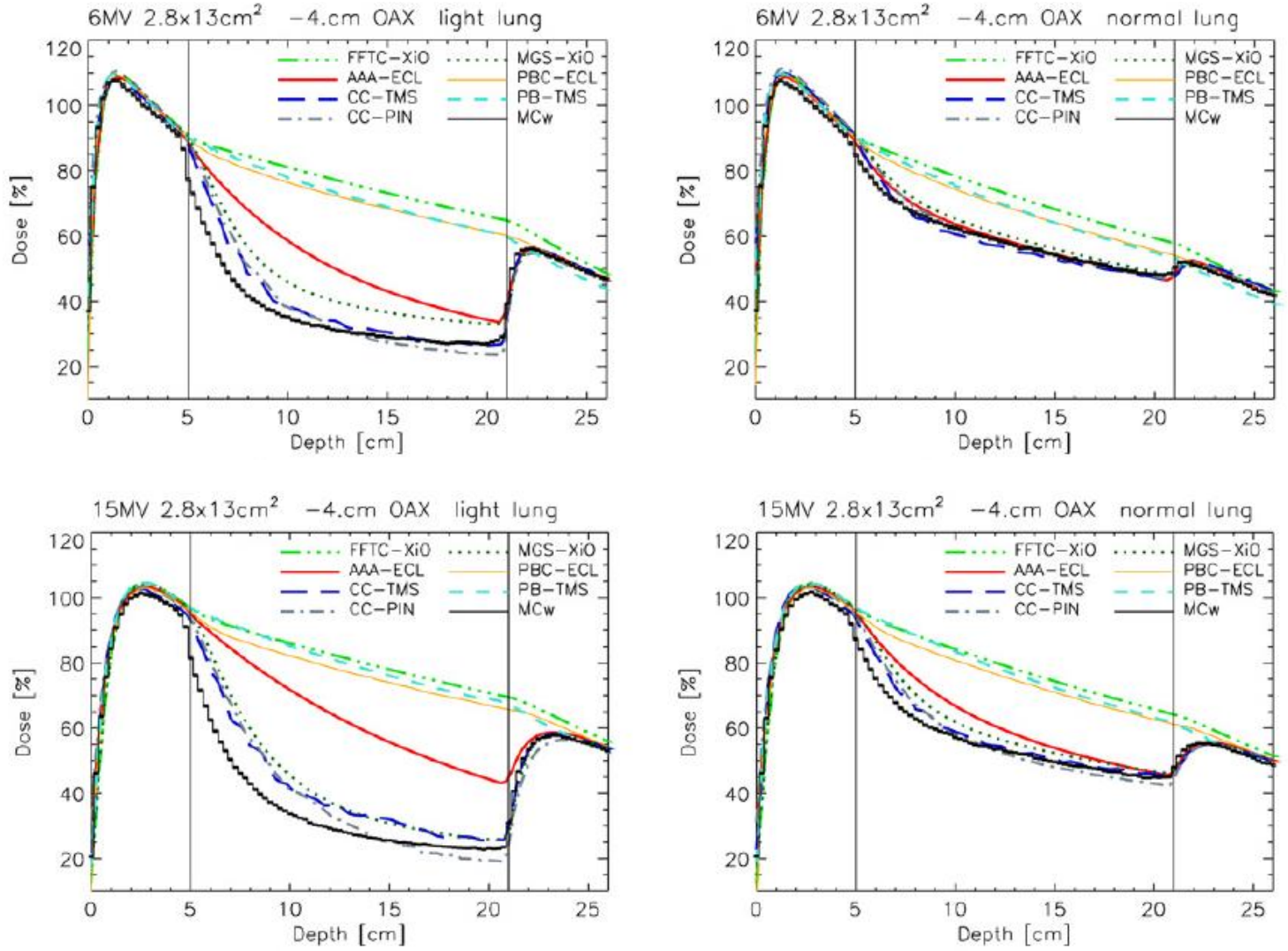

Fogliata A et al (2007) Phys Med Biol 52, 1363-85.

Approximations in dose calculation

Comparison of methods (pencil kernel, AAA, point kernel, MC)

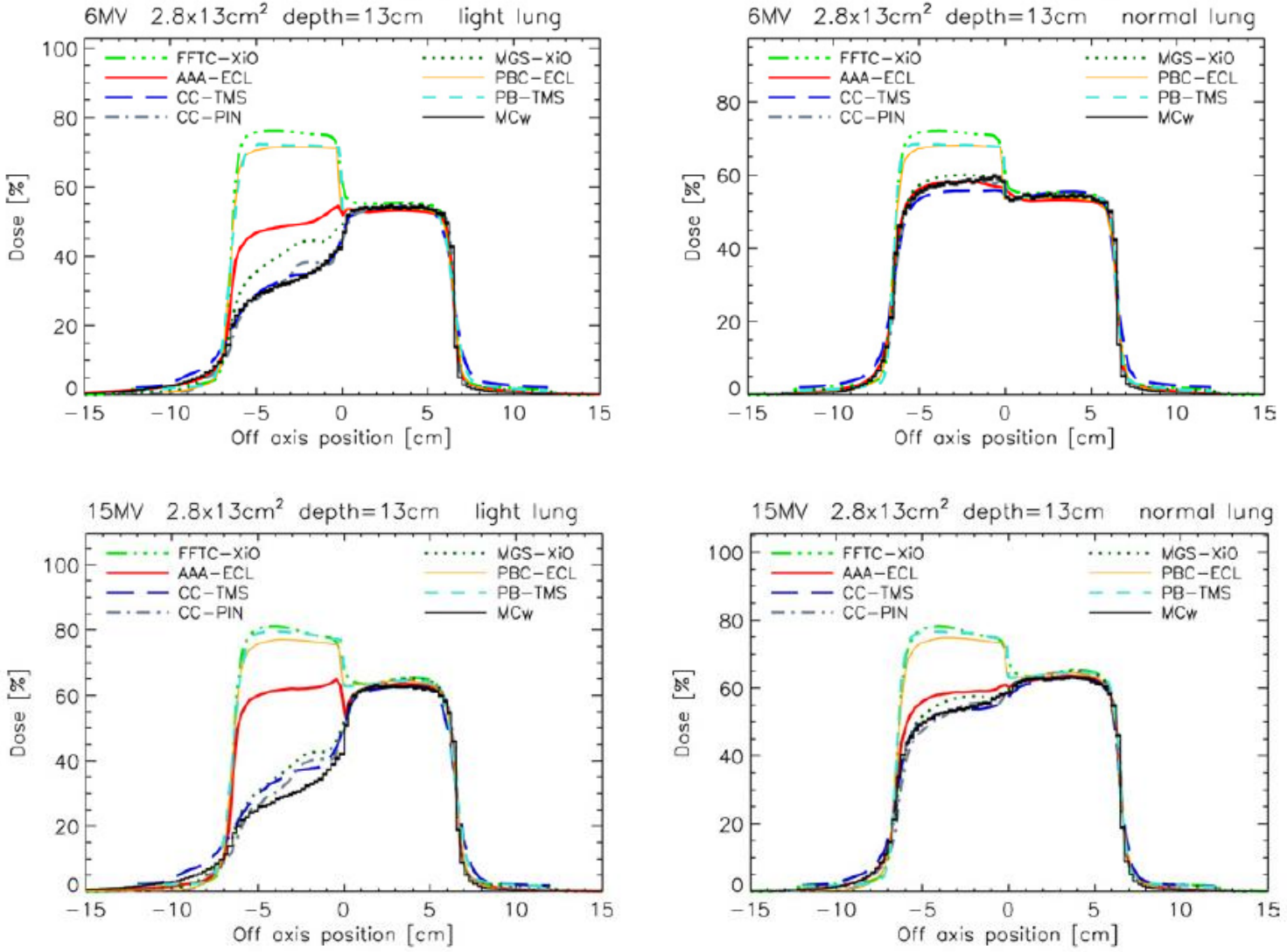

Fogliata A et al (2007) Phys Med Biol 52, 1363-85.

Approximations in dose calculation

Comparison of methods (pencil kernel, AAA, point kernel, MC)

15 MV photons

(Dose contr. normalization)

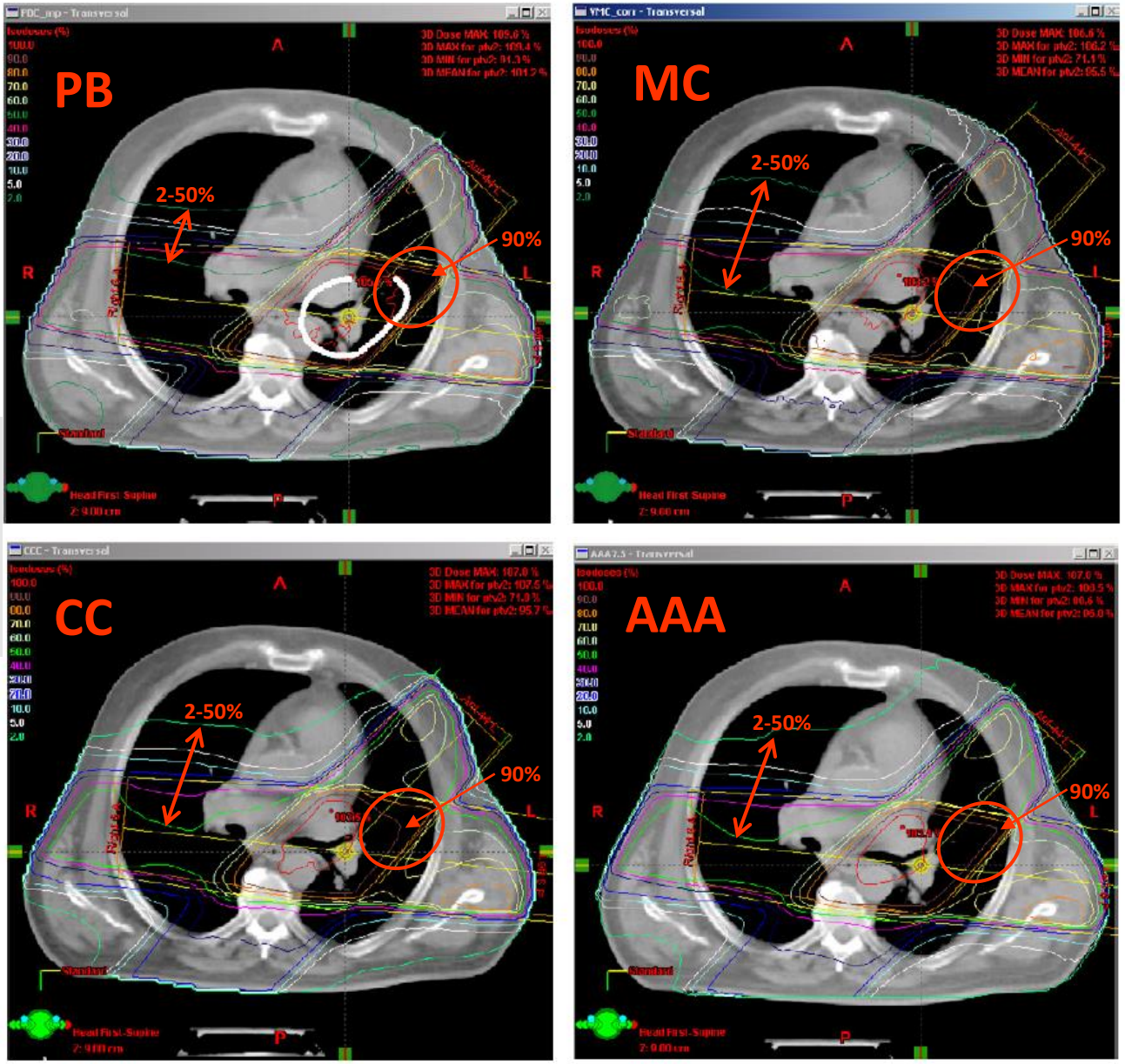

Hasenbalg F (2007) *Phys Med Biol. 52*, 3679-91

Approximations in dose calculation

Comparison of methods (pencil kernel, AAA, point kernel, MC)

Cumulative DVH for PTV and left lung (case from previous page)

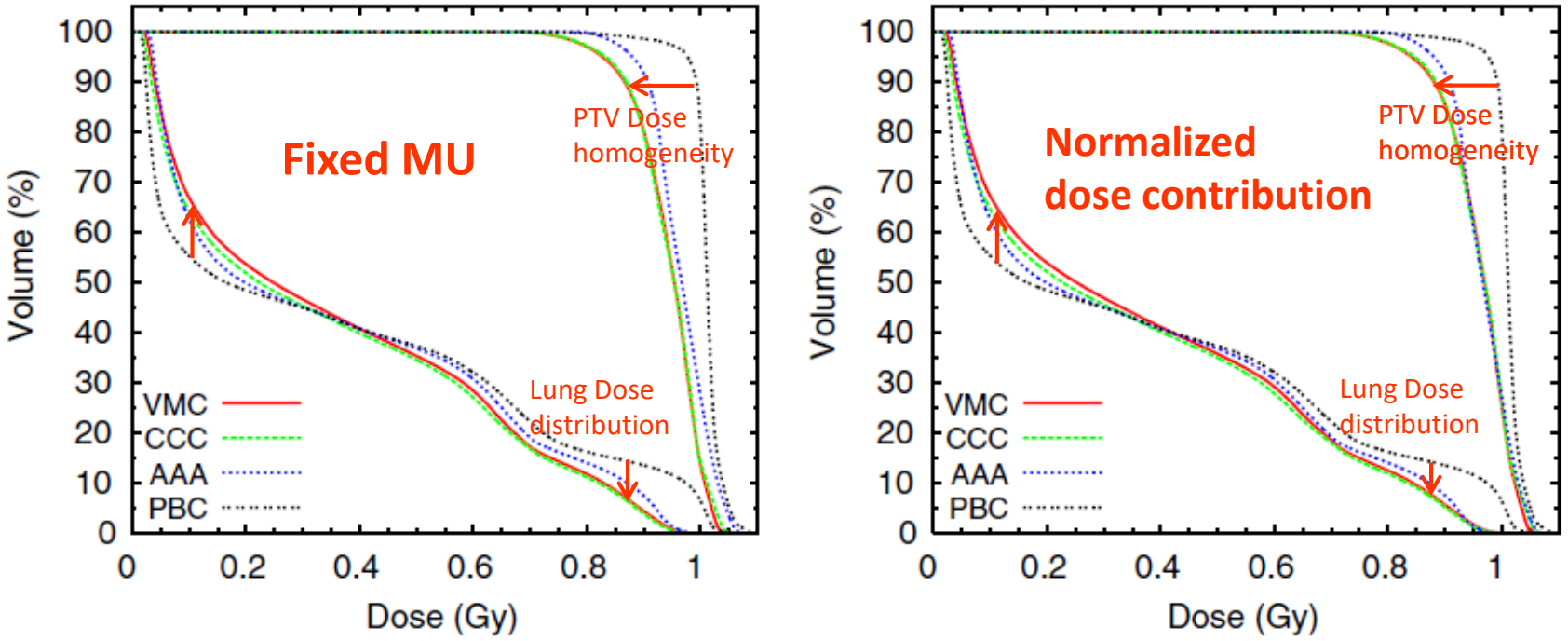

Hasenbalg F (2007) *Phys Med Biol. 52*, 3679-91

Approximations in dose calculation

Comparison of methods (pencil kernel, AAA, point kernel, MC)

6 MV photons

(Dose contr. normalization)

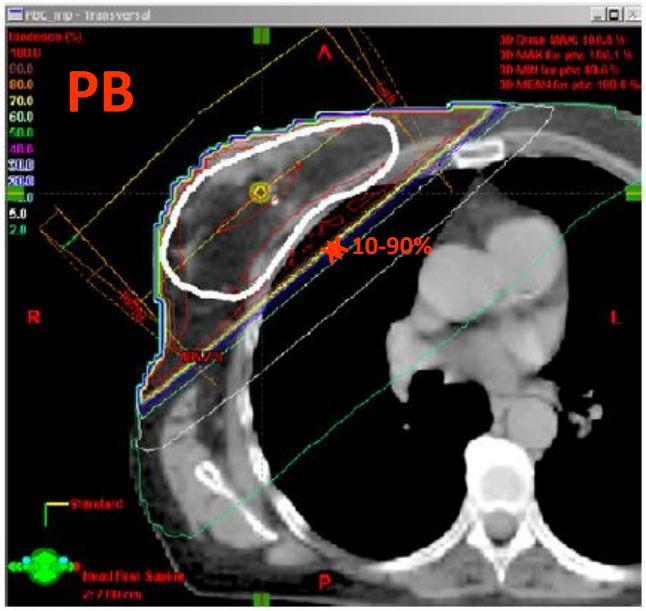

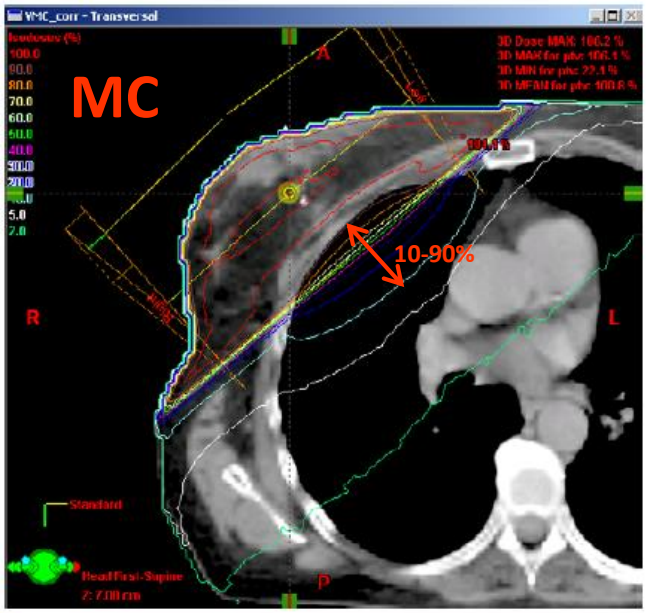

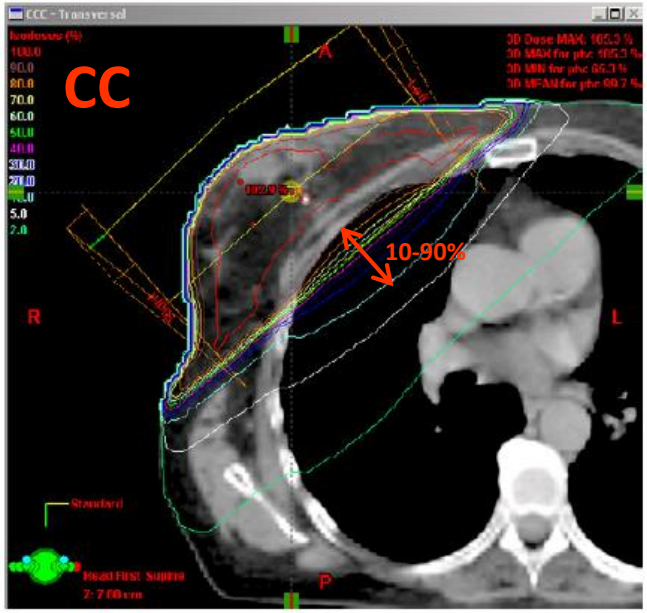

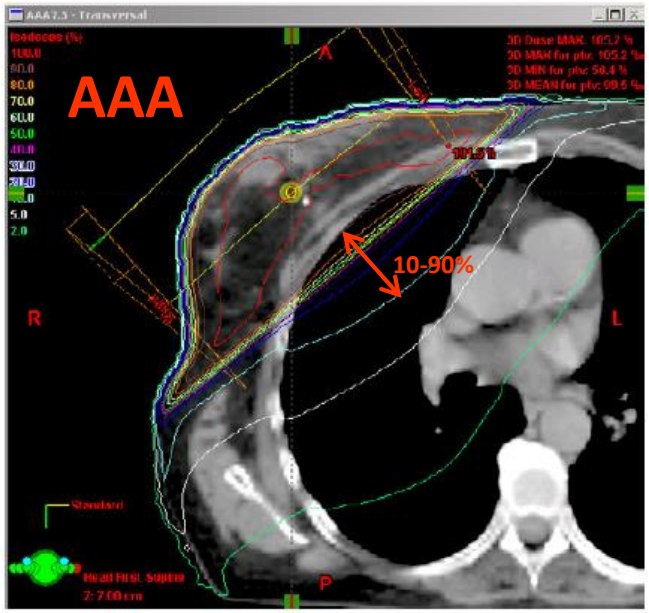

Hasenbalg F (2007) *Phys Med Biol. 52*, 3679-91

Future role of pencil kernel(beam) algorithms?
- fast algorithms for probabilistic planning!!

Planning paradigm	**Number of recalculations**
CRT forward	1
PTV based IMRT	100
Probabilistic planning	100000

Finally, the primary dose perturbation factor is given by

$$C_{\mathrm{p}}^{i}(\boldsymbol{r}) = \frac{\widetilde{\Psi}_{\mathrm{p}}^{i}(x,y) \otimes \frac{p_{\mathrm{p}}}{\rho}}{\Psi^{\infty}(x,y) \otimes \frac{p_{\mathrm{p}}}{\rho}}.$$

The correction factor for the scattered component,

$$C_{\mathrm{s}}^{i}(\boldsymbol{r}) = \frac{\widetilde{\Psi}_{\mathrm{s}}^{i}(x,y) \otimes \frac{p_{\mathrm{s}}}{\rho}}{\Psi^{\infty}(x,y) \otimes \frac{p_{\mathrm{s}}}{\rho}},$$

….a speedup of over 1000 times compared to the full pencil kernel calculations. The speedup versus collapsed cone would be greater…

Tilly and Ahnesjö (2015). Phys. Med. Biol. 60: 5439-54.

Role of pencil kernel(beam) algorithms?
- optimization!

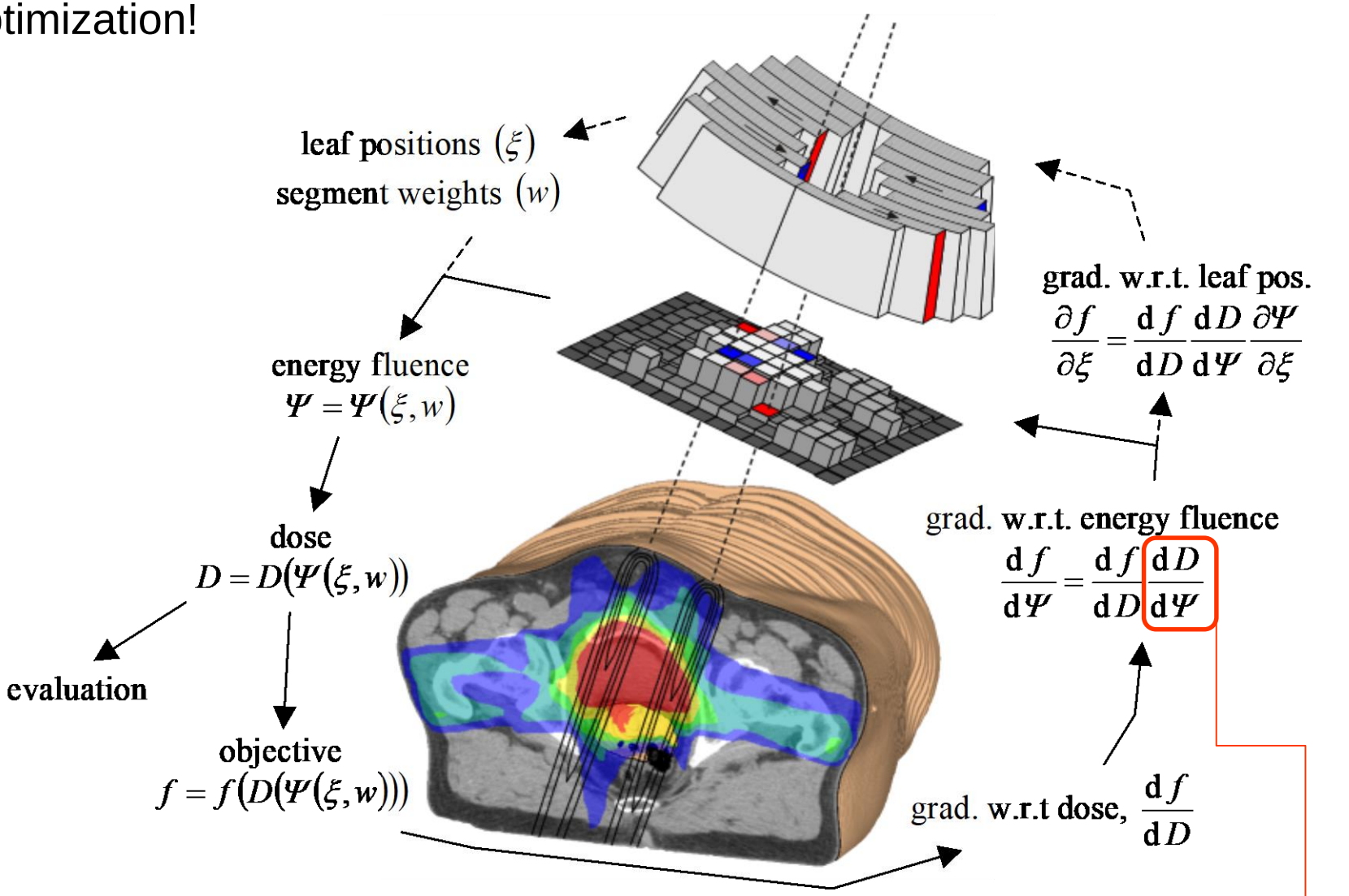

Pencil kernel!

First appearance

Schoknecht, G. (1971). "Die Beschreibung von Strahlenfeldern durch Separierung von Primär- und Streustrahlung IV. Berechnung von Streuverteilungen für parallele Photonenstrahlenfelder." Strahlentherapie 141(3): 326-331.

Equivalent field derivation

Bjärngard, B. E. and R. L. Siddon (1982). "A note on equivalent circles, squares, and rectangles." Medical Physics 9(2): 258-260.

How to apply in TPS

Mohan, R. and C. S. Chui (1987). "Use of fast Fourier transforms in calculating dose distributions for irregularly shaped fields for three-dimensional treatment planning." Med Phys 14(1): 70-77.

Ahnesjö, A., M. Saxner and A. Trepp (1992). "A pencil beam model for photon dose calculation." Med Phys 19(2): 263-273. **Oncentra**

Bourland, J. D. and E. L. Chaney (1992). "A finite-size pencil beam model for photon dose calculations in three dimensions." Medical Physics 19(6): 1401-1412.

Bortfeld, T., W. Schlegel and B. Rhein (1993). "Decomposition of pencil beam kernels for fast dose calculations in three-dimensional treatment planning." Medical Physics 20(2): 311-318. **Voxelplan, RayStation**

Storchi, P. and E. Woudstra (1996). "Calculation of the absorbed dose distribution due to irregularly shaped photon beams using pencil beam kernels derived form basic beam data." Physics in Medicine & Biology 41(4): 637-656. **Cadplan**

Ulmer, W. and Harder, D. (1995) "A Triple Gaussian Pencil Beam Model for Photon Beam Treatment Planning", Zeit. Med. Physik 5 25–30 **AAA**

Tillikainen, L. Siljamäki, L., Helminen, H., Alakuijala, J., and Pyyry, J., (2007) "Determination of parameters for a multiple-source model of megavoltage photon beams using optimization methods" Phys. Med. Biol. 52 1441–1467 **AAA**

Optimization vehicle

Gustafsson, A., B. K. Lind and A. Brahme (1994). "A generalized pencil beam algorithm for optimization of radiation therapy." Medical Physics 21(3): 343-356.

Limitations

Knöös, T., A. Ahnesjö, P. Nilsson and L. Weber (1995). "Limitations of a pencil beam approach to photon dose calculations in lung tissue." Phys Med Biol 40(9): 1411-1420.

Experimental kernel data

Ceberg, C. P., B. E. Bjarngard and T. C. Zhu (1996). "Experimental determination of the dose kernel in high-energy x-ray beams." Medical Physics 23(4): 505-511.

QA usage

Nyholm, T., J. Olofsson, A. Ahnesjö and M. Karlsson (2006). "Photon pencil kernel parameterisation based on beam quality index." Radiother Oncol 78(3): 347-351.

Probalistic planning

Tilly, D. and A. Ahnesjö (2015). "Fast dose algorithm for generation of dose coverage probability for robustness analysis of fractionated radiotherapy." Physics in Medicine and Biology 60(14): 5439-5454.

Remark:

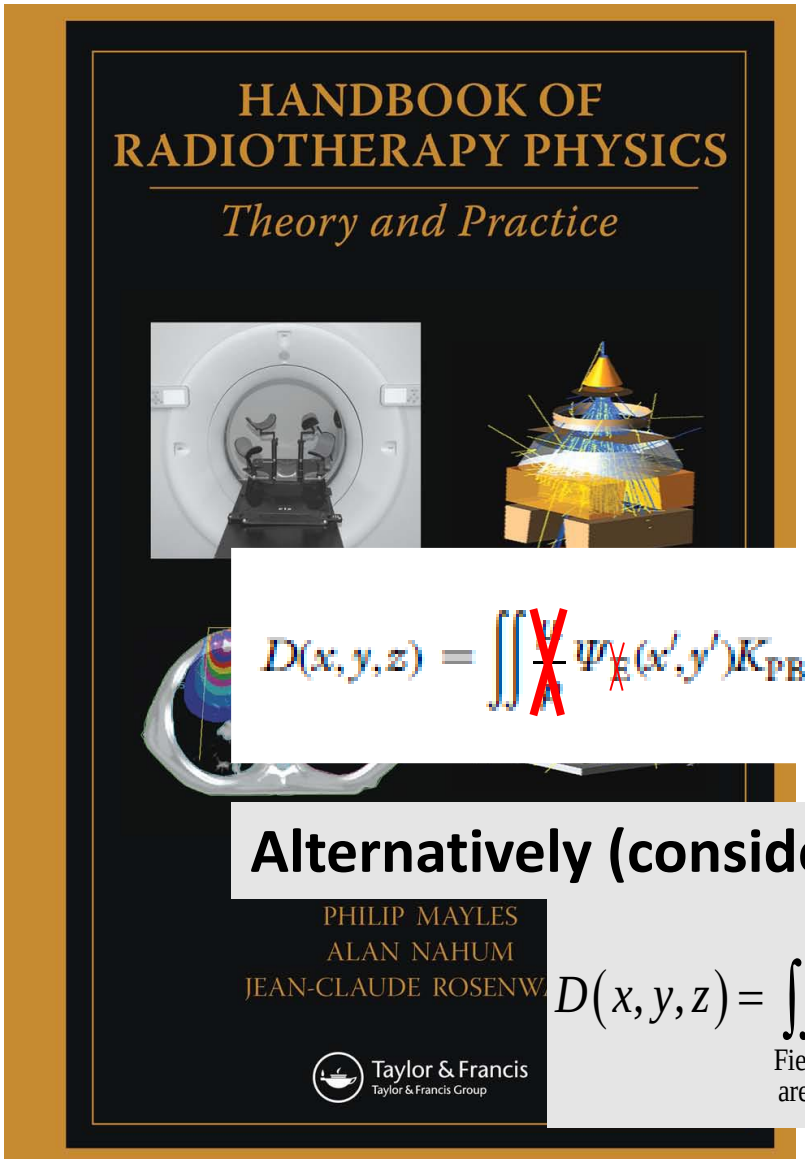

P574, equation missprint:

$$D(x,y,z) = \iint \frac{1}{A} \Psi_E(x',y') K_{PB}(x-x', y-y', z)\,dx'dy' \qquad (26.22)$$

Alternatively (considering energy spectrum):

$$D(x,y,z) = \underbrace{\iint}_{\text{Field area}} \underbrace{\int}_{\text{Beam spectrum}} \Psi_E(x',y') \cdot K_{PB}(E, x-x', y-y', z)\,dE\,dx'\,dy'$$

Conclusions

- Several different methods are available when characterizing, parameterizing and integrating pencil kernels

- pencil kernel implementations goes with a number of approximations and limitations

- Pencil kernel algorithms are widely used in clinical treatment planning systems for photon dose calculations. Their popularity is related to the fact that they offer a good **compromise** between flexibility, accuracy and speed.

Electron modelling
An overview

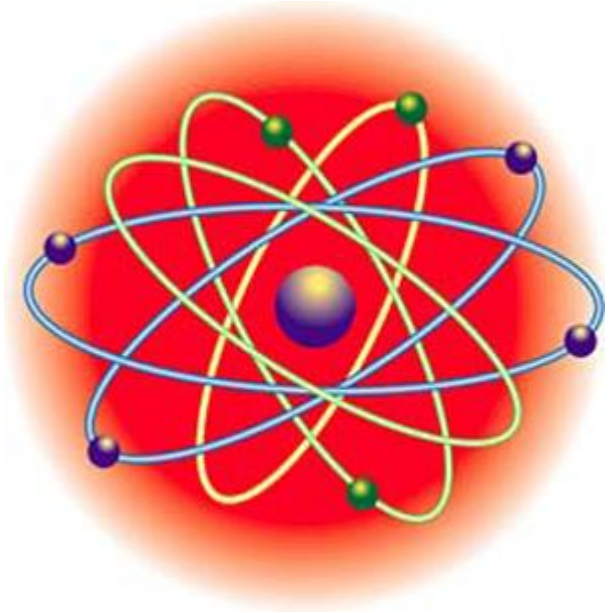

T Knöös

With some help from the faculty

Learning objectives

- To understand what beam models and dose engines we are using for treatment planning and dose calculation with electrons
  - Pencil Beams models
  - Monte Carlo simulation
- Comparison and Performance

Patient dose calculation

PENCIL BEAM METHODS…

Pencil beam dose kernels in water – MC generated

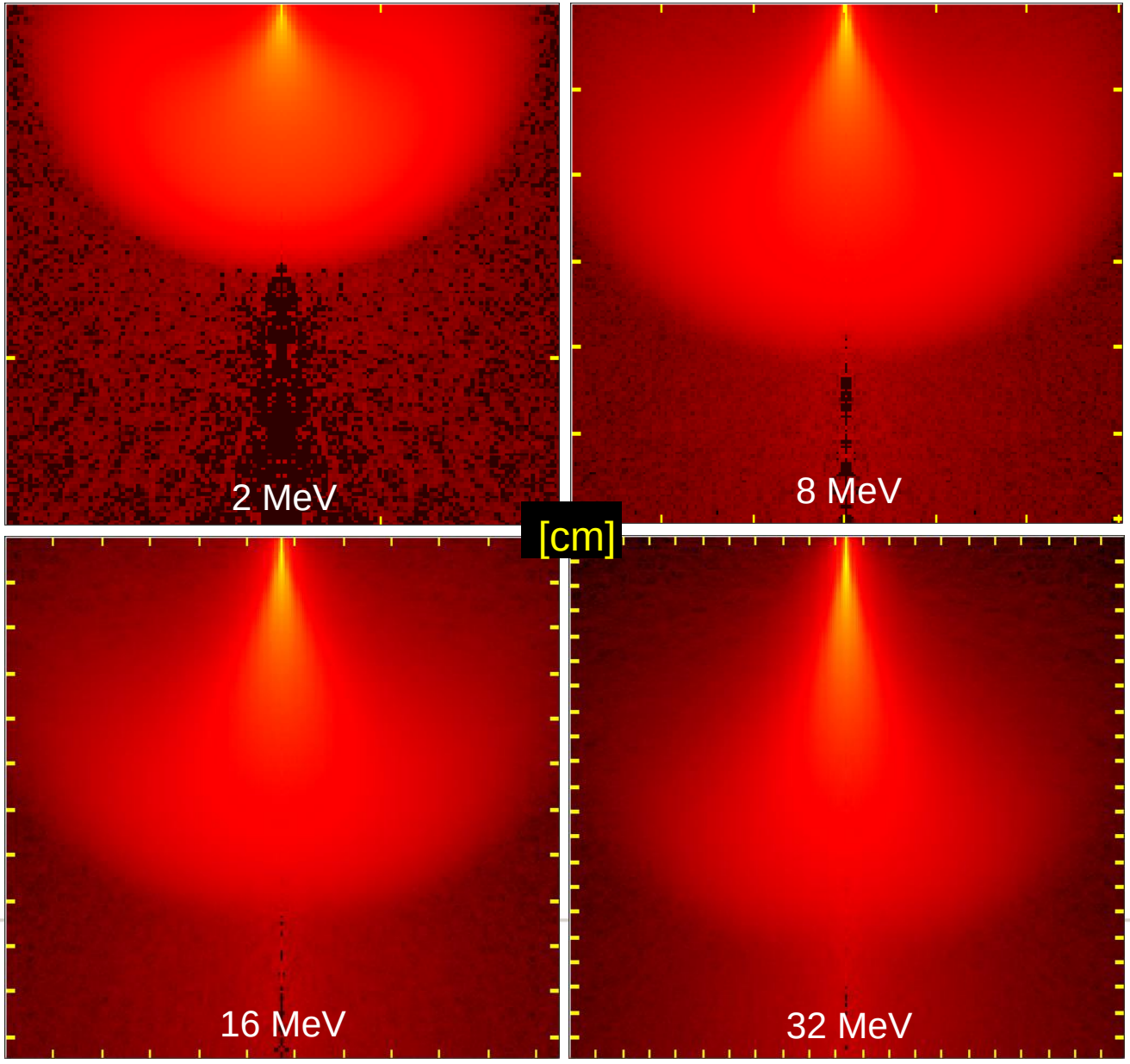

Length scale not the same

From A Ahnesjö

Fermi-Eyges theory for pencil beam propagation in media (incl slab media)

Fermi-Eyges theory describes the broadening of a pencil beam due to multiple scattering along its path. The result is Gaussian distributions of the electrons characterized by:

- Mean square of scattering angle: $\overline{\theta^2}$
- Mean radius-angle covariance: $\overline{r\theta}$
- Mean square of radius: $\overline{r^2}$

In a stack of slabs one gets, after slab *i*:

$$\overline{\theta_i^2} = \overline{\theta_{i-1}^2} + h_i T_i \left(\Sigma_{i-1} + k h_i S_i / 2 \right)$$

$$\overline{r\theta}_i = \overline{r\theta}_{i-1} + h_i \left[\overline{\theta_{i-1}^2} + \frac{1}{2} h_i T_i \left(\Sigma_{i-1} + k h_i S_i / 3 \right) \right]$$

$$\overline{r_i^2} = \overline{r_{i-1}^2} + h_i \left\{ 2\overline{r\theta}_{i-1} + h_i \left[\overline{\theta_{i-1}^2} + \frac{1}{3} h_i T_i \left(\Sigma_{i-1} + k h_i S_i / 4 \right) \right] \right\}$$

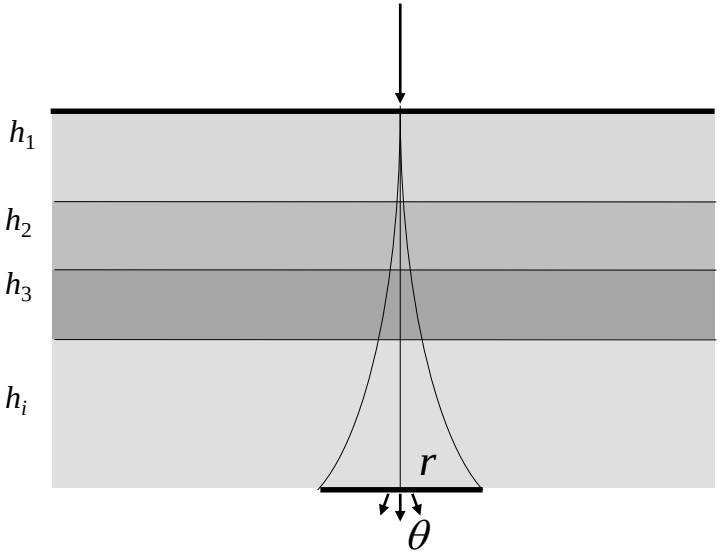

where

h_i thickness of stack *i*

T_i scattering power of stack *i*

S_i stopping power of stack *i*

$\Sigma_{i-1} = \Sigma_i + k h_i S_i$

k a scaling constant to increase T with depth (Brahme-Lax)

Mix of Hogstrom and Brahme/Lax papers

Pictorial description of pencil beam modeling

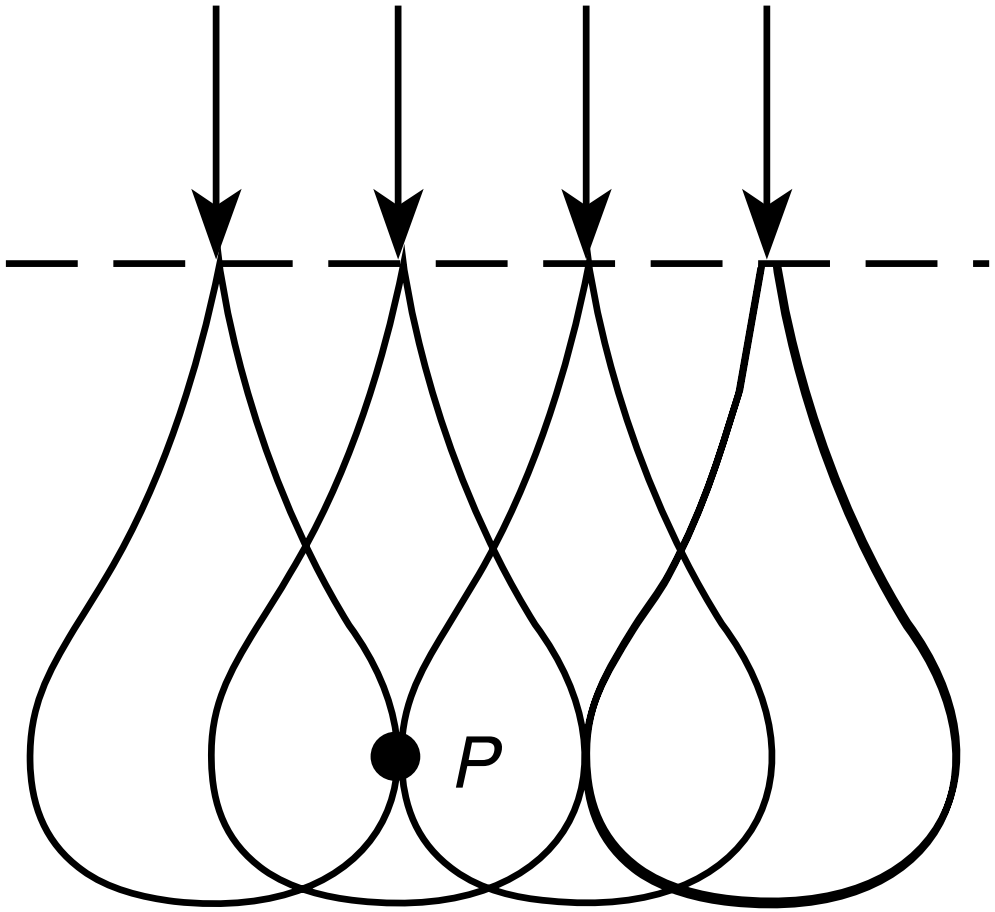

From Handbook of Radiotherapy Physics
Ed Mayles, Nahum and Rosenwald

Fermi-Eyges for electrons

- Referring to a Cartesian coordinate system (x,y,z) and an electron, incident perpendicularly on a medium at (0,0,0) in the z direction, the Fermi–Eyges expression for the probability of finding the electron at depth z with displacement between x and x+dx , y and y+dy is

$$p(x,y,z)\mathrm{d}x\,\mathrm{d}y = \frac{1}{2\pi\sigma^2_{\mathrm{MCS}}}\exp\left[-\frac{x^2+y^2}{2\sigma^2_{\mathrm{MCS}}}\right]\mathrm{d}x\,\mathrm{d}y$$

- Where

$$\sigma^2_{\mathrm{MCS}} = \frac{1}{2}\int_0^z (z-u)^2 T(u)\mathrm{d}u$$

- $T(u)$ is the linear scattering power of the medium at depth u
- MCS is multiple coulomb scattering

From Handbook of Radiotherapy Physics
Ed Mayles, Nahum and Rosenwald

Multiple Coulumb Scattering

- Particles (electrons) passing through matter suffer repeated elastic Coulomb scattering from nuclei
- Considering that usually nuclei have mass greater than the incoming particle, the energy transfer is negligible but each scattering centre adds a small deviation to the incoming particle's trajectory also

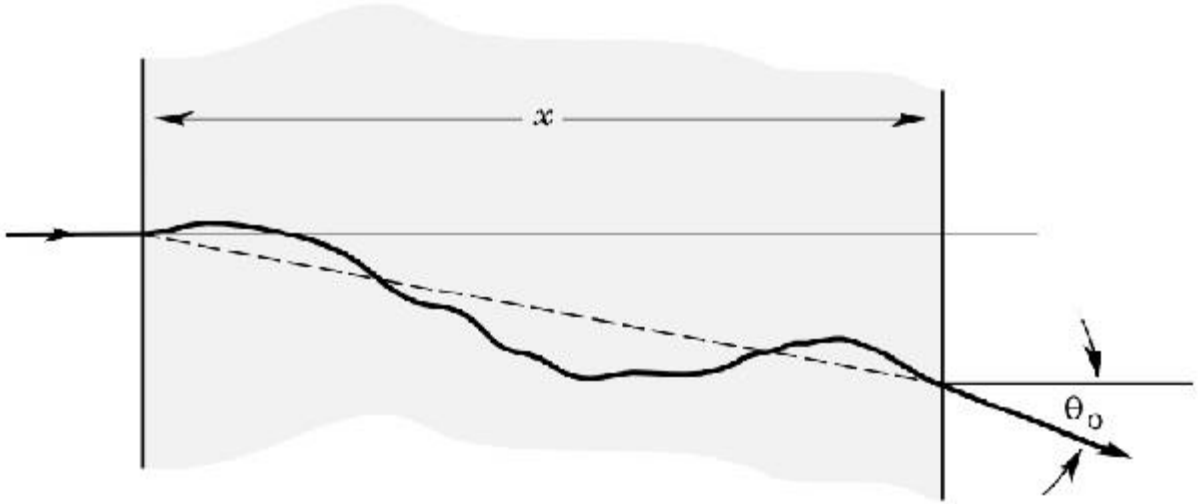

Fermi-Eyges for electrons

- Can be divided as $p(x,y,z)=p(x,z)\,p(x,y)$ where both are given as

$$p(x,z)\mathrm{d}x = \frac{1}{\sqrt{2\pi}\sigma}\exp\frac{-x^2}{2\sigma^2}\mathrm{d}x$$

- This is a Gaussian, or normal distribution, and s can be identified as the standard deviation , which is a measure of the width of the distribution. As the depth increases, σ_{MCS} increases and the pencil spreads out.
- Integration of a Gaussian is written with the erf function

$$\mathrm{erf}(x) \equiv \frac{2}{\sqrt{\pi}}\int_0^x \mathrm{e}^{-t^2}\mathrm{d}t$$

From Handbook of Radiotherapy Physics
Ed Mayles, Nahum and Rosenwald

Fermi-Eyges for electrons

- After some algebra you get

$$N(x,y,z) = \frac{1}{4}\left[\mathrm{erf}\left(\frac{A-x}{\sqrt{2}\sigma_{\mathrm{MCS}}}\right) + \mathrm{erf}\left(\frac{A+x}{\sqrt{2}\sigma_{\mathrm{MCS}}}\right)\right]\left[\mathrm{erf}\left(\frac{B-y}{\sqrt{2}\sigma_{\mathrm{MCS}}}\right) + \mathrm{erf}\left(\frac{B+y}{\sqrt{2}\sigma_{\mathrm{MCS}}}\right)\right]$$

- Recalling that erf(x) is very close to unity for x>2, it can be seen that N(x,y,z)=1 if both x and y are more than about 3 times the σ_{MCS} from the field edges, i.e. the dose profile is flat away from the edges of a broad beam, exactly as one would expect.
- The above result also implies that N (x,y,z) is constant with depth, i.e. the build-up due to scattering is not predicted.
- The Fermi–Eyges theory do not account for electron loss.
  - An empirical correction factor is necessary in order to reproduce measured depth–dose curves.

From Handbook of Radiotherapy Physics
Ed Mayles, Nahum and Rosenwald

How to get the dose distribution?

- To get a depth dose curve one has to correct the planar fluence of electrons

$$d(x,y,z) = p(x,y,z) \cdot g(z)$$

- The weighting factor g (z) is determined such that the dose as a function of depth on the central axis for a given field size exactly equals the measured central axis depth dose
  - Corrected to infinite SSD
  - Bremsstrahlung dose, is subtracted (assumed constant at all depths less than Rp

$$g(z) = \frac{D_{\text{meas,e}^-}(0,0,z)}{\text{erf}\left[\frac{A(1+z/\text{SSD})}{\sqrt{2}\sigma_{\text{med}}(z)}\right]\text{erf}\left[\frac{B(1+z/\text{SSD})}{\sqrt{2}\sigma_{\text{med}}(z)}\right]}$$

From Handbook of Radiotherapy Physics
Ed Mayles, Nahum and Rosenwald

Further additions

- The SSD dependence have to be added
- The dose due to bremsstrahlung was originally subtracted from the measured depth–dose curve.
  - This must now be added back to the electron dose, after putting back the inverse square law dependence.
  - It is assumed that the dose beyond the depth of the practical range is entirely due to photons.

From Handbook of Radiotherapy Physics
Ed Mayles, Nahum and Rosenwald

The widening of the pencil is limited

- The pencil-beam width (σ_{MCS}) as a function of depth agrees well with experiment at small and moderate depths.
- Then it continues to increase, whereas in reality it goes through a maximum and finally decreases.
- This is managed by the *g(x)* function or has to managed in other ways in some systems
- This is due to the reduction of the number of electrons in the beam at large depths due to range straggling

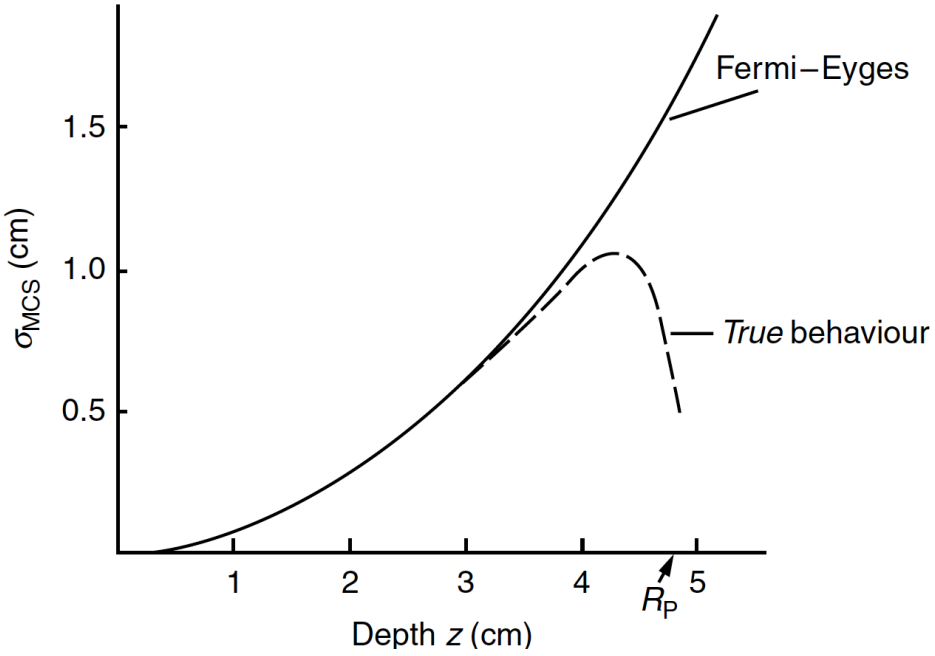

From Handbook of Radiotherapy Physics
Ed Mayles, Nahum and Rosenwald

Beam model plus dose engine (pencil beam)

Starting point

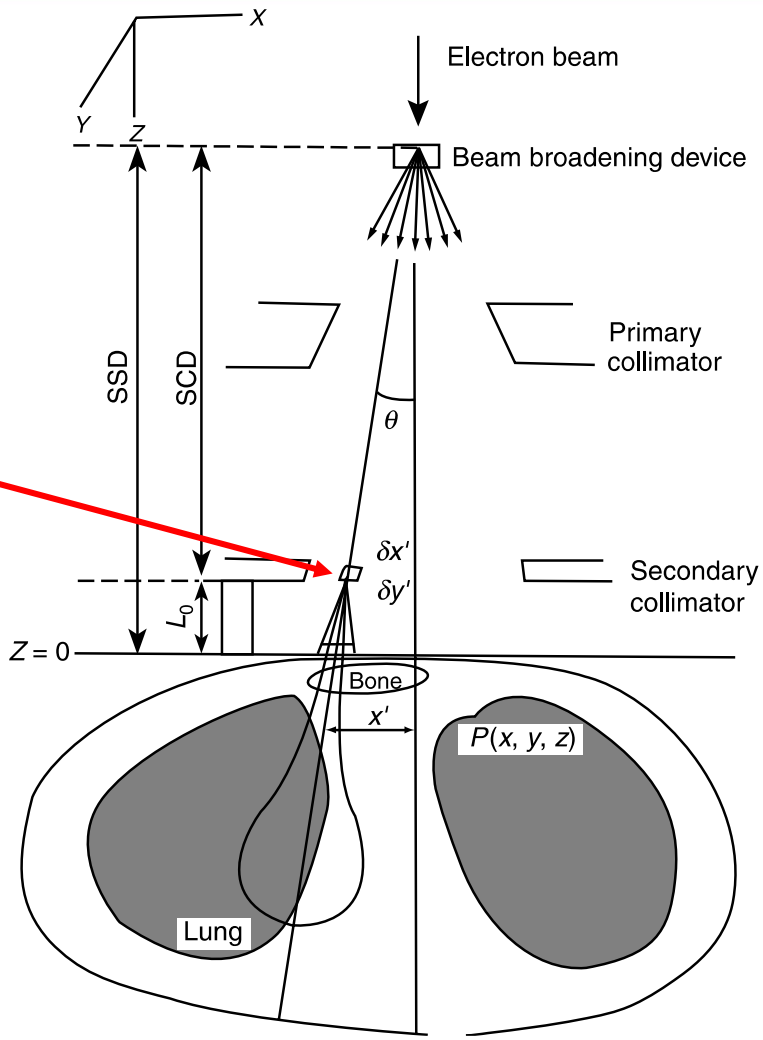

Hogstrom et al., Phys. Med. Biol., 26, 445–459, 1981.

The semi-infinite slab approximation in tissue

The pencil beams are propagated through tissue as if it was made of a stack of slabs, each with the local heterogeneities along each ray extended laterally into homogeneous slabs.

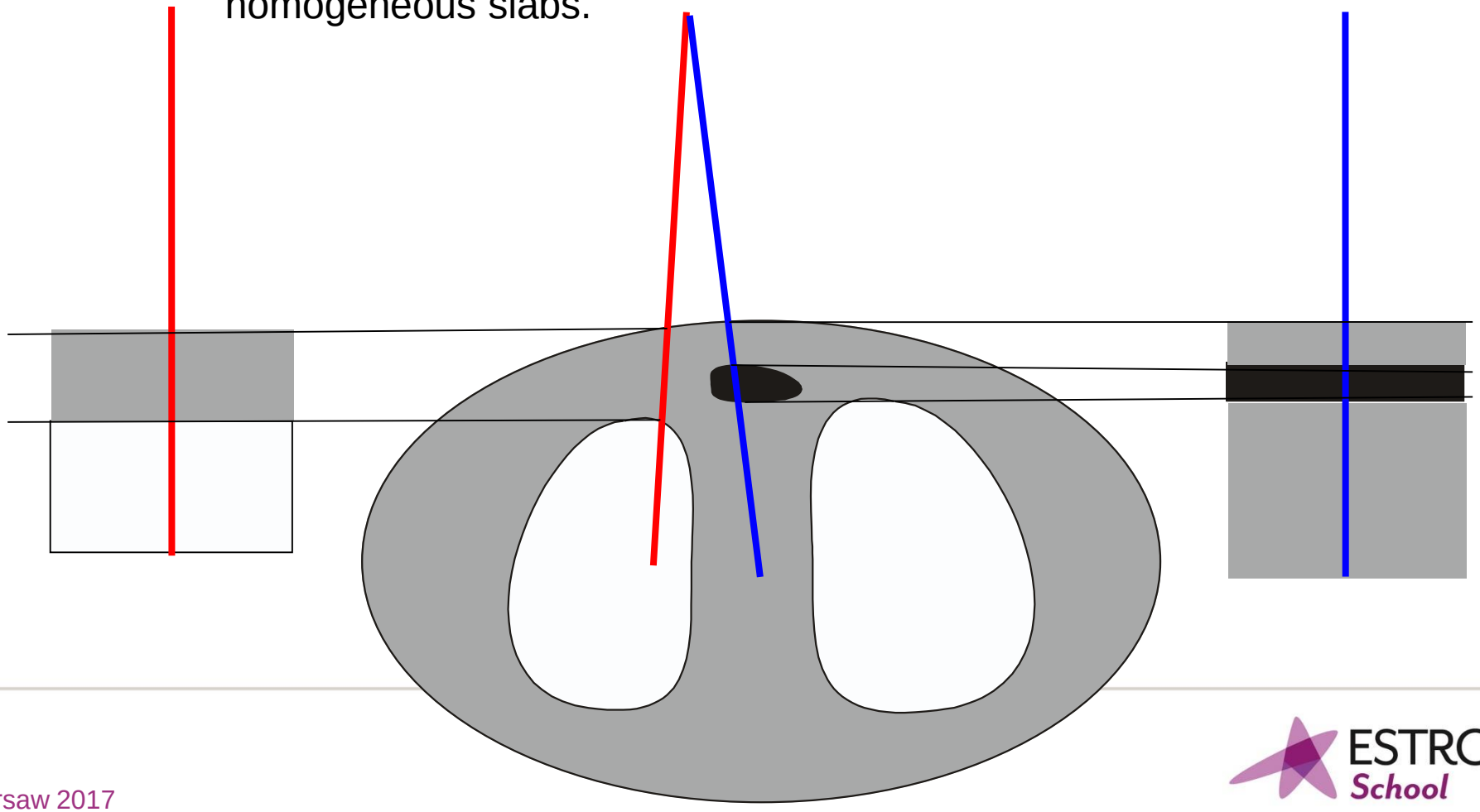

Pencil Beam example, penumbra modeling

At calculation points well inside field limits, PB width set to zero at patient level not to wash out effects from heterogeneities

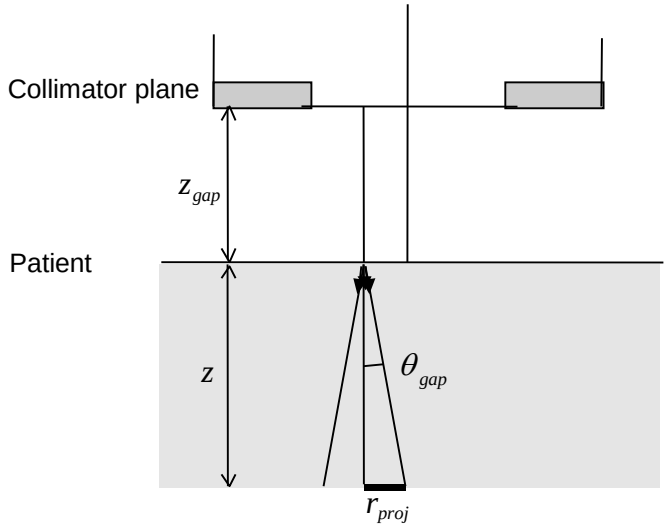

At calculation points in penumbra region, PB width set to zero at collimator level to correctly model penumbra width including effects of in air scattering

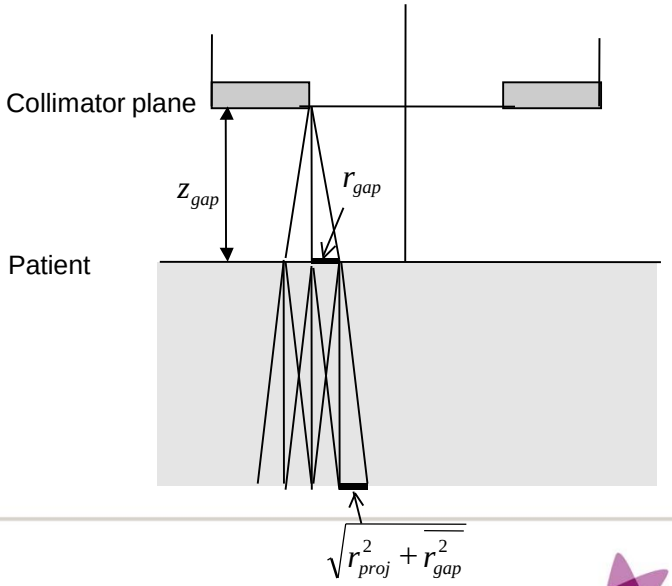

Hot and cold spots

In between regions of much scattered pencils and less scattered pencils, hot and cold spots will occur due to varying degree of lateral equilibrium.

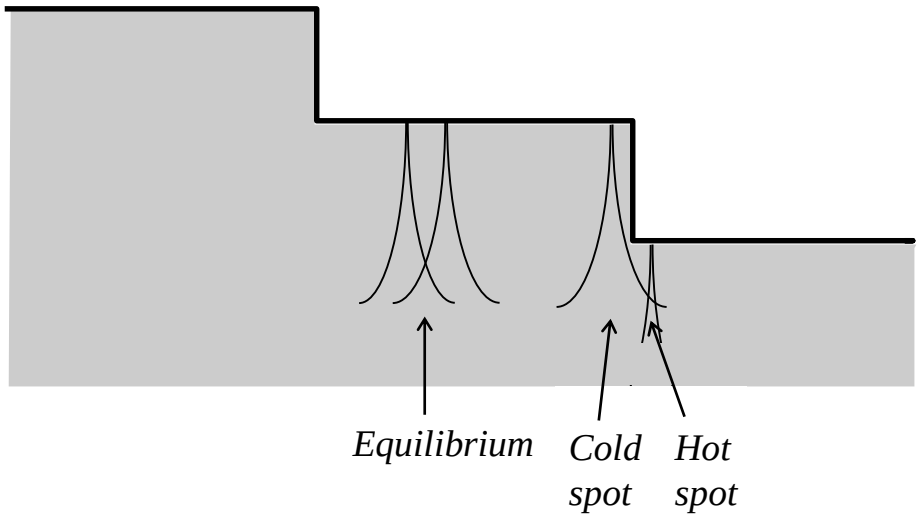

Unresolved issues with electron pencil beam models

Beam modeling:

PB methods assume Gaussian characteristics of the incident beam. Hence, influence from “non Gaussian” features (collimator scattering, etc) yield profile errors and make output factors hard to calculate (has to be table lookup driven).

Penumbra modeling through manipulation of incident pencil width may wash out effects of heterogeneities.

Heterogeneities:

Heterogeneities are well modeled at the first part of the depth range (since voxels are larger than the FE pencil width).

At the end of the electron range, effects of localized heterogeneities (smaller than the FE pencil width using semi-infinite slab approximation) get washed out PB by models. “Redefinition” and “phase space evolution” models fix that, to the cost of CPU&memory…

MONTE CARLO METHODS

Rationale for Monte Carlo dose calculation for electron beams

Slide from Cygler

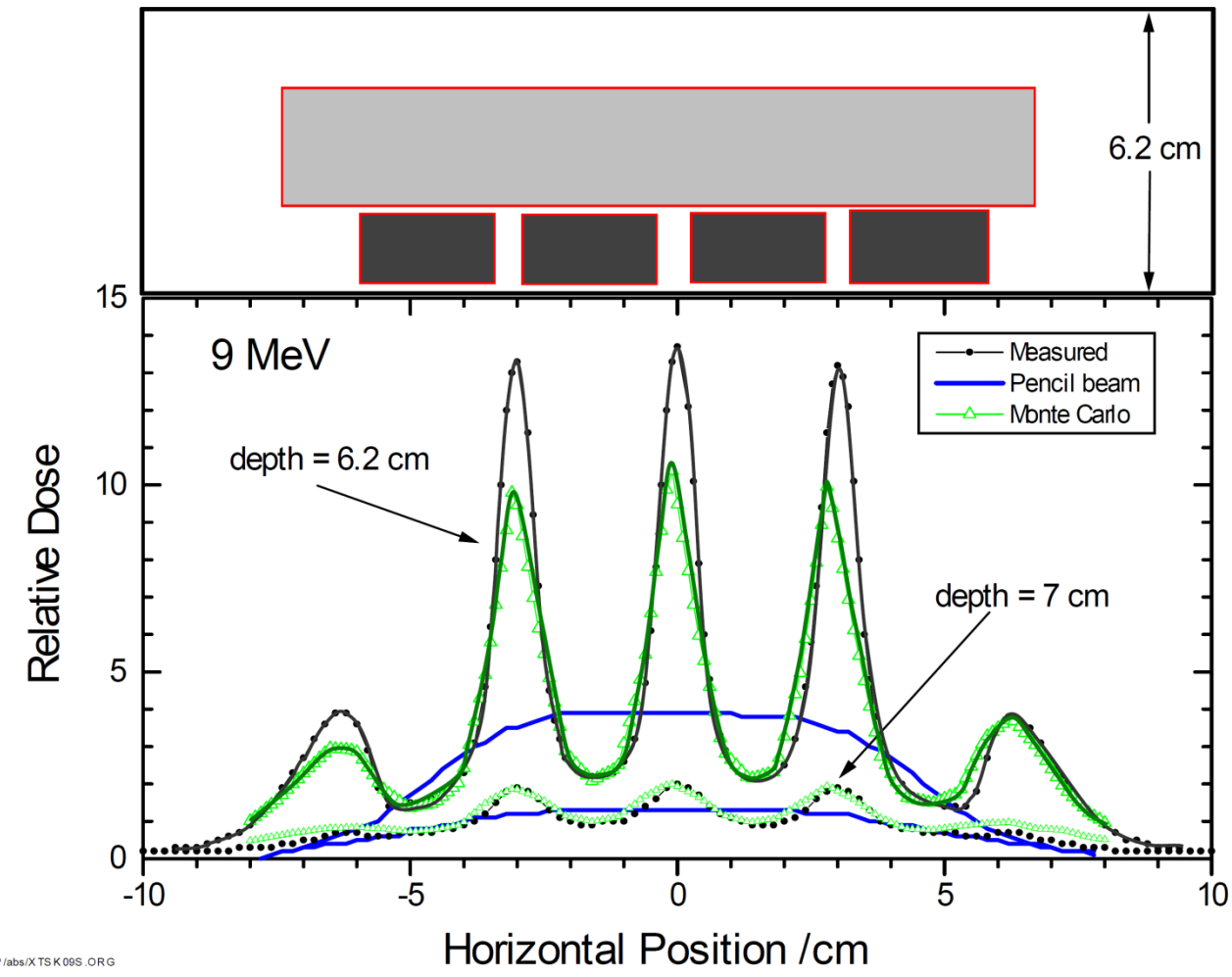

Ding, G. X., et al, Int. J. Rad. Onc. Biol Phys. (2005) 63:622-633

Monte Carlo in commercial TPS

- Elekta MONACO
  - First commercial Monte Carlo treatment planning for electron beams
  - Implementation of Kawrakow's VMC++ Monte Carlo dose calculation algorithm (2000)
  - Handles electron beams from all clinical linacs

- Varian Eclipse eMC 2004
  - Based on Neuenschwander's MMC dose calculation algorithm (1992)
  - Handles electron beams from Varian linacs only

PATIENT DOSE ENGINES

VMC++

- VMC was developed by I. Kawrakow, M. Fippel and K. Friedrich with K. Ulm at the U of Leipzig, 1996
  - VMC originally only for electrons
  - Extended later by M.Fippel to photons - xVMC
  - Re-implemented in C++ by I. Kawrakow at NRC - VMC++
- Recent work implements a series of additional variance reduaction techniques for photons to gain in calculation time
  - Exact MS theory developed at NRC
  - Boundary crossing algorithm (BCA) allowing multi-voxel CH steps
  - Optimization of sampling algorithms
    - Generated with emphasis on filling the multidimensional space of interest in as uniform a way as possible
- Used in Elekta Monaco

VMC++ accuracy and speed

- Sub-percent agreement with EGSnrc
- Is about 100 times faster than BEAMnrc for linac head simulations
- Is 50-150 times faster than EGS4/PRESTA for electron and photon beam simulations in the patient geometry for comparable accuracy.
- CPU times for in-patient simulations (10x10 beam, 5 mm voxels, 2% statistical uncertainty):
  - ~30 seconds for electrons

Electron beam calculations - Monaco

Beam characterization

- Measure fluence profiles in air with removed applicator, field settings varied with the photon collimators
- Optimize source phase space parameters to fit measured profiles
- Generate source phase space electrons and propagate them with the photon collimators at preset values and the applicator mounted (no insert) to the exit phase space
- Parameterize the exit phase space

Run time calculations

- Generate exit phase space electrons, discard those who stem from areas blocked by the insert
- Add collimator scatter electrons and treatment head photons
- Propagate the generated particles into the patient

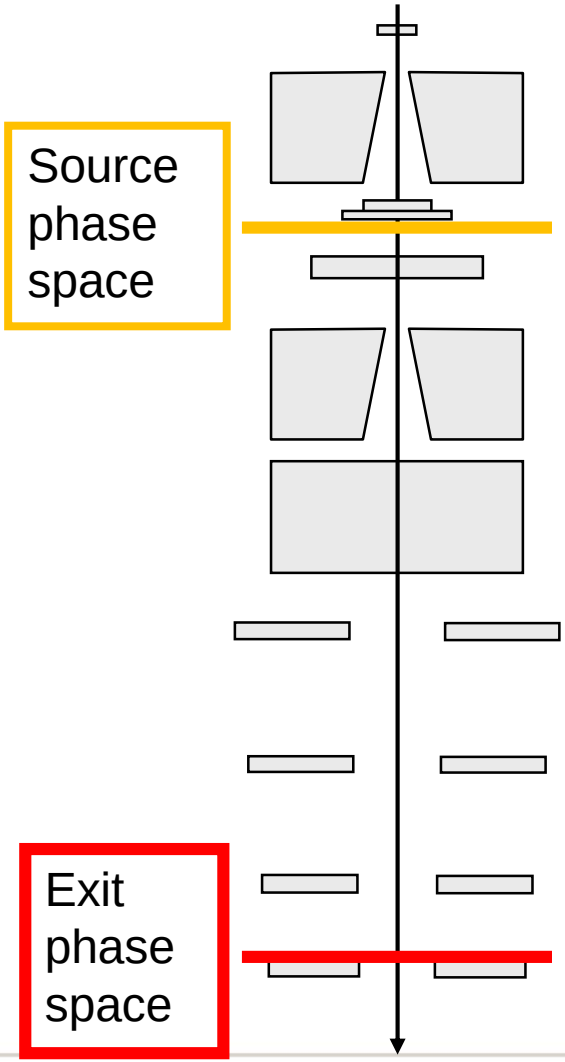

eMC Global MC input

- Local geometries are spheres of various sizes, material compositions and incident electron energies:
  - 5 materials: air, lung, water, lucite(PMMA) and solid bone
  - 5 sphere radii: 0.5, 1.0, 1.5, 2.0 and 3.0 mm
  - 30 incident energy values, between 0.2 and 25 MeV
- 200 000 electrons per sphere were simulated using Monte Carlo with EGSnrc Code System
- Results from simulations were collected to probability distribution functions (PDFs):
  - Exit point and direction of primary electron
  - Energy of primary electron
  - Secondary particles (e- & γ) and their energies

Macro Monte Carlo transport model in Eclipse

- An implementation of Local-to-Global (LTG) Monte Carlo:
- Local: Conventional MC simulations of electron transport performed in well defined local geometries ("kugels" or spheres).
  - Monte Carlo with EGSnrc Code System - PDF for "kugels"
  - 5 sphere sizes (0.5-3.0 mm)
  - 5 materials (air, lung, water, Lucite and solid bone)
  - 30 incident energy values (0.2-25 MeV)
  - PDF table look-up for "kugels"
  - This step is performed off-line.
- Global: Particle transport through patient modelled as a series of macroscopic steps, each consisting of one local geometry ("kugel")

A “kugel”

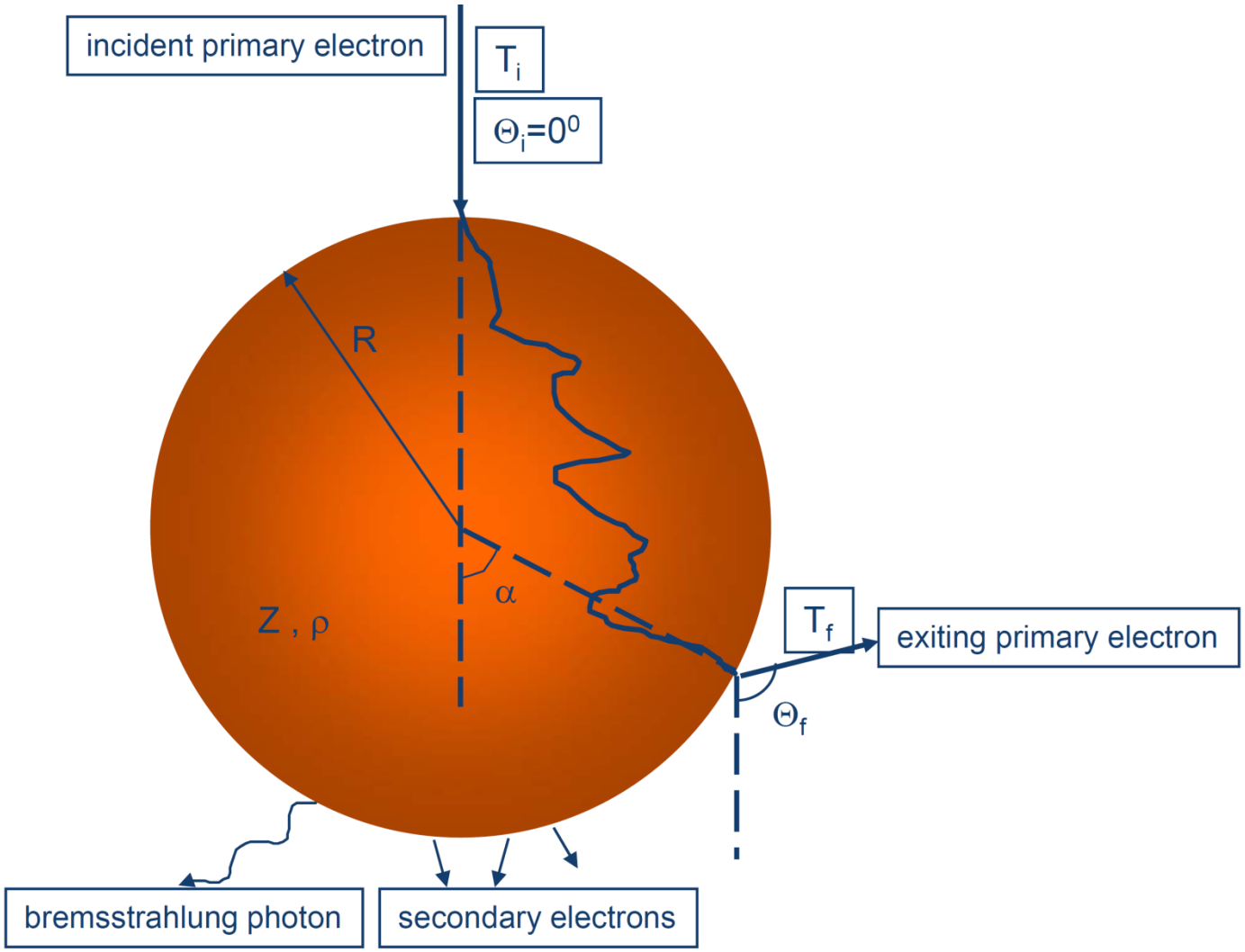

Kugel = sphere

MMC by Neuenschwander et al 1995

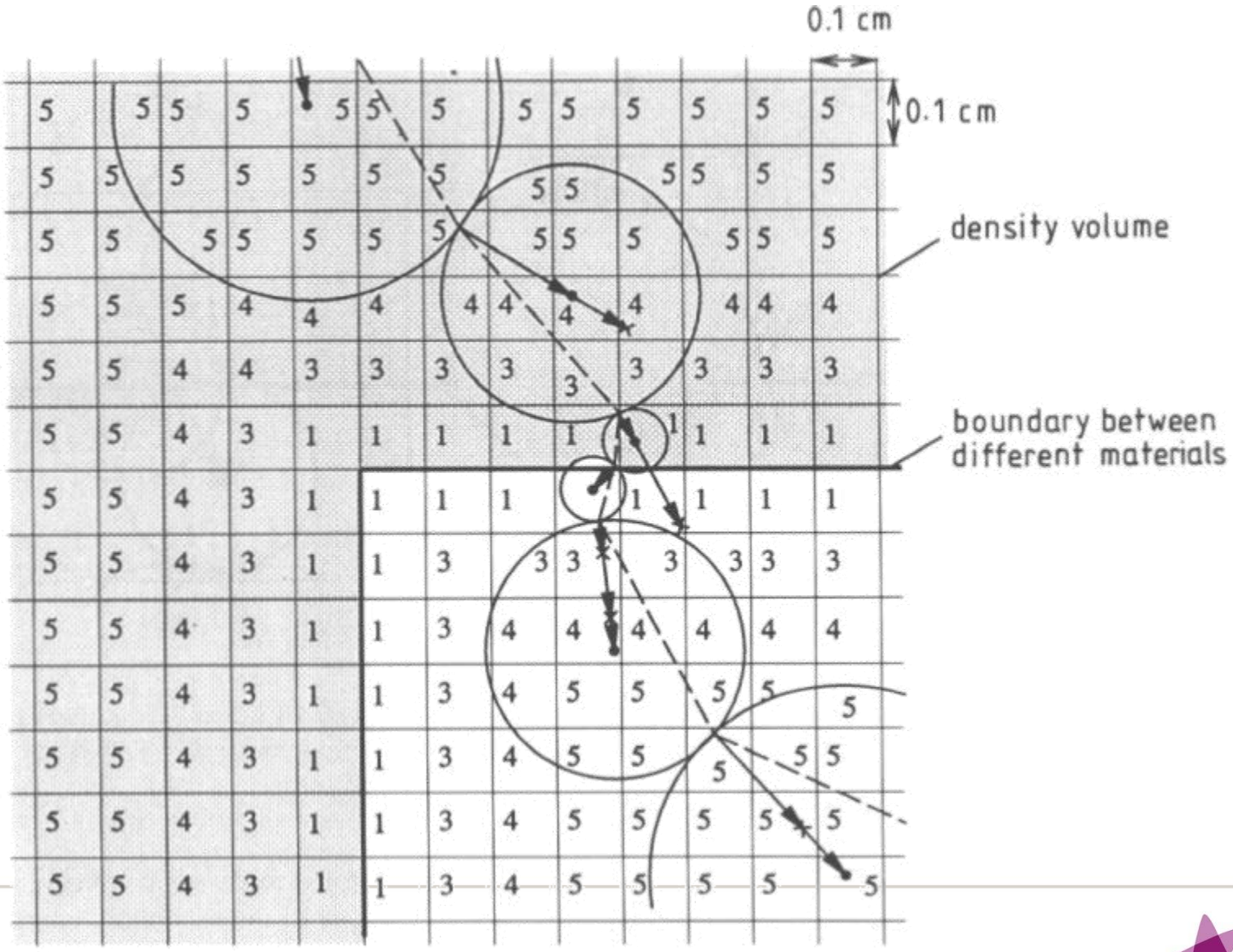

ESTRO School

MMC or kugel transport

- Global geometry calculations
  - CT images are pre-processed to user defined calculation grid
  - HU in CT image are converted to mass density
  - The maximum sphere radius and material at the center of each voxel is determined
- Homogenous areas
  - large spheres
- In/near heterogeneous areas
  - small spheres

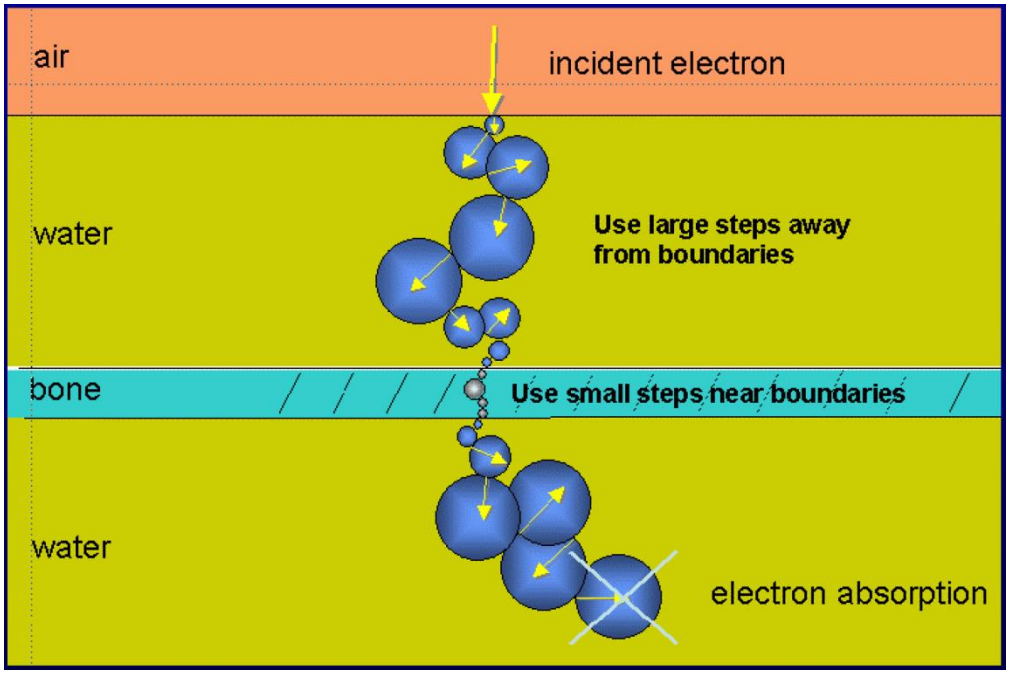

Adopted from DeMarco and Cygler

COMPARISONS

OMP MC vs EGSnrc

12 MeV – 14x14 cm^2 applicator

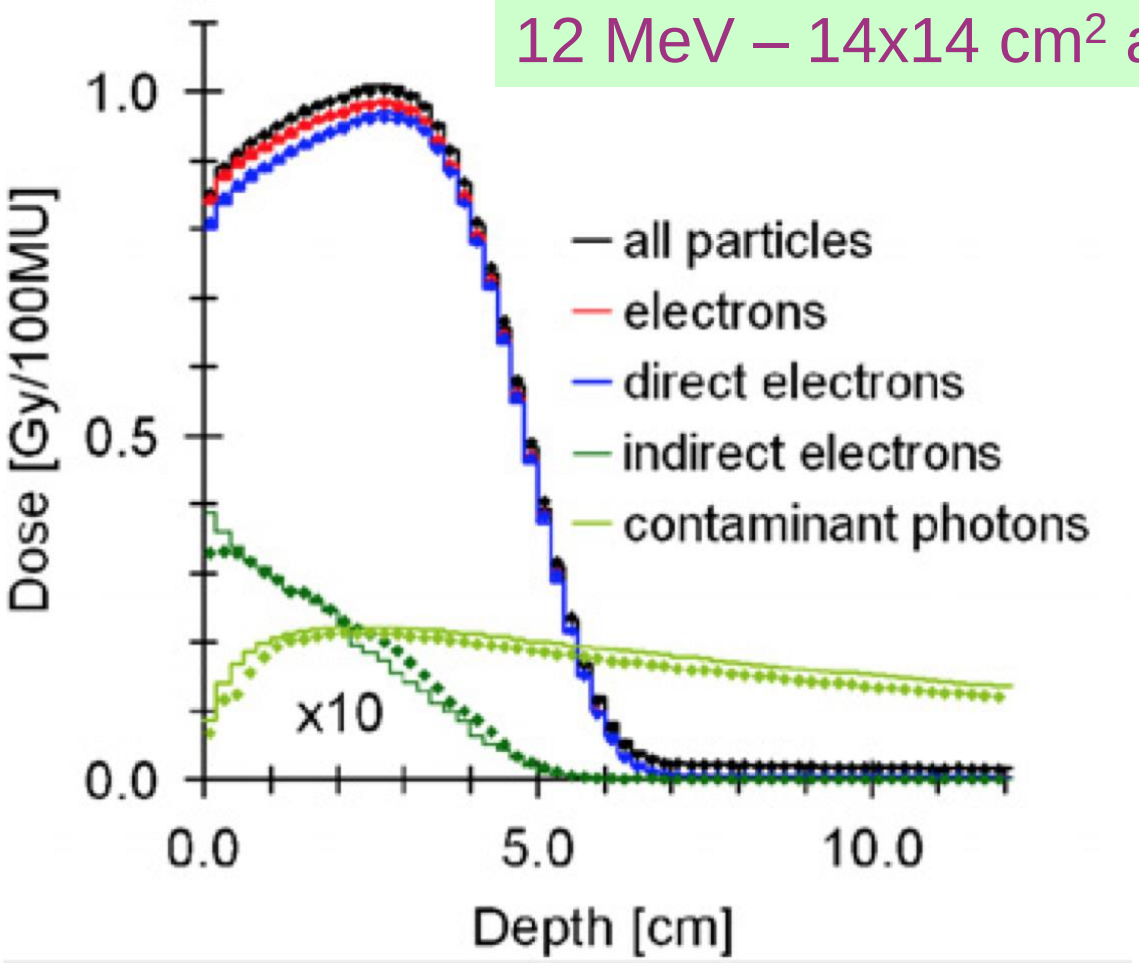

The possibility to separate different dose components for detailed performance QA

Wieslander and Knöös, PMB, 2006

OMP MC vs EGSnrc

Wieslander and Knöös, PMB, 2006

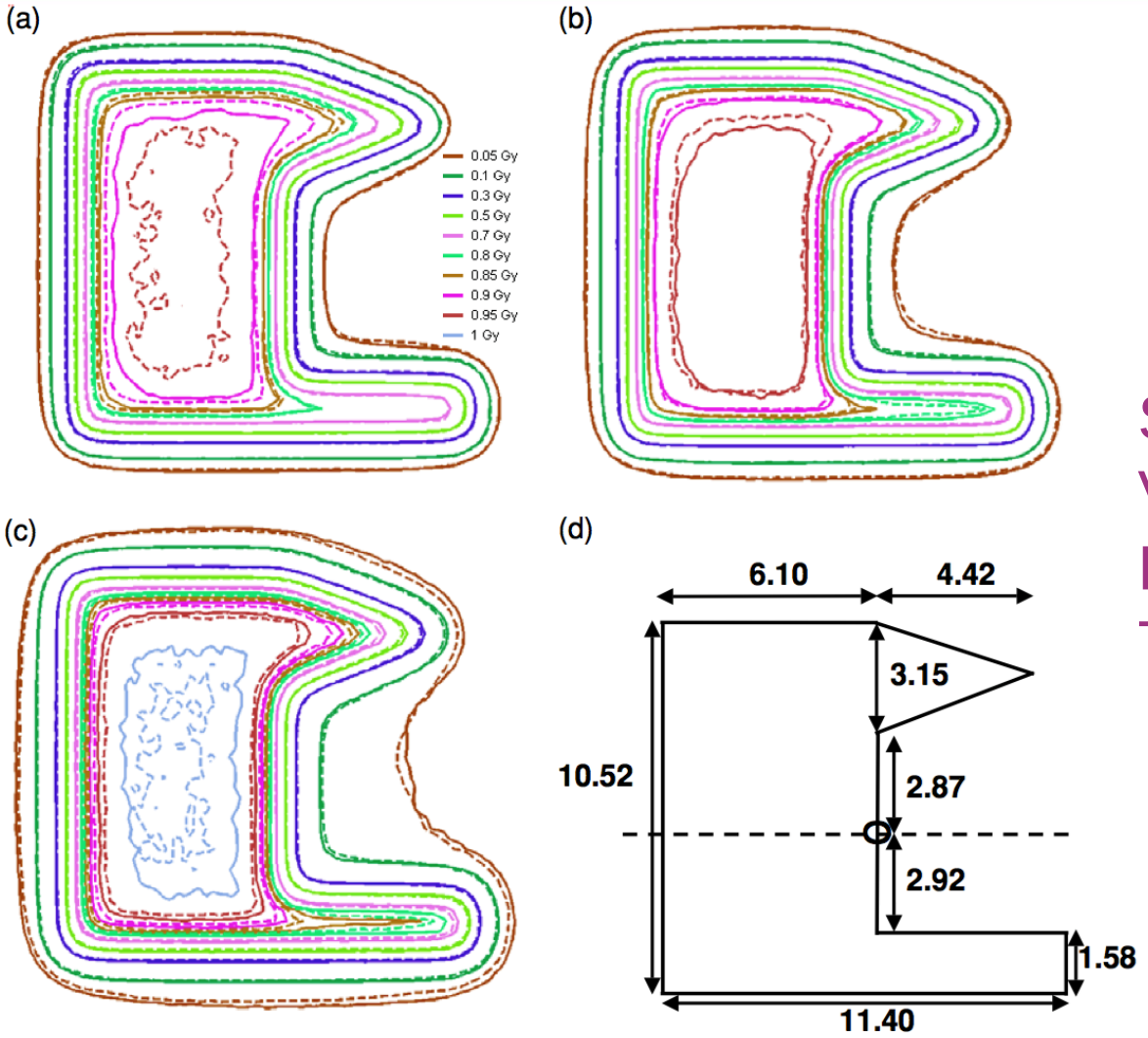

Solid lines
VA (EGSnrc)
Dashed lines
TPS (MC)

Figure 6. 2D isodose distributions in Gy/100 MU for the house field at 1.0, 2.0 and 3.0 cm for 6 (a), 12 (b) and 18 MeV (c), respectively. Solid lines represent the virtual accelerator and dashed lines the TPS. In panel (d), the design of the house field with dimensions given at SSD 100 cm is shown. The circle represents the centre of the 14 × 14 applicator.

OMP MC vs EGSnrc

VMC++ vs EGSnrc (solid)

PB vs EGSnrc (solid)

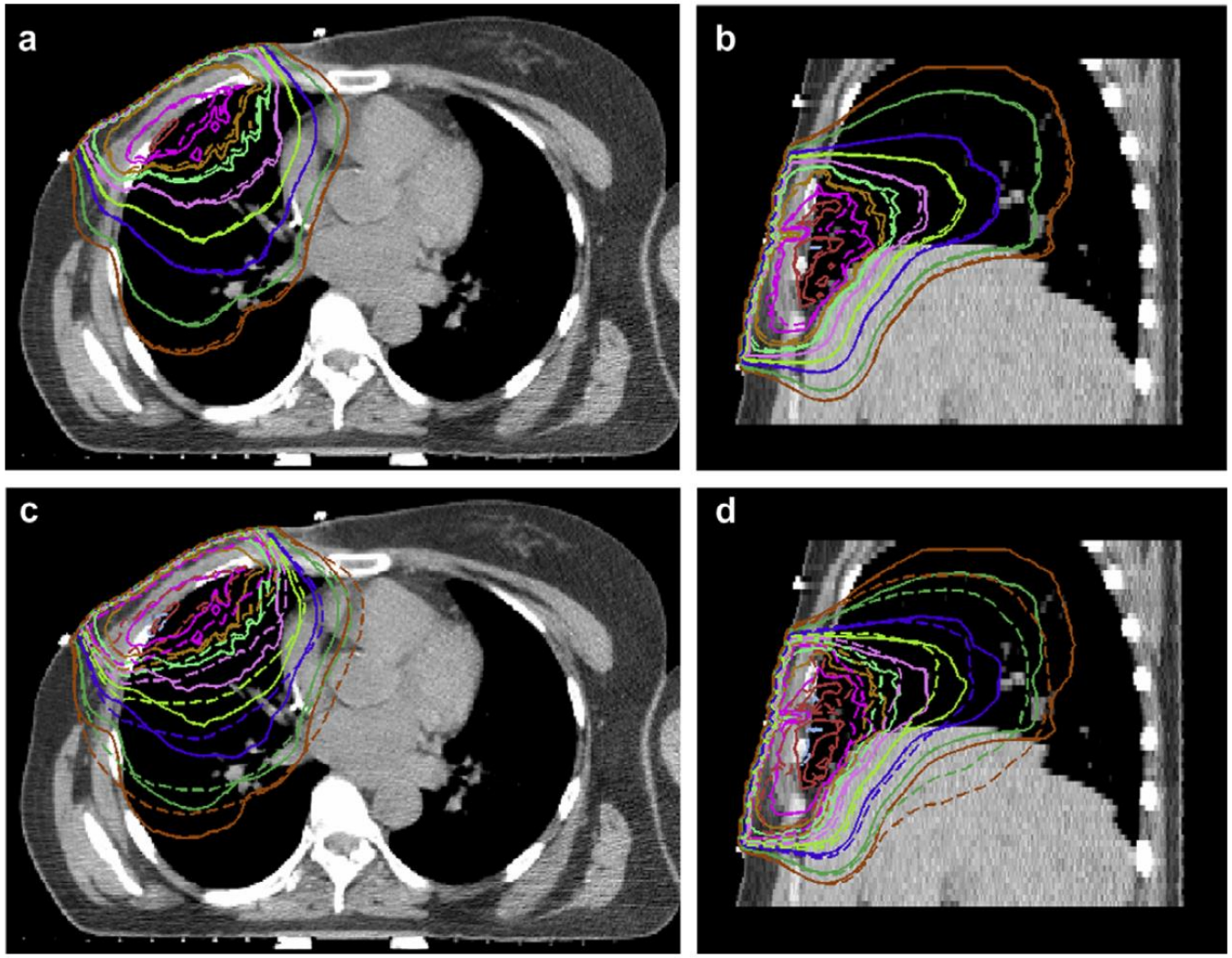

12 MeV electron, 100 MU
Isodose levels 0.05, 0.10, 0.30, 0.50, 0.70, 0.80, 0.85, 0.90, 0.95 and 1.00 Gy.

Wieslander and Knöös, RO 2007

OMP MC vs EGSnrc

VMC++ vs EGSnrc (solid)

PB vs EGSnrc (solid)

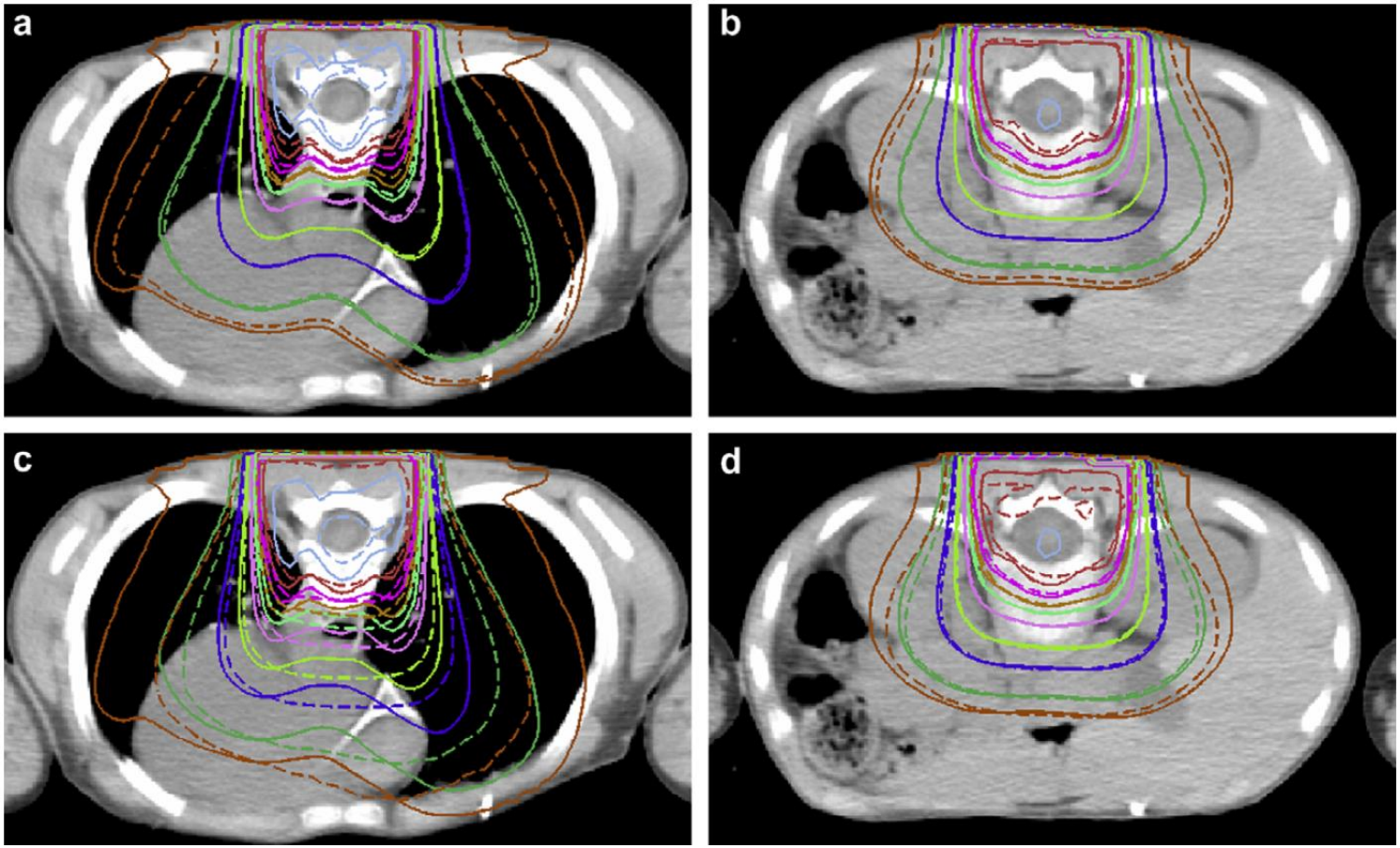

18 MeV electron, 100 MU
Isodose levels 0.05, 0.10, 0.30, 0.50, 0.70, 0.80, 0.85, 0.90, 0.95 and 1.00 Gy.

Wieslander and Knöös, RO 2007

Electrons in CMS eMC 9 MeV

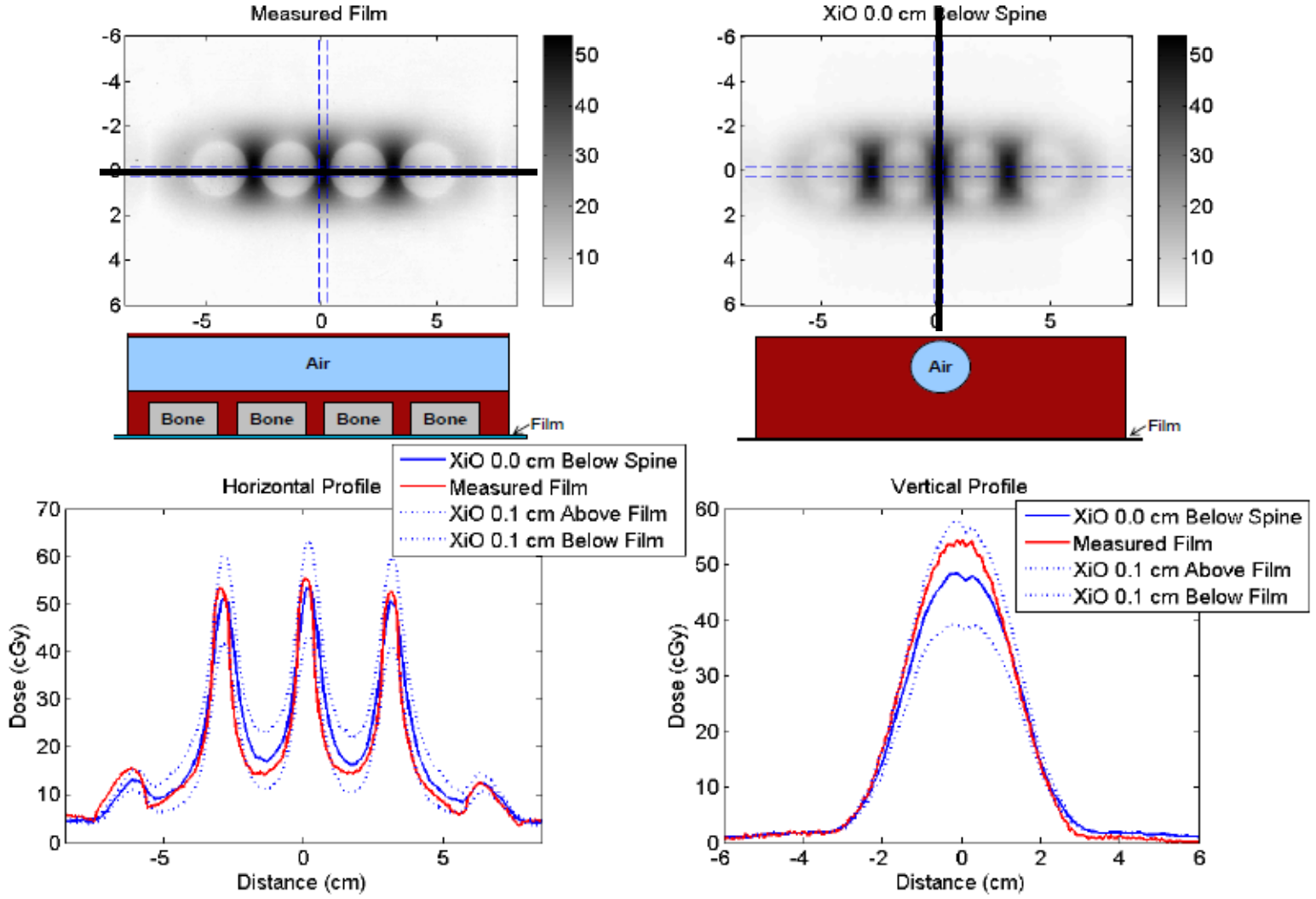

Vandervoort and Cygler, COMP 56th Annual Scientific Meeting, Ottawa June 2010

Electron In Eclipse I

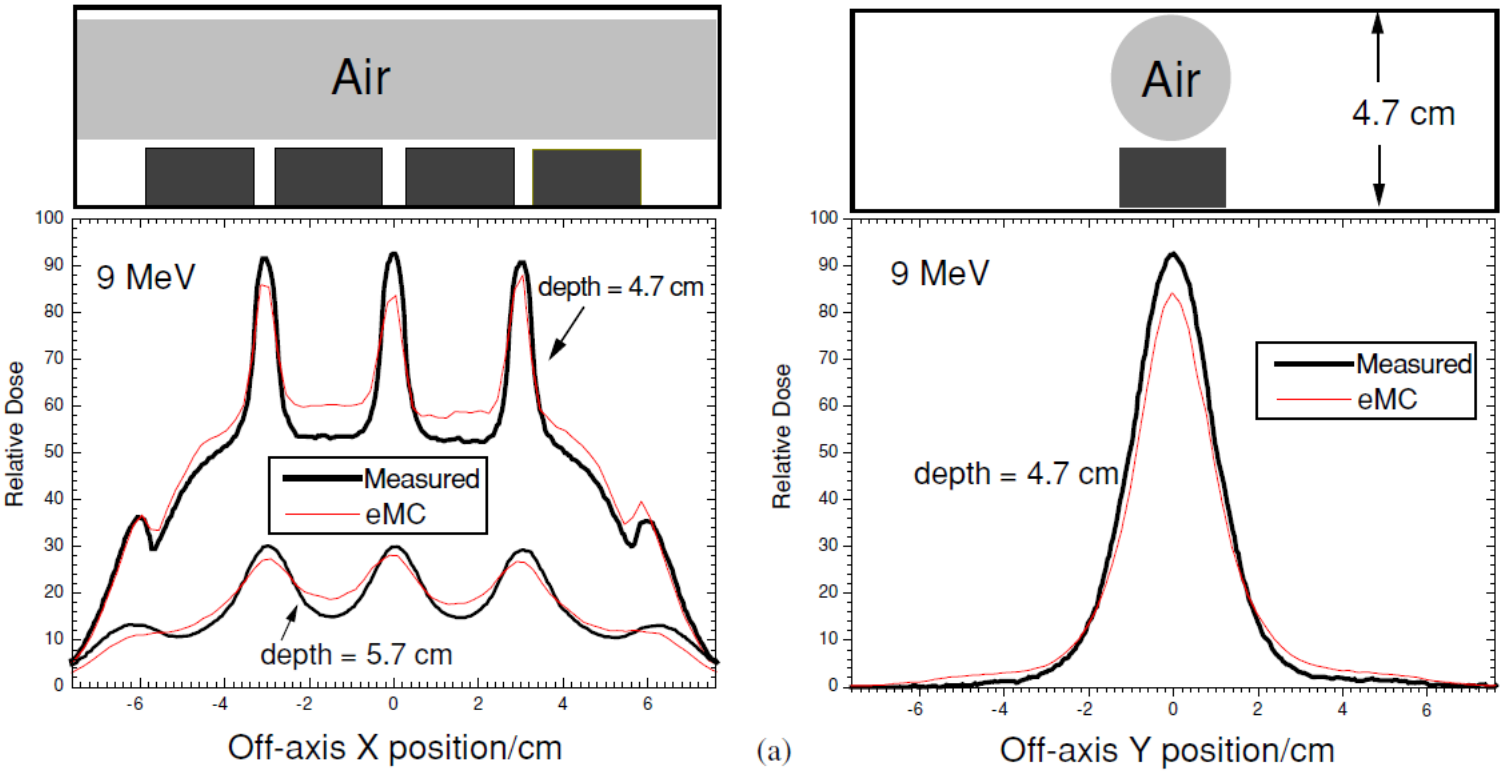

Ding et al PMB 2006

ESTRO School

Electron In Eclipse II

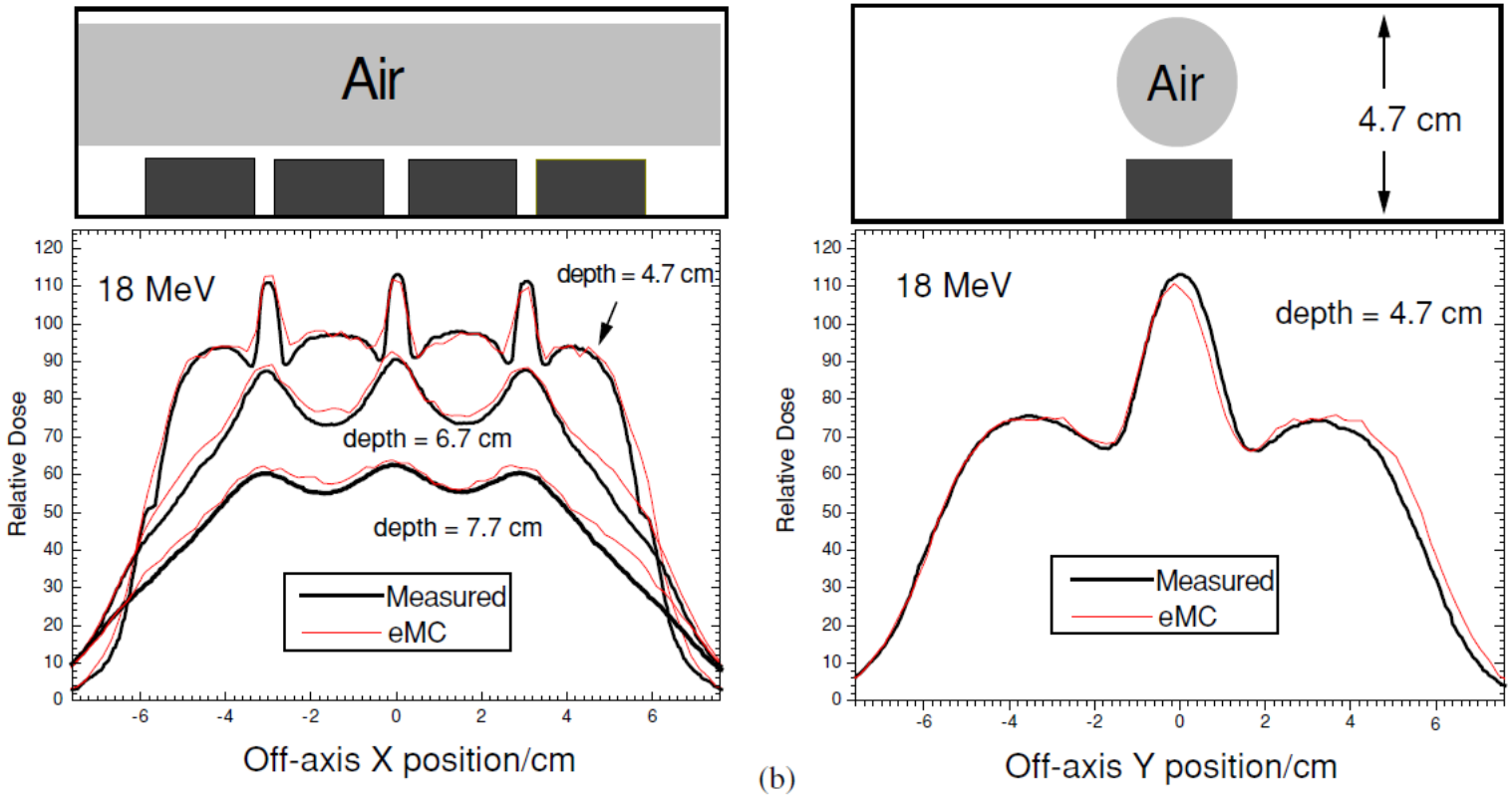

Ding et al PMB 2006

ESTRO School

Conclusions

- Commercial MC based TP system are available
  - easy to implement and use
  - MC specific testing required
- Fast and accurate 3-D dose calculations
- Single virtual machine for all SSDs
- Large impact on clinical practice
  - Accuracy improved
  - More attention to technical issues needed
  - Dose-to-medium calculated
  - MU based on real patient anatomy (including contour irregularities and tissue heterogeneities)
- Requirement for well educated physics staff

From Popple and Cygler at AAPM 2009

Thanks to the faculty who have contributed to these slides

Selected suggested reading

- IAEA TRS 380 (2000): Absorbed Dose Determination in External Beam Radiotherapy: An International Code of Practice for Dosimetry based on Standards of Absorbed Dose to Water- International Atomic Energy Agency, Vienna.
- IPEM Code of practice for electron dosimetry,(2003), Phys Med Biol, 48:2929
- IAEA TRS 381 (1997): The use of plane parallel chambers in high energy electron and photon beams - International Atomic Energy Agency, Vienna
- AAPM Task Group 25 (1991) : Clinical electron-beam dosimetry - Med. Phys. 18(1),pp 73-109.
- AAPM Task Group 70 (2009)Recommendations for clinical electron beam dosimetry: Supplement to the recommendations of Task Group 25 -Med. Phys. 36(7), 3240-3269.
- ICRU report 35 (1984): Electron beams with energies between 1 and 50 MeV- International Commission on Radiation Units and Measurements, Bethesda, Maryland.
- Green D and Williams PC (1985), Linear Accelerators for Radiation Therapy, IOP Publishing, ISBN 07503 0476 6
- Gibbons J P (2000), Monitor Unit Calculations for External Photon and Electron Beams, Advanced Medical Physics Publishing Inc, ISBN: 1-883526-08-6
- Khan F.M. (2003): The Physics of Radiation Therapy- Williams and Wilkins, Baltimore, Maryland.
- Klevenhagen S.C.(1993): Physics and Dosimetry of Therapy Electron Beams- Medical Physics Publishing, Madison, Wisconsin.
- Klevenhagen S.C.(1985): Physics of Electron Beam Therapy, Medical Physics Handbooks 13, Adam Hilger Ltd, ISBN 0-85274-781-0
- Klevenhagen S. C (1979) High Energy Electrons in Radiotherapy (Eindhoven: Philips).
- Hogstrom KR (1991) Treatment planning in electron beam therapy. Front Radiat Ther Oncol 25, 30-52+61-63.
- Hogstrom KR and Almond PR (2006). Review of electron beam therapy physics. Phys.Med. Biol. 51 (R544-R489).

- First impression

- Do you want more about electrons?

Out of field dose modeling and measurement in radiotherapy treatments

Brendan McClean

ESTRO Warsaw 2017

Saint Luke's
Radiation Oncology
Network

Learning Objectives

- Explain why we are interested in out of field dose (OFD)
- Understand the origin of OFD
- Investigate the effects of OFD
- Examine the accuracy of calculation of OFD with TPS
- Discuss the measurement of OFD

Why are we interested in out of field dose?

- Success of RT means longer survival of patients (Second Primary)
- New treatment techniques (VMAT)
- Improved optimisation based on DVC's
- Peripheral doses to IED's
- Differences in TPS?

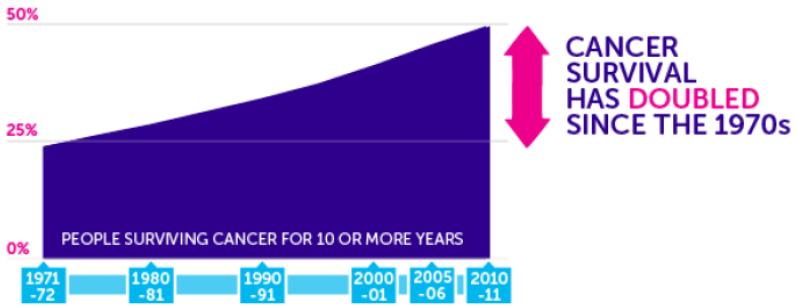

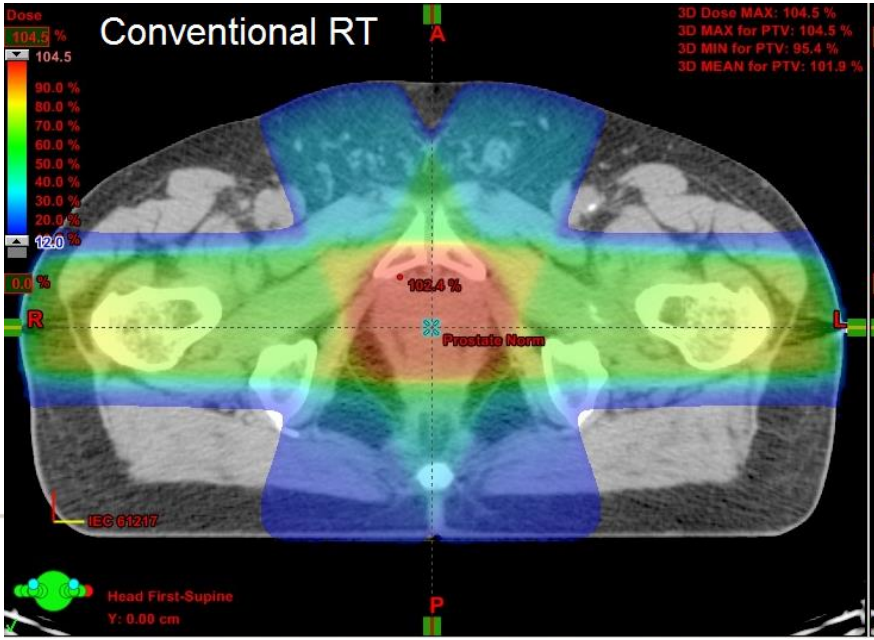

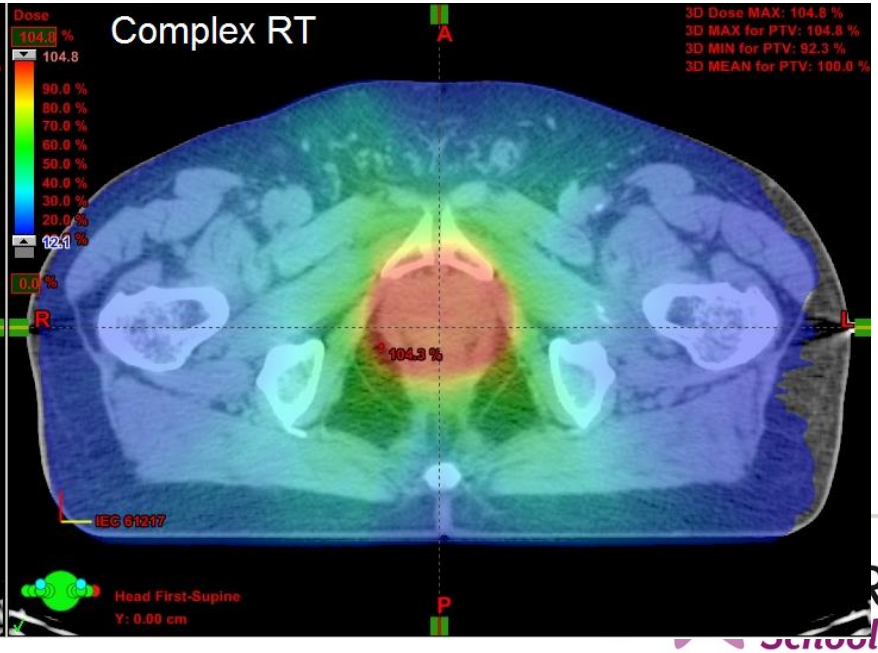

Origin of peripheral dose contributions: Patient Scatter

Treatment Site:	Right Oral Cavity
Technique:	6-field IMRT, 6 MV
Prescribed Dose:	66 Gy
Total Fractions:	33
Fractions Treated:	20

Without shield

Estimated dose to foetus:						
From full plan, unmodified:	0.017	Gy from	33	fractions	0.026%	
From treated fractions:	0.010	Gy from	20	fractions		
From remainder + lead:	0.003	Gy from	13	fractions		
From full plan, modified:	0.013	Gy from	33	fractions	-24% best case: difficult to shield obliques	

Patient scatter (AA)

Unavoidable

Decrease from target essentially as: $\frac{e^{-\mu \cdot r}}{r^n}$

n=1 column shaped scatter source

n=2 “blob” shaped scatter source

With shield

ESTRO School

Origin of peripheral dose contributions: Head Scatter

Sources are all irradiated parts of the treatment head: main source the ***flattening filter***

Limited by the collimating devices

Machine design dependent (FFF machines have less – approx 50%reduction **Georg, Knoos, McClean MP 2011**)

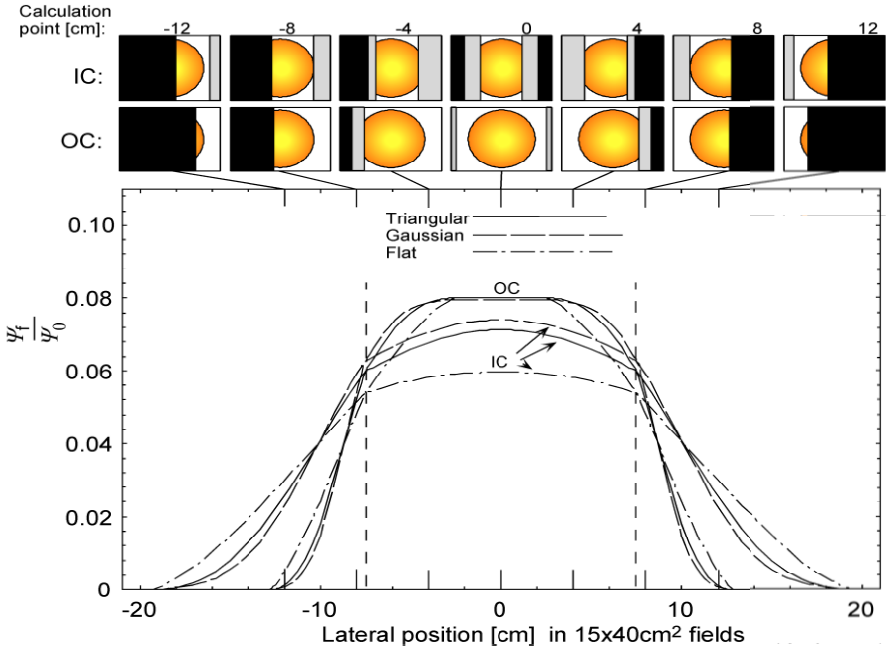

Ahnesjö 1994 Med. Phys. **21** 1227-35

Flattening filter or not? MLC or jaws?

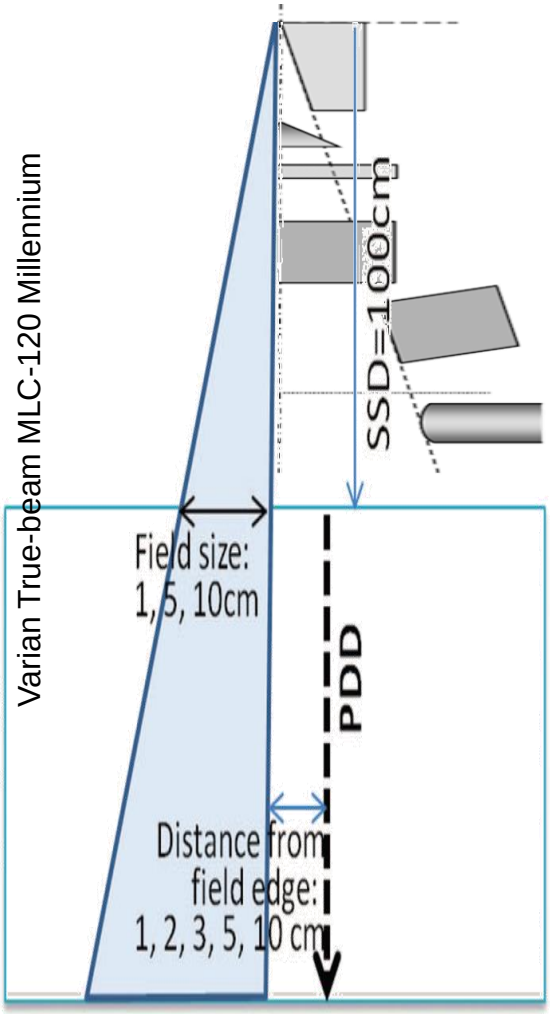

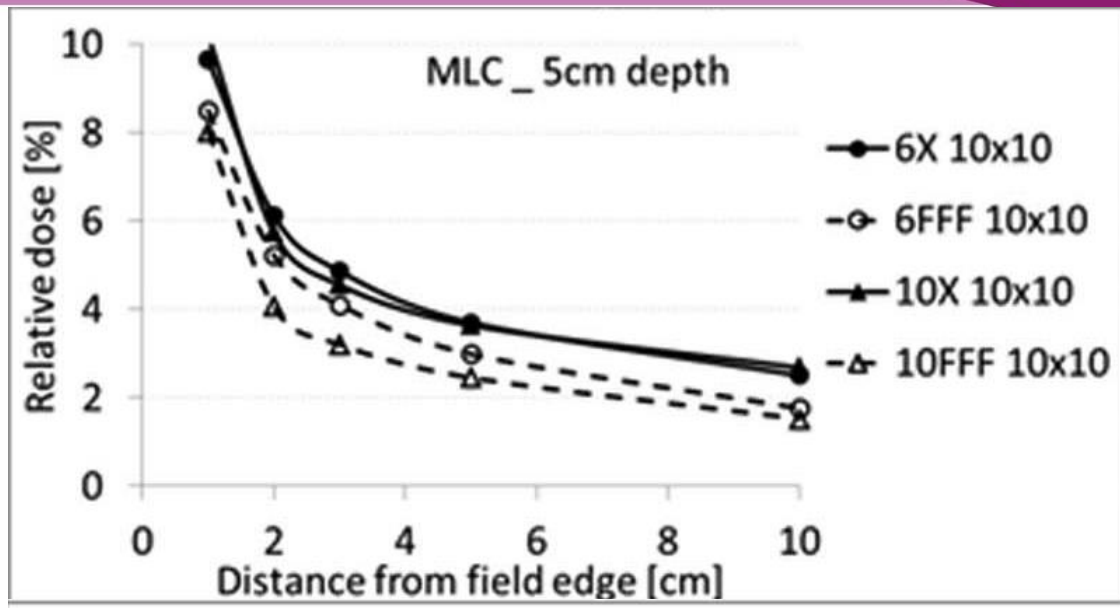

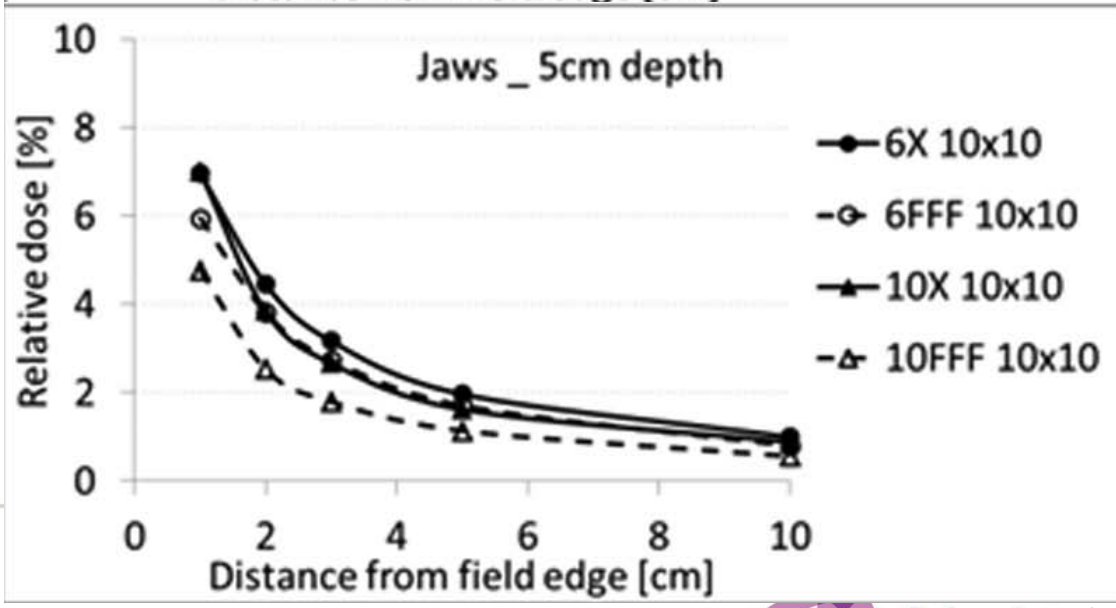

Fogliata etal 2013 MedPhys 40(10) p101706-1

Collimator leakage - intraleaf and interleaf

Two effects:

- Diffused dose from spiky interleaf fluence leakage
- *Intraleaf* attenuation

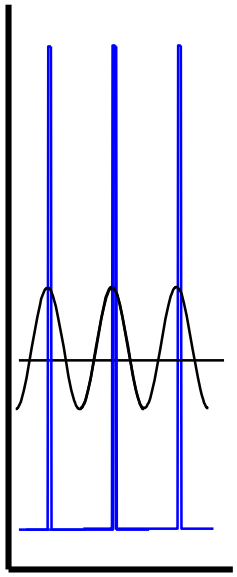

Intraleaf leakage very small:

$$e^{-\frac{\mu}{\rho}\rho \cdot t} \xrightarrow[\substack{8\text{ cm tungsten}\\ \text{at 3 MeV}}]{} e^{-0.0408\times 18.0\times 8.0} = 0.28\%$$

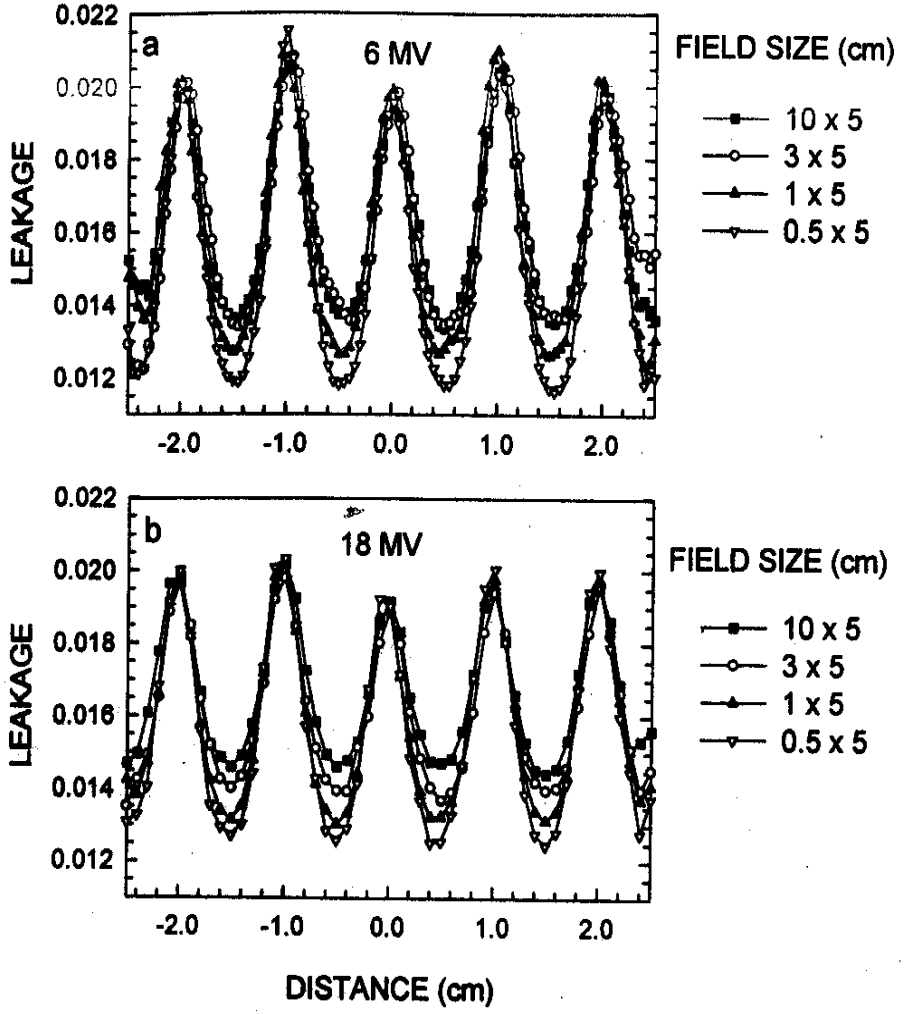

Measurements from Arnfield *et al*, 2000 Med. Phys. **27**

Origin of peripheral dose contributions

Anders A.

Patient scatter

- Unavoidable
- Decrease from target essentially as: $\frac{e^{-\mu \cdot r}}{r^n}$ *n*=1 column shaped scatter source; *n*=2 “blob” shaped scatter source

Head scatter

- Sources are all irradiated parts of the treatment head, main source the flattening filter
- Limited by the collimating devices
- Machine design dependent (FFF machines have less!)

Leakage, including scatter leakage

- Depends on collimator and shield thicknesses and material (density)
- Collimator design dependent
- **Treatment technique dependent**

Neutrons

- Mainly a high Z phenomena at photon energies above photonuclear threshold values
- Avoidable by lower beam energy

Only one factor user controllable on a daily basis, all other once per decade (replacement)!

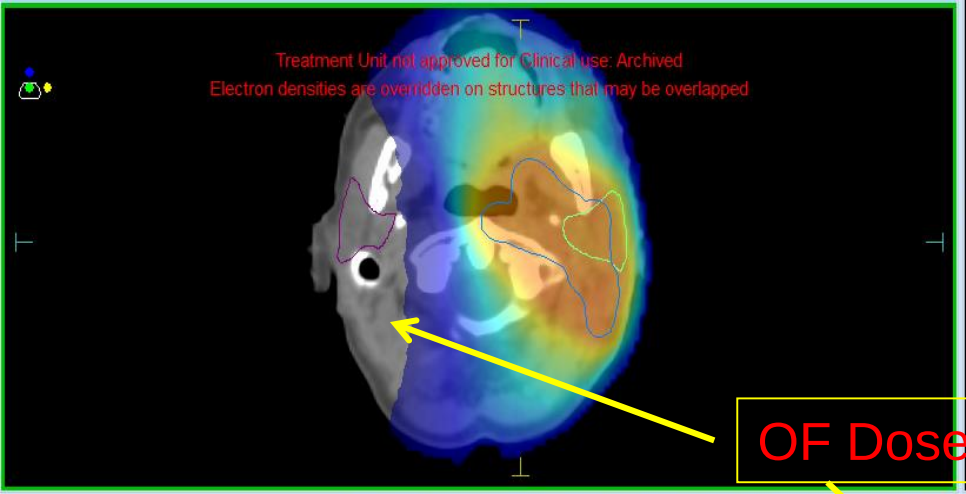

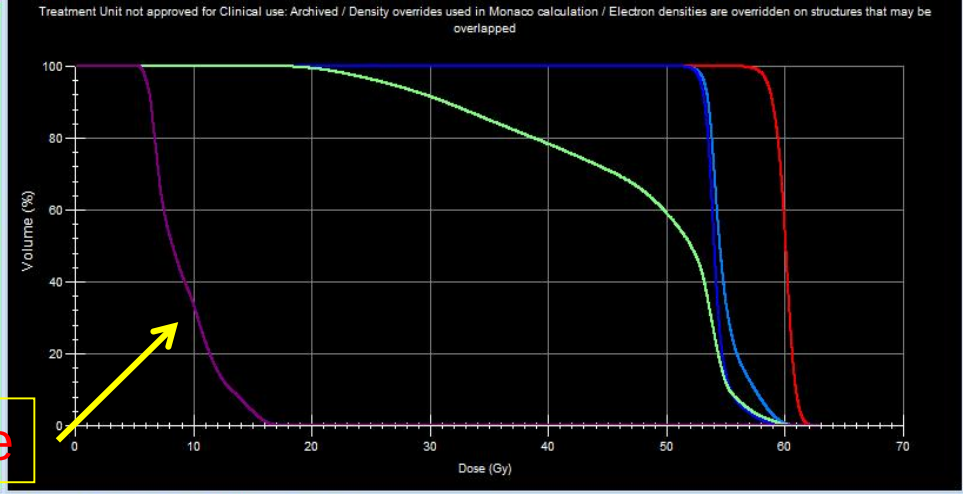

OF Dose

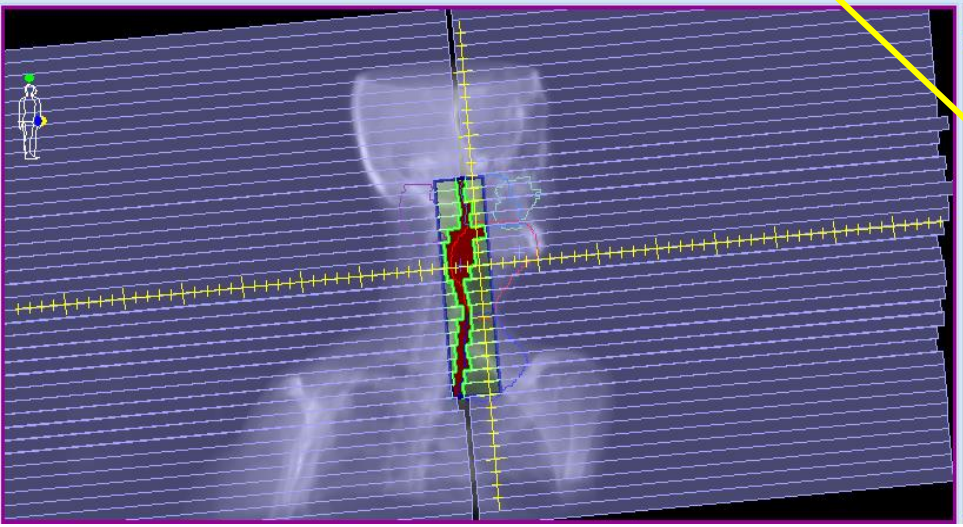

- **Effect of out of field doses?**
- **How accurate is the calculation of out of field dose?**
- **How do we measure it?**

Effect: Second Primary Malignancies (SPM)

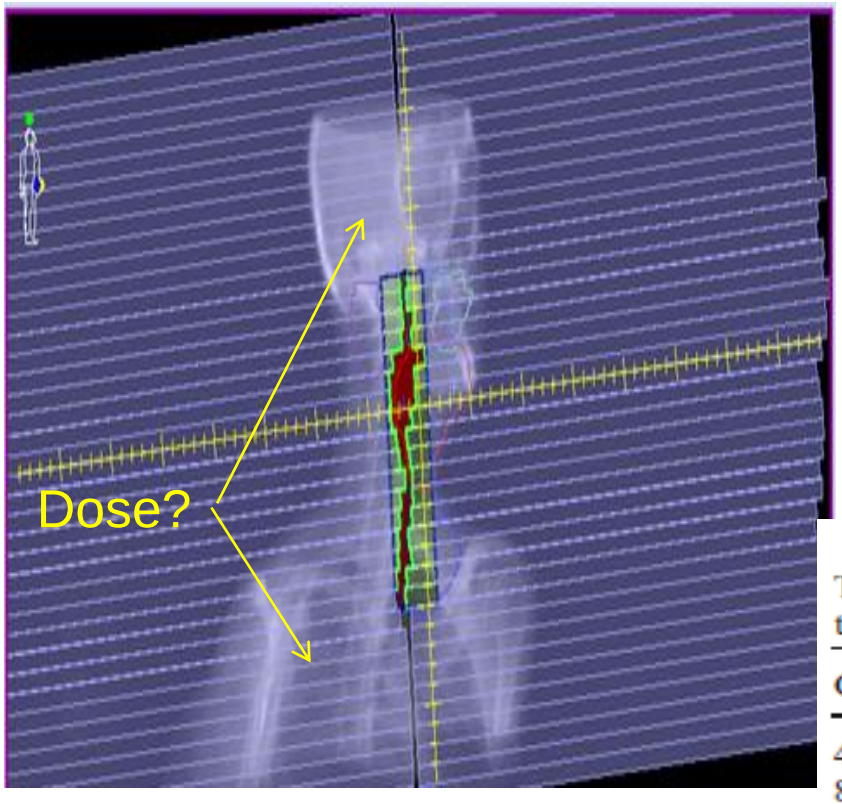

Implantable devices etc too…

- SPM's mostly in tissues >2Gy (fractionated)
  - Thresholds of 0.6Gy (adult) and 0.1Gy (children)
- Practical guidelines: aim for reducing volume <3.5Gy **Tubiana, R&O 2009**
- SPM incidence has reduced due to better conformality of dose (heart, lung, breast) **Tubiana, R&O 2009**
- Somewhat controversial but ***clear need for organ specific doses and distributions*** **K.Trott R&O 2009** (patient specific?)

Table 3. Fatal cancer risk for various organs in terms of a 70-Gy tumor dose[a] **Mesbahi etal, Jpn J Radiol 2010 28:398-403**

Cobalt-60	6 MV	9 MV	Organ
4.53E-06	5.31E-06	5.10E-06	Bladder
8.25E-03	8.50E-03	9.00E-03	Bone marrow
5.25E-05	6.60E-05	7.44E-05	Liver
3.82E-04	4.87E-04	5.55E-04	Lung
1.04E-02	1.11E-02	1.22E-02	Skin
5.53E-04	6.89E-04	7.25E-04	Stomach
5.22E-02	6.32E-02	7.34E-02	Thyroid

[a]Estimated using the MC calculated organ dose and coefficients in Table 2 for conventional radiation therapy of the nasopharynx

Energy spectrum out of field

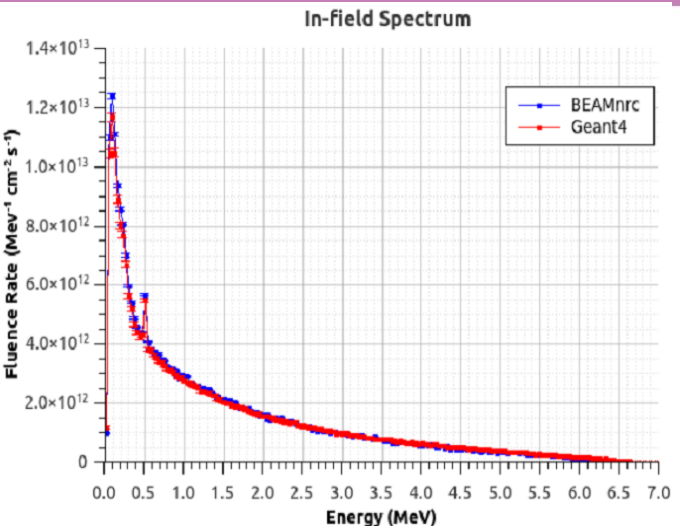

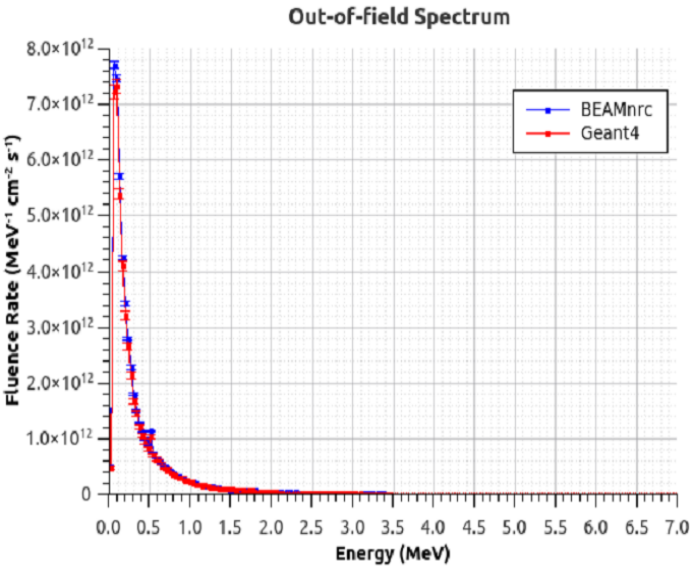

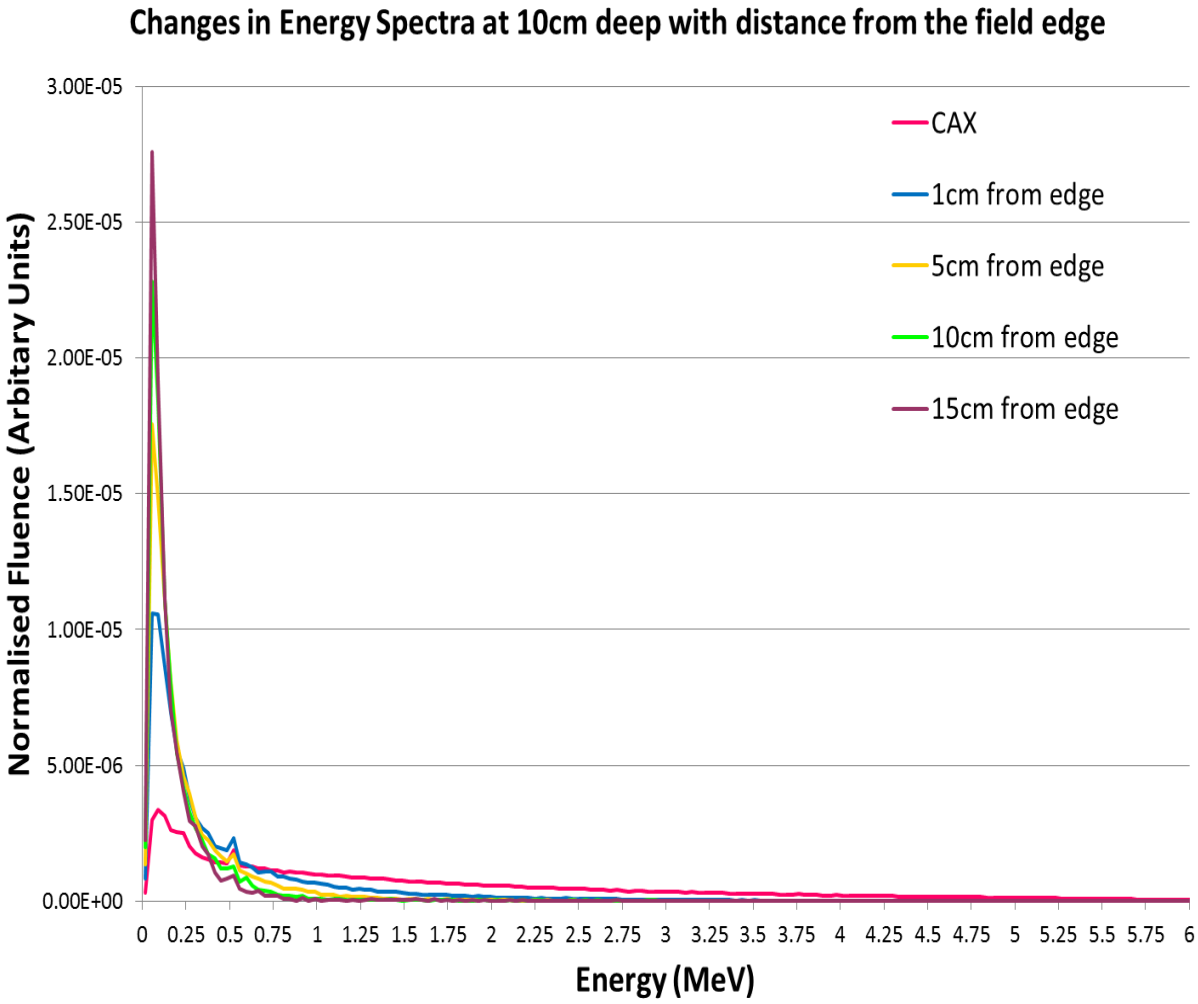

ESTRO School

Radiobiological Effect of OFD dose

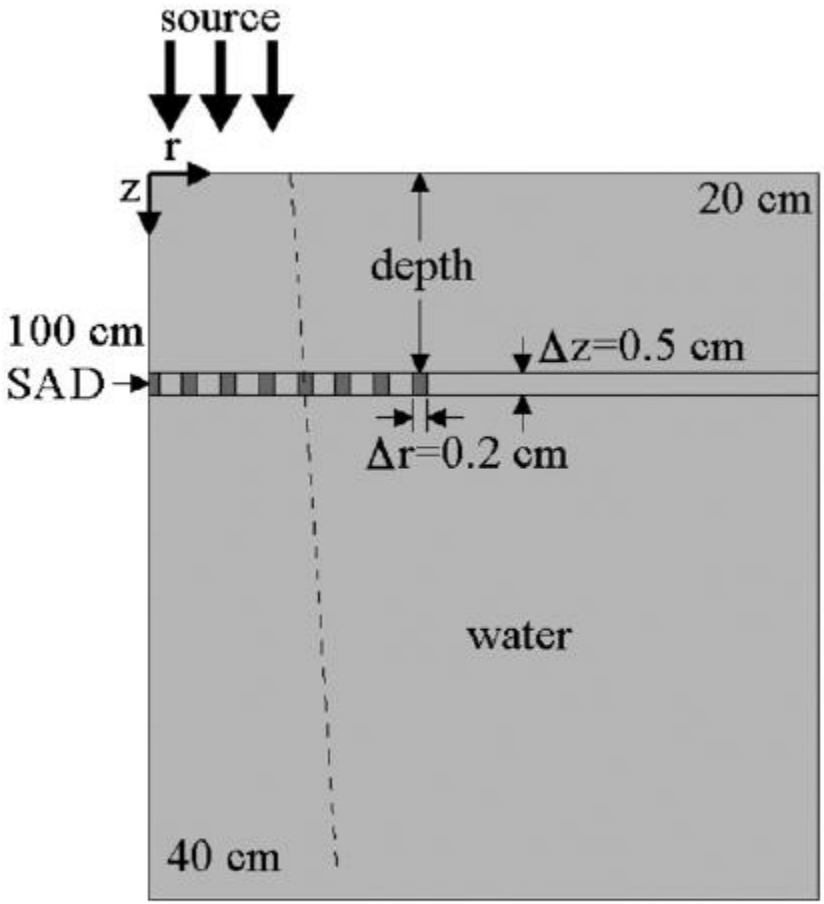

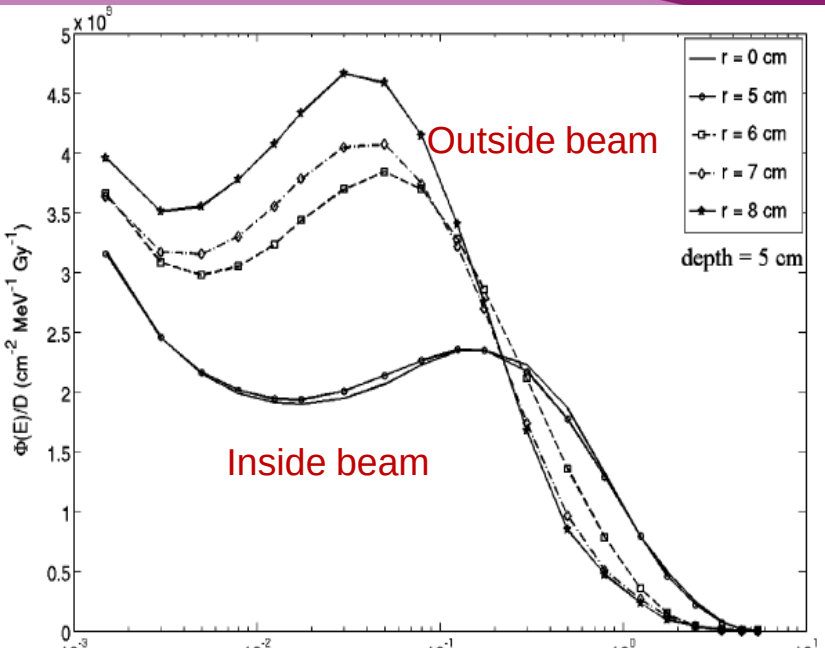

5cm radius 6MV beam

Increase of 25% in RBE 2cm from field edge

Kirkby et al PMB 2007

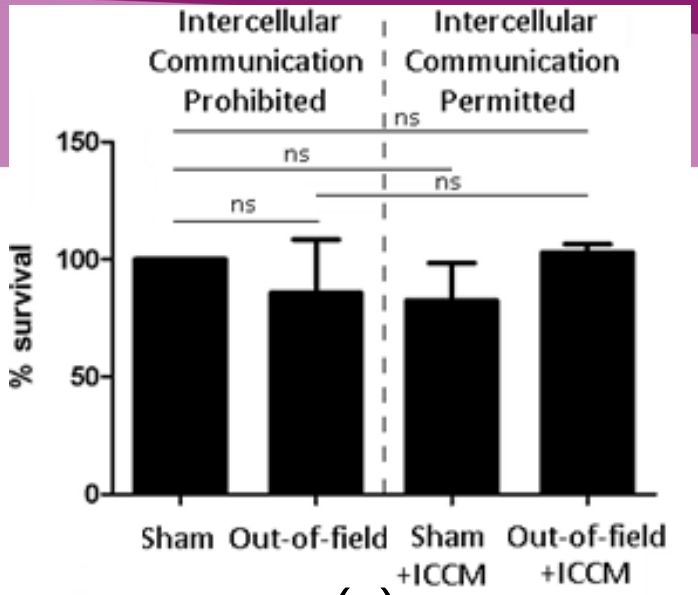

(a)

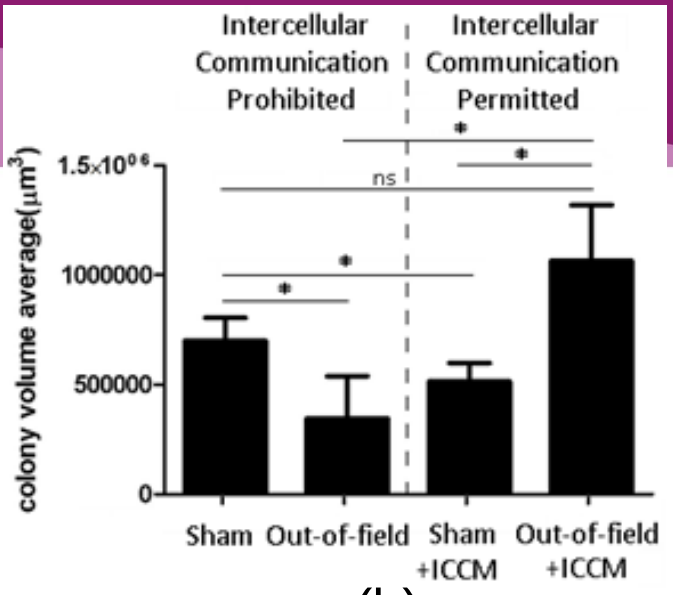

(b)

Shields et al. RADIATION RESEARCH 182, 499–506 (2014)

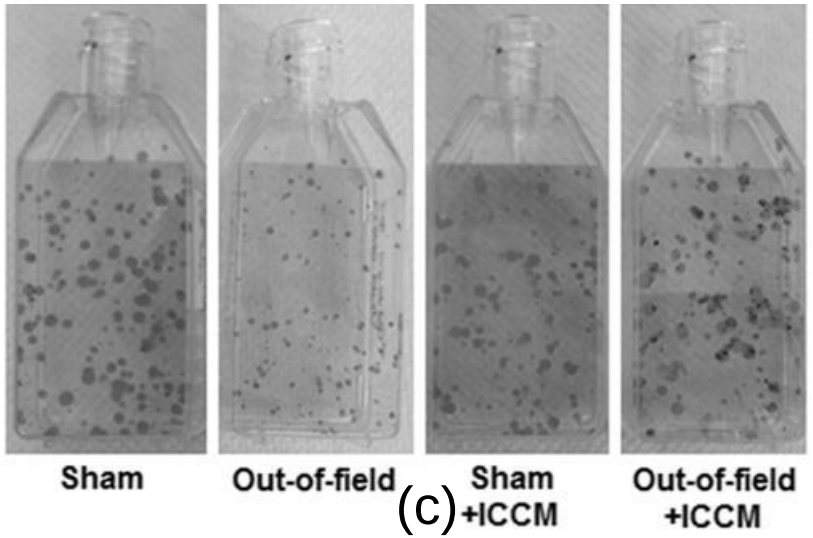

(c)

Figure 3(a) Percentage survival, (b) Average Colony Volume and (c) Photograph of clonogenic assay flasks of the sham and out-of-field cells both with and without ICCM transfer after irradiation of 2 Gy in-field.

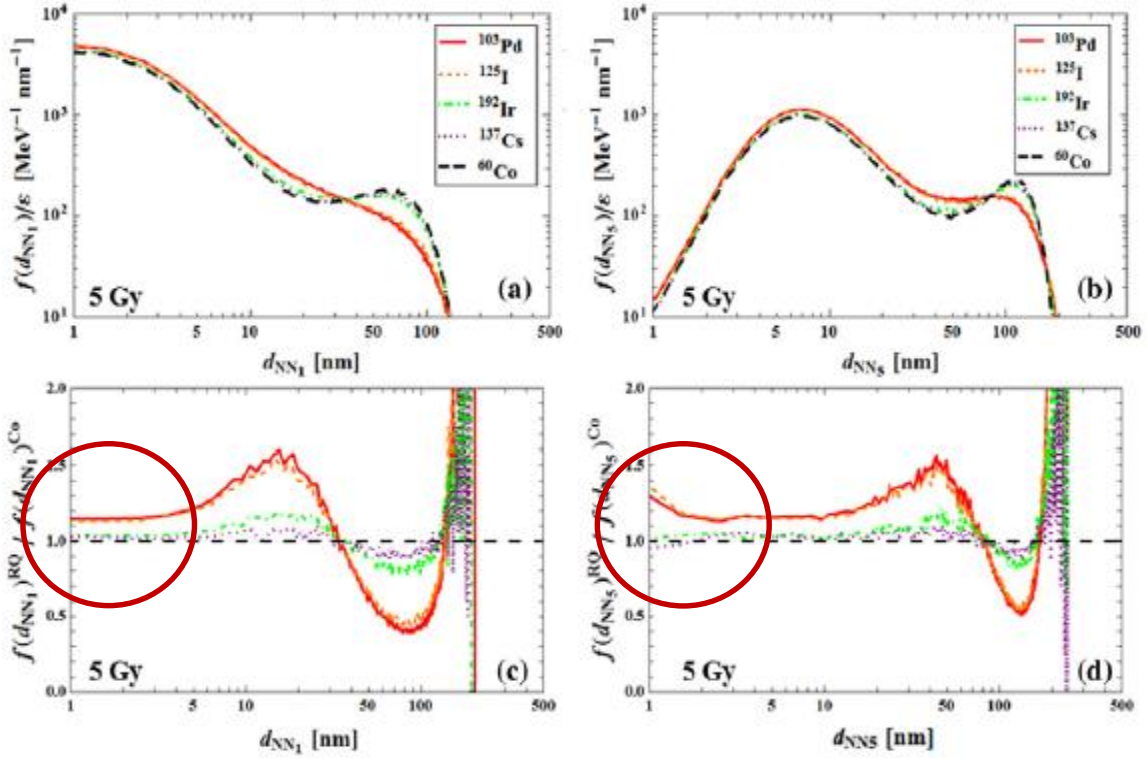

Figure 1. Frequency distributions of (*a*) the first $f(d_{NN_1})$ and (*b*) the fifth $f(d_{NN_5})$ nearest neighbour normalized per deposited energy ε, for the investigated sources. The density of scored EDs corresponds to a dose of 5 Gy using the multi-track approach. In the lower panel graphs, the ratios of the frequency distributions of the different radiation qualities (RQ) with respect to ^{60}Co are shown for the first (*c*) and the fifth (*d*) neighbouring EDs, demonstrating the presence of more dense ionizations for the low energy sources ^{103}Pd and ^{125}I.

Cluster pattern analysis of energy deposition sites for the brachytherapy sources 103Pd, 125I, 192Ir, 137Cs, and 60Co

ESTRO School

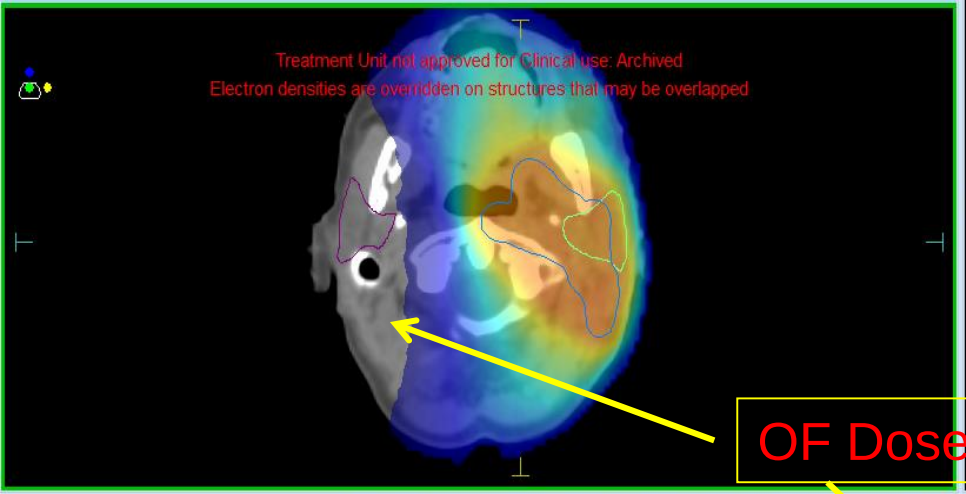

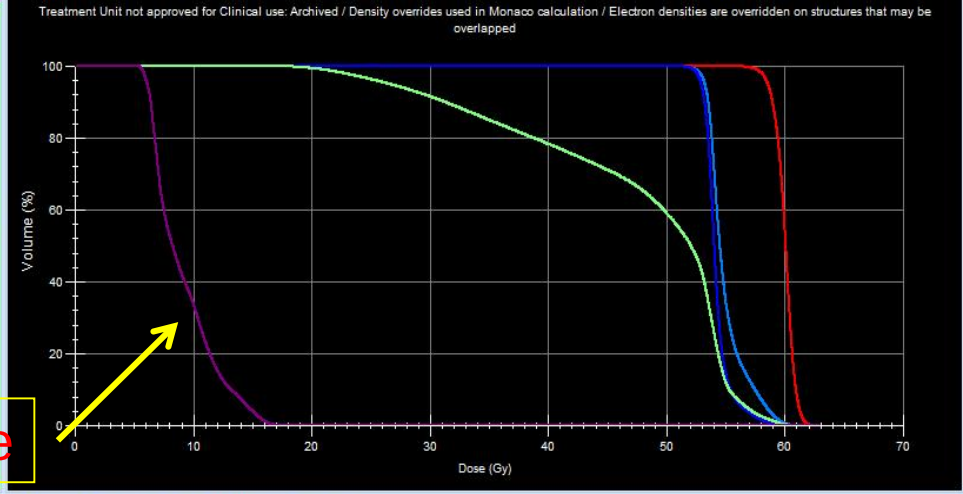

OF Dose

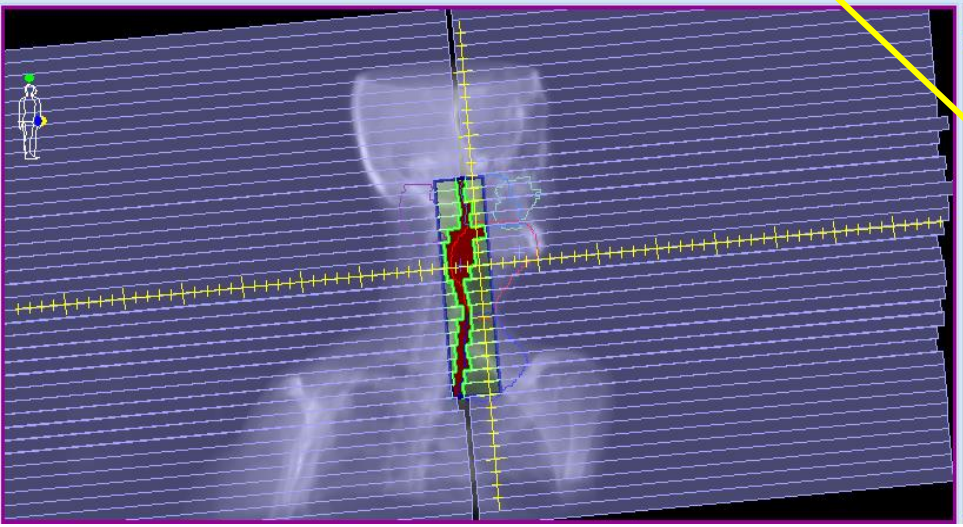

- **Effect of out of field doses?**
- **How accurate is the calculation of OFD?**
- **How do we measure it?**

TPS: General

Dose calculations bound to grids (fluence map/phase space & dose voxel matrix)

- lack of beam data to drive dose calculations outside the largest field

Main TPS concern is planning dose to target (and saving nearby risk organ)

- Dose in the beam channel and penumbras modeled correctly…
- …scatter usually OK but…
- …less focus on accurate leakage outside of penumbra, far away scatter & neutrons

- Few publications dealing with tests outside field edge
- Fewer guidelines on data gathering outside field edge

Geometrical models in TPS

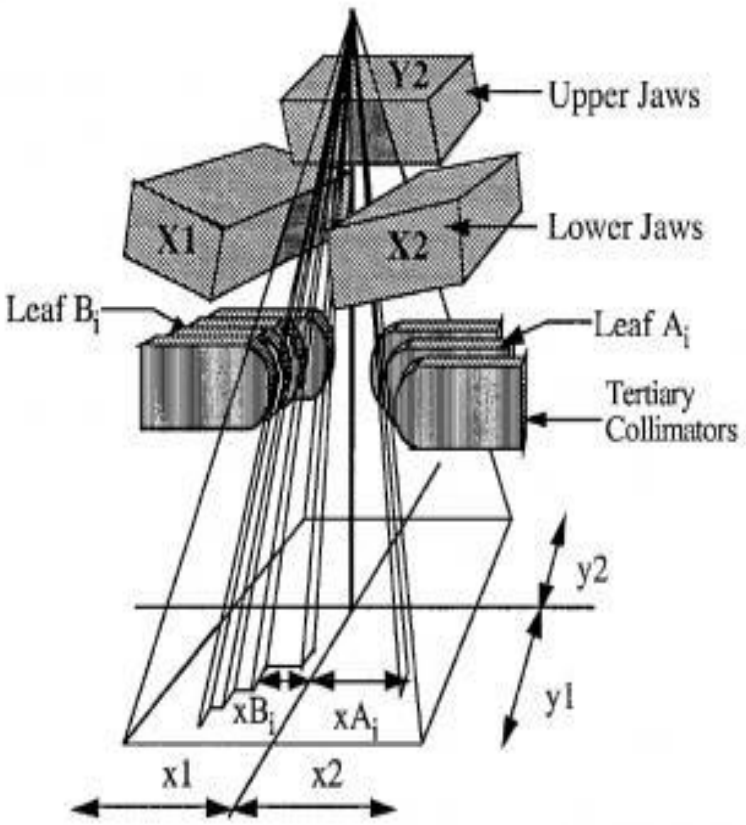

Geometrical models in Monte Carlo

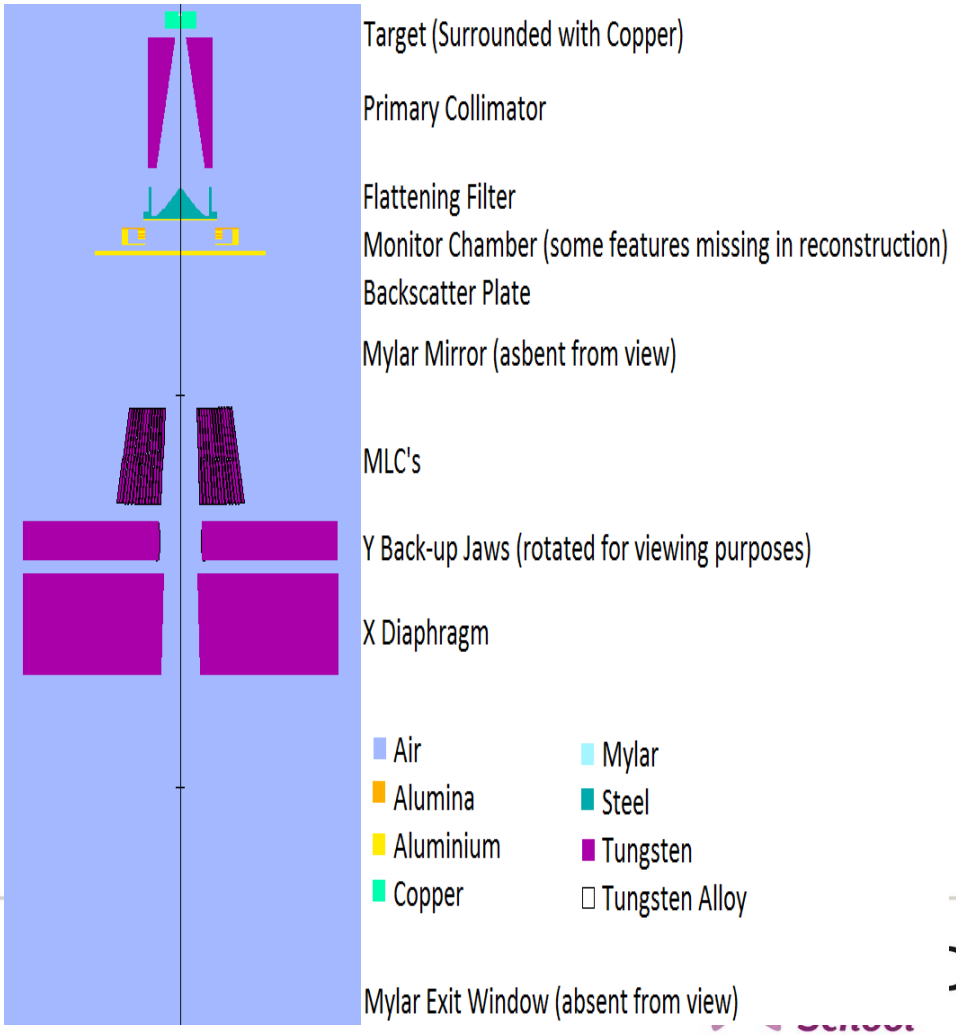

Geometrical models i

Geometrical models e Carlo

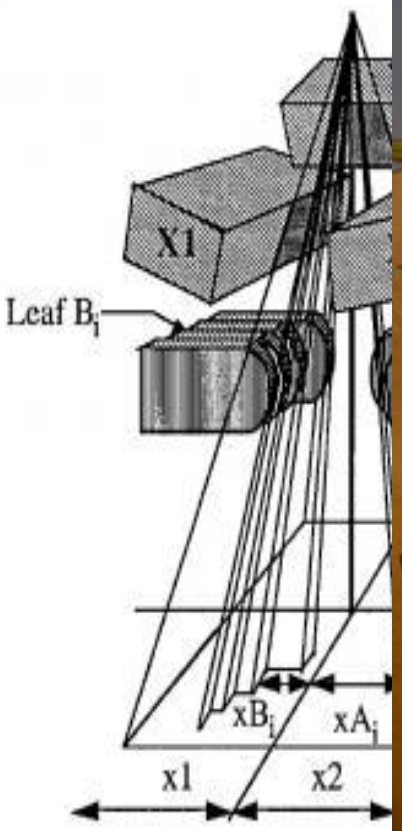

Target (Surrounded with Copper)

Primary Collimator

Flattening Filter

Monitor Chamber (some features missing in reconstruction)

Backscatter Plate

Mylar Mirror (asbent from view)

MLC's

Y Back-up Jaws (rotated for viewing purposes)

X Diaphragm

Air
Alumina
Aluminium
Copper
Mylar
Steel
Tungsten
Tungsten Alloy

Mylar Exit Window (absent from view)

Peripheral dose components

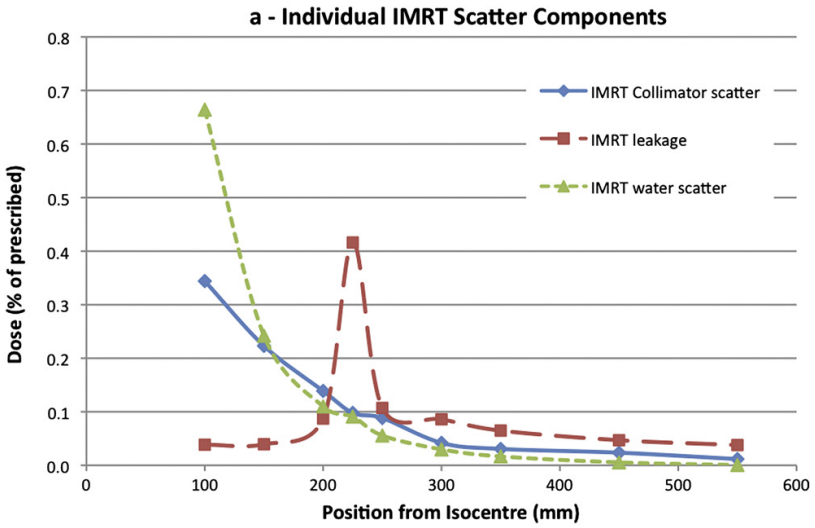

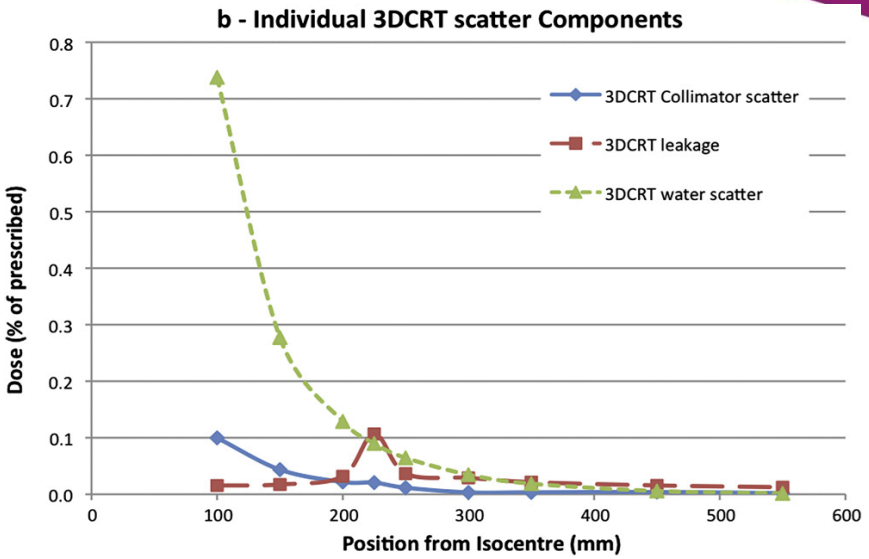

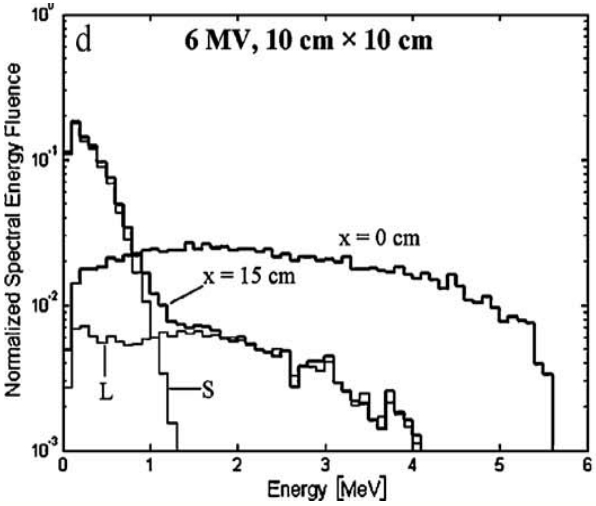

L - head leakage
S - phantom scatter

Ruben etal, IJROBP, Vol. 81, No. 5, pp. 1458–1464, 2011

Chofor etal, Z. Med. Phys. 21 (2011)

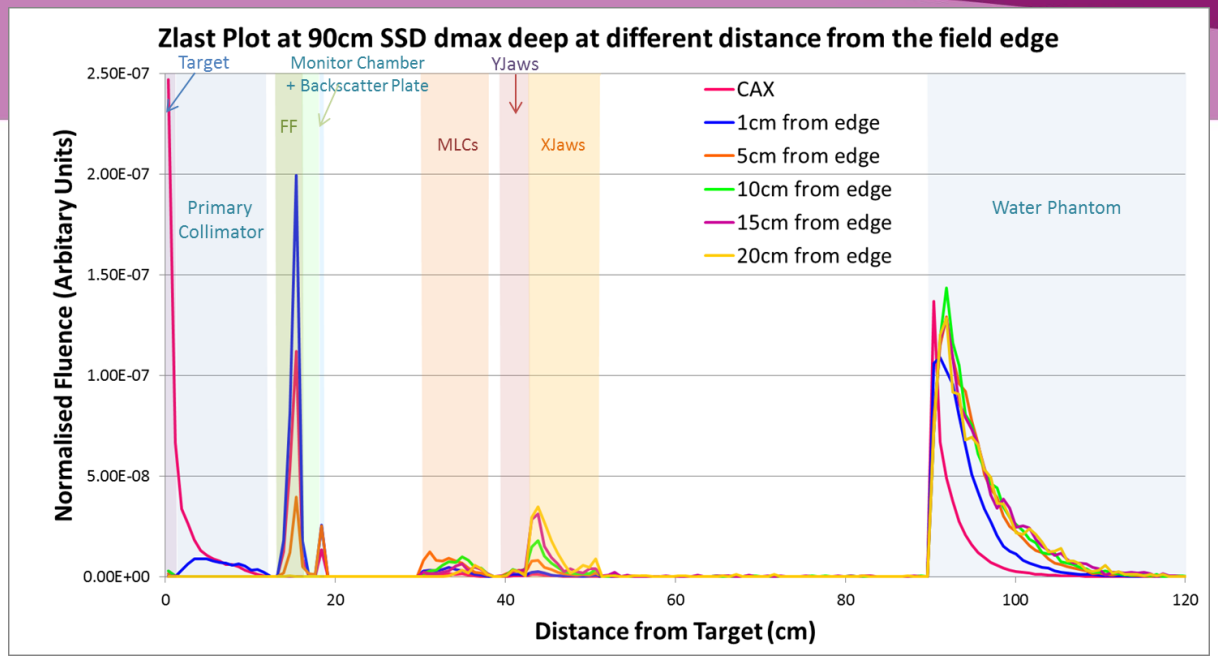
Zlast Plot at 90cm SSD dmax deep at different distance from the field edge
Target
Monitor Chamber
+ Backscatter Plate
YJaws
FF
MLCs
XJaws
Primary Collimator
Water Phantom
CAX
1cm from edge
5cm from edge
10cm from edge
15cm from edge
20cm from edge
Normalised Fluence (Arbitary Units)
2.50E-07
2.00E-07
1.50E-07
1.00E-07
5.00E-08
0.00E+00
0
20
40
60
80
100
120
Distance from Target (cm)

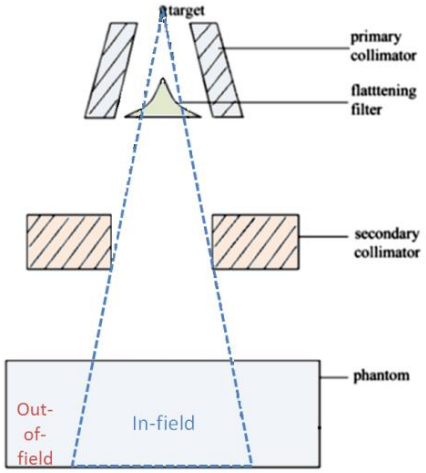
target
primary collimator
flatttening filter
secondary collimator
phantom
Out-of-field
In-field

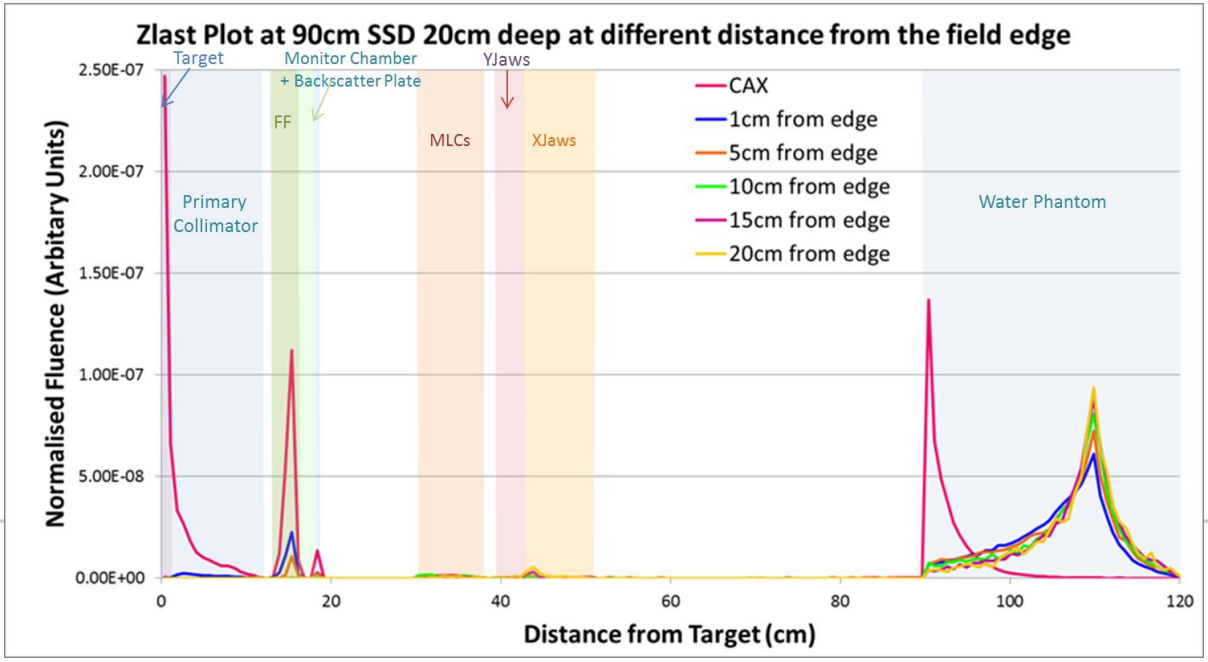
Zlast Plot at 90cm SSD 20cm deep at different distance from the field edge
Target
Monitor Chamber
+ Backscatter Plate
YJaws
FF
MLCs
XJaws
Primary Collimator
Water Phantom
CAX
1cm from edge
5cm from edge
10cm from edge
15cm from edge
20cm from edge
Normalised Fluence (Arbitary Units)
2.50E-07
2.00E-07
1.50E-07
1.00E-07
5.00E-08
0.00E+00
0
20
40
60
80
100
120
Distance from Target (cm)

Monte Carlo Modelling: Conclusions

- As the distance from the field edge increased so too did the number of low energy photons incident out-of-field
  - Implications for detector choice
  - Radiobiological Effectiveness
- The ZLAST plots indicate that modelling the peripheral components of the linac head would most likely have a negligible contribution to out-of-field dose

Treatment Planning System Accuracy Out-of-field

- Calculation of dose volume histograms (DVHs) to organs at risk (OARs)
- Dose optimisation
- Calculation of dose to implanted devices or foetus
- Studies have shown Eclipse AAA may underestimate the (local) dose out-of-field >50%
- Implication of incorrect modelling of out-of-field dose can also influence dose to the target (Kim et al. 2001 Med. Phys) – contributes >10%

Howell et al PMB 2010
Average 40% difference

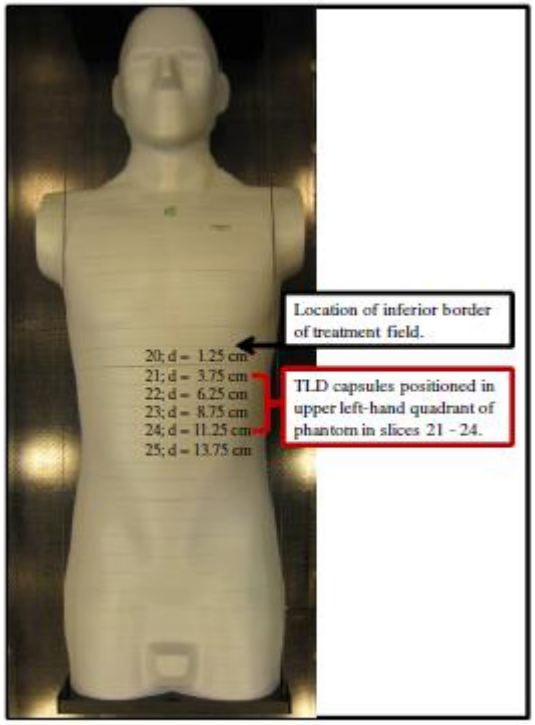

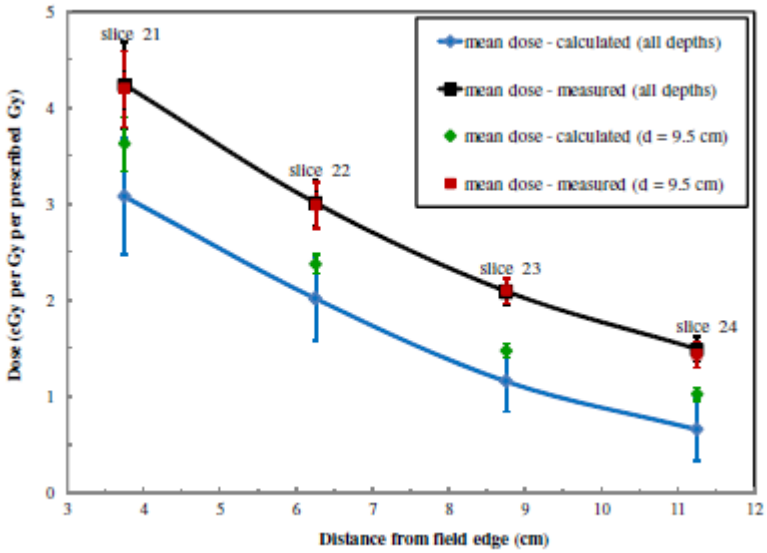

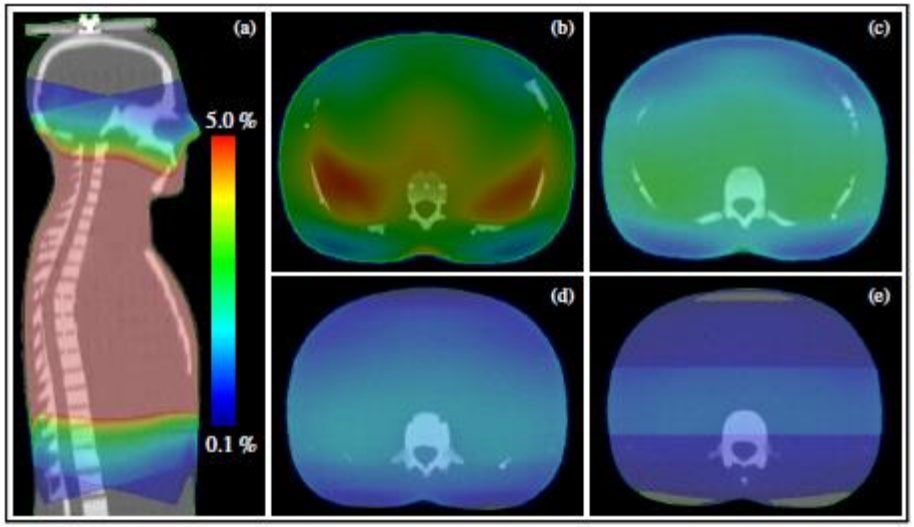

Also: Huang et al J. Appl Clin Med Phys 2013
Average 50% difference

Input data dependant? Detector dependant?

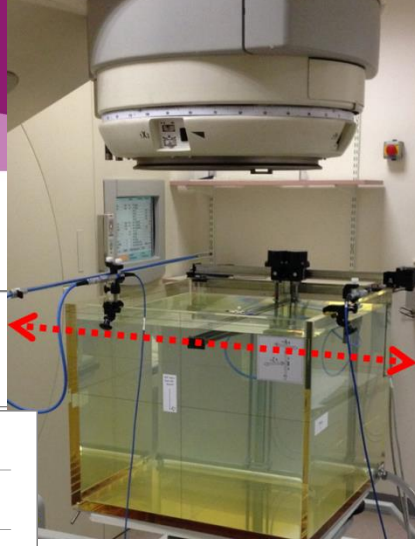

In-plane TPS profile comparison at 10cm

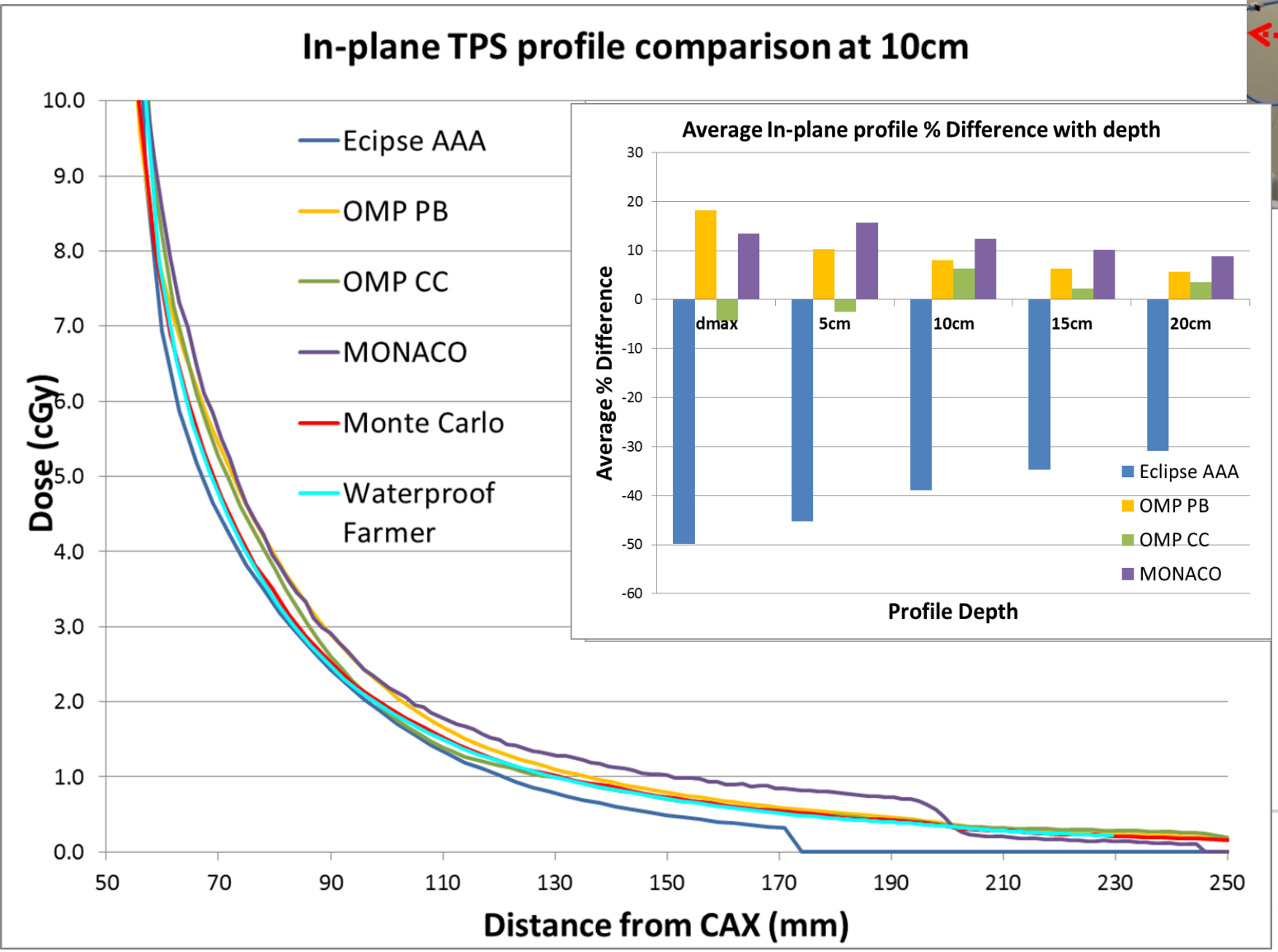

ESTRO School

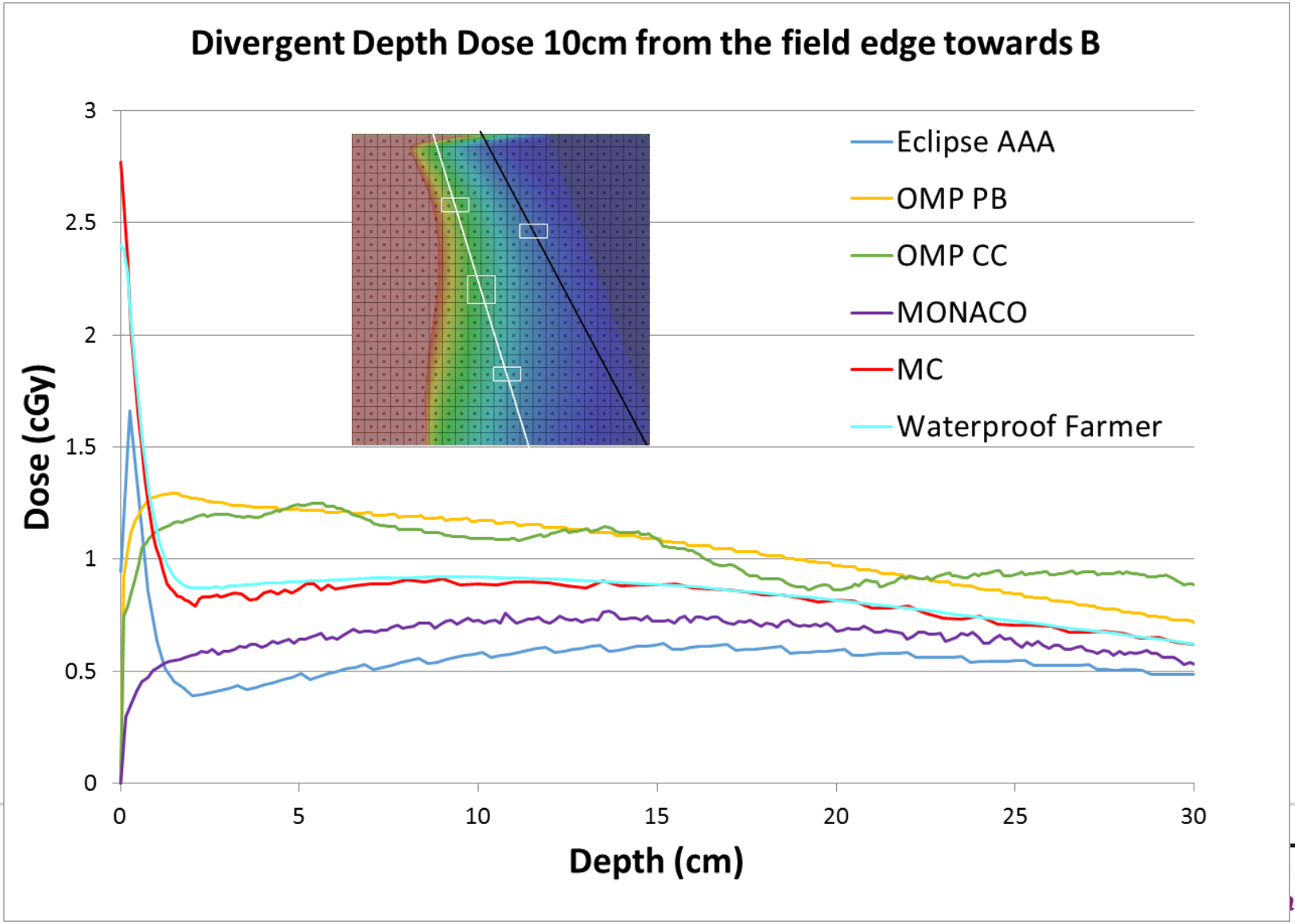
Divergent Depth Dose 10cm from the field edge towards B
Dose (cGy)
Depth (cm)
0
0.5
1
1.5
2
2.5
3
0
5
10
15
20
25
30
Eclipse AAA
OMP PB
OMP CC
MONACO
MC
Waterproof Farmer

Conclusions: TPS

- Considerable variation in out-of-field dose calculation by different TPSs
- Differences between MC and TPS increased with increasing distance from the field edge but improved with increasing depth
- Not all TPS underestimated the dose
- Accuracy of TPS could be improved by refining the acceptance criteria

Patient scatter

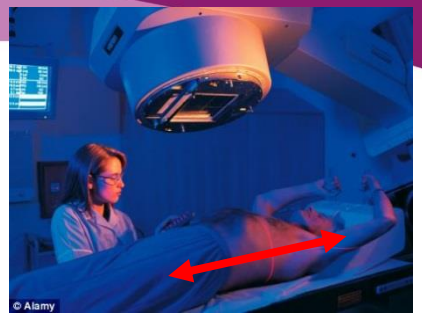

Pencil kernel models

* ***Best in class!***

- Heterogeneity scaling lacking (water patient)

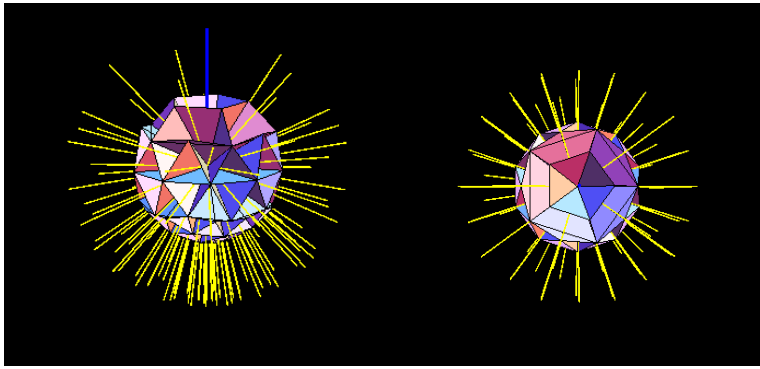

Point kernel

- Heterogeneity scaling typically included
- Collapsed Cone yield angular discretization effects at far away distances

Grid solvers

- Angular discretization effects?

Monte Carlo

- Low doses far away from field is extremely computer time demanding to achieve statistics

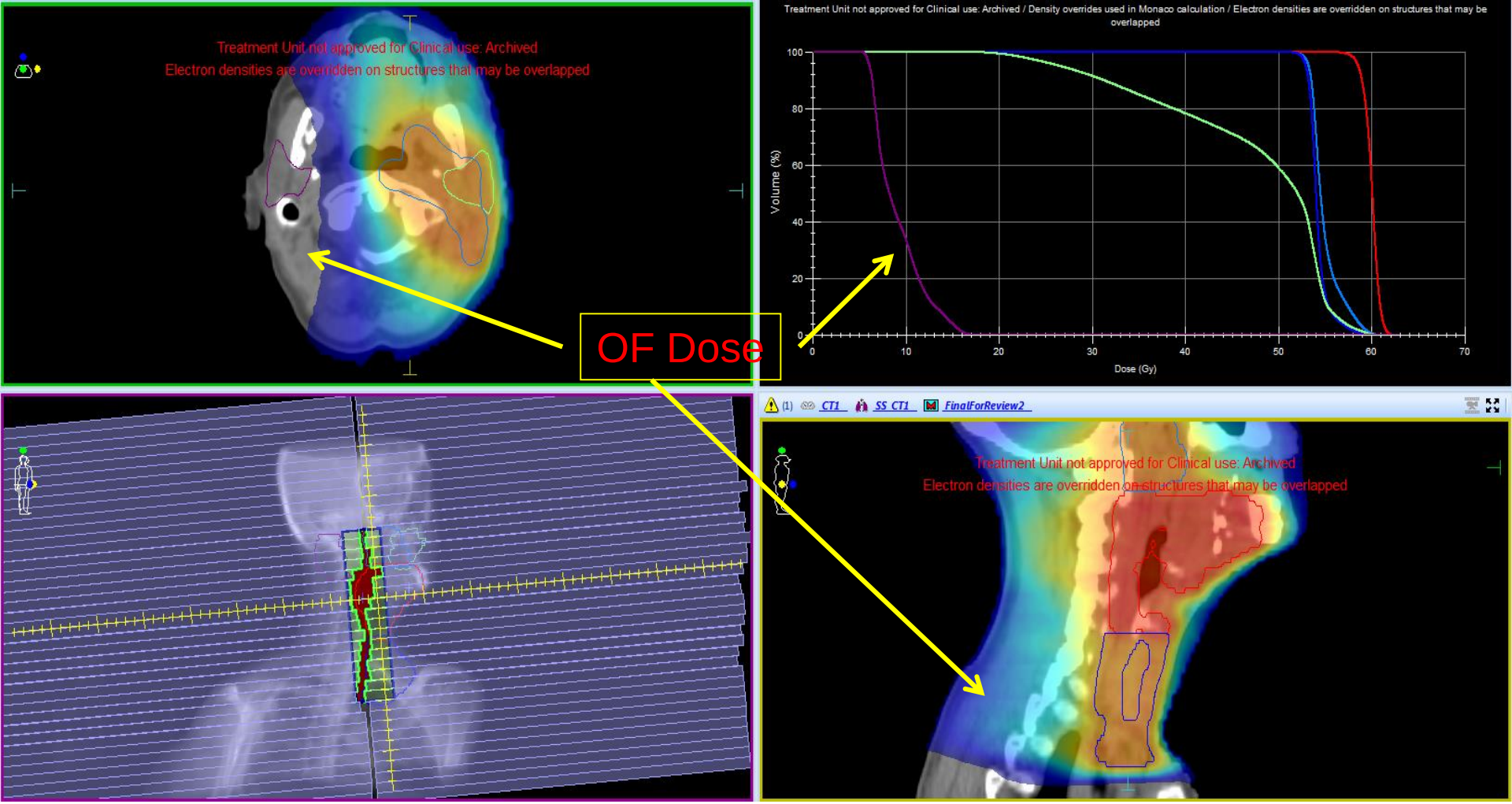

SLH H&N plan VMAT 2015. Marion Quinn

- **Effect of out of field doses?**
- **How accurate is the calculation of out of field dose?**
- **How do we measure it?**

Detector Study Aims

- Investigate the response of a range of clinically available detectors to out-of-field radiation
- Identify the most appropriate detector for out-of-field dosimetry by comparison to MC calculated out-of-field dose

Energy Dependence

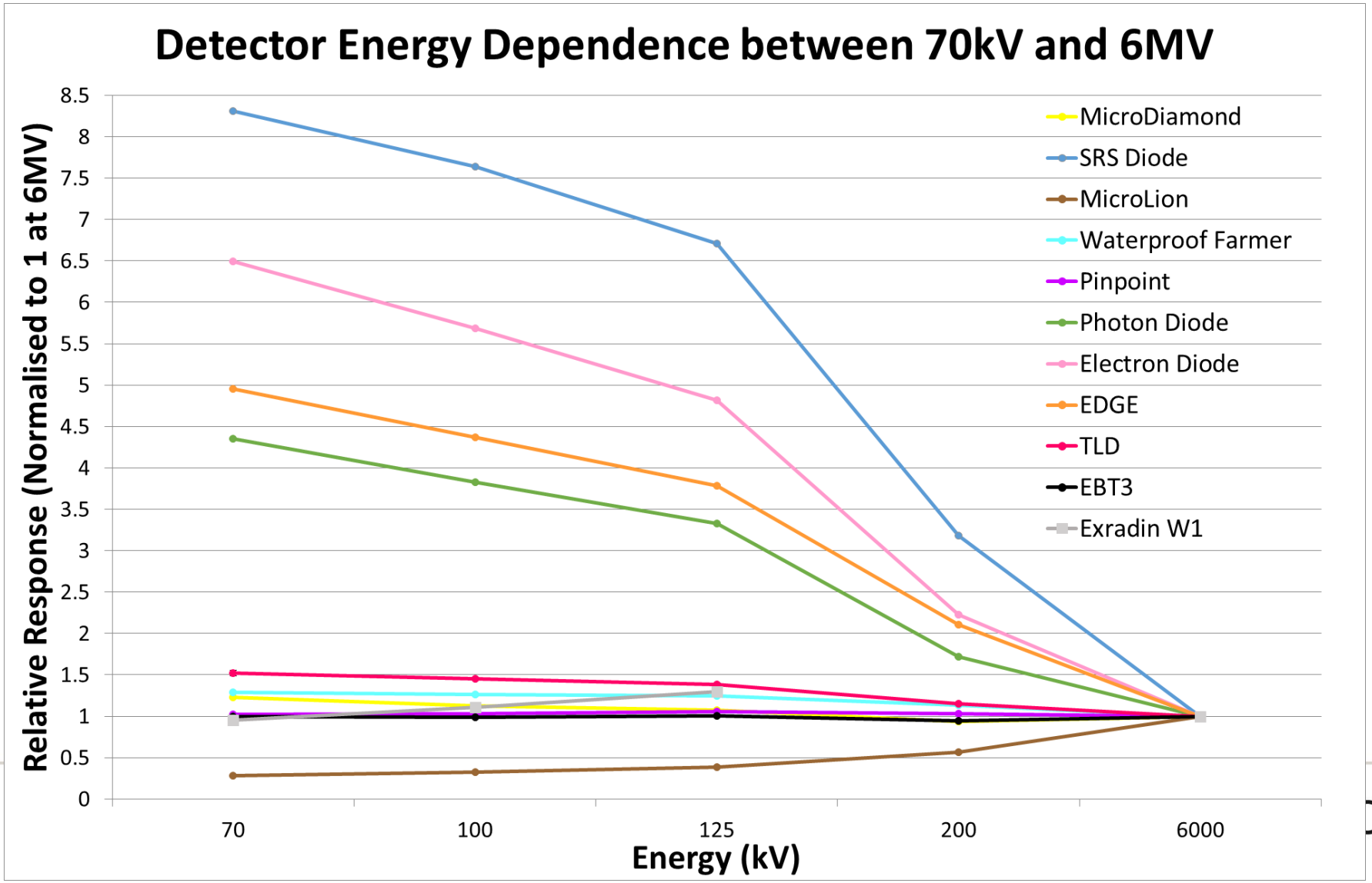

Results - Profiles

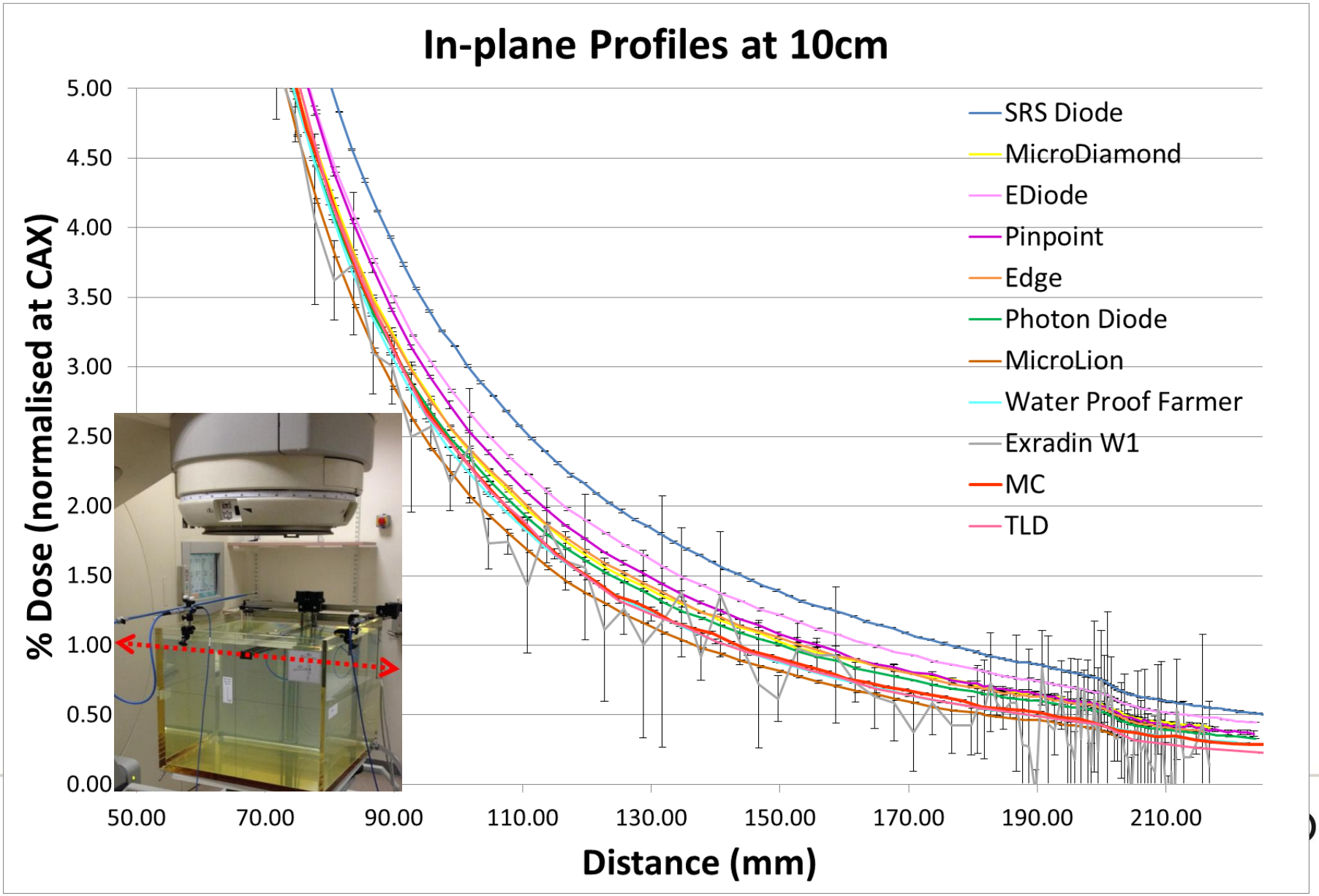

In-plane Profile Step

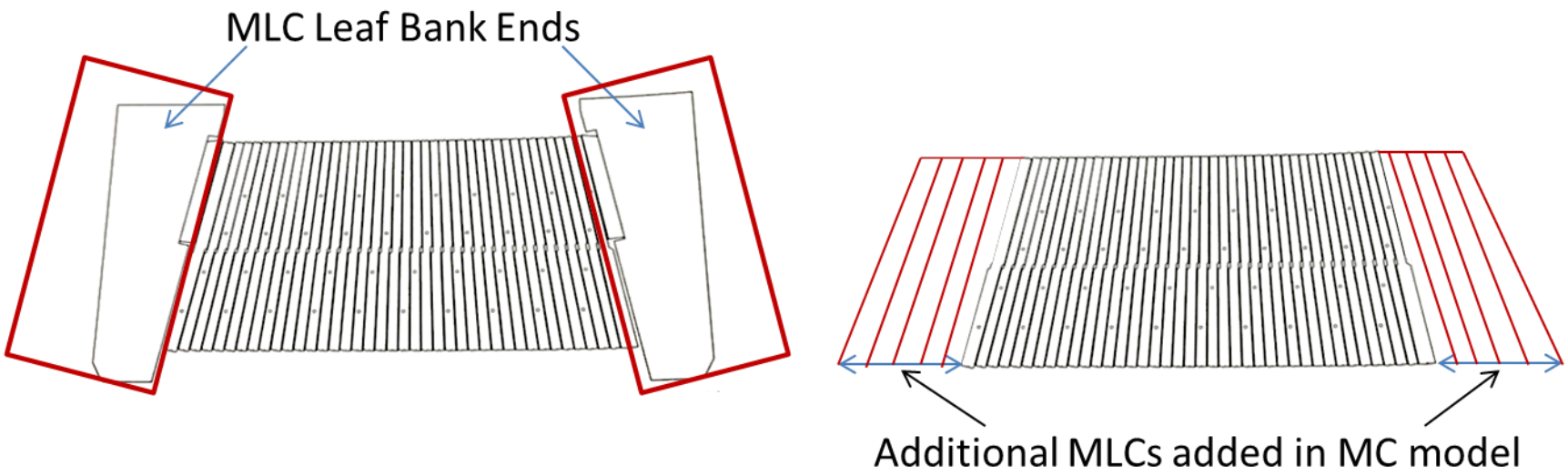

Divergent PDD

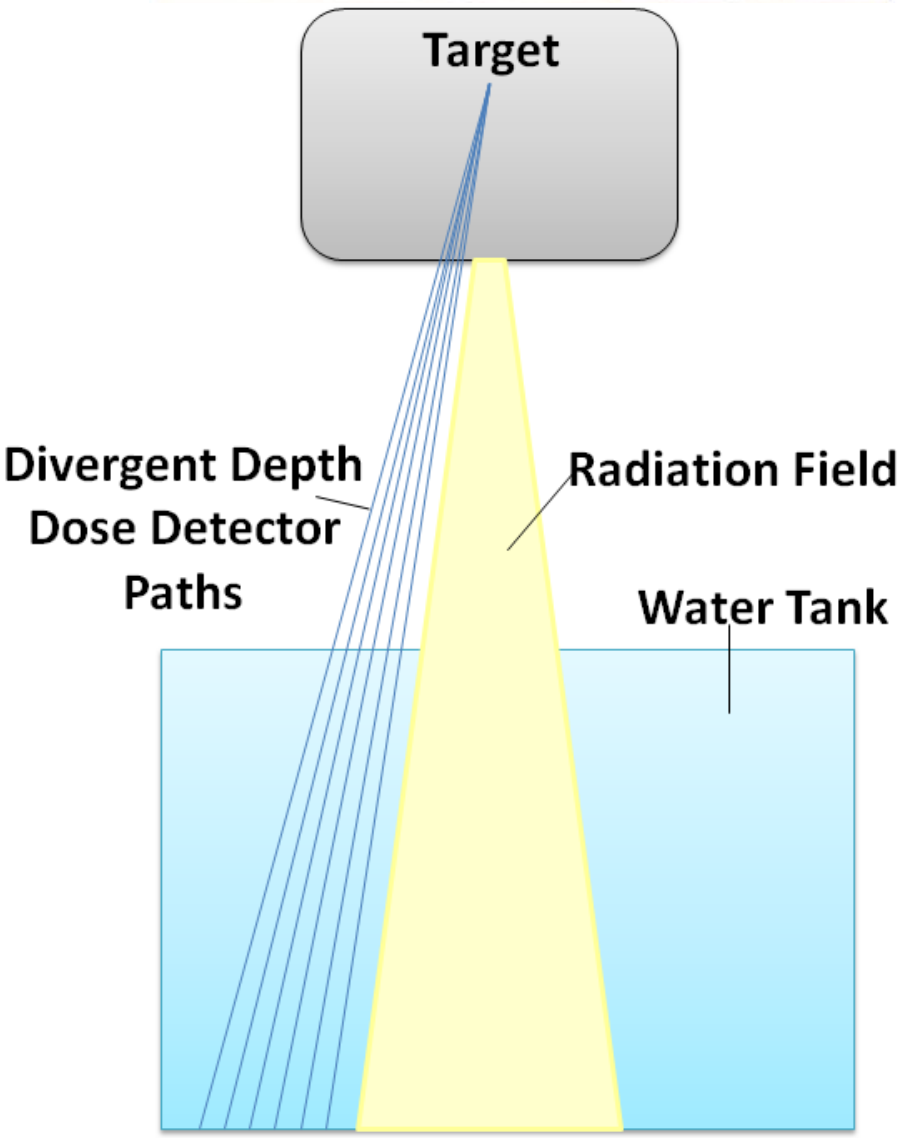

Divergent Depth Doses

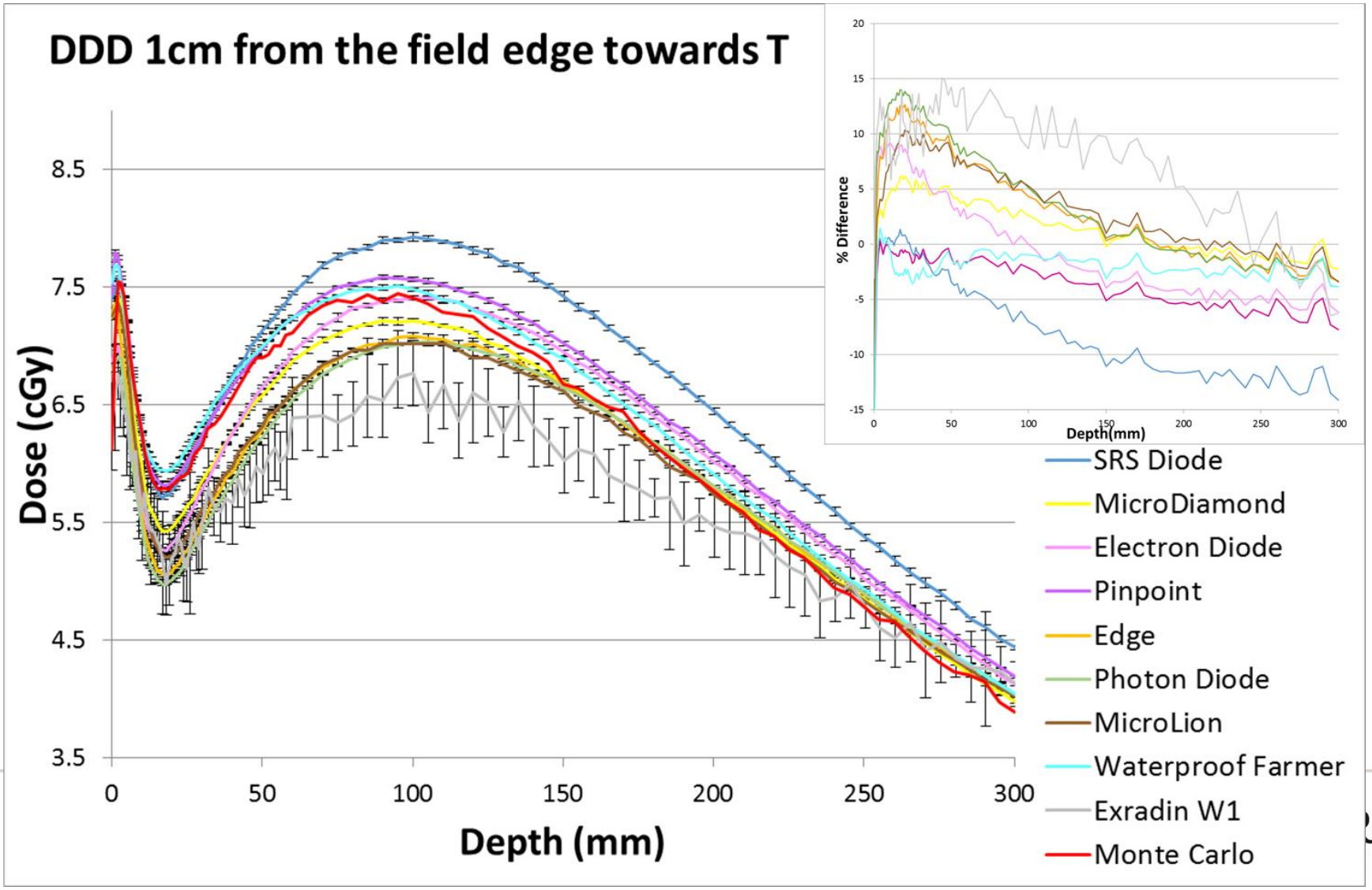

Divergent Depth Doses

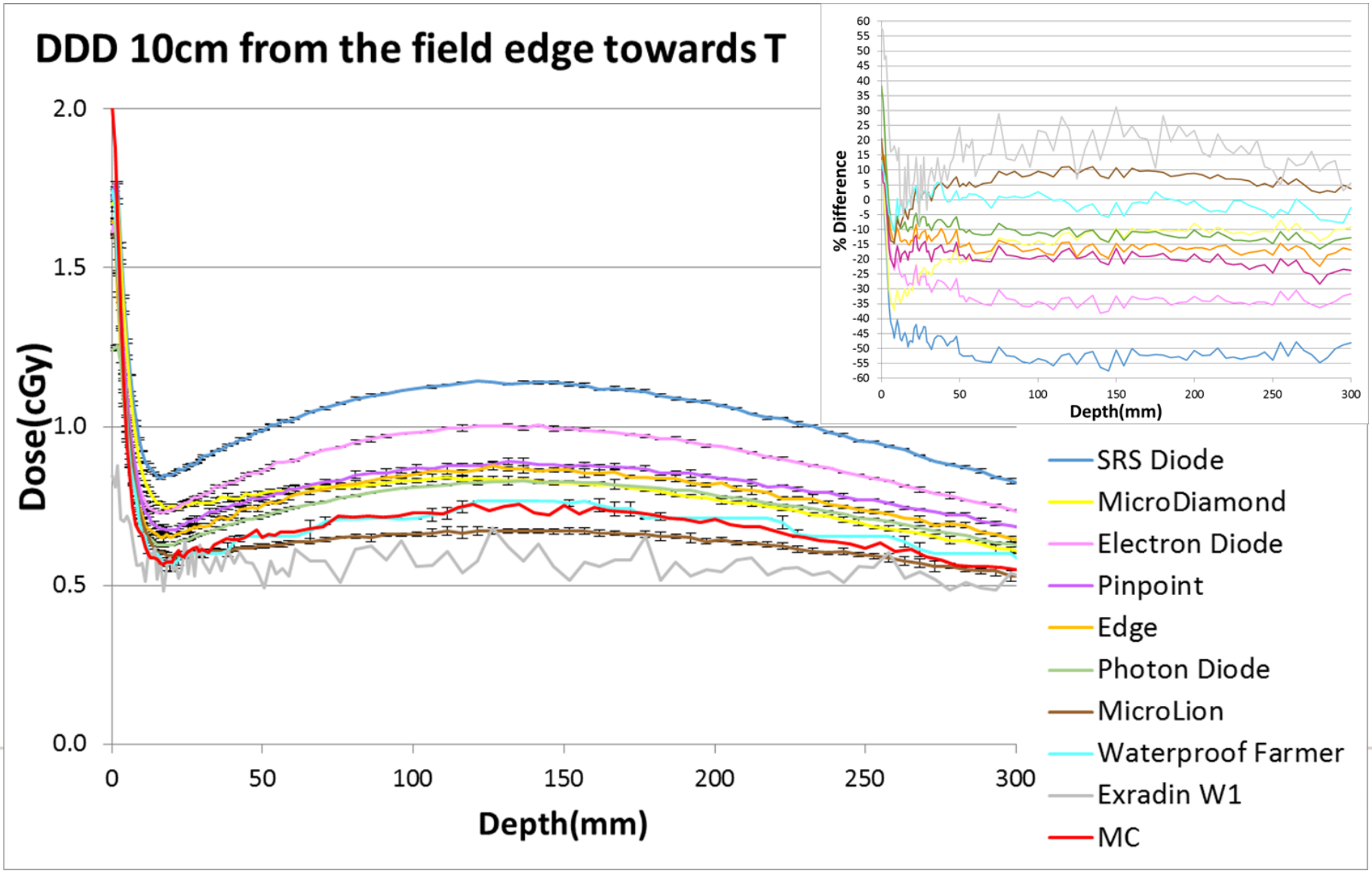

Divergent Depth Doses

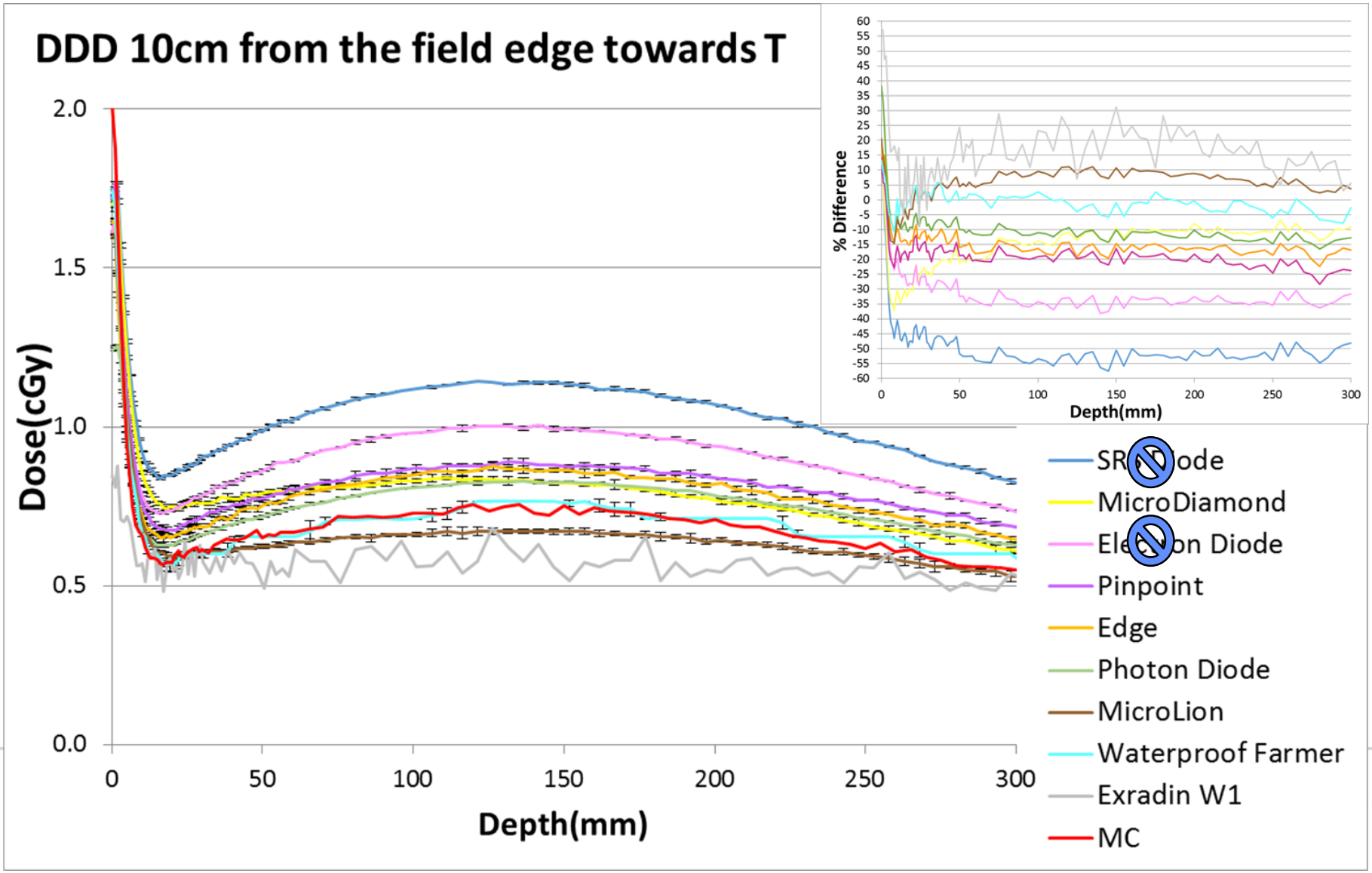

Conclusions: Detector Study

- Waterproof Farmer chamber agreed best with MC
- The SRS and Electron Diodes and Gafchromic EBT3 film is not recommended for out-of-field dosimetry
- Reproducible method of acquiring out-of-field depth doses required
- Presence of Dmin at depth of dmax in-field

Summary

- **Out of field doses in radiotherapy can be relatively high**
- **Modern treatment techniques can deliver low doses to larger volumes**
- **Need improved dose models and measurements to assess:**
  - **radiobiological impact – effects on cell types**
  - **clinical impact – improved optimisation and clinical DVC's**
  - **Cancer induction risks**
- **Careful selection of detectors for out of field measurements**
- **Guidelines for commissioning TPS for out of field doses?**

Grid based approaches

Crister Ceberg

Medical Radiation Physics

Lund University

Sweden

Learning objectives

After completing this module you should be able to

- Formulate the radiation transport equation
- Identify common simplifications
- Describe the solution using deterministic methods
- Discuss the performance of one such model

THE RADIATION TRANSPORT EQUATION

Vector fluence

$$\vec{\Phi}_{j,\Omega,E} = \vec{\Omega}\Phi_{j,\Omega,E}$$

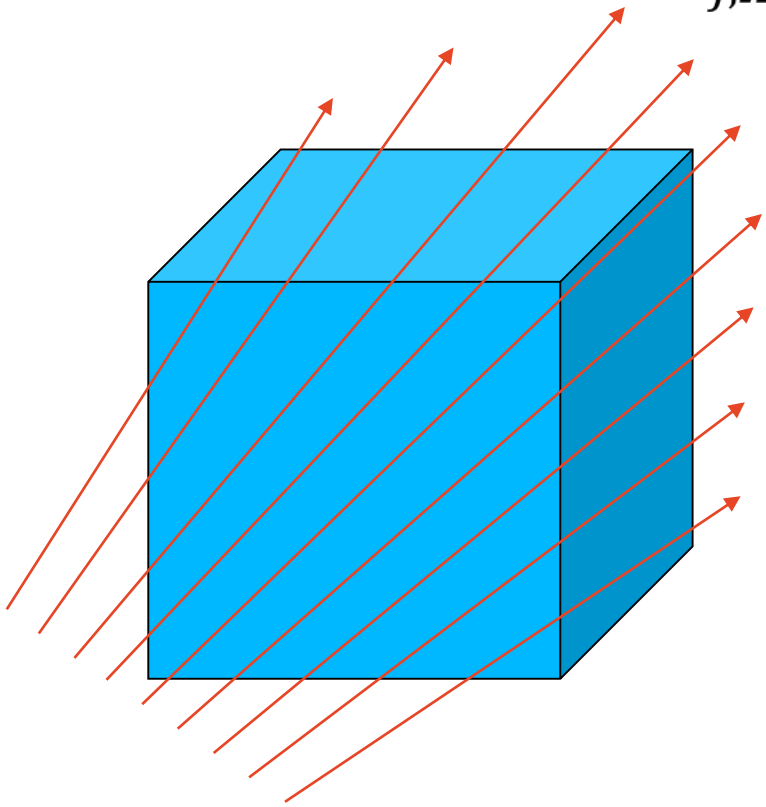

Net transport of particles out of a volume

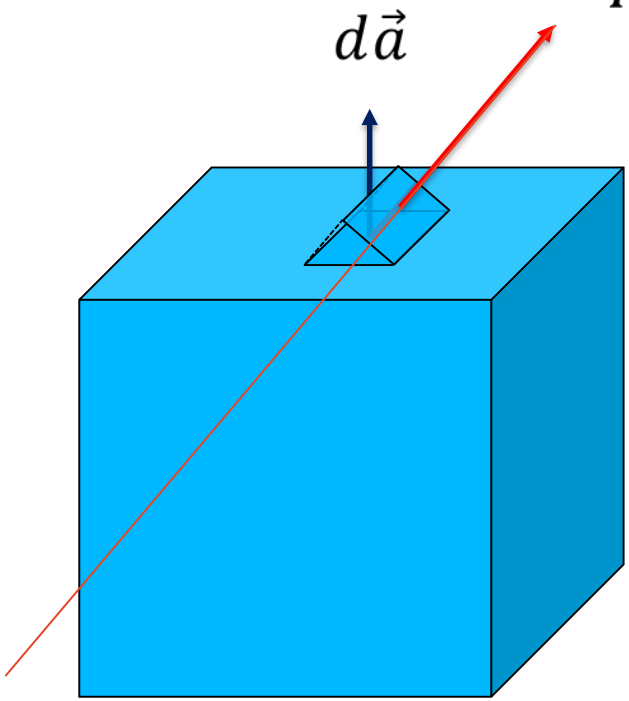

$$\vec{\Phi}_{j,\Omega,E} = \vec{\Omega}\Phi_{j,\Omega,E}$$

$$dn_{j,\Omega,E} = \vec{\Phi}_{j,\Omega,E} \cdot \overrightarrow{da}$$

$$n_{j,\Omega,E} = N^{in}_{j,\Omega,E} - N^{out}_{j,\Omega,E} = \oiint_A dn_j$$

$$n_{j,\Omega,E} = \oiint_A \vec{\Phi}_{j,\Omega,E} \cdot \overrightarrow{da}$$

$$n_{j,\Omega,E} = \iiint_V \nabla \cdot \vec{\Phi}_{j,\Omega,E} dV$$

For an infinitesimal volume

$$\frac{dn_{j,\Omega,E}}{dV} = \frac{d}{dV}\iiint_V \nabla \cdot \vec{\Phi}_{j,\Omega,E} dV = \nabla \cdot \vec{\Phi}_{j,\Omega,E}$$

Sink term

- Outscatter

Source terms

- Inscatter
- Radiation production

Outscatter

$$Outscatter: \; -\Phi_{j,\Omega,E}(\vec{\Omega}, E)\, \mu_j(E)$$

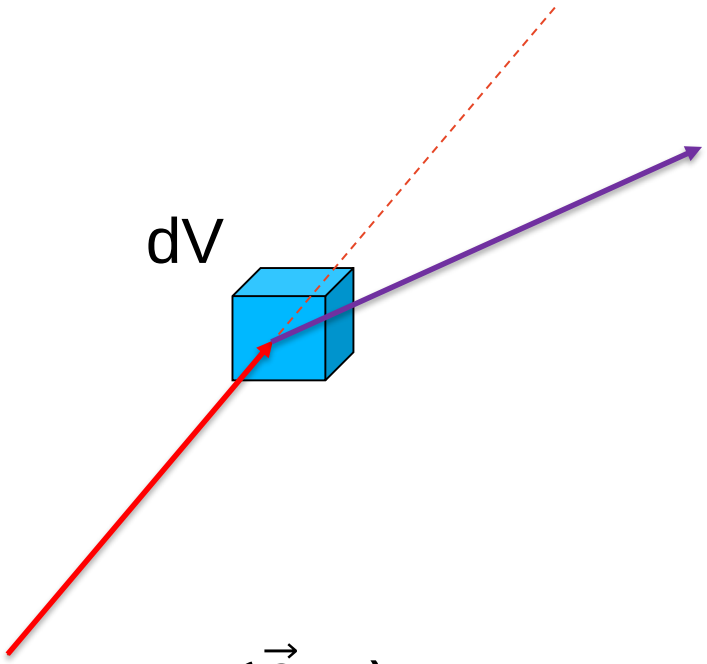

$$\mu = \rho \frac{N_A}{M} \sigma$$

Inscatter

$$Inscatter: +\sum_{j'} \int_{4\pi} d\Omega' \int_{E_{cut}}^{\infty} dE'\, \Phi_{j',\Omega,E}(\vec{\Omega}', E')\mu_{j'\to j,\Omega,E}(\vec{\Omega}', E'; \vec{\Omega}, E)$$

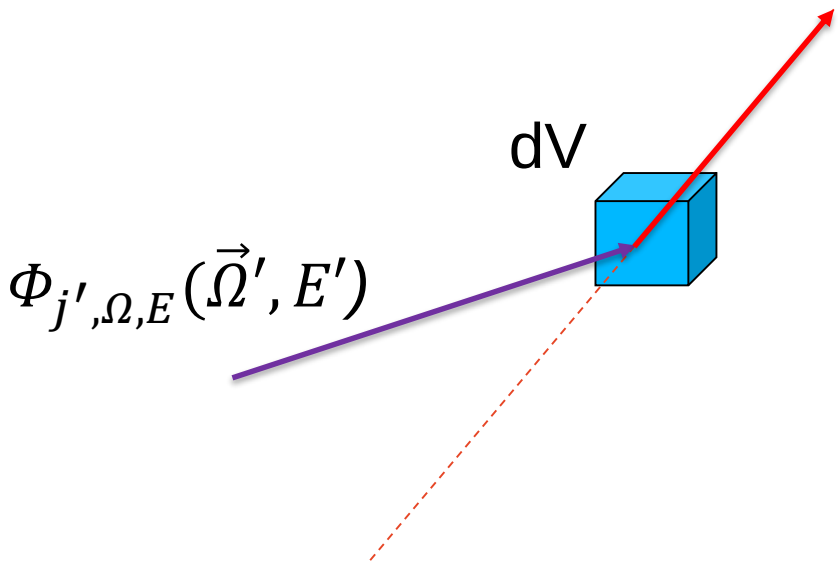

Radiation production

$$Radiation\ production: \quad + S_{j,\Omega,E}$$

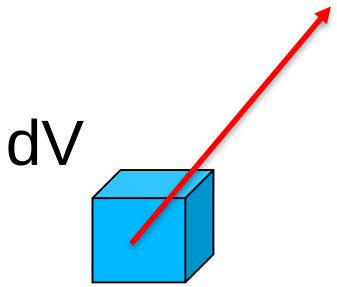

The radiation transport equation

For all particle types:

$$\nabla \cdot \vec{\Phi}_{j,\Omega,E}(\vec{\Omega},E) = -\Phi_{j,\Omega,E}(\vec{\Omega},E)\mu_j(E)$$

$$+\sum_{j'}\int_{4\pi} d\Omega' \int_{E_{cut}}^{\infty} dE'\, \Phi_{j',\Omega,E}(\vec{\Omega}',E')\mu_{j'\to j,\Omega,E}(\vec{\Omega}',E';\vec{\Omega},E)$$

$$+S_{j,\Omega,E}$$

Solving the radiation transport equation

$$\nabla \cdot \vec{\Phi}_{j,\Omega,E}(\vec{\Omega},E) = -\Phi_{j,\Omega,E}(\vec{\Omega},E)\mu_j(E) + \sum_{j'} \int_{4\pi} d\Omega' \int_{E_{cut}}^{\infty} dE'\, \Phi_{j',\Omega,E}(\vec{\Omega}',E')\mu_{j'\to j,\Omega,E}(\vec{\Omega}',E';\vec{\Omega},E) + S_{j,\Omega,E}$$

- Solve for $\Phi_{j,\Omega,E}\ (\Omega, E)$
  - Analytical solution is generally not feasible
- Convergent techniques
  - Monte Carlo
  - Deterministic methods

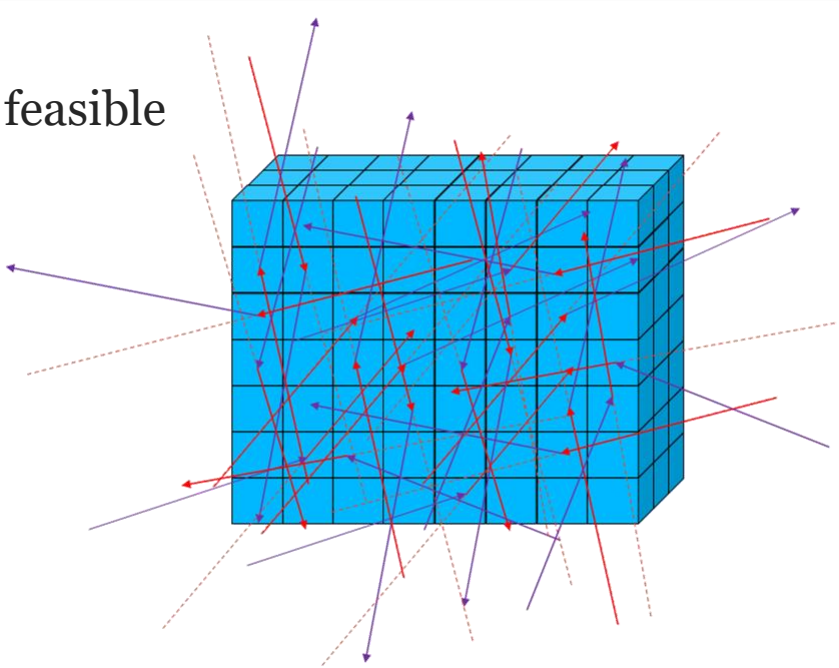

DETERMINISTIC MODELS

General simplifications

$$\nabla \cdot \vec{\Phi}_{j,\Omega,E}(\vec{\Omega},E) = -\Phi_{j,\Omega,E}(\vec{\Omega},E)\mu_j(E) + \sum_{j'} \int_{4\pi} d\Omega' \int_{E_{cut}}^{\infty} dE'\, \Phi_{j',\Omega,E}(\vec{\Omega}',E')\mu_{j'\to j,\Omega,E}(\vec{\Omega}',E';\vec{\Omega},E) + S_{j,\Omega,E}$$

- Particle types
  - Consider only photons and electrons
  - Positrons are treated as electrons
- Interaction types
  - Photons can produce electrons, electrons cannot produce photons
  - Bremsstrahlung neglected
- Primary and scattered fluence
  - External source of primary fluence
  - Raytracing of primary fluence
  - No internal source of primary radiation

Acuros® XB in Varian Eclipse

- Los Alamos National Laboratory
  - Developed a code named Attila
  - Around 2000
  - Wareing TA, McGhee JM et al.
- Transpire Inc.
  - Founded mid 2000
  - Wareing T, McGhee JM, Failla GA et al.
  - Developed Acuros for radiotherapy
- MD Anderson
  - Vassiliev O, Gifford KA, et al.
- Varian
  - Introduced Acuros XB in Eclipse v10.0

Source model (same as in AAA)

- Primary source – user-defined circular or elliptical source located at the target plane which models the bremsstrahlung photons created in the target that do not interact in the treatment head.
- Extra focal source – Gaussian plane source located at the bottom of the flattening filter, which models the photons that result from interactions in the accelerator head outside the target (primary in the flattening filter, primary collimators, and secondary jaws).
- Electron contamination – represents the dose deposited in the build-up region not accounted for by the primary and extra-focal source components.
- Photons scattered from wedge – represents the scatter from hard wedges, where present. Implemented with a dual Gaussian model, where the width of the Gaussian kernel increases with distance from the wedge.

Four step solution

1. Transport of primary photon fluence
2. Calculation of scattered photon fluence
3. Calculation of scattered electron fluence
4. Dose calculation

Transport of primary photon fluence

- Transport in 1D
- No electron transport
- Outscattering = attenuation
- No inscattering, no production

$$\nabla \cdot \vec{\Phi}_{j,\Omega,E}(\vec{\Omega},E) = -\Phi_{j,\Omega,E}(\vec{\Omega},E)\mu_j(E) + \sum_{j'} \int_{4\pi} d\Omega' \int_{E_{cut}}^{\infty} dE'\, \Phi_{j',\Omega,E}(\vec{\Omega}',E')\mu_{j'\to j,\Omega,E}(\vec{\Omega}',E';\vec{\Omega},E) + S_{j,\Omega,E}$$

$$\frac{d\Phi_\gamma}{dz} = -\Phi_\gamma \mu + 0 + 0$$

$$\Phi_\gamma(z) = \Phi_\gamma(0)e^{-\mu z}$$

Transport of primary photon fluence

- Point source of primary photons at $\vec{r}_p$
- No electron transport
- Outscattering = attenuation
- No inscattering

$$\nabla \cdot \vec{\Phi}_{j,\Omega,E}(\vec{\Omega},E) = -\Phi_{j,\Omega,E}(\vec{\Omega},E)\mu_j(E) + \sum_{j'} \int_{4\pi} d\Omega' \int_{E_{cut}}^{\infty} dE'\, \Phi_{j',\Omega,E}(\vec{\Omega}',E')\mu_{j'\to j,\Omega,E}(\vec{\Omega}',E';\vec{\Omega},E) + S_{j,\Omega,E}$$

$$\nabla \cdot \vec{\Phi}_{\gamma,\Omega,E}(\vec{\Omega},E) = -\Phi_{\gamma,\Omega,E}(\vec{\Omega},E)\mu(E) + S_{\gamma,\Omega,E}\left(\vec{r}_p, \vec{\Omega}_{\vec{r},\vec{r}_p}\right)$$

$$\Phi_{\gamma,\Omega,E}(\vec{r}) = \frac{S_{\gamma,\Omega,E}\left(\vec{r}_p, \vec{\Omega}_{\vec{r},\vec{r}_p}\right)}{4\pi\left|\vec{r}-\vec{r}_p\right|^2} e^{-\mu|\vec{r}-\vec{r}_p|}$$

1. Transport of primary photon fluence

$$\nabla \cdot \vec{\Phi}^{prim}_{\gamma,\Omega,E}\left(\vec{\Omega},E\right) = -\Phi^{prim}_{\gamma,\Omega,E}\left(\vec{\Omega},E\right)\mu_{\gamma}(E) + S_{\gamma,\Omega,E}\left(\vec{r}_p,\vec{\Omega}_{\vec{r},\vec{r}_p}\right)$$

$$\Phi^{prim}_{\gamma,\Omega,E}(\vec{r}) = \frac{S_{\gamma,\Omega,E}\left(\vec{r}_p,\vec{\Omega}_{\vec{r},\vec{r}_p}\right)}{4\pi\left|\vec{r}-\vec{r}_p\right|^2} e^{-\mu_{\gamma} z_{rad}(\vec{r},\vec{r}_p)}$$

2. Calculation of scattered photon fluence

$$\nabla \cdot \vec{\Phi}_{\gamma,\Omega,E}\left(\vec{\Omega},E\right) = -\Phi_{\gamma,\Omega,E}\left(\vec{\Omega},E\right)\mu_{\gamma}\ (E)$$
$$+\int_{4\pi} d\Omega' \int_{E_{cut}}^{\infty} dE' \Phi_{\gamma,\Omega,E}(\vec{\Omega}',E')\ \mu_{\gamma\rightarrow\gamma,\Omega,E}\left(\vec{\Omega}',E';\vec{\Omega},E\right)$$

where

$$\Phi_{\gamma,\Omega,E} = \Phi^{prim}_{\gamma,\Omega,E} + \Phi^{scat}_{\gamma,\Omega,E}$$

Inscattering term

$$\nabla \cdot \vec{\Phi}_{\gamma,\Omega,E}(\vec{\Omega},E) = -\Phi_{\gamma,\Omega,E}(\vec{\Omega},E)\mu_{\gamma}\ (E) + \underbrace{\int_{4\pi} d\Omega' \int_{E_{cut}}^{\infty} dE' \Phi_{\gamma,\Omega,E}(\vec{\Omega}',E')\ \mu_{\gamma\to\gamma,\Omega,E}(\vec{\Omega}',E';\vec{\Omega},E)}_{Q(\vec{\Omega},E)}$$

$$Q(\vec{\Omega},E) = \int_{4\pi} d\Omega' \int_{E_{cut}}^{\infty} dE' \Phi_{\gamma,\Omega,E}(\vec{\Omega}',E')\ \mu_{\gamma\to\gamma,\Omega,E}(\vec{\Omega}',E';\vec{\Omega},E)$$

Inscattering term – fluence

$$Q(\vec{\Omega}, E) = \int_{4\pi} d\Omega' \int_{E_{cut}}^{\infty} dE' \Phi_{\gamma,\Omega,E}(\vec{\Omega}', E') \mu_{\gamma\to\gamma,\Omega,E}(\vec{\Omega}', E'; \vec{\Omega}, E)$$

$$\Phi_{\gamma,\Omega,E}(\vec{\Omega}', E') = \sum_{l=0}^{\infty} \sum_{-l}^{+l} \varphi_l^m(E') Y_l^m(\vec{\Omega}')$$

$$\varphi_l^m(E') = \int_{4\pi} Y_l^m(\vec{\Omega}') \Phi_{\gamma,\Omega,E}(\vec{\Omega}', E') d\Omega'$$

Inscattering term – fluence

$$Q(\vec{\Omega}, E) = \int_{4\pi} d\Omega' \int_{E_{cut}}^{\infty} dE' \Phi_{\gamma,\Omega,E}(\vec{\Omega}', E') \mu_{\gamma\to\gamma,\Omega,E}(\vec{\Omega}', E'; \vec{\Omega}, E)$$

$$\Phi_{\gamma,\Omega,E}(\vec{\Omega}', E') = \sum_{l=0}^{\infty} \sum_{-l}^{+l} \varphi_l^m(E') Y_l^m(\vec{\Omega}')$$

$$\varphi_l^m(E') = \int_{4\pi} Y_l^{m*}(\vec{\Omega}') \Phi_{\gamma,\Omega,E}(\vec{\Omega}', E') d\Omega' \approx \sum_n w_n Y_l^{m*}(\vec{\Omega}'_n) \Phi_{\gamma,\Omega,E}(\vec{\Omega}'_n, E')$$

Inscattering term – cross section

$$Q(\vec{\Omega}, E) = \int_{4\pi} d\Omega' \int_{E_{cut}}^{\infty} dE' \Phi_{\gamma,\Omega,E}(\vec{\Omega}', E') \, \mu_{\gamma\to\gamma,\Omega,E}(\vec{\Omega}', E'; \vec{\Omega}, E)$$

$$\mu_{\gamma\to\gamma,\Omega,E}(\vec{\Omega}\cdot\vec{\Omega}', E', E) = \sum_{l=0}^{\infty} \frac{2l+1}{4\pi} m_{\gamma\to\gamma,\Omega,E}(E', E) P_l(\vec{\Omega}\cdot\vec{\Omega}')$$

$$m_{\gamma\to\gamma,\Omega,E}(E', E) = \frac{1}{2}\int_{-1}^{1} P_l(\vec{\Omega}\cdot\vec{\Omega}') \, \mu_{\gamma\to\gamma,\Omega,E}(\vec{\Omega}\cdot\vec{\Omega}', E', E) d(\vec{\Omega}\cdot\vec{\Omega}')$$

Inscattering term – reorder

$$Q(\vec{\Omega}, E) = \int_{4\pi} d\Omega' \int_{E_{cut}}^{\infty} dE' \Phi_{\gamma,\Omega,E}(\vec{\Omega}', E')\, \mu_{\gamma\to\gamma,\Omega,E}(\vec{\Omega}', E'; \vec{\Omega}, E)$$

$$Q(\vec{\Omega}, E) = \int_{4\pi} d\Omega' \int_{E_{cut}}^{\infty} dE' \left[\sum_{l=0}^{\infty}\sum_{-l}^{+l} \varphi_l^m(E') Y_l^m(\vec{\Omega}')\right]\left[\sum_{l=0}^{\infty} \frac{2l+1}{4\pi} m_{\gamma\to\gamma,\Omega,E}(E', E) P_l(\vec{\Omega}\cdot\vec{\Omega}')\right]$$

$$Q(\vec{\Omega}, E) = \int_{E_{cut}}^{\infty} \sum_{l=0}^{L}\sum_{-l}^{+l} \varphi_l^m(E'_i) Y_l^m(\vec{\Omega}') m_{\gamma\to\gamma,\Omega,E}(E'_i, E) dE'$$

Inscattering term – energy discretization

$$Q(\vec{\Omega}, E) = \int_{4\pi} d\Omega' \int_{E_{cut}}^{\infty} dE' \Phi_{\gamma,\Omega,E}(\vec{\Omega}', E')\, \mu_{\gamma\to\gamma,\Omega,E}(\vec{\Omega}', E'; \vec{\Omega}, E)$$

$$Q(\vec{\Omega}, E) = \int_{4\pi} d\Omega' \int_{E_{cut}}^{\infty} dE' \left[\sum_{l=0}^{\infty}\sum_{-l}^{+l} \varphi_l^m(E') Y_l^m(\vec{\Omega}')\right]\left[\sum_{l=0}^{\infty} \frac{2l+1}{4\pi} m_{\gamma\to\gamma,\Omega,E}(E', E) P_l(\vec{\Omega}\cdot\vec{\Omega}')\right]$$

$$Q(\vec{\Omega}, E) = \sum_{i}^{L}\sum_{l=0}^{+l}\sum_{-l} \varphi_l^m(E'_i) Y_l^m(\vec{\Omega}') m_{\gamma\to\gamma,\Omega,E}(E'_i, E)\Delta E'_i$$

3. Calculation of scattered electron fluence

$$\nabla \cdot \vec{\Phi}_{e,\Omega,E}\left(\vec{\Omega},E\right) = -\Phi_{e,\Omega,E}\left(\vec{\Omega},E\right)\mu_e(E)$$
$$+\int_{4\pi} d\Omega' \int_{E_{cut}}^{\infty} dE' \Phi_{\gamma,\Omega,E}(\vec{\Omega}',E')\,\mu_{\gamma\to e,\Omega,E}\left(\vec{\Omega}',E';\vec{\Omega},E\right)$$
$$+\int_{4\pi} d\Omega' \int_{E_{cut}}^{\infty} dE' \Phi_{e,\Omega,E}(\vec{\Omega}',E')\,\mu_{e\to e,\Omega,E}\left(\vec{\Omega}',E';\vec{\Omega},E\right)$$

- *Large-angle, large-energy*
- *Small-angle, small-energy (CSDA)*

3. Calculation of scattered electron fluence

$$\nabla \cdot \vec{\Phi}_{e,\Omega,E}(\vec{\Omega},E) = -\Phi_{e,\Omega,E}(\vec{\Omega},E)\mu_e(E) + \int_{4\pi} d\Omega' \int_{E_{cut}}^{\infty} dE' \Phi_{\gamma,\Omega,E}(\vec{\Omega}',E')\, \mu_{\gamma\to e,\Omega,E}(\vec{\Omega}',E';\vec{\Omega},E) + \int_{4\pi} d\Omega' \int_{E_{cut}}^{\infty} dE' \Phi_{e,\Omega,E}(\vec{\Omega}',E')\, \mu_{e\to e,\Omega,E}(\vec{\Omega}',E';\vec{\Omega},E)$$

$$\int_{4\pi} d\Omega' \int_{E_{cut}}^{\infty} dE' \Phi_{e,\Omega,E}(\vec{\Omega}',E')\, \mu_{e\to e,\Omega,E}(\vec{\Omega}',E';\vec{\Omega},E) + \frac{\partial}{\partial E}\left(L_\Delta \Phi_{e,\Omega,E}(\vec{\Omega}',E')\right)$$

Large system of linear equations

- One transport equation for each direction
  - In Acuros 32-512 discrete angles
- Cartesian mesh
  - Variably sized elements
  - Refinement in factors of 2
- Iterative solution
  - Yields $\Phi_{e,\Omega,E}\left(\vec{\Omega}, E\right)$ at each point

4. Absorbed dose calculation

- One transport equation for each direction
  - In Acuros 32-512 discrete angles
- Cartesian mesh
  - Variably sized elements
  - Refinement in factors of 2
- Iterative solution
  - Yields $\Phi_{e,\Omega,E}\left(\vec{\Omega}, E\right)$ at each point
- Absorbed dose is calculated as:

$$D = \int_{E_{cut}}^{\infty} \left[\int_{4\pi} \Phi_{e,\Omega,E}(\vec{\Omega}, E) d\Omega \right] \frac{S_{el}}{\rho} dE$$

PERFORMANCE

Calculation time

- Scaling with number of beams
  - Step 1 (the raytracing) is repeated for each beam
  - Step 2-4 are performed only once

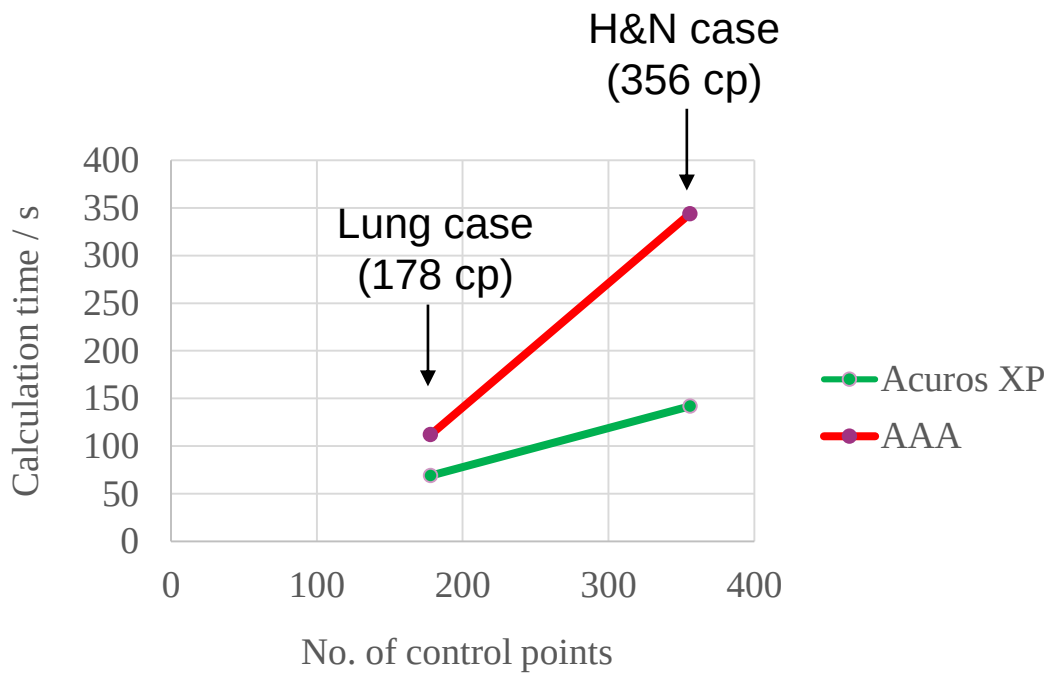

Dose calculation in homogeneous medium

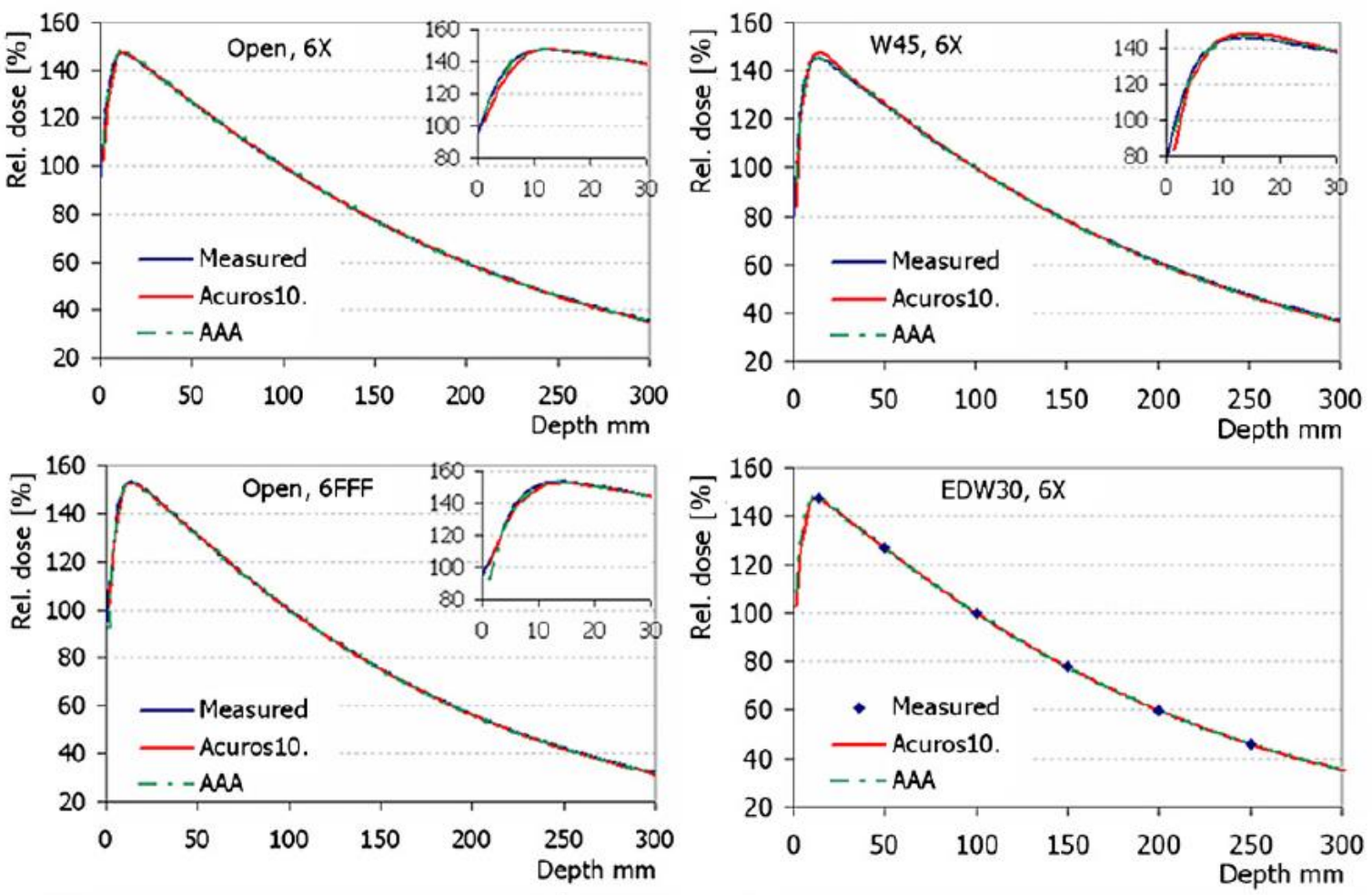

Fogilata et al., Phys Med Biol 56:1879, 2011

ESTRO School

Dose calculation in heterogeneous media

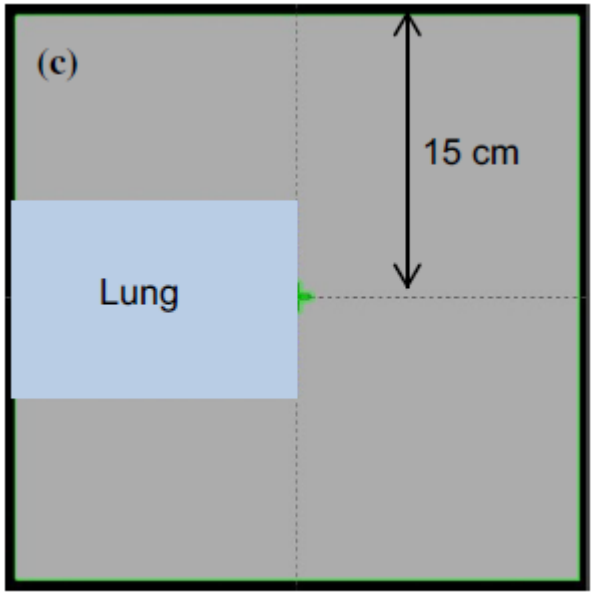

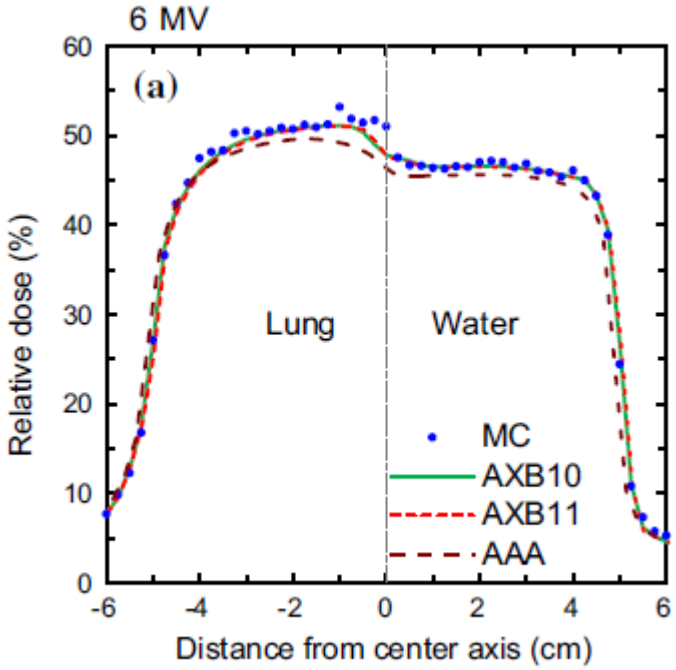

Onizuka et al., Radiol Phys Tech 9:77, 2016

Dose calculation in heterogeneous media

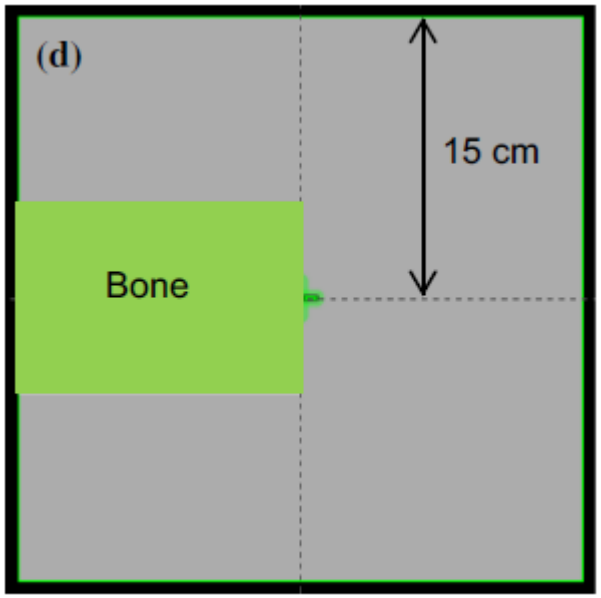

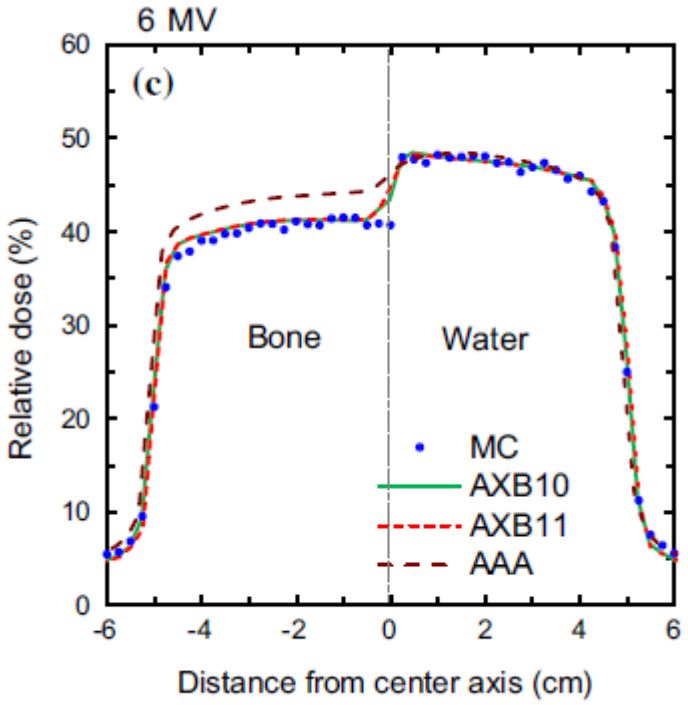

Onizuka et al., Radiol Phys Tech 9:77, 2016

Dose calculation in heterogeneous media

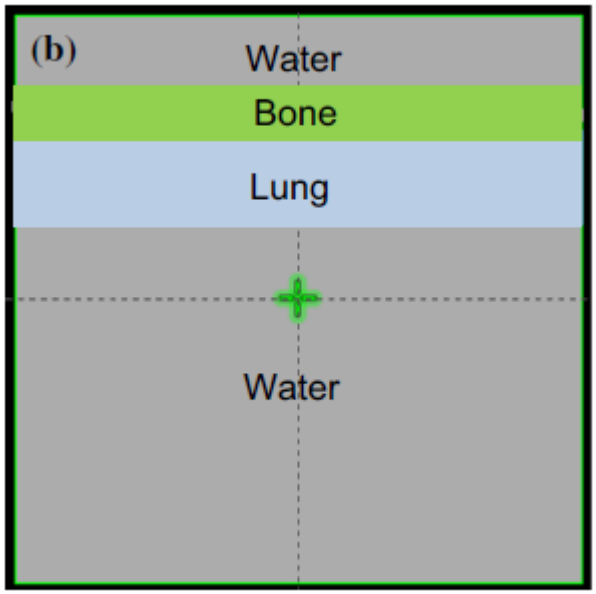

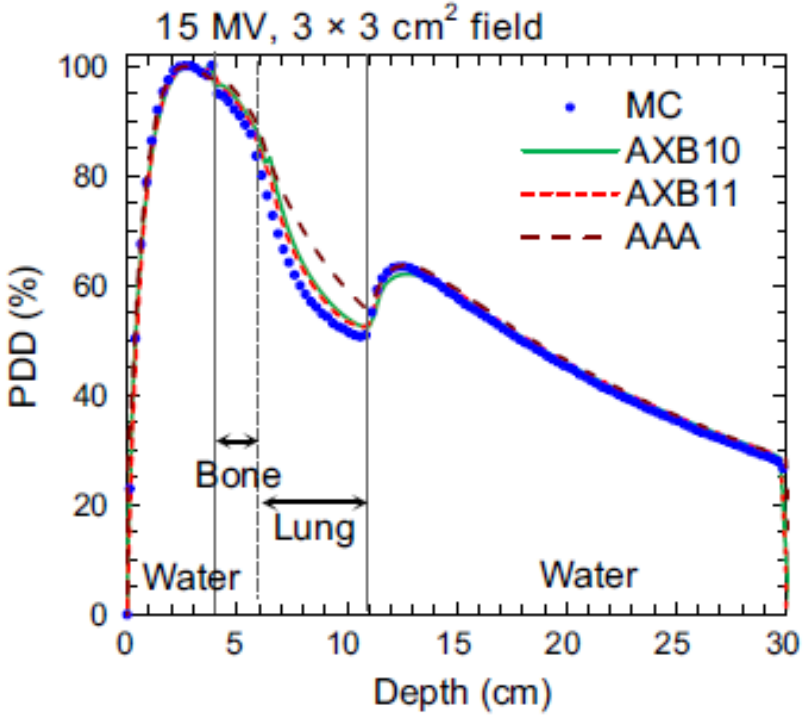

Onizuka et al., Radiol Phys Tech 9:77, 2016

ESTRO School

Dose calculation in heterogeneous media

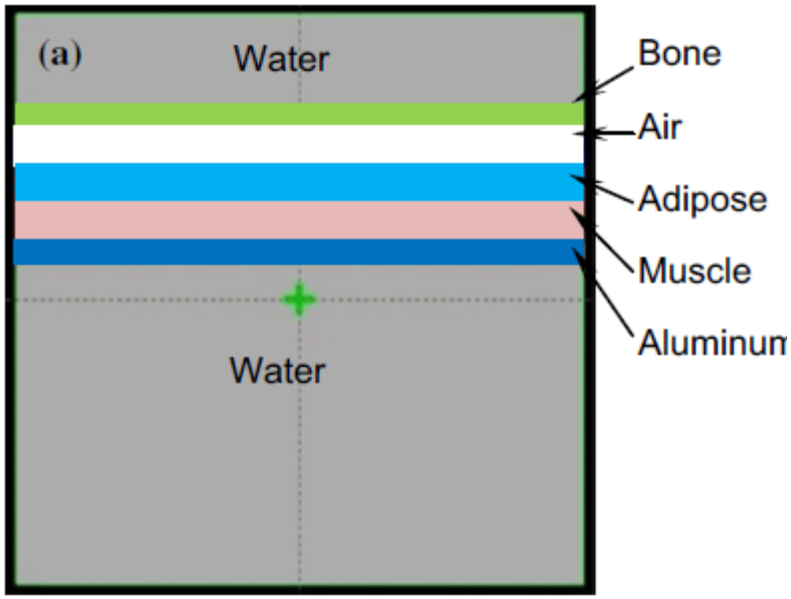

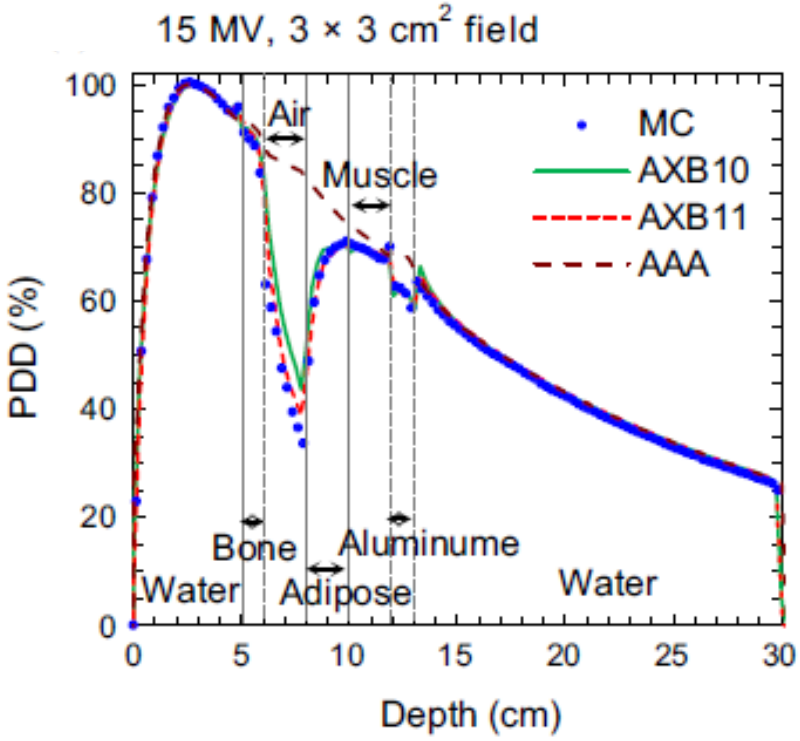

Onizuka et al., Radiol Phys Tech 9:77, 2016

ESTRO School

Dose calculation with air cavities

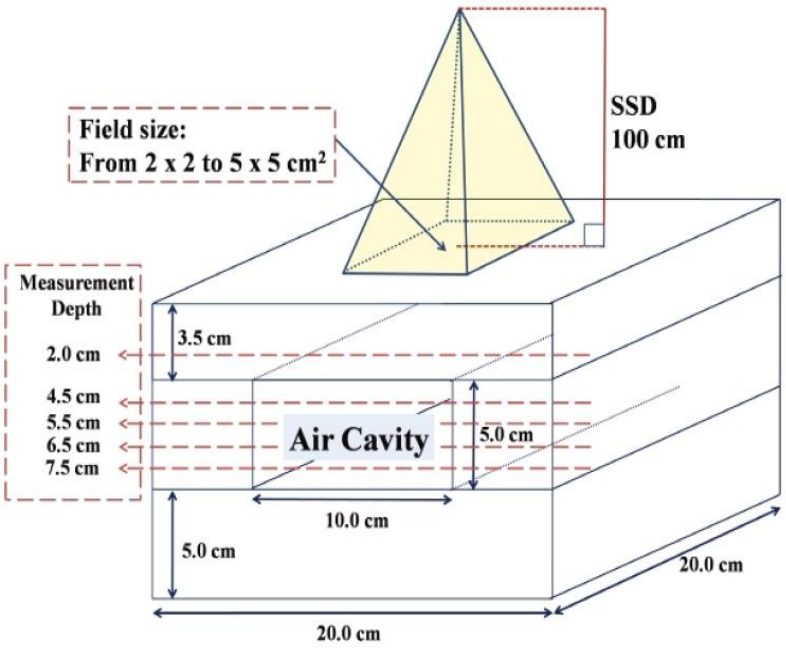

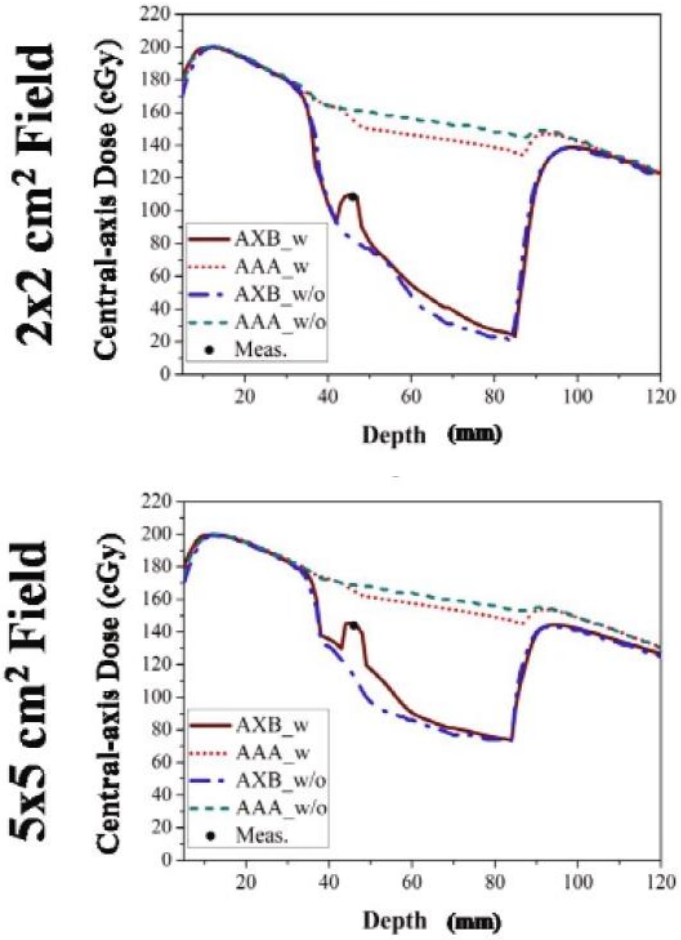

Kang et al., J Kor Phys Soc 67:2138, 2015

ESTRO School

Dose calculation with hip implants

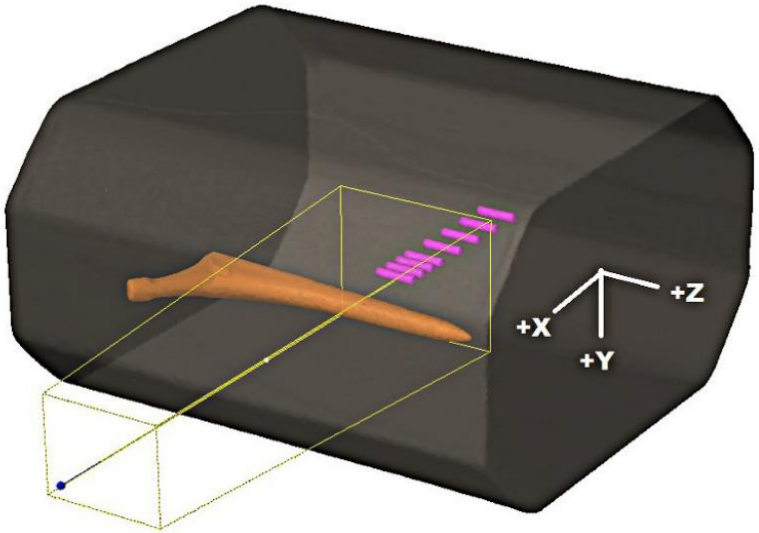

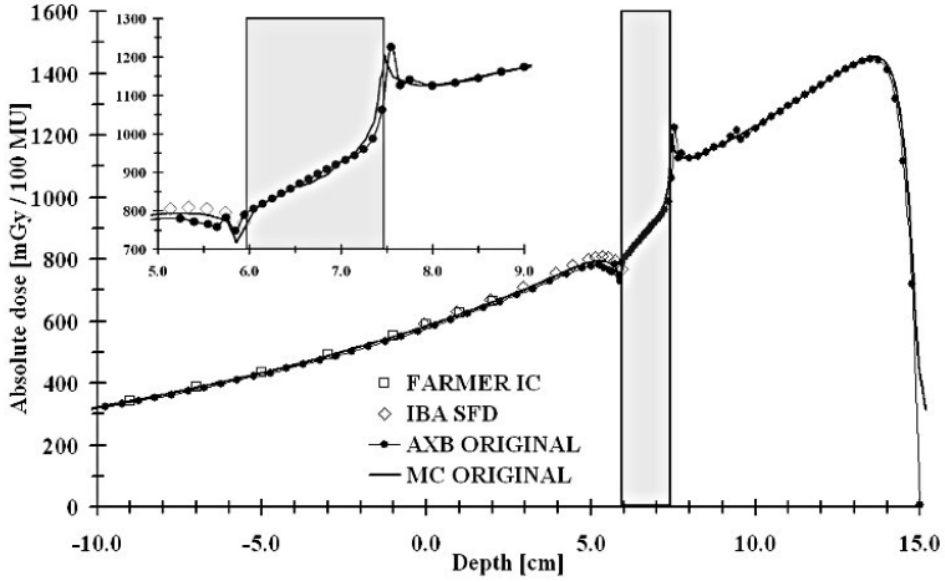

Ojala et al., JACMP 15:162, 2015

Dose calculation in a H&N phantom

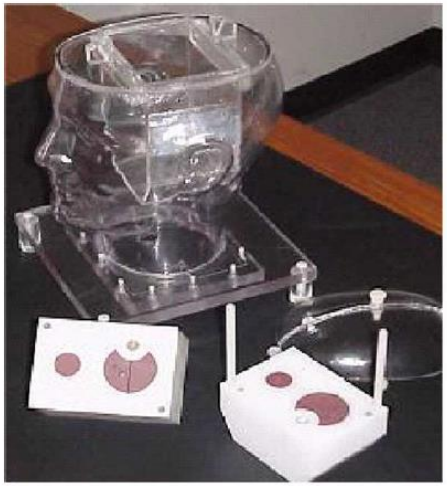

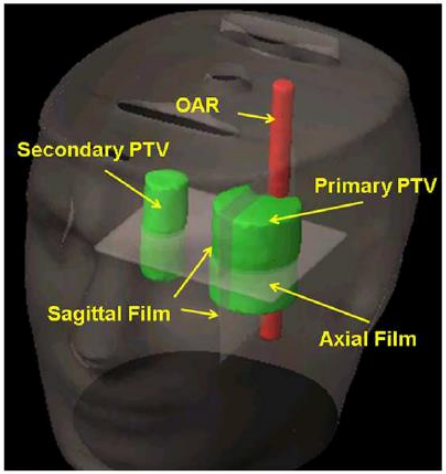

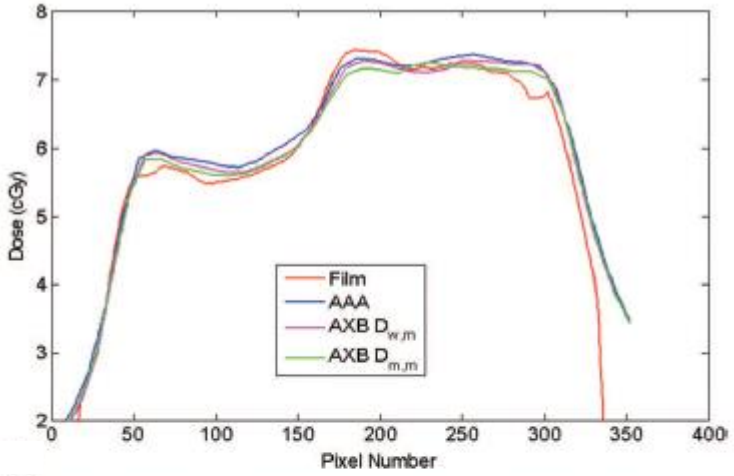

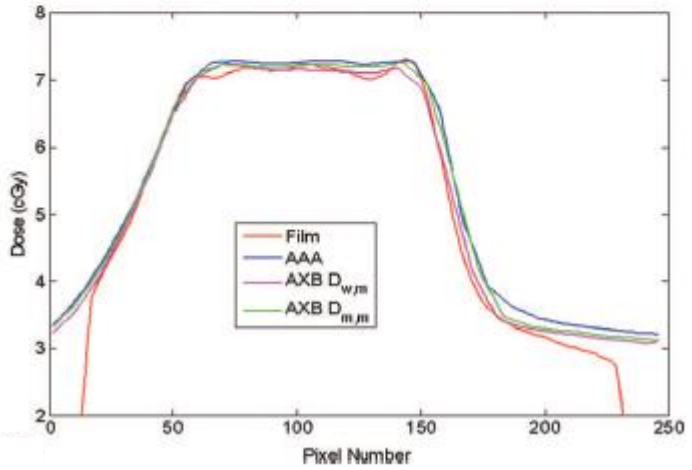

Han et al., Med Phys 39:2193, 2012

Summary

We have discussed

- The components of the radiation transport equation
- General simplifications
- The solution using deterministic methods
- The performance of one grid based solver

References

- KA Gifford, JL Horton, TA Wareing, G Failla, F Mourtada. Comparison of a finite-element multigroup discrete-ordinates code with Monte Carlo for radiotherapy calculations. Phys Med Biol 51:2253-2265, 2006.
- ON Vassiliev, TA Wareing, J McGhee, G Failla, MR Salehpour, F Mourtada. Validation of a new grid-based Boltzmann equation solver for dose calculation in radiotherapy with photon beams. Phys Med Biol 55:581-598, 2010.
- GA Failla, T Wareing, Y Archambault, S Thompson. Validation of a new grid-based Boltzmann equation solver for dose calculation in radiotherapy with photon beams. Varian white paper, 2105.
- GC Pomraning. The Fokker-Planck operator as an asymptotic limit. Math Mod Meth Appl Sci 2:21-36, 1992.

References

- A Fogliata, G Nicolini, A Clivio, E Vanetti, P Mancosu, L Cozzi. Dosimetric validation of the Acuros XB advanced dose calculation algorithm: fundamental characterization in water. Phys Med Biol 56:1879-1904, 2011.
- R Onizuka, F Araki, T Ohno, Y Nakguchi, Y Kai, Y Tomiyama, K Hioki. Accuracy of dose calculation algorithms for virtual heterogeneous phantoms and intensity-modulated radiation therapy in the head and neck. Radiol Phys Technol 9:77-87, 2016.
- SW Kang, TS Suh, JB Chung, et al. Dosimetric Accuracy of AAA and Acuros XB Dose Calculations within an Air Cavity for Small Fields of a 6-MV Flattening Filter-free Beam. J Korean Phys Soc 67:2138-2145, 2015.
- J Ojala, M Kapanen, P Sipilä, S Hyödynmaa, M Pitkänen. The accuracy of Acuros XB algorithm for radiation beams traversing a metallic hip implant — comparison with measurements and Monte Carlo calculations. J Appl Clin Med Phys 15:162-176, 2014.
- T Han, F Mourtada, K Kisling, J Mikell, D Followill, R Howell. Experimental validation of deterministic Acuros XB algorithm for IMRT and VMAT dose calculations with the Radiological Physics Center's head and neck phantom. Med Phys 39:2193-2202, 2012.

ESTRO School

WWW.ESTRO.ORG/SCHOOL

Small fields

Part II: Modelling

Mania Aspradakis
maria.aspradakis@luks.ch

Dose modelling dose in small & composite fields

IMRT = Σsmall fields

Dose = function (penumbra + leakage + head scatter)

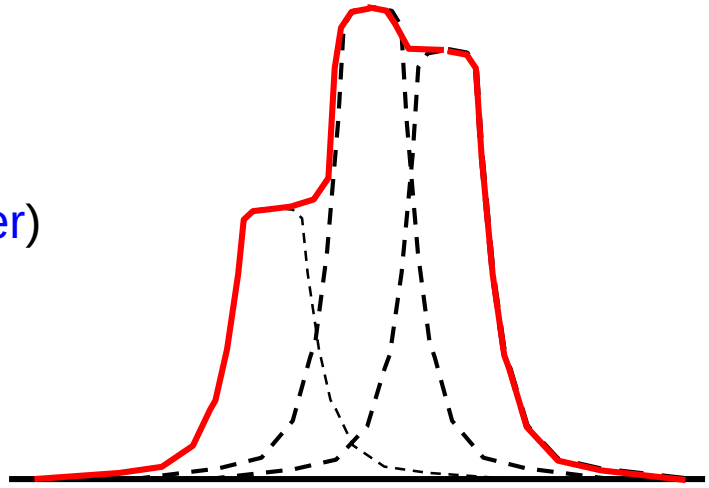

IMRT beam profile

Need accurate treatment head model to get this right

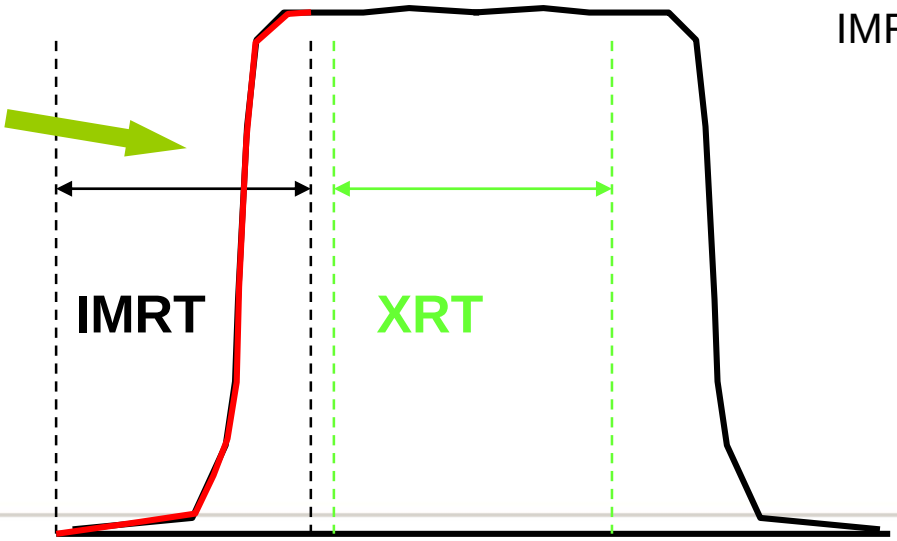

XRT beam profile

ESTRO School

Learning objectives

1. Highlight those aspects of beam modelling on treatment planning systems (TPS) that play major role on the accuracy of dose in plans comprising of small MV photon beams:

    1. finite size of beam source (also referred to as *focal spot*)
    2. jaw and MLC leaf edges
    3. resolution: influence of voxels size (calculation grid)
    4. Inhomogeneities

2. Review implementations on modern treatment planning systems (TPS)

Finite source and jaw edges

Primary beam source

Collimating devices shaping penumbra and shielding the primary souce

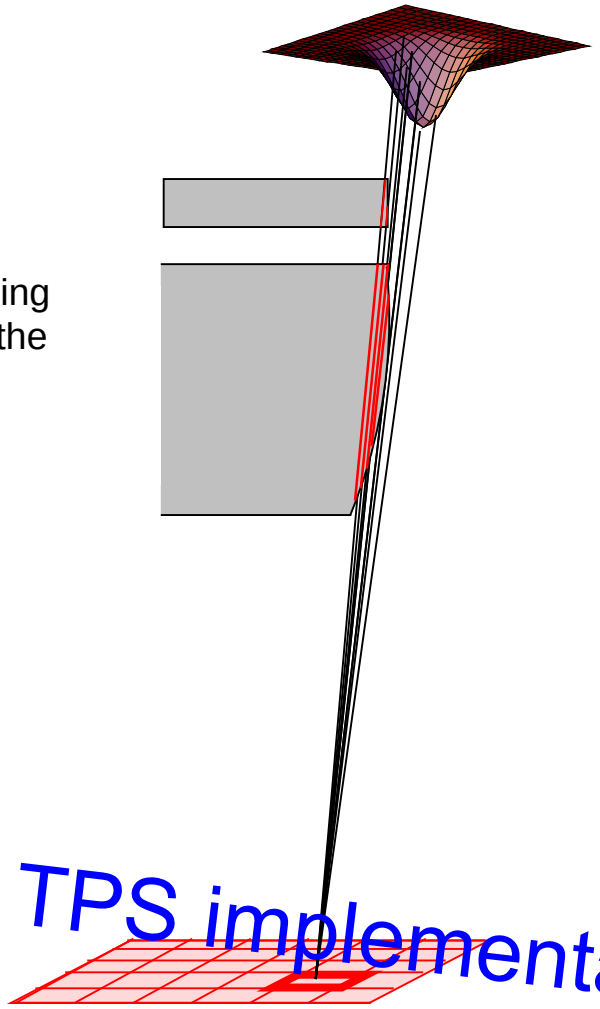

Energy fluence matrix

At narrow collimations

Dominating effect

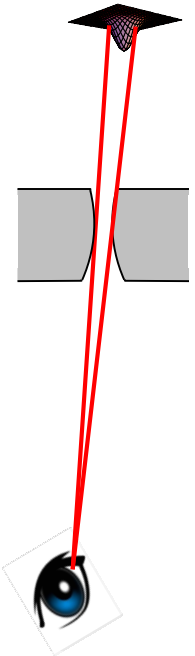

POI-eye-view of the source!

TPS implementations differ

From Anders Ahnesjö

ESTRO School

Modelling the finite beam source

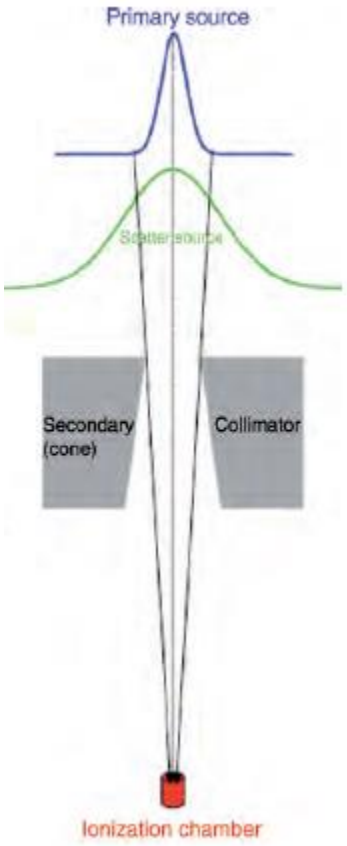

ICRU Report 83, Vol 10 (1), 2010

Source size modelling

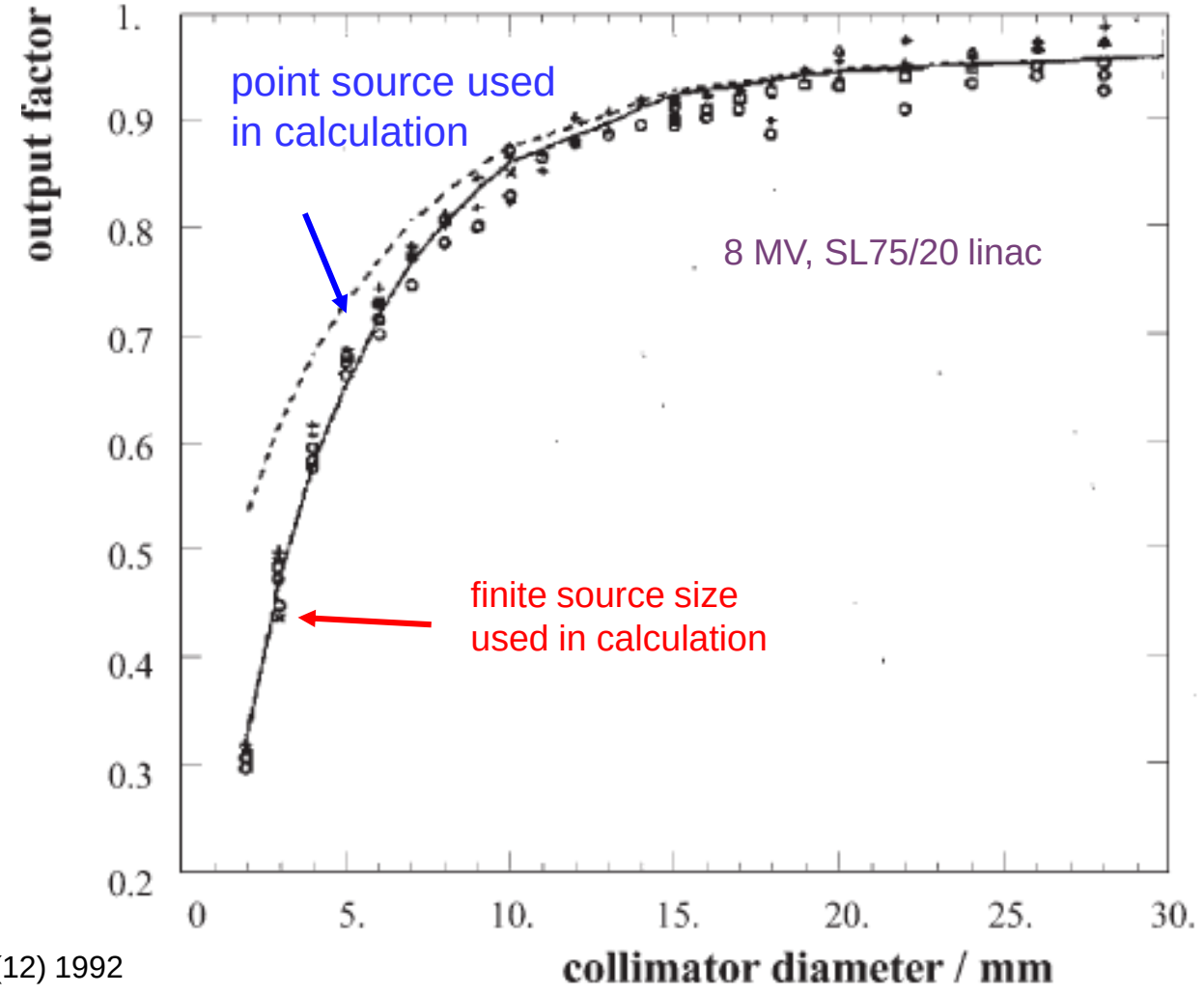

Treuer et al PMB 38(12) 1992

Source size: a modelling parameter

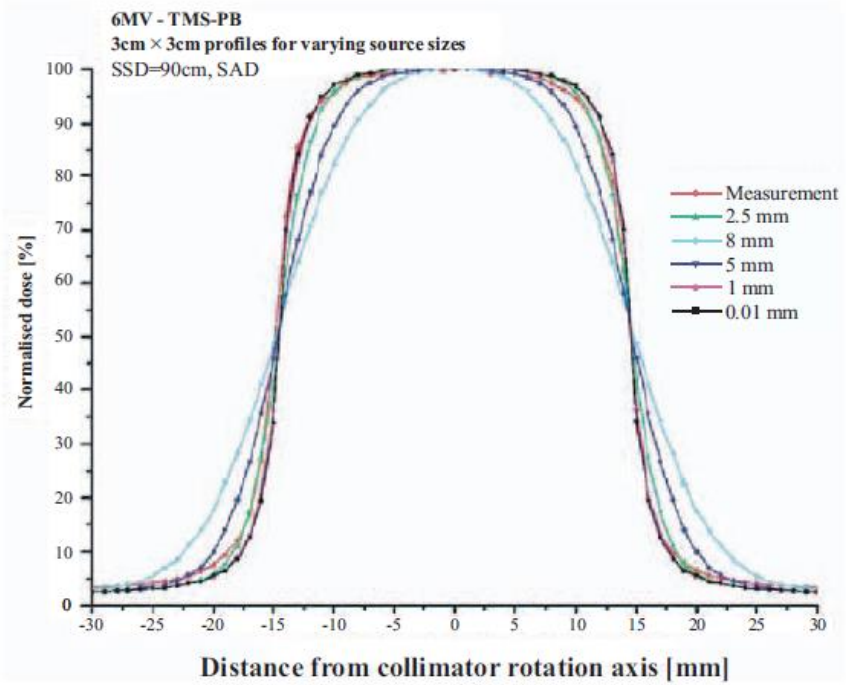

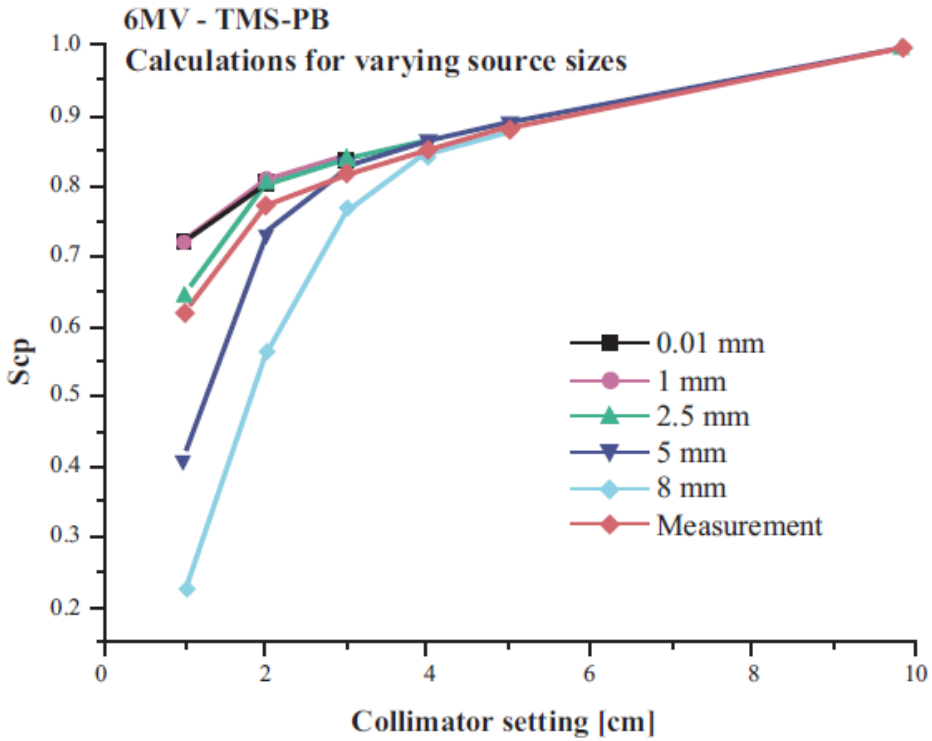

Aspradakis et al, (2005), Medical Dosimetry, 30(4), 233

ESTRO School

Dose for varying source size

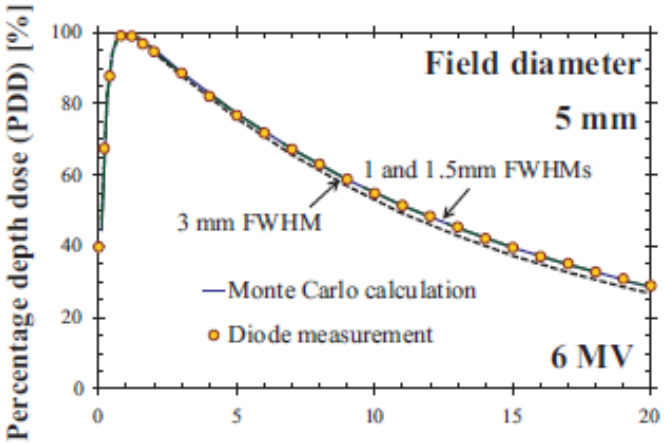

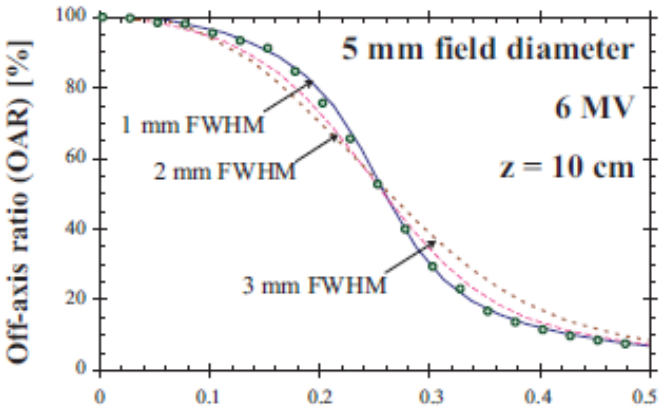

Sham et al (2008), Medical Physics, 35(7), 3317

ESTRO School

Source size modelling

How to treatment planning systems (TPS) account for the finite size of the direct beam source?

What follows is a quick survey amongst four of the most common commercial TPS on source modelling

(searching the manuals…!)

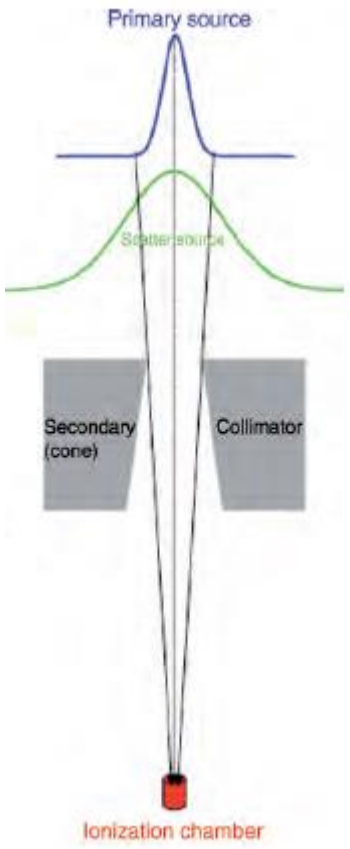

ICRU Report 83, Vol 10 (1), 2010

Source size modelling by TPSs - 1

Elekta Oncentra®, *Physics and Algorithms v4.3*

The direct fluence is obtained by modulating the open beam fluence with the attenuation from the different elements of the treatment head. The modulation at a certain point in the energy fluence matrix grid depends on the visibility of the source from that position

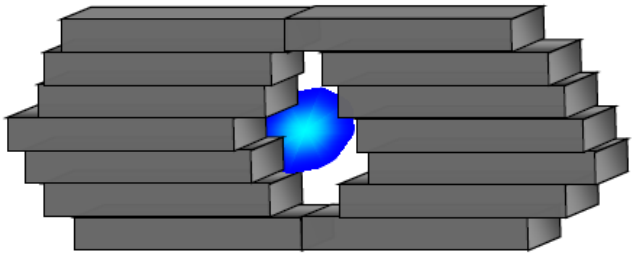

5.3.6 **Collapsed Cone Dose Calculation**

5.3.6.1 Beam Energy Fluence in Ray Tracing

The beam energy fluence used for the ray trace in Collapsed Cone is described by a fluence matrix that includes the effects of collimation and modulation of the beam.

The collimation is defined by the field shape, with energy fluence set to zero outside of the field (collimator leakage is book kept as part of the head scatter fluence). The effect of the finite source size is considered by convolving the projected source distribution with a constant energy fluence bounded by the actual field shape. The method takes into account the position of the collimating element along the beam axis, yielding a broader penumbra (i.e. smaller gradient) for collimators closer to the source.

ESTRO School

Source size modelling by TPSs - 1

Elekta Oncentra®, *Physics and Algorithms v4.3*

Source modelling is part of the calculation of direct photon energy fluence (the energy fluence of non-scattered photons reaching the patient which calculated on a 1mm matrix resolution).

- Beam source model: Elliptical, 2D Gaussian distribution
- Source size: Determined individually for each machine and beam energy using measured data (fitting measured profiles and small field output factors)
- Source is discretised on a 2D grid; amplitudes on each position renormalized to sum up to unity
- The resolution of the source grid depends on its size, the resolution of the energy fluence matrix and the distance to the collimators; derived at runtime (10×10 → 40×40)

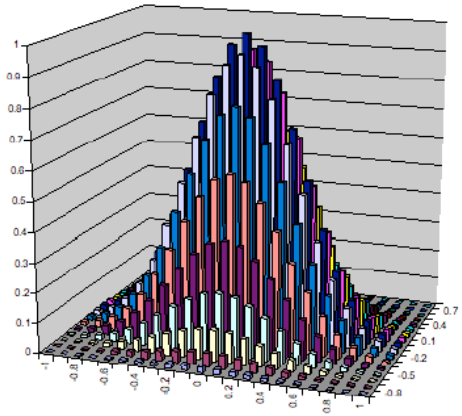

•Source of finite size (not point)
•Explicit source model
•Parameters of model determined from measured data

ESTRO School

Source size modelling by TPSs - 2

Philips Pinnacle^3, *Physics Reference Guide v9.10*

3.4.4 Out of Field model parameters

The penumbra and tails of the profiles are modeled with the Out of Field model parameters. To access the out of field photon model parameters, click the Out of Field tab in the Photon Model Editor window.

Effective Source Size parameters

The Effective Source Size parameters model the penumbra of a beam by blurring the incident fluence model. The shape of the blurring kernel is modeled as a Gaussian with the FWHM (or Full Width at Half Maximum—describes a gaussian distribution's width) equal to the projected effective source size.

The effective source size is scaled by (SAD - SCD)/SCD, where SCD is the source to collimator (jaw) distance and SAD is the source to axis distance. Note that each dimension is handled separately. This Gaussian blurring kernel is then convolved with the incident fluence to determine the incident fluence distribution.

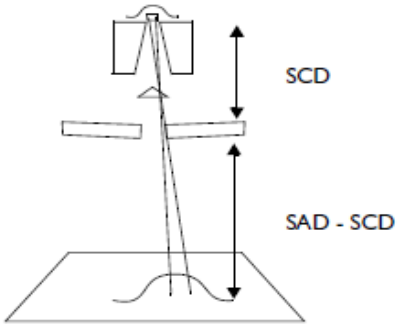

ESTRO School

Source size modelling by TPSs - 2

Philips Pinnacle^3, *Physics Reference Guide v9.10*

3.1.1 An overview of the model

The Pinnacle^3 photon beam model parameters characterize the radiation exiting the head of the linear accelerator. The starting point for photon modeling is a uniform plane describing the incident energy fluence. Then Pinnacle^3 adjusts the fluence model to account for the flattening filter, the accelerator head, and beam modifiers such as blocks, wedges, and compensators.

- The geometric penumbra is modeled by convolving the fluence array with a focal spot blurring function.

3.5 Automodeling sequences

Sequences to use for all field sizes (open and/or wedge)

- E_TuneAllInSections.OptSequence

3.5.1 E_TuneAllInSections

This sequence currently produces the best results for tuning an entire model. The sequence tunes the electron contamination parameters in conjunction with the spectrum while tuning the entire model. It also separates the X and Y focal spot size tuning and optimizes the left/right jaw transmission, top/bottom jaw transmission, MLC transmission, and arbitrary fluence profiles. The left/right jaw transmission optimization only uses X profiles, while the top/bottom jaw transmission only uses Y profiles. The MLC transmission is optimized after the jaw transmissions, and it only uses profiles that include the MLC.

- Point source assumed
- 'Effective source model' to model penumbra
- Parameters of model chosen during automodelling

ESTRO School

Source size modelling by TPSs - 3

RaySearch, Raystation, *RayPhysics Manual v4.7*

6.10 SUMMARY OF THE BEAM MODEL PARAMETERS

The beam model parameters are listed in the table below. Geometric parameters (not z) are defined at the projection onto the isocenter plane. Typical values are given in parenthesis.

Parameter	Description
Primary source • x width (0.05 cm – 0.3 cm) • y width (0.05 cm – 0.3 cm)	The width parameters specify the elliptical σ of the gaussian source intensity distribution at the source position.

8.5.2 Optimization steps

Auto modeling step	Affected Parameters	Target Function	Default curves	Selectable curves
Primary Source [iii]	Primary source widths in x and y.	Penumbra region.	Profiles of the smallest and the reference field size.	All profiles.

10.6 TIPS AND TRICKS

- If the steepness of the penumbra does not fit well, first tune the source sizes before attempting to adjust the collimator calibration parameters. Note that source sizes usually have a larger impact on the smaller fields.

ESTRO School

Source size modelling by TPSs - 3

RaySearch, Raystation, *RayPhysics Manual v4.7*

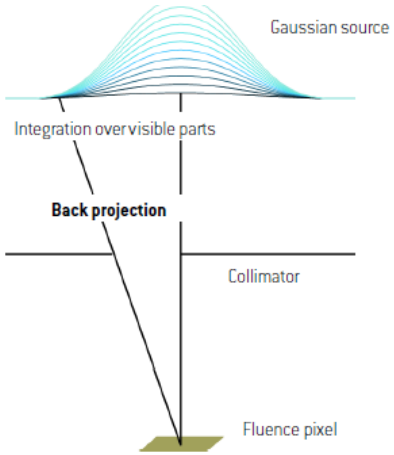

Figure 8. Source projection.

Projecting a spatially extended source through collimators onto a spatially extended fluence pixel involves a doubly two-dimensional integration: one over the source and one over the pixel. In RayStation the sources are projected using back projection.

In back projection, for each central pixel point in the fluence plane, integration is performed over the visible part of the sources. When projecting the sources through the collimators, the collimator positions specified in the **Fluence** tab in beam commissioning are used.

When the source size is small, on the scale of a few fluence pixels, the approximation that the average fluence in the pixel is the same as the fluence in the center of the pixel no longer holds. In that case an integration over the pixel has to be performed. This integration is performed by convolving the source distribution with the size of the pixel in the source plane.

The projection is done separately for the primary photon source, secondary (flattening filter) photon source, electron source and wedge scatter source considering the jaws and the MLC settings and block or circular cone openings when applicable. The electron source from the flattening filter can use the same projection as the photon flattening filter source.

- Source of finite size (not point)
- Explicit source model
- Parameters of model are chosen during beam configuration

Source size modelling by TPSs - 4

Varian Eclipse, *Eclipse Algorithms Reference Guide v13+*

Primary Source

In the photon beam source model, the primary source is a point source located at the target plane. The physical effects of the finite size of the primary source are modeled by the effective target spot size parameters (for more information on the parameters, see "AAA and Acuros XB Parameters" on page 71). The source models the bremsstrahlung photons created in the target that do not interact in the

Small Field Support

Tuning of the effective spot size parameters

The beam data includes parameters `Effective target spot size in X-direction` and `Effective target spot size in Y-direction`, which have a significant effect on the calculated absolute dose level for very small field sizes (<= 1x1 cm^2) and for the shape of the calculated penumbra for all field sizes.

These parameters should be manually adjusted for each treatment unit based on high-resolution measurements (such as film). After changing the parameter value, attention should be paid on the agreement in the absolute dose level for small field sizes and on the penumbra region for all field sizes.

Table 14 Example Values for Target Spot Size Parameters

Algorithm / Treatment Unit	Spot Size X-direction [mm]	Spot Size Y-direction [mm]
AAA / Varian treatment unit	0.0 1.0 if MLC in field	0.0 0.0 if MLC in field
Acuros XB / Varian treatment unit	1.0 1.5 if MLC in field	1.0 0.0 if MLC in field
AAA / Elekta Beam Modulator	2.5	0.0
Acuros XB / Elekta Beam Modulator	2.5	0.0
AAA / Other Elekta treatment units	0.0 1.0 if MLC in field	0.0 0.0 if MLC in field
Acuros XB / Other Elekta treatment units	1.0 1.5 if MLC in field	1.0 0.0 if MLC in field
AAA / Siemens treatment units	2.0	2.0
Acuros XB / Siemens treatment units	2.5	2.5

In all cases, fine-tuning of the spot size parameter values can be performed based on matching measurements and calculations.

- Point source assumed
- 'Effective source model' to model penumbra
- Parameters of model chosen during beam configuration

Dose for varying source size

Eclipse AAA v11; 6MV X-profiles from 1mm × 1 mm MLC-defined fields (jaws at 60mm × 60mm), dose calculation grid size = 1mm

AAA jaw-spot (SpotSizeX=SpotSizeY=0mm)

2%/1mm

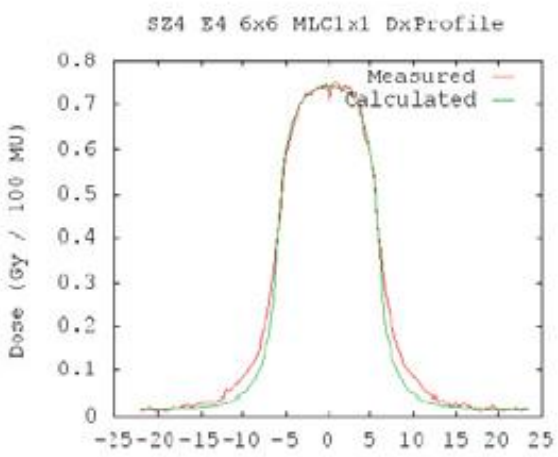

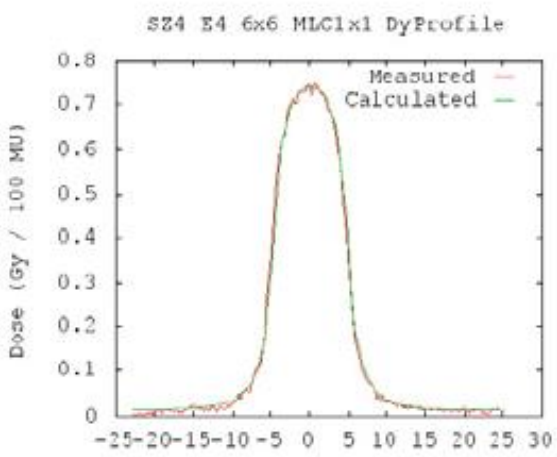

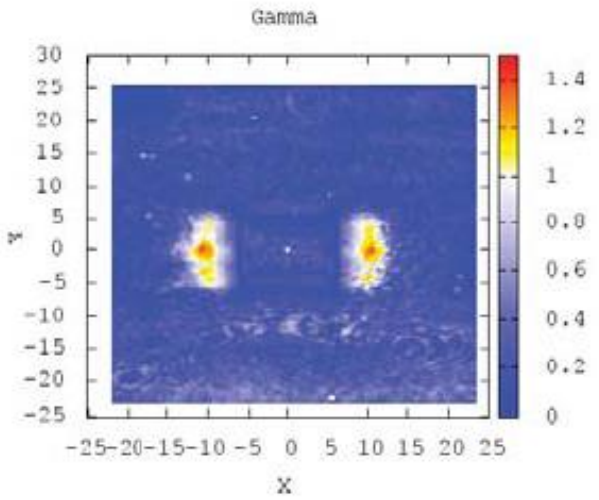

AAA MLC-spot (SpotSizeX=1mm, SpotSizeY=0mm)

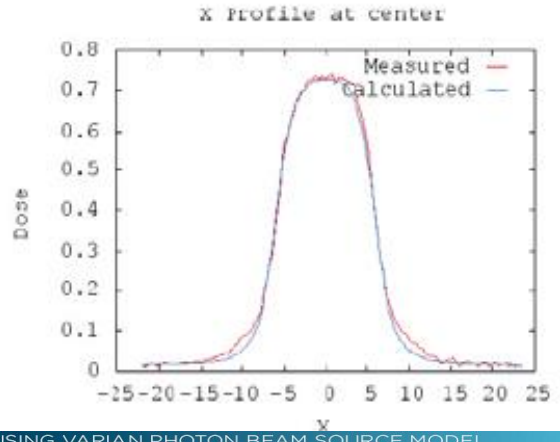

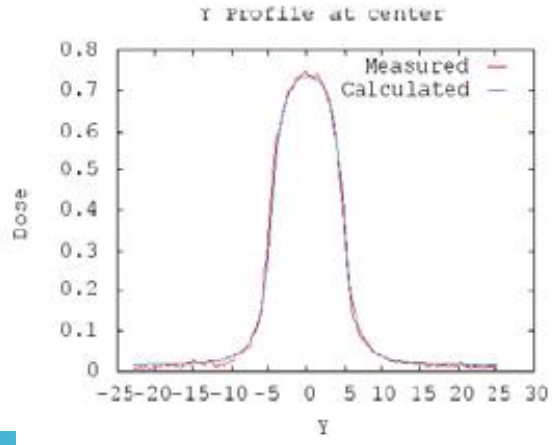

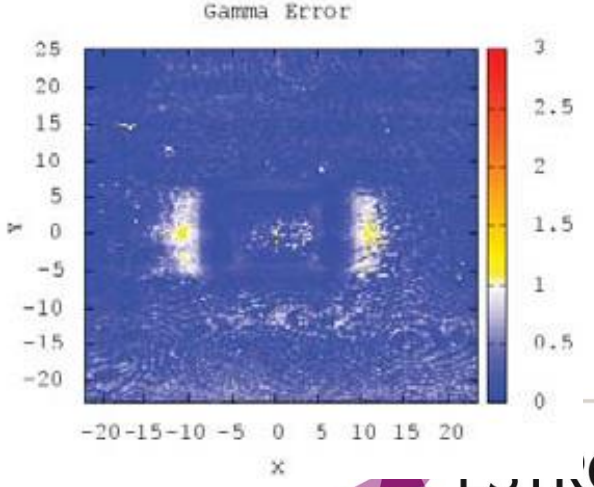

Dose for varying source size in small fields

Eclipse TPS: AAA v10.0.28, AXB 11.0.03, 6MV , DLG=0.2cm, Trans=1.8%, dose calculation grid size = 1mm

TABLE III. Small fields: output dose difference between calculations and measurements, in %, Acuros XB (AXB) and AAA algorithm, for the three spot sizes of 0.0, 0.5, 1.0, and 2.0 mm.

Algorithm_ SpotSize	3 × 3 (%)	2 × 2 (%)	1 × 1 (%)	0.8 × 0.8 (%)	Mean
AXB_0.0 mm	−0.1	0.1	0.1	1.7	0.5 ± 0.8%
AXB_0.5 mm	−0.1	0.1	−0.1	1.5	0.3 ± 0.8%
AXB_1.0 mm	−0.1	0.2	0.8	1.7	0.7 ± 0.8%
AXB_2.0 mm	0.0	0.0	−2.0	−7.5	−2.4 ± 3.6%
AAA_0.0 mm	0.2	0.1	0.3	0.3	0.2 ± 0.1%
AAA_0.5 mm	0.2	0.0	−0.2	−0.2	−0.1 ± 0.2%
AAA_1.0 mm	0.2	0.2	1.1	0.3	0.4 ± 0.5%
AAA_2.0 mm	0.4	−0.1	−2.0	−8.9	−2.7 ± 4.3%

Fogliata et al (2011) Med Phys 38(11), 6228-6237

ESTRO School

Modelling collimation

- Jaws
- Backup jaws to MLC
- MLC (leaf ends and edges, transmission)

Modelling collimation: position of backup jaws

consistency and robustness in delivery and in the modeling of dose

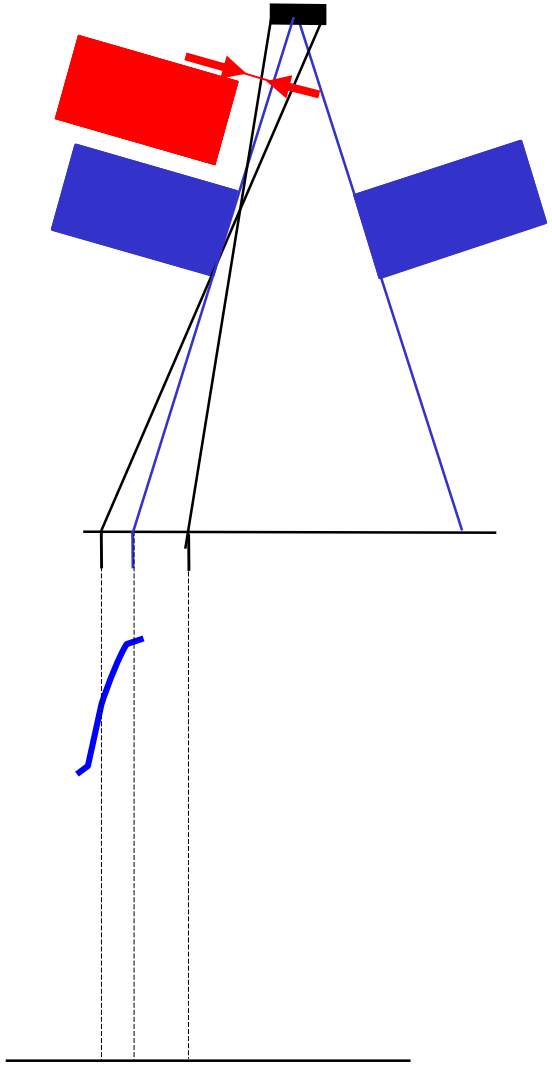

Consistent offset of any backup jaws from collimators defining the field edge would ensure consistency in the conditions shaping the penumbra and robust modelling of this by the TPS.

From Anders Ahnesjö

Modelling collimation: shape of MLC

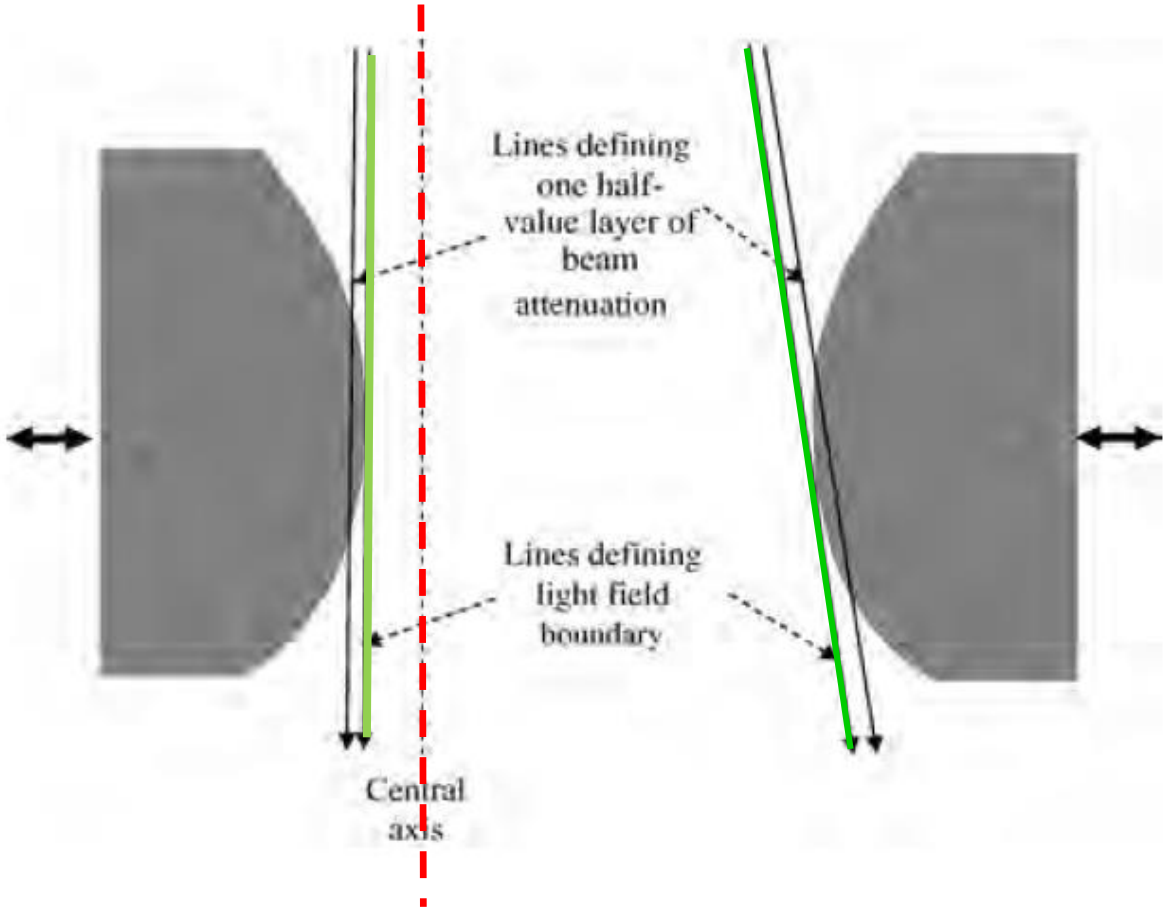

ICRU Report 83, Vol 10 (1), 2010

MLC leaf ends

Penumbra from rounded leaf is almost invariant of position

Elekta MLC geometry, source size 0.35 cm

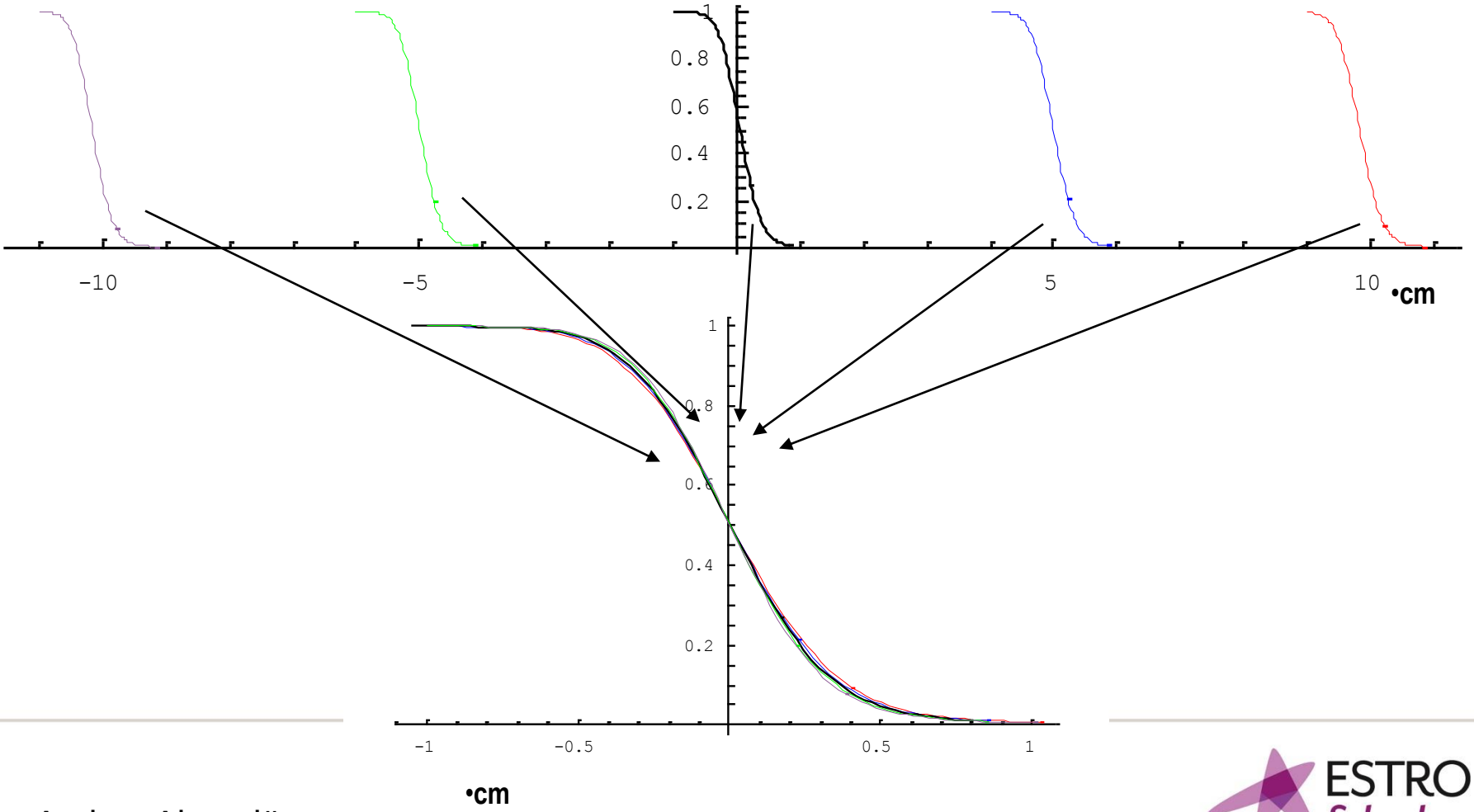

From Anders Ahnesjö

ESTRO School

Modelling the MLC leaf ends

The difference in radiation field edge and leaf tip position varies with off-axis location

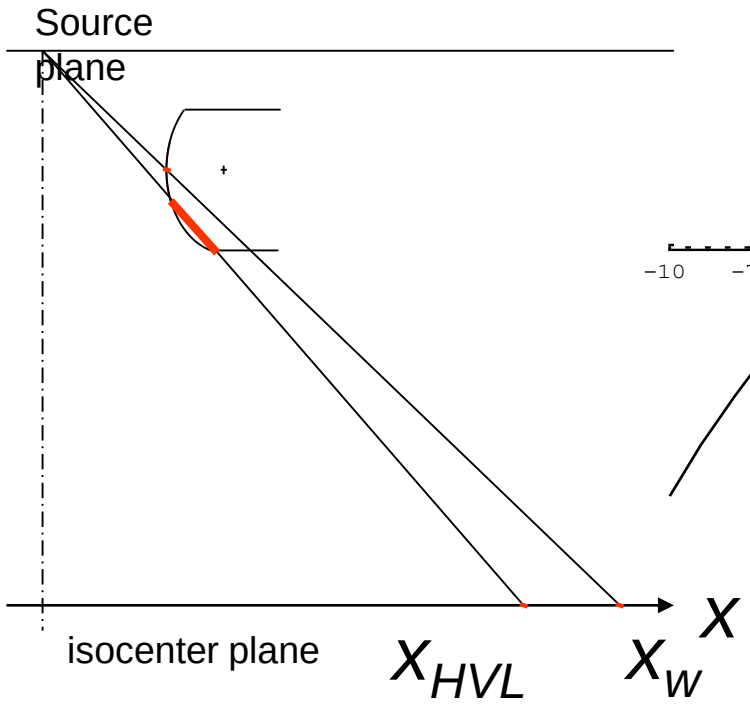

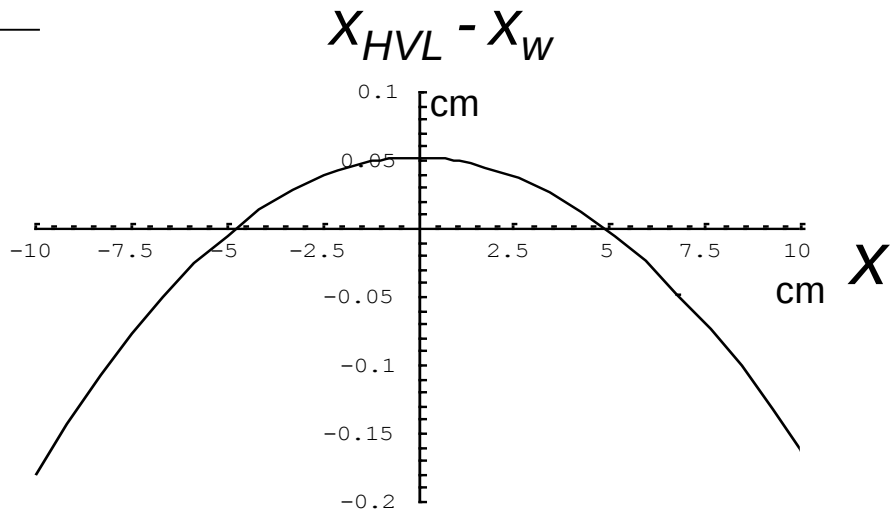

Delivery (linac): lookup table or parameterized correction to set leaf position

TPS : same method as used for delivery;
or
based on direct calculation of 50% transmission

→ potential inconsistency between dose calculations and delivery

From Anders Ahnesjö

Modelling the MLC

How to treatment planning systems (TPS) account for the influence of the MLC?

What follows is a quick survey amongst four of the most common commercial TPS on modelling the MLC

(searching the manuals…!)

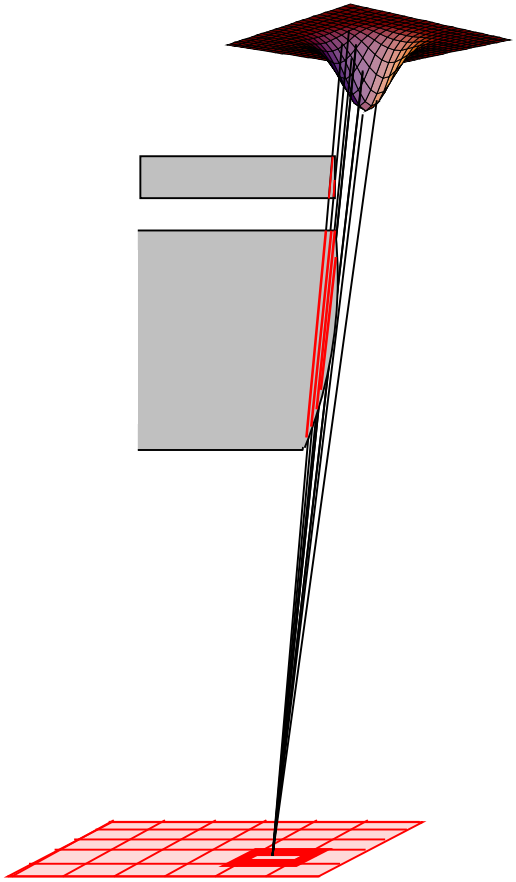

Modelling the MLC - 1

Elekta Oncentra®, *Physics and Algorithms v4.3*

5.3.2.1.2 Modulation Calculation

To determine the modulation at a given position in the energy fluence matrix, a ray trace is performed from each beam source grid point down through the treatment head to the "dose" point. Although the modulation

Dose points under the leaves/jaws will be totally blocked, except for the residual transmission through the jaw/leaf and dose points in the beam opening will see the full source. The intermediate region defines the geometrical penumbra where the source is partially blocked and where a detailed calculation of the modulation is required to describe its variation with the lateral position.

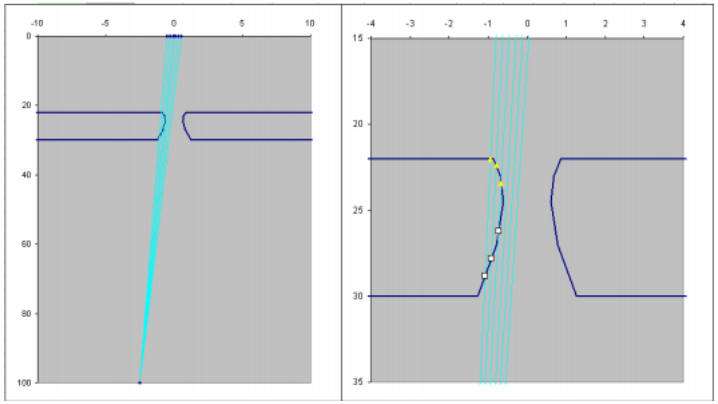

If the collimating element is an MLC, separate ray traces are done for each leaf contributing to the blocking of the source from the given dose point.

Note that the transmission through jaws and MLC leaves is part of the direct fluence.

Modelling the MLC - 1

Elekta Oncentra®, *Physics and Algorithms v4.3*

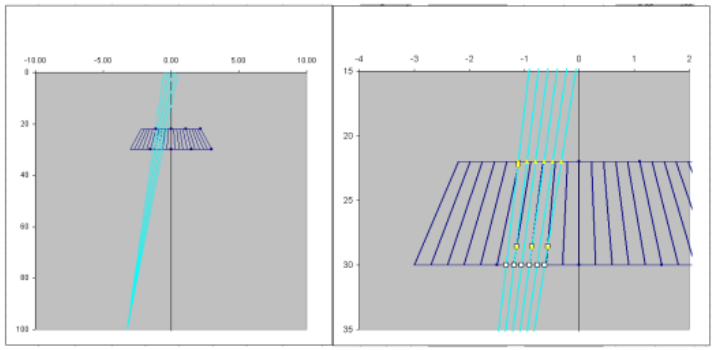

Figure 5-6 Ray tracing from the beam source grid down to a dose point on the isocenter plane through a leaf bank, overview (*left*) and detail (*right*). The triangles denote entry points and the squares exit points at individual leaves for each ray.

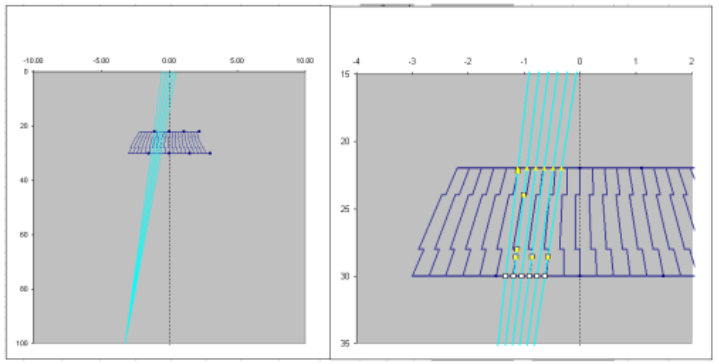

Figure 5-7 Ray tracing from the beam source grid down to a dose point on the isocenter plane through a leaf bank with tongue and groove, overview (*left*) and detail (*right*). The triangles denote entry points and the squares exit points at individual leaves for each ray.

If the collimating element is an MLC, separate ray traces are done for each leaf contributing to the blocking of the source from the given dose point.

Note that the transmission through jaws and MLC leaves is part of the direct fluence.

- MLC leaf ends are modelled rounded
- Ray-tracing through leaf ends
- Ray-tracing through leaf edges (between leafs)

ESTRO School

Modelling the MLC - 2

Philips Pinnacle^3, *Physics Reference Guide v9.10*

- Leaf-end shape is modelled rounded
- Leaf end radius of curvature: an adjustable ('global') parameter
- Leaf Offset: an adjustable ('global') parameter (an estimate of the increase in transmission through the leaf end relative to the transmission from the full MLC thickness

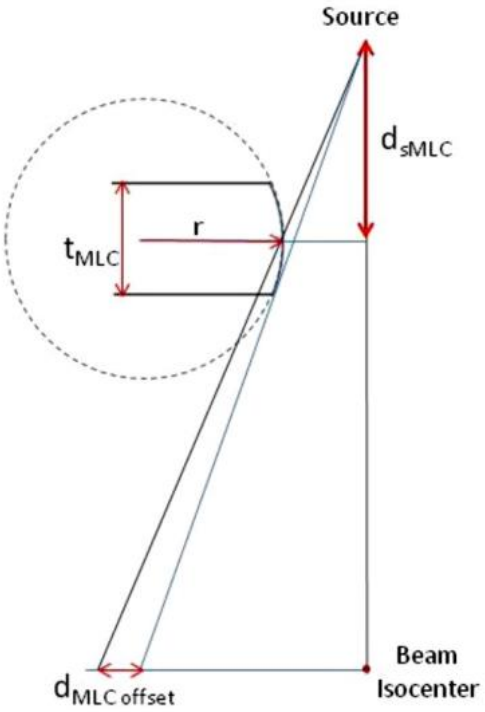

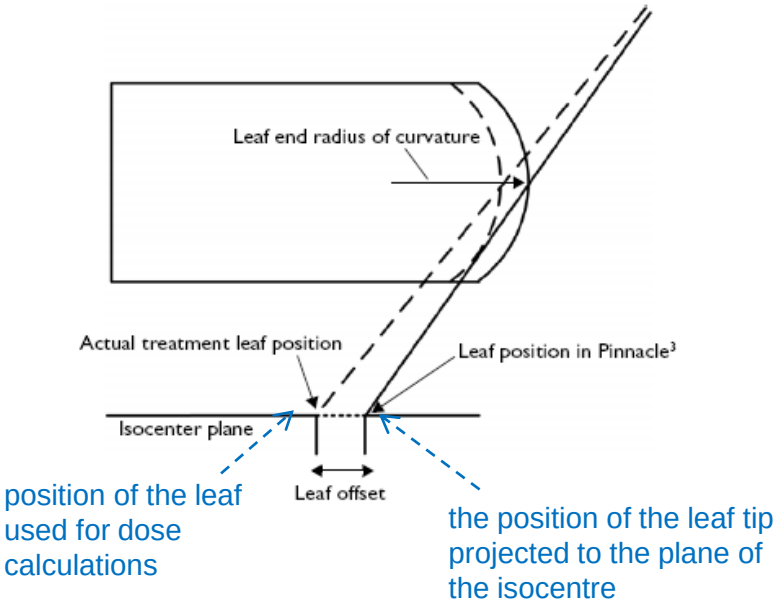

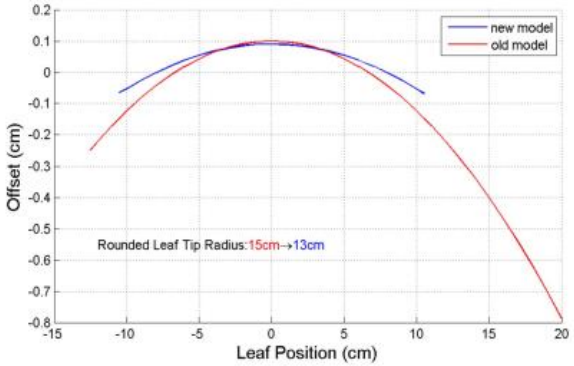

Young et al, J App Clin Med Phys, 17(6), 2016

ESTRO School

Modelling the MLC - 2

Philips Pinnacle^3, *Physics Reference Guide v9.10*

To model the tongue and groove effect, vary the widths from 0.005 to 0.200 cm and compare the models to the measured profiles. Increasing the width widens the penumbra in the direction perpendicular to the leaf motion. Decreasing the width sharpens the penumbra.

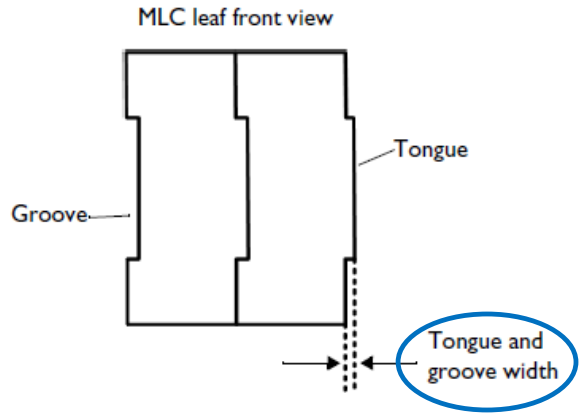

Typical values:
Leaf-end curvature: 8 – 15 cm
MLC leaf offset: 0.1cm
Tongue & groove width: 0.1cm
MLC intra-transmission: 1.5-2%, interleaf trans: 5%

Williams et al PMB, 51 (2006) N65-N78
Young et al, J App Clin Med Phys, 17(6), 2016

- MLC leaf ends are modelled rounded
- No explicit ray-tracing through leaf ends
- The difference between nominal leaf end and radiation field (one HVL of beam attenuation) is approximated by an off-set parameter and the leaf end curvature ('leaf off-set table')
- T&G modelled using an adjustable parameter (no ray tracing)

Modelling the MLC - 3

RaySearch, Raystation, *RayPhysics Manual v4.7*

In the energy fluence and dose computation, the MLC is treated as flat but a set of parameters are used to correct for 3D-effects.

MLC regions

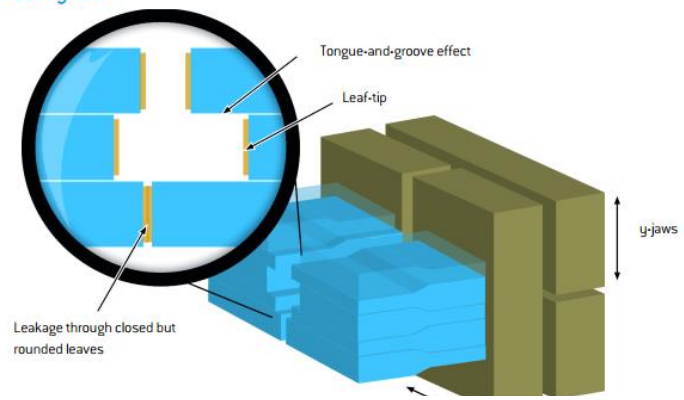

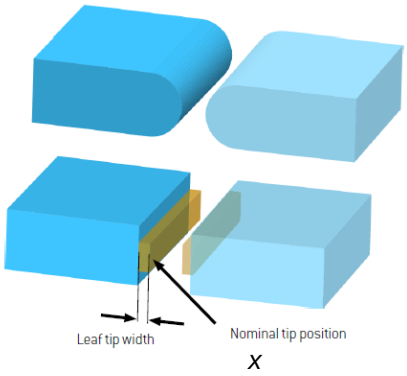

Leaf tip width

The tips of the MLC leaves are generally rounded in the xz-plane (yz-plane for a machine with MLC in the y-direction) in the beam limiting device coordinate system. The effect of the roundedness is included as a region just inside the leaf tip which has more transmission than the leaves. The transmission is taken to be the same as the tongue-and-groove region, which is the square root of the transmission through a leaf. As for the tongue-and-groove, the transmission is directly obtained from the MLC transmission, but the width of the leaf-tip region can be tuned during beam commissioning. The leaf-tip width is defined at the projection onto the isocenter plane. Since the leaf-tip region is positioned from the nominal tip position toward the leaf base, the effect of increasing the width is to increase the field size slightly and increase the width of the low dose region just outside or inside the penumbra along the MLC-leaf motion direction. If this increase in field size was not the intent the effect can be balanced by the collimator position offset (*Collimator position calibration – offset, gain and curvature on page 39*).

ESTRO School

Modelling the MLC - 3

RaySearch, Raystation, *RayPhysics Manual v4.7*

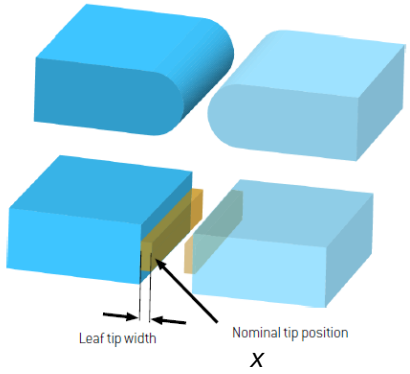

Collimator position calibration – offset, gain and curvature

The assumption that the collimators are flat introduces an error which to some extent is corrected for in a position calibration procedure. The calibration parameters are the offset, the gain and the curvature. For the MLC, these parameters correct the nominal leaf position to an effective leaf position that better match the measured fluence profiles. The correction is polynomial and x-symmetric.

$$x_{effective} = x - offset + gain \cdot x - curvature \cdot x^2 \quad left\ side$$

$$x_{effective} = x + offset + gain \cdot x + curvature \cdot x^2 \quad right\ side$$

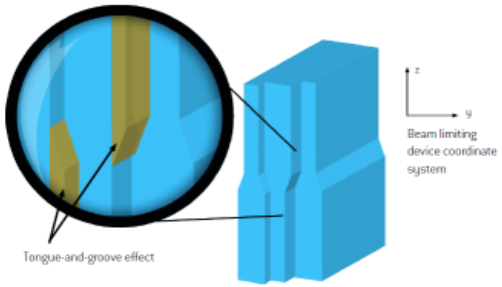

Figure 6. Tongue-and-groove.

Tongue and groove modelling

Width of the T&G area is the adjustable parameter: The transmission under this is set to the square root of the transmission through the leaves

Tongue-and-groove regions are only added for MLC leaf edges where the edge is exposed into the MLC opening. For MLC leaf edges that are closed against another MLC leaf, no tongue-and-groove regions are added. Interleaf leakage can be taken into account by increasing the average MLC transmission.

ESTRO School

Modelling the MLC - 3

RaySearch, Raystation, *RayPhysics Manual v4.7*

6.10 SUMMARY OF THE BEAM MODEL PARAMETERS

The beam model parameters are listed in the table below. Geometric parameters (not z) are defined at the projection onto the isocenter plane. Typical values are given in parenthesis.

Parameter	Description
MLC • Effective Dist. to Sour. (different for different vendors, 30 cm – 55 cm) • Transmission (0.01 – 0.03) • Tongue and groove (0 cm – 0.1 cm) • Leaf tip width (0 cm – 0.5 cm) • Collimator calibration coefficients x offset (0 cm – 0.1 cm), gain (0 – 0.01), curvature (0 [1/cm] – 0.001 [1/cm]), y gain (0)	Multi leaf collimator. The tongue and groove effect is connected to the leaf side and the effective offset and width to the leaf tip. Tongue-and-groove, leaf-tip-width and collimator calibration coefficients are defined at the projection onto the isocenter plane.

- MLC leaf ends are modelled straight (flat)
- No ray-tracing through leaf ends. Transmission through leaf tip is taken the same as the T&G transmission
- The MLC leaf tip position off-axis is corrected to account for difference in nominal position and radiation field edge (one HVL of beam attenuation through leaf end).
- T&G modelled using an adjustable parameter (no ray tracing)

ESTRO School

Modelling the MLC - 4

Varian Eclipse, *Eclipse Algorithms Reference Guide v13+*

Fluence delivery modelling algorithms: programs to convert optimal fluence patterns to deliverable fluence patterns, where the influence of the MLC is taken into account (Leaf Motion Calculator, LMC)

The fluence delivery algorithms deal with the rounded leaf end transmission by means of the *dosimetric leaf gap* configuration parameter. The algorithms model the shape of the leaf edges as sharp (as opposed to rounded) and take the rounded leaf transmission into account by shifting the leaf tip positions in the actual fluence calculation. Leaf tips are shifted by pulling each of them back by half the value of the dosimetric leaf gap parameter so that the gap between a fully closed leaf pair equals the dosimetric leaf gap parameter.

Modelling the MLC - 4

Varian Eclipse, *Eclipse Algorithms Reference Guide v13+*

Parameters in beam model configuration

- Dosimetric Leaf Gap (or separation, DLG or DLS)
- Transmission through MLC leaves

- DLG: represents the additional gap width needed to reflect the transmission through the rounded MLC leaf end
- MLC Transmission: includes inter and intra-leaf transmission

These parameters are measured by the user using a set of dynamic MLC fields (sliding window delivery patterns) defined by the vendor

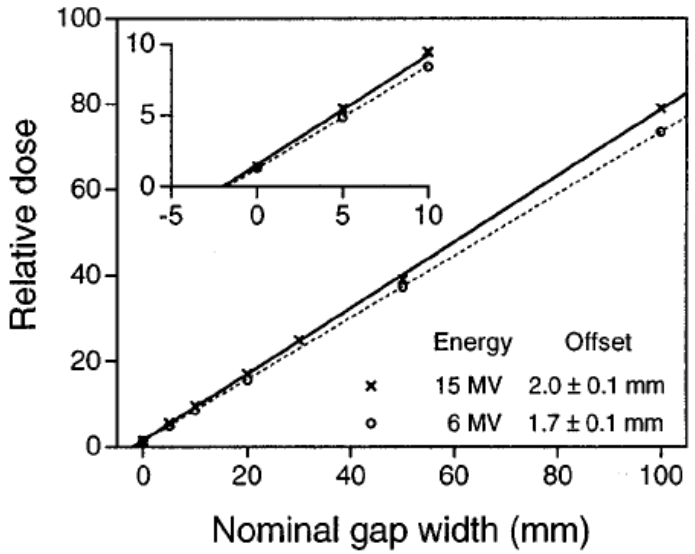

FIG. 7. Integrated dose vs MLC gap width measured in phantom with radiographic film for 6 and 15 MV x rays. The lines are linear fits to the data using least-squares regression. Extrapolation to zero integral dose determines the effective gap offset. The uncertainties are the standard errors of the data.

Lo Sasso, Med. Phys., 25(10), 1998m 1919-1927

- MLC leaf ends are modelled straight (flat)
- No ray-tracing through leaf ends
- DLG & MLC transmission are measured parameters serving as 'first guess' of the adjustable parameters needed per beam

Small fields: Influence of modelling MLC leafs

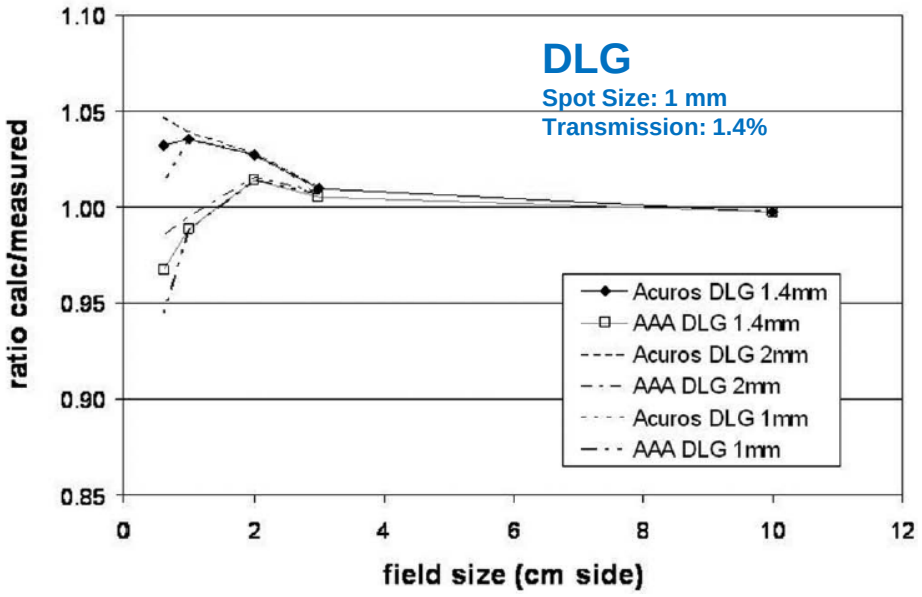

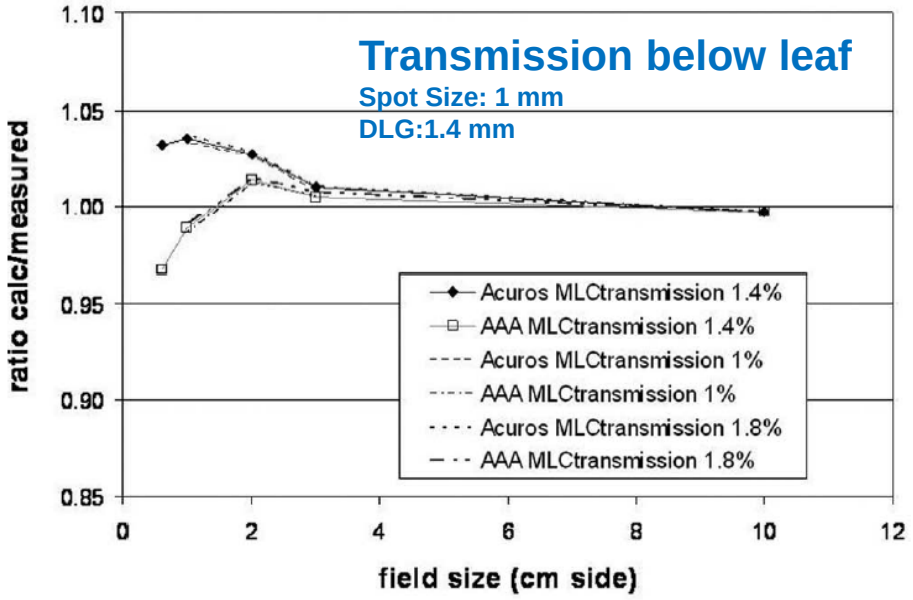

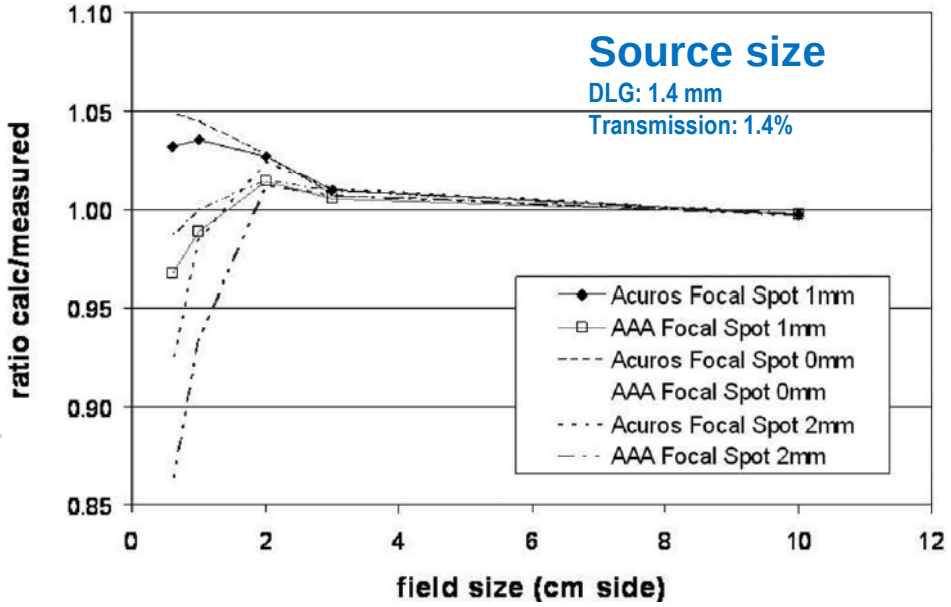

Kron et al (2012)
Med Phys 39(12), 7480-7489

ESTRO School

VMAT fields: Influence of modelling the MLC

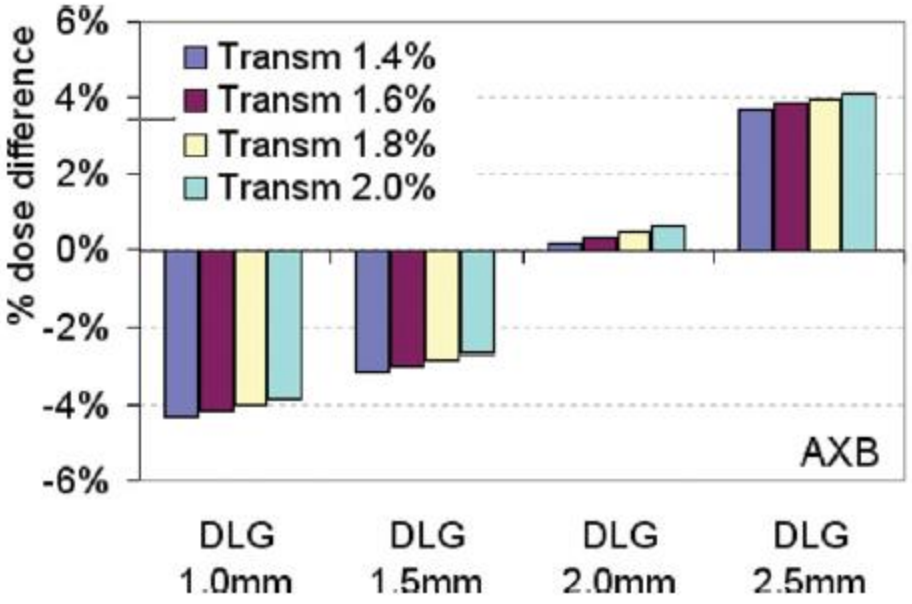

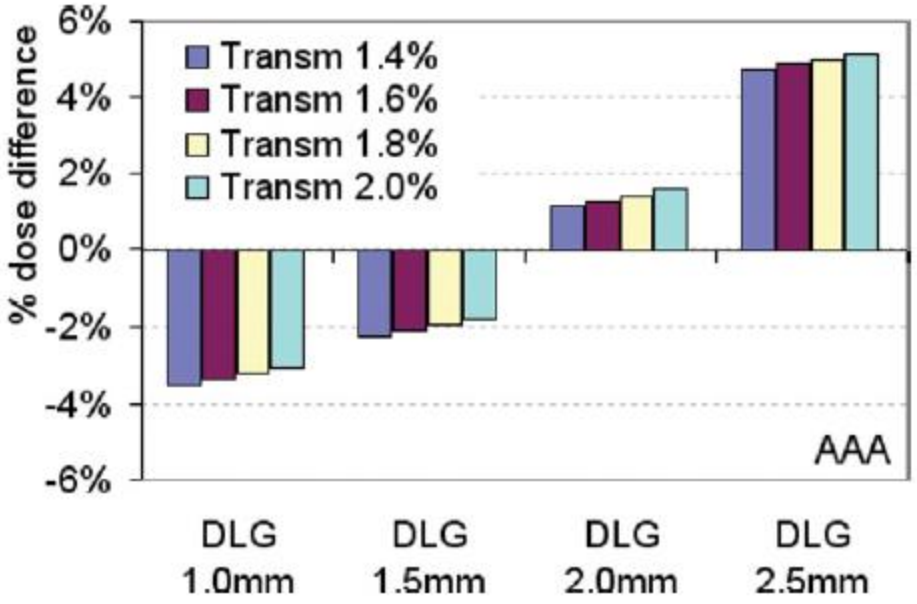

Fogliata et al (2011) Med Phys 38(11), 6228-6237

Small fields: the choice of collimation (jaws or MLC)

Jaw settings	MLC field size		Output factor (% diff from measurement) (%diff from symmetric jaw setting)		
[cm]	[cm]				
			Measurement	AAA v10.0.28	Acuros AAA v11.0.03
10 × 10	No MLC		1	1	1
12 × 12	3 × 3	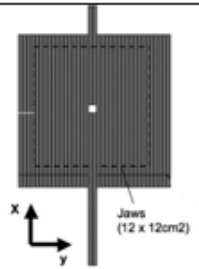	0.866	0.870 (0.5%)	0.874 (0.9%)
	1 × 1		0.724	0.716 (-1.1%)	0.750 (3.5%)
Beam: Varian Cliniac iX 6MV (TPR20,10 = 0.673), Millenium MLC (5mm width)					
All calculations with source size at 1mm, transmission 1.4%, DosLeafGap DLG=1.4mm, 1mm resolution					

Kron et al (2012)
Med Phys 39(12), 7480-7489

ESTRO School

Small fields: the choice of collimation (jaws or MLC)

Jaw settings	MLC field size		Output factor (% diff from measurement) (%diff from symmetric jaw setting)		
[cm]	[cm]				
			Measurement	AAA v10.0.28	Acuros AAA v11.0.03
10 × 10	No MLC		1	1	1
12 × 12	3 × 3	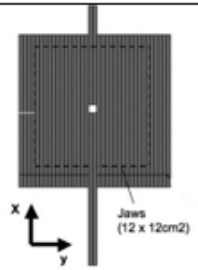	0.866	0.870 (0.5%)	0.874 (0.9%)
	1 × 1		0.724	0.716 (-1.1%)	0.750 (3.5%)
X1 = Y1 = 2 X2 = Y2 = 7.5	3 × 3	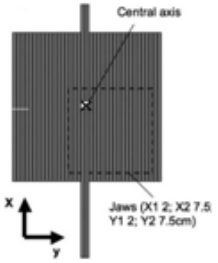	0.844 -2.5%	0.841 (-0.4%) -3.3%	0.842 (-0.2%) -3.7%
	1 × 1		0.719 -0.7%	0.725 (0.7%) 1.3%	0.696 (-3.2%) -7.2%

Beam: Varian Cliniac iX 6MV (TPR20,10 = 0.673), Millenium MLC (5mm width)

All calculations with source size at 1mm, transmission 1.4%, DosLeafGap DLG=1.4mm, 1mm resolution

Kron et al (2012)
Med Phys 39(12), 7480-7489

ESTRO School

Small fields: influence of collimation (jaws or MLC)

Jaw settings [cm]	MLC field size [cm]		Output factor (% diff from measurement) (%diff from symmetric jaw setting)		
			Measurement	AAA v10.0.28	Acuros AAA v11.0.03
10 × 10	No MLC		1	1	1
12 × 12	3 × 3	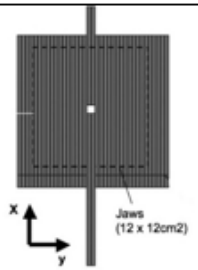	0.866	0.870 (0.5%)	0.874 (0.9%)
	1 × 1		0.724	0.716 (-1.1%)	0.750 (3.5%)
X1 = Y1 = 2 X2 = Y2 = 7.5	3 × 3	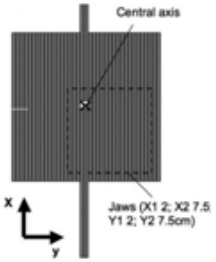	0.844 -2.5%	0.841 (-0.4%) -3.3%	0.842 (-0.2%) -3.7%
	1 × 1		0.719 -0.7%	0.725 (0.7%) 1.3%	0.696 (-3.2%) -7.2%
12 × 12	3 × 3 off set by 4cm	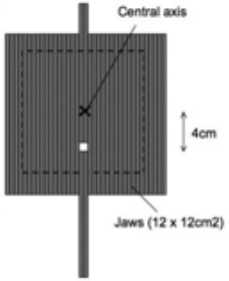	0.855 -1.3%	0.869 (-0.1%) -0.1%	0.866(-0.9%) -0.9%
12 × 12	1 × 1 off set by 4cm		0.732 1.1%	0.747 (4.3%) 4.3%	0.714(-5.0%) -4.8%
Beam: Varian Cliniac iX 6MV (TPR20,10 = 0.673), Millenium MLC (5mm width)					
All calculations with source size at 1mm, transmission 1.4%, DosLeafGap DLG=1.4mm, 1mm resolution					

Kron et al (2012)
Med Phys 39(12), 7480-7489

ESTRO School

Dose modelling dose in small & composite fields

On the choice of resolution in fluence and dose matrixes …

Calculation of fluence map – resolution

Eclipse AAA; 6MV X-profiles from 5mm × 5 mm MLC-defined fields (jaws at 40mm × 40mm)
Source size (X,Y)=(0,0), dose calculation grid size = 1mm

v8.6

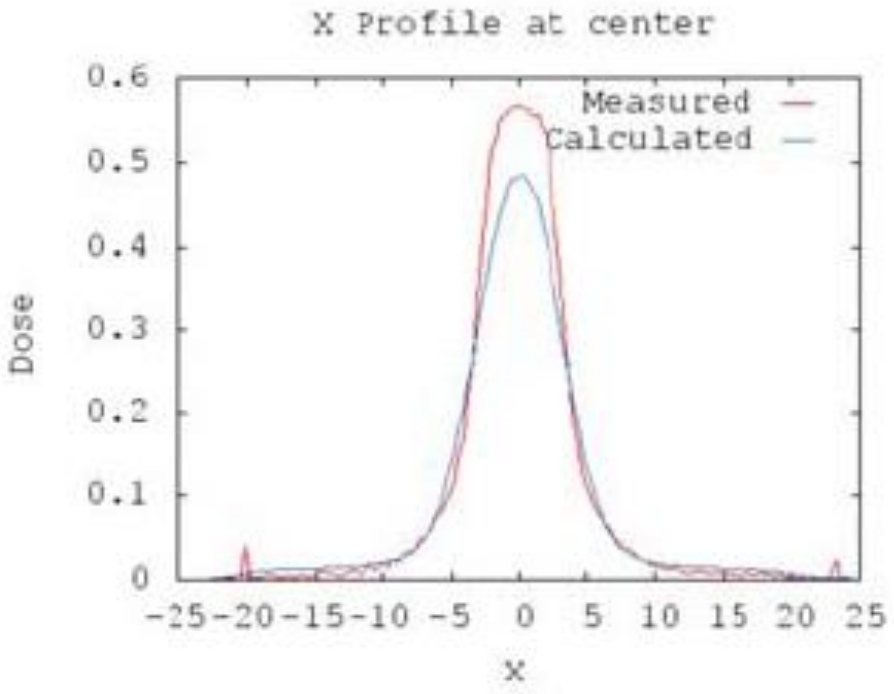

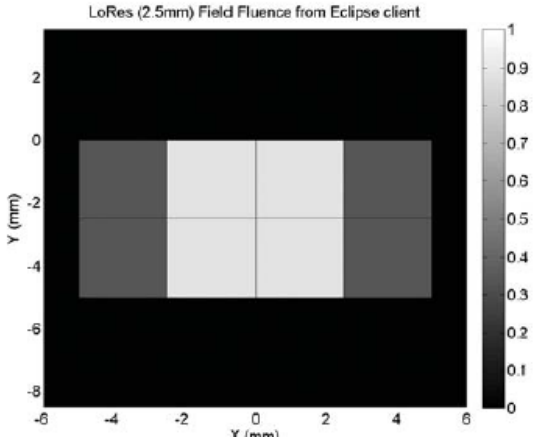

Initial fluence resolution 2.5mm

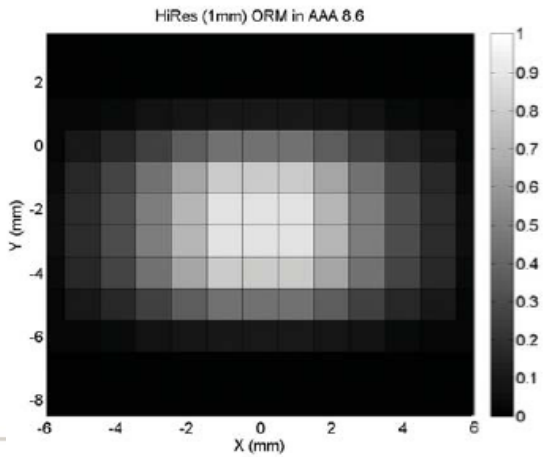

Resampled fluence resolution 1mm

Calculation of fluence map – resolution

Eclipse AAA; 6MV X-profiles from 5mm × 5 mm MLC-defined fields (jaws at 40mm × 40mm)
Source size (X,Y)=(0,0), dose calculation grid size = 1mm

v8.9

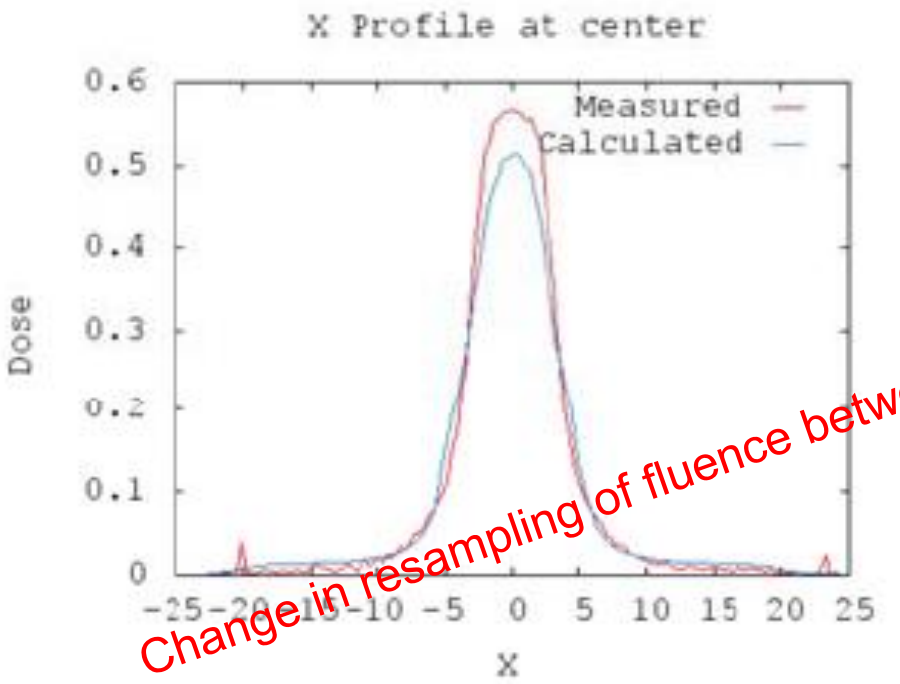

Change in resampling of fluence between versions of same TPS

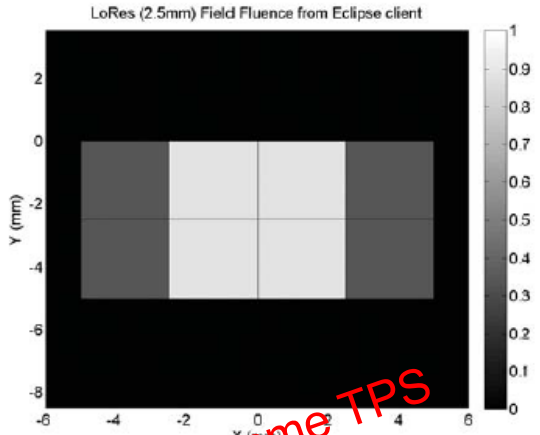

Initial fluence resolution 2.5mm

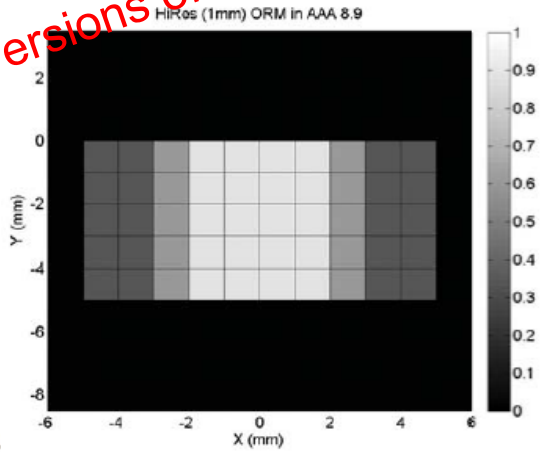

Resampled fluence resolution 1mm

Calculation of fluence map – resolution

Eclipse AAA; 6MV X-profiles from 5mm × 5 mm MLC-defined fields (jaws at 40mm × 40mm)
Source size (X,Y)=(0,0), dose calculation grid size = 1mm

v11

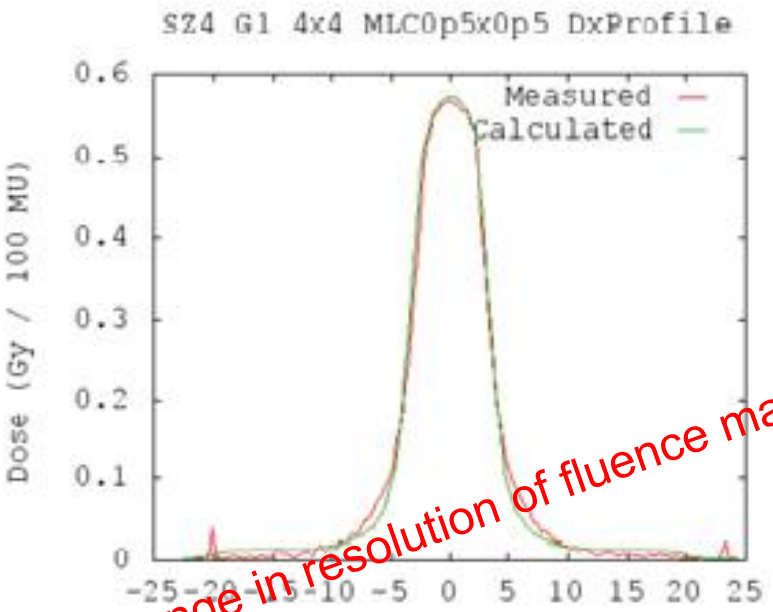

Initial fluence resolution 0.3125mm

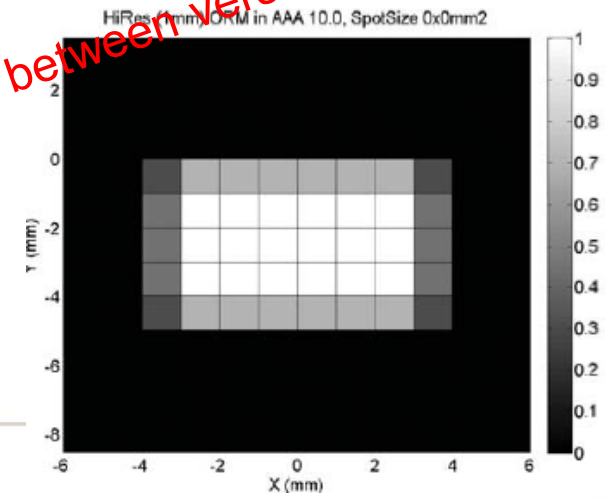

Resampled fluence resolution 1mm

Change in resolution of fluence matrix between versions of same TPS

Small static fields: size of fluence and dose voxels

Differences between doses computed between two versions of same model

AAA v8.6.15 vs AAA v10.0.25

Major difference between versions was the resolution of the **fluence matrix**

2.5mm vs 0.3125mm

Film EBT - Calc

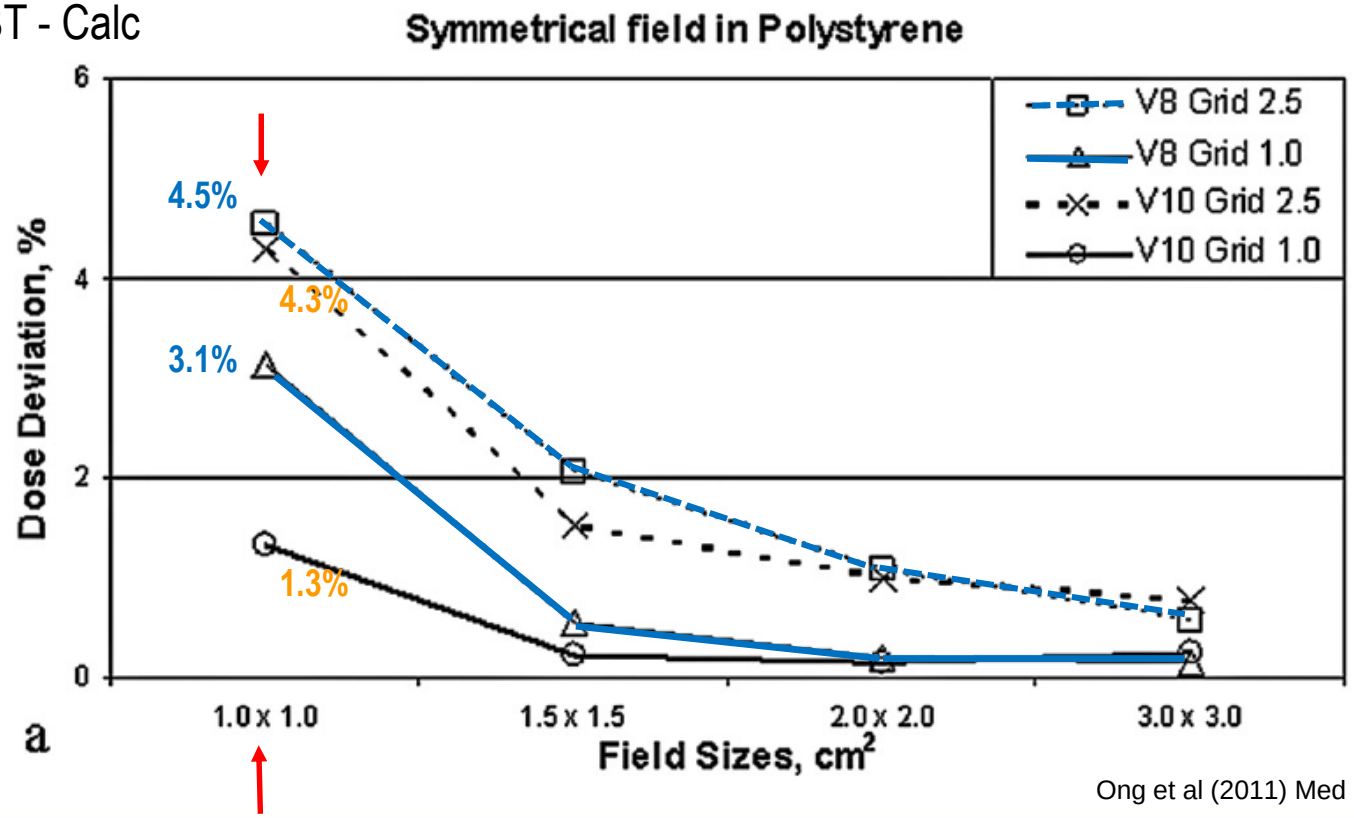

6MV
SSD=100cm
@6cm depth in polystyrene
MLC fields

Ong et al (2011) Med Phys 38(8), 4471-4479

ESTRO School

Small static fields: size of fluence and dose voxels

Differences between doses computed between two versions of same model

AAA v8.6.15 vs AAA v10.0.25

Major difference between versions was the resolution of the **fluence matrix**

2.5mm vs 0.3125mm

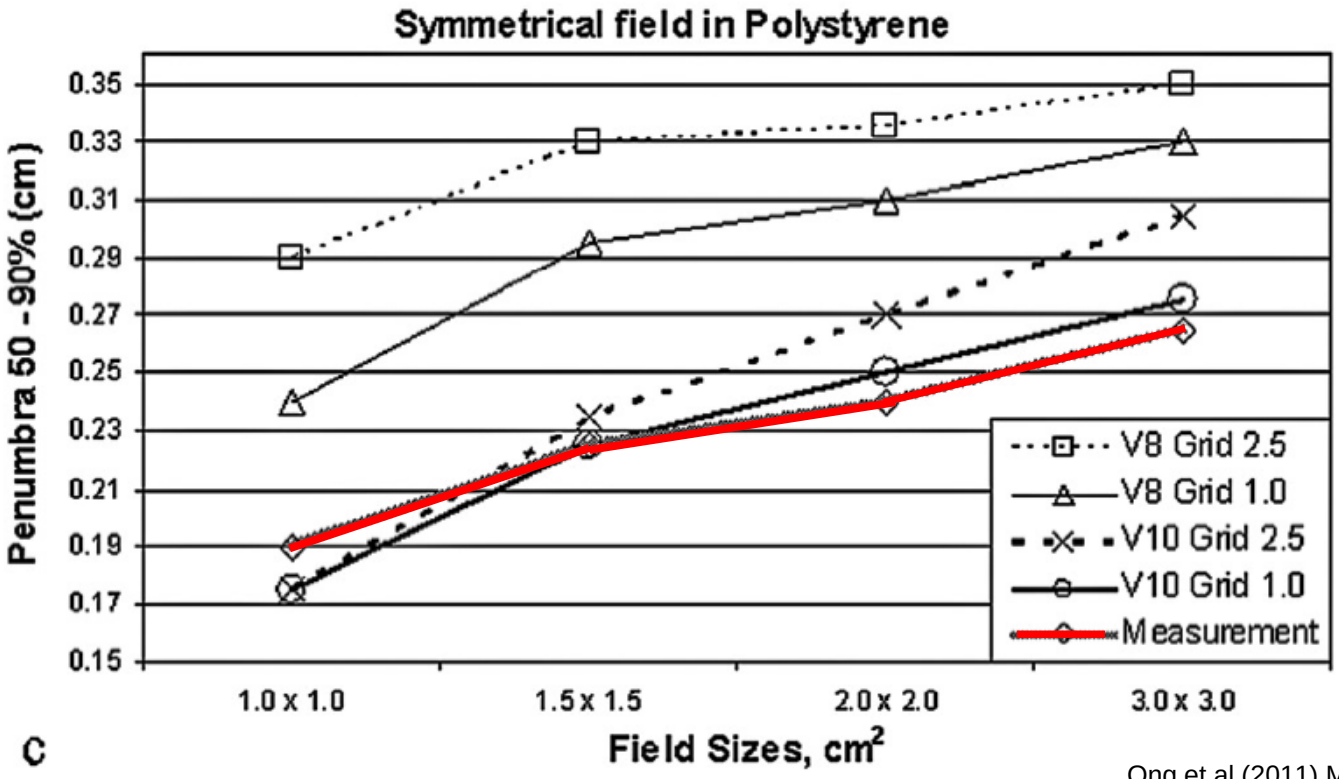

6MV
SSD=100cm
@6cm depth in polystyrene
MLC fields

Ong et al (2011) Med Phys 38(8), 4471-4479

ESTRO School

Small static fields: size of fluence and dose voxels

Differences between doses computed between two versions of same model

AAA v8.6.15 vs AAA v10.0.25

Major difference between versions was the resolution of the **fluence matrix**

2.5mm vs 0.3125mm

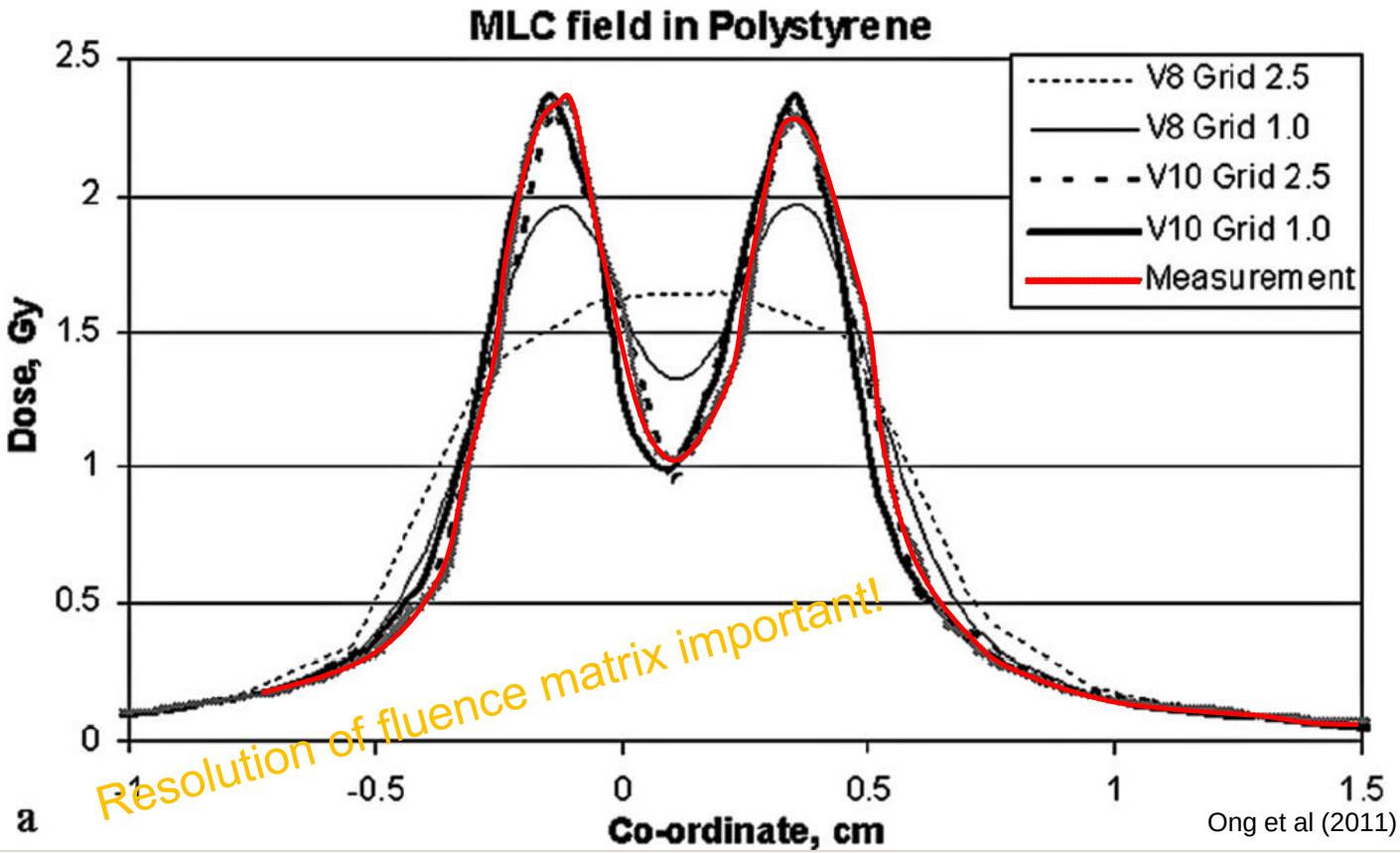

6MV
SSD=100cm
@6cm depth in polystyrene
HD-MLC two open leaves separated by one closed leaf

Ong et al (2011) Med Phys 38(8), 4471-4479

ESTRO School

Dose modelling in low density media

Modelling of source size & electron transport

energy fluence profile for an ideal point source

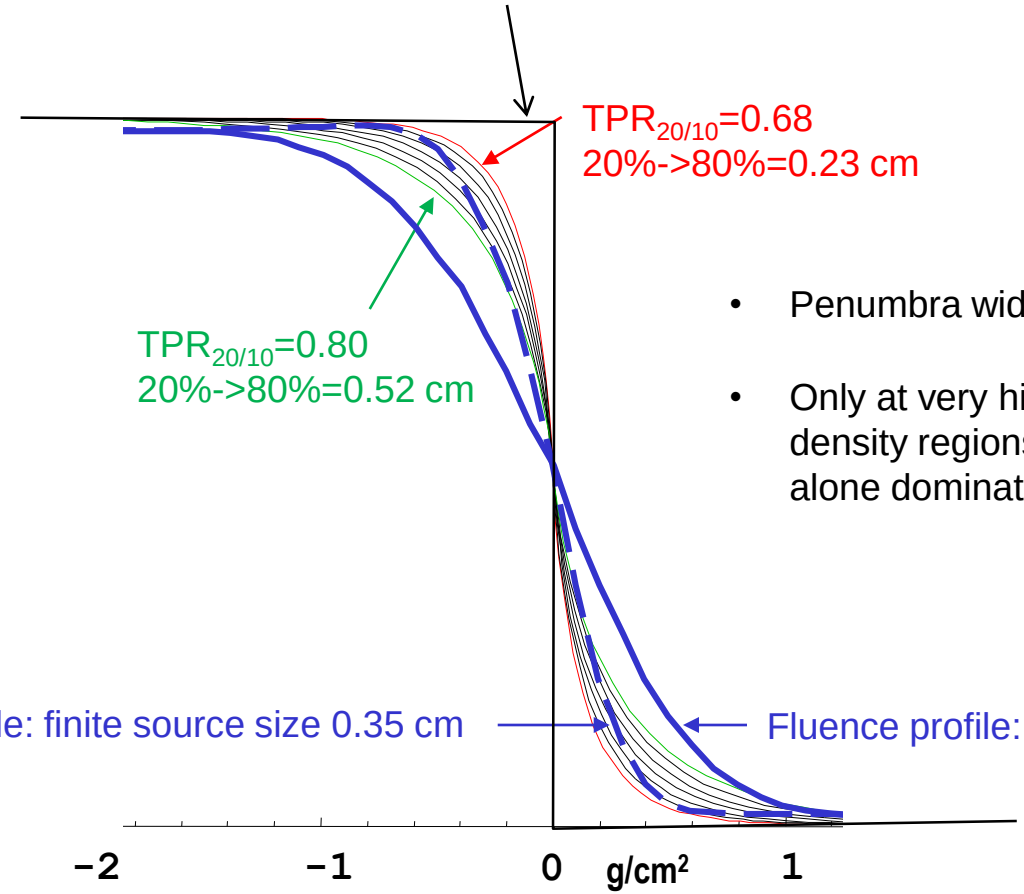

- Penumbra width influenced by source size
- Only at very high beam energies (or in low density regions) lateral electron transport alone dominates penumbra shaping

Nyholm *et al* Rad. Onc. 78, pp 347-51 and PMB 51 pp 6245-62
(Anders Ahnesjö)

ESTRO School

Small static fields: Influence of low density medium

Differences between doses computed between two versions of same model

AAA v8.6.15 vs AAA v10.0.25

6MV
SSD=100cm
@6cm depth
MLC fields

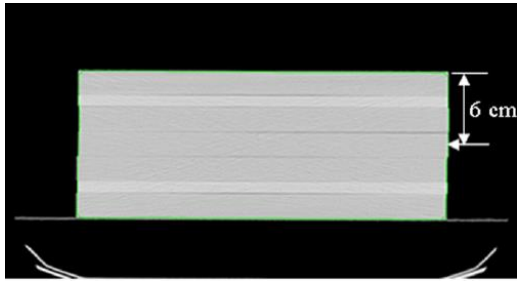

Film EBT - Calc

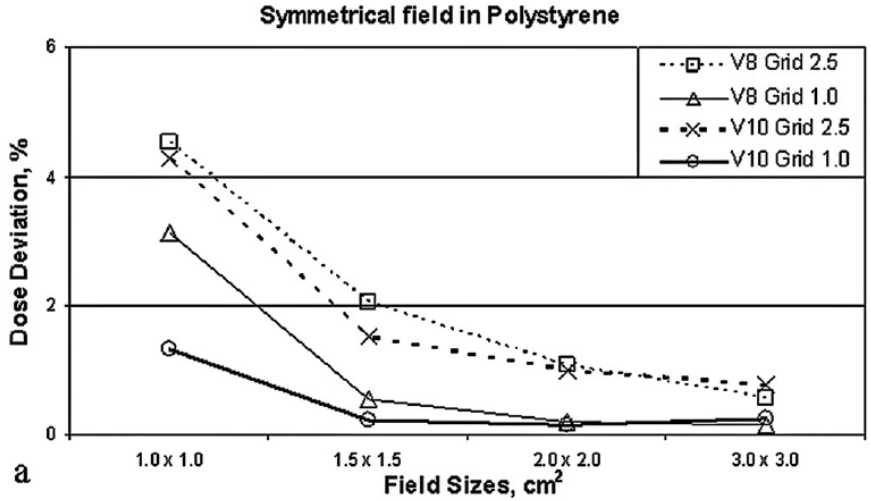

Ong et al (2011) Med Phys 38(8), 4471-4479

Small static fields: Influence of low density medium

Differences between doses computed between two versions of same model

AAA v8.6.15 vs AAA v10.0.25

Major difference between versions was the resolution of the **fluence matrix**

2.5mm vs 0.3125mm

6MV
SSD=100cm
@6cm depth
MLC fields

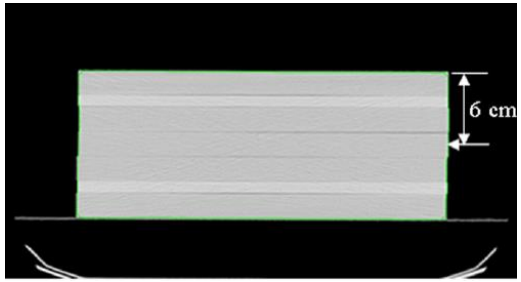

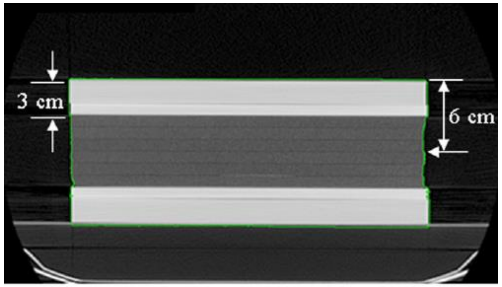

Film EBT - Calc

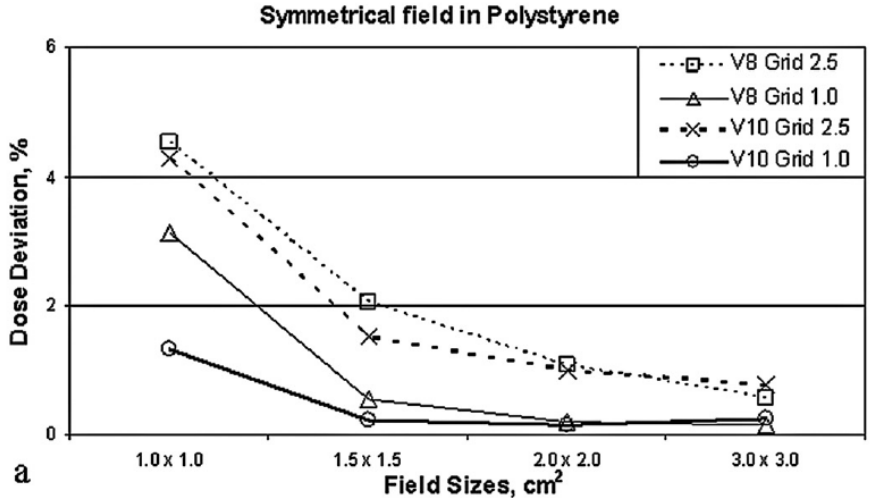

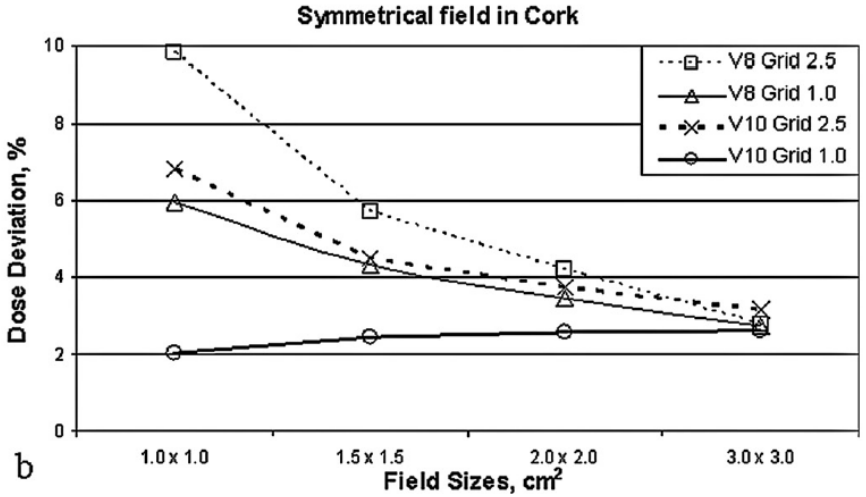

Ong et al (2011) Med Phys 38(8), 4471-4479

ESTRO School

Small static fields: Influence of low density medium

Differences between doses computed between two versions of same model

AAA v8.6.15 vs AAA v10.0.25

6MV
SSD=100cm
@6cm depth
MLC fields

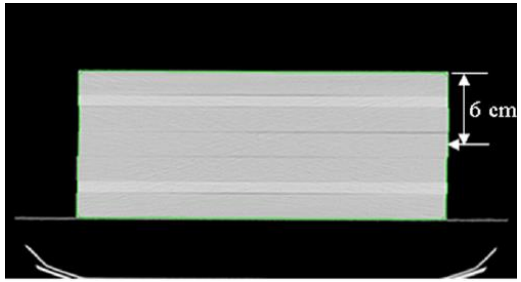

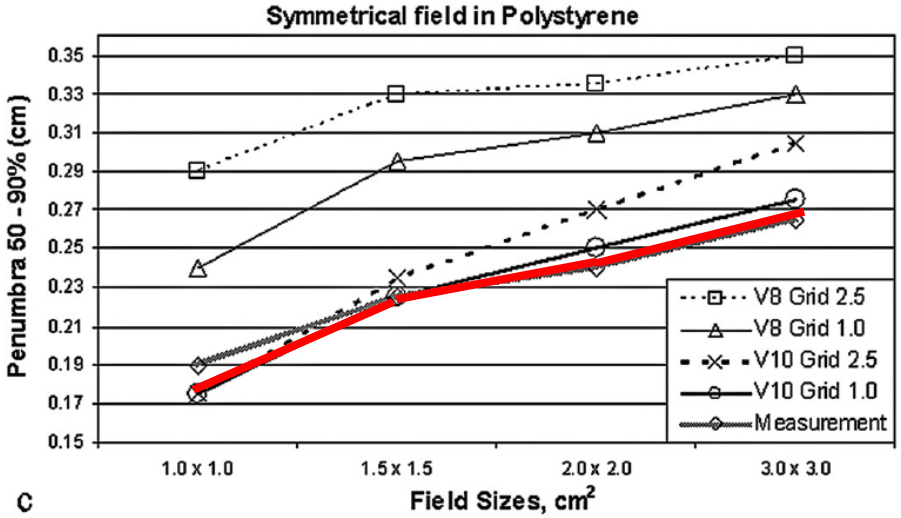

Onget al (2011) Med Phys 38(8), 4471-4479

ESTRO School

Small static fields: Influence of low density medium

Differences between doses computed between two versions of same model

AAA v8.6.15 vs AAA v10.0.25

Major difference between versions was the resolution of the **fluence matrix**

2.5mm vs 0.3125mm

6MV
SSD=100cm
@6cm depth
MLC fields

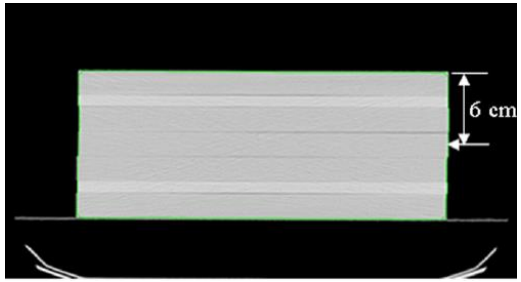

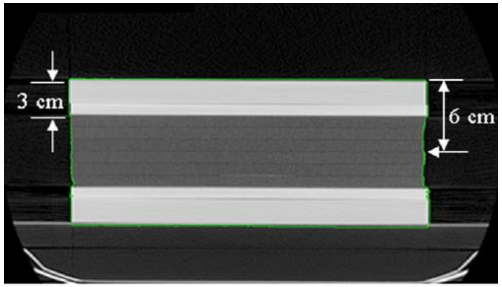

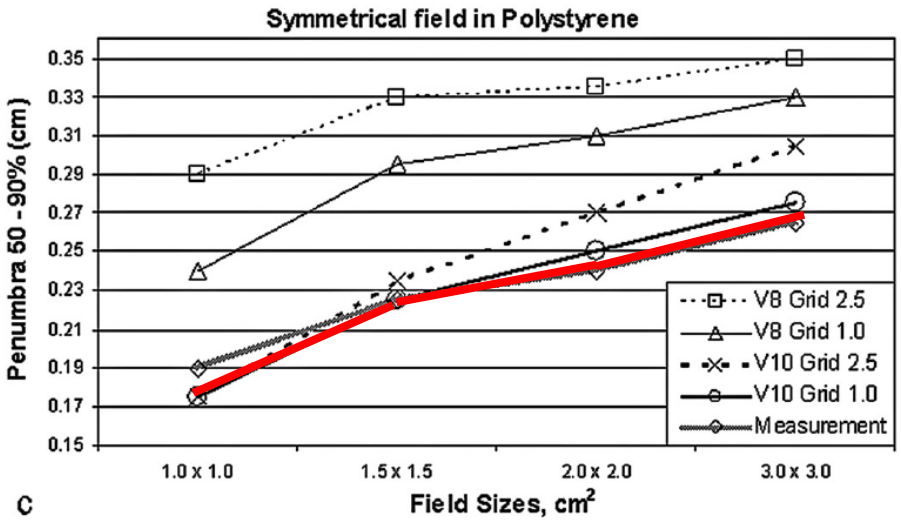

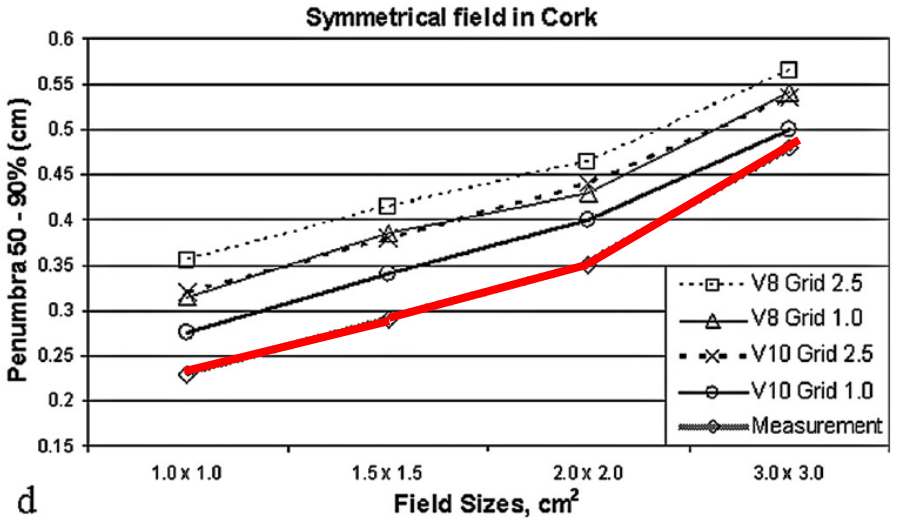

Onget al (2011) Med Phys 38(8), 4471-4479

ESTRO School

Small static fields: Influence of low density medium

Differences between doses computed between two versions of same model

AAA v8.6.15 vs AAA v10.0.25

Major difference between versions was the resolution of the **fluence matrix**

2.5mm vs 0.3125mm

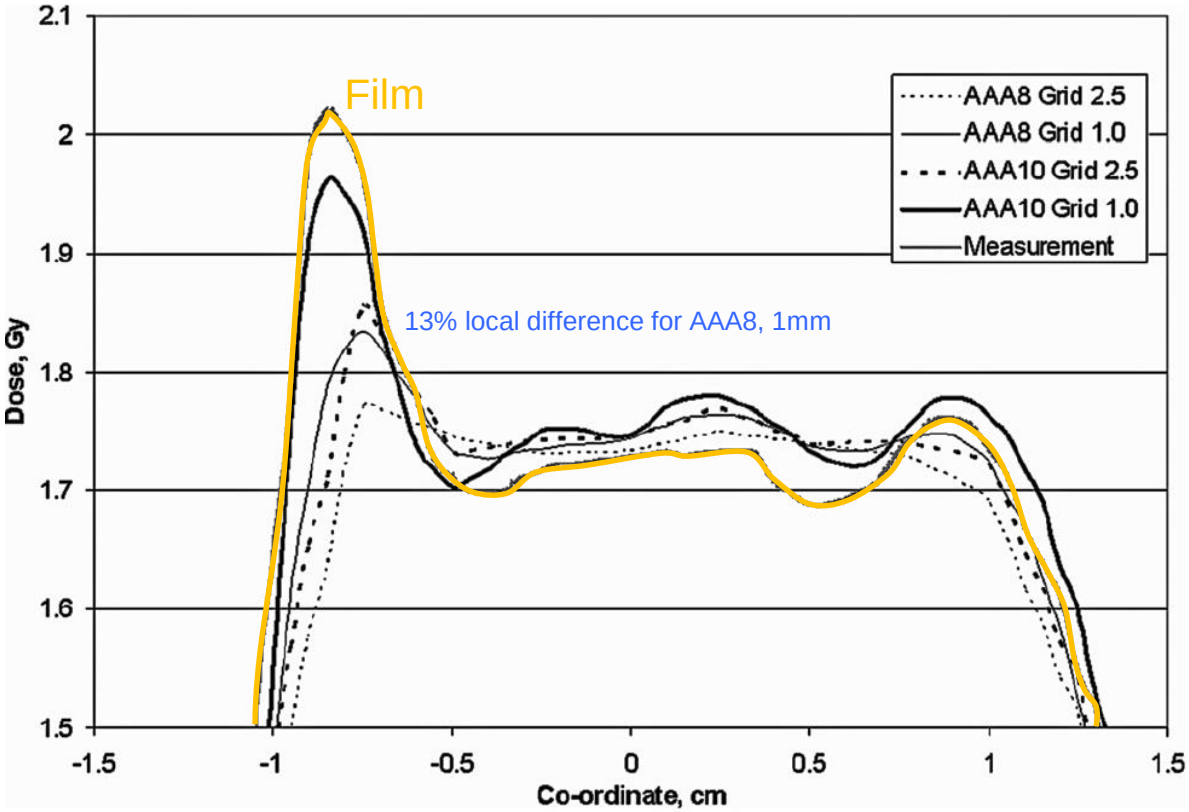

Clinical VMAT plan
6MV
Measurement in homogeneous polystyrene
EBT film

Ong et al (2011) Med Phys 38(8), 4471-4479

ESTRO School

Summary 1: TPS performance related to penumbra modelling (beam source modelling and lateral electron transport effects)

Type of dose calculation model	Homogeneous water medium	Heterogeneous tissues
Factor-based	Limited performance	
Pencil kernel (PB)	Dependant on beam source model	Lateral electron transport effects mostly ignored
Point kernel (conv/sup, CC, AAA)	Dependant on beam source model	Lateral electron transport effects approximately acounted for
Monte Carlo	Dependant on beam source model	Dependant on beam source model

Adapted from Anders Ahnesjö

Summary 2 : TPS modelling of small & composite fields

- Modelling of the direct beam source becomes important in narrow collimated modulated fields due to source occlussion
- In small and modulated fields the MLC is more involved in shaping primary energy fluence, so modelling this becomes important
- Explicit modelling of the direct beam source size and the effects due to the MLC is not common in most TPS. Implementations (approximations) vary.
- Fine resolution is required in dose but also energy fluence calculations for small field modelling
- Only at very high beam energies (or in low density regions) lateral electron transport alone dominates penumbra shaping $\rightarrow$ a beam model that accounts for finite source size and collimating jaw effects plays a primary role in the dose calculated by the TPS
- Most TPSs do not require small field measured data as default input to their beam configuration engines.

ESTRO School

WWW.ESTRO.ORG/SCHOOL

ESTRO School

WWW.ESTRO.ORG/SCHOOL

Dose per Monitor Unit (MU) formalisms
Factor-based approaches

Maria Mania Aspradakis
Maria.Aspradakis@luks.ch

Acknowledgement: Profs. Anders Ahnesjö & Dietmar Georg

ESTRO School

Learning Objectives

I. Dose per Monitor Unit (MU) formalism for first-principles (or model-based) photon dose calculations (how is the calculated dose related to MU?)

II. Dose per Monitor Unit (MU) formalism for factor-based dose calculations
   I. understand the main factors involved
   II. learn how these factors are determined
   III. appreciate how such factors relate to each other
   IV. the AAPM TG-71 / NCS12 / ESTRO factor-based dose per MU formalisms

III. Reflect on the purpose and usefulness of factor-based models in modern radiotherapy physics

Acknowledgement: Profs. Anders Ahnesjö & Dietmar Georg

Beam calibration: Dose per Monitor Unit

Beam output given as the absorbed dose [Gy] per Monitor Unit [MU] in water under <u>calibration conditions</u>

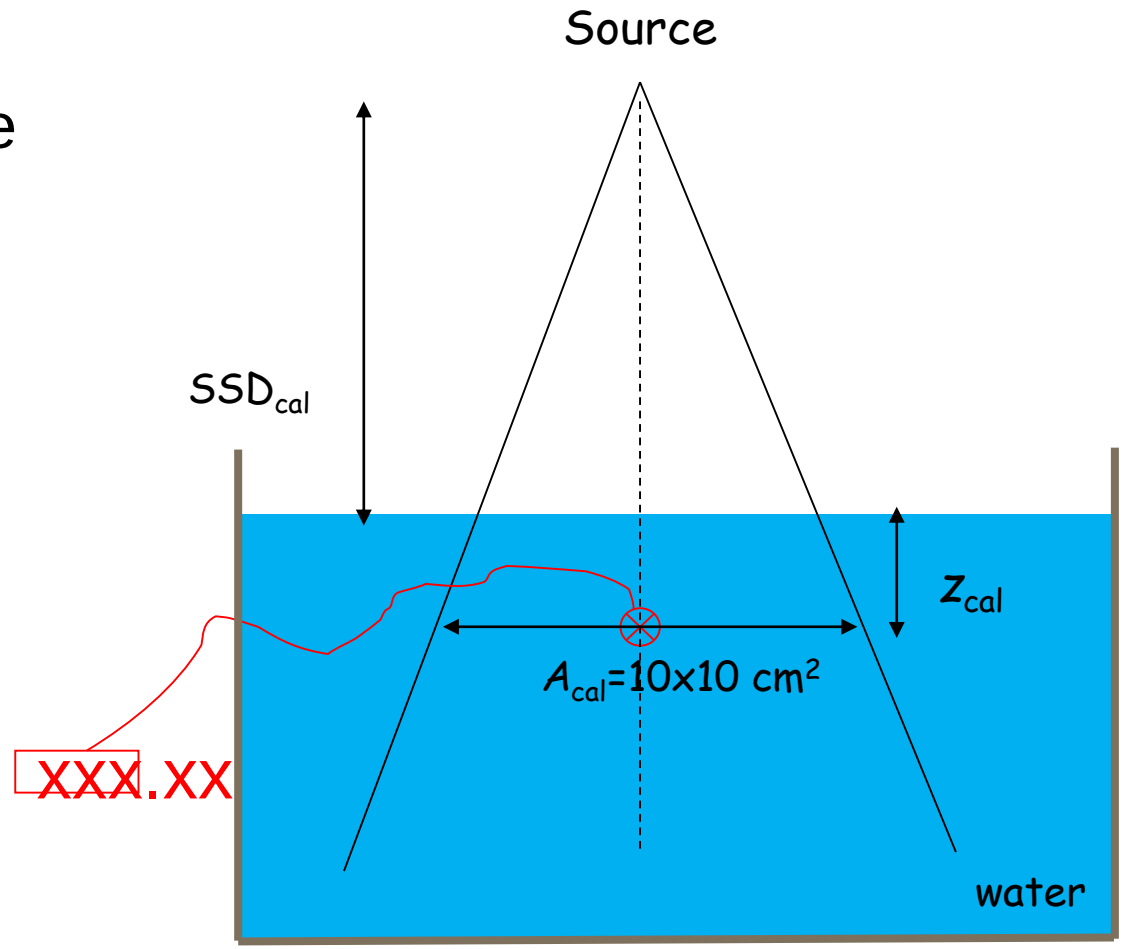

$$\left[D\left(A_{\text{cal}}; x_{\text{cal}}, y_{\text{cal}}, z_{\text{cal}} \right) / M \right]_{\text{Measured}}$$

Dose per MU formalisms: model-based dose calculations

$$\frac{D_{\text{calc}}(A;x,y,z)}{M} = \frac{D_{calc}(A;x,y,z)}{amount\ of\ \ radiation} \cdot F_{\text{calibration}}$$

The amount of radiation incident of the patient is either in terms of:

Particle (*beam phase space*) – e.g **Monte Carlo**

((type, energy, location, direction)$_{\text{particle 1}}$,
(type, energy, location, direction)$_{\text{particle 2}}$,
"
"
"
type, energy, location, direction)$_{\text{particle } N}$)

N of order 10^7

or

Energy fluence (*direct*, *head scatter*) – **kernel-based models**

$$\Psi(x,y) = \frac{\#\text{photons@(x, y)} \cdot \text{their energy}}{\text{beam cross section}}$$

ESTRO School

Calculation of monitor units per field for treatment

per field *i*:

$$M_{\mathrm{i}} = \frac{D_{\mathrm{presc}} \cdot w_{\mathrm{i}}}{D_{calc,i}\left(s_{\mathrm{d}}, d; SSD\right) / M}$$

with

$$w_{\mathrm{i}} = \frac{D_i\left(s_{\mathrm{d}}, d; SSD\right)}{\sum_{\mathrm{i}=1}^{\text{all fields}} D_{calc,i}\left(s_{\mathrm{d}}, d; SSD\right)}$$

ESTRO School

Dose per MU formalisms

model-based dose calculations

Dose per MU formalisms: model-based dose calculations

$$\frac{D(A;x,y,z)}{M} = \frac{D(A;x,y,z)}{\Psi_o} \cdot \frac{\Psi_o}{M}$$

Energy fluence of **direct photons** at isocentre in air

Calibration factor

relates the MU to the incident direct energy fluence under *reference calibration conditions*

$$\left.\begin{array}{l} \dfrac{D_{\text{ref,meas}}}{M} \\[2ex] \dfrac{D_{\text{ref,calc}}}{\Psi_o} \end{array}\right\} \quad \frac{\Psi_o}{M} = \frac{\left[D(A_{\text{ref}};x_{\text{ref}},y_{\text{ref}},z_{\text{ref}})/M\right]_{\text{meas}}}{\left[D(A_{\text{ref}};x_{\text{ref}},y_{\text{ref}},z_{\text{ref}})/\Psi_o\right]_{\text{calc}}}$$

No monitor backscatter accounted for!

ESTRO School

Dose per MU formalisms: model-based dose calculations

- The signal from the monitor chamber has a component that originates from particles which have backscattered from the upper part of the jaws into the chamber.
- The fraction of this signal depends on the aperture defined by the upper jaws and increases as this decreases.

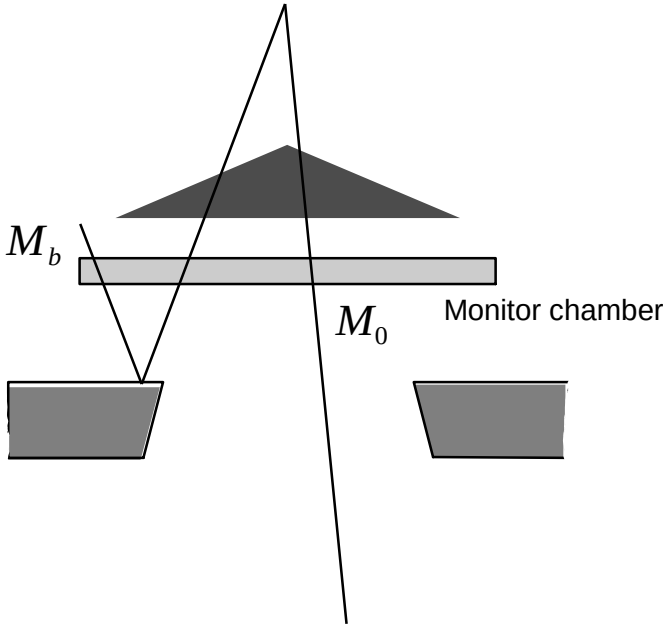

Fraction of the total of the monitor chamber which is attributed to particles that have backscattered into the monitor chamber

$$M = M_0 + M_b(A) = \left(1 + b\left(A\right)\right) M_0$$

or

$$\frac{M_0}{M} = \left(1 + b(A)\right)^{-1}$$

ESTRO School

Dose per MU formalisms: model-based dose calculations

Including monitor signal M_b caused by backscatter as a function of collimator aperture, the formalism is:

$$\frac{D(A;x,y;z)}{M} = \frac{D(A;x,y;z)}{\Psi_0}\frac{\Psi_0}{M_0}\cdot\left(1+b(A)\right)^{-1}$$

calibration factor

$$\frac{\Psi_o}{M_o} = \frac{\left[D(A_{ref};x_{ref},y_{ref},z_{ref})/M\right]_{meas}}{\left[D(A_{ref};x_{ref},y_{ref},z_{ref})/\Psi_o\cdot\left(1+b(A_{ref})\right)^{-1}\right]_{calc}}$$

Note: Different implementations in common TPSs described in the next lecture)

Dose per MU formalisms

factor-based dose (or MU) calculations

Dose per MU formalisms: factor-based dose calculations

$$\frac{D(A;x,y,z)}{M} = \frac{D(A;x,y,z)}{\Psi_o} \cdot \frac{\Psi_o}{M}$$

Basic factorisation:

$$\frac{D(\text{cond. a})}{M} \equiv \underbrace{D(\text{calibration})/M}_{\textit{calibration value}} \cdot \underbrace{\frac{D(\text{cond. a})/M}{D(\text{calibration})/M}}_{\textit{factor a}}$$

More general…:

$$\frac{D(\text{cond. a})}{M} \equiv \underbrace{D(\text{calibration})/M}_{\textit{calibration value}} \cdot \underbrace{\frac{D(\text{cond. n})/M}{D(\text{calibration})/M}}_{\textit{factor n}} \cdots \underbrace{\frac{D(\text{cond. b})/M}{D(\text{cond. c})/M}}_{\textit{factor b}} \cdot \underbrace{\frac{D(\text{cond. a})/M}{D(\text{cond. b})/M}}_{\textit{factor a}}$$

ESTRO School

Dose per MU formalisms: factor-based dose calculations

Nomenclature used in this presentation (in analogy, but not identical, to that in AAPM Task group report 71)

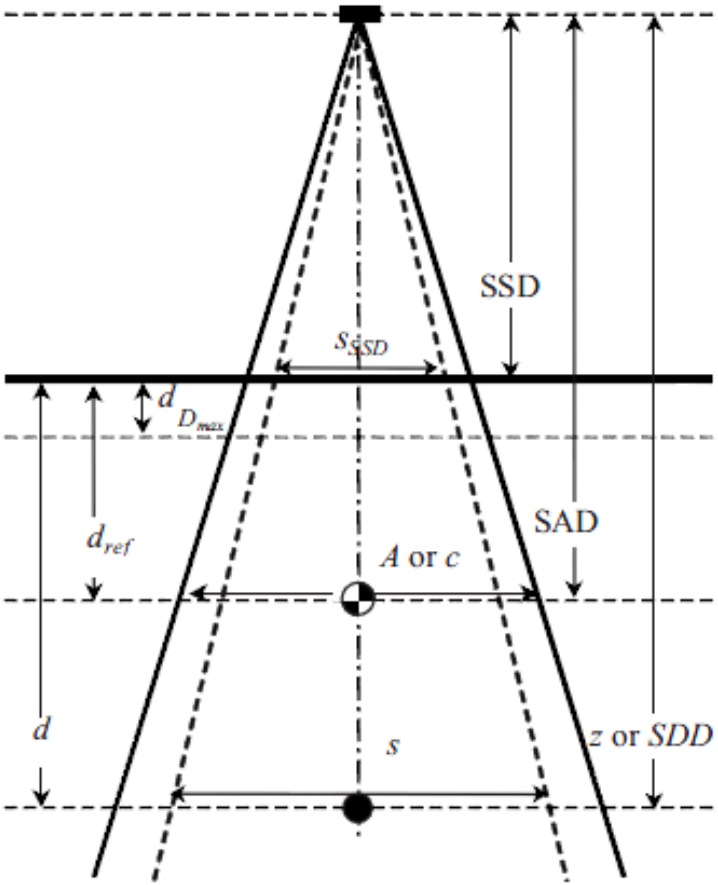

d_{ref} reference depth

$c_{ref} \equiv r_{ref}$ reference field size/collimator setting

c_{eqsq} collimator setting (equivalent square)

$s_{d,eqsq}$ field size at depth (equivalent square)

Calculation point at isocentre:

$$s_{d,eqsq} = c_{eqsq}$$

Dose per MU formalisms: factor-based dose calculations

Reference normalisation conditions

Isocentric

- c_{ref} = 10 x 10 cm²

  Field Size at isocenter

- d_{ref} = 10 cm
- SSD = SAD - d_{ref}

Tissue phantom ratio

TPR(c,d)

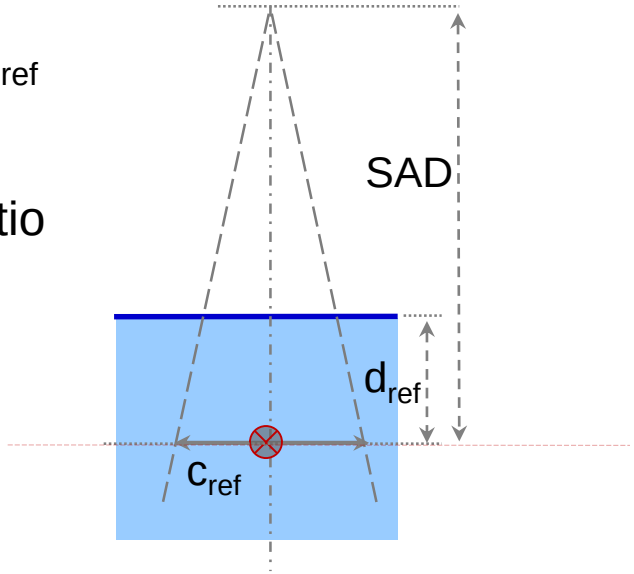

$$\frac{D(c_{ref}, d_{ref}; \mathrm{SAD})}{M} [cGy/MU]$$

Dose per MU formalisms: factor-based dose calculations

Reference normalisation conditions

Isocentric

- c_{ref} = 10 x 10 cm²

  Field size at isocenter

- d_{ref} = 10 cm
- SSD = SAD - d_{ref}

Tissue phantom ratio

TPR(c,d)

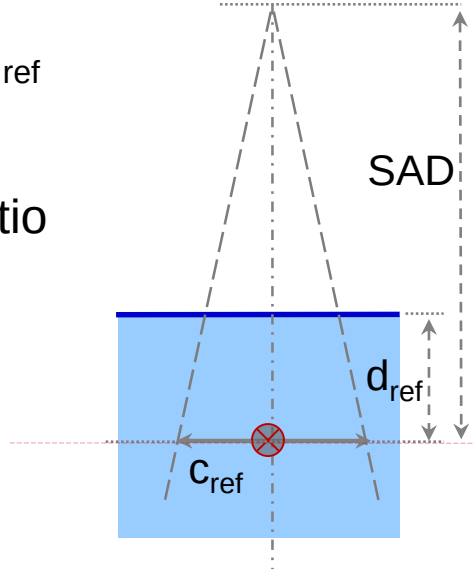

$$\frac{D(c_{ref},d_{ref};SAD)}{M}[cGy/MU]$$

Fixed SSD

c_{ref} = 10 x 10 cm²

Field size at surface

d_{ref} = 10 cm

SSD = SAD

Relative depth dose

RDD(s,d)

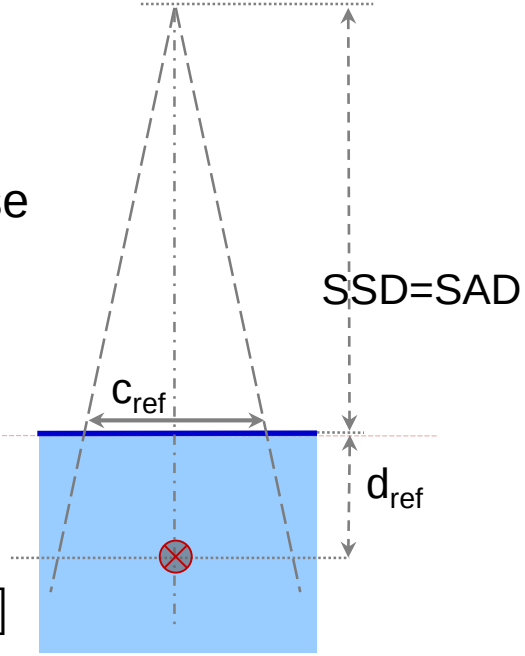

$$\frac{D(c_{ref},d_{ref};SSD)}{M}[cGy/MU]$$

ESTRO School

Dose per MU formalisms: factor-based dose calculations

Reference normalisation conditions: choice of reference depth d_{ref}

Reference depth in water of 10 cm recommended irrespective of beam quality index

- Previous recommendations where 5 cm for BQI < 0.70 and 10 cm for BQI > 0.70

Avoids unpredictable influence of contaminating electrons as far as possible

- Rule of thumb: depth of influence ~ $2 \cdot d_{Dmax}$ or MV/3

$\therefore$

10cm depth chosen for consistency in reference depth for beam calibration and MU calculation

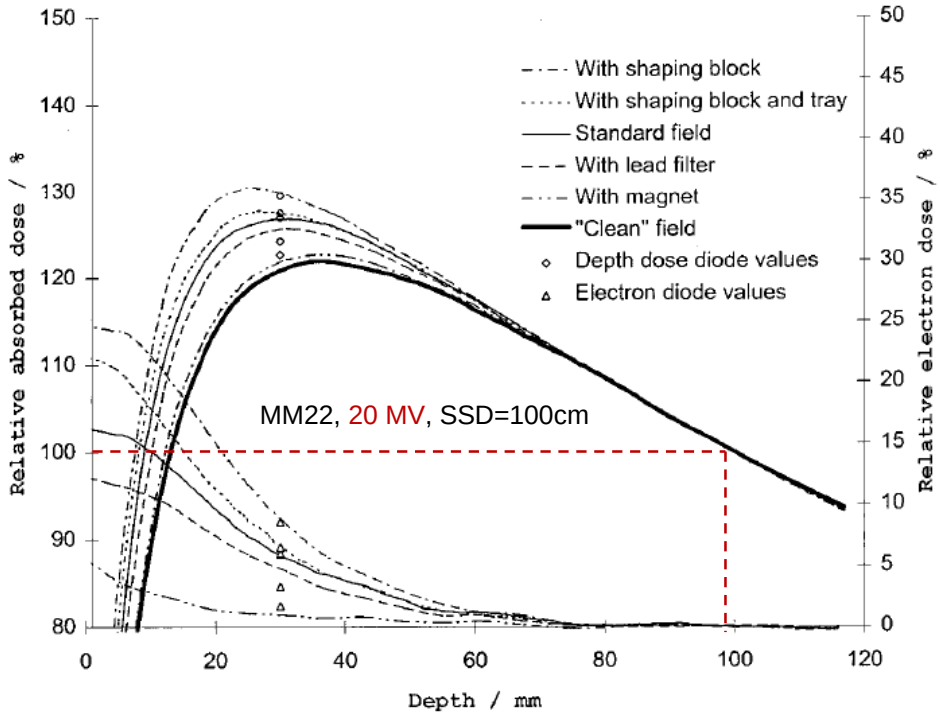

Sjögren and Karlsson, Med, Phys, 25(6), p916, 1998

ESTRO School

Dose per MU formalisms: factor-based dose calculations

Reference normalisation geometry

reference normalisation geometry could differ from linac calibration geometry (but for simplicity in this lecture we take the two to be the same)

$$\frac{D_{ref}(c_{ref}, d_{ref}; SSD_{ref})}{M}$$

Arbitrary treatment geometry

$$\frac{D(c, s_d, d; SSD)}{M}$$

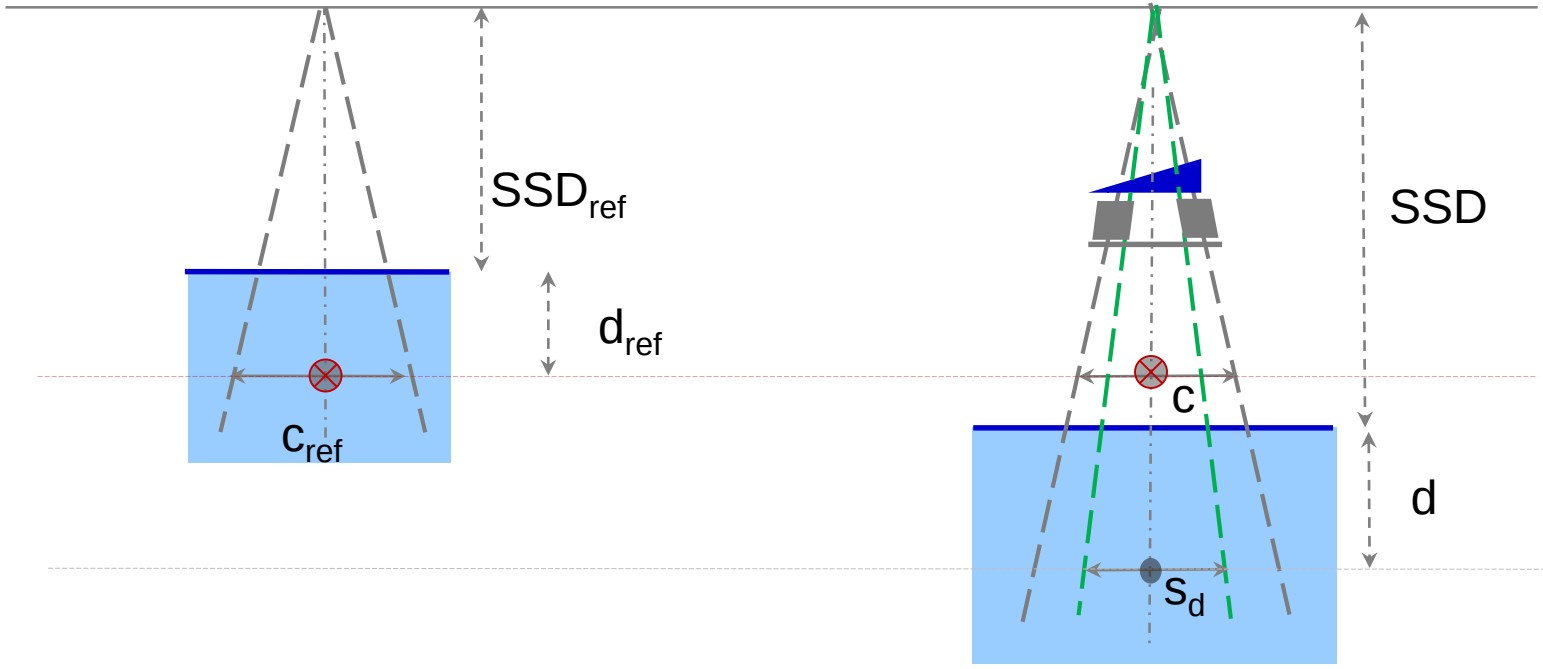

ESTRO School

Dose per MU formalisms: factor-based dose calculations

$$\frac{D(s_d, d; SSD + d)}{M} = \frac{D_{ref}(c_{ref}, d_{ref}; SSD_{ref})}{M} \cdot [factor(s)]$$

dosimetric quantities to account for all differences from
the reference irradiation geometry in terms of:

- distance from source (~ inverse square law)
- field size and depth (~ scatter dose in medium)
- modulation (~ beam intensity)
- attenuators in the beam path
- position off axis
- heterogeneities

ESTRO School

Dose per MU formalisms: factor-based dose calculations

basic scenario

Isocentric reference normalisation geometry

Isocentric treatment geometry: Open beam & calculation point at isocentre and on CAX

$$\frac{D_{ref}(c_{ref}, d_{ref}; SSD_{ref})}{M}$$

$$\frac{D(c, s_d, d; SAD)}{M}$$

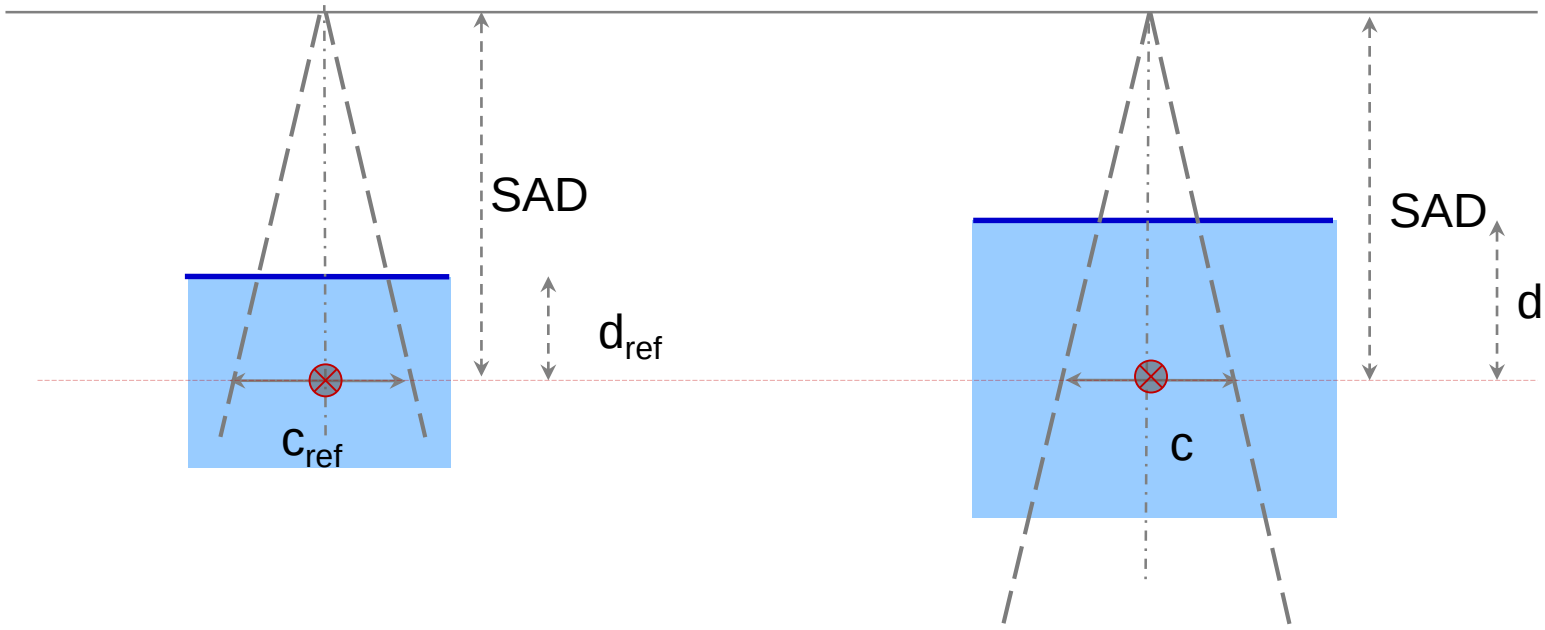

Dose per MU formalisms: factor-based dose calculations

Isocentric linac reference normalisation geometry

- **Step 1:** account for differences in dose at the calculation point due to changes in energy fluence from the different scatter conditions in the head of the linac
- Step 2:
- Step 3:

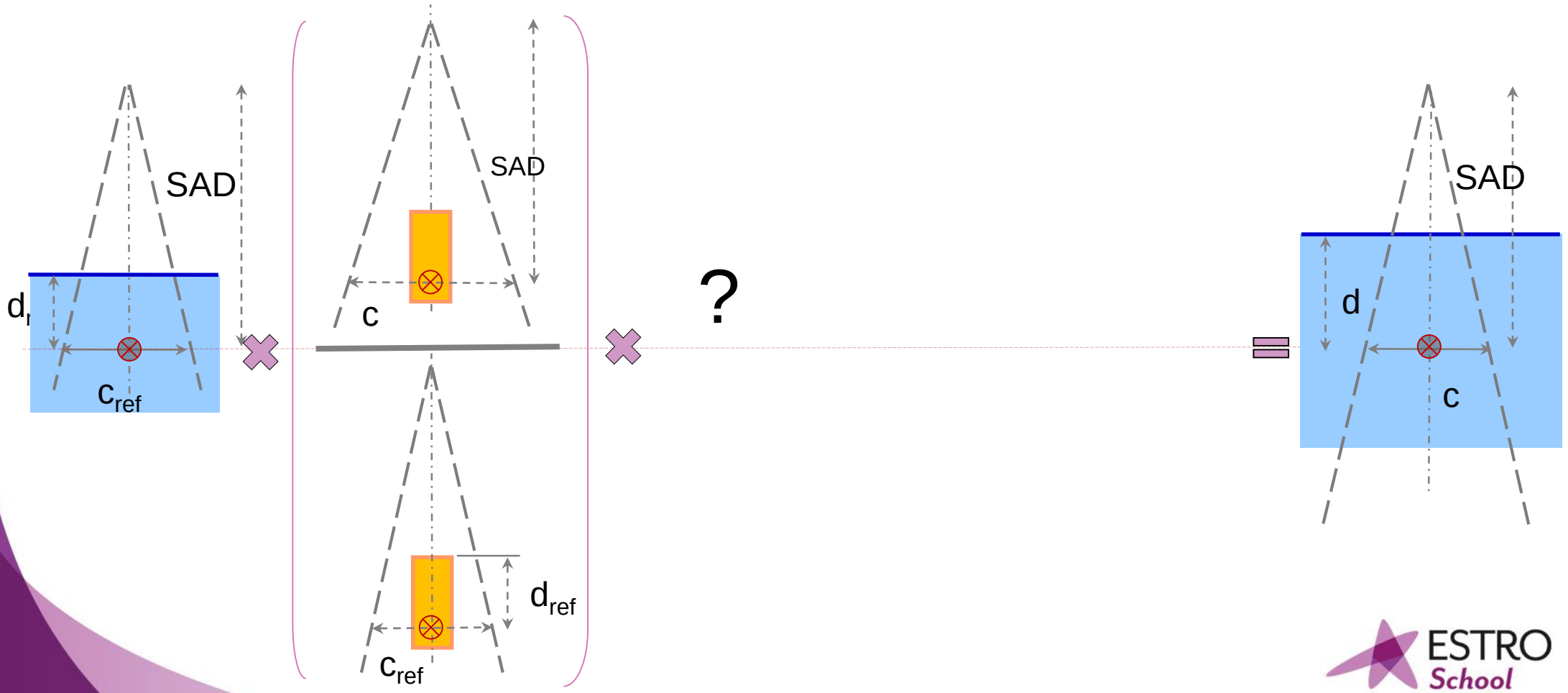

ESTRO School

Dose per MU formalisms: factor-based dose calculations

Isocentric linac reference normalisation geometry

- Step 1: account for differences in dose at the calculation point due to changes in scatter conditions in the head of the linac
- **Step 2**: account for differences in phantom scatter due to the change in field size (amount of phantom irradiated)
- Step 3:

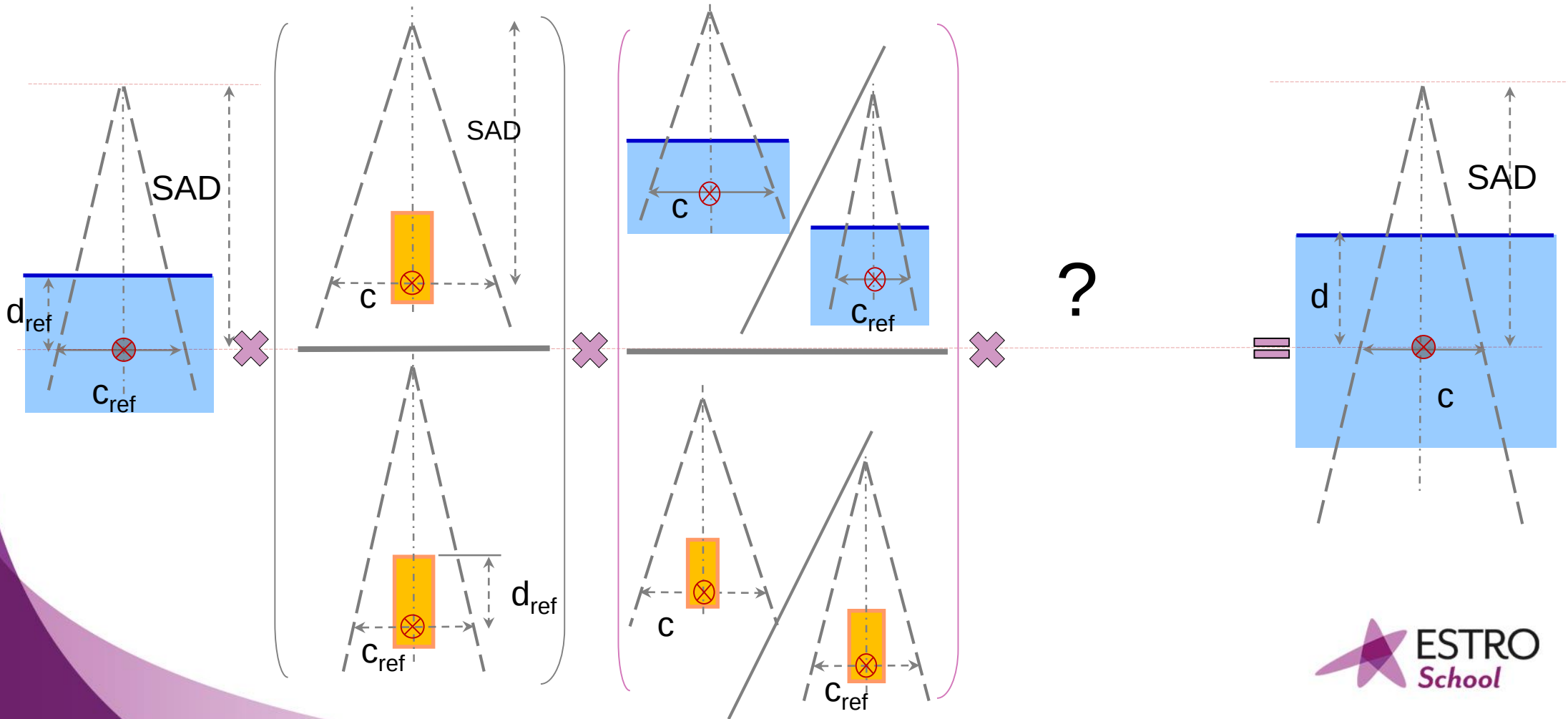

Dose per MU formalisms: factor-based dose calculations

Isocentric linac reference normalisation geometry

- Step 1: account for differences in dose at the calculation point due to changes in scatter conditions in the head of the linac
- Step 2: account for differences in phantom scatter due to the change in field size (amount of phantom irradiated)
- **Step 3**: account for differences in phantom scatter due to the change of depth

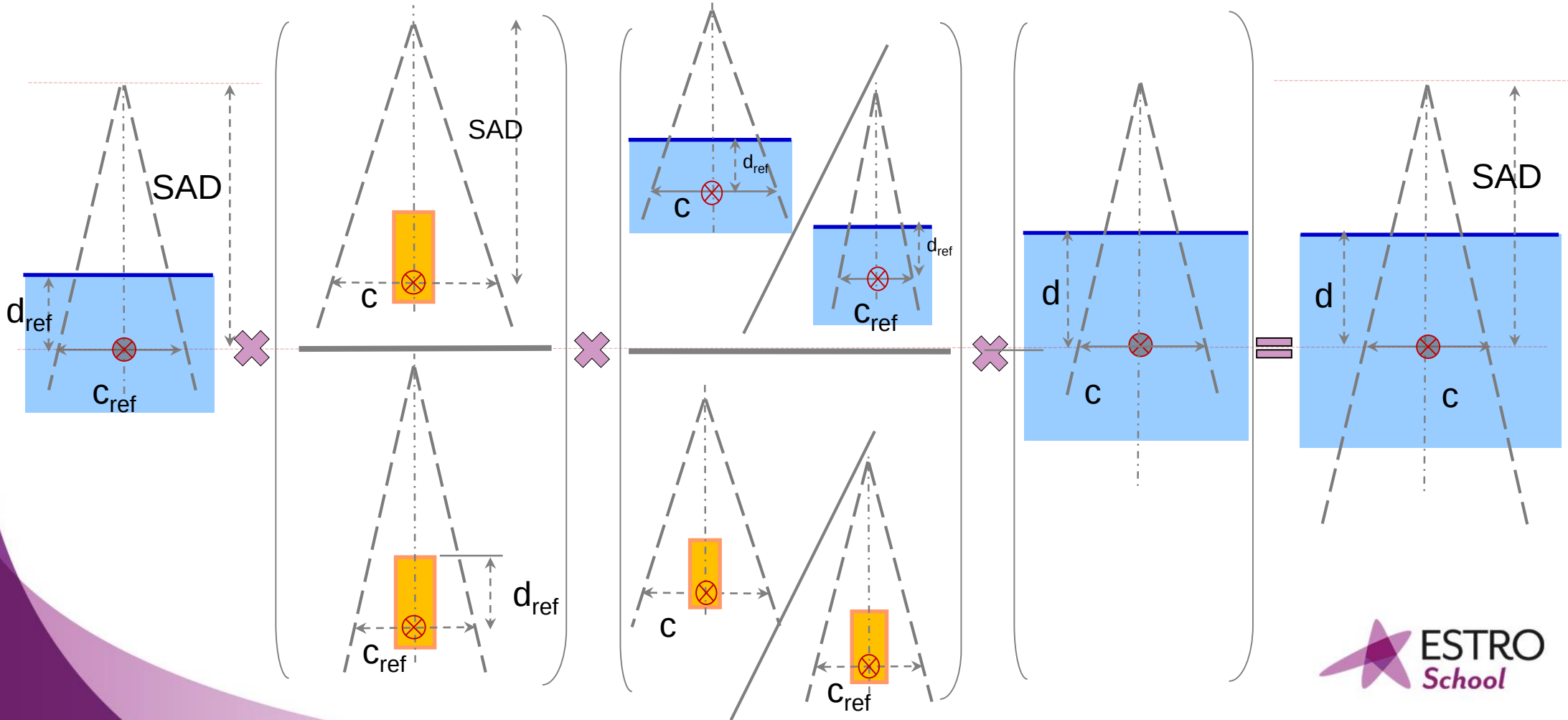

ESTRO School

Factor-based dose calculations

basic dosimetric quantities

In-air output ratio or output factor in air, Sc

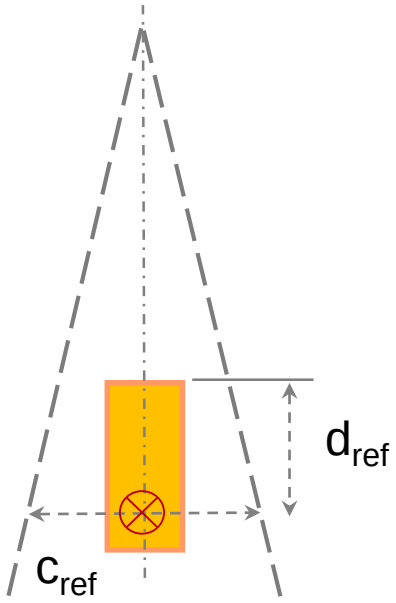

Report pf AAPM TG106: Accelerator beam data commissioning, Med Phys, 35(9), 2008
AAPM TG 74 report, Med Phys 36 (11), 2009

ESTRO School

Factor-based dose calculations: basic dosimetric quantities

In-air output ratio or output factor in air, Sc

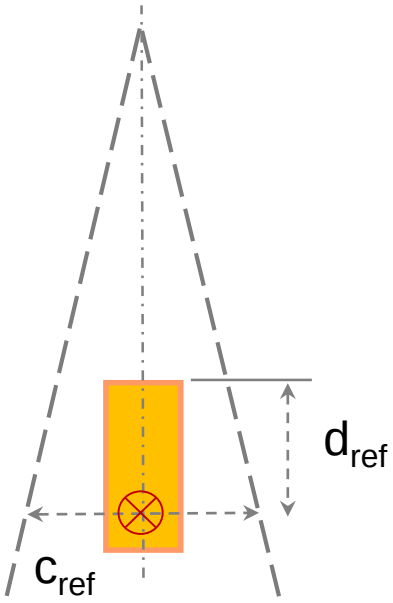

Is the ratio of **primary collision water kerma in free-space K_p** per monitor unit (MU) between an arbitrary collimator setting c and the reference collimator setting c_{ref} at the same location on the beam's central axis:

$$S_c(c) = \frac{K_p(c; d_{ref})/M}{K_p(c_{ref}; d_{ref})/M}$$

Also known as:

Mini-phantom output ratio

Collimator scatter factor

Head scatter factor

Sc quantifies fluence variations with collimator settings that can be used in beam modelling and dose calculations.

Usually d_{ref} = 10cm and c_{ref}=10cm

$$K_p = \int_{\text{primary spectrum}} \Psi_E \frac{\mu_{en}}{\rho} dE$$

Report pf AAPM TG106: Accelerator beam data commissioning, Med Phys, 35(9), 2008
AAPM TG 74 report, Med Phys 36 (11), 2009

ESTRO School

Factor-based dose calculations: basic dosimetric quantities

S_c : mini-phantom/buildup cap design – lateral considerations

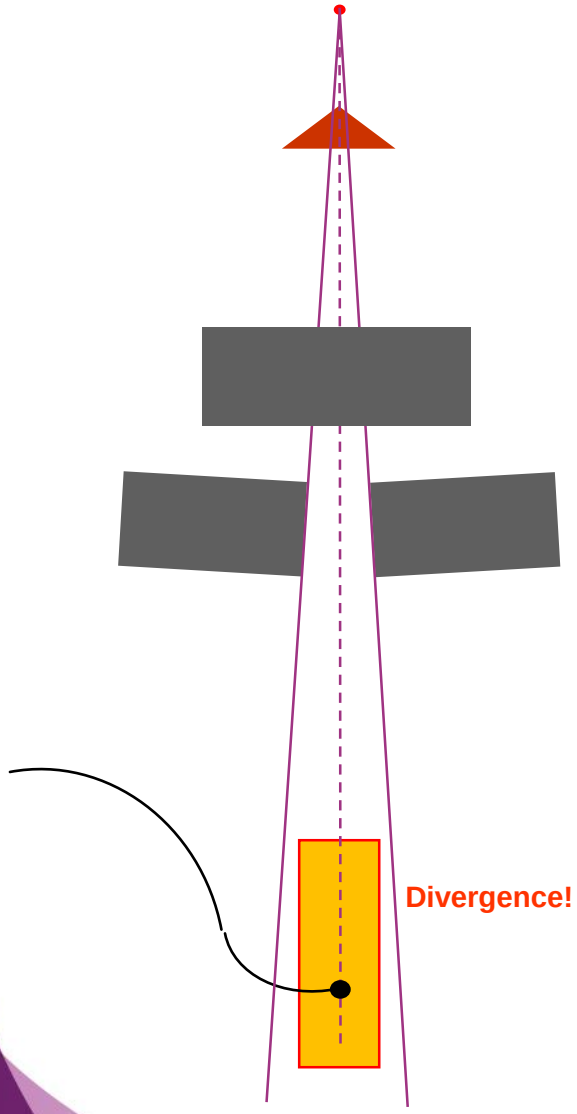

1. The entire mini-phantom/build-up cap should always be enclosed by the radiation field (incl. margin for penumbra).
2. The mp/bc should provide lateral CPE;
   $r_{CPE} \approx 5.973 \cdot TPR_{20,10} - 2.688$ [g/cm^2]
   Experimental investigations suggest that a wall thickness ≥ 1 g/cm^2 is sufficient.

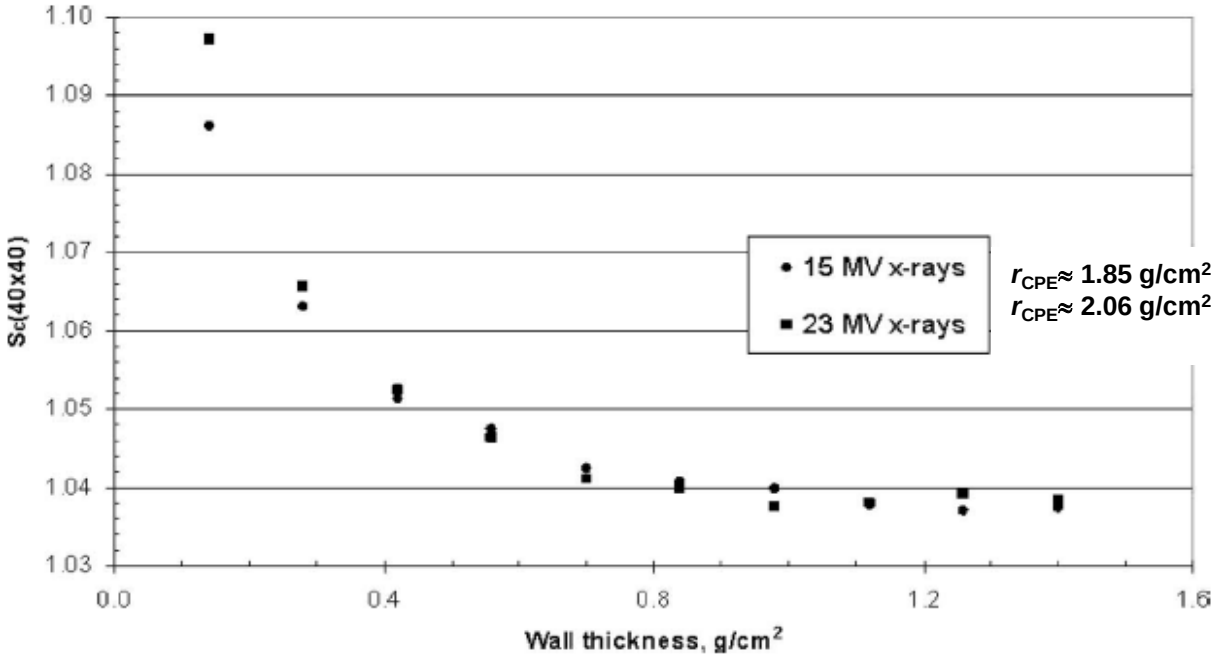

Jursinic PA (2006) , Med Phys 33, 1720-8,
Li et al MedPhys **22**, 1995, 1167-1170

Factor-based dose calculations: basic dosimetric quantities

S_c : mini-phantom/buildup cap design – depth considerations

The effective measurement depth in the mini-phantom/build-up cap must be large enough to stop contaminating electrons.

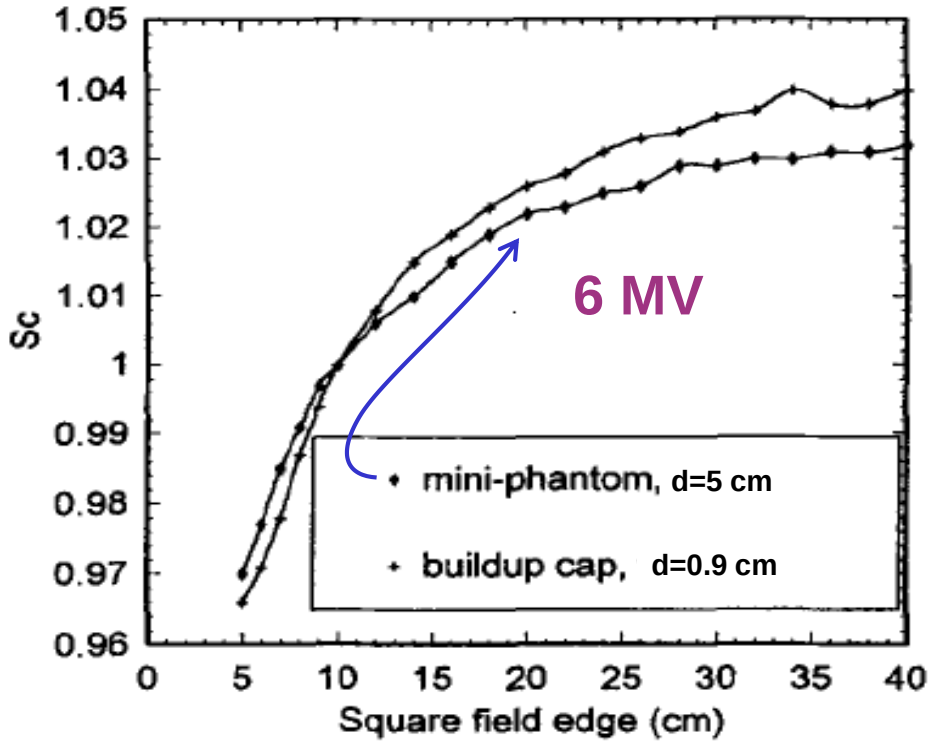

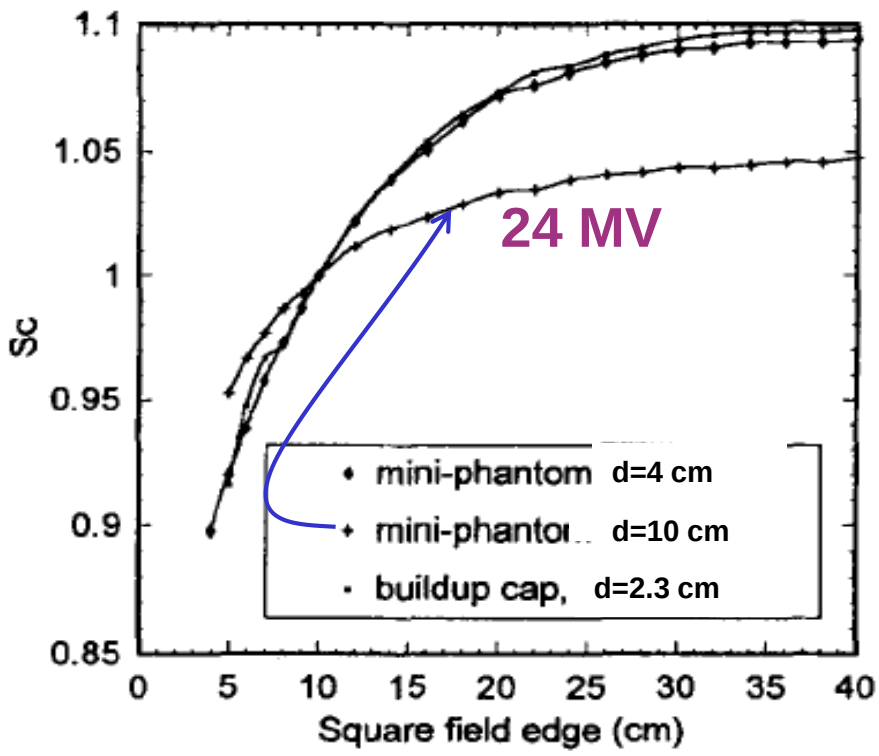

Frye DM, et al (1995) Med Phys 22, 249-53

Two rules of thumb used to eliminate e⁻ contamination:

$$d \geq 2 \cdot d_{max}$$

$$d \geq \mathrm{MV}/3 \ [\mathrm{cm}]$$

Factor-based dose calculations: basic dosimetric quantities

S_c : mini-phantom/buildup cap design – material considerations

- Water-equivalent material (solid water, acrylic (PMMA), graphite)
- For collimator settings < 5cm: miniphantom made of high Z material
- Using a high-*Z* material build-up cap should not introduce any deviations as long as the beam quality is constant...

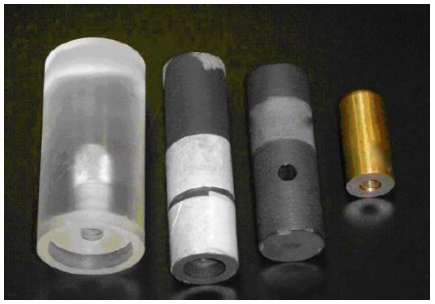

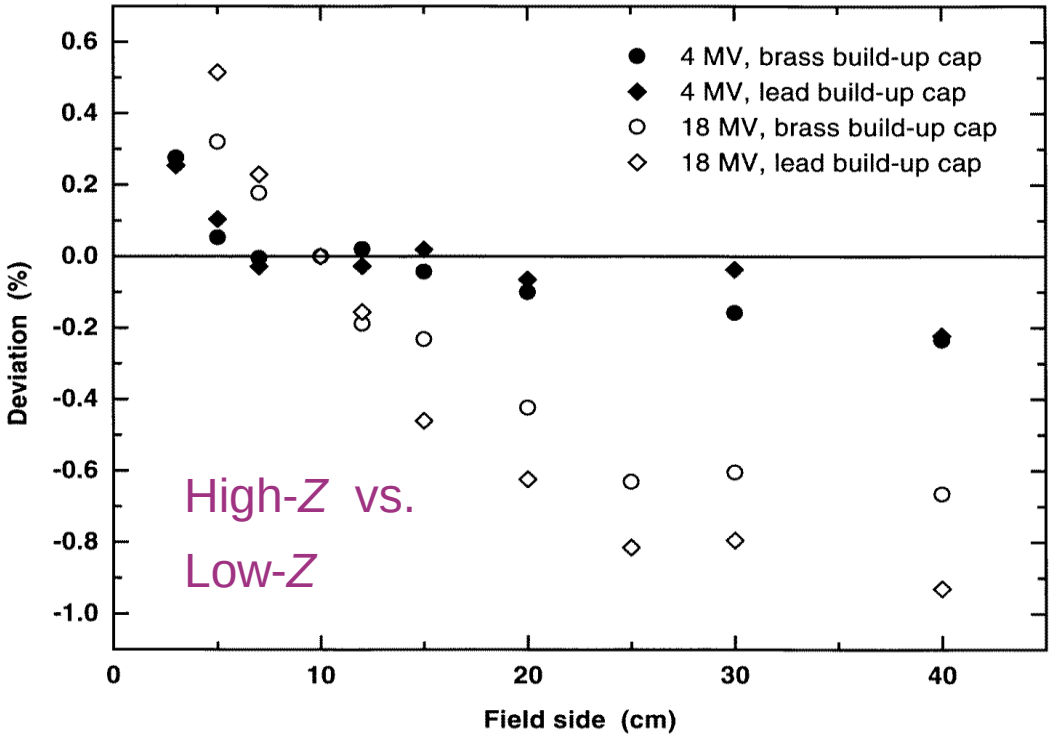

Recommendation: Only use high-*Z* buildup caps for very small fields and normalize these measurements to those in low-*Z* caps in the smallest possible overlapping field size (roughly 4x4 cm^2).

Weber L, Nilsson P, Ahnesjö A (1997) Phys Med Biol 42, 1875-86

ESTRO School

Factor-based dose calculations: basic dosimetric quantities

S_c : mini-phantom/buildup cap design

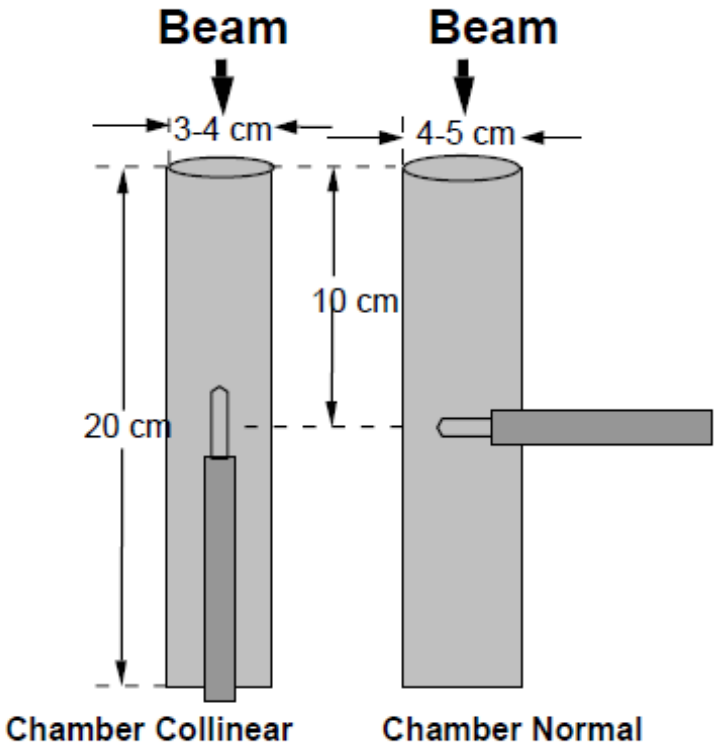

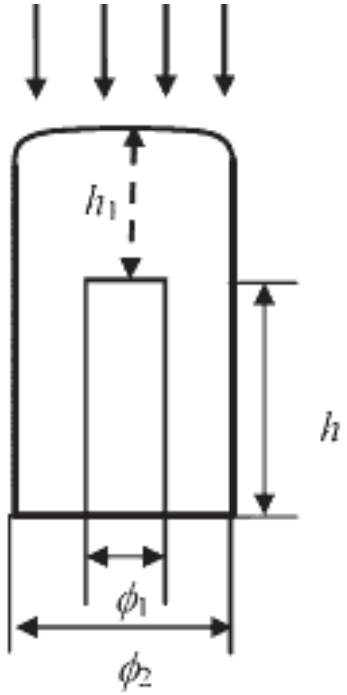

Figure 8.3 Brass mini-phantom design for square fields down to 15 mm × 15 mm and photon energies less than 25 MV recommended by Zhu et al. (2009): Thickness $h_1 \geq 12$ mm (or 10 g/cm², mass density $\rho = 8.4 - 8.7$ g/cm³) and inner diameter ϕ_1 equal to the outer diameter of the detector. Height h is sufficient to cover the detector sensitive volume. The outer diameter ϕ_2 of the mini-phantom can be such that its wall is thinner than the thickness required for CPE but not less than 12 mm for energies up to 18 MV. The total lateral dimension above the chamber should ensure lateral CPE for the photon energy (from Zhu et al. (2009) with permission)

Zhu et al, AAPM Report TG74: 'In-air output ratio Sc for megavoltage photon', *Med Phys 36 (11), 2009*

ESTRO School

Summary: in-air output ratio, Sc
isocentric conditions

- To quantify variations in energy fluence incident on the patient
- Function of the collimator setting
- Depends on the photon beam quality and on treatment head design
- Depends on the field orientation for rectangular beams (CEE)
- Almost independent of the source-detector distance
- Does not depend on depth if z > R contam. electrons

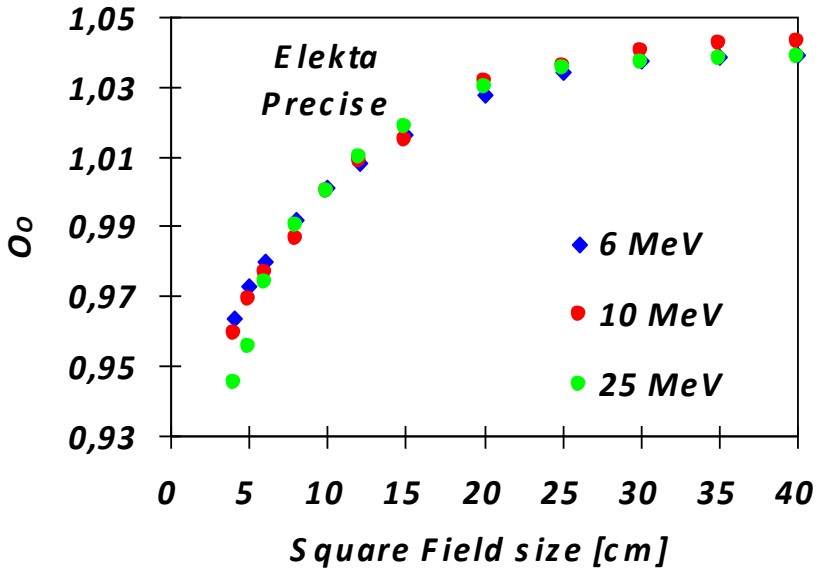

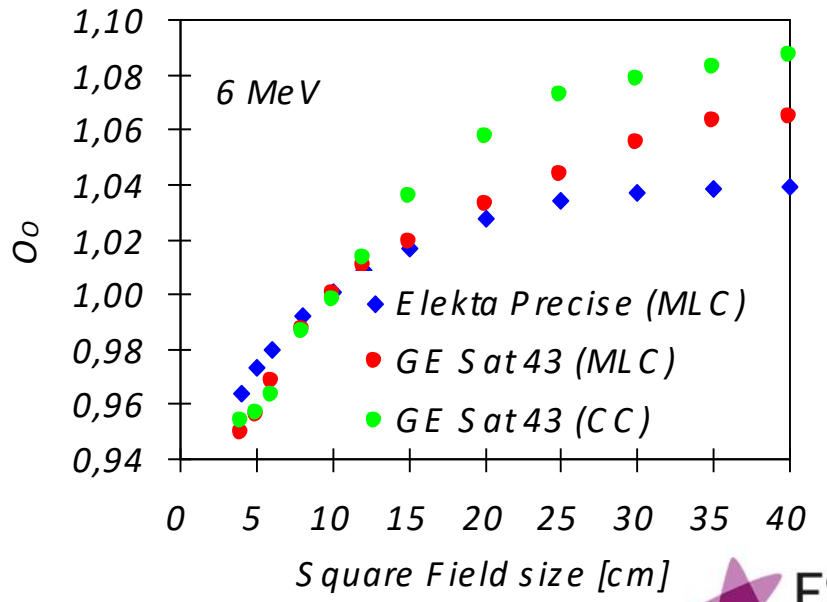

ESTRO School

Dose per MU formalisms: factor-based dose calculations

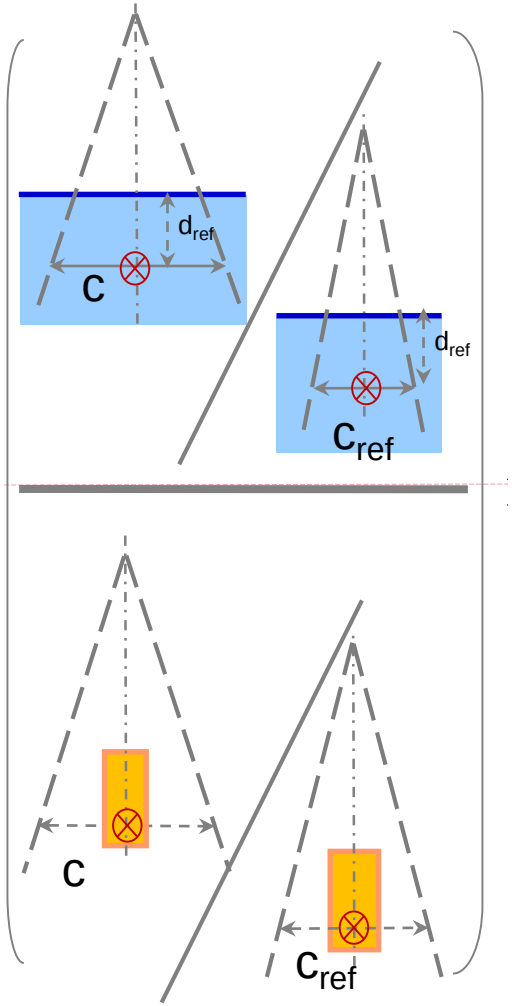

Factor-based dose calculations basic dosimetric quantities

Phantom **scatter factor**

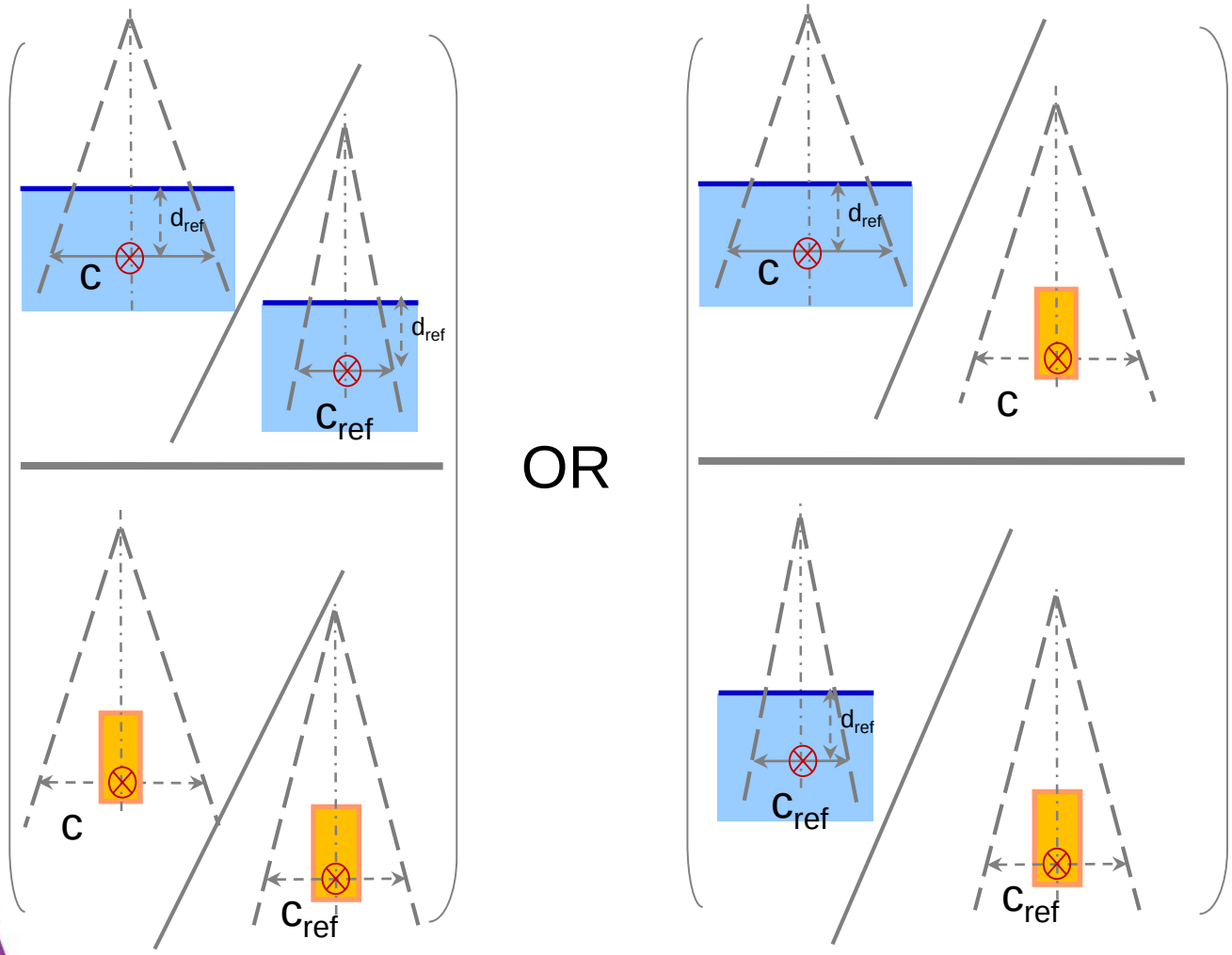

AAPM TG 74 report, Med Phys 36 (11), 2009

ESTRO School

Scatter Factor (SF)
The concept of buildup or (scatter) factor

$$B = \frac{\text{quantity due to primary} + \text{scattered radiation}}{\text{quantity due to primary radiation alone}}$$

In narrow beam geometry (only primary radiation): B=1

In broad beam geometry: B>1

Factor-based dose calculations basic dosimetric quantities

Phantom scatter factor, S_p

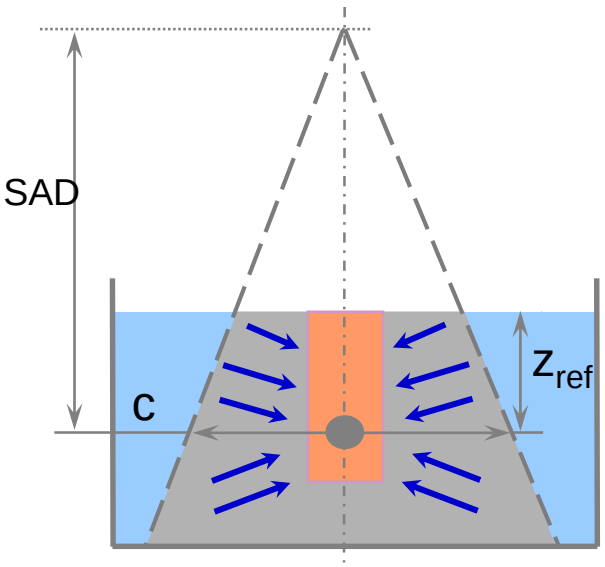

$$S_p(c) = \frac{D_{total}(c;d_{ref}) \,/\, D_{primary}(c;d_{ref})}{D_{total}(c_{ref};z_{ref}) \,/\, D_{primary}(c_{ref};d_{ref})}$$

S_p is the ratio of scatter factors between the actual field size c in the phantom and that of the reference field size c_{ref} , both at the reference depth d_{ref}:

S_p describes the effects of photon scattering in the phantom only

AAPM TG 74 report, Med Phys 36 (11), 2009

ESTRO School

Factor-based dose calculations basic dosimetric quantities

Phantom scatter factor, S_p

$$S_p(s) = \frac{D_{total}(s; z_{ref}) \,/\, D_{primary}(s; z_{ref})}{D_{total}(s_{ref}; z_{ref}) \,/\, D_{primary}(s_{ref}; z_{ref})} = \frac{D_{total}(s; z_{ref}) \,/\, D_{total}(s_{ref}; z_{ref})}{D_{primary}(s; z_{ref}) \,/\, D_{primary}(s_{ref}; z_{ref})}$$

$$D_{primary}(s) = K_p(s)\beta_p(s)$$ s: field size

if s = collimator setting c at the plane of the isocentre

$$S_p(c) = S_{cp} \Big/ \left(\frac{K_p(c)}{K_p(c_{ref})} \frac{\beta_p(c)}{\beta_p(c_{ref})} \right) = \frac{S_{cp}}{S_c\left(\frac{\beta_p(c)}{\beta_p(c_{ref})} \right)} \cong \frac{S_{cp}(c)}{S_c(c)}$$

dose to collision kerma ratio

$\cong$ 1 under lateral CPE

AAPM TG 74 report, Med Phys 36 (11), 2009

ESTRO School

Factor-based dose calculations basic dosimetric quantities

Phantom scatter factor, S_p

NCS report 12

field size (cm)	Quality index .600	.620	.640	.660	.680	.700	.720	.740	.760	.780	.800
4.0	0.859	0.877	0.892	0.904	0.914	0.921	0.926	0.931	0.931	0.932	0.931
5.0	0.888	0.902	0.913	0.923	0.930	0.937	0.942	0.946	0.948	0.950	0.952
6.0	0.916	0.926	0.934	0.941	0.947	0.952	0.957	0.961	0.963	0.966	0.968
7.0	0.940	0.947	0.953	0.959	0.963	0.967	0.970	0.973	0.975	0.977	0.979
8.0	0.962	0.967	0.970	0.974	0.976	0.978	0.981	0.983	0.985	0.987	0.989
9.0	0.983	0.985	0.986	0.987	0.988	0.989	0.990	0.992	0.993	0.994	0.995
10.0	1.000	1.000	1.000	1.000	1.000	1.000	1.000	1.000	1.000	1.000	1.000
12.0	1.029	1.026	1.024	1.022	1.019	1.017	1.015	1.013	1.011	1.010	1.010
14.0	1.053	1.049	1.044	1.039	1.035	1.030	1.027	1.024	1.021	1.018	1.017
16.0	1.072	1.065	1.059	1.054	1.048	1.043	1.037	1.033	1.029	1.026	1.023
18.0	1.085	1.078	1.072	1.066	1.060	1.054	1.047	1.042	1.037	1.032	1.027
20.0	1.097	1.090	1.084	1.077	1.070	1.063	1.056	1.050	1.043	1.036	1.030
22.0	1.115	1.106	1.097	1.089	1.079	1.071	1.063	1.056	1.048	1.041	1.034
24.0	1.124	1.114	1.106	1.097	1.087	1.079	1.070	1.062	1.053	1.044	1.037
26.0	1.130	1.122	1.114	1.105	1.094	1.086	1.077	1.068	1.058	1.049	1.040
28.0	1.136	1.128	1.120	1.111	1.101	1.092	1.082	1.072	1.062	1.052	1.042
30.0	1.142	1.134	1.126	1.117	1.107	1.097	1.087	1.076	1.066	1.055	1.045
32.0	1.148	1.140	1.132	1.123	1.112	1.102	1.091	1.080	1.069	1.057	1.047
34.0	1.154	1.146	1.137	1.128	1.116	1.106	1.095	1.084	1.072	1.060	1.049
36.0	1.160	1.152	1.142	1.132	1.121	1.110	1.098	1.087	1.075	1.063	1.051
38.0	1.167	1.157	1.147	1.137	1.124	1.113	1.101	1.089	1.077	1.065	1.053
40.0	1.175	1.163	1.153	1.140	1.128	1.116	1.104	1.091	1.079	1.067	1.055

Factor-based dose calculations basic dosimetric quantities

Phantom scatter factor, S_p

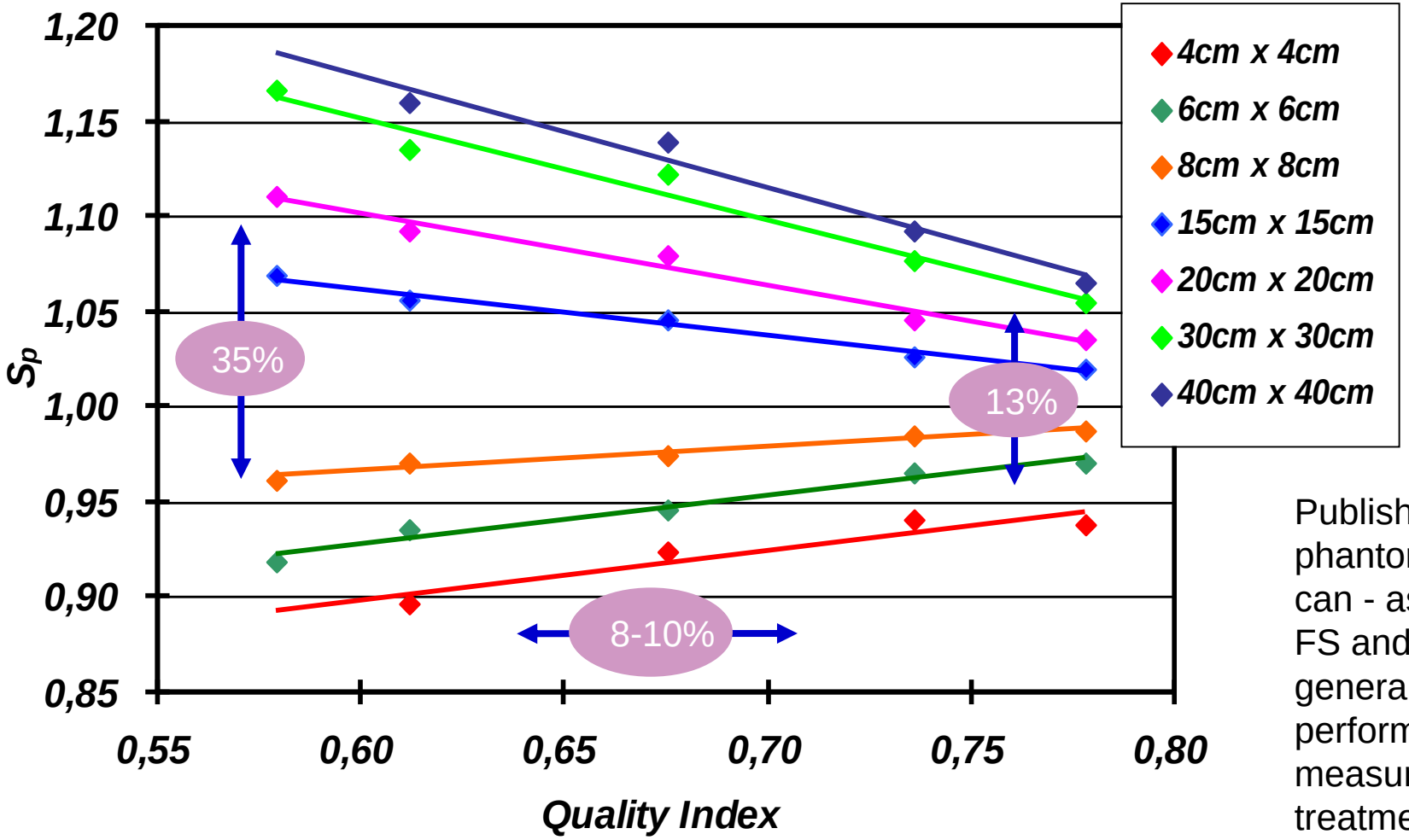

Published data on phantom scatter factors can - as a function of FS and QI - be in general used instead of performing measurements for each treatment unit individually

Georg et al 1999, PMB 44, 2987-3007; Sätherberg et al 1996, PMB 41, 2687-2694)

ESTRO School

Dose per MU formalisms: factor-based dose calculations

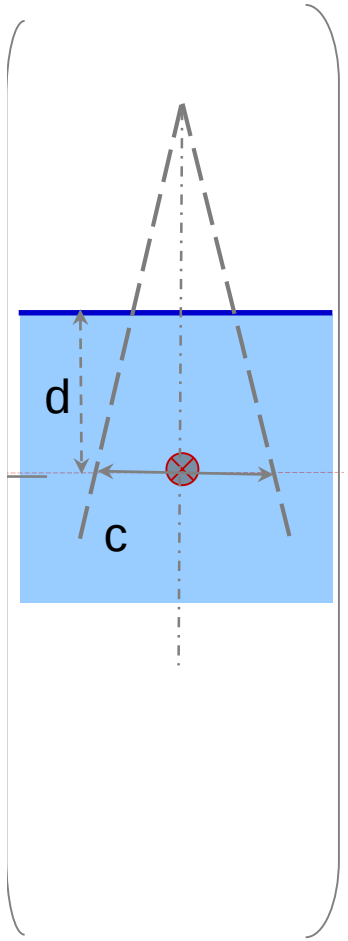

Factor-based dose calculations basic dosimetric quantities

Tissue Phantom Ratio, TPR for isocentric setup

$$T(s,d) = \frac{D(s,d,SAD)}{D(s,d_{\text{ref}},SAD)}$$

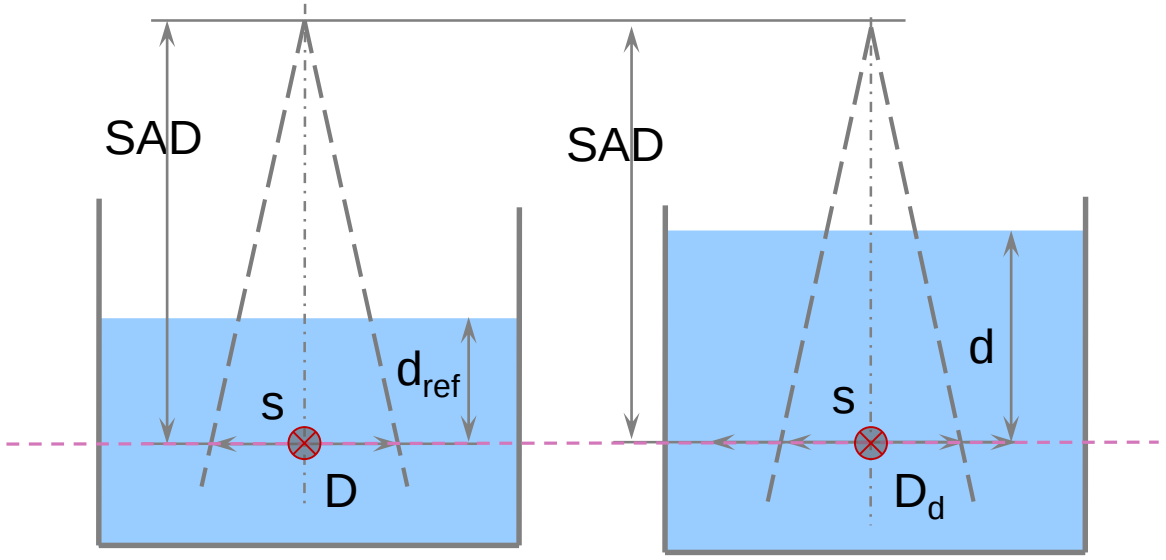

ESTRO School

Tissue-phantom ratios for a 10 x 10 cm² field obtained from BJR Suppl. 25 and from measurements on linacs used in ESTRO booklet nr. 6

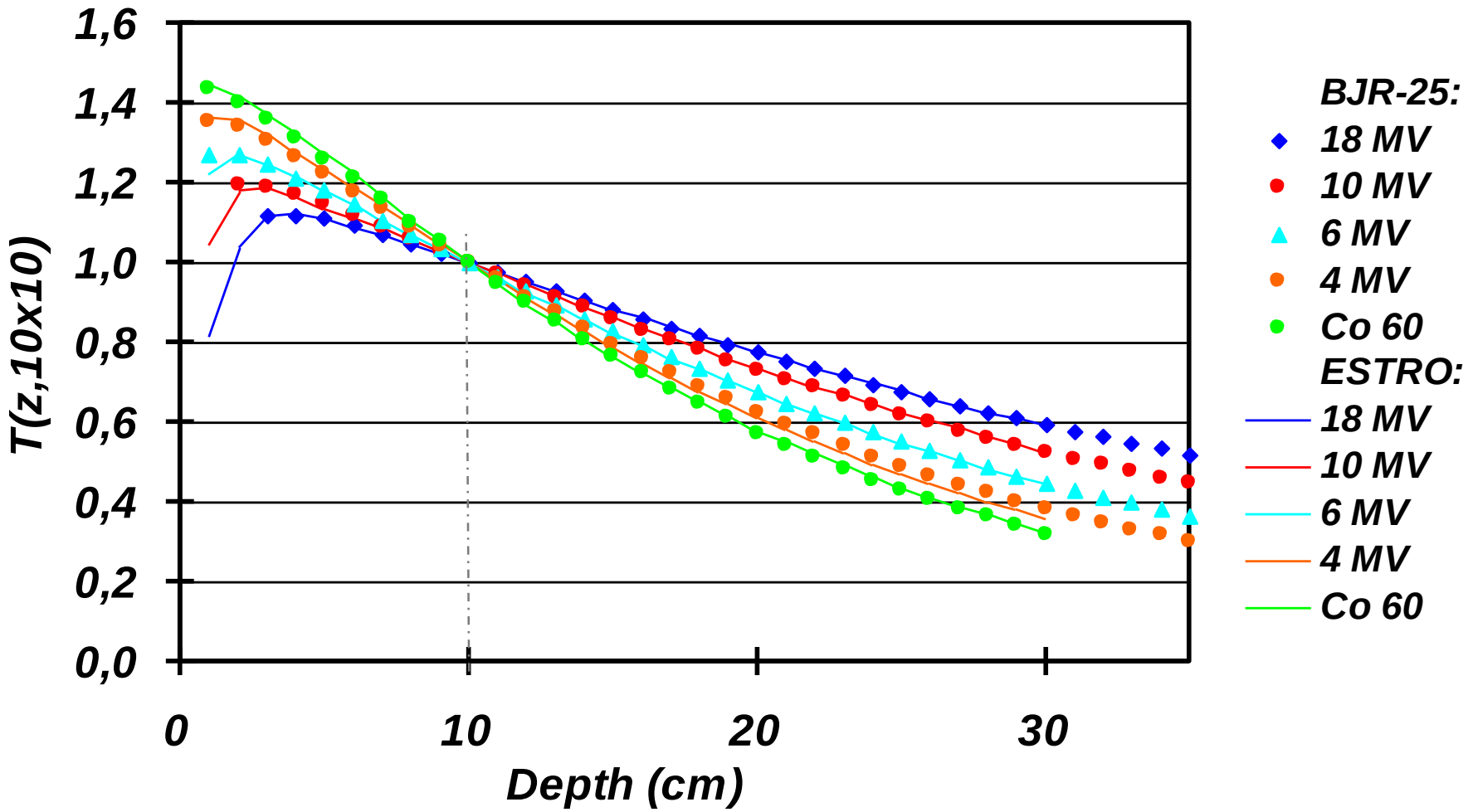

NORMALIZATION DEPTH: 10 cm in water

ESTRO School

Factor-based dose calculations basic dosimetric quantities

Relative depth dose (RDD, or PDD) at an SSD=SAD setup

$$SSD_{ref} = SAD$$

Relative depth dose, RDD

$$RDD_{\text{ref}}(s,d,SSD_{\text{ref}}) = \frac{D(s,d,SSD_{\text{ref}})}{D(s,d_{\text{ref}},SSD_{\text{ref}})}$$

or

Percentage depth dose, PDD

$$PDD(s,d,SSD_{\text{ref}}) = \frac{D(s,d,SSD_{\text{ref}})}{D(s,d_{\text{ref}},SSD_{\text{ref}})} \cdot 100$$

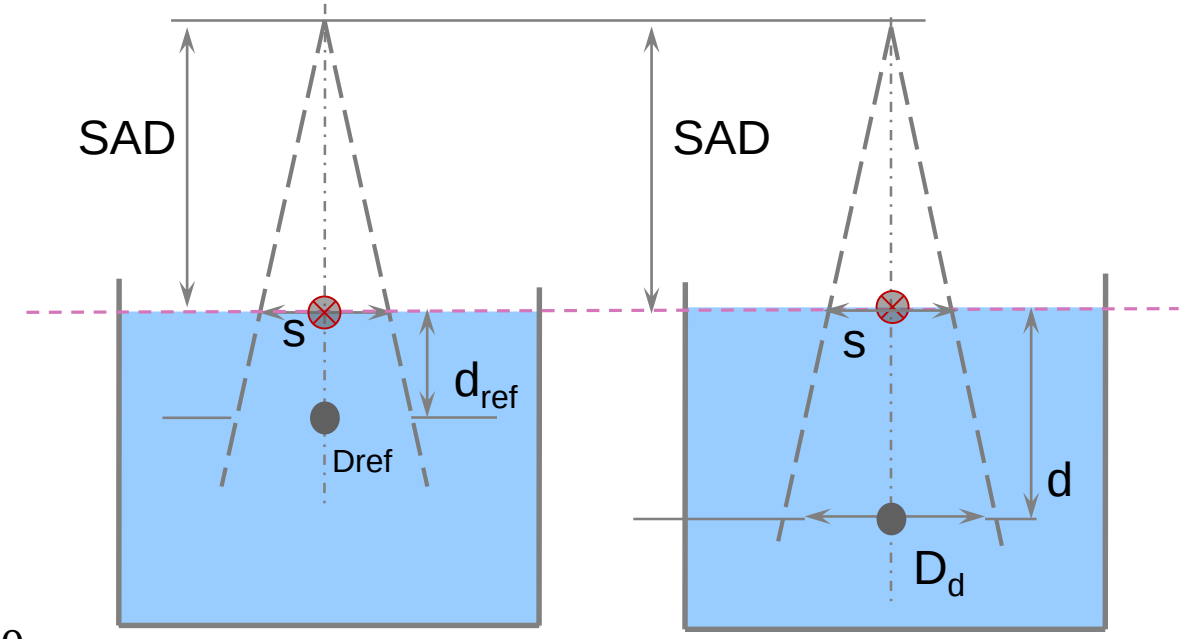

ESTRO School

Dose per MU formalisms: factor-based dose calculations

Isocentric formalism: dose per meterset at isocentre (at SAD and on CAX)

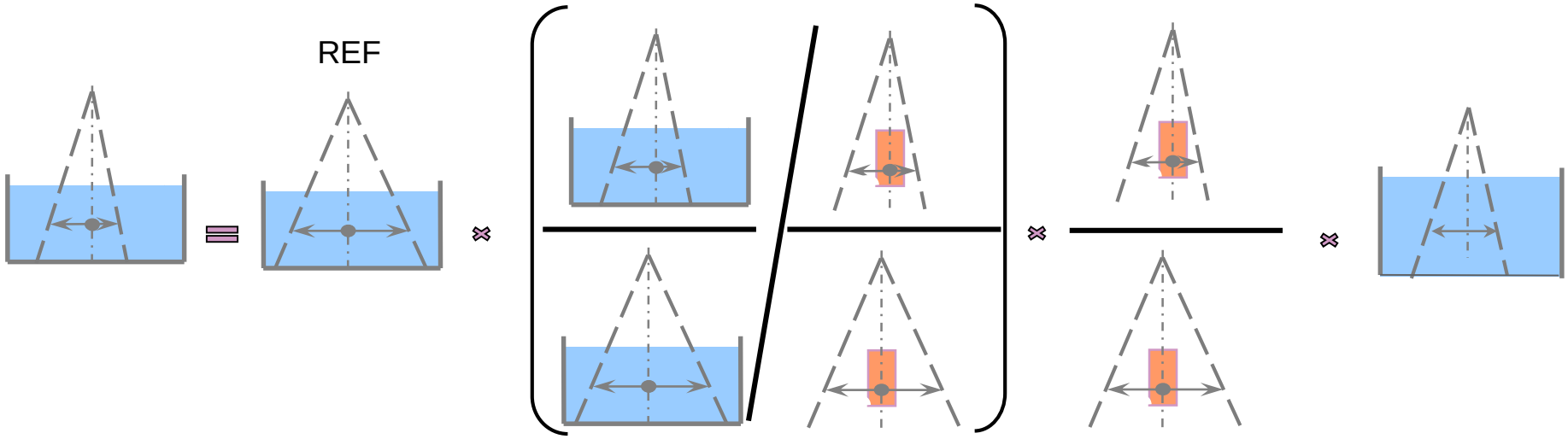

$$\frac{D(c_{\mathrm{d}}, d; SAD)}{M} = \frac{D(c_{\mathrm{ref}}, d_{\mathrm{ref}})}{M} \cdot S_{\mathrm{p}}(c_{\mathrm{eqsq}}) \cdot S_{\mathrm{c}}(c_{\mathrm{eqsq}}) \cdot TPR(c_{\mathrm{eqsq}}, d)$$

The formalism above applies when the reference normalization conditions are isocentric (SSD_{ref}=90cm and d_{ref}=10cm) and scatter factors are determined isocentrically.

ESTRO School

Dose per MU formalisms: factor-based dose calculations

Isocentric formalism: dose per meterset NOT at isocentre (on CAX)

Scaling energy fluence from that at isocentre to that at the calculation point not at SAD

$$\frac{D(s_{\mathrm{d}}, d; SSD)}{M} = \frac{D(c_{\mathrm{ref}}, d_{\mathrm{ref}})}{M} \cdot S_{\mathrm{c}}(c_{\mathrm{eqsq}}) \cdot \underbrace{S_{\mathrm{p}}(s_{d,\mathrm{eqsq}}) \cdot TPR(s_{\mathrm{d,eqsq}}, d) \cdot \left(\frac{SAD}{SSD + d}\right)^2}$$

On the assumption that phantom scatter ratios are independent of SSD

The field size used is that at the calculation point

ESTRO School

Dose per MU formalisms: factor-based dose calculations

How do factor-based formalisms deal with:

- non-square collimator settings
- fields shaped with blocks or MLCs
- modulation with hard wedges
- modulation with soft (dynamic/virtual) wedges
- other modulations (IMRT fields)
- Inhomogeneities
- points off axis

?

$$\frac{D(c, s_d, d; SSD)}{M}$$

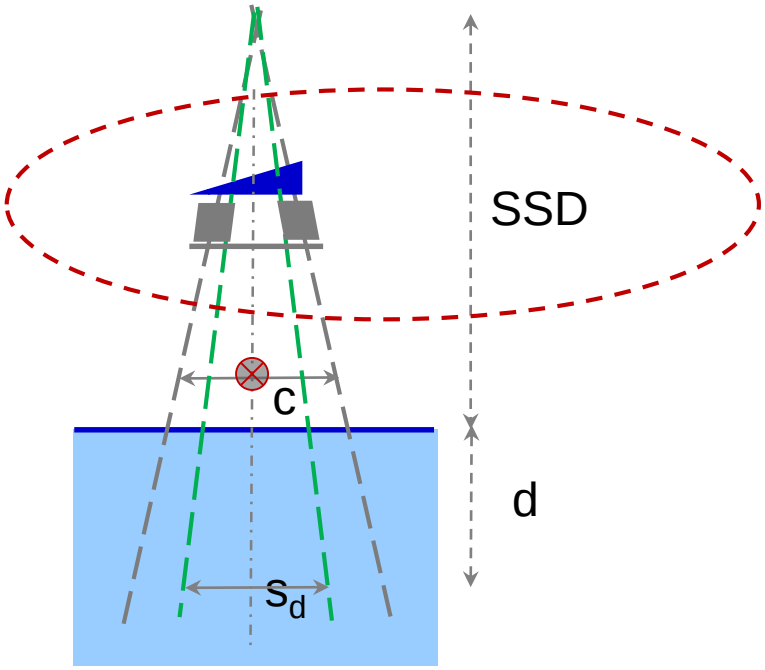

ESTRO School

Dose per MU formalisms: factor-based dose calculations

Isocentric formalism: dose per meterset at isocentre (at SAD and on CAX)

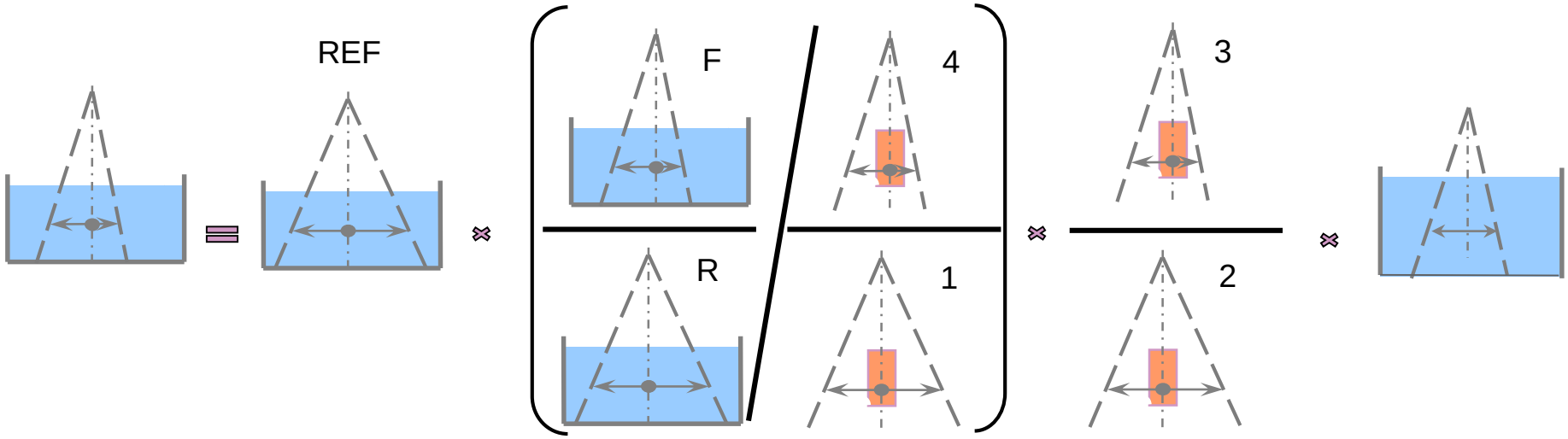

$$\frac{D(c_{\mathrm{d}}, d; SAD)}{M} = \frac{D(c_{\mathrm{ref}}, d_{\mathrm{ref}})}{M} \cdot S_{\mathrm{p}}(s_{\mathrm{eqsq}}) \cdot S_{\mathrm{c}}(c_{\mathrm{eqsq}}) \cdot TPR(s_{\mathrm{eqsq}}, d)$$

The formalism above applies when the reference normalization conditions are isocentric (SSD_{ref}=90cm and d_{ref}=10cm) and scatter factors are determined isocentrically.

ESTRO School

Equivalence between square and rectangular, circular or irregular fields

How this equivalency is defined and determined depends on the dosimetric quantity involved:

a. Dosimetric quantities relating to changes in scattered radiation in the phantom; TPR, S_p, S_{cp}
b. Dosimetric quantities relating to changes in energy fluence from the linac head reaching the phantom; S_c

a. The concept of equivalent square for quantities describing phantom scatter

Equivalent field is defined as 'the standard' (i.e. circular or square) field that has the same central axis depth dose characteristics as the given non-standard field *(Day and Aird 1996, BJR25, 138).*

The equivalency between standard and non-standard fields is determined by the requirement that the contribution to the dose along CAX from scattered photons for the two fields be equal. Namely, that the quantity describing phantom scatter (e.g *scatter factor*) in the standard and non-standard field at the point of calculation is equal.

Phantom scatter: equivalent square of a circular field

The equivalence between a square field and a circular field has be shown to be:

Bjärngard and Siddon Med Phys 9(2), (1982)

$$r = 0.5611\ S$$

This equation can be implemented in sector integration algorithms to calculate the equivalent square of irregularly shaped fields

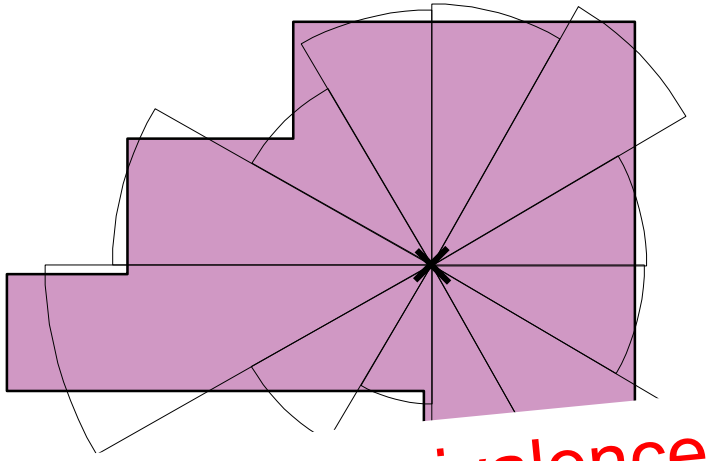

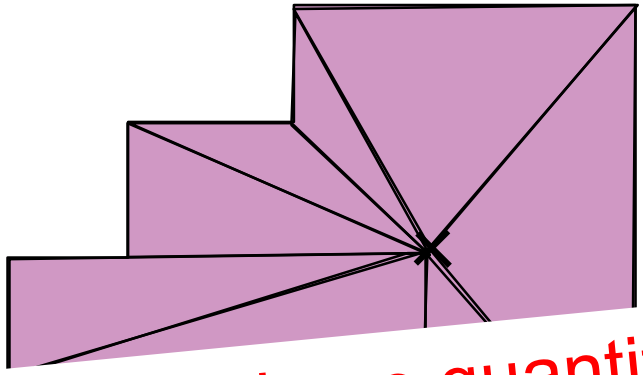

This concept of equivalence is applicable to those quantities where changes in phantom scatter need to be considered

Triangular decomposition
Siddon *et al* (1985), Med Phys 12(2)

g Biomed 2 192-199

ESTRO School

Phantom scatter: equivalent square of a rectangular field

Area over perimeter method

(Sterling et al 1964 BJR 37, 544; Patomaki 1968, BJR 41,381 etc)

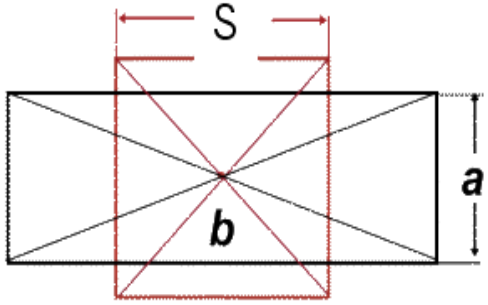

$$S = \frac{Area}{Perimeter}$$

or

"$4A/P$"

$$\frac{S^2}{4S} = \frac{a \cdot b}{2(a+b)}$$

$$S = 2\frac{a \cdot b}{a+b}$$

Method not based on sound physical principles, BUT used for years, with surprisingy accurate results (<1%) <u>for rectangular fields of length <20cm and length/width<4</u> *(Day and Aird 1996 BJR25, 138,McDermott, MedPhys 25(11), 2215, 1998).*

ESTRO School

Phantom scatter: equivalent square of a rectangular field

Tabulated data

NCS Report 12, Appendix 8.6 (1998): Tables constructed by averaging 4 energy specific tales for ^{60}Co, 6, 10, 25 MV photon beams(Venselaar et al, Phys Med Biol, 42: 2369-2381, 1997)

The equivalent square field, to be used for the determination of the phantom scatter factor and phantom scatter related quantities, is defined here as the square field which has the same phantom scatter contribution at the reference point in the beam: at 10 cm depth on the central axis, as the arbitrarily shaped field under consideration.

of QI of 0.573 to 0.783 (^{60}Co to 25 MV). It was shown that the use of the energy-specific tables could eventually lead to a difference of 0.5 - 1.0% in the value of S_p, compared to the use of the BJR-table, in which the use of the BJR-table systematically leads to a lower value of S_p. The relatively small differences

s1 \ s2	2.0	4.0	6.0	8.0	10.0	12.0	14.0	16.0	18.0	20.0	22.0	24.0	26.0	28.0	30.0	32.0	34.0	36.0	38.0	40.0
2.0	2.0																			
4.0	2.8	4.0																		
6.0	3.3	4.9	6.0																	
8.0	3.6	5.4	6.9	8.0																
10.0	3.7	5.7	7.4	8.8	10.0															
12.0	3.8	5.9	7.7	9.4	10.9	12.0														
14.0	3.9	6.0	7.9	9.9	11.6	12.9	14.0													
16.0	4.0	6.1	8.1	10.3	12.2	13.8	15.0	16.0												
18.0	4.0	6.2	8.3	10.6	12.7	14.5	15.9	17.1	18.0											
20.0	4.0	6.2	8.5	10.9	13.2	15.1	16.6	18.0	19.1	20.0										
22.0	4.0	6.3	8.6	11.2	13.7	15.7	17.3	18.7	20.0	21.1	22.0									
24.0	4.1	6.4	8.7	11.5	14.1	16.1	17.9	19.4	20.7	22.0	23.1	24.0								
26.0	4.1	6.4	8.8	11.7	14.4	16.6	18.4	19.9	21.4	22.7	24.0	25.1	26.0							
28.0	4.1	6.4	8.9	11.9	14.7	16.9	18.8	20.4	22.0	23.4	24.7	26.0	27.1	28.0						
30.0	4.1	6.5	9.0	12.0	14.9	17.2	19.1	20.9	22.5	24.0	25.4	26.7	28.0	29.1	30.0					
32.0	4.1	6.5	9.1	12.2	15.1	17.5	19.4	21.2	22.8	24.4	25.9	27.3	28.7	29.9	31.0	32.0				
34.0	4.1	6.5	9.1	12.3	15.3	17.7	19.7	21.5	23.2	24.8	26.4	27.9	29.3	30.6	31.9	33.0	34.0			
36.0	4.1	6.5	9.1	12.4	15.4	17.8	19.9	21.7	23.4	25.1	26.7	28.3	29.8	31.2	32.6	33.8	35.0	36.0		
38.0	4.1	6.5	9.2	12.5	15.5	17.9	20.0	21.9	23.7	25.3	27.0	28.7	30.2	31.7	33.2	34.6	35.8	36.9	38.0	
40.0	4.1	6.5	9.2	12.5	15.6	18.1	20.1	22.0	23.8	25.6	27.3	28.9	30.5	32.1	33.6	35.1	36.5	37.8	39.0	40.0

ESTRO School

b. The concept of equivalent square for quantities describing head scatter

Output in air, Sc: depends upon the orientation of the rectangular fields (on CEE)

Collimator Exchange Effect (CEE): is mainly caused by a difference in extra-focal scattered radiation that can reach the point of interest for the same collimator setting of the upper and lower jaw

- CEE is of the order of 1% to 2.5 % for (most) modern linacs
- for older type of linacs (e.g. Saturne) the difference in output in air with X-Y vs. Y-X setting can amount to 6%

Points Eye View of the extended source

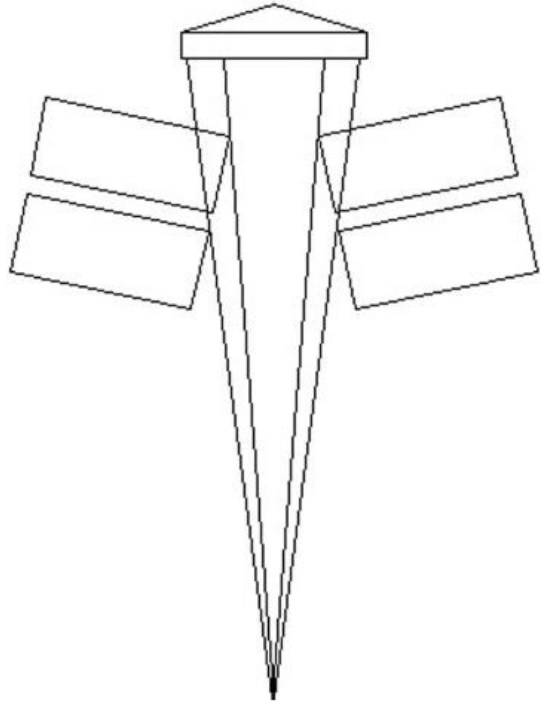

FIG. 12. Points eye view of upper and lower jaws. Schematic diagram of the treatment head showing flattening filter, monitor chamber, and upper and lower jaws. The lower jaws have been rotated by 90° for clarity.

AAPM TG 71 report, Med Phys 41 031501, 2014

Head scatter: equivalent square of a rectangular field

Empirical approach to account for different influence of collimator layers

$$c_e(x, \quad y) = \frac{(G+1)\cdot x \cdot y}{G \cdot x + y}$$

x ➔ lower jaw

y ➔ upper jaw

G **weighting factor**

depends on:

- treatment head design
- beam energy
- beam modifiers

Linac head

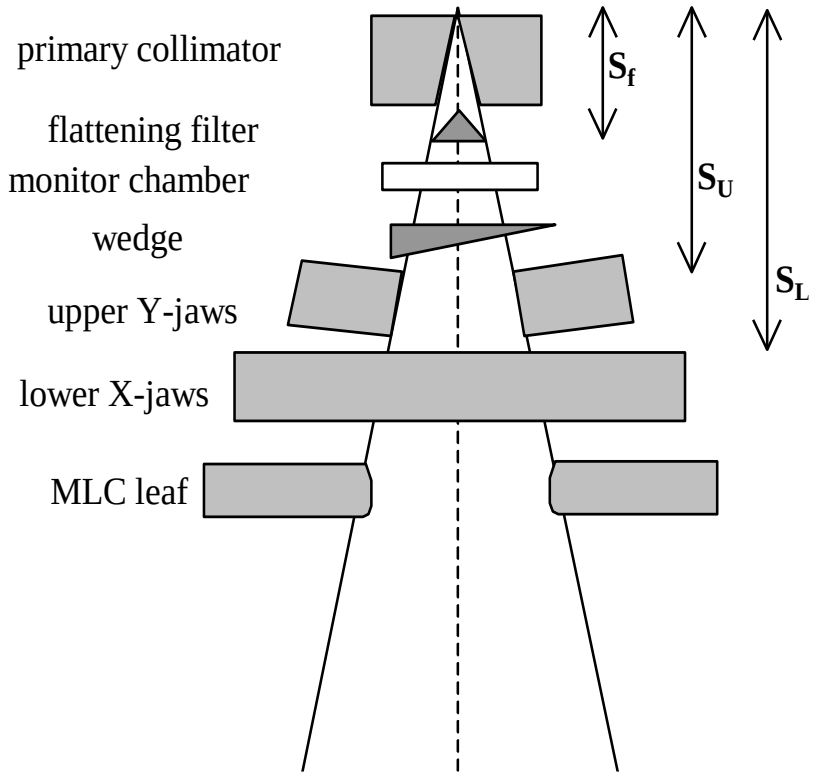

Vadash P and Bjärngard B E (1993) Med. Phys. 20, 733-734.

ESTRO School

Summary: equivalence between square, rectangular, circular or irregular fields

- Output in air ratio, S_c, in air is not symmetric in X and Y
  - Equivalent squares with individual weighting of collimator elements can lead to sufficiently accurate approximation
  - For elongated fields less accurate
- Phantom (volume) scatter factor, S_p, is symmetric in X and Y
  - Traditional equivalent square formula lead to sufficiently accurate approximation for S_p, TPR, RDD, PDD
  - For elongated fields less accurate
- Irregular blocked or MLC shaped fields require more sophisticated models

Dose per MU formalisms: factor-based dose calculations

How do factor-based formalisms deal with:

- non-square collimator settings
- fields shaped with blocks or MLCs
- points off axis
- modulation with hard wedges
- modulation with wedges
- other modulations (IMRT fields)
- Inhomogeneities

?

$$\frac{D(c, s_d, d; SSD)}{M}$$

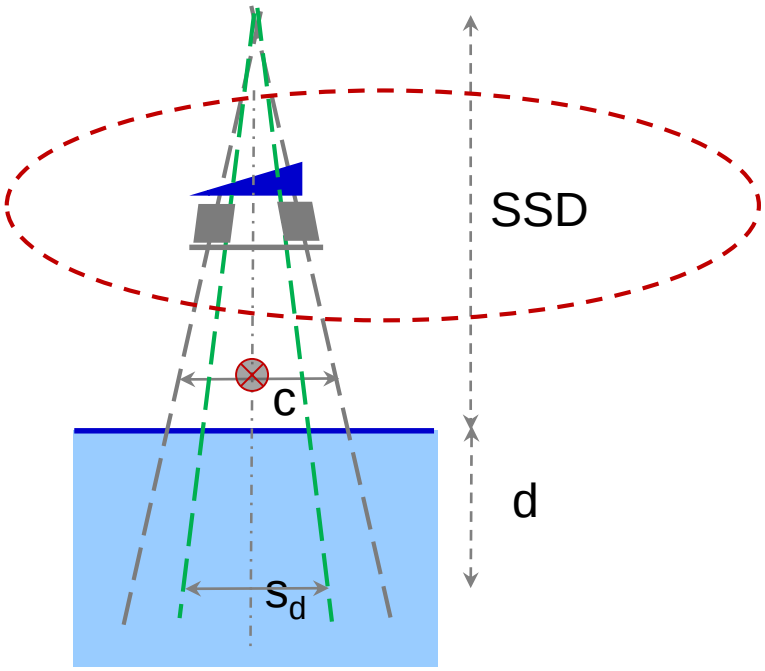

ESTRO School

Dose per MU formalisms: factor-based dose calculations

Irregular fields shaped with MLCs

- MLC design and position in linac head
  - Lower jaw replacement
  - Upper jaw replacement
  - Add-on (3rd level) configuration

- Depending on the MLC design, its influence on Sc and Sp needs to be considered separately:

  - Upper or lower jaw replacement MLC (e.g. Elekta, Siemens linacs)
    - ➢ The equivalent square from a sector intergration of the MLC aperture is used for both Sc and Sp

    Palta et al 1995 MP
    Das et al 1999 MP
    Georg et al 1999 PMB

  - Add-on (3rd level) configuration (eg Varian linacs)
    - ➢ Sc ⇐ eq. Sq. of secondary jaws
    - ➢ Sp ⇐ eq. Sq. from MLC aperture

    Klein et al 1995 IJROBP
    Boyer 1992 MP

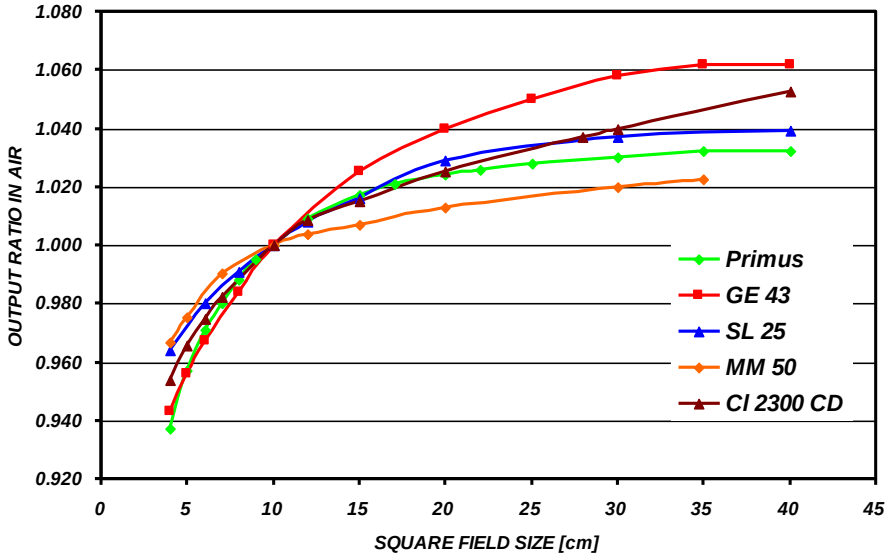

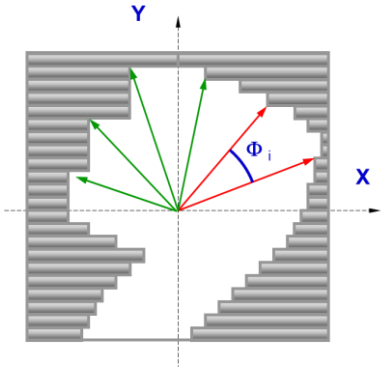

ESTRO School

Dose per MU formalisms: factor-based dose calculations

Calculations at points off-axis (asymmetric fields)

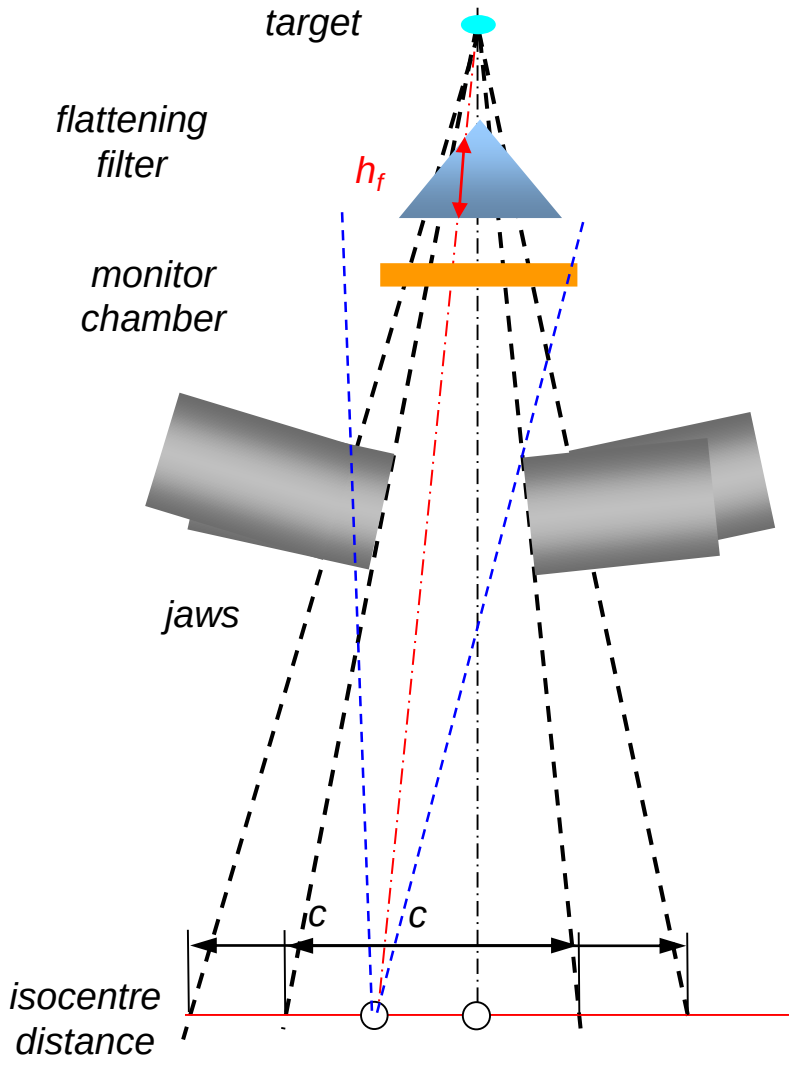

Dose per MU formalisms: factor-based dose calculations

Calculations at points off-axis (asymmetric fields)

$$\frac{D(s_d, d, x; SSD)}{M} = \frac{D(c_{ref}, d_{ref})}{M} \cdot S_c(c_{eqsq}) \cdot S_p(s_{d,eqsq}) \cdot TPR(s_{d,eqsq}, d) \cdot OAR(d, x) \cdot \left(\frac{SAD}{SSD + d}\right)^2$$

For off-axis positions up to 5cm
no significant variation from the values CAX
On-axis data used

Off-Axis Ratio: representing off-axis variations of primary fluence; different approaches to determine this experimentally

ESTRO School

Dose per MU formalisms: factor-based dose calculations

Modulation with physical wedges

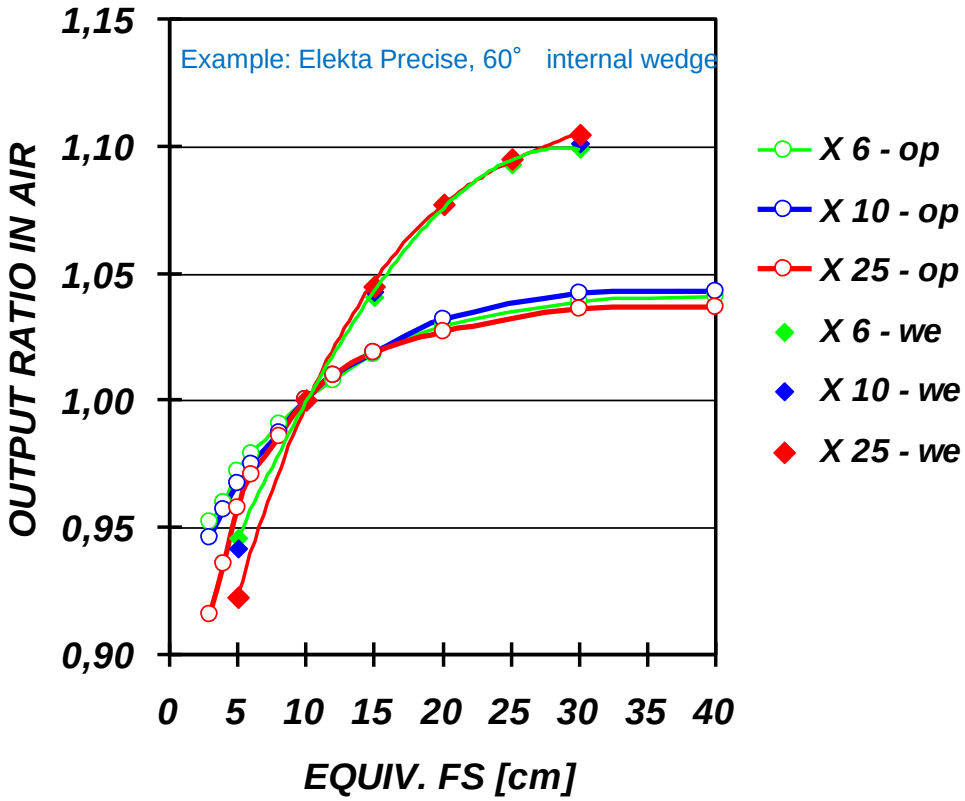

Variation open vs wedged fields:

- With FS
  - ➔ ~ 10% open
  - ➔ ~ 20% wedge
- Wedge angle
- Energy
- Linac specific

- Physical wedges introduce changes in the beam spectrum, which are dependent on wedge material and influence dosimetric parameters that vary with depth (TPR, RDD) as well as phantom scatter, Sp
- The position of the wedge, whether internal (motorised) or external (manually inserted) affects Sc
- Dosimetric parameters for wedged beams should not be confused with open beam data
- Irregular wedged beams need some special considerations for MU calculation / verification

⇒ Additional correction factors needed in the dose per MU formalism

ESTRO School

Dose per MU formalisms: factor-based dose calculations

Modulation with physical wedges

Example of a correction factor that can be determined from a model

Wedge Factor Calculation

$WF_W = e^{\mu W}$

where,

e - base of the natural log

μ = linear attenuation coefficient, $= \frac{\ln(WF_{CAX})}{W_{CAX}}$

W = thickness at the point of interest

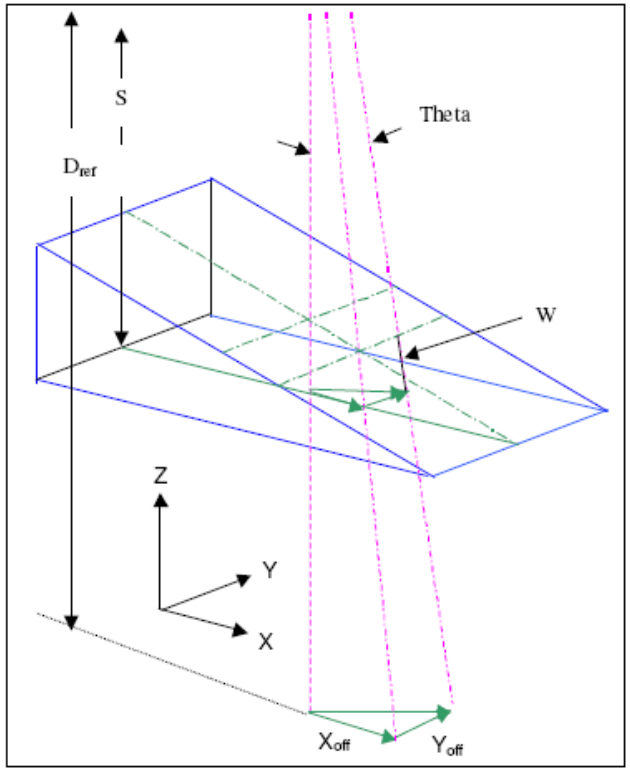

Off Axis Wedge Ratio using the physical dimensions

$$OAWR = \left(\frac{WF_W}{WF_{CAX}(d,f)} \right)$$

where,

WF_W = calculated wedge factor from thickness W

$WF_{CAX}(d,f)$ = interpolated central axis wedge factor at depth d, field size f from entered table

Off axis calculations with OAWR calculated from physical wedge dimensions:

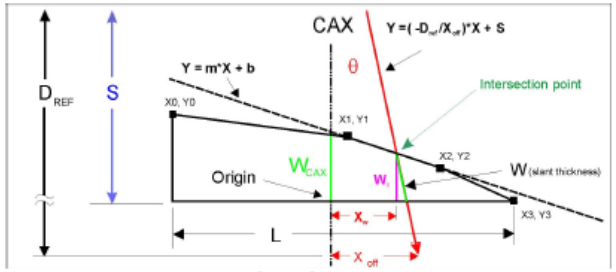

Wedge Diagram 1

For the interval $X_1 < X_w < X_2$, where $X_w = X_{off} * S/D_{ref}$,

$$W = \frac{1}{Cos(\theta)} \left[m \left[X_{off} \left(\frac{S}{D_{ref}} \right) - x_1 \right] + y_1 \right]$$

where,

W = thickness at the point of interest

S = source to wedge distance

$m = \frac{(y_2 - y_1)}{(x_2 - x_1)}$ = slope of the wedge at the point of interest

D_{ref} = reference distance

X_{off} = distance off axis along the sloping side of the wedge at D_{ref}

$\theta = Tan^{-1} \left(\frac{X_{off}}{D_{ref}} \right)$

From the manual of: Diamond: Dose Calculation Management s/w, version 2010

ESTRO School

Dose per MU formalisms: factor-based dose calculations

Modulation with physical wedges

Accounting for the presence of physical wedge in dose calculations is not trivial

Let us have a debate!

Is there a role for physical wedges in modern radiotherapy?

Should we continue to commission these for treatment planning?

POINT/COUNTERPOINT 

OA **Radiotherapy using hard wedges is no longer appropriate and should be discontinued**

Christopher F. Njeh, Tae Suk Suh and Colin G. Orton

Med. Phys. **43**, 1031 (2016); http://dx.doi.org/10.1118/1.4939262

ESTRO School

Dose per MU formalisms: factor-based dose calculations

Modulation with non-physical wedges

Non-physical wedges are delivered with one of the Y-jaws moving in or out during beam at variable dose rate and at variable speed.
Wedge factors:

- do not depend on depth (no beam hardening)
- vary with beam energy and off axis position

Varian EDW

- Y-jaw motion into field (0.5 cm from opposing) jaw; in variable speed and dose rate
- Jaw positions per MU: stored lookup (GSTT) tables; one per beam energy
- 7 wedge angles in total (as combination of 60° wedged and open fields)
- WF depends on energy, wedge angle, field size and off-axis position (along Y direction; asymmetric fields)
- WF ≈ 0.4 - 1

Siemens VW

- Y-jaw motion out of field, starting from 1 cm of opposing jaw
- Jaw positions per MU: calculated using a mathematical algorithm with energy dependent parameters.
- Multiple wedge angles between 10° and 60°
- WF depends on energy, wedge angle, field size and off-axis position (along Y direction; asymmetric fields)
- WF ≈ 1 from calculation points on CAX

In MU formalisms WF for non-physical wedges are either derived from measurements or are calculated (from GSTT data)

ESTRO School

Dose per MU formalisms: factor-based dose calculations

Inhomogeneities

Methods to account for inhomogeneities in factor-based dose/MU calculations :

Either scale dosimetric parameters appropriately

Or

Determine a correction factor as a function of scaled dosimetric quantities

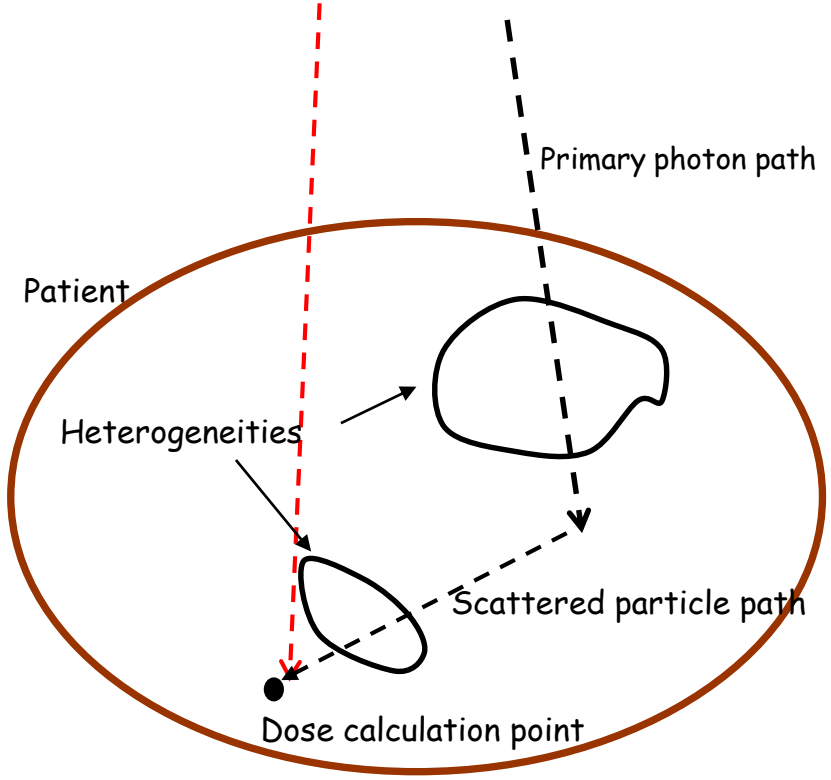

$$\left[\frac{D}{MU}(\ldots)\right]_{\text{heterogeneous}} = CF(\ldots)\left[\frac{D}{MU}(\ldots)\right]_{\text{homogeneous}}$$

Dose per MU formalisms: factor-based dose calculations

Inhomogeneities

Effective depth to a calculation point is the thickness of water equivalent tissue that would attenuate the radiation by the same amount as the actual tissue along a fan-line between the calculation point and the surface

If the radiation passes through *n* different tissues each if thickness d_i and density ρ_i

$$d_{\text{eff}} = \sum_{i=1}^{n} \rho_{\text{i}} d_{\text{i}}$$

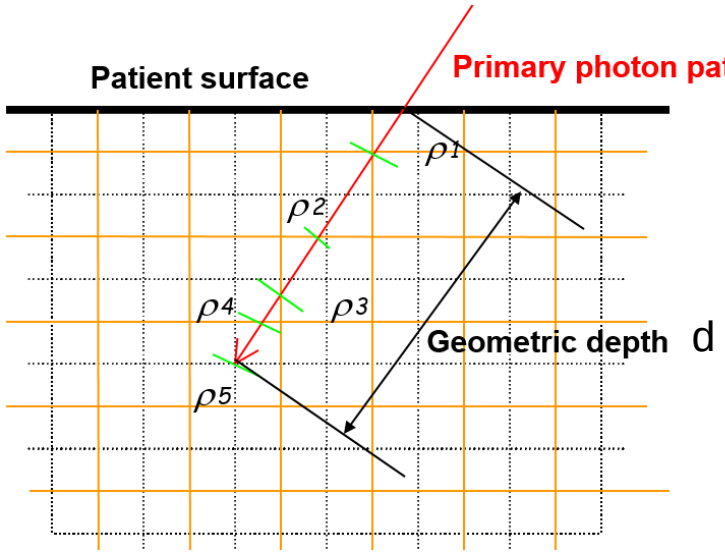

Note:
TPSs usually report an effective depth for a calculation point, but how exactly this is derived is not always apparent

ESTRO School

Dose per MU formalisms: factor-based dose calculations

Intensity modulated fields (IMRT)

Implementations vary based on delivery technique

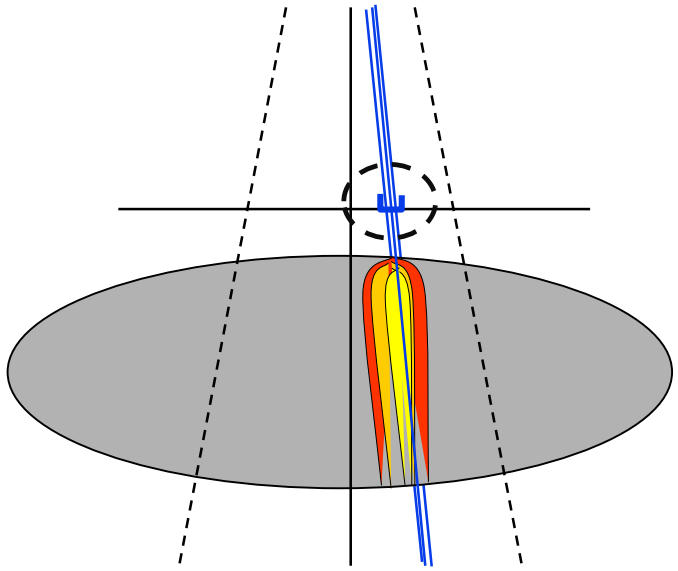

For IMRT techniques (Segmental-MLC or Dynamic-MLC), the *general approach* for the calculation of dose per MU from a modulated field is:

1. Split the modulated field into K segments
2. Sub-divide each segment into a number of beamlets, M
3. Calculate the dose per MU for each beamlet as an open field based on the factor-based formalism
4. Sum up the doses from each beamlet, with a weight proportional to the contribution of the segment to total dose, and accounting for the effect of MLC leakage and transmission.

$$\frac{D}{M} = \sum_{m}^{M} C_m d_m^{open}$$

open field (beamlet) dose derived from the dose per MU factor-based formalism

Beamlet weight depending on how it contributes to the dose from the segment. This weight is also adjusted dosimetric properties of the MLC (leakage and transmission)

ESTRO School

In conclusion:

I. Now you know the general formalism to calculation MU on TPSs using model-based dose engines

BUT, how does a commercial TPS (the TPS in your hospital?) calculate MU?

Stay tuned on the next lecture!

ESTRO School

In conclusion:

II. Now you are familiar with the ‘basic ingredients’ of factor-based dose per MU formalisms (AAPM TG-71 / NCS12 / ESTRO etc) and could relate dosimetric quantities to each other

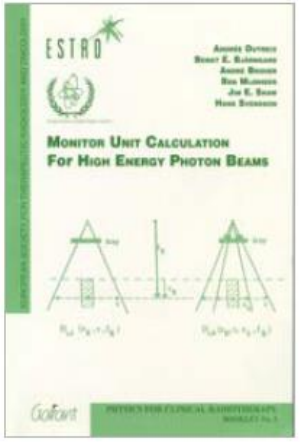

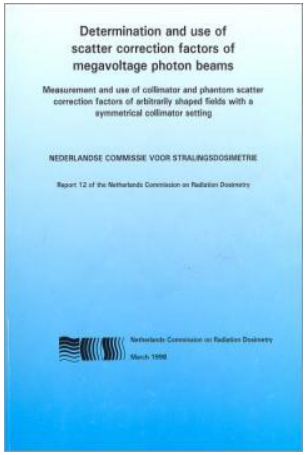

Monitor unit calculations for external photon and electron beams: Report of the AAPM Therapy Physics Committee Task Group No. 71

John P. Gibbons, John A. Antolak, David S. Followill, M. Saiful Huq, Eric E. Klein, Kwok L. Lam, Jatinder R. Palta , Donald M. Roback, Mark Reid, and Faiz M. Khan

Citation: Medical Physics **41**, 031501 (2014); doi: 10.1118/1.4864244
View online: http://dx.doi.org/10.1118/1.4864244
View Table of Contents: http://scitation.aip.org/content/aapm/journal/medphys/41/3?ver=pdfcov
Published by the American Association of Physicists in Medicine

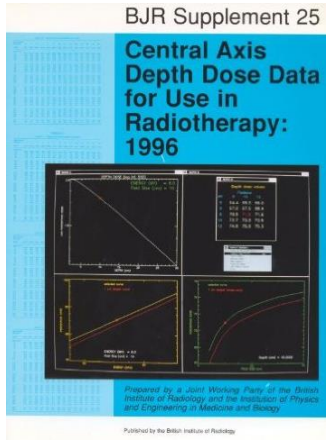

Report of AAPM Therapy Physics Committee Task Group 74: In-air output ratio, S_c, for megavoltage photon beams

Timothy C. Zhu[a)]
University of Pennsylvania, Philadelphia, Pennsylvania 19104
Anders Ahnesjö
Uppsala University, 751 85 Uppsala, Sweden and Nucletron AB, Box 1704, 751 47 Uppsala, Sweden
Kwok Leung Lam
University of Michigan, Ann Arbor, Michigan 48109
X. Allen Li
Medical College of Wisconsin, Milwaukee, Wisconsin 53226
Chang-Ming Charlie Ma
Fox Chase Cancer Center, Philadelphia, Pennsylvania 19111
Jatinder R. Palta
University of Florida, Gainesville, Florida 32610
Michael B. Sharpe
Princess Margaret Hospital, Toronto, ON M5G 2M9, Canada
Bruce Thomadsen
University of Wisconsin, Madison, Wisconsin 53705
Ramesh C. Tailor
RPC, UT MD Anderson Cancer Center, Houston, Texas 77030

Verification of monitor unit calculations for non-IMRT clinical radiotherapy: Report of AAPM Task Group 114

Robin L. Stern[a)]
Department of Radiation Oncology, University of California, Davis, Sacramento, California 95817
Robert Heaton
Radiation Medicine Program, Princess Margaret Hospital, 610 University Avenue, Toronto, Ontario M5G 2M9, Canada and Department of Radiation Oncology, University of Toronto, Toronto, Ontario M5G 2M9, Canada
Martin W. Fraser
Department of Radiation Oncology, Tufts Medical Center, 750 Washington Street #246, Boston, Massachusetts 02111
S. Murty Goddu
Radiation Oncology, Mallinckrodt Institute of Radiology, Washington University, 4921 Parkview Place Campus, Box 8224, St. Louis, Missouri 63110
Thomas H. Kirby
Global Physics Solutions, 5015 Larchmont NE, Albuquerque, New Mexico 87111
Kwok Leung Lam
Department of Radiation Oncology, University of Michigan Medical Center, Ann Arbor, Michigan 48109
Andrea Molineu
Radiological Physics Center, University of Texas MD Anderson Cancer Center, Houston, Texas 77030
Timothy C. Zhu
Department of Radiation Oncology, University of Pennsylvania, 2 Donner, 3400 Spruce Street, Philadelphia, Pennsylvania 19104-4283

ESTRO School

In conclusion:

III. Remember: in a factor-based formalisms, factors should cancel out!

$$\frac{D(\text{cond. a})}{M} \equiv \underbrace{D(\text{calibration})/M}_{\text{calibration value}} \cdot \underbrace{\frac{D(\text{cond. d})/M}{D(\text{calibration})/M}}_{\text{factor d}} \cdot \underbrace{\frac{D(\text{cond. c})/M}{D(\text{cond. d})/M}}_{\text{factor c}} \cdot \underbrace{\frac{D(\text{cond. b})/M}{D(\text{cond. c})/M}}_{\text{factor b}} \cdot \underbrace{\frac{D(\text{cond. a})/M}{D(\text{cond. b})/M}}_{\text{factor a}}$$

IV. The error in factor-based models is proportional to the number of factors:

$$\frac{D}{M} \equiv f_a \cdot f_b \cdots f_n \cdot D(calibration)/M \quad \Longrightarrow \quad \frac{\Delta D}{D} \leq \left|\frac{\Delta f_a}{f_a}\right| + \left|\frac{\Delta f_b}{f_b}\right| + \ldots$$

V. The number of measurements can be reduced by modelling some of the factors (e.g non physical wedge factor)

ESTRO School

In conclusion:

VI. Can you answer the following questions?

- What are the calibration conditions of the linacs in your hospital?
- What formalism do you use in your hospital to calculate MU? Isocentric or fixed-SSD?
- What are the normalisation conditions in the MU formalism you use?

ESTRO School

'Food for thought' and reflection…

- What is purpose and usefulness of factor-based models in modern radiotherapy physics?
- Is the check of dose at a point a sufficient, adequate check of a complex radiotherapy plan?
- What are the errors we aim to avoid? (at what level of tolerance we wish to work at?)

Prepare thoughts and/or questions for the MU workshop session later today

Let us have a debate!

ESTRO School

ESTRO School

WWW.ESTRO.ORG/SCHOOL

How TPSs calculate Monitor Units (MU)

Maria Mania Aspradakis
Maria.Aspradakis@luks.ch

Anders Ahnejsö
Anders.Ahnesjo@igp.uu.se

ESTRO School

Learning Objective

Understand the different implementations of the dose per meterset formalism on commercial TPSs using model-based dose calculations for MV photon beams

In the interest of time, only 4 TPSs, as representatives of commercial systems widely used, will be discussed:

- Philips Pinnacle v9.10
- Elekta Oncentra Masterplan
- Varian Eclipse v13.6
- Raysearch Raystation v4.7

Dose per MU formalisms: model-based dose calculations

$$\frac{D(A;x,y,z)}{M} = \frac{D(A;x,y,z)}{\Psi_0} \cdot \frac{\Psi_0}{M}$$

$D(A,x,y,z)$ integrated fluence and dose engine

Ψ_0 energy fluence of **direct photons** at isocentre in air

Calculation engine calibration factor relates MU to the direct energy fluence.

Commonly determined under ***ref****erence* ***cal****ibration conditions*

$$\frac{D_{\text{ref,meas}}}{M}$$

$$\frac{D_{\text{ref,calc}}}{\Psi_0} =$$

$$\frac{\Psi_0}{M} = \frac{\left[D(A_{\text{ref}};x_{\text{ref}},y_{\text{ref}},z_{\text{ref}})/M\right]_{\text{meas}}}{\left[D(A_{\text{ref}};x_{\text{ref}},y_{\text{ref}},z_{\text{ref}})/\Psi_0\right]_{\text{calc}}}$$

No monitor backscatter accounted for!
How monitor backscatter is handled varies in different TPSs

ESTRO School

Backscatter into the monitor chamber

- The signal from the monitor chamber can be affected from particles which have backscattered from the upper part of the jaws into the chamber (dependent on linac head and monitor chamber design,)
- At narrower collimations there is more backscatter than in larger fields $\Rightarrow$ monitor chamber reaches faster its pre-set value $\Rightarrow$ linac relative output decreases with decreasing field size

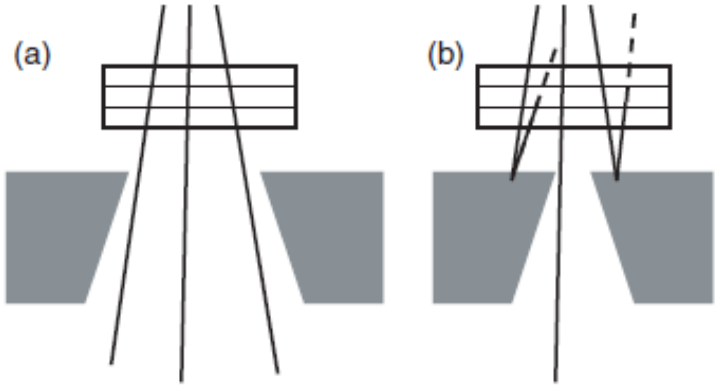

Figure 4. Schematic representation of backscatter to the monitor ion chamber from collimating jaws for different positions field sizes. When going from a large field (a) to a smaller one (b), the backscatter fraction increases.

Verhaegen & Seuntjens, Phys. Med. Biol, 48 (2003) R107-R164

ESTRO School

Backscatter into the monitor chamber

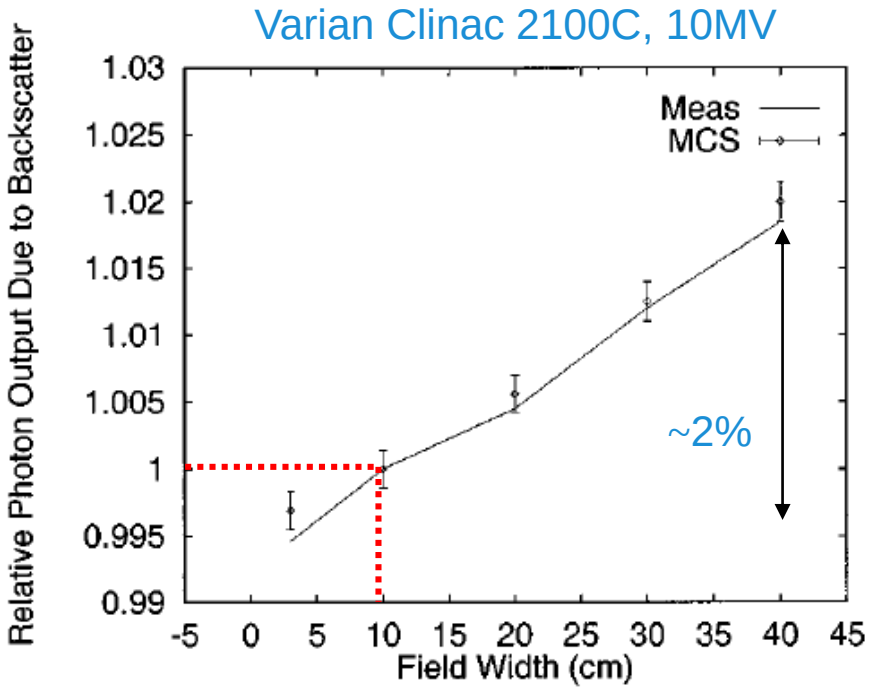

Liu et al Med, Phys. 27(4), 2009

FIG. 9. Relative photon output due to the backscatter, S_{cb}, of symmetric and square fields. The straight line (''meas'') shows data from measurement of electron target pulses. The discrete points (''MCS'') are from the Monte Carlo simulation. The one standard errors of the data are shown by the error bars.

- The effect is included in the measured output factors (S_{cp}, S_c), and thus in factor-based dose per MU formalisms. But needs to be accounted for separately in model-based dose per MU formalisms.

Dose per MU formalisms

The monitor signal caused by backscatter as a function of collimator aperture, can be modelled as an additional fraction b of the direct signal. The formalism would be:

$$\frac{D(A;x,y;z)}{M} = \frac{D(A;x,y;z)}{\Psi_0} \frac{\Psi_0}{M_0(1+b(A))}$$

$$\frac{\Psi_0}{M_0} = \frac{\left[D(A_{ref};x_{ref},y_{ref},z_{ref})/M\right]_{Measured}}{\left[(D(A_{ref};x_{ref},y_{ref},z_{ref})/\Psi_0)\right]_{Calculated}}(1+b(A_{ref}))$$

Explicit as a backscatter correction factor: $\frac{1+b(A_{ref})}{1+b(A)}$

ESTRO School

Dose per MU formalism: Elekta Oncentra MasterPlan

Dose per MU formalism: Elekta Oncentra MasterPlan

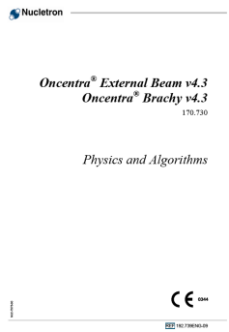
Nucletron

Oncentra® External Beam v4.3
Oncentra® Brachy v4.3
170.730

Physics and Algorithms

Dose engine results are linked to meterset values through:

$$D(\mathbf{r}) = M \frac{1 + b^{\text{calib}}}{1 + b(A)} \frac{(D/M)^{\text{calib}}_{\text{meas}}}{d^{\text{calib}}} d(\mathbf{r}) \qquad \text{(Eq. 5.8)}$$

where $(D/M)^{\text{calib}}_{\text{meas}}$ is the dose at the calibration point and geometry measured per meterset value, d^{calib} is the calculated dose for the same point and b^{calib} is the calculated backscatter signal fraction, all obtained for the same calibration geometry. For Cobalt-60 units the calibration dose rate is corrected for the decay of the source from the calibration date until the date when the dose calculation is performed.

All the internal Oncentra dose calculation engines yield the dose per energy fluence. More specifically, a dose engine d is defined by the relation:

$$d(\mathbf{r}) = \frac{D(\mathbf{r})}{\Psi_0} \qquad \text{(Eq. 5.5)}$$

where $D(\mathbf{r})$ is the absolute dose at position $\mathbf{r}$, including effects from head scatter etc. Thus dose engine calculates the dose scaled to absolute dose considering beam setup parameters, patient, etc.

ESTRO School

Including monitor signal M_b caused by backscatter depending on collimator setting

$$\frac{D(A;x,y;z)}{M} = \frac{D(A;x,y;z)}{\Psi_0}\frac{\Psi_0}{M_0}\cdot\left(1+b(A)\right)^{-1}$$

$$\frac{\Psi_0}{M_0} = \frac{\left[D(A_{ref};x_{ref},y_{ref},z_{ref})/M\right]_{Meas}}{\left[\left(D(A_{ref};x_{ref},y_{ref},z_{ref})/\Psi_0\right)\cdot\left(1+b(A_{ref})\right)^{-1}\right]_{Calc}}$$

Includes head scatter and phantom scatter

$$M = M_0 + M_b(A) = \left(1+b(A)\right)M_0$$

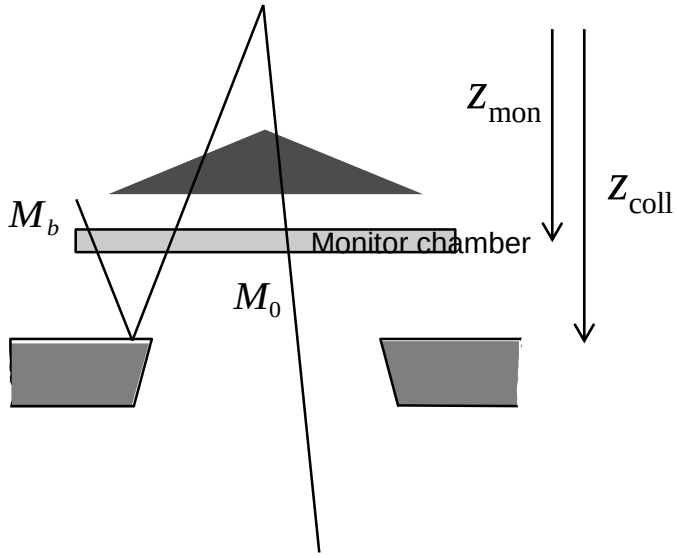

Plan with dose weighted fields and prescribed dose D_{pres}:

$$w_i = \frac{D(A_i;\text{prescription conditions})}{\sum_{i=1}^{\text{all fields}} D(A_i;\text{prescription conditions})}$$

$$M_i = \frac{D_{presc}\cdot w_i}{\frac{D(A_i;\text{at prescription point/conditions from field } i)}{M}}$$

Empirical factor from S_c measurements

$$b(A) = k_{back}\,F\,\frac{z_{mon}^2}{z_{coll}^2}$$

$$F = \iint_{\substack{\text{Irradiated}\\ \text{collimator}\\ \text{area}}} \frac{\cos^3\theta}{\pi\left(z_{coll}-z_{mon}\right)^2}\,\mathrm{d}A$$

ESTRO School

Output factor normalizition, <u>the</u> norm for comparison of calculations and measurements:

$$\frac{\left[D(A;x,y,z)/M\right]_{\text{Measured}}}{\left[D(A_{\text{ref}};x_{\text{ref}},y_{\text{ref}},z_{\text{ref}})/M\right]_{\text{Measured}}} \longleftrightarrow \frac{\left[D(A;x,y,z)/M\right]_{\text{Calculated}}}{\left[D(A_{\text{ref}};x_{\text{ref}},y_{\text{ref}},z_{\text{ref}})/M\right]_{\text{Calculated}}}$$

Global norm for deviations:

$$\frac{\left[D(A;x,y,z)/M\right]_{\text{Calculated}} - \left[D(A;x,y,z)/M\right]_{\text{Measured}}}{\left[D(A_{\text{ref}};x_{\text{ref}},y_{\text{ref}},z_{\text{ref}})/M\right]_{\text{Measured}}}$$

Local norm for deviations:

$$\frac{\left[D(A;x,y,z)/M\right]_{\text{Calculated}} - \left[D(A;x,y,z)/M\right]_{\text{Measured}}}{\left[D(A;x,y,z)/M\right]_{\text{Measured}}}$$

Dose per MU formalism: Varian Eclipse v13.6 TPS

Dose per MU formalisms: Varian Eclipse v13.6 TPS

Overview of Eclipse TPS (29. Feb 2016)

Multi-source beam model that describes:

- primary photon source
- extra-focal photon source
- electron contamination source
- (hard) wedge scatter source

Dose engines

- Pencil Beam Convolution (PBC v10.0.28)
- Pencil kernel - Anisotropic Analytical Algorithm for photons (AAA v13.6.23)
- Acuros External Beam for photons (Acuros XB v13.6.23)
- Cone Dose Calculation for photons (CDC v13.6.23)
- Generalised Gaussian Pencil Beam for electrons (GGPB v10.0.28)
- Electron Monte Carlo Algoritm (eMC v13.6.23)
- Proton Convolution Superposition (PCS v13.6.23)

Dose Optimisation algorithms for IMRT/VMAT planning

- Photon Optimiser (PO v13.6.23)
- Dose Volume Optimiser (DVO v13.6.23)
- Plan Geometry Optimiser algorithm (PGO V13.6.23)
- Progressive Resolution Optimiser (PRO v13.6.23)
- Nonlinear Universal proton Optimiser v13.6.23

Fluence Delivery modelling algorithms for IMRT planning

- Algorithms that correct optimal fluence maps to deliverable fluence maps based on constraints imposed by the MLC (Leaf Motion Calculator, LMC)

Portal Dose Image Prediction (PDIP v13.6.23)

Intermediate dose calculation using: Multi-Resolution Dose Calculation Algorithm (MRDC v13.6.23)

Depending on MLC motion (static or dynamic), the total MU of a beam are adjusted appropriately

ESTRO School

Dose per MU formalism: Varian Eclipse v13.6 TPS

Excerpt from Eclipse Photon & Electron Reference Guide, Dec2014

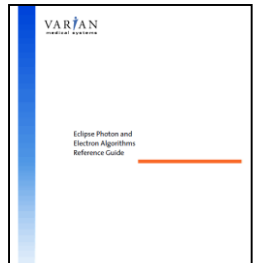

The final MU are calculated from the prescribed dose, plan normalization, field weight, field normalization and a normalization factor determined by the dose calculation algorithm. The normalization factor determined by the AAA and Acuros XB is the MU value for 1 Gy to 100% of the current field. AAA and Acuros XB calculate the monitor units at the normalization point MUnorm for open field, hard wedge, Enhanced Dynamic Wedges and physical compensators as in the equation:

Equation 2

$$MU_{norm} = CBSF(X,Y) \times \left(\frac{MU_{calib}}{D_{calib}}\right) \times \left(\frac{D_{ref}}{D_{norm}(X,Y)}\right) \times \frac{1}{WCF(X,Y)}$$

where

CBSF(X,Y) = Collimator backscatter factor for an open field with same collimator settings (more information: Equation 1 on page 23).

In case of treatment units where MLC defines the field size (for example Elekta), the collimator backscatter factor is calculated based on the effective field size in X and Y direction instead of the collimator jaw settings (X, Y).

MU_{calib} = User-defined value of parameter Reference Dose In MU at Calibration Depth. (For hard wedges, this parameter is read from the wedge parameters. More information: Hard Wedge Parameters on page 65.)

D_{calib} = User-defined value of parameter Reference Dose In Gy at Calibration Depth. (For hard wedges, this parameter is read from the wedge parameters. More information: Hard Wedge Parameters on page 65.)

D_{ref} = Dose calculated by the AAA or Acuros XB for the reference conditions (more information: Output Factor Geometry on page 84) at the calibration depth, which is the value of the Absolute Dose Scaling Factor parameter. (For hard wedges, this parameter is read from the wedge parameters.)

$D_{norm}(X,Y)$ = Dose calculated by the AAA or Acuros XB at the field normalization point, based on the selected field normalization method.

WCF(X,Y) = Wedge correction factor for hard wedge field with the collimator jaw settings (X,Y).

In case the field contains a block or an MLC, the wedge correction factor is calculated based on the effective field size in X and Y direction instead of the collimator jaw settings (X, Y).

The calculation of MU is based on output factor measurements performed for different field sizes in a certain reference geometry (more information: Output Factor Geometry on page 84), and calibration calculations made for the reference field size.

The change in the output factor as a function of field size is caused by changes in phantom scatter, head scatter and collimator backscatter into the monitor chamber. The phantom and head scatter effects are accounted for by the photon beam source model and the volumetric dose calculation algorithm (AAA or Acuros XB). The remaining change in the output factors is assumed to be caused by collimator backscatter. It is estimated from the measured output factor table as shown in the equation.

Equation

$$CBSF(X,Y) = \frac{OF_{ref}}{OF(X,Y)} \times \frac{D'(X,Y)}{D'_{ref}}$$

where

X,Y = Collimator settings ($X = X_2 - X_1$, $Y = Y_2 - Y_1$)

CBSF(X,Y) = Collimator backscatter factor for an open field with same collimator settings.

OF_{ref} = Output factor table value for reference field size. The value is normally 1.0. The reference field size is given by the parameter Absolute dose reference field size, defined in the AAA and Acuros XB Parameters (more information: Table 12 on page 59).

OF(X,Y) = Output factor table value for field size X,Y.

D'(X,Y) = Dose at the reference point calculated by the AAA or Acuros XB for the field size X,Y and the reference geometry when ignoring the effect of collimator back scatter.

D'_{ref} = Dose calculated by the AAA or Acuros XB for the reference conditions in the reference geometry (more information: Output Factor Geometry on page 84) when ignoring the effect of collimator back scatter.

The reference field geometry used in the measurement of the output factor table is indicated by the Source-Phantom Distance parameter defined in the output factor table in Beam Configuration (more information: Table 5 on page 48). The reference point depth from the surface of the phantom is given by the Detector depth from phantom surface parameter, also defined in the output factor table.

Dose per MU formalism: Varian Eclipse v13.6 TPS

$$CBSF(A) = \frac{D_{\text{calc}}(A)/\Psi_o}{D_{\text{calc}}(A_{\text{ref}})/\Psi_o} \cdot \frac{S_{\text{cp,meas}}(A_{\text{ref}})}{S_{\text{cp,meas}}(A)} = \frac{S_{\text{cp,calc}}(A)}{S_{\text{cp,meas}}(A)}$$

$$S_{\text{cp,calc}}(A)$$

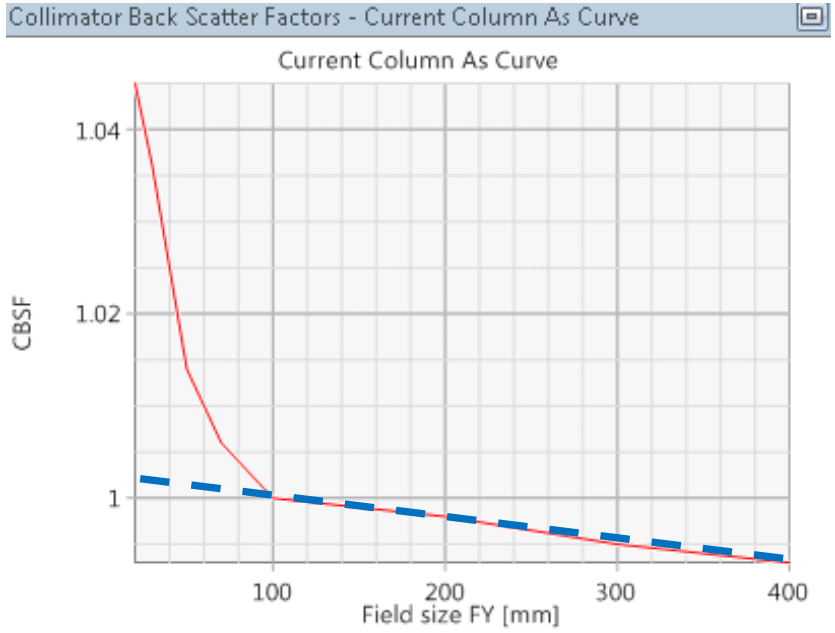

As a result of the beam configuration process, a table of CBSC(X,Y) factors for symmetric rectangular fields is generated and stored for each MV beam (input for this are the measured S_{cp} data)

Korhonen, Doctoral Dossertation, Helsinky University of Technology, 2009

Dose per MU formalism: Philips Pinnacle TPS

Dose per MU formalism: Philips Pinnacle TPS

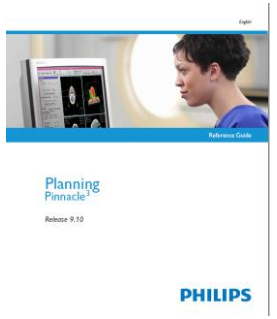

Convolution algorithm monitor unit calculations

Because the convolution algorithm can accurately compute phantom scatter (S_p), we can use the following equation to compute dose:

$$MU = \frac{D_{presc}}{ND \cdot OF_c \cdot TTF \cdot (D/MU)_{cal}}$$

ref

where:

D_{presc} is the prescription dose per fraction at the prescription point, in units of cGy.

ND is the Normalized Dose at the reference point.

OF_c is the computed correction factor determined during commissioning.

TTF is the total transmission factor.

$(D/MU)_{cal}$ is the dose per Monitor Unit at the calibration point.

Normalized dose is the ratio of dose per unit energy fluence at the prescription point to dose per unit energy fluence at the reference point for the calibration field (the point at which $(D/MU)_{cal}$ was measured) as determined by the convolution superposition calculation for the treatment geometry.

Philips Medical Systems

The convolution/superposition algorithm uses a head scatter model when computing the incident energy fluence. This head scatter model is intended to predict the increased output of the accelerator due to scatter in the head. During the computation of OF_p and OF_c the head scatter is included in the OF_p. Therefore, the OF_c represents the residual effects of head scatter not included in the model. Similarly, the effects of the wedge are also included in OF_p.

Pinnacle³ uses output factors generated using the following equation (which resembles S_c, S_p formalism):

$$OF_c = OF/OF_p$$

where

OF is the user-measured overall output factor.

OF_p is the computed phantom output factor, which includes the head scatter model and wedge effects.

OF_c is an internal normalization factor that will not match measured S_c values. OF_c is tabulated by equivalent square. The value used for a given field is interpolated linearly from the output factor table based on the equivalent square of the unblocked field. OF_c is also tabulated by wedge. If the beam has a wedge, an output factor for that wedge must be available.

ESTRO School

Dose per MU formalism: Philips Pinnacle TPS

The formalism in Pinnacle uses in essence the same approach as that in Eclipse. Unfortunately the manual does not explicitly describe what is accounted for by the *internal correction factor* correcting for *residual head scatter effects…*

$$MU = \frac{D_{presc}}{ND \cdot OF_c \cdot TTF \cdot (D/MU)_{cal}}$$

Pinnacle[3] uses output factors generated using the following equation (which resembles S_c, S_p formalism):

$$OF_c = OF/OF_p$$

$$CF_{\text{residual}}(A) = \frac{S_{\text{cp,meas}}(A)}{S_{\text{cp,calc}}(A)}$$

where

OF is the user-measured overall output factor.

OF_p is the computed phantom output factor, which includes the head scatter model and wedge effects.

OF_c is an internal normalization factor that will not match measured S_c values. OF_c is tabulated by equivalent square. The value used for a given

or

$$CF_{\text{residual}}(A) \cong \frac{1}{CBSF(A)}$$

ESTRO School

Dose per MU formalism: Raysearch Raystation

Dose per MU formalism: Raysearch Raystation

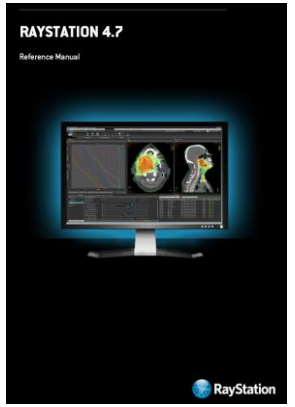

Output factor corrections – used in energy fluence computations

Part of the output factor increase with field size is caused by increased secondary scattering of energy from the sides into the center of the field (phantom scatter); this effect is part of the radiation transport in the collapsed cone dose calculation (*section 3.3 Collapsed cone dose computation on page 42*). A smaller part (for Varian, Elekta and Siemens LINACs) of the field size dependence is caused by the projection of extended sources through the collimators (head scatter). The phantom scatter and head scatter is generally not sufficient to completely describe the output factor variation. The remaining field size dependence, the output factor correction, is introduced into the energy fluence and dose computation to account for effects such as backscattering from collimators into the beam monitor. The output factor correction can be normalized to 1.0 for the reference field size; it generally increases slightly with field size. The output factor corrections can be fitted to the output factors in the auto-modeling or selected by the user to give a best fit to dose curves and output factor measurements. When computing the fluence for a segment the output factor corrections are computed using the field measure (*Field measure on page 33*).

Same as Pinnacle

Field measure

The field measure is calculated from the jaw or MLC openings, $I_{x\text{-jaw/MLC}}$ and $I_{y\text{-jaw/MLC}}$, using an equivalent square formula.

ESTRO School

In conclusion

- Similarities in physics background
- Large differences in the “explanation” in the manuals
- Advice to vendor: Make more effort in using present day standard physics terms
- Advice to users: make an effort to understand and review beam modelling results

Dose to medium vs dose to water
A discussion

Tommy Knöös with little help from my friends

Content

1. Where are the properties of the medium influencing the dose calculation
2. Explain the differences between the D(m-in-m) and D(w-in-m) and in particular why the values differ so much in materials such as bone
3. Explain what different TPS dose calculation algorithm do/report
4. Explain how the conversion to D(w-in-m) from D(m-in-m) is done in MC and AXB
5. Conclusions – what to do!

2.4 DOSIMETRIC QUANTITIES

2.4.3 Absorbed dose

- Absorbed dose is a quantity applicable to both indirectly and directly ionizing radiations.
- Indirectly ionizing radiation implies that the energy is imparted to matter in a **two step process**.
  - In the first step (resulting in kerma), the indirectly ionizing radiation transfers energy as kinetic energy to secondary charged particles.
  - In the second step, these charged particles transfer a major part of their kinetic energy to the medium (finally resulting in absorbed dose).
- Directly ionizing radiation implies that charged particles transfer a major part of their kinetic energy directly to the medium (resulting in absorbed dose).

PHOTONS

Photon beam attenuation

- Energy transfer from the photon beam - TERMA to the medium

$$T(E,z) = \frac{\mu_E}{\rho} \cdot \Phi(E,z) \cdot E$$

- Or when including ray tracing

$$T(E,z) = \frac{\mu_E}{\rho} \cdot \Phi_0(E, z=0) \cdot e^{-\mu_E \cdot z_{radiol}} \cdot E$$

- Mass-attenuation coefficients are dependent on the medium of where the energy is removed from the beam
- This energy is transferred to photons and electrons which propagates away from the interaction site
- Coefficient can be downloaded for elements and compounds
- https://www.nist.gov/pml/x-ray-mass-attenuation-coefficients

Mass energy and mass transfer coefficients

$$\frac{\mu_{tr}}{\varrho} = (f_{pe}\sigma_{pe} + f_{incoh}\sigma_{incoh} + f_{pair}\sigma_{pair} + f_{tripl}\sigma_{tripl}) \cdot N_a/u \cdot A$$

$$\frac{\mu_{en}}{\varrho} = (1 - g)\frac{\mu_{tr}}{\varrho}$$

Where:

f_i is the proportion of interaction i

σ_i is the cross section of interaction i per electron (the probability that the incident photon makes an effect in the target element),

ρ the density of the material target,

N_a is the Avogadro number (6.023 ^{23}/mol), u is the atomic mass unit, and A is the relative atomic mass of the target element

Absorption coefficients for bone and water

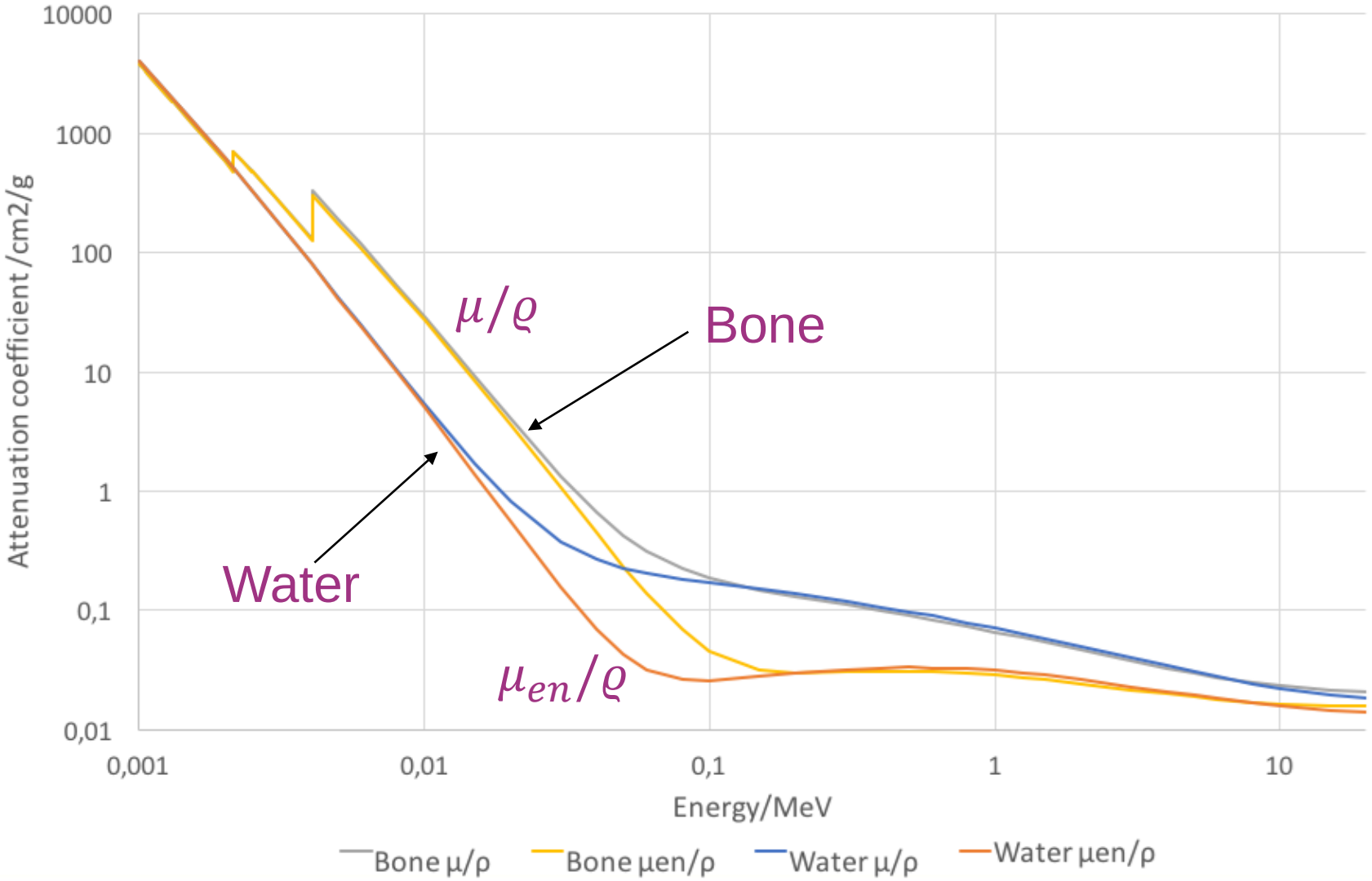

ESTRO School

Mass-absorption coefficient ratios

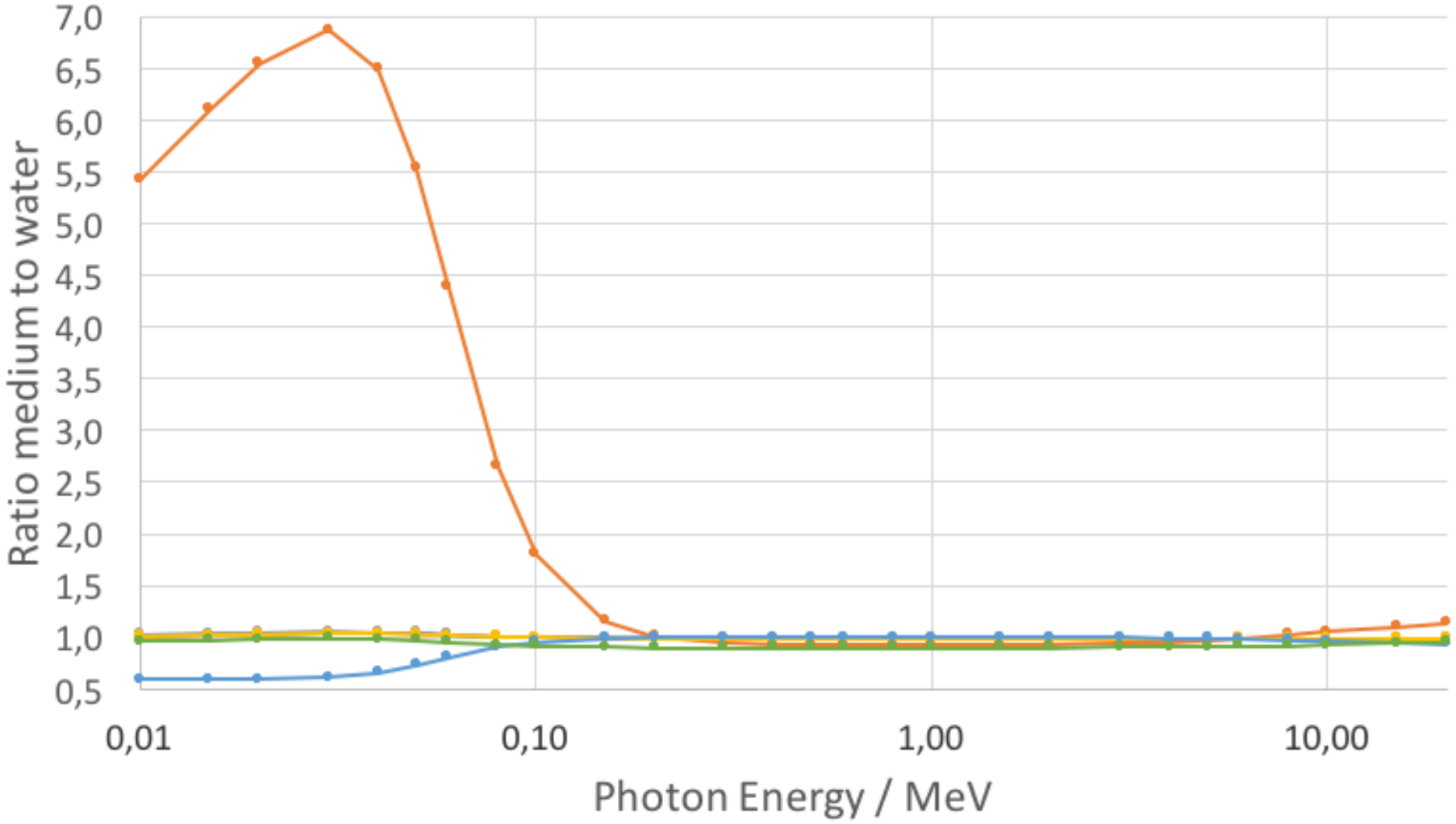

ESTRO School

Mass-absorption coefficient ratios

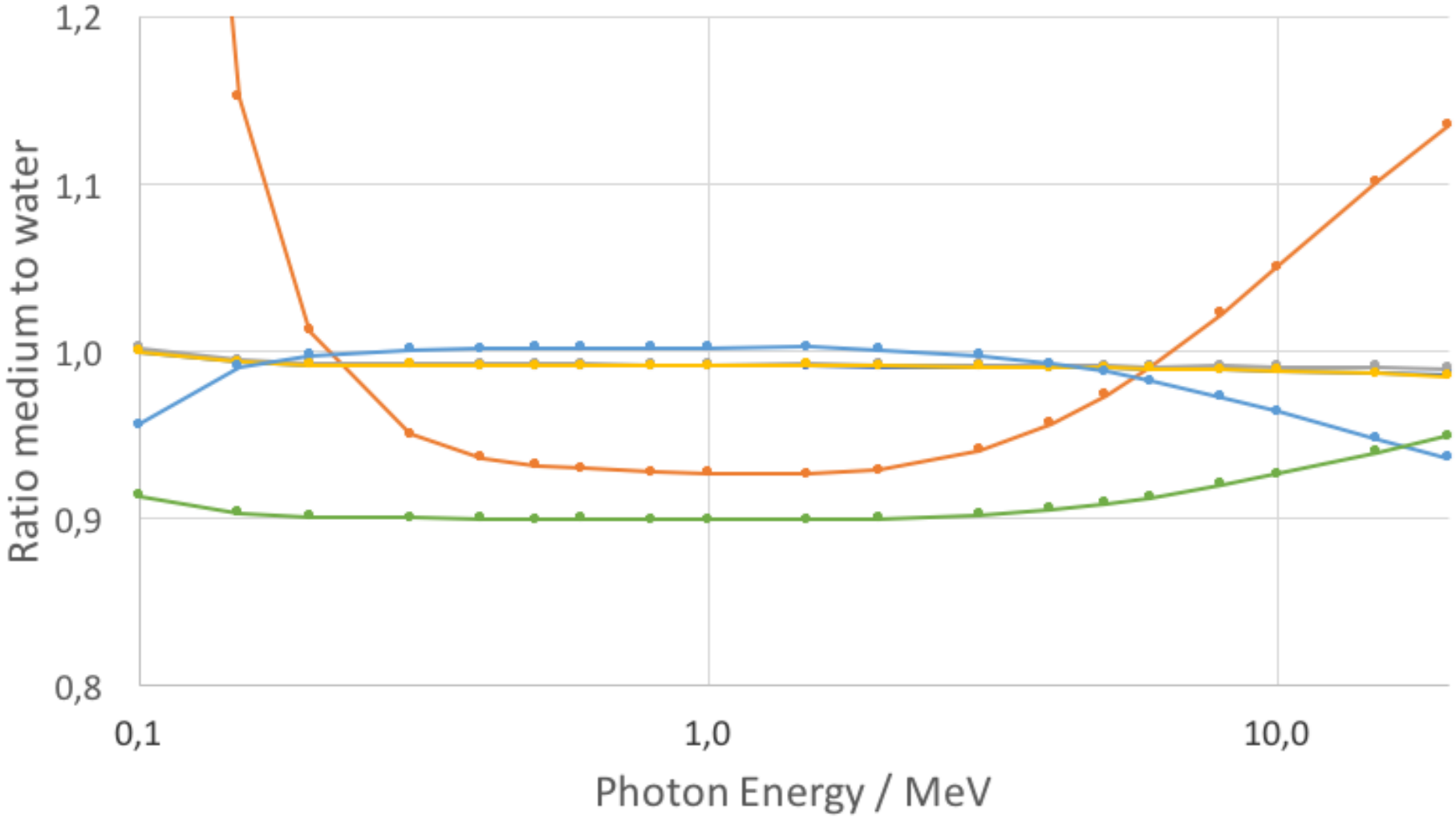

ELECTRONS

Electron slowing down or energy absorption

- Electrons slows down and looses energy by the mass-stopping power thus;

$$D = \int_0^{E_{max}} \Phi_{med}(E) \cdot \left(\frac{S_{el,med}(E)}{\rho} \right) dE$$

- Mass-stopping power is dependent on the medium where the electrons are slowing down

$$\left(\frac{S}{\rho} \right)_{tot} = \frac{1}{\rho} \cdot \frac{dE}{dx}$$

- Use ESTAR to calculate mass-stopping powers etc

- http://physics.nist.gov/PhysRefData/Star/Text/ESTAR.html

Mass stopping power

- The total mass stopping power consists of two components:
  - Mass electronic[1] or collision stopping power $\left(\frac{S}{\rho}\right)_{el}$ resulting from electron-orbital electron interactions (atomic ionizations and atomic excitations)
  - Mass radiation stopping power $\left(\frac{S}{\rho}\right)_{rad}$ resulting mainly from electron-nucleus interactions (bremsstrahlung production)

$$\left(\frac{S}{\rho}\right)_{tot} = \left(\frac{S}{\rho}\right)_{el} + \left(\frac{S}{\rho}\right)_{rad}$$

1) ICRU 85

2.5 INTERACTION COEFFICIENTS: ELECTRONS

2.5.4 Mass stopping power for electrons and positrons

- Formula according to the ICRU Report No. 37.

$$\frac{S_{col}}{\rho} = \frac{N_A Z}{A} \frac{\pi r_0^2 2 m_e c^2}{\beta^2} \left[\ln(E_K / I)^2 + \ln(1 + \tau/2) + F^{\pm}(\tau) - \delta \right]$$

with

N_A	=	Avogadro's constant	I	= mean excitation energy
Z	=	atomic number of substance	τ	= $E_K / (m_e c^2)$
A	=	molar mass of substance	δ	= density effect correction
r_0	=	electron radius		
$m_e c^2$	=	rest energy of the electron		
β	=	v/c		
v	=	velocity of electron	$F^{\pm}$	is given in the next slide
c	=	velocity of light		

IAEA

2.5 INTERACTION COEFFICIENTS: ELECTRONS

2.5.4 Mass stopping power for electrons and positrons

- *The mean excitation potential I is a geometric mean value of all ionization and excitation potentials of an atom of the absorbing material.*

- *I* values are usually derived from measurements of stopping powers in heavy charged particle beams, for which the effects of scattering in these measurements is minimal.
  - For elemental materials *I* varies approximately linearly with *Z*, with, on average, $I = 11.5 \times Z$.
  - For compounds, *I* is calculated assuming additivity of the collision stopping power, taking into account the fraction by weight of each atom constituent in the compound.

Mean excitation energy *I*

- *I*-values for body tissues may vary significantly from one patient to another, and they are responsible for the large uncertainties, up to the order of 10–15%, stated by ICRU-37 for the mass stopping powers of body tissues.

- …mass stopping-power ratios to water are more dependent on possible patient-to-patient differences on composition, and therefore on I -values, than on density…

- The key issue continues to be tissue segmentation due to individual tissue composition and I –values…

Mass stopping power for bone and water

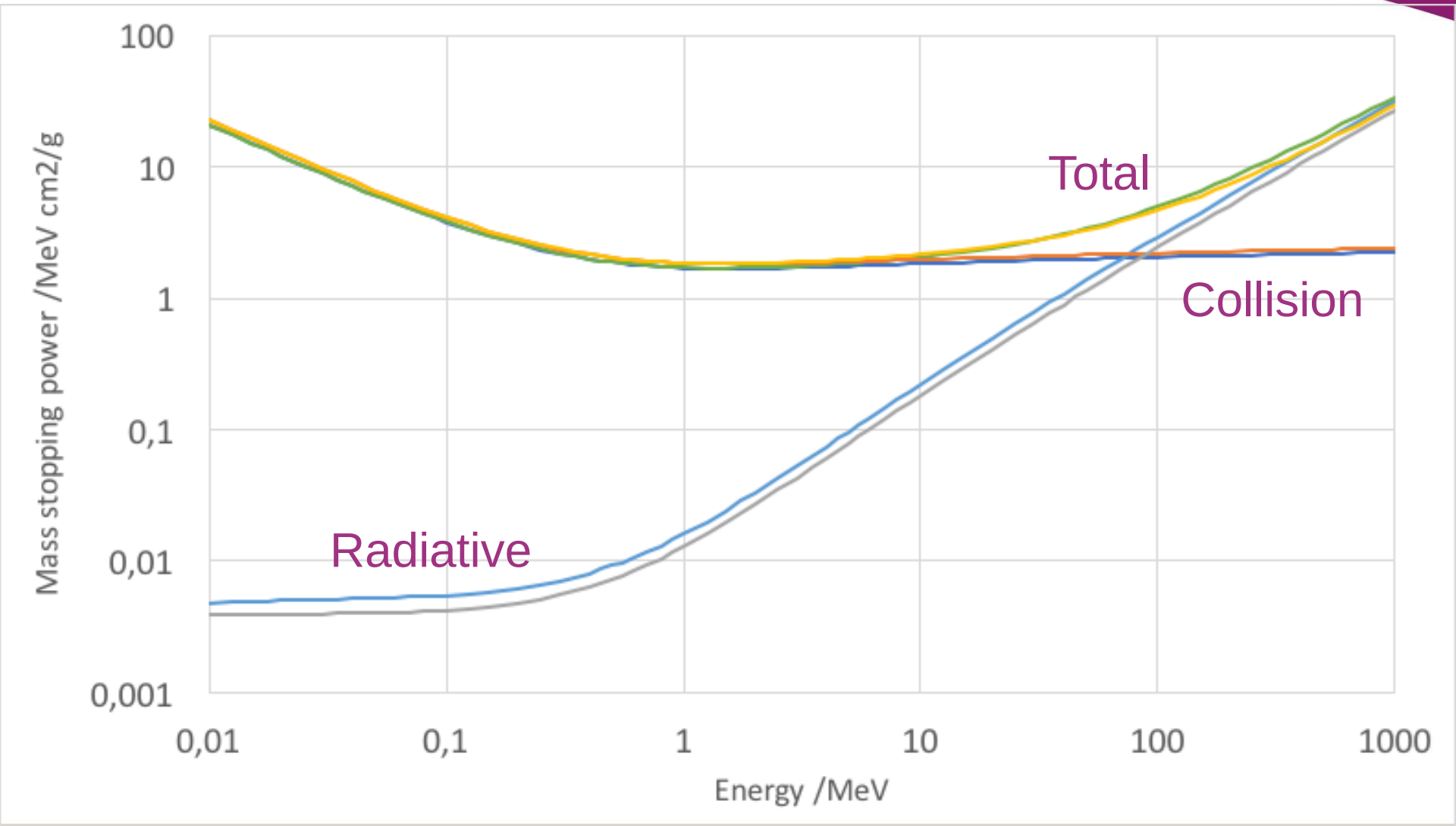

ESTRO School

Mass stopping-power ratios (electronic) from ESTAR

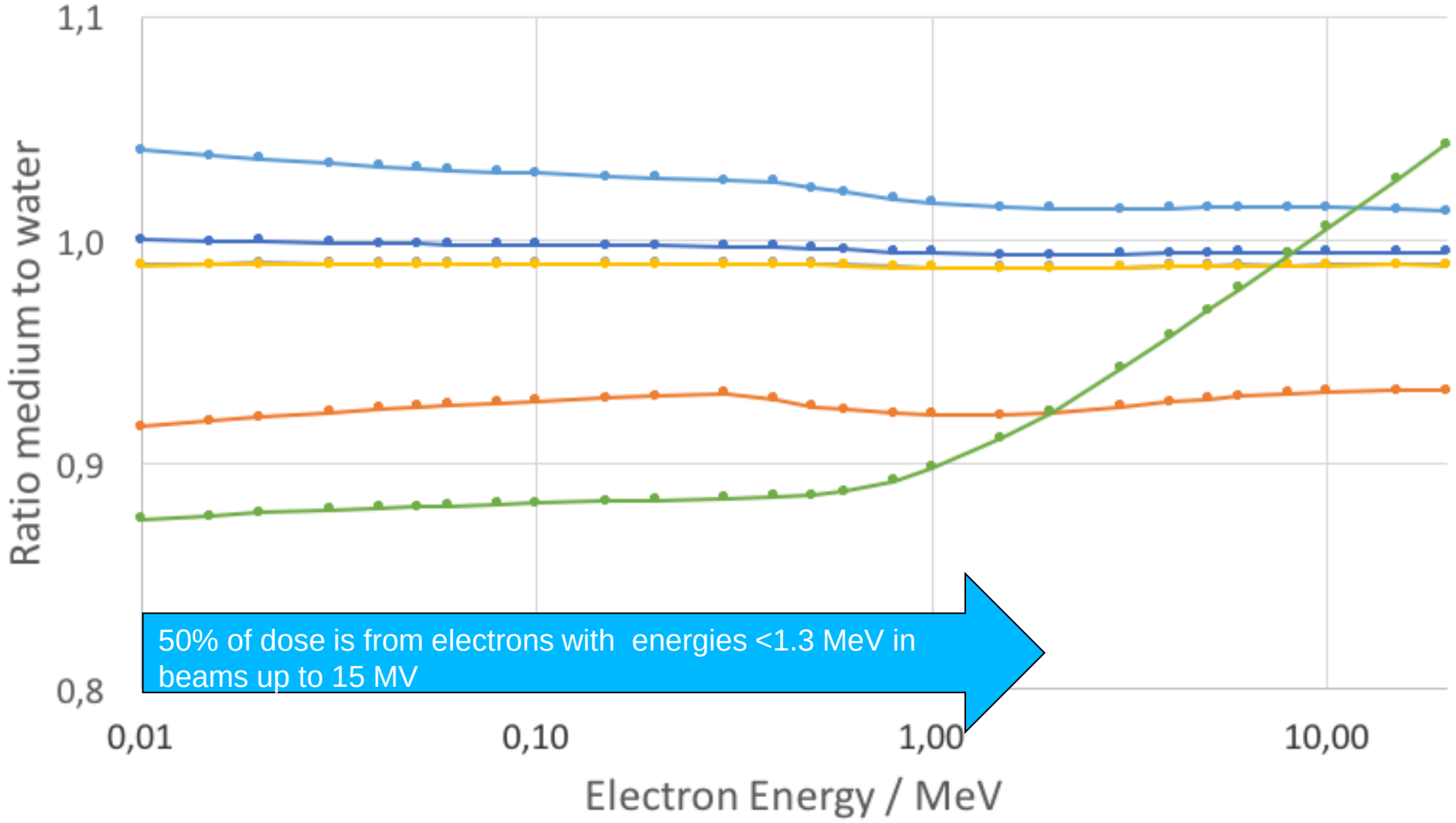

ESTRO School

Example of mapping of medium

Table 1 Material mass densities for automatic conversion, as implemented in the two Acuros XB versions

Material	Density Range [g/cm^3] Acuros XB version 10	Density Range [g/cm^3] Acuros XB version 11
Air	-	0.000-0.020
Lung	0.000-0.590	0.011-0.624
Adipose Tissue	0.590-0.985	0.554-1.001
Muscle, Skeletal	0.985-1.075	0.969-1.093
Cartilage	1.075-1.475	1.056-1.600
Bone	1.475-3.000	1.100-3.000

From Fogliata A, Nicolini G, Clivio A, Vanetti E, Cozzi L. Dosimetric evaluation of Acuros XB Advanced Dose Calculation algorithm in heterogeneous media. Radiat Oncol. 2011;6:82.

ALGORITHMS

Definition

- Introduce for classification of algorithms
  - $D_{transport,deposit}$
- Where *transport* can either be in *water* or in *medium* during ray-trace and/or calculation of TERMA or similar quantity
- And *deposit* is either energy deposit/absorbed in *water* or *medium*
- Example - $D_{water,water}$ for an algorithm where transport and deposit take place in water

Other notations exist

Pencil beam based models

- Transport
  - PB kernels determined in water from MC and/or measurements
  - Transport scaled by mass or electron density[1]
    - In principle one either use water as medium or
    - introduce a medium during scaling
  - Dose deposit in water

- Deposit
  - No conversion to medium during absorption

- Thus on general we have $D_{w,w}$ however it can in principle be $D_{m,w}$

[1] Scales best electron density according to Seco and Evans, Med Phys 2006, but important to check what the specific TPS requires

Point kernel based models

- Transport
  - Kernels determined in water
  - Ray tracing of "energy released- TERMA" have the possibilities to be done in the medium

$$T(E,z) = \frac{\mu_E}{\rho} \cdot \Phi_0(E, z=0) \cdot e^{-\mu_E \cdot z_{radiol}} \cdot E$$

  - An approximation is that only the energy released in the voxel depends on the medium not the attenuation
- Deposit
  - Transporting and depositing energy from the interaction point can be done either in water or in the medium, thus;
  - $D_{m,w}$ or $D_{w,w}$ or $D_{m,m}$ or $D_{w,m}$

Monte Carlo based models

- Transport
  - MC-models transports particles *generally* in the medium and interaction is determined from the actual medium
  - EGSnrc, GEANT, Penelope…
  - Patient model can be “fooled” to be water by varying density by changing look-up tables!

- Deposit
  - Energy deposit in each voxel is based on the medium
  - This can be converted to dose in water

- We have $D_{m,m}$ and/or $D_{m,w}$ and/or $D_{w,w}$
  - In commercial system these choices are probably not available

Grid based Boltzman solvers (GBBS) based models[1]

- Transport
  - Basically the model calculates the electron fluence in each voxel
  - This is done considering a system where the medium in each voxel is accounted during photon and electron transport

- Deposit
  - Since the differential electron fluence is determined one can apply either stopping electronic power for the medium or water to receive the absorbed dose

- We have either $D_{m,m}$ or $D_{m,w}$

[1)]Only one system available for radiotherapy

Pinnacle by Philips

- Primary transport for a beam is accomplished by projecting the incident energy fluence through the density representation of a patient to compute a TERMA (Total Energy Released per unit Mass) volume using poly-energetic rays, with water equivalent depth hardening and off-axis softening.
  - Transport in water
- A three-dimensional superposition of the TERMA with a poly-energetic energy deposition kernel is used to compute dose. A ray-tracing technique is used during the superposition to incorporate the effects of heterogeneities on lateral scatter.
  - To account for heterogeneities, the kernels are density-scaled during superposition. Superposition is performed using "collapsed cones."
  - Deposit in water
- No mention of medium in the manual, thus; $D_{w,w}$

Eclipse from Varian

- Unlike the classic pencil beam models, the AAA also considers changes in scatter perpendicular to the propagation direction (i.e. lateral direction).
- The longitudinal scaling is the standard radiological depth (equivalent path length) method based on the converted electron densities.

$$I_\beta(z,\rho) = I_\beta(z')\frac{\rho(0,0,z)}{\rho_{water}}$$

where $z' = \int_0^z \frac{\rho(0,0,t)}{\rho_{water}} dt$ ρ electron density

Equations from Varian's Eclipse Physics course

Eclipse from Varian

- For the lateral scaling, a discretization in 16 perpendicular directions is used and for each an equivalent path length is determined.

$$K_\beta(x,y,z) = \frac{\rho(x,y,z)}{\rho_{water}} \sum_{k=0}^{5} c_k(z') \frac{1}{r} e^{-\mu_k r_d(x,y,\rho)}$$

$$r_d(x,y,\rho) = \int_R \frac{\rho(\vec{t})}{\rho_{water}} \left| d\vec{t} \right|$$

- While the variable lateral scatter considerations improve the algorithm performance in lung, it does not change the fact that the medium is still uniformly considered water-equivalent and the dose is thus reported to water.
- Different heterogeneities can be modified as scaled water, thus $D_{w,w}$

Oncentra/Monaco[1] – (Pencil beam) and Collapsed Cone Convolution

- Patient tissue distribution is represented by a 3D density matrix where the properties in each voxel are either derived from pixel values in a CT image or from user specified values of mass or electron density.
- It is assumed that the specified density values correspond to tissue material of "standard" compositions (see ICRP 23 and ICRU 44).
- The Hounsfield number assigned to each standard tissue is mapped from the calculated electron density using relations given by Knöös et al [38].

- …for charged particle equilibrium conditions CC calculates dose to medium while PK calculates dose to a large water cavity in medium. Both algorithms *consider attenuation of the beam as per medium* thus;
- Pencil kernel $D_{m,w}$ and for point kernel $D_{m,m}$

[1)]Monaco do not supply a PB model initially

RaySearch – CT numbers

- ...convert the Hounsfield Units (HU) of the CT-images to mass densities...
- Considering Compton and especially pair production an effective density is determined based on the elemental composition of a number of pre-determined materials.

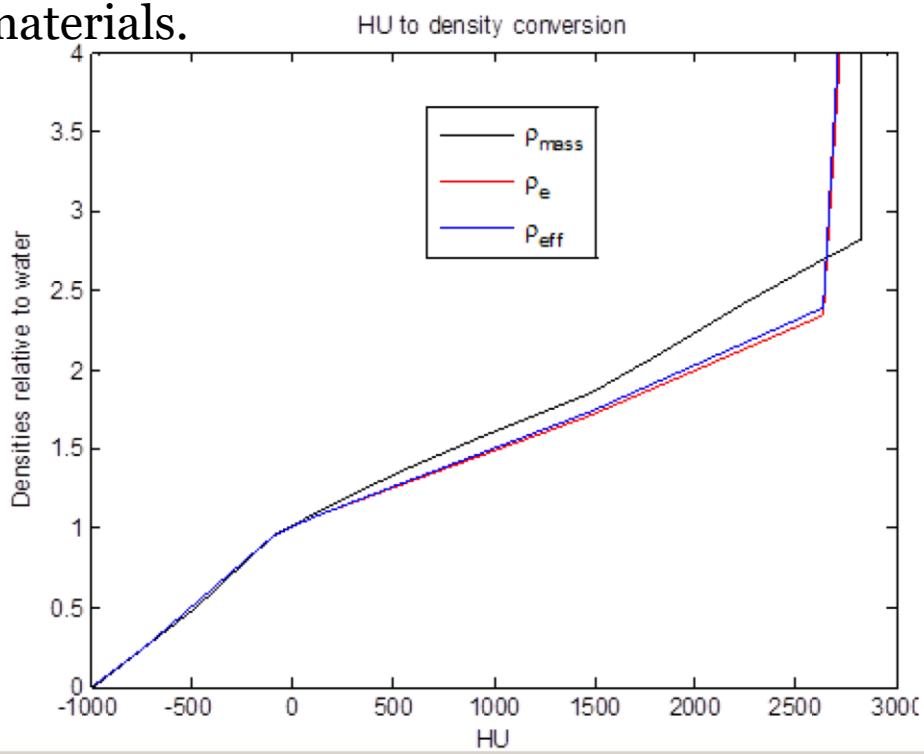

From RaySearch manuals

RaySearch – Algorithm – Collapsed cone

- Effective density basis for the TERMA calculation – implicitly transport in medium
- Collapsed cone implemented as dose-point of view
- Same effective density used during scaling of cones/pipes.
- …the electron stopping power is assumed to scale with the effective density i.e. they are assumed to be material dependent in the same way.
  - Water-like medium with a scaled mass-stopping power
  - This is converted to dose-in-water by the effective density ratio

- Thus; $D_{m,w}$ maybe???

Monaco from Elekta – Monte Carlo

- The dose calculation uses a continuous density material approximation.

- The technique used in XVMC is to correct/scale the cross section and stopping power data as a function of energy for water using empiric equations based on the density mapped from the patient CT data.

Cross sections are scaled by mass density

$\Sigma_{medium}(E)$ – cross section for a medium represented by mass density, ϱ_{medium}

ϱ_{medium} – mass density in the patient (ϱ_{water} =1)

$\Sigma_{water}(E)$ – cross section for water

$[f(\varrho)/\varrho]$ is the correction function which is always equal to unity for water.

$$\Sigma_{medium}(E) = [f(\varrho)/\varrho] \cdot \varrho_{medium} \cdot \Sigma_{water}(E)$$

Some additional considerations may be present in certain situations

Mass stopping power ratios

- Kawrakow et al

$$\frac{S_{\mathrm{el}}(\rho_{\mathrm{t}}, E)/\rho_{\mathrm{t}}}{S_{\mathrm{el}}^{\mathrm{w}}(\rho_{\mathrm{w}}, E)/\rho_{\mathrm{w}}} = f_c\left(\rho_{\mathrm{t}}/\rho_{\mathrm{w}}\right) = \begin{cases} \left(\rho_{\mathrm{t}}/\rho_{\mathrm{w}}\right)^{-0.17} & \rho_{\mathrm{t}} \geqslant 0.795 \text{ g cm}^{-3} \\ 1.039 & \text{all other } \rho_{\mathrm{t}} \end{cases}$$

- Monaco manual

$S^{m,w} = 1.039 - (0.05553 - 0.0617\rho)S_{corr}$	ρ≤0.821	Eqn. 56
$S^{m,w} = \rho^{-0.227} + 0.038(\rho - 1) - (0.05553 - 0.0617\rho)S_{corr}$	0.821<ρ≤0.9	Eqn. 57
$S^{m,w} = \rho^{-0.227} + 0.038(\rho - 1)$	0.9<ρ≤0.98	Eqn. 58
$S^{m,w} = 1.000$	0.98<ρ<1.02	Eqn. 59
$S^{m,w} = \rho^{-0.227} + 0.038(\rho - 1)$	1.02≤ρ<1.1	Eqn. 60
$S^{m,w} = \rho^{-0.227} + 0.038(\rho - 1) - (0.05553 - 0.0617\rho)S_{corr}$	ρ=1.1	Eqn. 61
$S^{m,w} = \rho^{-0.227} + 0.038(\rho - 1) - (0.012\rho - 0.013)S_{corr}$	1.1<ρ≤2.68	Eqn. 62
$S^{m,w} = 0.829$	2.68<ρ<2.72	Eqn. 63
$S^{m,w} = \rho^{-0.227} + 0.038(\rho - 1) - (0.012\rho - 0.013)S_{corr}$	2.72≤ρ	Eqn. 64

Where:

ρ – density (g/cc)

S_{corr} – a correction factor based on the mean energy of the photon spectra

$S^{m,w} = \frac{S_m}{S_w}$ - medium-to-water mass collision stopping power ($1/S^{w,m}$)

$S_{corr} = 1.0$	0.4* Ē ≤ 1.0	Eqn. 65
$S_{corr} = e^{-(0.4*\bar{E}-1.0)}$	1.0< 0.4* Ē	Eqn. 66

Mass stopping power ratios

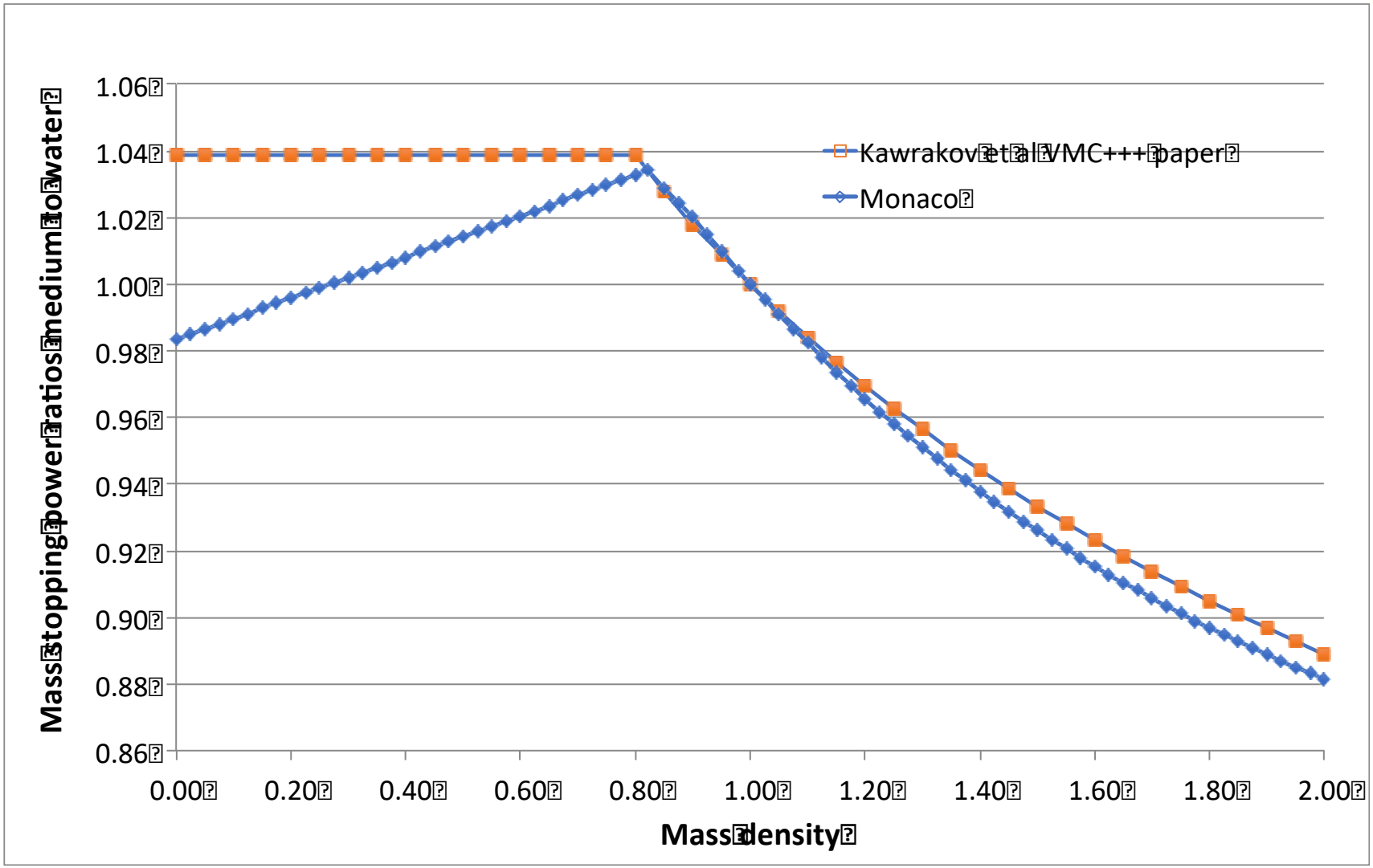

ESTRO School

Monaco MC

- Transport
  - Medium or scaled water interaction coefficients
- Deposit
  - Medium or scaled water mass stopping power
- Thus $D_{m,m}$
- Or maybe $D_{m,w}$ "scaled water"
- Or $D_{w,w}$ "scaled water"

Acuros - Varian

- Transport of particles in medium
- Electron fluence calculated in each voxel – differential in energy
- Mass stopping power applied either as tissue or medium when dose is determined
  - The default method used to determine the material composition of a given voxel in a 3D image is based on the HU value.
  - In the only commercial implementation of the GBBS, this is converted to *mass density* using the CT scanner calibration curve. For voxels with density <3 g/cm^3, only a biological material can be assigned: lung, adipose tissue, muscle, cartilage, or bone.
  - The material corresponding to a given HU is hard-coded into a lookup table..
- Thus $D_{m,m}$ or $D_{m,w}$ (user select)

CONCLUSIONS (AND RECOMMENDATIONS)

w-m-w slab 15 MV in Eclipse

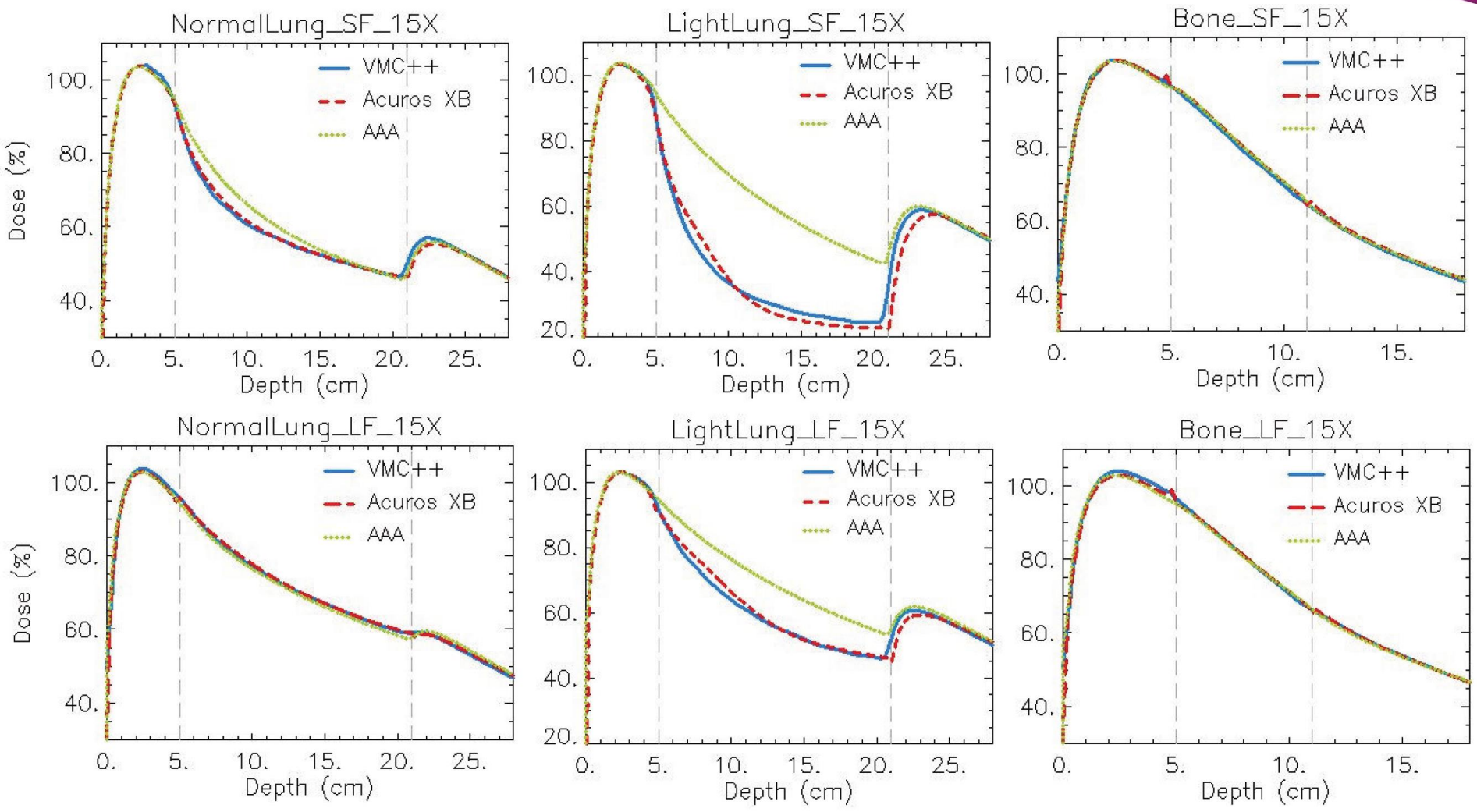

ESTRO School

Conclusion from Rana and Pokharel 2014

- D_{medium} or D_{water} in AXB is less likely to produce significant dosimetric differences in the clinical environment.

- …depends on the disease site, and even for the same type of disease (e.g., lung cancer), the results are patient specific…

Results for prostate and SBRT lung

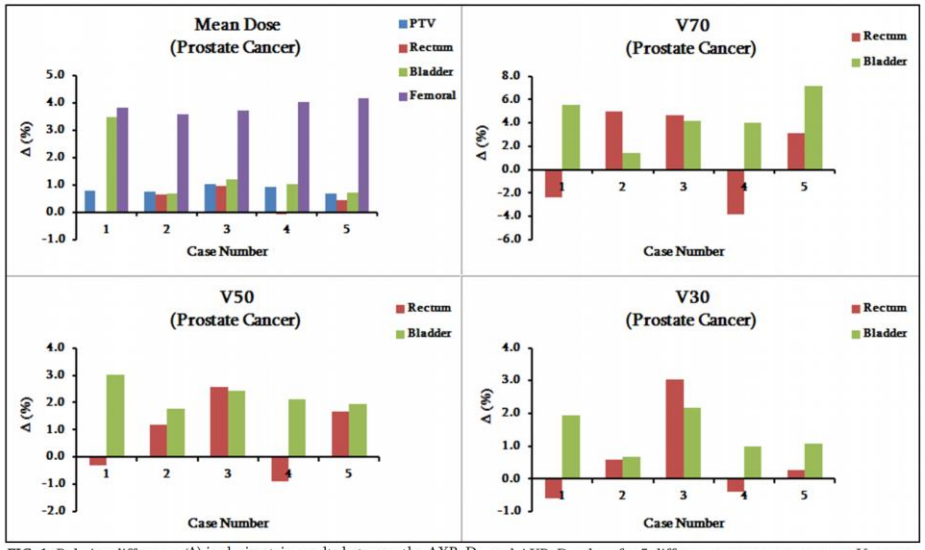

FIG. 1: Relative difference (Δ) in dosimetric results between the AXB_D$_w$ and AXB_D$_m$ plans for 5 different prostate cancer cases. V$_n$ means percentage volume irradiated by n Gy or more of a certain structure. The Δ is defined in Equation 1.

$$\Delta = \frac{D_{medium} - D_{water}}{D_{water}} \%$$

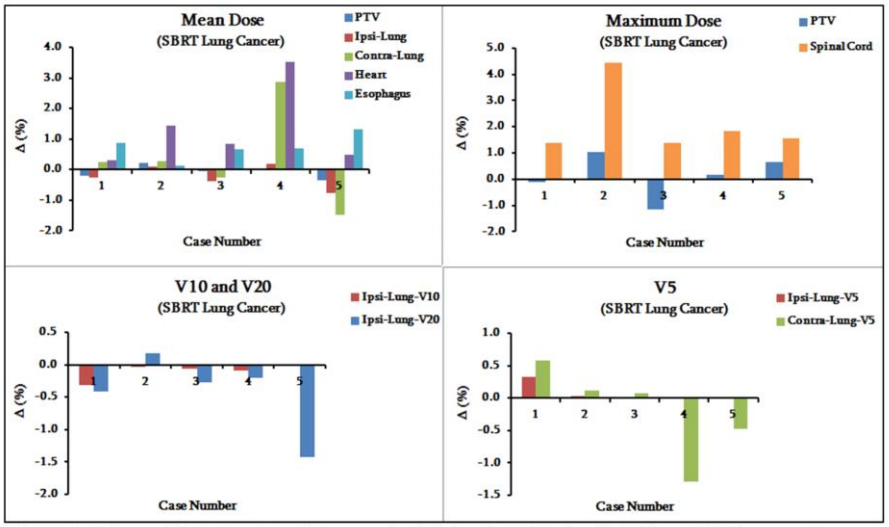

FIG. 2: Relative difference (Δ) in dosimetric results between the AXB_D$_w$ and AXB_D$_m$ plans for 5 different SBRT lung cases. V$_n$ means percentage volume irradiated by n Gy or more of a certain structure. The Δ is defined in Equation 1.

Rana S, Pokharel S. Dose-to-medium vs. dose-to-water: Dosimetric evaluation of dose reporting modes in Acuros XB for prostate, lung and breast cancer.

Int J Cancer Ther Oncol 2014; 2(4):020421. DOI: 10.14319/ijcto.0204.21

ESTRO School

Results for left and right breast

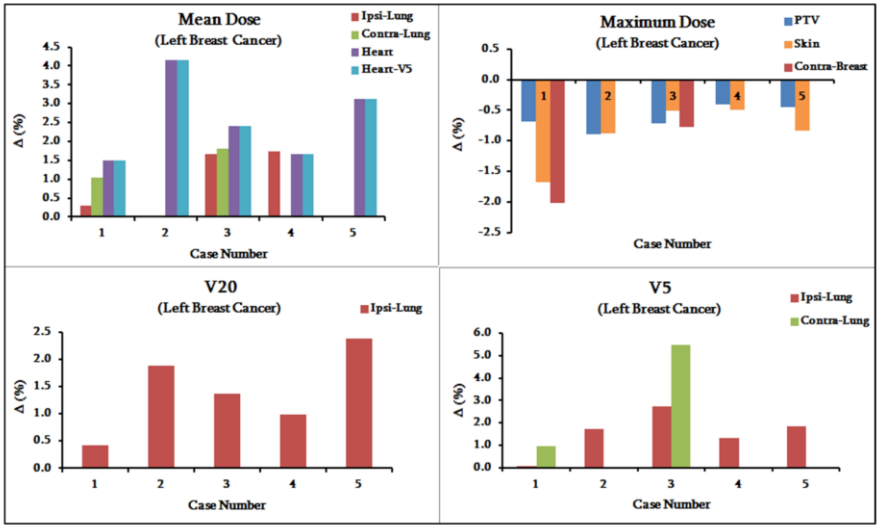

FIG. 3: Relative difference (Δ) in dosimetric results between the AXB_D$_w$ and AXB_D$_m$ plans for 5 different left breast cancer cases. V$_n$ means percentage volume irradiated by n Gy or more of a certain structure. The Δ is defined in Equation 1.

$$\Delta = \frac{D_{medium} - D_{water}}{D_{water}} \%$$

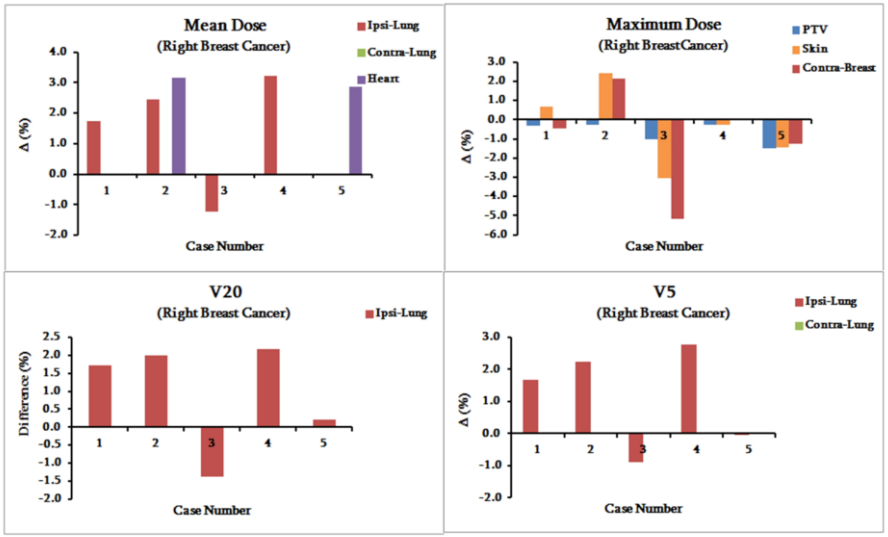

FIG. 4: Relative difference (Δ) in dosimetric results between the AXB_D$_w$ and AXB_D$_m$ plans for 5 different right breast cancer cases. V$_n$ means percentage volume irradiated by n Gy or more of a certain structure. The Δ is defined in Equation 1.

Rana S, Pokharel S. Dose-to-medium vs. dose-to-water: Dosimetric evaluation of dose reporting modes in Acuros XB for prostate, lung and breast cancer.

Int J Cancer Ther Oncol 2014; 2(4):020421. DOI: 10.14319/ijcto.0204.21

ESTRO School

In favour of using D_{water} compiled by Andreo

- Current clinical experience is mostly based on dose-to-water, hence the use of D_{water} allows direct **compliance with previous clinical experience** and with treatment planning based on analytical algorithms.
  - Doses reported in clinical trials, and therapeutic and normal-tissue tolerance criteria, are based on D_{water}.
- Reference dosimetry (beam calibration) of accelerators relies on dosimetry protocols yielding a **reference absorbed dose to water**, $D_{w,ref}$, which is used to normalize the output of the TPS.
  - This is the reference quantity at the clinic, irrespective of the type of calibration coefficient of the ionization chamber used, either in terms of absorbed dose-to-water or air-kerma.
- MCTP relies on the assumption that the codes used are '*accurate*', irrespective of the sometimes crude approximations made in the physical models of these systems, often simpler than those in general MC codes.

From P. Andreo, "Dose to 'water-like' media or dose to tissue in MV photons radiotherapy treatment planning: still a matter of debate," Phys. Med. Biol. 60, 309-337 (2015)

In favour of using D_{medium} compiled by Andreo

- Dose-to-tissue is the quantity '*inherently*' computed by MCTP. This may be of more clinical relevance than the doses on which historical clinical experience is based, which are approximate estimates of the true dose in the first place.

- The difference between D_{medium} and D_{water} for tissue-equivalent materials is **rather small** and '*is likely*' to have **minimal impact in clinical practice**.

- **Converting** D_{medium} back to D_{water} in order to overcome constraint in the D_{water} case involves '*additional complexity*' and introduces **additional uncertainty.**

From P. Andreo, "Dose to 'water-like' media or dose to tissue in MV photons radiotherapy treatment planning: still a matter of debate," Phys. Med. Biol. 60, 309-337 (2015)

Summary

- The dose discrepancy could be up to 10-15% due to the large difference between the stopping powers of water and these higher-density materials i.e. bone.
  - vertebrae, mandible, femoral heads…
- For soft tissues and lung, the dose discrepancy is only about 1 to 2%
- For air the discrepancy could be around 10-12%
  - air cavities in PTV, trachea, air cavities in intestines, rectum
  - Do we need to define air, is it OK with very low density soft tissue/water???

Slide inspired by N Reynaerts from his ESTRO 35 lecture

Clinical Significance – MV energies

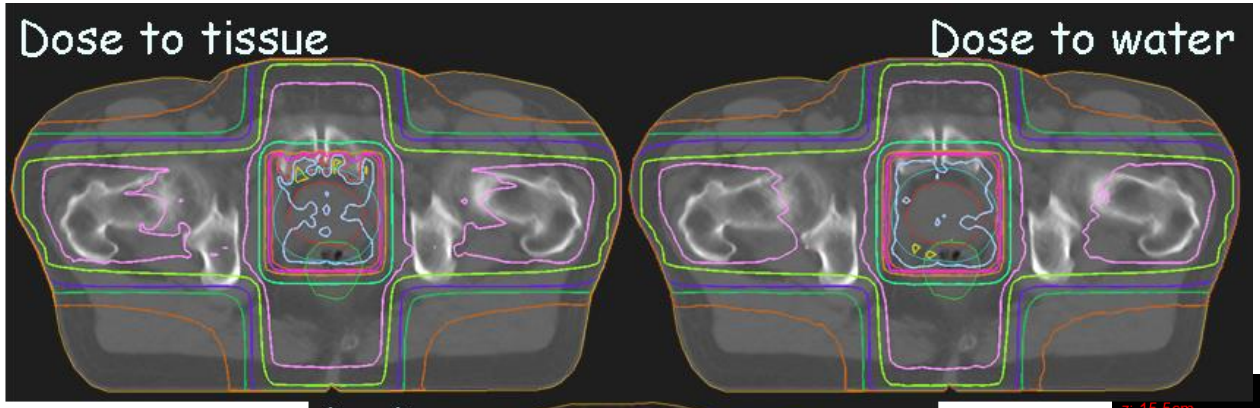

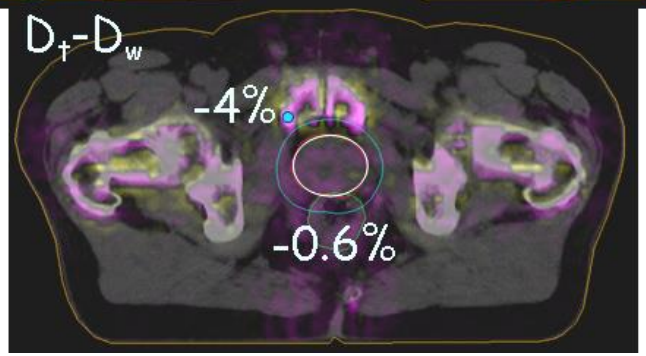

All materials either assigned to tissues or scaled water

Air cavity either air of lung(thin water)

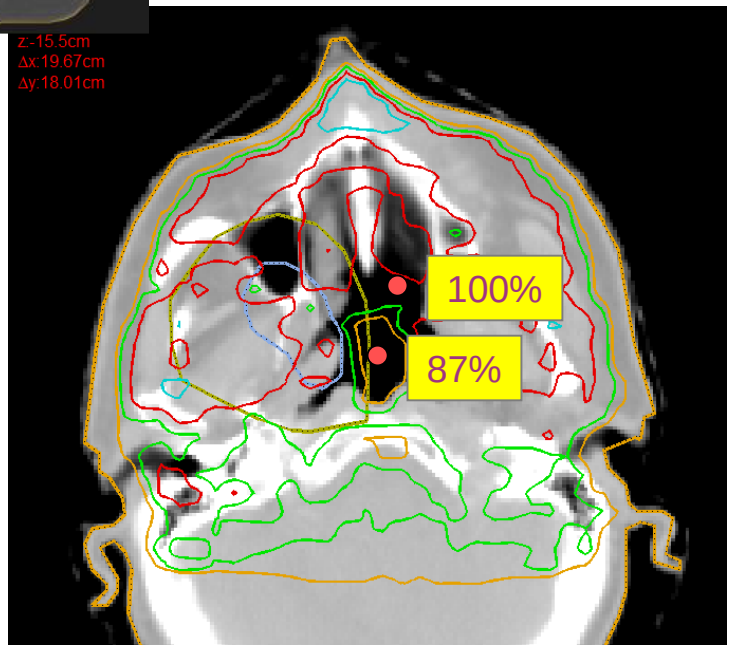

Knöös et al PMB 51 2006

Scaled water = dose to medium!

Monte Carlo simulation with different type of bone

Dose to bone, dose to bone converted using $\left(\frac{S_{el}}{\rho}\right)_{water,medium}$, dose to dense water

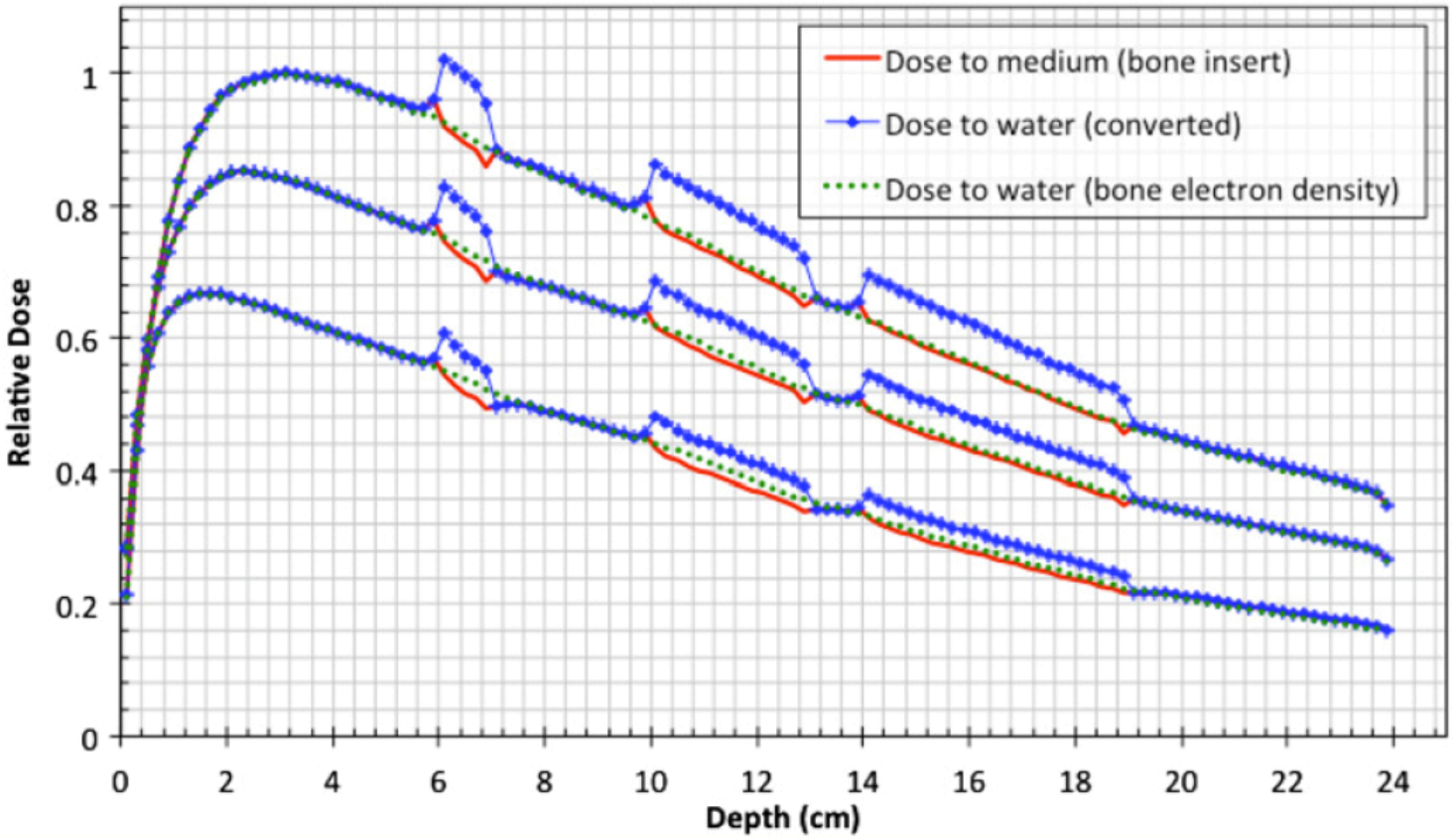

18 MV

10 MV

6 MV

Ma and Li, 2011

Conclusions

The results from this study show that contrary to the popular perception, conventional photon dose calculation using water with relative electron densities produces dose distributions that are much closer to Monte Carlo calculated dose-to-medium distributions than to dose-to-water distributions converted using mass stopping-power ratios of water to bone…

… explained by the fact that the photon dose deposition depends mainly on the electron density since the predominant mode of interaction is Compton scattering for photon beams of radiotherapy interest.

Thus, the dose deposition scaled based on the relative electron density is effectively dose to medium (with the corresponding electron density), as implemented in many commercial treatment planning dose algorithms in spite of their initial intentions or claimed applications.

Ma and Li, 2011

Conclusions

- Probably best to use D_{medium} when available
  - Too many uncertainties involved if converted to D_{water}
    - In Medium and in mass stopping power
- For most tissues – no big difference between the two dose reporting modes
- Scaled water gives result very similar to dose to medium models.
- Avoid air (and bone) in evaluation and optimisation processes
  - Large difference in mass stopping power, about 10 %

References

- J. V. Siebers, P. J. Keall, A. E. Nahum and R. Mohan, "Converting absorbed dose to medium to absorbed dose to water for Monte Carlo based photon beam dose calculations," Phys. Med. Biol. 45, 983-995 (2000).
- A. Brahme, "Current algorithms for computed electron beam dose planning," Radiother. Oncol. 3, 347-362 (1985).
- I. J. Chetty, B. Curran, J. E. Cygler, J. J. DeMarco, G. Ezzell, B. A. Faddegon, I. Kawrakow, P. J. Keall, H. Liu, C. M. Ma, D. W. Rogers, J. Seuntjens, D. Sheikh-Bagheri and J. V. Siebers, "Report of the AAPM Task Group No. 105: Issues associated with clinical implementation of Monte Carlo-based photon and electron external beam treatment planning," Med. Phys. 34, 4818-4853 (2007).
- P. Andreo, "Dose to 'water-like' media or dose to tissue in MV photons radiotherapy treatment planning: still a matter of debate," Phys. Med. Biol. 60, 309-337 (2015).
- C. M. Ma and J. Li, "Dose specification for radiation therapy: dose to water or dose to medium?," Phys. Med. Biol. 56, 3073-3089 (2011).
- A. Ahnesjo, M. Saxner and A. Trepp, "A pencil beam model for photon dose calculation," Med. Phys. 19, 263-273 (1992).
- T. Knöös, E. Wieslander, L. Cozzi, C. Brink, A. Fogliata, D. Albers, H. Nystrom and S. Lassen, "Comparison of dose calculation algorithms for treatment planning in external photon beam therapy for clinical situations," Phys. Med. Biol. 51, 5785-5807 (2006).

References - continue

- W. Ulmer, J. Pyyry and W. Kaissl, "A 3D photon superposition/convolution algorithm and its foundation on results of Monte Carlo calculations," Phys. Med. Biol. 50, 1767-1790 (2005).
- A. Van Esch, L. Tillikainen, J. Pyykkonen, M. Tenhunen, H. Helminen, S. Siljamaki, J. Alakuijala, M. Paiusco, M. Lori and D. P. Huyskens, "Testing of the analytical anisotropic algorithm for photon dose calculation," Med. Phys. 33, 4130-4148 (2006).
- I. Kawrakow, M. Fippel and K. Friedrich, "3D electron dose calculation using a Voxel based Monte Carlo algorithm (VMC)," Med. Phys. 23, 445-457 (1996).
- T. R. Mackie, J. W. Scrimger and J. J. Battista, "A convolution method of calculating dose for 15-MV x rays," Med. Phys. 12, 188-196 (1985).
- T. R. Mackie, A. F. Bielajew, D. W. O. Rogers and J. J. Battista, "Generation of photon energy deposition kernels using the EGS Monte Carlo code," Phys. Med. Biol. 33, 1 (1988).
- N. Papanikolaou, T. R. Mackie, C. Meger-Wells, M. Gehring and P. Reckwerdt, "Investigation of the convolution method for polyenergetic spectra," Med. Phys. 20, 1327-1336 (1993).
- W. Lu, G. H. Olivera, M.-L. Chen, P. J. Reckwerdt and T. R. Mackie, "Accurate convolution/superposition for multi-resolution dose calculation using cumulative tabulated kernels," Phys. Med. Biol. 50, 655-680 (2005).
- Kijewski, P.K., Bjarngard, B.E., 1978. The use of computed tomography data for radiotherapy dose calculations. Int. J. Radiat. Oncol. Biol. Phys. 4, 429–435

References - continue

- A. Ahnesjo, "Collapsed cone convolution of radiant energy for photon dose calculation in heterogeneous media," Med. Phys. 16, 577-592 (1989).
- M. Miften, M. Wiesmeyer, S. Monthofer and K. Krippner, "Implementation of FFT convolution and multigrid superposition models in the FOCUS RTP system," Phys. Med. Biol. 45, 817-833 (2000).
- M. Fippel, "Fast Monte Carlo dose calculation for photon beams based on the VMC electron algorithm," Med. Phys. 26, 1466-1475 (1999).
- C. M. Ma, J. S. Li, T. Pawlicki, S. B. Jiang, J. Deng, M. C. Lee, T. Koumrian, M. Luxton and S. Brain, "A Monte Carlo dose calculation tool for radiotherapy treatment planning," Phys. Med. Biol. 47, 1671-1689 (2002).
- T. Knöös, M. Nilsson, L. Ahlgren, 1986, A method for conversion of Hounsfield number to electron density and prediction of macroscopic pair production cross-sections, Radioth Oncol, 5, 337-345.
- Ojala J. The accuracy of the Acuros XB algorithm in external beam radiotherapy – a comprehensive review. Int J Cancer Ther Oncol. 2014;2(4):020417.
- Ojala JJ, Kapanen MK, Hyödynmaa SJ, Wigren TK, Pitkänen MA. Performance of dose calculation algorithms from three generations in lung SBRT: comparison with full Monte Carlo-based dose distributions. J Appl Clin Med Phys. 2014;15(2):4662–80.

References - continue

- Fogliata A, Nicolini G, Clivio A, Vanetti E, Cozzi L. Dosimetric evaluation of Acuros XB Advanced Dose Calculation algorithm in heterogeneous media. Radiat Oncol. 2011;6:82.
- Fogliata A, Nicolini G, Clivio A, Vanetti E, Cozzi L. On the dosimetric impact of inhomogeneity management in the Acuros XB algorithm for breast treatment. Radiat Oncol 2011 6:103.
- Rana S and Pokharel S. Dose-to-medium vs. dose-to-water: Dosimetric evaluation of dose reporting modes in Acuros XB for prostate, lung and breast cancer. Int J Cancer Ther Oncol 2014;2(4):020421.
- J. Y. Huang, D. Eklund, N. L. Childress, R. M. Howell, D. Mirkovic, D. S. Followill and S. F. Kry, "Investigation of various energy deposition kernel refinements for the convolution/superposition method," Med. Phys. 40, 121721 (2013).
- Ojala J, Kapanen M, Sipilä P, Hyödynmaa S, Pitkänen M. The accuracy of Acuros XB algorithm for radiation beams traversing a metallic hip implant - comparison with measurements and Monte Carlo calculations. J Appl Clin Med Phys. 2014;15(5)5:4912–27.
- Rana S, Rogers K, Lee T, Reed D, Biggs C. Verification and dosimetric impact of Acuros XB algorithm for stereotactic body radiation therapy (SBRT) and RapidArc planning for non-small-cell lung cancer (NSCLC) patients. Int J Med Phys Clin Eng Radiat Oncol. 2013;2:6–14.

Thanks

Discussion on independent monitor unit calculations

Brendan McClean and Tommy Knöös

Faculty

Participants

Discussion topics

- An **independent calculation of monitored units** (iMUc) is supposed to verify that the treatment planning system (TPS) is an accurate part of the complex system for the delivery of a safe and effective treatment.
- Planning systems are subjected to rapid evolution, they implement new complex technologies and therefore it is **not possible to verify all potential future clinical usage** in advance.
- Many factors, such as layout of anatomic structures, positioning of a patient, factors related to an accelerator (a dose calibration and mechanic parameters) **cause random and systematic failures** in a dose delivery.
- The source of some problems can be also caused by the **system databases and relating information transfer**; and the TPS containing besides other things other dose calculation algorithms.
- **Legislation** requires iMUc in many countries.

Questions?

- If one do PSQA measurements – is iMUc necessary?
- What tolerances should we have?
  - What frequency of alarms is acceptable? Alarm fatigue!!!
- Can a supervisor perform a iMUc?

When things go wrong

- Delivery of IMRT without MLC movements – would iMUc caught it?
- Scaling the plan twice with the prescription dose – would iMUc caught it?
- Mix of hard and soft wedges – would iMUc caught it?
- Linac recalibrated 5% wrong – would iMUc caught it?

Methods for comparison

Tommy Knöös

Learning objectives

- Comparisons
- Evaluation
- Dose difference
- Gamma evaluation
- Discussions

Contents

- Point by point
- Distributions
- Examples

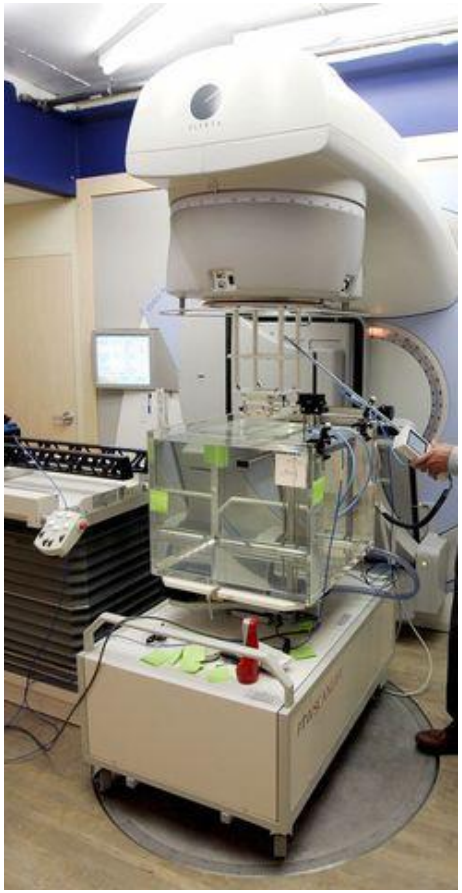

Comparisons between measurement and calculations

- Look at differences: do we use a substraction, a division (or ratio), in gray or in %?
  - Then, in % of what?
    - in % of max of beam dose or other “global” point/dose?
    - in % of “local” dose?
- What are the data that we have?
  - point dose values? How many?
  - Curves or measurement along a liner i.e. PDD, profiles…
  - 2D distributions e.g. from film or 2D-array system
  - 3D distributions?
- What are the criteria that we should use?
- Should we reject all, if only a few points exceed the criterion in a specified case?
- Is it OK with the same criteria for the whole distribution?
- Is it reasonable to have the same criteria in simple and in very complex cases?

How to express deviations?

Calculated and measured dose distributions can be compared according to

1) to the **local dose** value

$$d\%(i,B) = 100 \cdot \left(D_{calc}(i,B) - D_{meas}(i,B)\right) / D_{meas}(i,B)$$

2) to the dose at a **specific point inside the beam** under consideration

$$d\%(i,B) = 100 \cdot \left(D_{calc}(i,B) - D_{meas}(ref,B)\right) / D_{meas}(ref,B)$$

this is proposed in the IAEA TRS-1583

3) to the **dose in a reference field**

$$d\%(i,B) = 100 \cdot \left(D_{calc}(i,B) - D_{meas}(ref,R)\right) / D_{meas}(ref,R)$$

B – present beam, R – Ref beam

Suggestion

- Absorbed dose is given per monitor unit
- Dose is normalised to a reference field (output normalised)

$$d(i) = \frac{\left[\frac{D_c(i)/M_c}{D_c(ref)/M_c}\right]}{\left[\frac{D_m(i)/M_m}{D_m(ref)/M_m}\right]}$$

- ESTRO Booklet n°7 gives that monitor units are implicitly checked too
- Get rid of any fluctuation in the treatment output.

C.f. Anders lecture on MU calc in TPS

Criteria depending on position in photon beam

Points along the central axis of the beam beyond the depth of dose maximum: **low dose gradient area**.

Points on and off the central axis in the build-up and penumbra region. This region includes also points in the proximity of interfaces: **high dose gradient area**.

Points **inside** the beam (*e.g.*, inside 80% of the geometrical beam) but off the central axis: **low dose gradient area**.

Points **outside** the geometrical beam or below shielding blocks, jaws, MLC, *etc*… where the dose is lower than, for instance, 7% of the central axis dose at the same depth: **low dose gradient area**.

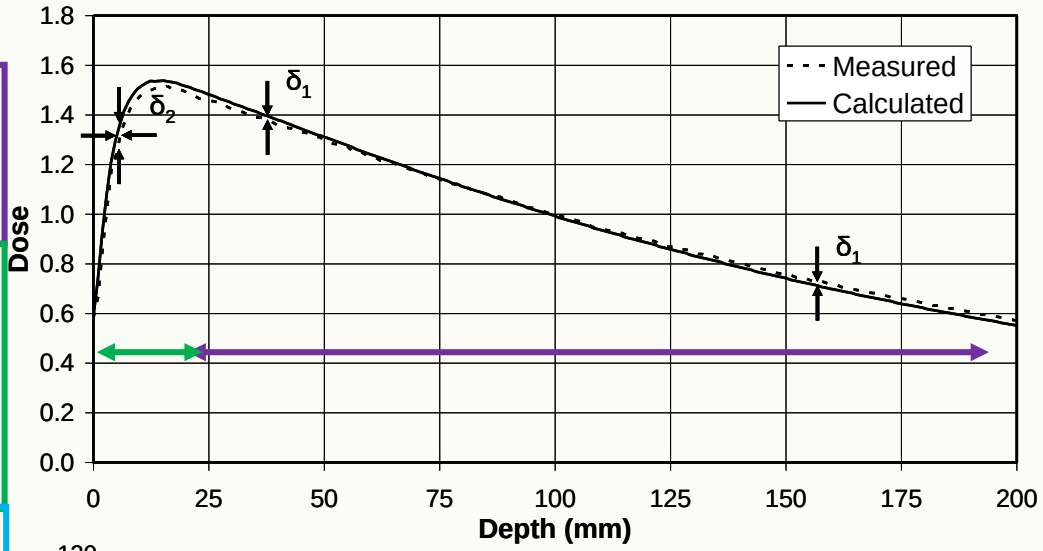

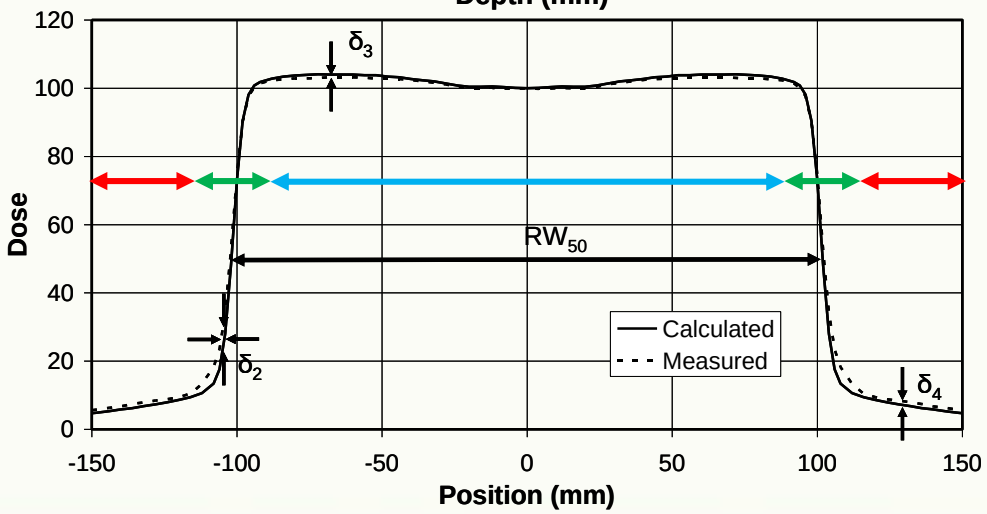

Adopted from Venselaar, 2001

Tolerances δ for the local dose deviation d%(i)

Region		Homogenous, simple geometry	Complex geometry (wedge, inhomogeneity, asymmetry, blocks / MLC)	More complex geometries****
δ_1	*Central beam axis data* – high dose, low dose gradient	2%	3%	4%
δ_2*	*Build-up region of central axis beam, penumbra region of the profiles* - high dose, high dose gradient	2 mm or 10%	3 mm or 15%	3 mm or 15%
δ_3	*Outside central beam axis region* - high dose, low dose gradient	3%	3%	4%
δ_4**	*Outside beam edges* – low dose, low dose gradient	30% (3%)	40% (4%)	50% (5%)
RW_{50} ***	***Radiological width* – high dose, high dose gradient.**	2 mm or 1%	2 mm or 1%	2 mm or 1%
$\delta_{50\text{-}90}$	***Beam fringe* – high dose, high dose gradient**	2 mm	3 mm	3 mm

(normalized at central axis same depth)

Adopted from Venselaar, 2001

Confidence limit

Statistical approach

The confidence limit is based on the determination of the mean deviation between calculation and measurement for a number of data points for comparable situations, and the standard deviation (1 SD) of the deviation, and is defined as:

$$\Delta = |\text{mean deviation}| + k * SD$$

k=1.5 - In later publications it was suggested to use a factor of 2, instead of the value of 1.5

(Venselaar *et al*., Radiother. Oncol. 60, 191–201, 2001)

Tolerances δ for the local dose deviation d%(i)

Region		Homogenous, simple geometry	Complex geometry (wedge, inhomogeneity, asymmetry, blocks / MLC)	More complex geometries****
δ_1	*Central beam axis data* – high dose, low dose gradient	2%	3%	4%
δ_2*				
δ_3				
δ_4**				
RW_{50} ***				1%
$\delta_{50\text{-}90}$	***Beam fringe*** **– high dose, high dose gradient**	2 mm	3 mm	3 mm

The tolerances, if applied to the confidence limit, can be exceeded in two ways; either because the mean deviation of all points is too large
or because a few data points show extreme deviations and therefore the SD is too large.

(normalized at central axis same depth)

Adopted from Venselaar, 2001

EXAMPLES – POINT AND LINE MEASUREMENTS (N=1)

Open field depth doses 6 MV

Depth dose curves normalized to the output at 10 cm depth of the 10cm x 10cm field.

Ratio, d(i), between calculated and measured dose per monitor unit values

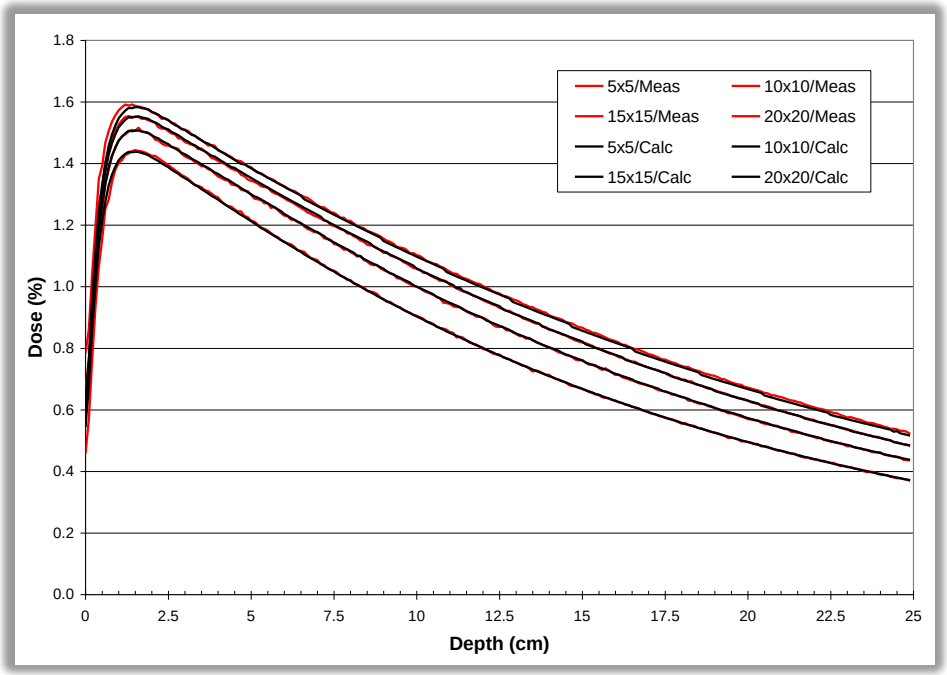

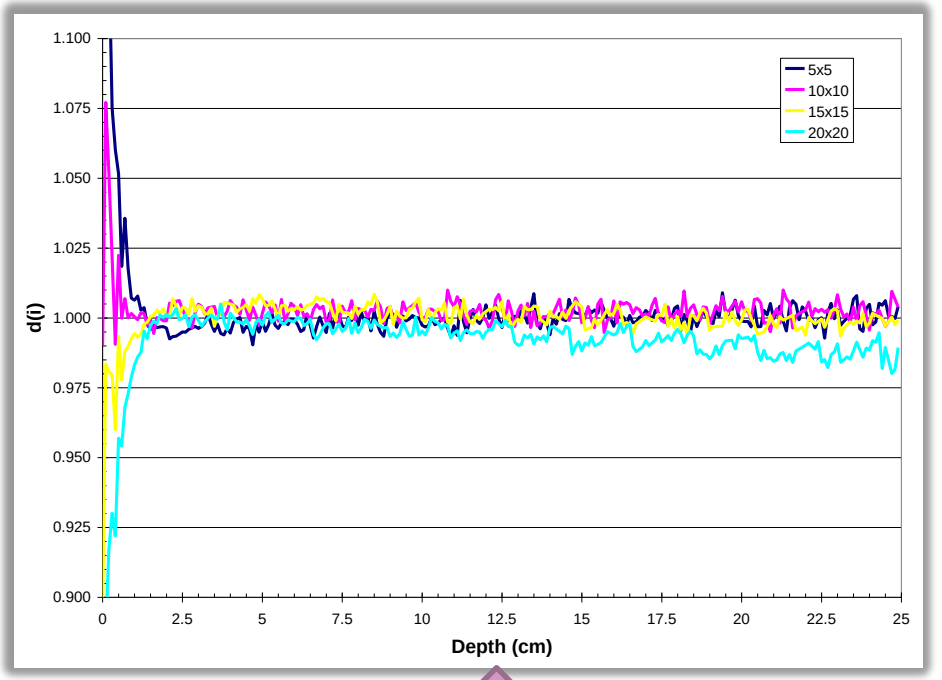

$$d(i) = \frac{\frac{D_c(i)/M_c}{D_c(ref)/M_c}}{\frac{D_m(i)/M_m}{D_m(ref)/M_m}}$$

ESTRO School

Evaluation of PDDs

Build-up region (0-2 cm)	Field size	Field size	Field size	Field size
Tol. 10 %	5x5 cm^2	10x10 cm^2	15x15 cm^2	20x20 cm^2
Average deviation (%)	3.7	0.7	- 1.3	- 3.7
Standard deviation (%)	6.2	2.1	2.4	5.1
Confidence limit (%)	**13.0**	3.9	5.0	**11.3**
Remaining curve (2-25 cm)				
Tol. 2 %	5x5 cm^2	10x10 cm^2	15x15 cm^2	20x20 cm^2
Average deviation (%)	- 0.1	0.2	0.1	- 0.6
Standard deviation (%)	0.3	0.3	0.3	0.5
Confidence limit (%)	0.5	0.7	0.6	1.4

Statistical evaluation of the deviations between calculated and measured data of the four 6 MV depth dose curves. Note that the confidence limits for the 5x5 cm2 and 20x20 cm2 do not fulfill the recommended 10% accuracy requirement of dose calculations of a TPS in the build-up region.

Dose and monitor unit calculation

Data from point measurements using an ionization chamber positioned at 20 cm depth along the central beam axis in a large water phantom, source-skin distance 90 cm, irradiated with a beam of 18 MV x-rays.

		Measured			Calculated			
	Type	Dose (Gy)	MU	(Dose/MU) meas	Dose	MU	(Dose/ MU) calc	*d(i) /d%(i)*
5x5	Open	0.557	100	0.00557	1.00	184.78	0.00541	0.971 / -2.9%
	60º Wedge	0.152	100	0.00152	1.00	677.73	0.00148	0.969 / -3.1%
10x10	Open	0.614	100	0.00614	1.00	165.46	0.00604	0.984 / -1.6%
	60º Wedge	0.173	100	0.00173	1.00	579.46	0.00173	1.000 / 0.0%
20x20	Open	0.673	100	0.00673	1.00	149.80	0.00668	0.993 / -0.7%
	60º Wedge	0.197	100	0.00197	1.00	527.66	0.00189	0.964 / -3.6%
30x30	Open	0.694	100	0.00694	1.00	145.35	0.00688	0.991 / -0.9%
	60º Wedge	0.206	100	0.00206	1.00	509.46	0.00196	0.951 / -4.9%
5x20	Open	0.597	100	0.00597	1.00	168.16	0.00595	0.997 / -0.3%
	60º Wedge	0.167	100	0.00167	1.00	593.02	0.00169	1.010 / +1.0%
20x5	Open	0.589	100	0.00589	1.00	172.77	0.00579	0.983 / -1.7%
	60º Wedge	0.164	100	0.00164	1.00	622.97	0.00162	0.979 / -2.1%

Dose and monitor unit calculation

Data from point measurements using an ionization chamber positioned at 20 cm depth along the central beam axis in a large water phantom, source-skin distance 90 cm, irradiated with a beam of 18 MV x-rays.

		Measured			Calculated			
	Type	Dose (Gy)	MU	(Dose/MU) meas	Dose	MU	(Dose/MU) calc	%(i)
5x5	Open	0.557	100	0.00557	1.00	184.78		%
	60º Wedge	0.152	100	0.00152	1.00	677.7		-3.1%
10x10	Open	0.614	100	0.00614	1.0			0.984 / -1.6%
	60º Wedge	0.173	100	0.00173			173	1.000 / 0.0%
20x20	Open	0.673	100			.80	0.00668	0.993 / -0.7%
	60º Wedge	0.197	10			527.66	0.00189	0.964 / -3.6%
30x30	Open	0.69			1.00	145.35	0.00688	0.991 / -0.9%
	60º Wedg			00206	1.00	509.46	0.00196	0.951 / -4.9%
5x20			100	0.00597	1.00	168.16	0.00595	0.997 / -0.3%
			100	0.00167	1.00	593.02	0.00169	1.010 / +1.0%
20x5		0.589	100	0.00589	1.00	172.77	0.00579	0.983 / -1.7%
	60º Wedge	0.164	100	0.00164	1.00	622.97	0.00162	0.979 / -2.1%

Obtaining the dose/MU either by fixed MU at measurents or fixed dose at calculation!

DISTRIBUTIONS (N>1)

Methods for dose distribution comparison

- Dose distribution overlays - requires that the user interpret the differences themselves
- Dose-difference distributions - has the limitation that very large dose differences can be caused by relatively small spatial discrepancies in steep dose gradient regions
- Distance-to-agreement - has the limitation of large distances in homogeneous areas
- Quantitative comparison tools
  - Composite tool
    - Combined DTA and dose difference in a binary way
  - Gamma and similar tools - useful when a large amount of dose data needs to be reviewed quickly, such as for routine patient QA. When discrepancies are identified, the clinical impact of those discrepancies can e.g. be determined using the dose difference tool.
- No single dose comparison tool provides all of the information necessary to quantitatively evaluate or compare dose distributions.

Inspired by Low et al 2011, Med Phys

Example - Composite evaluation 3% / 3 mm

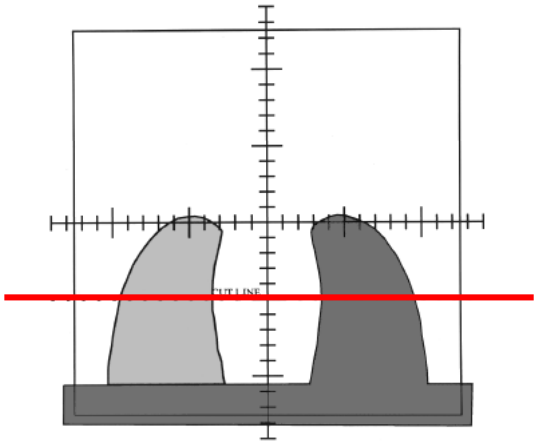

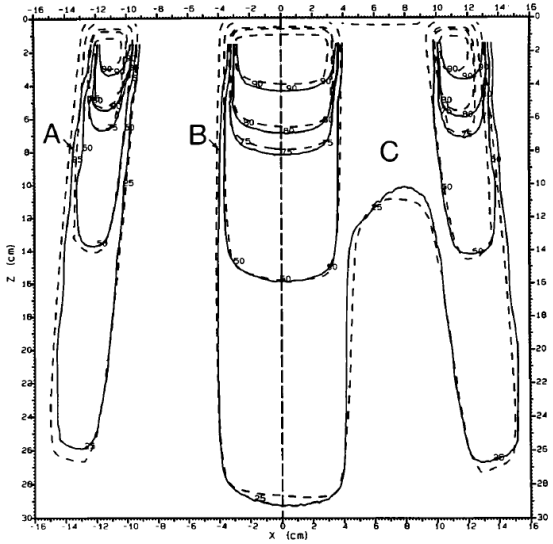

Dose diffence

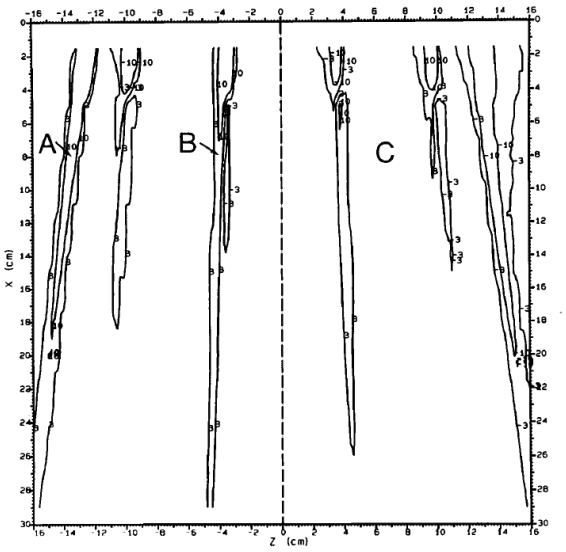

Distance to agreement

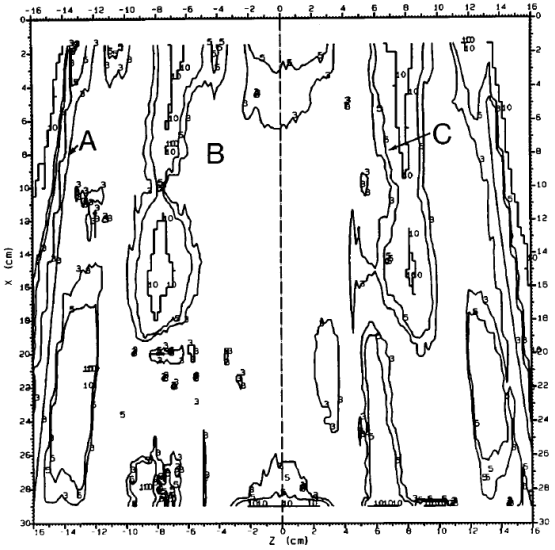

Composite

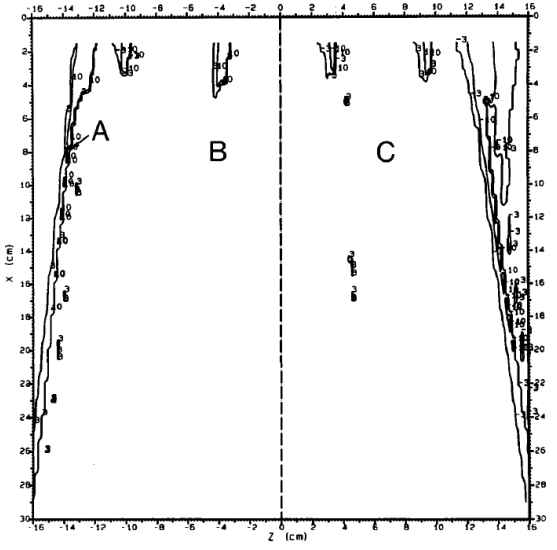

Harms et al Med Phys 1998

Gamma evaluation

- A more quantative measure
- Combining
  - Dose difference
  - Distance to agreement (DTA)
- Instead of binary composite function, use

$$\gamma(\mathbf{r}_m) = \min\{\Gamma(\mathbf{r}_m, \mathbf{r}_c)\} \forall \{\mathbf{r}_c\},$$

where

$$\Gamma(\mathbf{r}_m, \mathbf{r}_c) = \sqrt{\frac{r^2(\mathbf{r}_m, \mathbf{r}_c)}{\Delta d_M^2} + \frac{\delta^2(\mathbf{r}_m, \mathbf{r}_c)}{\Delta D_M^2}},$$

- With tolerances Δd and ΔD

Low et al Med Phys 1998

Gamma analysis

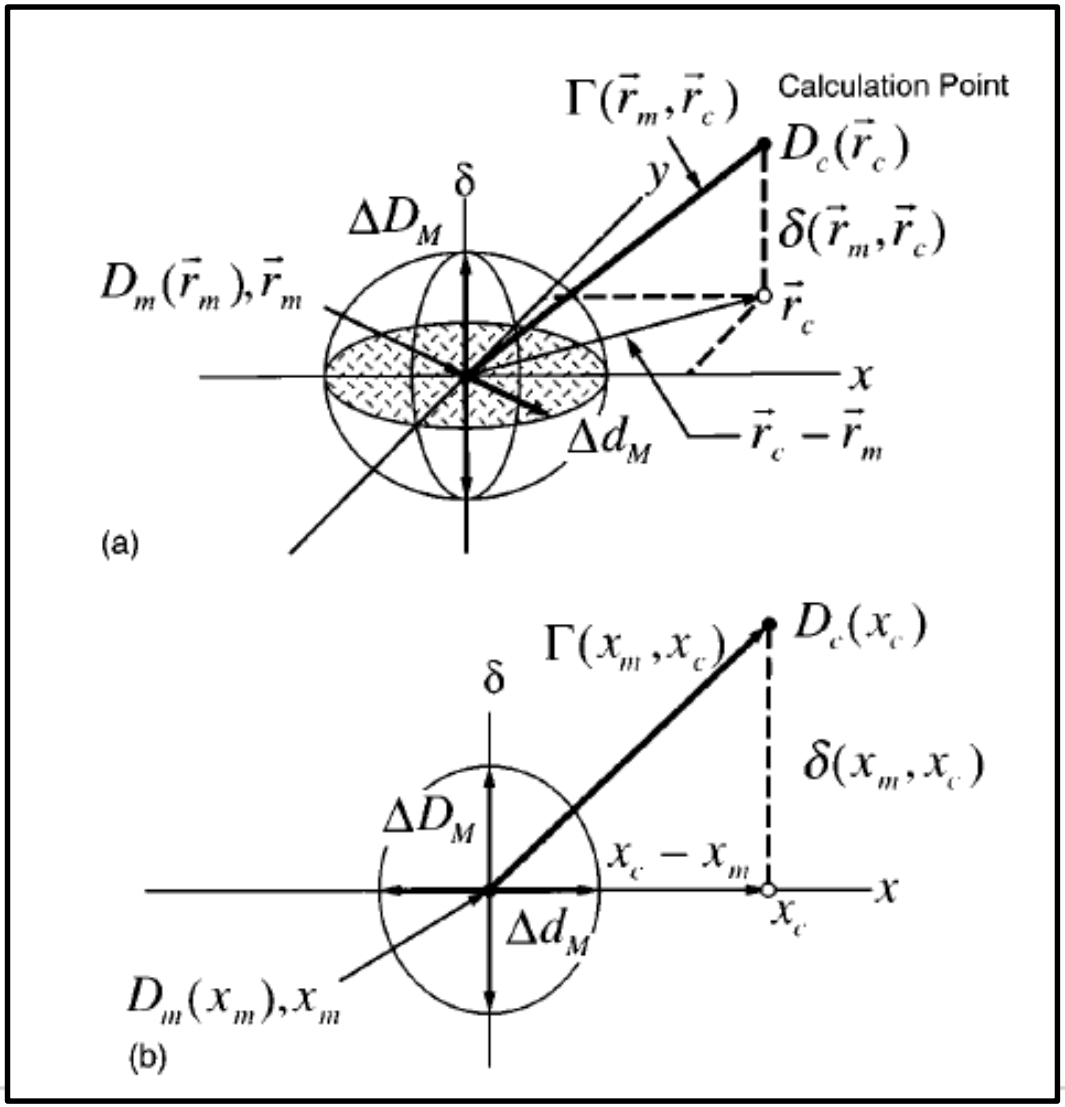

Two dimensional e.g. films or detector arrays

One dimensional e.g. Profiles and depth doses

ESTRO School

Gamma (γ) analysis in 2D (in the d-r room)

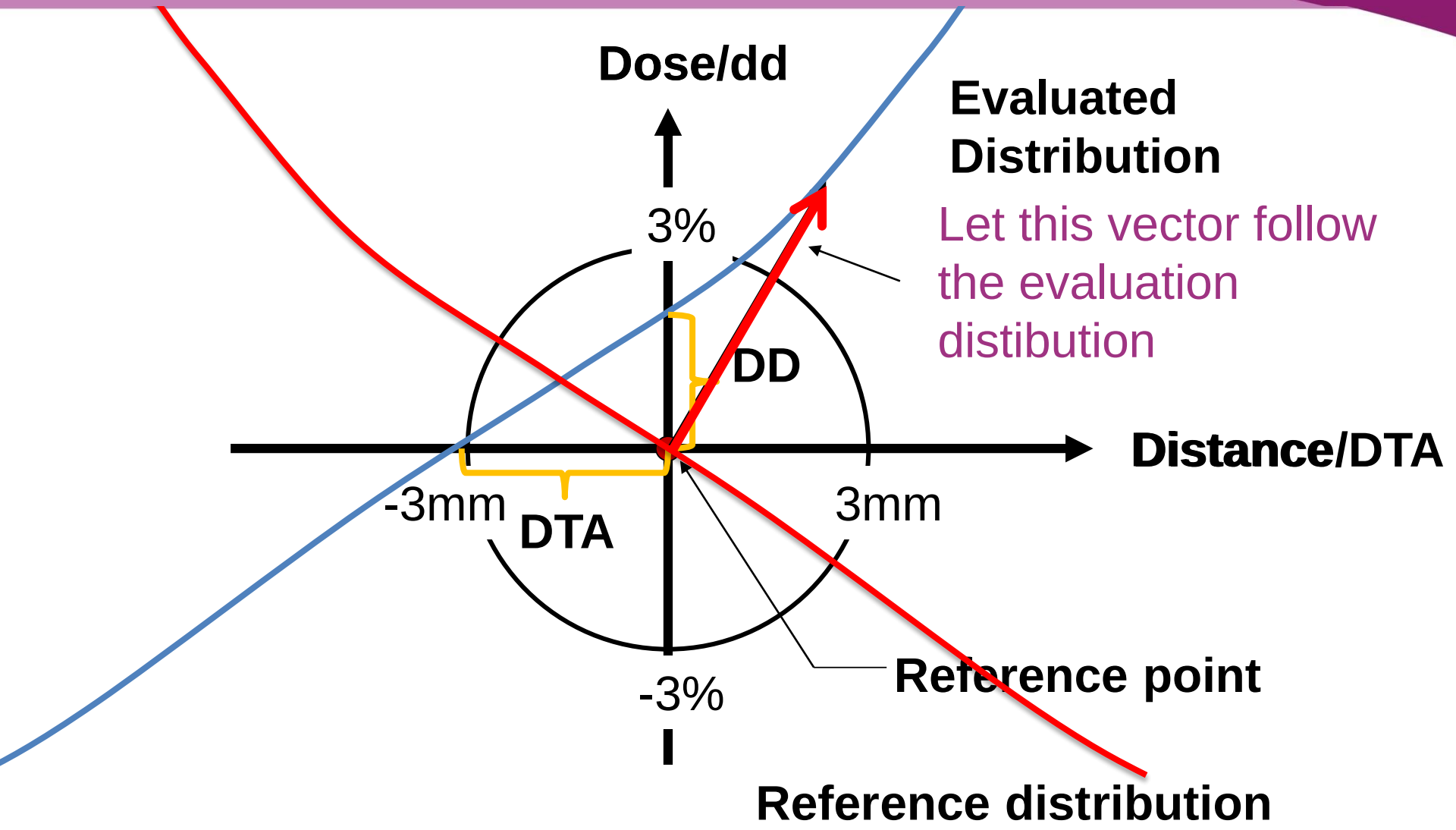

γ = min(Γ) minimum when vector is perpendiculat to the evalautation distribution

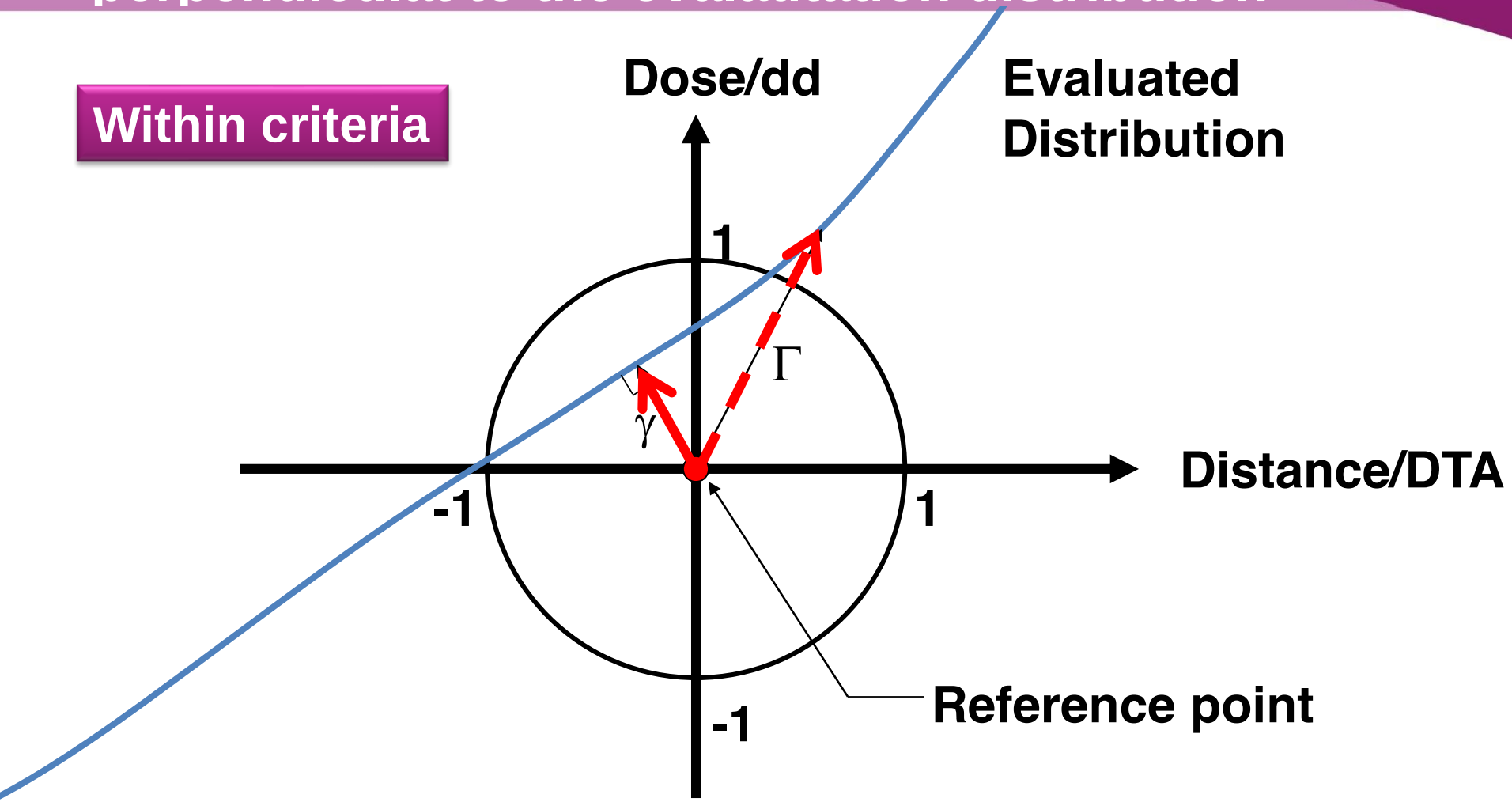

γ = min(Γ)

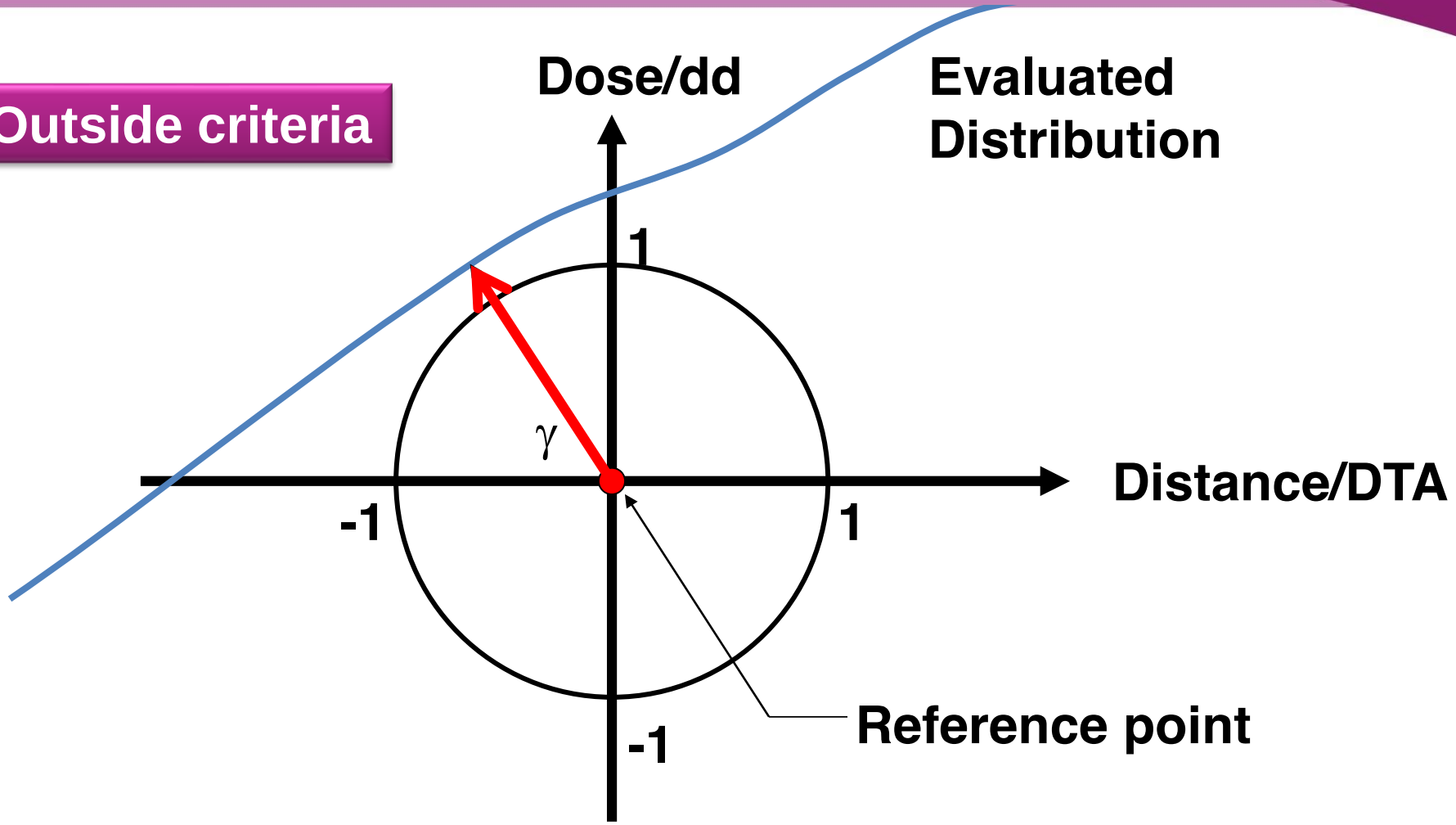
Outside criteria
Dose/dd
Evaluated
Distribution
1
γ
-1
1
Distance/DTA
-1
Reference point

Low dose gradient

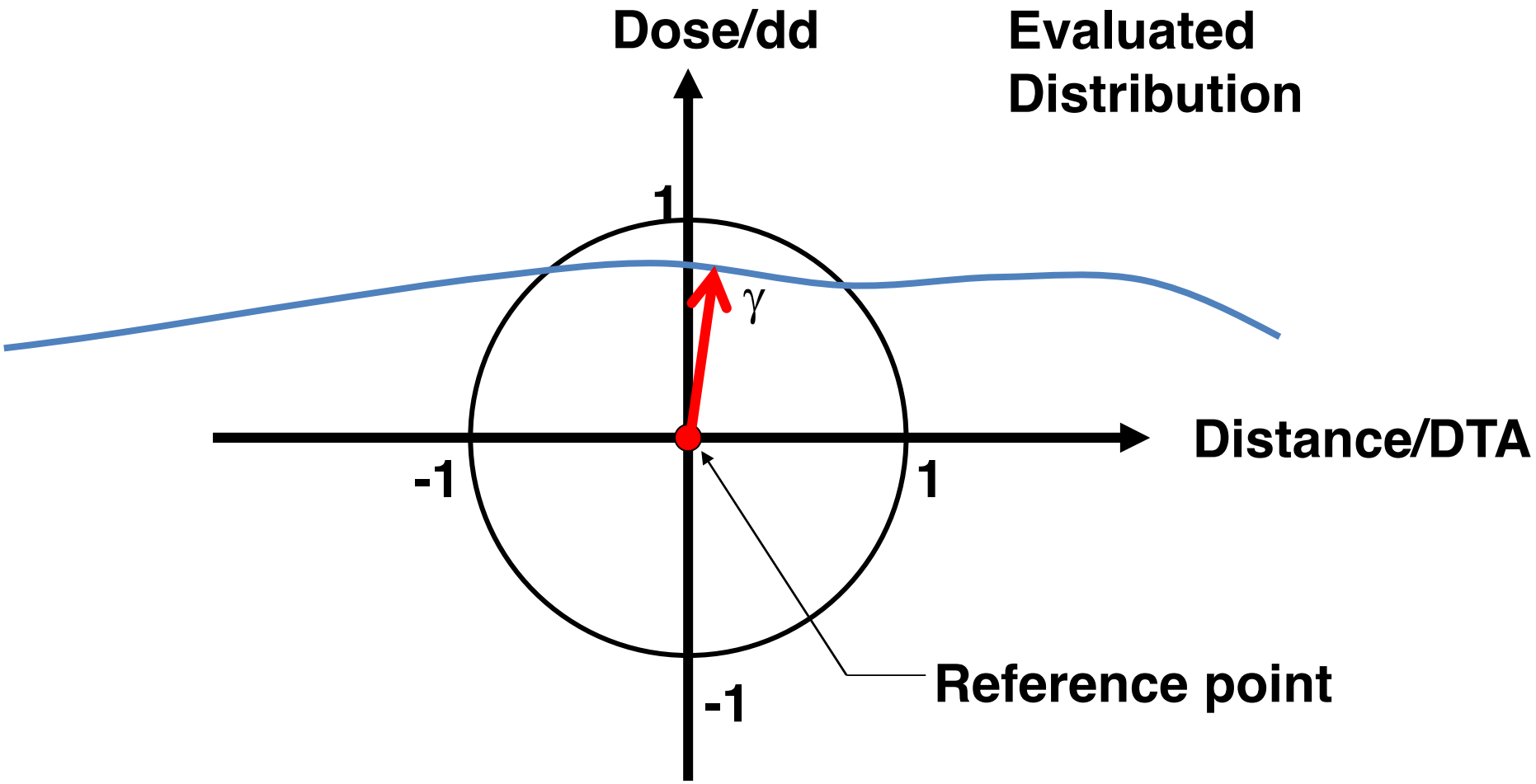

High dose gradient

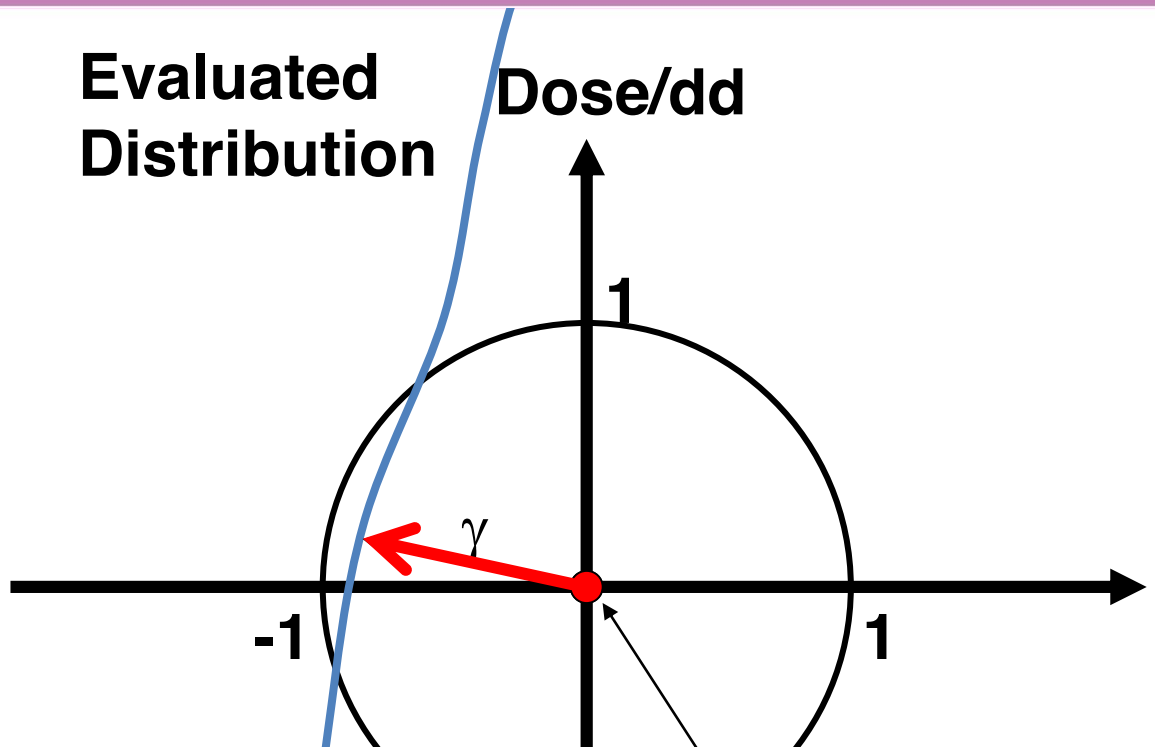

γ defaults to dose-difference and DTA in shallow and steep dose gradients, respectively

point

Gamma evaluation – value and angle

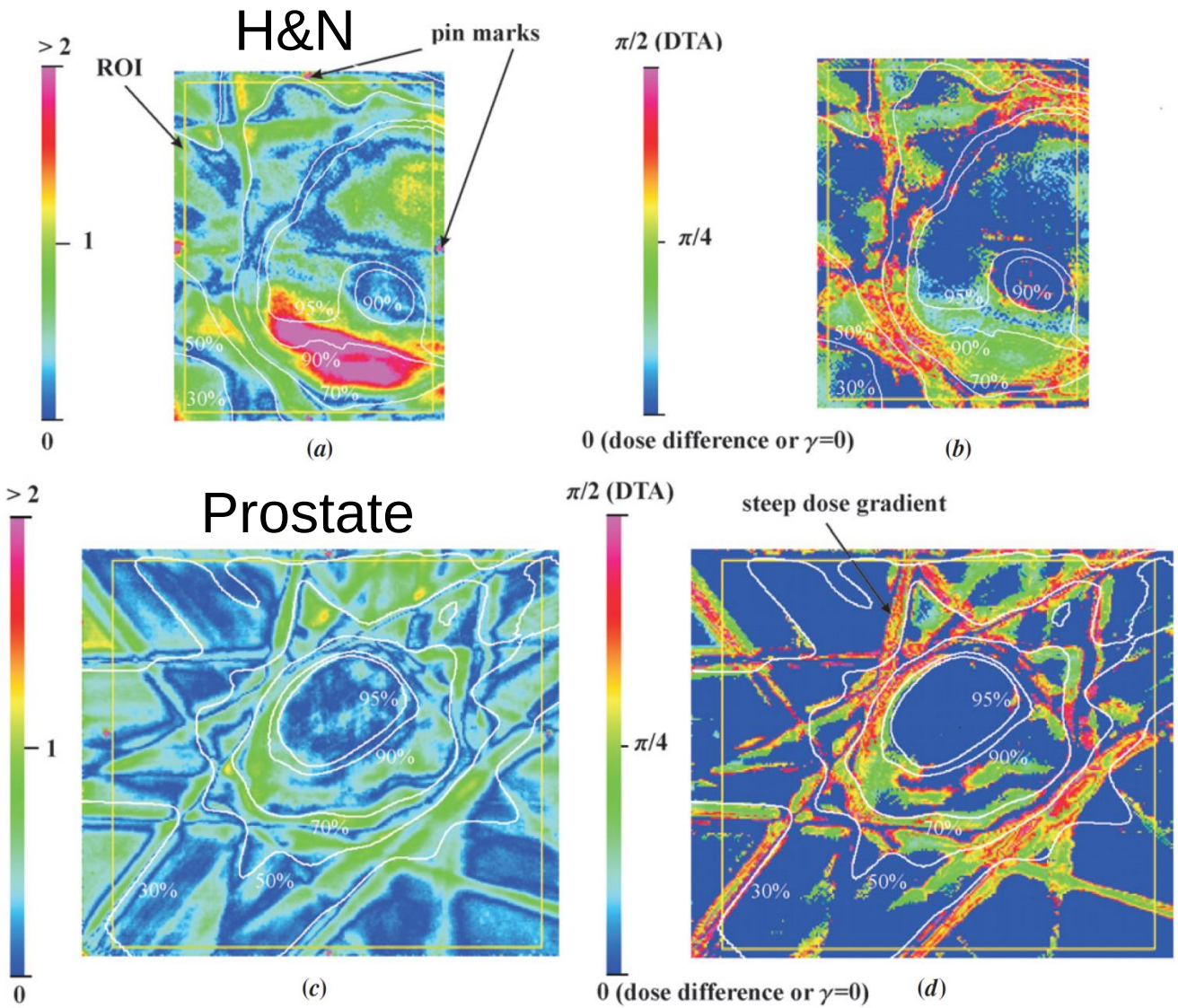

Gamma value

Gamma angle

With the angle added one can easily judge if it is DTA or dose that contributes to the deviation

White lines represent isodoses (30%, 50%, 70%, 90% and 95%) calculated with the TPS

3%/3mm

Stock et al PMB 2005

ESTRO School

EXAMPLES

Example on evaluation

Reference

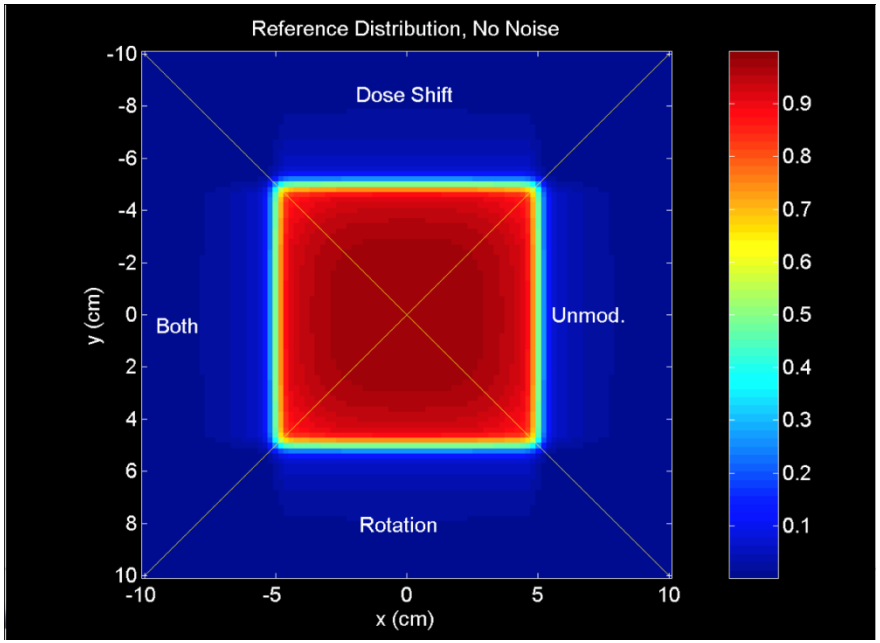

Evaluation

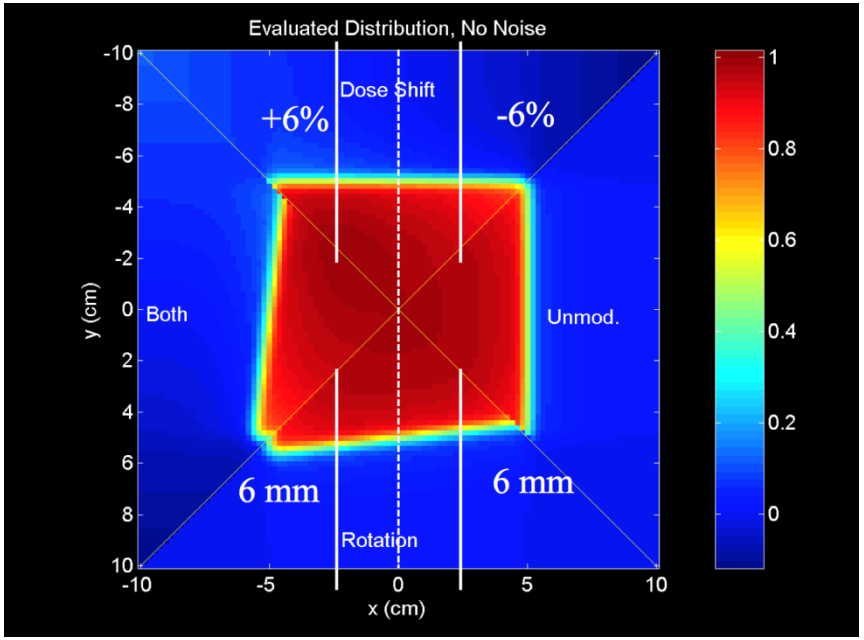

Low and Dempsey, Med Phys, 2003

ESTRO School

Analysis – Dose difference and DTA

Dose difference

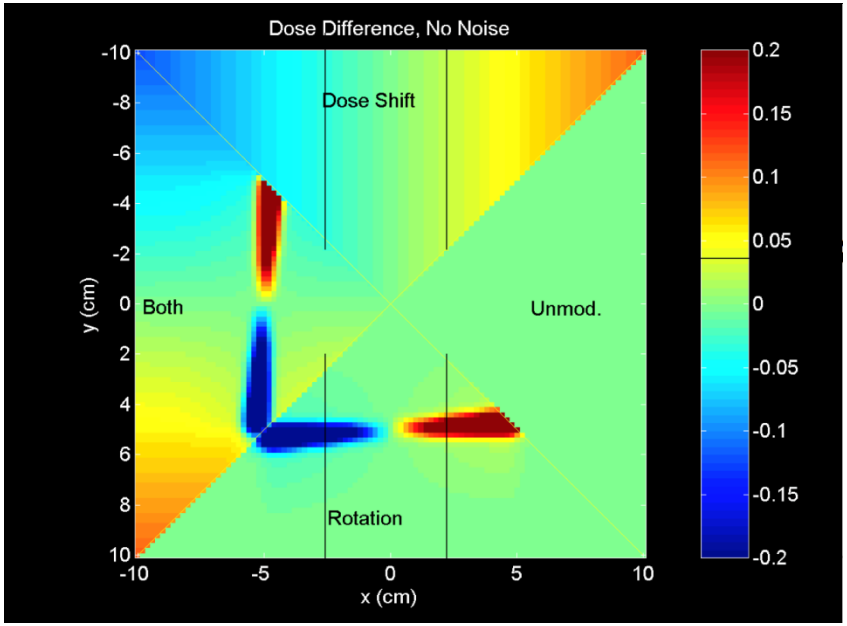

Distance to agreement

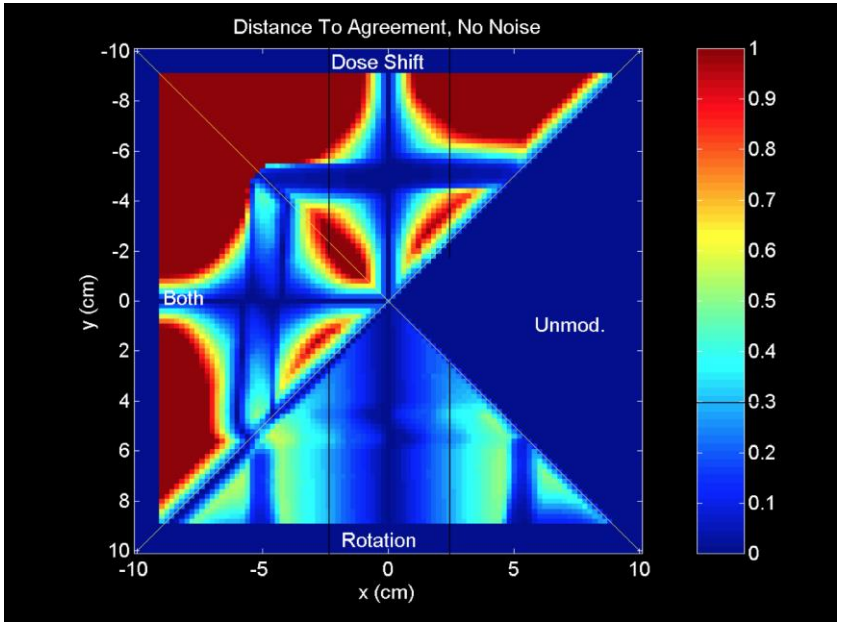

Low and Dempsey, Med Phys, 2003

Analysis – Composite and Gamma

Composite

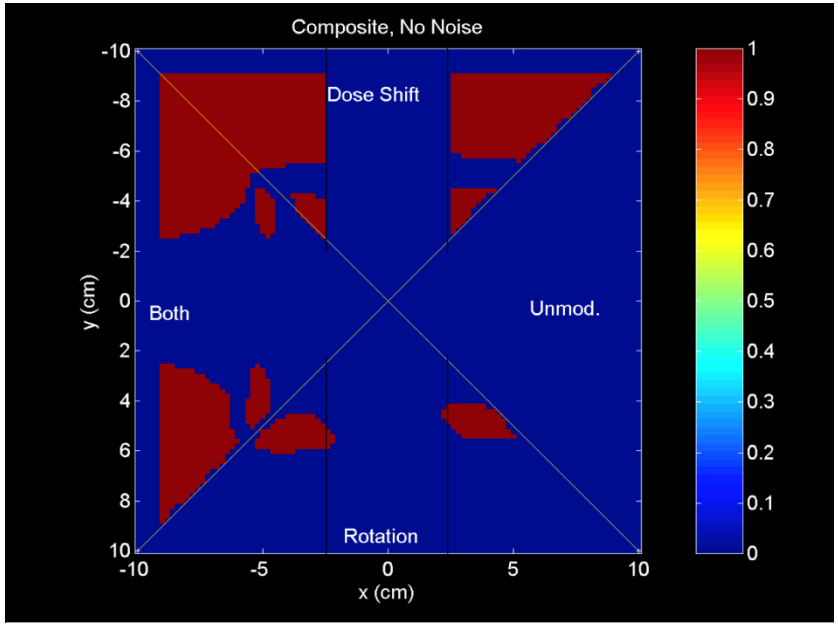

Gamma

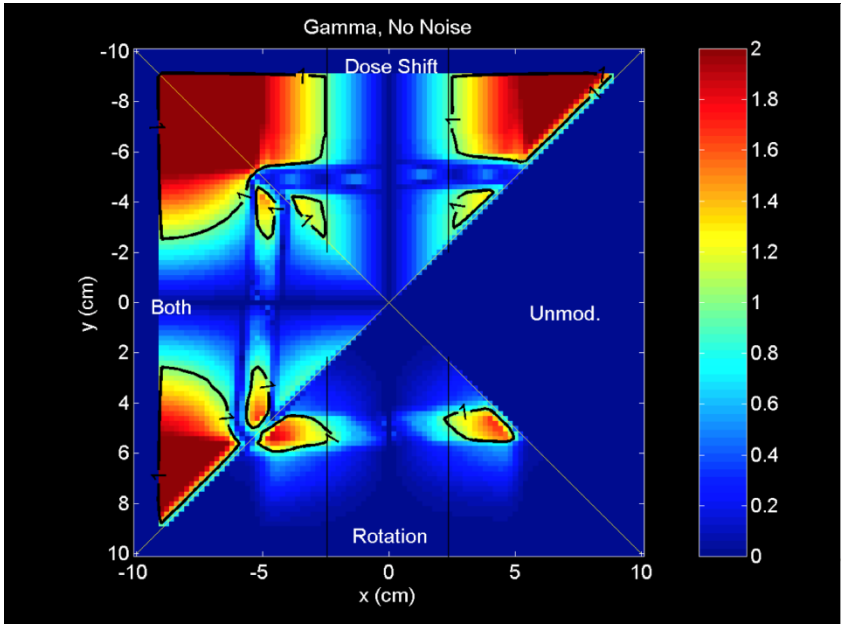

Low and Dempsey, Med Phys, 2003

Course evaluation grid - interpolation

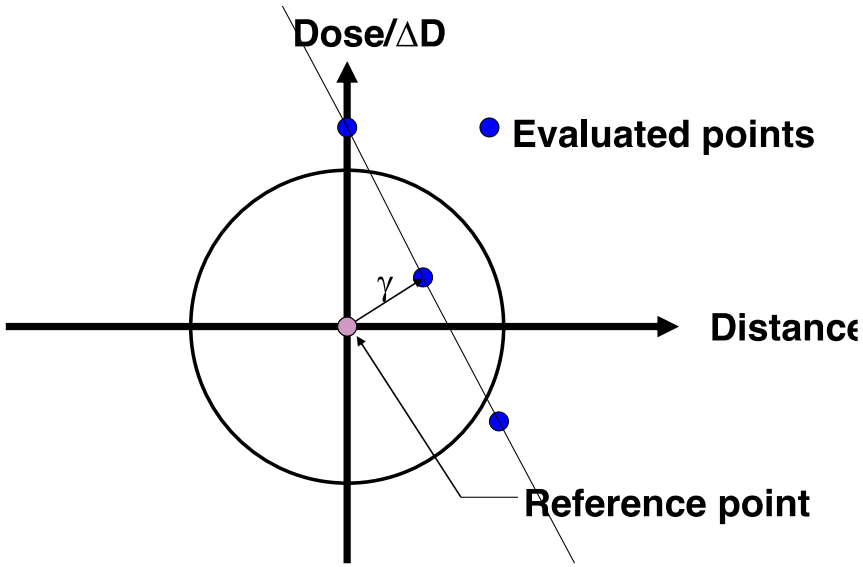

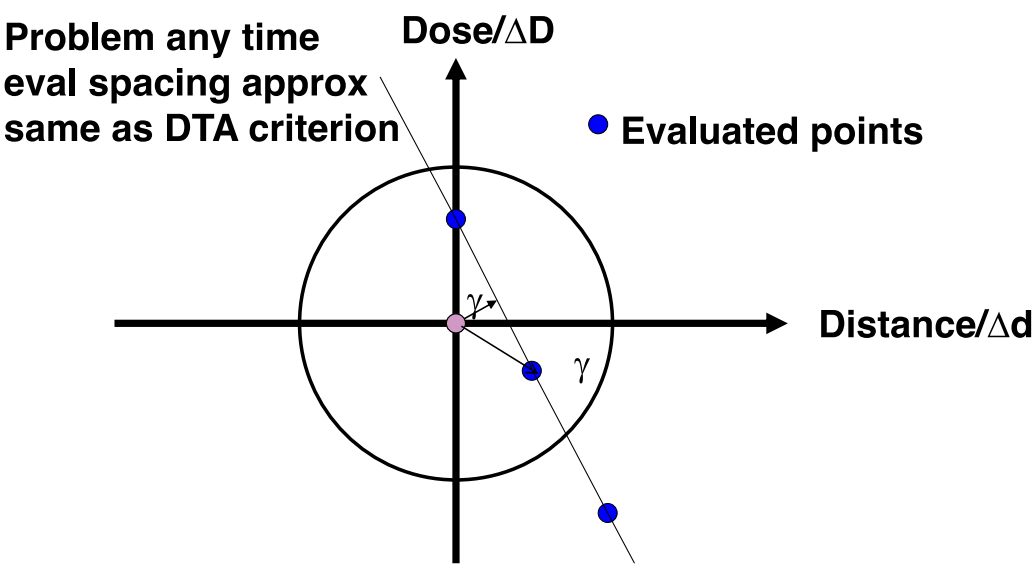

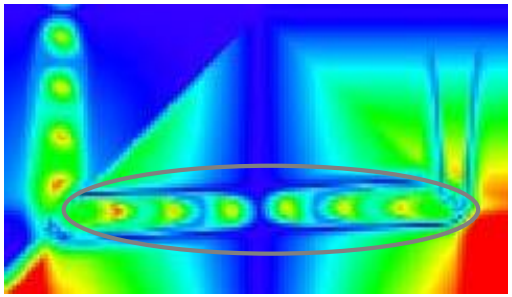

γ

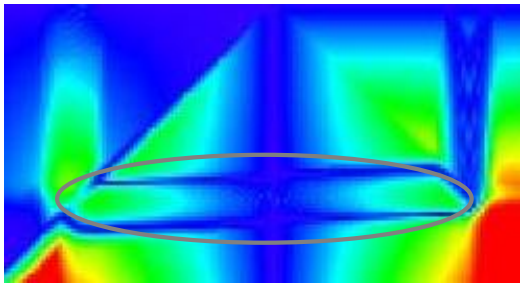

Uninterpolated

Interpolated voxels 8x

Adopted from Low UKRO 2013

Further reading - Ju et al. Med. Phys. 35, 879-887 (2008)

ESTRO School

Influence of Noise in calculated or measured distribution

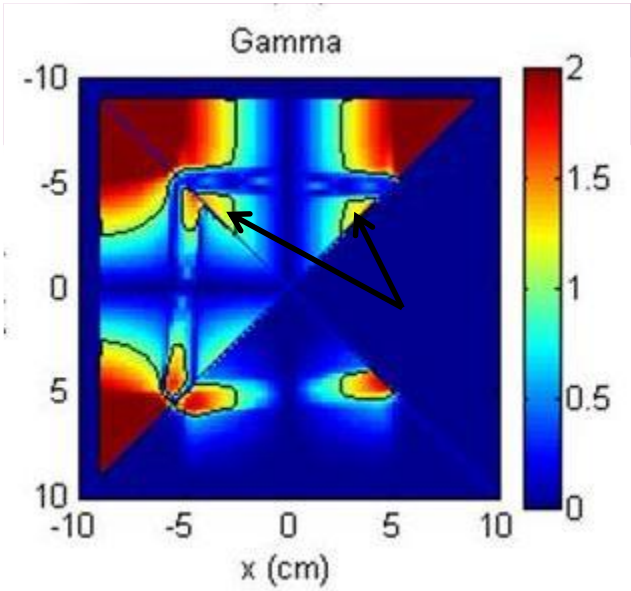

No Noise

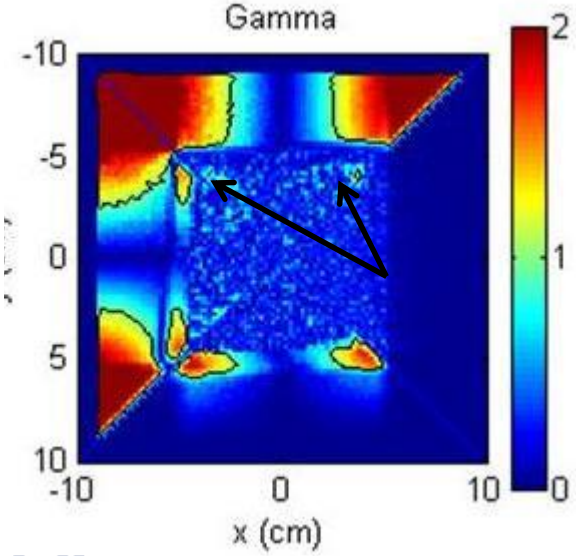

3% Noise
Evaluation

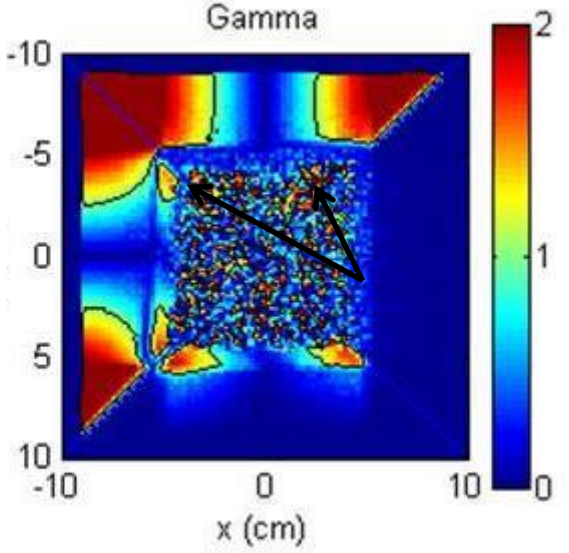

3% Noise
Reference

Underestimation

Low and Dempsey, Med Phys, 2003

Don’t loose the details

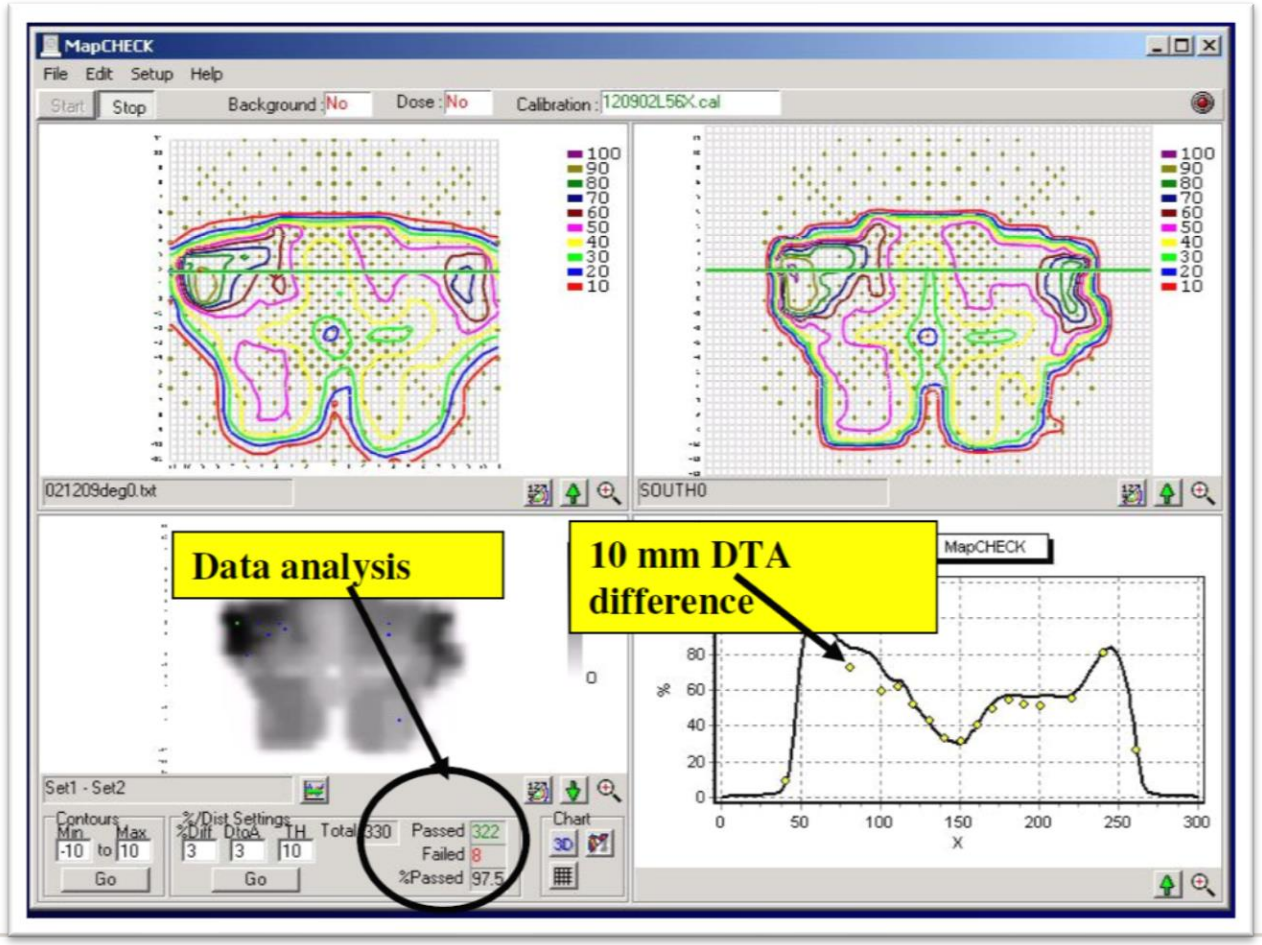

Comparison of a measured and calculated cross-plot (at 5 cm depth) of an intensity modulated field incident on a flat phantom. A diode-array (MapCheck; Sun Nuclear Corp.) was used for this comparison, which shows that 97.5% of the points meet 3% criteria even though DTA (distance to agreement) for a few points is 10 mm.

Can be crucial for organs at risk.

From J Palta AAPM 2005

Choice of reference point - important

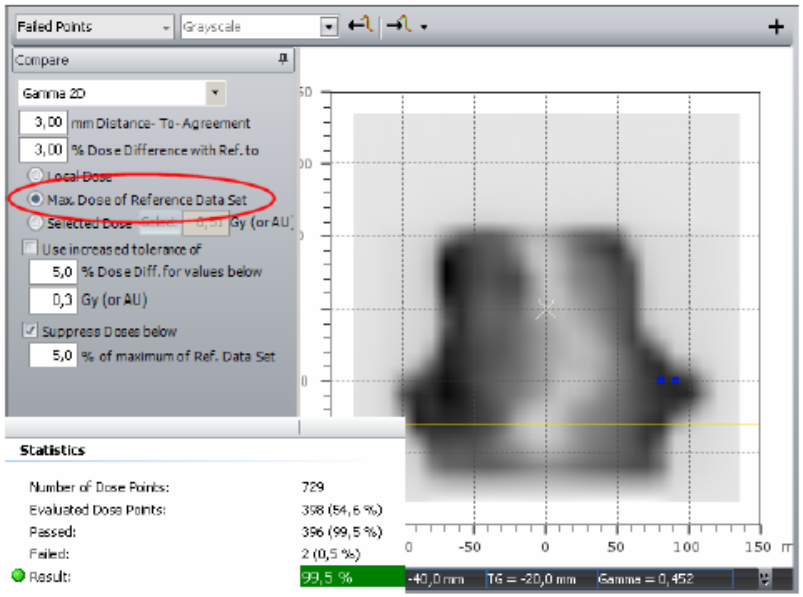

Figure 1: Comparison with a global dose point as reference

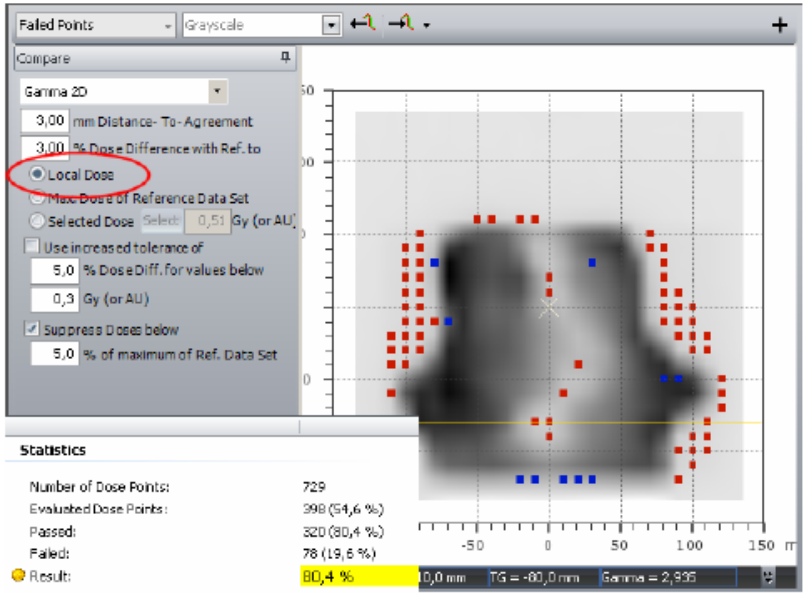

Figure 2: Comparison with local dose points as reference

Should IMRT patient QC be done field-by-field or for the composite plan?

- Assume a 5 field plan each beam contributes with 1/5 to the target

- Each beam are delivered within 3 % of calculation
- Except for one that is 15% off.
- This **plan** will not pass field-by-field QC
- For a composite plan you **will not** detect this, the plan is within 3%!!!

John Schreiner's Commandments

1. "know and understand your dosimetry system completely, including its limitations, before applying it to a particular validation task"

2. "engage in the clinical exchange of ideas and knowledge through publication in scientific journals, and, perhaps more importantly, through regular communication, meetings and workshops with colleagues locally, nationally and internationally"

Schreiner L J in J Med Phys 2011;36:189-91

Gamma Analysis 3%G/3mm

Example #1

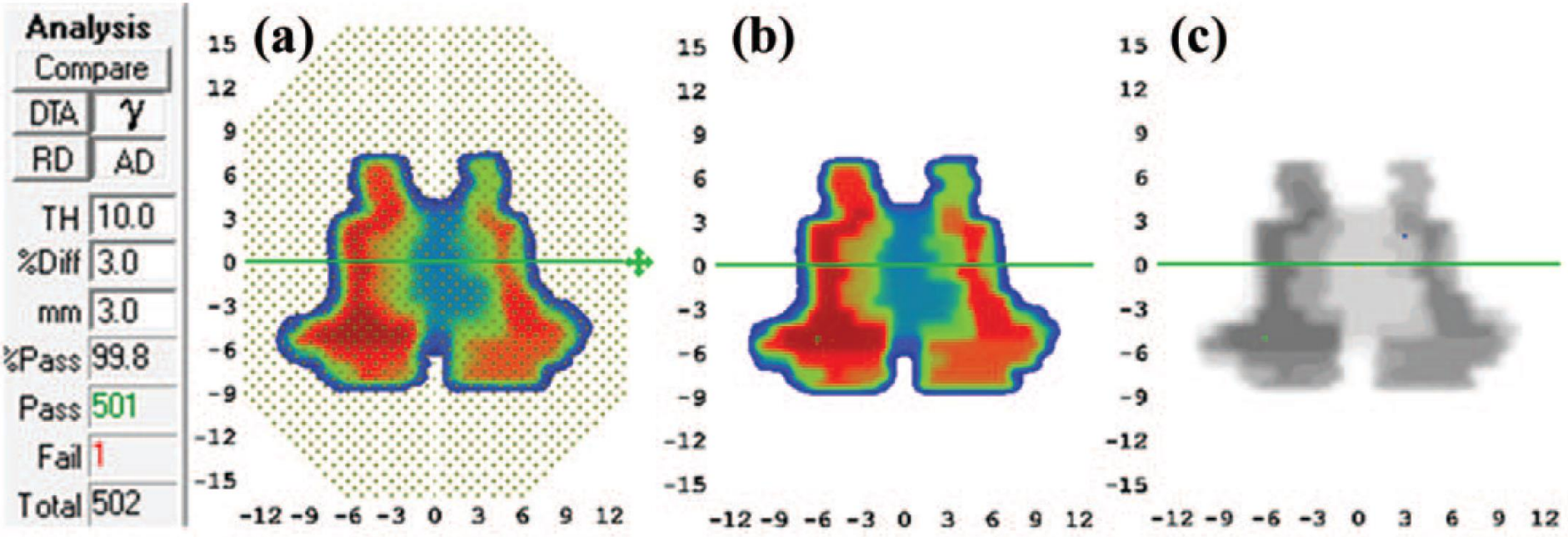

Med Phys 2013 – Nelms et al

ESTRO School

Line or Profile Analysis

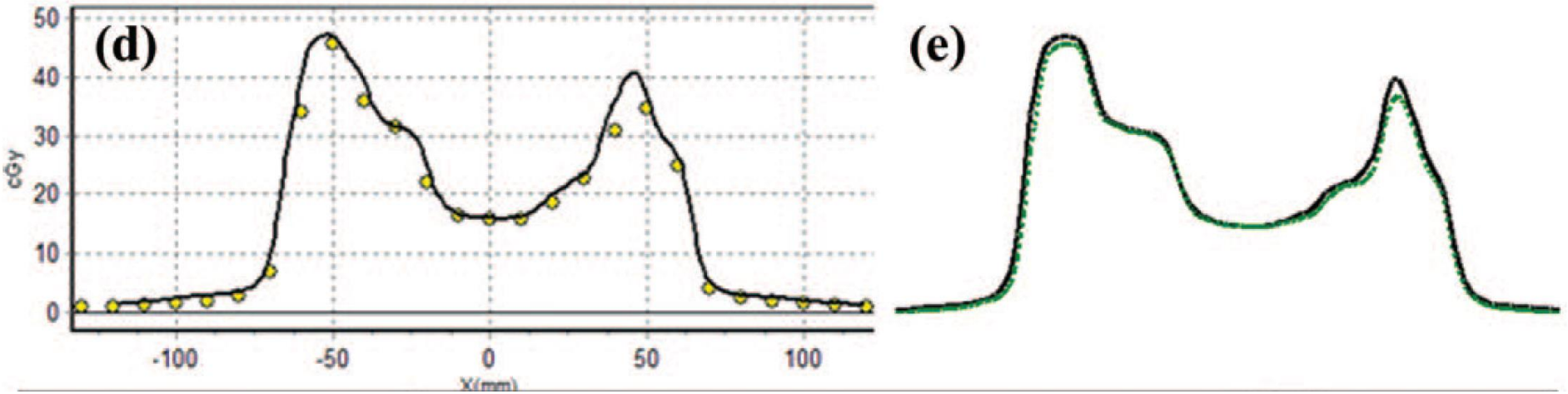

Measurements consistently lower

Med Phys 2013 – Nelms et al

Measurement Based 3D Calculation

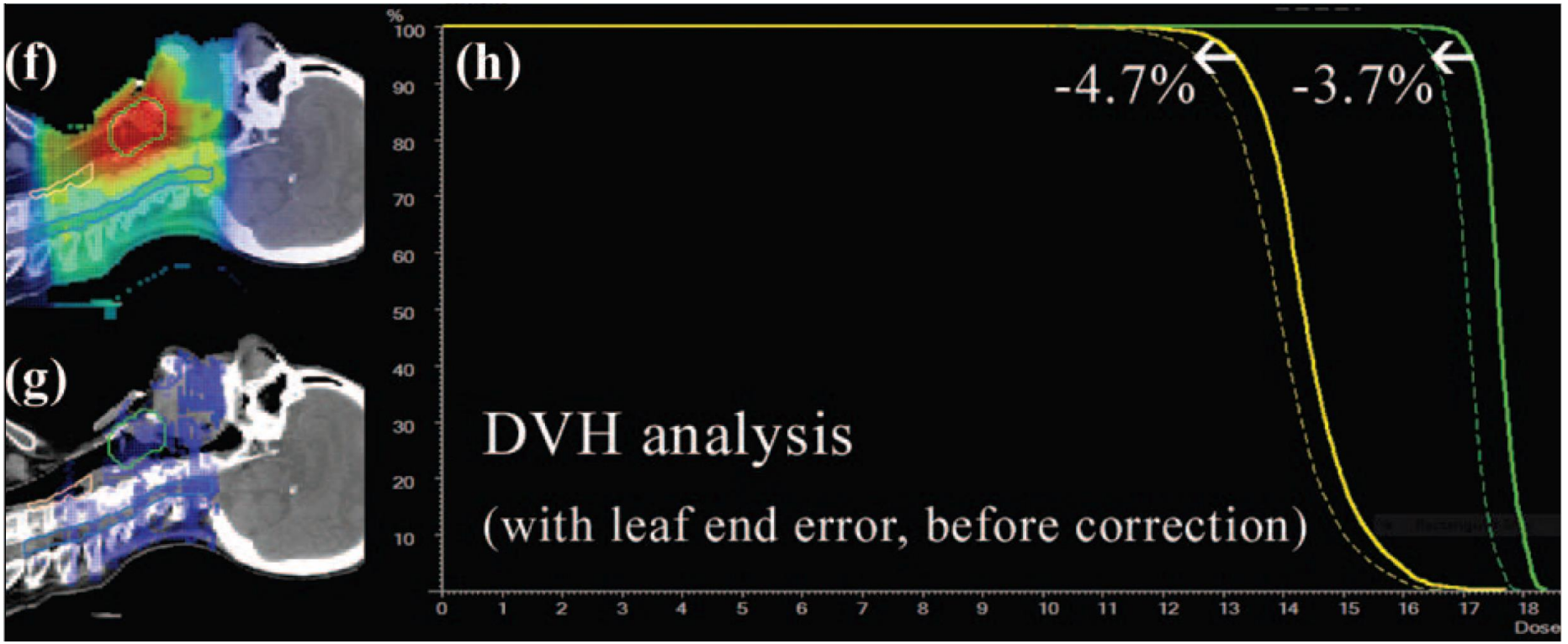

"Measured" dose in both target volumes are about 4% too low

Med Phys 2013 – Nelms et al

ESTRO School

3%G/3mm Fails but 2%L/2mm Detects T/G Errors

Example #2

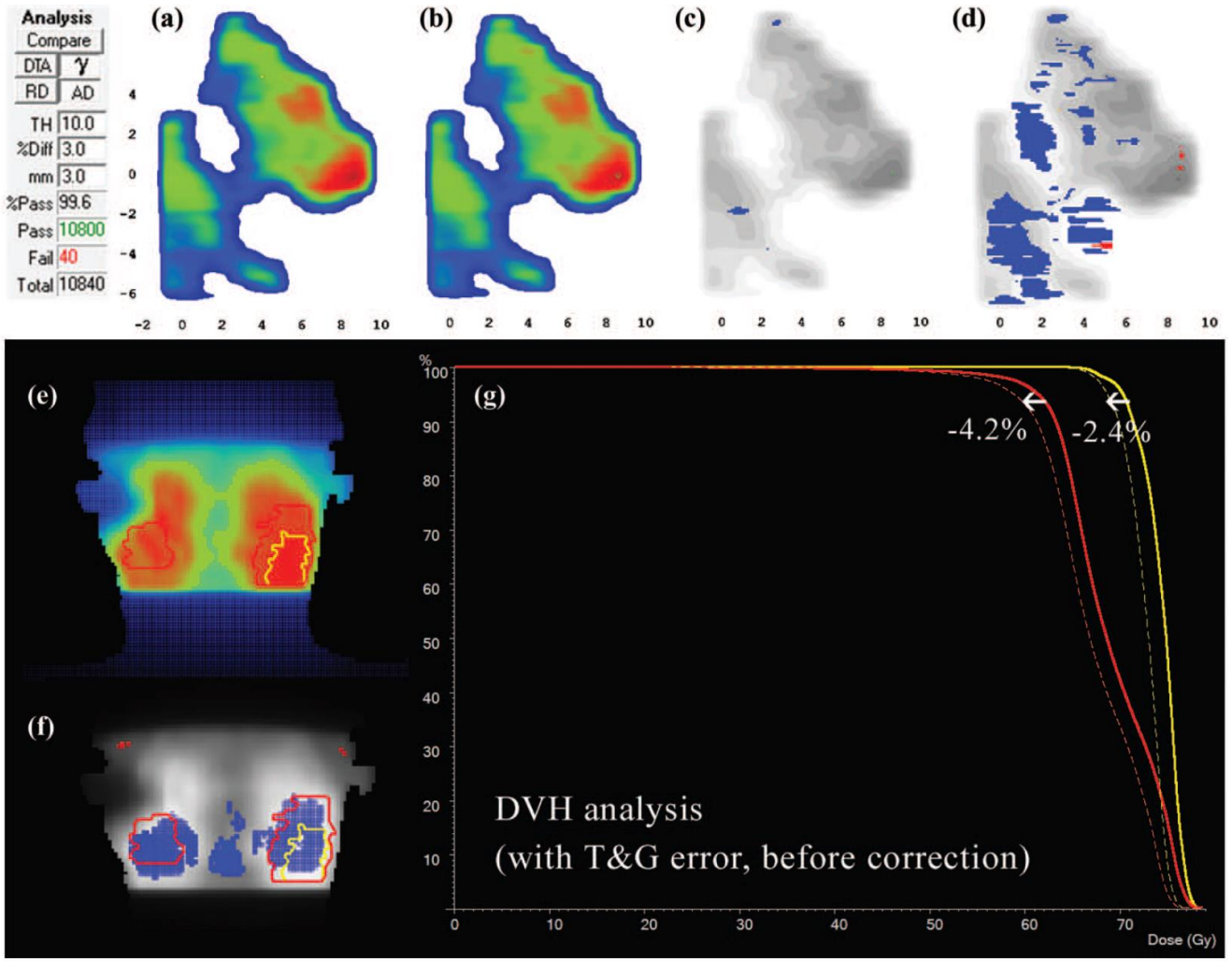

Med Phys 2013 – Nelms et al

ESTRO School

1st Commandment Explained

- Metric for γ-analysis
  - "Overreliance on the insensitive metric is
    - counterproductive to quality improvement and
    - can lead to the sense of complacency among the clinical physicists."
  - "IMRT and VMAT commissioning, along with product validation, would benefit from the retirement of the 3%/3 mm passing rates as a primary metric of performance, and
    - the adoption instead of tighter tolerances, more diligent diagnostics, and more thorough analysis."

Med Phys 2013 – Nelms et al

Data from two systems (Delta4 and Portal Dosimetry) for the same patients

Delta^4-phantom

- 2 diode matrices 3D-phantom
- PMMA
- TPS algorithm

EPID

Electronic Portal Imaging Device

- 2D-detector
- aSi (amorphous silicone)
- Portal Dosimetry Image Prediction (PDIP) algorithm

Courtesy A Karlsson Hauer

Delta^4 vs EPID

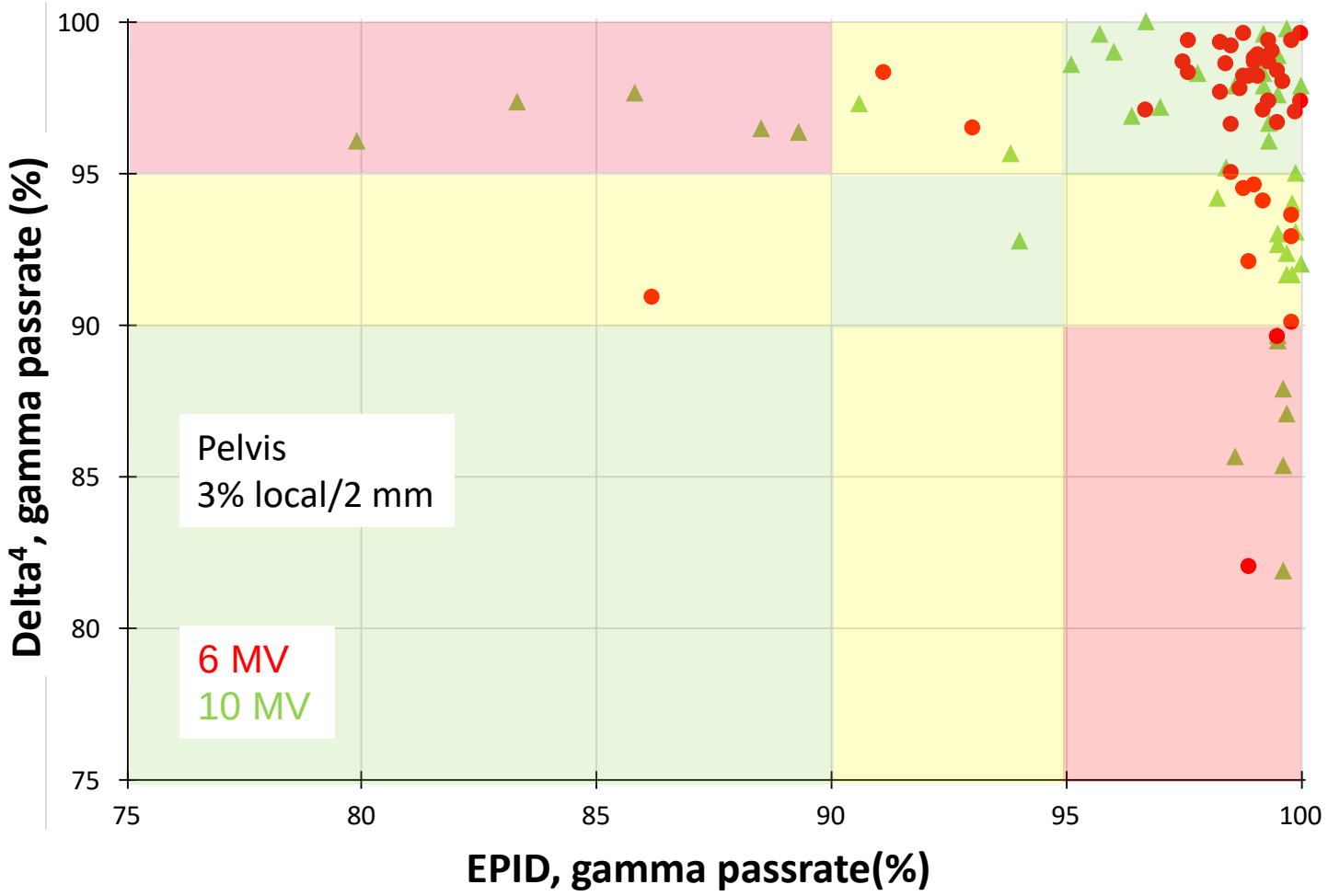

Courtesy A Karlsson Hauer

Criticism of the 3%/3 mm γ metric

- The common 3%/3 mm γ analysis metric is **not sensitive enough** to provide optimal results in IMRT/VMAT commissioning.
- Overreliance on the insensitive metric is **counterproductive** to quality improvement and can lead to the sense of complacency among the clinical physicists.
- Use of this metric also enables manufacturers to release products that may not be validated with sufficient rigor, hindering them from designing error out of the system before commercial release.
- "adoption of more sensitive metrics/tighter tolerances enables continual improvement of the accuracy of radiation therapy dose delivery"
- Adoption of sensitive metrics and tighter tolerances fit the larger goal to better standardize the methods and processes of commissioning and product validation, with the ultimate goal to increase quality…

Nelms et al, Med Phys 2013.

Taking patient specific QA further…

- "none of the approaches tested to verify IMRT plans by means of gamma analysis using 3%/3 mm or 2%/2 mm criteria solve the problem of evaluating treatment plans. **Neither is it clear whether global 3D gamma analysis is superior to local 3D gamma analysis.**" - Carrasco et al 2012
- "a suitable alternative for evaluating and reporting the measured planar differences is to **transfer their impact to the plan DVH** and then to compare the resulting DVHs with the **clinical tolerances of the PTV and OAR.**" - Carrasco et al 2012
- "the essence of patient-specific IMRT QA is to **ensure that the dose distribution that is going to be delivered to the patient is of the same comparable quality as the approved plan**, and such quality is evaluated by patient dose statistics and DVH curves." - Zhen – et al 2011
- "**The evolution from gamma passing rates to DVH based metrics is natural in this way.**" – Zhen –et al 2011

- "This study suggests that it is possible, and advisable, to **select γ- criteria** that specifically prioritize the property (either dose difference or distance to agreement) of **greatest clinical importance** for each treatment modality or anatomical site **while also identifying action levels that maintain acceptable QA pass rates**"

- "the adoption of more sensitive γ-criteria, specifically 2%/2 mm, 2%/3 mm, or 3%/2 mm could be beneficial"

Crowe et al Med Phys 2016

Conclusions

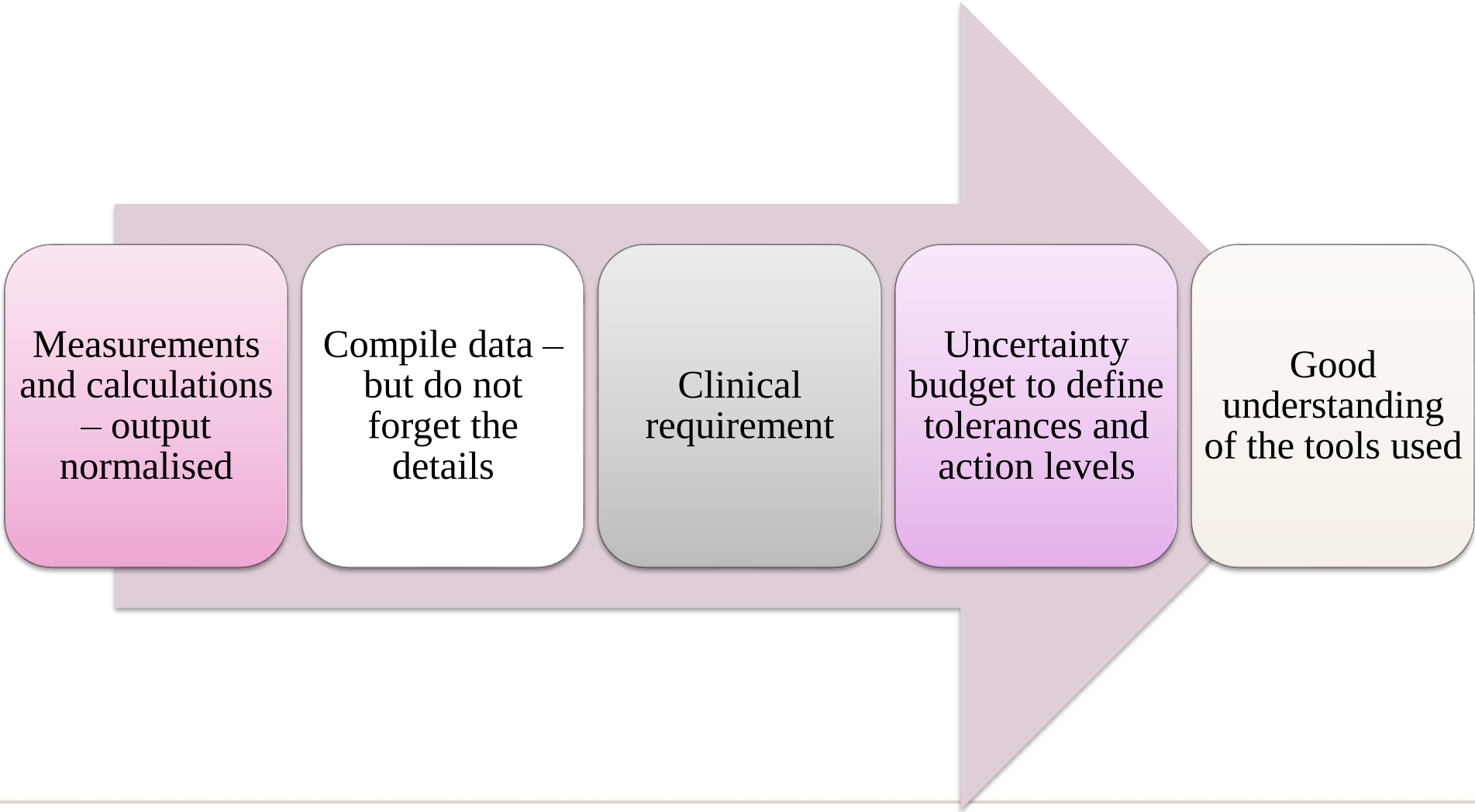

Thank You

Dose Modelling and Verification for External Beam Radiotherapy
2-6 April 2017, Warsaw, Poland

ESTRO

Uncertainties, Tolerance and Action limits

Brendan McClean
St Luke's Radiation Oncology Network, Dublin, Ireland

Previous versions JO, GH, NJ

Learning objectives

- to understand the need to report on the quality of a measurement result in addition to the result itself
- To understand the concepts of dosimetric tolerance limits and action limits.
- Get a feeling for how measurement or calculation uncertainties will influence action limits.
- to understand how to set action limits taking into account clinical tolerance limits and uncertainties.

Some important documents…..

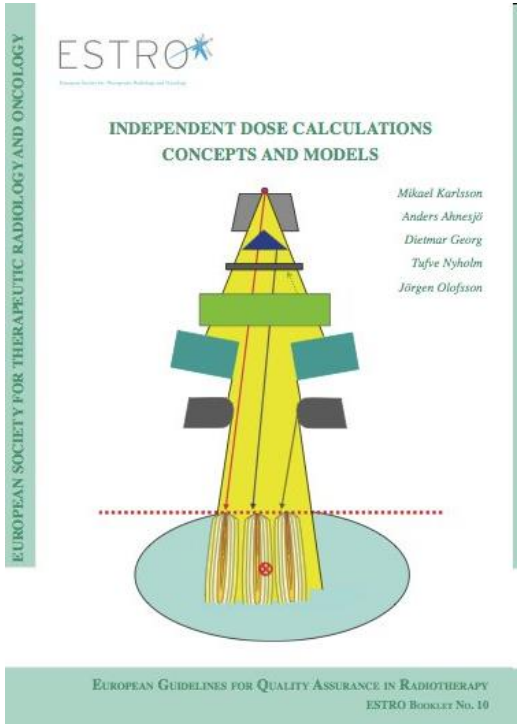

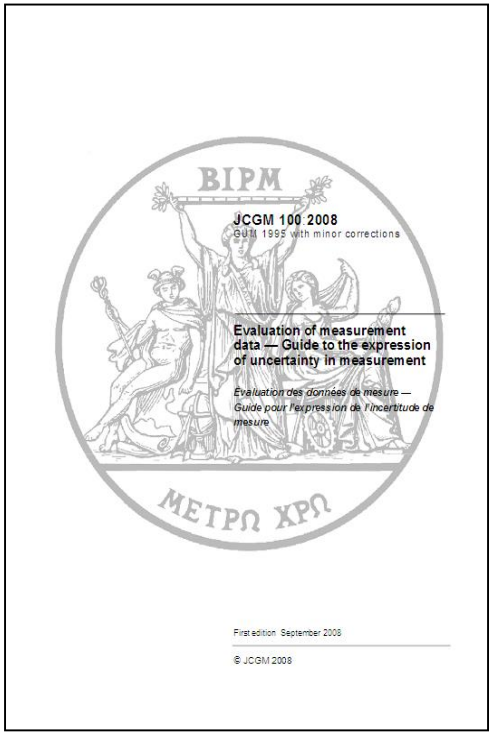

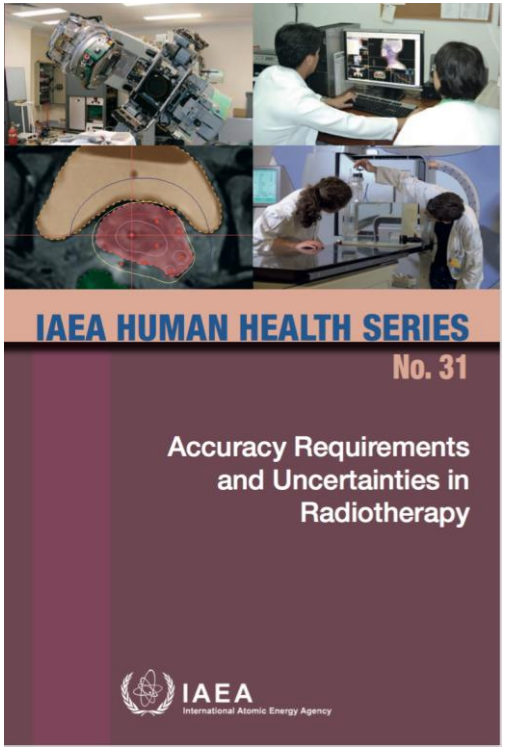

ESTRO School

Introduction

Medical physics is full of measurements which require an **accuracy as high as possible.**

Example: dose determination in reference dosimetry

$$D_w = M\ [C] \cdot N_{D,w}[Gy/C] \cdot k_Q$$

Where:

$$\text{true}(D_w) = \text{measured}(D_w) \pm \text{uncertainty interval}$$

or $$D_{w,true} = D_{w,m} \pm u$$

$D_{w,true}$ probably lies somewhere in the interval $\{D_{w,m} - u,\ D_{w,m} + u\}$, i.e. 2 u wide and centered around the measured value $D_{w,m}$

measured value **"True" value**

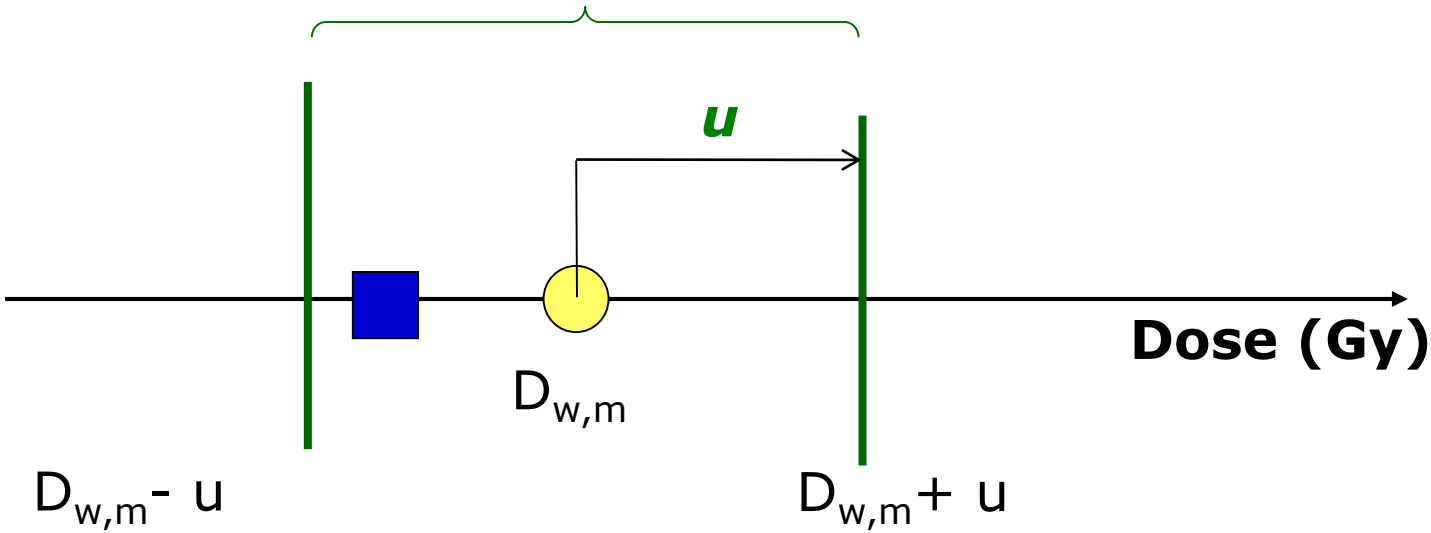

However this information is still incomplete, because we need a clear understanding what the word "**probably**" means.

Introduction

Example:
A dose is measured and found to be 1 Gy.
However, even assuming an identical uncertainty of measurement, this result might be reported either as:

(1 ± 0.01) Gy ⟸ with 99% confidence limits

or:

(1 ± 0.007) Gy ⟸ with 95% confidence limits

Same measurement, same accuracy, different reporting

Need a general and internationally accepted standard on how to best provide information also on the quality of a reported result.

…this is the standard:

the so-called GUM

http://www.bipm.org/en/publications/guides/gum.html

GUM: Accuracy and Precision

Frequently used to describe the **quality** of a measurement:

Accuracy: specifies the **closeness** of agreement between repeated independent measurements and the **true value**.

Precision: Is a measure of the **degree of reproducibility** of results.

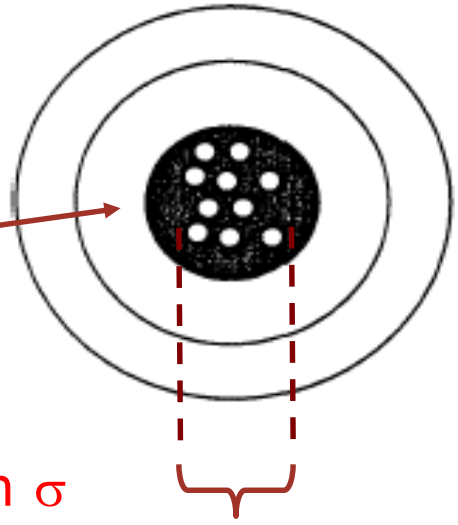

Note:
High precision

is equivalent to a small standard deviation σ

A short discussion on acccuracy and precision

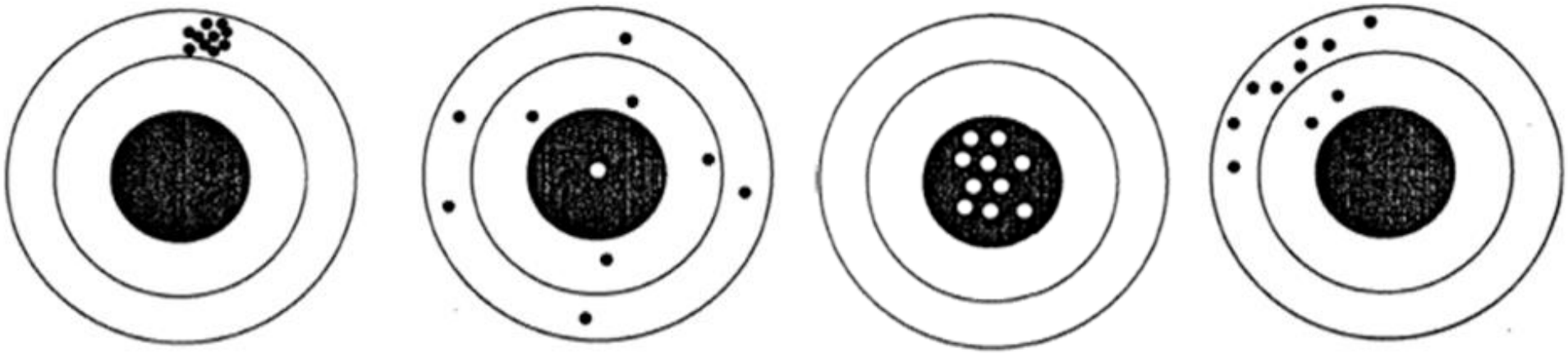

High precision and Low accuracy	Low precision and High accuracy	High precision and High accuracy	Low precision and Low accuracy

Note: Each of these situations refer to the target point, which can be taken as the **true value**

How to know the "true value"?

No measurement is perfect!

non-representative sampling

Personal bias

Finite resolution

etc….

Changes in influence quantities can affect the quality of measurements

Table 3.1. Some examples of influence quantities, reference conditions and standard test conditions for ionization chambers used for radiation therapy calibrations (IAEA, 2000a). ICRU 76

Influence quantities	Reference conditions	Standard test conditions
Ambient temperature	20 or 22°C	Reference ambient temperature ±2°C
Relative humidity	50 %	45–65 %[a]
Atmospheric pressure	101.325 kPa	86–103 kPa[a]
Stabilization time	30 min	>15 min
Electromagnetic fields	Negligible	<Value causing interference
Radioactive contamination	Negligible	Negligible
Radiation background	≤1.0 μGy/h	≤52.0 μGy/h

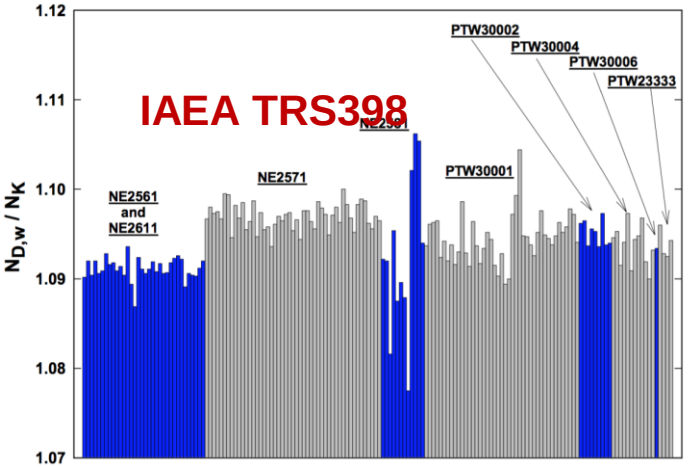

In principle, the quantity to be measured **cannot be completely** described without an **infinite** amount of information.

Introduces concept of **uncertainty**

(The use of '**error**' is discouraged)

Uncertainty

- Doubt!
- Parameter characterizing the dispersion of values of a measurement when it is performed repeatedly.

possible values of the measured parameter

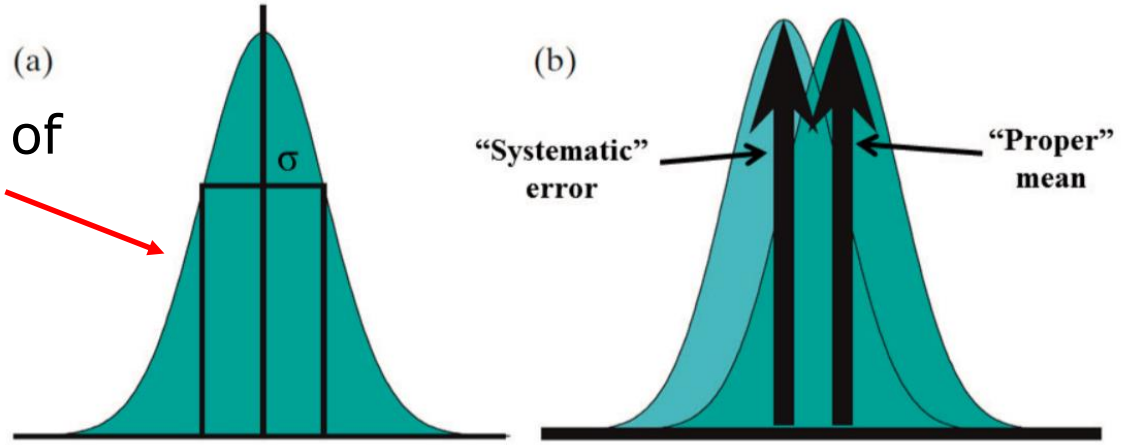

FIG. 3 (a) Uncertainty distribution for a particular measurement. (The vertical axis shows frequency; the horizontal axis shows the measurement value.) The standard deviation is shown by σ. (b) Comparison of two uncertainty distributions, one about the proper mean and the other with a systematic error. (Adapted from Ref. [28].)

IAEA Accuracy and Uncertainty 2017

The value of the measured parameter is a stochastic quantity

ESTRO School

Standard and Expanded Uncertainty

Want to define an interval about a measurement result
within which the true value can be confidently predicted to be

Standard Uncertainty = 1σ
Expanded Uncertainty = kσ where k=1 (67%),2 (95%) or 3 (99%)
k= coverage factor

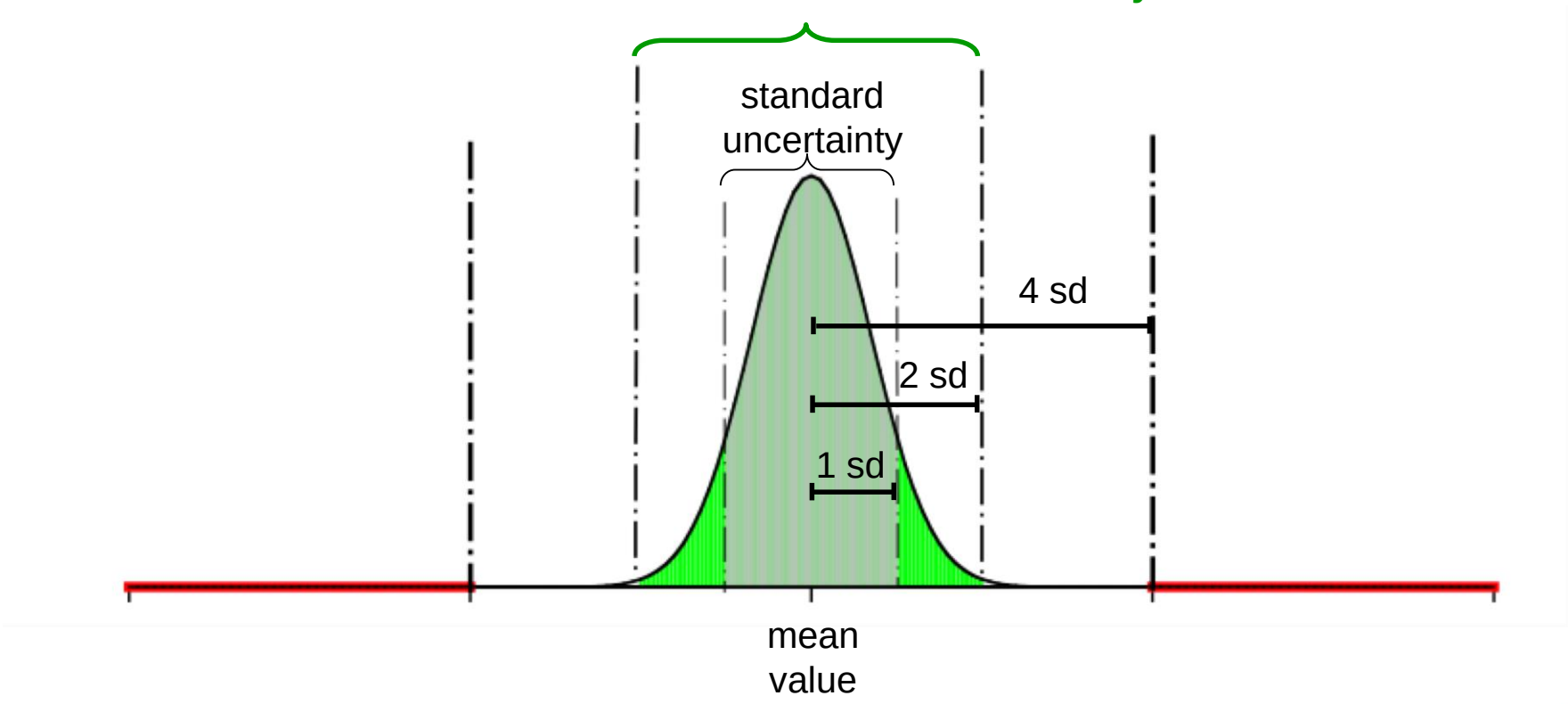

The coverage factor and expanded uncertainty

Example for a coverage factor and expanded uncertainty in a Calibration Certificate

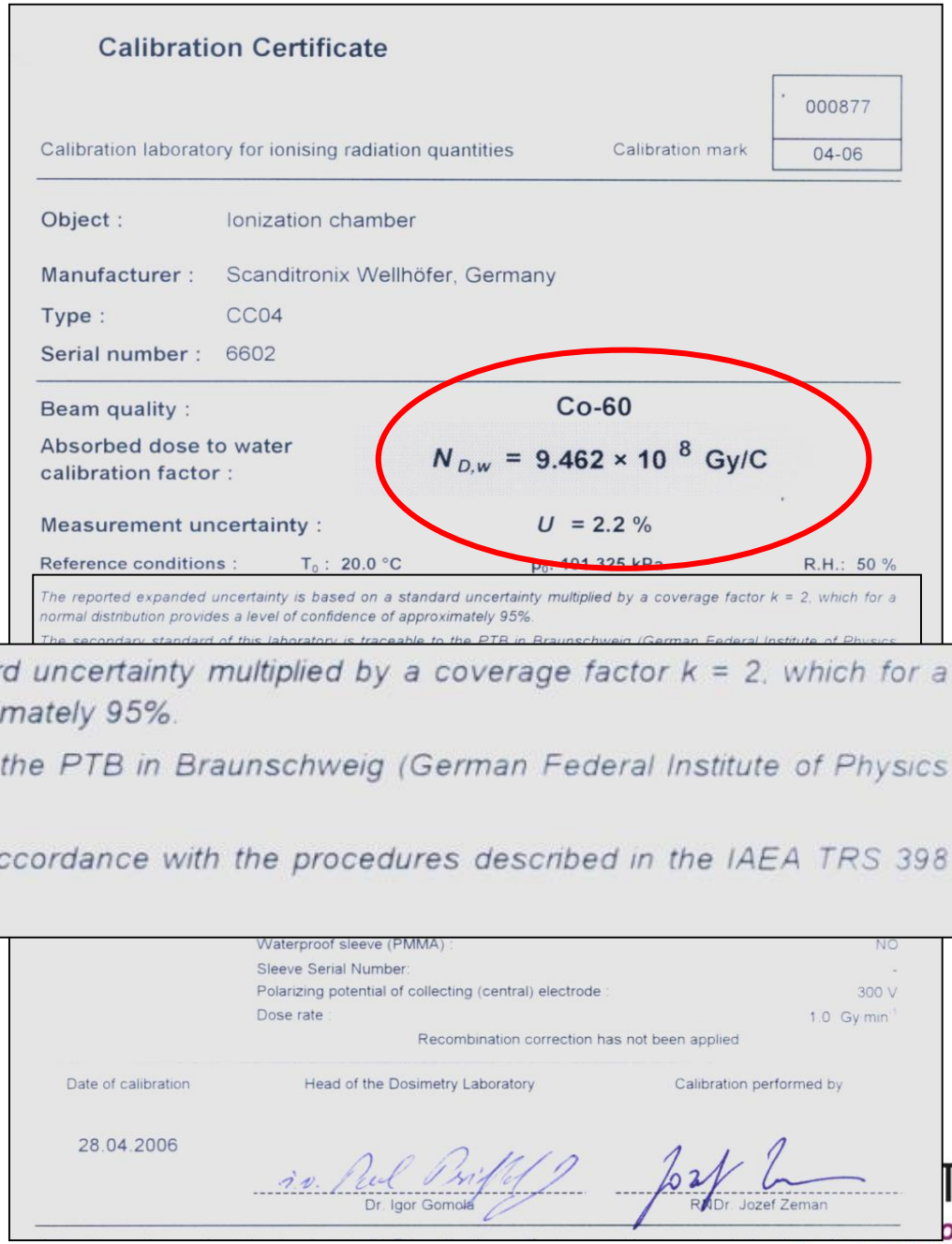

Calibration Certificate

000877

Calibration laboratory for ionising radiation quantities — Calibration mark: 04-06

Object : Ionization chamber

Manufacturer : Scanditronix Wellhöfer, Germany

Type : CC04

Serial number : 6602

Beam quality : Co-60

Absorbed dose to water calibration factor : $N_{D,w} = 9.462 \times 10^{8}$ Gy/C

Measurement uncertainty : $U = 2.2$ %

Reference conditions : T_0 : 20.0 °C — p_0: 101.325 kPa — R.H.: 50 %

The reported expanded uncertainty is based on a standard uncertainty multiplied by a coverage factor k = 2, which for a normal distribution provides a level of confidence of approximately 95%.

The secondary standard of this laboratory is traceable to the PTB in Braunschweig (German Federal Institute of Physics and Metrology).

Calibration reported in this certificate was carried out in accordance with the procedures described in the IAEA TRS 398 Code of Practice.

Waterproof sleeve (PMMA) : NO

Sleeve Serial Number: -

Polarizing potential of collecting (central) electrode : 300 V

Dose rate : 1.0 Gy min^{-1}

Recombination correction has not been applied

Date of calibration: 28.04.2006

Head of the Dosimetry Laboratory: Dr. Igor Gomola

Calibration performed by: RNDr. Jozef Zeman

Combined uncertainty

In most cases a parameter, eg Y, is not measured directly, but is determined from ***N*** other input quantities
$\boldsymbol{X_1}$, $\boldsymbol{X_2}$, **….**, $\boldsymbol{X_N}$, through a functional relationship ***f***:

$$Y = f(X_1, X_2, ...X_N)$$

The input quantities X_1, X_2, ..., X_N are – of course – also subject to probability distribution.

Combined uncertainty

A combined (standard) uncertainty is then obtained as the positive square root of the **sum of variances** weighted according to how the result is influenced by varying different influence components (only if not correlated).

$$u_c = + \sqrt{\sum_{i=1}^{N} \left(\frac{\partial f}{\partial x_i} \right)^2 \cdot u^2(x_i)}$$

$\frac{\partial f}{\partial x_i}$ = sensitivity coefficient

More on the uncertainty concept:

- The determination of the uncertainty of a result therefore requires an analysis of the **distribution** of any influence quantity.

- All components to the overall uncertainty are grouped into **two different categories** according to **how the associated probability distribution is being evaluated**:

NOT Random and Systematic errors!

Both based on probability distributions

Type A (evaluation of) uncertainty:

Those components which are evaluated by statistical analysis of repeated of observations

Type B (evaluation of) uncertainty:

Those components which are evaluated by any other means

Type A evaluation:

Step 1: Determine the **mean value** from a series of observations:

$$x_i = \frac{1}{N}\sum_{k=1}^{N} x_{i,k}$$

Step 2: Determine the **positive root of the estimate of the variance** of the mean value

$$u = +\sqrt{s(\bar{x}_i)^2} = \sqrt{\frac{1}{N\cdot(N-1)}\sum_{k=1}^{N}(x_{i,k}-\bar{x})^2}$$

Type B evaluation:

The uncertainty cannot be evaluated by repeating the measurement.

The corresponding distribution must be evaluated as a **a-priori distribution** based on **any other available information** such as:

- previous measurement
- experience
- general knowledge
- manufacturer's specification

Type B evaluation:

Typical examples for an **a-priori probability distribution** are:

1) Gaussian probability distribution

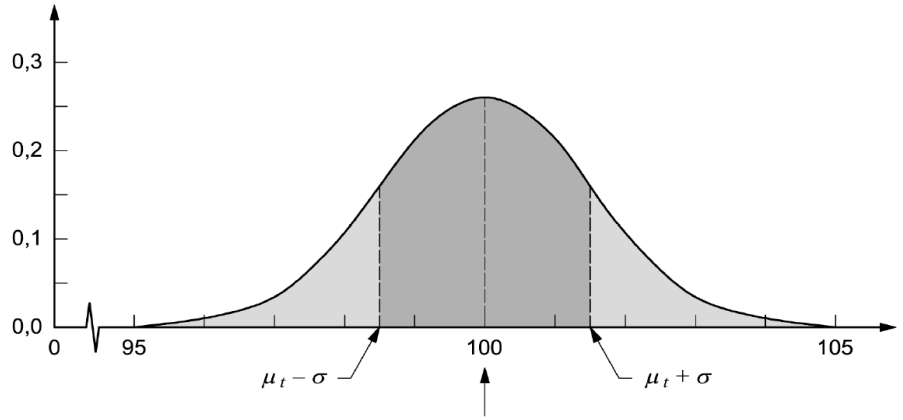

2) Rectangular probability distribution

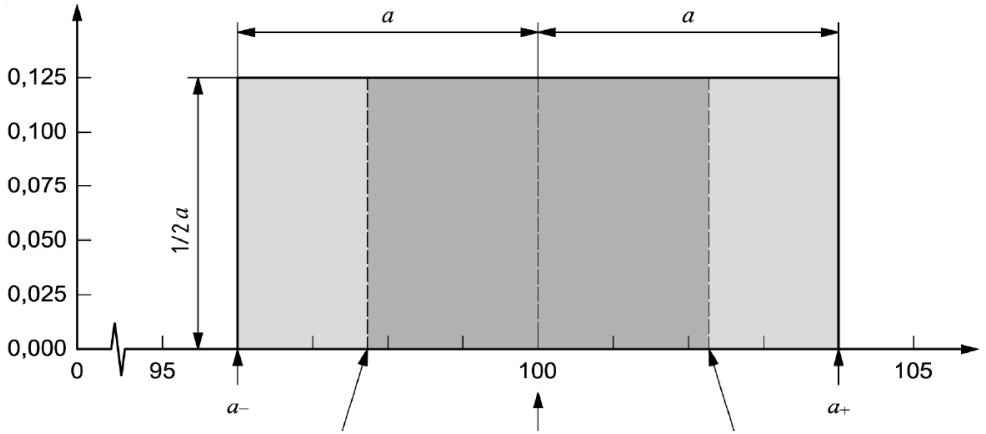

3) Triangle probability distribution

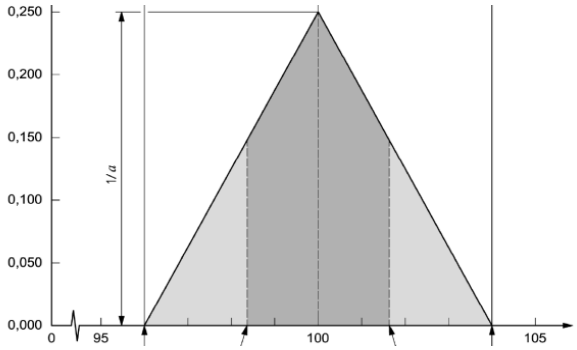

From GUM

Type B evaluation:

Example for a type B evaluation:

One of the input quantities in the dose determination is the correction factor for the air temperature and pressure

$$k_\rho = \frac{(273.2+T)}{(273.2+T_0)}\frac{P_0}{P}$$

Temperature measurement with a Thermometer

T = 293.25 K =20ºC

The thermometer has a traceable calibration.

However this only says that the measured value is correct within an interval of ±0.2° C. What is the underlying distribution??

All one can do is to **suppose** that there is a symmetric lower and upper bound of the interval {T-Δ T+Δ} and that any value between this interval has an **equal probability**.

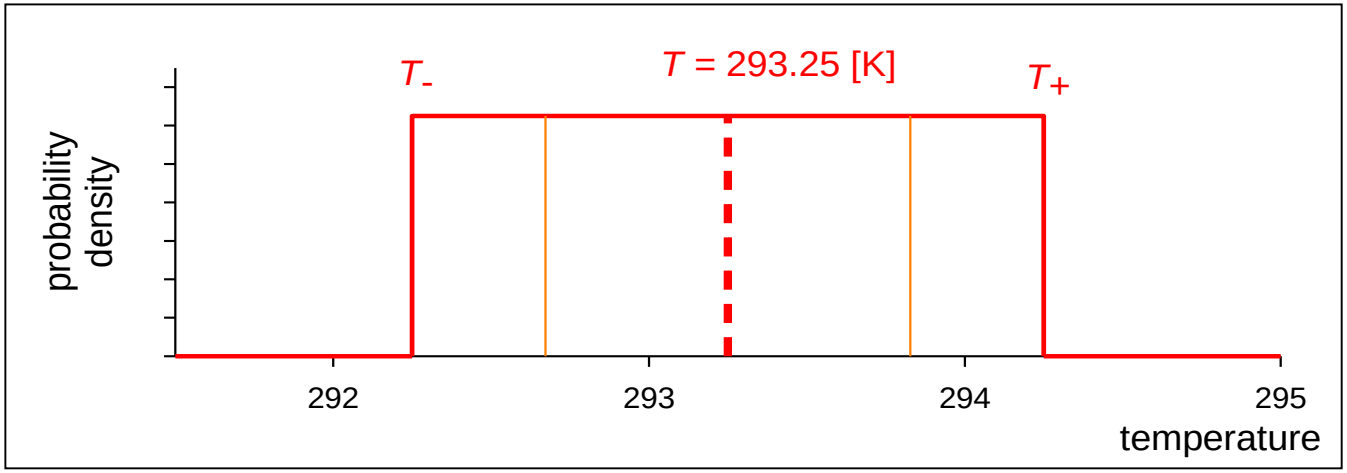

Standard uncertainty:

$$u_B = \sqrt{\sigma^2} = \frac{\Delta}{\sqrt{3}}$$

Corresponding standard uncertainty:

$$u_B = \frac{0.2\,°C}{\sqrt{3}}$$

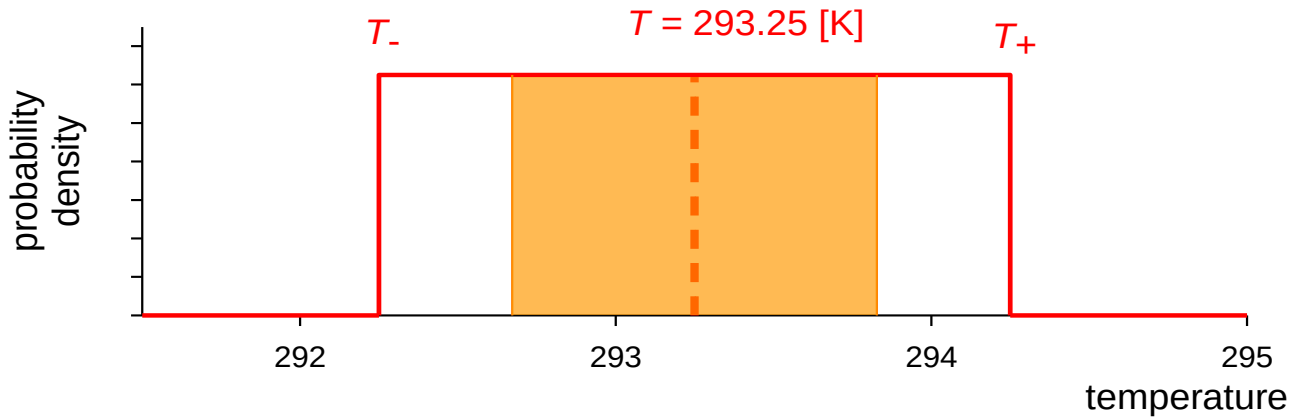

Outline of part 2

- Now we have the means to characterise uncertainty – how does that apply in comparing calculated and measured doses?
- ***Fact***: There is a True dose at every point in an irradiated object.
  - We estimate this dose with measurement or models
- Can assign a tolerance to individual points or to a set of points
  - Δ=|Ave Deviation| + 1.96σ Confidence Limit (Venselaar) (CI=95%, P=0.05)
  - See TK lecture for details
- Need to set Tolerance and Action limits and its relation to the uncertainty of measurements

Confidence Intervals

- This is the observed interval which ***potentially*** includes the unobservable true parameter of interest
- A CI of 95% is NOT the probability that the interval contains the true parameter
  - Observed data points are random samples of true population – so is the CI
- A CI of 95% refers to a number of experiments each of which has a CI set then the proportion of those intervals which contain the true value approaches the confidence interval
  - ie how frequently the observed intervals contain the true value of the parameter
  - Or a CL of 95% means 95% of the observed CI's will hold the true value of the parameter

Friday afternoon at the medical physics department…

Dose measurement

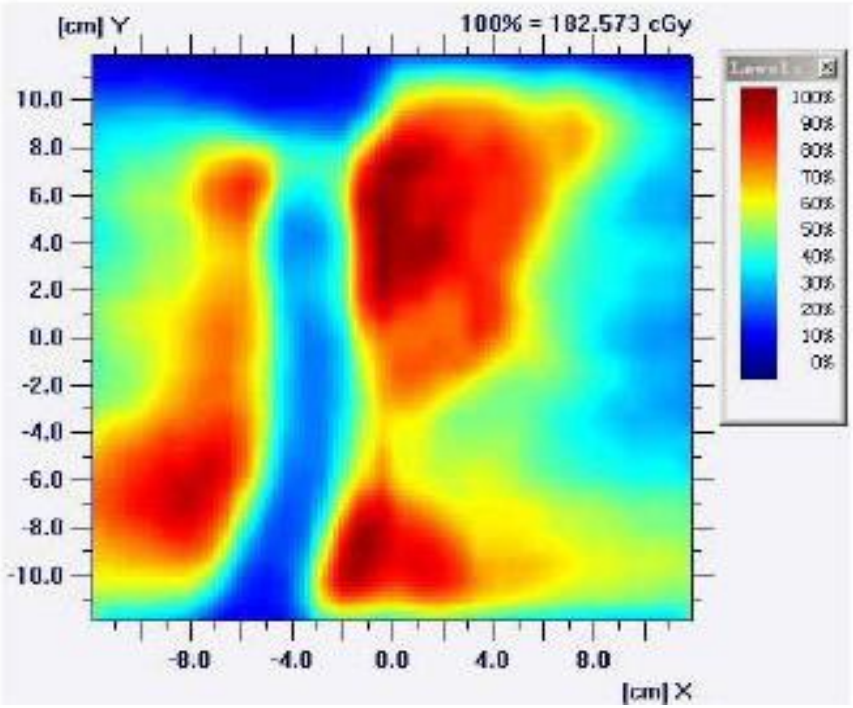

TPS dose calculation

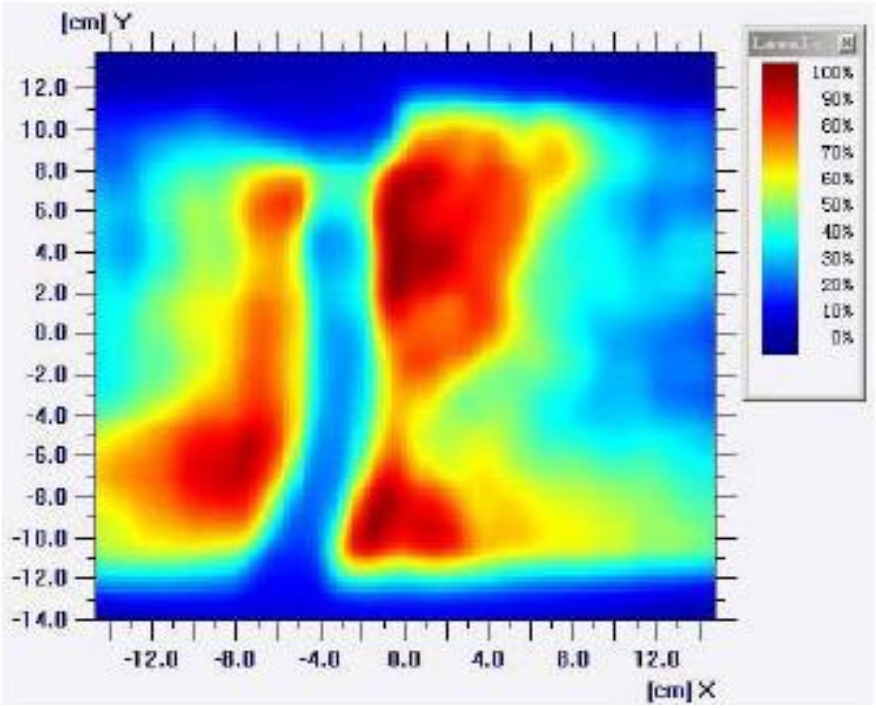

Not OK for treatment?

We need limits to make objective decisions!

From Jörgen Olofsson (Dose Modeling and dose verification ESTRO COURSE)

ESTRO School

How are those limits set?

For simplicity, let us consider verification of dose in one single (ICRU) point

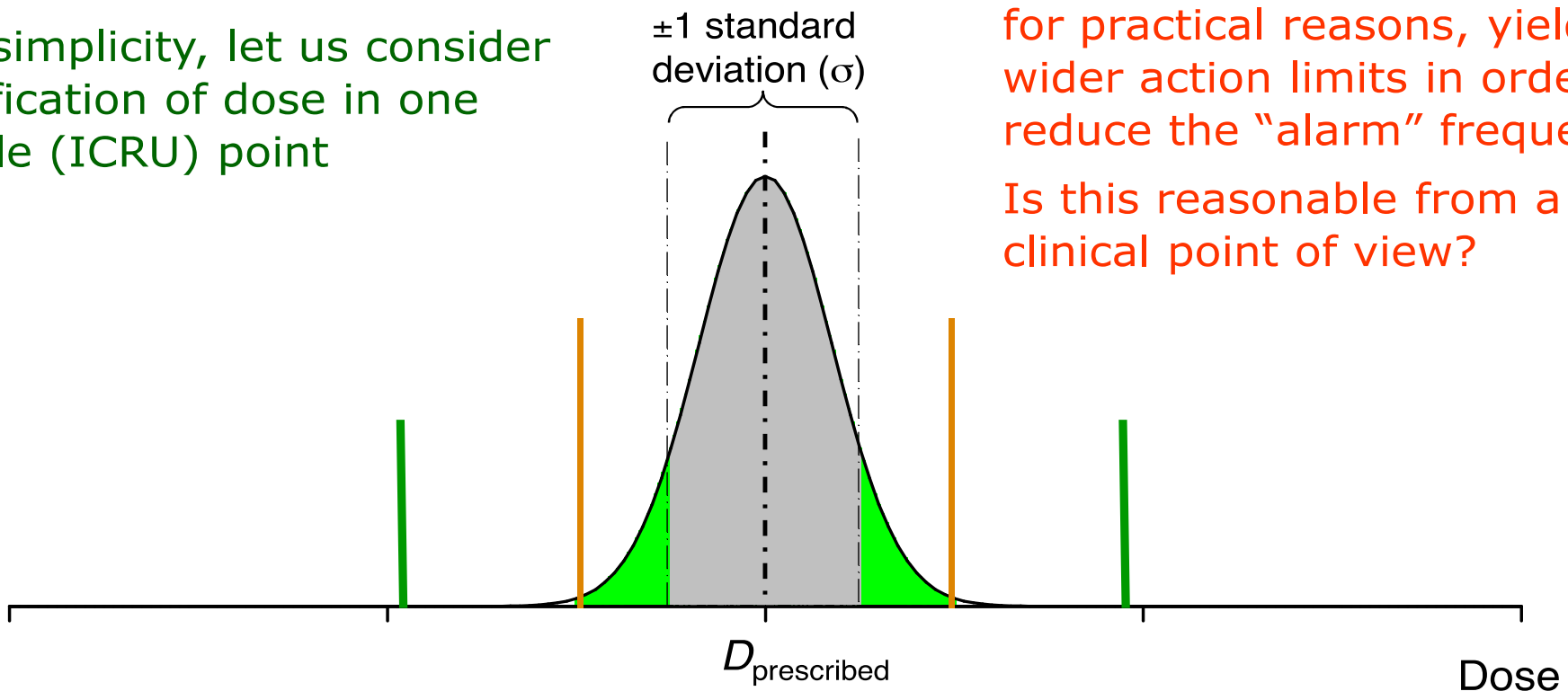

Hence, large uncertainties may, for practical reasons, yield wider action limits in order to reduce the "alarm" frequency.

Is this reasonable from a clinical point of view?

A reasonable (?) **tolerance** limit: **± 2σ**

A reasonable (?) **action** limit: **± 4σ** (= 2 × tolerance limit)

From Jörgen Olofsson (Dose Modeling and dose verification ESTRO COURSE)

Action limits - Traditional philosophy

- Prescribed dose (=TPS dose)
- Independent dose calculation/measurement

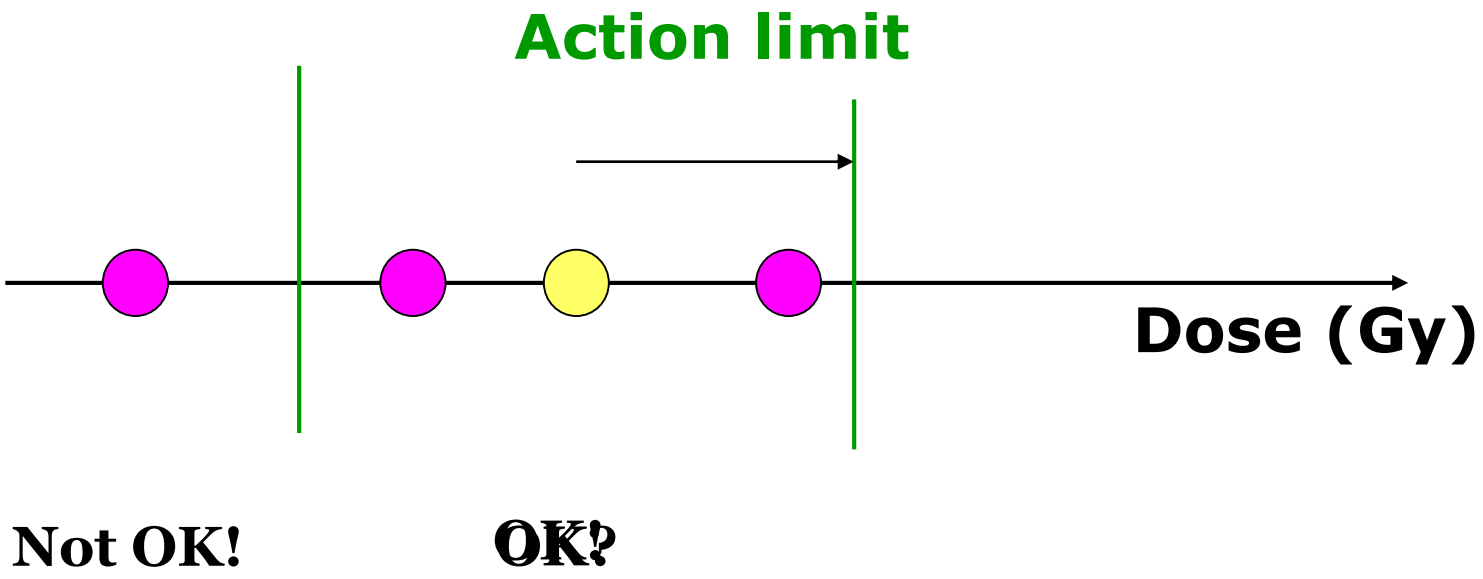

From Jörgen Olofsson (Dose Modeling and dose verification ESTRO COURSE)

ESTRO School

Reality

Prescribed dose (=TPS dose)

True dose (=Actually delivered dose)

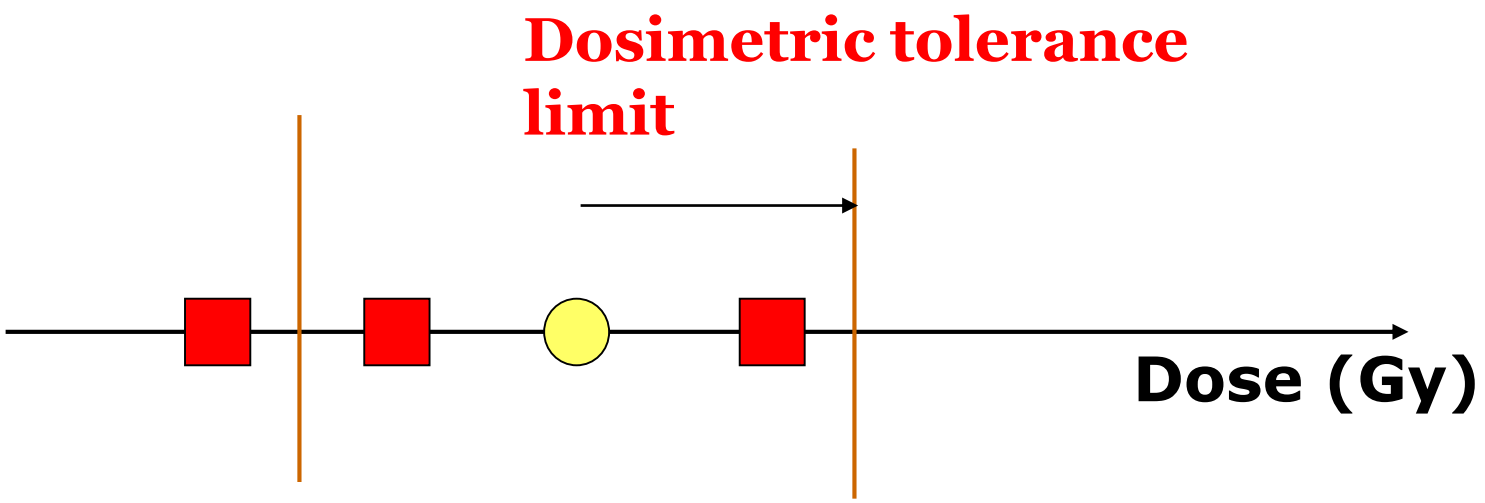

Not OK! **OK?** **Do we know the True dose?**

From Jörgen Olofsson (Dose Modeling and dose verification ESTRO COURSE)

ESTRO School

Action limits - Proposed philosophy

Prescribed dose

True dose

Independent dose calc/meas

Probability distribution for the true dose

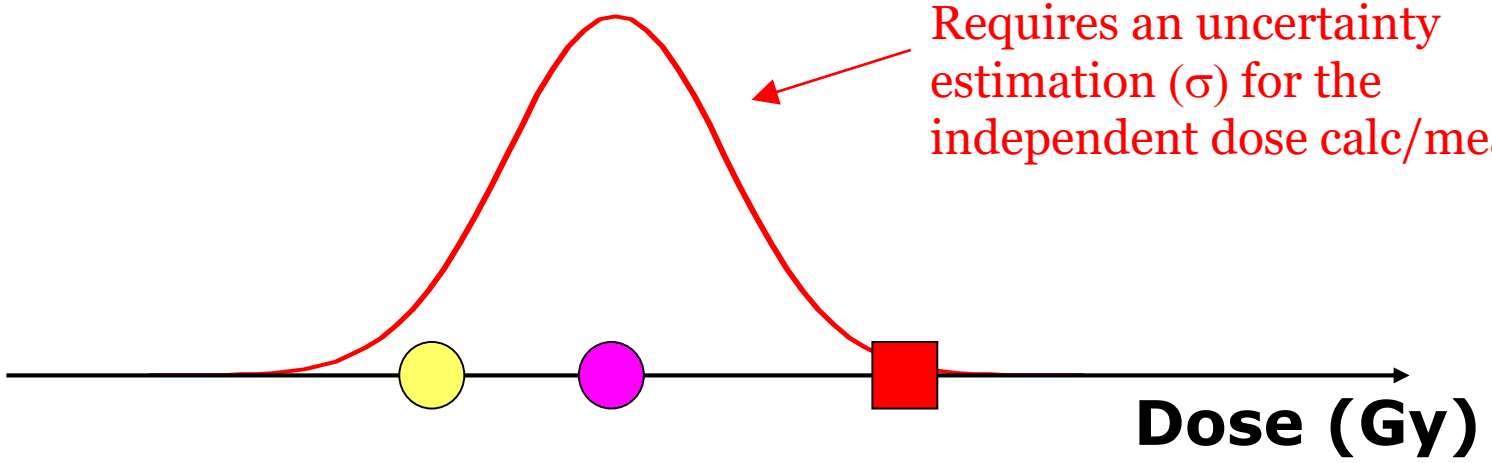

OK?

Not OK?

What is the Clinical tolerance limit?

From Jörgen Olofsson (Dose Modeling and dose verification ESTRO COURSE)

ESTRO School

- Clinical tolerance limits or specifications should be based on clinical experience.
- Clinical experience can be summarized through statistical analysis of the outcome of a particular treatment for a particular tumor disease.
- Examples:
  - Local tumor control as a function of dose.
  - Fraction of survivors after five years as a function of dose.
- At the same time, normal tissue complications must be taken into account.

From Jörgen Olofsson (Dose Modeling and dose verification ESTRO COURSE)

Minimum acceptable cure rate

Maximum acceptable complication rate

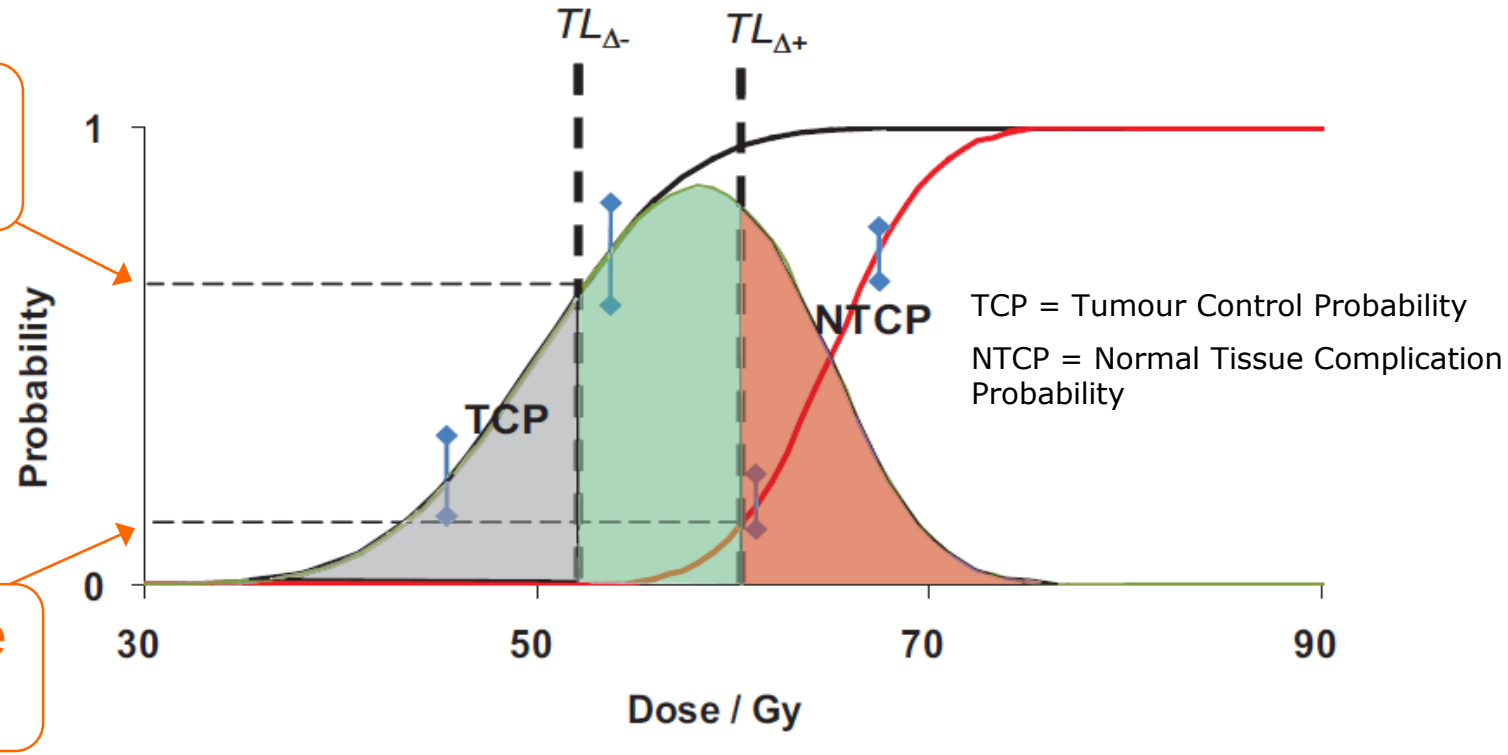

Figure 3.2 Illustration of the procedure to obtain dosimetric tolerance limits from TCP and NTCP data. $TL_{\Delta-}$ is set to a minimum acceptable cure rate and $TL_{\Delta+}$ to a maximum acceptable complication rate.

ESTRO Physics Booklet #10 [2]

ESTRO School

Action limits - Proposed philosophy

Step 1: Determine the uncertainty (σ) for the dose measurement, yielding the probability distribution for the true dose.

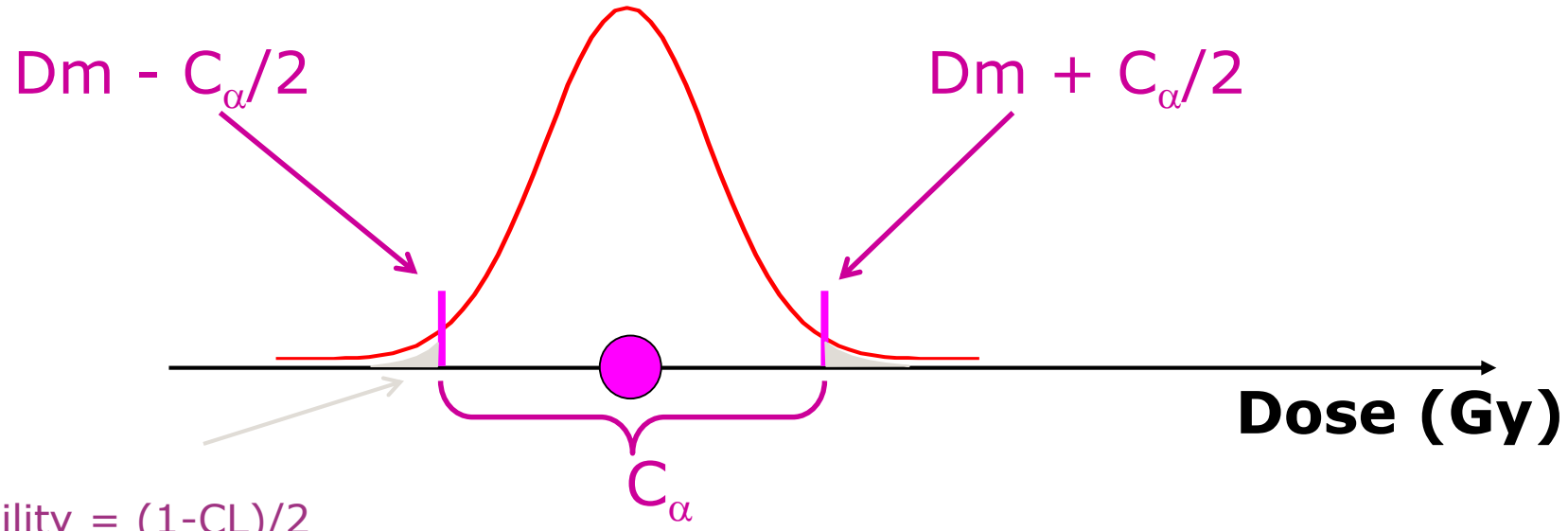

Error probability = (1-CL)/2
(i.e. 2.5% when CL=95%)

Step 2: Set a confidence level CL for the true dose, e.g. CL =95%, and determine the corresponding dose interval C_α.

From Jörgen Olofsson (Dose Modeling and dose verification ESTRO COURSE)

ESTRO School

Action limits - Proposed philosophy

Step 3: Adjust the true dose probability distribution such that the dose limits IDC-$C_\alpha/2$ and IDC+$C_\alpha/2$ coincide with the clinical tolerance limits.

Prescribed dose

Probability distribution for the true dose

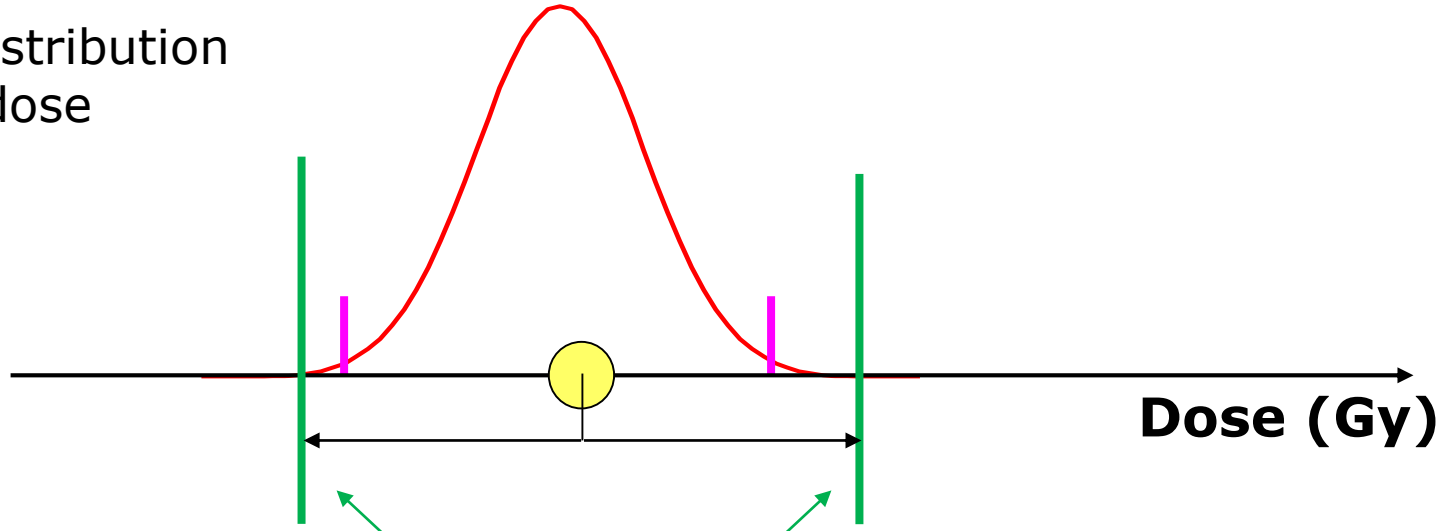

is set to a minimum acceptable cure rate

is set to a maximum acceptable complication rate

Clinical tolerance limits

From Jörgen Olofsson (Dose Modeling and dose verification ESTRO COURSE)

ESTRO School

Action limits - Proposed philosophy

Step 4: Define the center of the true dose probability distribution as the lower and upper **action limit**, respectively.

Prescribed dose

Probability distribution for the true dose

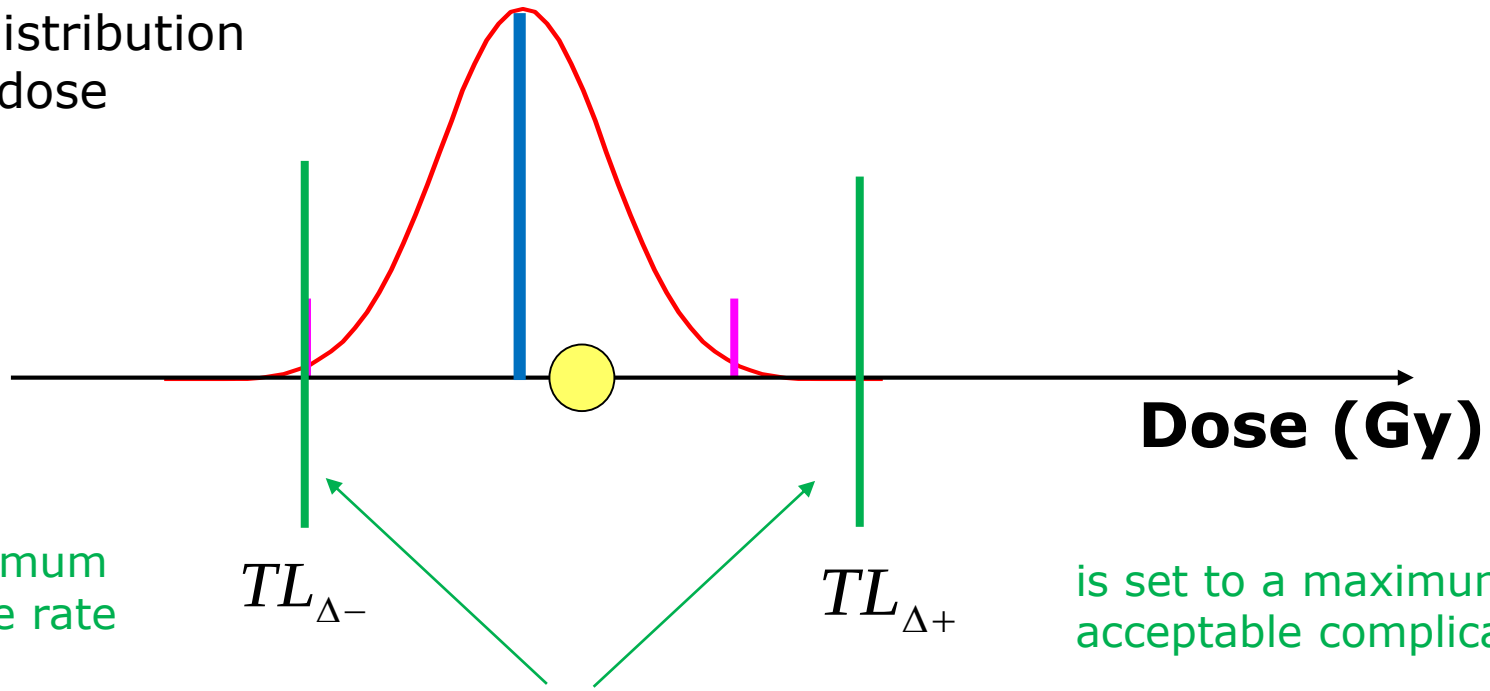

is set to a minimum acceptable cure rate

is set to a maximum acceptable complication rate

Clinical tolerance limits

From Jörgen Olofsson (Dose Modeling and dose verification ESTRO COURSE)

ESTRO School

Action limits - Proposed philosophy

Step 3: Adjust the true dose probability distribution such that the dose limits IDC-$C_\alpha/2$ and IDC+$C_\alpha/2$ coincide with the clinical tolerance limits.

Prescribed dose

Probability distribution for the true dose

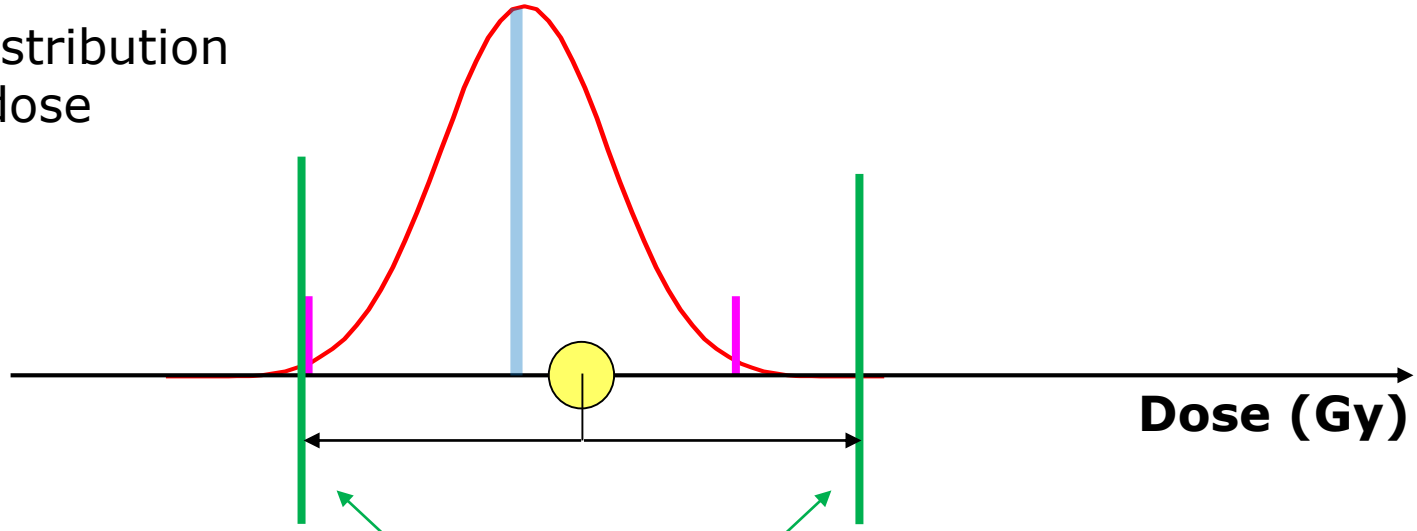

is set to a minimum acceptable cure rate

is set to a maximum acceptable complication rate

Clinical tolerance limits

T. From JörgenOlofsson (Dose Modeling and dose verification ESTRO COURSE)

ESTRO School

Action limits - Proposed philosophy

Step 4: Define the center of the true dose probability distribution as the lower and upper **action limit**, respectively.

Prescribed dose

Probability distribution for the true dose

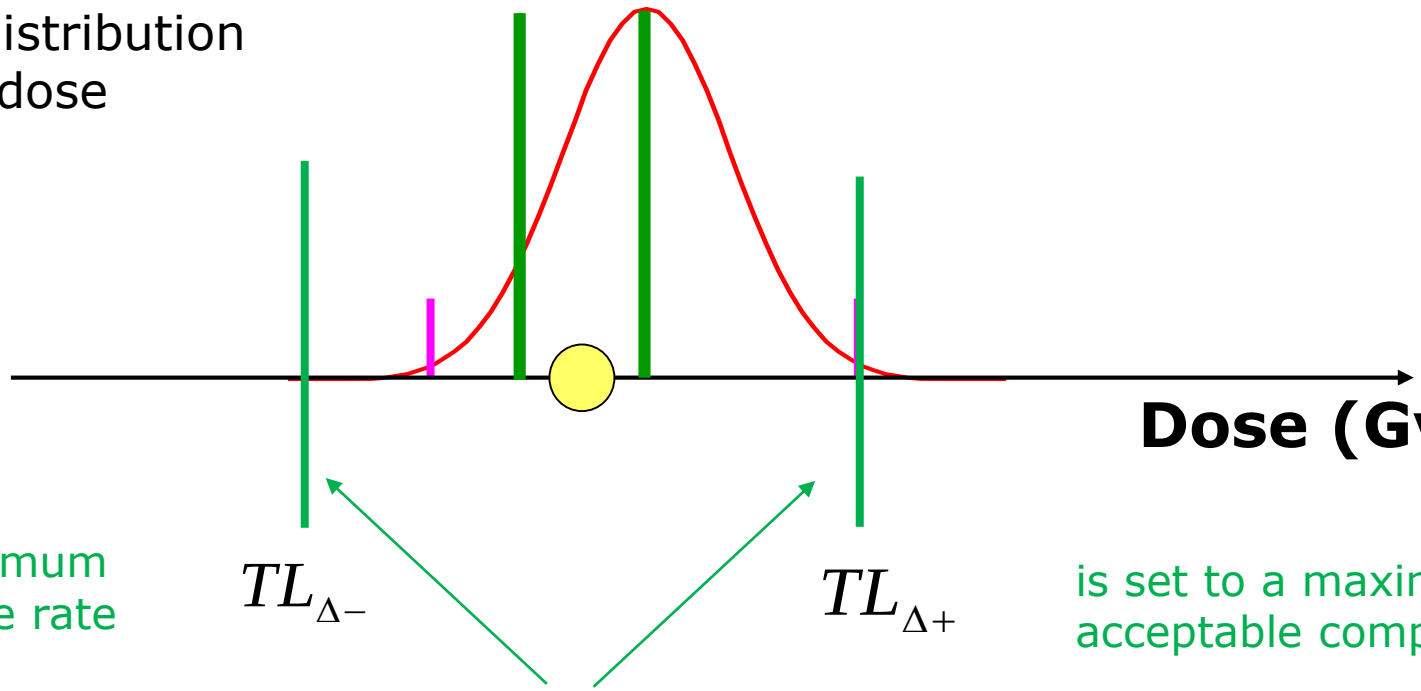

is set to a minimum acceptable cure rate

is set to a maximum acceptable complication rate

Clinical tolerance limits

From Jörgen Olofsson (Dose Modeling and dose verification ESTRO COURSE)

ESTRO School

Action limits - Proposed philosophy

Hence, the action limits should be calculated as

Clinical tolerance=specification

Measurement uncertainty

$$\Delta L_{\pm} = TL_{\pm} \pm \frac{C_{\alpha}}{2}$$

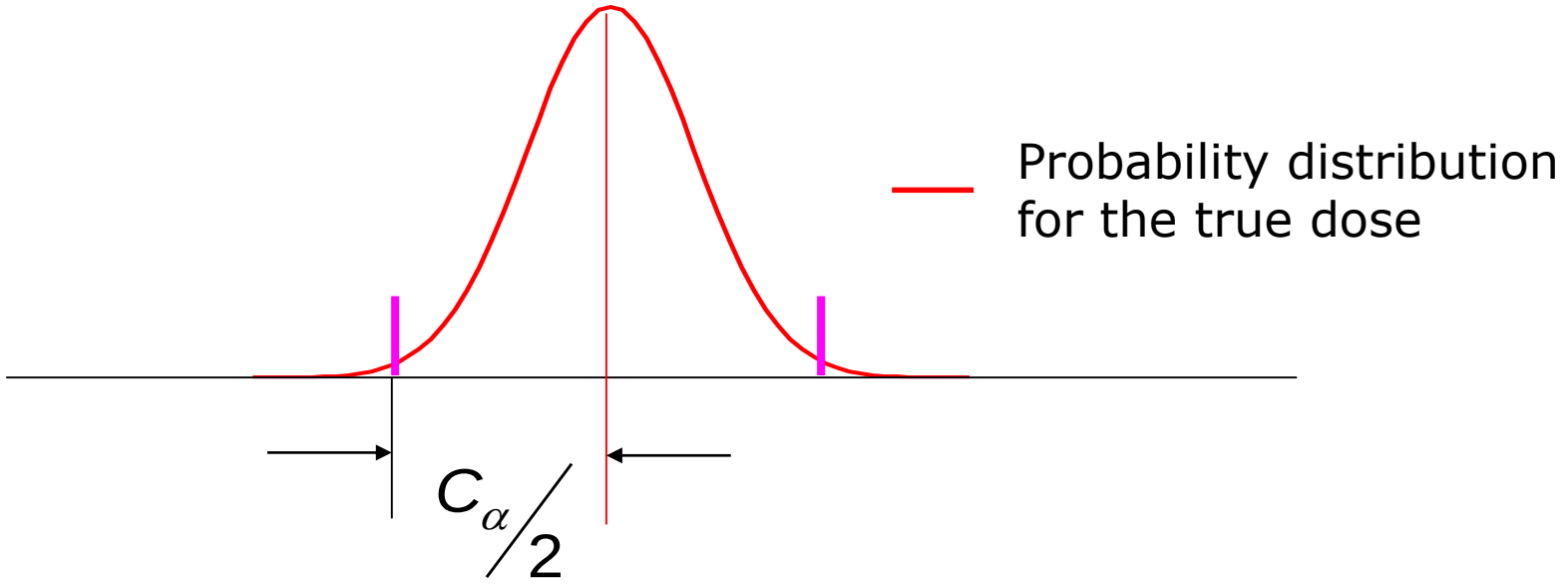

From Jörgen Olofsson (Dose Modeling and dose verification ESTRO COURSE)

ESTRO School

Example with small uncertainty:

Prescribed dose

Probability distribution for the true dose

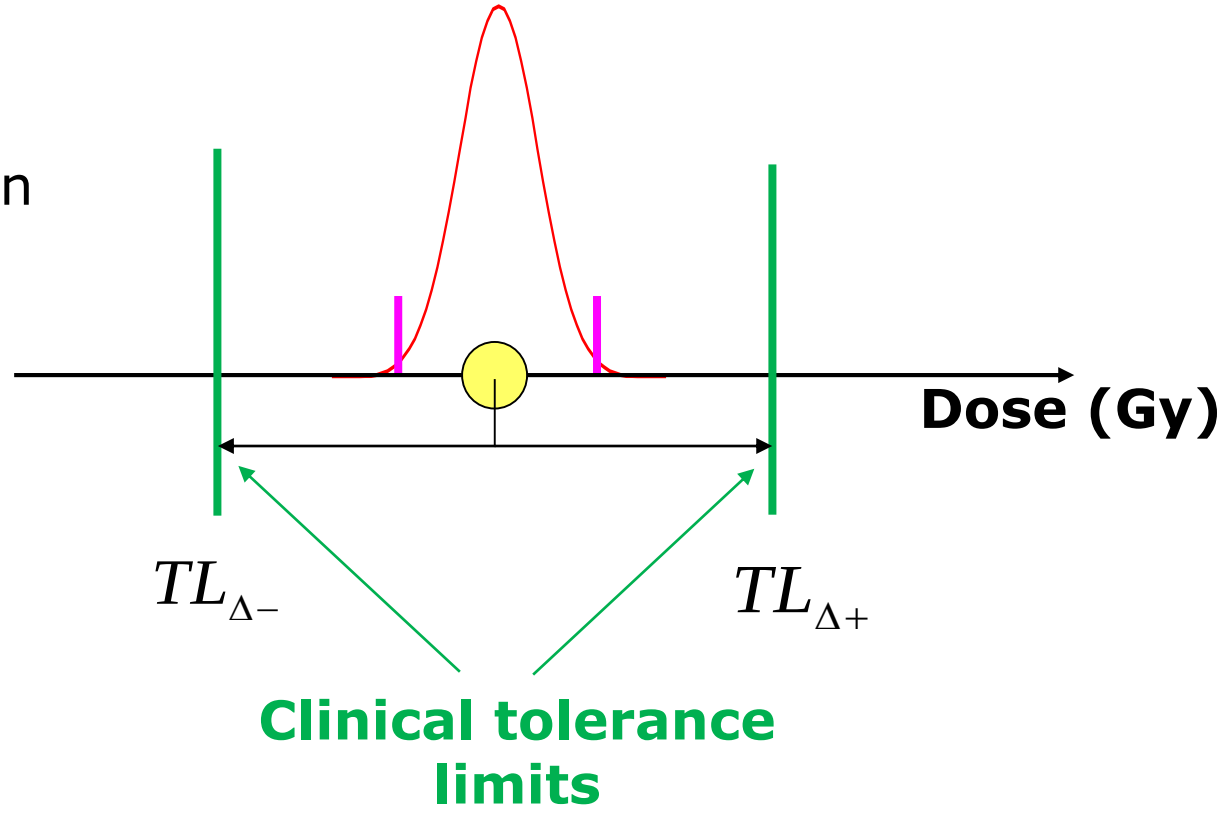

Example with small uncertainty:

Prescribed dose

Probability distribution for the true dose

Action limits smaller than tolerance limits

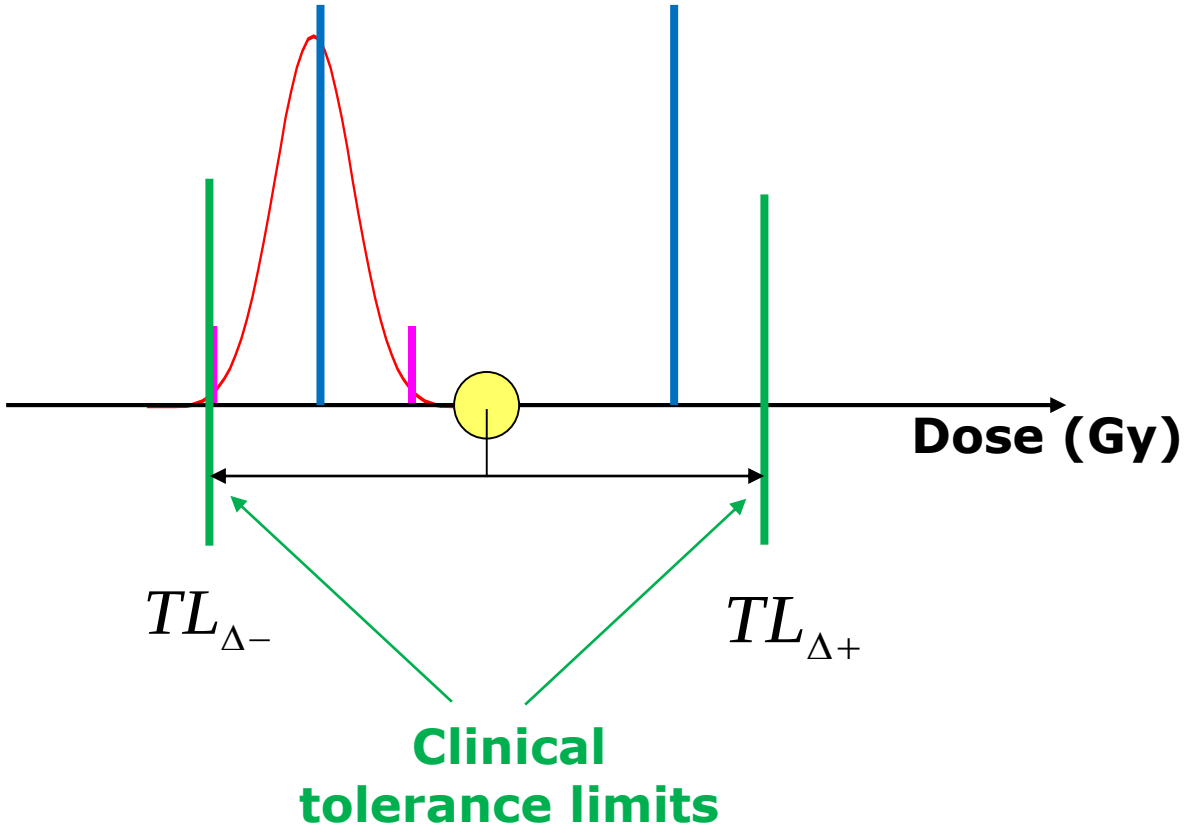

Example with large uncertainty:

Prescribed dose

Probability distribution for the true dose

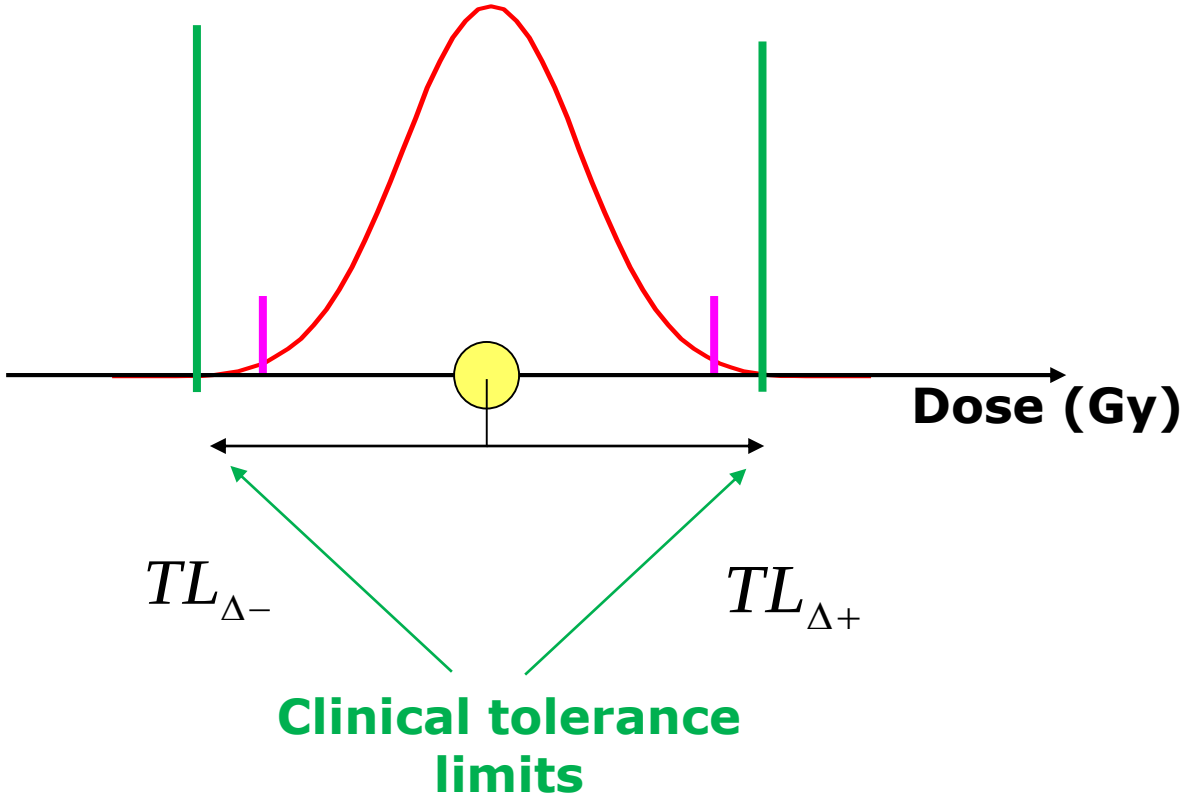

T. From JörgenOlofsson (Dose Modeling and dose verification ESTRO COURSE)

Example with large uncertainty:

Prescribed dose

Probability distribution for the true dose

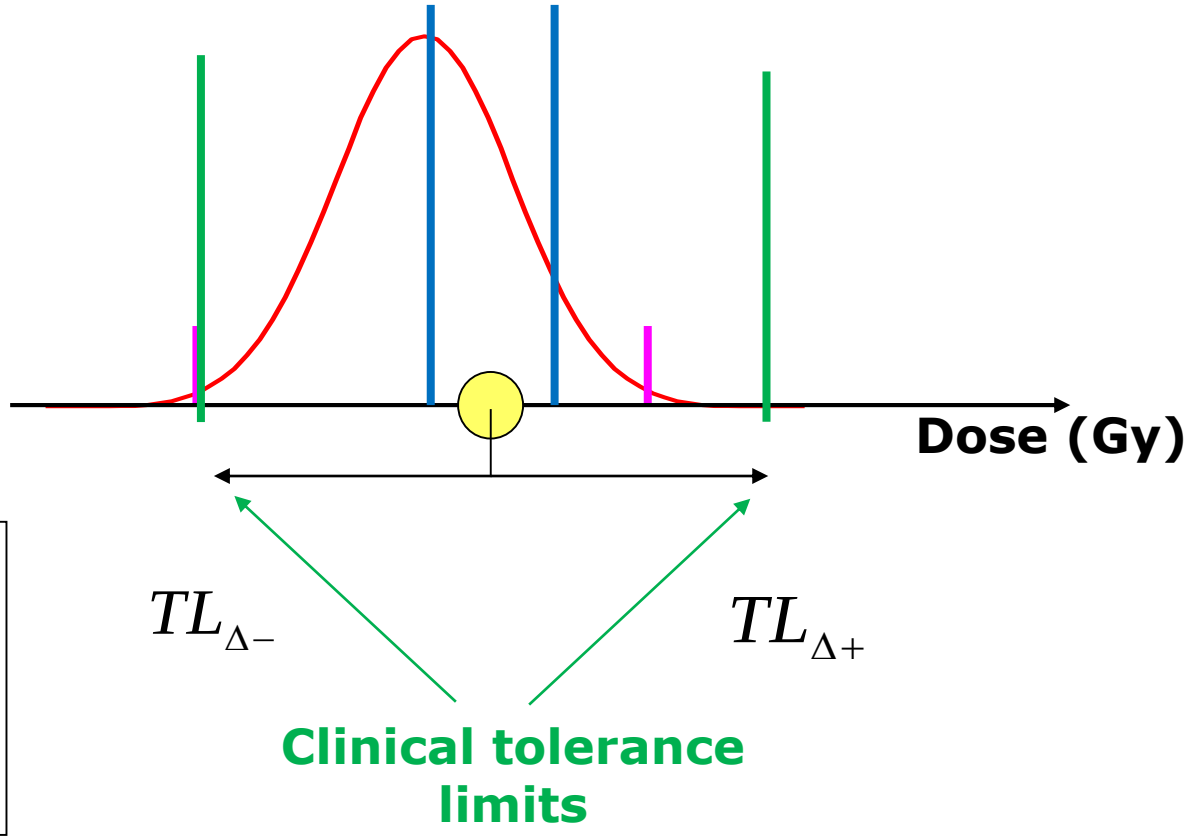

Action limits go to zero when dose measurement uncertainty increases

Relations between TL_Δ AL_Δ σ and α

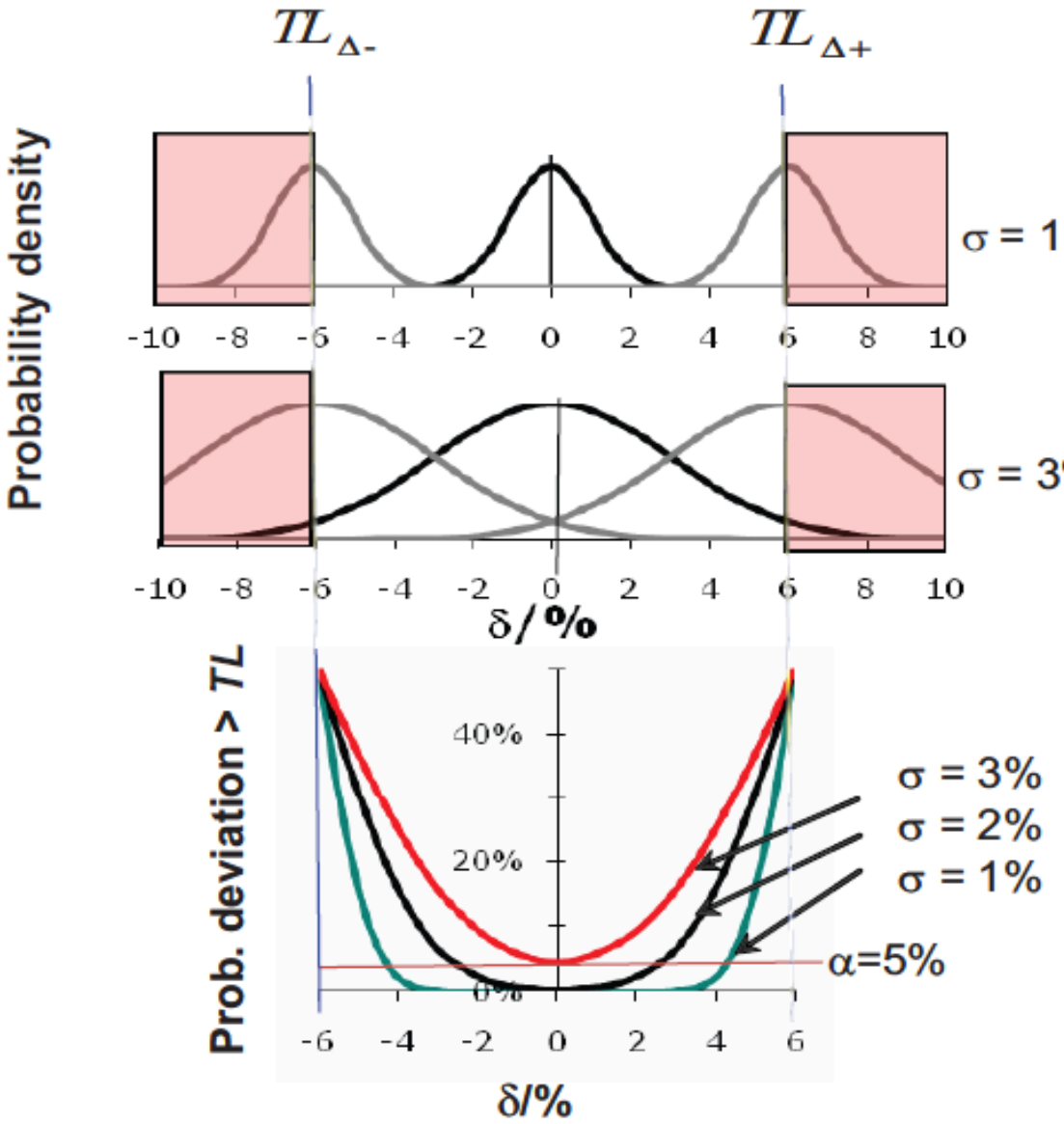

AL_+= 6-2=4

AL_+= 6-6=0

$$\Delta L_\pm = TL_\pm \pm \frac{C_\alpha}{2}$$

Dosimetric tolerance set to ± 6%

Different measurements standard deviations (σ)

What is the Action level (δ) if I set the confidence level in 95% (⟨ =5%)?

ESTRO School

Friday afternoon at the medical physics department…

Dose measurement

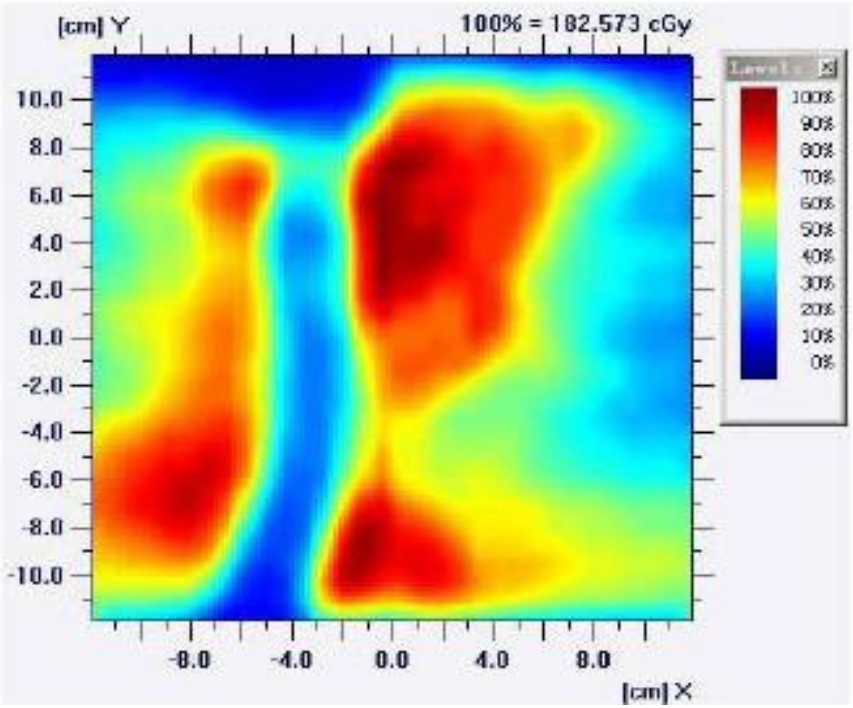

TPS dose calculation

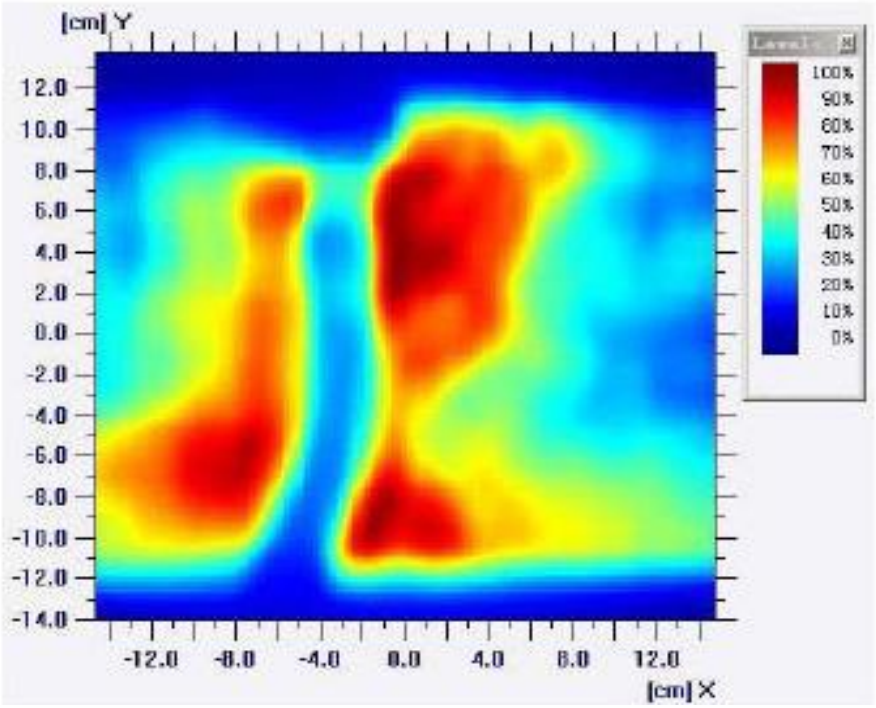

Not OK for treatment?

We need limits to make objective decisions!

From Jörgen Olofsson (Dose Modeling and dose verification ESTRO COURSE)

ESTRO School

A couple of questions

IMRT; Does it make sense to have different action limits for different treatment sites?

IMRT; Does it make sense to have different action limits for different treatment units?

IMRT; Does it make sense to have different action limits for different sites?

The uncertainty in the measurement: The same

If clinical tolerance limits depend on the site : YES

IMRT; Does it make sense to have different action limits for different treatment units?

The uncertainty in the measurement: The same

The clinical tolerance limits: The same

Conclusion

- Be critical when setting value driven tolerance and action limits
- The action limit must be set according to clinical tolerances and measurement uncertainty
- If your measuring equipment has large uncertainties it may not be suitable for QC

References

1. BIPM: Guide to the Expression of Uncertainties in Measurements (GUM). JCGM 100:2008
2. ICRU Report 76: Measurement QA for Ionising Radiation Dosimetry
3. Venselaar et al, Radiotherapy and Oncology 60 (2001) 191-201
4. E.B. Podgorsak (editor). Radiation Oncology Physics: A Handbook for Teachers and Students. International Atomic Energy Agency; Vienna, Austria, 2005, (ISBN 9201073046).
5. M. Karlsson, A. Ahnesjö, D. Georg, T. Nyholm and J. Olofsson (2010) Independent Dose Calculations – Concepts and Models, ESTRO Physics Booklet no. 10. ESTRO; Brussels, Belgium.

ESTRO School

References

International Organization for Standardization:
Guide to the Expression of Uncertainty in Measurement, ISO (1993), ISBN 92-67-10188-9

May be obtained also via:

http://www.bipm.org/en/publications/guides/gum.html

H. Jin, J. Palta, T Suh and S. Kim. A generalized *a priori* dose uncertainty model of IMRT delivery. Med. Phys. 35, 982 (2008)

M. Karlsson et al. ESTRO booklet nº10. Independent dose calculations concepts and methods. (2010).

M. Goitein, Calculation of the uncertainty in the dose delivered during radiation therapy. Med. Phys. 12(5) (1985)

Lujan et al. A method for incorporating organ motion due to breathing into 3D dose calculations. Med. Phys. 26 (5) (1999)

G.K Svensson et al. AAPM Report 13. Physical aspects of Quality Assurance in Radiotherapy. (1994)

Step 1: Construct the **a priori** probability density $p(x)$ for the temperature distribution:

$$p(x) = C \quad \text{for} \quad \mathrm{T} - \Delta \le \mathrm{x} \le \mathrm{T} + \Delta$$
$$p(x) = 0 \quad \text{otherwise}$$

The integral $\int_{-\infty}^{\infty} p(x)\,\mathrm{d}x$ must be unity.

$$\int_{-\infty}^{\infty} p(x)\mathrm{d}x = C \cdot x\Big|_{T-\Delta}^{T+\Delta} = C \cdot 2\Delta \qquad C = \frac{1}{2\Delta}$$

$$p(x) = \frac{1}{2\Delta} \quad \text{for} \quad T - \Delta \le x \le T + \Delta$$
$$p(x) = 0 \quad \text{otherwise}$$

Step 2: Calculate the **expectation value** ξ and the **variance** σ^2 of the temperature using that probability density $p(T)$

Expectation value:

$$\xi = \int_{-\infty}^{+\infty} x \cdot p(x)\mathrm{d}x = \frac{1}{2\Delta}\int_{T-\Delta}^{T+\Delta} x\,\mathrm{d}x = T$$

Variance:

$$\sigma^2 = \int_{-\infty}^{+\infty} (x-\xi)^2\, p(x)\,\mathrm{d}x = \frac{1}{2\Delta}\int_{T-\Delta}^{T+\Delta} (x-T)^2\,\mathrm{d}x = \frac{1}{3}\Delta^2$$

Standard uncertainty:

$$u_B = \sqrt{\sigma^2} = \frac{\Delta}{\sqrt{3}}$$

ESTRO School

WWW.ESTRO.ORG/SCHOOL

Phantoms for verification and patient specific quality assurance (PSQA)

Mania Aspradakis
maria.aspradakis@luks.ch

Learning Objectives

- Discuss how solid plastic phantoms are represented in TPS
- Review phantoms available for end-to-end testing and patient specific QA (PSQA)

Reference medium in radiotherapy dosimetry

Water is a good soft tissue equivalent material for high energy photon and electron beams.

Dosimetry for beam characterisation & TPS verification:

- Reference dosimetry: dosimetry Codes of Practice (CoP) use water as reference medium
- Relative dosimetry: relative depth functions (PDD, TPR), beam profiles, output factors etc. are measured in water

Phantoms for TPS verification: liquid water

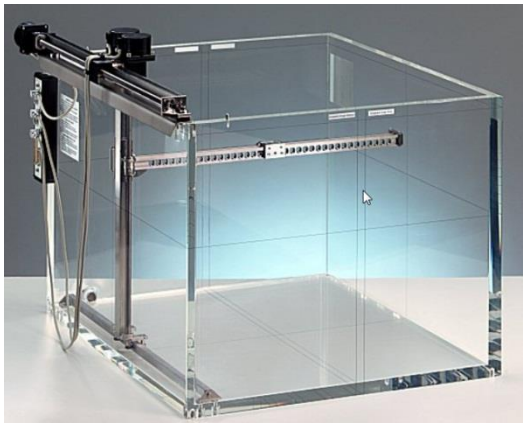

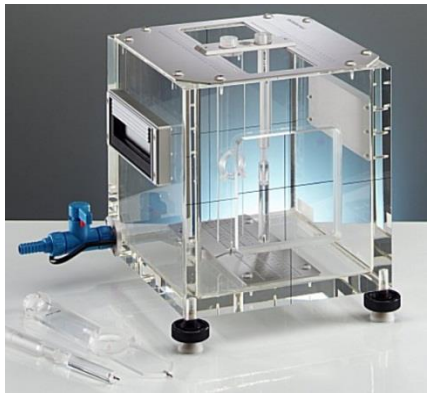

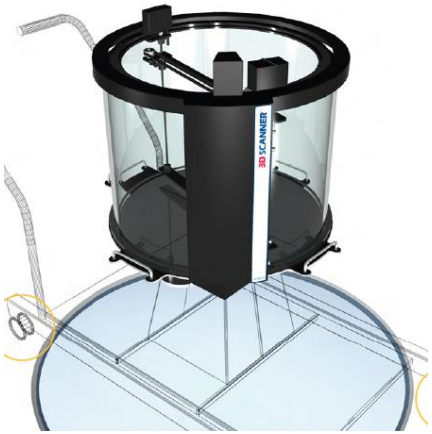

Advantages

- Widely used and available
- Known composition
- Detectors can be placed at any point inside the phantom
- Large enough to characterize the beam under full scatter conditions

Disadvantages

- Not all detectors are waterproof
- Not quick and easy to set up
- Too large to simulate the dimensions of a real patient and be used for the dosimetric verification of a treatment plan

How are phantoms represented in the TPS?

For the verification of doses calculated in liquid water against measurements in a **homogeneous water medium (water tank)**:

It suffices to perform the calculations in a virtual phantom, ‘drawn’ in the TPS, which is assigned the density of water

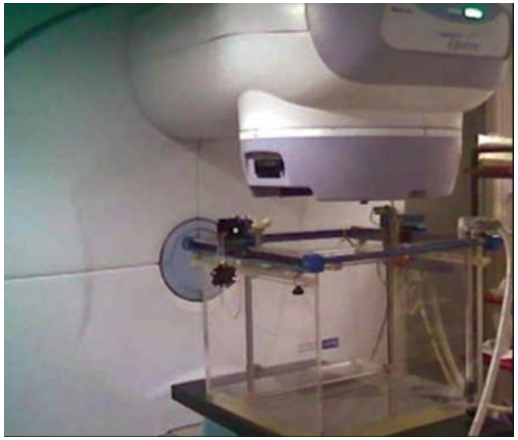

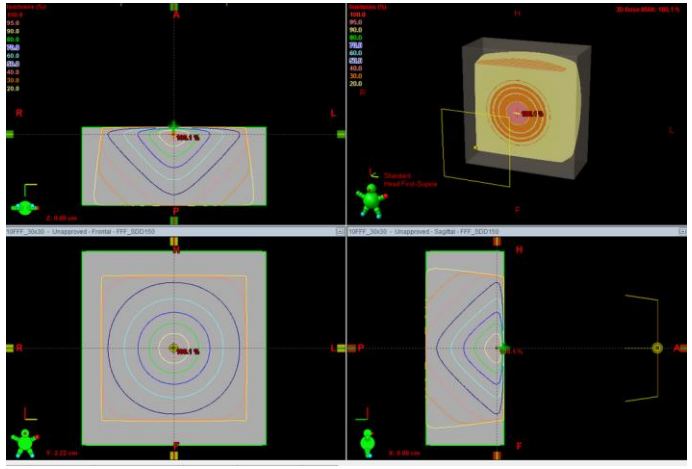

How are phantoms represented in the TPS?

For the comparison/verification of doses between different calculation methods in phantoms with heterogeneities

- It suffices to draw TPS virtual phantoms being assigned different densities

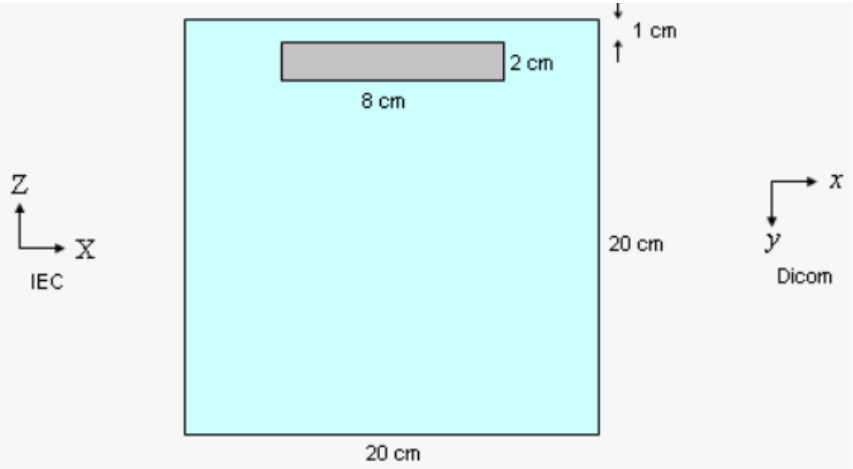

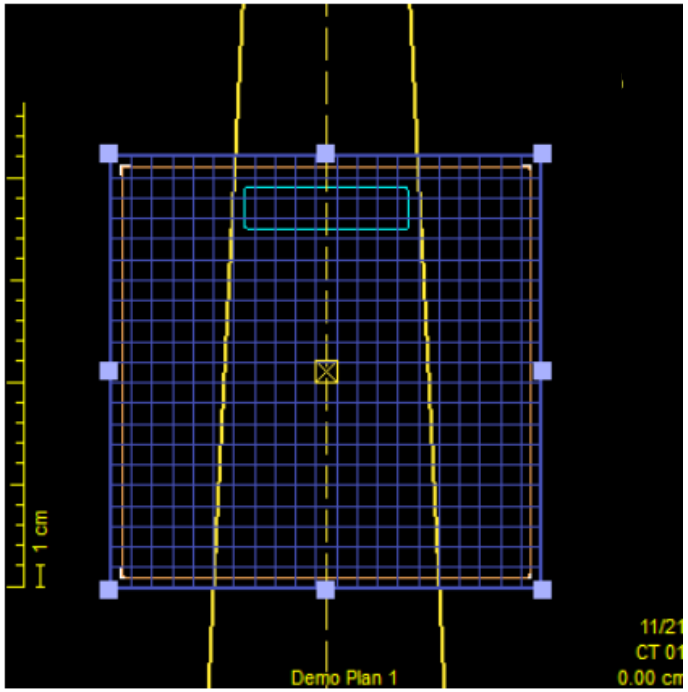

Phantoms for TPS verification and plan QA: solid plastic slabs

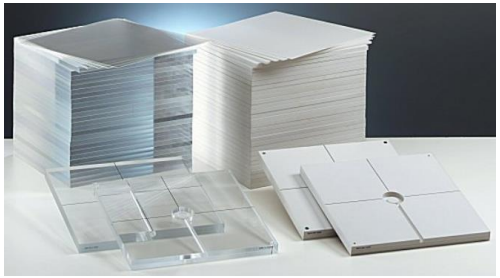

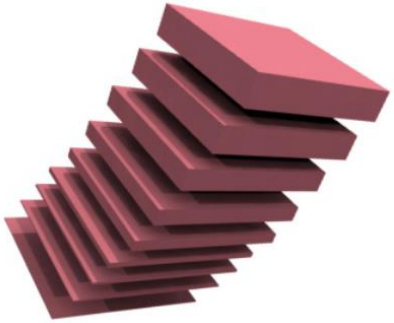

Advantages

- Robust
- Allow easy, quick and reproduceable setup
- Can be used with non water-proof detectors
- Easier to use with films

Disadvantages

- Water-equivalence depends on modality and energy (MV, kV, MeV)
- Expensive if manufactured to be water-equivalent
- Different samples of same type of plastic could vary in composition and from manufacturer specification
- Possible degradation with time
- Possible charge storage effects

Use of solid plastic materials for dosimetry

Determination of absorbed dose to water using an ionisation chamber in a solid plastic phantom:

The dosimetry formalism that converts ionisation measured in a solid plastic to dose in water necessitates that the density and composition of the material are known, as well as

- Appropriate detector perturbation factors (not widely available)
- Phantom conversion factor can be determined experimentally
- **Epoxy resin based solid phantoms** shown to be equivalent to within 1% to water

Formalism in Dosimetry Code of Practice
for dose to water from a measurement in plastic

$$D_{w,Q}\left(z_{\text{ref}}\right) = M_{s,Q}\left(z_{\text{eq}}\right) \underbrace{N_{\text{D,w,Q}_o}\, k_{\text{Q,Q}_o}}\, k_{w,s}^{Q}$$

from dose to water formalism

Relevant references:
Jan Seuntjens etal, 2005, Med.Phys. 32 pp2945-
Araki etal, 2009, Med.Phys. 36 (7) pp2992-
McEwen, Med Phys 33(4), 2006, p876-
Fujita, Y. et al (2010). J Radiat Res **51**(6): 707-713.

Use of solid plastic materials for dosimetry

Epoxy resin based solid phantoms shown to be equivalent to within 1% to water

TABLE I. Stated composition (% by weight) of epoxy-resin materials. For comparison, values are also given for liquid water.

Element	Virtual Water™	Solid Water™ RMI-457[a]	Plastic Water™[b]	Water	WT1
H	7.7	8.09	9.25	11	
C	68.7	67.22	62.82		
N	2.3	2.40	1.00		
O	18.9	19.84	17.94	89	
Ca	2.3	2.32	7.95		
Cl	0.1	0.13	0.96		
Br			0.03		
ρ [g cm^{-3}]	1.030	1.043	1.030	0.998 [t]	1.020
ρ_e [$\times 10^{23}$ g^{-1}]	3.237	3.249	3.238	3.343	3.249
$(\rho_e)_{pl,w}$	0.968	0.972	0.969		0.972
Z_{eff} [c]	6.35	6.35	6.83	7.22	6.35

McEwen, Med Phys 33(4), 2006, p876-

$$\rho_e = \rho_m \cdot N_A \cdot \left(\frac{Z}{A}\right)_{eff} \quad \text{cm}^{-3}$$

ESTRO School

Use of solid plastic materials for treatment planning calculations

A. Correct representation of phantom (medium and geometry) in the CT dataset

B. Correct representation and use of the phantom (medium and geometry) by the TPS

Use of solid plastic materials for treatment planning calculations

Accurate phantom reconstruction from a series of CT slices generally requires that

- Phantom dimensions are reproduced correctly
- There is no distortion in the images from image reconstruction
- The slice position and dimension is reproducible
- The slice thickness is correct
- The different materials in the phantom are correctly represented

For faithful simulation of radiation transport in media, the media properties must be considered:

- Electron Density
- Mass Density
- Chemical composition

Phantoms for TPS verification and plan QA: use of solid plastics

A comparison of absorbed doses calculated by a TPS in CT-scanned solid phantoms against measurements in these phantoms is valid if the different materials in phantom are correctly represented in the CT dataset.

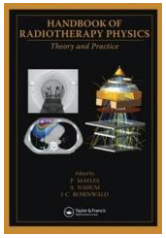

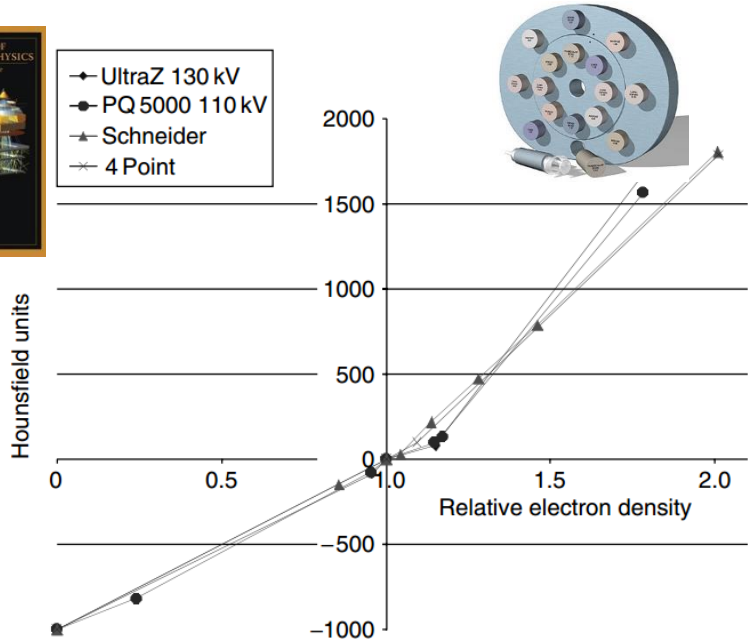

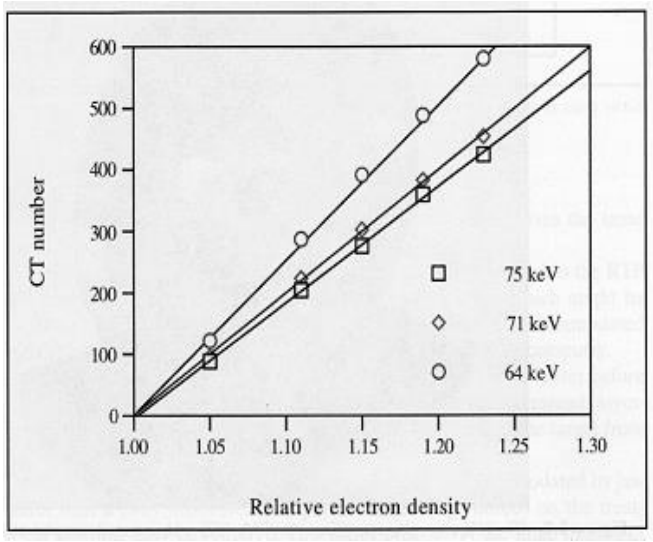

Metcalfe, Kron & Hoban,
The Physics of Radiotherapy X-ray and Electrons (2007)

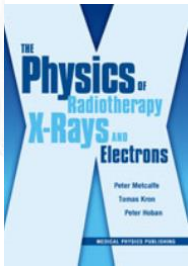

$$N_{CT} = \frac{\mu_m - \mu_w}{\mu_w} x\,1000$$

with

$$\mu(E) = \rho N_A \sum_i^N \left(\frac{w_i}{A_i} \sigma_i(E) \right)$$

ESTRO School

Phantoms for TPS verification and plan QA: use of solid plastics

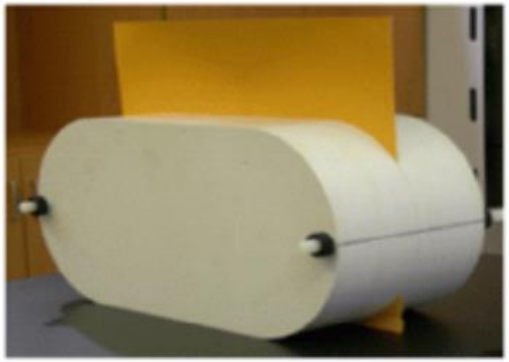

If the solid plastic material is not water equivalent in the kV beam energy region at which the CT scan is being performed, then the CT calibration curve will not correctly represent the relationship between relative density and Hounsfield numbers.

In such a case, it is best to override the material density with the density of the medium as given by its manufacturer

Use this description of the phantom for dose calculations and comparisons of these against measurement in the phantom

Phantoms for TPS verification and plan QA: use of solid plastics

To compare measured doses in **plastic phantoms** against doses calculated by TPSs, the phantoms needs to be corrected represented in the TPS

HN to relative electron density calibration

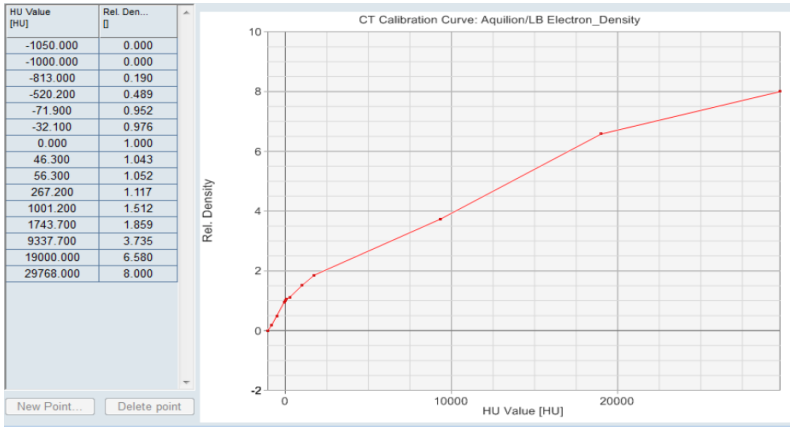

HU Value [HU]	Rel. Den... []
-1050.000	0.000
-1000.000	0.000
-813.000	0.190
-520.200	0.489
-71.900	0.952
-32.100	0.976
0.000	1.000
46.300	1.043
56.300	1.052
267.200	1.117
1001.200	1.512
1743.700	1.859
9337.700	3.735
19000.000	6.580
29768.000	8.000

Eclipse

If voxels are assigned to water-like media of varying relative electron density, and only this material property is used for the calculation dose (transport of particles and energy deposition),

comparison against measurements in terms of absorbed dose to water is straightforward (provided the all necessary perturbation corrections are considered in the measurement!)

Phantoms for TPS verification and plan QA: use of solid plastics

To compare measured doses in **plastic phantoms** against doses calculated by TPSs, the phantoms needs to be corrected represented in the TPS

HN to relative mass density calibration

HU Value [HU]	Density [g/cm3]
-1000.000	0.001
-815.500	0.195
-523.800	0.495
-77.700	0.967
-38.000	0.991
0.000	1.000
44.100	1.062
51.500	1.071
258.700	1.161
985.900	1.609
1715.400	2.000
7708.800	4.507

New Point... Delete point

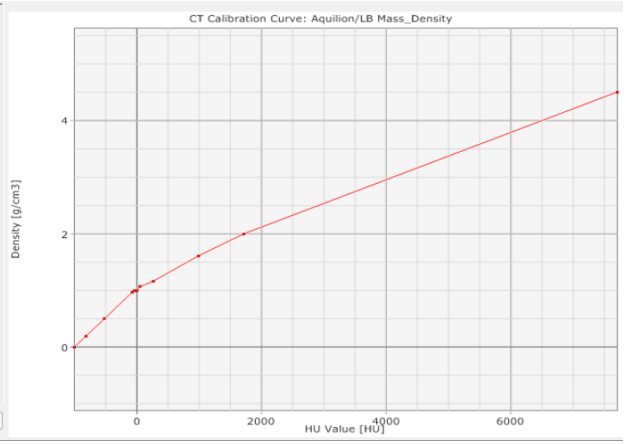

Eclipse

…and with assignment to material properties

Volume Type | Volume Code | Color and Style | Add-On Material | Brachy Applicator | Tolerance | Radioactive Source Model | Equivale

Table ID: AcurosXB-11.0 Set as Default Delete Table

Default Table ID: AcurosXB-11.0 Import from DCF

Physical Materials

ID	Name	Minimum Density [g/cm3]	Default Density [g/cm3]	Maximum Density [g/cm3]	Used in Automatic CT-to-Material Conversion
Acetal	Acetal		1.4200		no
Adipose_Tissue	Adipose Tissue	0.5539	0.9200		
Air	Air	0.0000	0.0012		
Aluminum	Aluminum	2.2750	2.7000		
Bone	Bone	1.1000	1.8500		
Cartilage	Cartilage	1.0556	1.1000		
Cork	Cork	0.1000	0.1900		
Epoxy	Epoxy		1.0400		
Lung	Lung	0.0110	0.2600		
Muscle_Skeletal	Muscle Skeletal	0.9693	1.0500		
PEEK	PEEK		1.3100		
PMMA	PMMA		1.1900		
Polystyrene	Polystyrene	0.5900	1.0500		
PTFE	PTFE		2.2000		
PVC	PVC		1.3800		
PVDF	PVDF		1.7700		
Radel	Radel		1.3000		
Stainless_Steel	Stainless Steel	6.2100	8.0000		
Ti6Al4V_ELC	Titanium Alloy	3.5600	4.4200		
Water	Water	0.0000	1.0000		
Wood	Wood	0.3000	0.7000		

Material	Density		
	Minimum (g/cm³)	Default (g/cm³)	Maximum (g/cm³)
Automatic CT to material conversion			
Air (STP)	0.0012	0.0012	0.0204
Lung (ICRP 1975)	0.0110	0.26	0.6242
Adipose Tissue (ICRP 1975)	0.5539	0.92	1.0010
Muscle, Skeletal (ICRP 1975)	0.9693	1.05	1.0931
Cartilage (ICRP 1975)	1.0556	1.10	1.60
Bone (ICRP1975)	1.10	1.85	3.00
Manual material assignment			
Aluminum	2.2750	2.70	3.56
Titanium Alloy	3.56	4.42	6.21
Stainless Steel	6.21	8.00	8.00
Water	0.0012	1.00	3.00
Wood	0.30	0.70	1.00
Cork	0.10	0.19	0.40
Polystyrene	0.59	1.05	1.0750
Epoxy		1.04	
PMMA		1.19	
Radel		1.30	
PEEK		1.31	
PVC		1.38	
Acetal		1.42	
PVDF		1.77	
PTFE		2.20	

The phantom medium must be manually assigned for the calculations

Phantoms for TPS verification and plan QA: use of solid plastics

To compare measured doses in **plastic phantoms** against doses calculated by TPSs, the phantoms needs to be corrected represented in the TPS

HN to relative mass density calibration

HU in Oncentra	Composition	$\frac{\rho_{mass}}{\rho_{mass,H_2O}}$	$\frac{\rho_{elec}}{\rho_{elec,H_2O}}$
-992	Air (outside patient)	0.00121	0.00109
-976	Air (inside patient)	0.00121	0.00109
-480	Lung (ICRU 44)	0	
-96	Adipose (ICRU 44)	0	
48	Muscle (ICRU 44)	1	
128	Cartilage (ICRP 23)	1	
528	2/3 Cartilage, 1/3 Bone	1	
976	1/3 Cartilage, 2/3 Bone	1	
1488	Bone (ICRP 23)	1	
1824	Bone (ICRP 23)	2	
2224	½ Bone, ½ Aluminum	2	
2640	Aluminum	2	
2832	Aluminum	2	
>2832	Iron	7	
-	Water	1	

Oncentra

	Hounsfield units	Density [g/cm³]
Air (outside patient)	-992	0.00121
Air (inside patient)	-976	0.00121
Lung (ICRU 44)	-480	0.5
Adipose (ICRU 44)	-96	0.95
Muscle (ICRU 44)	48	1.05
Cartilage (ICRP 23)	128	1.1
2/3 Cartilage, 1/3 Bone	528	1.35
1/3 Cartilage, 2/3 Bone	976	1.6
Bone (ICRP 23)	1488	1.8
Bone (ICRP 23)+	1824	2.1
1/3 Bone, 2/3 Aluminum	2224	2.4
Aluminum	2640	2.7
Aluminum+	2832	2.8
Iron	2833	7.8
Iron+	3096	7.8

RayStation

Table 2.2: The mass density relative to water and the atomic mass composition (%) of tissue materials used in RayStation 4.7 for effective density calculation.

	$\frac{\rho_{mc\text{-}material}}{\rho_{mc\text{-}water}}$	H	C	N	O	Na	Mg	P	S	Cl	Ar	K	Ca
Z		1	6	7	8	11	12	15	16	17	18	19	20
Z/A		0.992	0.5	0.5	0.5	0.478	0.494	0.484	0.499	0.479	0.451	0.486	0.499
Air	0.001203			75.5	23.2						1.3		
Lung	0.26	10.3	10.5	3.1	74.9	0.2		0.2	0.3	0.3		0.2	
Adipose	0.95	11.4	59.8	0.7	27.8	0.1			0.1	0.1			
Tissue	1	10.12	11.1	2.6	76.18								
Muscle	1.05	10.2	14.3	3.4	71	0.1		0.2	0.3	0.1		0.4	
Cartilage	1.1	9.6	9.9	2.2	74.4	0.5		2.2	0.9	0.3			
Bone	1.85	3.4	15.5	4.2	43.5	0.1	0.2	10.3	0.3				22.5
Alu-minum	2.7												
Iron	7.87												
Gold	19.32												
Osmium	22.57												

Phantoms for TPS verification and plan QA: use of solid plastics

To compare measured doses in **plastic phantoms** against doses calculated by TPSs, the phantoms needs to be corrected represented in the TPS

HN to relative mass density calibration

HU in Oncentra	Composition	$\frac{\rho_{mass}}{\rho_{mass,H_2O}}$	$\frac{\rho_{elec}}{\rho_{elec,H_2O}}$
-992	Air (outside patient)	0.00121	0.00109
-976	Air (inside patient)	0.00121	0.00109
-480	Lung (ICRU 44)	0.50	0.50
-96	Adipose (ICRU 44)	0.95	0.95
48	Muscle (ICRU 44)	1.05	1.04
128	Cartilage (ICRP 23)	1.10	1.08
528	2/3 Cartilage, 1/3 Bone	1.35	1.29
976	1/3 Cartilage, 2/3 Bone	1.60	1.52
1488	Bone (ICRP 23)	1.85	1.72
1824	Bone (ICRP 23)	2.10	1.95
2224	½ Bone, ½ Aluminum	2.40	2.15
2640	Aluminum	2.70	2.34
2832	Aluminum	2.83	2.46
>2832	Iron	7.87	6.60
-	Water	1.00	1.00

Oncentra

For some TPSs, the HN to relative mass density calibration does not include an assignment of HN to the density and composition of plastic materials, because plastics area not included in the list of available materials

In such cases, to avoid systematic deviations in the dosimetric validation of dose engines, an *effective mass density* is being assigned to the plastic medium.

- *An implementation of such a workaround can be found in Oncentra.*

- *An effective mass density as implemented in the RayStation, is computed for all media and aims to account for any systematic errors introduced in the assignment of mass density to CT-HN as a result of photon attenuation in the kV energy range (CT energies)*

Phantoms for TPS verification and plan QA

Examples of phantoms available for

- TPS dose verification
- end-to-end testing
- patient specific QA (PSQA)

Slabs of solid plastic

Use of plastic slabs with 2D detector arrays, for example…

MapCHECK/MapPHAN

MapCHECk (Sun Nuclear)

IMRT MatriXX (iba)

seven29 (PTW)

Verification of VMAT dose at different planes possible with such combinations

Simple geometric phantoms

Typical characteristics

- Simple design to mimic body anatomy (pelvis, thorax, head)
- Homogeneous medium
- Detectors can be placed at various points in the phantom
- Possibility to use various types of detectors (chambers diodes, film, TLD etc) in drilled cavities or with special inserts
- Can be manufactured in house
- Large variety of commercially available options
- More expensive if made of water-equivalent plastic

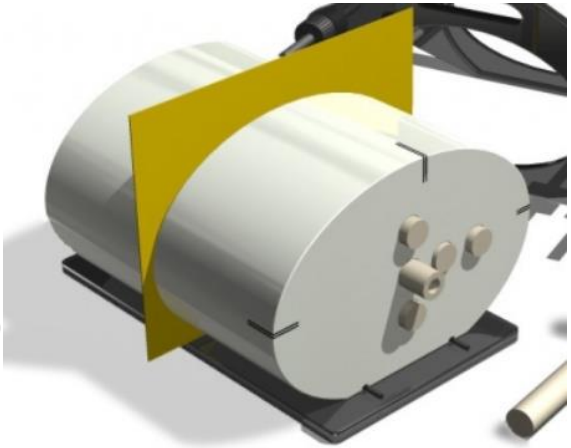

Simple geometric phantoms

Use of geometric phantoms with 2D detector arrays (2D → 3D)

Products & Solutions > Radiation Therapy > VMAT QA, IMRT QA, OCTAVIUS, DIAMOND, DICOM RT Studio > OCTAVIUS

OCTAVIUS® Systems

- 4D Patient and Machine QA
  - OCTAVIUS® 4D
- 2D Patient and Machine QA
  - OCTAVIUS® I | OCTAVIUS® II | OCTAVIUS® III
- OCTAVIUS® Detectors
  - OCTAVIUS® 1500 | OCTAVIUS® 1000 SRS | OCTAVIUS® 729

http://www.ptw-usa.com/octavius.html

Verification of VMAT dose at individual gantry positions possible, but with early versions of this product there were dimensional dependence issues…

http://www.wienkav.at/kav/kfj/91033454/physik/729/PMO.htm

ESTRO School

Measurement vs calculation

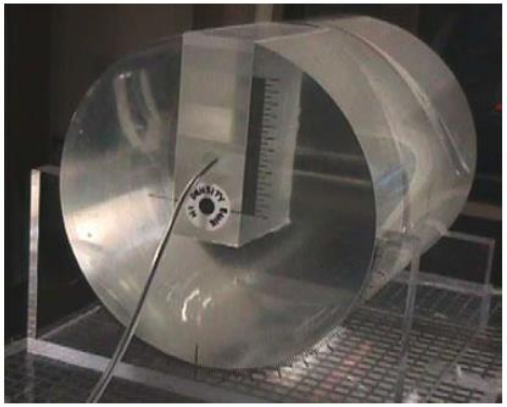

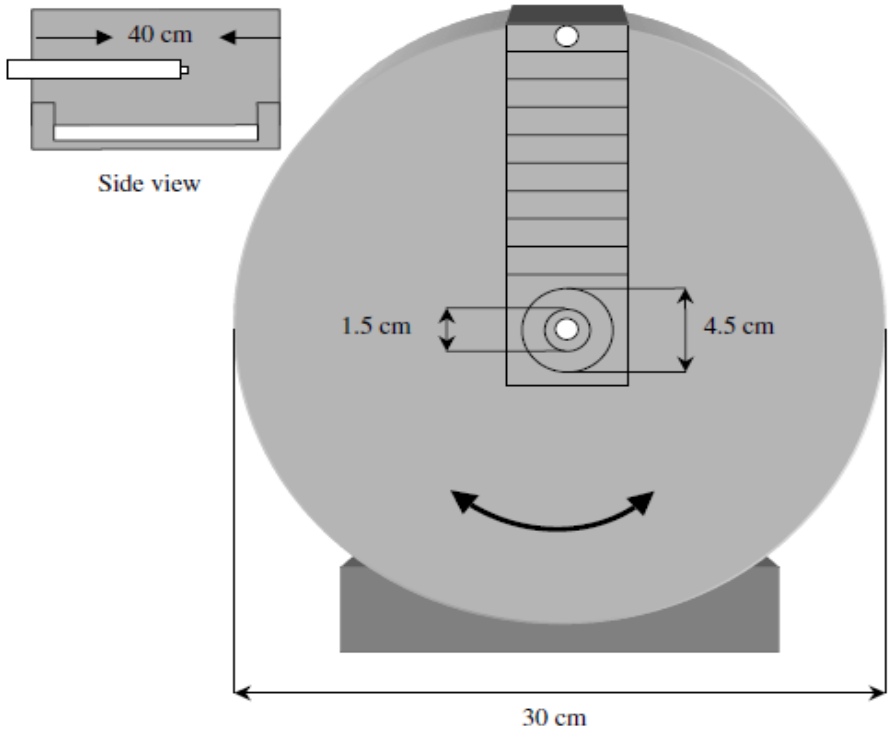

Ma et al, PMB 48 (2003) 561-572

Phantoms for TPS verification and plan QA

Dose determination in PMMA phantom

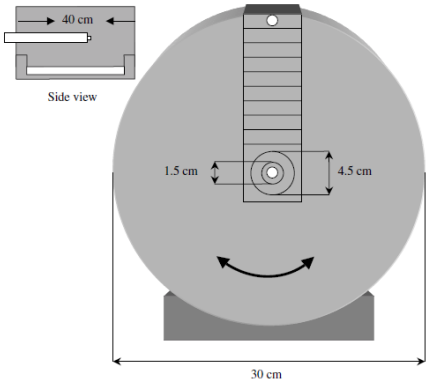

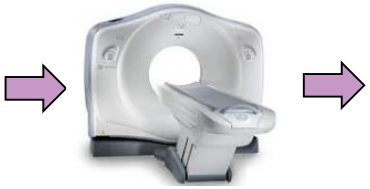

Formalism to derive dose to water from from ionisation measurements in PMMA

$$D_{w}^{clin} = D_{PMMA}^{clin}\left[\left(\frac{\bar{\mu}_{en}}{\rho}\right)_{PMMA}^{w}\right]_{cal}\left[CF_{PMMA\rightarrow w}^{scat}\right]_{cal}$$

$$D_{PMMA}^{clin} = M_{PMMA}^{clin}\; k_{ion}\left[N_{air}\left(\frac{\bar{S}}{\rho}\right)_{air}^{PMMA} p_{repl}\, p_{wall}\right]_{cal}$$

Chamber and medium specific perturbation factors are for the calibration geometry and not the clinical field

Ma et al, PMB 48 (2003) 561-572

Calculations of dose in phantom

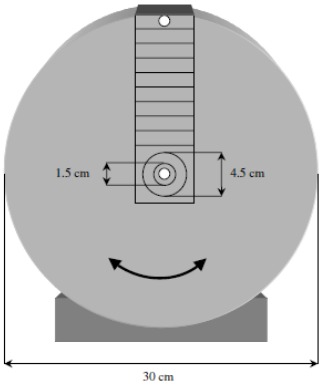

How accurate are the HN to density conversions for plastic phantoms?

Would it be better to create a virtual phantom with the density of PMMA?

How does the TPSs handle materials different from water?

Does the TPS calculates dose to PMMA in PMMA or dose to water in PMMA or...?

Questions we need to be asking ourselves

ESTRO School

Complex phantoms

Typical characteristics

- Shaped to body anatomy (pelvis, thorax, head) or even anthropomorphic
- Include inhomogeneities (low and high density inserts to simulate lung, air, bone cavities)
- Detectors can be placed at various points in the phantom
- Possibility to use various types of detectors in cavities or using special inserts (chambers, diodes, film, TLD etc).
- Only commercially available
- Expensive if made of epoxy resin material

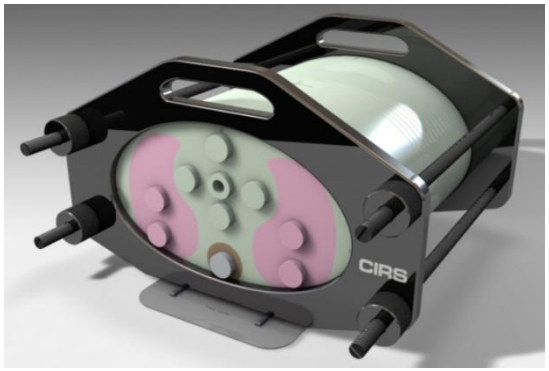

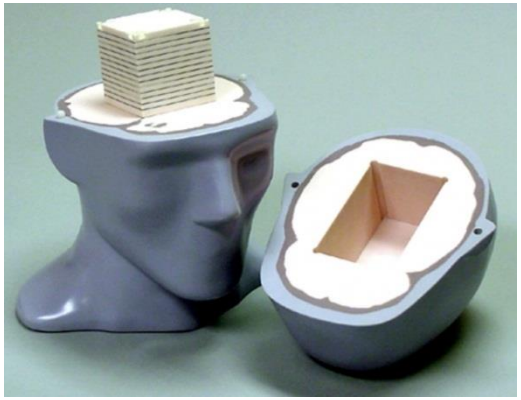

Complex phantoms

QUASAR™ Multi-Purpose Body Phantom

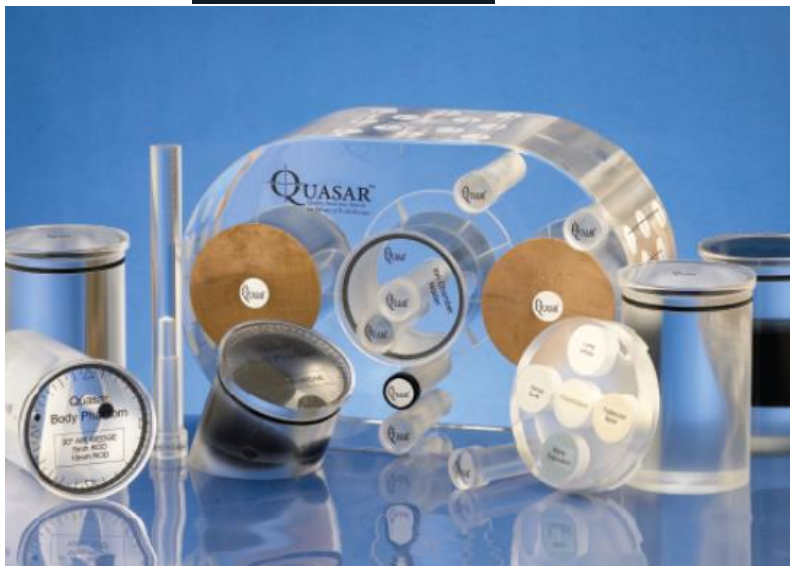

Non-dosimetric test capabilities:

- Geometric accuracy of 2D images and 3D image reconstructions
- 2D and 3D measurement tools including volume calculation accuracy
- Automatic, semi-automatic and manual boundary identification tools
- Auto-margining tools
- Representation and manipulation of contoured patient anatomy
- Dose volume histograms
- Conversion of CT numbers to relative electron densities
- Comparison of display on simulators, RTPS and other imaging workstations
- Image transfer, storage, retrieval, DICOM tools on all workstations

Dosimetric measurement capabilities:

- Verify dosimetry calculations with Ion Chamber measurements; compatible with Ion Chambers from major suppliers
- Measure in low or high dose areas with multiple measurement locations throughout the phantom
- Perform homogeneous density measurements with blank acrylic rods and inserts
- Use inhomogeneous inserts to test density corrections in an idealized near anthropomorphic geometry

http://modusqa.com/imrt/multi-purpose-body

Complex phantoms

IMRT Thorax Phantom

Model 002LFC showing optional water equivalent rod with ion cavity

OVERALL DIMENSIONS:	43.2 cm x 38.1 cm x 22.9 cm (17" x 15" x 9")
WEIGHT:	11.2 kg (30 lb)
MATERIALS:	Phantom Body: Tissue Equivalent Epoxy Materials Inserts: CIRS Tissue Equivalent Materials (epoxy resin based)

MODEL 002LFC INCLUDES

QTY	PART NO.	DESCRIPTION
1		Thorax section drilled to accommodate rod inserts
12		1 cm thorax sections
1		3 cm end section
5	002RW-S	Water equivalent solid rod inserts
1	002RB-S	Bone equivalent solid rod insert
4	002RL-S	Lung equivalent solid rod inserts
1		Set of CT to film fiducial markers
1		Alignment base
1		Holding device

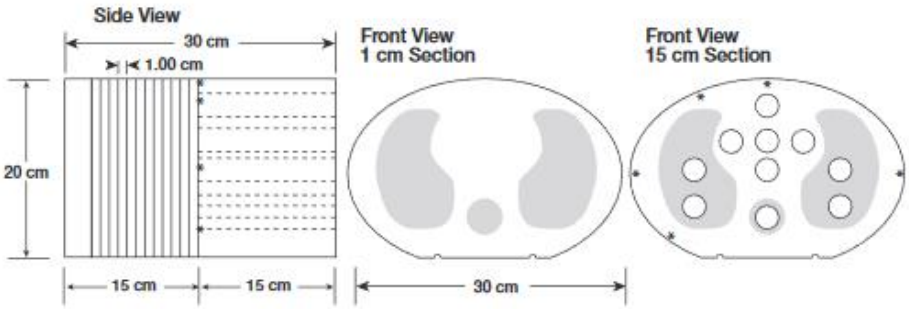

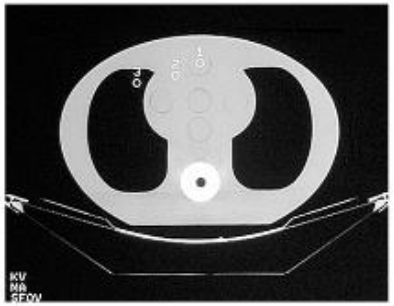

http://www.cirsinc.com/file/Products/002LFC/002LFC%20DS%20090116.pdf

ESTRO School

Complex phantoms

E2E® SBRT Phantom

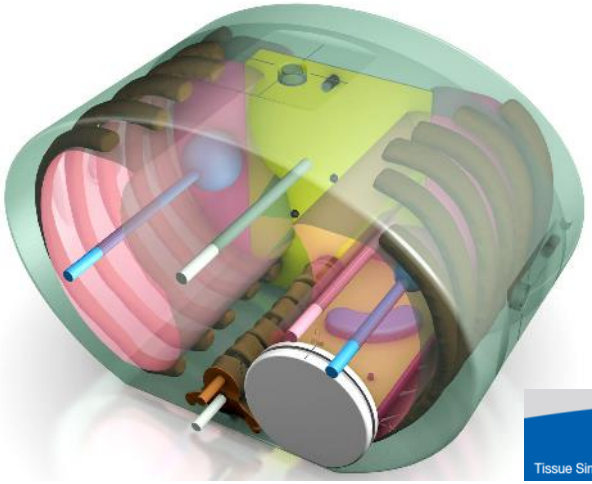

CIRS
Tissue Simulation & Phantom Technology

DIMENSIONS:	16.5 cm x 30 cm x 20 cm 6.5" x 11.8" x 7.9"
PHANTOM WEIGHT:	~7 kg (15 lb)
MATERIALS:	Proprietary Epoxy Resins

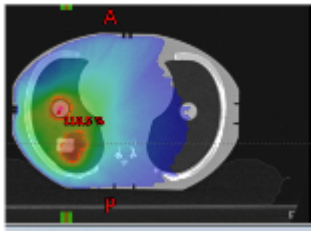

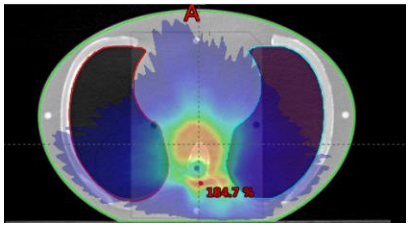

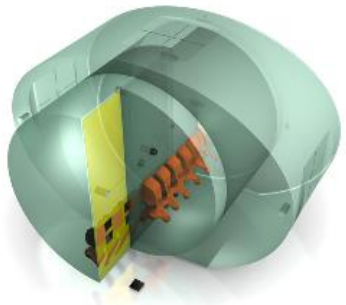

Model 036-01 SBRT Abdomen Phantom with 3D spine for film and nanoDot™ Dosimetry (cutaway to show internal structure)

Features

- Thorax with articulated spine, ribs and lungs
- Optional Abdomen with film insert
- High Resolution Anthropomorphic Characteristics
- Center point fiducial and offset target for daily system checks
- Ideal for commissioning an SBRT program
- Excellent test environment for Monte Carlo dose calculation verification
- Supports use and testing of Image Guidance capabilities
- Facilitates SBRT planning and delivery for Lung, Liver, and Spine treatments

http://www.cirsinc.com/file/Products/036/036A%20DS%20070716.pdf

ESTRO School

Complex phantoms

Lucy 3D QA Phantom

STANDARDIMAGING

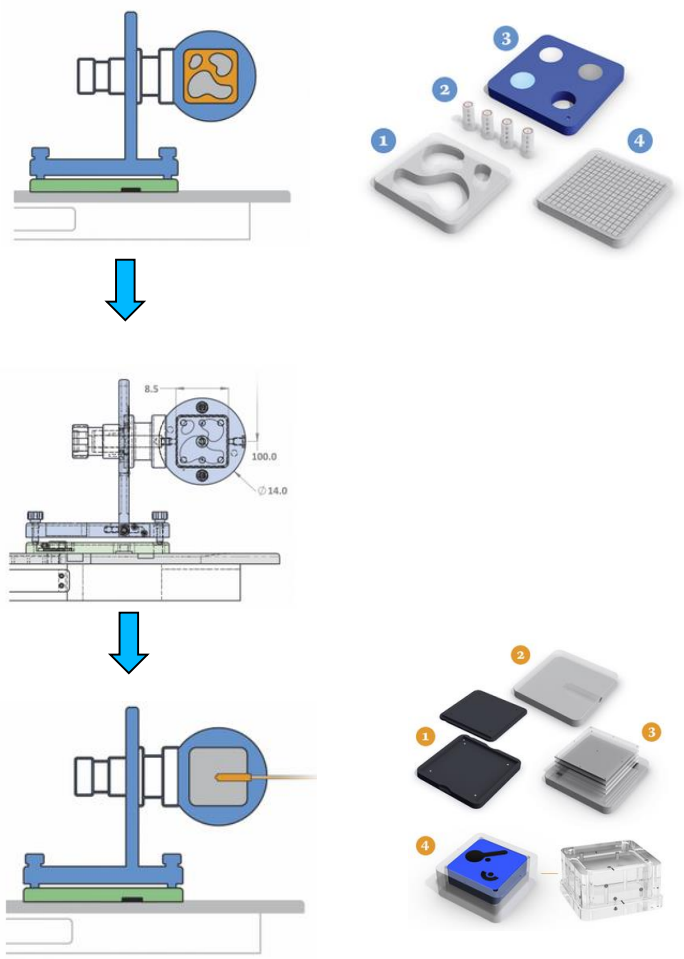

https://www.standardimaging.com/phantoms/lucy-3d-qa-phantom

ESTRO School

Complex phantoms

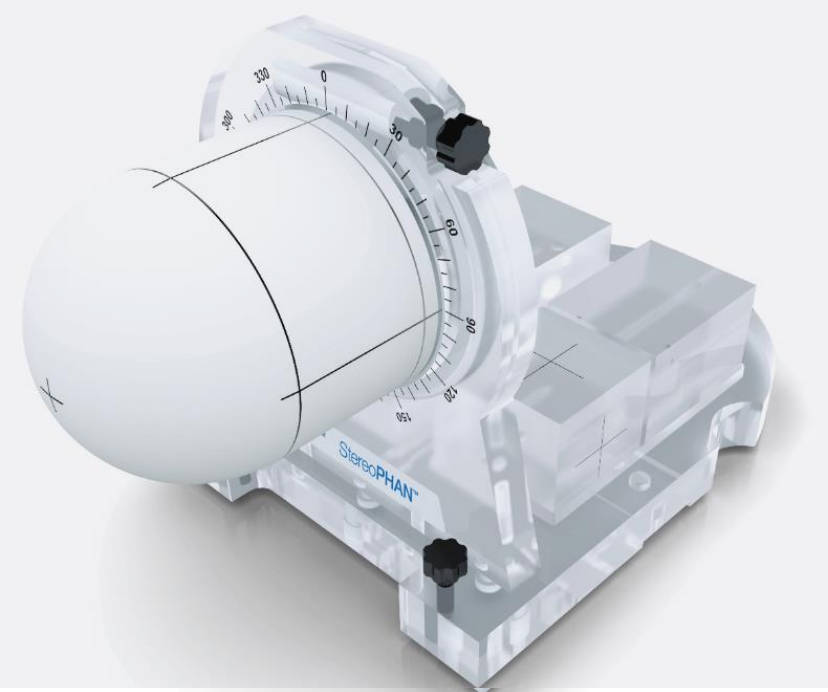

Standard Inserts

Film | Ion Chamber | CT/MRI | MRI Signal Generator | Universal Spacer

StereoPHAN™

End-to-End Stereotactic Commissioning & QA

SUN NUCLEAR corporation

Features & Benefits

- Stereotactic (SRS/SRT/SBRT) end-to-end testing and patient-specific QA
- Adapters for Head-Frames and CyberKnife
- Image fusion
  - Quality assurance of image fusion algorithms for CT and MRI imaging modalities
- Dosimetry
  - Absolute, relative and point dose dosimetry QA measurements at isocenter with ion chambers; relative dose distribution using film
  - Dosimetry detector cabling remains outside of beam for interference-free dose measurement regardless of measurement setup
- Geometric accuracy
  - Optical and geometric isocenter
  - Laser alignment
  - Indexed table positioning alignment and positioning coordinates
  - CBCT and MV/kV isocenter alignment
- Easy setup and assembly
  - No tools required for assembly
  - Stand base can be mounted to a couch that uses the prevalent Lok-Bar™ system
  - Phantom stand holds the inserts, making them easily accessible during testing
- Inserts
  - Single cube insert tests CT and MRI imaging, including slice position, thickness and alignment
  - Target volumes in CT/MRI cube eliminate need for CT/MRI markers
  - Flat surface of ion chamber insert enables easier cross-calibration to water than the curved surface of a spherical geometry
- All components fit into a durable rolling case suitable for storage and air travel

https://www.sunnuclear.com/documents/datasheets/stereophan.pdf

ESTRO School

Complex, anthropomorphic phantoms

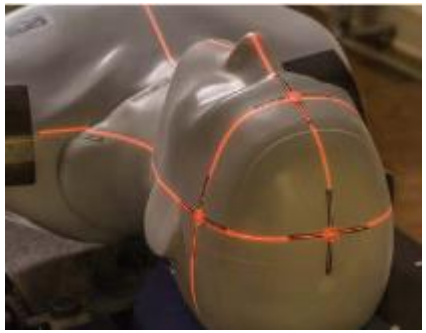

STEEV™
STEREOTACTIC END-TO-END VERIFICATION

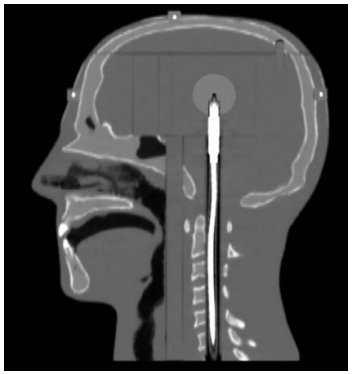

e2e SCAN PLAN LOCALIZE TREAT

CIRS
Tissue Simulation & Phantom Technology

http://www.meditron.ch/radiation-therapy/downloads/038%20PB%20071614.pdf

ESTRO School

Phantoms for TPS verification and plan QA: complex phantoms – 4D

Dose verification at motion

modusQA

QUASAR™ Respiratory Motion Phantom

A state-of-the-art breathing simulator for conducting QA testing on radiotherapy systems using patient respiratory waveforms.

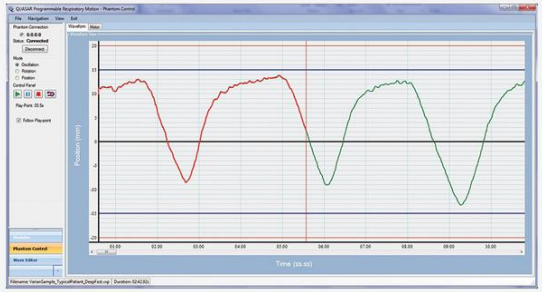

Software Capability Highlights

- Import patient-specific waveforms
- Create custom waveforms
- Edit patient-specific & custom waveforms
- Adjust the amplitude, stretching or compressing the timeline
- Filter out high frequency noise, low frequency drift and cardiac signals

http://modusqa.com/motion/phantom

ESTRO School

Phantoms for TPS verification and plan QA: complex phantoms – 4D

Dose verification at motion

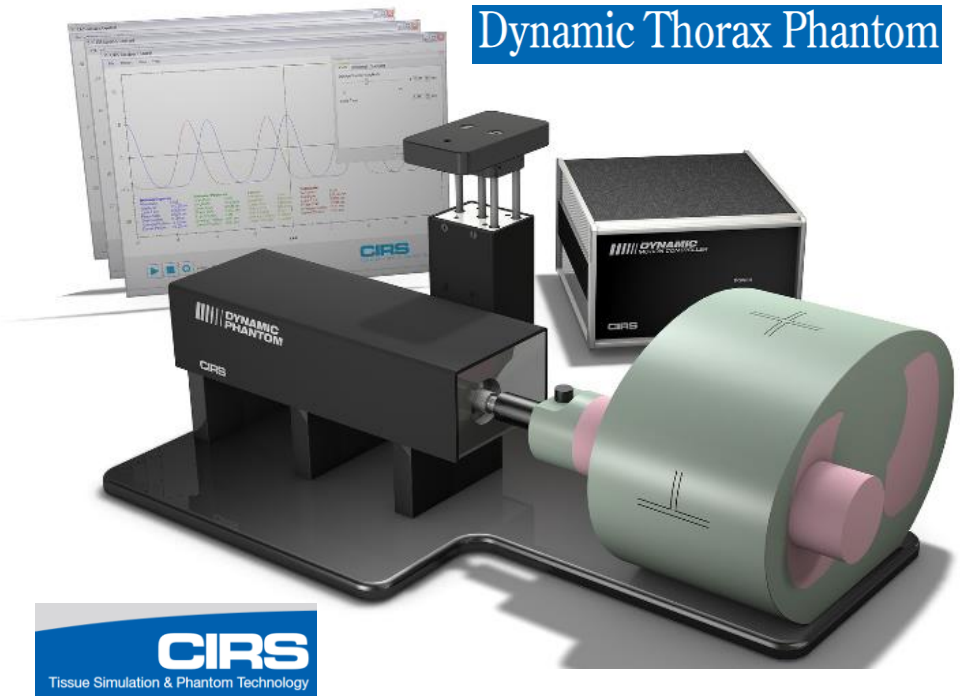

Features

- Complex 3D tumor motion within the lung
- Sub-millimeter accuracy and reproducibility
- Motion software enables different cycles, amplitudes and wave forms
- Tissue equivalent from 50 keV to 15 MeV
- Compatible with TLD, MOSFET, nanoDot™, Dose Gel, micro-chamber, PET/CT targets and film
- Surrogate breathing platform accommodates numerous gating devices

http://www.cirsinc.com/file/Products/008A/008A%20DS%20062515.pdf

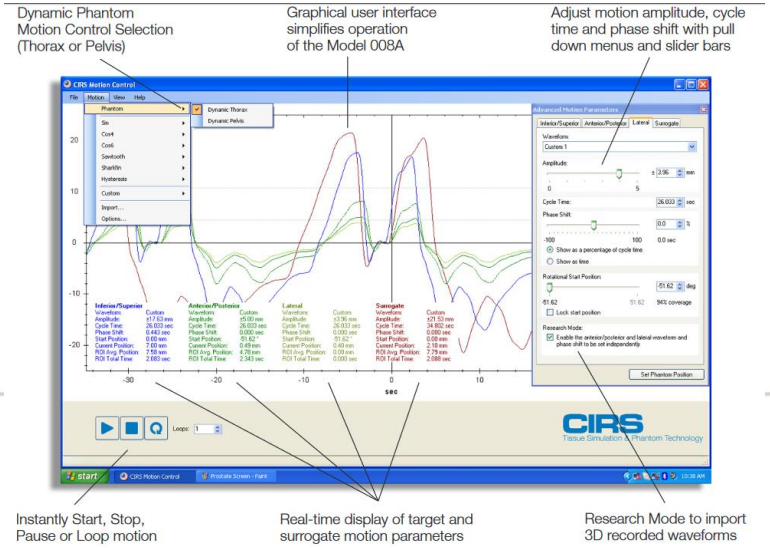

Integrated phantom-detector solutions

ArcCHECK®

SUN NUCLEAR corporation

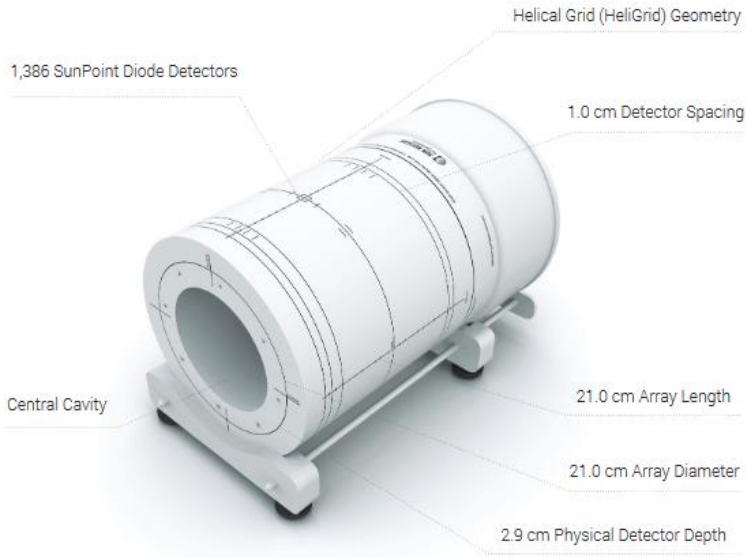

Detector Type:	SunPoint® Diode Detectors
Detector Quantity:	1,386
Detector Spacing (cm):	1.0
Array Diameter (cm):	21.0
Array Length (cm):	21.0
Cavity Diameter (cm):	15.0
Inherent Buildup (g/cm²):	3.3
Inherent Backscatter (g/cm²):	3.3
Detector Physical Depth (cm):	2.9
Array Geometry:	Helical Grid (HeliGrid) 1 cm offset
Phantom Material:	PMMA (Acrylic)
Active Detector Area (mm²):	0.64
Detector Sensitivity (nC/Gy):	32.0
Max Dose/Pulse (Gy):	0.003
Detector Volume (mm³):	0.019
Detector Stability:	0.5% / kGy at 6 MV

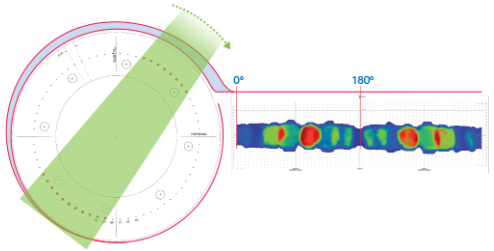

ArcCHECK Measurement

ArcCHECK displays BEV dose distribution throughout the entire arc delivery. More data is available to perform a more thorough QA analysis.

MultiPlug™

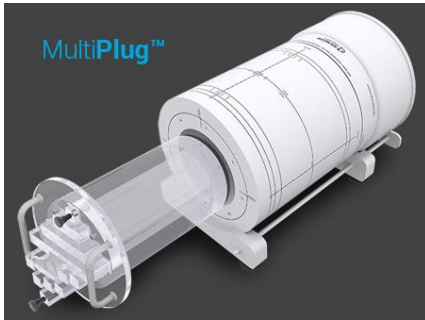

- Hounsfield Unit (HU) conversion testing
- Tissue equivalent inserts:
  - Muscle, Bone, Lung, Adipose, Titanium
- Dose in up to 25 locations
- Film cassette insert
- Bezel angle indicator for rotation within cavity
- Precision milled detector holder included
  - Solid insert included to achieve solid cavity

CavityPlug™

- Precision fitted to ArcCHECK cavity
- Measure dose in cavity center
- Precision milled detector holder included
  - Solid insert included to achieve solid cavity

https://www.sunnuclear.com/solutions/patientqa/arccheck3dvh

ESTRO School

Integrated phantom-detector solutions

Delta⁴®

ScandiDos

Cylinder phantom

Material	PMMA; optional Plastic Water DT®
Diameter	22 cm
Length	40 cm
Ion chamber insert in cylinder	Inserts for common cylindrical ion chambers available

Detectors

Type	p-Si
Total number	1069
Layout	Distributed on coronal and sagittal plane
Max field size	20 x 38 cm² (with merger of two consecutive measurements, otherwise 20 x 20 cm²)
Distance between detectors	
Central area (6 x 6cm²)	5 mm (or 2.5mm in longitudinal direction with merger of two consecutive measurements)
Outer area	10 mm
Size (radial x axial)	1 x 0.05 mm³ = 0,00004 cm³
Detector stability (6MV beam)	Better than 0.1% per kGy, typically 0.04%/kGy

Size and weight

Total length	71 cm
Total weight	27kg

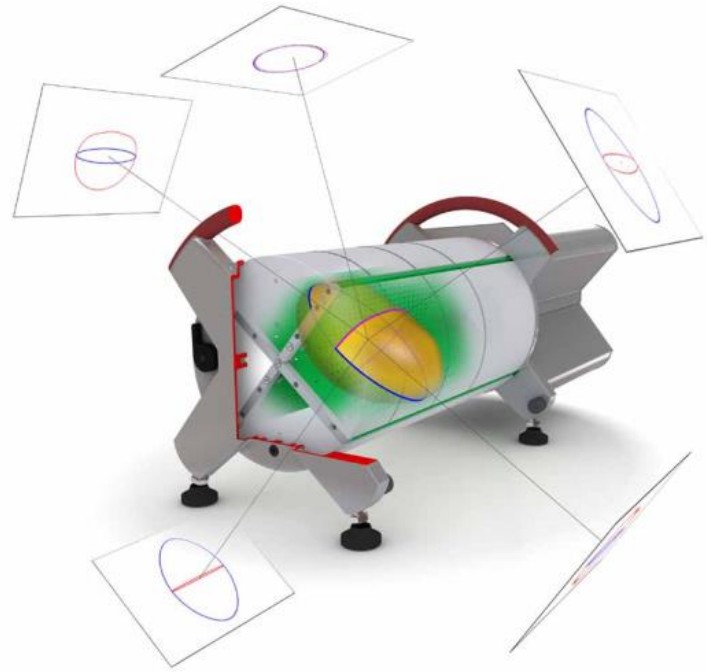

http://delta4family.com/products#phantom

ESTRO School

Summary: the use of plastic phantoms for TPS QA & PSQA

•Representation of solid plastics in CT datasets is influenced on whether the material is water-equivalent in the kV energy range.

•Systematic discrepancies in the verification of calculated dose in solid plastics can occur if these are not properly represented in the TPS.

•We have been working on the assumption that homogeneous solid phantoms which are shown to be water-equivalent for reference dosimetry and relevant dosimetry using an ionization chamber are also water-equivalent under a multiple beam arrangements (for the verification of treatment plans).

•The interpretation of measurements from complex phantoms with embedded detector systems might not be straightforward if there is limited understanding on how these phantoms are represented in the TPS and how the phantom software processes the measured signal by the detectors.

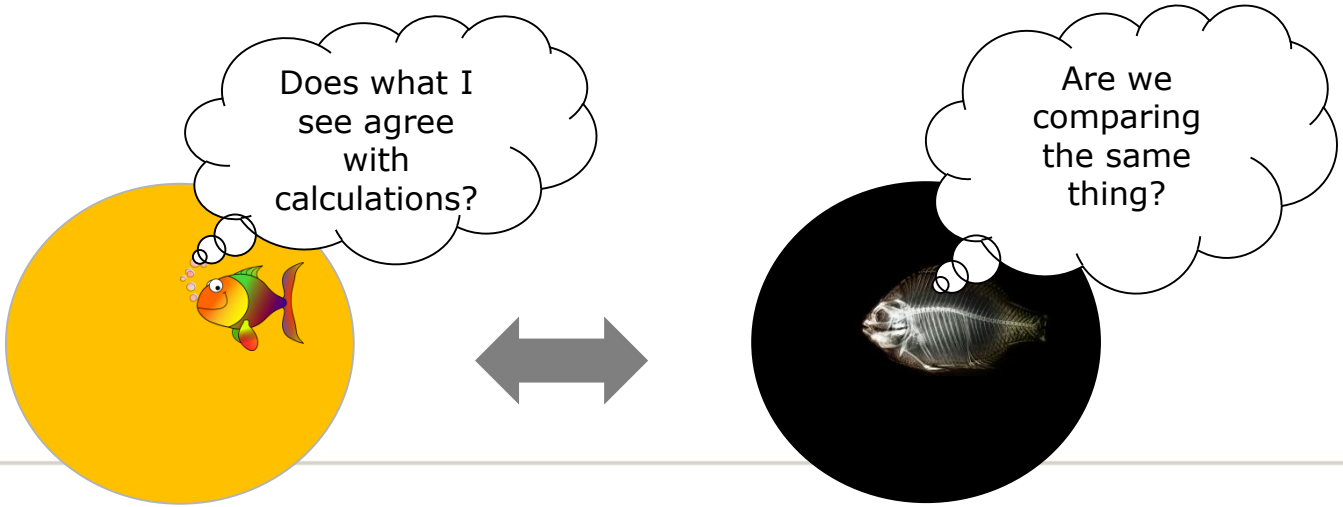

The detector in plastic phantom
(by Nuria Jornet)

TPS (often referred to as 'black box')

ESTRO School

ESTRO School

WWW.ESTRO.ORG/SCHOOL

ESTRO School

Dose measurements;

Part 2 The best detector for different jobs

detectors for verification measurements

Núria Jornet

Servei de Radiofísica
Hospital Sant Pau,
Barcelona

2D detectors: why are they needed?

2D dose detectors are needed for measurements in dynamic beam deliveries. Characterization of dose distribution would be cumbersome using 1D detectors (1 point per beam delivery).

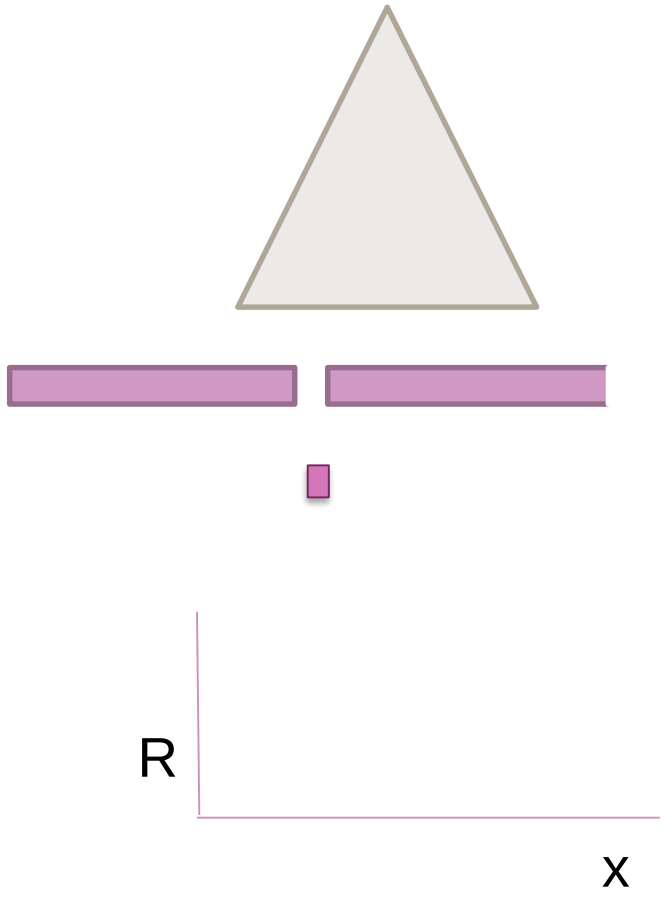

2D detectors: why are they needed?

2D dose detectors are needed for measurements in dynamic beam deliveries. Characterization of dose distribution would be cumbersome using 1D detectors (1 point per beam delivery).

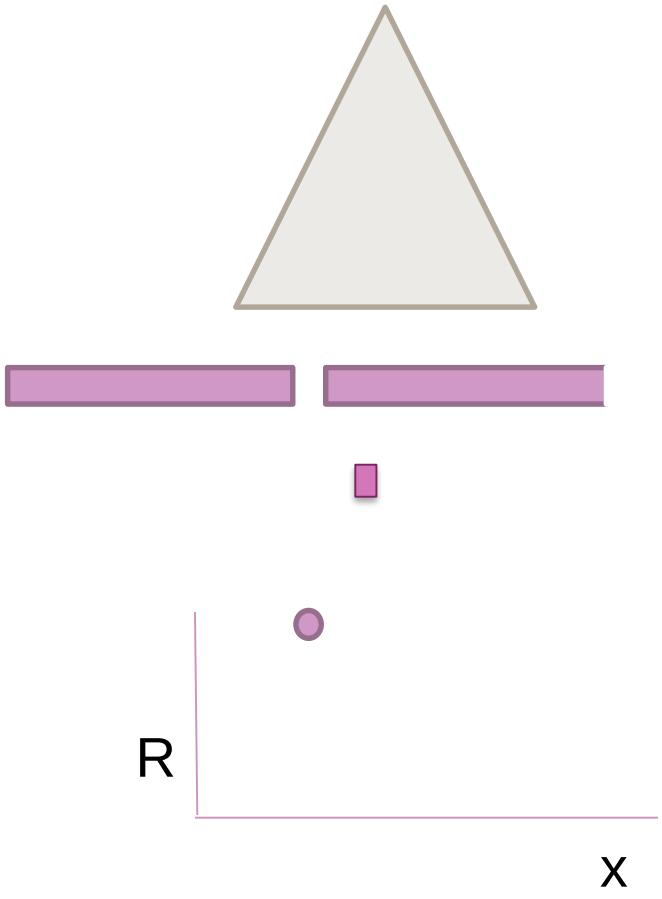

2D detectors: why are they needed?

2D dose detectors are needed for measurements in dynamic beam deliveries. Characterization of dose distribution would be cumbersome using 1D detectors (1 point per beam delivery).

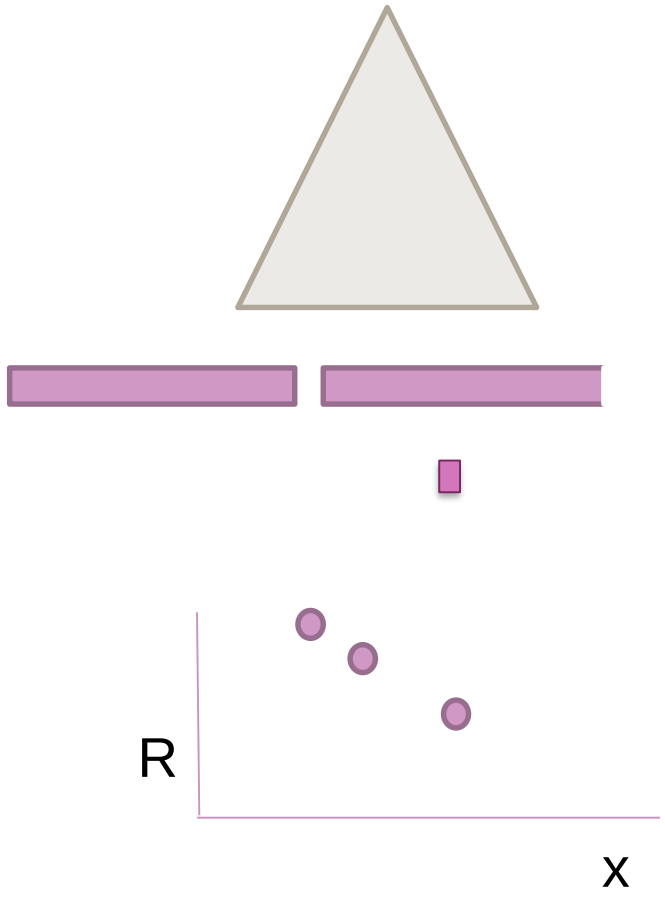

ESTRO School

2D detectors: why are they needed?

2D dose detectors are needed for measurements in dynamic beam deliveries. Characterization of dose distribution would be cumbersome using 1D detectors (1 point per beam delivery).

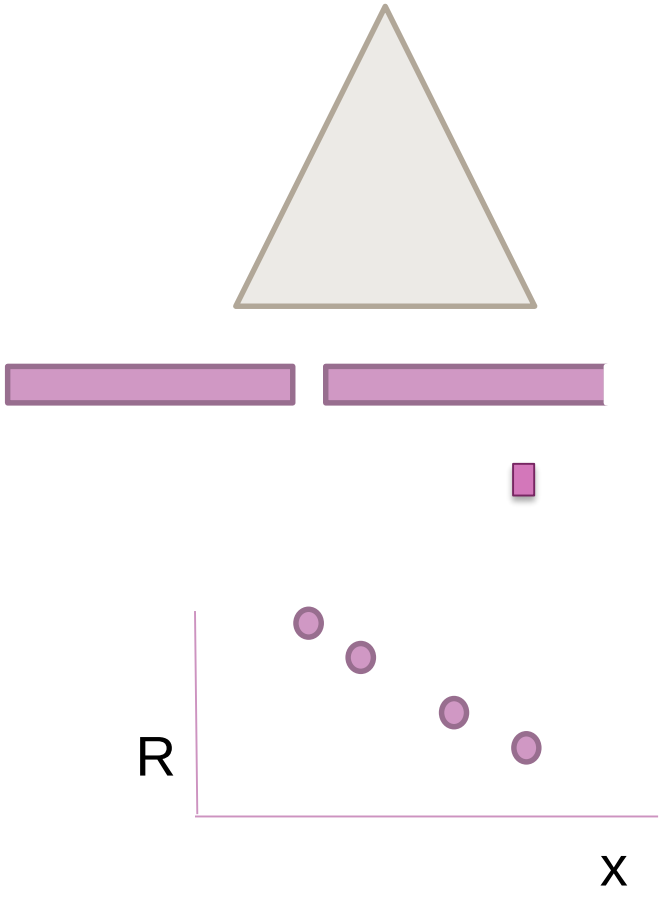

2D detectors: why are they needed?

2D dose detectors are needed for measurements in dynamic beam deliveries. Characterization of dose distribution would be cumbersome using 1D detectors (1 point per beam delivery).

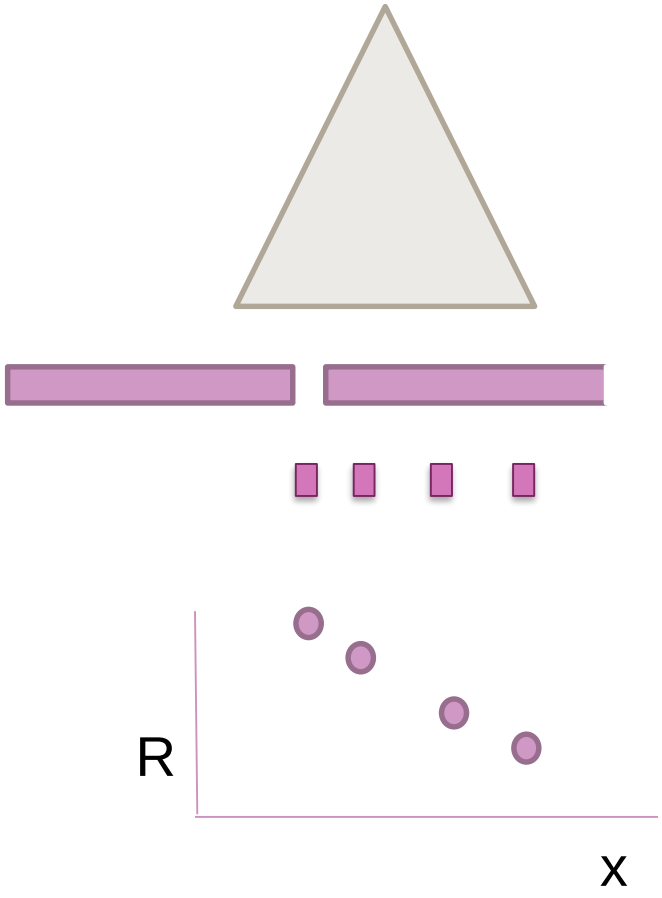

3D detectors: why are they needed?

Measurement-based plan validation for IMRT:

- Demonstrate that an IMRT plan can be delivered. Leaf sequences as calculated by the TPS may not take into account the limitations of the real device and the equipment may not perform as expected.
- Fluence modulation produces regions with high dose. These hot spots depend critically on accuracy of the delivery and treatment field set-up

The measurement system should:

- Cover the entire irradiated volume
- High resolution
- On line measurement

3D detector

GEL DOSIMETRY

2D·3D detectors wish list :

1D

- Linearity response with dose
- No-energy/dose rate/temperature response dependencies
- Isotropic response
- Repeatability and reproducibility
- Stability of the response with accumulated dose
- Stability of the response with time (fading)
- High sensitivit

2D-3D

- Response homogeneity
- High spatial resolution
- Low cost
- Re-usable
- Possibility to place the detector inside a phantom (any direction) **2D**
- Possibility for mailed dosimetry for audits

From 1D to 2D: challenges (passive detectors)

1. Coating: Distribute homogenously (constant thickness and concentration) the detector material over a surface.

2. Reading: System capable of retrieving 2D dose related parameters from the detector.

ESTRO School

The most known passive detectors are:

Radiochromic	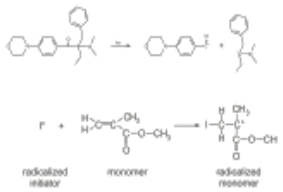	Commercially available: Gafchromic films Scanner Software
Silver Halide	Ag Ag^{+}	
Fricke	Fe^{2+} Fe^{3+}	
Thermoluminiscent	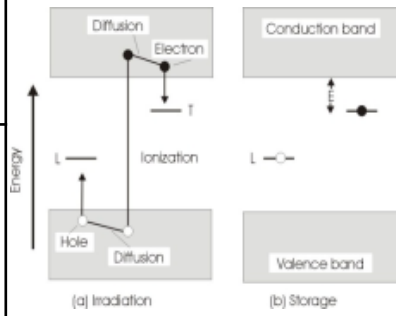	
Optical stimulated		Under development:
Alanine	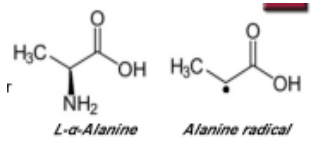	**Under development:**

From silver halide films to radiochromic

Silver halide films

1

2

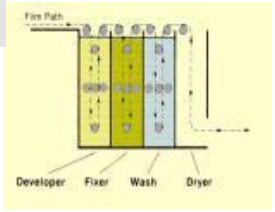

3

- No water equivalence
- Energy dependence

Radiochromic films

1

2

- Water equivalence
- No (little) energy dependence

Energy dependence (silver halide versus radiochromic)

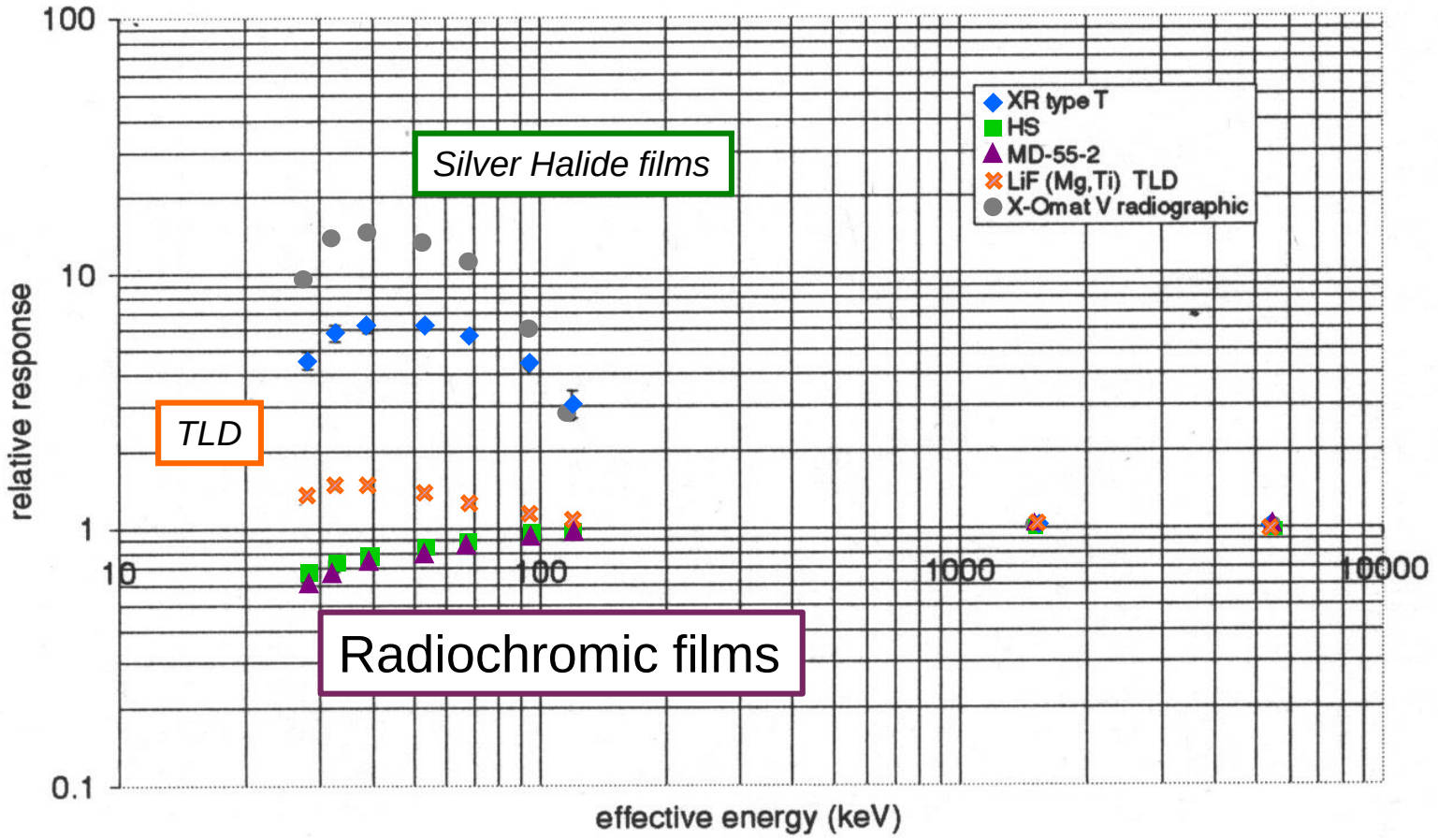

Cheung et al. PMB 49 (2004)

ESTRO School

From silver halide to radiochromic films

Silver halide films

1

2

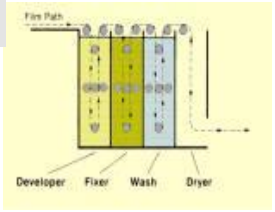

3

- No water equivalence
- Energy dependence
- High spatial resolution
- Saturation high doses
- Sensitive to visible light
- Needs developing
- Time consuming

Radiochromic films

- Water equivalence
- No (little) energy dependence
- High spatial resolution
- Saturation high doses
- Insensitive to visible light
- No need of processing-“Real time” development, stability reached in ~ 2 h
- Can be evaluated with flatbed scanner (transmission mode-fluorescent light source and a linear CCD array detector)

ESTRO School

Radiochromic film: principle of detection

❑ Film emulsion is a radiation sensitive monomer. The coloration process is based on radiation-induced polymerization. The polymer is blue in color and film absorbs light in the red part of visible spectrum.

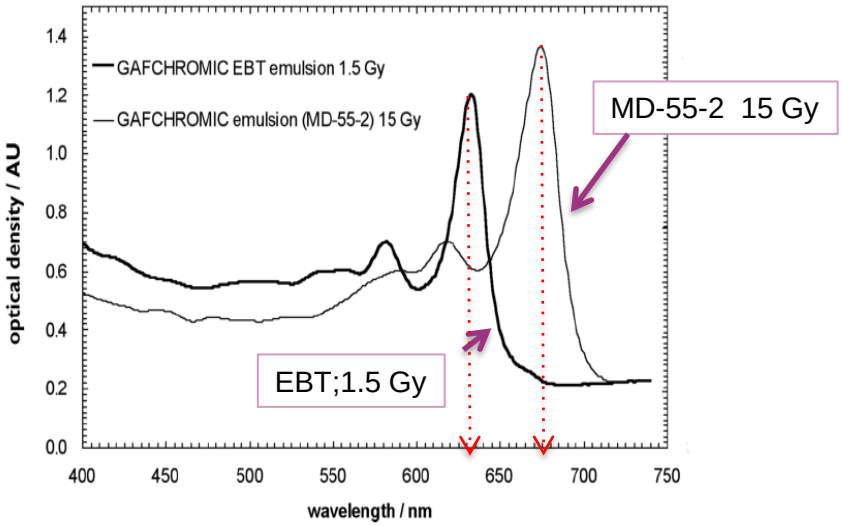

Soares et al. chapter 23 AAPM Summer School, 2009

$$OD = -\log_{10}(T) = -\log_{10}(I_0/I)$$

OD is proportional to absorbed dose

ESTRO School

Radiochromic film evolution…

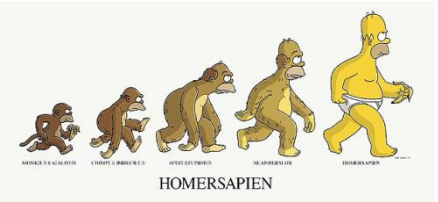

PRIOR EBT GAFCHROMIC FILMS
[HD-810; MD-55-2; HS]

- Low sensitivity
- Small size
- Inherent optical density non-uniformity in one sheet (15%)

  [Need of double-exposure]
- High price

POST EBT GAFCHROMIC FILMS (2004)
[EBT;EBT2;EBT3]

- Dose range 2cGy – 8 Gy
- Saturation ~ 10Gy (15Gy)
- Different sizes available
- Z_{eff} ~ 7.05 (chlorine addition)
- Significant better homogeneity

  [no need of double-exposure techniques]
- Lower price

Table 23-3. Radiochromic Film Characteristics for Readout at 633 nm

Film Model	Emulsion thickness (μm)	Sensitivity (mAU/Gy)	Useful range (Gy)
HD-810	6.5	3	10–1000
MD-55-2	32	20	1–100
HS	38	35	0.5–50
EBT	34	400 to 800[a]	0.05–10
XR-RV2	17		0.01–5
XR-QA	50	0.001–0.2	

[a] For a dose of 1 Gy, depending on film orientation.

ESTRO School

Remember that radiochromic film dosimetry is a two step process

FILM CHARACTERISTICS:

Composition of the dye
Homogeneity
Batch uniformity

SCANNING SYSTEM AND PROTOCOL

ESTRO School

Film structure and characteristics

The active layer is a radiation sensitive organic microcrystal monomer.

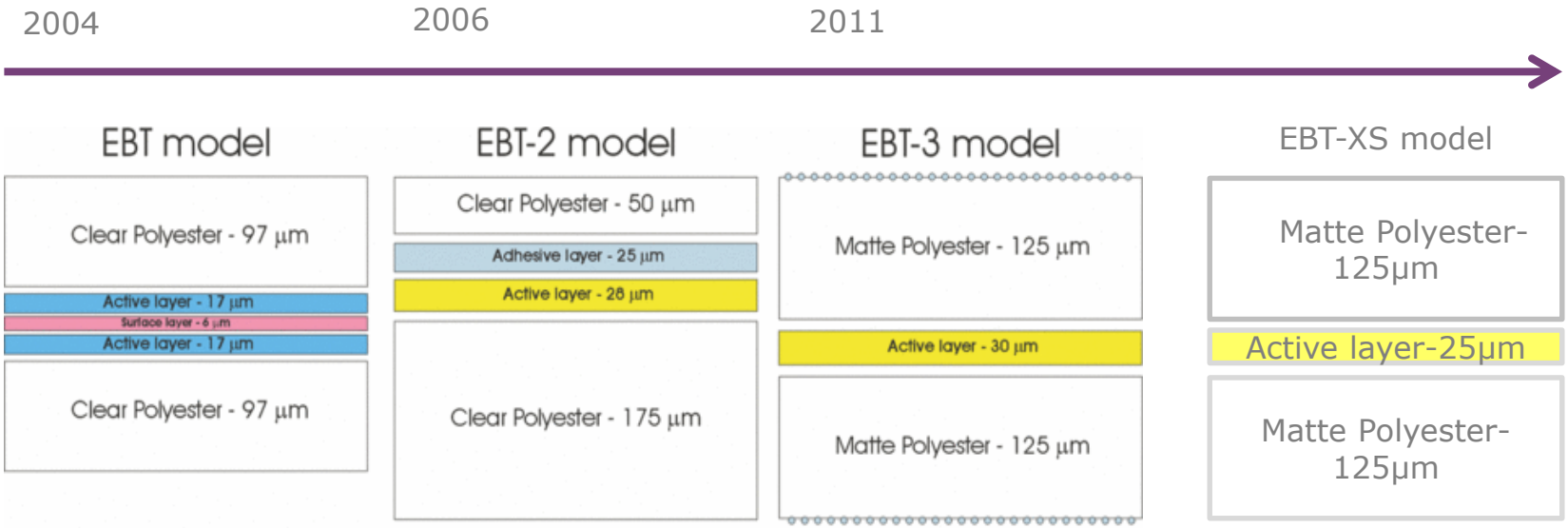

Symetric

Assymetric

Optimal Dose range:

2 cGy-10 Gy

Yellow dye to use blue channel to correct for non-homogeneity of the active layer

Decreases UV/light sensitivity

Symetric

Optimal Dose range:

2 cGy-10 Gy

Anti-newton rings (addition of silica particles on the surface)

Symetric

Optimal Dose range:

4 cGy- 40 Gy

Anti-newton rings

ESTRO School

Scanner requirements

- RGB flat bed color scanner
- Color depth: 48 bit (16 bits per color channel-red).

  [8 bit per chanel-256 “grey” levels; 16 bit 65535 “grey” levels]
- Scanner table: A4 / letter or A3
- Resolution: up to 3200 dpi (75 dpi enough)
- Disable all color correction options. Need of raw data
- If used in transmission mode need of a transparency adapter

Wilcox et al MP (34 (2007), Paelinck et al PMB 52 (2007)

- Translation of a line source focused to a line or area detector array, over the film.
- Spatial resolution: 0.34-0.042 mm in diameter.

Important. BEFORE USE

1. Check response, spatial integrity, susceptibility to image artifacts and time needed to reach steady-state operation conditions

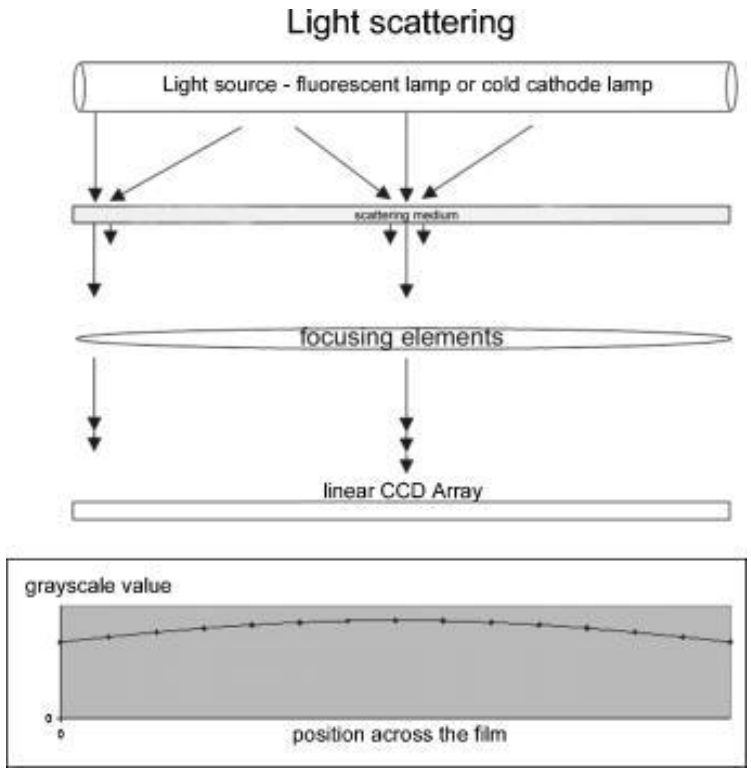

Fiandra et al. Med. Phys. 33 (2006)

ESTRO School

Scanner homogeneity

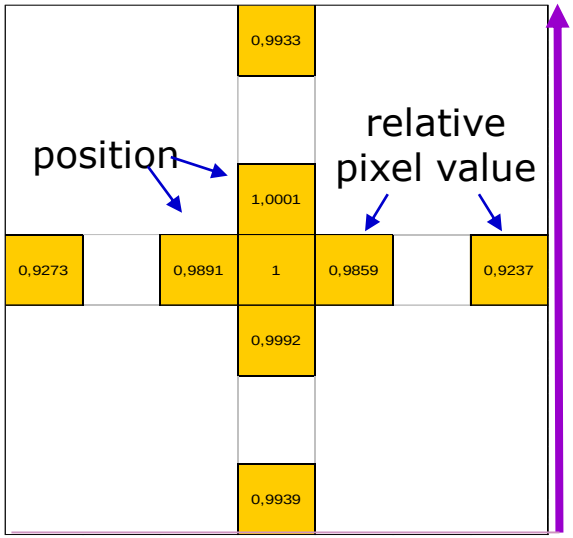

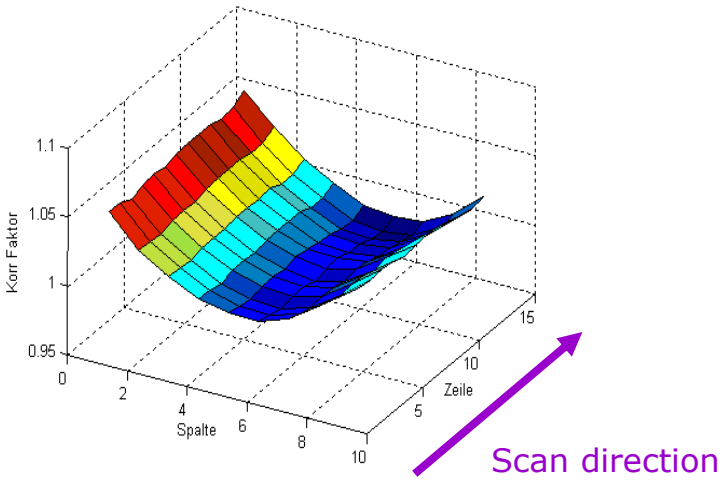

- Pixel value varies with position on the scanner plate due to light scattering differences:
  - small effects (<1%) when moving films parallel to scan direction
  - up to 8% variation when moving films perpendicular to the scan direction, dose dependent.
    <2% within 5 cm from the scanner axis for D<2Gy)
- 2D correction for "full" films
  - Dose dependent
  - Scanner dependent

EPSON Pro 1680 Expression scanner:

Paelinki et al PMB 52 (2007) and Fuss et al PMB 52 (2007)

Fiandra et al MP 33 (2006)

Epson 10000XL scanner:

Ferreira et al. PMB54 (2009)

ESTRO School

Scanner homogeneity: Newton rings

Newton rings:

Are interference patterns caused by the reflection of light in the glass on the scanner and the film surface (distance ≈ λ light).

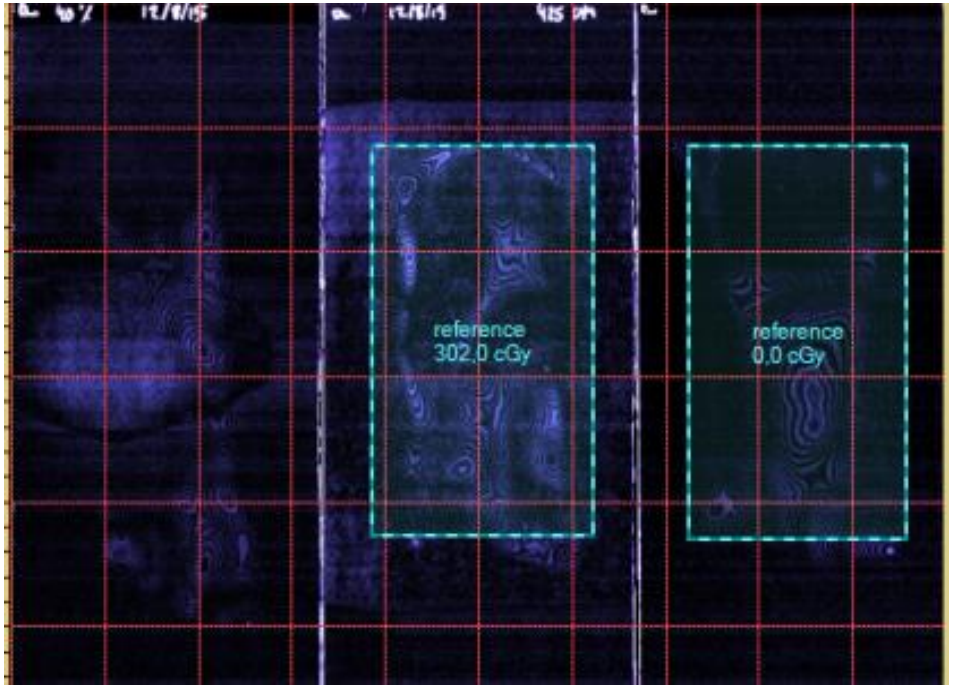

Calibration:
Determination of the sensitometric curve

- The film calibration procedure consists in acquiring a set of single measurements of net optical density NOD with the corresponding absorbed dose and obtaining a function which relates NOD for a given dose, called the sensitometric curve. The NOD is obtained by subtracting the average OD of a non-irradiated film to an irradiated film using regions of interest ROIs of constant sizes and uniform field doses

$$OD = -\log_{10}(T) = -\log_{10}(I_0/I)$$

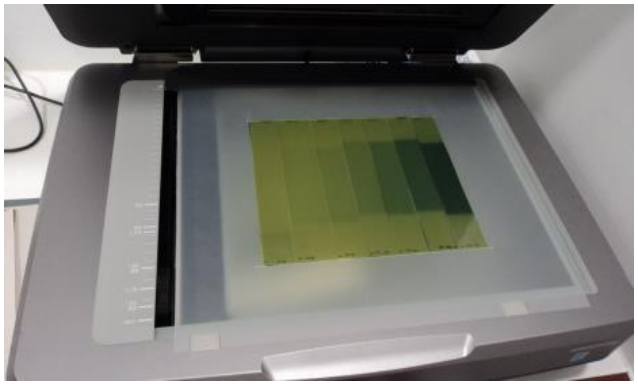

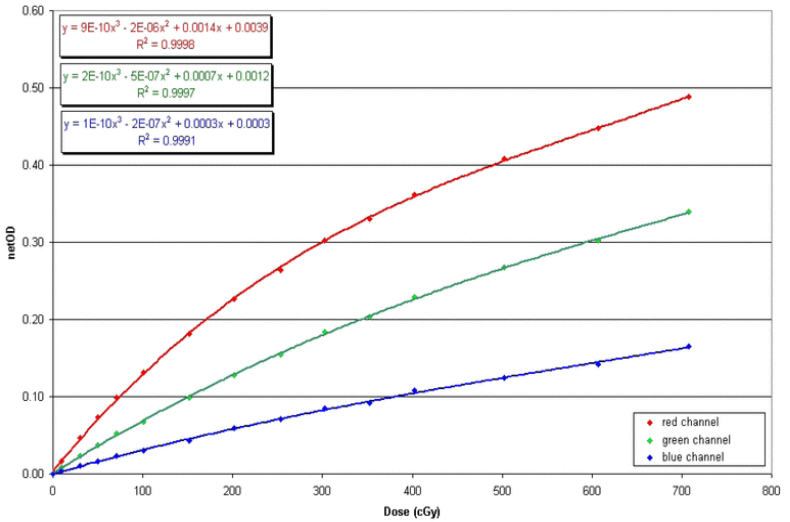

Calibration:
Determination Absorbed dose-pixel value

Remember that if using a 48 bits scanner :pixel value per color channel [0,65535]

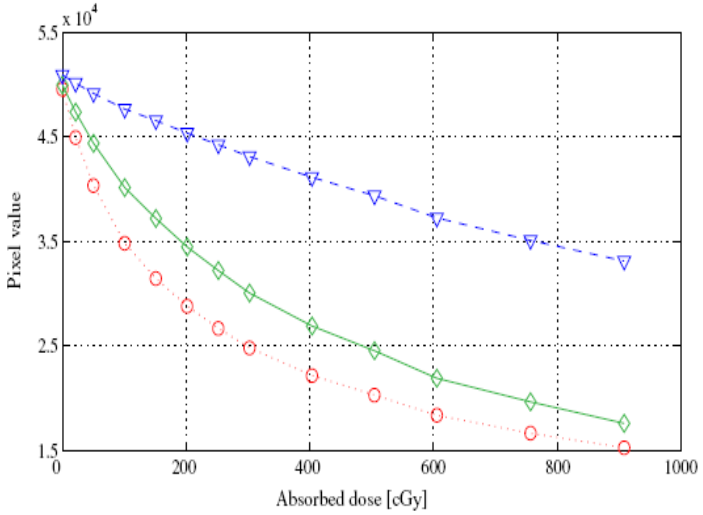

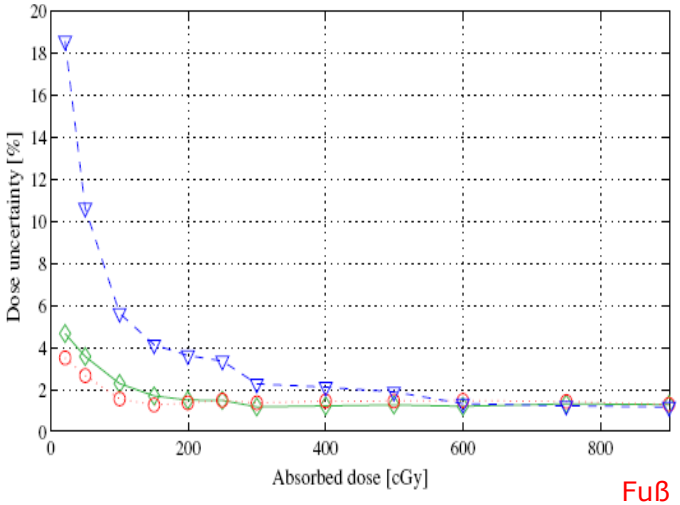

Fuß et al, PMB 52 (2007)

Some film dosimetry softwares use calibration curves: absorbed dose-pixel value

Fit to a polynomic function or to a rational function (shape corresponding to the dose-response characteristic of the film)

$$X(D) = a + b/(D-c)$$

ESTRO School

Calibration:
Determination of the absorbed dose-pixel value curve

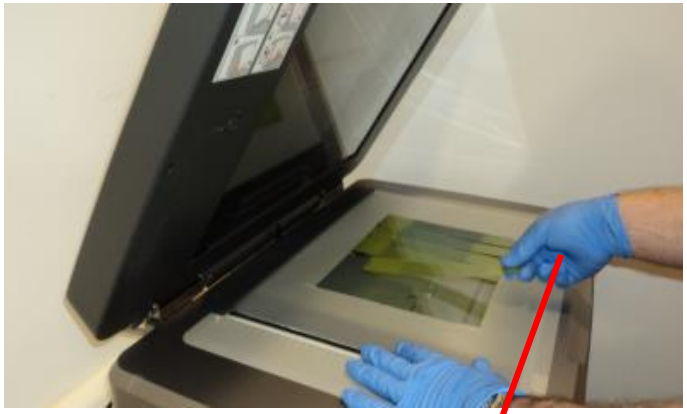

Use of globes to avoid scratches and fingerprints

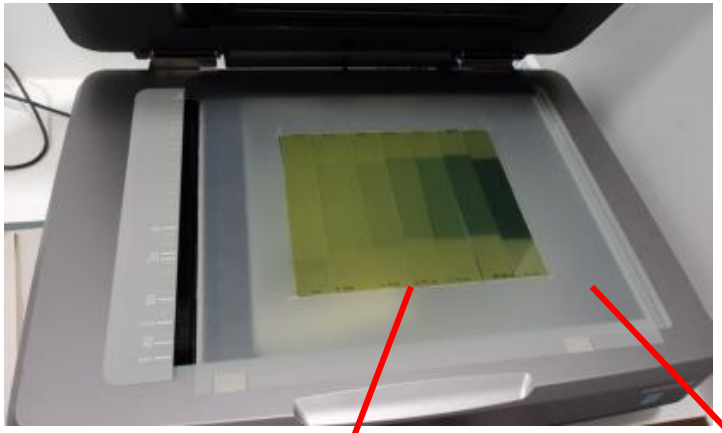

Frame to align only central part of the scanner is used

24 h between irradiation and digitization

Five scans before reading the calibration films.

7 film patches (7 dose levels)

Dose measured with a c.i. before and after film irradiation

Keep track on film orientation, landcape or portrait.

ESTRO School

Calibration:

Determination of the absorbed dose-pixel value curve

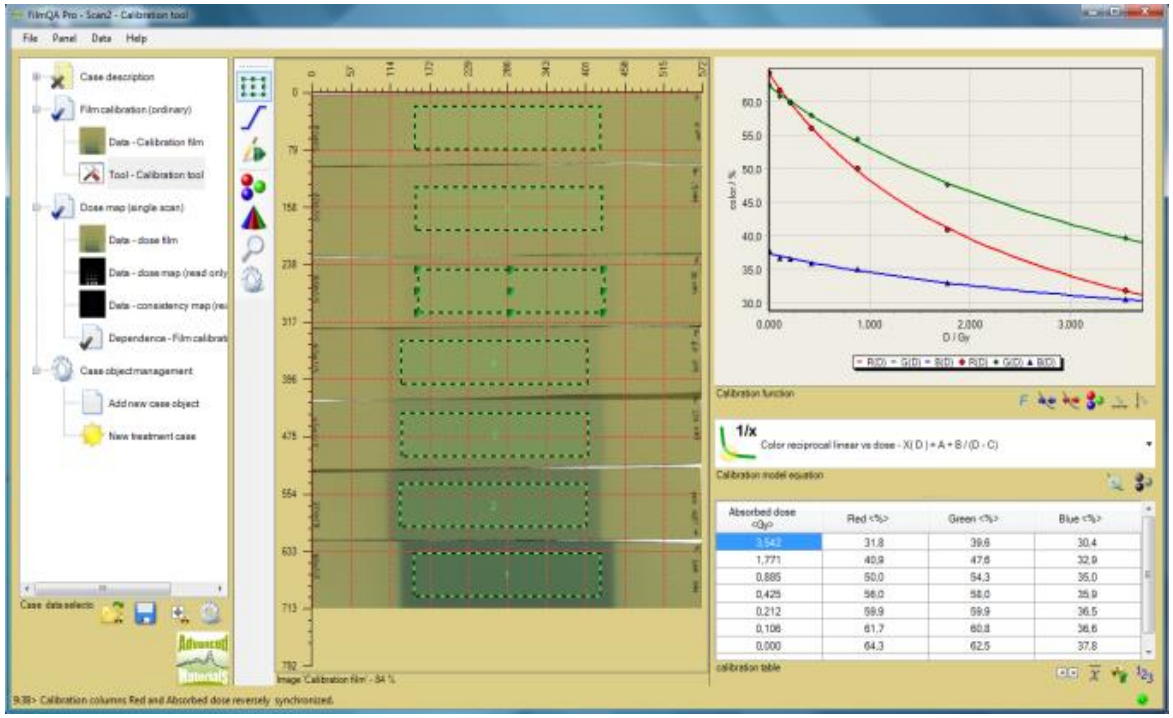

Selection of a ROI large enough to have a good pixel value average

ESTRO School

Calibration curve and scanner

- Optical density is a function of the wavelength of the light source
- Flat-bed color photo-document scanner use broad band fluorescent visible light sources
- OD it will also depend on the sensitivity of CCD array

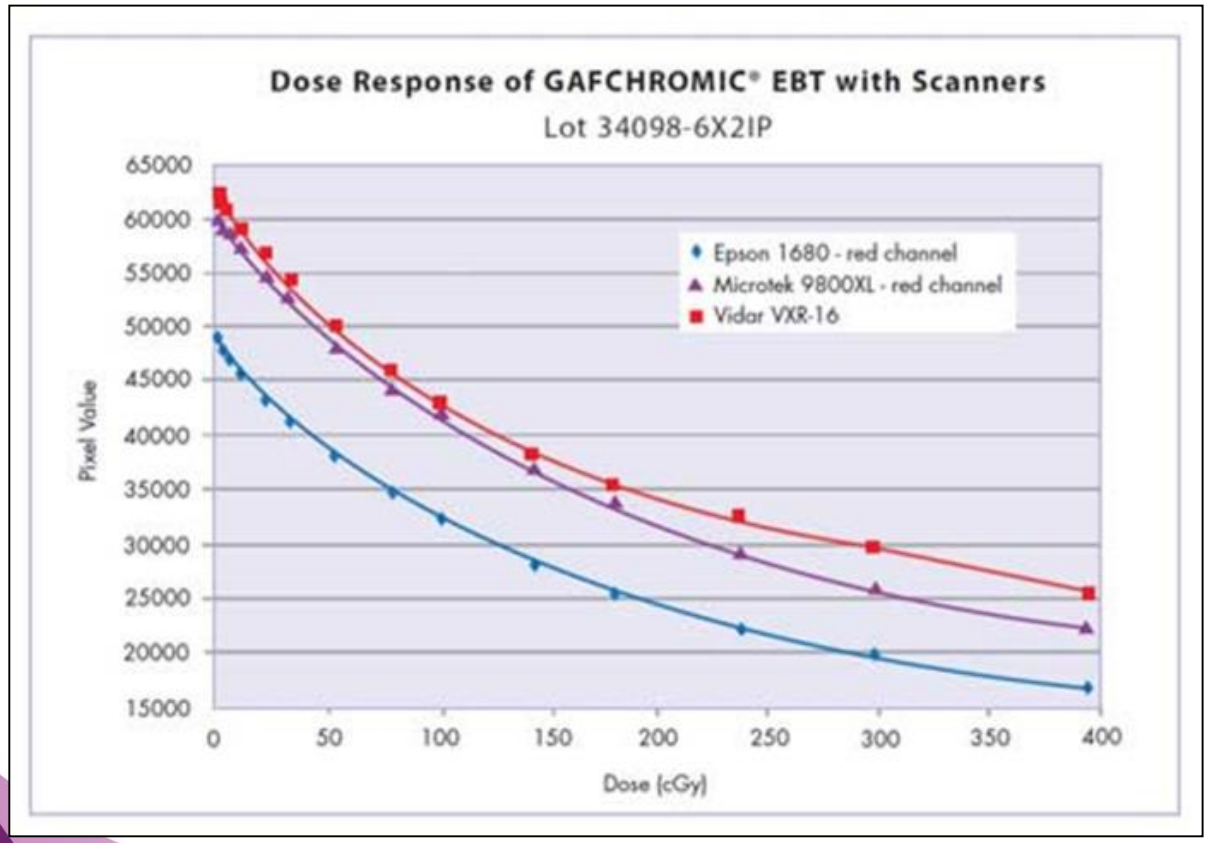

- Calibration curve is scanner dependent
- Need to have stable performance of the scanner before using it for calibration or for film digitization

ESTRO School

Dose response of EBT2 films dependence on Beam modality and energy

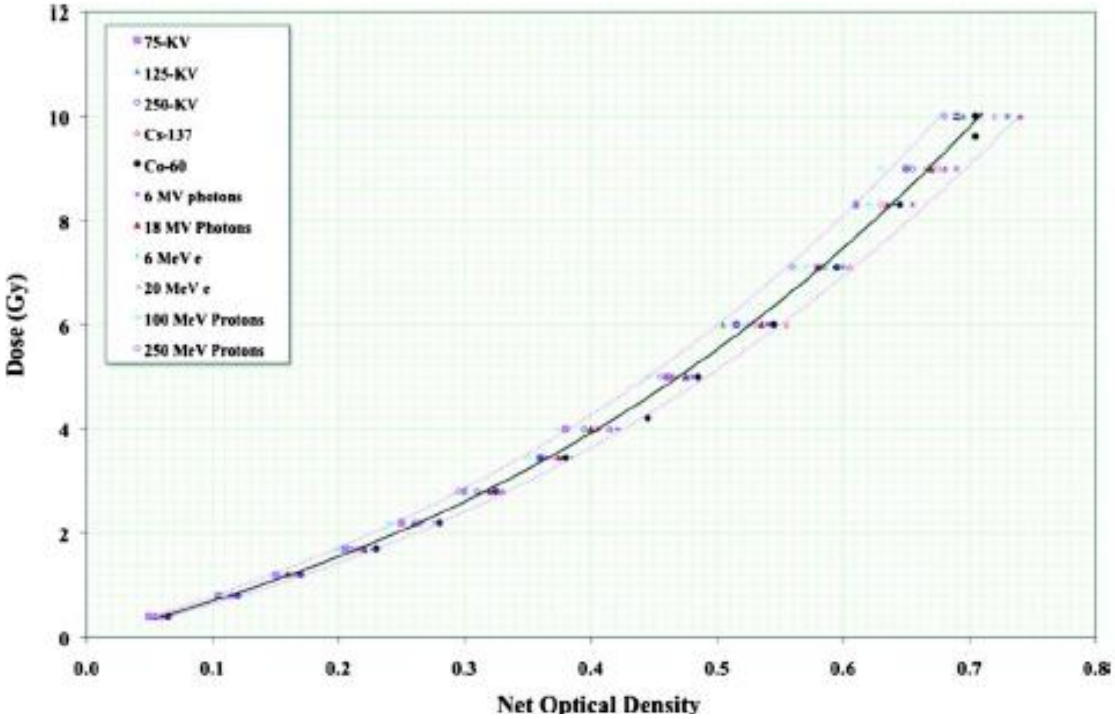

FIG. 3. Dose responses of EBT2 films for a range of beam energies from different radiation sources. The region between the two extreme curves represents the trend of all the data collectively and encompasses more than 95% of the data. The variation in data in this the region between the 3 and 10 Gy doses corresponds to $1\sigma = \pm 4.5\%$.

Figure from: Arjomandy et al. Med. Phys, 37(5), 2010

Variation within ±4.5% 1SD

RX from 75kV to 18MV
Protons 100-250 MeV
Electrons 6-20 MeV

RX from 100 keV to 25 MV
[all published studies, up to 2016]

Variation <0.6% (1SD)

ESTRO School

Film manufacturing

Film manipulation

Film Characterization

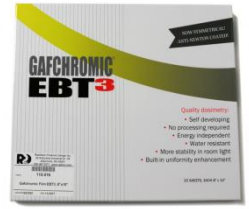

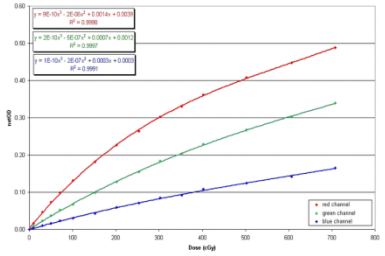

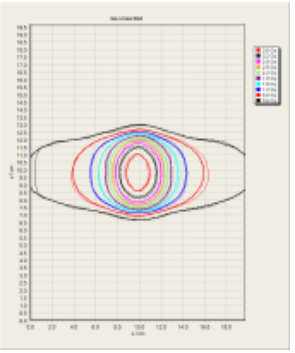

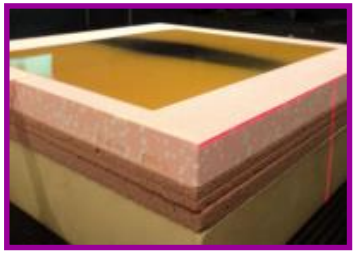

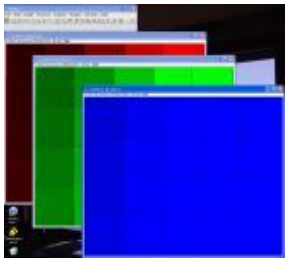

Irradiation process

Digitization process

ESTRO School

Method: single channel

10 x 10 cm^2
6 MV field

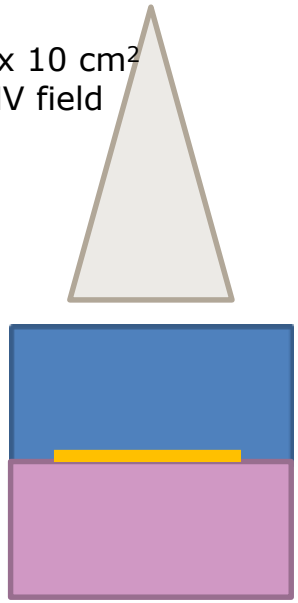

Irradiated EBT2 film (2.25Gy)

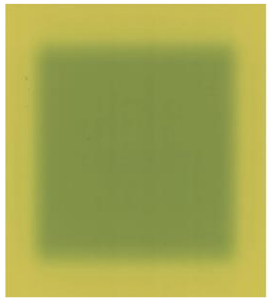

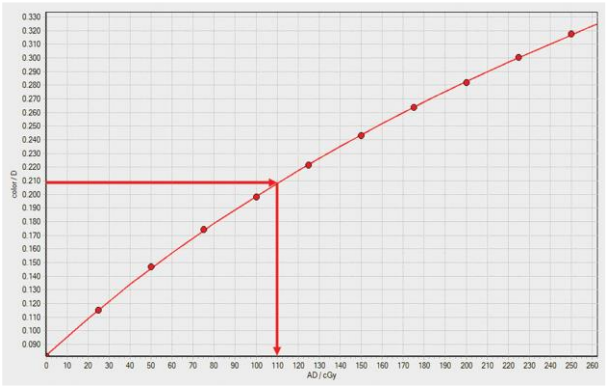

EBT2 calibration curve (red channel, 16bits)

Beer-Lambert law:

OD dye thikness

2D dose map

We can't discriminate between non-dose dependent parameters (i.e. thickness, non homogeneity scan response) and dose depedent parameters

Uncertainty budget

Images from: Micke et al. Med. Phys. 38(5) (2011)

ESTRO School

Method: Triple channel

10 x 10 cm^2
6 MV field

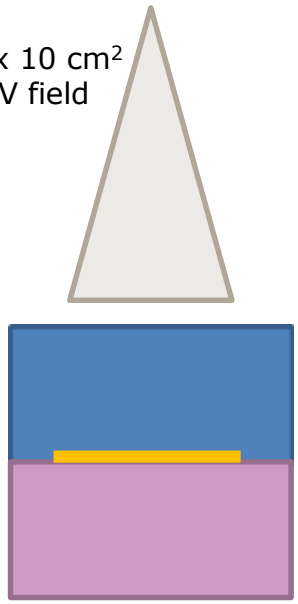

Irradiated EBT2 film (2.25Gy)

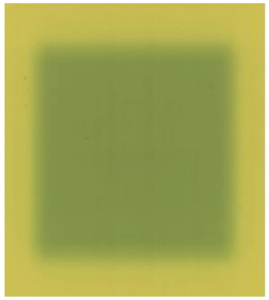

EBT2 calibration curve (red, bule and green channels, 16bits/channel)

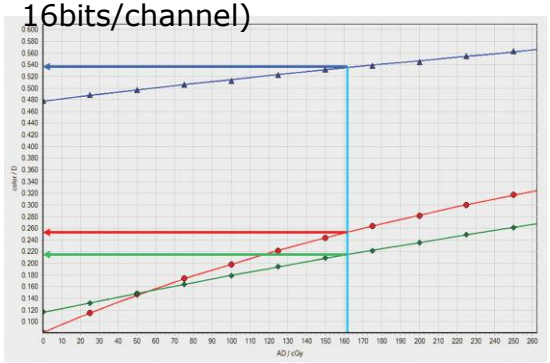

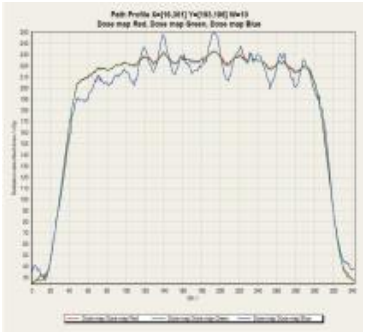

Consistency map (non dose dependent parameters/artifacts)

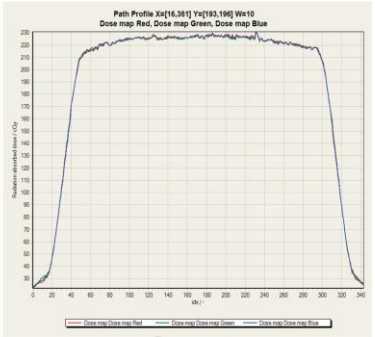

TIPS:

Size of calibration patches at least 10x10 cm^2

0-3 Gy: 8 patches

ADVANTAGES

Corrects for film thickness differences

Mitigates scanner lateral dependence

Increases de signal to noise ratio

Extends dose range

Micke et al. Med.Phys. 38 (2011)
Mendez et al. Med. Phys. 41 (2014)
Mendez, Med. Phys. 40(2013)

ESTRO School

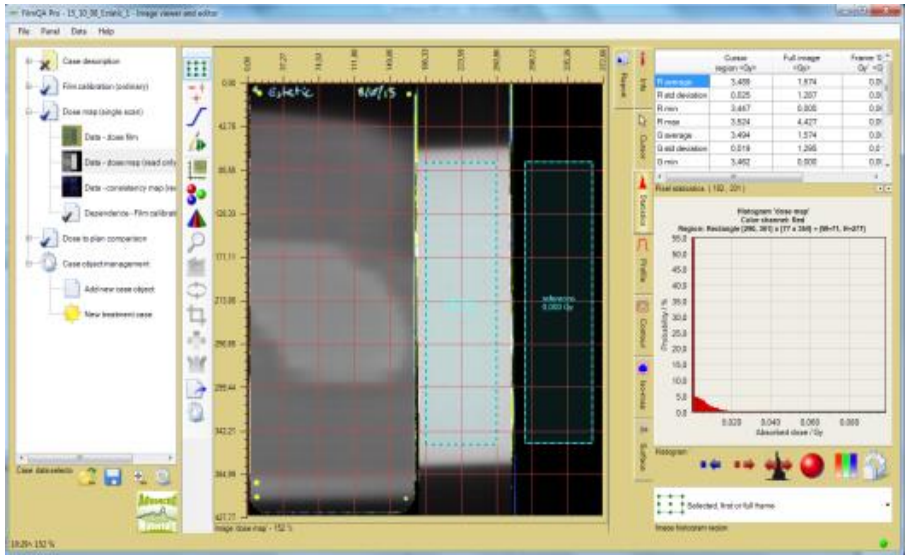

Film QA Pro (Ashland)

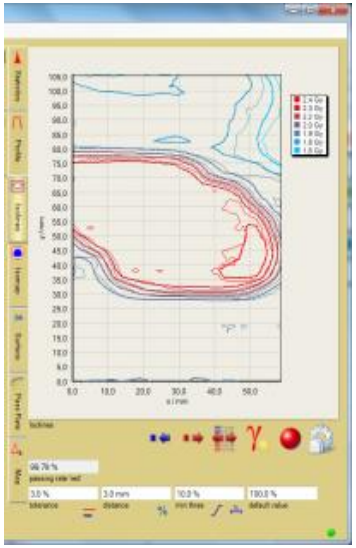

Dose distribution comparison

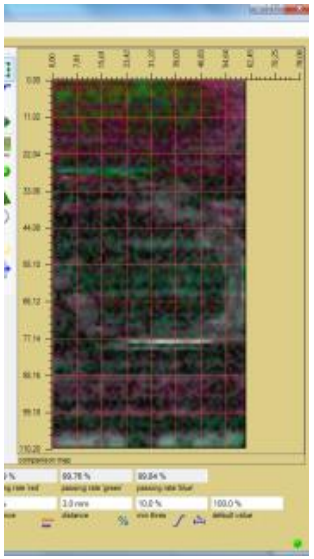

Gamma comparison

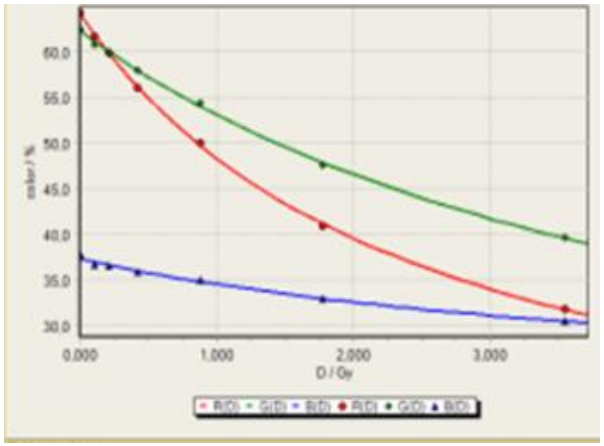

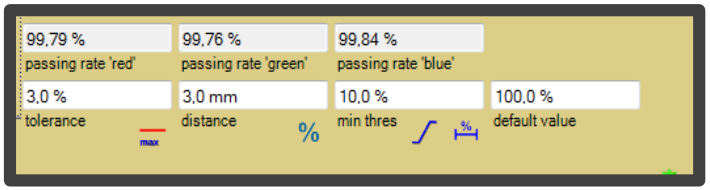

Uncertainties

Will strongly depend on the process used and the uncertainty budget has to be performed in each department once the process has been set.

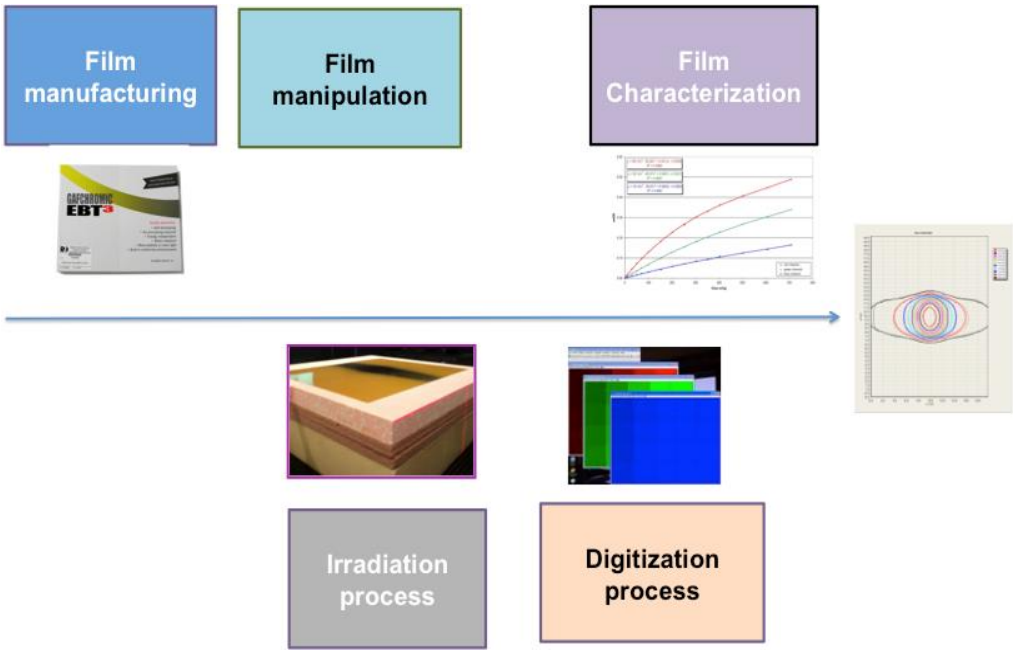

Uncertainties

- Published studies on EBT, red channel, uncertainty between 0.9% and 2% depending on the procedure.

- Uncertainty is reduced using 3 channel methods. The uncertainty depends on the model used for channel combination (Mendez et al. MP 41(1) 2014).

- None of these uncertainty calculations take into account the uncertainty in the dose measured by the ionisation chamber. (Reference conditions: relative standard uncertainty 1.5% for high energy X-ray beams (TRS398)).

Tips to succeed:

- Process consistency is key to obtaining accurate and precise results in film dosimetry.

- Not handle films with bare hands

- Control temperature during irradiation, storage and readout. Use the same conditions that for the films used for calibration

- Do not expose films to ultraviolet or sun light for hours.

- Although can be used in water, prolonged immersions will cause water to seep into the emulsion at the cut edges, be careful.

Tips to succeed:

- Process consistency is key to obtaining accurate and precise results in film dosimetry.
- The range of dose levels used for calibration must cover the measurement range.
- 5 films per point dose recommended for calibration
- If small square pieces are used for calibration keep track of the initial sheet orientation (remember coating direction).
- Use the same scanning protocol for calibration and for measuring
    - Need to be scanned in the same orientation [orientation of "needle like micro-crystals (EBT)]
    - For best results, scan one day following irradiation (min. two hours)
- Take into account corrections for the scanner: Linearity and non homogeneity.

From 1D to 2D: On line detectors

I can not wait
I need the results of verifications
NOW

2D: Detector arrays

Film dosimetry was the standard for 2D dose measurements.

BUT Trends towards so called "digital hospitals"

- No access to film processing machine

Wish to implement fast **real-time** procedures for measurements

2D detector arrays are an option

- No necessity to downscale MUs to the sensitive range (not for EBT- XT)
- Potential for absolute dose measurements
- Results available immediately after irradiation
- Mostly limited to single beam verification

2D: Detector arrays

- **Use different physical principles**

  IC, diodes, fluorescence screen, ..

- **Limited spatial resolution (>7 mm)**

  Impact on gamma-evaluation

- **Differences in build-up and backscatter (!)**

- **Software (import of d... distributions, evalua...**

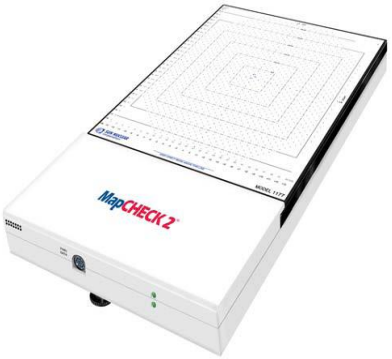

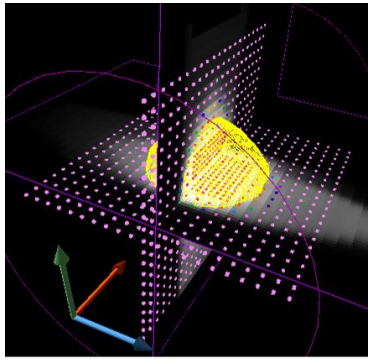

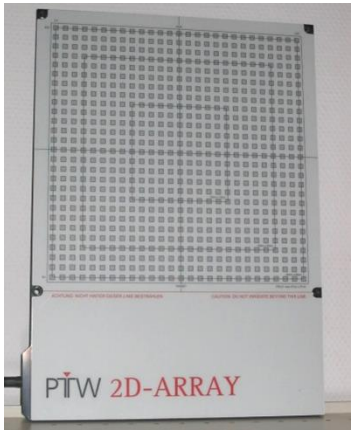

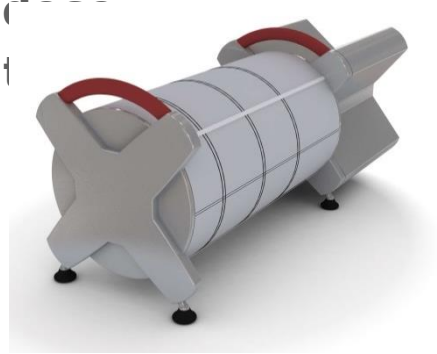

ESTRO School

2D: Detector arrays

MatriXX
(IBA)

1020 i.c.
0.080 cm^3
24x24 cm^2

Seven29
(PTW)

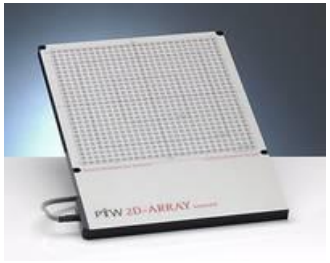

729 i.c.
0.125 cm^3
27x27 cm^2

Mapcheck2
(Sun Nuclear)

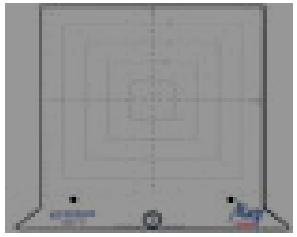

1527 diodes
0.000019 cm^3.
32x26cm^2
Build up 2cm –Backscatter 2.3cm

Limited spatial resolution.

Diodes : energy-dose-rate dependence, need recalibration (6 months)

i.c.: volume averaging effects

		Manufacturer	Sun Nuclear	IBA	PTW
		Product	MapCHECK	MatriXX	729
Advantage	1	Active Dimension (mm)	0.8 x 0.8	4.5 (diameter)	5.0 x 5.0
		Active Area (mm^2)	0.64	15.90	25.00
	2	Active Thickness (mm) Active Volume (cm^3)	0.03 0.000019	5.0 0.08	5.0 0.125
	3	Sensitivity (nC/Gy)	32.0	2.4	3.3

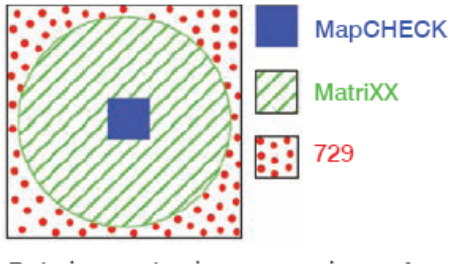

ESTRO School

2D: Detector arrays

MapCheck 2 (Sun Nuclear)

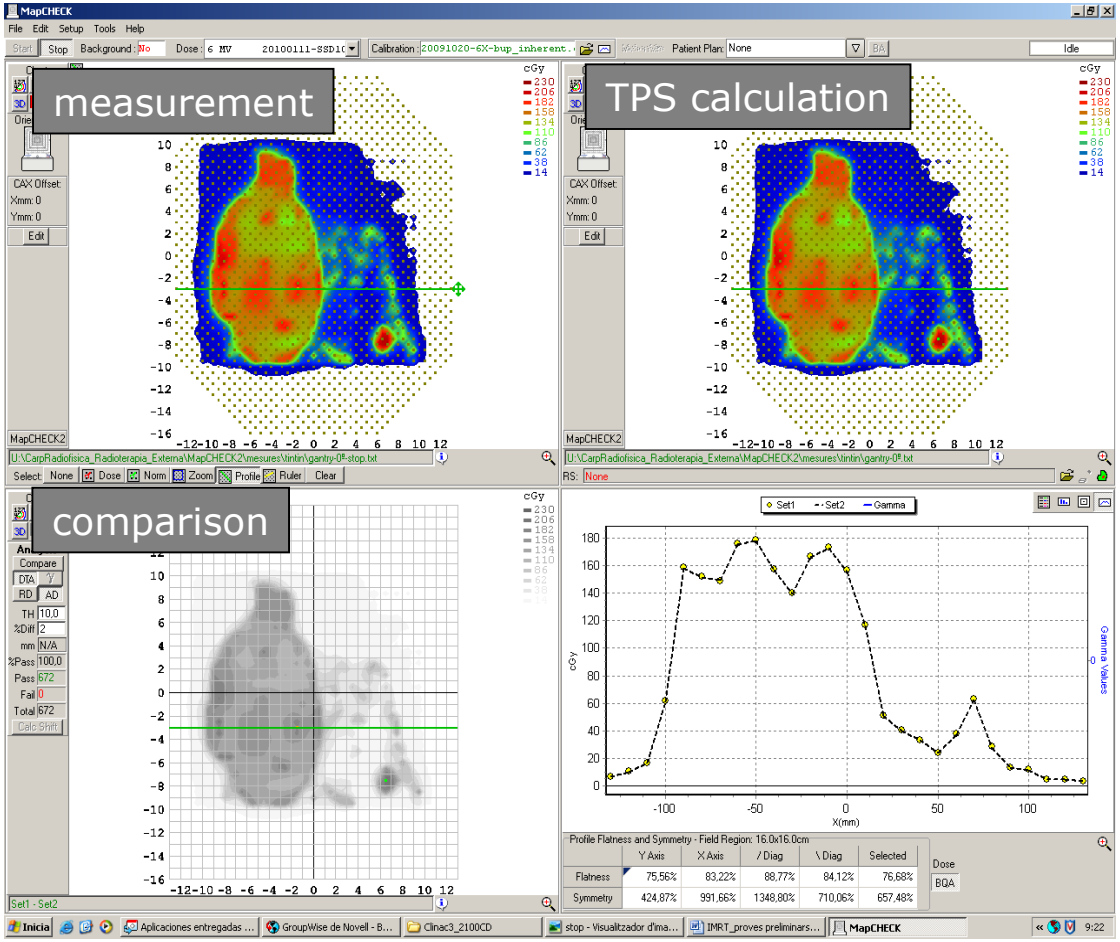

MapCHECK 2

1527 díodes
Resolution: 7.07 mm
Surface: 26 cm x 32 cm

MapPHAN (*virtual water*) + Plastic Water

SDD = 100 cm
z = 10 g/cm2

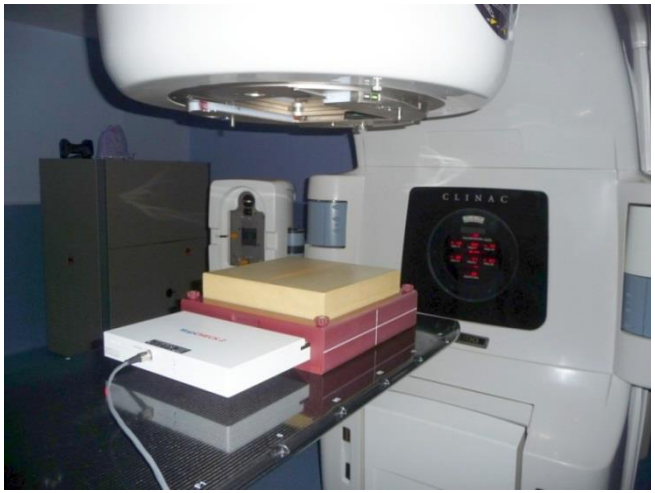

ESTRO School

2D: Detector arrays + phantom

Arrays PTW

The Modular Advantage For any application. Start now, upgrade later.	 OCTAVIUS® 4D **1500**	 OCTAVIUS® 4D **1000 SRS**	 OCTAVIUS® 4D **729**
Applications			
Patient Plan QA (field-by-field, composite)	●	●	●
LINAC QA	○	○	○
Dose Delivery QA	○	○	○
Treatment Techniques			
3D CRT	■	-	■
IMRT (static, dynamic)	■	-	■
Arc Therapy	■	-	▣
SRS/SBRT	▣	■	-
FF/FFF Beams	■	■	■
Coplanar/Non-Coplanar Beams	■	■	■

● included ○ optional **Suitability**: ■ excellent ▣ very good - not recommended

2D: Detector arrays
1000 SRS (PTW)

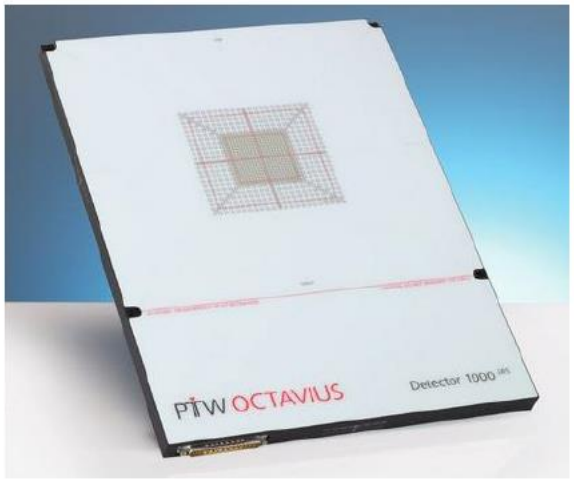

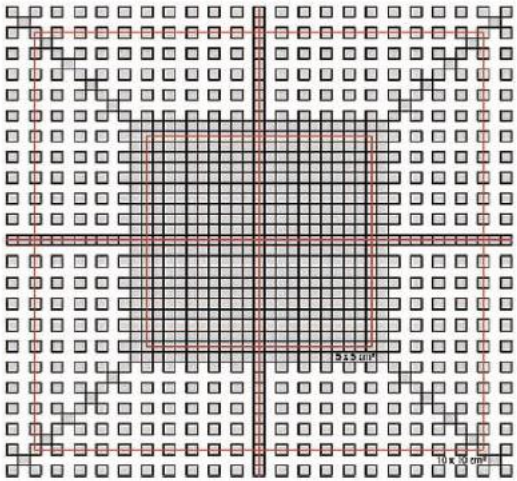

Detector type:	Liquid-filled ionization chambers
Number of detectors:	977
Detector size:	2.3 mm x 2.3 mm x 0.5 mm (0.0003 cm^3)
Detector spacing:	Center (5.5 cm x 5.5 cm): 2.5 mm center-to-center Outer area (11 cm x 11 cm): 5 mm center-to-center
Max. field size:	11 cm x 11 cm
Reference point:	9 mm below the surface of the array

ESTRO School

“3D” detector matrix

Delta4 (Scandidos)

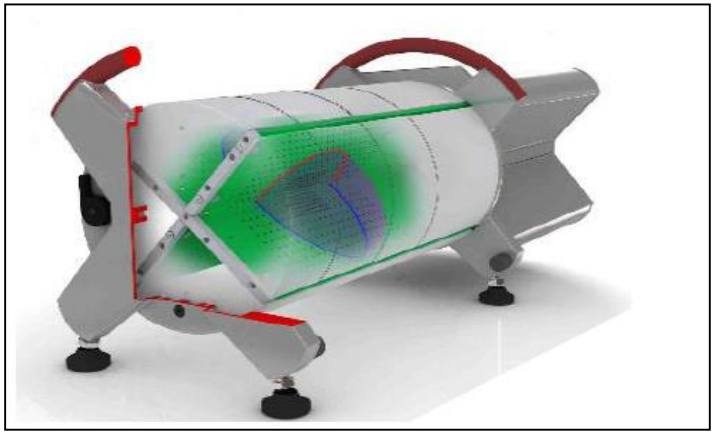

2 ortogonal planes

Detectors	Type p-Si
Total number	1069
Maximum deviation of detection point relative to markings on the phantom	0.5 mm
Detection area per plane	20 x 20 cm
Distance between detectors Central area (6x6cm)	5 mm
Outer area (20x20cm)	10 mm
Size (radial x axial)	1 x 0.05 mm^3 = 0.04 mm^3

James L Bedford et al Phys. Med. Biol. 54 (2009)

ArcCHECK (Sun Nuclear)

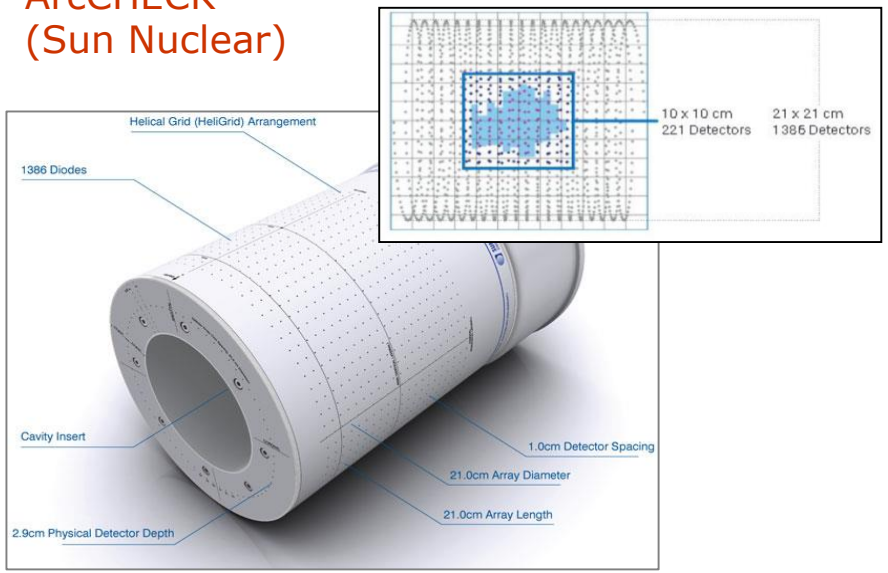

Cylindrical disposition

Detector Type	SunPoint® Diode Detectors
Detector Quantity	1386
Detector Spacing (cm)	1.0
Array Diameter (cm)	21.0
Array Length (cm)	21.0
Cavity Diameter (cm)	15.0
Inherent Buildup (g/cm^2)	3.3
Inherent Backscatter (g/cm^2)	3.3
Detector Physical Depth (cm)	2.9
Array Geometry	Helical Grid (HeliGrid) 1 cm offset
Phantom Material	PMMA (Acrylic)
Active Detector Area (mm^2)	0.64
Detector Volume (mm^3)	0.019

Daniel Létourneau et al. Med.Phys. 36 (2009)

ESTRO School

Detector array handling tips

- Determine the effective point of measurement. Water equivalent depth
- Calibrate the array following the manufacturer methodology

  (calibration coefficient +homogeneity factor)
- Check linearity with dose, dose rate dependence, field size dependence, angular dependence (important for static set-up)

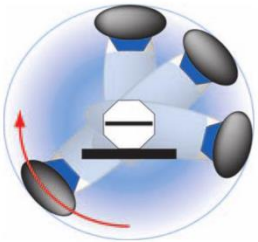

Angular dependence correction for MatriXX

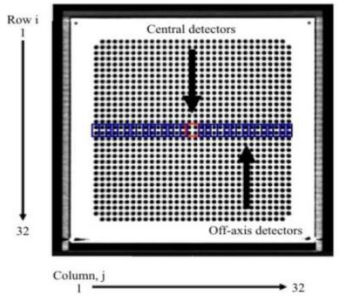

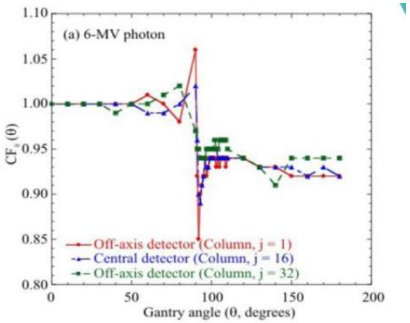

Y.Shimohigashi et al. Angular dependence correction of MatriXX and its application to composite dose verification. Journal Of Applied clinical medical physics. 13, (5), 2012.

- Compare your results with literature

ESTRO School

EPID as 2D Detector

Trends towards so called "digital hospitals"

- No access to film processing machine
- Film dosimetry limited to radiochromic films

Wish to implement fast **real-time** procedures for measurements

EPID are an option

No necessity to downscale MUs to the sensitive range

Potential for absolute dose measurements

Results available "immediately" after irradiation

Mostly limited to single beam verification

Good spatial resolution

Need of corrections to convert the resulting signal into fluence or dose in detector

EPID as 2D Detector

- Standard equipment on new linacs
- Suitable for dosimetry
- Potential for a variety of applications

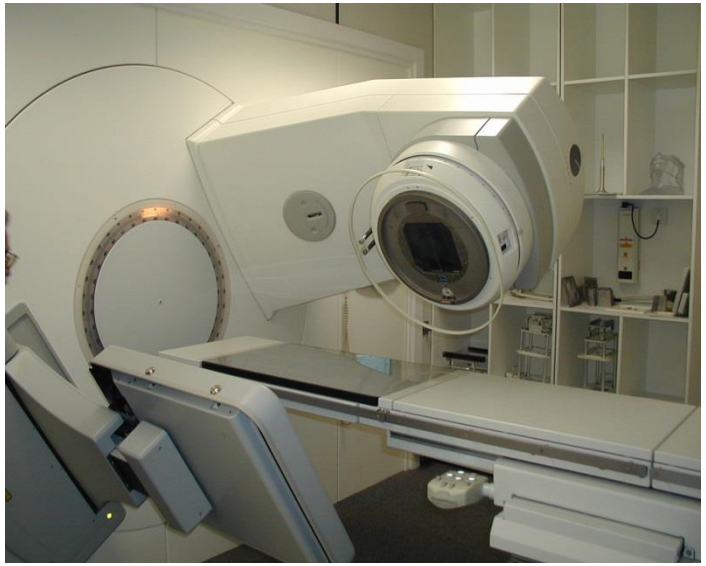

AMORPHOUS SILICON

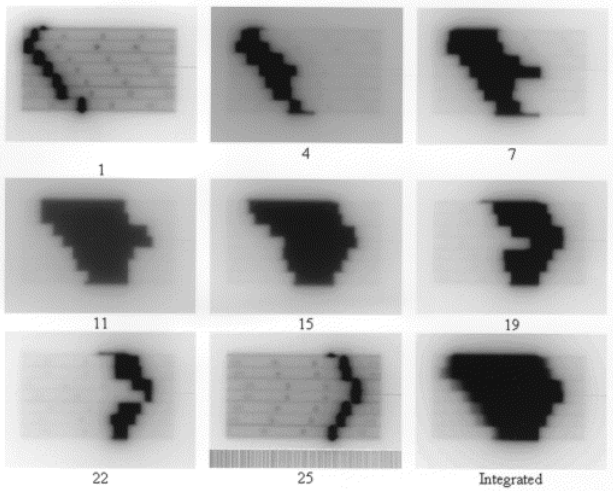

ESTRO School

Amorphous silicon (a-Si) type of EPID

Principles of operation

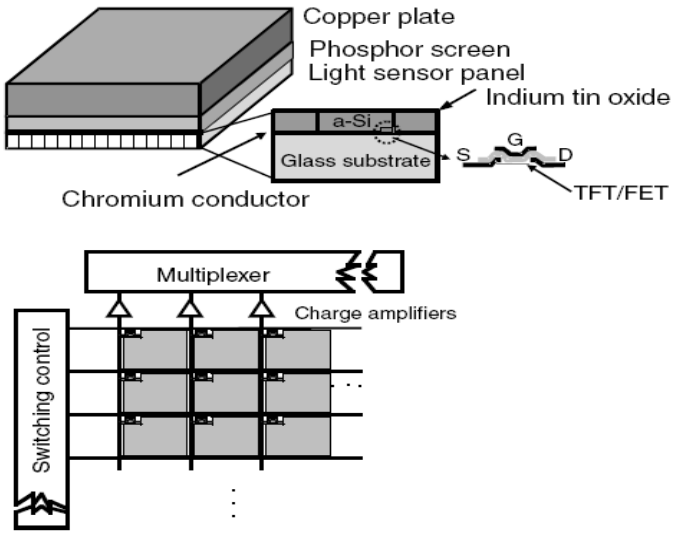

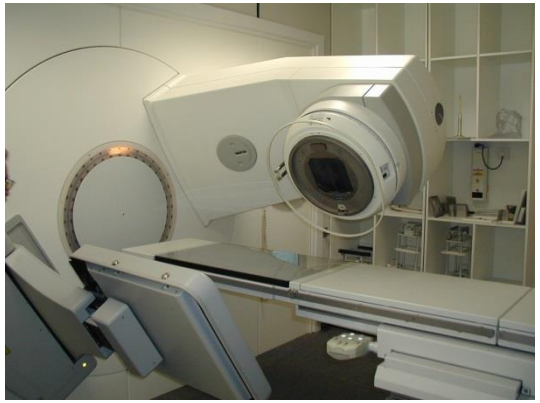

- Compton electrons produced in the copper plate
- Electrons produce light photons in the phosphor material
- The light sensor detector pixels are photodiodes and TFT transistors connected to readout and scanning electronics.

Nahum, Mayles, Rosenwald, Handbook of radiotherapy

Forward approach

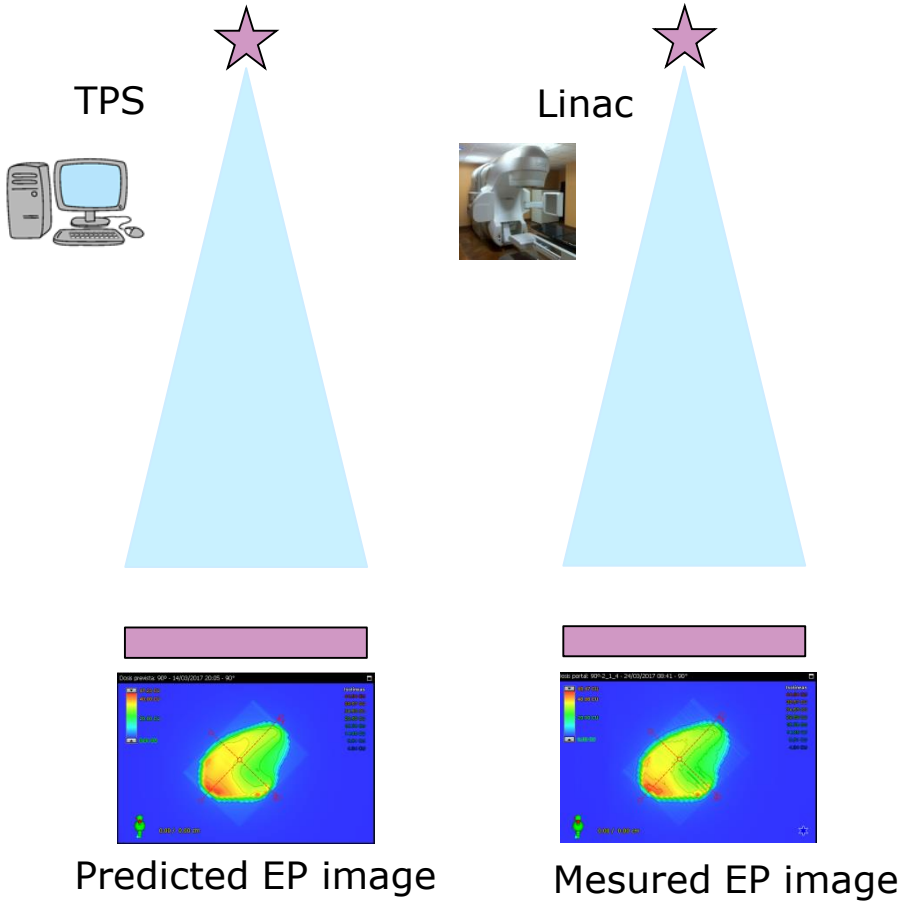

TPS has a model to
Predict EP image from
the calculated fluence

Portal Calibration:

Dark and Flood fields
Calibration response/dose
Correction for beam profile

EPID calibration

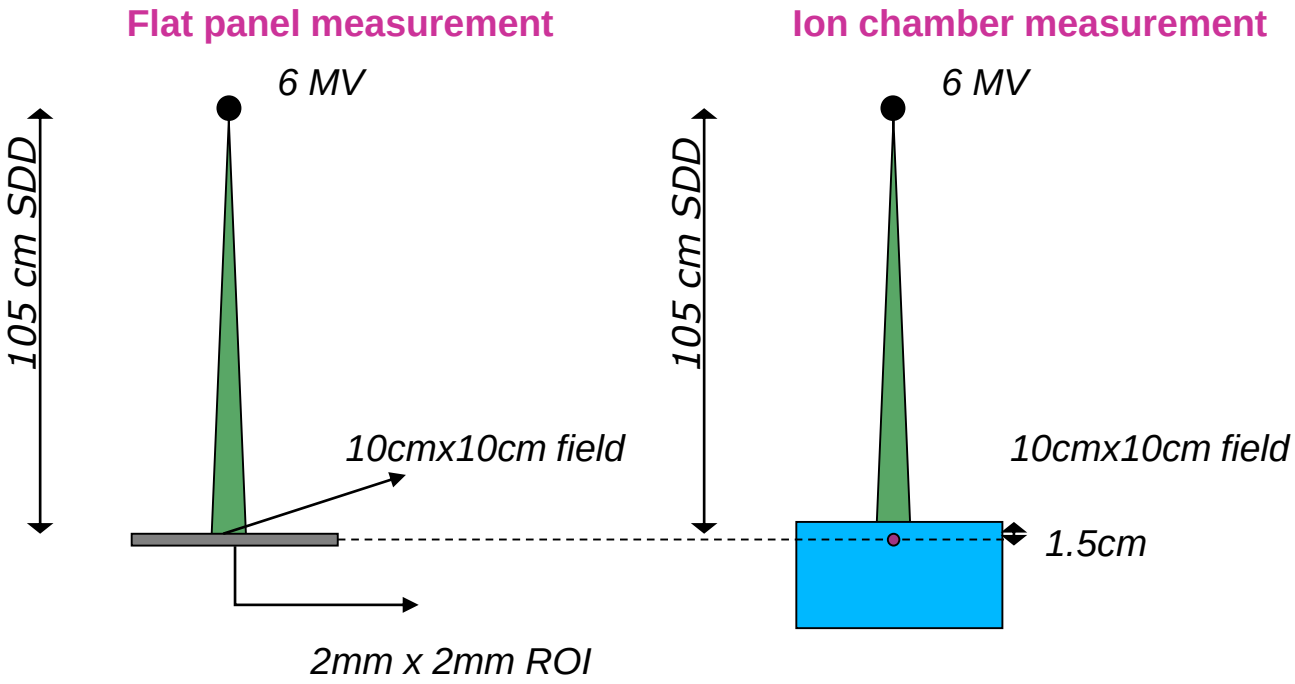

AMORPHOUS SILICON: linear with dose, need of selecting adquisition parameters to avoid saturation

Application example; Portal imaging (Varian)

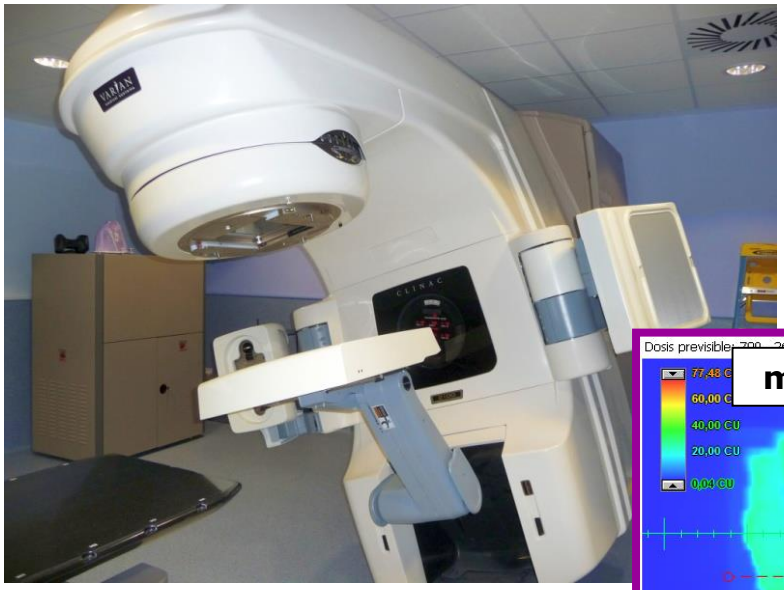

Amophous silicon (aSi1000): 1024 × 768 píxels

Resolution: 0.4 mm

Surface: 40 cm x 30 cm

SDD = 105 cm

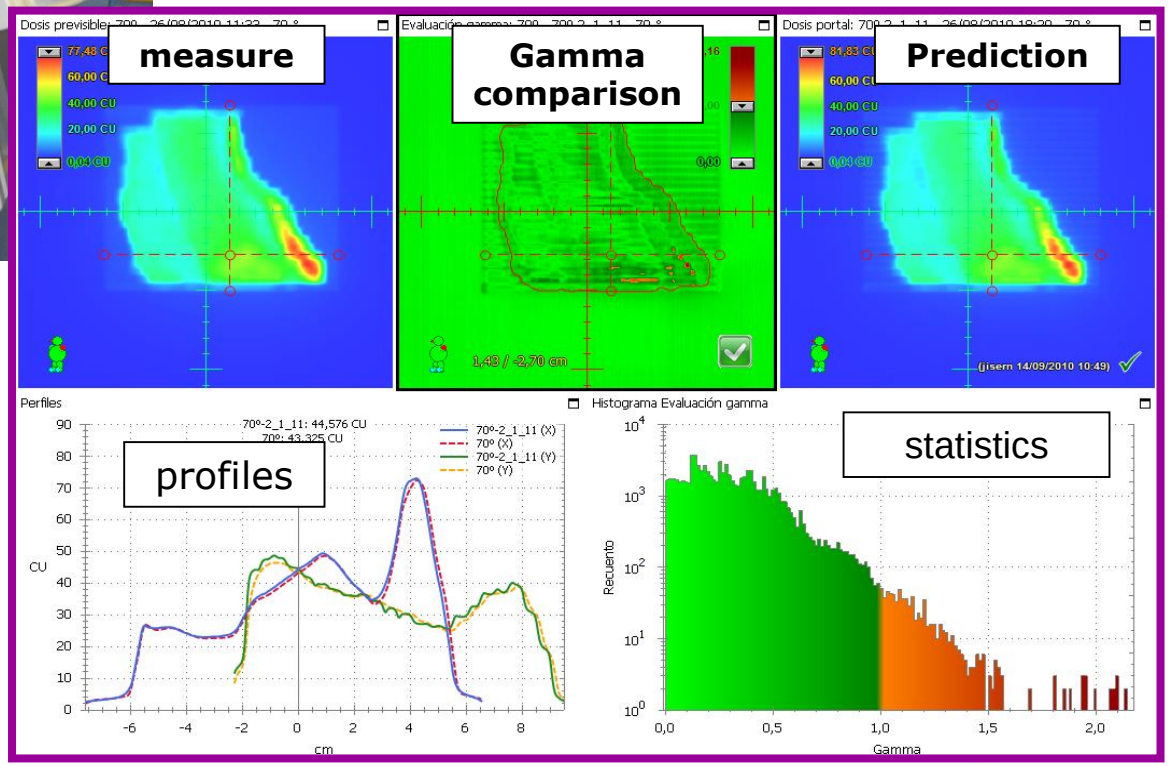

Reconstruction approach (virtual phantom)

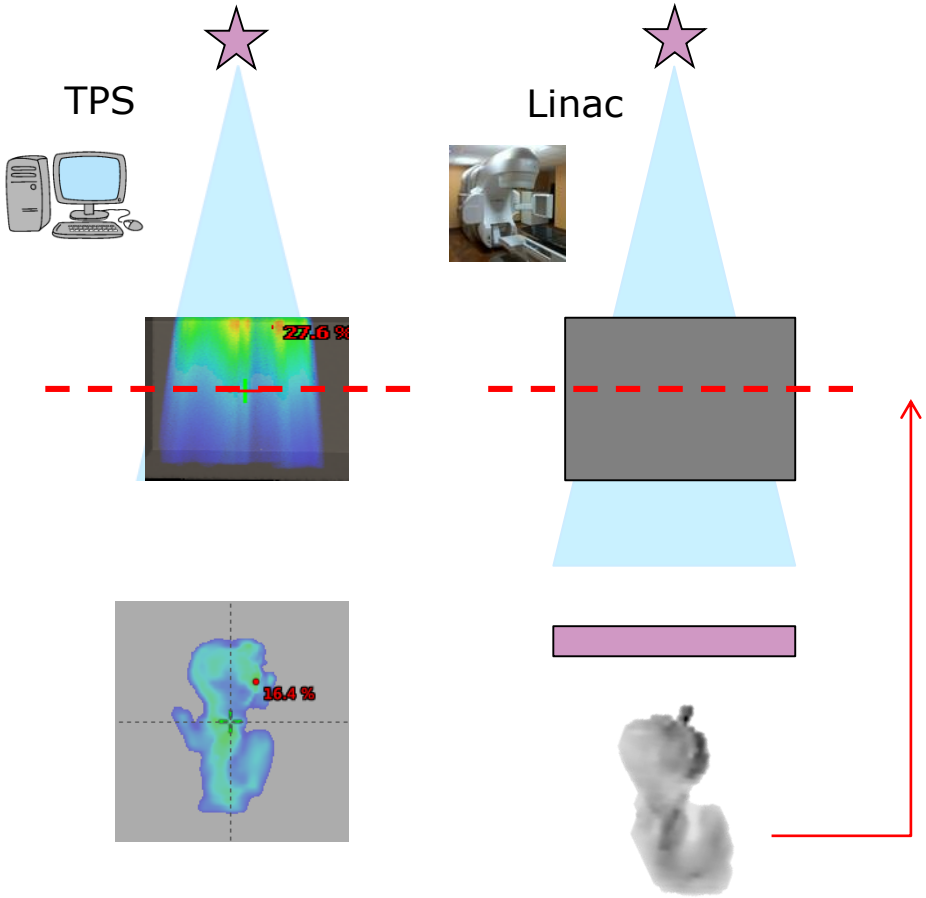

Portal Calibration:

Dark and Flood fields
Calibration response/dose
Correction for beam profile
Correction for arm backscatter

Calculate dose in a regular phantom

Dose in a plane
3D dose distribution

Mesured EP image

ESTRO School

Correct for arm back scatter (if needed)

Pixel to dose at 10 cm depth in a cylindrical phantom calibration

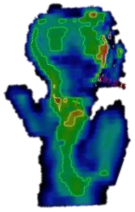

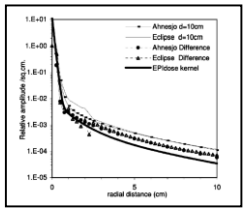

Convolution with a kernel to account for phantom scatter and electron transport

Off axis correction

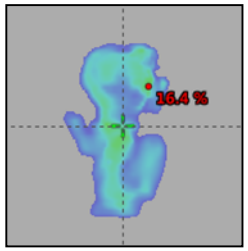

How is this Kernel constructed:

1. The relative dose as a funtion of field size matches the TPS calculation at the phantom center

2. Penumbra at edge of a typical field is broadened to the same extend it would be at the depth of the phantom center

W. Ansbacher, Med Phys (33;9), 2006
B. W. King et al. JAMP (17;6), 2016

ESTRO School

EPID CALIBRATION

Correction factors (at this moment to be used for pretreat verifications and linac QA)

THE INTENSITY AT EACH POINT IN THE IMAGE MUST BE CALIBRATED IN A QUANTITATIVE SENSE

- The dose response of each pixel point must be known
- The effects of scattered radiation in the detector must be understood
- The temporal stability of the detector must be known.

DEPENDING ON THE DETECTOR: DIFFERENT CORRECTION FACTORS CAN BE EXPECTED

- Field size
- Backscatter from the EPID arm (Varian aS500, aS1000).
  Not needed for aS1200 (backscatter shielding added)
- EPID SAG if used at different gantry angles

ESTRO School

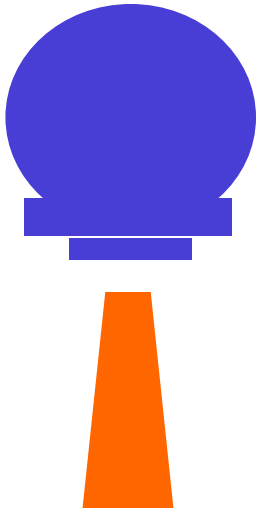

2D ARRAYS, EPID

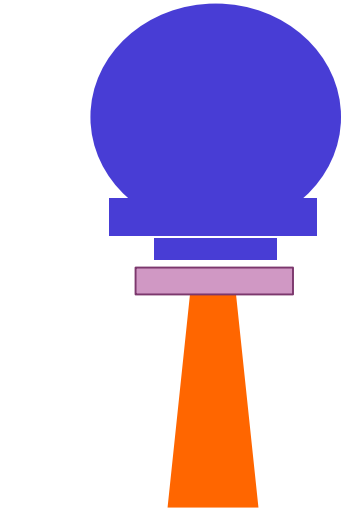

Transmission chamber

Periodic QC Dynamic wedges
Beam symetry and flatness

Pre-treatment verification IMRT
VMAT

WE CHECK DELIVERY

How can we know that the delivery
is as planned when treating the patient?

ESTRO School

Transmission chambers

"Dolphin" (IBA)

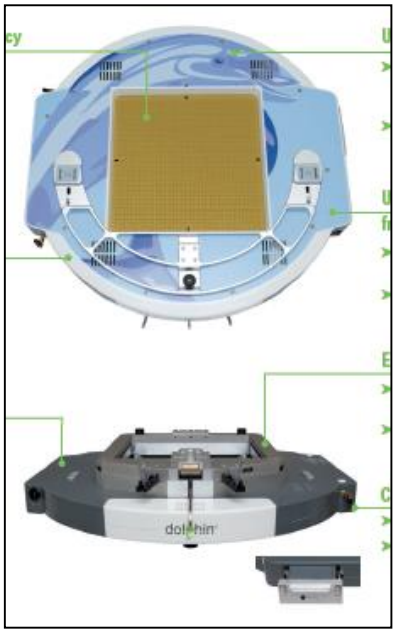

pp i.c. matrix
1513 i.c.
0.02 cm^{3-} 5mm center to center
Attenuation 1% (6MV)
Measures dose fluence
MC modelling of detector reponse

David (PTW)

Multiwire i.c.
nº of wires = nº leaf pairs

Attenuation 5% (6MV)
Measures dose-length product

Delta 4 TD (Scandidos)

diode matrix
4040 diodes
1mm (disc shaped)
2.5 x 5 mm spacing
Attenuation 1% (6MV)
Sensitivity decrease: 0.04% per kGy

Dose measurement accuracy 1.5%

MLC position accuracy 1mm

ESTRO School

Transmission chambers

"*Dolphin"*
(IBA)

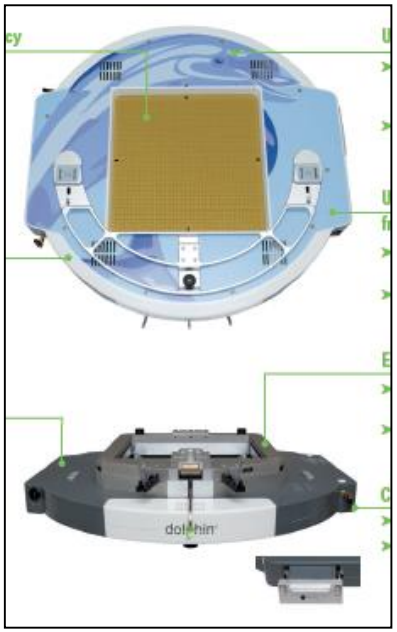

David
(PTW)

Delta 4 TD
(Scandidos)

LIMITED SPATIAL RESOLUTION

NEED TO REMOVE ELECTRON CONTAMINATION FROM THE HEAD

ESTRO School

2D detector's comparison: spatial-dose resolution

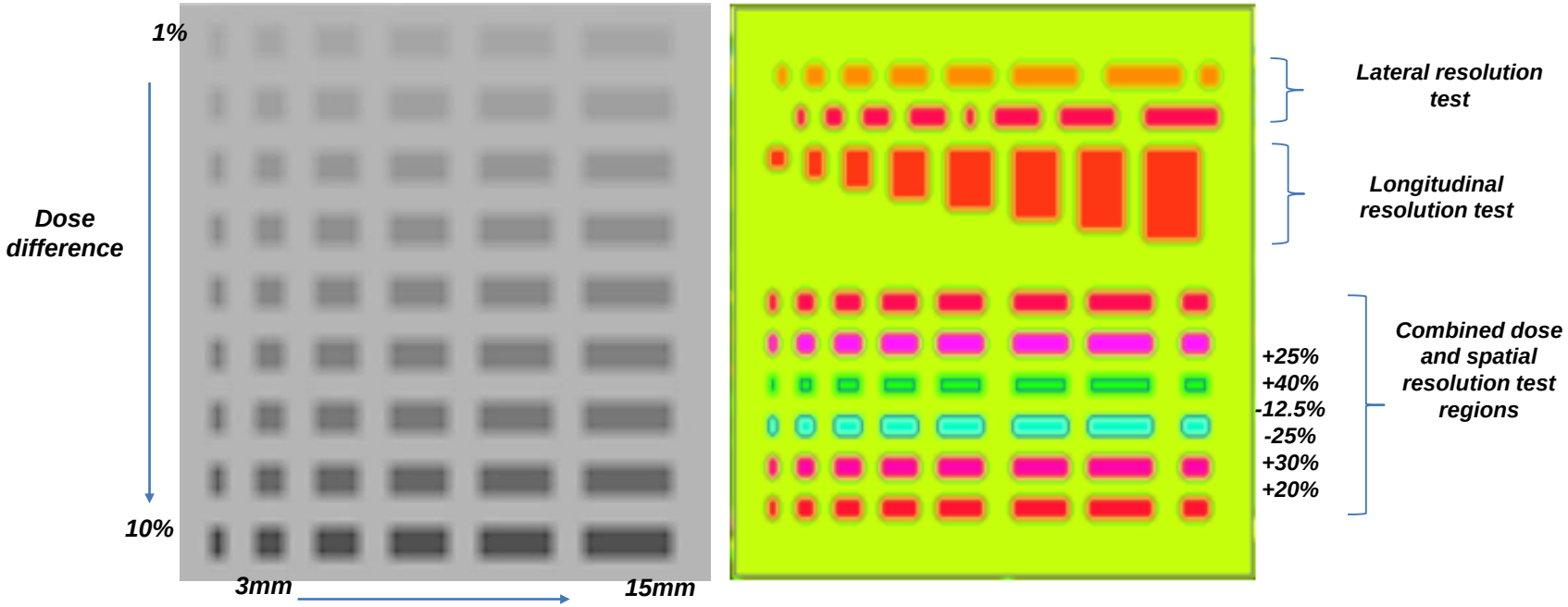

Single gantry test fields for resolution and sensitivity assessment. (left) the sensitivity test, and (right) the resolution test. In the resolution test the values in the lower half represent difference in % dose between the regions and the background (lime green) area.

2D detector's comparison: spatial-dose resolution

Gafchromic film | 2D array | 2D array | EPID

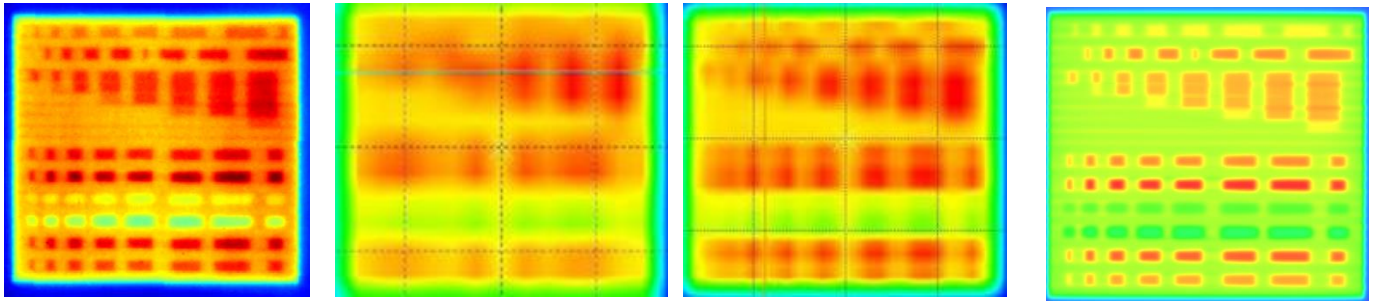

Single acquisition | Double acquisition

From Andrew Nisbet, ESTRO premetting Geneve 2013

ESTRO School

3D dosimetry systems

- **Films, 2D arrays, EPIDs: partial sampling of a 3D dose distribution**

- 3D dosimetry materials:

  - Polymer gels: Polyacrylamide gels (BANG gel, nPAG)
  - Fricke gels
  - Radiochromic plastics (PRESAGE)

- Reading systems:

  - Magnetic resonance (MR) imaging - Polymer
  - Optical- Computed Tomography (optical CT) - Radiochromic
  - Laser scanning – Polymer and Radiochromic

GEL DOSIMETRY SYSTEMS

- Gel dosimetry systems are true 3-D dosimeters.
- The gel dosimeter is a phantom that can measure absorbed dose distribution in a full 3-D geometry. HIGH RESOLUTION
- Short time in the treatment room.
- Gels are nearly tissue equivalent and can be molded to any desired shape or form.
- Large amount of information in patient geometry!
- Can be deformed (simulate organ deformation during irradiation)
- Excellent for new treatment implementation but still too labor intensive to be used in routine

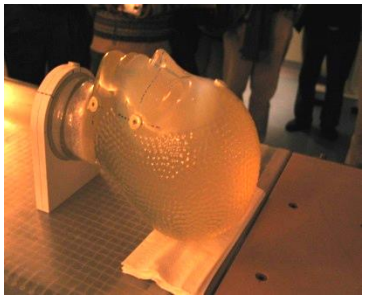

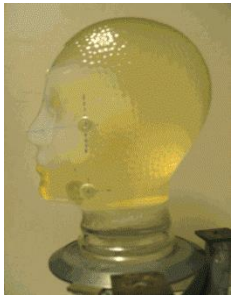

IRRADIATION (TREATMENT)

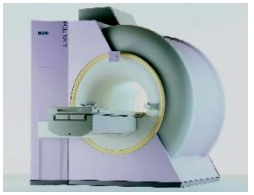

qMRI

$$R2 = \frac{1}{T2}$$

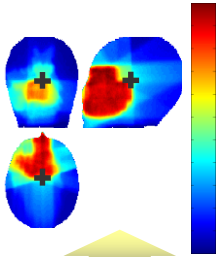

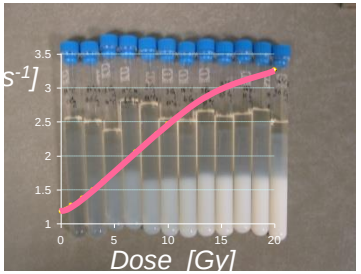

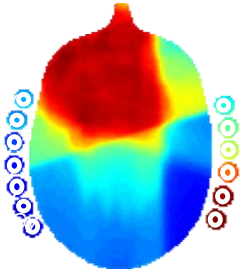

GEL FABRICATION

From Yves De Deene – Univ Ghent

ESTRO School

SUMMARY

How to choose the 2D dosimetry system

Its use:

Comissioning treatment units
Data adquisition for TPS
Comissioning TPS
QA treatment unit: Periodic QC.
Pretreatment QA
In vivo dosimetry

Dosimetric requirements:

Accuracy
Spatial resolution
Absolute vs relative dose measurements

Logistics:

Available phantoms
Time slots for QA in Treatment units
Time needed to calibrate the dosimetry system
Post processing time/complexity


Questions?

RECOMMENDED READING

•**General:**

•Clinical dosimetry measurements in radiotherapy. AAPM monograph nº34 (2009)

•**Film dosimetry:**

•AAPM TG69. Radiographic film for megavoltage beam dosimetry.Med.Phys. 34(6); 2006

•AAPM Report nº 63. Radiochromic film dosimetry. Med. Phys. 25(11); 1998

•Devic S., Seuntjens J. et al. Dosimetric properties of improved GafChromic films for seven different digitizers. Med. Phys. 31(9); 2004

•Devic S., Seuntjens J. et al. Precise radiochromic film dosimetry using a flat-bed document scanner. Med. Phys. 32(7); 2005

•Zeidan O.A., Stephenson S.A.L. et al. Characterisaton and use of EBT radiochromic film for IMRT verification. Med.Phys. 33(11); 2006

•Fuss M., Sturtewagen E. Dosimetric characterisation of GafChromic EBT film and its implication on film dosimetry quality assurance. Phys. Med. Biol. 52; 2007

•Bouchard H., Lacroix F. On the characterization and uncertainty analysis of radiochromic film dosimetry. Med. Phys. 36(6); 2009

•Devic. Radiochromic film dosimetry: Past, present and future. Phys. Medica 27 (2011)

•Méndez et al. On multichannel film dosimetry with channel-independent perturbations. Med. Phys. 41(1);2014

•Micke et al. Multichannel film dosimetry with nonuniformity correction. Med. Phys. 38 (2011)

ESTRO School

RECOMMENDED READING

•**Arrays:**

•Spezi E. et al. Characterisation of a 2D ion chamber array for the verification of radiotherapy treatments. Phys. Med. Biol. 50; 2005 [Seven29™ (PTW)]

•Herzen J. et al. Dosimetric evaluation of a 2D pixel ionization chamber for implementation in clinical routine. Phys. Med. Biol 52; 2007 [MatriXX (IBA)]

•Létorneau D. et al. Evaluation of a 2D diode arrray for IMRT quality assurence. Radiother. Oncol.70(2); 2004

•Létorneau D., Publicover J. et al. Novel dosimetric phantom for quality assurance of volumetric modulated arc therapy. Med.Phys. 36(5);2009

James L Bedford et al. Evaluation of the Delta4 phantom for IMRT and VMAT verification. Phys. Med. Biol. 54 ;2009

EPID:

W. Van Elmpt, L. McDermott et al. A literature review of electronic portal imaging for radiotherapy dosimetry. Radiother Oncol. 88(3);2008

Gel Dosimetry:

Oldham et al. High resolution gel-dosimetry by optical-CT and MR scanning. Med. Phys. 28(7);2001

ESTRO School

Acknowledgement
with many thanks to:

Dr. Jorgen Oloffson and Pablo Carrasco

ESTRO School

Patient specific QA

Núria Jornet

Servei de Radiofísica
Hospital Sant Pau,
Barcelona

Learning objectives

To understand what is meant by patient specific QA

To understant the role of in vivo dose measurements within QA in RT.

To get familiar with the different possibilities for in vivo dosimetry

To compare the different available systems. Cons and Prons.

To have an overview of how the different systems should be calibrated to be used for in vivo dosimetry.

Patient specific verifications, what does it refer to?

Machine QA

TPS QA

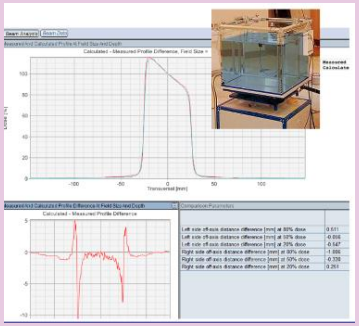

PATIENT

Imaging

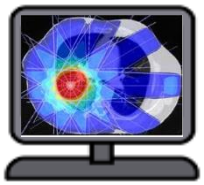

Treatment Planning

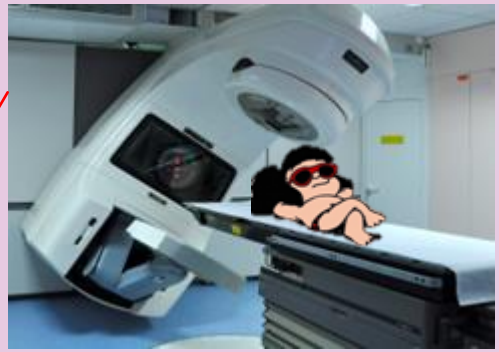

Treatment delivery

Data tranfer to treatment unit

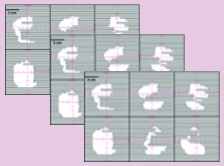

Usually a standard set of tests
Confidence that the equipment can be used safely to treat patients

Verify the treatment for that patient!

The treatment is delivered as planned

ESTRO School

Patient specific verifications: different layers

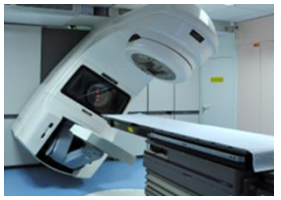

First layer:

-Treatment unit can deliver the treatment as planned

PRETREATMENT VERIFICATION

- Verification of data transfer for the actual patient plan ✗
- Beam data adquired during patient treatment
  - Log files ✗
  - Fluence
- Checking the dose distribution as delivered to the patient (patient changes). ✗

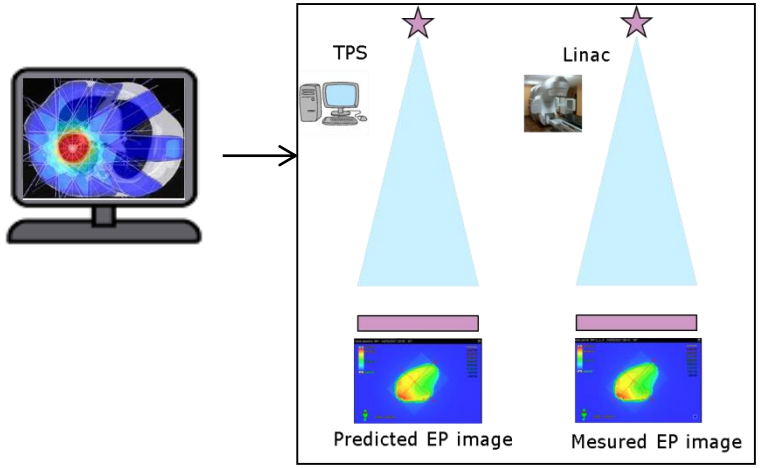

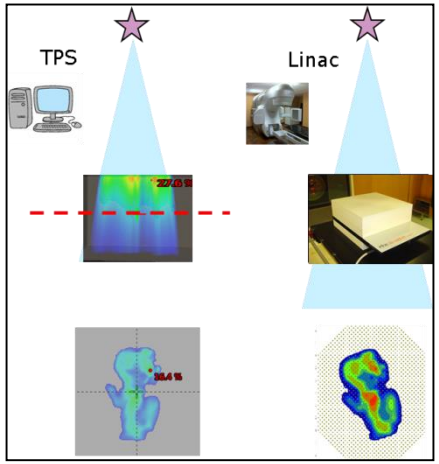

ESTRO School

Patient specific verifications: different layers

Second layer:

-Treatment unit can deliver the treatment as planned during patient treatment

TREATMENT VERIFICATION ON DELIVERY

- Verification of data transfer for the actual patient plan ✓
- Beam data adquired during patient treatment
  - Log files ✓
  - Fluence ✗
- Checking the dose distribution as delivered to the patient (patient changes). ✗

LOG FILES (MLC, gantry angle)

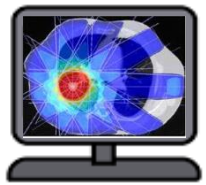

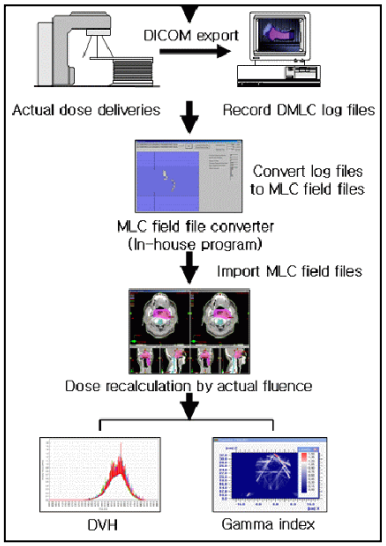

Mar 2013.Journal- Korean Physical Society

ESTRO School

Patient specific verifications: different layers

Second layer:

-Treatment unit can deliver the treatment as planned during patient treatment

TREATMENT VERIFICATION ON DELIVERY

- Verification of data transfer for the actual patient plan ✓
- Beam data adquired during patient treatment
  - Log files ✓
  - Fluence ✓
- Checking the dose distribution as delivered to the patient (patient changes). ✗

LOG FILES (MLC, gantry angle)

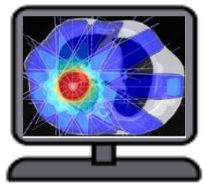

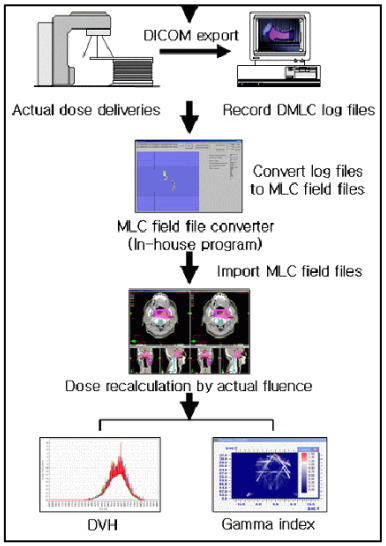

TRANSMISION DETECTORS

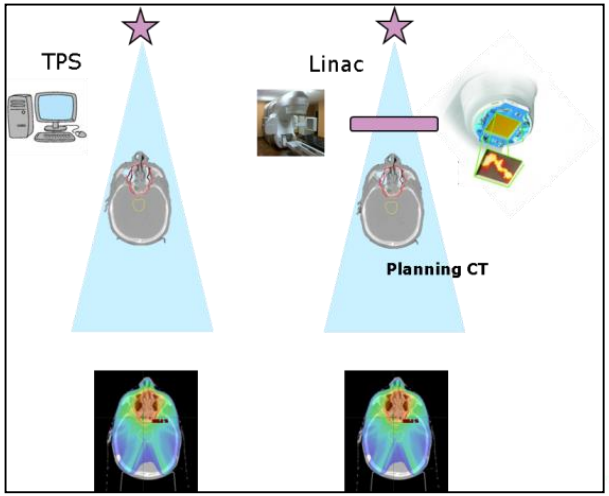

Mar 2013.Journal- Korean Physical Society

ESTRO School

Patient specific verifications: different layers

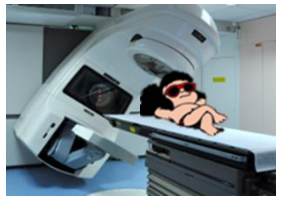

Third layer:

-Dose delivered to the patient agrees with the planned dose

- Verification of data transfer for the actual patient plan ✓
- Beam data adquired during patient treatment
  - Log files ✓
  - Fluence ✓
- Checking the dose distribution as delivered to the patient (patient changes). ✓

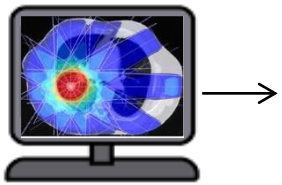

POINT MEASUREMENTS

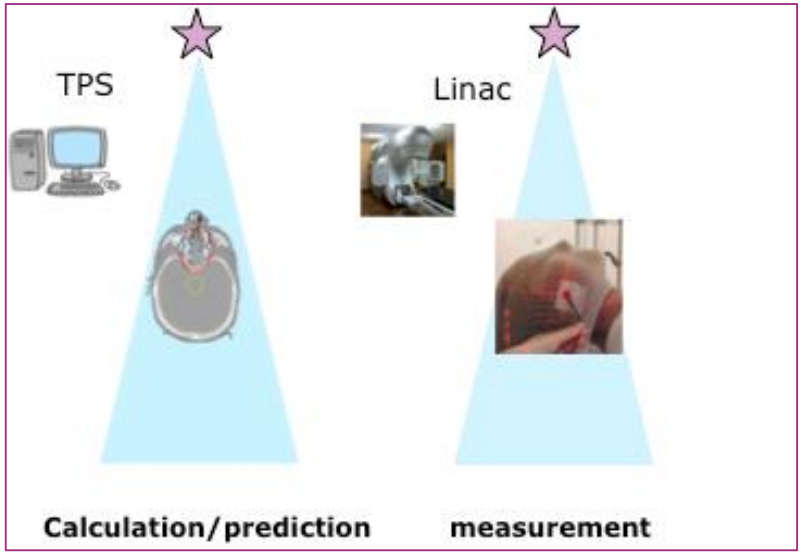

ESTRO School

Patient specific verifications: different layers

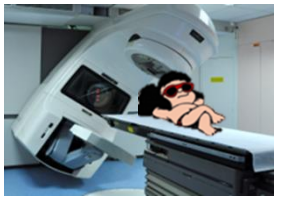

Third layer:

-Dose delivered to the patient agrees with the planned dose

- Verification of data transfer for the actual patient plan ✓
- Beam data adquired during patient treatment
  - Log files ✓
  - Fluence ✓
- Checking the dose distribution as delivered to the patient (patient changes). ✗

FORWARD APPROACH

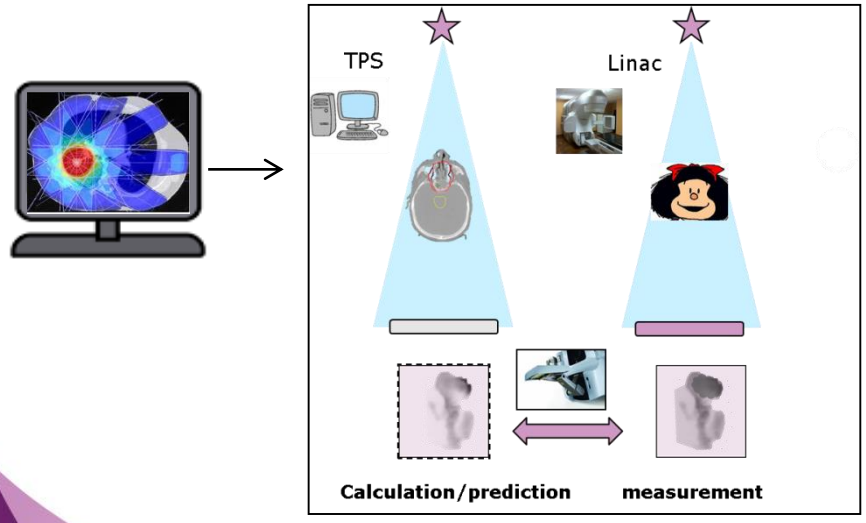

BACKWARD APPROACH (DOSE RECONSTRUCTION)

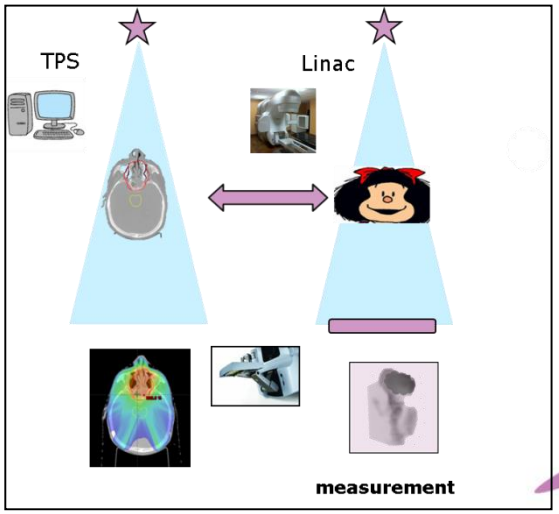

ESTRO School

Patient specific verifications: different layers

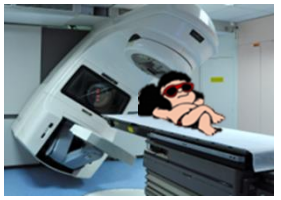

Third layer:

-Dose delivered to the patient agrees with the planned dose

- Verification of data transfer for the actual patient plan ✓
- Beam data adquired during patient treatment
  - Log files ✓
  - Fluence ✓
- Checking the dose distribution as delivered to the patient (patient changes). ✓

FORWARD APPROACH

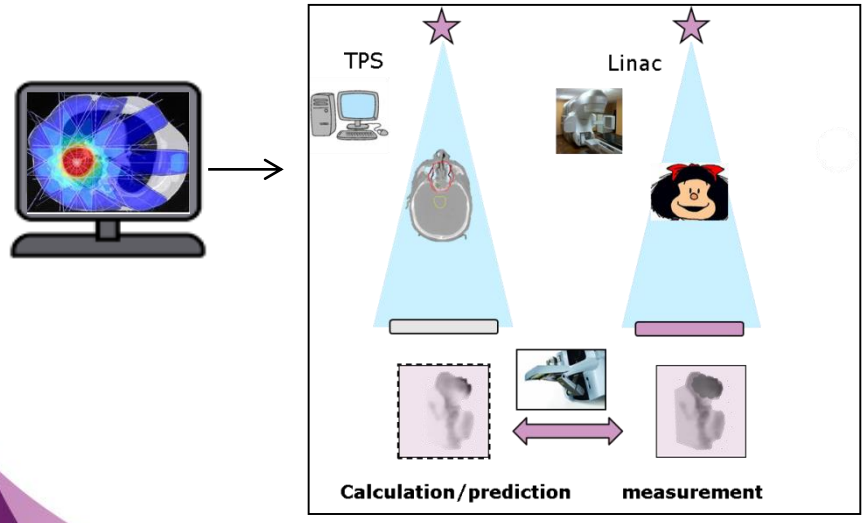

BACKWARD APPROACH (DOSE RECONSTRUCTION)

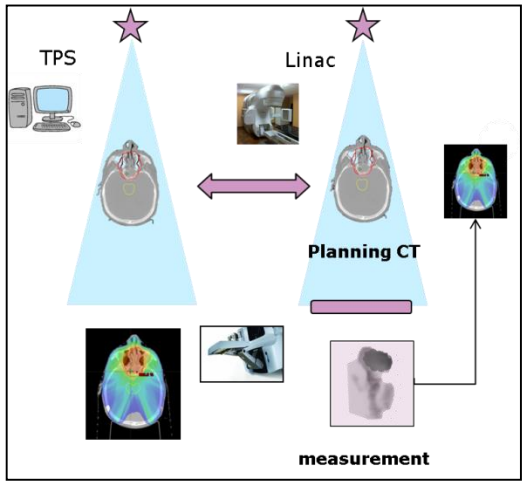

ESTRO School

Patient specific verifications: different layers

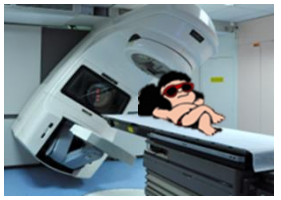

Third layer:

-Dose delivered to the patient agrees with the planned dose

- Verification of data transfer for the actual patient plan ✓
- Beam data adquired during patient treatment
  - Log files ✓
  - Fluence ✓
- Checking the dose distribution as delivered to the patient (patient changes). ✓

FORWARD APPROACH

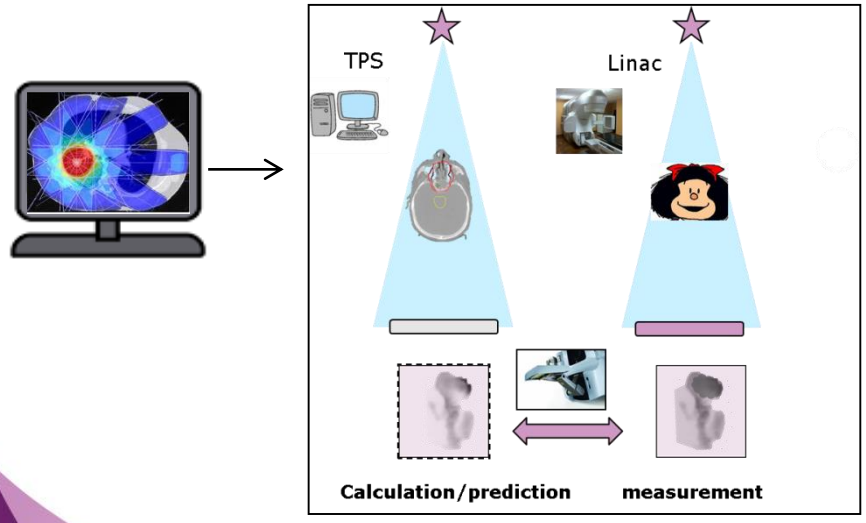

BACKWARD APPROACH (DOSE RECONSTRUCTION)

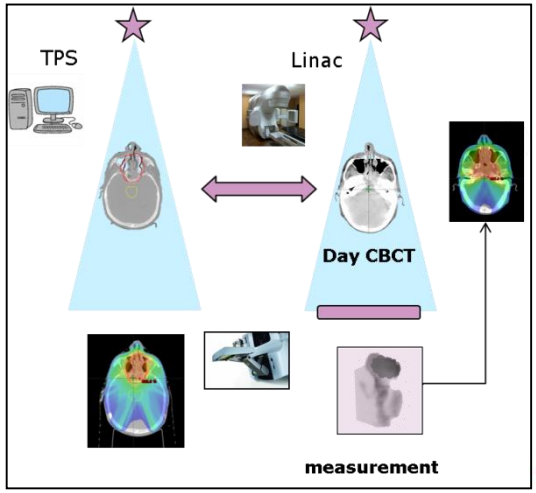

ESTRO School

Patient specific verifications: different layers

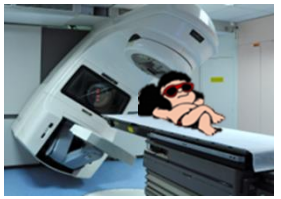

Third layer:

-Dose delivered to the patient agrees with the planned dose

- Verification of data transfer for the actual patient plan ✓
- Beam data adquired during patient treatment
  - Log files ✓
  - Fluence ✓
- Checking the dose distribution as delivered to the patient (patient changes). ✓

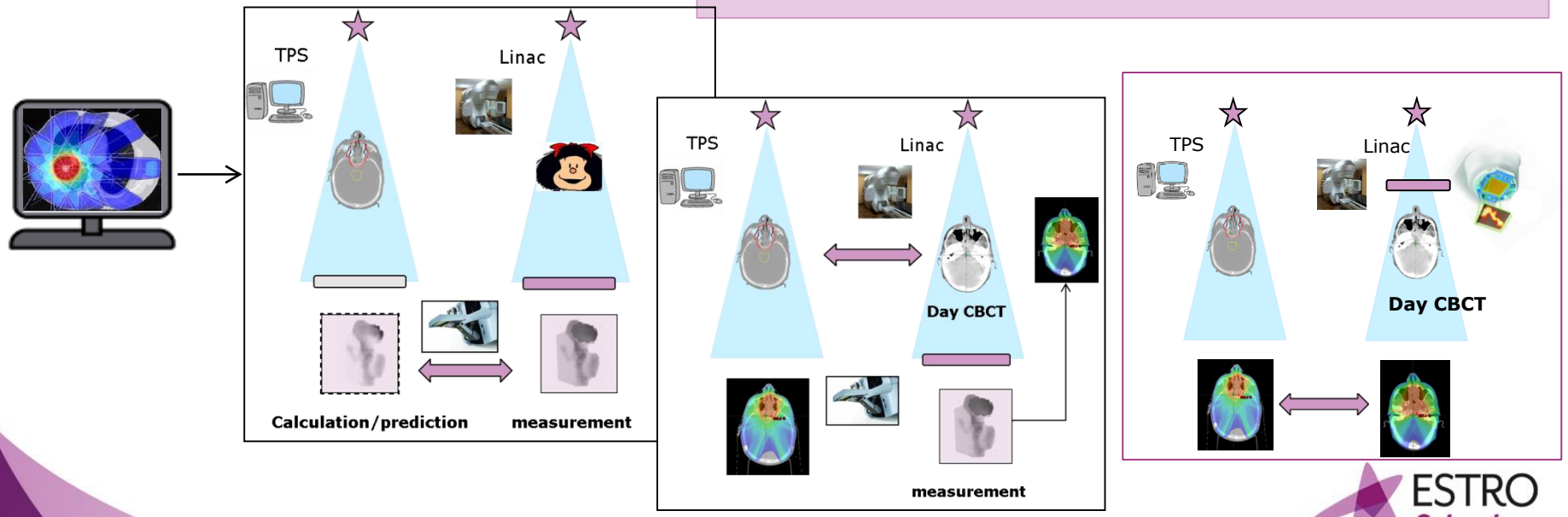

ESTRO School

Am I giving

the prescribed dose and

am I irradiating the planned volume?

ESTRO School

Definition of in vivo dosimetry

In vivo dosimetry is the measure of the dose delivered to the patient during the treatment.

Third layer:

-Dose delivered to the patient agrees with the planned dose

- Verification of data transfer for the actual patient plan ✓
- Beam data adquired during patient treatment
  - Log files ✓
  - Fluence ✓
- Checking the dose distribution as delivered to the patient (patient changes). ✓

FORWARD APPROACH

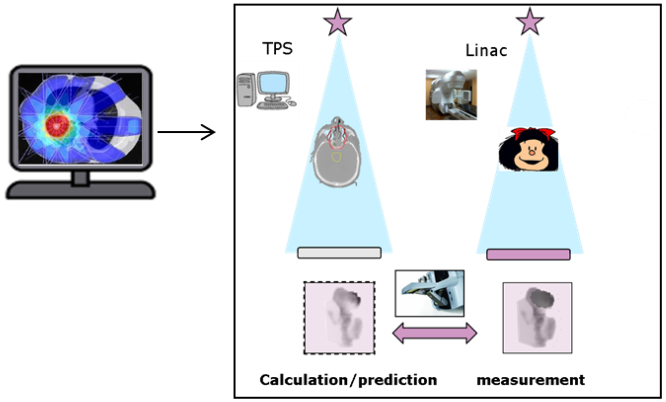

BACKWARD APPROACH (DOSE RECONSTRUCTION)

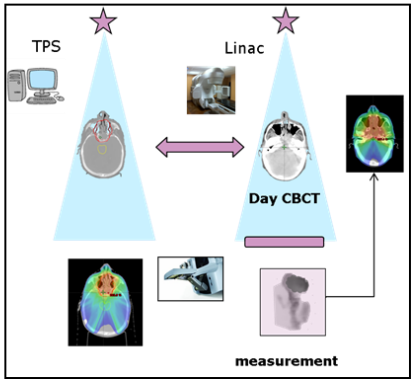

ESTRO School

Methods for in vivo dosimetry

In vivo dosimetry is the measure of the dose delivered to the patient during the treatment.

In vivo dosimetry can be done in two ways:

- A suitable detector can be inserted into the patient to measure the dose directly but **invasively**
- A detector can be placed against or at some distance from the patient to measure the dose **non-invasively**

  In this case the dose inside the patient is calculated with a suitable mathematical model, using the dose measured at the position of the detector.

EPID dosimetry, as well as the use of dosimeters positioned on the skin of a patient, belongs to the second category of in vivo dosimetry.

Point detectors for in vivo dosimetry

TLD	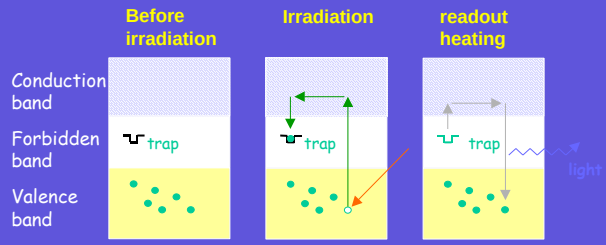 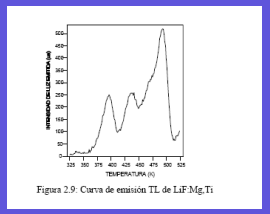 Figura 2.9: Curva de emisión TL de LiF:Mg,Ti	$\int G(T)dT \propto D$ **Sensitivity:** material;reader
Diode	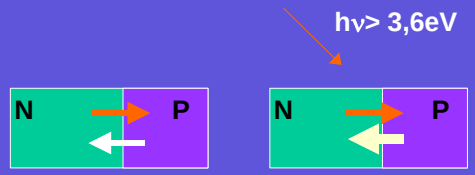 I_n (sat)= I_N (dif) I_{total} = 0 I_n (sat) + I_n (ion) >I_N (dif)	$I_T \propto D$ **Sensitivity:** doping; pre-irradiation dos
MOSFET	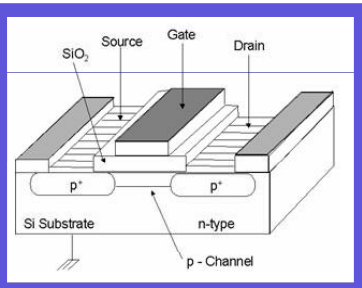 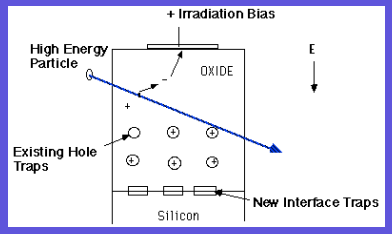	$\Delta V_{Threshold} \propto D$ **Sensitivity:** thickness SiO_2; bias during irradiation

ESTRO School

Point detectors for in vivo dosimetry

	pros	cons
TLD	No cables/No bias Tissue-equivalence (no E dependence) Permanent storage of dose (swallow traps) No T or Dose rate dependence Different shapes	No on-line measures Accurate read-out needs care Need of Post-processing Limited dose-response lineal.
Diode	No bias On-line measurements Long life High sensitivity	Non tissue-equiv. (E depend) Dose-rate dependence Sensitivity var. Accum. D Sensitivity variation witn T
MOSFET	No cables/No bias (depends on manufact.) “On-line” measurements No dose-rate dependence No T dependence (with some precautions)	Non tissue-equiv. (E depend) Limited life-time Low sensitivity

Can we use a detector characterization performed inside a phantom for entrance in vivo measurements?

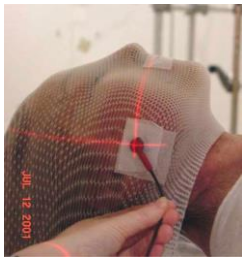

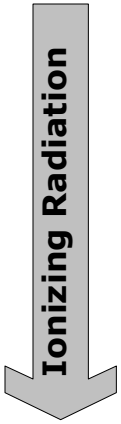

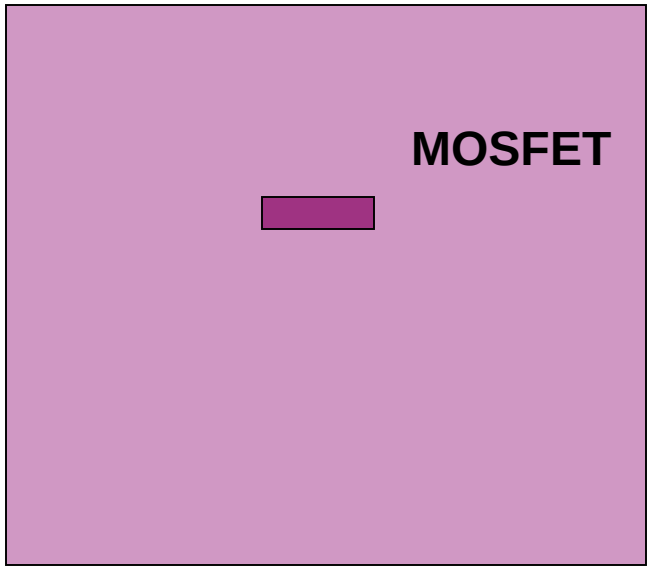

Energy dependence

	6 MV	18 MV	Co-60
$D/R\|_{z=5cm}$	0.337	0.348	0.318
SD	0.005	0.005	0.005

TN MOSFET
Panettieri et al. Phys. Med Biol

SSD dependence

Field size dependence

.....

ESTRO School

Can we use a detector characterization performed inside a phantom for entrance in vivo measurements?

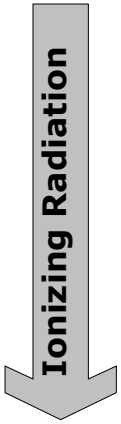

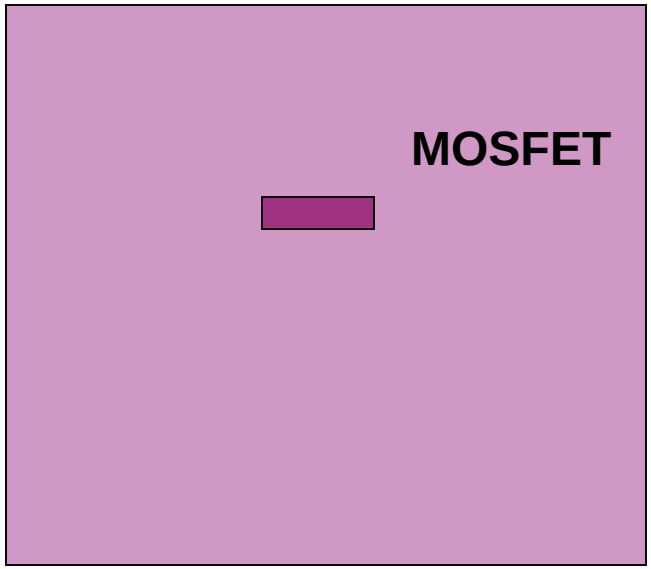

Energy dependence

	6 MV	18 MV	Co-60
$D/R|_{z=5cm}$	0.337	0.348	0.318
SD	0.005	0.005	0.005
CFenergy	1.000	**1.032**	0.944

TN MOSFET
Panettieri et al. Phys. Med Biol. 52

SSD dependence

Field size dependence

.....

Can we use a detector characterization performed inside a phantom for entrance in vivo measurements?

NO

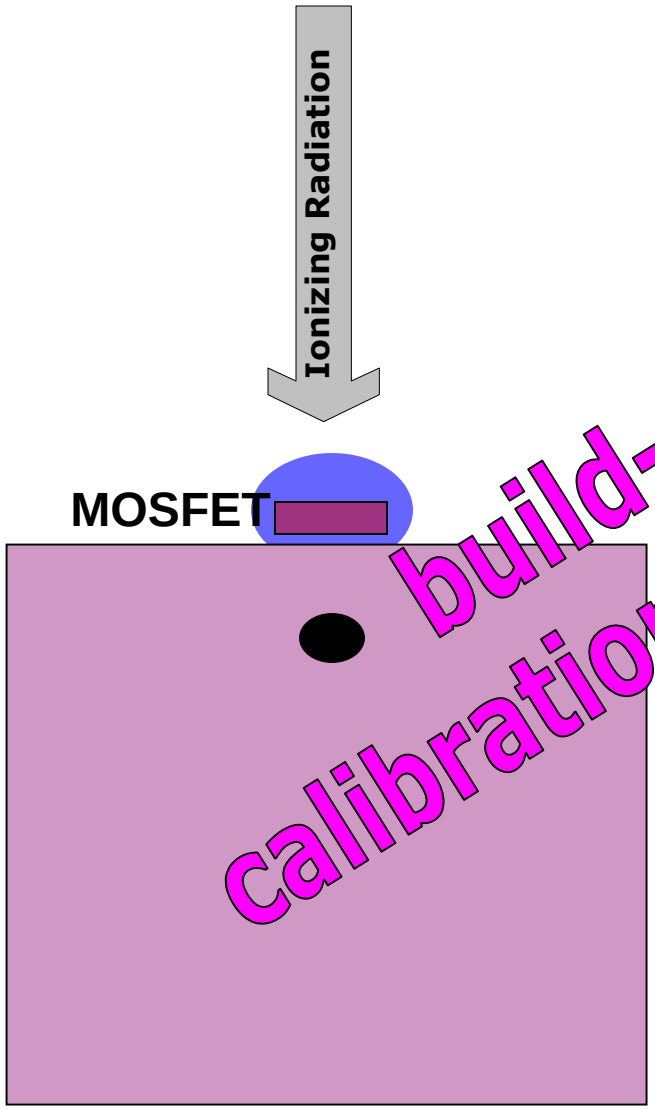

build-up cap calibration methodology

RE-EVALUATION

Energy dependence

	6 MV	18 MV
$D(z_{max})/R$	0.336	0.269
SD	0.002	0.004
CFenergy	1.000	**0.801**

TN MOSFET+brass cap

Panettieri et al. Phys. Med Biol. 52 (2007) 303-316

SSD dependence

Field size dependence

.....

ESTRO School

Calibration: Entrance dose
dose at the depth of dose maximum

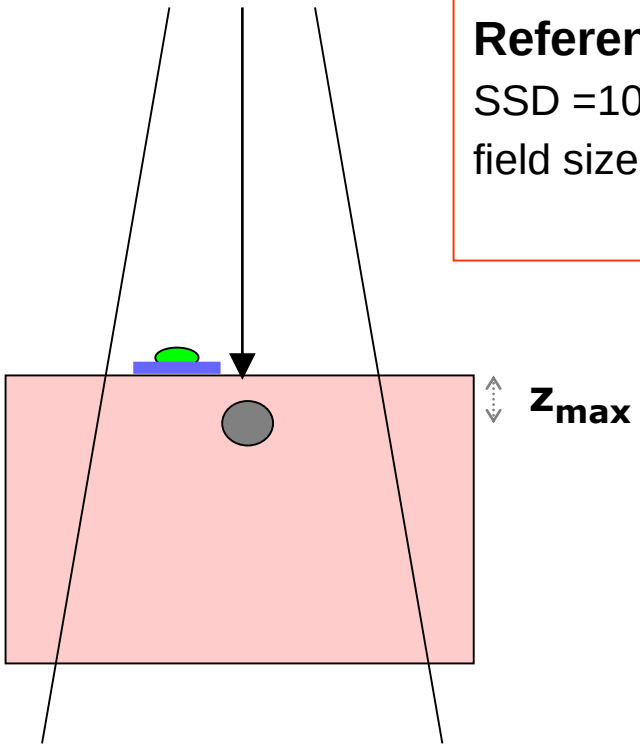

Reference conditions

SSD =100 cm

field size 10x10 cm^2

$$D_{ent} = R \times F_{cal}$$

$$F_{cal} = \frac{D_{ic}}{R_{in\,vivo}}$$

Calibration: Entrance dose
dose at the depth of dose maximum

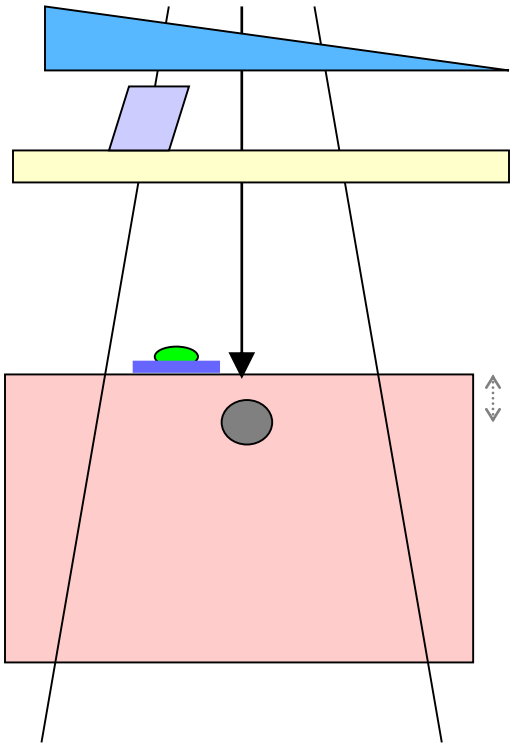

Ideal situation:

When changing the irradiation conditions the reading of the in vivo detector changes in the same proportion as changes the i.c. reading

$$D_{ent}(r, SSD, wedge, T) = R(r, SSD, wedge, T) \times F_{cal}$$

Reality:

Detector+ **build up** response dependence in dose rate, energy, temperature may differ of those of an i.c.

Due to the calibration geometry the detectors "see" different scatter conditions.

ESTRO School

Calibration: Entrance dose
dose at the depth of dose maximum

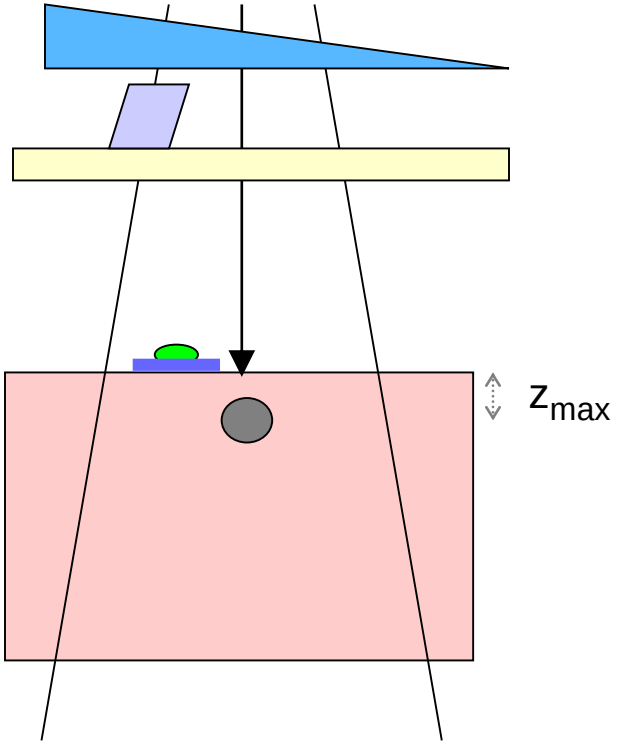

$$CF_{field} \times CF_{SSD} \times CF_{angle} \times CF_{wedge} \times CF_{i}$$

$$CF = \frac{\text{absorbed dose}_{IC}}{\text{absorbed dose}_{\text{in vivo detector}}}$$

ESTRO School

How large are those factors?

Do they vary a lot between different detectors?

Commercialised in vivo detectors-diodes

	EDP30	EDPHL-3G	P30	QED 1116	Isorad-p 1164	Isorad-3	PTW T60010H
Manufacturer	IBA	IBA	ONCOlog Medical	Sun Nuclear	Sun Nuclear	Sun Nuclear	PTW
Die - type	p	p	n	p	p	n	p
Die – dimensions-area (mm^2)	1.76	1.76	6.8	0.64	1.54	1.54	1
Die- thickness (µm)	60	60	100	-	-	-	2.5
Build up cap -shape	hemispherical	hemispherical	cylindrical	hemispherical	cylindrical	cylindrical	hemispherical
Build up cap - material	Tantalum	Tantalum	Tungsten	Brass	Tungsten	Tungsten	Tungsten
Build up cap- water equivalent thickness (mm)	14	14	30	30.4	26	26	30
Preirradiation dose- modality	8 kGy at 10 MeV	confidential	25 kGy	10 kGy at 10 MeV	10 kGy at 10 MeV	10 kGy at 10 MeV	0 Gy

ESTRO School

Commercialised in vivo detectors-diodes
Acceptance tests

	EDP30	EDPHL-3G	P30	QED 1116	Isorad-p 1164	Isorad-3	PTW T60010H
Stability after irradiation (5 min)	-0.58%	-0.40%	0.33%	-0.06%	- 0.20%	0.43%	0.00%
Intrinsic precission (sd) (10 irradiations)	0.16%	0.10%	0.05%	0.07%	0.10%	0.64%	0.09%
Lineality response/dose (r^2)	1.0000E00 (0.2 Gy-7 Gy)	1.0000E00 (0.2Gy-7 Gy)	1.0000E00 (0.2 Gy-3.5 Gy)	1.0000E0 (0.2 Gy- 7 Gy)	1.0000E00 (0.2 Gy-7 Gy)	1.0000E00 (0.2 Gy-7 Gy)	1.0000E00 (0.2 Gy-2.3 Gy)
Depth of the diode measurement point (water equivalent depth)	1.4 cm	1.4 cm	3.0 cm	2.2 cm	3.3 cm	3.3 cm	3.5 cm
SVWAD (per 100 Gy)	3.4%	1%	0.2%	0.8%	0.3%	0.3%	1.8%
Dose decrease at 5 cm depth	2.5%	2.5%	10.4%	5.6%	14%	14%	11%

ESTRO School

Commercialised MOSFET detectors

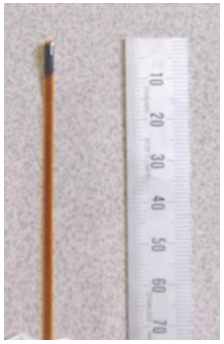

An Autosense patient dosimetry system model TN-RD-60 (Thomson&Nielsen):

dual MOSFETs model TN-502-RD

a 9-bias supply box

a reader

a windows based TABULA TM software

High sensitivity mode

+

Build up caps

OneDose system SICEL

single MOSFETs (Radfet)

no bias during irradiation

pre-calibrated

single use

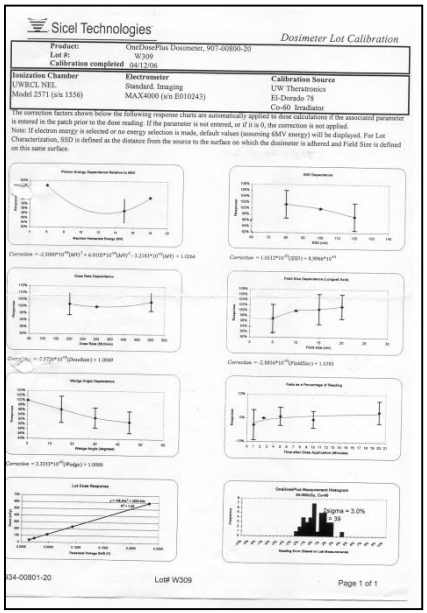

TL detectors

LiF (enriched 7Li (99.95%), DTL 937 powder doped with Na, Mg and Ti,philtech company)

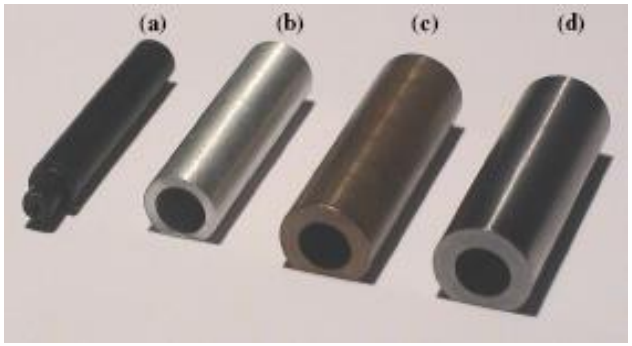

Build up caps

Ans Swinnen, PhD thesis 2005

Correction factors; Field size.
Diodes

RX 18 MV

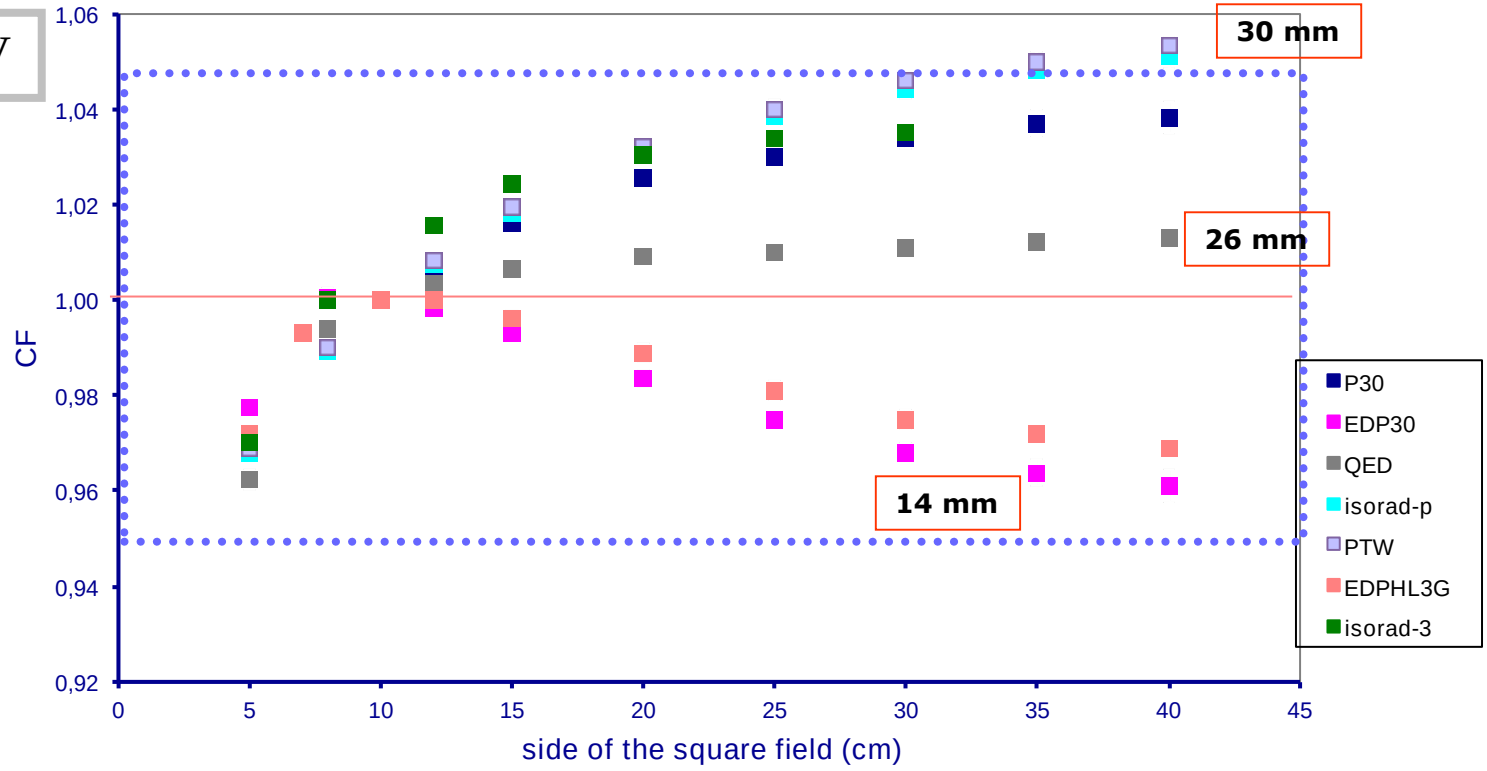

$$CF_{field\,size} = \frac{OF_{ic}(c, z_{max})}{OF_{diode}(c)} \qquad OF(c) = \frac{R(c)}{R(10x10)}$$

Jornet et alt, Med. Phys. 2000, Jornet et alt, Estro Booklet,2001

ESTRO School

Correction factors; Field size.
TLD MOSFET

RX 18 MV

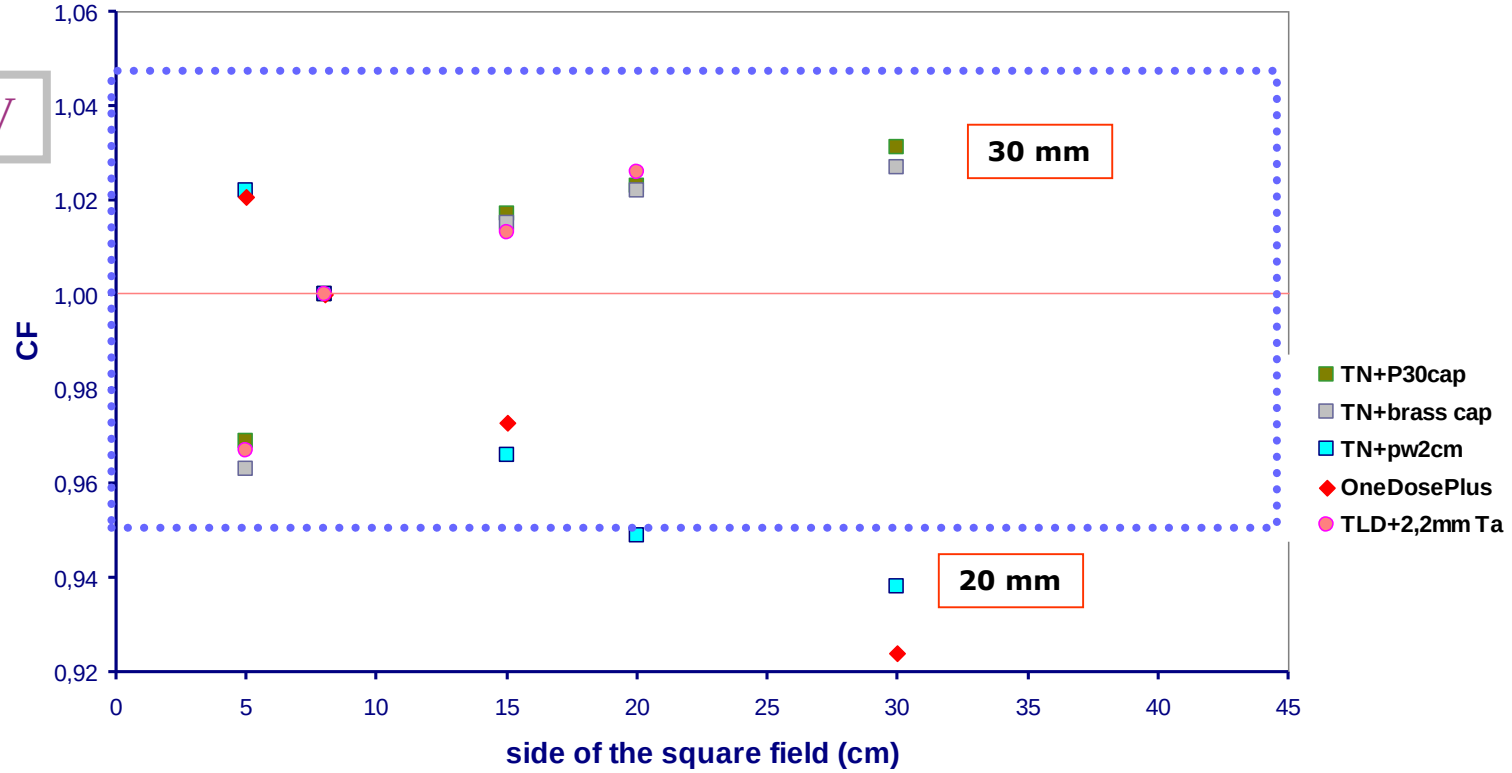

$$CF_{field\,size} = \frac{OF_{ic}(c, z_{max})}{OF_{diode}(c)}$$

$$OF(c) = \frac{R(c)}{R(10x10)}$$

Not using any build up cap…

RX 18 MV

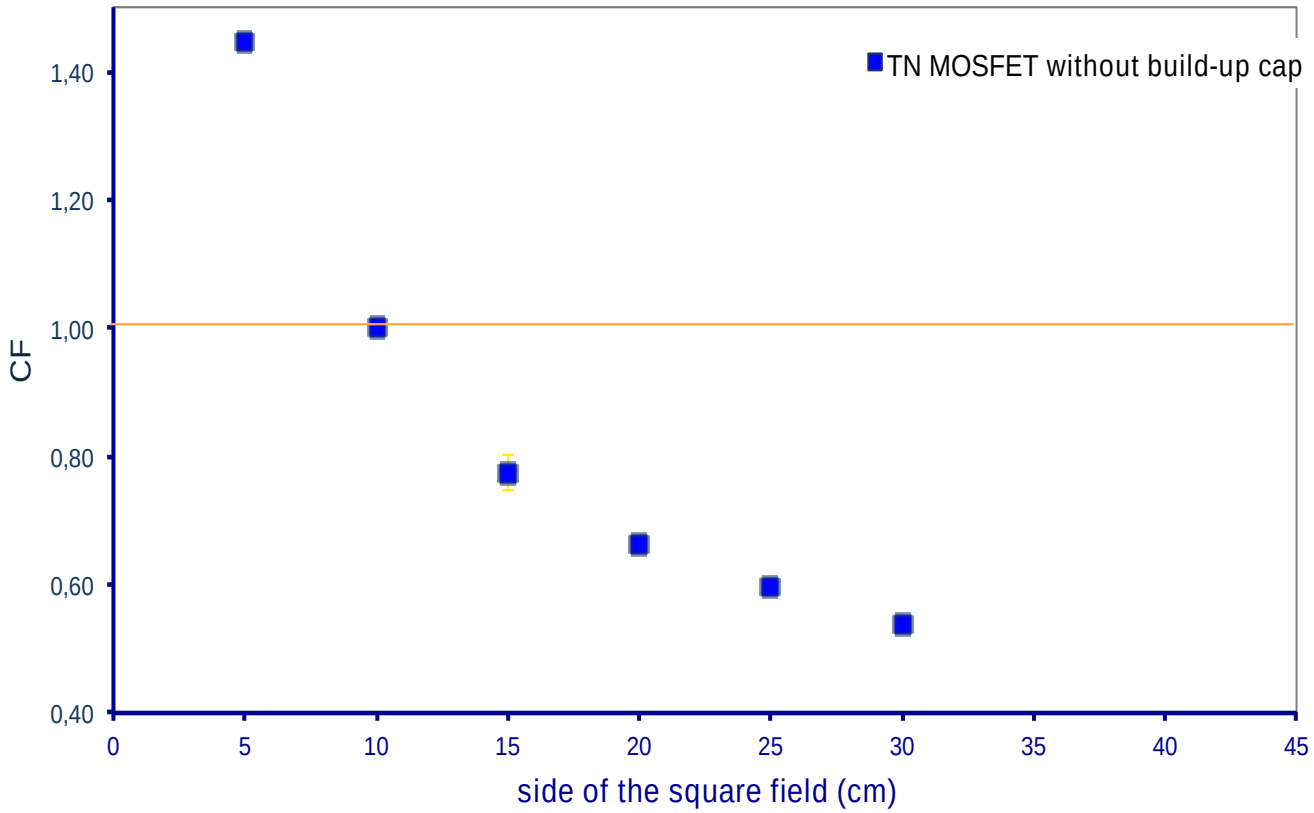

$$CF_{field\,size} = \frac{OF_{ic}(c, z_{max})}{OF_{diode}(c)}$$

$$OF(c) = \frac{R(c)}{R(10 \times 10)}$$

Uncertainties, Tolerance limits and action levels

ESTRO School

Tolerance limits and action levels

$$u'_{total} = \sqrt{u'^{2}_{measurement} + u'^{2}_{Fcal} + u'^{2}_{CF}}$$

"The overall accuracy of entrance in vivo measurements is determined by the combined uncertainty in the calibration factor, the correction factors and the accuracy and reproducibility in diode position"

In our case it is equal to **2% (1sd)**. So without any additional cause of error 68% of all measurements would have a dispersion of ±2% and 95% of ±4%."

Essers and Mijnheer, Int.J.Radiat.Oncol.Biol.Phys., 1999

ESTRO School

Uncertainty in entrance dose measurements

18 MV X-rays

Physical quantity of procedure	Relative standard uncertainty (%)		
	OneDosePlus	MOSFET (T&N)	diode
Step 1: Calibration under reference conditions			
Dose measured with the ionisation chamber	**2.0%**	**2.0%**	**2.0%**
Reading of the in vivo detector	**2.6%**	**0.7%**	**0.1%**
Reproducibility of the setting		**0.5%**	**0.3%**
Combined standard uncertainty of step 1	**3.3%**	**2.2%**	**2.0%**
Step 2: Correction factors			
Field correction factor	**3.0%**	**0.8%**	**0.1%**
SSD correction factor	**2.0%**	**0.8%**	**0.2%**
Combined standard uncertainty of step 2	**3.6%**	**1.1%**	**0.2%**
Step 3: measure on the patient			
Reading of the in vivo detector[1]	**3.3%**	**0.7%**	**0.1%**
Combined standard uncertainty of step 3	**3.3%**	**0.7%**	**0.1%**
Combined standard uncertainty of steps 1+2+3	**5.9%**	**2.6%**	**2.0%**

[1] reproducibility on positioning on patients was not tested.

ESTRO School

Uncertainty in entrance dose measurements

18 MV X-rays

Physical quantity of procedure	Relative standard uncertainty (%)
	TLD Ans Swinen PhD thesis 2005
TLD calibration with IC	**1.7%**
TLD reading of "unknown detector"	**1.0%**
Non-lineality	**0.5%**
Fading	**<0.5%**
Combined standard uncertainty of step 1	**2.1%**
Step 2: Correction factors	
Field correction factor	**1.5%**
SSD correction factor	**1.5%**
Combined standard uncertainty of step 2	**2.1%**
Step 3: measure on the patient	
Reading of the in vivo detector[1]	**1.2%**
Combined standard uncertainty of step 3	**1.2%**
Combined standard uncertainty of steps 1+2+3	**3.2%**

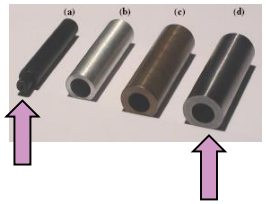

[1] reproducibility on positioning on patients was not tested.

ESTRO School

What to compare?

ENTRANCE DOSE MEASUREMENT

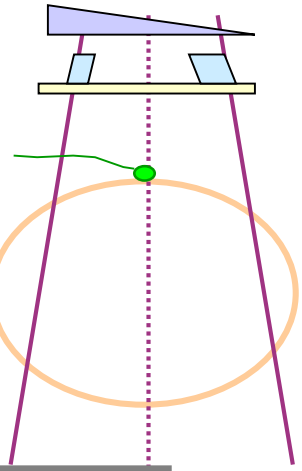

Reading

calibration

$$D_{entrance} = R \times F_{cal} \times \Pi\, CF$$

ENTRANCE DOSE CALCULATION

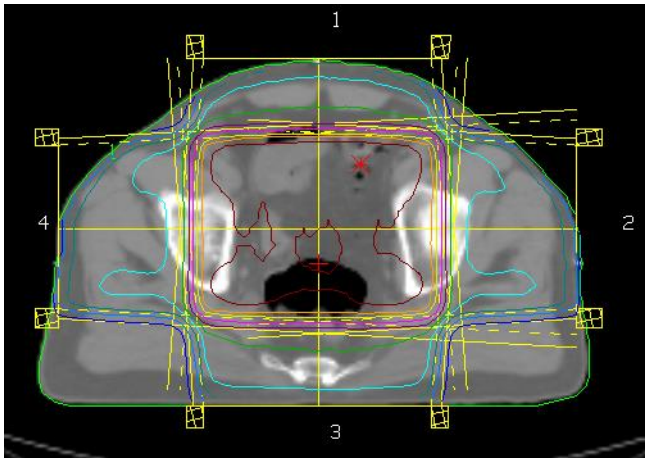

Calculate expected entrance dose from the ICRU point prescription dose

Should we use the TPS or an independent calculation??

ESTRO School

What to compare?

ICRU point dose ⟺ **PRESCRIBED DOSE to ICRU point**

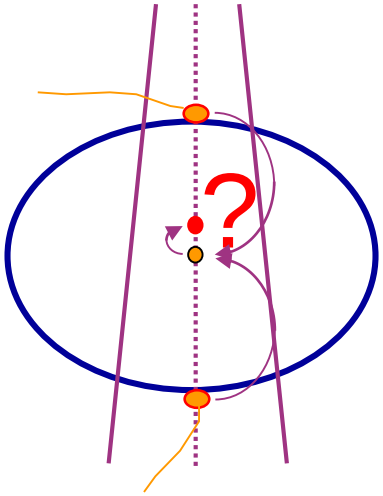

R_{ent} R_{ex}

↓ calibration

D_{ent} D_{ex}

↓ algorithm

$D_{1/2}$ ⇨ D_{ICRU}

ESTRO School

Dosimetric errors (examples)

In vivo dosimetry

D_{ex} = 0.336 Gy

Heterogeneity correction

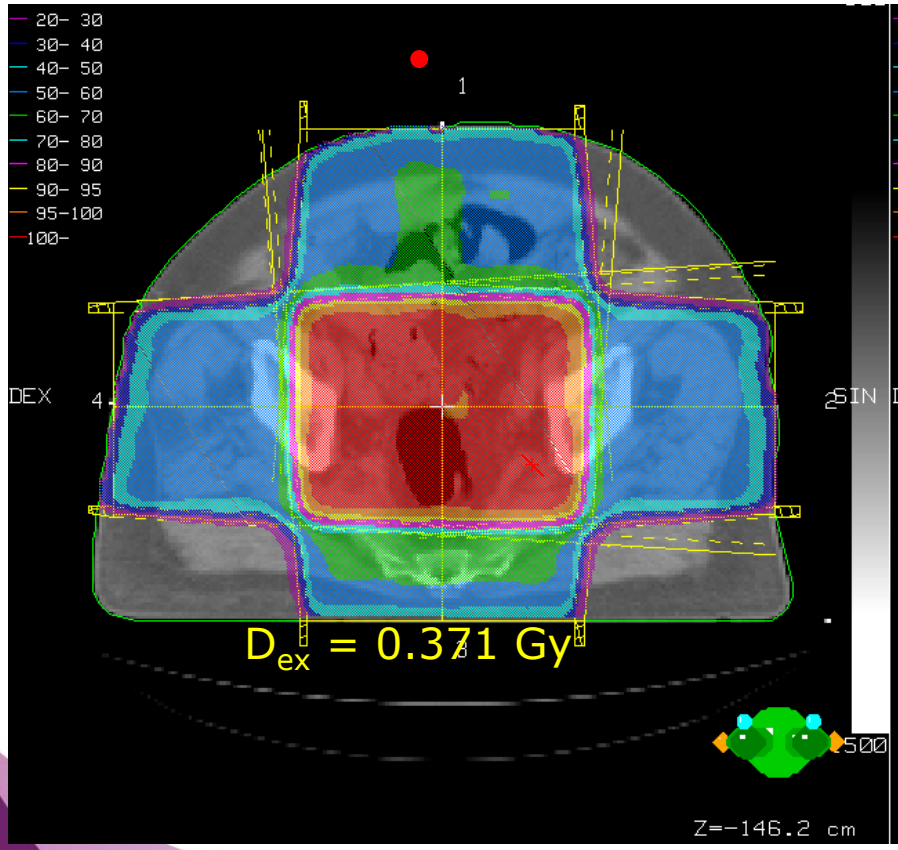

Without heterogeneity correction

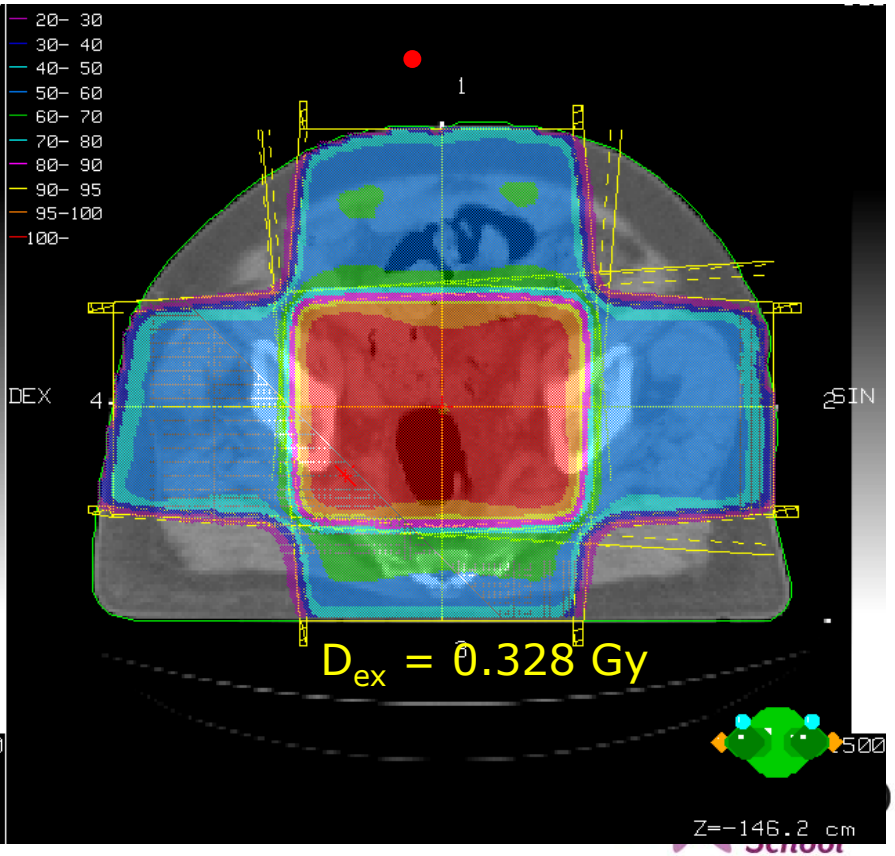

Dosimetric errors (examples)

In vivo dosimetry

D_{ex} = 0.336 Gy

Heterogeneity correction

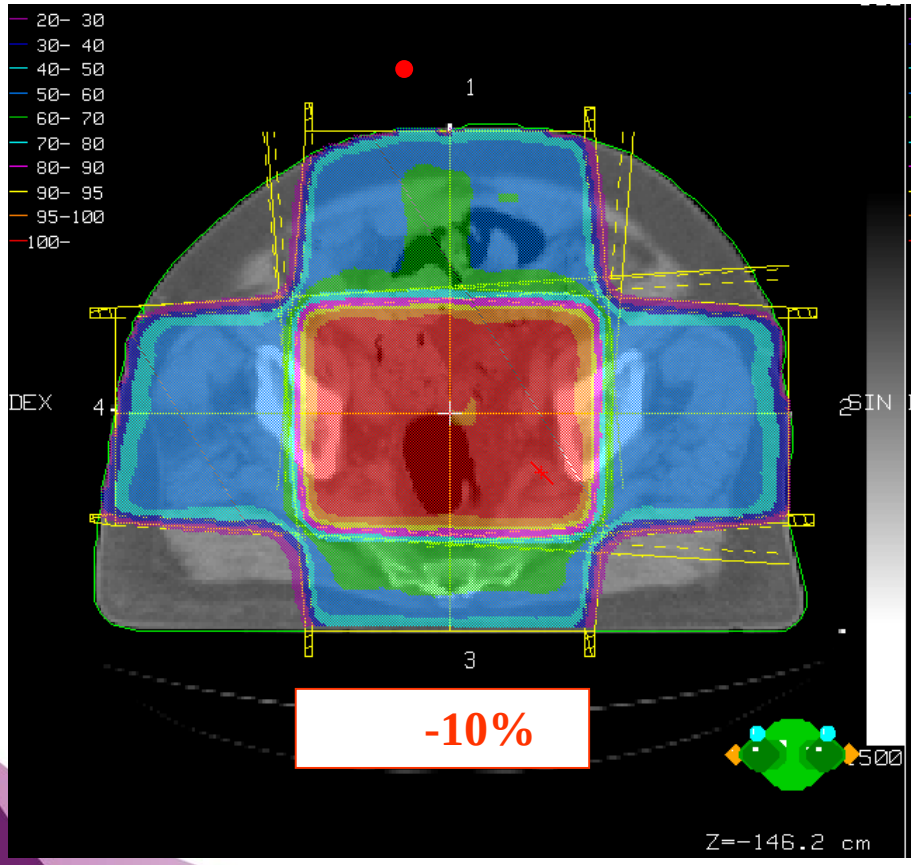

Without heterogeneity correction

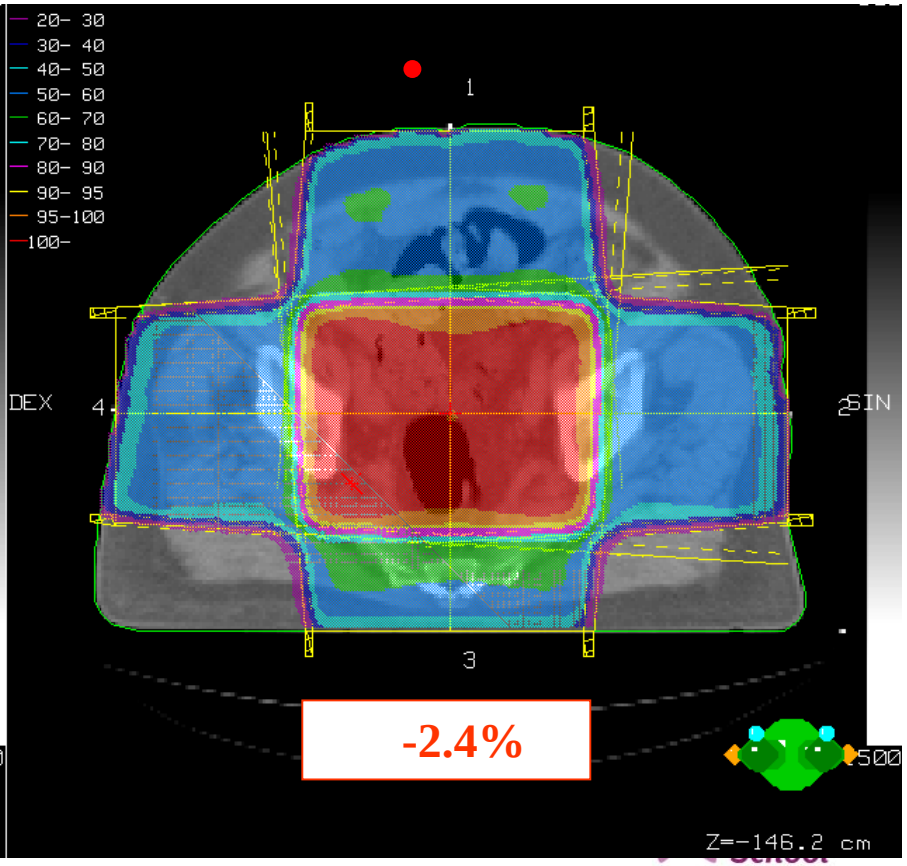

Point in vivo dosimetry and IMRT

Inhomogeneous fluence distributions ➡ Positioning the detector is critical

Field size, energy spectra and dose rate variation ➡ Correction factors ??

A practical approach to diode based *in vivo* dosimetry for intensity modulated radiotherapy

Nils Kadesjö*, Tufve Nyholm, Jörgen Olofsson

Department of Radiation Sciences, Umeå University, Sweden

- Intelligent calibration of diodes
- The use of EqualDose software to select the point to place the diode and to calculate expected dose

Point in vivo dosimetry and IMRT

Calibration

Effective depth: The diodes will be calibrated to give the dose at a depth for which the CF_{field} is minimized

$$O(d) = \sum_{n=1}^{N_f} \left(\frac{D_C(d; f_n) R_M(f_{norm})}{R_M(f_n) D_C(d; f_{norm})} - 1 \right)^2$$

Positioning

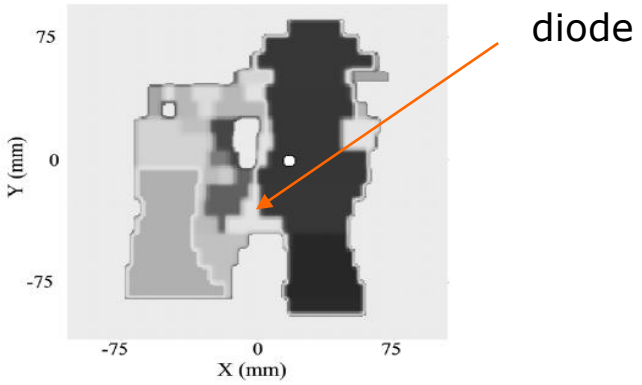

Calibration factor:

$$k = \frac{1}{N_f} \sum_{n=1}^{N_f} \frac{R_M(f_n)}{D_C(d_E; f_n) \cdot MU_n}$$

Where R_M is the detector reading and Dc is the calculated dose per MU.

Expected reading:

$$R_C = k \cdot MU \cdot D_C(\boldsymbol{x}, SSD, d_E; A)$$

For a calculation point x in a treatment head setting A.

ESTRO School

Point in vivo dosimetry and IMRT

Results

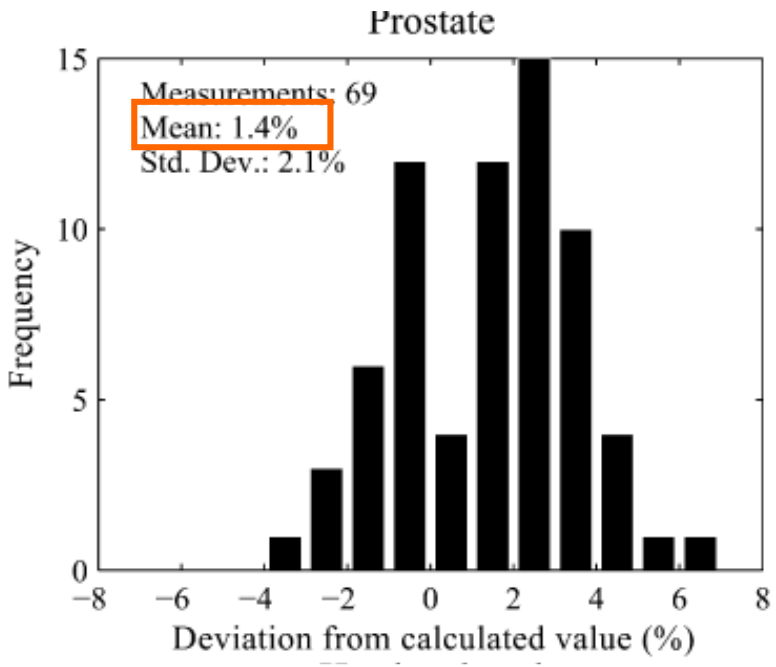

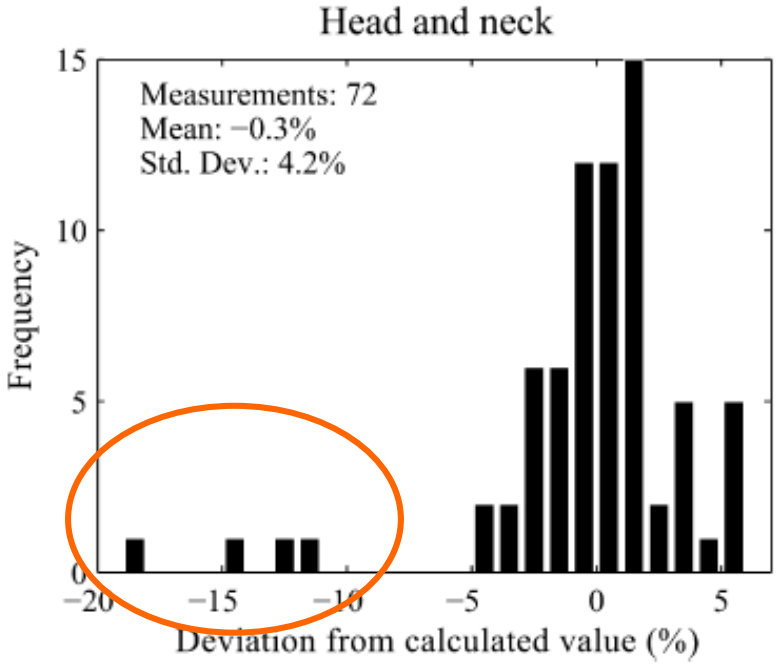

Temperature 0.2%/ºC

Action level at 5%. Final safeward to avoid severe errors. Complementary to pretreatment verification and checks the data transferred to the treatment unit

ESTRO School

Invasive techniques
Implantable MOSFET Detector

THE UNIVERSITY OF TEXAS
MD ANDERSON
CANCER CENTER
Making Cancer History®

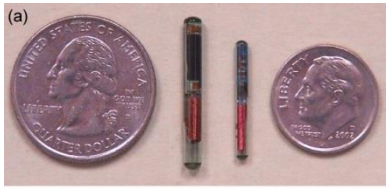

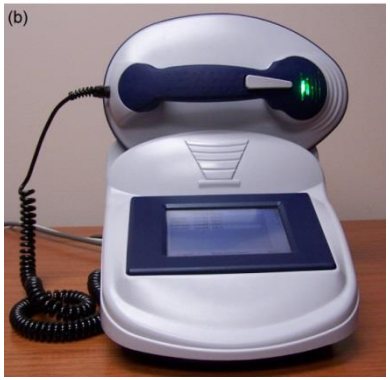

- The DVS detector is **permanently implantable** and is read with an external hand-held RF reader. It is **factory calibrated** and designed for daily use over an entire treatment course.

- **New detector**: 2.1 mm diameter and 20 mm length
  doble-MOSFET
  internal temperature sensor

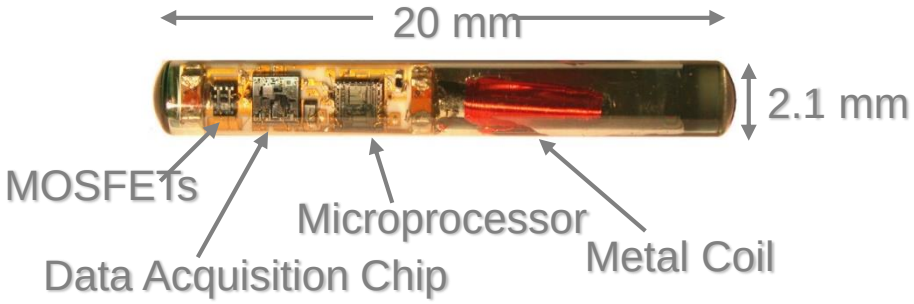

ESTRO School

Implantable MOSFET Detector (DVS)

- Electronics assembly contains 2 MOSFETs and support circuitry
- Bi-directional antenna coil provides dosimeter power and communications channel
- Hermetically sealed in bio-compatible glass capsule
- Filled with medical grade epoxy

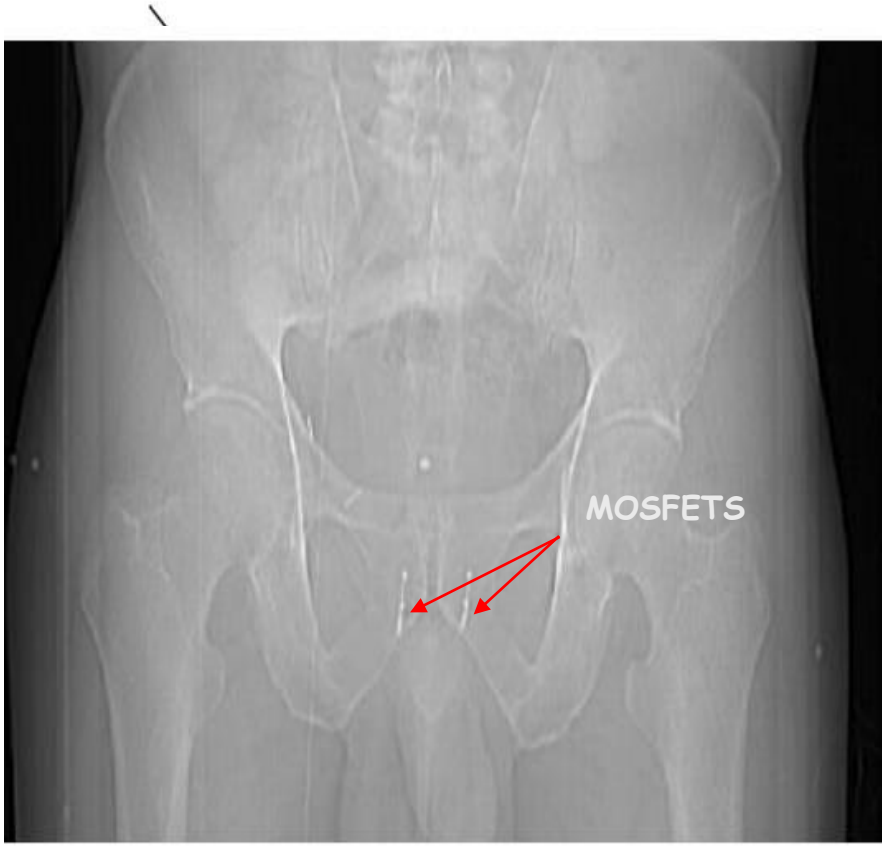

Joanna Cygler, MOSFET dosimetry, AAPM Summer School, 2009

Calibration Process for DVS

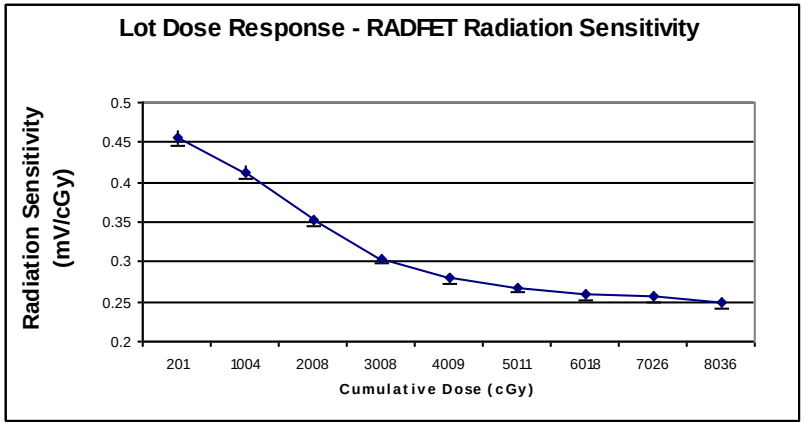

Dose response curve

- A cumulative dose response calibration curve is obtained for a specific lot by irradiating a statistically significant representative sample from the lot up to **80Gy** (*maximum dose range of the dosimeter*).

Verified by UW-ADCL (sample lot sent for testing)

- Calibration is valid for use with daily doses of 150-250 cGy
- Reported accuracy for each lot has a calibration certificate with values within:
  - <5.5% (2σ) up to 20 Gy
  - <6.5% (2σ) up to 74 Gy (accuracy decreases for doses > 74 Gy).

INITIAL CLINICAL RESULTS OF AN *IN VIVO* DOSIMETER DURING EXTERNAL BEAM RADIATION THERAPY

CHARLES W. SCARANTINO, M.D., PH.D.,*† CHRISTOPHER J. RINI, M.S.,* MIGDALIA AQUINO, B.S.,* TAMMY B. CARREA, B.S.,* ROBERT D. ORNITZ, M.D.,† MITCHELL S. ANSCHER, M.D.,‡ AND ROBERT D. BLACK, PH.D.*

*Sicel Technologies Inc., Morrisville, NC; †Radiation Oncology, Rex Cancer Center, Raleigh, NC; ‡Radiation Oncology, Duke University Medical Center, Durham, NC

- Standard irradiation techniques (CRT)
- Dose calculation TPS: heterogeneity correction off
- Old type of detectors: [dim 3mmx25mm] single MOSFET
- Detectors precalibrated at the factory: accuracy <3.5 (1SD)
- Daily doses [1.5-3 Gy]

Migration:

Patient ID	Tumor site	Movement of sensor	Sensor AEs
01-01	Lung	None	None
01-02	Rectum	None	None
01-03	Thigh	None	None
01-04	Lung	None	None
01-05	Lung	2.2 cm movement of one device*	None
01-06	Rectum	None	None
01-07	Rectum	None	None
02-01	Prostate	None	None
02-02	Prostate	None	None
02-03	Prostate	None	None

* Device was placed in unconsolidated tissue.

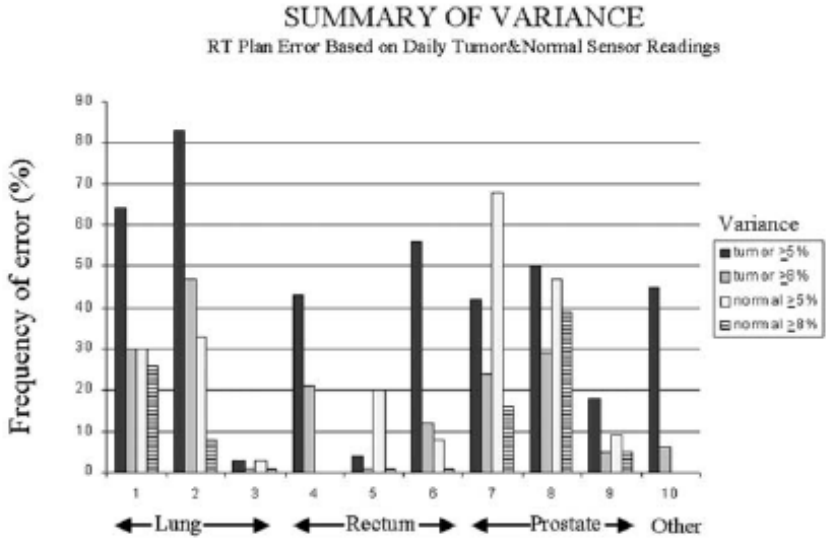

Fig. 6. The frequency of dose variations at the ≥5% and ≥8% levels. Deviations beyond 5% are generally considered to be unacceptable for planning purposes. The 8% mark represents the level at which changes in outcome are noted to occur.

From 1D to 2D and 3D *in vivo* dosimetry

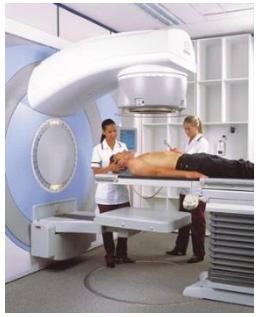

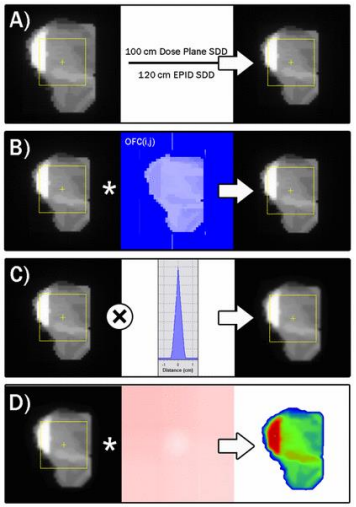

Nelms et al. JAMP vol 11(2) 2010

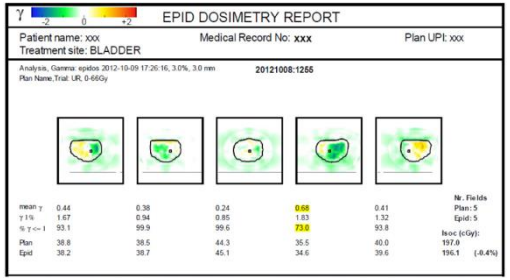

Olaciregui-Ruiz et al. Phys.M ed.Biol.58 (2013)

2D detectors [EPID]

1 – Forward from transit images

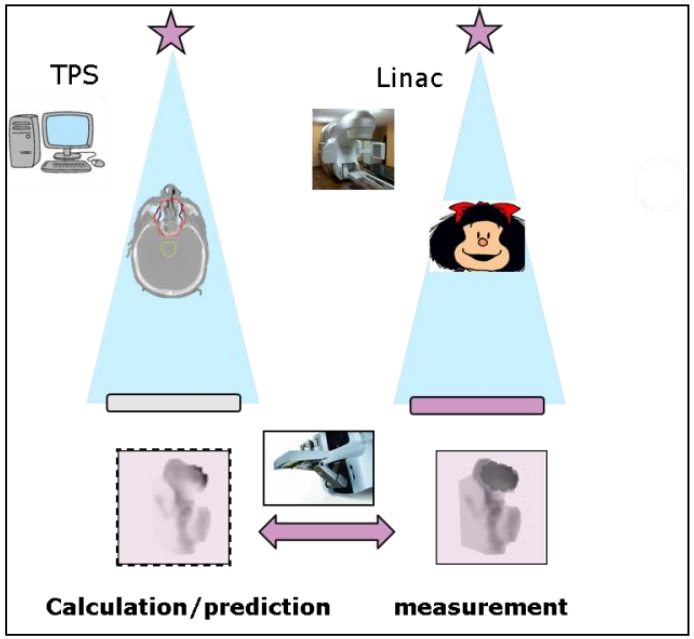

- Measure transit EPID dose (D_{EPID_meas})
- Extend patient CT data to EPID level and calculate TPS EPID dose (D_{EPID_calc})
- Compare measured with calculated EPID dose

$$D_{EPID\_meas} = D_{EPID\_calc} ?$$

McNutt	Med Phys (23) 1996
Pasma	IJROBP (45) 1999
Van Esch	Radiother Oncol (60) 2001

ESTRO School

2D detectors [EPID]

2 - Predict primary fluence from open images

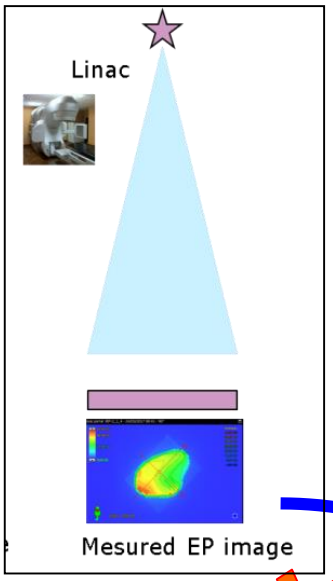

- Measure 'open' EPID image (i.e. without attenuating medium)
- Convert to dose at EPID level
- Deconvolve EPID dose with lateral scatter kernel to estimate primary fluence
- Use primary fluence as input to calculate dose distribution in patient/phantom

This is not in vivo dosimetry

dose calculation algorithm

Steciw	*Med Phys (32) 2005*
Renner	*J Appl Clin Med Phys (6) 2005*
van Elmpt	*Med Phys (33) 2006*

ESTRO School

2D detectors [EPID]

3. Predict primary fluence from transit images

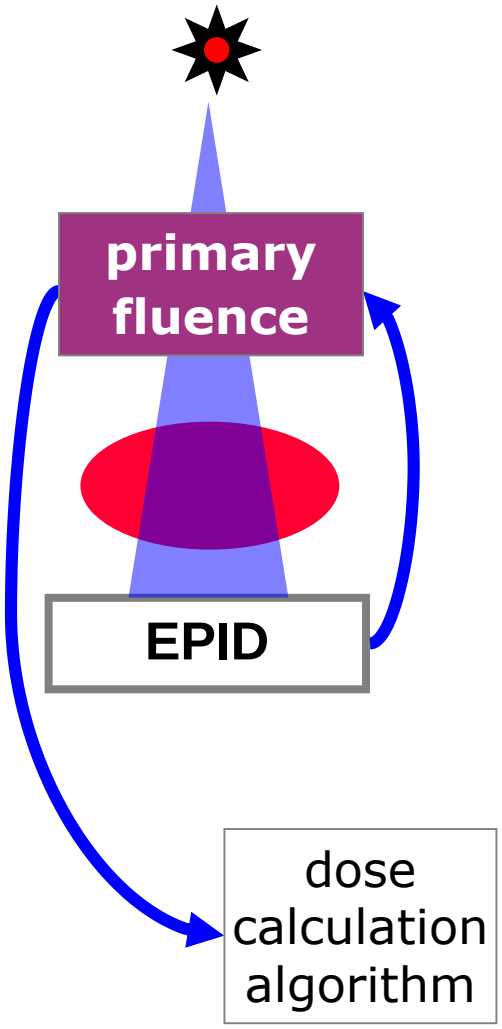

- Measure transit EPID dose
- Convert to dose at EPID level
- Deconvolve EPID dose with lateral scatter kernel and back-project through patient/phantom to estimate primary fluence
- Use primary fluence as input to calculate dose distribution in patient/phantom

Hansen	Med Phys (23) 1996
Kapatoes	Med Phys (28) 2001
Partridge	Med Phys (29) 2002

2D detectors [EPID]

4. Back-project to dose grid from transit images

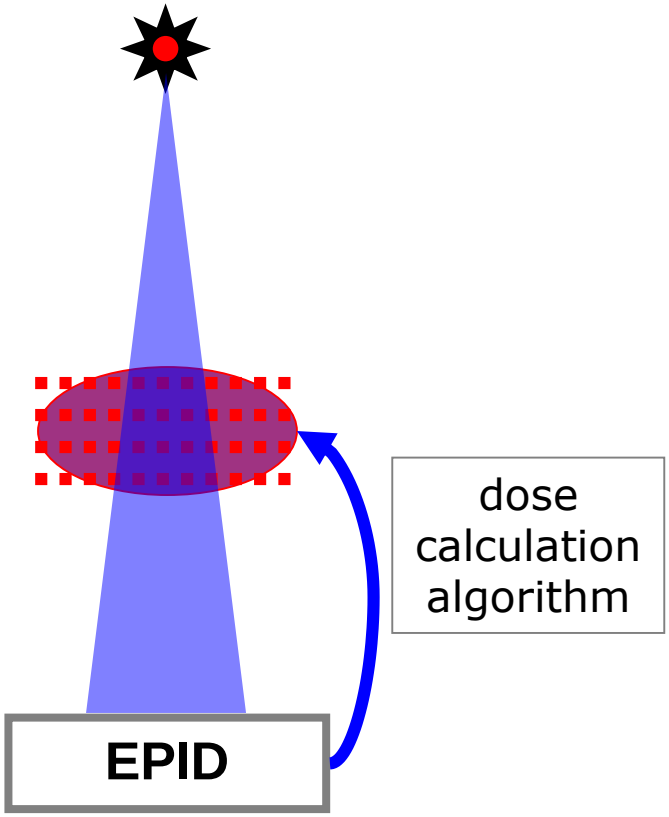

- Measure open and transit EPID dose image
- Estimate and subtract EPID and patient/phantom scatter
- Back-project primary dose to multiple planes to form dose grid using CT data
- Total dose = primary (based on transmission)+ patient scatter

Louwe	Med Phys (30), 2003
Wendling	Med. Phys. (33), 2006
	Med. Phys.(36), 2009
Olaciregui-Ruiz	Phys. Med.Biol. (58), 2013
Ian M Hanson	Phys. Med.Biol. (59), 2014

ESTRO School

How does the algorithm work?

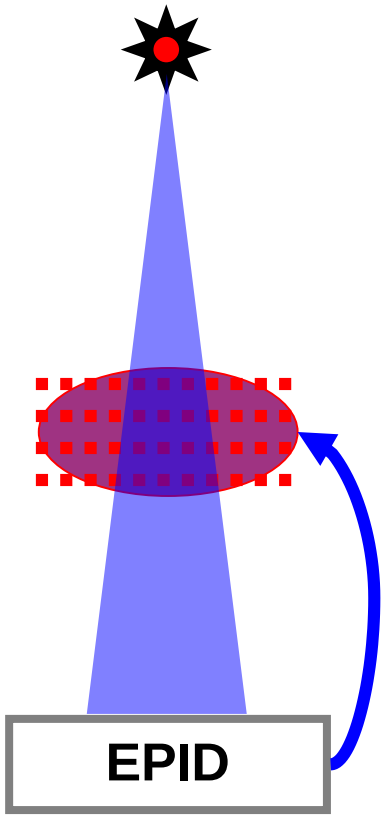

dose calculation algorithm

4. The attenuation of the beam by the phantom or patient.
5. The distance from the radiation source to the EPID plane and to the dose-reconstruction plane.
6. The scatter within the phantom or patient

Dose to any point inside the patient

1. EPID Dose Response
2. Lateral Scatter within the EPID
3. Scatter from the patient

Primary dose map at EPID plane

ESTRO School

2D detectors [EPID]

Calibration for *absolute* dosimetry

EPID measurement **Ion chamber measurement**

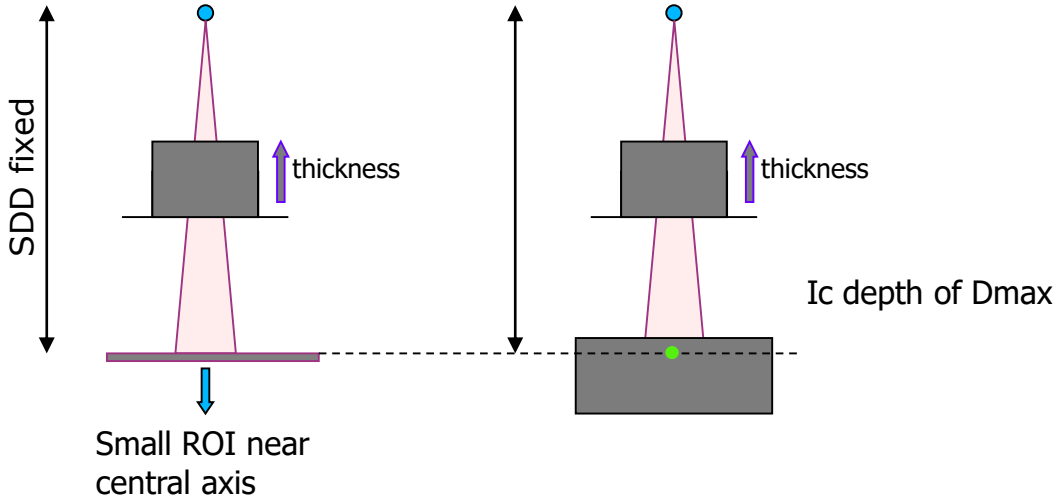

1. **Dose Response of the EPID**
2. Lateral Scatter within the EPID
3. Scatter from the patient

Apply a sensitivity matrix correction (get back the image before the flood field correction)

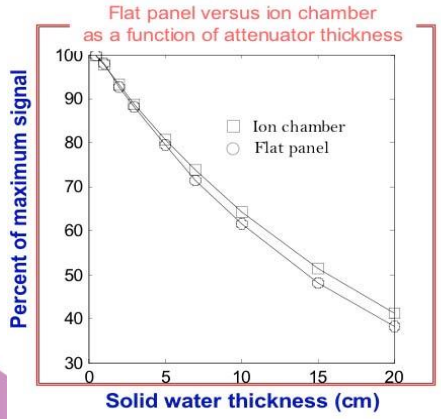

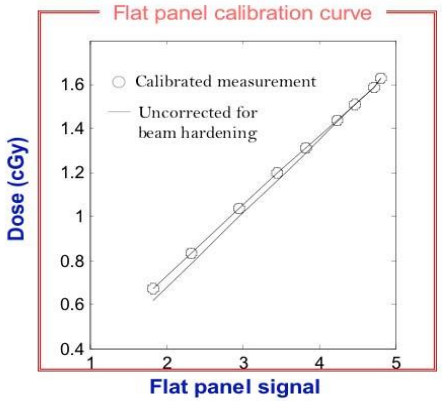

Chen et al. Med. Phys 33(3), 2006

http://radonc.ucsf.edu/research_group/jpouliot/tutorial/main.htm

ESTRO School

2D detectors [EPID]

Detector scatter kernel

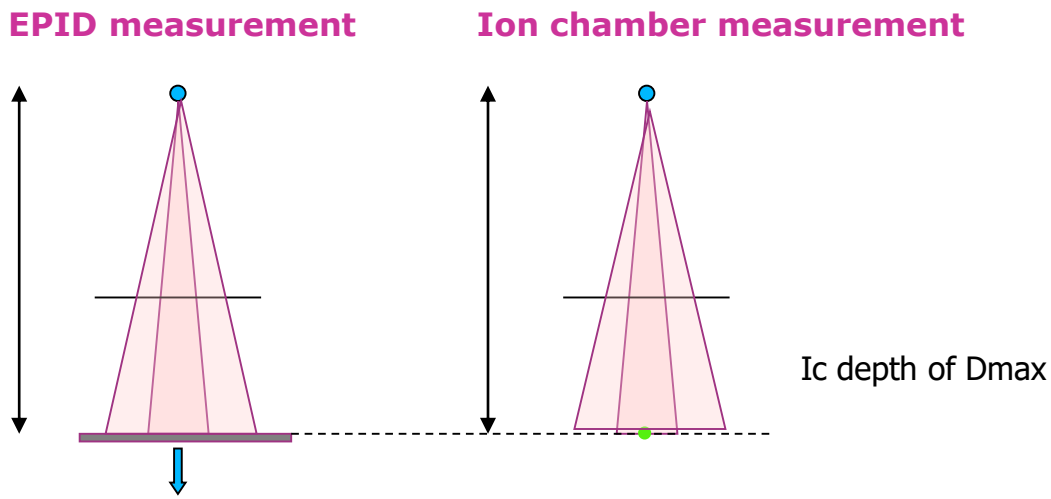

1. Dose Response of the EPID
2. **Lateral Scatter within the EPID**
3. Scatter from the patient

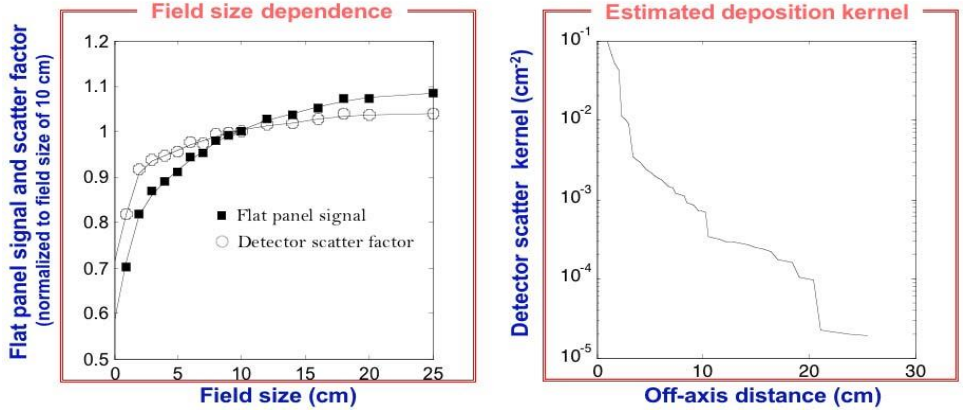

2D: need a **second Kernel** to model penumbra.
Compare profiles in the EPID with those measured in a water phantom.

http://radonc.ucsf.edu/research_group/jpouliot/tutorial/main.htm

ESTRO School

2D detectors [EPID]

Scatter from the patient

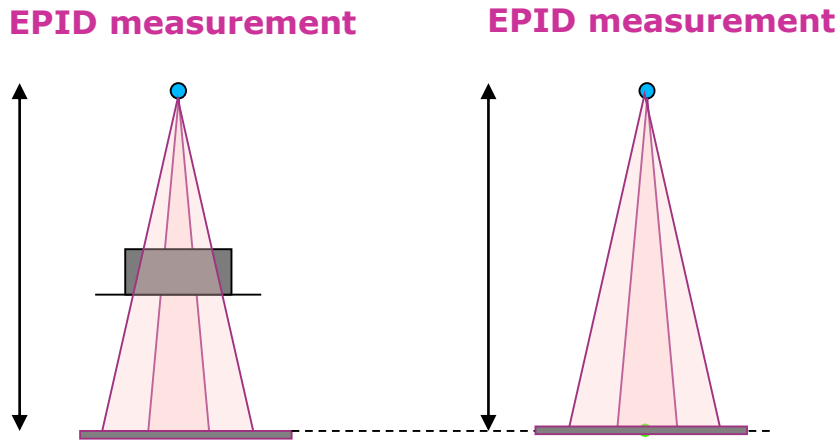

1. Dose Response of the EPID
2. Lateral Scatter within the EPID
3. **Scatter from the patient**

Use the fact that when field size goes 0 the scatter becomes negligible

ESTRO School

Dose reconstruction in the patient: How does the algorithm work?

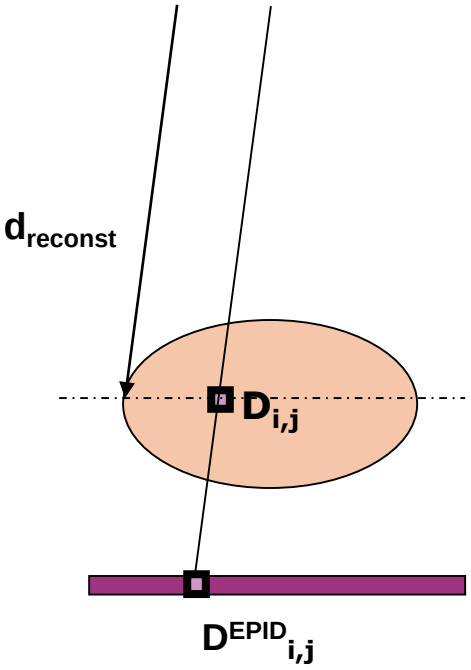

$$Pr_{ij}(d_{reconst}) = Pr_{ij}^{EPID} \cdot \left(\frac{d_{reconst}}{d_{EPID}} \right)^{-2} \cdot AC_{ij}(d_{reconst})$$

Attenuation

Uses external contours (d) to distribute the attenuation Within the patient, gives the reconstruction-plane dependent Attenuation correction

$$AC_{ij}(d_{reconst}) = \frac{T^{primary}(d_{ij}^{radiol})}{T_{ij}^{primary}}$$

Experimental value:
Ratio between EPID doses with and without the patient

$$D_{i,j}(d_{reconst}) = Pr_{ij}(d_{reconst}) + Sc_{ij}(d_{reconst})$$

Primary Dose | Scatter Dose

ESTRO School

Dose reconstruction in the patient: How does the algorithm work?

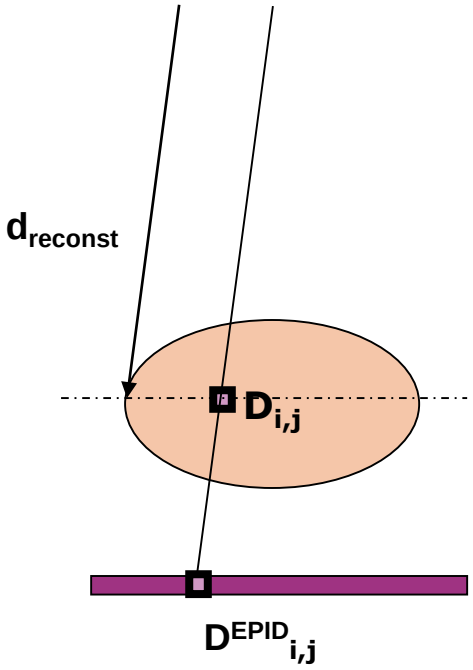

$$D_{i,j}(d_{reconst}) = Pr_{ij}(d_{reconst}) + Sc_{ij}(d_{reconst})$$

Primary Dose | Scatter Dose

Scatter Kernel (accounts for field size dependence)

$$Sc_{ij}(d_{reconst}) = \left\{ \Pr_{ij}(d_{reconst}) \cdot SPR^{ref}\left[T_{ij}^{primary} \right] \right\} \otimes K_{ij}^{mid}$$

Scatter to primary ratio: Depends on the depth

Need to know the Primary Dose to the EPID

EPID calibration + modelling

8-11 h measurements
2h modelling

Per linac, per beam

ESTRO School

3D in vivo dose reconstruction

5-field IMRT prostate cancer treatment

18 MV beam
TPS: Pinnacle
3D gamma (3% of dose at isoc./3 mm DTA)

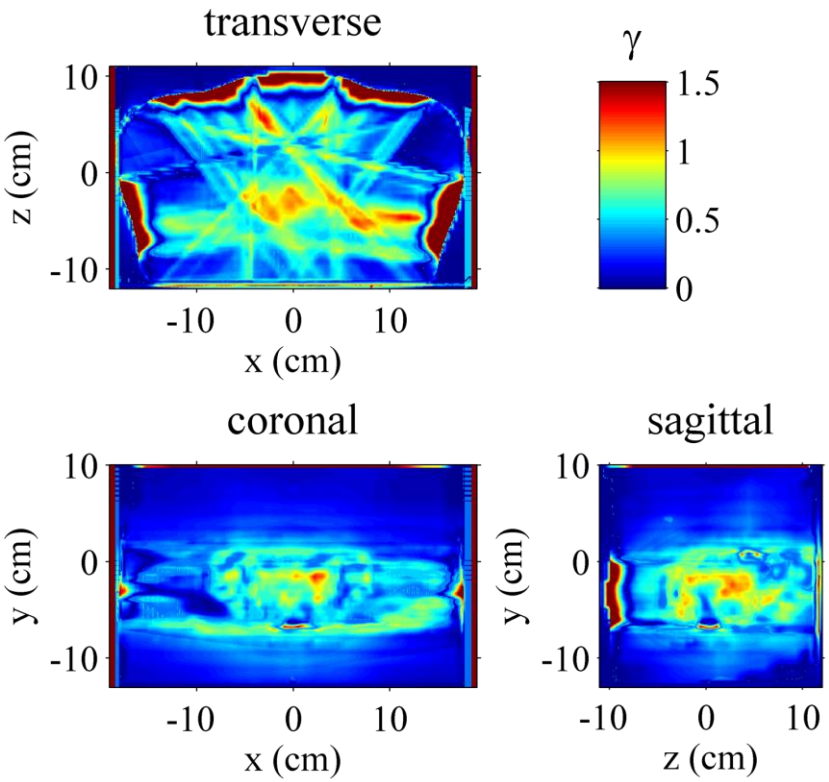

Within 20% isodose line of plan (including build-up regions):

- mean g-value = 0.58; SD = 0.41
- percentage of points with a g-value ≤ 1 = 95%

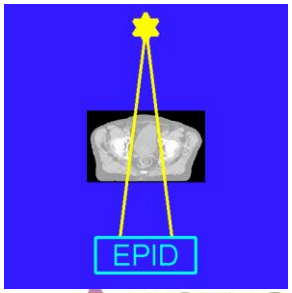

ESTRO School

EPID in vivo dosimetry-commercial solutions

Product Name	How they work
Dosimetry Check (Math Resolutions)	From EP images they calculate the fluence at a plane before the patient. This fluence is used instead that calculated by a beam model to calculate the dose to patient (dose engine)
EpiGrayTM (DosiSoft) (IBA)	The EP image is converted to EP dose (deconvolution by scatter from the portal and patient), This "primary dose" is backprojected into the patient (attenuation) and convolved with a scatter kernel.
iViewDose (Elekta)	The EP image is converted to EP dose (deconvolution by scatter from the portal and patient), This "primary dose" is backprojected into the patient (attenuation) and convolved with a scatter kernel.
PerFraction (Sun Nuclear)	Beam model +syntetic MLC logfiles (from EP images) DOES not use the transmission information ONLY WORKS FOR DYNAMIC FIELDS

ESTRO School

Should I spend

any time

in implementing in vivo

dosimetry?

ESTRO School

Errors in radiation oncology: A study in pathways and dosimetric impact

Eric Klein, Robert E. Drzymala, James A. Purdy and Jeff Michalski

Journal of applied Med. Phys. 2005

Error type:	Typical # of fraction in which it was detected	Method of detection	# of events	#of record and verify
Incorrect treatment coordinate(s)	first	Port film	19	7
Wrong gantry angle	first	Port film	15	8
Wrong or omitted cerrobend block	first	Port film	15	N/A
Incorrect calculation	2 to 5 fractions	In vivo dosimetry; physicist chart review	11	N/A
Wrong field size	first	Port film.	9	8
Incorrect collimator angle	first	Port film	8	3
Missing compensation filter	2 to 5 fractions	In vivo dosimetry; physicist chart review	6	N/A
Incorrect MU	2 to 5 fractions	In vivo dosimetry	5	4
Wrong photon energy	2 to 5 fractions	In vivo dosimetry	3	3
Missing or incorrect MLC shape	first	Port film	3	
Incorrect wedge direction	1,5,16 fractions	Later diode check; physics check	3	
Incorrect number of fractions for given set of fields	1 to 3 fractions	Physicist review	3	2
Incorrect or rotated compensating filter	2 or 11 fractions	Therapist discovery; in vivo dosimetry	2	N/A
Patient treated head to gantry but scanned foot to gantry	First fraction	Port film	1	N/A

Errors over a 30 months on 7 linacs equiped with R&V system.
No complete electronic transfer of treatment set-up data.

Detected errors 49/3900

With entrance in vivo dose measurements **30/3900**

ESTRO School

Major RT accidents

Entrance in vivo dose measurements

Identification	Cause of the accident	Consequence	Number of patients involved
USA (1974-1976)	Wrong decay curve for Co-60	Overdose (up to 50%)	426
UK (1982-1990)	Double correction of MU by ISQ after the implementing a new TPS.	Underdose (5-30%)	1045
Costa Rica (1996)	Error in the calibration of a Cobalt unit. Misunderstanding of the time units (0.3 minutes were taken as 30 seconds instead of 18 seconds)	Overdose (up to 60%)	115
Panama (2000)	Forcing a fifth block in a TPS that admitted four as a maximum	The time was doubled. 100% overdose.	28
USA and Canada (1985-1987)	Software of an old accelerator was incorporated in a new accelerator. Errors in modality and energy.		6 (3 of them died)
Poland (2001)	Two faults in two circuits at the same time + inoperative interlock lead to the accelerator operating with an ineffective beam monitoring system.	Overdose (doses in one fraction of 80-100 Gy)	5
USA (1987-1988)	After changing a cobalt source all files except one (dose calculation with trimmers) were actualised in the TPS. One new doctor decided treating patients with the trimmers. Treatment time was calculated using the dose-rate of the old source	Overdose (up to 75%)	33
Spain (1990)	After a breakdown of a linear accelerator a company technician repaired it. However a meter display indicated an energy selection problem. This indication was disregarded. All patients treated with electron beams were treated with the maximum available electron energy.	Overdose	27
France (2004-2005)	TPS calculation performed with static wedges while the patient was treated with dynamic wedges	Overdose (by 7%-34%)	23

Remarks

- Entrance and/or exit dose in vivo dose measurements still a valid method for QC of the delivered dose at one point

- Limitations of point detectors on the surface of the patient for IMRT techniques, SBRT…

- Need of solutions: Implantable detectors (point dose inside the area of interest)

need — EPIDs (2D information, labour intensive, of dose calculation algorithms)

[need — Transmission chambers+conebeam CT of dose calculation algorithms]

NEED TO KNOW THE DELIVERED AND NOT THE PLANNED DOSE TO EVALUATE THE SUCCESS OF A TREATMENT.

ESTRO School

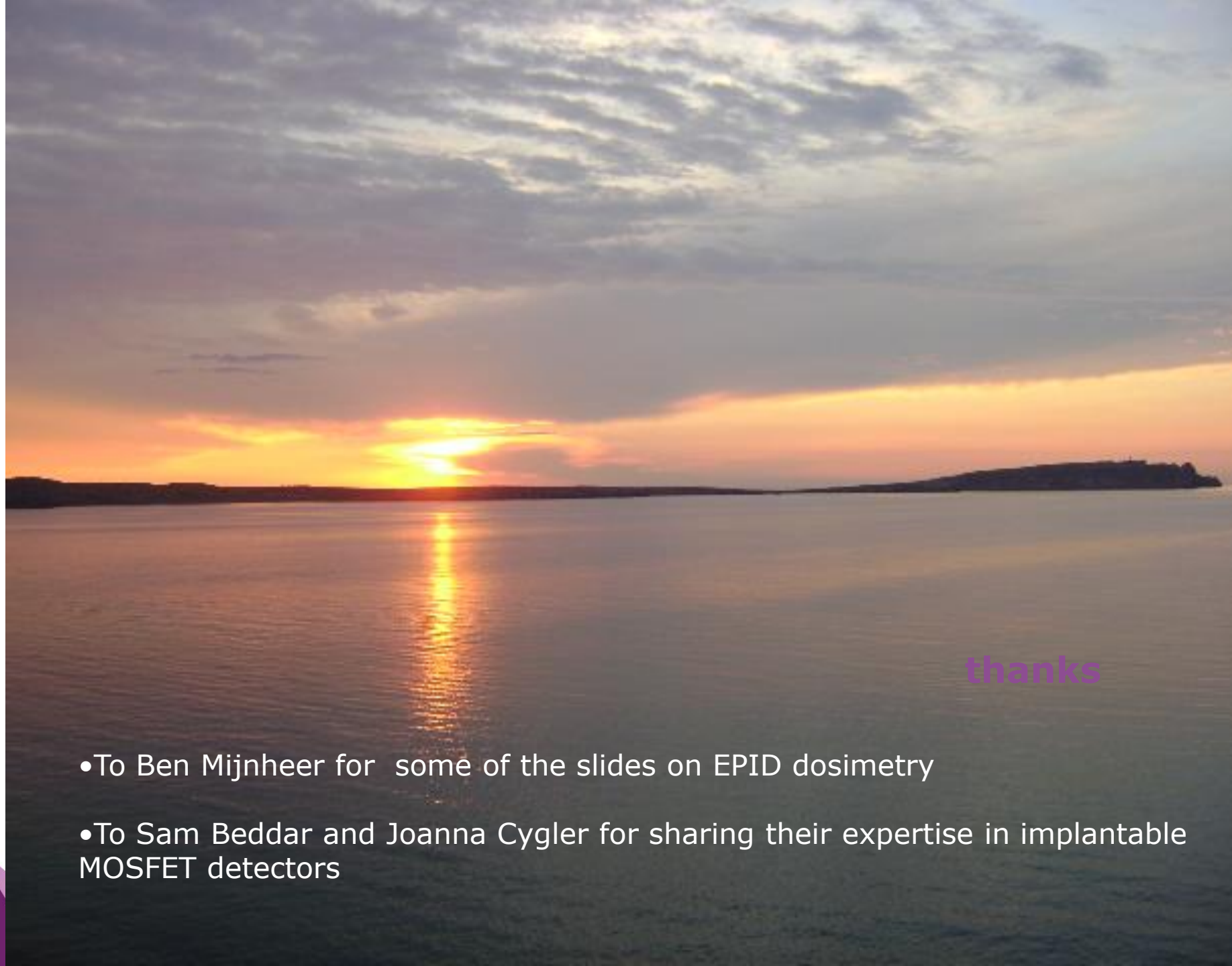

thanks

•To Ben Mijnheer for some of the slides on EPID dosimetry

•To Sam Beddar and Joanna Cygler for sharing their expertise in implantable MOSFET detectors

Recommended reading

General

•ESTRO Booklet nº1. Methods for in vivo dosimetry in External Radiotherapy. www.estro-education.org/publications/Pages/ESTROPhysicsBooklets.aspx

•ESTRO Booklet nº5. Practical Guidelines for the Implementation of in vivo dosimetry with diodes in external radiotherapy with photon beams. www.estro-education.org/publications/Pages/ESTROPhysicsBooklets.aspx

• AAPM report 87, "Diode in vivo dosimetry for patients receiving external beam radiation therapy" Report of Task Group 62 of the Radiation Therapy Committee," Medical Physics Publishing. (2005).

Diodes and MOSFET

N. Jornet, P. Carrasco, D. Jurado, a Ruiz, T. Eudaldo, and M. Ribas, "Comparison study of MOSFET detectors and diodes for entrance in vivo dosimetry in 18 MV x-ray beams," Med.Phys., vol. 31,, p. 2534. (2004)

EPID

•Van Elmpt, W. et al. "A literature review of electronic portal imaging for radiotherapy dosimetry". Radiother. Oncol. 88(3), pp.289-309. (2008)

•S.M.J.J.G. Nijsten, B.J. Mijnheer, et al. "Routine individualised patient dosimetry using electronic portal imaging devices.," Radiother and oncol, vol. 83, pp. 65-75.(2007)

IMRT

•Higgins, P.D. et al. "In vivo diode dosimetry for routine quality assurance in IMRT". Med. Phys., 30(12), pp.3118. (2003)

•Kadesjö, T. Nyholm, and J. Olofsson, "A practical approach to diode based in vivo dosimetry for intensity modulated radiotherapy.," Radiother. and oncol., vol. 98, pp. 378-81 (2011)

Implantable MOSFET

•T.M. Briere, M.T. Gillin, and a S. Beddar, "Implantable MOSFET detectors: Evaluation of a new design," Med.l Phys., vol. 34, pp. 4585. (2007)

•G.P. Beyer, C.W. Scarantino, et al., "Technical evaluation of radiation dose delivered in prostate cancer patients as measured by an implantable MOSFET dosimeter.," Int. J. Radiat. Oncol. biol. Phys., vol. 69, pp. 925-35. (2007)

ESTRO School

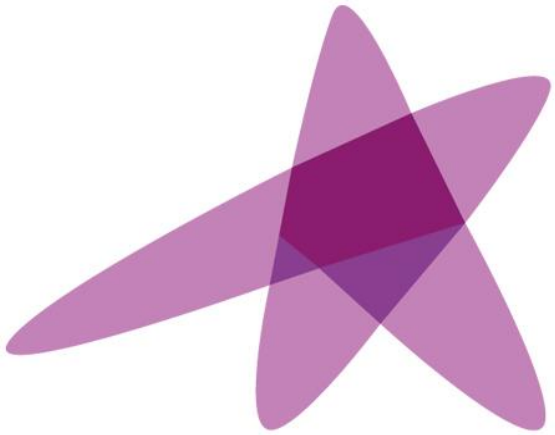

ESTRO School

WWW.ESTRO.ORG/SCHOOL

TPS QA:

Commissioning, Performance Testing

Núria Jornet

Servei de Radiofísica
Hospital Sant Pau, Barcelona

Learning Objectives

- Understand what is meant by QA for TPS
- Identification of some documentation available
- Review responsibility for
  - Vendor
  - User
- Define the nature of the information we want to know about our black boxes
- Commissioning and performance testing examples
  - To be able to design specific tests to know how accurate is the TPS for the clinical conditions in which will be used.

TPS commissioning is crucial to ensure safety and quality in the RT treatment.

- TPS is an essential component of RT
- TPS is used to plan treatment arrangements to provide optimal dose distributions.
- It is a hub of RT process

ESTRO School

Computer planning system – 'Hub' of RT

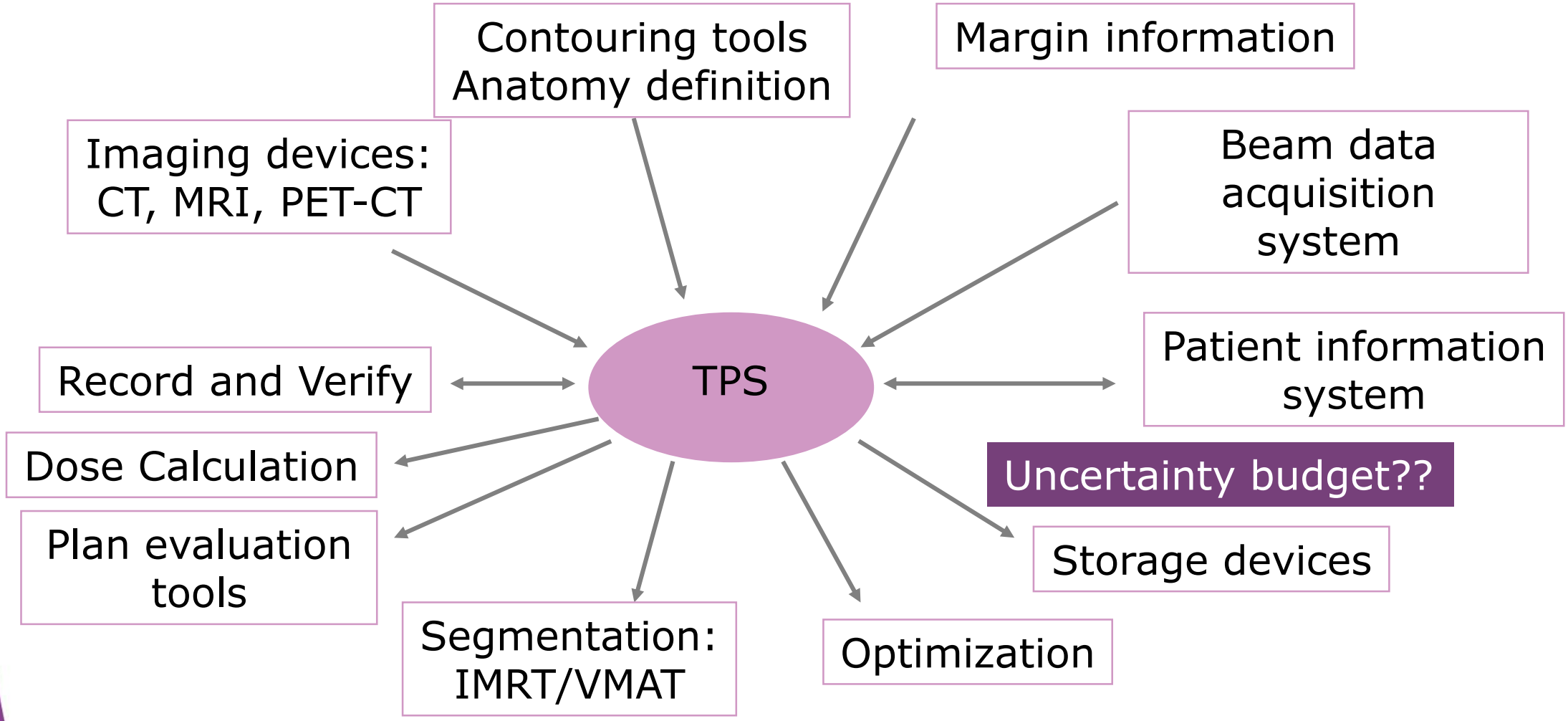

ESTRO School

Computer planning system – 'Hub' of RT

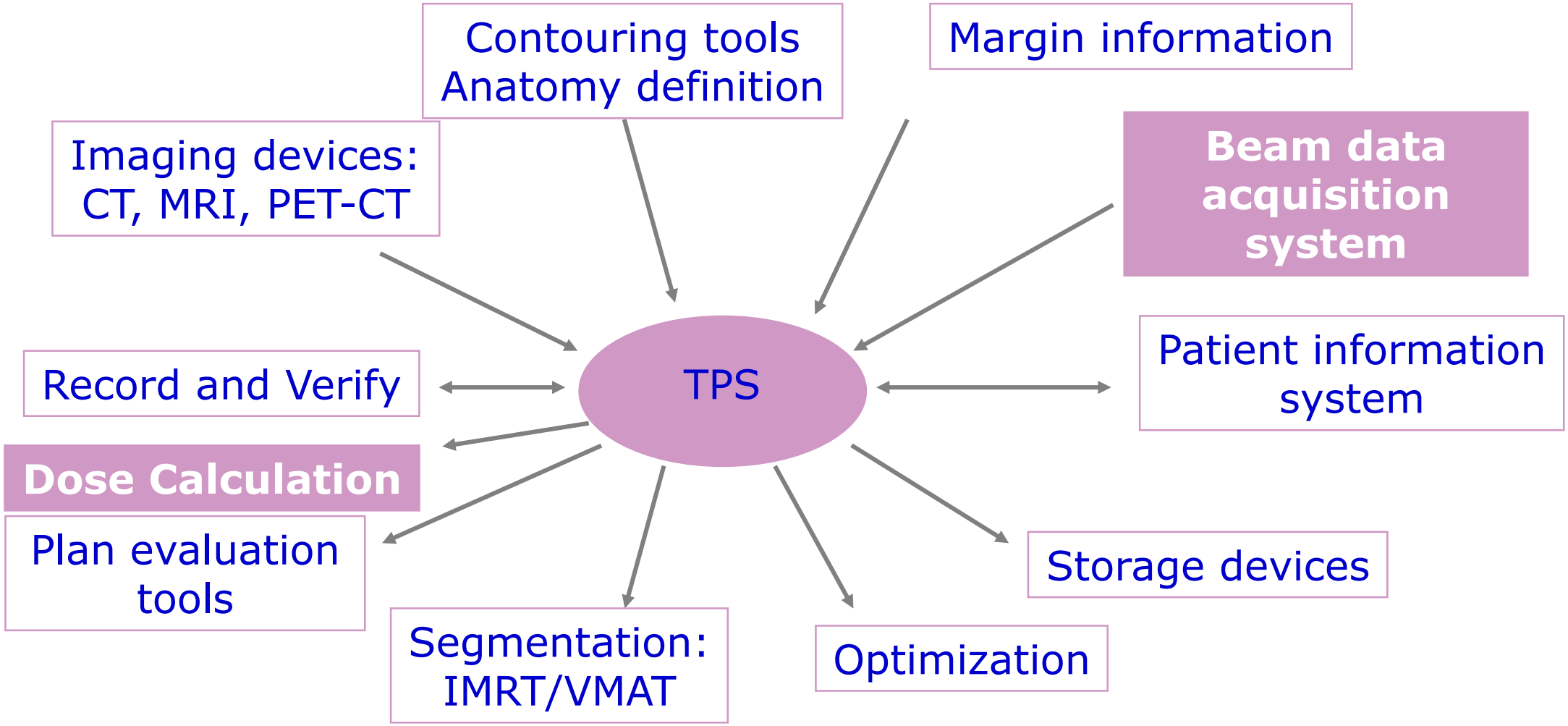

"Dose algorithms are the most unique, critical and complex software in a TPS" (Van Dyk)

ESTRO School

We need to assess that radiation beam parameters and other data needed for dose calculation are adequately modeled in the system and properly validated.

Who should test the TPS? Responsibilities.

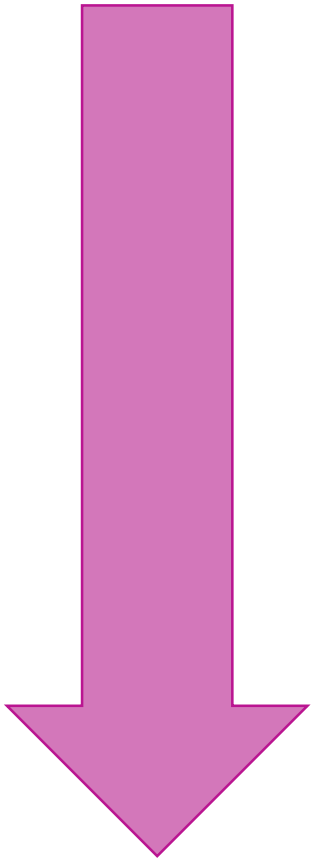

1) Generic performance — Vendor

2) Generic performance in users environment — Vendor/user

3) Specific performance in users environment — User

ESTRO School

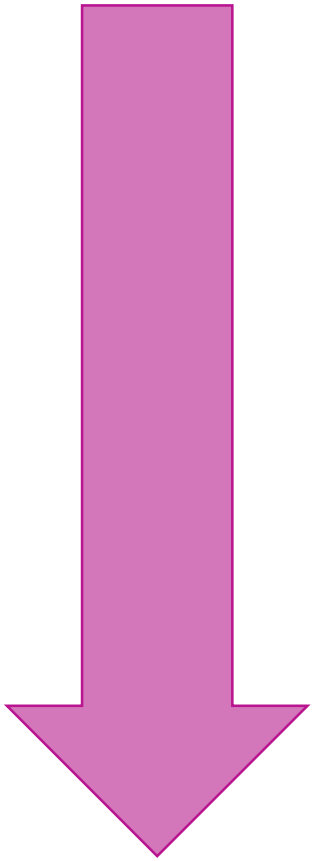

1) Generic performance

Acceptance

2) Generic performance in users environment

Acceptance
Site tests

3) Specific performance in users environment

Commissioning

ESTRO School

Once the TPS has been "accepted"

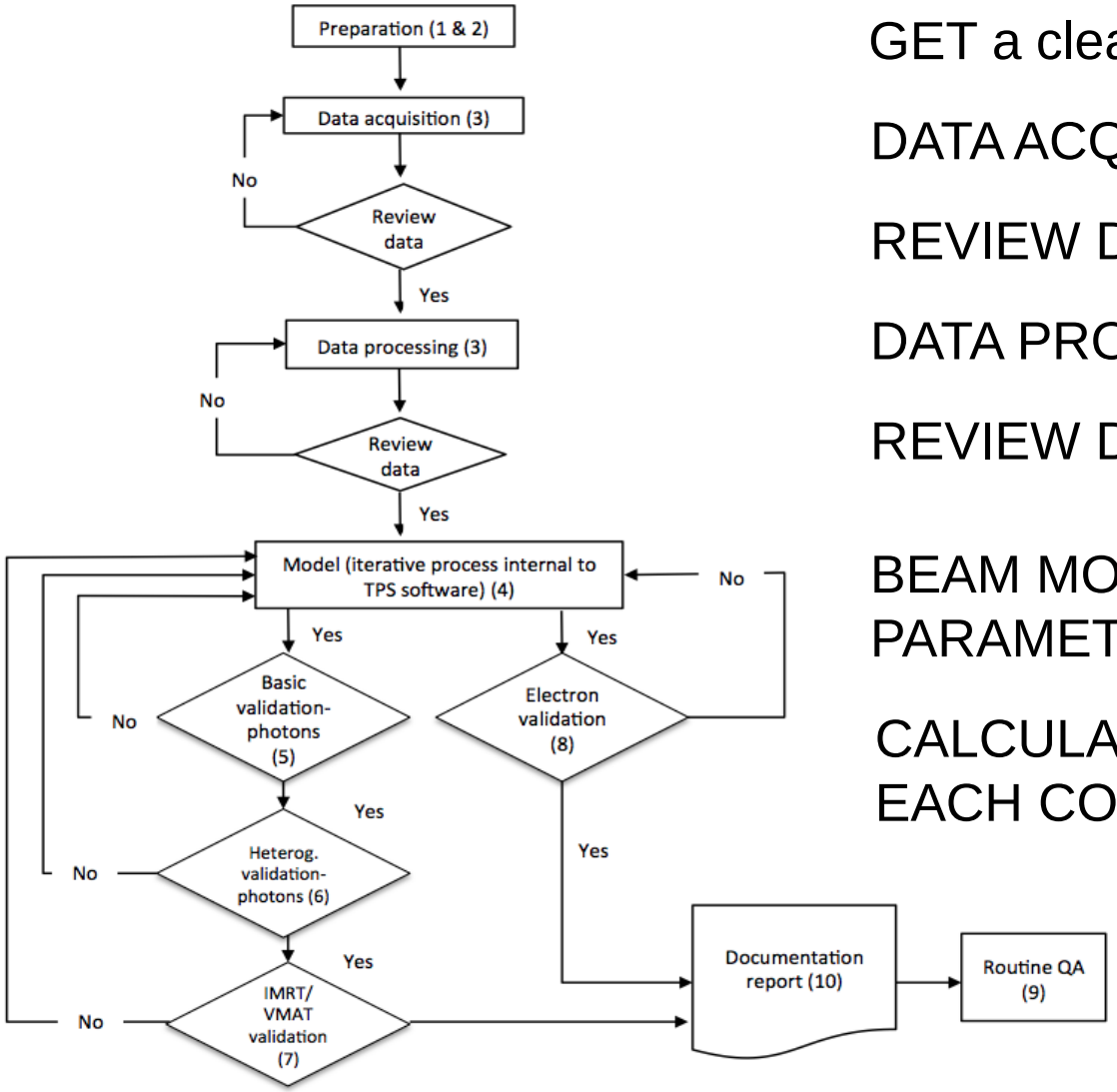

GET a clear UNDERSTANDING of the algorithm

DATA ACQUISITION for BEAM MODELING

REVIEW DATA

DATA PROCESSING

REVIEW DATA

BEAM MODEL (MAY NEED SOME PARAMETER ADJUSTEMENTS)

CALCULATION VALIDATIONS FOR EACH CONFIGURED BEAM

6-8 WEEKS FOR 2 X-Ray energies and 5 electron energies
Two full time equivalent Medical Physics Experts

ESTRO School

Commissioning – Dose Calculation

Create work plan

- Identify the algorithm type and special issues
- Define an efficient plan for data collection, dose distribution comparisons and analysis of results

Perform measurements

- Plan and Measure
- Transfer
- Analyse and Prepare data for TPS

Check and configure

- Verify input data
- Confirm machine/beam configuration
- Determine beam modelling fitting parameters

Beam modelling

Plan Comparison tools

Perform Calculation Checks

- Compare beam specific calculations with measured data
- Beam, algorithm and clinical specific calculations

Standards

Comparison and Analysis

- Verify that the calculations perform as expected in the user's hands
- Verify behaviour over the range of expected clinical usage and at the limits set for clinical use
- Verify calculation techniques and plan comparison tools

Performance testing

Commissioning – Dose Calculation

Create work plan	• Identify the algorithm type and special issues • Define an efficient plan for data collection, dose distribution comparisons and analysis of results
Perform measurements	• **Plan and Measure** • **Transfer** • **Analyse and Prepare data for TPS**
Check and configure	• Verify input data • Confirm machine/beam configuration • Determine beam modelling fitting parameters
Perform Calculation Checks	• Compare beam specific calculations with measured data • Beam, algorithm and clinical specific calculations
Comparison and Analysis	• Verify that the calculations perform as expected in the user's hands • Verify behaviour over the range of expected clinical usage and at the limits set for clinical use • Verify calculation techniques and plan comparison tools

Importance of data acquisition

- The data set is proposed by the manufacturer.

  Don’t reduce the required data set!

- Keep in mind that the quality of your measurements has a direct impact on the accuracy of your calculations!

- Equipment and methodology have to be chosen wisely for each of the requested data (reference dose, output factors, profiles and Depth Dose curves...)

Equipment: Data acquisition and TPS commissioning

Detectors

Detector	*Use*	*Comments*	*Reference*
Scanning ion chambers	Beam scanning for photons and electrons	Typical scanning chambers have an air cavity of 4–6 mm diameter, (minimum of 2 chambers for measurement and reference)	TG-106 (Das et al.[5])
Electron diodes and film	Beam scanning for electrons, output factors (film)	QMP must confirm the effective point of measurement	TG-25 (Khan et al.[45]), TG-70 (Gerbi et al.[46])
Small field detectors	• Small field scanning & output factors[a], • IMRT/VMAT point measurement • MLC intraleaf measurement & penumbra	Carefully select the detector type and size to fit the application. When scanning for penumbra, diodes are recommended.	TG-106 (Das et al.[5]), TG-120 (Low et al.[18]) Yunice, et al.[16]
Large ion chamber	Aggregate MLC transmission factors	Interleaf transmission	LoSasso et al.[20]
Film and/or array detector	2D dose distributions, including dynamic/virtual wedge and planar fluence maps, intraleaf measurements[b]	• Absolute dosimetry preferred; relative dosimetry adequate. • Desirable if the device can be mounted on the gantry and/or in a phantom at different geometries	TG-106 (Das et al.[5]), TG-120 (Low et al.[18]), IAEA TRS-430[7]

AAPM Medical Physics Practice Guideline 5.a: Commissioning and QA of Treatment Planning Dose Calculations-Megavoltage Photon and Electron Beams. JAMP 12016

ESTRO School

Equipment: Data acquisition and TPS commissioning

Phantoms

Equipment	*Use*	*Comments*	*Reference*
3D water phantom	Beam scanning	Must have sufficient scanning range and lateral/depth scatter	TG-106 (Das et al.[5]), TG-70 (Gerbi et al.[46])
Buildup cap or miniphantom	In-air output factor measurement	Measurements required for some planning systems, most second check systems	Yunice, et al.[16]
Water-equivalent phantom material in slab form	Buildup and backscatter for measurements	> 20 cm of total thickness in varying increments, width and length ≥ 30 cm, cavity for detector(s)	TG-106 (Das et al.[5]), TG-120 (Low et al.[18]), IAEA TRS-430[7]
CT density phantom	CT number to electron or mass density calibration	Should include tissue-equivalent materials spanning the clinical range of low-density lung to high-density bone.	TG-66 (Mutic et al.[13])
Heterogeneity phantom with lung-equivalent material	End-to-end testing	Include cavities for detectors, useful for annual QA reference test	TG-65 (Papanikolaou & Stathakis[26]), IAEA TRS-430[7]
Anthropomorphic phantom	Anatomic model testing, end-to-end testing, use testing	Include cavities for detectors	IAEA TRS-430[7]
IMRT/VMAT or arc therapy phantom	VMAT or arc therapy	Options include a solid phantom holding a planar array, 3D detector arrays, film inside a phantom, other	TG-120 (Low et al.[18])

JAMP 17(1), 2017

ESTRO School

Equipment: Data acquisition and TPS commissioning

Other

Equipment	*Use*	*Comments*	*Reference*
Electrometers and cables	Beam scanning, output calibration, relative and absolute dosimetry	ADCL calibration, low noise and leakage with wide dynamic range and linear response	TG-106 (Das et al.[5])
Software for data processing	Processing, comparing, and analyzing profiles, depth-dose curves, and other beam data	May be included with the 3D water tank scanning software	TG-106 (Das et al.[5])

JAMP 17(1), 2017

ESTRO School

Data acquisition for CT calibration

Why is it important:

Dose calculation algorithm will be commissioned comparing measurements with dose calculation in homogeneous and heterogeneous phantoms

The accuracy of dose calculation in patients will depend on the CT mapping to some physical descriptor that will be used in the calculation (electron density, mass density, composition)

Check the calibration curve
for the range of clinically relevant densities and CT settings (kVp)

Commissioning – Dose Calculation

Create work plan

- Identify the algorithm type and special issues
- Define an efficient plan for data collection, dose distribution comparisons and analysis of results

Perform measurements

- Plan and Measure
- Transfer
- Analyse and Prepare data for TPS

Check and configure

- **Verify input data**
- **Confirm machine/beam configuration**
- **Determine beam modelling fitting parameters**

Perform Calculation Checks

- Compare beam specific calculations with measured data
- Beam, algorithm and clinical specific calculations

Comparison and Analysis

- Verify that the calculations perform as expected in the user's hands
- Verify behaviour over the range of expected clinical usage and at the limits set for clinical use
- Verify calculation techniques and plan comparison tools

Always review data before its input to the TPS

Check for measuring errors:

Critically look at your data (i.e. changes with energy, field size…)

Compare with a reference data set (vendor or another hospital with the same equipment)

BUT ALSO, review after its input to the TPS

Check for processing errors

ESTRO School

Modelling

Once the beam data and machine parameters have been introduced, the beam model should be completed according vendors instructions

The amount of adjustable parameters depends on the vendor

i.e. Varian: second source (size, mean energy, relative intensity), MLC (DLS, transmission), spot size.

Therefore modeling is an iterative process when a compromise for the different clinical situations in which it be used has to be reached.

Evaluate the goodness of the model by Comparing PDDs and profiles using the softare beam commissioning application

Commissioning – Dose Calculation

Create work plan	• Identify the algorithm type and special issues • Define an efficient plan for data collection, dose distribution comparisons and analysis of results
Perform measurements	• Plan and Measure • Transfer • Analyse and Prepare data for TPS
Check and configure	• Verify input data • Confirm machine/beam configuration • Determine beam modelling fitting parameters
Perform Calculation Checks	• **Compare beam specific calculations with measured data** • **Beam, algorithm and clinical specific calculations**
Comparison and Analysis	• Verify that the calculations perform as expected in the user's hands • Verify behaviour over the range of expected clinical usage and at the limits set for clinical use • Verify calculation techniques and plan comparison tools

Calculation checks

Basic dose calculation algorithm validation (dose distribution and MU):

Homogeneous phantom, regular fields

Dose calculation in heterogeneous media (dose distribution and MU):

Heterogeneous phantoms

IMRT and VMAT dose calculation (dose distribution and MU):

Tune model parameters

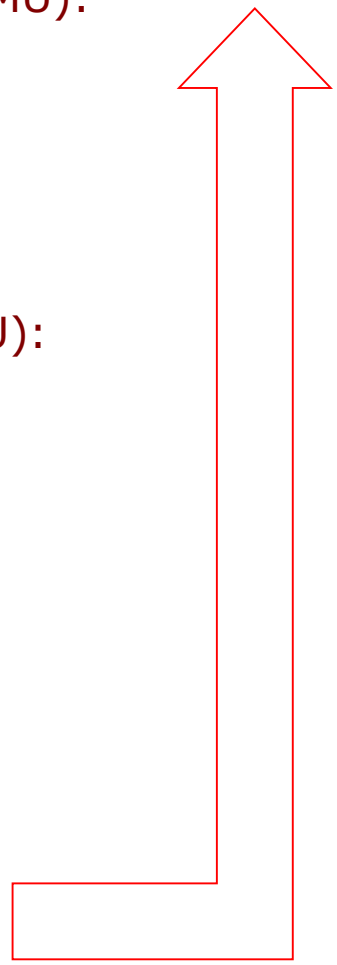

1. Basic dose algorithm validation
TPS model comparison tests

- Needs to be completed for each configured beam.
  - Each physical wedge is a unique beam (different energy fluence spectrum)
  - Nonphysical wedges can be considered an extension of the correspondent open field (is not a different beam)
- No extra measurements are needed. Confirmation that the dose calculated in the planning module agrees with those in the modeling module.

1. Basic dose algorithm validation

TPS model comparison tests

Test	*Comparison*	*Description*	*Tolerance*
5.1	Dose distributions in planning module vs. modeling (physics) module	Comparison of dose distribution for large (> 30×30cm^2) field.	Identical[a]
5.2	Dose in test plan vs. clinical calibration condition[b]	Reference calibration condition check	0.5%
5.3	Dose distribution calculated in planning system vs. commissioning data	PDD and off axis output factors for a large and a small field size	2%

[a] Identical to within the expected statistical uncertainty (considering noise and calculation grid size).
[b] TPS absolute dose at reference point.

ESTRO School

1. Basic dose algorithm validation

TPS model comparison tests

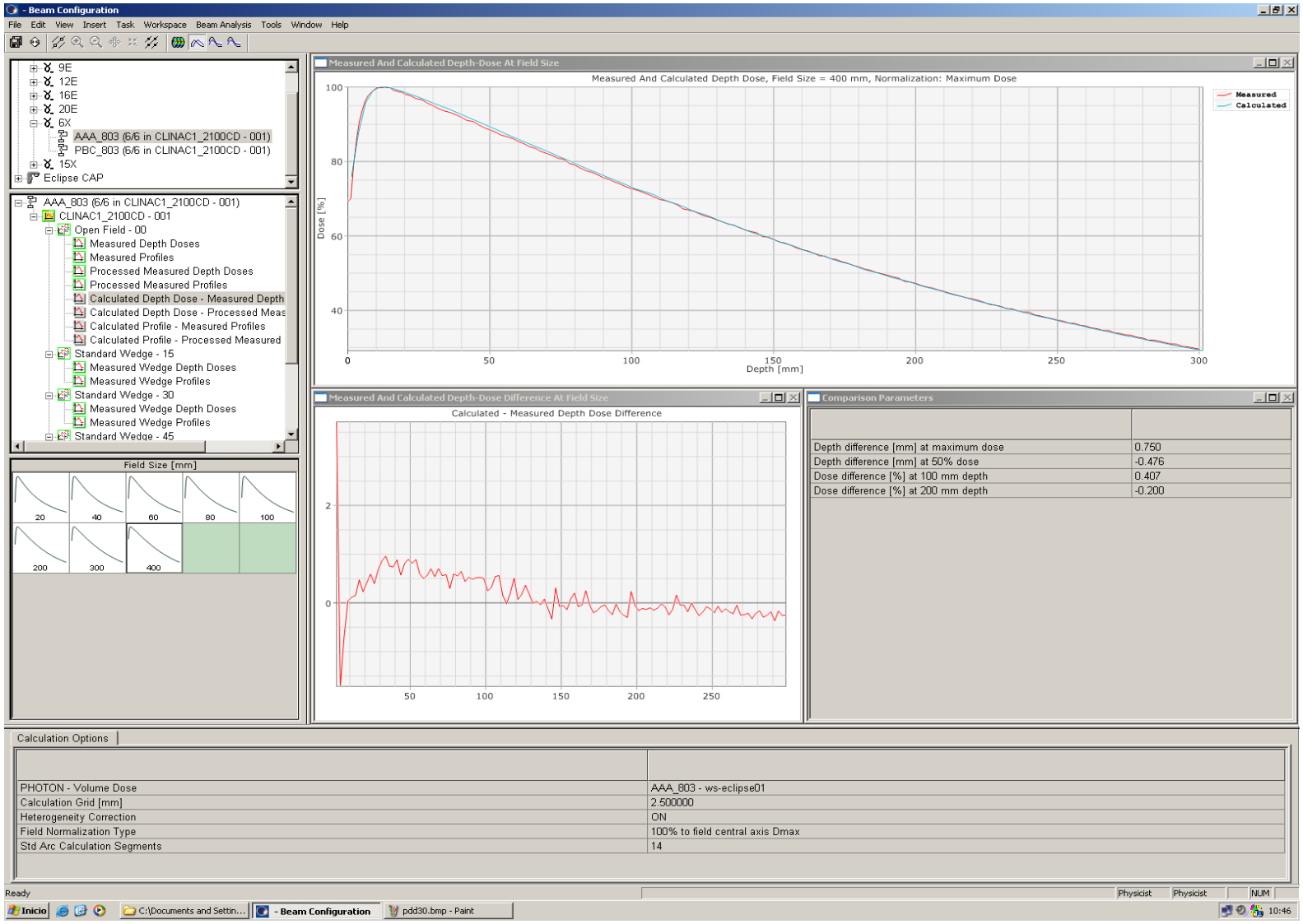

Varian Eclipse

ESTRO School

1. Basic dose algorithm validation

TPS model comparison tests

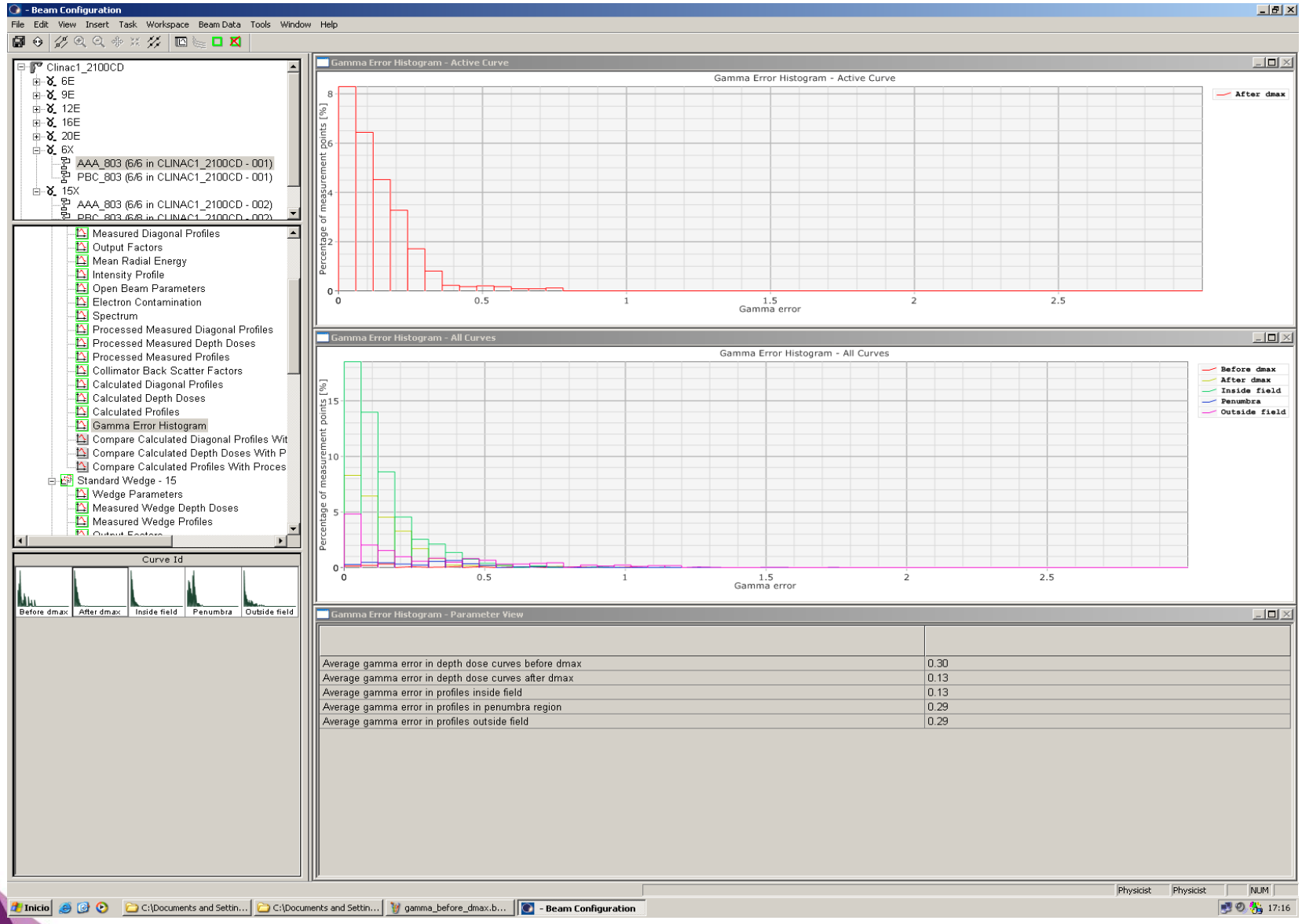

Varian Eclipse

ESTRO School

1. Basic dose algorithm validation

Validation tests using field configurations different from those used in the modelling phase

- Moving to more clinically relevant conditions but still using regular homogeneous (water) phantoms.
  - Tests samples can be taken from TRS230
  - A minimum subset of tests is proposed in AAPM Medical Physics Practice Guideline 5.a (JAMP 17(1), 2016)
- Extra measurements in a water phantom are needed.

AAPM set of test-cases

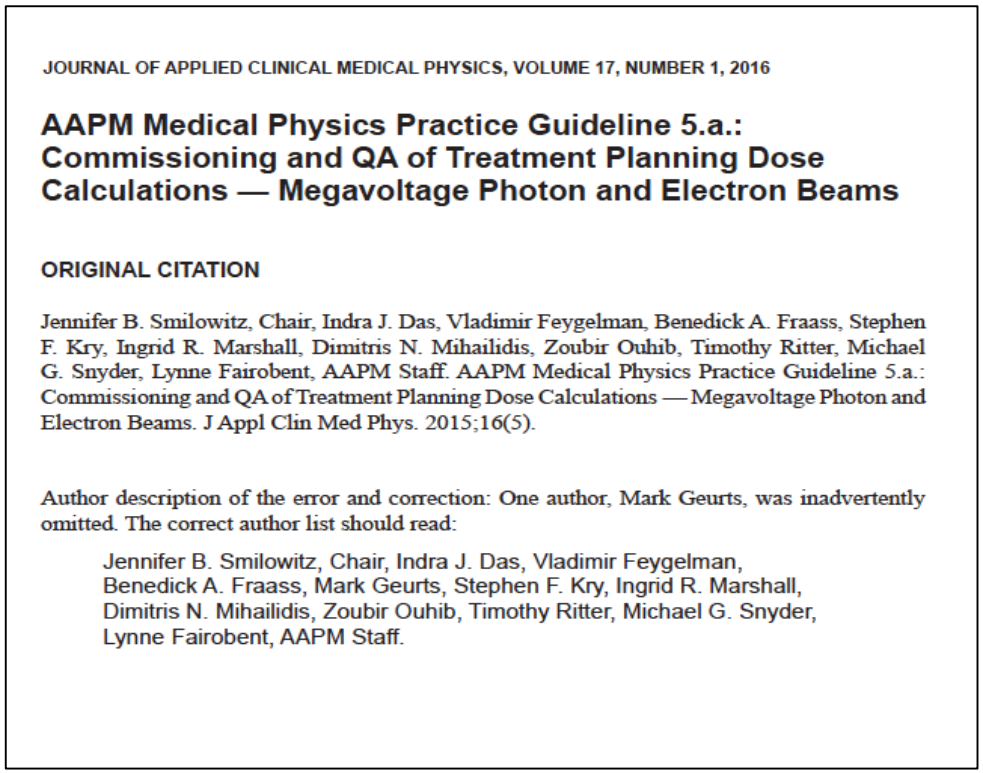

JOURNAL OF APPLIED CLINICAL MEDICAL PHYSICS, VOLUME 17, NUMBER 1, 2016

AAPM Medical Physics Practice Guideline 5.a.: Commissioning and QA of Treatment Planning Dose Calculations — Megavoltage Photon and Electron Beams

ORIGINAL CITATION

Jennifer B. Smilowitz, Chair, Indra J. Das, Vladimir Feygelman, Benedick A. Fraass, Stephen F. Kry, Ingrid R. Marshall, Dimitris N. Mihailidis, Zoubir Ouhib, Timothy Ritter, Michael G. Snyder, Lynne Fairobent, AAPM Staff. AAPM Medical Physics Practice Guideline 5.a.: Commissioning and QA of Treatment Planning Dose Calculations — Megavoltage Photon and Electron Beams. J Appl Clin Med Phys. 2015;16(5).

Author description of the error and correction: One author, Mark Geurts, was inadvertently omitted. The correct author list should read:

Jennifer B. Smilowitz, Chair, Indra J. Das, Vladimir Feygelman, Benedick A. Fraass, Mark Geurts, Stephen F. Kry, Ingrid R. Marshall, Dimitris N. Mihailidis, Zoubir Ouhib, Timothy Ritter, Michael G. Snyder, Lynne Fairobent, AAPM Staff.

- Minimal tests for TPS commissioning
- Simple phantoms
  - From regular slab phantom to anthropomorphic phantoms
- Includes IMRT, SBRT

ESTRO School

1. Basic dose algorithm validation

Validation tests using field configurations different from those used in the modelling phase

Test	*Description*	*Sample tests from literature*[7]
5.4	Small MLC-shaped field (non SRS)	Photon Test 1
5.5	Large MLC-shaped field with extensive blocking (e.g., mantle)	Photon Test 3
5.6	Off-axis MLC shaped field, with maximum allowed leaf over travel	Photon Test 2
5.7	Asymmetric field at minimal anticipated SSD	Photon Test 6
5.8	10×10 cm^2 field at oblique incidence (at least 20°)	Photon Test 10
5.9	Large (> 15 cm) field for each nonphysical wedge angle[b]	–

[a] For all tests, measurements in the high-dose region, penumbra, and low-dose tail regions should be compared to calculated values at various depths (including slightly beyond dmax, midrange/10–15 cm, and deep/25–30 cm). SSDs, other than those used at commissioning and that reflect the clinically expected range, should be used. The MLC should be used for tests 5.4–5.6. The MLC or jaws may be used for tests 5.7–5.9.

[b] Tests 5.4–5.8 are intended for each open and (hard) wedged field. Nonphysical wedges are considered an extension of the corresponding open field in terms of spectra and only require the addition of Test 5.9.

JAMP 17(1), 2017

ESTRO School

2. Heterogeneity correction validation

- Important to understand the implementation of the heterogeneity corrections and also their limitations.
- Important to know what dose is being reported:
  - Dose to water or dose to media
- Any heterogeneous phantom available can be used. A reasonable phantom is a slab phantom with water equivalent+low density material+water equivalent.
- Use small fields (5x5 cm2) because discrepancies are maximized.

2. Heterogeneity correction validation

Test	*Objective*	*Description*	*Reference*
6.1	Validate planning system reported electron (or mass) densities against known values	CT-density calibration for air, lung, water, dense bone, and possibly additional tissue types	TG 65,[26] IAEA TRS-430[7]
6.2	Heterogeneity correction distal to lung tissue	5×5 cm^2, measure and calculate dose ratio above and below heterogeneity, outside of the buildup region	IAEA TRS-430,[7] Carrasco et al.[28]

[a] Tolerances are relative to local dose unless otherwise noted.

JAMP 17(1), 2017

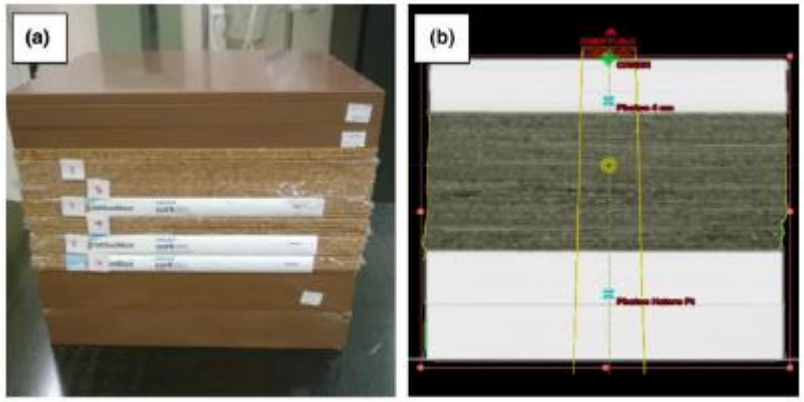

ESTRO School

2. Heterogeneity correction validation

Test	*Objective*	*Description*	*Tolerances*[a]	*Reference*
6.1	Validate planning system reported electron (or mass) densities against known values	CT-density calibration for air, lung, water, dense bone, and possibly additional tissue types	–	TG 65,[26] IAEA TRS-430[7]
6.2	Heterogeneity correction distal to lung tissue	5×5 cm^2, measure and calculate dose ratio above and below heterogeneity, outside of the buildup region	3%	IAEA TRS-430,[7] Carrasco et al.[28]

[a] Tolerances are relative to local dose unless otherwise noted.

JAMP 17(1), 2017

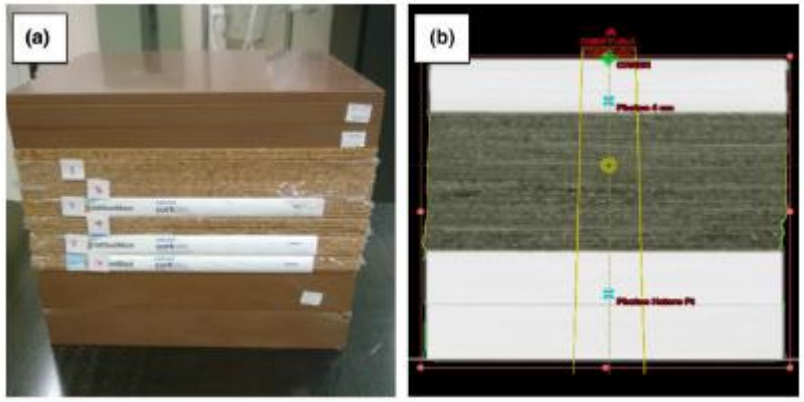

ESTRO School

3. IMRT/VMAT calculation validation

- Accurate dosimetric commissioning of an IMRT system remains a challenge
- Results of IMRT credentialling by IROC shows that only 82% of institutions passed the credentialling end to end test (5%-7mm)
- Most of the failures were due to the basic beam modeling inaccuracies.

3. IMRT/VMAT calculation validation

Test	*Objective*	*Description (example)*	*Detector*	*Ref*
7.1	Verify small field PDD	≤ 2×2 cm^2 MLC shaped field, with PDD acquired at a clinically relevant SSD	Diode or plastic scintillator	Yunice et al.[16]
7.2	Verify output for small MLC-defined fields	Use small square and rectangular MLC-defined segments, measuring output at a clinically relevant depth for each[a]	Diode, plastic scintillator, minichamber or microion chamber	Cadman et al.[58]
7.3	TG-119 tests	Plan, measure, and compare planning and QA results to the TG119 report for both the Head and Neck and C-shape cases	Ion chamber, film and/or array	TG-119 (Ezzell et al.[37])
7.4	Clinical tests	Choose at least 2 relevant clinical cases; plan, measure, and perform an in-depth analysis of the results	Ion chamber, film and/or array	Nelms et al.[42]
7.5	External review	Simulate, plan, and treat an anthropomorphic phantom with embedded dosimeters.	Various options exist[b]	Kry et al.[39]

JAMP 17(1), 2017

ESTRO School

3. IMRT/VMAT calculation validation

Measurement Method	*Region*	*Tolerance*
Ion Chamber	Low-gradient target region OAR region	2% of prescribed dose 3% of prescribed dose
Planar/Volumetric Array	All regions	2%/2 mm[a], no pass rate tolerance, but areas that do not pass need to be investigated
End-to-End	Low-gradient target region	5% of prescribed dose

[a] Application of a 2%/2 mm gamma criterion can result in the discovery of easily correctable problems with IMRT commissioning that may be hidden in the higher (and ubiquitous) 3%/3 mm passing rates.[39]

JAMP 17(1), 2017

ESTRO School

Commissioning – Dose Calculation

Create work plan	• Identify the algorithm type and special issues • Define an efficient plan for data collection, dose distribution comparisons and analysis of results
Perform measurements	• Plan and Measure • Transfer • Analyse and Prepare data for TPS
Check and configure	• Verify input data • Confirm machine/beam configuration • Determine beam modelling fitting parameters
Perform Calculation Checks	• Compare beam specific calculations with measured data • Beam, algorithm and clinical specific calculations
Comparison and Analysis	• **Verify that the calculations perform as expected in the user's hands** • **Verify behaviour over the range of expected clinical usage and at the limits set for clinical use** • **Verify calculation techniques and plan comparison tools**

Any specific treatment

Treatment technique not covered by the vendor

User's interest to:

- Search for limitations
- Understand limitations and put in place processes to prevent non-verified use

A user doing special measurements

PERFORMANCE TESTING

ESTRO School

Remember...

- Testing all components of a treatment-planning process can be a formidable task.
- Physicist must ascertain extent and complexity of treatment-planning needs of clinic
- Based on this information, physicist must establish elements of acceptance, commissioning, and QA of the TPS.

How to design clinical tests?

ESTRO School

Not really… We can go through documents…

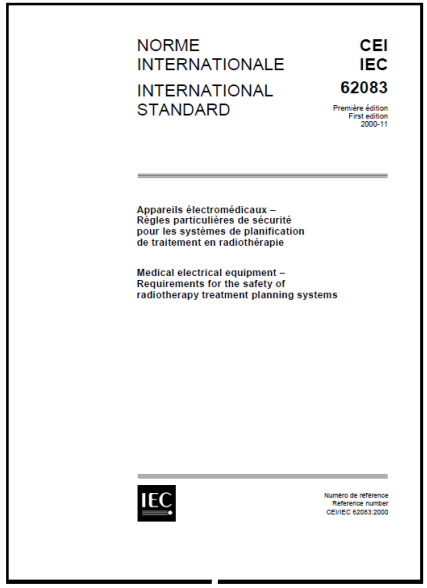
NORME INTERNATIONALE
INTERNATIONAL STANDARD

CEI IEC 62083

Première édition
First edition
2000-11

Appareils électromédicaux – Règles particulières de sécurité pour les systèmes de planification de traitement en radiothérapie

Medical electrical equipment – Requirements for the safety of radiotherapy treatment planning systems

IEC

Numéro de référence
Reference number
CEI/IEC 62083:2000

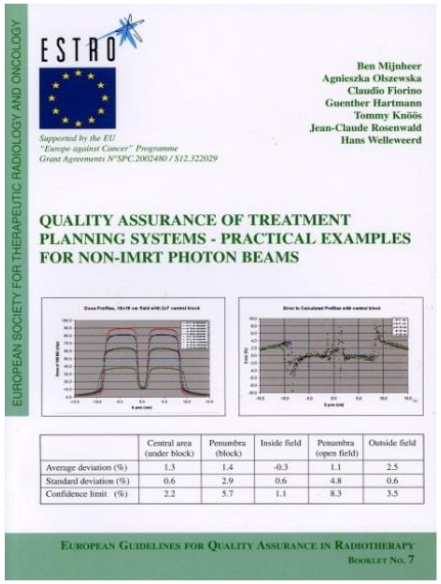
ESTRO

EUROPEAN SOCIETY FOR THERAPEUTIC RADIOLOGY AND ONCOLOGY

Ben Mijnheer
Agnieszka Olszewska
Claudio Fiorino
Guenther Hartmann
Tommy Knöös
Jean-Claude Rosenwald
Hans Welleweerd

Supported by the EU
"Europe against Cancer" Programme
Grant Agreements N°SPC.2002480 / S12.322029

QUALITY ASSURANCE OF TREATMENT PLANNING SYSTEMS - PRACTICAL EXAMPLES FOR NON-IMRT PHOTON BEAMS

	Central area (under block)	Penumbra (block)	Inside field	Penumbra (open field)	Outside field
Average deviation (%)	1.3	1.4	-0.3	1.1	2.5
Standard deviation (%)	0.6	2.9	0.6	4.8	0.6
Confidence limit (%)	2.2	5.7	1.1	8.3	3.5

EUROPEAN GUIDELINES FOR QUALITY ASSURANCE IN RADIOTHERAPY
BOOKLET No. 7

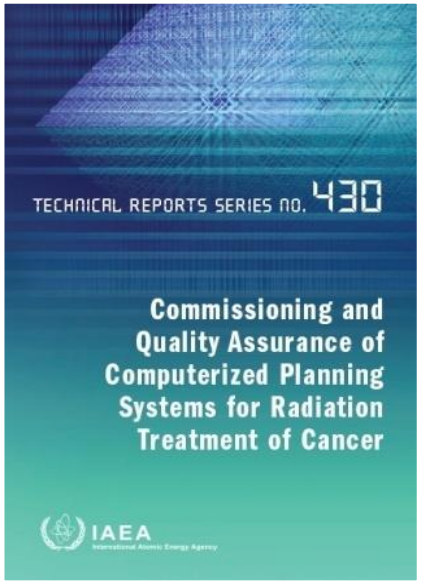
TECHNICAL REPORTS SERIES NO. 430

Commissioning and Quality Assurance of Computerized Planning Systems for Radiation Treatment of Cancer

IAEA
International Atomic Energy Agency

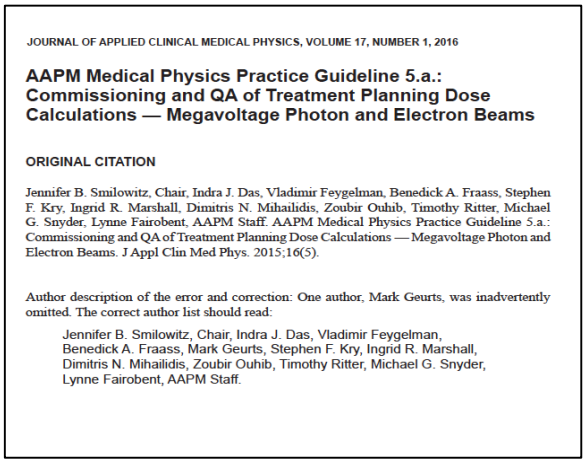
JOURNAL OF APPLIED CLINICAL MEDICAL PHYSICS, VOLUME 17, NUMBER 1, 2016

AAPM Medical Physics Practice Guideline 5.a.: Commissioning and QA of Treatment Planning Dose Calculations — Megavoltage Photon and Electron Beams

ORIGINAL CITATION

Jennifer B. Smilowitz, Chair, Indra J. Das, Vladimir Feygelman, Benedick A. Fraass, Stephen F. Kry, Ingrid R. Marshall, Dimitris N. Mihailidis, Zoubir Ouhib, Timothy Ritter, Michael G. Snyder, Lynne Fairobent, AAPM Staff. AAPM Medical Physics Practice Guideline 5.a.: Commissioning and QA of Treatment Planning Dose Calculations — Megavoltage Photon and Electron Beams. J Appl Clin Med Phys. 2015;16(5).

Author description of the error and correction: One author, Mark Geurts, was inadvertently omitted. The correct author list should read:

Jennifer B. Smilowitz, Chair, Indra J. Das, Vladimir Feygelman, Benedick A. Fraass, Mark Geurts, Stephen F. Kry, Ingrid R. Marshall, Dimitris N. Mihailidis, Zoubir Ouhib, Timothy Ritter, Michael G. Snyder, Lynne Fairobent, AAPM Staff.


American Association of Physicists in Medicine
Radiation Therapy Committee Task Group 53:
Quality assurance for clinical radiotherapy treatment planning

Benedick Fraass[a]
University of Michigan Medical Center, Ann Arbor, Michigan
Karen Doppke
Massachusetts General Hospital, Boston, Massachus.
Margie Hunt
Fox Chase Cancer Center, Philadelphia, Pennsylvania and Memorial Sloan Kettering Cancer Center, New York,
Gerald Kutcher
Memorial Sloan Kettering Cancer Center, New York, New Yor.
George Starkschall
M. D. Anderson Cancer Center, Houston, Texas
Robin Stern
University of California, Davis Medical Center, Sacramento, California.
Jake Van Dyke
London Regional Cancer Center, London, Ontario, Canada

(Received 15 December 1997; accepted for publication 4 August 1998.

In recent years, the sophistication and complexity of clinical treatment ·lanning and treatment planning systems has increased significantly, particularly including three-c, ·ensional (3D) treatment planning systems, and the use of conformal treatment planning and deli. ·ry techniques. This has led to the need for a comprehensive set of quality assurance (QA) guidelines. ·at can be applied to clinical treatment planning. This document is the report of Task Group 53 ·f the Radiation Therapy Committee of the American Association of Physicists in Medicine. The ·rpose of this report is to guide and assist the clinical medical physicist in developing and im. ·lementing a comprehensive but viable program of quality assurance for modern radiotherapy tre. ·tment planning. The scope of the QA needs for treatment planning is quite broad, encompassing in. ·e-based definition of patient anatomy, 3D beam descriptions for complex beams including multi. ·f collimator apertures, 3D dose calculation algorithms, and complex plan evaluation tools including. ·dose volume histograms. The Task Group recommends an organizational framework for the te. ·of creating a QA program which is individualized to the needs of each institution and addresses ·e issues of acceptance testing, commissioning the planning system and planning process, routi. quality assurance, and ongoing QA of the planning process. This report, while not prescribing specific QA tests, provides the framework and guidance to allow radiation oncology physicists to design comprehensive and practical treatment planning QA programs for their clinics. © *1998 American Association of Physicists in Medicine.* [S0094-2405(98)03416-5]

Key words: treatment planning, quality assurance, 3D treatment planning

PREFACE

This document is the report of Task Group 53 of the Radiation Therapy Committee of the American Association of Physicists in Medicine (AAPM). The purpose of this report is to guide and assist the radiation oncology physicist in developing and implementing a comprehensive but viable program of quality assurance for radiotherapy treatment planning. This report is the first guidance on the topic of treatment planning quality assurance (QA) from the AAPM, although there are several related reports,[1] including the recent report from Task Group 40 on Comprehensive QA for Radiation Oncology.[2] Further expansion of AAPM recommendations regarding treatment planning quality assurance is likely after the radiation oncology community accumu. ·es some experience with the approach recommended in this ·. ·port.

In recent years, the increased complexity of the treatment planning process required to support such procedures as conformal radiotherapy has led to the need for a comprehensive set of quality assurance guidelines that can be applied to treatment planning systems that support this complex process. This Task Group has been charged by the AAPM to prepare this report recommending the scope and content of necessary quality assurance procedures and the frequency of tests, from acceptance testing, characterization and commissioning to routine quality assurance of clinical system use.

1773 Med. Phys. 25 (10), October 1998 0094-2405/98/25(10)/1773/67/$10.00 © 1998 Am. Assoc. Phys. Med. 1773

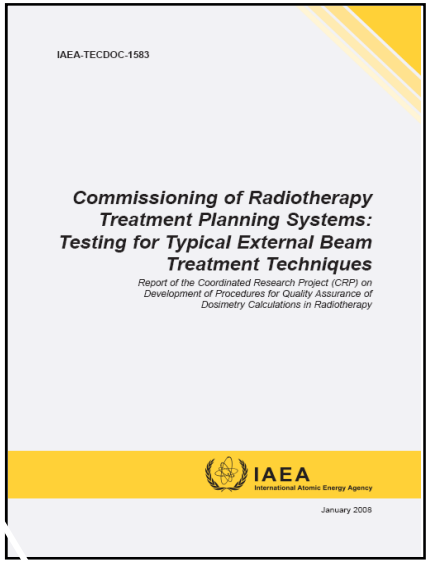
IAEA-TECDOC-1583

Commissioning of Radiotherapy Treatment Planning Systems: Testing for Typical External Beam Treatment Techniques

Report of the Coordinated Research Project (CRP) on Development of Procedures for Quality Assurance of Dosimetry Calculations in Radiotherapy

IAEA
International Atomic Energy Agency

January 2008

Medical electrical equipment – Requirements for the safety of radiotherapy treatment planning systems

American Association of Physicists in Medicine
Radiation Therapy Committee Task Group 53:
Quality assurance for clinical radiotherapy treatment planning

ESTRO School

We can take tests from these documents and adapt to our own necessities.

American Association of Physicists in Medicine
Radiation Therapy Committee Task Group 53:
Quality assurance for clinical radiotherapy treatment planning

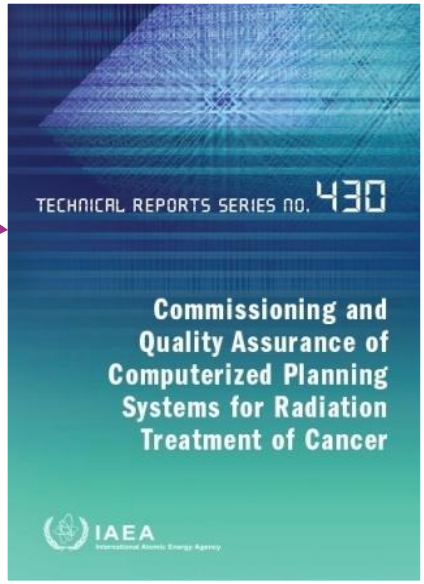

Framework
Large number tests
Many for system vs
Individual user

Extension with emphasis on practical tests

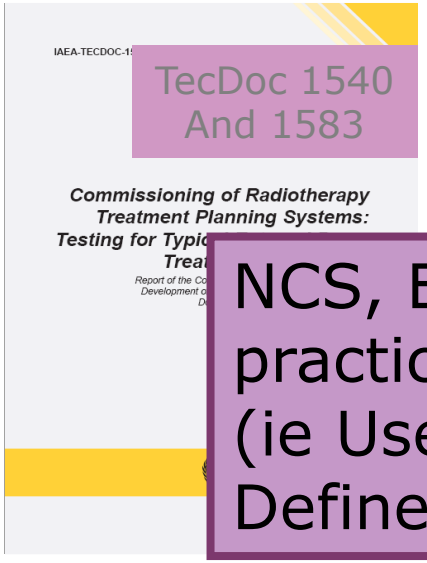

TecDoc 1540
And 1583

NCS, ESTRO, TecDocs focus on
practical approach and **how** to do tests
(ie User focused)
Defines minimum set of tests

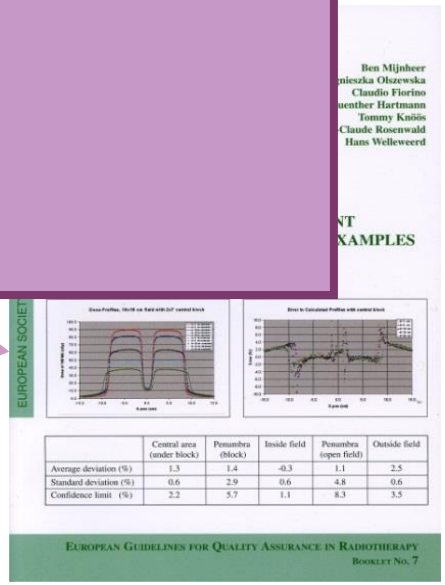

QUASIMODO
Booklets 7 and 9

ESTRO School

Design of a QC test:

1. Definition of a specification: *(Capability of calculating DVH)*
2. The measurement of performance associated to that specification
3. The comparison of the measurement with the standard
4. The possible action steps if the perfomance fails out of the tolerance

Need to know what is an acceptable deviation from a known standard

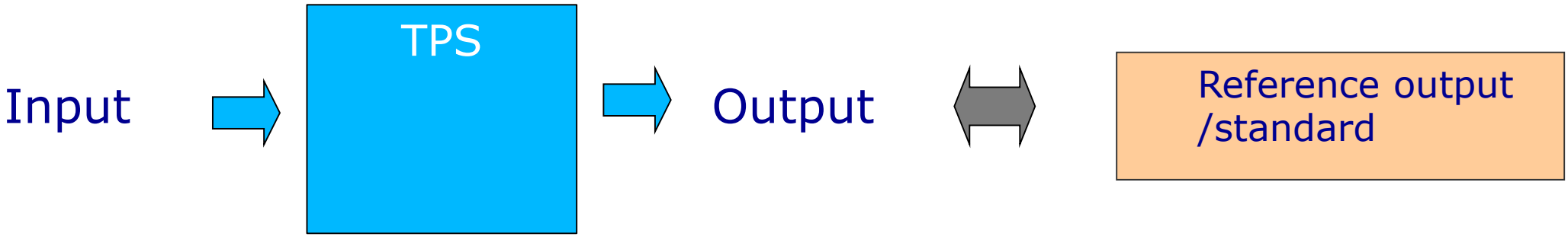

If Δ[output-standard]<tolerance*s*

The TPS performs well

Performance testing – dose calculations

If Δ[output-standard]<tolerances

The TPS performs well

How to design tests cases

- First step: Use test cases proposed in international recommandations. Ex. TG53, IAEA...

- Second step: Design your own test cases addressing your typical clinical situations.

IAEA set of test-cases

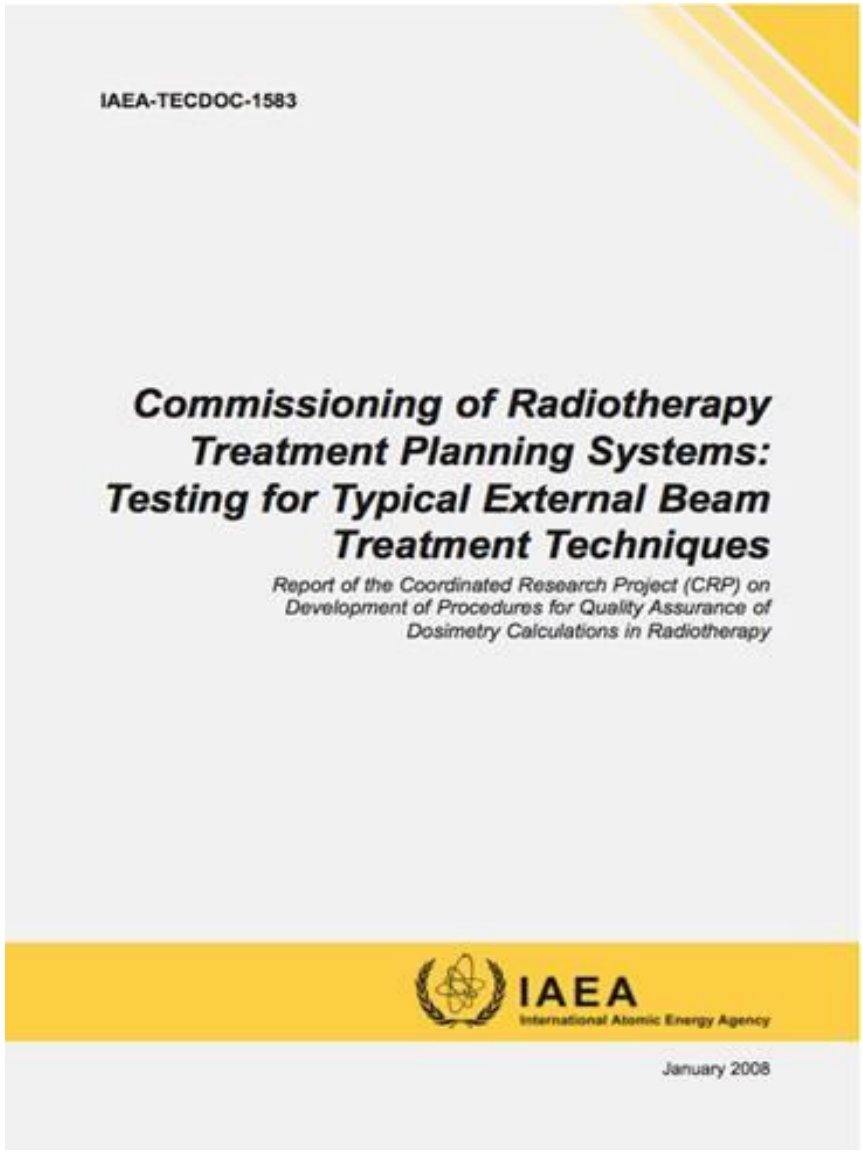

- Practical guidance for the implementation of TRS 430
- Includes clinical commissioning tests. Based on the use of a specific phantom

  (CIRS TORAX PHANTOM).

Covers only standard techniques.

ESTRO School

Test cases (TRS-430)

Non dosimetric tests:

- Verification of digitized contours
- Verification of the CT number-electron density conversion

Dosimetric tests:

- Testing for reference conditions on CT data
- Oblique incidence, lack of scattering, tangential fields
- Significant blocking on field corners
- Four field box
- Automatic expansion and customized blocking
- Oblique incidence with irregular fields and beam center blocked
- Three fields, two wedge paired, asymmetric collimation
- Non coplanar fields, collimator and couch rotation

Example

Case 1: Testing for reference conditions based on CT data

The purpose of this test is to verify the calculation for the reference field. A 10 cm x 10 cm field with a gantry angle of 0° and collimator angle of 0° is used to confirm the basic beam data. The measurement points are defined in the middle of holes 1, 3, 5, 9 and 10: see Figure A.3 and Table A.2.

Table A.2 Geometry for case 1

Case	Number of beams	Set-up	Reference point	Measurement point	Field Size [cm] L x W	Gantry angle	Collimator angle	Beam modifiers
1	1	SSD=SAD 100 cm (linac) 80 cm (Co-60)	3	1 3 5 9 10	10x10	0	0	none

Test cases (TRS-430)

ESTRO School

Table A.3. Comparison of measured and calculated data for case 1

Case	Location of measuring point	Calculated dose [Gy]	Measured dose [Gy]	Deviation [%]	Agreement criterion [%]
1	1				2
	3				2
	5				2
	9				4
	10				3

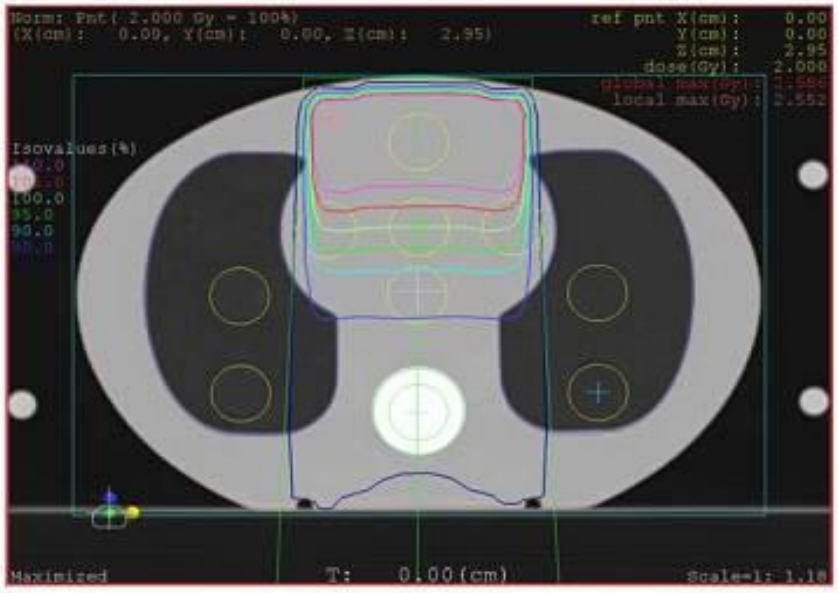

Figure A.5. A sample dose distribution in central plane for case 1.

Instructions for Case 1:

(1) Perform the treatment plan with the RTPS according to Table A.2 and document it.
(2) Calculate with RTPS MU/time needed to deliver 2 Gy to the reference point #3.
(3) Report the computed dose at points 1, 5, 9 and 10.
(4) Perform manual MU/time calculation and compare result with RTPS MU/time calculated values.
(5) Set up the phantom on the couch of the treatment machine with Head first supine towards gantry.
(6) Align the phantom with lasers intersection at the centre of hole #5.
(7) Set gantry angle to 0°.
(8) Set SSD=100 cm (80 cm for C0-60 or nominal SSD).
(9) Set collimator rotation to 0°.
(10) Set field size: Length (Y) = 10 cm Width (X) = 10 cm
(11) Insert ionisation chamber into the tissue plug and place it into hole #3.
(12) Irradiate the phantom with the RTPS calculated MU/time.
(13) Register the value of the measured doses. Repeat irradiation at least three times and determine average value.
(14) Change the position of the ionisation chamber to the next hole #5.
(15) Repeat steps 12 and 13 after changing the position of the chamber.
(16) Change the position of the ionisation chamber to the next hole #1.
(17) Repeat steps 12 and 13 after changing the position of the chamber.
(18) Insert ionisation chamber into the bone-equivalent plug and place it into hole #10.
(19) Repeat steps 12 and 13 after changing the position of the chamber.
(20) Insert ionisation chamber into the lung-equivalent plug and place it into hole #9.
(21) Repeat steps 12 and 13 after changing the position of the chamber.
(22) Fill in Table A.3 with calculated and measured data and compare results.

Performance testing – references

If Δ[output-standard]<tolerances

The TPS performs well

Performance testing – references

MEASUREMENTS: Algorithm input data (usually specified by the vendor)

Try to use a different measurement system from the one used to get the data for beam configuration

Performed in the department with their own measuring equipment/phantoms.

Audit (i.e. mailed phantom+TLD+Films)

Benchmark data (published)

CALCULATIONS: Other TPS/calculation algorithm, version, MonteCarlo

ESTRO School

Setting up tolerances

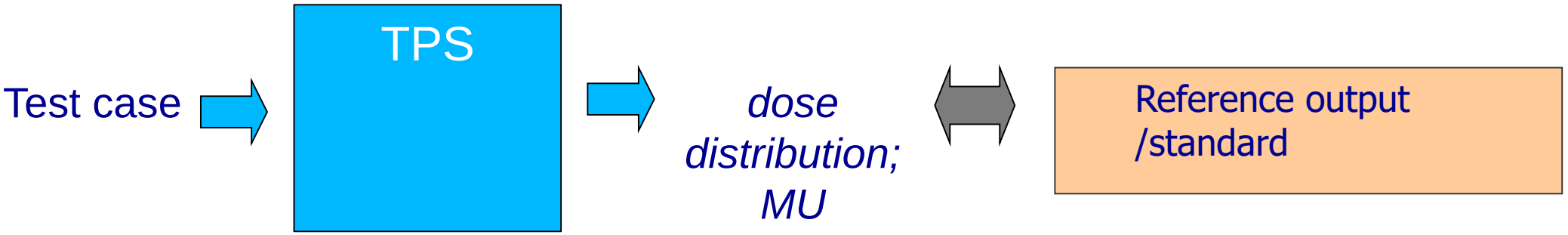

If Δ[output-standard]<tolerances

The TPS performs well

Different regions may have different tolerances

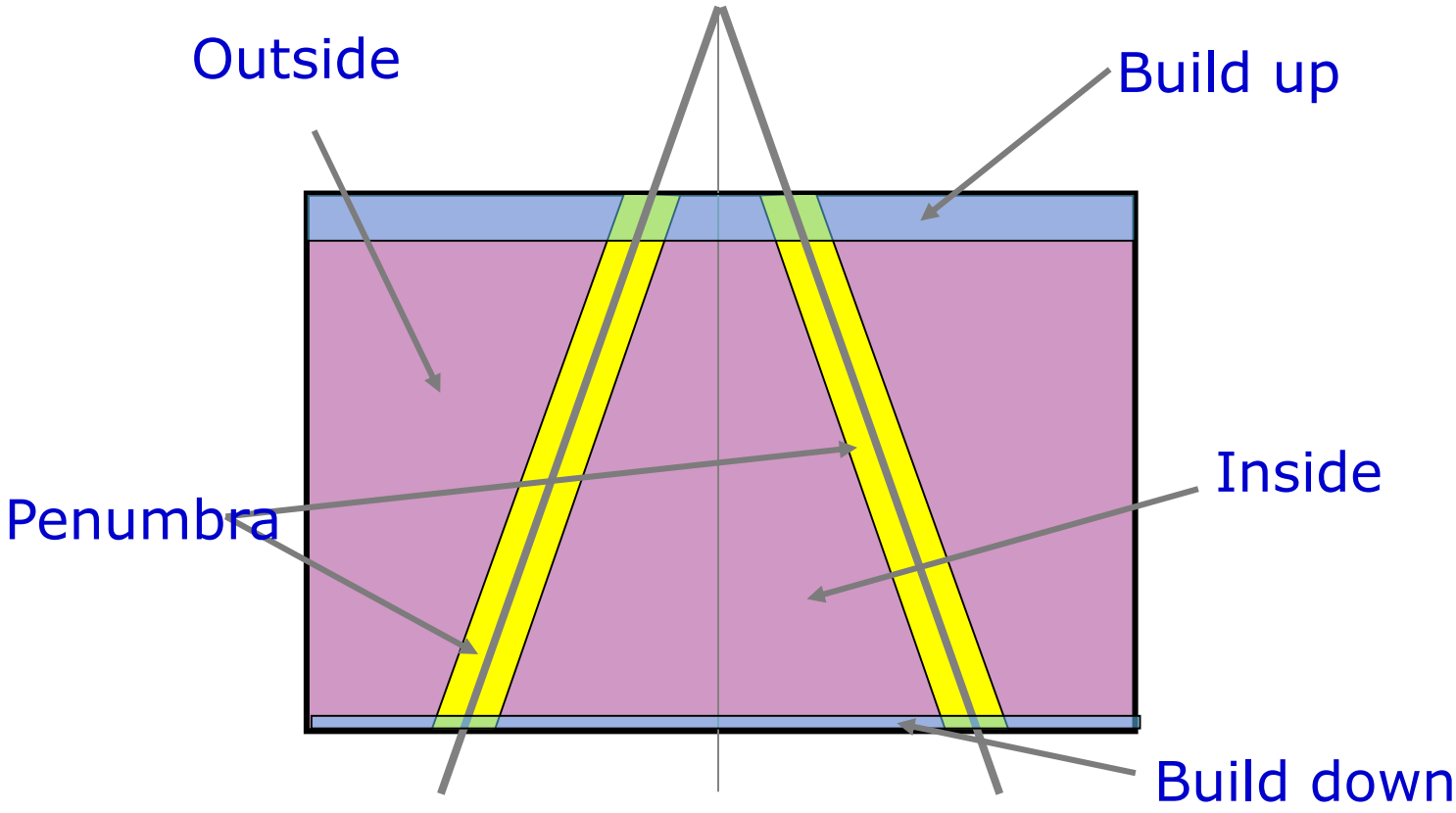

- Establish limits of dose algorithm
- Quantify or interpret in different regions
- Agree criteria of acceptance

How define the tolerances

The final criteria should reflect both what is achievable in clinical practice with up-to-date equipment, and the radiobiological requirements for accuracy [dose delivery in the patient, one should strive for an overall accuracy of 3.5% (1 SD) in the value of the dose delivered to the ICRU reference point]

- Different methods for comparison of dose distribution
- How to fix tolerances

ESTRO School

Performance testing – dose calculations

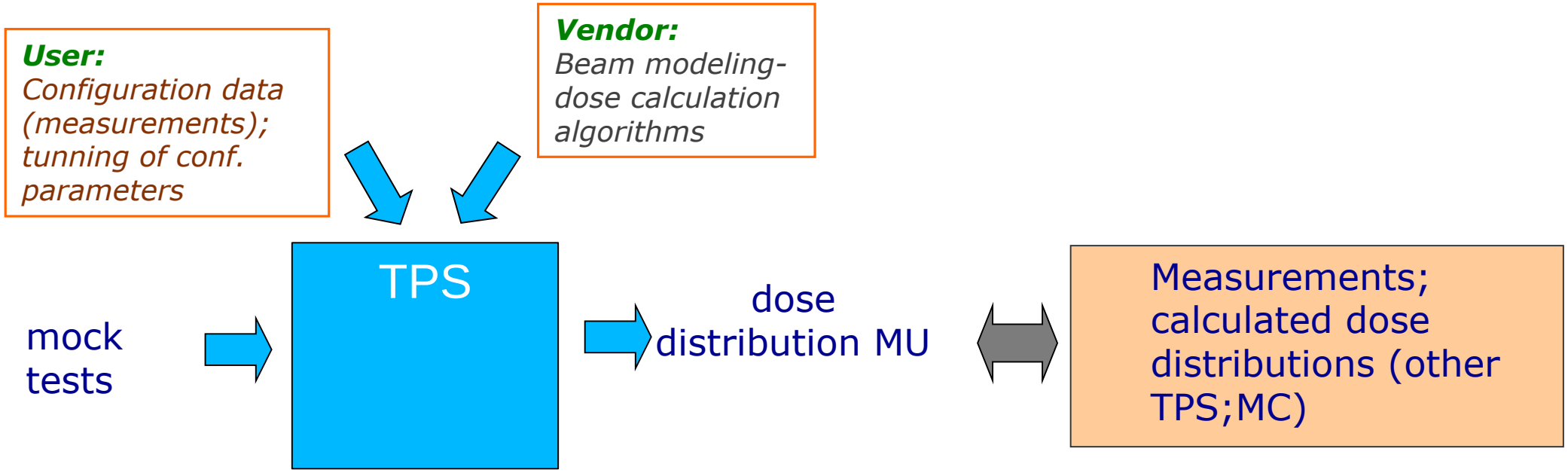

If Δ[output-standard]<tolerances

The TPS performs well

Testing dose calculation algorithms

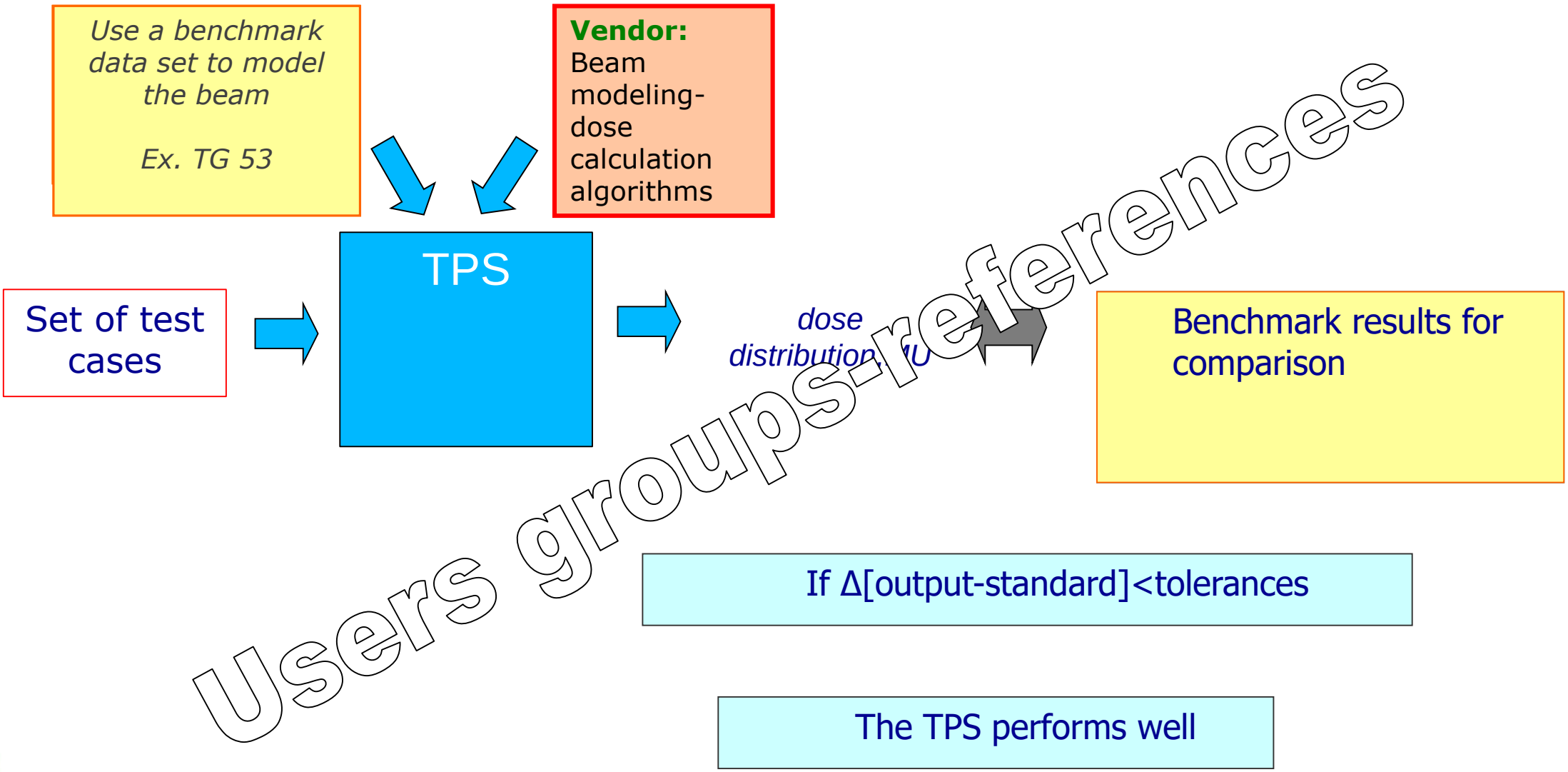

AAPM TG23 (1994): Beam data from two beams/13 test cases

3D test cases not included

wedge field case: 45º and normal incidence

asymmetric collimation not covered

absolute dose determination not included

AAPM TG53 (1998): Data set reviewed and upgraded

More tests are prepared i.e. 3D test included

NCS Beam Data set from two modern Elekta linacs (3 energies)

Possibility to adapt data set with latest technical developments.

Specific demands of basic beam data could be realized

New tests prepared

AAPM TG67 (to be published): update of beam data and test cases

TG 67 [Radiation Therapy Committee]

AAPM Radiation Therapy Committee Task Group 67 Benchmark Datasets for Photon Beams

CAX %dd, open fields	Open and wedge field profiles, in air	Output factors (Sc,p) at dmax
CAX %dd, wedge fields	Open field profiles, 2 SSD's	Output factors measured at 10 cm depth
CAX %dd, 90 cm SSD, open and wedged	Off axis HVL	Collimator factors (Sc)
Diagonal profile for max collimator setting, in phantom	MLC penumbra profiles	Phantom scatter factors (Sp) (either published data or values derived from Sc,p and Sc values)
Diagonal profile for max collimator setting, in air	MLC/Collimator jaw transmission	Collimator transmission
Diagonal profile for max square field	MLC setting and radiation field offset	Wedge transmission factors
Star profiles for max field size, open and wedge	Wedge profiles, nominal SSD	Tray transmission factors
Open field profiles, nominal SSD	Physical wedge dimensions	Absolute dose reference condition and value
Open field profiles, 90 cm SSD	Block edge profiles	Absolute dose for 100cm SSD

Performance testing – Test package example

Application of a test package in an intercomparison of the photon dose calculation performance of treatment planning systems used in a clinical setting

Jack Venselaar[a,*], Hans Welleweerd[b]

[a]Department of Radiotherapy, Dr B. Verbeeten Institute, P.O. Box 90120, 5000 LA Tilburg, The Netherlands
[b]Department of Radiotherapy, University Medical Center, P.O. Box 8500, 3508 GA Utrecht, The Netherlands

Received 26 May 2000; received in revised form 12 December 2000; accepted 9 January 2001

- Use of a common data set as input for 7 commercial planning systems
- Test package
- Comparison: Percentage deviations of the local dose except points ourside the penumbra or under blocs where the deviation was expressed relatively to the dose on the central axis of the open beam.
- Confidence límit:
- Tolerance: depending on the region

$$\Delta = |\text{average deviation}| + 1.5 \times SD$$

ESTRO School

Performance testing – example

Values of the criterion for the confidence limit for the different types of test geometries[a]

Description	Tolerance
	in % of local dose
1 Homogeneous, simple geometry	
Output factors	1
Central axis data of square fields	2
Off-axis data	3
2 Complex geometry (wedged fields, inhomogeneities, irregular fields, asymmetrical collimator setting)	
Central and off-axis data	3
3 More complex geometries, i.e. combinations of #2	
Central and off-axis data	4
	In % relative to the dose at the same depth, but at the central axis of the open beam
4 Outside beam edges	
In simple geometry	3
In complex geometry (see #2)	4
In more complex geometry (combinations of #2)	5

ESTRO School

Performance testing – drawnbacks of this approach

Advantages:

- The results only depend on beam modeling and the calculation algorithms as implemented in the TPS.
- Ideal for TPS comparison as avoids uncertainties due to different set of measurements performed at different sites at different times.

Disadvantages:

- Different planning systems need different data
- Some of them require tunning of parameters
- Need of modeling a “new beam” with no clinical application
- Difficult to have a good data set for beam configuration that can be used in all planning systems.

Performance testing – Beam model

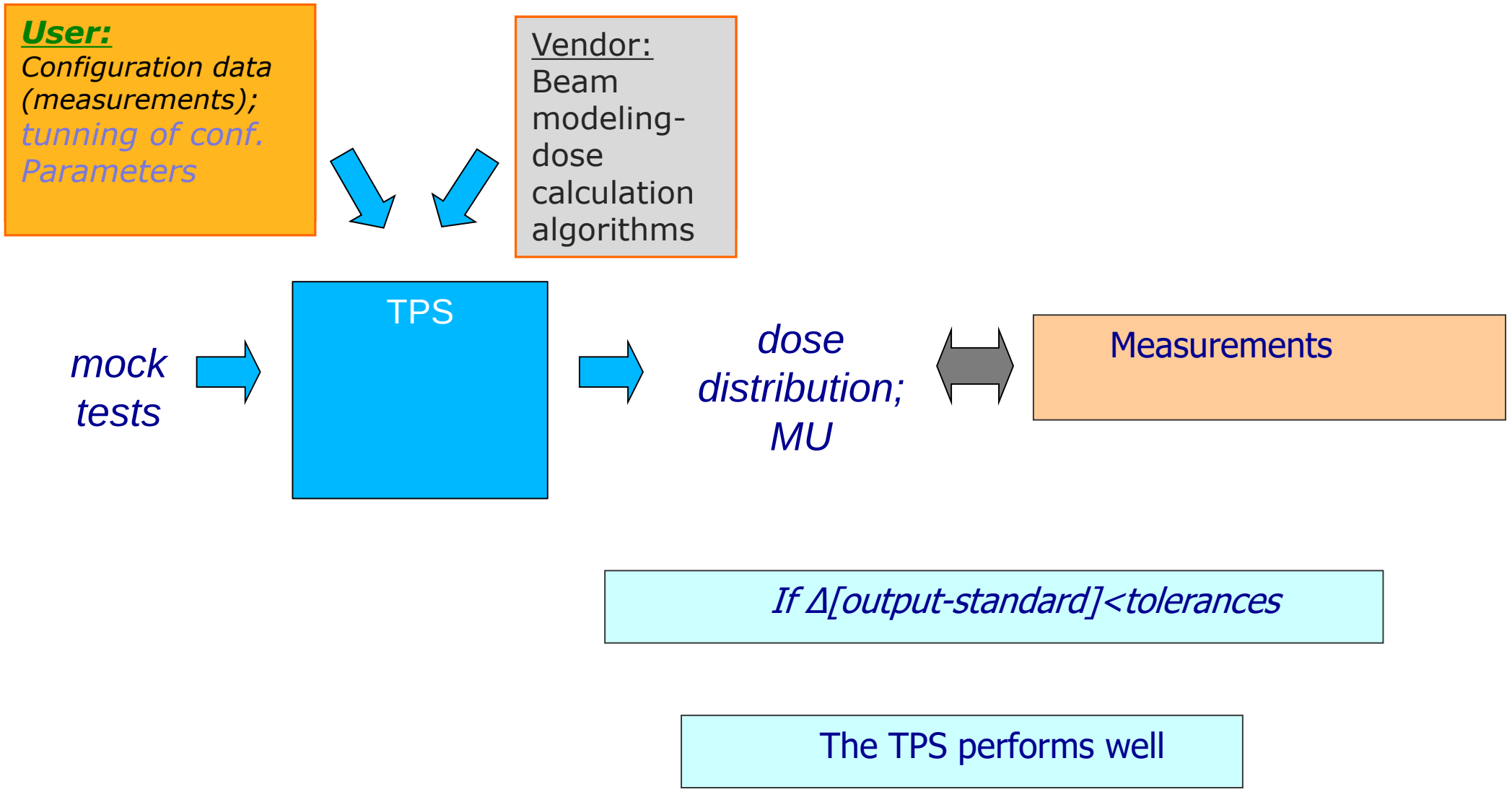

Performance testing – ex. Feed back configuration parameters

Automated beam model optimization

Daniel Létourneau[a] and Michael B. Sharpe
Radiation Medicine Program, Princess Margaret Hospital, Toronto, Ontario, Canada and Department of Radiation Oncology, University of Toronto, Toronto, Ontario M5G 2M9, Canada

Amir Owrangi
Radiation Medicine Program, Princess Margaret Hospital, Toronto, Ontario M5G 2M9, Canada

David A. Jaffray
Radiation Medicine Program, Princess Margaret Hospital, Toronto, Ontario M5G 2M9, Canada; Department of Radiation Oncology, University of Toronto, Toronto, Ontario M5S 2E3, Canada; and Department of Medical Biophysics, University of Toronto, Toronto, Ontario M5G 2M9, Canada

(Received 23 November 2009; revised 26 January 2010; accepted for publication 8 March 2010; published 22 April 2010)

Performance testing – ex. Feed back configuration parameters

Automated beam model optimization
Med Phys 37 (2010)

Background

- Beam model accuracy for IMRT calculation (calculation performance depends on the tunning by the user of multiple parameters
- Pinnacle (Philips Medical Systems)
- IMRT and SBRT requirement of measurement data for TPS commissioning and beam model accuracy have increased.

Aim

- Development and validation of an automated beam model optimisation system (ABMOS)

Performance testing – ex. Feed back configuration parameters

User:
Configuration data (measurements); tunning of conf. Parameters

Vendor: Beam modeling- dose calculation algorithms

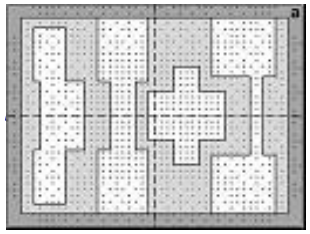

TPS

Planar fluence prediction

High resolution 2D array measurements

MapCheck (Sun Nuclear) sampling 0.2 mm

Configuration parameters

Jaw and MLC transmission
Radiation source size
Extrafocal radiation contribution
MLC rounded lef-end transmission

Cost function= 1-Gamma evaluation pass rate

2%-1mm Th 10% Tolerance 85% points

ESTRO School

Automated beam model optimization

Med Phys 37 (2010)

Results

TABLE II. Comparison of beam model parameter values for the initial and the optimized beam model for the Synergy S treatment unit.

Beam model parameters		Initial beam model	Optimized beam model
MLC transmission:	$\%T_{MLC}$ (%)	0.400	0.175
Jaw transmission:	$\%T_{X\text{-jaws}}$ (%)	0.400	1.590
	$\%T_{Y\text{-jaws}}$ (%)	0.400	1.590
MLC interleaf leakage:	L_{height} (%)	2.000	2.208
	L_{width} (cm)	0.150	0.071
Orthogonal source size:	S_X (cm)	0.035	0.066
	S_Y (cm)	0.035	0.042
Extrafocal scatter source:	G_{height} (%)	8.500	8.500
	G_{width} (cm)	1.850	1.850
Second degree polynomial:	a	-1.140×10^{-3}	-1.630×10^{-3}
$(\mathrm{Pos}(z)=az^2+bz+c)$	b	-1.530×10^{-5}	-1.530×10^{-5}
(Rounded leaf-end correction)	c	6.996×10^{-2}	6.235×10^{-2}

IMRT beam pattern

46.1% to 87.3%

Pretreatment results

(3%-2mm Th 10%)

Prostate: 91.4% to 98.2%
Paraspinal: 77.1% to 96.4%

ESTRO School

Performance testing – ex. Accuracy of configuration data-volume averaging

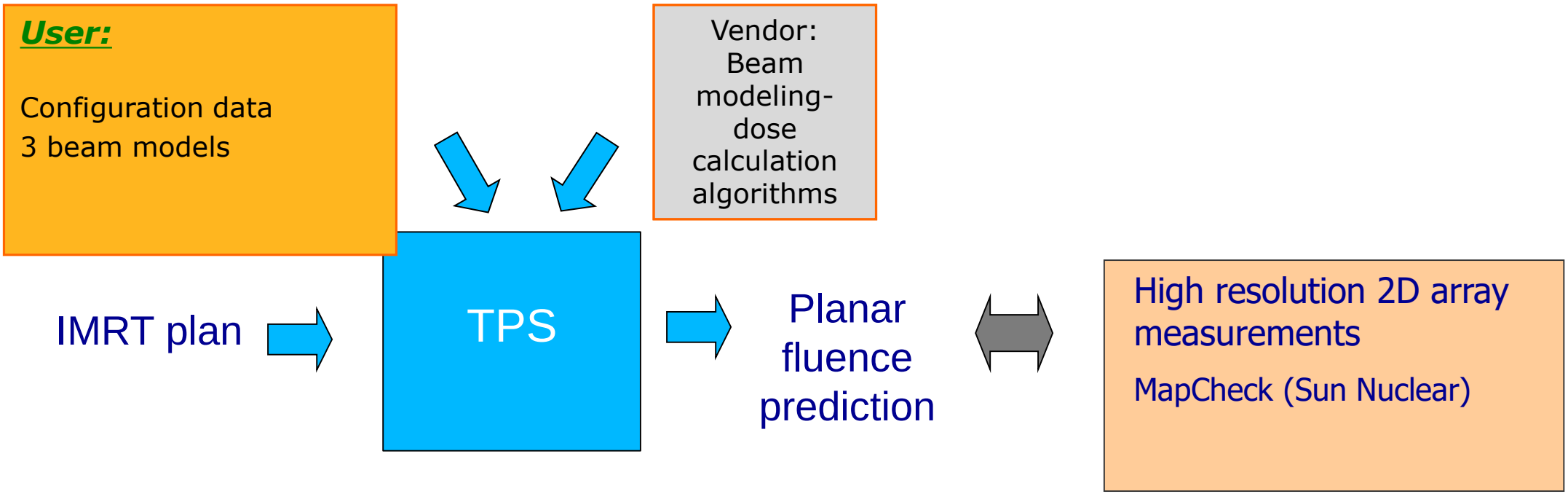

Three beam models (profiles)

- 6mm diameter ion chamber
- 4mm diameter ion chamber
- True profiles (analytic fitting/deconvolution)

Gamma analysis (3%-3mm)

Guanghya Yan et al. Med Phys 35(8) 2008

ESTRO School

Performance testing – ex. Accuracy of configuration data-volume averaging

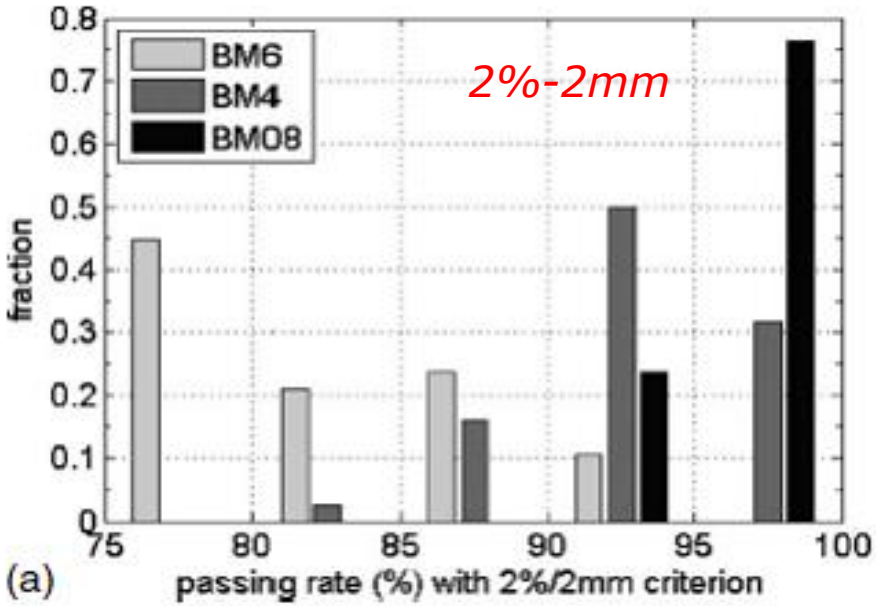

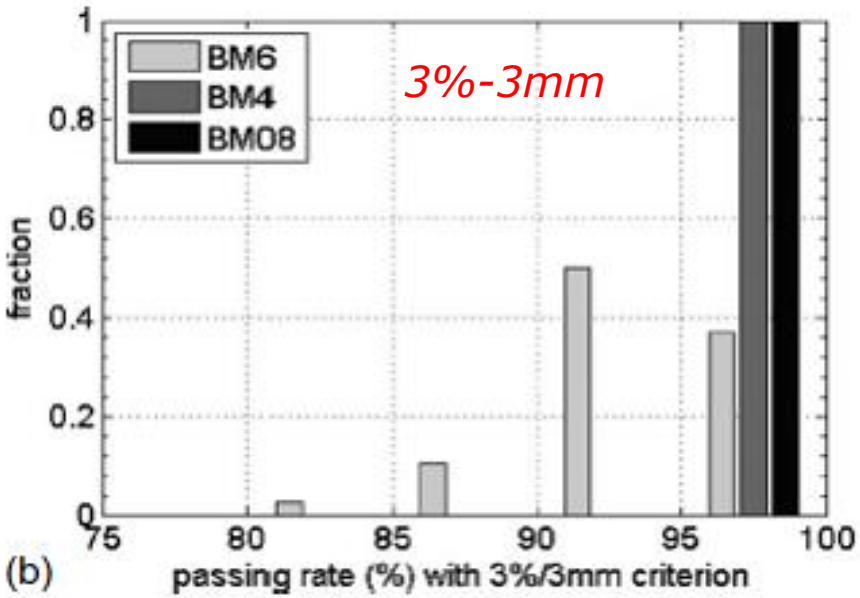

Gamma analysis (2%-2mm; 3%-3mm)

Three beam models (profiles)

- 6mm diameter ion chamber (BM6)
- 4mm diameter ion chamber (BM4)
- True profiles (analytic fitting/deconvolution)(BM08)

The use of the appropiate detector has a direct impact in the results of gamma evaluation; agreement between planning and delivery

Guanghya Yan et al. Med Phys 35(8) 2008

ESTRO School

Performance testing: Small field dose calculation accuracy for general purpose TPS

General purpose TPS are not necessarily designed to be used in small fields

ESTRO School

Performance testing: Small field dose calculation accuracy for general purpose TPS

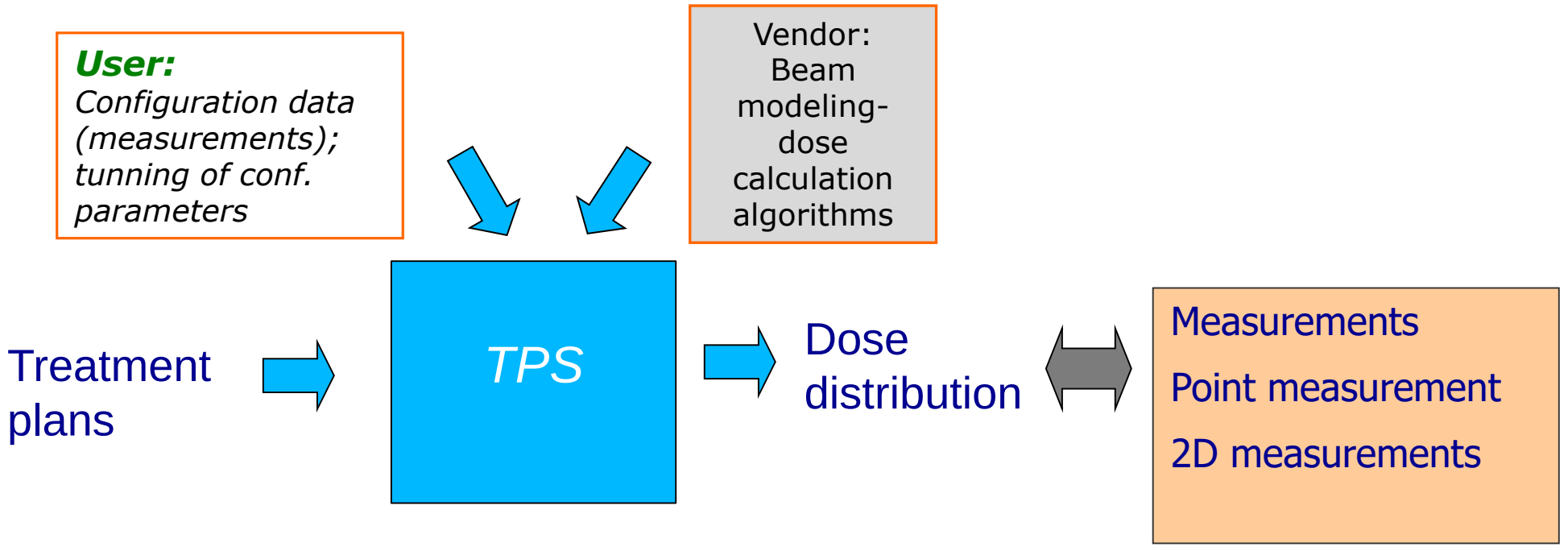

Dose differences and Gamma analysis (3%-2mm)

Flogliata et al. Med Phys 35(8) 2008

ESTRO School

Small field dose calculation accuracy

General purpose TPS are not designed to be used in small fields

Design performance tests to check the capability of the calculation algorithms for small fields

- Define the conditions for the test:
  - simple/baseline conditions
  - treatment plans
- Select the data against which the TPS calculation will be compared (reference data)
  - Measurements: detector/phantom
  - Calculation: other TPS/algorithm; MC...
- Compare TPS calculation with the reference data;
  - Tolerance levels.

ESTRO School

Small field dose calculation accuracy

Accuracy of Acuros XB and AAA dose calculation for small fields with reference to RapidArc® stereotactic treatments

Antonella Fogliata,[a)] Giorgia Nicolini, Alessandro Clivio, Eugenio Vanetti, and Luca Cozzi
Oncology Institute of Southern Switzerland, Medical Physics Unit, CH-6500 Bellinzona, Switzerland

(Received 5 July 2011, revised 25 August 2011; accepted for publication 4 October 2011, published 27 October 2011)

- **Define the conditions for the test**:

  simple/baseline conditions

  treatment plans

- **Select the data against which the TPS calculation will be compared** (reference data)

  Measurements: detector/phantom

  Calculation: other TPS/algorithm; MC...

- **Compare TPS calculation with the reference data;**

  Tolerance levels. 3%-2mm (>95% points)

ESTRO School

User:
Configuration data (measurements); tunning of conf. parameters

Vendor:
Beam modeling-dose calculation algorithms

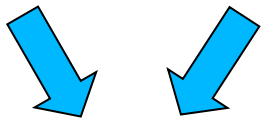

TPS

Patient cases

Rapid Arc IMRT Eclipse
PTV (0.3-7 cm^3)
Single partial arc (110º-250º)
2Gy at isocenter
Maximum dose rate:600MU/min

Dose distribution

Measurements
Point measurement
2D measurements

Dose differences and Gamma analysis (3%-2mm)

Optimisation and dose calculation using different:

DLG (dosimetric leaf gap)
LT (leaf transmission)
Spot size parameter (0, 0.5, 1, 2 mm)
Acuros XB and AAA.

Flogliata et al. Med Phys 35(8) 2008

Measurements

Point measurements: PTW-Octavius phantom-Diamond detector at the isocenter

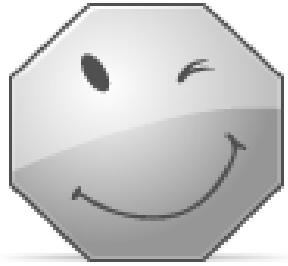

polystyrene

2D dose distributions: EPID+GLAaS algorithm

Results evaluation

Compare TPS calculation with the reference data; tolerance levels:

Point measurements:

Measurement compared to the mean dose in a circular structure of 4mm diameter (simulation of the detector sensitive area)

2D measurements:

2D gamma analysis (2mm;3% of the maximum dose; evaluation inside the jaw setting, no low dose threshold).

Results

The DLG has a higher impact on discrepancies

The best results are obtained for DLG 2mm and TL 1.4%

This applies for the two algorithms

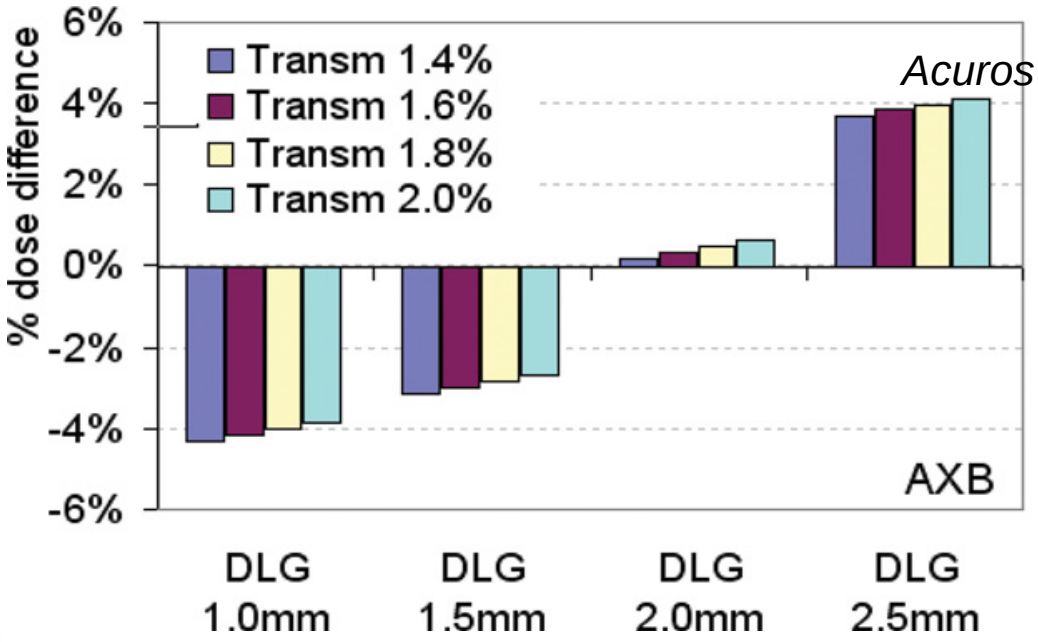

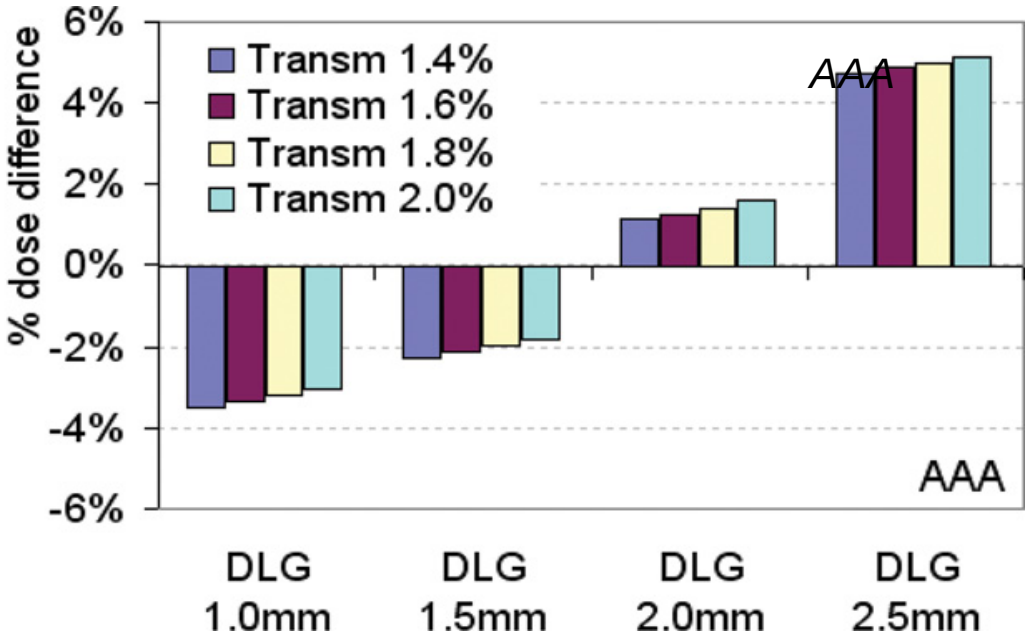

Results

Spot size

AAA: 0-2 mm
Acuros XB: 0.5-1mm-2 mm

Default values in red

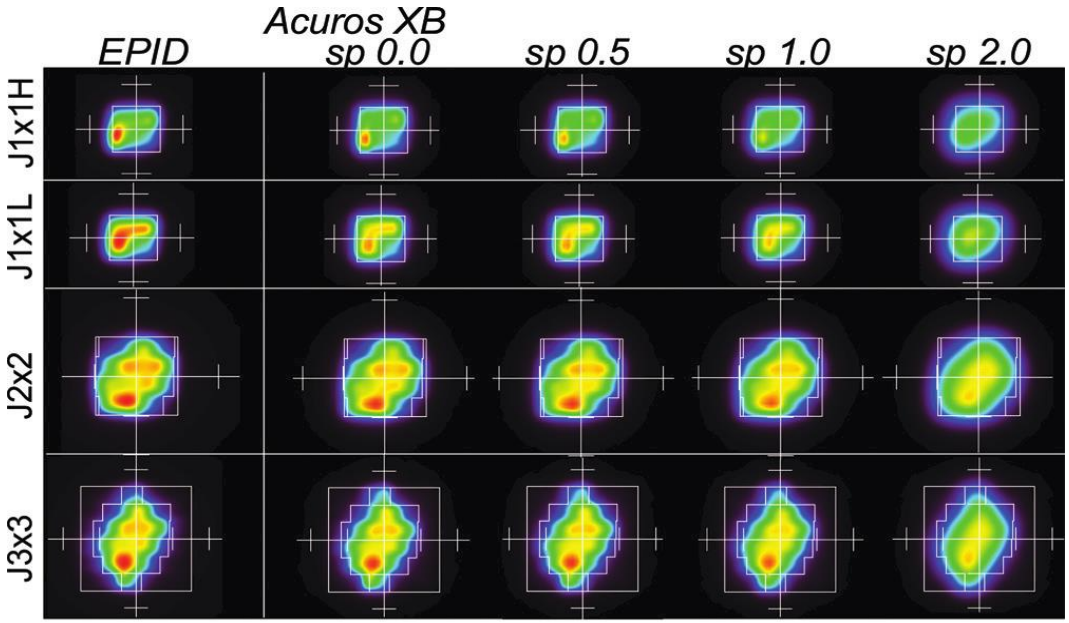

Acuros

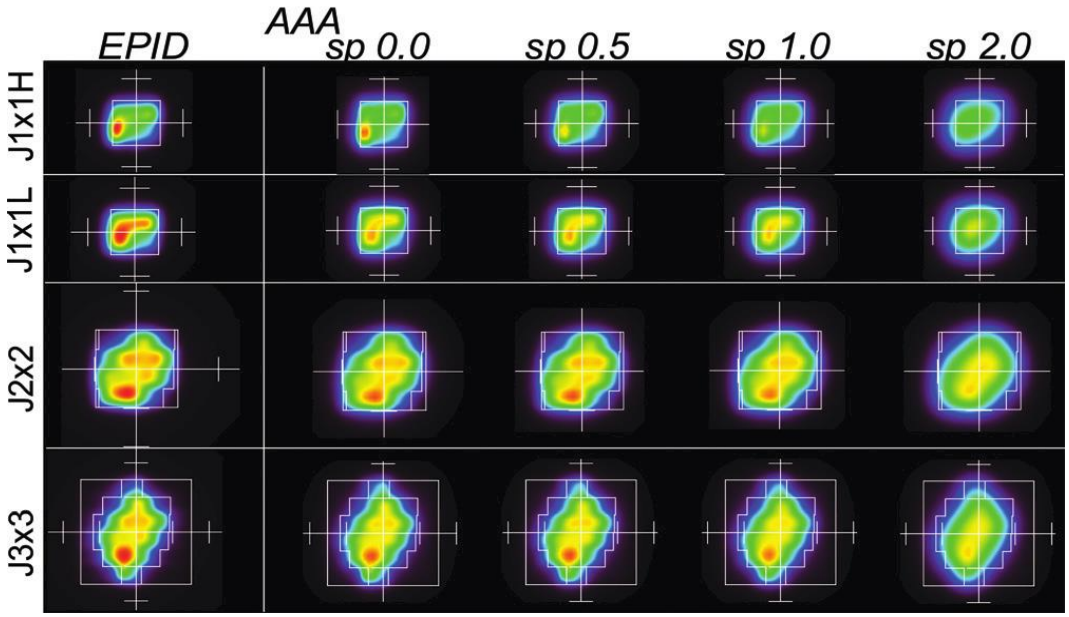

AAA

Stereotactic specific configuration including OF for small fields (MU calculation).

Modify the Spot size to a value between 0.5-1 mm.

ESTRO School

Performance testing new TPS version-upgrade or routine QA

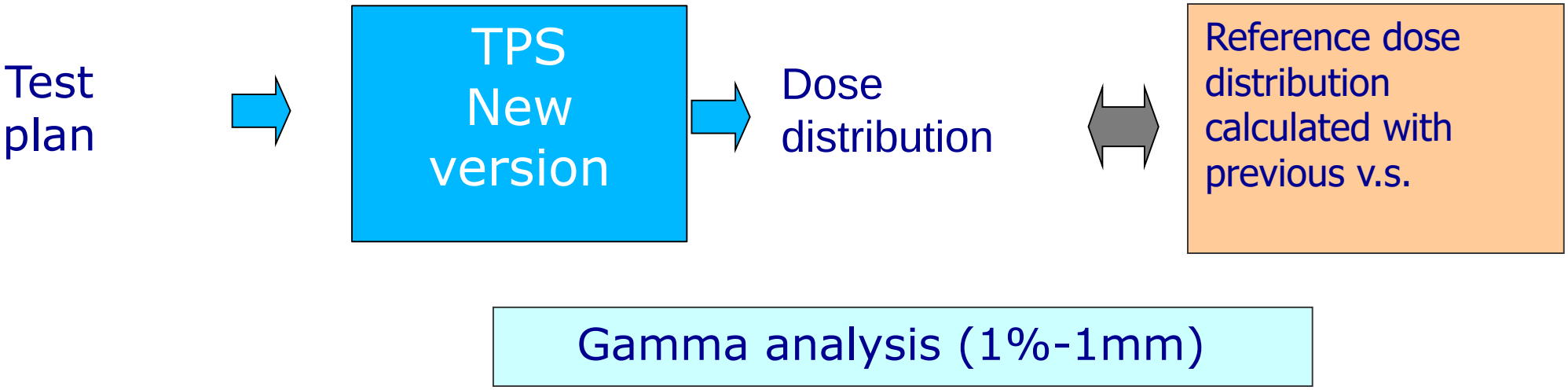

Change of vs: Example Eclipse

$$I_1 = \sqrt{\frac{1}{4N}\sum_{i=1}^{N}\left\{\left(\frac{\Delta z_{\max}}{1\text{mm}}\right)^2 + \left(\frac{\Delta z_{50}}{1\text{mm}}\right)^2 + \left(\frac{\Delta D_{10}}{1\%}\right)^2 + \left(\frac{\Delta D_{20}}{1\%}\right)^2\right\}_i}$$

$$I_2 = \sqrt{\frac{1}{6N}\sum_{i=1}^{N}\left\{\Delta d_{20}^2 + \Delta d_{50}^2 + \Delta d_{80}^2 + \Delta d'^2_{20} + \Delta d'^2_{50} + \Delta d'^2_{80}\right\}_i}$$

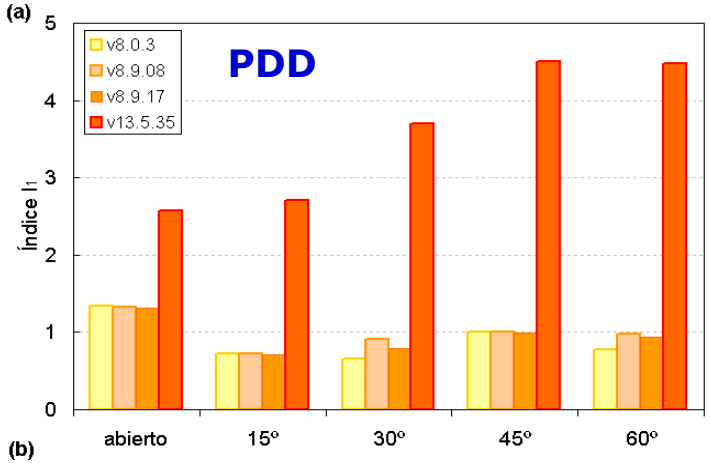

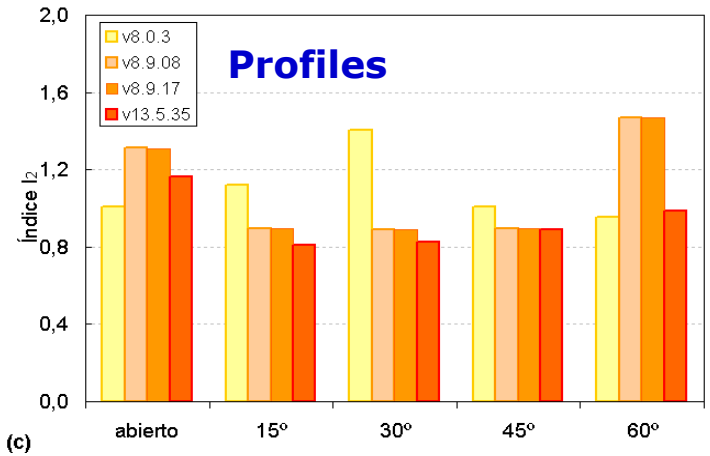

(c)

$$I_3 = \sqrt{\frac{1}{N}\sum_{i=1}^{N}\Delta D_{\text{abs}}^2}$$

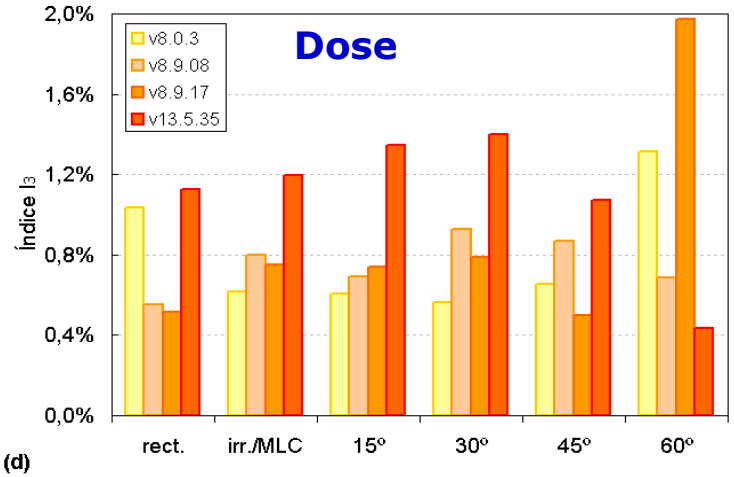

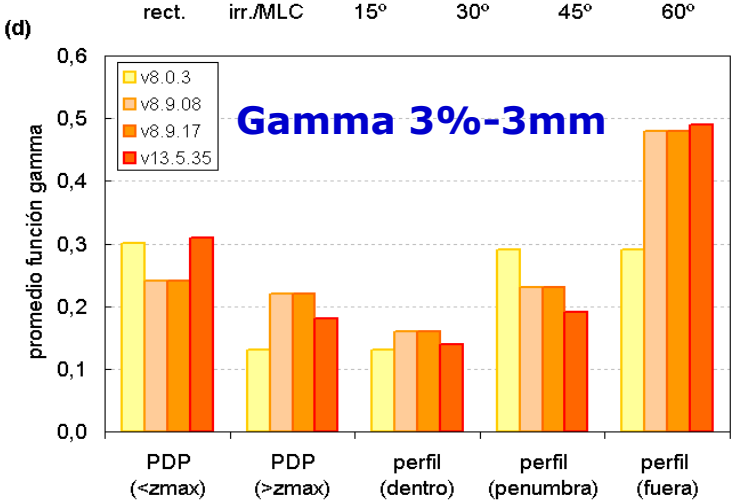

PDD differences up to 8mm and 3%.

MU differences up to 2%

Vs 13.5 uses a calculated spectra while the previous vs use a theoretical spectra.

Thanks to Artur Latorre-Mussoll Servei de Radiofisica Hospital Sant Pau

ESTRO School

Regular QA is needed to ensure dose calculation consistency

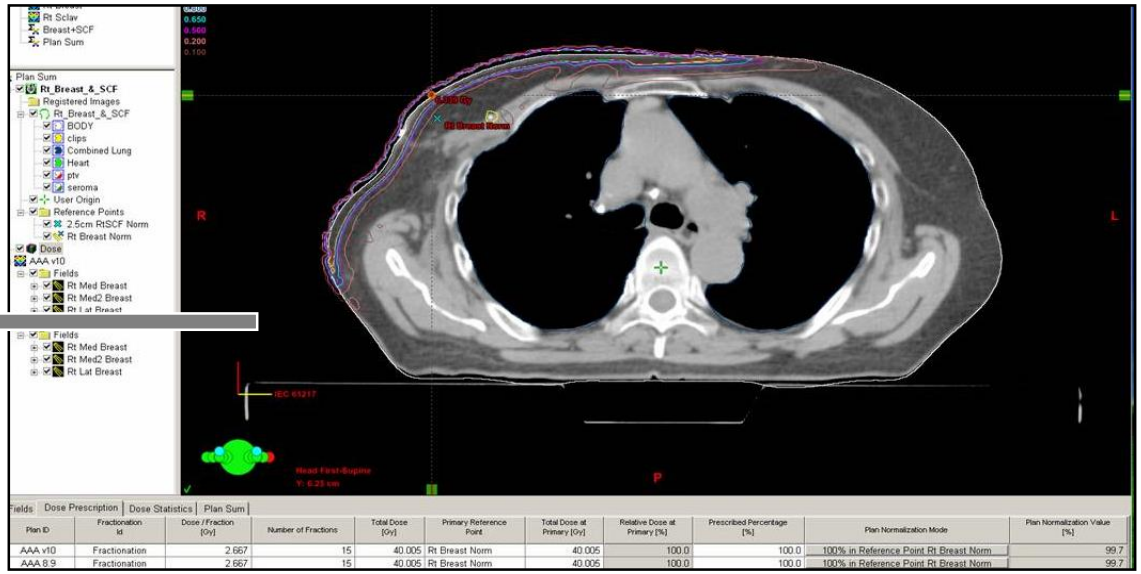

Plan ID	Fractionation Id	Dose / Fraction [Gy]	Number of Fractions	Total Dose [Gy]	Primary Reference Point	Total Dose at Primary [Gy]	Relative Dose at Primary [%]	Prescribed Percentage [%]	Plan Normalization Mode	Plan Normalization Value [%]
AAA v10	Fractionation	2.667	15	40.005	Rt Breast Norm	40.005	100.0	100.0	100% in Reference Point Rt Breast Norm	99.7
AAA 8.9	Fractionation	2.667	15	40.005	Rt Breast Norm	40.005	100.0	100.0	100% in Reference Point Rt Breast Norm	99.7

Subtraction plans for routine QA or after a version change

Check dose distribution and also MU

Tolerance 1%-1mm

If larger differences are observed RECOMMISSIONING

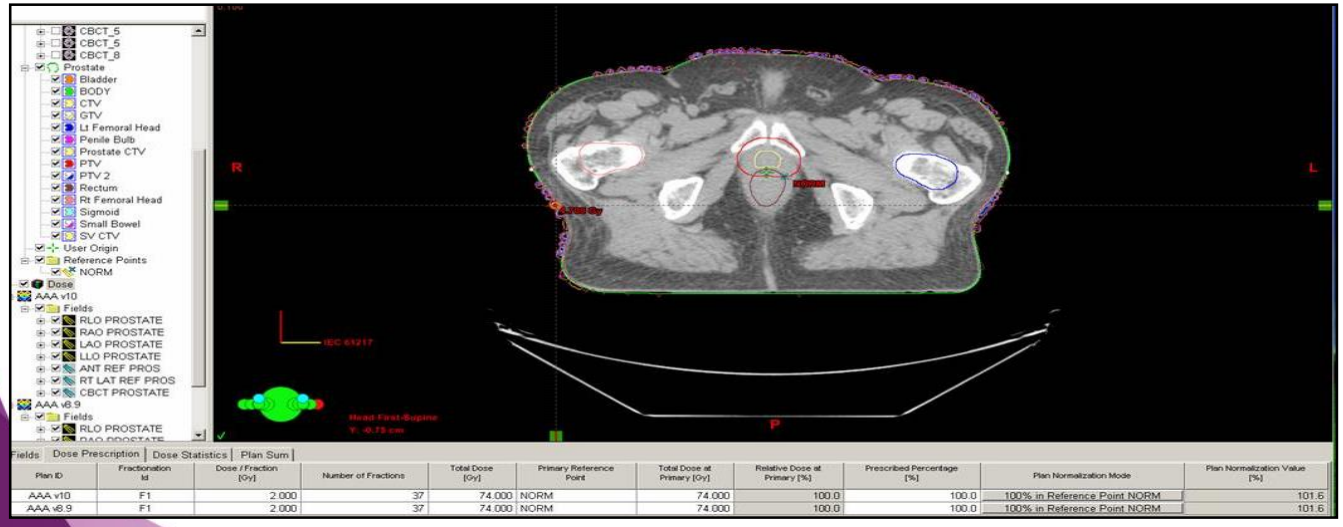

Plan ID	Fractionation Id	Dose / Fraction [Gy]	Number of Fractions	Total Dose [Gy]	Primary Reference Point	Total Dose at Primary [Gy]	Relative Dose at Primary [%]	Prescribed Percentage [%]	Plan Normalization Mode	Plan Normalization Value [%]
AAA v10	F1	2.000	37	74.000	NORM	74.000	100.0	100.0	100% in Reference Point NORM	101.6
AAA v8.9	F1	2.000	37	74.000	NORM	74.000	100.0	100.0	100% in Reference Point NORM	101.6

ESTRO School

Summary-Recap

- TPS has a direct effect on patient outcome so a high quality QA process is essential
- Enormous number of parameters involving physics – getting the answers to these questions???
- Role of the QMP is critical
  - Understand models and limitations
  - Ensure TPS is used consistent with linac commissioning data
  - Ensure high quality input data
  - Awareness of changes anywhere in the RT Chain
  - Design QA process *for your clinic*
  - Training at start and on -going essential
- Establish periodic QC programme
- External audits

ESTRO School

Design QA process *for your clinic*

- Think on the clinical situation for which the TPS will be used
- Design tests that mimic these clinical situations
- Think carefully on which data/measurements will you use as reference for comparison and on the method for comparison.
- Clearly define tolerances to confirm that your TPS perfoms well.

ESTRO School

References

Guidelines/International recommendations:

Frass B, Doppke K, Hunt M, et al. American Association of Physicists in Medicine Radiation Therapy Committee Task Group 53; Quality Assurance for Clinical Radiotherapy treatment planning. Med Phys 1998;25(10): 1773-1829

International Atomic Energy Agency. Commissioning and quality assurance of computerized planning systems for radiation treatment of cancer. TRS 430. Vienna: International Atomic Energy Agency;2004

International Atomic Energy Agency. Commissioning of Radiotherapy Planning Systems: Testing for typical external beam treatment techniques. IAEA TECDOC 1583. Vienna; International Atomic Energy Agency; 2008

Mijhneer B, Olszewska A, Fiorino C, et al. ESTRO booklet nº7 Quality Assurance of treatment planning systems-practical examples for non-IMRT proton beams;2004 [free download from ESTRO webpage].

Smilowitz JB, Das IJ, Feygelman V, et al. AAPM Medical Physics Practice Guideline 5.a: Commissioning and QA of Treatment Planning Dose Calculations-Megavoltage Photon and Electron Beams. JAMP 2016; 17(1):14-34

ESTRO School

DVH and Dose based metrics

Brendan McClean

Feidhmeannacht na Seirbhíse Sláinte
Health Service Executive

Saint Luke's
Radiation Oncology
Network

Learning Objectives

- Identify the need for accurate DVH construction
- Investigate the limitations and assumptions of DVH calculation
- Examine QC requirements for DVH use

The ideal DVH(?)

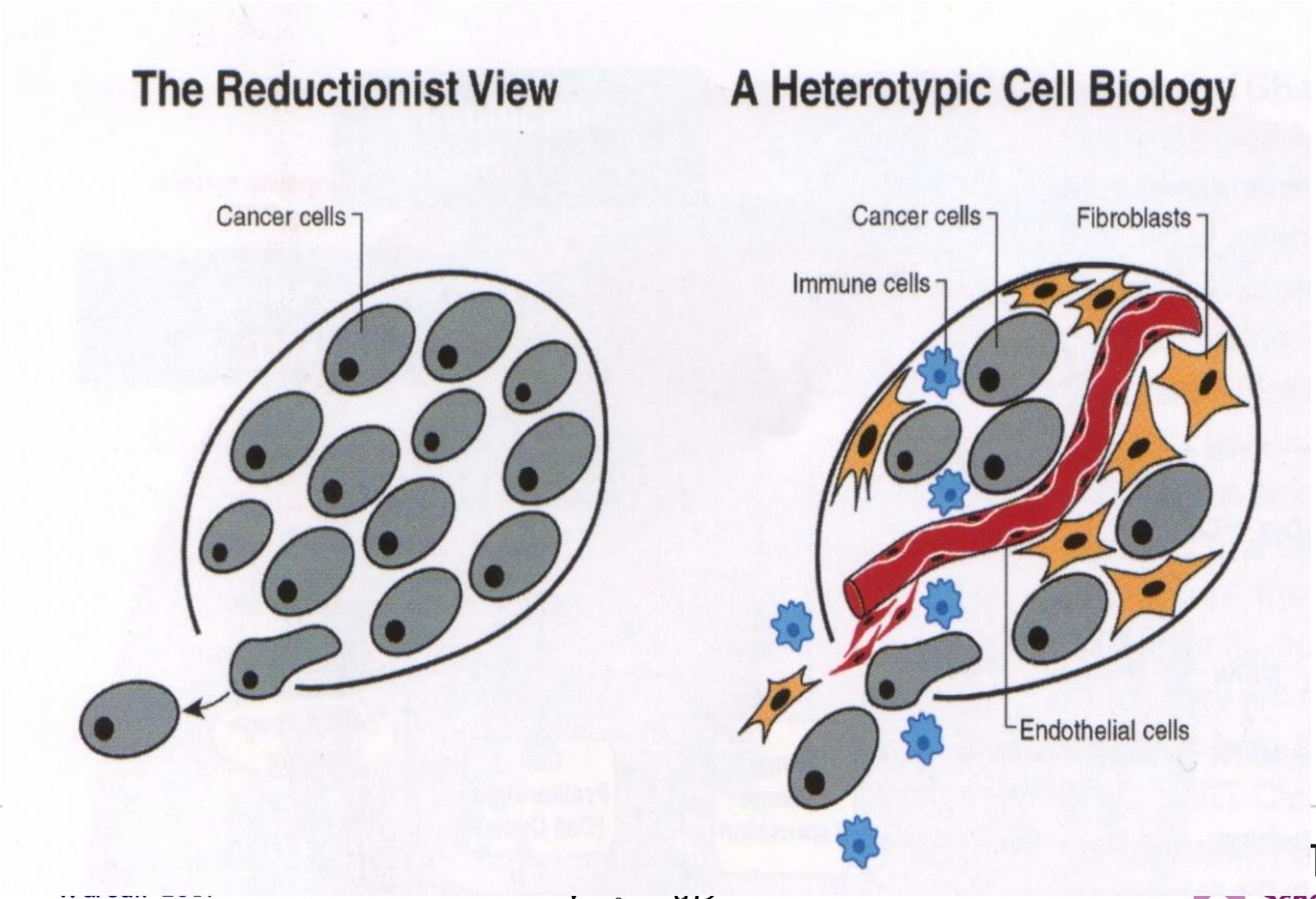

Potential downsides of DVH

- Loss of organ specific spatial information
  - Single hot spot vs multiple hot spots?
  - Assume all regions are of equal functional importance
- Does not consider fraction size variations
- Does not account for changes during treatment
- Image segmentation differences among clinicians, dose calculations algorithms, patient populations, preferred beam arrangements, whole course DVH's for OAR risk etc.
- Comparison with Gamma Analysis?

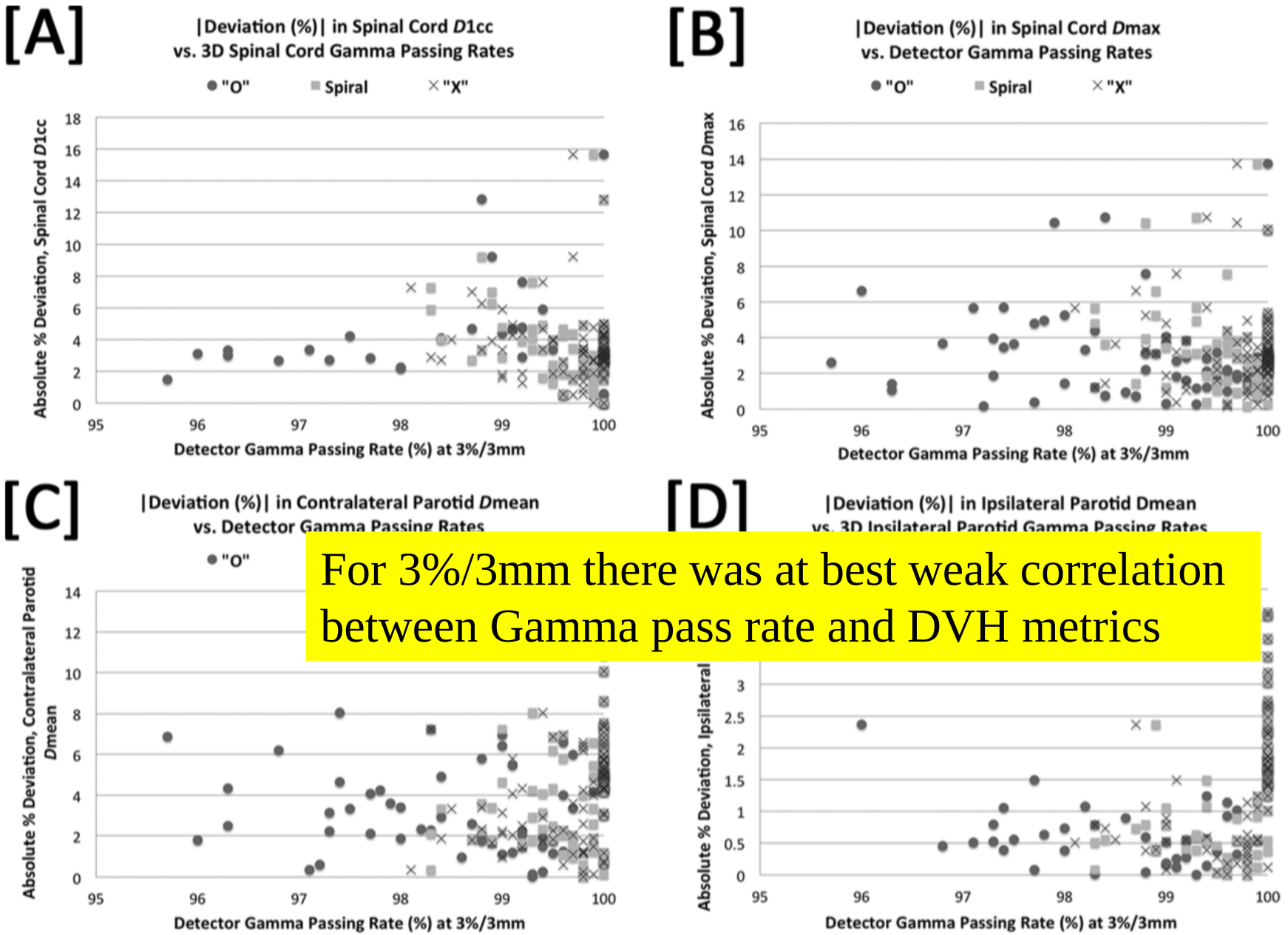

For 3%/3mm there was at best weak correlation between Gamma pass rate and DVH metrics

Need Accurate DVH's…..

- Various metrics calculated from DVH
  - *Calculation of biological indices*
- Used to correlate local control
  - *Clinical Trial outcome analysis*
- Used to report dose homogeneity
- IMRT Optimisation (Dose Volume Constraints)
- Used to correlate with morbidity for OAR's
  - *Clinical decisions are based on these*
- Used to develop dose constraints for prospective treatment planning
- Move from passing rates to DVH based QA metrics?
- ***Accuracy in DVH construction essential***
  - Need dose calculation to compute dose in small fields, inhomogeneous tissue, non-equilibrium regions
  - **'Use of dose volume reporting is dependent on accurate dose calculation algorithms' (ICRU83)**

Marks et al, IJROBP vol 76 No.3 S10-S19

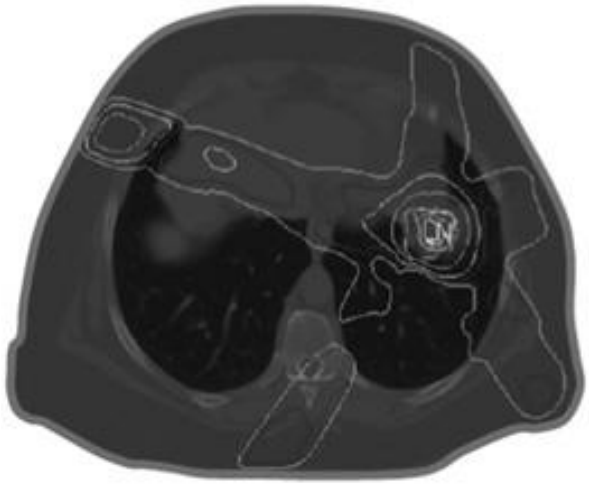

3D dose distribution

Discard spatial, anatomic, physiologic data

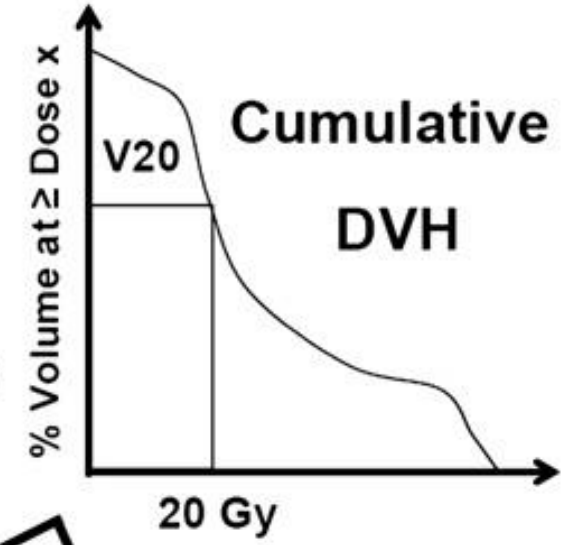

Extract unambiguous data

- Single Point: e.g. V20
- Global: e.g. mean dose

Compute model-based NTCP estimates

Sample DVC's (Head and Neck)

Patient Name: <Full Name>

Patient ID Number: <Patient Id 1>

Consultant: <Primary Care Physician Name (Default)>

Date of Birth:

Date: <Current Date>

Diagnosis: <All Primary Diagnoses With Staging Info (Default)>

Dose	95%	107%
70	66.5	74.9
63	59.9	67.4
60	57.0	64.2
56	53.2	59.9
50	47.5	53.5
46	43.7	49.22

Dose PTV1	Fractions	Dose PTV2	Fractions	Dose PTV3	Fractions
Gy		Gy		Gy	

EVALUATION OF PTV 3DCRT

	Dose	Optimal	Acceptable Variation	Result	D2%	D50%	D98%
PTV1	D_{min} D_{max}	≥95% <107%	>90% <110%	% %			
PTV2	D_{min} D_{max}	≥95% <107%	>90% <110%	% %			

EVALUATION OF PTV/GTV for IMRT/VMAT

	Dose	Optimal	Acceptable Variation	Result	D2%	D50%	D98%
gtvpri70	$V_{95\%}$	>100%	N/A	%	N/A	N/A	N/A
gtvnrt70	$V_{95\%}$	>100%	N/A	%	N/A	N/A	N/A
gtvnlt70	$V_{95\%}$	>100%	N/A	%	N/A	N/A	N/A
ptv1	$V_{95\%}$ D_{max}	>99% <107%	>95% <110%	% %			
evalptv2 (NA for SIB)	$V_{95\%}$ D_{max}	>99% <107%	>95% <110%	% %			
Evalptv3 (NA for SIB)	$V_{95\%}$ D_{max}	>99% <107%	>95% <110%	% %			

evalptv1	cc @ 107%	<1.5cc	<6.5cc	cc
evalext-ptv	cc @ 110%		<1cc[22]	cc

OAR	Dose	Constraint Optimal	Acceptable Variation	Result		Toxicity Endpoint
Spinal cord	D_{max}	<45Gy[22]	<50Gy[13] (0.2%) <60Gy[13] (6%risk) <69Gy[13] (50%risk)	Gy		0.2% myelopathy
Spinal cord 4mm	D_{max}	<47Gy	50Gy<1cc[22]	Gy		
Brainstem	D_{max} D_{1-10cc}	<54Gy[3+23]	60Gy[23] (0.03cc) <59Gy[3] (risk<5%)	Gy Gy		Neuropathy /necrosis
Brainstem 3mm	D_{max}	<54Gy[22]	<60Gy[22] (<1%)	Gy		
Chiasm	D_{max}	<54Gy[1-3]	55-60Gy[1+2] (Risk3-7%) >60Gy[1+2] (Risk7-20%)	Gy		Optic Neuropathy
Chiasm 3mm	D_{max}	<54Gy[22]		Gy		
Pituitary	D_{max}	<45Gy	<50Gy[12]	Gy		Panhypo-pituitarism
Temporal Lobe	$D_{0.5cc}$	<69Gy[21]				
pharyngeal constrictors	D_{mean}	≤50Gy[20]	<60Gy[20]	Gy		Symptomatic dysphagia and aspiration
mandible ptv	D_{max}	<70Gy[17] or prescribed dose	<73Gy to 1.5cc <75Gy to 1cc[22]	Gy		
Oral cavity ptv	D_{median}	<46Gy[16]		Gy		
				Left	**Right**	
Parotid[18]	D_{mean}	<25Gy[17-19]	<26Gy[17-19]	Gy	Gy	Long-term salivary function<25%
	V_{30Gy}	<50%[17-19]		Gy	Gy	
Cochlea	D_{mean}	<45Gy[10-11]		Gy	Gy	Sensory-neural hearing loss
Eye	D_{max}	<50Gy[4]		Gy	Gy	Retinopathy
Lens	D_{max}	<6Gy[4-5]		Gy	Gy	Cataract
Optic Nerve	D_{max}	<54Gy[1-3]	55-60Gy[1+2] (Risk3-7%) >60Gy[1+2] (Risk>7-20%)	Gy	Gy	Optic Neuropathy
Optic Nerve 3mm	D_{max}	<54Gy[22]		Gy	Gy	

(some) Dose metrics from DVH's

D_{50} is close to 'old' ICRU reference point

ICRU 83

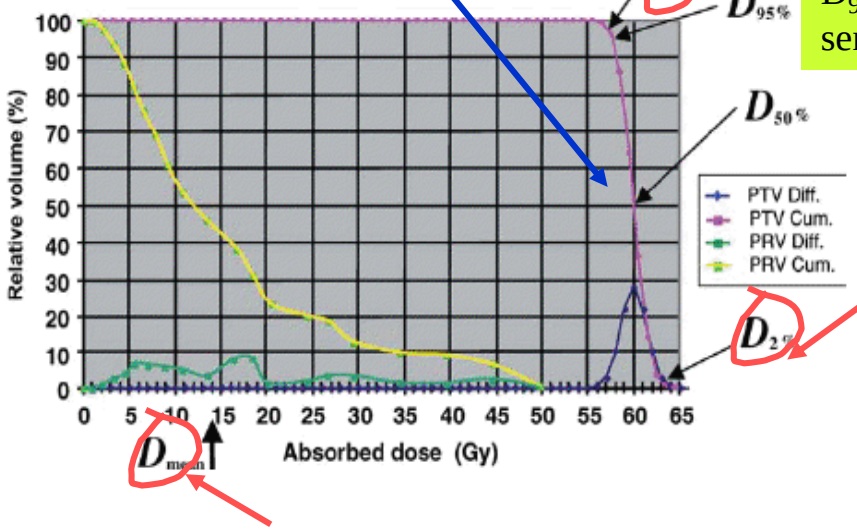

$D_{98\%}$ 'near minimum' since $D_{100\%}$ is highly sensitive to calculation and accuracy of CTV

$D_{2\%}$ 'near maximum' rather than previous maximum absorbed dose

$$HI = \frac{D_{2\%} - D_{98\%}}{D_{50\%}}$$

$$D_{mean} = \frac{1}{V}\int_0^{D_{max}} D\frac{dV(D)}{dD}\,dD$$

D_{median} is dose received by 50% of volume
If differential DVH is symmetric and unimodal for PTV then median and mean doses are nearly the same

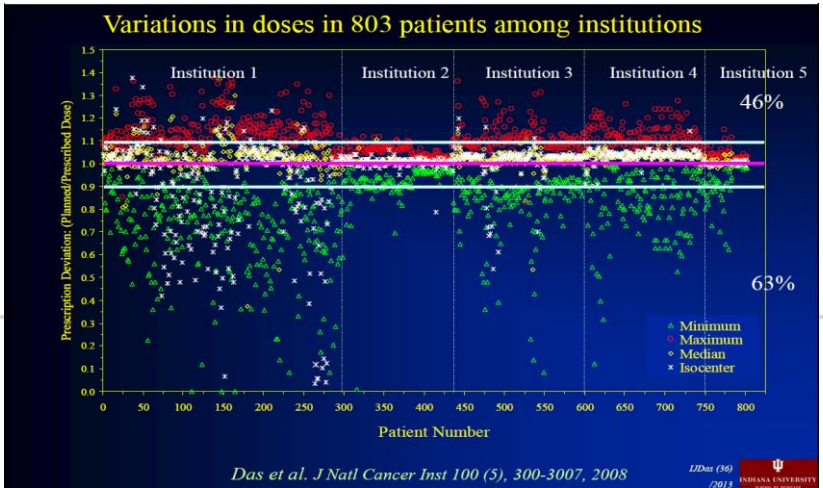

Reduction of DVH to a single relevant parameter

- Only if there is a volume effect model of dose response
  - Most common is a power law
  - $D_v = D_1 \, v^{-n}$

- NTCP varies with dose
- For a given dose, the NTCP is dependent on the fraction of volume irradiated - partial volume effect

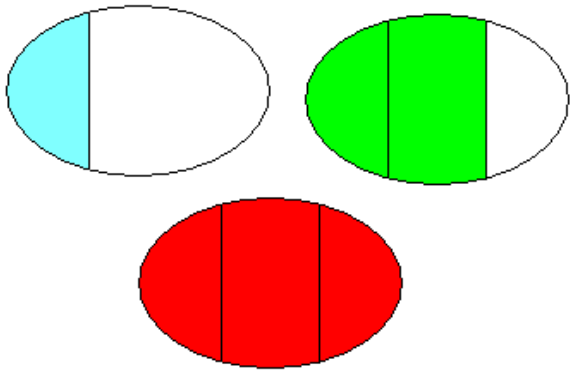

Irradiation to 1/3, 2/3 and 3/3 of the Volume

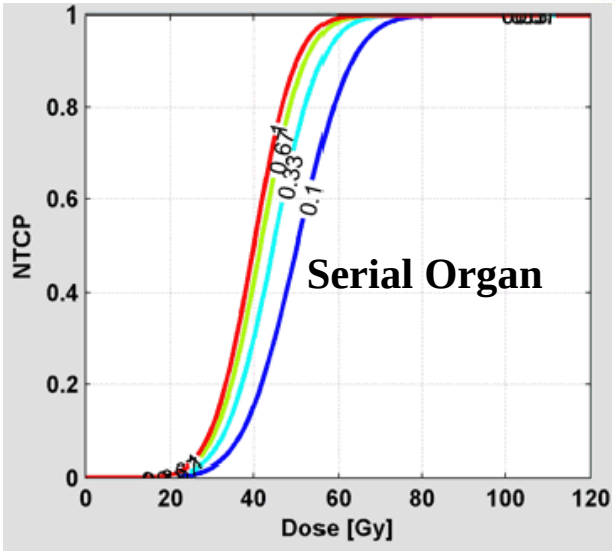

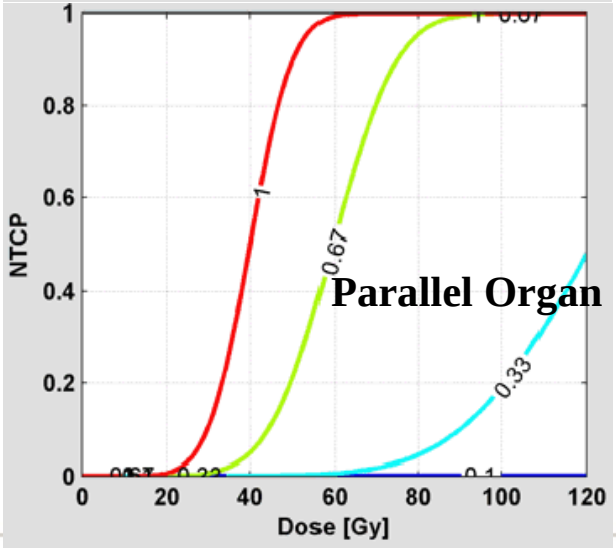

Power Law

$$\frac{D_i^{WO}}{D_i} = \left(\frac{v_i}{v_{total}} \right)^n \qquad D_i^{WO} = D_i (v_i)^n$$

D^{WO}_i = Dose to the Whole Organ

D_i = Dose to the partial volume when the NTCP is the same as the Dose to the whole organ

v_i = volume expressed in fractions

n = tissue specific parameter that describes organ architecture dependence

DVH Reduction

- Power Law gives a relationship between Dose and fractional volume while keeping the NTCP constant

- As a result we can transform the DVH by…
  - Converting bin doses to an equivalent dose to the whole organ (D_{eff} method)

    OR
  - Converting bin volumes into volumes for a particular reference dose (V_{eff} method)

- Then: Substitute V_{eff} or D_{eff} into Lyman Equations to get NTCP as dose is now uniform to organ

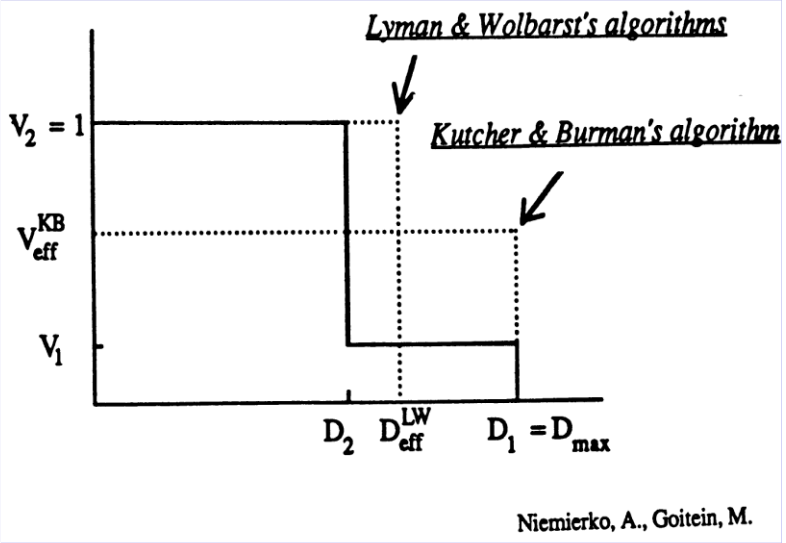

Assumes each dose bin obeys Power Law
Uniform irradiation to each dose bin

Histogram Reduction Method

* **Reduces a non-uniform dose distribution to an equivalent uniform dose to a partial volume**

$$V_{eff} = \sum \left(\frac{D_i}{D_m} \right)^{\frac{1}{n}} \Delta V_i$$

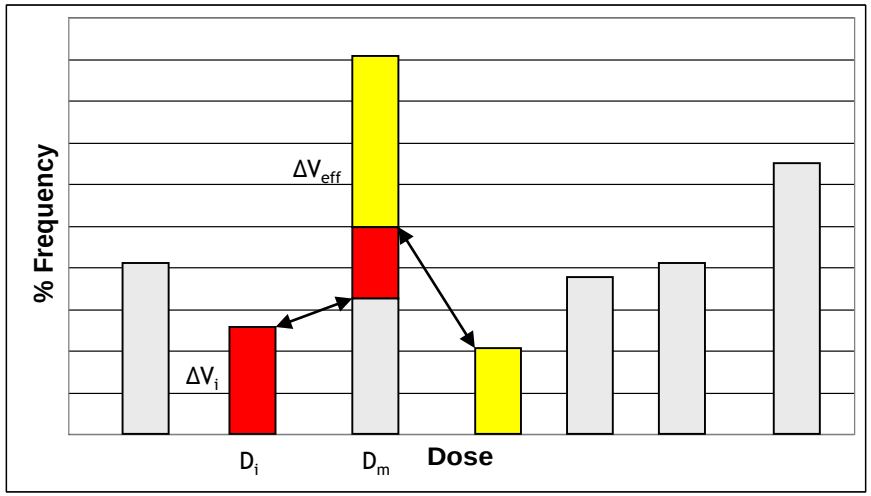

Histogram Reduction Method

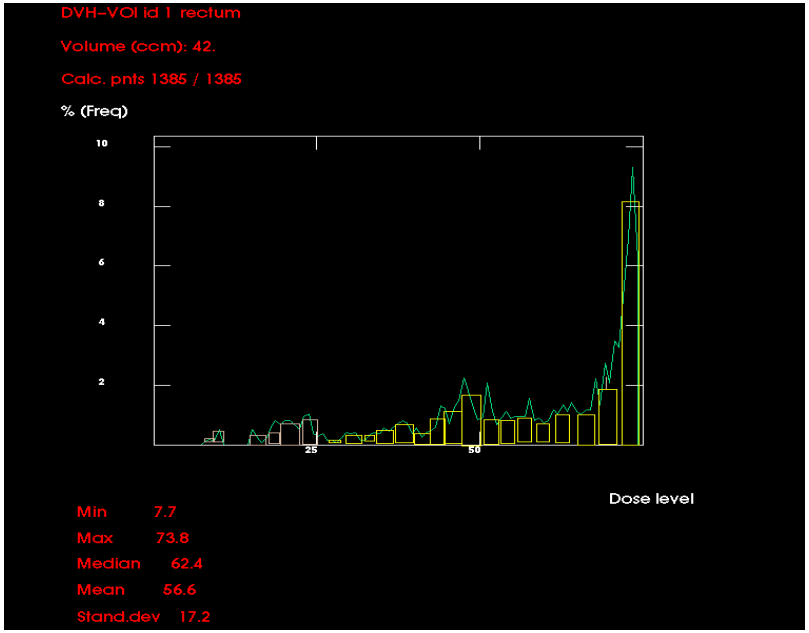

* Effective volume is calculated using the frequency DVH

* Model assumes that each volume element of the DVH independently obeys the same dose volume relationship as the whole organ

Equivalent Uniform Dose (EUD)

- "Quantity of dose that if given uniformly would give the same net cell kill as the non-uniform dose"

1. EUD (tumours only) (Niemierko 1997)

$$EUD = 2Gy \frac{\ln\left[\sum_i v_i (SF_2)^{\frac{D_i}{2Gy}}\right]}{\ln(SF_2)}$$

2. Generalised EUD (gEUD) (Niemierko 1999)

(Applicable to normal tissues and tumours)

The generalised EUD…

$$gEUD = \left(\sum_{i=1}^{N} v_i D_i^a \right)^{\frac{1}{a}} \qquad D_{eff} = \left[\sum_i \Delta V_i (D_i)^{\frac{1}{n}} \right]^n$$

D_i is the dose in the ith voxel; v_i is the fraction of the ROI occupied by the voxel.

a is a "biological" parameter, derived from clinical observation and chosen to reflect the desired radiobiological property, eg:

a < 1 (eg for tumours)….Low doses are given higher weight, so that cold spots "pull down" the gEUD.

a > 1 (eg for critical organs)….Large doses are given higher weight, so that hot spots "push up" the gEUD.

a = 1….The calculated EUD is simply the mean dose.

Niemierko, Med.Phys., (1999).

Equivalent Uniform Dose

- **Any two dose distributions are equivalent if they cause the same radiobiological effect**

- **Includes the biological effect of fractionation**

It is not a radiobiological or biologically based model (purely empirical)

- **When the dose is uniform, EUD tends towards the mean dose**

EUD will be affected by accuracy of DVH!

Accuracy and limitations

- **Factors affecting DVH accuracy:**
  - Accuracy to which VOI is delineated (Main contribution)
  - Dose bin size
  - Distance Map voxel size
  - Sampling method and sampling resolution
  - Shape of VOI
  - Dose Calculation Algorithm (difference in modelling heterogenities, penumbra…)
  - Dose voxel size

Gross Tumour Volume (GTV)

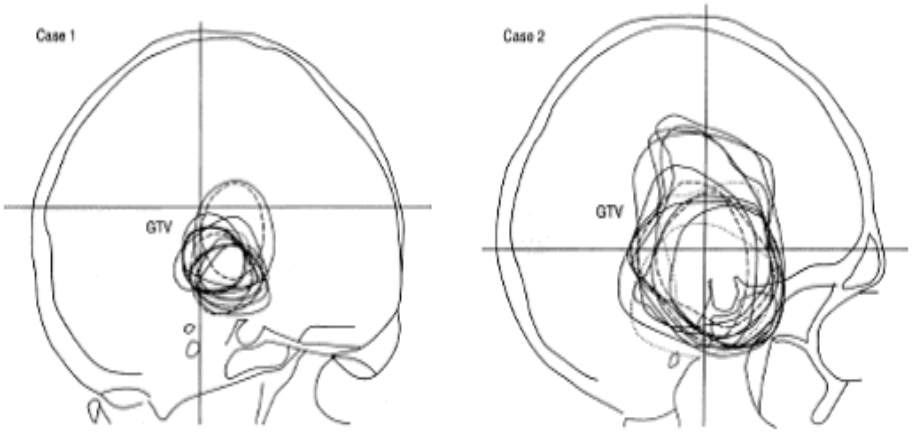

- Taken from ICRU Rpt. 50

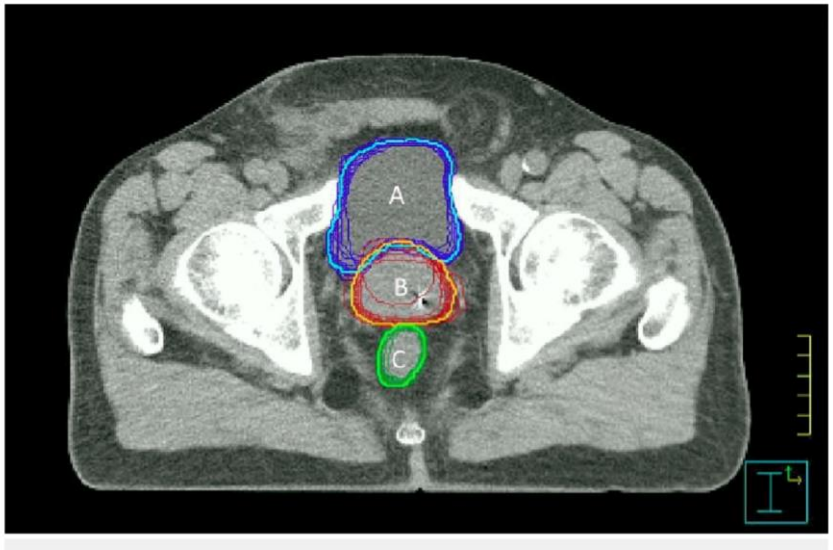

Barghi et al 2013

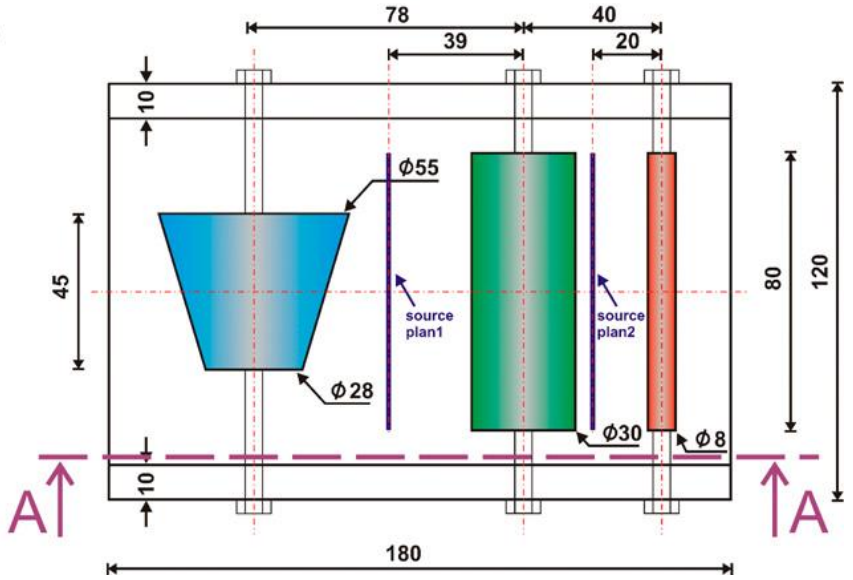

From Kirisits et al MP 2007

Also: Inter-observer variation(1SD) 13% small cylinder, 5% large cylinder, 3% cone shape (Kirisits et al RO 2007)

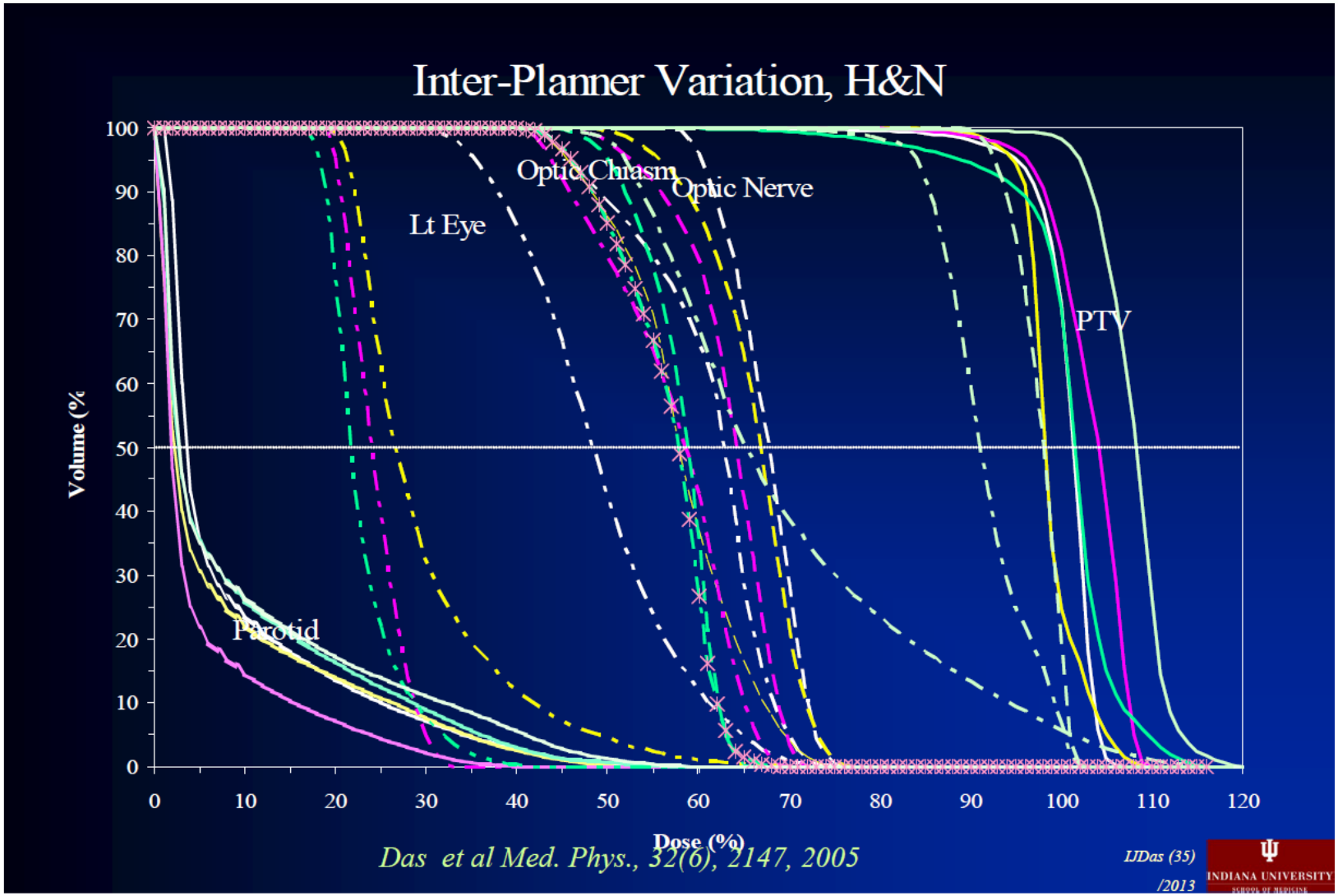
Inter-Planner Variation, H&N
Optic Chiasm
Optic Nerve
Lt Eye
PTV
Parotid
Volume (%
Dose (%)
Das et al Med. Phys., 32(6), 2147, 2005
IJDas (35)
/2013
INDIANA UNIVERSITY

Accuracy and limitations

- **Factors affecting DVH accuracy:**
  - Accuracy to which VOI is delineated (Main contribution)
  - Dose bin size
  - Distance Map voxel size
  - Sampling method and sampling resolution
  - Shape of VOI
  - Dose Calculation Algorithm (difference in modelling heterogenities, penumbra…)
  - Dose voxel size

Accuracy: Distance Map Voxel Size

- Predefined (usually for each VOI type i.e. target or OAR etc.)
- Automatic Voxel Size to achieve both reasonable accuracy and speed
- This can have an affect on the volume accuracy of the DVH

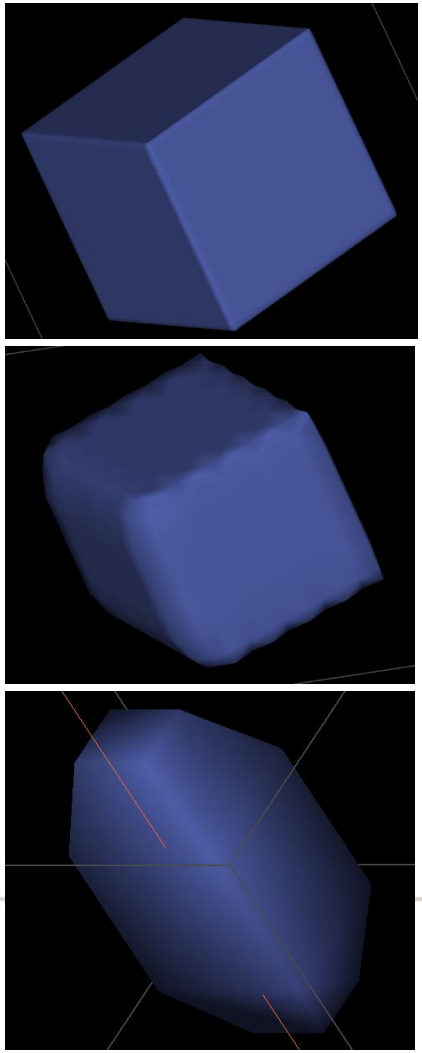

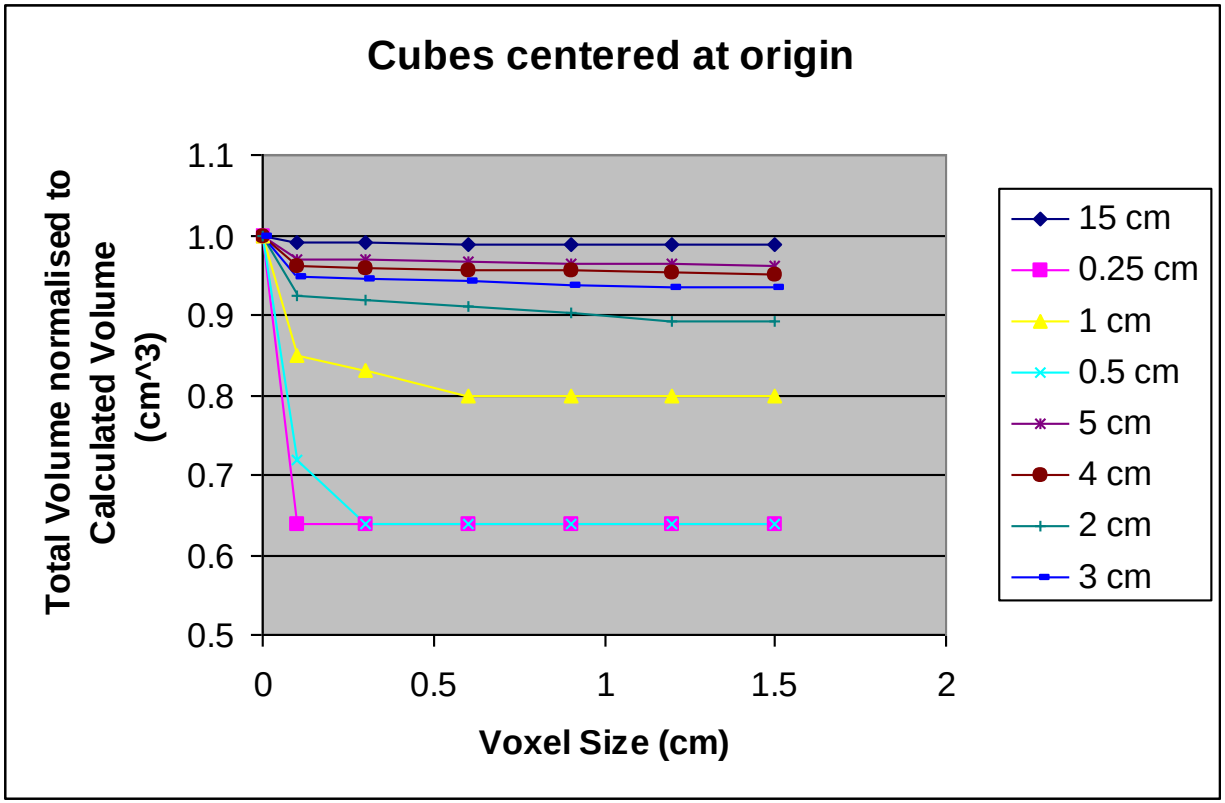

From Paul Kinsella St Luke's

Volume Tests

Depends on approach To shape 'ends'

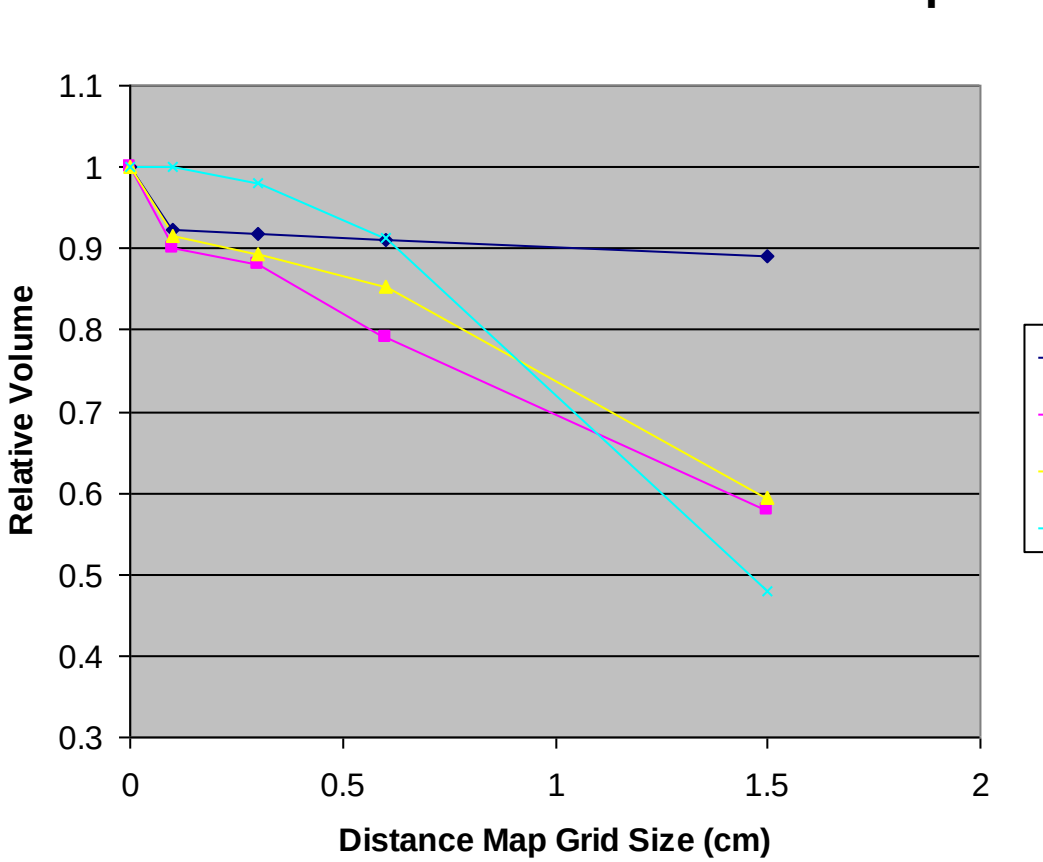

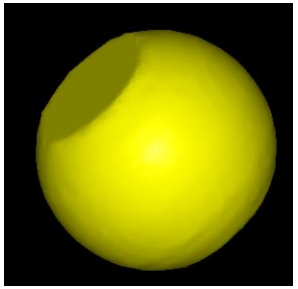

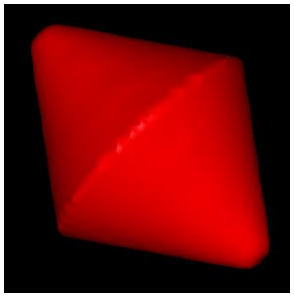

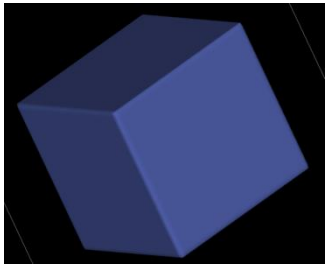

From Paul Kinsella St Luke's

TPS calculate dose, calculation of volumes not the primary function!

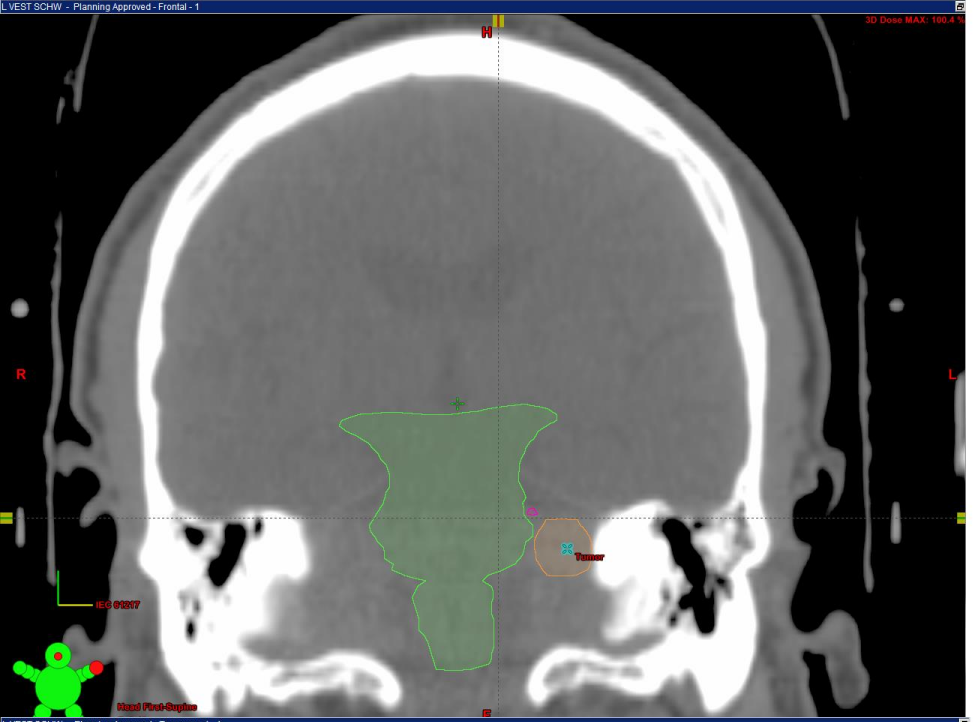
L VEST SCHW - Planning Approved - Frontal - 1
3D Dose MAX: 100.4 %
H
R
L
Tumor
IEC 61217
Head First-Supine

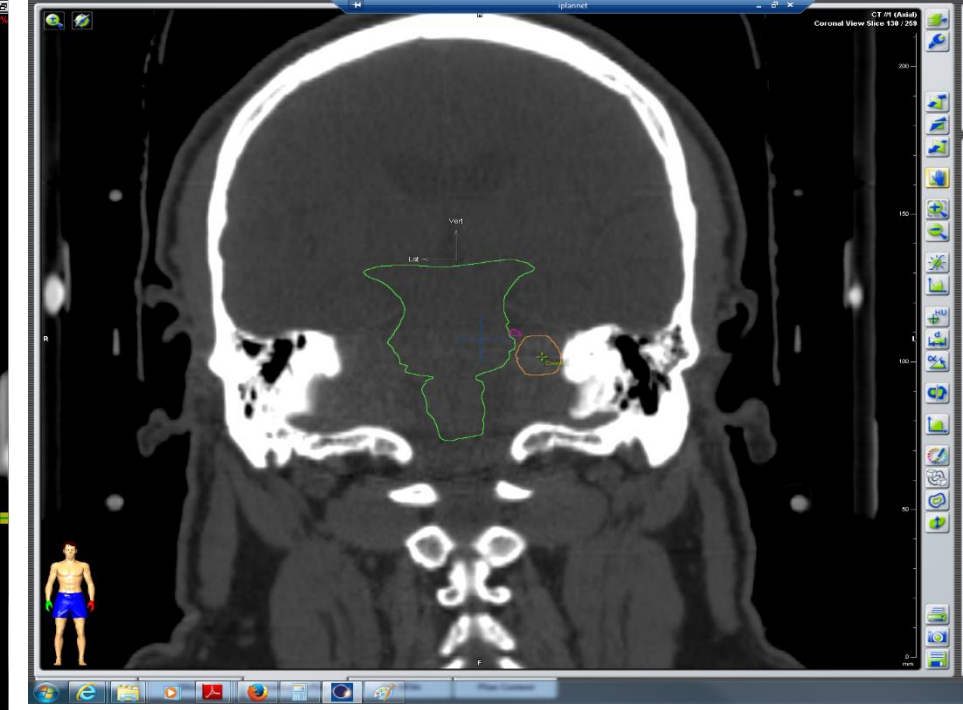
iplannet
CT /1 (Axial)
Coronal View Slice 138 / 259
Vert
Lat
R
L
F

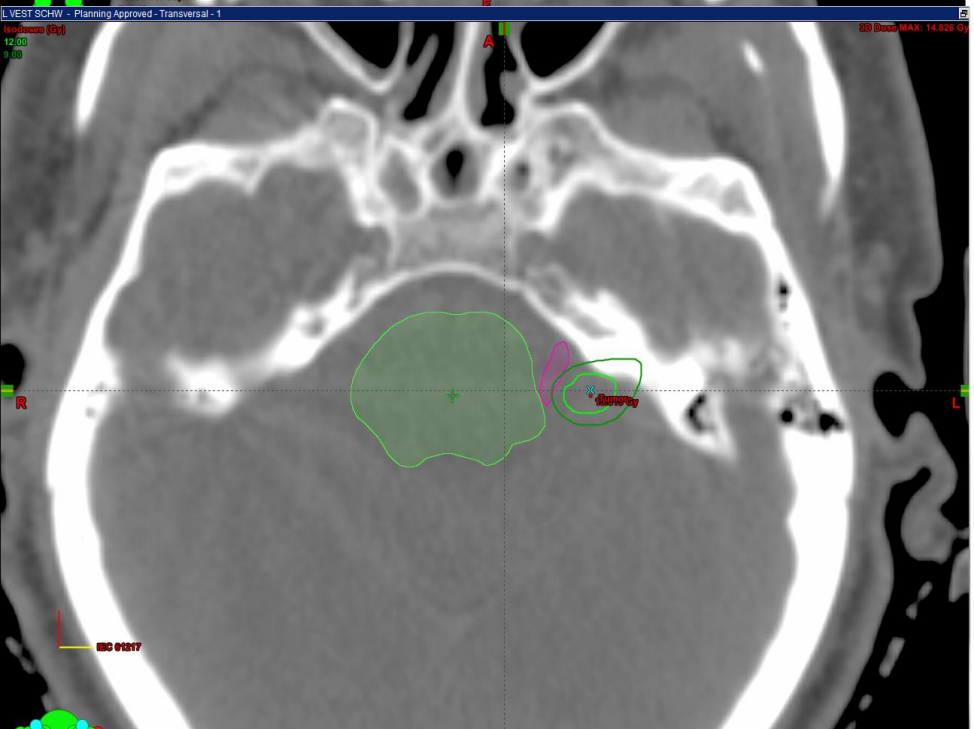
L VEST SCHW - Planning Approved - Transversal - 1
Isodoses (Gy)
12.00
9.00
3D Dose MAX: 14.826 Gy
A
R
L
Biopsy
IEC 61217

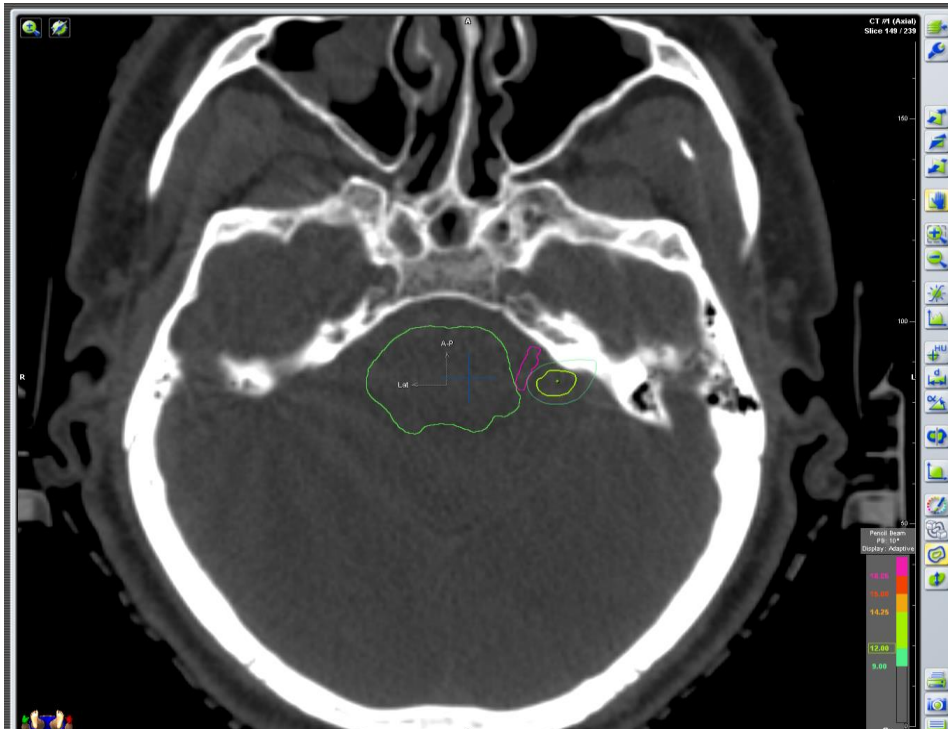
CT /1 (Axial)
Slice 148 / 239
A-P
Lat
R
L
Pencil Beam
Display : Adaptive
14.25
12.00
9.00

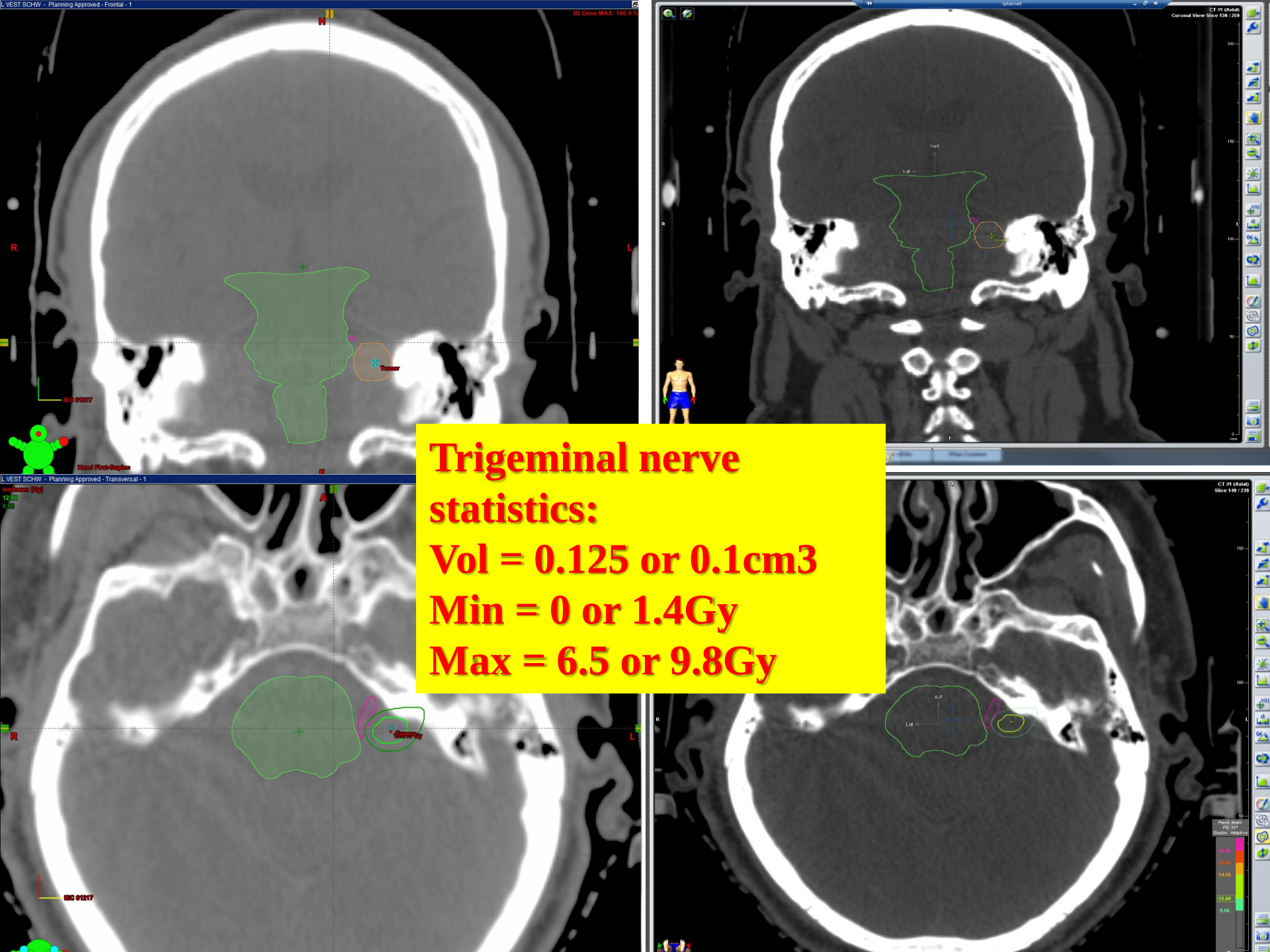
Trigeminal nerve statistics:
Vol = 0.125 or 0.1cm3
Min = 0 or 1.4Gy
Max = 6.5 or 9.8Gy

Accuracy and limitations

- **Factors affecting DVH accuracy:**
  - Accuracy to which VOI is delineated (Main contribution)
  - Dose bin size
  - Distance Map voxel size
  - Sampling method and sampling resolution
  - Shape of VOI
  - Dose Calculation Algorithm (difference in modelling heterogenities, penumbra…)
  - Dose Voxel Size

Effect of Dose Calculation on DVH metrics

Dose deposition approximations (patient)

15 MV photons

(Dose contr. normalization)

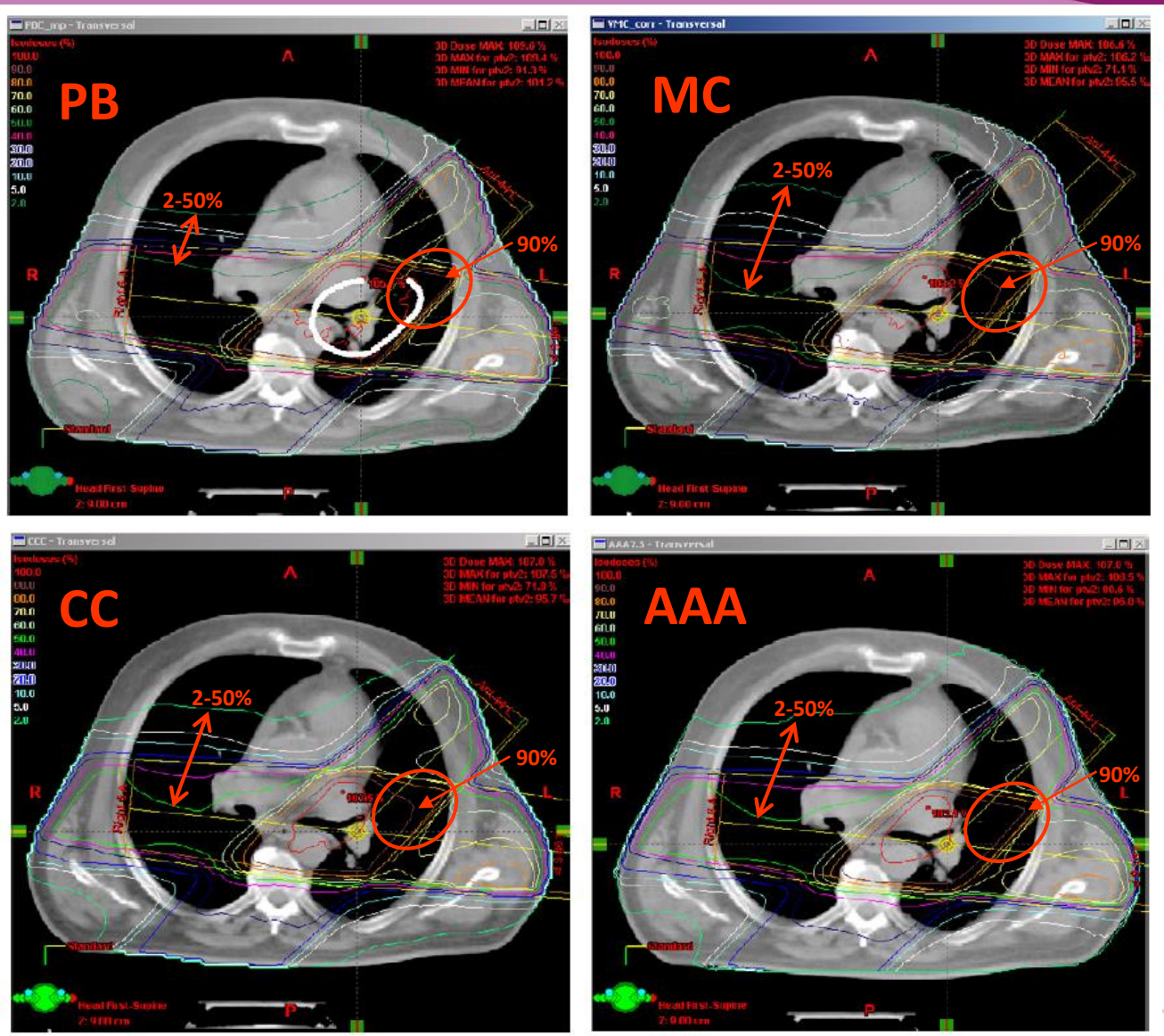

Hasenbalg *et al* [17]

Dose deposition approximations (patient)

Cumulative DVH for PTV and left lung (case from previous page).

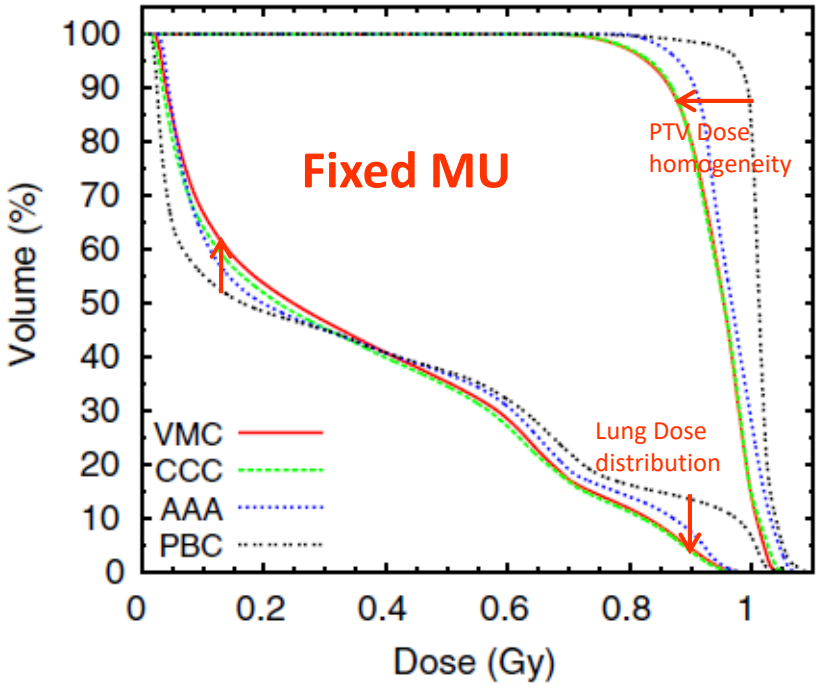

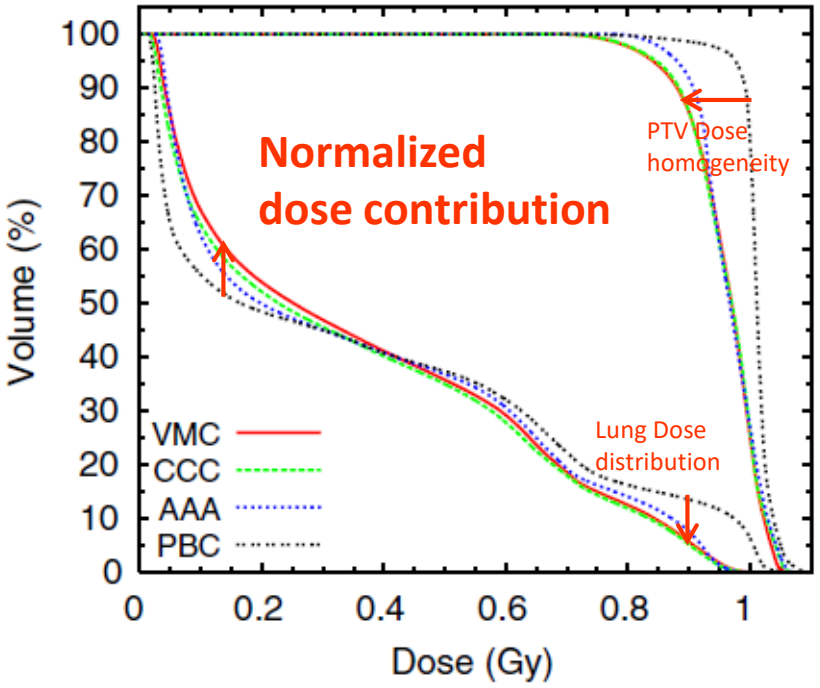

Hasenbalg *et al* [17]

From JO

Including dose calculation uncertainty in DVH construction

- Uncertainty in a dose point has both type A and type B uncertainty components
  - (both for measured data)
- A probability density function can be used to model uncertainty:

- Used Rectangular, Gaussian and Triangular distributions

$$f_i(\delta_i) = f\left(\frac{\delta_i - D(z_i)}{\sigma_i}\right)$$

Henriquez and Caastrillon MP 2010

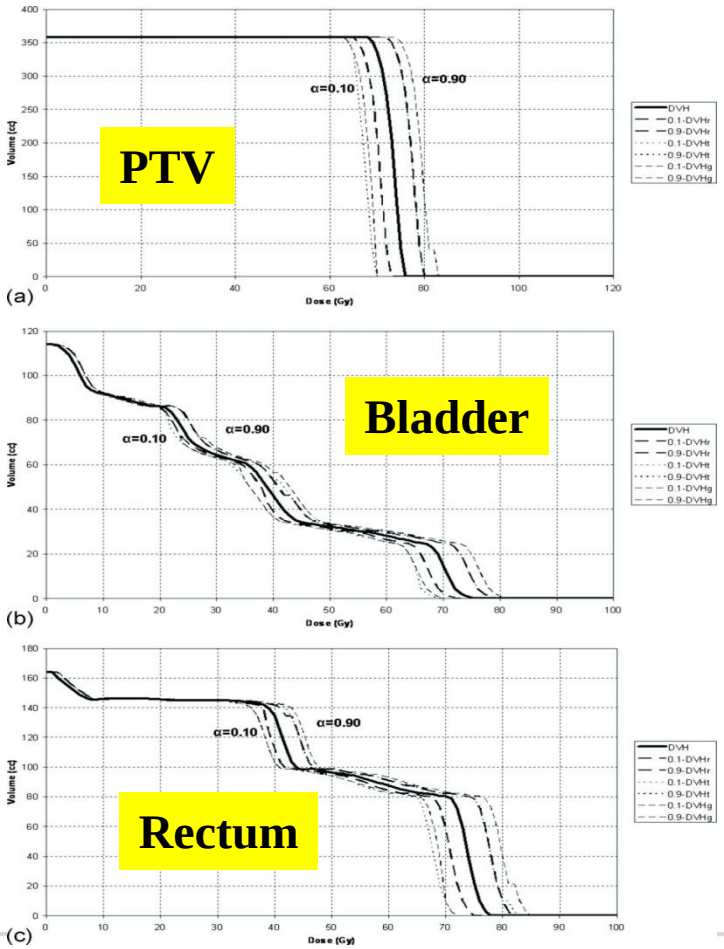

Prostate

Including dose calculation uncertainty in DVH construction

- Uncertainty in a dose point has both type A and type B uncertainty components
  - (both for measured data)
- A probability density function can be used to model uncertainty:

- Used Rectangular, Gaussian and Triangular distributions

$$f_i(\delta_i) = f\left(\frac{\delta_i - D(z_i)}{\sigma_i}\right)$$

Henriquez and Caastrillon MP 2010

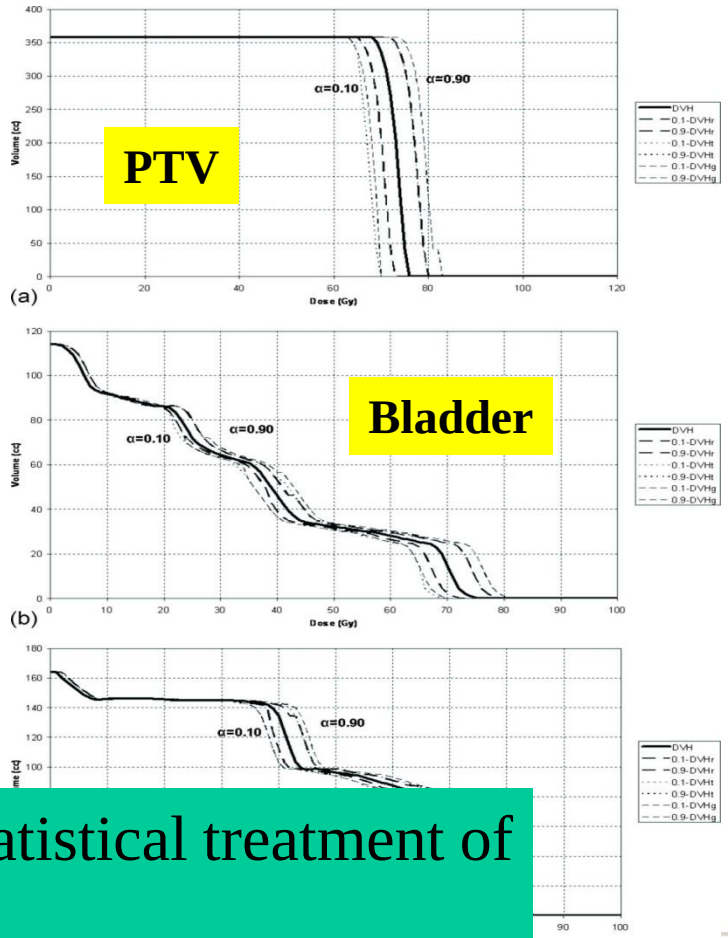

Report uncertainty in DVH to enhance statistical treatment of Clinical trial results?

Prostate

AAA vs Acuros

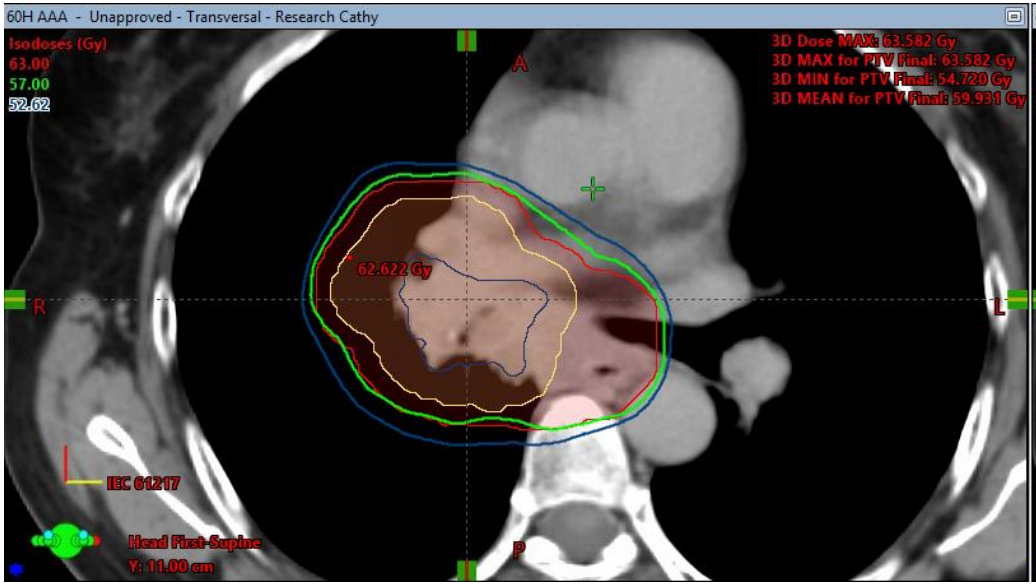

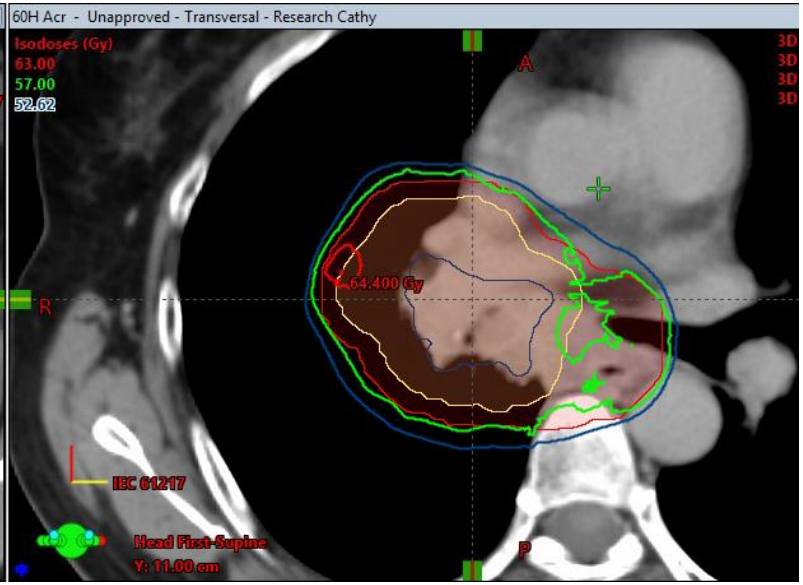

AAA

Acuros (Dm)

AAA vs ACUROS for 60Gy Lung plan – same MU

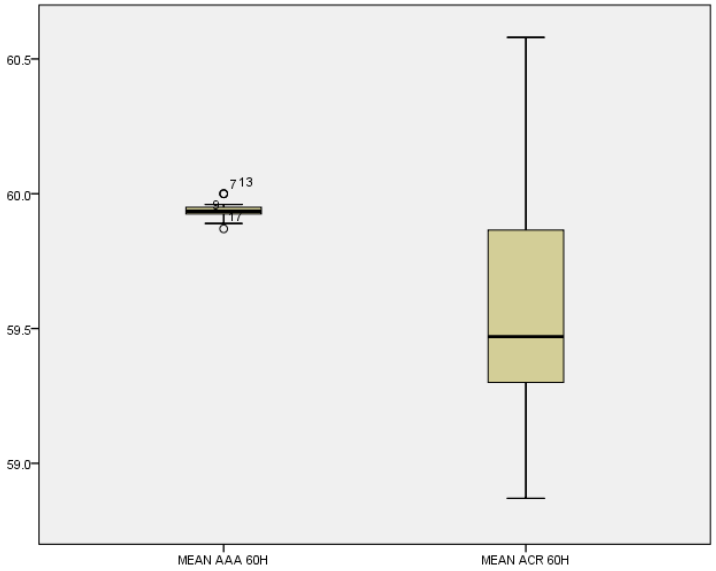

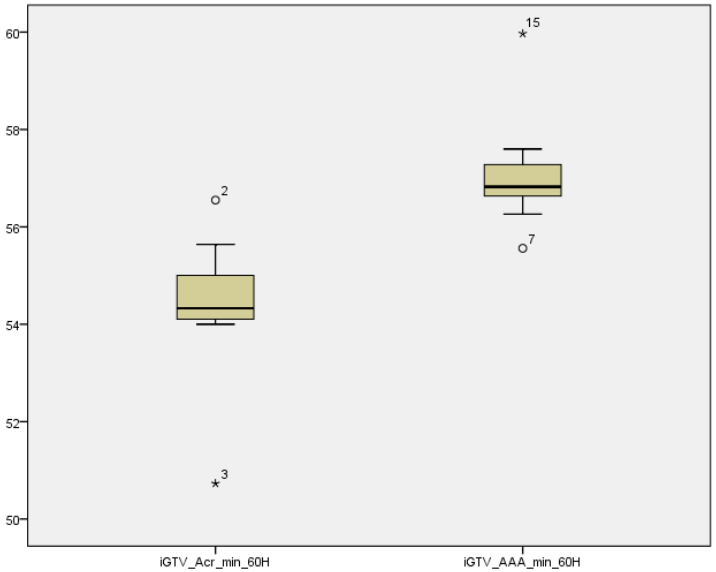

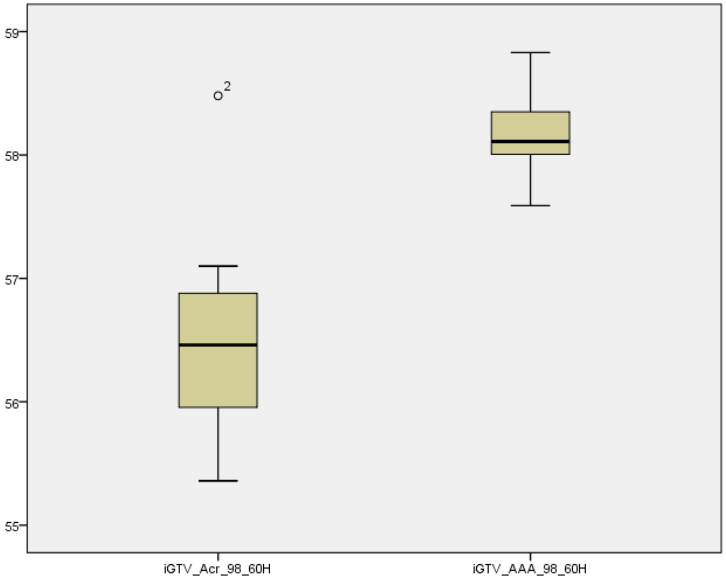

Box and Whisker plots

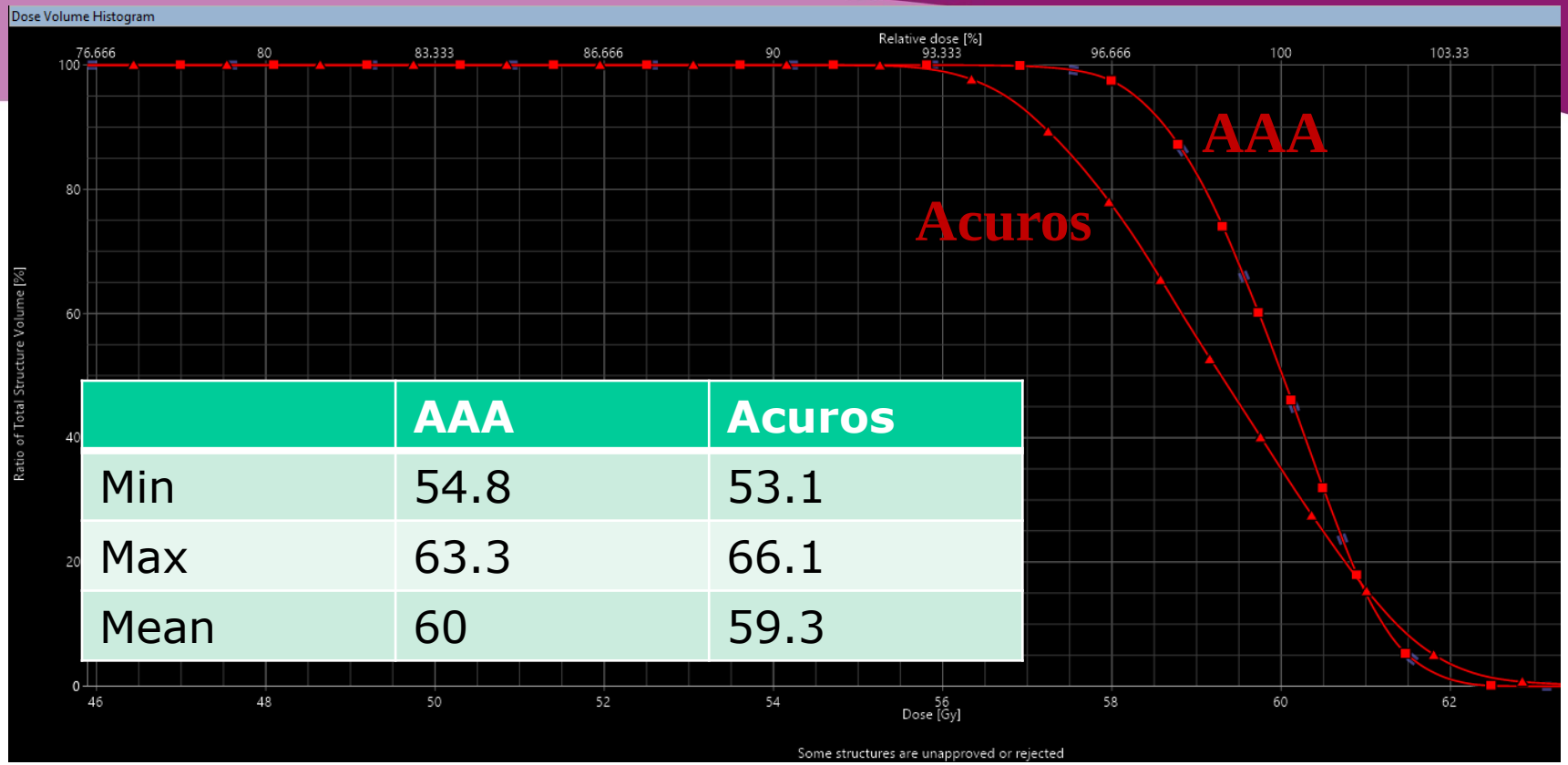

	AAA	Acuros
Min	54.8	53.1
Max	63.3	66.1
Mean	60	59.3

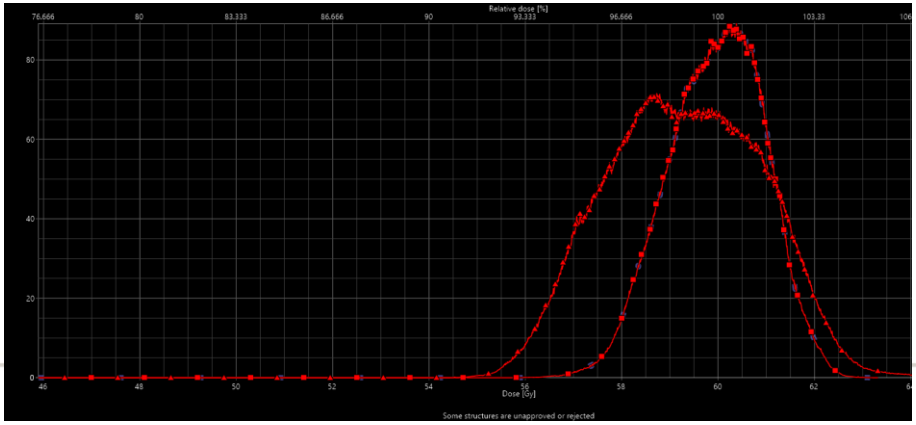

Effect of improved dose calculation

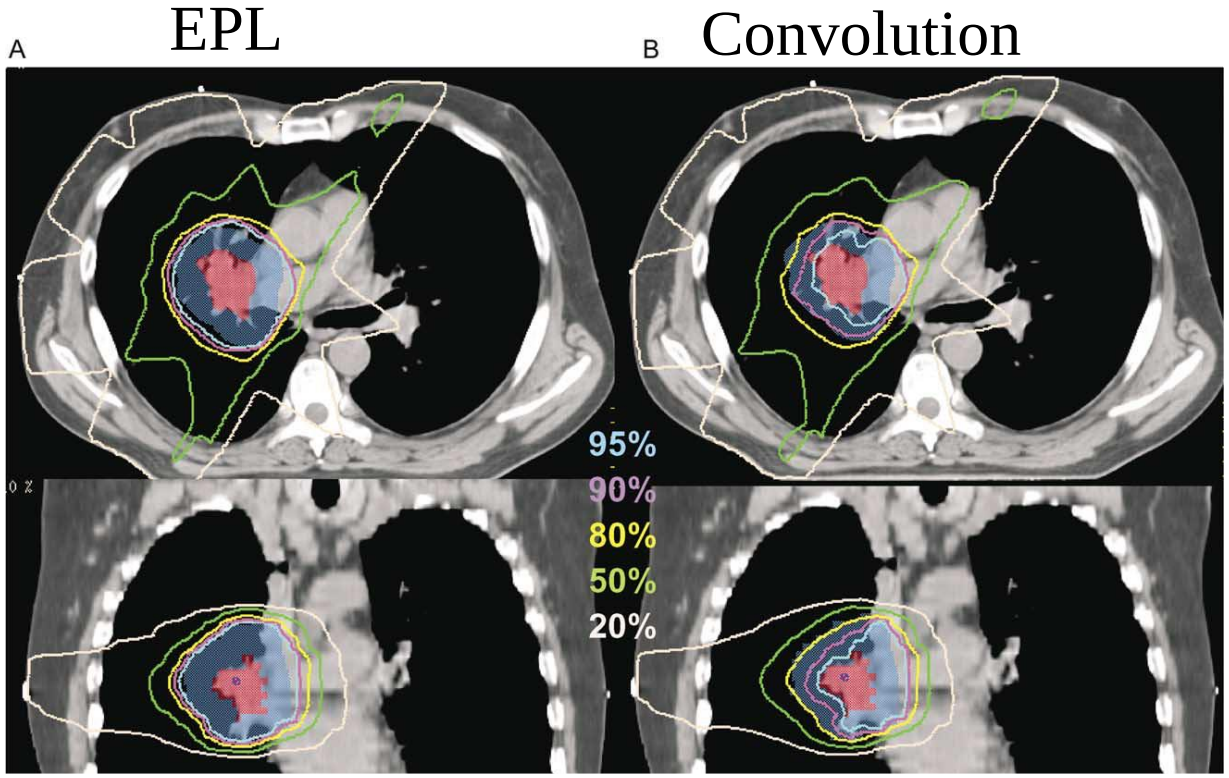

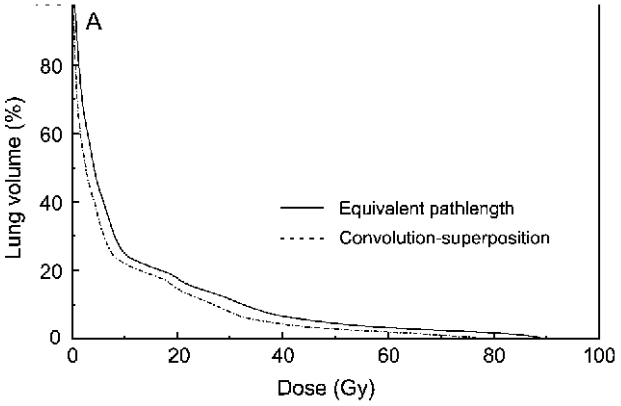

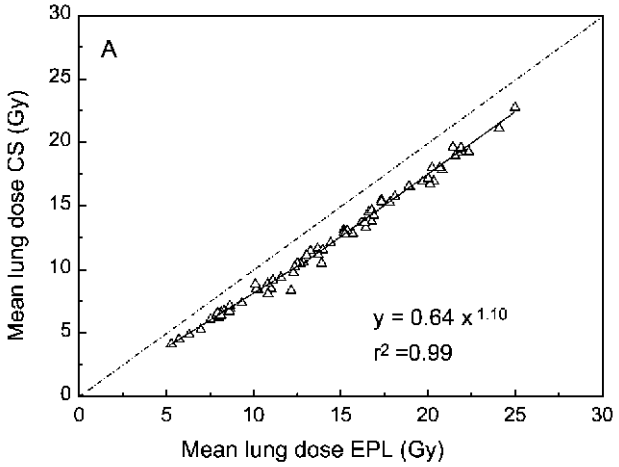

De Jaeger et al RadOnc 69 (2003)

Another example……

Hedin, Back JACMP 14 2013

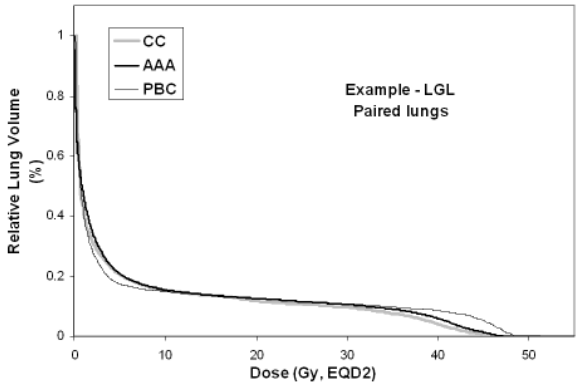

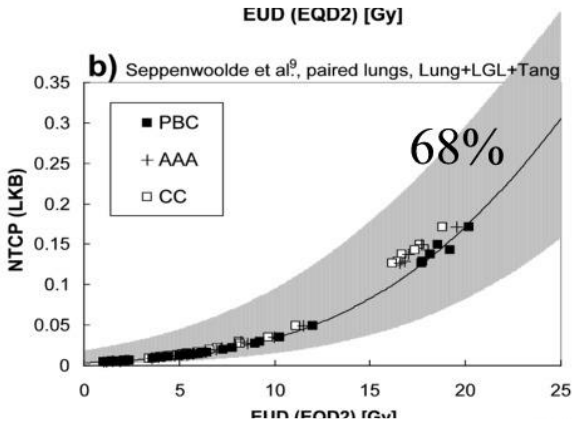

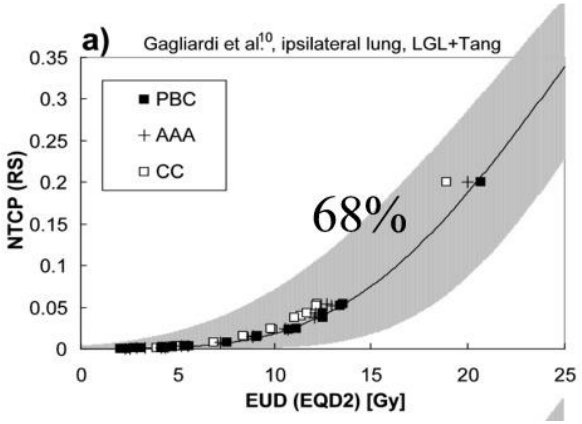

Conclude:
NTCP differences are within the confidence levels of NTCP!

Summary

- Important to ensure DVH calculation is accurate as it is central to clinical decisions
- Physicists should be familiar with the influence of different parameters on DVH construction
- DVH construction should be tested (QC)
- Clinical trials:
  - recording contouring practice?
  - DVH metric calculation methods? Predictive power?
  - DVH uncertainties?
  - Consistency among vendors?

ADDITIONAL SLIDES

Dose Constraints

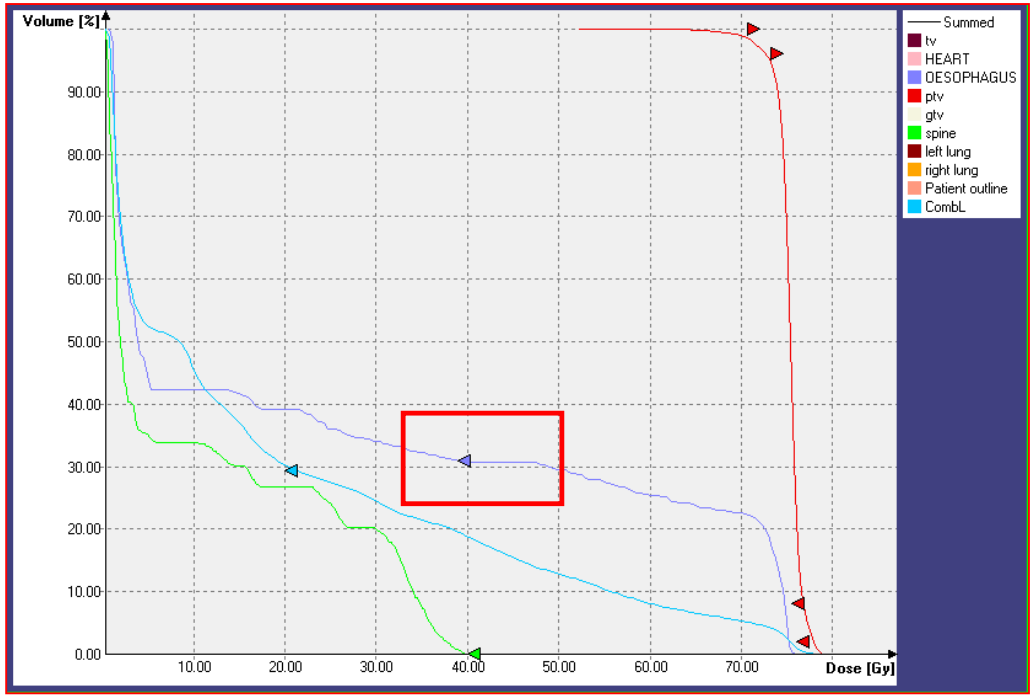

Power Law: n

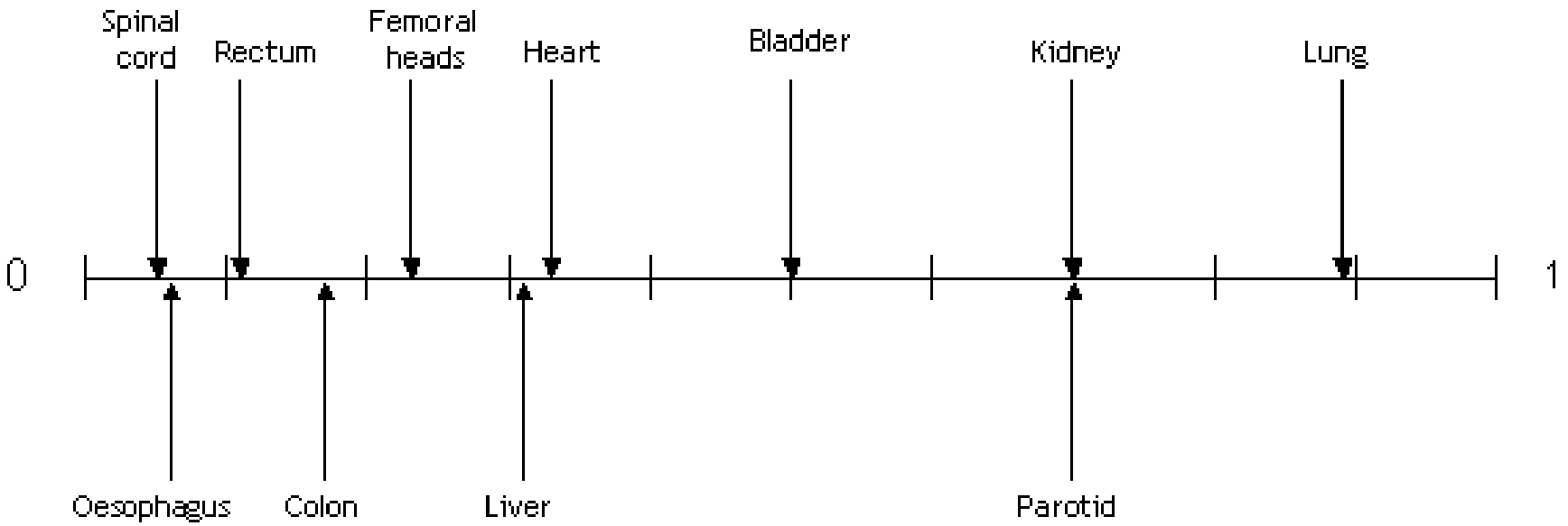

Max dose more important

Mean dose more important

1. DVH Reduction: V_{eff}

[4] [5] [6]

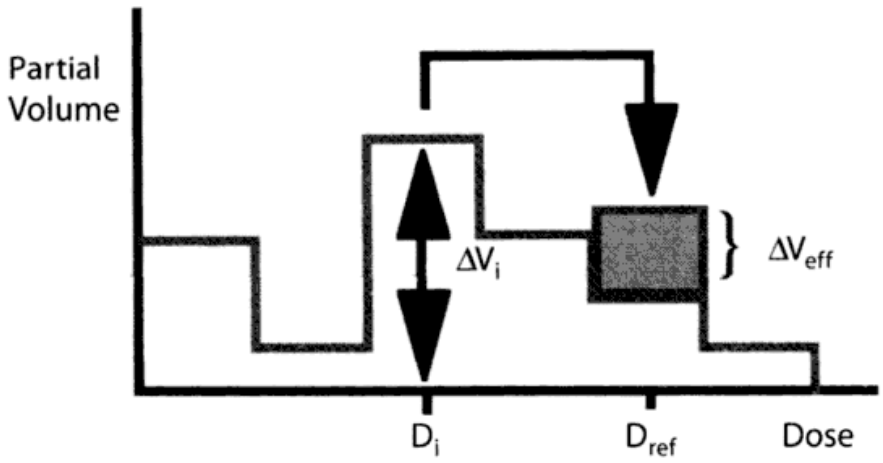

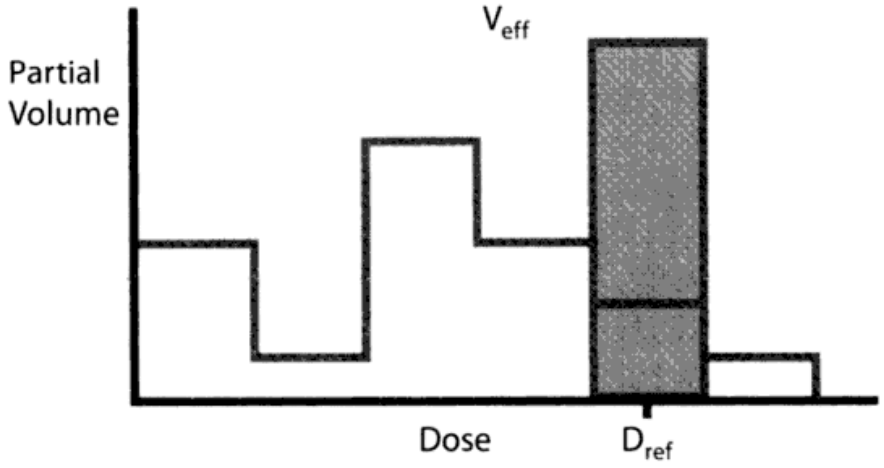

$$V_{eff} = \Sigma \{ v_i \bullet (D_i / D_{ref})^{1/n} \}$$

- $\Delta V_i > \Delta V_{eff}$
- NTCP remains the same before and after transform

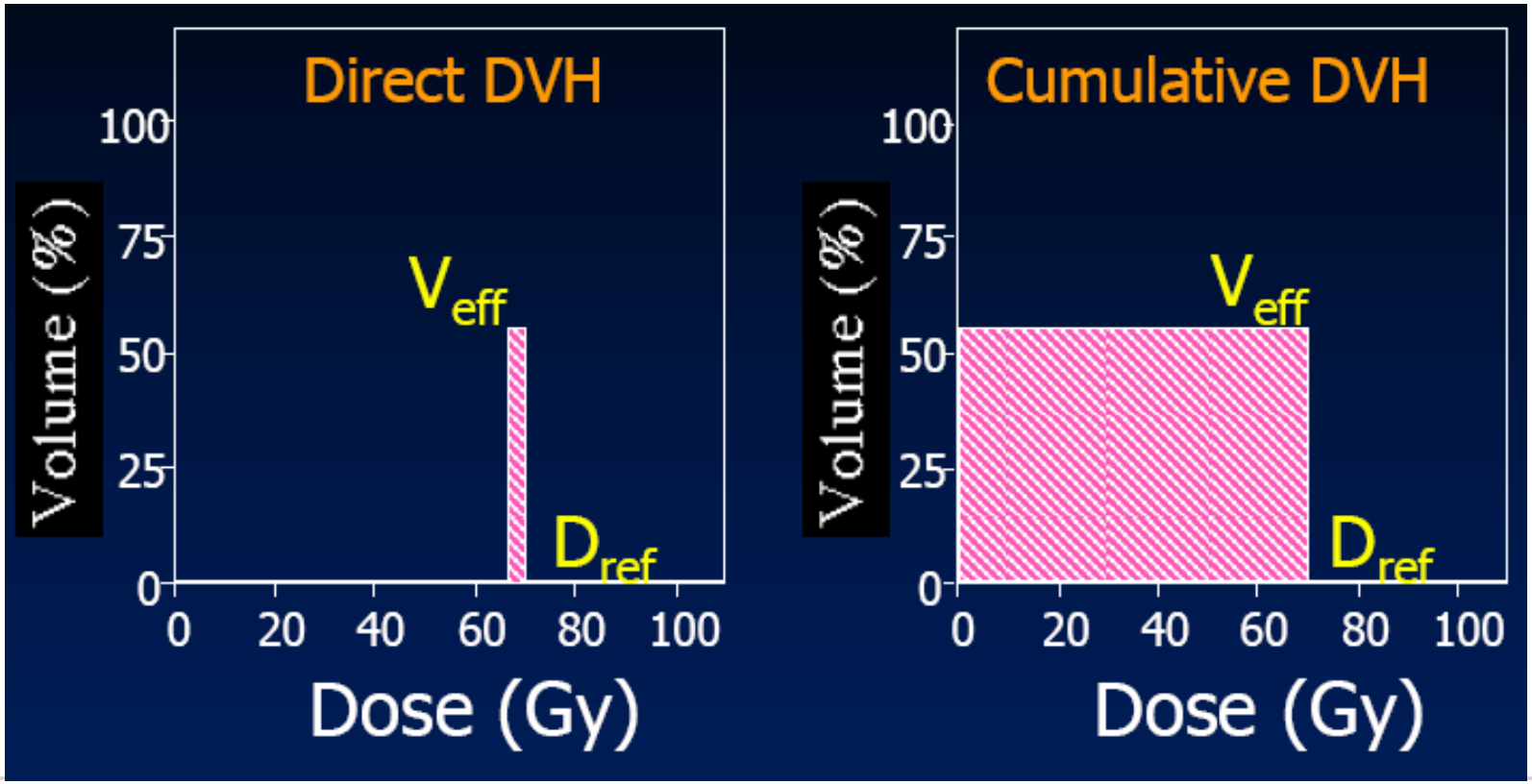
Direct DVH
Volume (%)
100
75
50
25
0
V_{eff}
D_{ref}
0 20 40 60 80 100
Dose (Gy)
Cumulative DVH
Volume (%)
100
75
50
25
0
V_{eff}
D_{ref}
0 20 40 60 80 100
Dose (Gy)

Cumulative DVH…

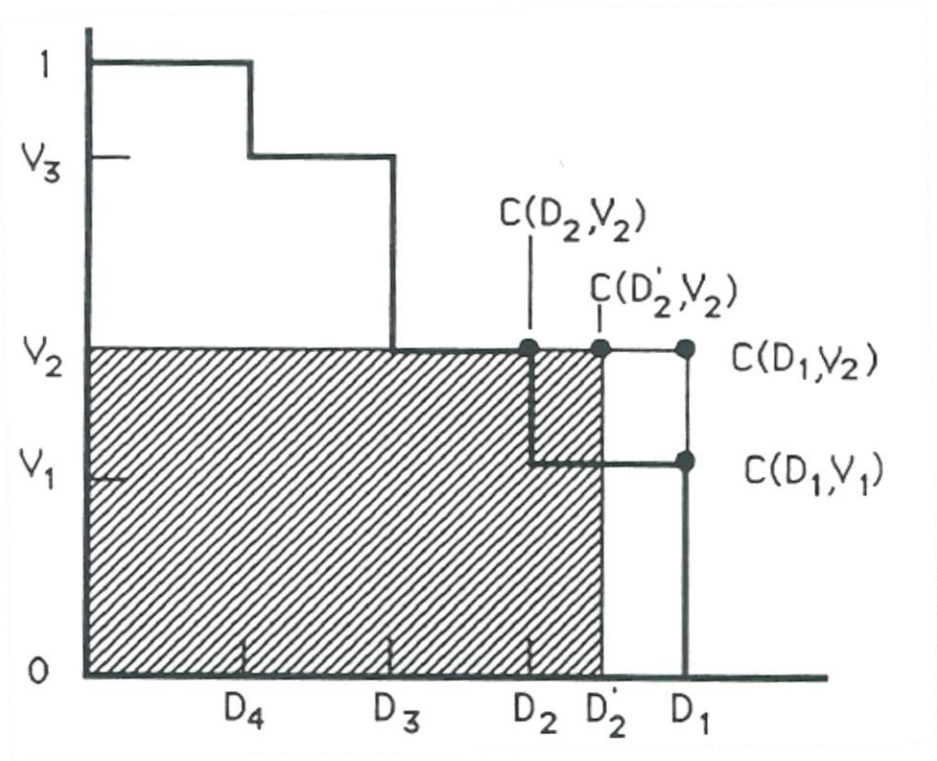

[7] [8] [9]

$$D_{eff} = \left[\sum_i \Delta V_i (D_i)^{\frac{1}{n}} \right]^n$$

- Again, NTCP is equivalent before and after transform

Examples of parameter a…

Brainstem: 4.6

Spinal cord: 7.4

Parotid: 5.0

Larynx: 7.4

Tumour: -8.0

Observations about the generalised EUD... (R. Dale Imperial College London)

- It is NOT a radiobiological or biologically-based model – it is purely empirical.
- It has the advantage that it may be tailored to match the clinical observations, which themselves inherently reflect the whole range of complex processes involved.
- As with all empirical models, care needs to be taken to ensure that it is not applied outside the set of circumstances for which the operative parameters have been derived.

Dose Constraints

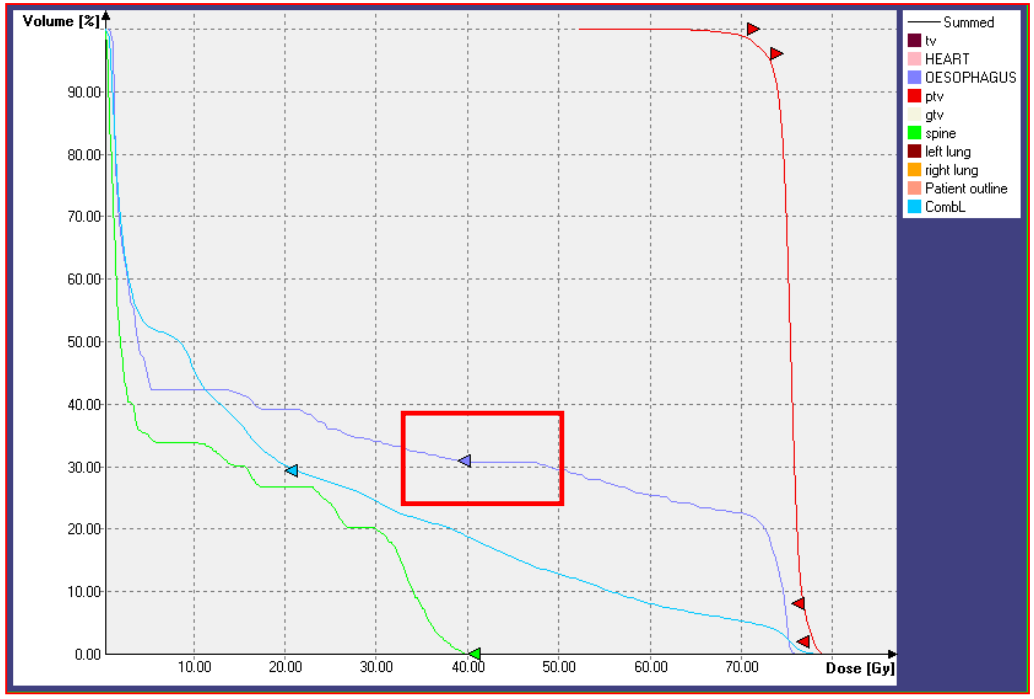

Probabilistic planning and margins

Crister Ceberg

Medical Radiation Physics

Lund University

Sweden

Learning objectives

After completing this module you should be able to

- Identify and categorize geometrical uncertainties
- Construct CTV-to-PTV margins
- Discuss the limitations of PTV-based treatment planning
- Describe the basics of CTV-based treatment planning

UNCERTAINTIES

The target of radiotherapy (breast cancer)

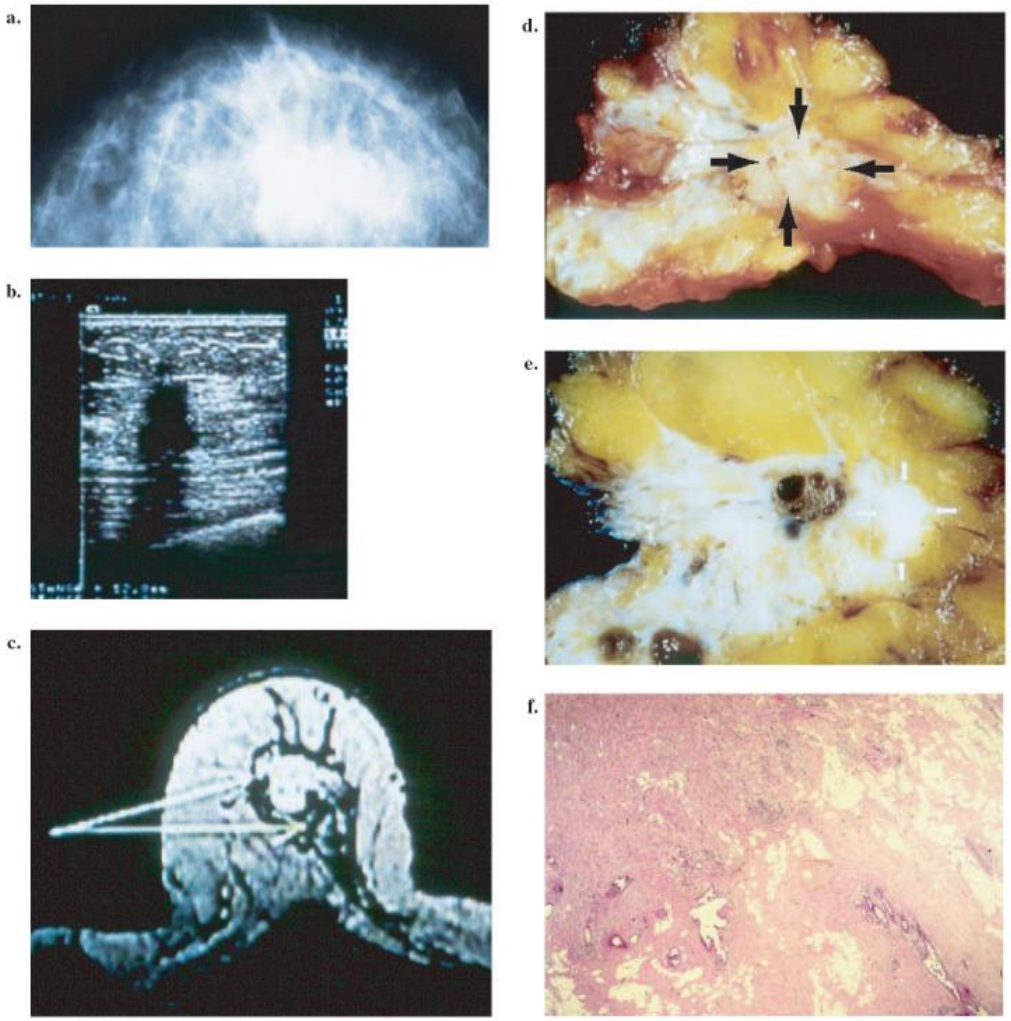

a. Mammography
b. Ultrasonography
c. MRI
d. Surgical specimen
e. Fixed specimen
f. Histology

ICRU 71

ICRU recommendations

ESTRO School

Clinical Target Volume, CTV

- Demonstrable extent and location of
  - Primary tumour
  - Metatstatic regional nodes
  - Distant metastases
- Subclinical malignant disease
  - Microscopic spread at the boundary
  - Possible infiltration into nodes
  - Potential metastatic involvement

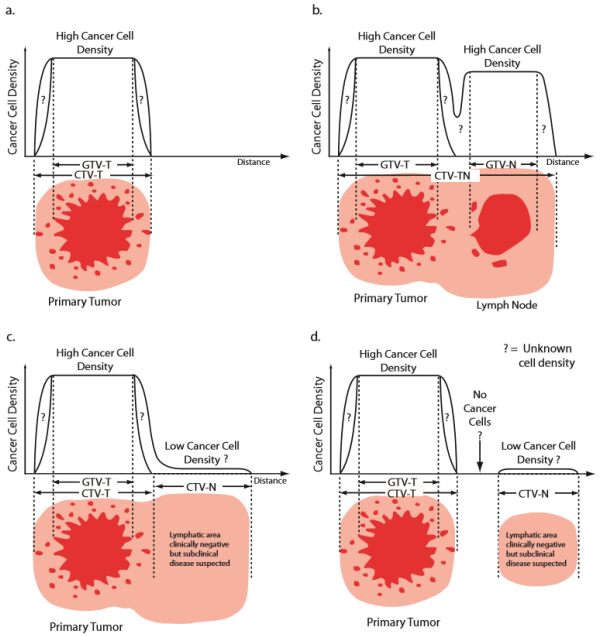

ICRU 71

ESTRO School

Intraobserver variation

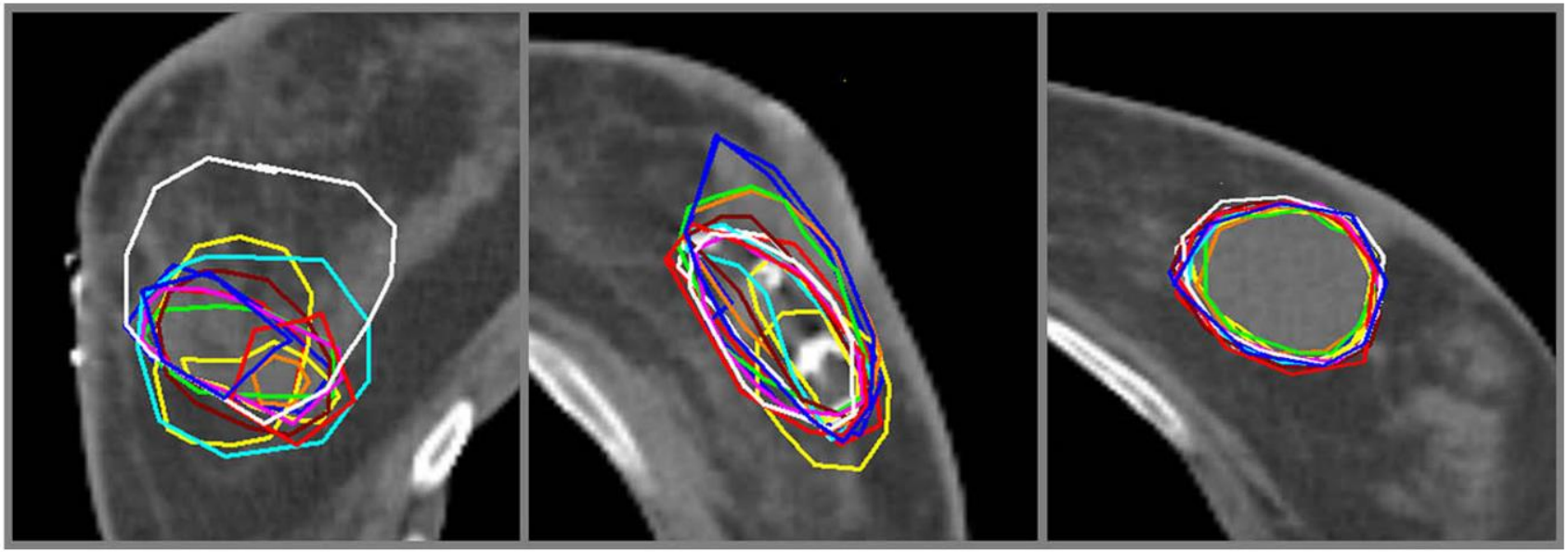

van Mourik et al., Radiother Oncol, 94:286, 2010

Additional uncertainties

- Internal uncertainties (target position, size and shape)
  - Tumour growth/treatment response
  - Weight gain/loss
  - Breathing
  - Bowel and rectal filling
  - Bladder filling
  - Heartbeat, swallowing, coughing
- External uncertainties (patient and beam positioning)
  - Muscle relaxation/tension
  - Fixation and immobilisation
  - Mechanical and dosimetric uncertainty

MARGINS

Planning Target Volume, PTV

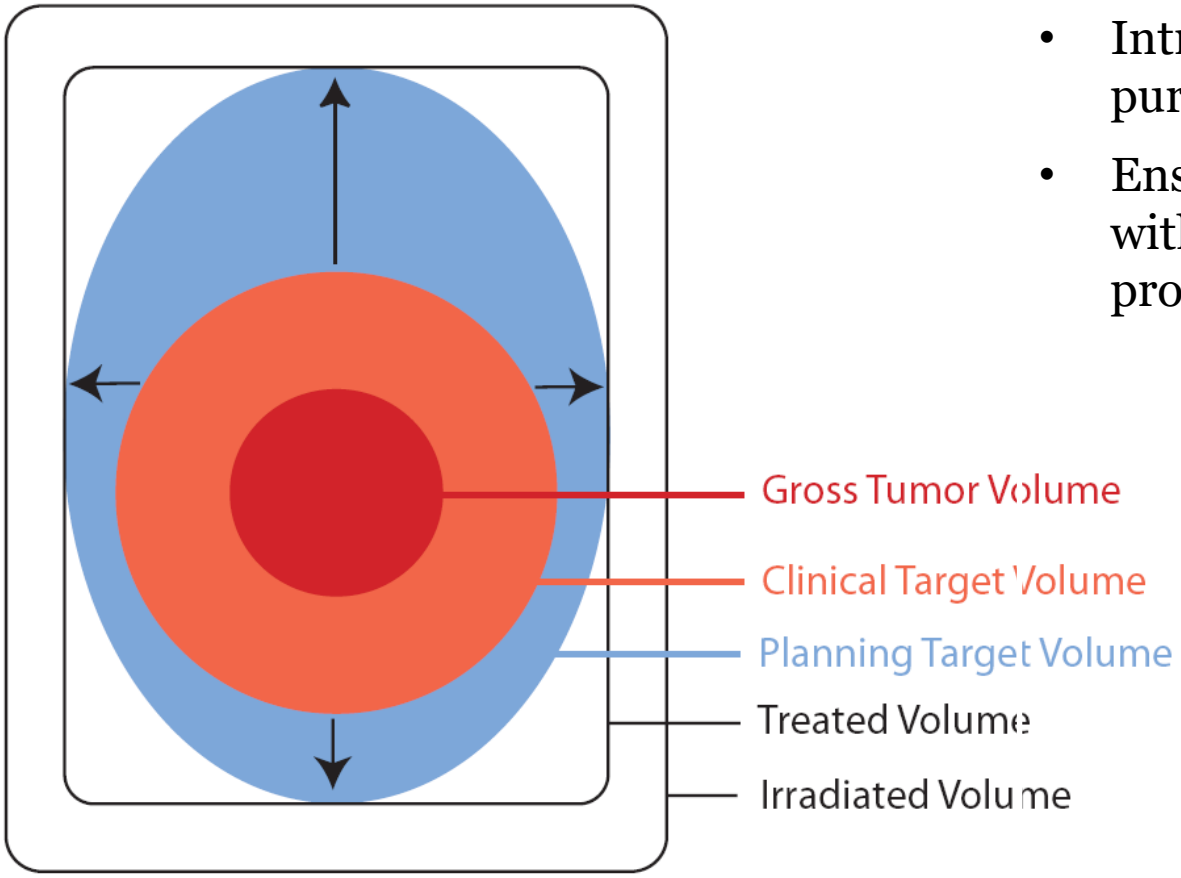

ICRU 71

- Introduced in ICRU 50 as a purely geometrical concept
- Ensures coverage of CTV with a clinical acceptable probability

Ensure coverage…

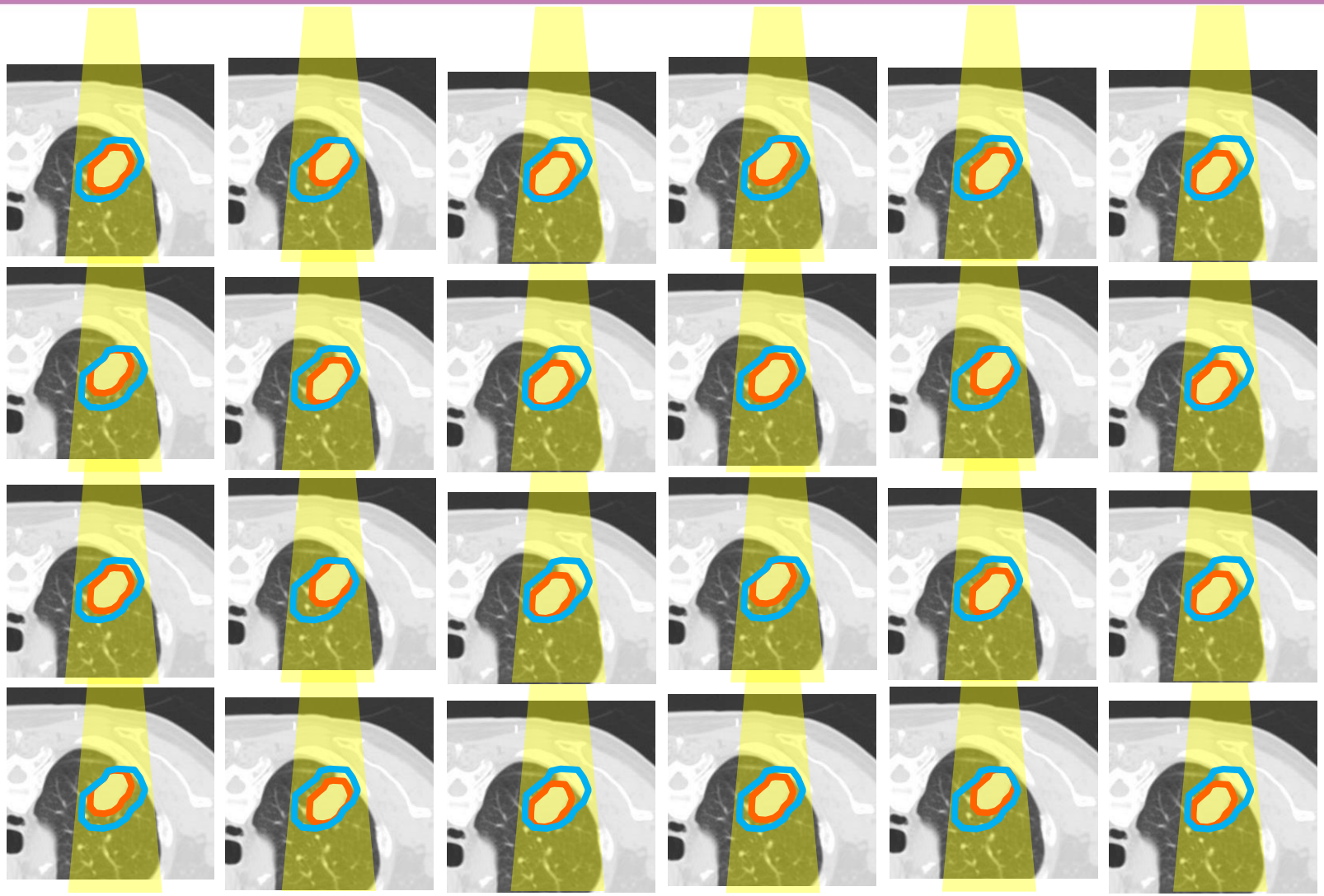

… with a clinically acceptable probability

Verellen et al., Nature Rev Cancer 7:949, 2007

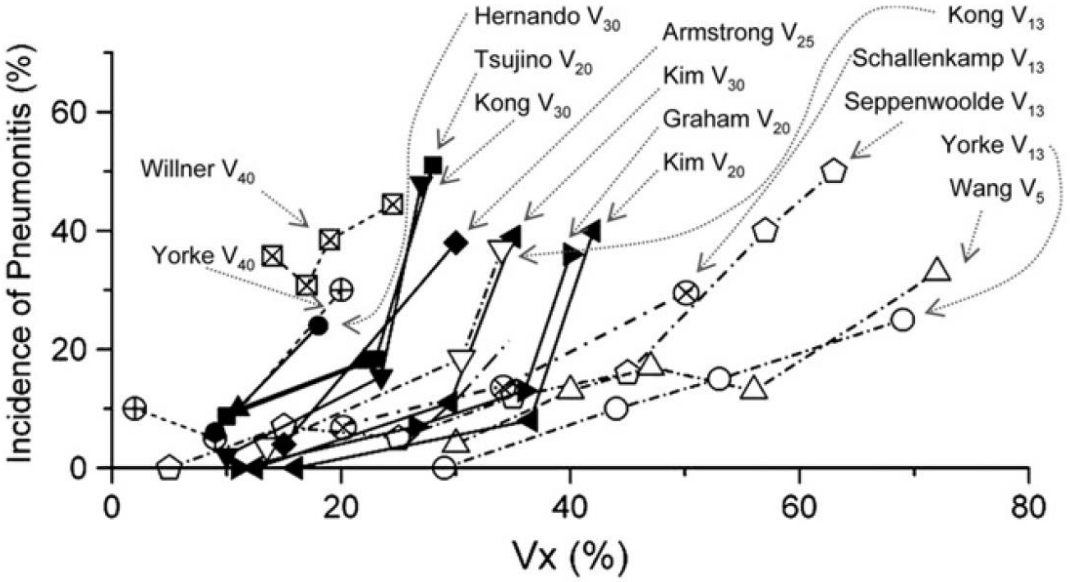

Marks et al., IJROBP 76:S70, 2010

ESTRO School

Margin recipes

Author	Region	Recipe	Comments
Bel *et al.* (1996)	PTV	0.7σ	Statistical uncertainties only (linear approximation)—Monte Carlo.
Antolak and Rosen (1999)	PTV	1.65σ	Statistical uncertainties only, block margin?
Stroom *et al.* (1999a)	PTV	$2\,\Sigma + 0.7\sigma$	95 % absorbed dose to on average 99 % of CTV tested in realistic plans.
van Herk *et al.* (2000)	PTV	$2.5\,\Sigma + 0.7\,\sigma$ (or more correctly): $2.5\Sigma + 1.64\,(\sigma - \sigma_e)$	Minimum absorbed dose to CTV is 95 % for 90% of patients. Analytical solution for perfect conformation.
McKenzie (2000)	PTV	$2.5\,\Sigma + \beta + (\sigma - \sigma_e)$	Extension of van Herk *et al.* (2000) for fringe dose due to limited number of beams. The factor β depends on the beam organization.
Parker *et al.* (2002)	PTV	$\Sigma + \sqrt{(\sigma^2 + \Sigma^2)}$	95 % minimum absorbed dose and 100 % absorbed dose for 95 % of volume. Probability levels not specified.
van Herk *et al.* (2002)	PTV	$2.5 + \Sigma + 0.7\sigma + 3$ mm (or more correctly): $\sqrt{2.7^2\Sigma^2 + 1.6^2\sigma^2} - 2.8$ mm	Monte Carlo based test of 1 % TCP loss due to geometrical errors for prostate patients, fitted for various σ and Σ.
Ten Haken *et al.* (1997), Engelsman *et al.* (2001a, 2001b)	PRV (liver and lung)	0	No margin for respiration, but compensation by absorbed-dose escalation to iso-NTCP, reducing target-dose homogeneity constraints.
McKenzie *et al.* (2000)	PRV	A	Margin for respiration on top of other margins when respiration dominates other uncertainties.
van Herk *et al.* (2003)	PRV (lung)	$0.25\,A$ (caudally); $0.45\,A$ (cranially)	Margin for (random) respiration combined with random setup error of 3 mm SD, when respiration dominates other uncertainties ($A > 1$ cm).
McKenzie *et al.* (2002)	PRV	$1.3\,\Sigma \pm 0.5\,\sigma$	Margins for small and/or serial organs at risk in low (+) or high (−) absorbed-dose region.

ICRU 83

Margin recipes

Author	Region	Recipe	Comments
Bel *et al.* (1996)	PTV	0.7σ	Statistical uncertainties only (linear approximation)—Monte Carlo.
Antolak and Rosen (1999)	PTV	1.65σ	Statistical uncertainties only, block
			beams. The factor β depends on the beam organization.
Parker *et al.* (2002)	PTV	$\Sigma + \sqrt{(\sigma^2 + \Sigma^2)}$	95 % minimum absorbed dose and 100 % absorbed dose for 95 % of volume. Probability levels not specified.
van Herk *et al.* (2002)	PTV	$2.5 + \Sigma + 0.7\sigma + 3$ mm (or more correctly): $\sqrt{2.7^2\Sigma^2 + 1.6^2\sigma^2} - 2.8$ mm	Monte Carlo based test of 1 % TCP loss due to geometrical errors for prostate patients, fitted for various σ and Σ.
Ten Haken *et al.* (1997), Engelsman *et al.* (2001a, 2001b)	PRV (liver and lung)	0	No margin for respiration, but compensation by absorbed-dose escalation to iso-NTCP, reducing target-dose homogeneity constraints.
McKenzie *et al.* (2000)	PRV	A	Margin for respiration on top of other margins when respiration dominates other uncertainties.
van Herk *et al.* (2003)	PRV (lung)	$0.25A$ (caudally); $0.45A$ (cranially)	Margin for (random) respiration combined with random setup error of 3 mm SD, when respiration dominates other uncertainties ($A > 1$ cm).
McKenzie *et al.* (2002)	PRV	$1.3\,\Sigma \pm 0.5\,\sigma$	Margins for small and/or serial organs at risk in low (+) or high (−) absorbed-dose region.

van Herk *et al.* (2000)

A CTV-to-PTV margin to ensure that the absorbed dose in the CTV is >95% for 90% of the patients

ICRU 83

Simplifications

- Clinical target volume
  - Spherical
  - Rigid transformation (translation)
- Dose calculation
  - Invariant body contour
  - Homogeneous medium
  - Inifinite number of fractions
- Normal distribution
  - Treatment execution errors
  - Treatment preparation errors

Two types of errors

- Treatment execution errors
  - Random variation between fractions

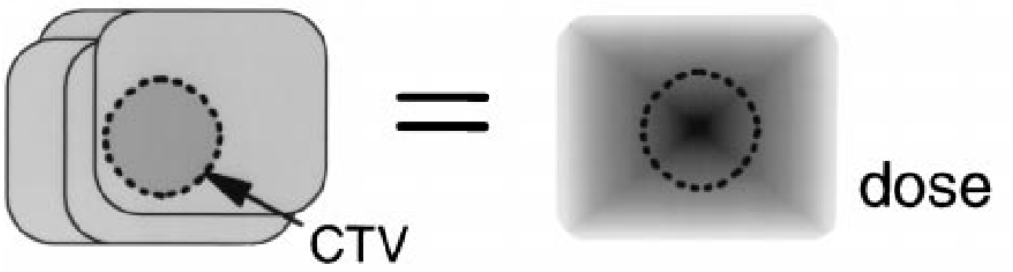

σ

- Treatment preparation errors
  - Random variation between patients
  - Systematic deviation for a single patient

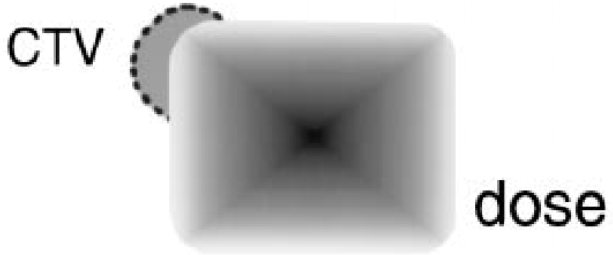

Σ

van Herk et al., IJROBP 47:1121, 2000

Treatment execution errors

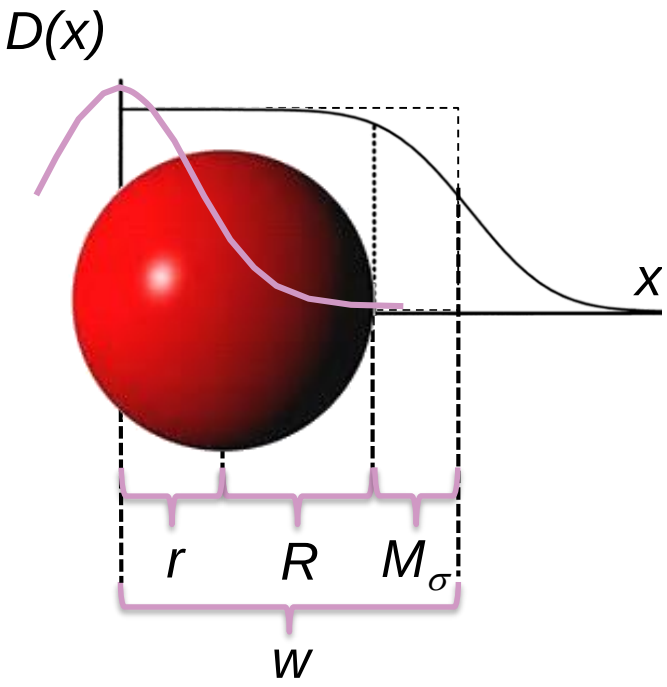

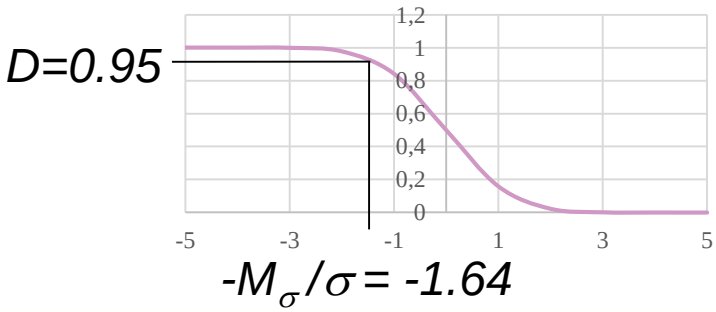

Dose profile ideal step function, blurred due to treatment execution errors:

$$D(x) = H(w-x) * \frac{e^{-\frac{x^2}{2\sigma^2}}}{\sqrt{2\pi}\sigma}$$

$$D(x) = \frac{1}{2}\left[1 - \mathrm{erf}\left(\frac{x-w}{\sqrt{2}\sigma}\right)\right]$$

$$D_{min} = D(r+R)$$

$$D_{min} = 95\% \Rightarrow M_\sigma = 1.64\sigma$$

ESTRO School

Treatment preparation errors

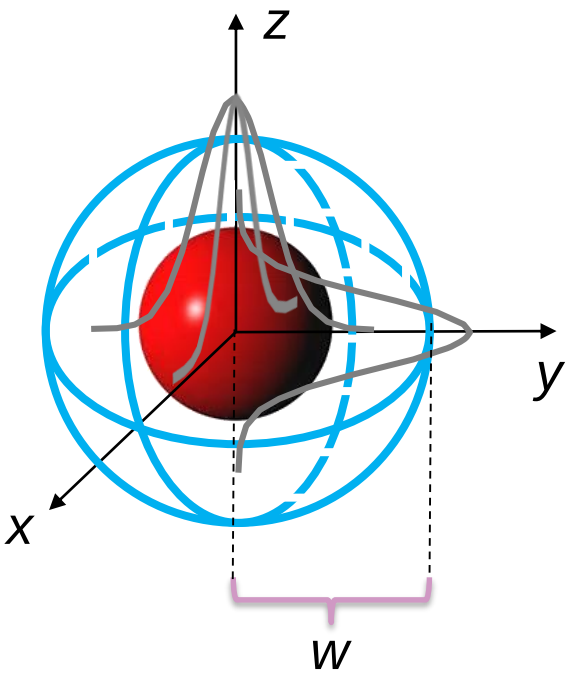

Probability that target position r ($r^2=x^2+y^2+z^2$) is within radius w:

$$P(r<w)=\int_0^w \left[\frac{e^{-\frac{x^2}{2\Sigma^2}}}{\sqrt{2\pi}\Sigma}\cdot\frac{e^{-\frac{y^2}{2\Sigma^2}}}{\sqrt{2\pi}\Sigma}\cdot\frac{e^{-\frac{z^2}{2\Sigma^2}}}{\sqrt{2\pi}\Sigma}\right]4\pi r^2 dr$$

$$P(r<w)=erf\left(\frac{w}{\sqrt{2}\Sigma}\right)-e^{-\frac{w^2}{2\Sigma^2}}\sqrt{\frac{2}{\pi}}\frac{w}{\sigma}$$

P=0.9

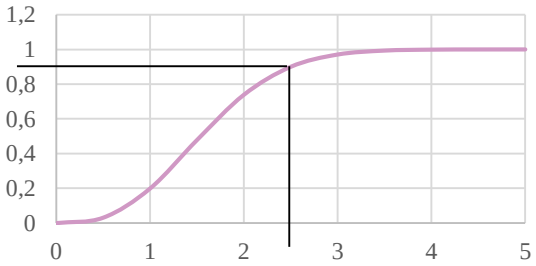

w/Σ=2.5

$$P=0.9 \Rightarrow r<w=2.5\Sigma$$

$$\Leftrightarrow r+R<R+2.5\Sigma \Rightarrow M_\Sigma=2.5\Sigma$$

ESTRO School

Total margin

$$M = M_{\Sigma} + M_{\sigma} = 2.5\Sigma + 1.64\sigma$$

$$\Sigma = \sqrt{\Sigma_m^2 + \Sigma_s^2 + \Sigma_d^2}$$

$$\sigma = \sqrt{\sigma_m^2 + \sigma_s^2 + \sigma_p^2}$$

m – organ motion during preparation

s – set-up error during preparation

d – target delineation error

m – organ motion during treatment

s – set-up error during treatment

p – dosimetric penumbra

Total margin

$$M = M_{\Sigma} + M_{\sigma} = 2.5\Sigma + 1.64\sigma$$

$$\Sigma = \sqrt{\Sigma_m^2 + \Sigma_s^2 + \Sigma_d^2}$$

$$\sigma = \sqrt{\sigma_m^2 + \sigma_s^2 + \sigma_p^2} - \sigma_p$$

In practice, the margin is determined with respect to the 95% isodose surface

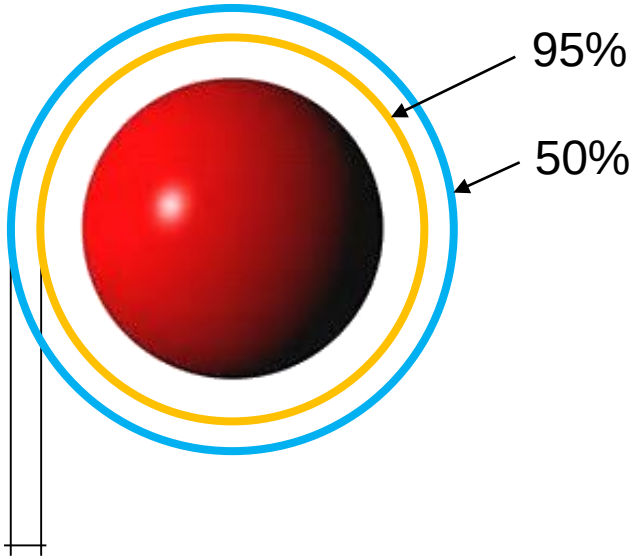

Subtracted from margin

Total margin

$$M = M_\Sigma + M_\sigma = 2.5\Sigma + 1.64\sigma$$

$$\Sigma = \sqrt{\Sigma_m^2 + \Sigma_s^2 + \Sigma_d^2}$$

$$\sigma = \sqrt{\sigma_m^2 + \sigma_s^2 + \sigma_p^2} - \sigma_p$$

$$M = M_\Sigma + M_\sigma = 2.5\Sigma + 0.7\sigma'$$

$$\sigma' = \sqrt{\sigma_m^2 + \sigma_s^2}$$

A 5 mm distance between the 95% and 50% isodose surface corresponds to σ_p=3.2 mm

$$1.64\left(\sqrt{\sigma'^2 + 0.32^2} - 0.32\right)$$

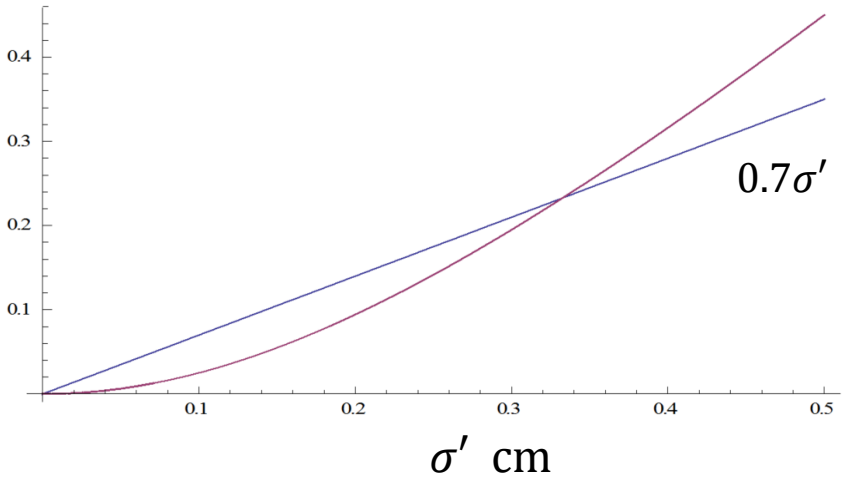

Limitations of margin recipes

- Idealised patient geometry
  - Spherical target
  - No change in body contours
  - No account for organs at risk
  - Motion only includes translation
  - Normal distribution of errors
- Idealised dose delivery
  - Perfect conformity
  - Not affected by changes in geometry
  - Calculation only considers minimum dose
  - Infinite number of fractions
  - Normal distribution of errors

PROBABILISTIC PLANNING

Probabilistic treatment planning

PTV-based planning

- One single CTV is delineated
- A **margin** is added by the planner to form PTV
- Treatment planning is based on PTV to ensure a certain dose coverage probability for the CTV

CTV-based planning

- Multiple CTVs are delineated by sampling known variations
- Robust treatment planning to account for **all CTV instances**
- Treatment planning is based directly on dose coverage histograms for the CTV

Dose-volume coverage maps

Systematic error
- Sampled from normal distribution
- Used to shift the CTV

Random error
- Normal distribution
- Infinite number of fractions
- Convolution of dose (or fluence)

Calculate DVH for CTV
- One entire treatment course

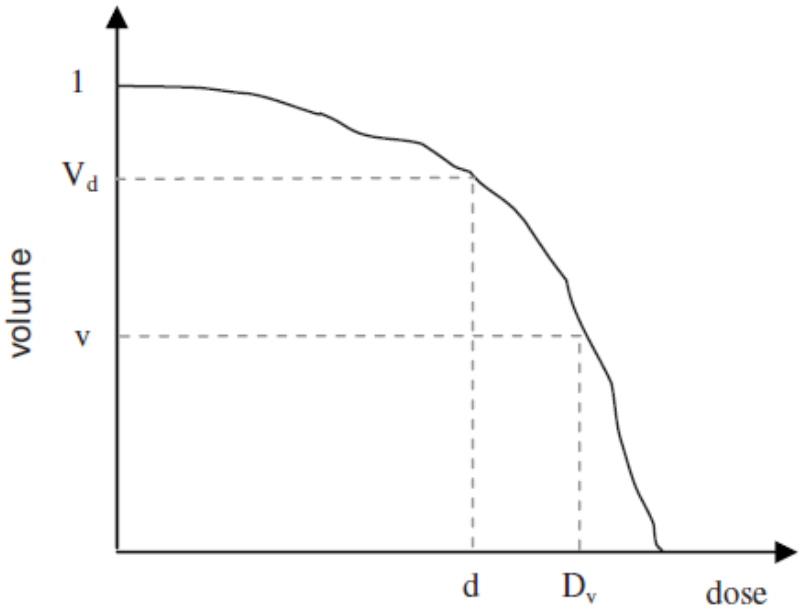

Gordon et al., Med Phys 37:550, 2010

Dose-volume coverage maps

Systematic error
- Sampled from normal distribution
- Used to shift the CTV

Random error
- Normal distribution
- Infinite number of fractions
- Convolution of dose (or fluence)

Calculate DVH for CTV
- One entire treatment course
- Create coverage map

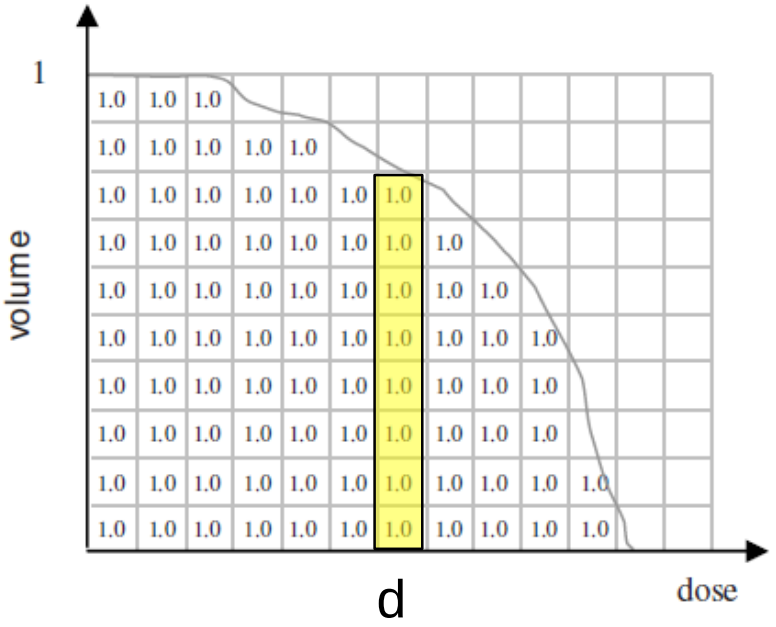

Gordon et al., Med Phys 37:550, 2010

ESTRO School

Dose-volume coverage maps

Repeat for N treatments

Systematic error
- Sampled from normal distribution
- Used to shift the CTV

Random error
- Normal distribution
- Infinite number of fractions
- Convolution of dose (or fluence)

Calculate DVH for CTV
- One entire treatment course
- Create coverage map

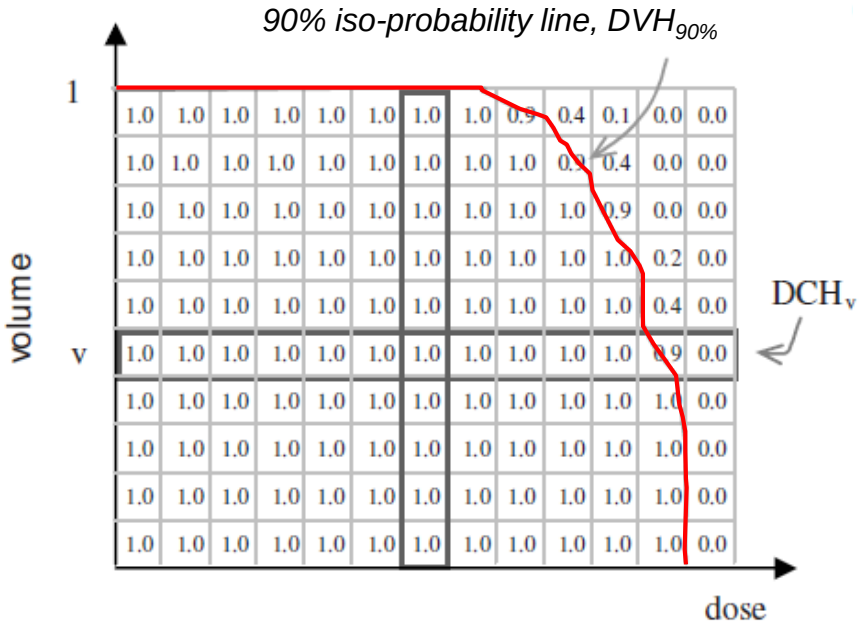

Gordon et al., Med Phys 37:550, 2010

ESTRO School

Dose-coverage histogram (DCH)

Repeat for N treatments

Systematic error
- Sampled from normal distribution
- Used to shift the CTV

Random error
- Normal distribution
- Infinite number of fractions
- Convolution of dose (or fluence)

Calculate DVH for CTV
- One entire treatment course
- Create coverage map

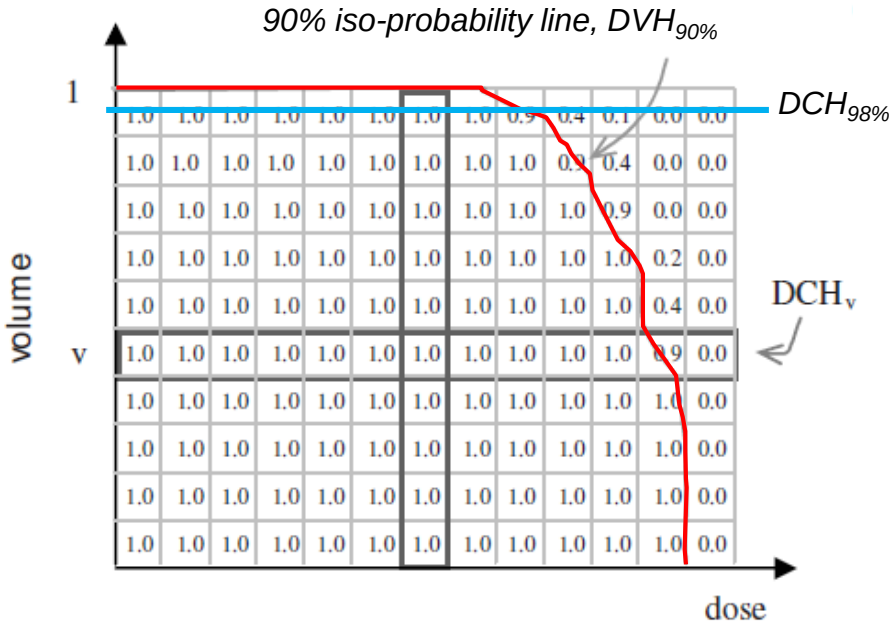

Gordon et al., Med Phys 37:550, 2010

ESTRO School

DCH as optimization criteria

Repeat for N treatments

Systematic error
- Sampled from normal distribution
- Used to shift the CTV

Random error
- Normal distribution
- Infinite number of fractions
- Convolution of dose (or fluence)

Calculate DVH for CTV
- One entire treatment course
- Create coverage map

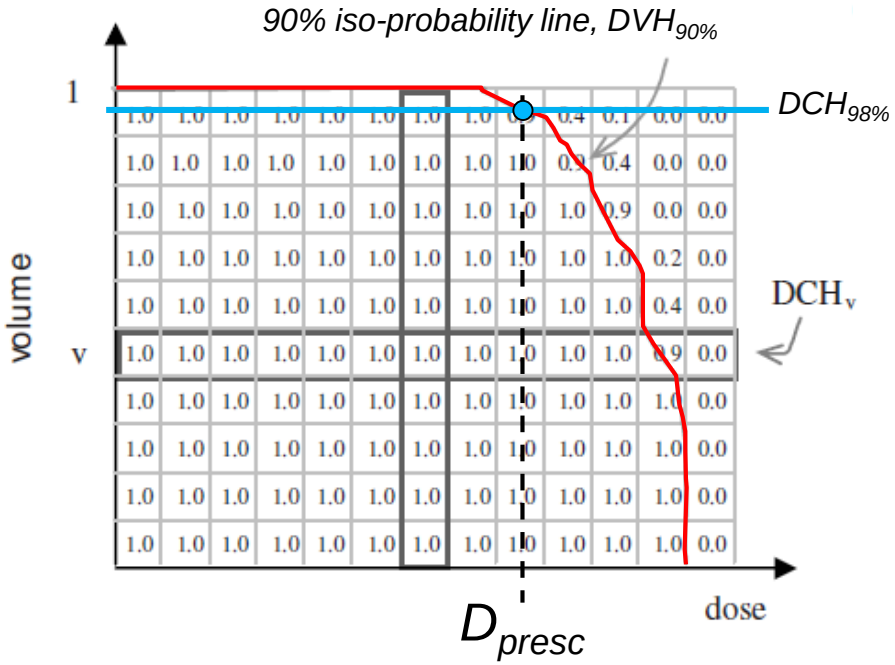

Example of optimization objective:

$$P\left(D_{98\%} \geq D_{presc}\right) \geq 90\%$$

Gordon et al., Med Phys 37:550, 2010

ESTRO School

Statistical shape models

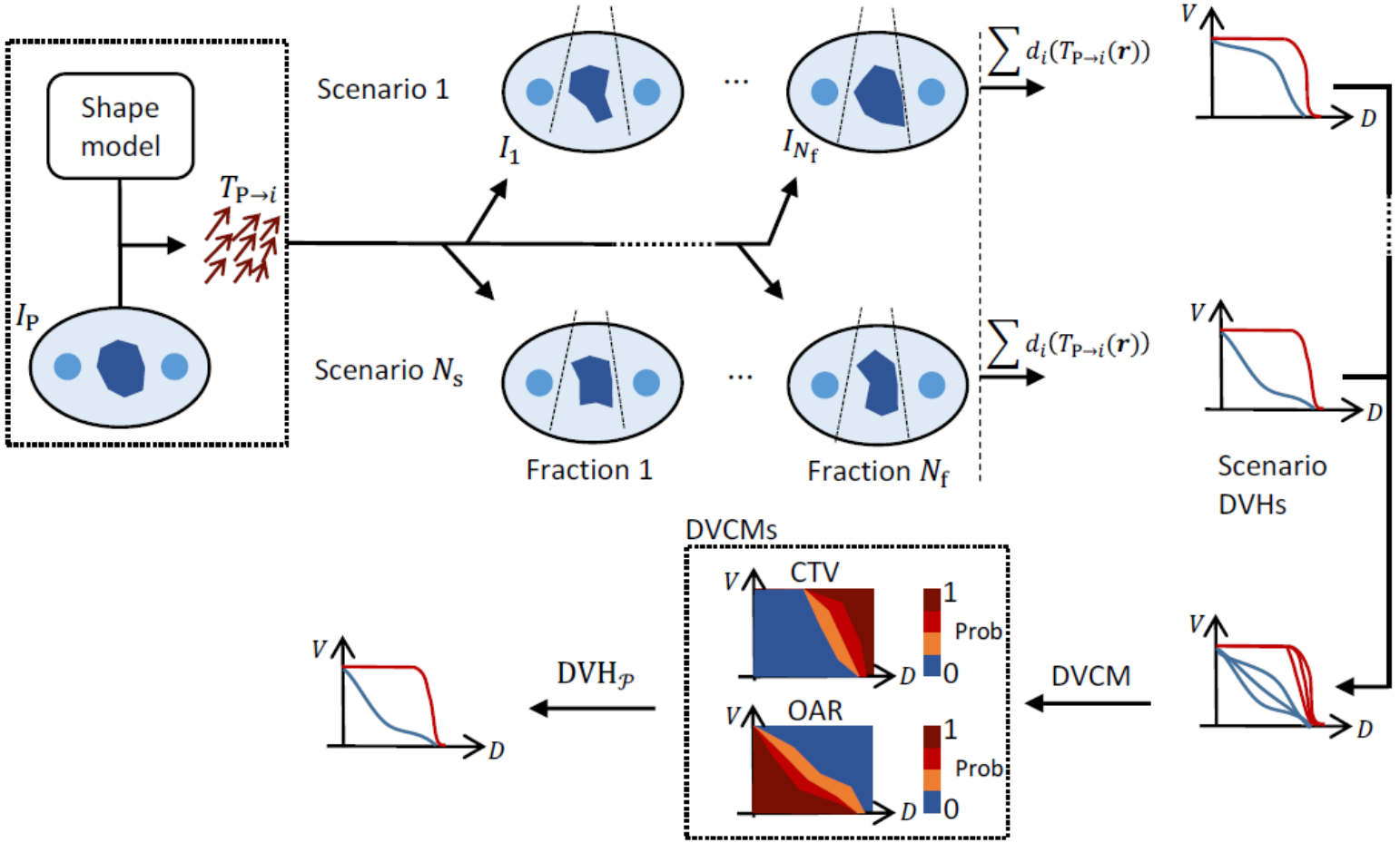

Tilly et al., Phys Med Biol, 2016

ESTRO School

Challenges

- Further development of statistical shape modelling
- Uncertainties associated with deformable registration
- Intrafraction motion and interplay effects
- Efficient optimization techniques
- **Fast dose calculation algorithms!**

Summary

We have discussed

- Various geometrical uncertainties
- The construction of CTV-to-PTV margins
- The limitations of margin recipes
- The basics of probabilistic planning

References

- AM van Mourik, PHM Elkhuizen, D Minkema, JC Duppen, C van Vliet-Vroegindeweij. Multiinstitutional study on target volume delineation variation in breast radiotherapy in the presence of guidelines. Radiother Oncol 94:286-291, 2010.
- D Verellen, M De Ridder, N Linthout, K Tournel, G Soete, G Storme. Innovations in image-guided radiotherapy. Nat Rev Cancer 7:949-960, 2007.
- LB Marks, SM Bentzen JO Deasy, et al. Radiation dose-volume effects in the lung. Int J Radiat Oncol Biol Phys 76:S70-S76, 2010.
- ICRU. Prescribing, recording, and reporting photon-beam IMRT. ICRU Report 83. Bethesda; 2010.

References

- M van Herk, P Remeijer, C Rasch, J V Lebesque. The probability of correct target dosage: dose-population histograms for deriving treatment margins in radiotherapy. Int J Radiat Onc Biol Phys 47:1121, 2000.
- D Tilly. Probabilistic treatment planning based on dose coverage – how to quantify and minimize the effects of geometric uncertainties in radiotherapy. Doctoral thesis. Acta Universitatis Uppsaliensis, Uppsala, 2016.
- JJ Gordon, N Sayah, E Weiss and JV Siebers. Coverage optimized planning: probabilistic treatment planning based on dose coverage histogram criteria. Med Phys 37:550, 2010.
- D Tilly, AJ van de Schoot, E Grusell, A Bel, A Ahnesjö. Dose coverage calculation using a statistical shape model – applied to cervical cancer radiotherapy. Phys Med Biol, 2016.